The Waterberg Platinum-Group Element Deposit, South Africa

UNIVERSITY OF THE
WITWATERSRAND,
JOHANNESBURG

2018

PhD Thesis

Matthew James Gerard McCreesh

Student number: 368485

Supervised by

Judith A. Kinnaird

&

Marina A.Yudovskaya

Declaration:

I declare that this dissertation is my own, unaided work. It is being submitted for the Degree of Doctor of Philosophy at the University of the Witwatersrand, Johannesburg, South Africa. It has not been submitted before for any degree or examination in any other University.

_____

(Signature of Candidate)

Date: _____

Abstract:

The Waterberg platinum-group element deposit of the Bushveld Complex is located within the Southern Marginal Zone of the Limpopo Mobile Belt, north of the Hout River Shear Zone. The Bushveld succession is approximately 1.2 km thick, and dips 34° to 38° towards the northwest. The succession is composed of basal Marginal sills, an Ultramafic Sequence, a troctolite-gabbronorite-anorthosite sequence, and an Upper Zone. The overlying Waterberg Group was deposited between ~2.05 to ~1.95 Ma, after extensive erosion of the roof rocks and the Upper Zone and before the intrusion of a dolerite sill associated with the ~1.1 Ga Umkondo Igneous Province.

The magmatic history of the Waterberg deposit stratigraphy is believed to have started with the intrusion of the basal Marginal sill composed of fine-grained pyroxenite and gabbronorite similar to the Marginal Zone lithologies elsewhere in the Bushveld Complex. These sill-like intrusions interacted with the granitic gneiss footwall of the Southern Marginal Zone to form a basal granofels unit. The overlying Ultramafic Sequence is the most primitive unit of the Waterberg stratigraphy, and hosts the lower F zone mineralisation. This sequence is dominated by a basal orthopyroxenite, overlain by serpentinised harzburgite. Chromite occurs as disseminated clusters with rare discontinuous chromitite stringers. The overlying troctolite-gabbronorite-anorthosite sequence forms a magmatic erosional contact with the underlying Ultramafic Sequence. The basal troctolite is interpreted to have formed from magma mixing between the residual melt of the harzburgite and the influx of a gabbroic melts. The troctolite grades upwards into gabbronorite and anorthosite with sporadic occurrences of inverted pigeonite, which are typical characteristics of the Main Zone elsewhere in the Bushveld Complex. The top contact of this sequence is associated with the upper T zone mineralisation and the occurrence of cumulus magnetite, an indicator mineral of the Upper Zone elsewhere in the Bushveld Complex. The Upper Zone is composed of disseminated cumulus magnetite, however it lacks the magnetitite layers seen in the rest of the Bushveld Complex.

The two PGE-Cu-Ni-Au mineralised intervals vary from 3 m to 60 m thick. The upper T zone is restricted to the southern portion of the project area, whereas the lower F zone extends for a known 17 km along strike. The lower F zone mineralisation is dominated by sperrylite and Pt-Pd bismuthotellurides and these platinum-group metals are mainly associated with primary magmatic base-metal sulphides, which have undergone alteration during serpentinisation followed by the formation of secondary sulphide assemblages. The sulphur isotopic signatures suggest that the F zone mineralisation is mantle-derived with no contamination involved in the formation of the mineralisation. The upper T zone mineralisation hosted by more felsic-rich lithologies is dominated by Pt-Pd bismuthotellurides. The mineralised zone contains relics of primary magmatic sulphides and is characterised by the development of a chalcopyrite-millerite-pyrite assemblage, associated with hydrothermal quartz and hydrous silicates. The fluid–induced style of platinum-group metal remobilisation, high Au/PGE ratios, and high proportion of native gold in the high-grade T zone mineralisation in cumulus magnetite-bearing lithologies is unique to the Bushveld Complex. The genesis of the T zone is interpreted to result from the prolonged fractionation of the troctolite-gabbronorite-anorthosite sequence with the residual melt interacting with the first influx of Upper Zone fertile melt. The sulphur isotopic results indicate that the mineralisation is mantle-derived and that no significant contamination is involved in the formation of the T zone ores.

Although there are similarities with the Bushveld succession south of the Hout River Shear Zone and with the rest of the Bushveld Complex, significant differences in the thickness and type of lithologies, mineral and whole-rock geochemistry and mineralisation of the arcuate intrusion of the Waterberg segment, compared with the eastern, western and northern limbs of the Bushveld Complex, suggests that the Waterberg Bushveld body may represent a structurally controlled separate compartment wedge between the Hout River Shear Zone to the south and the Palala Shear Zone to the north.

Acknowledgements:

I would like to acknowledge the following people for their assistance and contributions with many different aspects in the research thesis. First and foremost I would like to express my gratitude to my supervisors: First, Prof Judith Kinnaird for taking me on for a PhD and giving me this amazing opportunity. Her constant assistance and guidance made this project possible. Secondly, I would like to thank Dr Marina Yudovskaya for all her constant assistance in sample preparation and guidance throughout the whole project.

This project would have not been possible without the funding and access to the core yard for core-logging, sampling and magnetic susceptibility survey down the cores. I would like to thank Platinum Group Metals (PTM) Ltd, especially to Mike Jones, Thys Botha and the geologists on site Aleck Mkhabela, Sibusiso Sithole and Given Matjomane.

During this research project I have had the opportunity of carrying out many different types of analyses in different laboratories in South Africa. I would like to thank Mike Butler at the iThemba Laboratories in Johannesburg for introducing me to sulphur isotope analyses. To Dr Gelu Costin at Rhodes University, Grahamstown, thank you for guidance and the opportunity to learn how to operate the Jeol JXA 8230 Superprobe. The use of the Jeol JXA 8230 Superprobe, instrument was sponsored by NRF/NEP grant 40113 (UID 74464), which I gratefully acknowledge. I would like to thank the team from the Earth Lab at the University of the Witwatersrand for performing all the XRF analyses and for the assistance with XRF sample preparation. Furthermore, I would like to thank the technical staff of the School of Geosciences, particularly Caiphus F Majola, Musa Cebekhulu and Joe Aphane for assistance with preparing samples for polished thin sections, polished ore blocks as well as assisting in mineral separation processes. Thanks also go to Kofi Acheampong for assistance in the field when performing the magnetic susceptibility surveys on the boreholes and assistance with sample preparations.

I would like to thank the professors, lectures and other members of staff of the School of Geosciences at the University of the Witwatersrand, who provided access to sample preparation, microscopes, use of the Niton (Handheld XRF) and advice on how to perform certain aspect to my thesis.

Finally, I would like to thank my family and girlfriend Catherine van Eyk for all the support and encouragement throughout the entire journey and for being there when times were tough. I would also like to thank my girlfriend for helping with sample preparation and for her patience and understanding especially when I had to work late.

Contents:

Declaration

Abstract

Acknowledgements

Chapter 1: Introduction

1.1 Prelude……1

1.2. Platinum Group Elements (PGE)……1

1.2.1. Physical Properties of Platinum-Group Elements (PGE)……..1

1.2.2. Distribution of PGE within the Earth's Crust……2

1.2.3. Formation of Magmatic Ni-Cu-(PGE) Sulphide Deposits……...3

1.2.4. Uses of Platinum-Group Elements (PGE)……..5

1.3. Purpose of Study……...6

1.3.1. Problem Statement…….....6

1.3.2. Aim and Objectives……..7

1.3.3. Structure of this Thesis……..7

1.3.4. Methodology……..9

1.3.5 Other Presentations, Reports and Publications the author was involved with…….....9

Chapter 2: Regional Geology

2.1 Kaapvaal Craton……11

2.1.1. Regional Structural History……11

2.2 Bushveld Complex……..13

2.2.1. Rustenburg Layered Suite……...14

2.2.1. A. Marginal Zone (MnZ)……15

2.2.1. B. Lower Zone (LZ)……17

2.2.1. C. Critical Zone (CZ)……...18

2.2.1. D. Main Zone (MZ)……..24

2.2.1. E. Upper Zone (UZ)……24

2.2.2. Bushveld Granites……25

2.2.3. Age of the Bushveld Complex……26

2.2.4. Emplacement of the Bushveld Complex……..27

Chapter 3: Geology of the Northern Limb

3.1. Introduction to the Northern Limb……...……30

3.2. Structures of the Northern Limb……..32

3.3. Stratigraphy of the Northern Limb……..33

3.3.1. Footwall……34

3.3.2. Marginal Zone……..35

3.3.3. Lower Zone……..35

3.3.4. Critical Zone, GNPA Member and the Platreef.……36

3.3.4. A. GNPA Member……36

3.3.3. B. The Platreef……36

3.3.5. Main Zone……41

3.3.6. Upper Zone……..42

3.4. Mineralisation in the Northern Limb…….……..……43

3.4.1. Mineralisation in the Lower Zone……43

3.4.2. Mineralisation in the Platreef……43

3.4.3. Mineralisation in the Main and Upper Zone……47

3.5. Ages of the Northern Limb………48

Chapter 4: Manuscript 1 - The Waterberg Platinum-Group Element Deposit: Atypical Mineralisation in Mafic-Ultramafic Rocks of the Bushveld Complex, South Africa.

4.1. Candidates contribution……..……50

4.2. Abstract……...51

4.3. Introduction……...52

4.4. Geology of the Northern Limb……...53

4.5. Regional Geology of the Waterberg Project……..……57

4.6. Methodology……59

4.7. Project Geology……..……62

4.7.1. Magnetic susceptibility variations……..……67

4.7.2. Mineralization…..……..69

4.8. Discussion……74

4.8.1. Model for the formation of the Waterberg intrusion……84
4.9. Conclusions……..86
Chapter 5: Manuscript 2 - Platinum-group minerals of the Waterberg deposit, Bushveld Complex: implication for the formation of the PGE mineralisation
5.1. Candidates contribution……..……87
5.2. Abstract……...88
5.3. Introduction……...89
5.3.1. Bushveld Complex Geology……89
5.3.2. The Platreef……...91
5.3.3. Waterberg Project Setting……...92
5.3.3. A. Waterberg Project Geology……93
5.4. Methodology……96
5.5. Results……97
5.5.1. Waterberg Stratigraphy along the Boreholes WB034, WB099 and WB195……...97
5.5.2. Stratigraphy of the Mineralised zones……...98
5.5.3. Downhole PGE variations through the F and T zones……...99
5.5.4. Sulphide Assemblages of the F zone……102
5.5.5. Sulphide Assemblages of the T zone……106
5.5.6. PGM Mineralisation……109
5.6. Discussion……...118
5.6.1. Comparison of the F and T zone with other Bushveld mineralised intervals……118
5.6.2. Relationships between PGM, BMS and rock-forming minerals……..123
5.6.3. Model of the Waterberg Bushveld Succession……..125
5.7. Conclusion……..128
Chapter 6: Manuscript 3 - Whole rock geochemistry and mineral chemistry of the Waterberg PGE deposit, South Africa: implication for the Bushveld stratigraphy and the formation of the PGE mineralisation.
6.1. Candidates contribution……..……..132
6.2. Abstract……133
6.3. Introduction……134
6.4. Sample material……..……..138
6.5. Analytical Methods……..……141

6.6. Results……142
6.6.1. Magnetic Susceptibility……..142
6.6.2. Petrology……..143
6.6.3. Mineral chemistry……...146
6.6.4. Whole rock geochemistry……..150
6.6.5. Mineralisation……..154
6.7. Discussion……...156
6.7.1. Correlation with the Mineralised Intervals of the Northern Limb……158
6.7.2. Mineral Chemistry and Magnetic Susceptibility Stratigraphy Comparisons…….163
6.8. Conclusion……167
Chapter 7: Manuscript 4 - Sulphur Isotopes of the Waterberg PGE deposit, South Africa: implication for the formation of the PGE mineralisation
7.1. Candidates contribution……..169
7.2. Abstract……170
7.3. Introduction……170
7.4. Regional Geology……..171
7.4.1. Transvaal Supergroup……...171
7.4.2. Bushveld Complex……172
7.4.3. Northern Limb……172
7.4.4. Waterberg Project……..174
7.5. Previous Sulphur Isotope Works on the Northern Limb……177
7.6. Sampling and Methodology……182
7.7. Results……..182
7.7.1. Sulphur Isotopes……182
7.8. Discussion……...185
7.9. Conclusion……...188
Chapter 8: Manuscript 5 - Geochemistry and PGE of the lower mineralised zone of the Waterberg Project, South Africa
8.1. Candidates contribution……..189
8.2. Abstract……190
8.3. Introduction……191
8.4. Geology……191

8.4.1. The Northern Lobe and the Platreef……193
8.4.2. Local geology……..196
8.5. Methodology……..……199
8.6. Results……..201
8.6.1. Field relationships and petrography……201
8.6.1. A. Marginal orthopyroxenite……..201
8.6.1. B. Marginal gabbronorite……...202
8.6.1. C. The ultramafic sequence……..202
8.6.1. D. The Troctolite-Gabbronorite-Anorthosite Sequence……205
8.6.2. Geochemistry……..206
8.6.2. A. Major and trace element variation diagrams……206
8.6.2. B. Multi-element normalized plots……207
8.6.2. C. PGE and Au……...208
8.6.2. D. PGE and Cr assay data provided by Platinum Group Metals……212
8.6.3. Lateral variation in lithology and mineralization……213
8.7. Discussion……...216
8.7.1. Discussion of the data presented……216
8.7.2. Correlation with the Aurora Project……220
8.7.3 Correlation with the Platreef……..223
8.7.4. A preliminary model……...225
8.8. Conclusion……..……...229

Chapter 9: Discussion and Conclusion

9.1. Introduction……231
9.2. Stratigraphic Correlations of the Waterberg Project……..……231
9.3. Waterberg Mineralisation……..……244
9.4. Magma Emplacement……..……255
9.4.1. Model of Waterberg Stratigraphy……257
9.4.2. Hydrothermal Activity and Redistribution of PGE……259
9.4.3. Contamination……260
9.5. Conclusion……..……...261
9.6. Recommendation……..……262
References……...……264

List of Figures and Tables:

Chapter 1: Introduction

Table 1.1: Physical and chemical properties of platinum-group elements (PGE) (Westland, 1981)……..2

Figure 1.1: The distribution of Pt, Pd and Rh resources of major mining operations around the World (Johnson Matthey, 2011)……..3

Figure 1.2: Pie charts showing the main uses and demands for PGE (Pt, Pd, Rh, Ru and Ir) from 2011 to 2013 (Johnson Matthey, 2011; Cowley, 2014)……5

Chapter 2: Regional Geology

Figure 2.1: Schematic showing tectonomagmatic evolution of the Kaapvaal Craton. Key: TML - Thabazimbi-Murchison Lineament, CL - Colesberg Lineament, PSZ - Palala Shear Zone, TSZ - Triangle Shear Zone, LB - Limpopo Belt (Modified from Silver *et al*., 2004; Holwell, 2006)……..12

Figure 2.2: Simplified geological map of the Bushveld Complex (Modified from Kinnaird *et al*., 2005) as well as the location of the Waterberg project (star) between the Hout River Shear Zone (HRSZ) and the Palala Shear Zone (PSZ). TML; Thabazimbi Murchison Lineament……14

Figure 2.3: Generalised stratigraphy of the Rustenburg layered Suite through the Western and Eastern limbs of the Bushveld Complex. The figure is compiled from a number of sources (Cameron, 1978; 1980; 1982; von Gruenewaldt, 1973; Molyneux, 1974, Vermaak, 1976; SACS, 1980; Mitchell, 1990; Teigler *et al*., 1992; Nex *et al*., 1998; Wilson, 2015, primarily modified from Eales and Cawthorn, 2006)……..16

Figure 2.4: SE-NW schematic section showing variations in the pre-Merensky and Merensky pyroxenites in the southwestern Bushveld Complex (Redrawn from Naldrett *et al*., 2009)……21

Figure 2.5: Schematic section through stratigraphic succession including the Merensky Reef in the northwestern section of the western limb of the Bushveld Complex (descriptions from Smith *et al*., 2004; Robert *et al*., 2007; Viljoen, 1999 and Redrawn from Naldrett *et al*., 2009)……..21

Chapter 3: Geology of the Northern Limb

Table 3.1: Summary of the geology and mineralisation along the strike of the Platreef (Modified from Holwell, 2006; McDonald and Holwell, 2011)……46

Figure 3.1: Geological map of the northern limb of the Bushveld Complex (after van der Merwe, 1978; Ashwal *et al*., 2005; Modified from McDonald *et al*., 2017). Boundaries of farms mentioned in text are shown……..31

Figure 3.2: Schematic stratigraphy of the eastern and western limbs (left side) (Eales and Cawthorn, 1996), the stratigraphy south of the Ysterberg-Planknek Fault on Grasvally (middle) (Hulbert, 1983), and the stratigraphy for the northern limb north of the Ysterberg-Planknek Fault (right side) (Kinnaird *et al*., 2005; Kinnaird and Nex, 2015)……33

Figure 3.3: Lithostratigraphy of the Transvaal Supergroup floor rocks beneath the Rustenburg Layered Suite of the northern limb of the Bushveld Complex. The oldest floor rocks of Archean granite-gneisses occur in the north and the youngest floor rocks occur in the southern sector of the northern limb. Data from Button

(1973), Martini (1979), Catuneanu and Eriksson (1999), Bekker *et al*. (2004) and Van der Merwe (2008) for the Mokopane area, the image was redrawn from Kinnaird and Nex (2015)……34

Figure 3.4: Stratigraphy of the northern limb south of the Ysterberg-Planknek Fault (Modified from McDonald *et al*., 2005)……34

Figure 3.5: Schematic longitudinal section through the Platreef along the entire strike length (Redrawn from Kinnaird *et al*., 2005). Note that between Witrivier and Altona a significant strike length is not shown……39

Figure 3.6: A comparison of the noble metal abundance of the Platreef, the Merensky Reef and UG2, showing the predominance of palladium in the Platreef of the northern limb. Data for the Merensky Reef and the UG2 from Barker (2012), and for the Platreef based on data for Sandsloot from the Anglo Platinum annual report (2011). Diagram modified from Kinnaird *et al*. (2017)……..47

Chapter 4: The Waterberg Platinum-Group Element Deposit: Atypical Mineralisation in Mafic-Ultramafic Rocks of the Bushveld Complex, South Africa.

Table 4.1: Geochemical Analytical Data for Selected Samples from Waterberg……..68

Table 4.2: Grade Values for Precious and Base Metals in the F and T Zones……..73

Table 4.3: Potential Correlation of Upper Zone Rocks in the Waterberg Project with Those in the Eastern and Western Limbs of the Complex (subzones of the eastern and western limbs from Eales and Cawthorn, 1996)……..83

Table 4.4: JORC-Compliant Data for the Aurora Project in the Main Zone South of the Hout River Shear Zone is added for Comparison (Venmyn-Rand, 2010)……..84

Figure 4.1: Map showing the distribution of major lithologic units in northern South Africa. Abbreviations: HRSZ =Hout River shear zone, JHB = Johannesburg, NMZ = Northern marginal zone, SMZ = Southern marginal zone, TML = Thabazimbi-Murchison lineament. The small box indicates the Waterberg area. After Dorland *et al*. (2006)……53

Figure 4.2: Geology of the northern limb of the Bushveld Complex (A) map, showing locations that are mentioned in the text. HRSZ = Hout River shear zone, PYF = Planknek-Ysterberg fault, TML = Thabazimbi-Murchison lineament (B) stratigraphy of the Waterberg project area……..54

Figure 4.3: Selected photographs of cores showing different lithologies of the Waterberg sediments. (A). Medium- to coarse-grained red-bed sandstone interbedded with purple brown banded arkose and light-green epidotised zones and a very fine grained chocolate-brown mudstone (WB017). (B). Coarse-grained conglomerate containing quartz pebbles and various types of lithic fragments (WB047). (C). Cross trough-bedded and hummocky cross-stratification in variably coloured fine-grained sandstone (WB027). (D). Typical variably coloured sandstone of the Setlaole Formation of the Waterberg Group (WB096)…59

Figure 4.4: Schematic map showing the location of the boreholes discussed together with major shear zones and dikes within the project area……61

Figure 4.5: Contact between Bushveld gabbro and the overlying Waterberg sediments. (A), Coarse Waterberg conglomerate overlying altered and weathered Bushveld lithologies with remnants of a paleosol (WB004). (B). Sharp contact of altered light-greenish gabbro with relics of decomposed silicates and

overlying foliated hematitised siltstone, which may represent the original volcanic roof rocks into which the Waterberg igneous rocks were intruded (WB038) (Yudovskaya *et al*., 2015)……..62

Figure 4.6: Selected photos of footwall rocks. (A). Banded agmatite formed from the interaction between Bushveld magma and the footwall granite gneiss (WB017). (B). Granite gneiss with rare chalcopyrite and pyrrhotite (WE005D0). (C). Agmatite with well-defined banding of felsic- and pyroxenite-rich layers (WE035). (D). Highly altered agmatite (WE035). From McCreesh 2016……64

Figure 4.7: Selected images showing the variation in the ultramafic lithologies. (A). Strongly serpentinized harzburgite from WB132. (B). Feldspathic pyroxenite (Feldsp. PX) at the top and a unit that has been completely serpentinized below (WB027). (C). Feldspathic pyroxenite with blebs of pyrrhotite and chalcopyrite and veinlets of serpentine (WE035). (D). Harzburgite/feldspathic harzburgite with large oikocrysts of orthopyroxene (WB017). From McCreesh (2016)……..65

Figure 4.8: Lithologic variation in the troctolite-norite-anorthosite sequence. (A). Gabbronorite (WB0170). (B). Troctolite (WB163). (C). Pegmatoidal unit (WE001). (D). Anorthosite (WB017). From McCreesh (2016)……66

Figure 4.9: Upper zone lithologies from different cores. (A). Weakly altered ferrogabbro with pinkish altered olivine (WB017). (B). A 2-m-thick magnetite layer (in core tray slots 3 and 4 from the top) only seen in borehole WB001. From McCreesh (2016)……67

Figure 4.10: The magnetic susceptibility values (SI units) plotted against the depth for WB027 (left) and WB099 (right). The high magnetic susceptibility in the Ultramafic sequence is due to secondary magnetite formed from the serpentinisation of olivine. Olivine persists upward at the base of the troctolite-gabbronorite-anorthosite sequence. The increase in magnetic susceptibility values in the T zone is where the boundary is drawn between the troctolite-gabbronorite-anorthosite sequence and the Upper zone, even though there may be no notable lithologic change. From McCreesh (2016)……69

Figure 4.11: Schematic idealized section through the Bushveld intrusive rocks of the Waterberg project, showing the location of the mineralized F and T zones within the stratigraphy. The variability in Pt + Pd + Au grade is shown for both zones and the histograms reflect PGE grades that are typically up to 7 g/t……..70

Figure 4.12: Photomicrographs of sulfide mineralization in the F zone. (A). Magnetite replacement of sulfides. (B). Chalcopyrite, pentlandite, magnetite, and platinum group minerals in olivine. (C). Magnetite replaces chromite and sulfides. (D). Chromite with sulfide inclusion. Abbreviations: Ccp = chalcopyrite, Chr = chromite, Mgt = magnetite, Ol = olivine, Pn = pentlandite, PGM = platinum group minerals, Po = pyrrhotite……71

Figure 4.13: Noble metal minerals from the F zone in core sample WB034 (A). Electrum Au_6Ag_4 = 1,060.3-m depth. (B) Palladioarsenide Pd_2As = 1,060.3-m depth. (C). Majakite PdNiAs + stibiopalladinite, bright (Pd_5Sb_2) + pyrrhotite - 1061 m. (D). Sperrylite ($PtAs_2$) and cobaltite CoAsS = 1,018-m depth. Scale bars are 30 µm in length……71

Figure 4.14: The F zone showing the 2 PGE + Au (ppm) grade and abundances for Cr, Ni, Cu, and S in core WB027. From McCreesh (2015)……72

Figure 4.15: Compositional variation of MgO (wt. %), Mg number, and Cr/MgO (ratio) through core WB017. Dashed lines indicate the mineralized units. TGA sequence = troctolite-gabbronorite-anorthosite, T zone = T mineralized zone, UmS = Ultramafic zone, WB = Waterberg sedimentary sequence. McCreesh *et al*. (2015)……73

Figure 4.16: Schematic section through the T zone, showing the variability of the rock types and the host rocks of the mineralization in the T1 and T2 layers. The column to the left shows the lithology, while the column to the right for each borehole shows the stratigraphic affiliation of the various units……74

Figure 4.17: Photomicrographs of sulfide mineralization in the T zone. (A). Flame-textured pentlandite in pyrrhotite and pyrite. (B). Pyrite after magnetite and pyrrhotite. (C). Au and pyrrhotite in chalcopyrite. (D). Pyrite growing along the boundary of pyrrhotite and chalcopyrite. All images in reflected light. Abbreviations: Ccp = chalcopyrite, Ilm = ilmenite, Pn = pentlandite, Po = pyrrhotite, Py = pyrite……..75

Figure 4.18: The mineralized T zone showing the distribution of 2PGE+Au (ppm) grade within T1 and T2. Variations in the Cr, Ni, Cu, and S % in core WB099 are also shown. Note how the high PGE do not correlate with zones of high Cr %. Samples were analysed for Pt, Pd, and Au (all ppm) by standard 25-g lead fire-assay using a silver collector. Rh was assayed using the same method but with a palladium collector. After preconcentration by fire assay the resulting solutions were analysed using ICP-OES for copper, nickel, cobalt, and chromium. This technique results in "almost" total digestion. Data by courtesy of PTM in McCreesh (2015)……..76

Figure 4.19: Classification of the Main zone rocks in the Western Bushveld (Nex *et al*., 1998). Waterberg features indicate comparative mineralogy and tentative correlation on the Waterberg project Main zone rocks; opx = orthopyroxene……78

Figure 4.20: Profiles through the Main zone-Upper zone boundary in various parts of the Bushveld Complex, showing the position of a pyroxenitic layer that may be ortho- or clinopyroxene dominated, relative to where cumulus magnetite is recognized. Modified from Ashwal *et al*. (2005). GVG 1970 = von Gruenewaldt (1970)……78

Figure 4.21: Multielement chondrite-normalized plot for mafic-ultramafic rocks, showing the overall similarity of the different rock sequences in the Waterberg project area. There is a similarity to all Bushveld lithologies from the eastern and western limbs with a negative Nb-Ta and a positive Sr anomaly. Lower zone pyroxenites beneath the Platreef on Turfspruit also show a negative Nb-Ta anomaly, a variable negative Ti anomaly, and gently sloped Y and HREE. Data shown are from unpublished data of one of the authors (54 samples, Huthmann *et al*., unpub. data). Chondrite values from Sun and McDonough (1989)……80

Figure 4.22: Variations in the V, Cr, and Co (ppm) of borehole WB017. The solid black line represents the Main-Upper zone boundary determined using the magnetic susceptibility results. The black dashed lines represent the F and T zones. From McCreesh *et al*. (2015)……81

Figure 4.23: A schematic diagram comparing the stratigraphy in Waterberg cores with that for other areas of the northern limb, showing the distinctive lithologic differences between the different areas in the upper Main zone. (A). Bellevue core (Ashwal *et al*., 2005). (B). Waterberg stratigraphy showing how the thickness of the succession varies between the Waterberg and the Bellevue cores. (C). Sections through the Main zone in other areas, showing the position of mineralization. From McCreesh (2016)……..83

Figure 4.24: A comparison of the noble metal abundance of the Waterberg T and F mineralized zones compared to the Platreef, Merensky reef, and UG2, showing the predominance of palladium in the Waterberg deposit. Data for the Merensky reef and UG2 from Barker (2012), for the Platreef based on data for Sandsloot from the Anglo Platinum annual report (2011), and for Waterberg from PTM 43-101……..84

Figure 4.25: Schematic diagram showing the contrast in thickness between the Waterberg intrusive package in the far north of the northern limb of the Bushveld Complex and the intrusive sequence south of the Hout River shear zone. Modified from Kinnaird (2005)……..85

Chapter 5: Platinum-group minerals of the F and T zones, Waterberg Project, Far Northern Bushveld Complex: implication for the formation of the PGE mineralisation.

Table 5.1: Abundances and proportions (area %) of the PGM types in the heavy separates from the Waterberg deposit. The F zone is represented by mineralisation in feldspathic harzburgite to melatroctolite in the borehole WB034. The T zone is represented by mineralisation in gabbronorite and magnetite gabbro in the borehole WB099. D – apparent grain diameter in microns……..110

Table 5.2: Proportions (area %) of the PGM types in the polished sections of poikilitic leucogabbronorite of the T2 subzone in core WB195 according to the MLA results and grain counting under the scanning electron microscope (SEM)……111

Table 5.3: Representative electron microprobe analyses of PGM (wt. %) in the F zone from the cores WB034 and WB091……114

Table 5.4: Representative electron microprobe analyses of PGM (wt. %) in the T zone from the core WB195……116

SUPPLEMENTARY TABLE 5. Sulphide composition (wt. %) in the F mineralised zone (WB034 and WB091) by electron microprobe analysis……130

SUPPLEMENTARY TABLE 6. Sulphide composition (wt. %) in the T mineralised zone (WB195) by electron microprobe analysis……..131

Figure 5.1: Schematic geological map of the Bushveld Complex and enlarged map of the northern limb including the extension of the Waterberg Project in the far north. Modified after 1:250 000 geological map of the northern limb (van der Merwe, 1976)……90

Figure 5.2: Schematic stratigraphic columns for WB034, WB099 and WB195 boreholes in the Waterberg project exploration area. The first column shows the lithology whereas the second column shows stratigraphic units: UmS – Ultramafic Sequence, TGA – Troctolite-Gabbronorite-Anorthosite sequence, UZ – Upper Zone, and UDS – Umkondo Dolerite sill as well as F and T mineralised zones……94

Figure 5.3: Typical lithologies of the mineralised zones from WB161 (F zone) and WB195 (T zone): (a) medium-grained feldspathic orthopyroxenite with disseminated sulphides within the F zone, (b) feldspathic harzburgite to mela-troctolite with disseminated sulphides within the F zone, (c) coarse-grained leucogabbro/anorthosite with interstitial chalcopyrite from the T2 subzone, (d) medium- to coarse-grained feldspathic harzburgite with disseminated sulphides from the T1 subzone. Photo of half-core cut samples 5 cm in diameter; a depth (m) is shown on the left……..95

Figure 5.4: Variations of 2PGE+Au, Cu, Ni, S and Cr abundances, Pt/Pd, Cu/Pd and Au/Pt through the F zone within the Ultramafic Sequence in the WB034 section. Data of 0.5 m sampling are shown by courtesy of Platinum Group Metals (PTM)……..101

Figure 5.5: Variations of 2PGE+Au, Au, Cu, Ni, S and Cr abundances, Pt/Pd, Cu/Pd and Au/Pt through the T zone in the WB099 section. Data of 0.5 m sampling are shown by courtesy of Platinum Group Metals (PTM)……..102

Figure 5.6: Photomicrographs of sulphides in the F zone under reflected light: (a) pyrrhotite (Po) and pentlandite (Pn) with minor chalcopyrite and magnetite (Mgt) rimming an altered olivine (Ol) grain (WB165–1118.1),

(b) chalcopyrite and pyrrhotite (Ccp, Po) replaced by secondary magnetite (Mgt) with minor inclusions of moncheite (Mch), and pyrrhotite along the cleavage in silicates (WB034–1060.85), (c) euhedral crystals of sperrylite (Spe), surrounded by chalcopyrite and pyrrhotite (Ccp, Po), replaced by secondary magnetite (Mgt) in serpentinite (WB034-1060.85). (d) Ni-rich pentlandite (Pn) associated with covellite (Cv) and bornite (Bn) and rimmed by magnetite (Mgt) (WB165–1109.4), (e) chalcopyrite and pentlandite (Ccp, Pn) replaced by valleriite-like mineral 1 (Val 1) (WB034–1060.85), (f) Ni-rich chalcopyrite (Ccp) interstitial between chromite (Chr) grains, replaced by magnetite (Mgt). Valleriite-like mineral 2 (Val 2) is developed after phlogopite and serpentine in brecciated chromite (WB034–1060.85); (a-d and f) – plane polarised, (e) – cross-polarised light……104

Figure 5.7: BSE images of PGM and sulphide assemblages of the F zone in polished sections in core WB034: (a) lenses and lamella of probable sugakiite (Sug, an 12 and 36, Suppl. Table 5) in association with chalcopyrite (Ccp, an. 13-14, Suppl. Table 5) and pyrrhotite (Po, an. 22-23, Suppl. Table 5) in sulphide bleb rimmed by magnetite (Mgt) (1060.85 m), (b) inclusion in chromite (Chr) composed of amphibole (Amp), chalcopyrite (Ccp), pentlandite (Pn) and pyrrhotite (Po). Tiny particles of Pd-Bi-Te mineral are located along fractures in chromite (1060.85 m), (c) brecciated sperrylite (PtAs2, an. 1-6, Table 3) and hollingworthite (RhAsS, an. 8 and 9, Table 3) among pyrrhotite (Po) and chalcopyrite (Ccp) replaced by serpentine (Serp) (1060.85 m), (d) euhedral hollingworthite (RhAsS, an. 10-13 in Table 3) with Ir- and Pt-richer cores in association with kotulskite (PdTe), pyrrhotite (Po) and pentlandite (Pn) in feldspathic harzburgite (1060.93 m)……105

Figure 5.8: Photomicrographs of sulphide assemblages of the T zone: (a) millerite-chalcopyrite-pyrrhotite (Mil, Ccp and Py) association after a primary sulphide bleb inside a larger titanomagnetite-ilmenite intergrowth (Ti-Mgt and Ilm) in gabbronorite (Cpx – clinopyroxene) (WB165-493 m), (b) relics of primary interstitial pentlandite-chalcopyrite (Pn, Ccp) assemblage rimmed by quartz (Q) crust among cumulus clinopyroxene (Cpx) (WB195-902.3 m), (c) millerite (Mil) within pyrite-chalcopyrite (Py, Ccp) symplectitic intergrowths (WB165-493 m); (d) millerite (Mil) and chalcopyrite (Ccp) intergrowth with pyrite-magnetite (Py, Mgt) symplectite within silicates (Sil) (WB165-493 m), (e) chalcopyrite (Ccp) and chalcopyrite-pyrite symplectites rimmed by quartz (Q) and pyrite (Py) (WB195-902.3 m), (f) pyrite (Py) rimmed by quartz-amphibole (Q, Amp) crust interstitial to cumulus clinopyroxene (Cpx) (WB195-902.7 m); (a-e) reflected light, (f) cross-polarised transmitted light……108

Figure 5.9: BSE images of typical PGM grains in heavy mineral separates of the F zone in core WB034: (a) majakite (PdNiAs) with prints of secondary silicates (1060.3 m), (b) euhedral sperrylite ($PtAs_2$) with epitaxitic hollingworthite (RhAsS) on its faces (1061.6 m), (c) an intergrowth of maslovite (PtBiTe) and sperrylite ($PtAs_2$) with epitaxitic hollingworthite (RhAsS) (1067 m), (d) native gold (Au_9Ag_1) with inclusions of majakite (PdNiAs) (1061.6 m), (e) Au-Ag alloy (Au_5Ag_5) with inclusions of cobaltite (Fe,Co,Ni)AsS (1018.00 m), (f) inclusions of stibiopalladinite (Pd_5+x$(Sb)_2$+x) in menshikovite ($Pd_3Ni_2As_3$) (1060.3 m)……112

Figure 5.10: BSE images of rare PGM from the F zone in core WB034: (a) intergrowing Pt-Fe alloy and pyrrhotite on surface of a pyrrhotite (Po) particle (1067 m), (b) surface of atheneite $(Pd,Hg)_3As$ with ingrowths and prints of fine-grained hydrous silicates (1019 m)……113

Figure 5.11: BSE images of typical PGM assemblages in the heavy separates of the T zone in core WB099: (a) merenskyite ($PdTe_2$) intergrown with chalcopyrite (Ccp) (700 m), (b) an euhedral layered crystal of moncheite $(Pd,Pt)Te_2$ (705 m), (c) an intergrowth between layered moncheite ($PtTe_2$) and native gold

(Au_9Ag_1) with inclusions of kotulskite (PdTe) associated with chalcopyrite (Ccp) (705 m), (d) sperrylite ($PtAs_2$) and native gold (Au_9Ag_1) associated with chalcopyrite (Ccp) (705 m), (e) palarstannide $Pd_5(Sn,As)_2$ on native gold (Au_9Ag_1) with secondary silicates (705 m), (f) $Au_{75}Ag_{25}$ alloy associated with hydrous silicates (Sil) (705 m)……116

Figure 5.12: BSE images of PGM assemblages of the T zone in polished sections in core WB195: (a) disseminated kotulskite (PdTe) (an. 8, Table 4) on margins of chalcopyrite (Ccp) bleb with minor pentlandite (Pn) and pyrite (Py). PGM dissemination extends into neighbouring amphibole-quartz (Amp, Q) intergrowth (898.7 m), (b) an unidentified mineral (Pd_4SnTe) (an. 6-7, Table 4) within altered clinopyroxene (Cpx) and secondary silicates. An aureole of Pd-Sn dissemination in silicates surrounds the coarser particle (905.6 m), (c) heterogeneous grain of braggite (Pt,Pd,Ni)S (an. 1-5, Table 4) of variable composition in an intergrowth with pentlandite (Pn) within secondary amphibole (Amp). The grain is crosscut by micro-veinlets of Pt-rich braggite. Note a tail of disseminated braggite in secondary silicates (905.6 m), (d) euhedral crystal of Au-Ag alloy ($Au_{75}Ag_{25}$) in a hole encrusted by euhedral pyrite (Py) (898.7 m)……117

Figure 5.13: PGM statistics from the MLA study of the T zone core sample WB195-898.7: (a) grain size distribution, (b) PGM associations with silicates or base metal sulphides (BMS)……118

Figure 5.14: Chemical compositions (wt. %) of pentlandite (Ni and Co vs Fe), and pyrrhotite and troilite (Ni and S vs Fe) from the F and T zones at the Waterberg project. The data are compared with compositions from the Turfspruit reef in the Platreef (Yudovskaya *et al*., 2017), the Upper Zone in the eastern Bushveld (von Gruenewaldt, 1976) and the Merensky Reef at Rustenburg (Kawohl and Frimmel, 2016)……124

Figure 5.14: The conceptual model for the emplacement of the entire Waterberg magmatic succession and formation of the mineralised zones: (a) the initial influxes interact with the Archaean basement to form marginal sills of fine-grained pyroxenite and gabbronorite, and granofels under lateral dilation, (b) the channelised emplacement of ultramafic melts to form feldspathic orthopyroxenite (FP) and overlying harzburgite (FH). Thermal-mechanical erosion creates embayments in the footwall whereas mixing initiates exsolution of sulphide-droplets, (c) emplacement of the troctolitic sheet-like bodies extending laterally due to roof uplift and floor depression, (d) magma mixing between resident ultramafics and gabbroic melts at the base of the TGA sequence, (e) prolonged fractionation of the TGA melt column resulting in a build-up of S, Cu, Ni and PGE+Au in the residual melt. The influx of fertile magma of the Upper Zone affinity, magma mixing and formation of the T zone, (f) the area experiences uplift and erosion. Palaeosol forms after weathered Bushveld rocks, (g) deposition of the Waterberg Group sediments, (h) intrusions of the Umkondo dolerite sills……128

Chapter 6: Whole rock geochemistry and mineral chemistry of the Waterberg PGE deposit, South Africa: implication for the Bushveld stratigraphy and the formation of the PGE mineralisation.

Table 6.1: Different Pt:Pd and Ni:Cu ratios from the two mineralised zone in the Waterberg project from WB017 and WB099; OV-FPYX – olivine-feldspathic pyroxenite; GN – gabbronorite; HARZ – harzburgite; FPYX – feldspathic pyroxenite. The location of these borehole cores are seen in Figure 6.2……156

Figure 6.1: Schematic geological map of the Bushveld Complex and enlarged map of the northern limb including the extension of the Waterberg Project in the far north, as well as the location of boreholes WB017 and WB099. Modified after 1:250 000 geological map of the northern limb (van der Merwe, 1976). PTM:

Platinum Group Metals Ltd; HRSZ: Hout River Shear Zone; YPF: Ysterberg-Planknek Fault; TML: Thabazimbi-Murchison Lineament……..138

Figure 6.2: Lithological columns of the boreholes (a) WB017 and (b) WB099 showing the stratigraphy and lithologies intercepted at depth on the Waterberg PGE deposit. WB, Waterberg sediments; UZ, Upper Zone; T1 and T2, T zone; TGA sequence, troctolite-gabbronorite-anorthosite sequence; UmS, Ultramafic Sequence……141

Figure 6.3: Photomicrographs of the different lithologies seen in the Waterberg Bushveld succession (a) fine- to medium-grained orthopyroxene with minor interstitial plagioclase (orthopyroxenite WB099 – 1315.77 m) (b) subrounded olivine associated with interstitial clinopyroxene and plagioclase (harzburgite WB099 – 1228.50 m) (c) (troctolite WB165 – 749.90 m) (d) euhedral plagioclase and subhedral clinopyroxene and orthopyroxene with an ophitic texture (gabbronorite WB099 – 1021.18) (e) euhedral plagioclase and exsolution between clinopyroxene and orthopyroxene (gabbronorite WB099 – 628.50 m) (f) euhedral plagioclase, symplectic texture associated with orthopyroxene and magnetite and inverted pigeonite (magnetite gabbronorite WB099 – 551.80 m). Images a-f are taken in cross polarised, transmitted light……145

Figure 6.4: Variation in composition of pyroxene, plagioclase and olivine mineral separates in the Waterberg Bushveld stratigraphy……146

Figure 6.5: The compositional variations in orthopyroxene mineral separates through the stratigraphy of the Waterberg Bushveld succession from borehole WB099: Mg# (Opx), MnO (wt. %), TiO_2 (wt. %), Cr_2O_3 (wt. %) and NiO (wt. %)……148

Figure 6.6: The compositional variations in clinopyroxene mineral separates through the stratigraphy of the Waterberg Bushveld succession from borehole WB099: Mg# (Opx), MnO (wt. %), TiO_2 (wt. %), Cr_2O_3 (wt. %) and NiO (wt. %)……149

Figure 6.7: The proportions of olivine, orthopyroxene (Opx), clinopyroxene (Cpx), plagioclase and quartz (Qtz) and orthoclase (Or) through the stratigraphy of WB099. The olivine (Mg#) and plagioclase (An#) are also shown through the stratigraphy of borehole WB099……150

Figure 6.8: Whole-rock major and trace element geochemical variations with depth and lithology in borehole WB017. (a) SiO_2:Al_2O_3 (wt. %); (b) Fe_2O_3 (wt. %); (c) TiO_2 (wt. %); (d) Sr (ppm); (e) Al_2O_3/FeO+MgO; (f) Sr/Al_2O_3; (g) CaO/Al_2O_3 (wt. %); (h) Mg#. WB, Waterberg sediments; UZ, Upper Zone; T1 and T2, T zone; TGA sequence, troctolite-gabbronorite-anorthosite; UmS, Ultramafic Sequence ……..152

Figure 6.9: Whole-rock trace element geochemical variations with depth and lithology in borehole WB017. (a) Cr (ppm); (b) V (ppm); (c) Co (ppm); (d) Rb (ppm) and (e) Cr/MgO ratio. WB, Waterberg sediments; UZ, Upper Zone; T1 and T2, T zone; TGA sequence, troctolite-gabbronorite-anorthosite; UmS, Ultramafic Sequence……...153

Figure 6.10: Variations of 2PGE+Au, Pt/Pd, Au, Cr, Cu, Ni, S, Au, Au/Pt and Cu/Pd abundances through the WB017 section of the Ultramafic Sequence. Data of 0.5 m sampling are shown by courtesy of Platinum Group Metals (PTM)……155

Figure 6.11: Variations of 2PGE+Au, Pt/Pd, Cr, Cu, Ni, S, Au, Au/Pt and Cu/Pd abundances through the WB017 section of the upper T zone. Data of 0.5 m sampling are shown by courtesy of Platinum Group Metals (PTM)……..156

Figure 6.12: Binary variation diagrams for the ultramafic mineralised zones and the Troctolite Horizon of orthopyroxene mineral-chemistry from different Northern limb sites; Sandsloot Platreef, Turfspruit Platreef and Akanani down dip Platreef (data from Yudovskaya *et al*., 2011), Union Merensky Reef and Rustenburg Merensky Reef (data from Naldrett *et al*., 2009), Waterberg project F zone (this study), Bellevue drillcore (BV1) Troctolite Horizon (data from Ashwal *et al*., 2005), Moordkopje drillcore (MO1) Platreef (data from Roelofse and Ashwal, 2012), Aurora project Unit 1 (McDonald *et al*., 2017). The comparison of Mg# (opx) vs. Cr_2O_3 (wt. %), NiO (wt. %) and MnO (wt. %)……161

Figure 6.13: Binary variation diagram for mineralised intervals in the Northern limb, PGE+Au (ppm) grades versus Cr (ppm) concentrations (A) Waterberg Project (this study); (B) Aurora Project (both the ultramafic unit and the upper Main Zone mineralised zones) (McDonald *et al*., 2017) and the upper Main Zone mineralisation on the Moorddrift farm (Maier and Barnes, 2010); (C) Platreef Townlands (Manyeruke *et al*., 2005), Sandsloot (McDonald *et al*., 2005; Ihlenfeld and Keays, 2011), Overysel and Tweefontein (Ihlenfeld and Keays, 2011), diagram modified from McDonald *et al*., 2016……..164

Chapter 7: Sulphur Isotopes of the Waterberg PGE deposit, South Africa: implication for the formation of the PGE mineralisation

Table 7.1: Results of the conventional sulphur isotope analyses for the Waterberg Project performed at iThemba Laboratory. WB - Waterberg sediments, UZ - Upper Zone, TZ - T-mineralised zone, TGA - troctolite-gabbronorite-anorthosite sequence, FZ - F-mineralised zone, MnS - Marginal Sills, TRNZ - Transitional zone of granofels, BAS – Archean basement……..184

Figure 7.1: (a) Sketch geological map of the Bushveld Complex and enlarged map of the northern limb including the extension of the Waterberg Project in the far north and also the location of boreholes in the Waterberg segment. (b) Stratigraphy of the Waterberg project area……175

Figure 7.2: Sulphur isotope results for the northern limb (A) summary of previous sulphur isotope data on the northern limb (Liebenberg 1968; Buchanan *et al*., 1981; Hulbert, 1983; Buchanan and Rouse 1984; Manyeruke *et al*., 2005; Sharman-Harris *et al*., 2005; Holwell *et al*., 2007; Holwell *et al*., 2013; Sharman *et al*., 2013; Smith *et al*., 2016 McDonald *et al*., 2017; Yudovskaya *et al*., 2017). (B) Sulphur isotope data from the Klipspringer Kimberlite (Westerlund *et al*., 2004) and (C) the sulphur isotope results from the Waterberg Project in this study……180

Figure 7.3: The sulphur isotope composition in ‰ $\delta^{34}S$ versus the stratigraphy of the Waterberg succession excluding the values obtained for the Waterberg sediments. The mantle-derived sulphur isotope ranges are adopted from Westerlund *et al*. (2004)……..185

Chapter 8: Geochemistry and PGE of the lower mineralised zone of the Waterberg Project, South Africa

Table 8.1: Representative geochemical results for rocks analyzed during this study……209

Figure 8.1: Map showing the distribution of major lithological units in northern South Africa. JHB Johannesburg; SMZ Southern Marginal Zone; NMZ Northern Marginal Zone; TML Thabazimbi-Murchison lineament;

HSRZ Hout River Shear Zone VNS Villa Nora Segment. The small rectangle indicates the Waterberg area. Modified after Dorland *et al*. (2006)…….192

Figure 8.2: A: Geological map of the Northern Lobe of the Bushveld Complex showing the town of Mokopane and selected mining and exploration projects. HRSZ - Hout River Shear Zone; YPF - Ysterberg-Planknek Fault; TML - Thabazimbi-Murchison lineament. Red Rectangle highlights the area of interest. B: Simplified stratigraphic column for the Waterberg succession. Both the marginal gabbronorite and the pyroxenite may not be present or occur at varying position and with varying thickness in the Ultramafic Sequence…….194

Figure 8.3: Textural relationships in examples of rock types from drill core in the Waterberg Project. A: Upper contact of the TGA Sequence troctolite showing discrete zones of gabbroic and troctolitic rocks interpreted to represent mingling of cumulates; B: Typical Ultramafic Sequence. In the top tray the sharp contact between overlying troctolite and harzburgite is visible; C: Variations in the troctolite zone showing leucotroctolite and zones of abundant orthopyroxene oikocrysts; D: Variations in olivine abundance in the troctolite zone. The oikocryst-rich melatroctolite is characterized by significant spikes in Cr content; E: Orthopyroxenite autolith in troctolite. Note the small pyroxenite fragments in the troctolite and the presence of possibly remobilized sulfides in both rocks; F: Chromite in TGA Sequence troctolite adjacent to an alteration halo and remobilized sulfides; G: Mildly altered mineralized zone with 6.5 g/t Pt+Pd+Au; H: Vari-textured zone of Cr-enriched serpentinite and sulfide remobilization……..198

Figure 8.4: Subcrop map of the area shown in Fig. 2. Shown are the positions of the drill holes investigated in detail (red) and the cross- and long-section from Figs. 13 and 14. The stippled line marks the approximate outline of a 1 g/t 3E grade shell projected to surface. It has a 30 dip to the west. The sedimentary rocks overlying the succession are approximately 240 m thick in the east, and their thickness increases slightly to the west……..200

Figure 8.5: Rock textures of the Waterberg body under cross-polarized transmitted light. A: Small olivine crystals rimed by peritectic orthopyroxene in olivine-bearing leuconorite in the uppermost part of the TGA Sequence; B: Corroded olivine and euhedral plagioclase laths in orthopyroxene oikocryst in olivine norite; C: Coarse olivine and plagioclase of smaller size in troctolite; D: chadacrysts of olivine and chromite enclosed by orthopyroxene in poikilitic chromitite of the Ultramafic Sequence; E: Coarse grains of olivine with plagioclase inclusions among interstitial clinopyroxene in lherzolite of the Ultramafic Sequence; F: Recrystallized orthopyroxenite with triple junction texture of orthopyroxene grains……..204

Figure 8.6: Sulfide assemblages of the F Zone under reflected light. A: Primary magmatic sulfide bleb composed of pentlandite (Pn), pyrrhotite (Po) and chalcopyrite (Ccp) in harzburgite. Sperrylite (Spe) occurs at the margin on contact with olivine (Ol); B: Interstitial pyrrhotite partly replaced by secondary magnetite (Mgt) in harzburgite. Kotulskite (PdTe) is located inside magnetite and remobilized along the contact between sulfides and silicates (Sil). Olivine is completely replaced by serpentine…….204

Figure 8.7: Binary variation diagrams of MgO vs major elements. Except for two samples of feldspathic pyroxenite, the UmS group of samples comprises only harzburgite. The lines in the SiO_2 vs. Fe_2O_3 plot demonstrate the different trends of troctolite and harzburgite (see text). Lbd Labradorite; Bt Bytownite; Aug Augite; Di Diopside; En Enstatite……..208

Figure 8.8: Binary variation diagrams of MgO vs trace elements…….213

Figure 8.9: Primitive mantle normalized (Sun and McDonough, 1989) multi-element plots for all six groups of rocks with thick lines showing the average for each group of samples. It can be seen that except for a stratigraphic increase in absolute concentrations the patterns are almost identical. Variations in marginal gabbronorites and pyroxenites are believed to result from contamination by assimilation…….215

Figure 8.10: Box plots displaying Tb/Yb_N, Ce/Sm_N and Th/Sm_N values for groups of samples. Color scheme as in Fig. 8.7. Most variation is exhibited by marginal gabbronorites and pyroxenites, which is interpreted to represent contamination by assimilation. The box represents the inter quartile range with the median represented as horizontal line and the mean as a black circle……..216

Figure 8.11: Top: Binary variation diagrams of S vs Cu, Pt and Pd. S vs Cu show an excellent correlation, however the correlation between S and Pt and Pd is weak; Bottom: Chondrite normalized PGE plots for the samples analyzed in this study. Light grey represents PGE distribution from the Turfspruit and Sandsloot high-grade reef-style mineralization in the Northern Lobe (from Yudovskaya *et al*., 2017)……219

Figure 8.12: A-C: Binary variation diagrams of chalcophile elements vs sulfur. There is an excellent correlation between Cu and S and a very weak correlation between S and Pt/Pd. D: Ternary diagram showing the relative proportions of Pt, Pd and Au for the assays for the project area. E) Pt+Pd+Au vs Cr diagram highlighting the anti-correlation of precious metals and Cr-rich lithologies. Data filtered for Pt and Pd >0.1ppm, c. 9500 assays. Sulfide-bearing zones were preferentially sampled by PTM geologists……221

Figure 8.13: Cross section through the study area as shown in Fig. 8.3. Columns presented show dominant lithology, the grade of Pt+Pd+Au, Cr%, Pt/Pd and Cu/Pd extracted from PTM's database. PGE units have been omitted……223

Figure 8.14: Long section through the study area as shown in Fig. 8.3. Color scheme as in Fig. 8.13. Columns presented show dominant lithology, the grade of Pt+Pd+Au, Cr%, Pt/Pd and Cu/ Pd extracted from PTM's database. In contrast to the previous section, harzburgite thickness and associated PGE grade decreases towards the N and S. PGE units have been omitted……224

Figure 8.15: Simplified 3D model of the project area. A: Shown is the geometry of the basement and in yellow a >1g/t 3E (Pt+Pd+Au) grade shell. The mineralization envelope has a chonolith-shape and is trending in a NE direction. Also shown is the position of holes studied (Fig. 8.13). B: This panel shows the distribution of the olivine-bearing rocks of the Ultramafic and lower TGA Sequence as logged in PTM's database. The erosional unconformity bringing Waterberg Group sediment in contact with mafic rocks and the dolerite sills are also shown. Note the vertical offset between the two dolerite sheets, perhaps indicating fault control. (For interpretation of the references to color in this figure legend, the reader is referred to the web version of this article)……..226

Figure 8.16: Ternary diagram for Pt, Pd and Au displaying data for the Waterberg Project, the Aurora Project (McDonald *et al*., 2017) and Turfspruit (Yudovskaya *et al*., 2017). It can be seen, that Aurora rocks are relatively Au-rich whereas F Zone rocks from the Waterberg Project are Pd-rich……..227

Figure 8.17: Conceptual model for the emplacement of the lower part (excluding the T Zone mineralization) of the Waterberg Succession. A: Emplacement of marginal orthopyroxenites as finger-like elongated bodies. Lateral dilation with continuing magma flow. B: Emplacement of harzburgitic magma and sulfides by thermo- mechanical erosion of earlier intrusive phases and the host rock. C: Emplacement of troctolitic

magma, marking the departure from a finger-like geometry and the formation of magma sheets. D: After the emplacement and fractionation of more magma, the area experienced extensive uplift and the deposition of Waterberg Group Sediments on an erosional unconformity…….229

Chapter 9: Discussion and Conclusion

Table 9.1: Compilation of available orthopyroxene compositional data from the ultramafic/mafic intervals including the Platreef in the northern limb and the Critical Zone of the eastern and western limbs of the Bushveld Complex……235

Table 9.2: Shows the similarities and differences between the mantle normalised multi-element variations of the Waterberg TGA sequence (troctolite), the Troctolite Horizon in the Bellevue drill core and the Platreef on Sandsloot, Zwartfontein and Overysel (data from Jones, 2013; Kinnaird *et al*., 2015)…….237

Table 9.3: A summary of the difference between the J-M reef of the Stillwater Complex, The Rum Intrusion of NW Scotland and the F zone mineralisation associated with the Bushveld Complex (Data from Brown, 1956; McCallum *et al*., 1980; Todd *et al*., 1982; Barnes and Naldrett, 1985; Turner *et al*., 1985; Emeleus *et al*., 1996; Power *et al*., 2000; Latypov *et al*., 2013; O'Driscoll *et al*., 2014)……248

Table 9.4: A summary of the differences and similarities of the upper mineralised intervals between the Moorddrift farm, the Aurora project and the Waterberg project (Harmer *et al*., 2004; Manyeruke, 2007; Maier *et al*., 2008; Harmer and McDonald, 2010; Barnes and Maier, 2010; McDonald *et al*., 2017)……..252

Table 9.5: A summary of the difference and similarities between the Waterberg T zone (Bushveld Complex) and the Platinova Reef (Skaergaard Intrusion) (Wager and Deer, 1939; Wager and Brown, 1968; Bird *et al*., 1991; Anderson *et al*., 1998; Nielsen *et al*., 2005; Holwell and Keays, 2014; Keays and Tegner, 2015; Holwell *et al*., 2015; Keays and Tegner, 2016)……254

Table 9.6: A summary of the differences between the F and T mineralised intervals in the Waterberg Stratigraphy……255

Figure 9.1: A schematic diagram of the differences and similarities in the magmatic stratigraphic across the Bushveld Complex. (Data from von Gruenewaldt, 1973; Molyneux, 1974; Cameron, 1978; Hulbert, 1983; Hulbert and von Gruenewaldt, 1985; Mitchell, 1990; Teigler *et al*., 1992; Eales and Cawthorn, 1996; Ashwal *et al*., 2005; Kinnaird *et al*., 2005; Cawthorn *et al*., 2006; Maier and Barnes, 2010; Yudovskaya *et al*., 2011; Roelofse and Ashwal, 2012; Smith, 2014; Wilson, 2015)……238

Figure 9.2: The magnetic susceptibility results of borehole LAP 30 from the Aurora project indicate that the upper mineralisation is associated with the Upper Zone……..251

Figure 9.3 (above): Schematic diagram showing the contrast between the Waterberg intrusive package in comparison with the exposed northern limb of the Bushveld Complex south of the Hout River Shear Zone (Modified from Kinnaird, 2005; Kinnaird *et al*., 2017)……..256

Chapter 1
Introduction

1.1 Prelude

In the last two decades, the demand for platinum-group elements (PGE) and the resultant increase in the PGE prices has led to a worldwide boom in PGE exploration and mining. Since the discovery of PGE in the last 1920's, mines have been developed and opened along the Merensky Reef and the Upper Group 2 (UG2) of the eastern and western limbs of the Bushveld Complex and in recent years the exploration and mining activities have increased on the Platreef ore body of the northern limb. Anglo American's Mogalakwena mining complex is not just the largest open pit platinum mine in the world but also the most profitable. Other companies such as Ivanplats and Platinum Group Metals (PTM) have started extensive exploration and mining development on the northern limb, making this area the new platinum hub of the world. The new Waterberg PGE deposit was discovered in 2011 by Platinum Group Metals and is located north of the Hout River Shear Zone in the Southern Marginal Zone of the Limpopo Mobile Belt, where the layered, mineralised Bushveld lithologies are overlain by a thick succession of Waterberg Group sediments. This new discovery of mineralised Bushveld lithologies is the focus of the study and will be compared with the rest of the Bushveld Complex.

1.2. Platinum Group Elements (PGE)

1.2.1. Physical Properties of Platinum-Group Elements (PGE)

The platinum-group elements (PGE) are platinum (Pt), palladium (Pd), rhodium (Rh), ruthenium (Ru), iridium (Ir) and osmium (Os), which are generally grouped with gold (Au) and silver (Ag) and are all termed 'precious or noble' metals. The PGE occupy the second and third row of Group VIII of the Periodic Table together with Fe, Ni and Co which are some of the least abundant elements on Earth. Based on the atomic weight or density and position within the Periodic Table, the platinum-group elements are divided in two subgroups; the heavy Ir-subgroup consists of osmium (Os), iridium (Ir) and platinum (Pt) (Table 1.1), and the lighter Pd subgroup consists of ruthenium (Ru), rhodium (Rh) and palladium (Pd) (Table 1.1) (Cabri, 1972). A more common grouping based on geochemistry has separated the platinum-group elements into a high temperature Ir-group (IPGE) consisting of Ru, Os and Ir, and a low temperature Pd-group (PPGE) consisting of Rh, Pd and Pt (Barnes *et al*., 1985; Tredoux *et al*., 1995).

Chemically, the PGE are highly siderophile, meaning that PGE tend to bond with metallic iron and with one another in complete and partial solid solutions. PGE tend to bond with Fe, Ni and other elements

such as Sn, Pb, Sb, Te and Bi (Berlincourt *et al*., 1981). The most important property of PGE in terms of this study, is that the PGE dissolve in molten bases of the Groups 15 and 16 of the Periodic Table which produces the natural occurrence of platinum-group minerals (PGM) forming a wide range of sulphides, tellurides, arsenides, bismuthides, antimonides and selenides.

Table 1.1: Physical and chemical properties of platinum-group elements (PGE) (Westland, 1981).

Property	Ruthenium	Rhodium	Palladium	Osmium	Iridium	Platinum
Chemical Symbol	Ru	Rh	Pd	Os	Ir	Pt
Atomic number	44	45	46	76	77	78
Atomic weight	101.07	102.94	108.42	190.23	192.22	195.08
Density (g/cm^3)	12.45	12.41	12.02	22.59	22.56	21.45
Colour	Silvery White	Silvery White	Silvery White	Bluish White	Silvery White	Silvery White
Melting point (^{o}C)	2334	1960	1554	3033	2446	1769
Boiling point (^{o}C)	3900	3727	3140	5027	4130	3827
Resistivity at O^{o}C (μΩcm)	6.8	4.33	9.93	8.12	4.71	9.85
Hardness (annealed, VHN)	240	101	40	350	220	40
Atomic radius (cm^{-3})	1.336	1.342	1.373	1.35	1.355	1.385
Thermal conductivity (watts/m/^{o}C)	105	150	76	87	148	73
Tensile strength (kg/mm^2)	165	71	17	-	112	14
Crystal system	Hexagonal	Isometric	Isometric	Hexagonal	Isometric	Isometric

1.2.2. Distribution of PGE within the Earth's Crust

The Earth's core is believed to have been the principle reservoir of PGE during the early formation of the planet (Azbel *et al*., 1993; McDonough and Sun, 1995; Righter, 2003). Although, some authors have suggested that the mantle is more abundant in PGE than the core, the PGE are thought to concentrate at chondritic proportion within the mantle (Borisov *et al*., 1994). The concentrations of PGE in the mantle are thought to occur during partial melting, where PGE prefer to remain in the melt and are transported and further concentrated in crystallising magma chambers (Mungall and Naldrett, 2008).

The abundance of platinum (Pt) and palladium (Pd) is similar in the Earth's crust at approximately 5 parts per billion (ppb), whereas rhodium (Rh), iridium (Ir) and ruthenium (Ru) are much rarer at approximately 1 part per billion (ppb) (Johnson Matthey, 2011). There are few concentrations of PGE that are economically viable (~2 – 10 ppm), in the Earth's crust, and these are generally associated with Ni-Cu deposits in high temperature processes associated with mafic to ultramafic igneous rocks (Barnes *et al*., 1985; Crocket, 1981, 2002; Misra, 2000). The majority of the economic PGE resources can be divided into two types of deposits associated with either Ni-Cu sulphides or chromitite (Fig. 1.1) (Misra, 2000; Mungall *et al*., 2004; Naldrett, 2004; Arndt *et al*., 2005; Maier, 2005). Type I PGE mineralisation occurs as stratiform or stratabound deposits in large layered intrusions with Ni and Cu as by products (e.g. Bushveld Complex - South Africa, Great Dyke – Zimbabwe and Stillwater Complex – USA). Type II PGE

mineralisation occurs in massive Ni-Cu sulphides deposits, although mined primarily for Ni and Cu with recoverable amounts of PGE, particularly Pd as by products (e.g. Noril'sk – Russia, Sudbury Igneous Complex – Canada, Jinchuan Intrusion – China, Kambalda Intrusion Western Australia and Nkomati – South Africa). The largest producer of PGE in the world is the Bushveld Complex and which is the subject of this study and is discussed in further detail within subsequent Chapters.

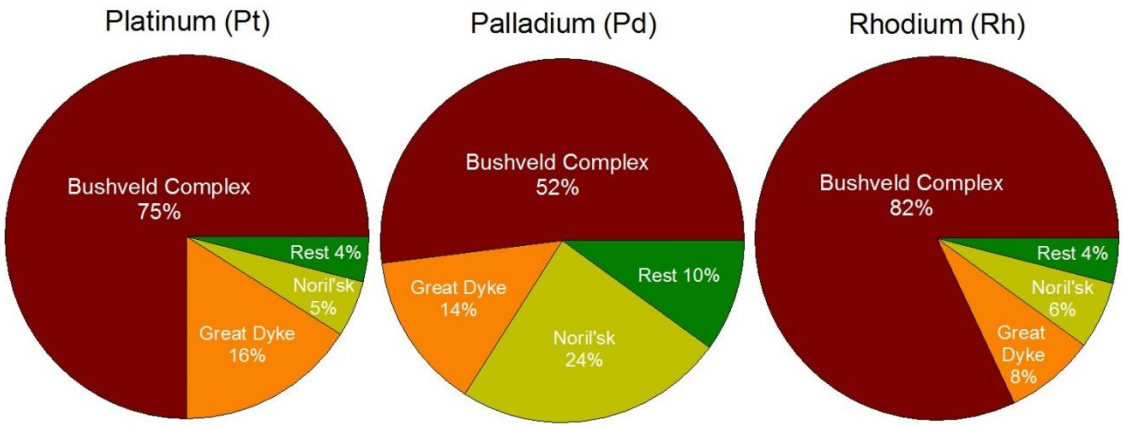

Figure 1.1: The distribution of Pt, Pd and Rh resources of major mining operations around the World (Johnson Matthey, 2011).

1.2.3. Formation of Magmatic Ni-Cu-(PGE) Sulphide Deposits

PGE are derived from the mantle and are concentrated in the crust in a variety of ways; the two main processes are (1) the development of mantle partial melts and their intrusion into the crust or (2), the emplacement of a mantle slab in a subduction/ collision zones (Naldrett *et al*., 2008). The first process is generally the most important and the accepted method for the formation of enriched layered intrusions and Ni-Cu sulphides deposits in the Earth's crust (Naldrett *et al*., 2008).

Most authors agree that there are fundamental processes or stages to consider during the formation of magmatic Ni-Cu-(PGE) sulphide deposits (Arndt *et al*., 2005; Maier, 2005; Naldrett *et al*., 2008; Naldrett, 2011). These include (i) the development of a parental magma through partial melting of the mantle which is enriched in PGE; (ii) the parental magma ascending into the upper crust without reaching sulphur saturation; (iii) the magma becoming sulphur saturated resulting in the segregation of an immiscible sulphide liquid that separates from the silicate liquid; (iv) the sulphide liquid interacting with a large mass of silicate magma scavenging PGE; and (v) finally the immiscible sulphide liquid needs to be concentrated to an economic potential.

The development of an immiscible sulphide liquid is generally considered the most important mechanism to concentrate PGE (Maier, 2005; Naldrett *et al*., 2008; Naldrett, 2011). There are a number of processes that may trigger sulphide saturation. (i) Sulphur saturation may be reached through prolonged fractionation of a silicate melt; crystallising silicates and oxides during fractionation does not incorporate sulphur, which therefore increases the sulphur content in the residual melt (Maier, 2005). (ii) Differentiation of Fe-rich minerals such as olivine, pyroxenes, chromite and magnetite causes a decrease in sulphur solubility which leads to sulphur saturation (Haughton *et al*., 1974; Shima and Naldrett, 1975; Hulbert and von Gruenewaldt, 1982; Li *et al*., 2001; Maier *et al*., 2003). (iii) Sulphur saturation can be triggered by addition of external silica, which decreases the sulphur solubility of magma (Irvine, 1975; Li and Naldrett, 1993). (iv) Furthermore, an increase in oxygen fugacity may cause the precipitation of chromite and magnetite, decreasing the FeO content of the magma, which in turn decreases the sulphur carrying capacity of the magma (Haughton *et al*., 1974; Buchanan and Nolan, 1979). (v) Mixing of compositionally contrasting magma which are sulphur undersaturated, may trigger sulphur saturation (Naldrett and von Gruenewaldt, 1989; Li *et al*., 2001). (vi) The addition of external Fe and sulphur from localised footwall lithologies can also aid in achieving or triggering sulphur saturation as seen in parts of the Platreef of the Bushveld Complex (Buchanan *et al*., 1981; Buchanan and Rouse, 1984; Sharman-Harris *et al*., 2005; Holwell *et al*., 2007).

Once the sulphide liquid has developed, the enrichment of PGE is dependent on the R factor (R factor refers to the sulphide liquid to silicate liquid mass ratio) (Campbell and Naldrett, 1979), and the sulphide melt equilibrating with a large volume of silicate magma (Arndt *et al*., 2005; Maier, 2005; Naldrett, 2011). Where the R factor is low, between 100 and 2000, the Ni and Co contents of sulphides will be adequate for most Ni sulphide ore bodies and the PGE concentration will be particularly low (Naldrett, 2010). However, if the R factor is significantly higher between 10,000 and 100,000 the Ni and Co content will be slightly higher than at the lower R factor, although the PGE concentration will be much higher and similar to the range that characterised the Merensky Reef of the Bushveld Complex (Naldrett, 2010; 2011).

High PGE tenors are also attained through the settling of dense sulphide droplets through a large volume of magma, where sulphides scavenge PGE. However, some authors have suggested that conduit systems are responsible for sulphide and PGE enrichment, through interaction with multiple influxes of sulphur undersaturated magma (e.g. Kerr and Leitch, 2005).

Furthermore, to develop an economic PGE deposit, the PGE-rich sulphide liquid must accumulate in sufficient amounts. Most PGE-rich sulphide liquids accumulate at the base of large igneous layered intrusions or above impermeable layers such as a chromitite layer to form economic stratabound or stratiform deposits (e.g. Bushveld Complex; Merensky Reef, UG2 chromitite, Platreef).

1.2.4. Uses of Platinum-Group Elements (PGE)

The platinum-group elements as well as approximately 90 other elements comprise less than 2% by weight of the Earth's crust. The scarcity and unqiue chemical properties of PGE influence price and demand for these elements. PGE have various applications both in their pure form and as alloys with other PGE or other metals. PGE have great catalytic properties due to their outer electronic structure and due to the global awareness of cleaner energy, Pt, Pd and Rh are in demand in the auto-motive business (Fig. 1.2). These PGE act as catalysts to reduce carbon monoxide, hydrocarbons and nitrogen oxides to legalised emission levels (Onvwiona and Uqursal, 2006). PGE are highly resistant to wear and tarnishing, making them suitable for jewellery (Fig. 1.2). Other distinctive properties of PGE which create a demand for these rare elements include; resistance to chemical erosion, excellent high temperature characteristics and stable electronical properties. Both Ru and Ir are used in the electrical and electrochemical industries due to the favourable properties. See Figure 1.2 below for all the different uses of PGE excluding osmium, which is little used because it is hard and brittle and in powdered form it produces a toxic gas when exposed to air.

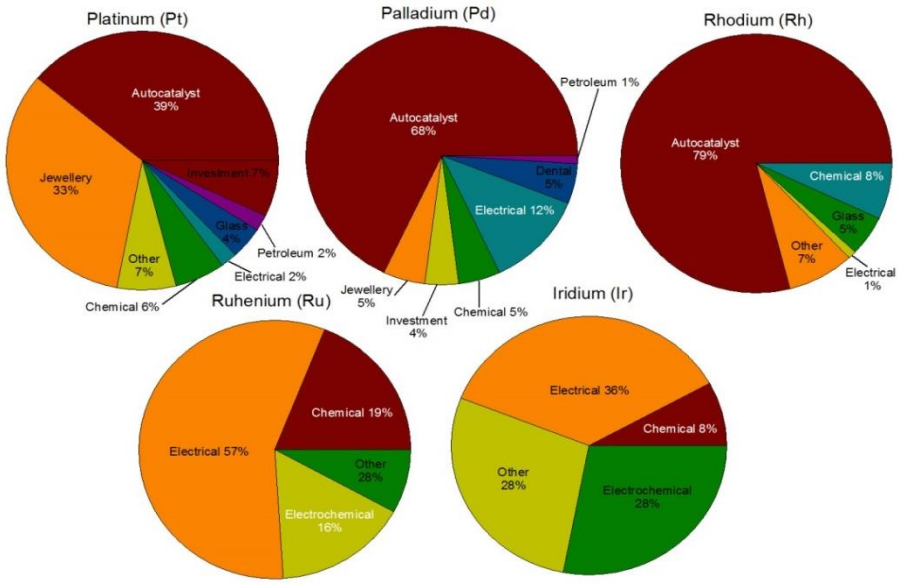

Figure 1.2: Pie charts showing the main uses and demands for PGE (Pt, Pd, Rh, Ru and Ir) from 2011 to 2013 (Johnson Matthey, 2011; Cowley, 2014).

1.3. Purpose of Study

1.3.1. Problem Statement

Since the discovery in 1924 of PGE in the Bushveld Complex (Merensky, 1925), there has been extensive exploration, mining and academic research in the area. The exploration and extensive underground mining operations in the eastern and western limbs of the Bushveld Complex to date has allowed for a sufficient accumulation of quality scientific data with regard to understanding the stratigraphy and formation of the PGE mineralisation, hosted primarily within the Merensky Reef and the UG2. However, some aspects of the stratigraphic position and genesis of mineralisation are still debated by a number of authors, Kruger and Marsh (1982) have challenged the stratigraphic boundaries of SACS (1980) based on initial Sr isotope ratios. Seabrook *et al*. (2005) studied the Sr isotopic and Cr/MgO ratios of rocks through the Critical Zone from below the Merensky Cyclic Unit into the base of the Main Zone at the top of the Bastard Cyclic Unit. These authors concluded that there were two magmas present during the crystallisation of these cyclic units, a Main Zone type magma contributing plagioclase and a Critical Zone type magma contributing orthopyroxene. They stressed that the compositions of these cyclic units were the result of mineral mixing rather than magma mixing (Seabrook *et al*., 2005). On the contrary, Wilson and Chunnett (2006) concluded from trace element data from the Merensky Reef and surrounding lithologies, that they formed from a degree of mixing or mingling of two distinctive magmas (T and U type). A number of authors have also argued about the genesis of PGE and chromite mineralisation in the Critical Zone e.g. Kinloch and Peyerl (1990), Wilson *et al*. (1999), Barnes and Maier (2002), Smith *et al*. (2004), Seabrook *et al*. (2005), Wilson and Chunnett (2006), Mitchell and Scoon (2007) and Latypov *et al*. (2016) for the Merensky Reef; and Eales (2000), Mathez and Mey (2005), Mondal and Mathez (2007), Mukherjee *et al*. (2017) and Pebane and Latypov (2017) for the UG chromitite layers.

In more recent years, the attention has been focused on the northern limb, where PGE have been exploited closer to the surface hosted in the stratabound Platreef deposit. The low-cost and high tonnage open pit mining operation of Anglo Platinum's Mogalakwena mining complex has driven other companies to explore for possible PGE deposits in the rest of the northern limb and allowed for more scientific research to occur in the northern limb. Prior to the 2000's, the northern limb had little scientific attention, only minor research on the tin mineralisation (Pringle, 1986), chromitites (Hulbert and von Gruenewaldt, 1986) and minor overviews of PGE mineralisation were performed for the central Platreef, where historical mining and exploration had been concentrated (Buchanan, 1988; White, 1994;

Lee, 1996; Viljoen and Schurmann, 1998). With mining operations and continuous exploration the scientific research has increased significantly for the northern limb.

In recent years, a number of authors have asked where the upper mineralisation occurs in the Bushveld Complex as seen in the Skaergaard Intrusion of East Greenland. Due to recent exploration in the northern limb, in situ PGE mineralisation has been discovered higher up in the stratigraphy, on Moorddrift farm (Maier and Barnes, 2010; Holwell *et al*., 2013) south of Mokopane, on Aurora in the far northern exposed rocks of the northern limb (Harmer *et al*., 2004; McDonald and Harmer, 2010; McDonald *et al*., 2017) and on the Waterberg Project north of the Hout River Shear Zone where this study takes place. In the western limb of the Bushveld Complex Wilhelm *et al*. (1997) found widespread soil geochemical anomalies for Ni, Cu, Pt, Pd and Au associated with the upper Main Zone and Main Zone-Upper Zone boundary. However, PGE analyses have been performed on the Pyroxenite Marker of both the eastern and western limb and have failed to find any PGE enrichment (Maier *et al*., 2001). Furthermore, the mineralisation in the upper stratigraphy of the Bushveld Complex is currently restricted to the northern limb of the complex.

1.3.2. Aim and Objectives

This study aims to identify and evaluate the stratigraphy and the geological processes involved in developing the mineralised interval seen in the Waterberg Project. In order to achieve this, the following aspects were undertaken:-

- Determine the role of magmatism, contamination and hydrothermal processes in the development of the two mineralised intervals of the Waterberg Project intercepted by drilling.
- Establish the whole-rock and mineral chemistry of the stratigraphy and mineralised intervals to compare with northern limb and the rest of the Bushveld Complex.
- Develop a genetic model for the Waterberg Project stratigraphy and the mineralisation.
- Determine whether the mineralisation in the Waterberg Project can be linked with other mineralised intervals in the northern limb.

1.3.3. Structure of this Thesis

This thesis is subdivided into 9 chapters and four of these chapters are presented as journal-style submitted or accepted papers. Due to this, there is overlap in the journal-style chapters as geological

setting and certain interpretations are repeated although, each journal-style chapter investigates and inter-operates one or more of the aims and objectives described above.

Chapter 2: This chapter provides an introduction to the regional geology of the Kaapvaal craton, the Southern Marginal Zone of the Limpopo Mobile Belt and the Bushveld Complex, summarizing key aspects of the extensive literature available. It focusses on the stratigraphy, ages, mechanisms of emplacement for the eastern and western limbs of the Bushveld Complex

Chapter 3: This chapter provides an introduction to the northern limb of the Bushveld Complex, with summaries of the structures, stratigraphy, ages and mineralisation. The mineralisation is discussed for the Platreef and the more recent discovery of upper stratigraphic mineralised intervals in the northern limb.

Chapter 4 - Manuscript 1 is titled: *The Waterberg Platinum-Group Element Deposit: Atypical Mineralisation in Mafic-Ultramafic Rocks of the Bushveld Complex, South Africa.*

Authors: Judith A. Kinnaird, Marina A. Yudovskaya, Matthew J. G. McCreesh, Florian Huthmann and Thys J. Botha. This article was published in *Economic Geology*, v. 112, p. 1367-1394.

Chapter 5 - Manuscript 2 is titled: *Platinum-group minerals of the Waterberg deposit, Bushveld Complex: implication for the formation of the PGE mineralisation.*

Authors: Matthew J. G. McCreesh, Marina A. Yudovskaya, Judith A. Kinnaird and Christen Reineke. This article was submitted to *Mineralogical Magazine* and is currently in press.

Chapter 6 - Manuscript 3 is titled: *Whole-rock geochemistry and mineral chemistry of the Waterberg PGE deposit, South Africa: implication for the Bushveld stratigraphy and the formation of the PGE mineralisation.*

Authors: Matthew J. G. McCreesh, Marina A. Yudovskaya and Judith A. Kinnaird. This article is currently in preparation.

Chapter 7 - Manuscript 4 is titled: *Sulphur isotopes of the Waterberg PGE deposit, South Africa: implication for the formation of the PGE mineralisation.*

Authors: Matthew J. G. McCreesh, Marina A. Yudovskaya and Judith A. Kinnaird. This article has been submitted to the *South African Journal of Geology.*

Chapter 8 – Manuscript 5 is titled: *Geochemistry and PGE of the lower mineralised zone of the Waterberg Project, South Africa.*

Authors: Florian Huthmann, Marina A. Yudovskaya, Judith A. Kinnaird, Matthew J. G. McCreesh and Ian McDonald. This article was submitted and accepted by *Ore Geology Reviews*.

Chapter 9 contains a detailed discussion and conclusion and summarizes the key aspects of the journal-style chapters 4-8 and draws all the conclusions together made in the previous chapters and in addition combines all the data to produce a genetic model for the formation of the stratigraphy and mineralisation associated with the Waterberg PGE deposit. The chapter also contains a recommendations section for future research. This chapter is followed by the appendices containing the current published papers as available in print and all the data gathered during the course of the Ph.D.

1.3.4. Methodology

To achieve the aims and objectives of this thesis, a number of geological techniques were used. These included core logging, sampling for mineralogical studies, magnetic susceptibility measurements, polished thin section and ore block studies for petrology and mineralisation, whole-rock geochemical analyses, and microprobe studies. A detailed methodology is given in each manuscript with all the details of the preparations and methods of each analysis performed in the thesis.

This aim of the research is to provide a better understanding of the stratigraphy in the Waterberg area as well as style and nature of the mineralisation, as the style differs in comparison to the rest of the Bushveld Complex.

1.3.5 Other Presentations, Reports and Publications the author was involved with

Presentations

- McCreesh, M. G. J., Kinnaird, J. A. and Yudovskaya, M. (2015). *A comparison of the two unique mineralised packages associated with Main Zone rocks in the Waterberg extension project of the northern limb, Bushveld Complex*. In extended Abstract; Platreef Workshop, 6th, Mokopane, South Africa, May 8-10th, p. 36-39.

- Yudovskaya, M., Kinnaird, J. A., McCreesh, M. J. G. and Frei, D. (2015). *The lithology at the contact between the Bushveld Mafic-Ultramafic sequence and overlying Waterberg sediments on the Waterberg*. In extended Abstract; Platreef Workshop, 6th, Mokopane, South Africa, May 8-10th, p. 59-61.

Report

- McCreesh, M. J. G. and Kinnaird, J. A. (2014). *Petrographic study of the sill and footwall from the boreholes of the Waterberg Project*. (Internal report) p 1-4.

Thesis

- McCreesh, M. J. G. (2016). *An investigation of the mineralisation in the Waterberg PGE deposit, South Africa*. MSc thesis, University of the Witwatersrand (unpublished), 226pp.
- McCreesh, M. J. G. (2013). *A study of the Main Zone-Upper Zone boundary beneath a thick succession of Waterberg sediments in the far north of the Northern Limb of the Bushveld Complex*. Honours Thesis, University of the Witwatersrand, Johannesburg, South Africa (unpublished), pp. 89.

Chapter 2
Regional Geology

This chapter focuses on the regional geology surrounding the study area, which includes the Kaapvaal Craton, Southern Marginal Zone of the Limpopo Belt and the Bushveld Complex (eastern and western limbs). An understanding of the wider geological setting of the region is crucial for the interpretation of the emplacement and the formation of the mineralised intervals within the Waterberg Project area.

2.1 Kaapvaal Craton

The Kaapvaal Craton contains a variety of Archean granite greenstone terranes and older tonalitic gneisses (3.6 – 3.2 Ga) intruded by younger variations of granitic bodies (3.3 – 3.0 Ga) (Robb *et al*., 2006). The accretion and stabilisation of the Kaapvaal Craton occurred between 3.7 and 2.5 Ga (De Wit *et al*., 1992), due to the emplacement of granitoid batholiths that thickened and stabilised the continental crust during early stage magmatism and sedimentary processes (Robb *et al*., 2006). The Kaapvaal Craton hosts some of the world's most important economic deposits, eg: gold (Barberton Greenstone belt and Witwatersrand basin), platinum-group metals (Bushveld Complex) and copper (Phalaborwa Carbonatite Complex) and various other economic commodities.

2.1.1. Regional Structural History

The Kaapvaal Craton is an amalgamation of crustal blocks that were assembled between 3.7 – 2.6 Ga, which can be divided into two periods (De Wit *et al*., 1992). During the first stage between 3.7 and 3.1 Ga, the initial separation of the continental lithosphere from the mantle by interoceanic obduction and amalgamation was followed by within-shield melting, granite formation and chemical differentiation to the upper lithosphere which created the Kaapvaal shield (De Wit *et al*., 1992). The second stage occurred from 3.1 to 2.6 Ga, which has been defined as the formation of the Kaapvaal Craton by Silver *et al*. (2004), using mantle fabrics revealed by seismic anisotropy which is summarised in Fig. 2.1. Firstly an unknown orogeny prior to 2.9 Ga imparted a mantle fabric on the Zimbabwe Craton (Fig 2.1a). Around, 2.9 Ga the Pietersburg and Kimberley blocks collided with the Kaapvaal Shield, imparting an arc-like mantle fabric which formed the Thabazimbi-Murchison Lineament (TML, Fig. 2.1b). During the Limpopo orogeny between 2.6 and 2.7 Ga, the Limpopo Belt was formed between the Kaapvaal and Zimbabwe craton (Fig. 2.1c) and at the same time the Great Dyke and Ventersdorp Supergroup were intruded (Silver *et al*., 2004).

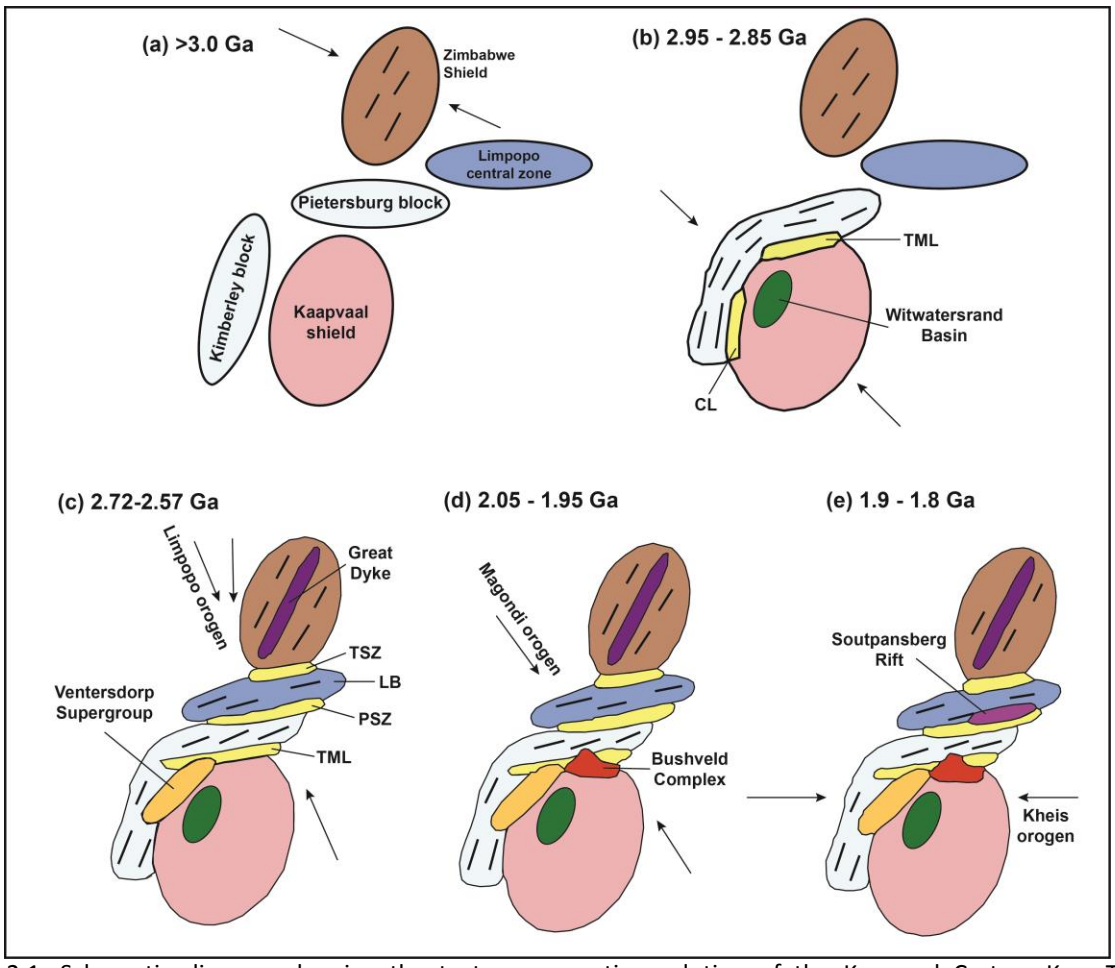

Figure 2.1: Schematic diagram showing the tectonomagmatic evolution of the Kaapvaal Craton. Key: TML - Thabazimbi-Murchison Lineament, CL - Colesberg Lineament, PSZ - Palala Shear Zone, TSZ - Triangle Shear Zone, LB - Limpopo Belt (Modified from Silver *et al*., 2004; Holwell, 2006).

The Hout River Shear Zone (Fig. 2.2) marks the boundary between the Southern Marginal Zone of the Limpopo Belt and the edge of the stable Archean Kaapvaal Craton (Van Reenen, 1986; Van Reenen *et al*., 1990; Roering *et al*., 1992) and is interpreted to represent a composite structure that was thrust southwards during the Paleoproterozoic collision between the Zimbabwean and Kaapvaal cratons (Schaller *et al*., 1999; Barton *et al*., 2006; Kramer *et al*., 2006; Smirnov *et al*., 2013; Rajesh *et al*., 2014). However, there is still debate regarding the timing of the Limpopo orogeny which ranges from 3.4 Ga to 2.0 Ga. The Limpopo Mobile belt is believed to have been active for 700 Ma of long-lived tectonothermal history (Hickman, 1978; Treloar *et al*., 1992; Berger *et al*., 1995; Good and de Wit, 1997; Blenkinsop *et al*., 2004; Kramers *et al*., 2006; Kramers and Mouri, 2011). The Southern Marginal Zone is a complex terrane that consists of a variety of grey granitoid gneisses, metasedimentary granulites, meta-mafic and meta-ultramafic lithologies associated with Archean gneisses (Du Toit *et al*., 1983; Nicoli *et al*., 2015). There are several major shear zones (Matok Shear Zone, Petronella Shear Zone and

Annaskraal Shear Zone) which trend parallel to the Hout River Shear Zone (Van Reenen *et al*., 1992). The Southern Marginal Zone and the structures associated with the area are important in the interpretation of the emplacement of the Waterberg Bushveld succession (Fig. 2.2). During the Magondi orogen around 2.0 Ga, shear zones in the Limpopo Belt were reactivated and the Bushveld Complex intruded along the TML (Fig. 2.1d) (Silver *et al*., 2004). The final stage of the regional structural history is the Kheis orogeny between 1.9 and 1.8 Ga (Cornell *et al*., 1998), which generated the Soutpansberg rift (Fig. 2.1e).

2.2 Bushveld Complex

The mafic-ultramafic component of the Bushveld Complex is the largest known preserved layered igneous intrusion in the World (Eales and Cawthorn, 1996; Cawthorn *et al*., 2007). Traditionally the Bushveld Complex was estimated to cover approximately 65,000 km^2 (Willemse, 1969; Cawthorn and Walraven, 1998). Recent geophysical studies and extensive exploration increased this total areal extent to approximately >90,000 km^2 (Finn *et al*., 2015). The exposed Bushveld Complex extends from Zeerust in the west to Burgersfort in the east and from the Bethal lobe in the south to Villa Nora in the north (Cawthorn *et al*., 2006) (Fig. 2.2). The Bushveld Magmatic Province as a whole is subdivided into four major magmatic suites; the felsic volcanics of the Rooiberg Group with an estimated volume of >300,000 km^3 (Twist and French, 1983; Buchanan *et al*., 2002; Buchanan, 2006), the ultramafic-mafic layered rocks of the Rustenburg Layered Suite (RLS), the Rashoop Granophyre Suite (Walraven, 1985), and the largest known example of A-type granites, the Lebowa Granite Suite (Kleeman, 1985; Kleeman and Twist, 1989). The Bushveld Complex is the world's most valuable mineral province hosting some of the largest resources of Pt and Pd which currently account for 75% and 40% respectively, of the annual global production (Johnson Matthey, 2011), Cr and V with accessory minerals such as Cu, Ni, Au, Sn, Fe, while fluorite and dimension stone are also products of the Complex.

The Bushveld Complex has been spatially divided into five major limbs or lobes (Fig. 2.2); the roughly symmetrical eastern and western limbs, a heavily eroded far western limb, the northern limb which includes the Villa Nora Fragment and a southern (Bethal) limb (Du Plessis and Walraven, 1990; Eales and Cawthorn, 2006). The latter is covered by younger sediments and was discovered based on gravity highs and confirmed with drill core (Buchanan, 1975).

There are still debates as to whether the limbs of the Bushveld Complex connect at depth. Initially Hall (1932) suggested that the limbs connect at depth due to the lithological similarities between the limbs, although, early gravity data lacked gravity highs in the centre of the eastern and western limbs

suggesting that the layered rocks were not continuous at depth (Cousins, 1959; Meyer and De Beer, 1987). Some authors described the various limbs to be disconnected, deep and narrow bodies (Sharpe, 1981; Hatton and Schweitzer, 1995) or steeply dipping conical intrusions (Meyer and De Beer, 1987). However, a reinterpretation of the gravity data and additional seismic data by Cawthorn and Webb (2001) and Webb *et al*. (2004), suggested an isostatic subsidence which eliminated the gravity anomaly. Based on the re-evaluation the connectivity of the eastern and western limb is now considered possible, but the connectivity with the rest of the limbs still remains unresolved (Cawthorn, 2015).

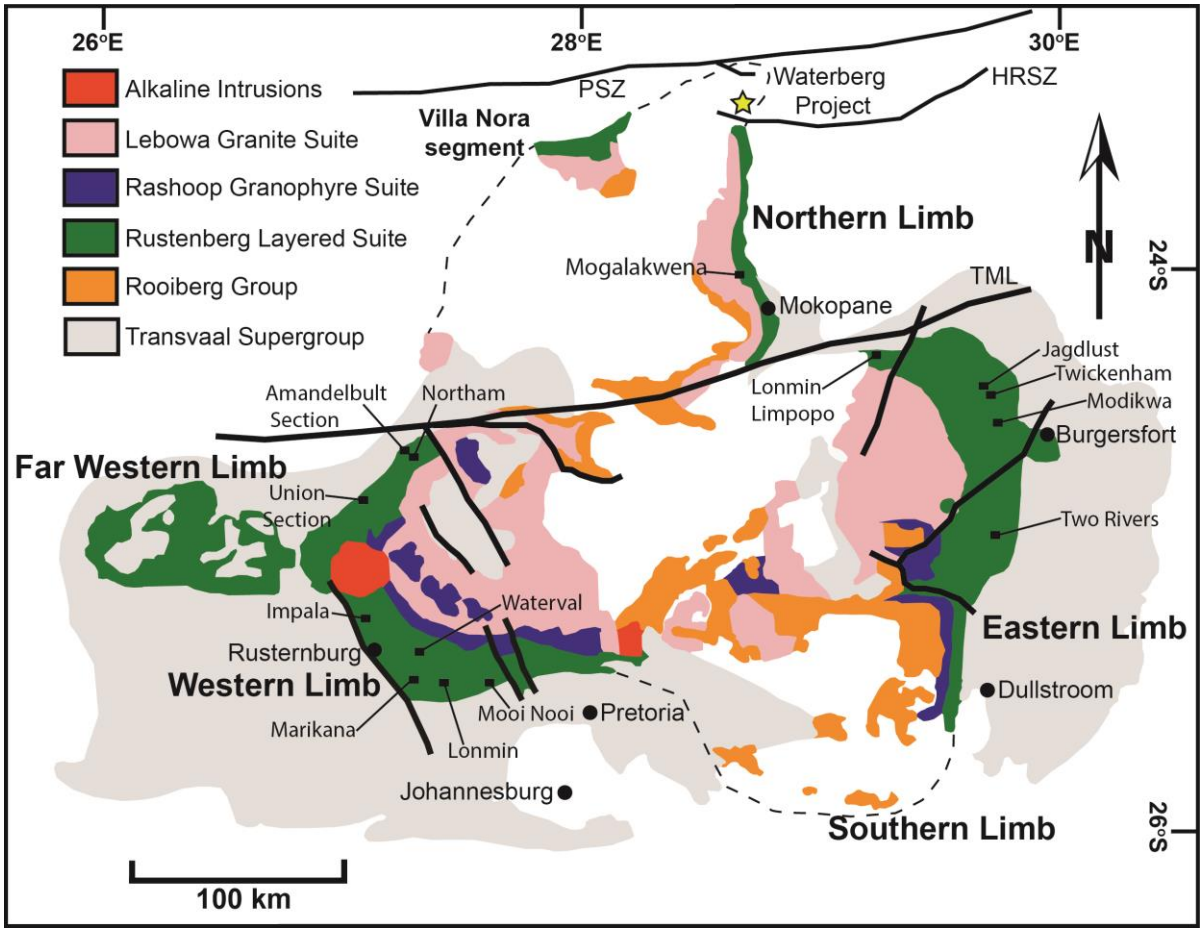

Figure 2.2: Simplified geological map of the Bushveld Complex (Modified from Kinnaird *et al*., 2005) as well as the location of the Waterberg project (star) between the Hout River Shear Zone (HRSZ) and the Palala Shear Zone (PSZ). TML; Thabazimbi Murchison Lineament.

2.2.1. Rustenburg Layered Suite

Although the alkaline and felsic intrusives and volcanics are included in the Bushveld Complex (Hatch and Corstorphine, 1905), most scientific literature restricts the Bushveld Complex to only the layered mafic-ultramafic rocks of the Rustenburg Layered Suite (RLS). The emplacement of the Rustenburg Layered Suite occurred along a regional unconformity between the preceding Rooiberg Group and the

Transvaal Supergroup or Archean Granite Basement (White, 1994; Eales and Cawthorn, 1996; Cawthorn *et al*., 2002). The layered rocks have a maximum vertical thickness of approximately 8-9 km (SACS, 1980; Walraven *et al*., 1990; Eales and Cawthorn, 1996). The layered intrusion of the Bushveld Complex shows a range of rock types from dunite to apatite-bearing diorites. The Rustenburg Layered Suite in the eastern and western limbs is traditionally subdivided into five stratigraphic zones based on mineralogical and petrological variations (Hall, 1932); the Marginal Zone (MnZ), Lower Zone (LZ), Critical Zone (CZ), Main Zone (MZ) and the Upper Zone (UZ). A simplified stratigraphy of the Rustenburg Layered Suite for the eastern and western limbs is shown in Fig. 2.3.

2.2.1. A. Marginal Zone (MnZ) and Basal Ultramafic Sequence (BUS)

The Marginal Zone is generally composed of medium-grained, poorly layered heterogeneous rocks which form the base of the Bushveld Complex, although, it is not everywhere developed (Eales and Cawthorn, 1996). These are generally noritic rocks with minor pyroxenite. The Marginal Zone rocks contain variable amounts of quartz and biotite, reflecting the assimilation of underlying shale units (Cawthorn *et al*., 2006). This sequence of rocks reaches a maximum thickness of 800 m (Fig. 2.3) (Vermaak, 1976; Engelbrecht, 1985; 1990; Kinnaird *et al*., 2002; Cawthorn *et al*., 2006). Eales and Cawthorn (1996) indicated that the Marginal Zone does not represent a true chilled margin at the base of the Bushveld Complex and rather formed from rapid crystallisation of the magma.

Early studies by Sharpe (1981), Harmer and Sharpe (1985), Sharpe and Hulbert (1985) and Davies and Tredoux (1985), divided the Marginal Zone rocks into three groups based on stratigraphic position and composition. These groups include (i) the composition of the noritic rocks with a quenched texture in contact with the Lower Zone and Lower Critical Zone were taken to represent the B1 parental magma of the Bushveld or the composition of ultramafic rocks that were within the footwall of the Lower Zone were termed B1 UM parental magma. (ii) Gabbronorites that were in contact with the Upper Critical Zone were termed B2 (Bushveld 2 magma) and (iii) Marginal Zone rocks in contact with the Main Zone were termed B3 magma. Barnes *et al*. (2010) suggested that all the Marginal Zone rocks are tholeiitic in composition which represent the Bushveld B1-3 magmas. Early works suggested that these B1-3 magmas were the parental magmas of the Bushveld Complex.

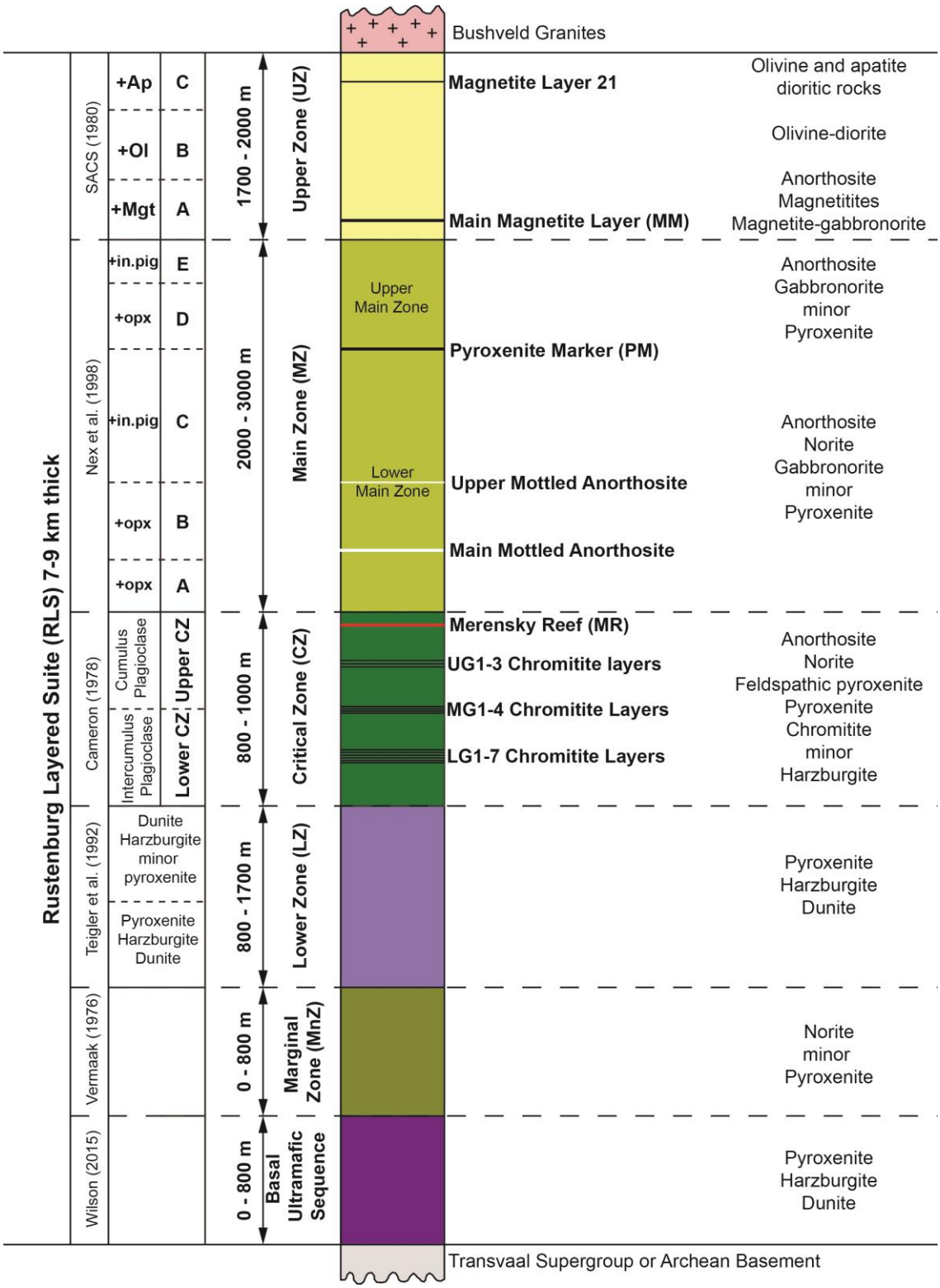

Figure 2.3: Generalised stratigraphy of the Rustenburg layered Suite through the Western and Eastern limbs of the Bushveld Complex. The figure is compiled from a number of sources (Cameron, 1978; 1980; 1982; von Gruenewaldt, 1973; Molyneux, 1974, Vermaak, 1976; SACS, 1980; Mitchell, 1990; Teigler *et al*., 1992; Nex *et al*., 1998; Wilson, 2015, primarily modified from Eales and Cawthorn, 2006).

A Basal Ultramafic Sequence (BUS) has been identified beneath the noritic Marginal Zone in the Clapham area in the eastern limb of the Bushveld Complex (Wilson, 2015). This previously unknown section is approximately 750 m thick and is composed of pyroxenites, harzburgites and dunites. Olivine and orthopyroxene through the BUS have the most magnesian compositions in the Bushveld Complex (Mg# > 0.91) (Wilson, 2012; Wilson, 2015; Wilson and Zeh, 2015). The lowest 10 m of the BUS section preserves different lithologies as well as a true chilled margin against quartzite floor rocks of the Transvaal Supergroup (Wilson, 2012). Wilson and Zeh (2015) suggested that a more ultramafic parental magma is required to form the overlying Lower and Critical Zone than the previously proposed B1 magma (Sharpe, 1981; Harmer and Sharpe, 1985; Hatton, 1995; Barnes *et al*., 2010). Similar high-Mg compositions of olivine and orthopyroxene have been reported for the recent discovery of an 800 m thick succession of Lower Zone rock beneath the Platreef in the northern limb (Yudovskaya *et al*., 2013). Wilson (2012) and Yudovskaya *et al*. (2013) indicated that the high Mg# of olivine (91) cannot be produced from the B1 magma with 13.5 wt. % MgO; rather the initial parental magma requires a higher MgO of around 19 wt. % similar to magmas which produce komatiites. The recent discovery of the BUS opens the debate on the origin of the Bushveld parental magma (Wilson, 2012; Naldrett *et al*., 2012; Eales and Costin, 2012; Yudovskaya *et al*., 2013; Wilson and Zeh, 2015).

2.2.1. B. Lower Zone (LZ)

The Lower Zone (Fig. 2.3) of the Bushveld Complex is composed of ultramafic lithologies that include dunite, harzburgite and pyroxenite (Bronzitites) (Cameron, 1978; Teigler and Eales, 1996). The Lower Zone in the Olifants River trough of the eastern limb is approximately 1300 m thick and has been subdivided into a basal pyroxenite and overlying harzburgite and an upper pyroxenite which all contain less than 1 % chromite (Cameron, 1978). In the western limb the Lower Zone was studied in detail from drill-cores. Here the Lower Zone was subdivided into two units: a lower pyroxenite and olivine-bearing rocks in equal proportions and an upper subzone with less pyroxenite (Teigler and Eales, 1996). There is no cumulus plagioclase recorded in the Lower Zone of the western limb apart from within a noritic layer midway up the succession which has been identified in both the eastern and western limbs of the complex (Lee and Tredoux, 1986; Teigler, 1990). In the far western limb, the Lower Zone contains nine cyclic units of dunite-harzburgite-pyroxenite reaching an approximate thickness of 1050 m (Engelbrecht, 1985). The southern or Bethal limb contains tens of meters of Lower Zone harzburgite which are overlain by more evolved magnetite-rich lithologies (Buchanan, 1975).

Cameron (1978) defined the base of the Critical Zone as where interstitial plagioclase increased from 2 modal % to 6 modal %. However, this boundary could not be used in the western limb due to the lack of plagioclase. Teigler *et al*. (1992) suggested the boundary between the Lower Zone and Critical Zone to occur where olivine is absent, indicating that the upper feldspathic pyroxenite defined by Cameron (1978) would now form part of the lower Critical Zone. The boundary suggested by Teigler *et al*. (1992) is the more accepted stratigraphy for the Lower Zone of the Bushveld Complex (Eales and Cawthorn, 1996; Cawthorn *et al*., 2006; Cawthorn, 2015).

2.2.1. C. Critical Zone (CZ)

The Critical Zone (Fig. 2.3) hosts two of the world's largest platinum-group element deposits, the Upper Group 2 Chromitite (UG2) and the Merensky Reef, and also has some of the largest chromite reserves hosted by the Lower (LG), Middle (MG) and Upper (UG) Group chromitite layers (Cousins and Feringa, 1964; Eales, 1987; Hatton and von Gruenewaldt, 1987; Schurmann *et al*., 1998). The Critical Zone displays spectacular layering of chromitites, pyroxenites, norites and anorthosites. This zone is subdivided into the lower Critical Zone (C_LZ) where intercumulus plagioclase is present and the upper Critical Zone (C_UZ) that is characterised by the appearance of cumulus plagioclase (Cameron, 1978; 1980). There are nine cyclic units identified in the lower Critical Zone and eight in the upper Critical Zone, with the UG2 and Merensky Reef at the base of cyclic unit 5 and 7 of the upper Critical Zone (Eales and Cawthorn, 1996; Cawthorn *et al*., 2006). At the base of each cyclic unit there is an enrichment of Mg/(Mg+Fe) content, interpreted as a replenishment of magma (Kruger and Marsh, 1982; Cawthorn *et al*., 2006).

Chromitites

Most of the chromitite layers can be traced for more than 100 km in both the eastern and western limbs of the complex (Hatton and von Gruenewaldt, 1987; Schurmann *et al*., 1998). The chromitite layers are grouped into the LG consisting of 1-7 layers, the MG 1-4 and the UG 1-3 chromitite layers, although there are lateral variations on the number of layers present in the eastern and western limbs (Hatton and von Gruenewaldt, 1987). The layers generally consist of between 60 and 90 modal % of chromite grains (De Waal, 1975). The chromitite layers range from <2 cm to 2 m in thickness and may consist of single or multiple seams. Naldrett *et al*. (2012) provided a detailed description of the chromitites and their geochemical variations within their groups.

There are numerous models on the formation of the chromitite layers in the Critical Zone which include: (i) gravity settling (Sampson, 1932; Wager *et al*., 1960; Irvine, 1979; Hiemstra, 1979); (ii) magma mixing (Irvine, 1977; Irvine *et al*. 1983 Eales *et al*., 1990); (iii) contamination by a siliceous component (Irvine, 1975); (iiii) pressure change (Cameron, 1977); (v) emplacement of chromitites suspensions (Eales, 2000; Eales and Costin, 2012); (vi) in situ crystallisation from chromite saturated magma (Latypov and Egorova, 2012; Latypov *et al*., 2017). Although there is no agreement on the proposed models, Sr isotopes indicate new influxes of magma at each chromitite layer (Kinnaird *et al*., 2002). The olivine associated with LG-1 and LG-4 is a result of magma mixing between a primitive and an evolved magma (Kinnaird *et al*., 2002). The overlying chromitites associated with orthopyroxene (LG5 to MG1) or orthopyroxene and plagioclase (MG2 and above) are interpreted to have formed from mixing of compositionally distinct magmas (Irvine, 1977; Irvine *et al*., 1983; Barnes *et al*., 2010), a U-type magma poor in Al_2O_3 but enriched in MgO, Cr and SiO_2 and an A type magma of tholeiitic composition (Harmer and Sharpe, 1985; Irvine and Sharpe, 1986).

PGE mineralisation

The UG2 chromitite layer and the Merensky Reef represent the economically important layers for 3PGE in the eastern and western limbs. The UG2 chromitite layers represent the largest single known PGE resource (58%) in the World, significantly higher than the PGE resource associated with the Merensky Reef (32%) (Naldrett *et al*., 2008). The UG2 is situated between 20 – 400 m below the Merensky Reef, ranging from 0.4 to 2.5 m thick, but is only rarely observed with thicknesses over 1 m (Schouwstra, 2000; Cawthorn *et al*., 2011). The UG2 can be traced at surface for almost the entire 400 km strike length of the eastern and western limbs of the Bushveld Complex (McLaren and De Villiers, 1982). The UG2 reef is situated at the base of the UG2 Cyclic Unit and in the eastern limb the hangingwall is often associated with a pyroxenite whereas in the western limb the UG2 is overlain by olivine-rich pyroxenite (Naldrett *et al*., 2008; Cawthorn *et al*., 2011). The footwall of the UG2 in both limbs is either a pegmatoidal pyroxenite or anorthosite (Naldrett *et al*., 2008; Cawthorn *et al*., 2011). The UG2 reef package is generally composed of 30-35% chromite cemented by interstitial orthopyroxene and plagioclase (Schouwstra, 2000), although within individual chromitite the proportion of chromite may increase to 75-90% (Mathez and Mey, 2005). Due to textural and compositional variations through the UG2, it is interpreted to have formed from multiple composite layers (Lee, 1996; Voordouw *et al*., 2010; Cawthorn *et al*., 2011; Junge *et al*., 2015) The UG2 chromitite has an average grade of 5g/t of 4PGE (Pt, Pd, Rh and Au) although the distribution of grade is not uniform within the layer (Hiemstra, 1985; 1986; Lee, 1996). The average Pt/Pd ratios for the UG2 are different for the eastern (1.0) and western (2.3) limbs. North of

the Steelpoort fault in the eastern limb there is a UG3 cyclic unit in addition to the UG2 (Gain, 1985). The UG2 chromitite layer contains minor base metal sulphides (pentlandite>chalcopyrite>pyrrhotite ± pyrite) (Merkle, 1992; Cawthorn, 2015).

The Merensky Reef is defined as "a mineralised zone within or closely associated with ultramafic lithologies at the base of the Merensky Cyclic Unit" (Cawthorn *et al*., 2002; Naldrett *et al*., 2009). Detailed descriptions of the Merensky Reef and its stratigraphic setting in the western limb of the Bushveld Complex have been given by Leeb-du Toit (1986), Viljoen and Hieber (1986), Viljoen (1986a; 1986b), Viljoen (1999), Wilson *et al*. (1999), Barnes and Maier (2002), Cawthorn *et al*. (2002), Smith *et al*. (2004), Godel *et al*. (2006), Naldrett *et al*. (2008), Naldrett *et al*. (2009) and Naldrett *et al*. (2015). The simplest form of the Merensky Reef from bottom to top is; (a) a footwall anorthosite, norite or pyroxenite; (b) a lower chromitite layer that ranges between 2 cm to >40 cm thick; (c) a varying thickness (0 - 12 m) of feldspathic pyroxenite (which tends to be pegmatoidal towards the top 60 cm) although in some areas this interval may host feldspathic harzburgite to dunite in addition to the feldspathic pyroxenite; (d) an upper chromitite layer between 2 to 10 mm thick; (e) overlain by 35 to 225 cm of orthopyroxenite (Naldrett *et al*., 2008; Naldrett *et al*., 2009; Naldrett *et al*., 2012).

In the southwestern Bushveld there is evidence of two influxes of magma. These magmas deposited a basal chromitite followed by orthopyroxenite with PGE-rich sulphides (Naldrett *et al*., 2015). The lower chromitite layer and overlying pyroxenite is referred to as the Pre-Merensky Cyclic Unit (PMCU) followed by the upper chromitite and overlying pyroxenite, norite and anorthosite as the Merensky Cyclic Unit (MCU) (Naldrett *et al*., 2015) (Fig. 2.4). The PMCU in the southeast of the western limb can be as thick as 10 m overlying interbanded norite and anorthosite footwall (Fig. 2.4). In the Rustenburg area the PMCU varies in thickness from 60 cm (Thick Reef), to < 10 cm (Thin Reef) to zero (Contact Reef). Where the PMCU is < 60 cm thick it generally has a pegmatitic texture (Wager, 1929; Viljoen, 1999; Viring and Cowell, 1999; Cawthorn *et al*., 2002; Scoon and Mitchell, 2004; Roberts *et al*., 2007; Naldrett *et al*., 2009) (Fig. 2.4). A high degree of discordance occurs in the central and northwestern parts of the southwestern Bushveld Complex where the Merensky Reef has been termed the "Rolling Reef" (Fig. 2.4). The chromitite seam at the base of the PMCU is not always present and there are generally uneconomic amounts of PGE-rich sulphides associated with the PMCU contact with the underlying norite/ anorthosite footwall (Naldrett *et al*., 2009) (Fig. 2.4). A significant amount of disseminated PGE-rich sulphides occur at the contact between the PMCU and the MCU, which extend 1 m above and below the contact (Naldrett *et al*., 2009) (Fig. 2.4).

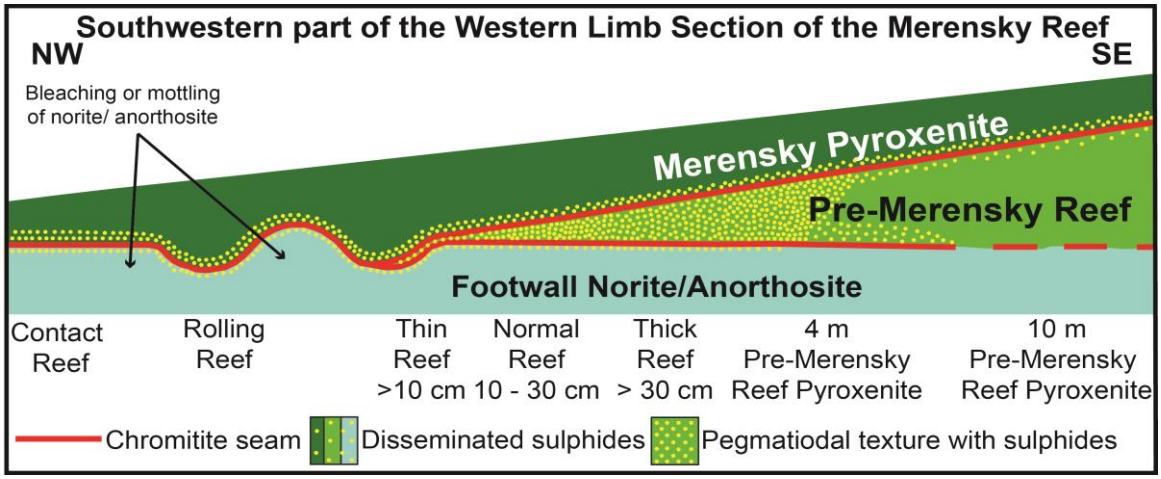

Figure 2.4: A SE-NW schematic section showing variations in the pre-Merensky and Merensky pyroxenites in the southwestern Bushveld Complex (Redrawn from Naldrett *et al*., 2009).

The Merensky Reef in the northwestern part of the Bushveld Complex shows remarkable differences relative to the southwestern parts. The Merensky Reef in the northwestern part of the Bushveld Complex is much thicker and olivine is the main constituent in the lower parts of the reef (Naldrett *et al*., 2012). Another major difference is that potholing is a very common feature of the Merensky Reef in the northwestern parts of the Bushveld Complex (Fig. 2.5). Much of the Merensky Reef in this area lies at a level up to 16 m below the "normal reef" and is termed the "Regional Pothole Reef" (Naldrett *et al*., 2009) (Fig. 2.5).

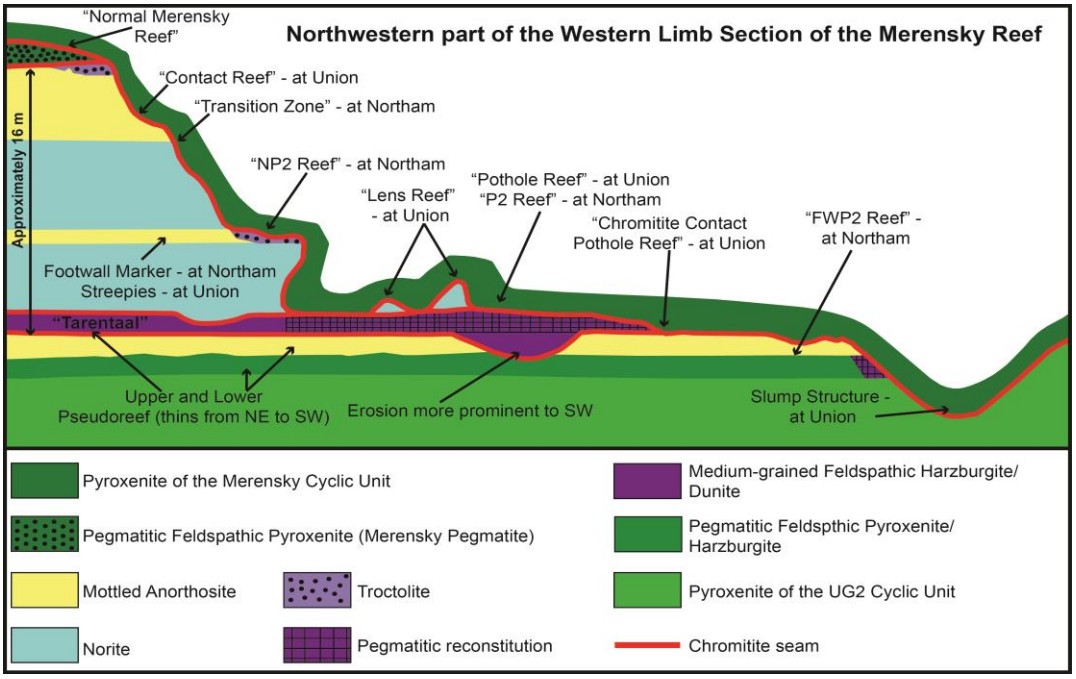

Figure 2.5: Schematic section through stratigraphic succession including the Merensky Reef in the northwestern section of the western limb of the Bushveld Complex (descriptions from Smith *et al*., 2004; Robert *et al*., 2007; Viljoen, 1999 and Redrawn from Naldrett *et al*., 2009).

In the eastern limb of the Bushveld Complex the interval between the Merensky Reef and the UG2 chromitite layers is much greater at between 120 and 410 m apart (Mitchell and Scoon, 2007; Naldrett *et al*., 2008). The Merensky Reef in the eastern limb shows remarkable differences relative to the western limb and is defined as the "Wide Reef Facies" in the eastern limb (Wilson *et al*., 2005; Mitchell and Scoon, 2007). Typically the footwall is composed of pyroxenite or in some places it may be norite, with a pegmatitic texture toward the upper 30 – 50 cm. Above this is a bottom chromitite layer and 70 to 250 cm of pyroxenite capped by the top chromitite seam (Mitchell and Scoon, 2007). The hangingwall is composed of 30 – 50 cm of pyroxenite grading upwards into norite, leuconorite and anorthosite of the MCU. Sulphides occur above and below the upper chromitite layers as well as below the lower chromitite layer when present (Naldrett *et al*., 2015).

In general, the Merensky Reef contains up to 3 - 5% PGE-bearing sulphides (pyrrhotite > chalcopyrite > pentlandite) (Lee, 1996). The distribution of PGE in the vertical profile of the Merensky Reef is extremely variable, although the highest grades tend to occur in the thin chromitite layers, especially the lower chromitite (Crocket *et al*., 1976; Lee, 1983; Viljoen, 1994; Viljoen and Schurmann, 1998; Naldrett *et al*., 2012). PGE grades of the Merensky Reef are highest (>6 g/t Pt) in the northwestern part of the western limb and lower (4 – 5 g/t) in the southwest of the western limb. The PGE grades in the eastern limb are significantly lower than those in the western limb, between 2 - 3 g/t, which is the reason why the Merensky Reef in the eastern limb was termed uneconomic for 20 years (Naldrett *et al*., 2015).

Apart from the UG2 and Merensky Reef, some of the other chromitite layers in the Critical Zone contain significant amounts of PGE; the lower LG1 to LG4 have the lowest PGE contents, LG5 to MG2 have somewhat higher PGE content and the overlying MG3 to UG3 have the highest PGE content with poor concentrations of base metal sulphides (Lee, 1983; Lee and Parry, 1988; Scoon and Teigler, 1994; Mitchell and Scoon, 2007; Naldrett *et al*., 2009; Naldrett *et al*., 2015).

Genesis of PGE mineralisation

A number of hypotheses address the origin of PGE mineralisation in the upper Critical Zone of the eastern and western limbs of the Bushveld Complex (e.g. Naldrett and von Gruenewaldt, 1989; Ballhaus and Sylvester, 2000; Miller and Anderson, 2002; Maier and Barnes, 2002; Wilson and Chunnett, 2006; Naldrett *et al*., 2009). Many of these authors agree that the mineralisation is a result of magma mixing, a concept initially proposed by Campbell *et al*. (1983). Naldrett *et al*. (2009) suggested that the PGE mineralisation formed from magma mixing between a resident (T-type) magma present in the Bushveld chamber mixing with a more primitive (U-type) magma enriched in PGE and characterised by low Cu/Pd

ratios. Rare earth element data confirms the presence of two compositionally distinct magmas (Maier and Barnes, 1998). Furthermore, evidence from Sr isotopes and Cr/Mg ratios as well as series of minicycles developed from different degrees of magma mixing termed “magma mingling” occur in the upper Critical Zone (Seabrook *et al*., 2005; Wilson and Chunnett, 2006).

There is an ongoing debate as to whether magma mixing between a T-type and a U-type magma composition would produce sulphide immiscibility (Cawthorn, 2002; Li *et al*., 2001). Li and Ripley (2005; 2009) suggested that sulphide immiscibility is possible from magma mixing of these compositions, provided that both magmas are close to sulphide saturation at the time of magma mixing. The U-type magma was interpreted to be significantly enriched in PGE with up to 200 ppb rather than 2 ppb. The concept of upgrading this magma was through complete dissolution of sulphide in the staging chamber (Naldrett *et al*., 1992). Naldrett *et al*. (2009) further proposed that the early magmas en route to the Bushveld Complex deposited sulphides in the staging chamber. The upgrading of sulphides resulted from interaction with a sulphide-undersaturated flowing magma, dissolving FeS from pre-existing sulphides (Maier, 2005). This would lead to progressive enrichment of elements such as PGE, Ni and Cu in residual sulphides (Kerr and Leitch, 2005; Naldrett *et al*., 2009).

Some authors have argued against magma mixing and deem it not necessary to induce sulphide saturation. Cawthorn (2005) and Mavrogenes and O’Neil (1999) suggested that sulphide immiscibility as well as the formation of chromitite layers is a result of negative effect from the increase in pressure on sulphide solubility. Boudreau and Meurer (1999) developed the concept of a vapour refining model, where volatiles released into a cooling pile of igneous cumulates ascend, dissolving elements including S, PGE, Ni and Cu. Willmore *et al*. (2000) proposed that the addition of S and PGE-rich vapour to a crystallising magma at the top of a cumulate pile would induce sulphide immiscibility and further concentrate PGE within the sulphides.

Contact between Critical and Main Zone

The boundary between the Critical Zone and the overlying Main Zone is not sharply defined (Mitchell and Manthree, 2002). The boundary is currently taken at the top of the Giant Mottled Anorthosite at the top of the Bastard Cyclic Unit which is the uppermost cyclic unit in the Critical Zone (SACS, 1980). However, Kruger (1990) revealed that Rb-Sr data show a significant change in Sr isotope ratios, and a major unconformity at the base of the Merensky Reef, indicating a major influx of new magma. Thus isotopically, the boundary between the Critical and Main Zone can be placed at the base of the

Merensky Cyclic Unit where large oikocrysts of pyroxenes occur (Kruger and Marsh, 1982; Kruger, 1990). According to Seabrook *et al*. (2005) the initial strontium isotope ratio and Cr/MgO within orthopyroxene from the eastern limb shows that the Merensky Reef and Bastard unit are composed of minerals from both the Critical and Main Zone magmas and interpreted that this interval is a transition zone.

2.2.1. D. Main Zone (MZ)

The Main Zone is the thickest zone in the Rustenburg Layered Suite (Fig. 2.3), devoid of olivine and chromite in the eastern and western limbs. The Main Zone is mainly composed of norite and gabbronorite with minor anorthosite and pyroxenite layers in the eastern and western limbs (Eales and Cawthorn, 1996). The Main Zone is 2200 m thick in the western limb and has been subdivided into the lower Main Zone comprising Norite Units I-II, overlain by Gabbronorite Units I-IV (upper Main Zone) separated by the Pyroxenite Marker (Mitchell, 1990). However, a more recent study by Nex *et al*. (1998), subdivided the western Main Zone into 5 subdivisions A-E based on the appearance of primary orthopyroxene and inverted pigeonite (Fig. 2.3). The Main Zone is 3100 m thick in the eastern limb (von Gruenewaldt, 1973; Molyneux, 1974). Von Gruenewaldt (1973) subdivided the Main Zone in the eastern limb into three subzones based on the appearance of primary orthopyroxene and pigeonite. The Main Mottled Anorthosite (Fig. 2.3) has a strong magnetic signature which is traceable in both the western and eastern limbs (Viljoen and Scoon, 1985). There is a reversal in mineral compositions and a break in Sr-isotopic ratios associated with the Pyroxenite Marker (Fig. 2.3) which is seen in both the eastern and western limbs (Sharpe, 1985; Kruger, 1990; Mitchell, 1990, Cawthorn *et al*., 1991).

2.2.1. E. Upper Zone (UZ)

The Upper Zone (Fig. 2.3) is the laterally most extensive zone in the Rustenburg Layered Suite (Kruger, 2005). The base of the Zone is defined by the appearance of cumulus magnetite. The Upper Zone is approximately 2000 m thick (SACS, 1980). The Upper Zone contains 24 magnetitite layers in the eastern limb and they are divided into four groups with up to seven magnetitite layers per group (Molyneux, 1974; Cawthorn and Molyneux, 1986; Tegner *et al*., 2006). The thickest of these magnetitite layers is 6 m thick, with others ranging from a few centimeters to 2 m thick. The Main Magnetitite Layer near the base of the Upper Zone is 2 m thick and is mined for its vanadium content (Eales and Cawthorn, 1996). The magnetitite layers have sharp contacts at the base of each layer and gradational tops (Cawthorn *et al*., 2006). The Upper Zone has been subdivided into three subzones based on the appearance of cumulus minerals (cumulus magnetite, olivine and apatite). In the eastern limb, subzone A comprises 700 m of anorthosite and magnetite ferrogabbro with the Main Magnetitite Layer 130 m from the base

followed by seven more magnetitite layers. Subzone B occurs with the appearance of olivine, which forms a 580 m thick succession of anorthosite, troctolite and ferrogabbro with a further seven magnetitite layers. The appearance of cumulus apatite marks the boundary of subzone C, which is composed of olivine diorite, anorthosite and another seven magnetitite layers (Molyneux, 1970; von Gruenewaldt, 1971). Similar subzones based on mineralogy evolutions are seen in the Upper Zone in the different limbs of the Bushveld Complex (Buchanan, 1977; Ashwal *et al*., 2005; Tegner *et al*., 2006).

Genesis of Magnetitite Layers

The formation of magnetitite layers in the Bushveld Upper Zone has been debated by several authors. Wager and Brown (1968) suggested that current sorting or gravity segregation were the physical controls behind the formation of the magnetitite layers. Cawthorn and McCarthy (1981) and Cawthorn and Ashwal (2009) argued that the layers formed from a sudden change in magma composition due to pressure change causing a shift in the phase boundaries, such that the liquid was within the magnetite field and produced monomineralic layers. This is similar to the proposal by Cameron (1978) for the formation of a layer in the Critical Zone where there was an abrupt change in pressure. Reynolds (1985), von Gruenewaldt (1993) and Van Tongeren and Mathez (2012) suggested that there was an immiscible Fe-rich liquid that produced the numerous magnetitite and nelsonite layers in the Upper Zone. A more recent study by Fischer *et al*. (2016), shows apatite-hosting inclusions with melt compositions of Fe-rich melts and Si-rich melts, which best explains the coexistence of both Si-rich and Fe-rich immiscible melts. Fischer *et al*. (2016) also argued that there was not a complete segregation, resulting in crystallisation of similar phases although in different proportions. However, partial segregation of Fe-rich melts and Si-rich melts may explain the evolution of melanocratic (Fe-rich) and leucocratic (plagioclase-rich) gabbros in the Upper Zone.

2.2.2. Bushveld Granites

The Bushveld granites are known as the Lebowa Granite Suite, which are sheet-like bodies 1.5-3.5 km thick that cover an area of approximately 30 000 km^2 (Molyneux and Klinkert, 1978; De Beer *et al*., 1987; Kleeman and Twist, 1989; Harmer and von Gruenewaldt, 1991; Kinnaird *et al*., 2004). The granites intruded near the contact of the Rustenburg Layered Suite and are overlain by the felsic volcanics of the Rooiberg Group and Rashoop Granophyre Suite (Lenthall, 1973; Hatton and Schweitzer, 1995; McNaughton *et al*., 1993). The Lebowa Granite Suite is composed of at least seven different granites (SACS, 1980; Wilson, 2000). The Nebo Granite consists of 2-3 km thick sheets, is coarse-grained and pinkish grey in colour. The Nebo Granite is composed of alkali feldspar, quartz, hornblende, biotite and

accessory minerals (Strauss, 1954; SACS, 1980; MacCaskie, 1983; Coetzee and Twist, 1989). The Bobbejaankop Granite which has a distinct brick-red colour mainly due to alteration, is medium-grained, composed of alkali feldspars and mafic minerals; biotite which has mostly been altered to chlorite is associated with mineralisation (fluorite and cassiterite) from late-stage hydrothermal fluids (Crocker, 1989; Kleemann and Twist, 1989; McNaughton *et al*., 1993). The Lease Granite is medium- to fine-grained and distinguished by low amounts of mafic minerals and the abundance of alkali feldspar phenocrysts (Kinnaird *et al*., 2004). These granites are sill and dyke-like bodies found within the Nebo and Bobbejaankop Granite (Kinnaird *et al*., 2004). The Makhutso Granite is medium- to coarse-grained, composed of perthite, quartz and oligoclase and identified by large amounts of biotite (Walraven, 1988). The Makhutso Granite is the least abundant and the youngest of the Bushveld granites, evident from the cross-cutting relationships and xenoliths of both Nebo and Klipkloof Granite (Walraven, 1988).

2.2.3. Age of the Bushveld Complex

Early work by Kruger *et al*. (1986) and Walraven *et al*. (1990) considered a well constrained age at 2.06 Ga (± 3 and ± 27 Ma respectively) for the Bushveld Complex. More recently, Buick *et al*. (2001) presented U-Pb isotope data from newly grown titanite from within a calc-silicate xenolith in the Upper Zone of the eastern limb that yield an age of 2058.9 ± 0.8 Ma. These authors concluded that the titanite preserved the crystallisation age of the Bushveld Complex rather than the cooling age. These ages together which the 2061 ± 2 Ma age of the Rooiberg Group roof rocks (Walraven, 1997) would tightly constrain the emplacement of the entire Rustenburg Layered Suite of the eastern and western limbs between 2059 Ma and 2061 Ma. However, more recently, high precision U-Pb zircon dating of the Merensky Reef of the western limb, revealed a significantly younger age of 2054.4 ± 1.3 Ma (Scoates and Friedman, 2008), while the same study revealed a U-Pb rutile age of 2055.0 ± 3.9 Ma which was interpreted as the cooling age. Hutchinson *et al*. (2004) provided a minimum age for the Platreef at 2053.7 ± 3.2 Ma. Due to the sheer size of the Bushveld Complex and the dispute on the sequence of intrusion and extrusive events, it may indicate that the crystallisation of the Rustenburg Layered Suite was not at the same time across all parts of the complex. However, most recent high precision U-Pb dates provided ages of 2055.91 ± 0.26 Ma for quenched Marginal Zone rocks and an age of 2054.89 ± 0.37 Ma for cumulus rocks in the centre of the Rustenburg Layered Suite (Zeh *et al*., 2015). These authors suggested that the Bushveld Complex crystallised and cooled within 1.02 ± 0.63 Ma which is similar to the timescale suggested by Cawthorn and Walraven (1998).

2.2.4. Emplacement of the Bushveld Complex

The mechanism of emplacement for the Bushveld Complex remains unresolved. The earliest theories of emplacement include Mills Davis (1925) suggesting *"an active molten rock magma of common or normal composition deep in the Central Transvaal area and its gradual advance upwards through thousands of feet of strata until it emerged through devious ways through the quartzites and shales of the Pretoria Group and…spread out like a colossal cake"*. Wagner (1929) characterised the complex as a lopolith and suggested intrusion into horizontal strata; however, he did not propose a mechanism for the intrusion. Cousins (1959) interpreted the Bushveld Complex as a series of disconnected lopoliths.

Hatton (1995) suggested that the emplacement of the Bushveld Complex was an intrusive event with magma volume equivalent to that of a continental flood basalt province. Calculations using MgO and SiO_2 contents suggest that the melting took place between 18 and 40 km depth (Hatton, 1995). Hatton (1995) further suggested that only a buoyant mantle plume could perpetrate the basal crust and cause melting at these depths to form the Bushveld magma. Cawthorn *et al*. (2002), however, argued that MgO and SiO_2 content could not be used to determine the depth of the melting due to the effects from crustal contamination and fractionation. These authors further identified a mantle xenolith (aged 3.0 Ga) within a kimberlite pipe that intruded the Bushveld Complex and argue that these xenoliths would not have been preserved if a plume had penetrated the mantle. Cawthorn *et al*. (2002) concluded that melting took place at much greater depth in the asthenosphere and argued that magma, rather than a plume, penetrated the lithospheric upper mantle. A xenolith from the Premier kimberlite in the eastern Kaapvaal Shield yielded Re/Os ages of around 2.0 Ga for a xenolith sourced from the upper lithosphere, and xenoliths from a deeper source yielded Re/Os ages of around 3.0 Ga typical of the Kaapvaal ages (Carlson *et al*., 1999). The younger ages are interpreted to have resulted from substantial modification of the mantle by magmatic events which correspond to the emplacement age of the Bushveld Complex (Carlson *et al*., 1999). If the plume model is adopted for the Bushveld Complex, the lower lithospheric mantle, the source for the older xenoliths would also be affected by the resetting of Re/Os. Sulphide inclusions from ~2.0 Ga diamonds recovered from the Premier and Venetia kimberlite on opposite sides of the igneous complex, show initial Os isotope ratios which are more radiogenic than those found in the ore deposits of the Bushveld Complex (Richardson and Shirey, 2008).

No feeder systems have been positively identified for the Bushveld Complex. However, several feeder systems have been inferred through geometric studies (Kinloch, 1982). It has been assumed that areas displaying positive gravity anomalies may represent pipe-like feeders (Sharpe *et al*., 1981). Du Plessis

and Kleywegt (1987) noted that these anomalies in the eastern and western limbs occur where the mafic rocks are at their greatest thickness, resulting in positive gravity anomalies that can only be interpreted as feeders.

Van der Merwe (1976) associated the strongest positive gravity anomaly with a feeder zone, located in the northern limb west of Mokopane. Furthermore, Van der Merwe (1976) found no gravimetric evidence of connectivity between the northern and eastern limbs and suggested that they are separated by the Thabazimbi-Murchison Lineament (TML). Kruger (2005), on the basis of $^{87}Sr/^{86}Sr$ ratios, suggested that the Main Zone magma intruded through the feeder zone west of Mokopane and north of the TML. The Main Zone magma first flowed northwards into the northern limb, followed by magma flowing south into the eastern and western limb to form the Merensky Reef at the base of the Main Zone (Kruger, 2005; Finn *et al*., 2015). However, this model of emplacement has been questioned as it implies that the Platreef and the Merensky Reef are coeval and directly related (e.g. McDonald and Armitage, 2003; McDonald *et al*. 2005).

Naldrett *et al*. (2008) suggested a "pudding basin" model for the emplacement of marginal mineralisation in the Bushveld Complex. These authors noted the absence of more evolved cumulates and suggested that expulsions of partially fractionated magma moved up and along the margins of the basin due to overpressure induced by constant influxes of new magma. The model proposes that the filling space of two adjacent pudding basins of similar size was by a feeder at the base of the lowest basin. Naldrett *et al*. (2008) interpreted the limbs of the Bushveld Complex to represent different pudding basins with different levels of erosion. They also indicate that the eastern and western limbs represent a single basin rather than two separate pudding basins.

Some authors have proposed that linear feeders represented by shear zones acted as magma conduits (Cawthorn *et al*., 2002; Friese, 2004). The Steelpoort fault is regarded as one of these linear feeders by Cawthorn *et al*. (2002), as there are differences in stratigraphic thicknesses in units of the Lower and Critical Zone on either side of the fault (Hatton and von Gruenewaldt, 1987). This has been interpreted to be a result of differential flow of magma to either side of the feeder zone (Cawthorn *et al*., 2002). These authors also proposed that other large shear zones and faults separating compartments in the Bushveld Complex may represent linear feeders or magma conduits. Friese (2004) suggested that the Bushveld magmas utilised the Thabazimbi-Murchison Lineament, the Palala Shear Zone and the Barberton-Magaliesburg Lineament as magma conduits. Where he suggested that at critical levels in the

crust the magmatic pressure would be equivalent to the lithostatic pressure and allow for lateral spread of the sill-like intrusion of the complex.

Chapter 3
Geology of the Northern Limb

3.1. Introduction to the Northern Limb

This chapter provides a literature review on the northern limb of the Bushveld Complex, particularly its stratigraphy, age, structural history and mineralisation in relation to the main body of the Bushveld Complex.

The exposed northern limb of the Bushveld Complex is located in the Limpopo Province of South Africa. It crops out as a slightly sinuous N-S striking, WSW-dipping body, over a strike length of 110 km (van der Merwe, 1976; Gain and Mostert, 1982). The Rustenburg Layered Suite north of the Thabazimbi-Murchison Lineament (TML) is generally shallowly buried (< 1500m depth) with an approximate area of ~160 km x ~125 km (Finn *et al*., 2015), which also includes the Villa Nora Fragment exposed in the far northern part of the northern limb. The Villa Nora Fragment is an area of exposed layered Bushveld rocks that strike in an east-west direction and have a southward dip (Kinnaird *et al*., 2005). The thickness of the northern limb is not well constrained but varies from <1000 to <12000 m with an average of <4000 m (Finn *et al*., 2015). South of Mokopane the Rustenburg Layered Suite of the northern limb is north-east trending with a westward dip between 15° and 27°. Northwards the strike changes to northwest and eventually due north, with westward dips decreasing upwards through the layered mafic rocks from 45° to 10° (van der Merwe, 2008).

To the north, the northern limb is covered by younger Waterberg Group sediments and to the south the Karoo sediments are juxtaposed against the layered mafic rocks and the Zebediela and Ysterberg-Planknek faults, which are subordinate branches of the Thabazimbi-Murchison Lineament (TML) (Fig. 3.1). The TML represents a pre-Bushveld collisional suture zone (ca. 2960 Ma Meso-Archean) between the Pietersburg and Central Kaapvaal terranes which has experienced repeated reactivation and is still active at the present day (Good and de Wit, 1997; McDonald *et al*., 1999). The TML is believed to have controlled the emplacement of the Bushveld Complex either by acting as a feeder (Kinnaird *et al*., 2005) or as a permanent / temporary barrier separating the movement of Bushveld magmas (Kruger, 2005). Van der Merwe (1978) suggested that the emplacement of the northern limb magma was controlled by the intersection point of the three major tectonic lineaments, west of Mokopane. It is still not clear if the northern limb was ever connected to the rest of the Bushveld Complex at the time the Bushveld magma intruded the Transvaal sediments (Kinnaird *et al*., 2005).

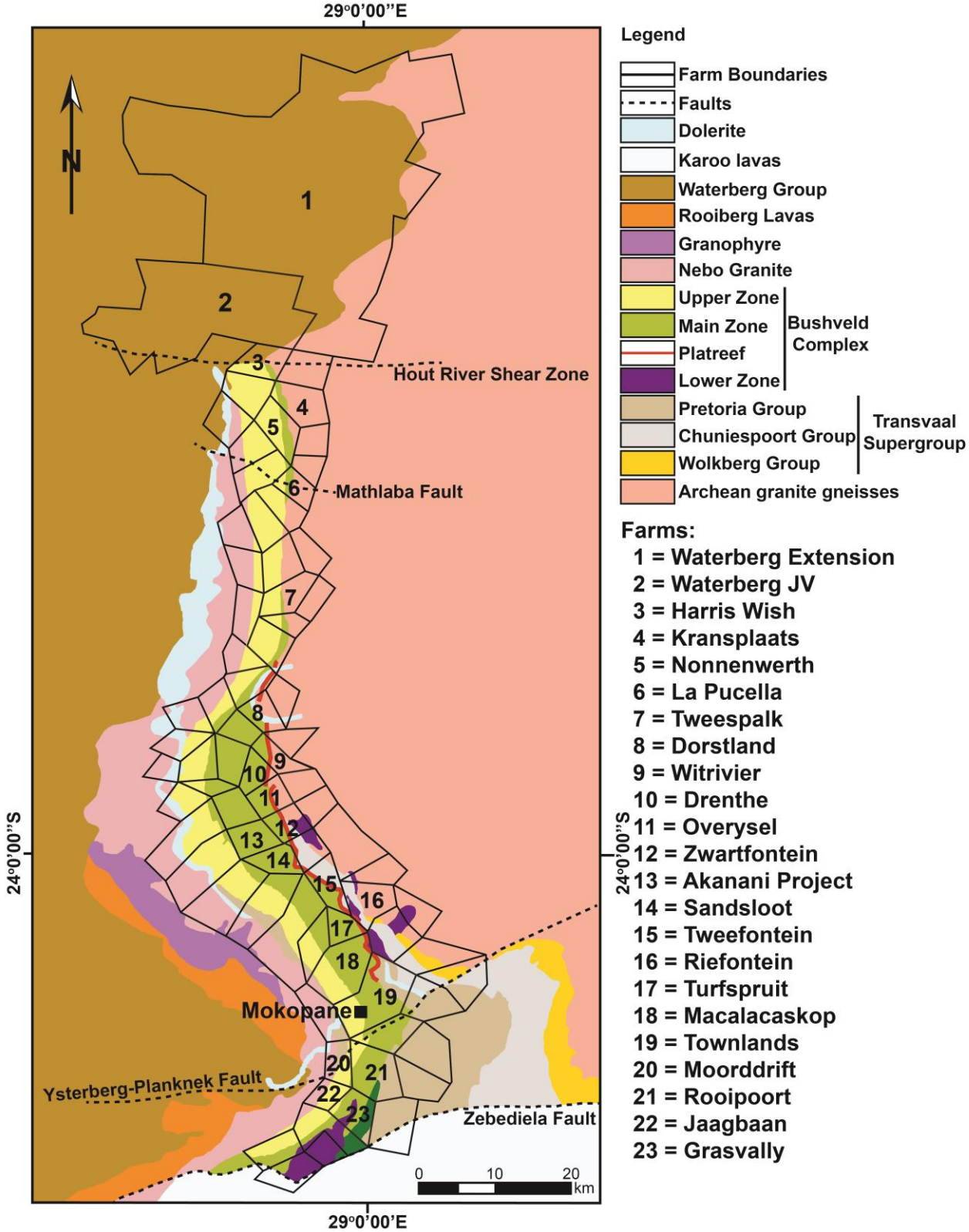

Figure 3.1: Geological map of the northern limb of the Bushveld Complex (Modified from van der Merwe, 1978; by Ashwal *et al*., 2005 and McDonald *et al*., 2017). Boundaries of farms mentioned in the text are shown.

3.2. Structures of the Northern Limb

The Rustenburg Layered Suite of the northern limb is disturbed by a number of faults. Truter (1947), van Rooyen (1954) and de Villiers (1967) recognised three sets of major faults; (i) N and NNW striking faults; (ii) NE-ENE striking faults; and (iii) NW trending faults. The NE-ENE trending faults appear to be the earliest and most important structures that divided the rock types and setting of the northern limb. Hulbert (1983) recognised four phases of fault deformation; (i) N-S trending reverse faulting; (ii) WNW trending faults; (iii) NE-striking faults that are assumed to have occurred post-Waterberg; (iv) the NE trending Zebediela and Ysterberg-Planknek faults that are considered to mark the final stages of faulting in the southern sector of the northern limb, which occurred post-Karoo deposition (van der Merwe, 1978). The final NE-striking faults have a normal displacement with a downthrow to the south (White, 1994).

Friese (2004) carried out a detailed structural investigation on the northern limb including the Villa Nora segment. Friese (2004) interpreted the following sets of structures that are listed from oldest to youngest.

- Shallow, NW dipping, SE verging thrusts and associated ENE trending, sub-horizontal, low-amplitude regional folds within the Archaean basement.
- NW to WNW trending, moderate to steeply dipping extensional faults within the Transvaal Supergroup. These were formed by reactivation of the structures that are similarly orientated, formed in the Archaean basement during the Murchison Orogeny that formed the TML.
- ENE to NNE trending, steep to subvertical, mainly SE dipping, dextral strike slip shear zones with associated NE verging, layer-parallel thrusts. This system developed in the Transvaal Supergroup by reactivation of the upper section of a Neoarchean (~2.78-2.64 Ga) sinistral strike slip system. Friese (2004) states that these structures developed in both the Transvaal Supergroup and the Bushveld Complex. It is noteworthy that the Bushveld Complex did not exist at the time of the Limpopo Orogeny (2.7-2.6 Ga) (Armitage, 2011).
- N-S striking, moderately west dipping extensional faults with imbricate, normal dip slip and sinistral strike slip duplexes in their immediate hangingwall. These faults transgress the Archean basement, Transvaal Supergroup and Bushveld mafics.

- NW dipping, SE verging thrusts and associated ENE trending, sub-horizontal, low amplitude regional folds of pre- to syn-Rustenburg Layered Suite age. These were formed by mild SE directed stress within the northern Kaapvaal Craton at an early stage of the Magondi Orogeny at ~2.1-2.058 Ga.
- WNW to WSW trending extensional fractures and joints with minor displacement that cut all other structural features.

All the structures have undergone several phases of reactivation, except for the youngest group of structures. The present magnitude and sense of displacement is an accumulation of movements that have taken place over more than 2 Ga (Friese, 2004; Armitage, 2011; Finn *et al*., 2015). In addition to the regional structural investigation, local detailed studies have been carried out by van der Merwe (1976) on the northern limb, Nex (2005) on Tweefontein Hill and Armitage *et al*. (2007) south of Mokopane.

3.3. Stratigraphy of the Northern Limb

The stratigraphy of the northern limb does not correlate exactly with the stratigraphy of the other limbs south of the TML, although all stratigraphic zones of the Rustenburg Layered Suite can be recognised. These differences are seen north of the Zebediela fault, a branch of the TML. Figure 3.2 summarises the traditional view of the stratigraphic relationship between the northern limb and the rest of the limbs of the Bushveld Complex. Furthermore, there are stratigraphic differences seen north and south of the Ysterberg-Planknek fault, which will be discussed below.

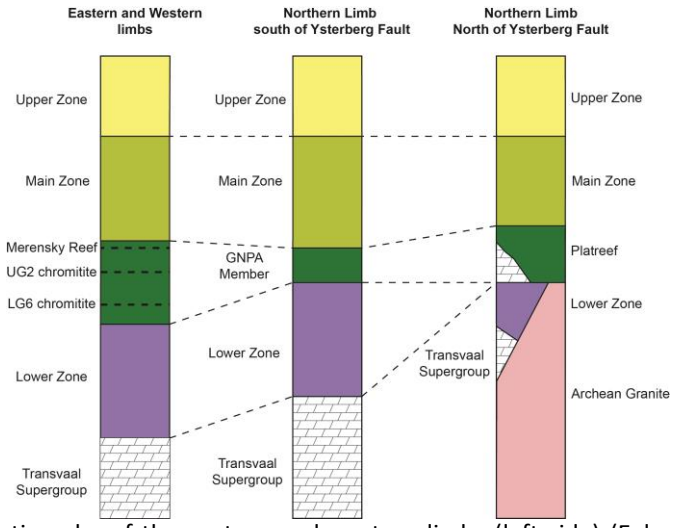

Figure 3.2: Schematic stratigraphy of the eastern and western limbs (left side) (Eales and Cawthorn, 1996), the stratigraphy south of the Ysterberg-Planknek fault on Grasvally (middle) (Hulbert, 1983), and the stratigraphy for the northern limb north of the Ysterberg-Planknek fault (right side) (Kinnaird *et al*., 2005; Kinnaird and Nex, 2015).

3.3.1. Footwall

A characteristic feature of the northern limb is the pronounced transgression of the layered mafic succession northwards from the TML, through different Transvaal Supergroup sediments (Fig. 3.3). The <12 km thick Transvaal Supergroup sediments (Button, 1986), were deposited on the Archean basement between 2670 to 2100 Ma (Eriksson *et al*., 2001). The footwall units of the layered cumulates, northwards, consist of: a thin basal clastic unit of the Black Reef Formation, interbedded quartzites and shales of the Magaliesberg Quartzite Formation, clastics with minor volcanics of the Timeball Hill Formation, shales of the Duitschland Formation, the Penge banded iron formation, the Malmani Subgroup dolomites and in the far north the Rustenburg Layered Suite rests on Archean basement granites and gneisses (Eriksson *et al*., 2001) (Fig. 3.1).

Transvaal Supergroup	Pretoria Group	Smelterskop Fm.	Andestic Lavas, arenites and intercalated shales
		Magaliesberg Fm.	Sandstone with minor mudstone lenses
		Silverton Fm.	Shales with intercalated pyroclastic volcanics
		Daspoort Fm.	Sandstone, quartzites and minor mudstones
		Strubenskop Fm.	Shales with subordinate sandstones
		Dwaalheuwel Fm.	Sandstones
		Timeball Hill Fm.	Clastic sediments (mudstone, quartzites, conglomerates & minor volcanics)
		Duitschland Fm.	Shale with significant dolomites, minor conglomerates and quartzites
	Chunniespoort Group	Penge Fm.	Banded ironstone with ferruginous shale and quartzite at the base
	Chunniespoort Group / Malmani Subgroup	Frisco Fm.	Chert-poor dolomite becoming more chert-rich towards the top. Thin layers of carbonaceous mudstone throughout, more areneceous towards the top
		Eccles Fm.	Chert-rich dolomite interbedded with chert-poor dolomite and minor siltstones and mudstones
		Lyttelton Fm.	Chert-poor dolomite with infrequent minor quartzites and mudstones
		Monte Christo Fm.	Chert-poor dolomite interbedded with abundant chert layers, minor quartzite and mudstones
		Oaktree Fm.	Chert-poor carbonate with thin quartzite and mudstone units, ubiquitous laminated chert.
		Black Reef Fm.	Coarse-grained quartzite, interbedded with pebble beds, sandy shales and minor andesitic lava.

Figure 3.3: Lithostratigraphy of the Transvaal Supergroup floor rocks beneath the Rustenburg Layered Suite of the northern limb of the Bushveld Complex. The oldest floor rocks of Archean granite-gneisses occur in the north and the youngest floor rocks occur in the southern sector of the northern limb. Data from Button (1973), Martini (1979), Catuneanu and Eriksson (1999), Bekker *et al*. (2004) and Van der Merwe (2008) for the Mokopane area. The image was redrawn from Kinnaird and Nex (2015).

3.3.2. Marginal Zone

The Marginal Zone is generally poorly exposed in the northern limb, although where there is outcrop exposed there are noritic to doleritic rocks from a few centimeters to tens of metres thick (van der Merwe, 1976). These exposed rocks have a number of inclusions of carbonate rocks, hornfels, quartzite and granite. Another feature seen in the Marginal rocks of the northern limb is an olivine-bearing chilled margin along the contact with the Lower Zone at the base of the Uitloop satellite I near Mokopane (van der Merwe, 1976). In a recent study by Yudovskaya *et al*. (2013) Marginal Zone rocks were found between the Platreef and the Lower Zone. These Marginal Zone rocks are intercalated within a package of country rocks approximately 100 m thick (Yudovskaya *et al*., 2013).

3.3.3. Lower Zone

The Lower Zone cumulates are comprised of at least 1600 m of 37 cyclic units of pyroxenite, dunite, harzburgite and chromitite on the Grasvally, Volspruit and Zoetveld farms (Hulbert, 1983; Hulbert and von Gruenewaldt, 1986: Smith *et al*., 2014). This sequence of ultramafic rocks differs from the Lower Zone in the rest of the complex in that it contains orthopyroxene with a higher enstatite content and olivine with higher forsterite content (van der Merwe, 1976; Maier *et al*., 2013), and chromitite layers with the highest Cr_2O_3 content and Cr# in the entire Bushveld Complex (Hulbert, 1983; Maier *et al*., 2013). Hulbert (1983) defined three subzones; the Volspruit pyroxenite; the Drummondlea harzburgite chromitite; and the Moorddrift harzburgite pyroxenite (Fig. 3.4). The Drummondlea harzburgite chromitite hosts two economically important chromitite seams (Fig. 3.4) that crop out over a strike length of 5 km (Hulbert and von Gruenewaldt, 1985).

The Lower Zone north of the Ysterberg-Planknek fault was previously only identified as several satellite bodies composed of orthopyroxene and orthopyroxene-olivine cumulates with occasional chromitite layers (de Villiers, 1970; van der Merwe, 1976; Gain and Mostert, 1982). A recent study by Yudovskaya and Kinnaird (2010) identified a layer of Lower Zone underlying the Platreef. Yudovskaya *et al*. (2013) reported a Lower Zone sequence up to 800 m thick on the farms Turfspruit and Sandsloot. The Lower Zone in these areas is separated from the Platreef by an interval of country rocks 100 m thick intercalated with Marginal Zone rocks and minor crosscutting granitic veins (Yudovskaya *et al*., 2013). Here, the Lower Zone is composed of dunite-harzburgite-pyroxenite cycles with sporadic chromite seams and contains one of the most magnesian-rich olivine compositions identified in the whole Bushveld Complex (Yudovskaya *et al*., 2013). The high Mg# of up to 91 and high Ni contents associated with these rocks are comparable to rocks at Grasvally (Hulbert and von Gruenewaldt,1985) and to the

Basal Ultramafic sequence (BUS) discovered in the Clapham section of the eastern limb of the Bushveld Complex (Wilson, 2012; Wilson, 2015).

3.3.4. Critical Zone, GNPA Member and the Platreef

3.3.4. A. GNPA Member

The Critical Zone as it is seen in the eastern and western limbs of the Bushveld Complex is not developed in the northern limb. South of Mokopane, between the Ysterberg-Planknek fault and the Zebediela fault, is a succession of rocks, up to 350 m thick, composed of pyroxenite, norites, anorthosites and chromitites known as the Grasvally Norite-Pyroxenite-Anorthosite (GNPA) member (Fig. 3.4) (Hulbert 1983; McDonald *et al*. 2005; Maier *et al*. 2008; Smith 2014; Smith *et al*. 2014, Holwell *et al*. 2015). Hulbert (1983) originally divided the GNPA member into a lower pyroxenitic subzone 1 and an upper noritic subzone 2. Recent drilling into the GNPA member on the adjacent farm, Rooipoort, has shown that the GNPA member occurs over a strike length of 5-6 km. De Klerk (2005) introduced new terminology and three new stratigraphic subdivisions; the Lower Mafic Unit (LMF), the Lower Gabbronorite Unit (LGN) and the Mottled Anorthosite Unit (MANO).

The chromitite layer of the GNPA member has been called the 'UG2-like chromitite' by Hulbert (1983) and has been directly correlated with the UG2 chromitite of the Critical Zone in the eastern and western limbs of the Bushveld Complex by van der Merwe (1998). However, although the Cr_2O_3 content of chromite from the GNPA member and the UG2 chromitite may be similar, the PGE pattern in the GNPA member chromitite does not show any resemblance to that of the UG2 chromitite (von Gruenewaldt *et al*., 1989), and the chromitite of the Grasvally area generally has higher TiO_2 and Al_2O_3 than the UG2 (Hulbert, 1983). North of the Ysterberg-Planknek fault the Platreef is the stratigraphic equivalent of the Critical Zone elsewhere in the Complex. According to Holwell *et al*. (2015) the Platreef formed from compositionally similar or related magmas to the GNPA member. McDonald *et al*. (2005) argues that the correlation between the GNPA member and the Platreef with the upper Critical Zone is not plausible due to different magma compositions and Cu/Pd ratios.

3.3.3. B. The Platreef

The Platreef is defined by Kinnaird and McDonald (2005) as ''*mafic units enriched in Ni-Cu-PGE that occur between the Archaean granite-gneiss basement or the Transvaal Supergroup and the gabbronorites of the Main Zone, north of the Planknek fault*'. This definition includes the Ni-Cu-PGE ore

bodies on the farms Witrivier, Drenthe, Overysel, Zwartfontein, Sandsloot, Vaalkop, Tweefontein, Turfspruit, Macalacaskop and Townlands from north to south, but does not include the mineralisation south of the Ysterberg Planknek fault (Hulbert, 1983: von Gruenewaldt *et al*., 1989; Maier and Barnes, 2010; Holwell *et al*., 2013; Smith *et al*., 2014), or the mineralisation of the Aurora project to the north (Harmer *et al*., 2004; McDonald and Harmer, 2010; McDonald *et al*., 2017).

In 1925, Merensky described an ultramafic body at the base of the Bushveld Complex north of Mokopane and referred to it as a "Pyroxenite body" composed mainly of pyroxenite and/or olivine-bearing pyroxenite that was highly serpentinised. Wagner (1929) described the Platreef as a basal package of pyroxenite, norite, serpentinite and xenoliths of footwall rocks hosting Ni-Cu-PGE mineralisation that transgresses various Transvaal Supergroup sedimentary footwalls and is overlain by gabbronorite ascribed to the Main Zone. The term Platreef was first proposed by van der Merwe (1976, 1978) who described it as a porphyritic appearance that grades upwards into a feldspathic pegmatitic pyroxenite, which he ascribed to the base of the Main Zone.

The Platreef can be traced for approximately 30 km along strike north of the Ysterberg-Planknek fault. Northwards the Platreef transgresses progressively older Transvaal Supergroup sediments and eventually abuts against Archean basement on the northern portion of Zwartfontein farm (Fig. 3.5). The Platreef is approximately 400 m thick in the south and <50 m thick in the north (Fig. 3.5). The Platreef strikes in a north to northwest direction and dips towards the west at 40-45°, although down dip the angle gradually deceases to an almost horizontal angle with a more regularly layered sequence termed "the Flatreef" (Grobler *et al*., 2012; Kekana, 2015; Nodder *et al*., 2015; Grobler *et al*., 2018). The overall geometry of the Platreef seems to have been controlled by the irregular footwall topography.

The Platreef hosts one of the world's largest deposits of PGE as well as significant reserves of Ni and Cu (Naldrett, 2010). It is estimated that the Platreef contains reserves of 16.3 million ounces of Pt+Pd (Cawthorn, 1999). The Platreef is <400 m thick on Turfspruit and Sandsloot (Kinnaird and Nex, 2015) and is amenable to open pit mining (Bye, 2001). Anglo Platinum currently operates 4 open pits on the Sandsloot, Zwartfontein and Overysel farms, collectively known as the Mogalakwena Mine Complex. This is currently the largest open pit platinum mine in the world and has a life-of-mine extending well beyond 2060 (Bye, 2001). Several other companies have started exploring for Cu-Ni-PGE deposits on the northern limb, making the northern limb one of the most intensively explored areas for Cu-Ni-PGE deposits in the world in recent times.

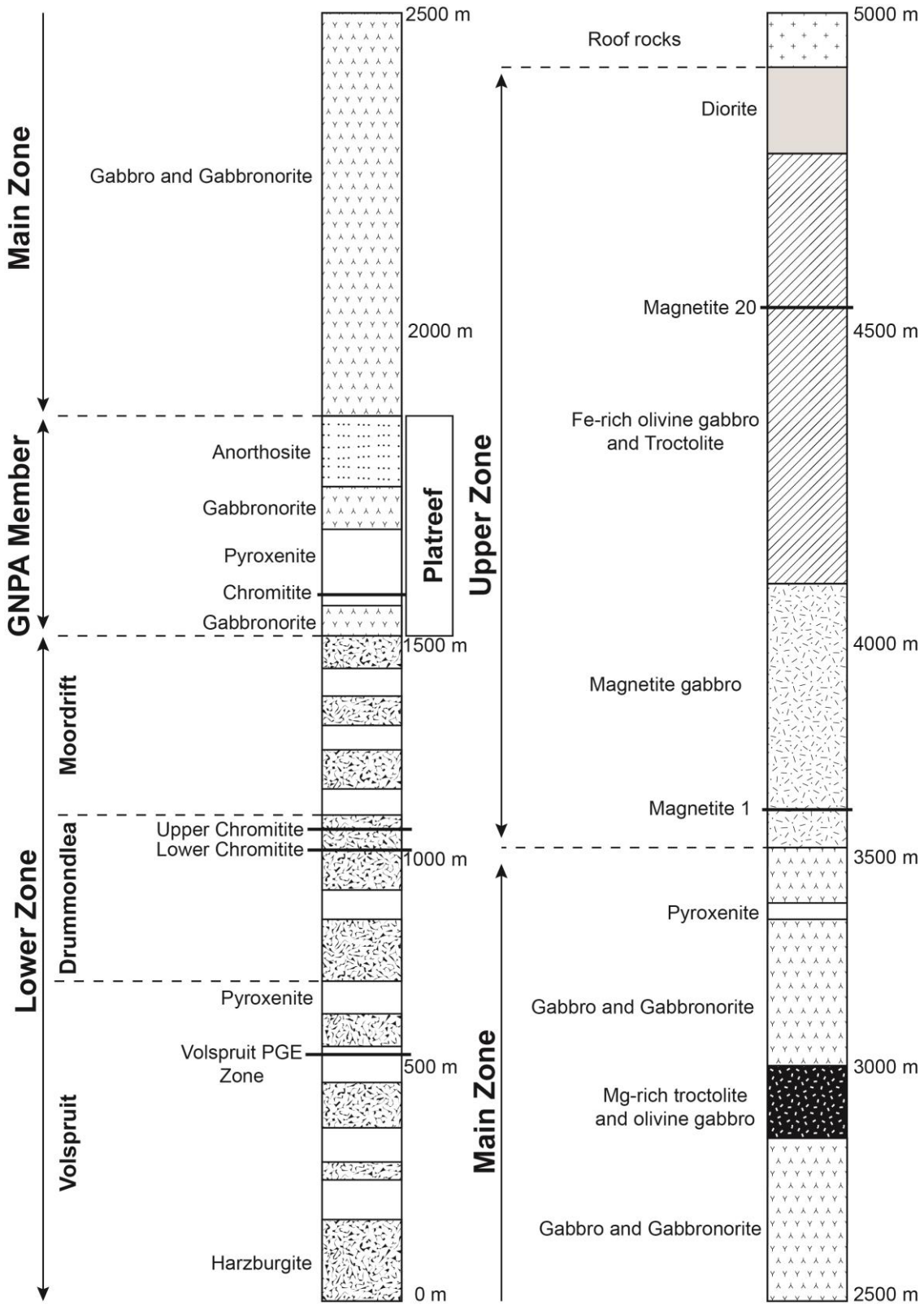

Figure 3.4: Stratigraphy of the northern limb south of the Ysterberg-Planknek fault (Hulbert, 1983; von Gruenewaldt *et al*., 1989; Modified from McDonald *et al*., 2005).

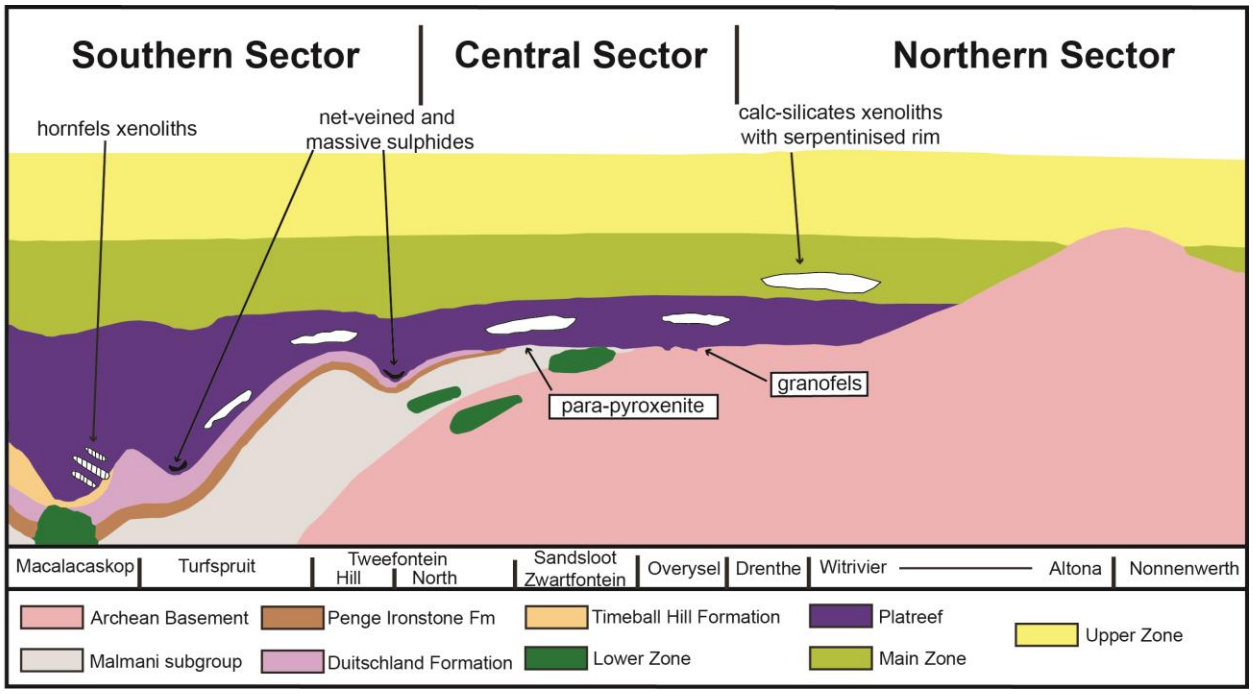

Figure 3.5: Schematic longitudinal section through the Platreef along the entire strike length (Redrawn from Kinnaird *et al*., 2005). Note that between Witrivier and Altona a significant strike length is not shown.

The Platreef is a very complex body of diverse lithologies that include igneous, hybrid and contact metamorphic rocks such as feldspathic pyroxenites, gabbronorites, igneous and metamorphic peridotites, serpentinites and a range of hybrid lithologies. The northern limb is divided into three different sectors along strike based on these variations and underlying footwall lithologies (Fig. 3.5) (Kinnaird *et al*., 2005; McDonald and Holwell, 2011). Chromitites are generally rare (Yudovskaya and Kinnaird, 2010), but recent deep drilling has indicated an increase in chromitites with depth (Yudovskaya *et al*., 2017).

The Platreef not only differs based on the degree of contamination and the transgressive footwall rocks but also in having a different style of mineralisation. Kinnaird (2005) indicated that the Platreef consists of several sill-like intrusions differing in chemistry and PGE distribution. The lowest sills in the southern sector overlying reactive Transvaal sedimentary lithologies are more contaminated than the upper sills (Sharman-Harris *et al*., 2005; Sharman *et al*., 2013). Where the lowest sills are overlying granite-gneiss basement lithologies towards the north there is less contamination close to the footwall. However, a dolomite raft within the middle sill may be the source of the contamination in the northern sector (Sharman-Harris *et al*., 2005; Holwell *et al*., 2007). This reinforces the importance of the host rocks for the different sectors of the Platreef.

The Platreef is considered to have formed from multiple complex sill-like intrusions of mafic and ultramafic compositions (Kinnaird *et al*., 2005; Maier *et al*., 2008). There are a number of aspects where the Platreef differs from the Critical Zone, although the major difference is the high degree of contamination with the Transvaal footwall lithologies at the base of the Platreef (Kinnaird *et al*., 2005; Maier *et al*., 2008). As a result of the contamination, the Platreef lacks the cyclicity typical for much of the Bushveld Complex. Regular occurrences of chromitite and anorthosite layers are absent from the Platreef package. However, recent studies down dip of the Platreef on the farm Turfspruit, Sandsloot and the Akanani project have revealed some similarities to the Critical Zone as seen in the rest of the Bushveld Complex (Dunnett *et al*., 2012; Grobler *et al*., 2012; Kekana, 2015; Nodder *et al*., 2015; Yudovskaya *et al*., 2017). The regular occurrence of chromitite layers down dip marks the conversion from Platreef to Critical Zone, as there are rare discontinuous chromitite layers seen in the shallow Platreef (Yudovskaya and Kinnaird, 2010). Similar cyclic units to the Merensky Reef and UG2 have been identified down dip of the Platreef (Grobler *et al*., 2012; Nodder *et al*., 2015). A thick (up to 20 m) PGE-rich reef bounded by chromitite layers occurs at the top contact of the down dip Platreef and the Main Zone, which is similar to the Merensky Reef in the eastern and western limbs (Grobler *et al*., 2012; Yudovskaya *et al*., 2017). This pristine magmatic PGE-rich reef has characteristics which resemble the Merensky Reef such as stratigraphic position, silicate compositions, PGE grades, sulphur isotopic compositions and platinum-group mineral characteristics (Grobler *et al*., 2012; Kekana, 2015; Yudovskaya *et al*., 2017).

Source and Emplacement of the Platreef

A number of authors suggest that the Platreef magma was fed from the Thabazimbi-Murchison Lineament (TML) (White, 1994; Kinnaird, 2004; Kruger, 2005; Kinnaird, 2008). Van der Merwe (1978) suggested that the gravity high northwest of Mokopane is the possible feeder for the Platreef and northern limb. An alternative feeder has been suggested by McDonald *et al*. (2009) and Yudovskaya *et al*. (2010), located downdip of Akanani, west of the central sector of the Platreef. This suggestion was based on mineral chemistry (highest Mg#), olivine-rich lithologies, high temperature PGM and high PGE tenors.

Pronost *et al*. (2008) used Nd isotope data from the Platreef and Main Zone and concluded that they have a common origin. Other studies have indicated that there is a significant time break between the Platreef and intrusion of the overlying Main Zone (Holwell and Jordaan, 2006; Weise, 2010).

However, many authors (e.g. Wagner, 1929; White, 1994) correlated the Platreef directly with the upper Critical Zone due to the pyroxenitic platinum-bearing ore body overlain by Main Zone lithologies. Cawthorn *et al*. (2002) suggested that the magma which formed the UG2 chromitite layer in the eastern limb may have flowed northwards to form the Platreef, due to the similar Pt/Pd ratios in both mineralised zones. Naldrett *et al*. (2008) suggested that the Platreef formed from different magmas than those which formed the main Bushveld Complex. These magmas produced the UG2 and Merensky Reef.

Nell (1985) suggested that the metamorphic aureole in the Mokopane area formed from the phases of thermal metamorphism associated with the magma emplacement. The first stage was related to the emplacement of the Lower Zone magma (750°C at 1.5 kb pressure). The second stage was associated with the emplacement of the upper Critical Zone followed by the Main and Upper Zone magmas (900°C and 4-5 kb pressure). Kruger (2005) also presented a two-stage emplacement model for the Platreef based on Cr/MgO ratios. The model suggested that the Platreef formed from an intermediate magma between the Main and Lower Zone, where the Main Zone magma assimilated Lower Zone lithologies.

McDonald *et al*. (2005) presented an alternative view, suggesting that the Platreef and GNPA member are not Critical Zone but were derived from magma mixing between the Lower Zone and Main Zone magmas. However, observations made by van der Merwe (1978) indicated that the Lower Zone was fully consolidated and tilted before the next influx of magmas. These observations were, however, only recorded for the satellite bodies of the Lower Zone and not for the Lower Zone package south of the Ysterberg-Planknek fault or the newly discovered thick successions of Lower Zone beneath the Platreef (Yudovskaya *et al*., 2013).

3.3.5. Main Zone

The contact between the Platreef and Main Zone shows that the gabbronorite cuts down into the Platreef in the Zwartfontein south pit (Holwell and Jordaan 2006). A fine-grained leuconorite is observed at the base of the Main Zone with textures that exhibit eroded Platreef, indicating that the Main Zone was emplaced after the Platreef had crystallised and began to cool (Holwell *et al*. 2005). In addition, there are xenoliths of reef pyroxenite found in the hangingwall gabbronorites (Holwell *et al*. 2005). This boundary has been described as a chilled margin between the Platreef and the Main Zone (Holwell *et al*. 2005; Holwell and Jordaan 2006).

The Main Zone of the northern limb is generally comparable with the Main Zone in the rest of the Bushveld Complex. However, north of the Ysterberg Planknek fault the Main Zone hosts a 110-160 m

thick sequence of olivine-bearing norite called the Troctolite Horizon, approximately 1100 m above the top of the Platreef (Van der Merwe, 1976; Ashwal *et al*., 2005). To date the Troctolite Horizon has only been described for the northern limb and is absent elsewhere in the Main Zone of the Bushveld Complex. In general, there is little to no olivine in the Main Zone of the eastern and western limbs of the Bushveld Complex (Eales and Cawthorn, 1996). Rare earth element patterns and incompatible trace element ratios suggest a Main Zone signature for the olivine-rich horizon rather than a Critical Zone origin as proposed by Ashwal *et al*. (2005). Tanner *et al*. (2014) identified Cr-rich pyroxenes associated with the Troctolite Horizon and ascribed this to a new pulse of ultramafic magma and indicated that the horizon may be prospective for PGE exploration. Recently PGM have been found in the Troctolite Horizon. Sperrylite ($PtAs_2$) enclosed in cleavage planes of plagioclase, electrum and PGM-tellurides entrapped in base metal sulphides and no sulphide-dominant PGM (braggite, cooperite and vysotskite) have been found (Kennedy *et al*., 2015).

In addition, the orthopyroxene-dominated Pyroxenite Marker of the eastern and western limbs of the Bushveld Complex, is absent in the Main Zone of the northern limb (Ashwal *et al*., 2005; Cawthorn, 2012). Ashwal *et al*. (2005) identified a pyroxene-rich layer in the Bellevue drillcore, which is in a similar stratigraphic position to the Pyroxenite Marker, although in the northern limb it consists of inverted pigeonite rather than primary orthopyroxene. On this basis Ashwal *et al*. (2005) and other authors (e.g. McDonald *et al*., 2005) have discounted the presence of the Pyroxenite Marker all-together in the northern limb. However, Maier and Barnes (2010) have correlated this pyroxene-rich layer in the northern limb with the Pyroxenite Marker seen in the eastern and western limbs.

In addition, other contrasts recognised is the thickness of the eastern and western limbs Main Zone succession is between 2.5 km and 4 km thick (Nex *et al*., 1998), whereas, the Main Zone in the northern limb has an approximate thickness of 2200 m (Van der Merwe, 1976; Ashwal *et al*., 2005; Mangwegape *et al*., 2016).

3.3.6. Upper Zone

The Upper Zone overlies the Main Zone and has an approximate thickness of 1400 m (Ashwal *et al*., 2005; McDonald *et al*., 2005). The boundary between the Upper Zone and Main Zone is determined by the first appearance of cumulus magnetite, similar to the rest of the Bushveld Complex (van der Merwe, 1976; SACS, 1980; Ashwal *et al*., 2005). The Upper Zone of the northern limb is composed of alternating layers of gabbro, anorthosite, magnetite-bearing gabbro and olivine-bearing diorites (Ashwal *et al*.,

2005). Within the Upper Zone there are twenty distinct magnetites ranging in thickness from a few cm to 10s of meters (Ashwal *et al*., 2005; Longridge, 2015; Viljoen, 2016). Over the thickness of the Upper Zone of the northern limb, the vanadium content of the magnetite decreases from >2% V_2O_5 near the base, to <0.3% towards the top, whereas titanium has an inverse relationship, increasing upwards (Longridge, 2015; Viljoen, 2016). A magnetite layer referred to as the Q layer in the northern limb by Bushveld Minerals (Longridge, 2015; Viljoen, 2016), forms a distinctive assemblage of magnetite layers approximately 45 m thick, consisting of massive, disseminated and stringer magnetite (Viljoen, 2016). This Q layer has been identified as a major potential iron and titanium resource for the Upper Zone of the northern limb (Longridge, 2015; Viljoen, 2016).

The Upper Zone also outcrops in the Villa Nora fragment. The main lithologies in this area include leuconorite, leucogabbro and anorthosite (Hattingh and Pauls, 1994). The lower parts of the Upper Zone in the Villa Nora fragment are truncated by the Abbottspoort fault.

3.4. Mineralisation of the Northern Limb

3.4.1. Mineralisation in the Lower Zone

South of the Ysterberg-Planknek fault on the Grasvally farm the Lower Zone differs from the Lower Zone in the eastern and western limbs of the Bushveld Complex. The Lower Zone in this area hosts two persistent chromitite layers with the highest Cr content in the Bushveld Complex (Hulbert and von Gruenewaldt, 1985), as well as the Volspruit zone containing Ni-PGE mineralisation with measured reserves of 31.6 Mt of ore (1.28 g/t Pt + Pd + Au; 0.14 wt. % Ni) (Hulbert and von Gruenewaldt, 1985; Sylvania, 2010).

North of the Ysterberg Planknek fault the Lower Zone was previously deemed to be restricted to isolated bodies in sedimentary rocks and granite gneisses (Van der Merwe, 1978). The Uitloop and Zwartfontein bodies (Fig. 3.1) contain PGE-Ni-Cu and Cr mineralisation (Van der Merwe, 1978). Yudovskaya *et al*. (2013) have identified PGE sulphide mineralisation (up to 1.3 g/t Pt + Pd) hosted in the newly discovered Lower Zone lithologies beneath the Platreef, on the Turfspruit farm and regarded this mineralised interval as a possible analogue of the Volspruit PGE mineralisation zone in the Grasvally area (Yudovskaya *et al*., 2013; Yudovskaya *et al*., 2014). However, no such mineralised interval was found in the Lower Zone lithologies beneath Sandsloot (Yudovskaya *et al*., 2013).

3.4.2. Mineralisation in the Platreef

The Platreef carries Ni-Cu-PGE mineralisation of three different types: massive sulphide bodies at the base, marginal or contact disseminated ore in hybrid rocks, and exoskarns as well as reef style mineralisation hosted by feldspathic pyroxenite and harzburgite at the top, near the boundary with the Main Zone (Yudovskaya *et al*., 2017). The PGE mineralisation in the Platreef is mainly associated with base metal sulphides (pyrrhotite, pentlandite, chalcopyrite and minor pyrite), however in detail the PGE may be decoupled (Kinnaird *et al*. 2005; Hutchinson and Kinnaird, 2005; Holwell *et al*., 2006). The PGE mineralisation is hosted mainly by the pyroxenitic package and in the immediate footwall metasedimentary rocks and Archean granites (Wagner 1929). The mineralisation in the individual sills of the Platreef is variable, and not all the sills are well mineralised (Viljoen and Schurmann, 1998; Kinnaird *et al*., 2005). Some authors indicate that the mineralisation is bottom loaded in the southern sector and top loaded in the central and northern (e.g. White, 1994), although this is an oversimplification of the Platreef mineralisation (Kinnaird *et al*., 2005). There is still an ongoing debate regarding any mechanisms that might have controlled the distribution of the mineralisation in the Platreef. The grades are generally lower and more variable in the Platreef compared to the Merensky Reef and UG2 in the eastern and western limbs (White, 1994; Gain and Mostert, 1982; Armitage *et al*., 2002; Hutchinson and Kinnaird, 2005; Holwell *et al*., 2006; Nichol and Kinnaird, 2008).

In the feldspathic pyroxenite of the Platreef, the sulphides occur as interstitial blebs and in some parts along strike close to the footwall contact, the sulphide content is up to 30 modal % as seen in cores (Kinnaird, 2004). On the farms Turfspruit and Tweefontein Hill, the occurrence of net-textured and massive sulphides is common (White, 1994; Nex 2005; Hutchison and Kinnaird, 2005). These large occurrences of sulphides are interpreted to have formed from an upgrade of the original sulphur content in the magma by assimilation of sulphide-rich footwall (Sharman-Harris *et al*., 2005). On the farm Tweefontein Hill, the sulphides were interpreted to have accumulated in a structural downwarp associated with gravitational settling (Viljoen and Schurmann, 1998; Nex, 2005). High grade mineralisation can be hosted by serpentinised zones within the footwall, as well as within serpentinised calc-silicate xenoliths in the reef (Gain and Mostert, 1982; Armitage *et al*., 2002). The PGE grades (3PGE+Au) can be up to 15 g/t (Kinnaird and Nex, 2015), and have been recorded as high as 26 g/t (Hutchinson and Kinnaird, 2005), although are more commonly 2-4 g/t (Kinnaird *et al*., 2005). Nickel and copper concentrations commonly range between 0.15 to 0.35 % and 0.1 to 0.25 %, respectively (Kinnaird and Nex, 2015).

The variable footwall plays a controlling role in the PGM assemblage of the disseminated marginal style mineralisation along the strike of the Platreef (Table 3.1) (Holwell and McDonald, 2006; Nichol and Kinnaird, 2008). In the southern and northern sectors, where the footwall is unreactive quartzite and anhydrous gneiss, these floor rocks allow for limited fluid activity and the PGE mineralisation was controlled by sulphide liquids (Holwell and McDonald, 2006; Maier *et al*., 2008). In the central sector, highly reactive footwall rocks such as dolomite and shale of the Malmani Subgroup and Duitschland Formation were dehydrated during metamorphism or assimilation and the fluid released remobilised PGE and BMS forming low temperature PGE mineralisation (Hutchison and Kinnaird, 2005). High-grade zones may locally occur within the disseminated sulphides in exoskarn, hybrid and magmatic rocks (Holwell *et al*., 2006; Klemd *et al*., 2016). Generally, contact style mineralisation and massive sulphides in the basal Platreef are typically characterised by a significantly lower tenor, a higher BMS abundance, lower Pt/Pd <1 and a higher Cu/Pd ratio (Yudovskaya *et al*., 2017). The changing footwall lithologies along strike of the Platreef are suggested to have been a controlling factor over the mineralisation, in particular, the platinum-group mineralogy (Viljoen and Schurmann 1998; Holwell and McDonald, 2005; Holwell *et al*., 2006; Holwell *et al*., 2007). Viljoen and Schurmann (1998) provided a brief overview of the PGM hosted in the Platreef and in more recent studies more detailed work on platinum-group minerals (PGM) assemblages have been done (Armitage *et al*., 2002; Hutchinson and Kinnaird, 2005; Holwell *et al*., 2006; Yudovskaya *et al*., 2011; van der Merwe *et al*., 2012; McCutcheon, 2012; Klemd *et al*., 2016; Yudovskaya *et al*., 2017). The most common PGM throughout the Platreef are Pt and Pd phases, dominated by tellurides, bismuthides and sperrylite with locally common antimonides and sulphides (Holwell *et al*., 2006; Yudovskaya *et al*., 2011; McCutcheon, 2012). The PGM include moncheite, kotulskite, sobolevskite, michenerite and sperrylite (Holwell *et al*., 2006; Yudovskaya *et al*., 2011). Holwell *et al*. (2006) investigated PGM on Sandsloot which showed that Pt-Fe alloys were rare in normal pyroxenite reef, although they were more common where olivine replaced reef was found. Pt-Fe alloys were also found in chromitites by Yudovskaya *et al*. (2011).

Where the Platreef rests on granite or gneiss of the Archean basement, PGE sulphides (e.g. cooperite and braggite) have been found, showing the strongest association between PGE and BMS in the Platreef. In addition, bismuthides and tellurides were also present (McDonald and Holwell, 2011). Alternatively, where the Platreef intrudes volatile country rocks (sediments of the Transvaal Supergroup), PGM mineralogy is altered due to the effects of fluid activity and/or contamination (Yudovskaya *et al*., 2011; McCutcheon, 2012). Here, the PGM assemblage is dominated by arsenides, antimonides and stannides.

Table 3.1: Summary of the geology and mineralisation along the strike of the Platreef (Modified from Holwell, 2006; McDonald and Holwell, 2011).

Sector	Farms	Footwall	Platreef			Mineralisation		Reference
			Thickness	Lithologies	xenoliths	BMS	PGM	
Northern Sector	Drenthe	Archean granite	250 m	Feldspathic pyroxenite, norite, chilled pyroxenite at the base, serpentinite	Dolomite/ calc-silicates, granite	Disseminated blebs	Sulphide alloys	Mostert (1982), Gain and Mostert (1982), Naldrett (2005), Kinnaird *et al*. (2005), Kinnaird and Nex (2015)
	Witrivier	Archean granite	250 m	Feldspathic pyroxenite, norite, chilled pyroxenite at the base, serpentinite	calc-silicates, granite	Disseminated blebs	Sulphide alloys	Kinnaird and Nex (2015)
	Overysel	Archean granite	100 m	Feldspathic pyroxenite, norite, chromitite, serpentinite	Calc-silicates	Disseminated blebs, massive sulphides in footwall	Tellurides, sulphides, arsenides, bismuthides	Kinloch (1982), Cawthorn *et al*. (1985), White (1994), Holwell and McDonald (2005), Holwell and McDonald (2006), Kinnaird and Nex (2015).
	Zwartfontein	Archean granite (N), Dolomite (Malmani Subgroup) (S)	200 m	Feldspathic pyroxenite, peridotite, norite, serpentinite.	Calc-silicates	Disseminated blebs within serpentinised rocks	Tellurides, alloys, arsenides	Wagner (1929), van der Merwe (1978), Kinloch (1982), White (1994), Viljoen and Schurmann (1998), Friese (2004), Holwell and Jordaan (2006), Kinnaird and Nex (2015).
Central Sector	Vaalkop	Dolomitic skarn (Malmani Subgroup)	500 m	Feldspathic pyroxenite, harzburgite, chromitite.	Calc-silicates	Disseminated blebs	-	Yudovskaya and Kinnaird (2010),
	Sandsloot	Dolomite (Malmani Subgroup)	10-600 m	Feldspathic pyroxenite, pegmatites, clino-pyroxenite, peridotites, serpentinite	Calc-silicates, serpentinite	Disseminated blebs common in footwall	Tellurides, alloys, antimonides, arsenides	Wagner (1929), White (1994), Viljoen and Schurmann (1998), Harris and Chaumba (2001), Bye and Bell (2001), Armitage *et al*. (2002), Friese (2004), McDonald *et al*. (2005), Holwell *et al*. (2005), Holwell *et al*. (2006), Kinnaird and Nex (2015).
	Tweefontein (North)	Dolomite (Malmani Subgroup)	150 m	Feldspathic pyroxenite, pegmatites, chromitites, serpentinite	Calc-silicates, BIF	Disseminated blebs, massive sulphides	Sulphides	Wagner (1929), Buchanan *et al*. (1981), Buchanan and Rouse (1984), White (1994), Viljoen and Schurmann (1998), Nichol and Kinnaird (2008); Kinnaird and Nex (2015).
	Tweefontein (Hill)	BIF (Penge Fm), shales (Duitschland Fm)	220 m	Feldspathic pyroxenite, norite, micronorite at base	Hornfels	Disseminated blebs, massive and net-textured sulphides	Tellurides, arsenides	Wagner (1929), Viljoen and Schurmann (1998), Nex (2005), Nyama *et al*. (2005, 2006), McCutcheon (2012).
Southern Sector	Turfspruit	Shales, calcrete, quartzite (Duitschland Fm)	<400 m	Feldspathic pyroxenite, harzburgite, gabbronorite, norite, pegmatites, serpentinites.	Hornfels, calc-silicate	Disseminated blebs, massive and net-textured sulphides	Bismuthides, antimonides, tellurides, antimonides, sulphides	Buchannan and Rouse (1984), Hutchinson and Kinnaird (2005), Kinnaird *et al*. (2005), Sharman-Harris *et al*. (2005), Mothetha and Kinnaird (2005), Hutchinson and McDonald (2008); Kinnaird and Nex (2015), Yudovskaya *et al*. (2017)
	Macalacaskop	Shale (Duitschland Fm) (N), quartzite (Timeball Hill Fm.) (S)	300 m	Feldspathic pyroxenite, serpentinites.	Hornfels, calc-silicate	Disseminated blebs, massive sulphides	Bismuthides, antimonides, tellurides, antimonides	Kinnaird *et al*. (2005), Hutchinson *et al*. (2004), Sharman-Harris *et al*. (2005), Kinnaird and Nex (2015).
	Townlands	Quartzite and shale (Timeball Hill Fm.)	150 m	Feldspathic pyroxenite, gabbronorite, interbedded hornfels	Hornfels, calc-silicate	Disseminated blebs	-	White (1994), Maier (2002), Manyeruke *et al*. (2005), Kinnaird and Nex (2015).

At Overysel, no evidence for hydrothermal activity is present and the PGE telluride and base metal sulphide relationship is regarded as a 'primary' association (McDonald and Holwell, 2011)

The reef style mineralisation occurs in uncontaminated pristine layers of feldspathic pyroxenite and harzburgite rimmed by persistent chromite seams at the top and the base (Yudovskaya *et al*., 2017). BMS abundance (<5%), Pt/Pd ratios (>1), sulphide tenor (as high as 600 ppm PGE) and PGM assemblages closely resemble those of the Merensky reef mineralisation: chromitites host predominant Pt-Pd sulphides grading into Pt-Fe alloy, whereas sperrylite and Pt-Pd bismuthotellurides become more abundant downwards (Yudovskaya *et al*., 2017). The Platreef mineralisation can be divided into three groups; the Lower sills of the Platreef are generally enriched in Pd, 2:1 Pd/Pt, whereas the middle sills of the Platreef are generally 1:1 Pd/Pt (Kinnaird *et al*., 2005). The upper sills of the Platreef are enriched in Pt similar to the Merensky Reef and the UG2 elsewhere in the Bushveld Complex (Fig. 3.6) (Yudovskaya *et al*., 2017).

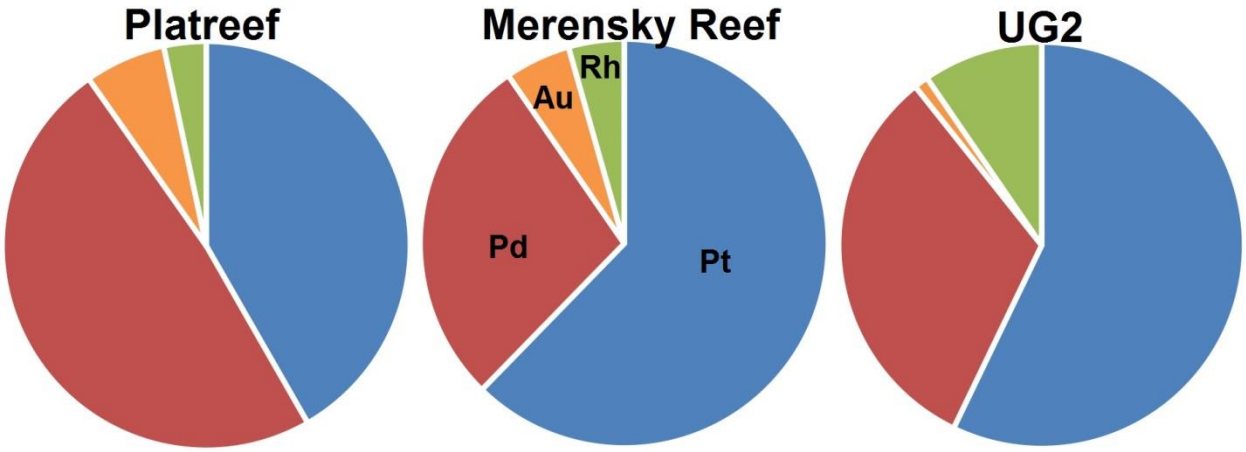

Figure 3.6: A comparison of the noble metal abundance of the Platreef, the Merensky Reef and UG2, showing the predominance of palladium in the Platreef of the northern limb. Data for the Merensky Reef and the UG2 from Barker (2012), and for the Platreef based on data for Sandsloot from the Anglo Platinum annual report (2011). Diagram modified from Kinnaird *et al*. (2017).

3.4.3. Mineralisation in the Main and Upper Zone

The Moorddrift farm is located south of Mokopane between the Ysterberg Planknek fault and the Zebediela fault (Fig. 3.6). Here, PGE mineralisation was discovered in the upper Main Zone hosted by mottled anorthosite, gabbronorite and gabbro and is associated with a pyroxenite layer (Maier and Barnes, 2010). The least disturbed sequence is a stratiform reef-style ~10 m thick package of mineralisation below the pyroxenite layer. Within the extensively disturbed zones in some localities PGE mineralisation may have been redistributed over 300 m (Holwell *et al*. 2013). The sulphide

mineralisation consists of pyrrhotite, pentlandite and chalcopyrite as well as secondary pyrite. The platinum-group assemblages are typical of magmatic ore deposits, with Pt and Pd tellurides and sperrylite within the ~10 m thick reef style package (Holwell *et al*. 2013), whereas, a decrease in tellurides and an increase in antimonides occurs in the hydrothermally and brecciated disturbed package (Holwell *et al*. 2013).

The Aurora Project is a group of seven farms located in the far northern end of the northern limb south of the Hout River Shear Zone (Fig. 3.1). PGE mineralisation is developed near the base of the Rustenburg Layered Suite in this area overlying Archean granite-gneiss basement, as well as higher up in the stratigraphy (Harmer *et al*., 2004; Manyeruke, 2007; Maier *et al*., 2008; McDonald *et al*., 2017). A JORC-complaint resource of 125 Mt of sulphide ore at 1.34 g/t Pt + Pd + Au, 0.08% Cu and 0.05% Ni (Venmyn-Rand, 2010) has been reported for this area south of the Hout River Shear Zone. Harmer *et al*. (2004) was the first to describe the mineralisation as hosted in anorthosite and leucogabbroic rocks, although later studies by Manyeruke (2007) and Maier *et al*. (2008) suggested that the mineralisation is contact-style PGE mineralisation and argued that the mineralisation represents a northern facies of the Platreef. McDonald and Harmer (2010) and McDonald *et al*. (2017) further argued on the basis of petrology, geochemical and PGE analyses that the mineralisation is hosted in lithologies associated with the Main Zone.

McDonald *et al*. (2017) subdivided the stratigraphy on the Aurora project into three major units. From the footwall upwards these units are divided based on lithologies and indicator minerals: at the base, Unit 1, consisting of peridotites and melagabbronorites; Unit 2 is composed of gabbronorites and leuco-gabbronorites with rare troctolites and magnetite gabbros; and Unit 3 contains gabbronorites with cumulus pigeonite (McDonald *et al*., 2017). PGE mineralisation is associated with finely disseminated sulphides close to the top contact of Unit 1, although the highest PGE grades are mainly associated with the gabbroic rocks in Unit 2 (McDonald *et al*., 2017). The most common PGM are Pd tellurides and electrum, with smaller amounts of Pt tellurides and Pt arsenides (Harmer and McDonald, 2010). Most of the PGM are associated with silicate minerals such as plagioclase and clinopyroxene. Where PGM are associated with sulphides, they are generally associated with chalcopyrite and pyrite (Harmer and McDonald, 2010).

3.5. Age of the Northern Limb

The age of the Bushveld Complex has been accepted by most authors as 2.06 Ga (Walraven *et al*., 1990) for all three limbs, although, in more recent years some authors have cast doubt on the assumption that the northern limb formed at the same time as the eastern and western limbs of the Bushveld Complex (e.g. McDonald *et al*., 2005). Hattingh (1995) proposed that the intrusion of the northern limb happened later than the rest of the complex. Based on palaeomagnetic data, he interpreted that in the main part of the complex, the remnant magnetisation of the Critical Zone was fixed before the Main and Upper Zone, followed by the magnetisation of the Main Zone in the northern limb and the youngest remnant magnetisation is observed in the Upper Zone of the northern limb (Hattingh, 1995). Ruiz *et al*. (2004) provided an age of 2011 ± 50 Ma from Re-Os isotope date for sulphides from the Platreef on the farm Turfspruit, which falls into the 2.06 Ga age due to the large error. Hutchinson *et al*. (2004) provided a much more accurate age of 2053.7 ± 3.2 Ma for zircons that were extracted from a granitic vein cross cutting the Platreef. In a more recent study, two zircons from chromitite in the upper Platreef on Vaalkop yielded new SHRIMP zircon ages at 2056.2 ± 4.4 Ma (Yudovskaya *et al*., 2013), which are within error of the ages recorded by Hutchinson *et al*. (2004) for the Platreef. These age dates for the Platreef are also within error of the age 2055.0 ± 3.9 Ma (Scoates and Friedman, 2008) obtained for the Merensky Reef. However, Yudovskaya *et al*. (2013) also reported ages for zircons obtained from the lower Platreef chromitite on Sandsloot which yielded ages of 2042.1 ± 4.2 Ma and 2038.3 ± 4.7 Ma.

3.6) Summary of the Northern limb:

The northern limb is located in the Limpopo Provinces of South Africa. The northern limb has a grossly similar stratigraphic sequence and orientation as the rest of the Bushveld Complex. However, north of the Ysterberg fault (Thabazimbi-Murchison Lineament) the Critical Zone is absent and instead the Platreef is present in the northern limb. The Platreef is believed to be equivalent to the Critical Zone of the eastern and western limb, due to its stratigraphic position between the Lower Zone and Main Zone. The northern limb is transgressive in nature due to the different footwall rocks, with Transvaal sediments and Archean granites in the far north of the northern limb. The northern limb is also currently the only limb of the Bushveld Complex where zones of continuous mineralisation have been found in the Main and Upper Zone stratigraphy.

Chapter 4

The Waterberg Platinum-Group Element Deposit: Atypical Mineralization in Mafic-Ultramafic Rocks of the Bushveld Complex, South Africa.

This chapter contains the full text of the paper " The Waterberg Platinum-Group Element Deposit: Atypical Mineralization in Mafic-Ultramafic Rocks of the Bushveld Complex, South Africa" by Kinnaird, J. A. Yudovskaya, M., McCreesh M. J. G., Huthmann, F. and Botha, T. J. is published by *Economic Geology*, v 112, p. 1367-1394. The PDF document as published can be found in Appendix A1.

This paper was written by Judith Kinnaird and represents a summary of several years of work conducted by the authors. As such, it contains work conducted, and ideas proposed by all the authors. It is suggested, that the first four authors are each responsible for 25% of the work, whilst the fifth author facilitated access to core and company information. This publication was submitted to an American Journal and the spelling differs from the previous chapters. The following list contains sections written or figures drafted by the author of this dissertation:

4.1. Candidate's contribution:

- The candidate performed aspects of the field work: core logging, magnetic susceptibility survey and collecting samples.
- Several paragraphs in this article were written by or taken almost without change from my MSc thesis. This includes for example paragraphs associated with the petrology section of this paper. In particular the section on emplacement models relied heavily on ideas developed by Marina Yudovskaya, Florian Huthmann and this author.
- Several figures, tables and plots were conceived and prepared by the candidate. This includes maps and the stratigraphic column as seen in Figures 3, 6, 7, 8, 9, 10, 11, 14, 16, 18, 20 and 23, data plots such as 15 and 22 and a schematic overview. It also includes all non-microscope photo plates.
- Figures 15 and 22 are based on geochemical analyses conducted by the candidate.
- Figure 10 is based on magnetic susceptibility measurements conducted by the candidate.
- All the polished thin sections were analysed and photomicrographs taken by Marina Yudovskaya and the candidate.
- The candidate was involved with the discussion during the preparation stages of the manuscript.

4.2. Abstract

The exposed northern limb of the Bushveld Complex forms the eastern part of a much larger basin, ~160 x -125 km in size based on geophysical data. Within this basin, the recently discovered ultramafic-mafic succession that extends 24 km northeast from the Hout River Shear Zone has been shown to have a Bushveld intrusion age of 2.06 Ga. The succession is typically 1 km thick, dips west at 34° to 38°, and comprises a basal Ultramafic sequence, a troctolite-gabbronorite-anorthosite sequence, and an Upper Zone. Overlying Waterberg red beds were deposited between ~2.05 and ~1.93 Ma. The basal Ultramafic sequence comprises a lower orthopyroxenite <60 m thick overlying Archean granite gneisses with an intervening agmatite, which is interpreted to be remobilised footwall gneiss interfingered with pyroxenite. The upper portion of the Ultramafic sequence is composed of serpentinised harzburgite. The troctolite-gabbronorite-anorthosite sequence is <850 m thick and is dominated by gabbronorites with minor anorthosites at the top and thick troctolite layers <50 m thick, which are locally pegmatoidal, toward the base. The boundary with the Upper Zone is defined by increased magnetic susceptibility due to increased cumulus magnetite. The Upper Zone of ferrogabbro and magnetite gabbronorite varies between 0 and 500 m in thickness. Disseminated magnetite is ubiquitous but magnetitite layers that are characteristic of the Upper Zone elsewhere in the Bushveld Complex are lacking, except in one drillcore from the extreme south of the project.

There are two PGE-Cu-Ni-Au mineralized intervals, a lower F zone and an upper T zone that vary from 3 to 60 m in thickness. The T zone is restricted to the southern portion of the project, whereas the F zone extends 17 km along strike. In both there is a correlation between visible chalcopyrite and pentlandite abundance and grade of PGE. The F zone of the Ultramafic sequence hosts disseminated sulfides with accessory chromite. Platinum group minerals (PGM), based on more than 1,000 grains recovered, are dominated by sperrylite with lesser Pt-Pd bismuthotellurides, Au-Ag alloys, Pd arsenides, and Pt-Rh sulfoarsenide with a grade of <7 g/t Pt + Pd + Au. The precious metal budget comprises 64% Pd, 30% Pt, 1% Rh, and 5% Au with 0.16% Ni and 0.07% Cu. Mineralization occurs over an interval of ~10 m although in the central portion of the north-easterly oriented body, the "Super F zone" thickens to 60 m, with grades of 3 g/t over this interval. The T zone occurs in a lithologically variable sequence close to the boundary between the troctolite-gabbronorite-anorthosite sequence and the Upper zone. In the south, the T zone is ~30 m thick but increases northward to >50 m thick. An upper T1 and lower T2 are separated by a barren middling that is sometimes absent. Grade in both T1 and T2 is indicated as 3.88 g/t Pt + Pd + Rh + Au, although locally with up to 14 g/t. PGM are less varied than in the F zone and are dominated by Pt-Pd bismuthotellurides. Both T1 and T2 zones have a consistent and unusually gold-enriched metal ratio

of ~49% Pd, ~29% Pt, 1% Rh, and 21% Au with 0.08% Ni and 0.16% Cu. Neither the T nor F mineralized zones has direct correlatives in other limbs of the Bushveld Complex.

Although there are comparisons with the Bushveld succession elsewhere, significant differences in thickness and type of lithologies, geochemistry, and mineralization of this arcuate intrusion of the Waterberg segment, compared to the eastern, western, and northern limbs of the Bushveld Complex, suggest that the Waterberg ultramafic-mafic body may represent a structurally controlled separate compartment north of the Hout River shear zone.

4.3. Introduction

The exposed northern limb of the Paleoproterozoic Bushveld Complex (Fig. 4.1) has a N-S-oriented sinuous outcrop that is up to 15 km in width with exposure extending 100 km from the Zebediela fault in the south, to the Hout River shear zone in the north (Fig. 4.1). The limb has been regarded as forming part of a much larger lobe of the Bushveld Complex, up to 160 × 125 km in size as suggested by aeromagnetic and gravity data (Kinnaird *et al*., 2005; Finn *et al*., 2015). Many previous workers believed that the limb terminated at the Hout River Shear zone (HRS zone, Fig. 4.1) and linked in an arcuate form with the Villa Nora fragment of the exposed Upper zone, which is truncated in the north by the Abbottspoort fault, part of the Zoutfontein-Palala shear zone (Grobler and Whitfield, 1970). However, papers in the 1980s (e.g., Vermaak and von Gruenewald, 1986) suggested that the northern limb of the Bushveld extended undercover, north of known outcrops, and the discovery in 2011 by Platinum Group Metals Ltd. of a buried mineralized ultramafic-mafic succession north of the Hout River shear zone in the Waterberg project has confirmed some of these earlier interpretations. The Waterberg PGM deposit was found by Platinum Group Metals Ltd. following a new generative geologic model and geophysics to target drilling through the Waterberg sedimentary succession. The succession shows a number of contrasts with Bushveld stratigraphy elsewhere, not least because economic grades of PGE mineralization occur in a gabbronorite-dominated sequence that could be correlated with Main zone rocks, or because a sedimentary succession directly overlies weathered mafic Bushveld rocks. In addition, geophysical studies by Finn *et al*. (2015) have confirmed that mafic Bushveld rocks continue under the Waterberg and Karoo sedimentary units as far north as the Palala shear zone and west to the Lebowa granite north of the Thabazimbi-Murchison lineament, confirming the suggestion by van der Merwe (1976), Kinnaird *et al*. (2005), and others of the extent of the northern limb. This would increase the total areal extent of the Bushveld Complex to >90,000 km². Our paper aims to summarize the current knowledge of this new platinum deposit, one of the most globally significant PGE discoveries of recent times. It is meant to be a general overview of the regional geology, and a series of papers will follow giving more specific details on mineralogy, geochemistry, isotopic characteristics, and mineralization.

4.4. Geology of the Northern Limb

The Archean basement consists of tonalitic gneiss intruded by heterogeneous potassic granites. The <12-km-thick Transvaal Supergroup sediments were deposited on the Archean basement between 2670 to 2100 Ma (Eriksson *et al*., 2001) and comprise a thin basal clastic unit (Black Reef Formation) followed by a sequence of dolomites, ironstones, and minor shales (Malmani Subgroup, Penge Formation, Duitschland Formation). These are overlain disconformably by the Pretoria Group (Timeball Hill Formation), which is dominantly a clastic succession with minor volcanics. North of the

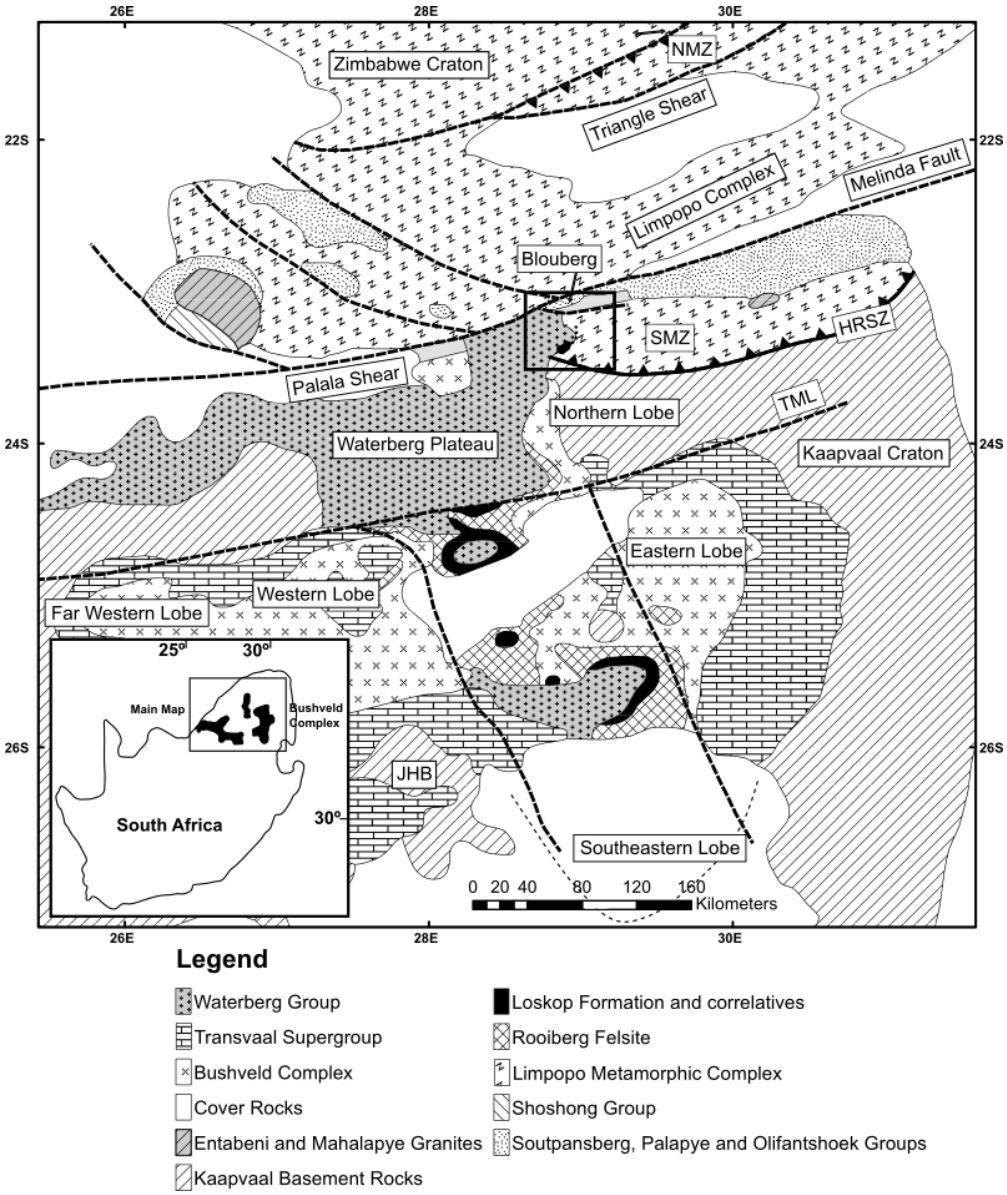

Figure 4.1: Map showing the distribution of major lithologic units in northern South Africa. Abbreviations: HRSZ =Hout River shear zone, JHB = Johannesburg, NMZ = Northern marginal zone, SMZ = Southern marginal zone, TML = Thabazimbi-Murchison lineament. The small box indicates the Waterberg area. After Dorland *et al*. (2006).

Planknek-Ysterberg fault (PYF, Fig. 4.2), one of the faults in the Thabazimbi-Murchison lineament array, the Bushveld Complex intruded Transvaal Supergroup metasediments and Archean basement (Fig. 4.2A). The Thabazimbi-Murchison lineament, which extends east-northeast–west-southwest for more than 500 km, has been active since 2960 Ma (Good and de Wit, 1997) to the present day. The sequence which strikes north-northwest has correlates with the eastern and western limbs, such that the Marginal, Lower, Main, and Upper zone units are widely recognized zones elsewhere in the Bushveld Complex (e.g., Kinnaird, 2005; McDonald *et al*., 2005). The Platreef, which occurs between the Lower and Main zones, is the stratigraphic equivalent of the Critical zone. South of the Planknek-

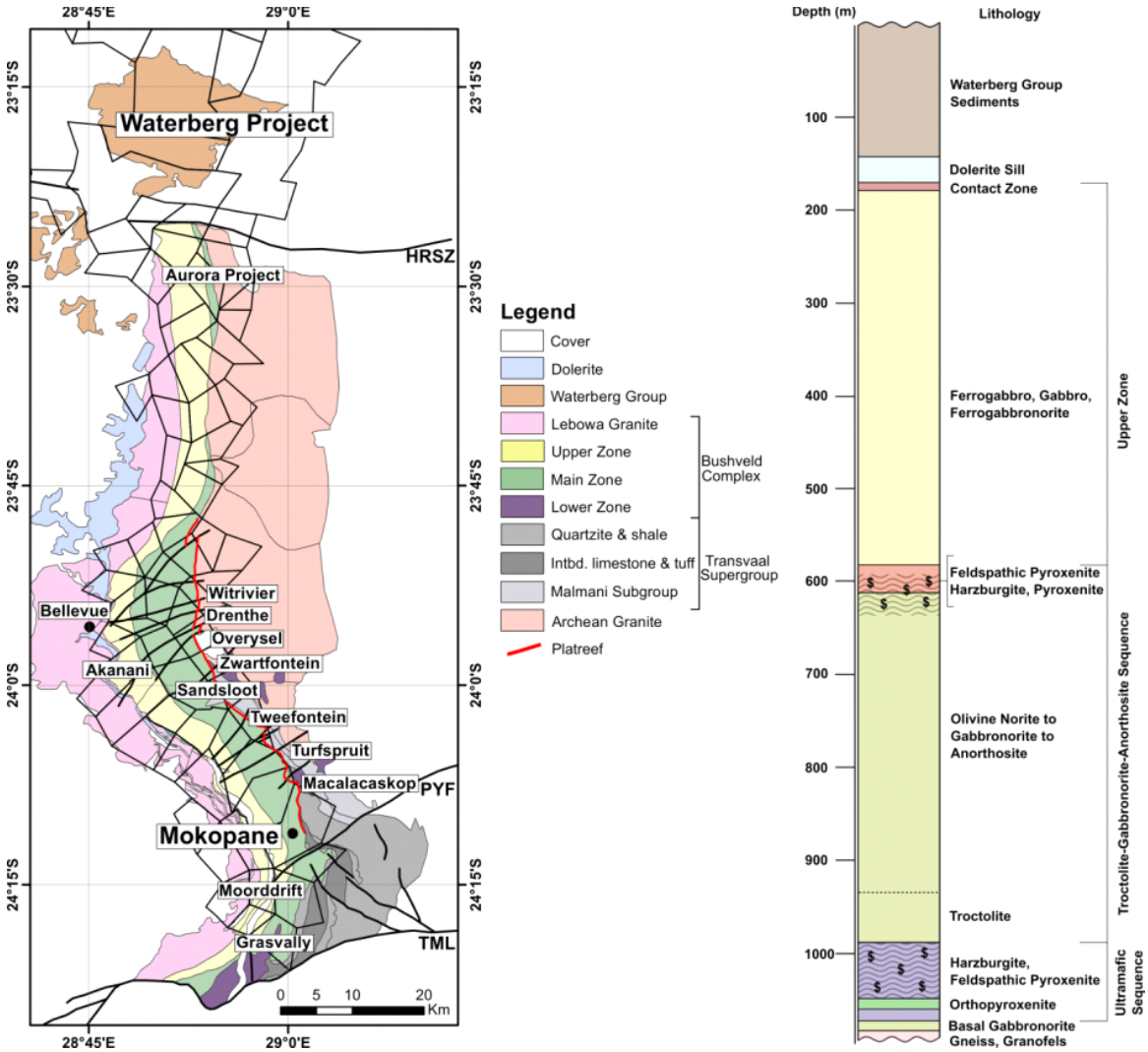

Figure 4.2: Geology of the northern limb of the Bushveld Complex (A) map, showing locations that are mentioned in the text. HRSZ = Hout River shear zone, PYF = Planknek-Ysterberg fault, TML = Thabazimbi-Murchison lineament (B) stratigraphy of the Waterberg project area.

Ysterberg fault, a series of ~400 m of intercalated gabbronorites, norites, pyroxenites and anorthosites (the GNPA member) equated with the upper Critical zone by Hulbert (1983), overlie the Lower zone ultramafic cumulates in Grasvally. The layered sequence strikes northeast and dips 15°

to 27° W and rests on quartzites of the Magaliesburg Formation, near the top of the Transvaal Supergroup. The Lower zone of the northern limb was believed to be limited to satellite bodies cutting Archean granite (van der Merwe, 1976) as shown in Figure 2A. However, a Lower zone sequence, up to 800 m thick, was confirmed by drilling beneath the Platreef on Sandsloot and Turfspruit (Fig. 4.2A; Yudovskaya *et al*., 2013a). The ultramafic sequence is composed of dunite-harzburgite-pyroxenite cycles with sporadic chromite seams and contains one of the most magnesian rich olivine compositions identified in the whole Bushveld Complex with a Mg number [Mg/(Mg + Fe)] up to 91 and a Ni content that varies from <0.4 wt. % NiO in Turfspruit to 0.66 wt. % NiO in Sandsloot. These Lower zone sequences are more similar to the Grasvally section of the northern limb (Hulbert and von Gruenewaldt, 1985) and the Clapham section of the eastern limb (Wilson, 2012) than to the earlier described sections of the western limb (Teigler and Eales, 1996).

The Platreef is a composite body of geochemically distinct mafic-ultramafic sills (Hutchinson and Kinnaird, 2005; Kinnaird, 2005; Manyeruke *et al*, 2005), dominantly of feldspathic pyroxenites that are variably mineralized in PGE, Ni, and Cu between the footwall and the Main zone (Van der Merwe 1978; Armitage *et al*., 2002; Kinnaird *et al*., 2005; Manyeruke *et al*., 2005; Kinnaird and McDonald, 2005; McDonald *et al*., 2005). The Platreef may be more than 500 m thick locally, in part due to the incorporation of thick interlayers of metasedimentary rocks. Where Lower zone rocks do not form the footwall to the Platreef, it overlies successively older Transvaal metasedimentary rocks northward. In the south the Platreef rests on shales, banded ironstones, calc-silicates, siltstones, and quartzite of the Chuniespoort Group, in the central sector the footwall is of Malmani dolomite, while to the north, the Platreef rests on a footwall of Archean granite-gneiss. Just above the top of the Platreef there is often a spotted anorthosite, overlain by a 300-m-thick succession of intercalated noritic rocks and pyroxenite layers that grade upward into the gabbronorites of the Main zone. Zircons from the upper Platreef give a concordant age of 2056.2 ± 4.4 Ma (MSWD = 0.05; Yudovskaya *et al*., 2013b), which is indistinguishable within error of a SHRIMP zircon age of 2053.7 ± 3.2 Ma for a granite dike crosscutting the Platreef (Hutchinson *et al*., 2004). New data from Turfspruit confirms that while the Platreef generally dips westward between 30° to 60° close to surface, the dip gradually lessens with depth downplunge into a more regularly layered sequence, termed the Flatreef, that looks more like the typical Critical zone (Grobler *et al*., 2012).

Mineralization is a combination of PGE and/or sulfide enrichment that varies within each of the individual sills and not all of the sills are well mineralized (Kinnaird, 2005; Manyeruke *et al*., 2005; Yudovskaya *et al*., 2011). Typically, mineralization is bottom-loaded in the south and top-loaded in the central and northern sectors, although this is an oversimplification (Kinnaird and Nex, 2015). The main PGE bearing reef with PGE grade and tenor identical to those of the Merensky reef

(Naldrett *et al*., 2008, 2012) is located close to the Main zone boundary in the same stratigraphic position as the Merensky reef. However, the thickness of the PGE reefs at Sandsloot and Turfspruit in the northern limb is much greater and may locally reach 90 m. Whereas there is a floor rock control on PGM mineralogy in contaminated parts of the Platreef, the mineralization in the upper sill carries predominantly Pt alloy and sulfides typical of the Merensky reef (Yudovskaya *et al*., 2017). Chromitite seams occur as discontinuous lenses at a constant stratigraphic level in the shallow Platreef (Yudovskaya and Kinnaird, 2010), but they become persistent and more numerous with depth. The Platreef is becoming a major world focus for platinum group element (PGE) production as current open pits are expanded and new underground operations are developed. Overviews of the recent work on the Platreef are given in Kinnaird (2005), Kinnaird *et al*. (2005), McDonald and Holwell (2011), and Kinnaird and Nex (2015).

The Main zone, which is <2,000 m thick in the northern limb, overlies the Platreef. It is dominated by gabbronorites, with lesser norites, especially toward the base, pyroxenites, and anorthosites. The distinctive >100-m-thick sequence of olivine-bearing norites and gabbronorites, 1,100 m from the base, which is unique to the northern limb, was mapped as a troctolite for about 35 km along strike by van der Merwe (1978).

The Upper zone is transgressive, resting on the Main zone in the south but on Archean footwall in the far north of the exposed northern limb (Fig. 4.2A). It is distinguished from the Main zone by the appearance of magnetite and apatite. In the Bellevue drill core (Fig. 4.2A), it is ~1,188 m thick and is dominated by magnetite-rich olivine gabbro and olivine ferrodiorite, with minor gabbronorite, plagioclase-magnetite cumulates, magnetitite, pyroxenite, and anorthosite (Ashwal *et al*., 2005). Magnetitite layers are characteristic with 32 discrete layers in the Bellevue core (Fig. 4.2A), ranging in thickness between 7 cm and 13 m (Ashwal *et al*., 2005). Commercial prospecting of these layers has identified at least 18 individual vanadiferous titanomagnetite layers elsewhere in the northern limb, ranging in thickness from a few centimeters to 10s of meters, with a number of zones with heavily disseminated (but not massive) magnetite (Longridge, 2015). PGE mineralization in the northern limb is not restricted to the Platreef. South of the Planknek-Ysterberg fault, mineralization at Moorddrift (Fig. 4.2A) has been noted close to a pyroxenitic layer in the Main zone (Maier and Barnes, 2010; Holwell *et al*., 2013). North of Overysel (Fig. 4.2A) the Main zone thins progressively until Upper zone cumulates rest directly on basement gneiss (Fig. 4.2A), then northward the Main zone reappears at surface directly in contact with Archean granite. Here mineralization occurs in two main horizons, each generally between 5 and 25 m thick, with a thinner discontinuous deeper horizon close to the basal contact with Archean granite gneiss (Manyeruke, 2007; Maier *et al*., 2008; McDonald *et al*., 2017).

The felsic rocks that overlie the Upper zone include the older Rooiberg felsites, which predate the mafic rocks, and the younger Lebowa Granite Suite.

4.5. Regional Geology of the Waterberg Project

The Hout River shear zone marks the boundary between the southern Marginal zone of the Limpopo belt and the stable Archean craton. It has been regarded as representing a composite structure along which the southern Marginal zone of the Limpopo belt was thrust southward during a Paleoproterozoic collision between the Zimbabwean and Kaapvaal cratons (Schaller *et al*., 1999; Barton *et al*., 2006; Smirnov *et al*., 2013; Rajesh *et al*., 2014), although there is still little consensus regarding aspects of the timing of the Limpopo orogeny (e.g., Treloar *et al*., 1992; Holzer *et al*., 1998; Barton *et al*., 2006). Long-lived tectonothermal activity over more than 700 Ma has been suggested (Good and de Wit, 1997; Kramers and Mouri, 2011). The southern Marginal zone is comprised of granulite facies granitic gneiss, amphibolitic gneiss, and minor quartzite. Within the southern Marginal zone there are several major shear zones that trend parallel to the Hout River shear zone (van Reenen *et al*., 1992) through the Waterberg project area (Fig. 4.1).

The term Waterberg relates to a geographic area so the term is used to describe a number of different geologic features of very different ages. In this paper, we use the term Waterberg project to refer to studies on the mineralized intrusion of Bushveld age north of the Hout River shear zone. The sedimentary term, the Waterberg Group, refers to a sedimentary succession which began deposition around ~2,050 Ma, while the Waterberg platinum veins of Bushveld age (e.g., McDonald *et al*, 1995) occur near Naboomspruit. The Karoo-aged Waterberg coalfield west of Lephalale is completely unrelated to any of the other geologic uses of the term.

The Waterberg platinum project is focused on a >3.5- × 24-km lobate intrusion north of the Hout River shear zone (Figs. 4.1, 4.2A). The Waterberg PGM deposit was found by Platinum Group Metals Ltd., following a new generative geologic model and geophysics to target drilling through Waterberg sediments. The intrusion consists of a layered package of troctolites, gabbros, gabbronorites, norites, and anorthosites with harzburgite, dunites, and orthopyroxenites toward the base (Fig 4.2B). U/Pb zircon age dating of the ultramafic-mafic succession gives intrusion ages of 2059 ± 3 and 2053 ± 5 Ma (Huthmann *et al*., 2016), indicating that the Waterberg intrusion is coeval with the intrusion of the Bushveld Complex (Walraven and Hattingh, 1993; Walraven, 1997; Buick *et al*., 2001; Scoates and Friedman, 2008; Zeh *et al*., 2015). The igneous rocks are covered by up to 750 m of sedimentary rocks of the Waterberg Group, a Paleoproterozoic red-bed succession of coarse siliciclastic rocks developed in a continental fault bound basin that covers large parts of the Archean Kaapvaal craton and the Limpopo belt (Callaghan *et al*., 1991; Barker *et al*., 2006).

The development of the Transvaal basin from ~2670 Ma (Eriksson and Reczko, 1995; Eriksson, *et al*., 2001) and the Waterberg basin from ~2050 Ma (Dorland *et al*., 2006) evolved from relatively small protobasins, to large basins with a massive sedimentary infill, to shrinking basins. The two major cycles were not necessarily separated by the intrusion of the Bushveld Complex, as Coertze *et al*. (1977) described sedimentation continuing throughout Bushveld magmatism on a local scale, especially in the Ootse basin in Botswana. The main Waterberg basin evolved as a continental fault-bounded basin, possibly extending far beyond its present fault-bounded margins (Barker *et al*., 2006). The total thickness of the Waterberg Group is variously estimated to be between 2,700 and 7000 m (Barker *et al*., 2006) although ~5 km is generally accepted (du Plessis, 1987; Callaghan *et al*., 1991; Dorland *et al*., 2006). A volcanic quartz porphyry in the oldest formation has yielded zircon SHRIMP ages of 2054 ± 4 and 2051 ± 2 Ma (Dorland *et al*., 2006), which are synchronous with Bushveld granite magmatism. Coertze *et al*. (1977) suggested that the quartz porphyry lavas were an extrusive equivalent of the Nebo granite of the Bushveld Complex.

The oldest formations of the Waterberg Group are confined to the central Bushveld Complex and deposition of sediments migrated northward over time, with the Setlaole Formation overlying the project area. This formation (Fig. 4.3) consists of medium- to coarse-grained granule-rich red-bed arenites with alteration (chloritisation/epidotisation); medium-grained, dark-brown, banded arkose; very fine grained chocolate-brown mudstone and purple shales with upward-fining channels, and a coarsening down sequence to a basal poorly sorted coarse grained pebble conglomerate composed of quartz pebbles 0.1 to 5 cm in size with minor amounts of detrital mica, hematite, apatite, and zircon. The amount of detrital hematite grains, 1 to 10 mm in size, is variable and may reach 50 to 70 vol %, forming discrete layers of hematite sandstone up to 1 m thick. It is notable that there are no Bushveld igneous lithologies in the lithic clasts. The Setlaole Formation, which reaches a maximum thickness of 450 m in the area, shows evidence of channel flows and cross-trough bedding in drill core and is interpreted to have formed as a proximal fluvial facies, deposited on a narrow braid-plain (Jansen, 1976, 1982; Callaghan *et al*., 1991). Zircons from the basal conglomerate of the Setlaole Formation gave a maximum age of deposition of ca. 2045 Ma (Huthmann *et al*., 2016). Abundant zircons of Archean age in the sample may indicate that the Limpopo belt to the north was the source for some of the sediments, which is consistent with the paleocurrent directions (Barker *et al*., 2006), while Paleoproterozoic zircons are interpreted to have been derived from the now-eroded roof rocks of the Waterberg intrusion.

The Makgabeng Formation overlies the Setlaole Formation. The Makgabeng Formation is composed of fine- to medium-grained pale-red banded sandstones that are generally horizontal. It is exposed in the mountain cliffs in the western part of the project area. There is evidence of a former

fluvial system at the base, although dunes occur higher up in the formation. Ripple marks, interference ripple marks, adhesion warts, and desiccation cracks indicate interdune and localized playa lake deposits (Eriksson *et al*., 2000). The hematitic coloration to the sands and gravels reflect an oxygenated atmosphere at this time.

A major dolerite sill, which is up to 200 m but typically ~80 m thick, occurs in most drill cores of the project area. It may be hosted within the Waterberg sediments, or within the Bushveld intrusion, but commonly occurs at the contact between the mafic igneous rocks and the Waterberg sedimentary succession. It has distinctive thick chilled margins on both contacts. The sill has been confirmed to belong to the Umkondo igneous province with a U/Pb baddeleyite age of 1125 ± 5 Ma (Huthmann *et al*., 2016). There is a cover of unconsolidated soils, weathered sediments, and younger Karoo sediments which are usually only a couple of meters thick.

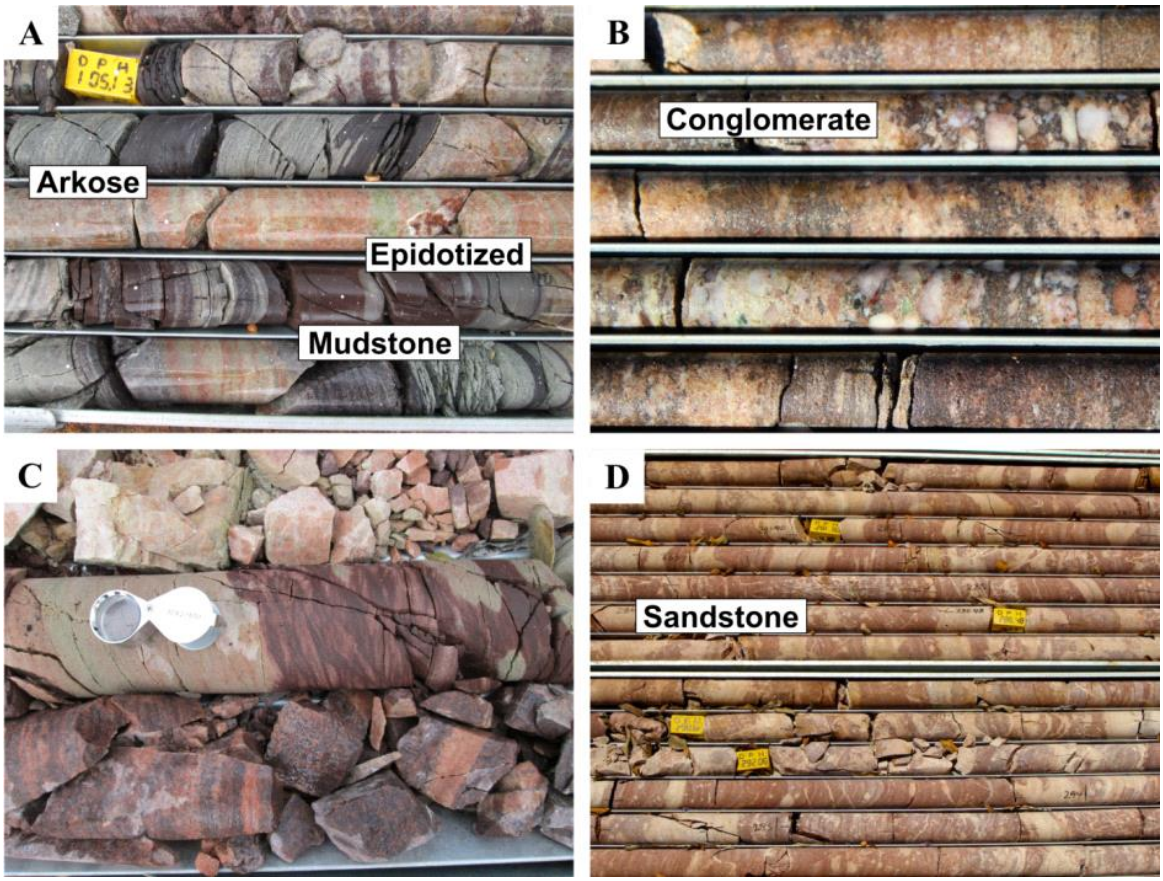

Figure 4.3: Selected photographs of cores showing different lithologies of the Waterberg sediments. (A). Medium- to coarse-grained red-bed sandstone interbedded with purple brown banded arkose and light-green epidotized zones and a very fine grained chocolate-brown mudstone (WB017). (B). Coarse-grained conglomerate containing quartz pebbles and various types of lithic fragments (WB047). (C). Cross trough-bedded and hummocky cross-stratification in variably coloured fine-grained sandstone (WB027). (D). Typical variably coloured sandstone of the Setlaole Formation of the Waterberg Group (WB096).

4.6. Methodology

The study is based on detailed logging and sampling during 2011 to 2016. Data in this paper are based on 15 boreholes as shown in Figure 4, although many additional boreholes were checked for

exact lithologic boundaries and potential mineralization. A Kappa-Meter KM-7 pocket meter was used to determine the magnetic susceptibility prior to documentation and sampling. An average of three readings was recorded at 1-m intervals. This method was found to be indispensable for determining the change from Main to Upper zone lithologies elsewhere in the northern limb (Ashwal *et al*., 2005) and has since been used on a regular basis by the exploration team. Quarter-core sampling (20–30 cm in length) was undertaken through the entire borehole core and representative samples selected for specific rock types. Samples were cut along the core axis and one-half was milled for geochemical analyses, and the other half was used for polished sections and mineral separation.

Samples were crushed, milled in a tungsten carbide mill, and analyzed at the School of Geosciences, University of the Witwatersrand. Whole-rock major elements, Co, Ni, Cu, and Cr were analyzed by X-ray fluorescence (XRF) using pressed pellets and matrix-matched standards. Trace element contents were determined by ICP-MS and a detailed description of analytical procedure can be found in Wilson (2012). A set of 28 representative samples was analyzed for major and trace elements at Cardiff University, UK. The analysis of 250 mg powder was carried out using a JY Horiba Ultima 2 inductively coupled plasma-optical emission spectrometer (ICPOES) and Thermo X7 series ICP-MS (McDonald and Viljoen, 2006). The accuracy of the analysis was assessed by analysis of the certified reference materials (CRM) JB1a, JP1, and BIR- 1. Platinum group elements, Au, and S in core samples from WB003 were analysed by Genalysis (Perth, Western Australia), using collection by means of the standard Ni-S fire assay method and determination by ICP-MS with an Elan Sciex 6100 system. International reference material AMIS0278 was analysed to ensure the accuracy of the PGE data. Detection limits for PGE were better than 1 ppb for all PGE and 2 ppb for Au. Sulfur was analysed by infrared spectrometry after melting in an induction furnace with a detection limit of 0.01 wt. % S. The PGE distribution in all other boreholes as shown in plots and columns is provided from the exploration assay database courtesy of Platinum Group Metals. Half core samples were analysed every half-meter in high-grade intervals and every meter in weakly mineralized intervals. Fire assay was used for Pt, Pd, Rh, and Au, and Cu, Ni, and S were determined by XRF analysis at Set Point Laboratory in Johannesburg. The compositions of olivine, orthopyroxene, and sulfides were analysed on a Jeol JXA 8200 microprobe at IGEM RAS (Moscow) with a measurement precision of 2 to 3% based on measurements of secondary standards. Petrography and mineralogy were studied in more than 150 polished thin sections and 12 heavy mineral concentrates. Platinum group minerals and zircon were separated in tribromomethane from a fraction <0.5 mm and laid out as rows on carbon tape. More than 1,000 PGM have been recovered. Chemical compositions of PGM and sulfides in the polished sections and grains in the separates were semiquantitatively identified with a

LINK EDS spectrometer attached to a FEI200 scanning electron microscope at the Microscopy and Microanalysis Unit of the University of the Witwatersrand. Images of minerals were obtained in a back scattered electron (BSE) mode with the same instrument.

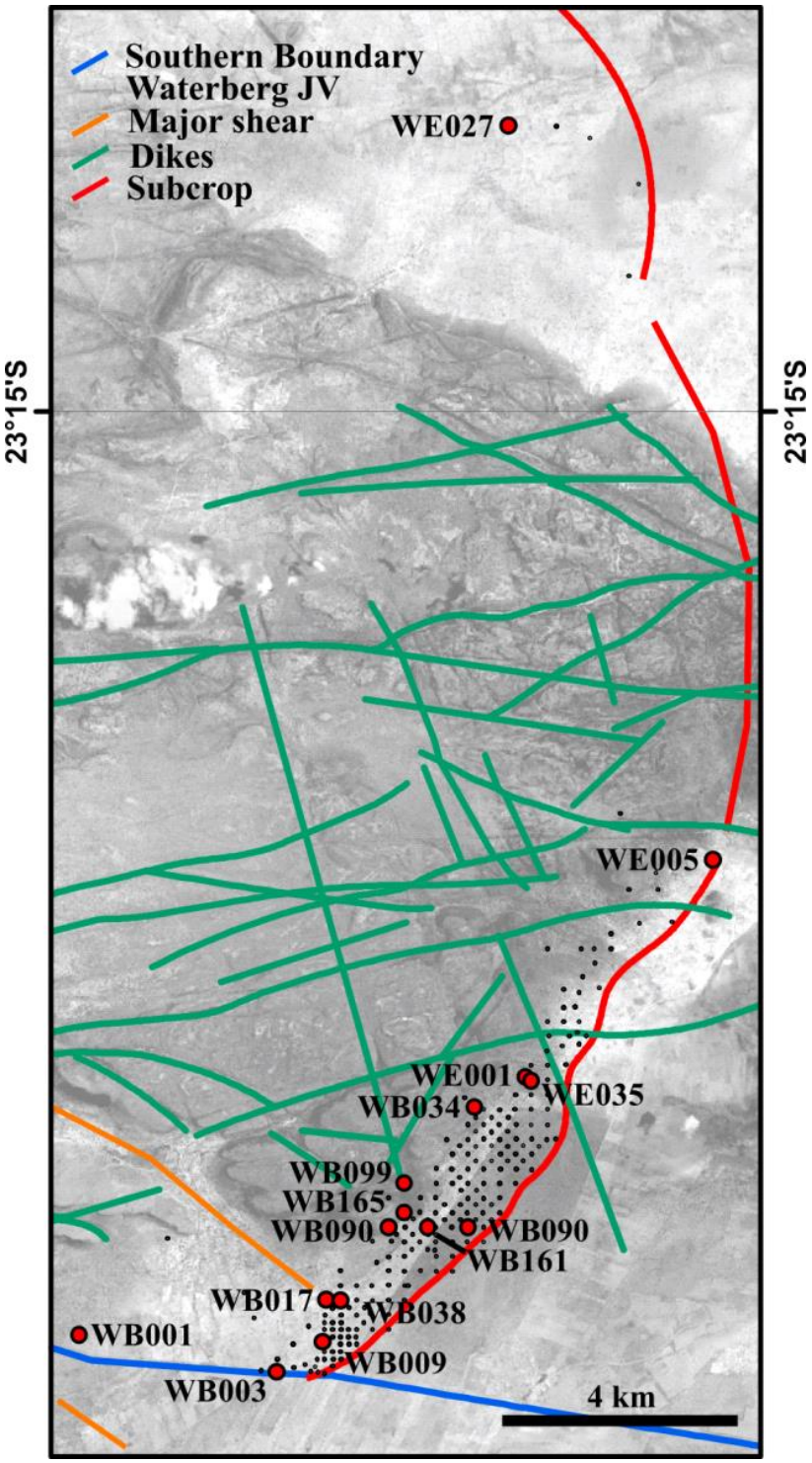

Figure 4.4: Schematic map showing the location of the boreholes discussed together with major shear zones and dikes within the project area.

4.7. Project Geology

The Waterberg platinum project lies 85 km north of Mokopane in the Limpopo province (Fig. 4.2A) centered at 23°22'01" south and 28°49'42" east. The magmatic succession comprises a basal Ultramafic sequence, comprising harzburgite and feldspathic pyroxenite, overlain by a troctolite-gabbronorite-anorthosite and in some areas by Upper zone ferrogabbro and magnetite gabbronorite with overlying Waterberg red beds (Fig. 4.2B). A general westward dip of 34° to 38° occurs although some blocks may be tilted at different angles depending on structural and/or tectonic controls. The top contact of the Bushveld Complex is complex and while often very sharp and mylonitised is commonly marked by a red siltstone (Fig. 4.5) or less commonly by a prominent fine-grained white-gray tuffaceous layer at the contact.

Figure 4.5: Contact between Bushveld gabbro and the overlying Waterberg sediments. (A), Coarse Waterberg conglomerate overlying altered and weathered Bushveld lithologies with remnants of a paleosol (WB004). (B). Sharp contact of altered light-greenish gabbro with relics of decomposed silicates and overlying foliated hematitised siltstone, which may represent the original volcanic roof rocks into which the Waterberg igneous rocks were intruded (WB038) (Yudovskaya *et al*., 2015).

The red aluminous- and hematite-rich siltstone is <10 m thick. It is strongly altered and sheared between the Upper zone and the overlying sediments (Yudovskaya *et al*., 2015). It comprises <70% hematite with a fine-grained matrix composed mostly of silica and phengite particles with subordinate chlorite and gibbsite. Silica is dispersed as colloform chalcedony, although it locally recrystallized into coarser aggregates of particles 5 to 100 µm in size. Phengite composition is mostly K dominant, although subordinate separate domains of Na-dominant mica (paragonite) occur in intergrowths (Yudovskaya *et al*., 2015). Hematite, with ilmenite exsolution lamellae, occurs as anhedral interstitial grains formed after magnetite, as coarse-grained margins to decomposed mineral and rock fragments and also as disseminations in the matrix. Numerous relics of mafic minerals, replaced by secondary assemblages, indicate that the lower part of the siltstone is a paleosol that developed on weathered Bushveld gabbros.

In some cores, the upper part is white-gray in colour, lacks the mafic silicate pseudomorphs, and instead contains multiple fractured quartz clasts <5 mm in size. This layer is richer in silica (<72 wt. % SiO_2) and potassium with respect to the underlying paleosol. The mineral composition of the matrix is similar to that of hematitised paleosol, but hematite and ilmenite are not so abundant whereas accessory fluorite, apatite, monazite, dumortierite, Al-Si chlorides, and fluorides are common (Yudovskaya *et al*., 2015). The fractured quartz porphyroclasts, K-dominant mica compositions, occurrence of coarse zircon intergrown with quartz, and low Ti content are not consistent with a gabbroic paleosol origin. We interpret this discontinuous layer between weathered Bushveld and overlying Waterberg conglomerate as of pyroclastic or tuffaceous origin that is likely to represent the original roof rocks into which the Waterberg igneous rocks were intruded.

The footwall to the intrusive sequence is an Archean granite or granite gneiss. Commonly however, a banded agmatite formed from the interaction between Bushveld magma and the footwall has developed between the intrusive sequence and the floor rocks (Fig. 4.6). Often the agmatite shows well defined banding of alternating felsic- and pyroxenite-rich layers. Rare chalcopyrite and pyrrhotite occur within both granite gneiss and agmatite. In a few boreholes there are xenoliths of calc-silicate in the pyroxenite at the base of the intrusive package, suggesting that at least locally a dolomite formed the footwall.

For the nomenclature of igneous rocks in subsequent sections, we follow the convention of Bushveld geologists and distinguish between cumulus and intercumulus minerals, thus for example, when plagioclase and orthopyroxene are cumulus, we use the term norite, whereas when orthopyroxene is cumulus and the plagioclase is intercumulus, the rock is classified as feldspathic pyroxenite.

The basal Ultramafic sequence, which is <100 m thick, trends northeast from the Hout River shear zone and dips moderately to the northwest. There are two components, a lower feldspathic orthopyroxenite (FP) unit that is <60 m thick, and an overlying harzburgite (FH) unit (Fig. 4.2B). The pyroxenites, which are interpreted as the initial magma to intrude the area, are interfingered with what are interpreted as Marginal zone fine-grained equigranular gabbronorite sills such that in some cores, gabbronorite forms the basal lithology (Fig. 4.2B). The pyroxenites are generally medium grained, dominated by up to 90% cumulus orthopyroxene with a high Mg number of up to 84, 10 to 15% clinopyroxene, and 2 to 5% chalcopyrite, pentlandite, and pyrrhotite in the upper part, but with up to 15% where semi-massive sulfides occur. Rare chromitite stringers have been identified in a few cores.

The harzburgite sequence in the Ultramafic sequence is 80 to 100 m thick and locally pegmatoidal toward the base, with lesser olivine-bearing gabbronorite, olivine-bearing norite,

pyroxenite, feldspathic pyroxenite, and serpentinized units that have been extensively chloritized and serpentinized (Fig. 4.7). It is possible that some of these units such as the olivine-bearing gabbronorite or feldspathic pyroxenite may be younger intrusive sills. The harzburgites have <65% olivine with orthopyroxene and lesser interstitial plagioclase and clinopyroxene. There is generally a high degree of alteration (Fig. 4.7B) with fractures in olivine filled with secondary magnetite and serpentine. Clinopyroxene occurs as small intercumulus grains, whereas orthopyroxene forms large oikocrysts and in some samples rims of orthopyroxene partially or completely surround olivine crystals.

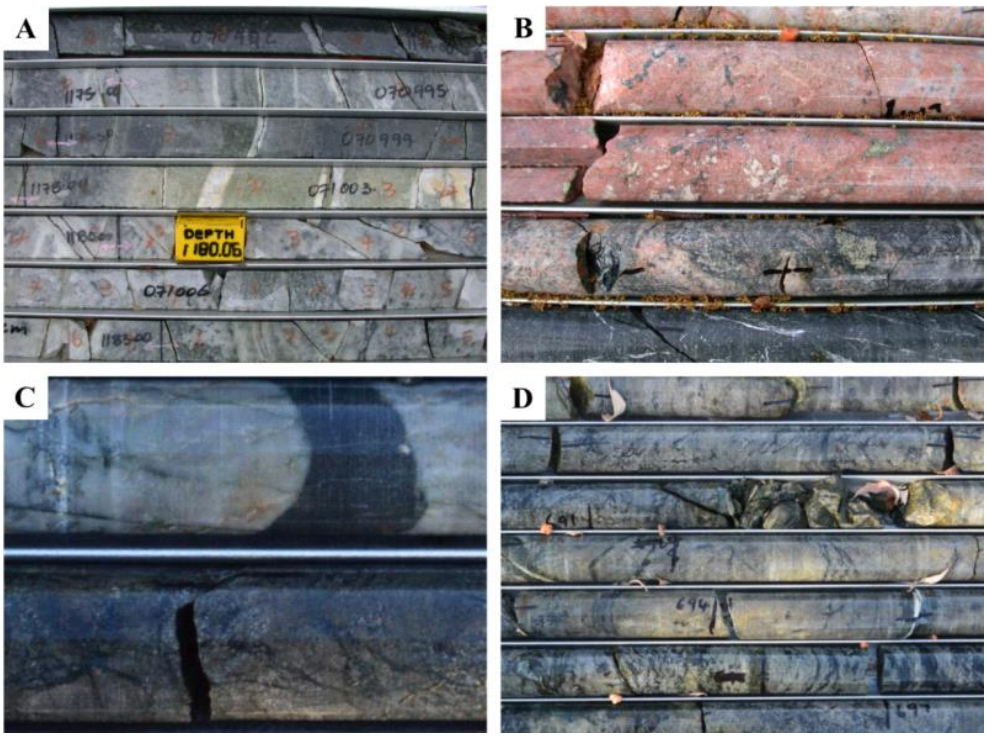

Figure 4.6: Selected photos of footwall rocks. (A). Banded agmatite formed from the interaction between Bushveld magma and the footwall granite gneiss (WB017). (B). Granite gneiss with rare chalcopyrite and pyrrhotite (WE005D0). (C). Agmatite with well-defined banding of felsic- and pyroxenite-rich layers (WE035). (D). Highly altered agmatite (WE035). From McCreesh 2016.

Medium-grained feldspathic pyroxenites have <30% interstitial plagioclase and <45% cumulus orthopyroxene 5 mm in size, although some samples contain up to 50% clinopyroxene that varies from 1 to 5 mm in size. Chalcopyrite, pentlandite, and pyrrhotite (2–5%) within the unit are associated with PGE mineralization (Fig. 4.7C). The troctolite-gabbronorite-anorthosite sequence (TGA, Fig. 4.2B) is a lithologically varied unit that reaches a maximum of 850 m in thickness. The troctolite unit at the base of the troctolite-gabbronorite-anorthosite sequence ranges in thickness from 40 to 100 m and varies in composition from melatroctolite and rare dunite to olivine norite and leucotroctolite, all with a medium- to coarse-grained equigranular texture intercalated with lenses of pyroxenite ranging up to a meter in size (Fig. 4.8). Most of the sequence comprises 50 to 80% olivine.

In thin section, altered olivines are usually subrounded and range from 3 to 7 mm in size. Sericitised plagioclase, 2 to 5 mm in size, forms <40%, while orthopyroxene (up to 10%) is either intercumulus surrounding or rimming olivine or forming occasional centimetre-sized oikocrysts. Both olivine and pyroxene may host chromite crystals up to 50 µm in size. The upper portion of the troctolite is heterogeneous and grades upward into olivine-bearing gabbroic rocks. The gabbronorites are medium- to coarse-grained (melanocratic, leucocratic, and altered) with varying proportions of orthopyroxene, subordinate clinopyroxene, inverted pigeonite, and <50% plagioclase of labradorite-bytownite composition. Grain size varies from 0.5 to 5 mm with minor pegmatoidal patches. Orthopyroxenes are generally subhedral and range from 0.5 to 4 mm and may form <50% of the mineralogy locally becoming a norite or olivine-bearing norite. Selected chemical analyses of the gabbronorites are shown in Table 1.

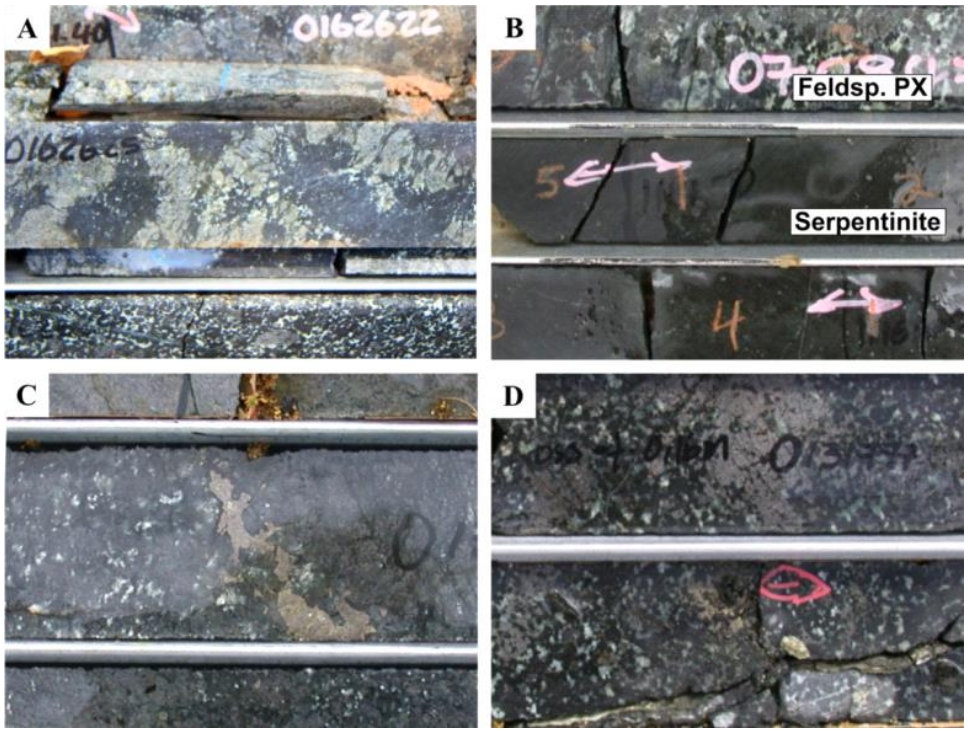

Figure 4.7: Selected images showing the variation in the ultramafic lithologies. (A). Strongly serpentinized harzburgite from WB132. (B). Feldspathic pyroxenite (Feldsp. PX) at the top and a unit that has been completely serpentinized below (WB027). (C). Feldspathic pyroxenite with blebs of pyrrhotite and chalcopyrite and veinlets of serpentine (WE035). (D). Harzburgite/feldspathic harzburgite with large oikocrysts of orthopyroxene (WB017). From McCreesh (2016).

Toward the top of the troctolite-gabbronorite-anorthosite sequence in the southern part of the project area, a mineralized zone (the T zone) occurs within a variable package of pyroxenite, feldspathic pyroxenites, troctolite/harzburgite, norite to anorthosite that is locally pegmatoidal. In the north of the project area the zone is either poorly developed or missing. The anorthosite is generally medium-grained sometimes becoming pegmatitic. It is often a light greenish-gray to milky-

white colour due to alteration of the plagioclase, with <10% oikocrysts of orthopyroxene forming a mottled and spotted texture locally.

The Upper zone is dominated by magnetite gabbro and gabbronorite (Fig. 4.9) with ferrogabbro at the top in some borehole cores. In the southwest close to the Hout River shear zone the unit may be as thick as 350 m, but northward it thins and is completely absent in the north-central project area, but it reappears in the far north where it can be 70 to 500 m thick. In core, the gabbro shows an inequigranular texture with large plagioclases, ranging from 2 to 5 mm in size, within a finer grained groundmass of orthopyroxene, clinopyroxene, and magnetite (0.5–5 mm) that may comprise up to 20% of the groundmass. However, magnetite is also intergrown with pyroxene crystals. The olivine-bearing gabbronorite has a similar composition to the magnetite-bearing gabbronorite apart from the presence of added olivine, although the former tends to have higher degrees of alteration. The uppermost portions of the Upper zone are characterized by brick-red alteration and a highly sheared contact zone. Geochemical analyses of typical magnetite-bearing gabbronorite and ferrogabbro are shown in Table 1.

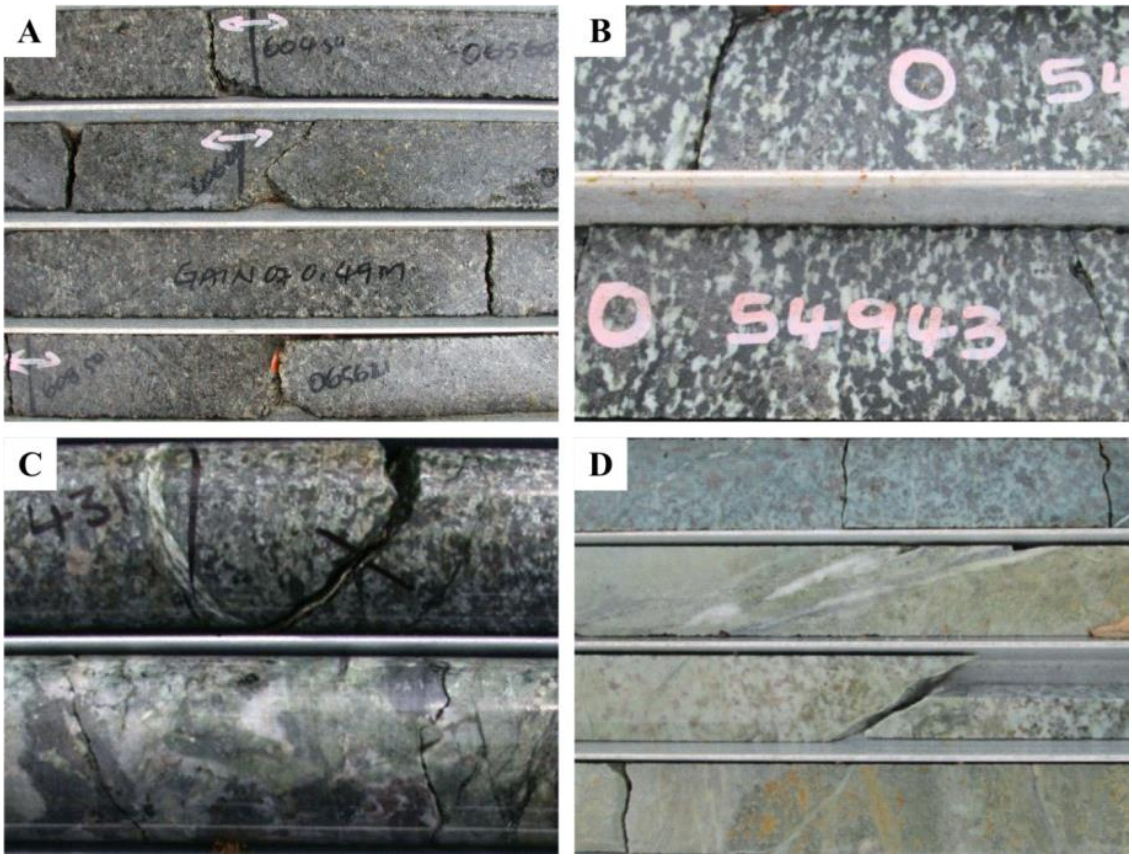

Figure 4.8: Lithologic variation in the troctolite-norite-anorthosite sequence. (A). Gabbronorite (WB0170). (B). Troctolite (WB163). (C). Pegmatoidal unit (WE001). (D). Anorthosite (WB017). From McCreesh (2016).

Where the Upper zone is missing, either the troctolite-gabbronorite-anorthosite sequence troctolite or pyroxenite of the Ultramafic sequence is in contact with the overlying Waterberg Group. Where this occurs, the troctolite-gabbronorite-anorthosite sequence rocks at the contact

show similar alteration to that of the Upper zone rocks elsewhere. The Upper zone is overlain by the relatively flat-lying Waterberg sedimentary package that varies from 120 to 760 m thick, with dip angles ranging from to 2° to 5°.

4.7.1. Magnetic susceptibility variations

Magnetic susceptibility profiles based on more than 15,000 measurements through six cores were created in order to distinguish between the different stratigraphic units. In the Ultramafic sequence, magnetic susceptibility measurements (Fig. 4.10) highlight pyrrhotite in feldspathic pyroxenite and secondary magnetite formed from the serpentinisation of olivine. The magnetic susceptibility values range from 1.00 to 10.00 SI units with a maximum of >40.00 SI units associated with harzburgite intervals. Through the troctolite-gabbronorite-anorthosite sequence, magnetic susceptibility values decrease upward from olivine-bearing to olivine-free lithologies, such that the majority of the troctolite-gabbronorite-anorthosite sequence has susceptibility values that are very low. These low values continue into the lower part of the T zone where susceptibility values range from 0.01 to 3.00 SI units. Upward in the T1 zone, values are from 0.01 to 5.00 with maximum values of <12.00 SI units associated with olivine-rich intervals. Upward in the succession the magnetic susceptibility becomes consistently higher, reflecting the incoming of magnetite as a primary mineral crystallizing from an Upper zone magma influx. The position of the sustained increase in magnetic susceptibility value is where the boundary is now drawn between the troctolite-gabbronorite-anorthosite sequence and the Upper zone. Distinct chemical changes support this rationale, even though there may be no notable lithologic change.

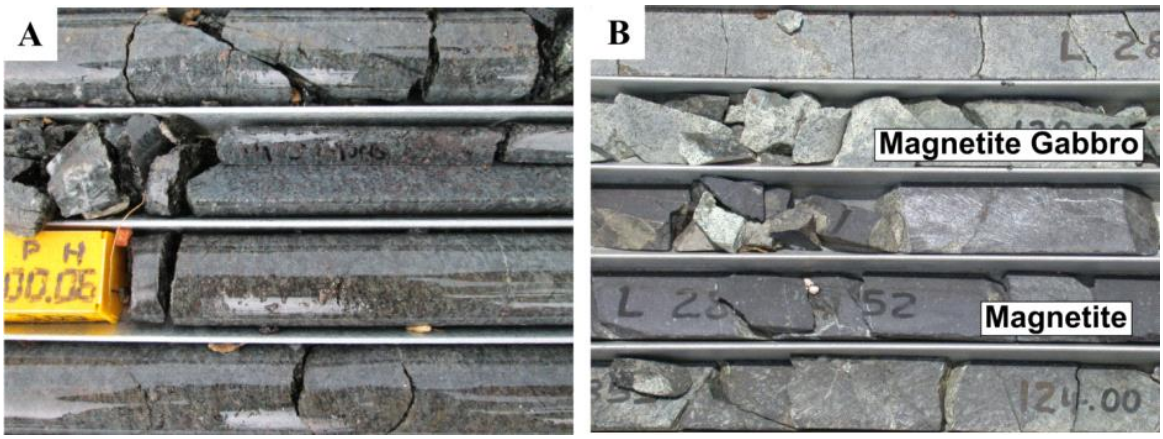

Figure 4.9: Upper zone lithologies from different cores. (A). Weakly altered ferrogabbro with pinkish altered olivine (WB017). (B). A 2-m-thick magnetite layer (in core tray slots 3 and 4 from the top) only seen in borehole WB001. From McCreesh (2016).

Although the Ti and V content of magnetite varies through the Upper zone, there is little or no change in the magnetic susceptibility values (Klemm *et al*., 1985; Cawthorn and Molyneux, 1986; Clark and Emerson, 1991; Clark, 1997; Ashwal *et al*., 2005). According to Clark and Emerson (1991) titanomagnetite ranges from 1 to 50 SI units, depending on the size of the titanomagnetite crystal.

Table 4.1: Geochemical Analytical Data for Selected Samples from Waterberg.

Units	FW	FP	FP	FP	FP	FH	FH	FH	FH	MZ	MZ	MZ	MZ	UZ	UZ	UZ	UZ
Rock Type	**GG**	**FPYX**	**FPYX**	**FPYX**	**FPYX**	**HZ**	**TOC**	**TOC**	**TOC**	**GN**	**GN**	**GN**	**GN**	**MGN**	**MGN**	**FG**	**FG**
(wt. %)																	
SiO_2	64.24	51.65	49.97	48.67	54.86	44.10	45.70	48.48	46.79	50.61	51.37	51.04	49.90	51.88	48.64	52.48	52.37
Al_2O_3	21.70	5.18	13.46	4.61	4.26	10.27	15.75	24.66	14.68	17.02	24.58	21.91	21.54	12.94	14.47	18.12	7.54
Fe_2O_3	0.08	1.69	1.60	0.91	1.16	1.53	1.11	0.42	0.99	1.10	0.46	0.65	0.50	1.31	1.59	1.03	1.64
FeO	0.63	13.65	12.96	7.37	9.42	12.35	8.99	3.38	8.02	8.94	3.72	5.31	4.02	10.57	12.87	8.37	13.25
MnO	0.01	0.24	0.18	0.14	0.20	0.18	0.14	0.07	0.16	0.18	0.07	0.11	0.10	0.22	0.21	0.12	0.28
MgO	0.28	22.50	14.07	35.51	25.33	22.63	17.86	6.78	17.41	8.85	5.32	7.35	5.45	12.45	12.83	6.94	15.27
CaO	6.09	3.75	6.09	2.60	4.59	6.70	9.25	13.64	10.73	10.81	10.78	11.33	15.86	8.73	6.86	10.25	8.20
Na_2O	6.06	0.42	1.10	0.22	0.37	0.34	1.00	2.03	0.94	1.92	2.89	2.07	2.23	1.55	1.62	2.24	0.88
K_2O	0.38	0.05	0.11	0.04	0.06	0.24	0.15	0.31	0.23	0.14	0.54	0.16	0.13	0.13	0.17	0.26	0.22
TiO_2	0.07	0.15	0.15	0.11	0.13	0.08	0.10	0.08	0.10	0.37	0.09	0.13	0.15	0.23	0.22	0.29	0.36
P_2O_5	0.04	0.02	0.01	0.02	0.02	0.02	0.02	0.02	0.01	0.02	0.02	0.02	0.01	0.02	0.02	0.02	0.02
Cr_2O_3	0.00	0.31	0.22	0.39	0.31	0.04	0.12	0.09	0.18	0.06	0.04	0.02	0.04	0.05	0.01	0.04	0.07
NiO	0.00	0.36	0.12	0.25	0.12	0.45	0.10	0.02	0.10	0.02	0.01	0.02	0.01	0.03	0.06	0.02	0.04
(ppm)																	
Sc	2.28	38.01	37.33	15.73	27.93	14.68	20.55	18.02	25.41	34.88	18.08	20.39	41.07	38.10	23.43	33.93	53.69
V	8.82	208.55	333.70	62.96	102.64	53.60	44.80	48.53	79.27	170.87	41.87	76.56	127.05	151.98	86.01	173.77	241.08
Cr	19.41	2118.90	1431.24	2388.51	2001.94	219.42	627.74	757.96	1052.97	383.81	252.24	97.40	202.95	275.18	56.75	190.73	383.94
Co	0.55	175.26	67.98	99.20	80.76	135.63	29.59	97.47	88.48	57.03	25.69	41.53	28.88	69.24	107.55	59.85	92.87
Ni	6.89	2819.35	881.34	1899.45	936.99	2840.78	157.20	793.96	776.19	170.97	96.30	140.62	113.64	194.64	464.59	150.58	260.11
Cu	9.42	1282.28	208.00	58.18	63.95	1242.38	28.70	37.03	50.26	58.42	51.92	71.09	40.94	63.78	60.53	81.80	71.50
Zn	10.35	88.87	103.92	59.81	96.64	82.76	23.40	62.83	56.56	61.39	29.14	38.89	27.62	77.46	89.16	46.40	99.29
Ga	21.82	5.44	12.28	3.79	5.13	7.16	13.36	9.17	9.79	12.18	15.86	16.49	14.34	11.63	11.88	16.07	9.22
Rb	8.60	5.39	7.24	3.62	4.63	10.59	9.91	5.95	7.43	5.00	13.96	4.56	2.34	4.07	6.55	4.94	8.41
Sr	1692.94	36.94	189.36	32.46	29.49	67.46	556.18	132.49	141.82	186.21	306.05	222.37	278.55	156.51	174.67	194.84	74.99
Y	2.29	3.34	2.02	0.78	2.38	1.78	0.88	1.34	3.16	6.29	2.09	4.96	6.68	7.16	3.73	6.79	11.42
Zr	81.79	6.83	5.44	7.40	4.37	2.88	6.54	5.19	4.91	14.61	16.28	10.77	8.58	11.86	15.57	13.84	23.93
Nb	1.69	2.01	0.79	1.08	0.65	0.45	1.15	1.46	0.61	3.01	1.59	1.71	1.37	3.47	3.74	2.36	3.45
Mo	0.51	0.86	0.79	0.39	d.l.	0.04	0.20	1.13	0.85	0.13	0.21	0.00	0.03	0.20	0.90	0.37	1.31
Ba	292.24	21.07	60.76	24.44	17.19	42.66	112.54	37.65	45.61	66.32	186.59	58.09	40.42	78.14	78.34	100.20	80.62
Pb	10.26	8.29	6.23	6.30	5.82	6.47	2.52	0.97	4.44	4.01	4.31	5.53	3.93	3.52	4.52	3.22	2.51

Abbreviations: FG = ferro-gabbro, FH = F-zone harzburgite, FP = F-zone pyroxenite, FPYZ = feldspathic pyroxenite, FW = footwall, GG = granite/granofels, GN = gabbronorite, HZ = harzburgite, MGN = magnetite-bearing gabbronorite, MZ = Main Zone, TROC = troctolite, UZ = Upper Zone.

This magnetic susceptibility technique is now used as a routine method by PTM as it provides a reliable technique that can be applied readily and cheaply to identify a boundary that can be correlated across all the borehole cores.

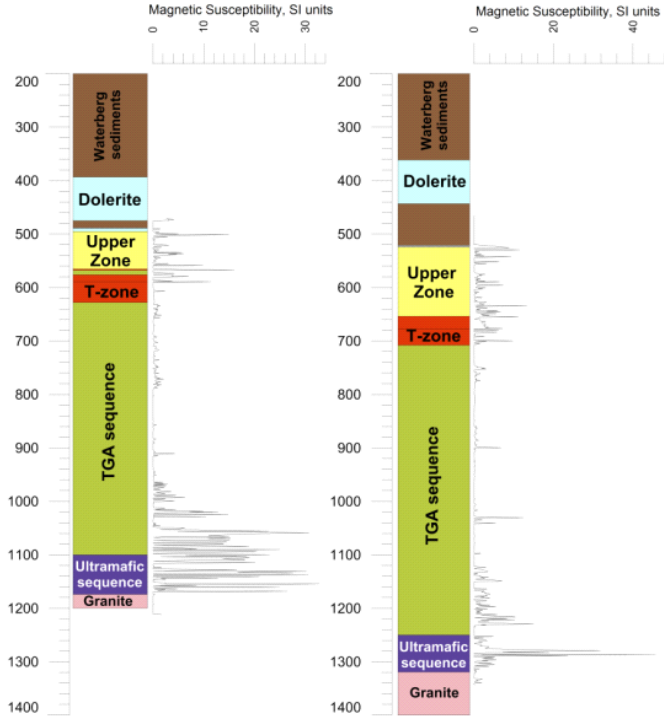

Figure 4.10: The magnetic susceptibility values (SI units) plotted against the depth for WB027 (left) and WB099 (right). The high magnetic susceptibility in the Ultramafic sequence is due to secondary magnetite formed from the serpentinisation of olivine. Olivine persists upward at the base of the troctolite-gabbronorite-anorthosite sequence. The increase in magnetic susceptibility values in the T zone is where the boundary is drawn between the troctolite-gabbronorite-anorthosite sequence and the Upper zone, even though there may be no notable lithologic change. From McCreesh (2016).

4.7.2. Mineralization

There are two mineralized intervals, a lower F zone and an upper T zone (Fig. 4.11). These mineralized zones are 3.0 to 60 m thick. The T zone outlined so far is restricted to the southern portion of the project area, whereas the F zone has been intersected along a strike length of 17 km. From the Hout River shear zone the succession thickens northward with greater separation between the two mineralized zones. There is a correlation between visible chalcopyrite and pentlandite abundance and the grade of PGE in both the T and F zones.

F zone: The F mineralized zone occurs in the Ultramafic sequence pyroxenite and harzburgite. In the southern portion, the F zone is typically <10 m thick but in the central portion, the “Super F zone” thickens to 60 m in true thickness, with grades of 2 to 4 g/t 2PGE + Au over this interval. The basal pyroxenite has variable grade: when the PGE grade is good in the pyroxenite then grade is also high in the harzburgite unit above. The mineralization generally comprises blebs, net textured to disseminated pyrrhotite, chalcopyrite and pentlandite with accessory chromite,

chalcocite, and pyrite (Fig. 4.12). Chromite crystals are often enclosed in silicates, while chromite itself may host sulfide inclusions (Fig. 4.12D) and rare chromitite stringers have been identified in two boreholes. Magnetite has often replaced sulfides and chromite. More than 600 PGM grains have been recovered for study. PGM (Fig. 4.13) are variable with dominant sperrylite and subordinate Pt-Pd bismuthotellurides, Au-Ag alloys, Pd arsenides, and Pt-Rh sulfarsenides. More textural details will be described in a subsequent paper. Variations in Cr, Ni, Cu, and PGE in one of the borehole cores are shown in Figure 14. The overall grade is given in Table 2. There is an anticorrelation between the Cr and PGE grade, with the highest PGE values coincident with the lowest Cr values. The changes in MgO%, Mg number, and Cr/MgO across the interface of the F zone and the troctolite-gabbronorite-anorthosite sequence are shown in Figure 15. Selected chemical analyses are shown in Table 4.1.

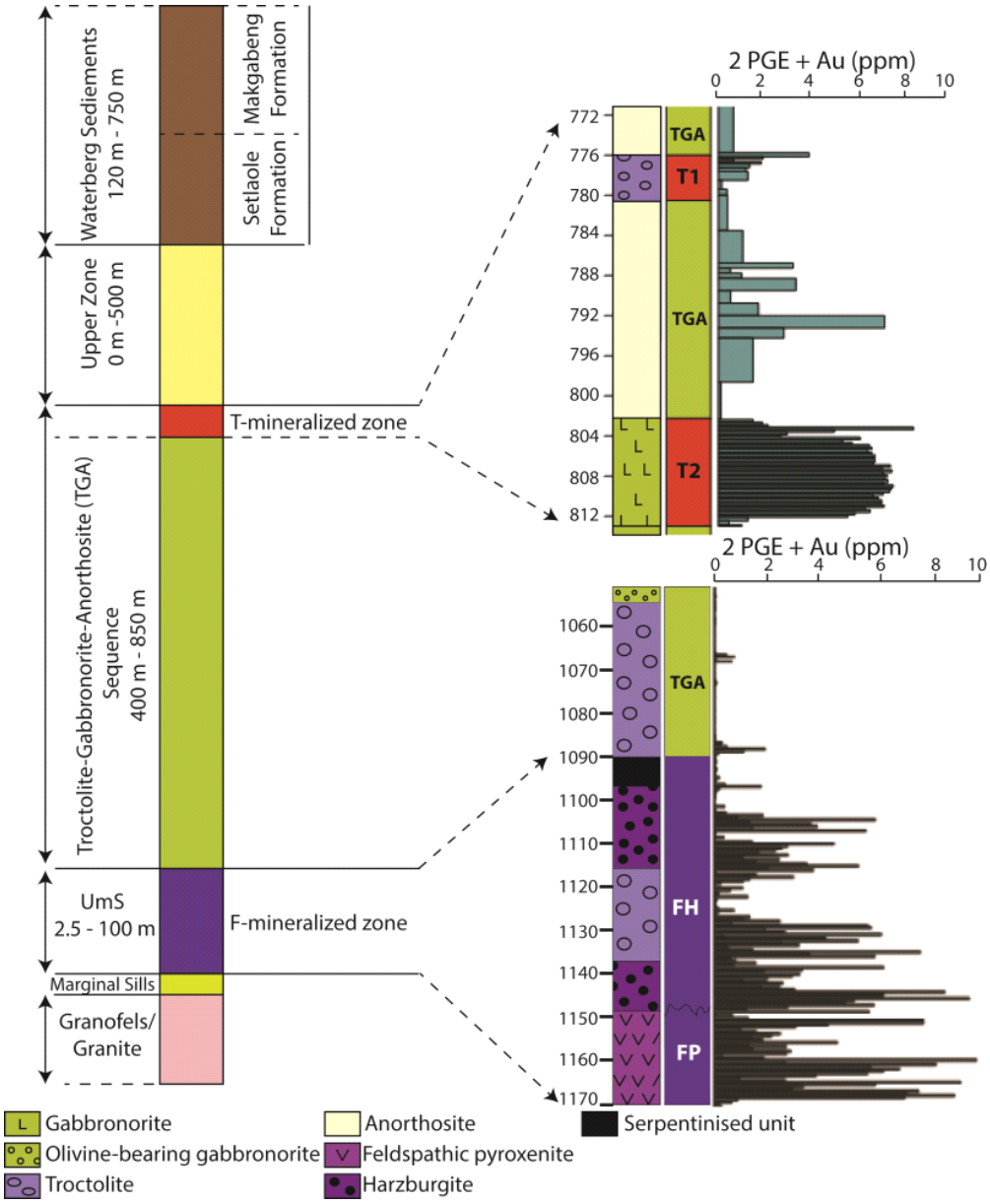

Figure 4.11: Schematic idealized section through the Bushveld intrusive rocks of the Waterberg project, showing the location of the mineralized F and T zones within the stratigraphy. The variability in Pt + Pd + Au grade is shown for both zones and the histograms reflect PGE grades that are typically up to 7 g/t.

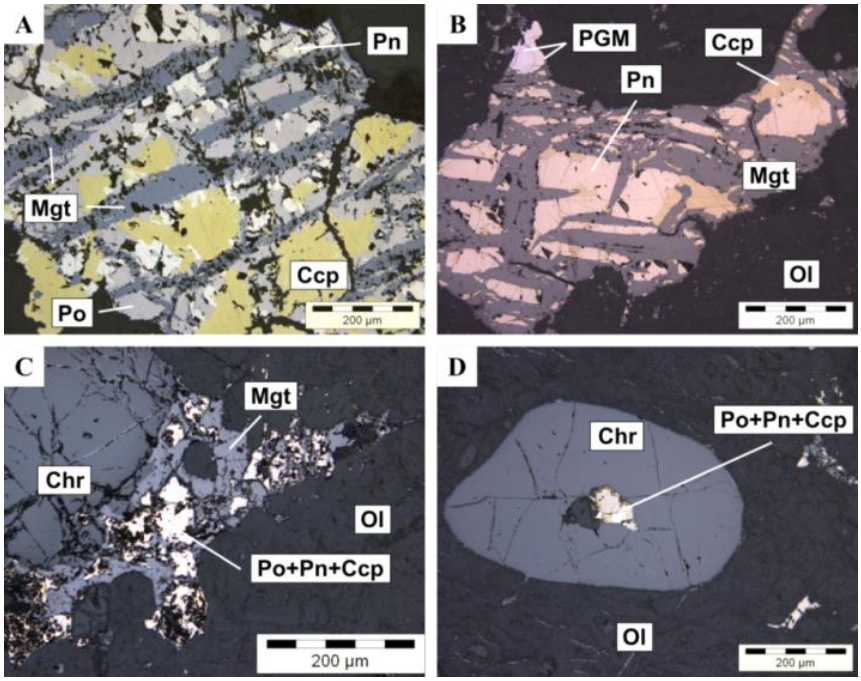

Figure 4.12: Photomicrographs of sulfide mineralization in the F zone. (A). Magnetite replacement of sulfides. (B). Chalcopyrite, pentlandite, magnetite, and platinum group minerals in olivine. (C). Magnetite replaces chromite and sulfides. (D). Chromite with sulfide inclusion. Abbreviations: Ccp = chalcopyrite, Chr = chromite, Mgt = magnetite, Ol = olivine, Pn = pentlandite, PGM = platinum group minerals, Po = pyrrhotite.

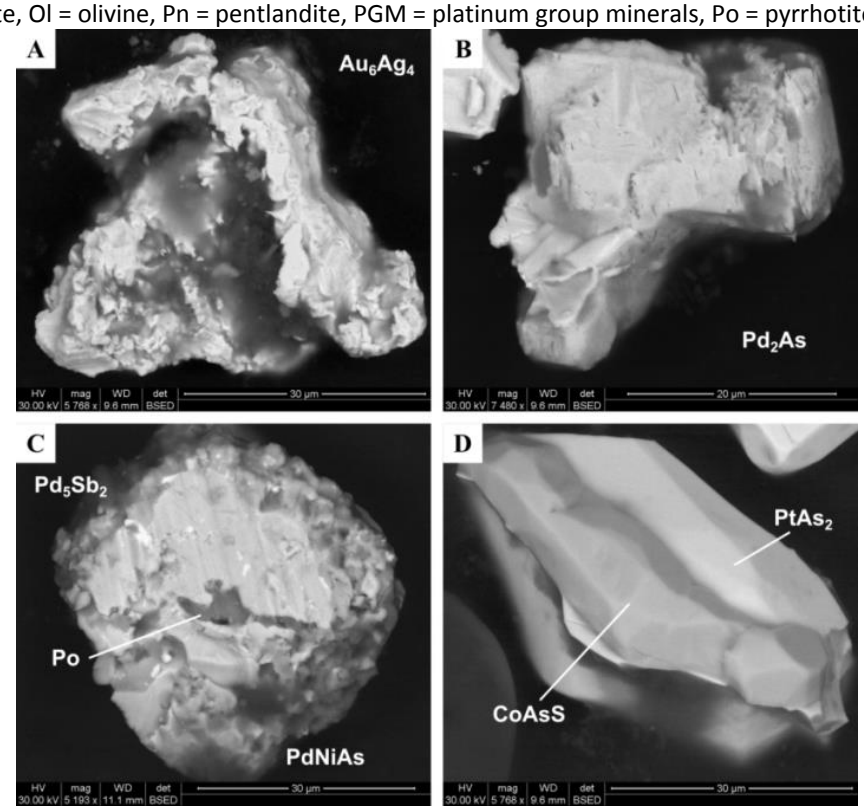

Figure 4.13: Noble metal minerals from the F zone in core sample WB034 (A). Electrum Au_6Ag_4 = 1,060.3-m depth. (B) Palladioarsenide Pd_2As = 1,060.3-m depth. (C). Majakite PdNiAs + stibiopalladinite, bright (Pd_5Sb_2) + pyrrhotite - 1061 m. (D). Sperrylite ($PtAs_2$) and cobaltite CoAsS = 1,018-m depth. Scale bars are 30 µm in length.

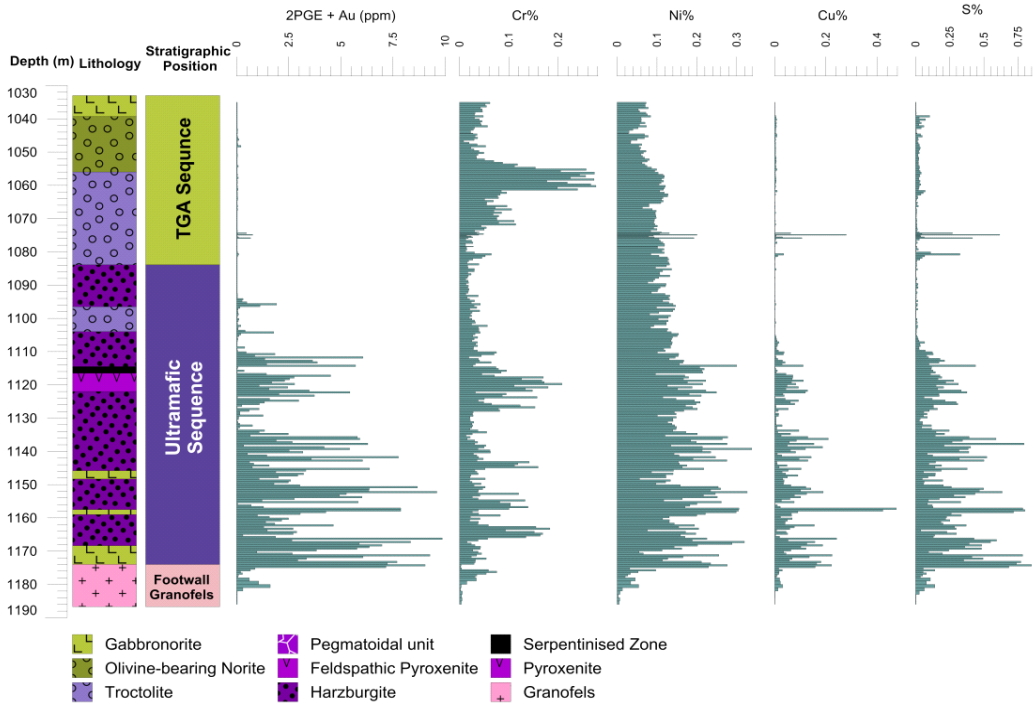

Figure 4.14: The F zone showing the 2 PGE + Au (ppm) grade and abundances for Cr, Ni, Cu, and S in core WB027. From McCreesh (2015).

T zone: The T zone (Fig. 4.11) occurs at the top of the troctolite- gabbronorite-anorthosite sequence just beneath the contact of the overlying Upper zone and at its shallowest is at 130 m in depth, subcropping against the Waterberg sedimentary rocks. In core sample WB003 in the south of the project area, the T zone is ~30 m thick but thickens northward to <50 m thick. The zone is characterized by its lithologic variability and includes anorthosite, pegmatoidal gabbros, pyroxenite, troctolite, harzburgite, gabbronorite, and norite. The T mineralized zone is subdivided into two mineralized zones the lower T2 unit and the upper T1 layer (Fig. 4.16). These units can be traced for several kilometers along strike. T2 mineralization is hosted in homogeneous gabbronorite/gabbro that is locally pegmatoidal and is characterized by distinctive, elongated milky-white plagioclase <1 cm in size. It may grade into a feldspathic pyroxenite (Fig. 4.16). The T2 ranges from 2 to 15 m thick with disseminated and blebby pyrrhotite, pentlandite, chalcopyrite, and pyrite with minor millerite, sphalerite, and bornite. PGM are less varied than in the F zone and are dominated by Pt-Pd bismuthotellurides. Both T zones have a consistent and unusual metal ratio with 21% Au in the precious metals (Table 4.2). T2 grades downward into an unmineralized gabbronorite/norite unit. Grade values for precious and base metals in the F and T zones are given in Table 2. Grade values given are derived from a total of 298,538 m of diamond drilling in 231 drill holes and 373 deflections. (PTM, October 2016). The indicated mineral resources in millions of tons have been based on a cut-off grade of 2.5 g/t and a depth of 1,250 m, although both the T and F zones continue below this depth.

Table 4.2: Grade Values for Precious and Base Metals in the F and T Zones

	Pt	Pd	Au	Ru	Cu (%)	Ni (%)	Proportion of precious metals (%)	Indicated resources (Mt)	Inferred resources (Mt)
T zone	1.13	1.9	0.81	0.04	0.16	0.08	Pt 29, Pd 49, Au 21, Rh 1	31.54	19.917
F zone	1.05	2.23	0.17	0.04	0.07	0.16	Pt 30, Pd 64, Au 5, Ru 1	186.725	77.295

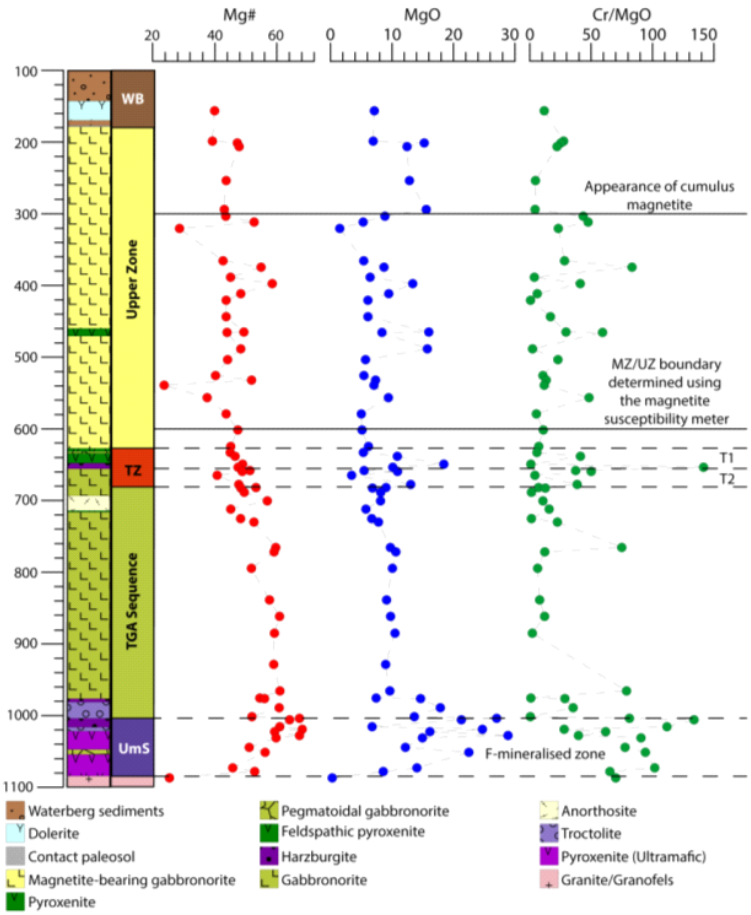

Figure 4.15: Compositional variation of MgO (wt. %), Mg number, and Cr/MgO (ratio) through core WB017. Dashed lines indicate the mineralized units. TGA sequence = troctolite-gabbronorite-anorthosite, T zone = T mineralized zone, UmS = Ultramafic zone, WB = Waterberg sedimentary sequence. McCreesh *et al*. (2015).

The middling between the T2 and T1 is not always present. Where it occurs it varies in thickness from ~20 cm to 35 m and comprises pegmatoidal leucogabbro or a varitextured pegmatoidal anorthosite that is compositionally similar to the pegmatoidal anorthosite in the T1 hanging wall (Fig. 4.16). This hanging wall can range from 0 to 20 m in thickness. The middling and hanging-wall units only locally have good grade. The T1 mineralized zone is hosted in a variety of rock types, including troctolite (Fig. 4.16), which may grade into a feldspathic harzburgite or sometimes to an olivine-bearing feldspathic pyroxenite. All show minor chloritisation and serpentinisation in olivine-bearing intervals. The thickness of T1 varies from 3.5 to 5 m. Sulfides are common (Fig. 4.17) as blebby to net-textured chalcopyrite and pentlandite, with minor disseminated pyrrhotite, as flame-textured pentlandite in pyrrhotite and pyrite, as pyrite replacing magnetite and pyrrhotite, or rimming earlier sulfides. The limited variations in MgO%, Mg number, and Cr/MgO

within the troctolite-gabbronorite-anorthosite sequence are shown in Figure 4.15, while the variations in Cr, Ni, Cu, and PGE in one of the borehole cores are shown in Figure 18. The Pt + Pd + Rh + Au grade is typically 1 to 7 g/t (Table 4.2). Selected chemical analyses are shown in Table 1. The hanging wall to T1 is generally a pegmatoidal anorthosite or coarse-grained leucogabbronorite that varies in thickness from 2 to <100 m although it is absent in a few cores (Fig. 4.16). This unit may host PGE mineralization together with chalcopyrite, pentlandite, and pyrrhotite.

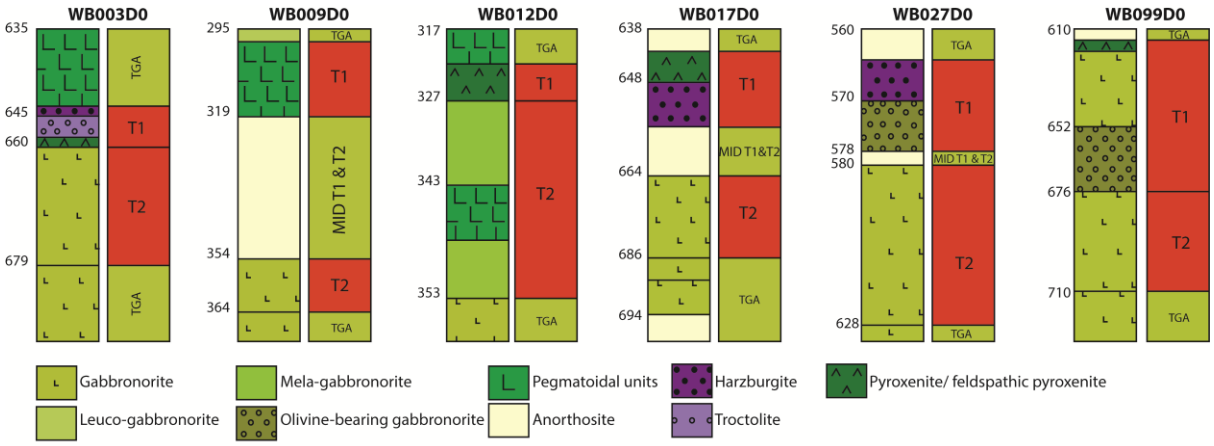

Figure 4.16: Schematic section through the T zone, showing the variability of the rock types and the host rocks of the mineralization in the T1 and T2 layers. The column to the left shows the lithology, while the column to the right for each borehole shows the stratigraphic affiliation of the various units.

4.8. Discussion

When the PGE mineralization was discovered at the Waterberg project, a significant question was whether the intrusion was of Bushveld age, related to the Great Dyke (2575 Ma; Oberthür *et al*, 2002) or to other Paleoproterozoic intrusions in the Limpopo belt. Having established that the intrusion on the Waterberg project is of similar age to the Bushveld Complex (Huthmann *et al*., 2016), the challenge is to compare and contrast the project stratigraphy and mineralization with that of the eastern, western, and northern limbs of the complex. It is apparent that there are significant similarities, but also notable differences, even with the northern limb immediately to the south of the Hout River shear zone. In the Waterberg platinum project, a Waterberg sedimentary sequence caps the eroded Bushveld rocks, whereas south of the Hout River shear zone, thick differentiated granite sheets cap the Upper zone.

Ultramafic sequence: Harzburgite and orthopyroxenite are typical constituents of both the Lower and Critical zones elsewhere in the Bushveld Complex. The amount of interstitial plagioclase in the Waterberg ultramafic rocks commonly exceeds 10 to 15 vol %, which is higher than the plagioclase proportions in the Lower zone rocks (2–6 vol % according to definition of Cameron, 1978) and is more comparable with the proportions in the Critical zone and the Platreef. The most common texture of the Waterberg harzburgite is poikilitic, whereas granular harzburgite transitional

into dunite as in the Lower zone at Grasvally (Hulbert and von Gruenewaldt 1985), Clapham (Wilson, 2012), and Turfspruit (Yudovskaya *et al*., 2013a) was not observed in the Waterberg rocks. Kink bands and chromite-pyroxene lamellae, which were described in Lower zone olivine (Wilson *et al*., 2012; Yudovskaya *et al*., 2013a), were not found in olivine from Waterberg harzburgite. The laminar fabric of preferred elongated orthopyroxene that is considered to be a typomorphic feature of the Lower zone pyroxenite (Boorman *et al*., 2004) was also not observed in Waterberg. The regular chromite seams with sharp boundaries common in the Lower Critical and in the Lower zones on Grasvally and Clapham are absent at Waterberg. Instead, chromite concentrates into bands of disseminated grains with irregular diffuse outlines resembling the appearance of Platreef chromitite in the northern limb of the Complex as described by Yudovskaya and Kinnaird (2010). Chemical compositions of the most primitive olivine and chromite analysed so far are also more consistent with the Critical zone lineage as Fo in olivine varies from 77 to 83 and Cr_2O_3 content in chromite does not exceed 32 wt. %. Furthermore, apart from at Grasvally there is no PGE or Cr mineralization known in the Lower zone anywhere else in the Bushveld Complex.

Troctolite-gabbronorite-anorthosite sequence: Originally the troctolite unit in the Waterberg project was thought to correlate with the troctolite in the Main zone of the northern limb, identified by van der Merwe (1976) and observed in the Bellevue drill core (Ashwal *et al*., 2005).

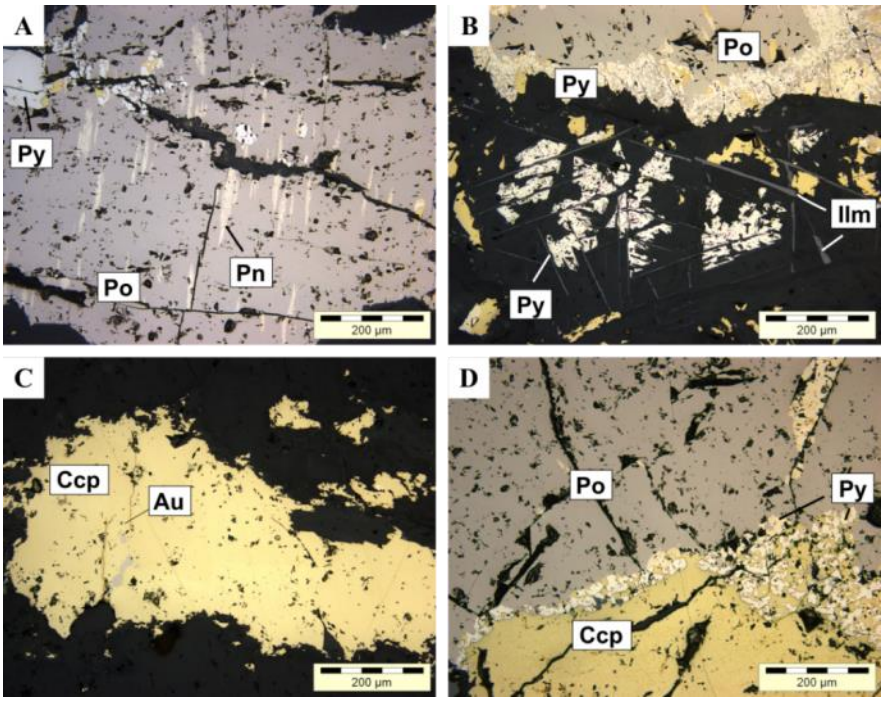

Figure 4.17: Photomicrographs of sulfide mineralization in the T zone. (A). Flame-textured pentlandite in pyrrhotite and pyrite. (B). Pyrite after magnetite and pyrrhotite. (C). Au and pyrrhotite in chalcopyrite. (D). Pyrite growing along the boundary of pyrrhotite and chalcopyrite. All images in reflected light. Abbreviations: Ccp = chalcopyrite, Ilm = ilmenite, Pn = pentlandite, Po = pyrrhotite, Py = pyrite.

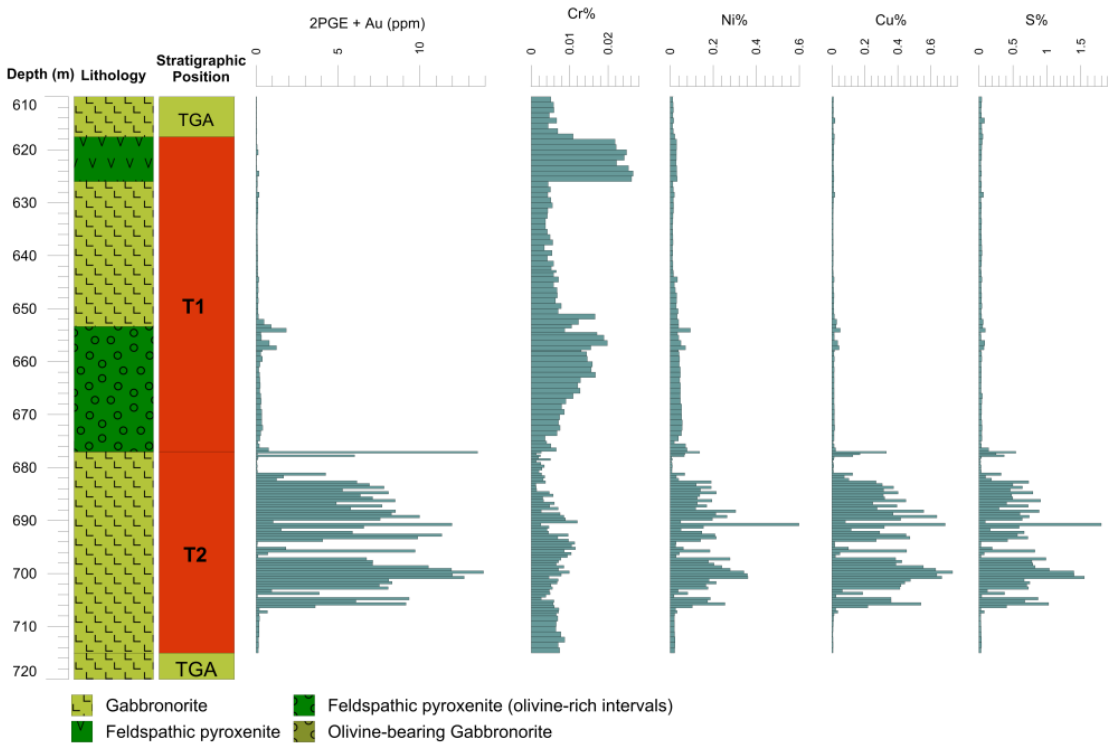

Figure 4.18: The mineralized T zone showing the distribution of 2 PGE + Au (ppm) grade within T1 and T2. Variations in the Cr, Ni, Cu, and S % in core WB099 are also shown. Note how the high PGE do not correlate with zones of high Cr %. Samples were analysed for Pt, Pd, and Au (all ppm) by standard 25-g lead fire-assay using a silver collector. Rh was assayed using the same method but with a palladium collector. After preconcentration by fire assay the resulting solutions were analysed using ICP-OES for copper, nickel, cobalt, and chromium. This technique results in "almost" total digestion. Data by courtesy of PTM in McCreesh (2015).

Both have high magnetic susceptibility signatures, which resulted from the formation of secondary magnetite during the alteration of olivine, and there is an overall similarity in chondrite-normalized multielement signatures. However, there are lithologic and mineralogical contrasts. According to Ashwal *et al*. (2005) the troctolite package in the Bellevue drill core is mainly composed of olivine-norite, gabbro, and gabbronorite with minor leucocratic varieties and pyroxenite horizons, rather than being a true troctolite, with the average modal abundance of olivine in the olivine-bearing sequence of 21.1% and decreasing irregularly upward. In contrast, the troctolite unit in the Waterberg stratigraphy is composed of cumulus feldspar and 25 to 65% olivine, with interlayers of pyroxenite or feldspathic pyroxenite (cumulus orthopyroxene and clinopyroxene with minor interstitial feldspars). Above the troctolite, the troctolite-gabbronorite-anorthosite sequence of the Waterberg project is dominated by medium to coarse-grained gabbronorite and norite, with minor anorthosite, feldspathic pyroxenite, pyroxenite, and pegmatoidal units. The sequence is characterized by higher Al, Sr, and low Cr concentrations compared to the Ultramafic sequence, the occurrence of inverted pigeonite in parts of the succession, an overlying magnetite-bearing zone, and a Cr/MgO ratio of less than 80 (Fig. 4.15) a parameter which Seabrook *et al*. (2005) believe to be characteristic of Main zone rocks. However, there are also notable contrasts. The Main zone in the western limb of the Complex is ~2,200 m thick (Mitchell, 1990), up to 3,940 m thick in the Roossenekal area of the eastern limb (von Gruenewaldt, 1973), and ~1,370 m thick in the Bellevue

core south of the Hout River shear zone (Ashwal *et al*., 2005). In contrast the maximum thickness of the troctolite-gabbronorite-anorthosite sequence in the Waterberg area is 850 m (core sample WB099). The subzones of the Main zone of the eastern and western limbs of the Complex are determined by the occurrence or absence of primary orthopyroxene, clinopyroxene/augite, and inverted pigeonite in the western limb. Nex *et al*. (1998) identified five subzones (Fig. 4.19). The occurrence of inverted pigeonite in the basal troctolite-gabbronorite-anorthosite sequence of the Waterberg project suggests a potential correlation with the Hexrivier unit of subzone C (Fig. 4.19) as both are characterized by up to 10% olivine, although subzone C is not fully developed in the Waterberg stratigraphy. Upward, the homogeneous equigranular gabbronorite with primary orthopyroxene, which lacks inverted pigeonite, could be correlated with subzone D of Nex *et al*. (1998). The upper troctolite-gabbronorite-anorthosite sequence of the Waterberg project, which is characterized by the reappearance of inverted pigeonite oikocrysts, with plagioclase and augite, could be correlated with subzone E (Nex *et al*., 1998; McCreesh, 2013), although this subzone is not always present in the Waterberg project. Within the Main zone of the eastern and western limbs of the Bushveld Complex, a distinctive pyroxenite marker is noted (von Gruenewaldt, 1973; Klemm *et al*., 1985; Cawthorn *et al*., 1991: Nex *et al*., 2002; Ashwal *et al*., 2005), as shown in Figure 4.20. This marker horizon is where Kruger (1994) regarded the influx of the Upper zone magma to have occurred, although SACS (1980) regard the boundary as marked by the appearance of cumulus magnetite, shown in Figure 4.20 as the horizon of "magnetite-in." For the Main zone of the Bellevue core there are two distinct pyroxene-rich horizons, the lower one is at a depth of 2,806.80 m (2.3 m thick) and an upper one at 1,971.80-m depth that is 1.88 m thick (Ashwal *et al*., 2005). The upper clinopyroxene-rich horizon in the Bellevue drill core occurs at the same stratigraphic position as the T1 zone in the Waterberg exploration area and both are dominated by clinopyroxene (McCreesh, 2013). This latter pyroxenite horizon is also at the appropriate stratigraphic position of the Pyroxenite Marker described by Cawthorn *et al*. (1991) in the eastern and western limbs of the Bushveld Complex (Fig. 4.20), although Ashwal *et al*. (2005) did not equate the pyroxenite layer 380 m below the Marginal-Upper zone boundary with the Pyroxenite Marker because the Pyroxenite Marker elsewhere in the Bushveld Complex is dominated by orthopyroxene (von Gruenewaldt, 1973; Cawthorn *et al*., 1991: Nex *et al*., 2002; Ashwal *et al*., 2005). Nevertheless, these distinctive clino- or orthopyroxenite horizons all seem to mark the position of an influx of new Upper zone magma around the Bushveld Complex at approximately the same stratigraphic level (Fig. 4.20).

Subzones	Units	cumulus mineralogy	textures	Waterberg features
E		plagioclase, augite and inverted pigeonite no primary opx.	similar to subzone C with occasional interstitial magnetite. Reticulated framework of inverted pigeonite on weathered surfaces	plagioclase, augite and inverted pigeonite
D		plagioclase, augite, primary opx no inverted pigeonite	slightly oikocrystic primary opx otherwise generally equigranular. In outcrop, large euhedral primary opx and prominent needles of augite at the base	homogeneous equigranular gabbronorite with primary opx
	Hexrivier	plagioclase, augite, inverted pigeonite no primary augite	microgabbronorite	inverted pigeonite at the base, with <10% olivine
C			cumulus plagioclase with oikocrystic inverted pigeonite and minor interstitial and subgranular augite. Frequent myrmekite. Reticulated framework of pigeonite on weathered surface	
	Springbok			
	Zebra	3 pyroxenes	rhythmically layered	
B		plagioclase, augite, primary opx	cumulus plagioclase with discrete primary opx, usually large crystals. In outcrop, distinctive large euhedral grains of primary opx	
A		plagioclase and primary opx		

Figure 4.19: Classification of the Main zone rocks in the Western Bushveld (Nex *et al*., 1998). Waterberg features indicate comparative mineralogy and tentative correlation on the Waterberg project Main zone rocks; opx = orthopyroxene.

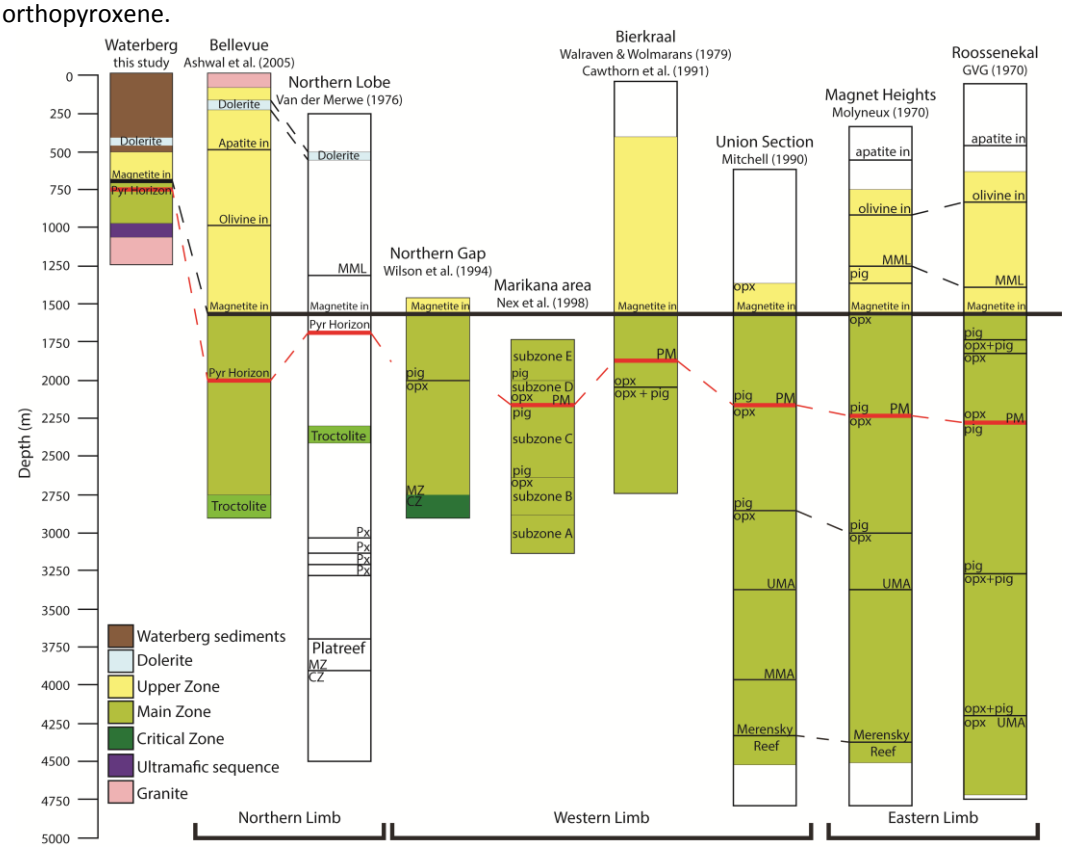

Figure 4.20: Profiles through the Main zone-Upper zone boundary in various parts of the Bushveld Complex, showing the position of a pyroxenitic layer that may be ortho- or clinopyroxene dominated, relative to where cumulus magnetite is recognized. Modified from Ashwal *et al*. (2005). GVG 1970 = von Gruenewaldt (1970).

Upper zone: Although fine-grained cumulus magnetite occurs in the Upper zone of the Waterberg project, as observed in core samples and identified based on magnetic susceptibility, typical magnetitite layers are lacking except in one borehole in the far south of the project property where a 2.5-m-thick magnetite layer occurs in core sample WB001, a borehole core from south of the Hout River shear zone. The widespread occurrence of disseminated magnetite has led to the recognition of this unit as the equivalent of the Upper zone.

In the Waterberg area the Upper zone, which is dominated by magnetite gabbro and gabbronorite (Fig. 4.9) with occasional ferrogabbro at the top, varies between 0 and 500 m in thickness (WE027), whereas south of the Hout River shear zone, the Upper zone in the Bellevue drill core is <1,188 m thick and is composed mainly of magnetite gabbro (41.1%), olivine ferrodiorite (21.4%), and minor gabbronorite, magnetite- bearing plagioclase cumulate rocks, and pyroxenites with 32 magnetitite layers or magnetite-rich rocks (Ashwal *et al*., 2005). The Upper zone in the eastern and western limbs is approximately 2,000 m thick and contains 26 magnetitite layers (Molyneux; 1970, 1974; Cawthorn *et al*., 2006; Tegner *et al*., 2006). The lack of magnetitite layers in the Waterberg project, in spite of the occurrence of abundant magnetite, may possibly relate to dynamic magma movement so that magnetite layers couldn't form, or because the smaller volume of the Upper zone magma was not capable of coalescing magnetite to form distinctive layers.

In the Upper zone of the Bushveld Complex, the most evolved rocks are quartz monzonite with up to 65 wt. % SiO_2 (Cawthorn, 2013) but these are not found in the Waterberg area. The relatively unevolved chemical composition and coarse-grained texture of Upper zone gabbro in the Waterberg project suggest that significant erosion of the Upper zone may have occurred with at least 1 km of roof rocks and Upper zone removed before sedimentation in this part of the Waterberg basin began. Geochemical analyses of typical magnetite bearing gabbronorite and ferrogabbro are shown in Table 4.1.

Geochemical comparisons with other Bushveld mafic-ultramafic rocks: The mantle-normalized trace element patterns of Waterberg rocks (Fig. 4.21) are remarkably similar to the profiles of other mafic-ultramafic rocks in the Bushveld. The patterns are identical in shape to the profile of the Archean midcrustal rocks of the Kaapvaal craton (Lana *et al*., 2004) that emphasizes an overwhelming crustal contamination of Bushveld melts. The abundances of incompatible elements in ultramafic rocks are determined by their concentrations in the cumulus minerals (which are commonly not high) but mostly by the proportion of intercumulus liquid and products of its crystallization. On this basis, feldspathic harzburgite and pyroxenite are characterized by the highest and most variable proportion of intercumulus assemblages as expressed in the wide ranges of element variations in the profile (Fig. 4.21). Troctolite and olivine gabbronorite are predominantly

adcumulates with a low concentration or absence of mesostasis that results in a relative depletion in incompatible elements.

Boundary between the Main and Upper zones: The recognition of exactly where the boundary lies between the Main and Upper zones in the eastern and western limbs of the Bushveld Complex is debatable. Based on the initial Sr isotope ratios, the boundary is at the orthopyroxene-bearing Pyroxenite Marker (Kruger; 1990, 1994). Mineralogically, the boundary defined by Molyneux, (1974) and SACS, (1980) at the first sustained occurrence of cumulus magnetite is well above the isotopic boundary. In the western Bushveld in the Marikana area, the position of the new magma influx is ~100 m below the Pyroxenite Marker based on whole-rock major element and mineral data (Nex *et al*., 2002). However, using trace element data the new magma influx is 135 to 150 m below the pyroxenite horizon, depending on which trace element is used (Nex *et al*., 2002). For the eastern limb south of Roosenekal, Klemm *et al*. (1985) also suggests the influx of a new magma prior to the formation of the Pyroxenite Marker.

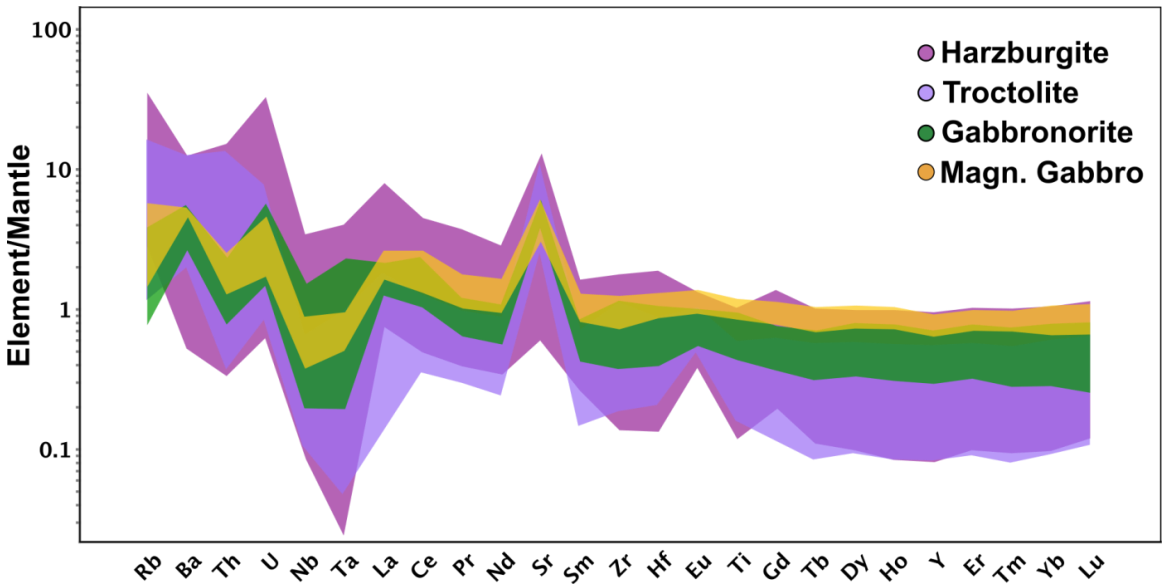

Figure 4.21: Multielement chondrite-normalized plot for mafic-ultramafic rocks, showing the overall similarity of the different rock sequences in the Waterberg project area. There is a similarity to all Bushveld lithologies from the eastern and western limbs with a negative Nb-Ta and a positive Sr anomaly. Lower zone pyroxenites beneath the Platreef on Turfspruit also show a negative Nb-Ta anomaly, a variable negative Ti anomaly, and gently sloped Y and HREE. Data shown are from unpublished data of one of the authors (54 samples, Huthmann *et al*., unpub. data). Chondrite values from Sun and McDonough (1989).

Ashwal *et al*. (2005) defined the boundary between the Main and Upper zones in drill core from the Bellevue borehole in the northern limb on the basis of a change in magnetic susceptibility. Through the Main zone cumulates, magnetic susceptibility values are between 0.02 and 0.05 SI units, while the Upper zone generally has higher values up to 5.00 SI units, although anorthositic horizons have very low magnetic susceptibility (Ashwal *et al*., 2005). In the Waterberg project, there is a significant change in magnetic susceptibility at the T zone, with disseminated magnetite

responsible for the significant increase in susceptibility values, even though magnetite only becomes apparent as a cumulus phase in visual inspection of core ~100 m higher in the stratigraphy. Geochemical profiles suggest that mineralization in the T zone of the Waterberg project occurs at a level where there was a new influx of magma mixing with the evolving resident magma (Figs. 4.15, 4.22). The boundary between the troctolite-gabbronorite- anorthosite sequence and Upper zone in the Waterberg stratigraphy has therefore been drawn on the changes in magnetic susceptibility and this position is in agreement with the noted geochemical changes.

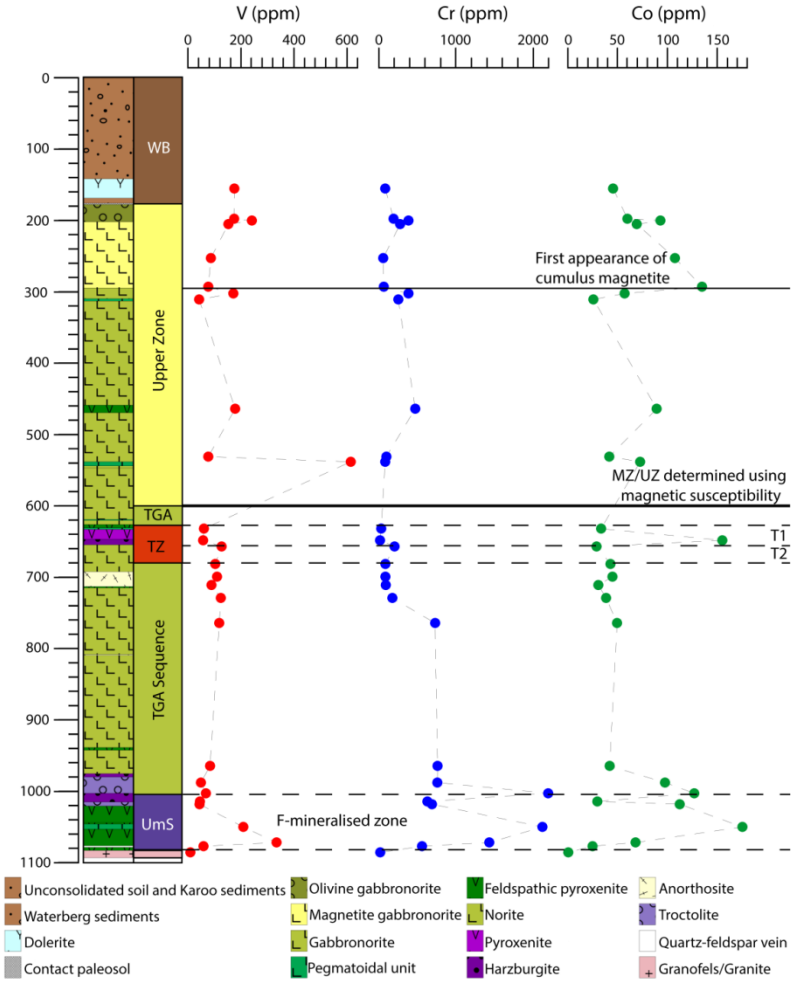

Figure 4.22: Variations in the V, Cr, and Co (ppm) of borehole WB017. The solid black line represents the Main-Upper zone boundary determined using the magnetic susceptibility results. The black dashed lines represent the F and T zones. From McCreesh *et al*. (2015).

Mineralization: In the Waterberg project, the dominance of Pd over Pt is atypical for mineralization of the eastern and western limbs of the Complex, although the Platreef overall is also Pd dominated with a Pd/Pt ratio of 2/1 in the basal Platreef and Pd slightly higher than Pt for the overall Platreef (Kinnaird, 2005; McDonald and Holwell, 2011). The PGE grade in the T zone in the Waterberg project is unusual as elsewhere in the Bushveld Complex, the Main zone has generally lower grade PGE with Pt and Pd in the 1- to 20-ppb level (Maier *et al*., 2013), although localized PGE

enrichment has been noted both in the northern and western limbs with reported grades lower than in the current prospect (Maier and Barnes, 2010; Kinnaird and Nex, 2015; McDonald *et al*., 2017). There is no mineralization reported in the clinopyroxenite horizon of the Bellevue core, which is in the same stratigraphic position as the T zone of the Waterberg project (Fig. 20). In the western limb of the Complex, stream-sediment samples showed enhanced Pt + Pd + Au concentrated toward the top of the Marginal zone that could be traced for more than 100 km (Wilhelm *et al*., 1997). Nine Pyroxenite Marker samples from the western limb averaged 23 ppb Pt, 10 ppb Pd, and 1.27 ppb Au according to Maier *et al*. (2001) so they concluded that while the Pyroxenite Marker may locally contain elevated sulfide and PGE contents, the layer is a poor target for PGE.

Platinum group element mineralization in the northern limb south of the Hout River shear zone is not restricted to the Platreef. PGE mineralization was identified in 1971 in Main zone anorthosite, gabbronorite, and pyroxenite layers in Moorddrift, south of the Planknek-Ysterberg fault, with grades of <6.67-ppm PGE (Maier and Barnes, 2010). Later drilling found PGE enrichment along a strike length of ~1 km. Highest grades were 3.21-ppm PGE over 4.6 m, with seven PGE-enriched zones in a thickness of ~400 m associated with the Pyroxenite Marker, with the most important "reef" (0.5–~4.3 m thick) in and just below the main pyroxenite. This unit contains 1 to 5% modal disseminated pyrite, chalcopyrite and pyrrhotite with accessory millerite and pentlandite (Maier and Barnes, 2010). This could be similar to the Waterberg mineralization in the T1 zone, although the PGE in Moorddrift are Pt rather than Pd dominant. However, according to Cawthorn (2012), the Pyroxenite Marker described by Maier and Barnes (2010) is not equivalent to the Pyroxenite Marker in the eastern and western limbs of the Bushveld Complex based on the chemical variations of Cr/MgO, MgO, and Mg number. The position of the mineralization in Moorddrift relative to the pyroxenite horizon is shown in Figure 4.23.

North of Overysel (Fig. 4.2A), the Main zone thins progressively until Upper zone cumulates rest directly on basement gneiss (Fig. 4.2A); then northward the Main zone reappears at surface directly in contact with Archean granite (van der Merwe, 1976). At the northern end of the exposed part of the northern limb, the Aurora project (Fig. 4.2A), which comprises seven farms just south of the Waterberg project boundary, has PGE-Cu-Ni mineralization in leucogabbro, anorthosite, and minor troctolite units (Manyeruke, 2007; Maier *et al*., 2008; McDonald and Harmer, 2010; McDonald *et al*., 2017). However, according to McDonald *et al*. (2017) this mineralization occurs above the pyroxenite/melagabbronorite unit (Fig. 4.23), although the pyroxenite horizon is also dominated by clinopyroxene, similar to both the Bellevue drill core and the Waterberg site. Mineralization in the Aurora project is associated with more felsic rocks than the Platreef and highest PGE grades occur

where Cr is lowest (McDonald *et al*., 2017) so it cannot be linked to the Platreef, and links to the Pyroxenite Marker are also debatable.

Mineralization in Aurora was initially identified from geochemical soil anomalies between 1974 and 1992 by the Union Corporation and 43 boreholes were drilled by Genmin on the farm Nonnenwerth to verify the occurrence (Venmyn-Rand, 2010). Pan Palladium subsequently defined an inferred resource based on a further 92 boreholes across 18 km of strike during the period 2002 to 2010 (Table 4.3). The mineralization in Aurora has been suggested to be correlative of the T zone mineralization on the Waterberg project to the north as it is also gold rich and palladium dominated (e.g., McDonald *et al*., 2017), although the overall PGE grade is much lower (Table 4.4).

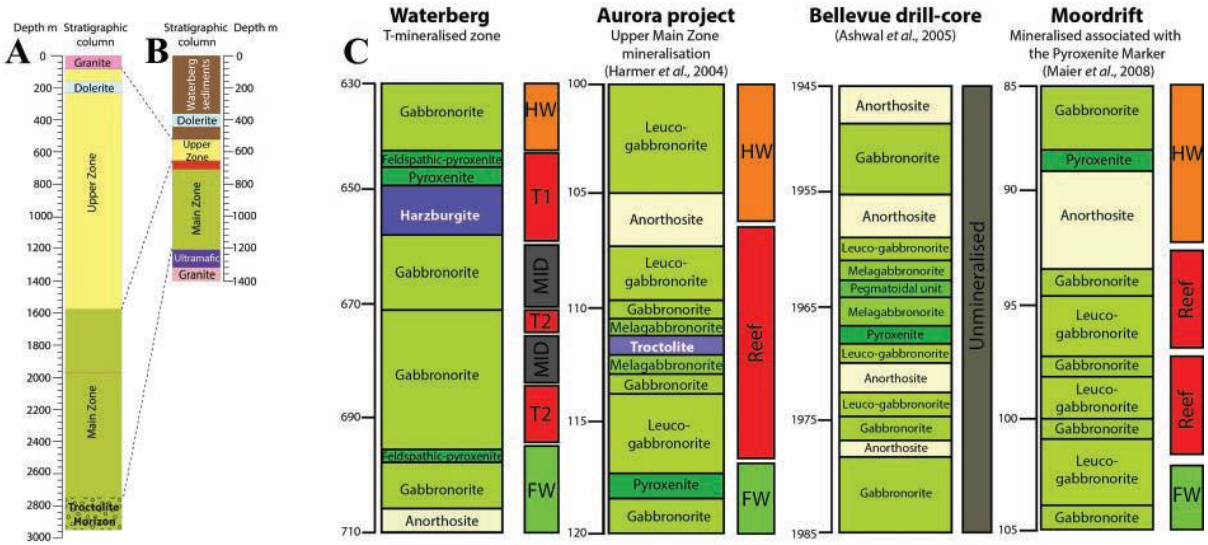

Figure 4.23: A schematic diagram comparing the stratigraphy in Waterberg cores with that for other areas of the northern limb, showing the distinctive lithologic differences between the different areas in the upper Main zone. (A). Bellevue core (Ashwal *et al*., 2005). (B). Waterberg stratigraphy showing how the thickness of the succession varies between the Waterberg and the Bellevue cores. (C). Sections through the Main zone in other areas, showing the position of mineralization. From McCreesh (2016).

The average grades for the F and T zones of the Waterberg project compare with the grade of 4.09 g/t for the Merensky reef in the eastern limb, 6.07 g/t in the western limb (Barker, 2012), and the UG2 grades of 4.39 g/t in the eastern limb, and5.1 g/t in the western limb (Barker, 2012). However, as Figure 4.24 shows both the T and F zone mineralization on the Waterberg project are very Pd dominated and compare more closely with the lower part of the Platreef than with the Merensky reef or UG2. The thick Super F zone in the Waterberg mineralization may have resulted from variations in basement topography with the formation of higher grade and thicknesses where embayments or large-scale changes in magma-flow direction facilitated the accumulation of magmatic sulfides.

Table 4.3: Potential Correlation of Upper Zone Rocks in the Waterberg Project with those in the eastern and western limbs of the Complex (subzones of the eastern and western limbs from Eales and Cawthorn, 1996).

Subzones	Lithology	Waterberg Features
Apatite Upper zone C	Olivine-apatite diorite	NA
Olivine Upper zone B	Ferrogabbronorite, olivine-magnetite, gabbronorite	Ferrogabbro, olivine-magnetite-gabbro
Magnetite Upper zone A	Magnetite-bearing gabbronorite, magnetite layers	Magnetite-bearing gabbronorite, magnetite layers (very south)

Table 4.4: JORC-Compliant Data for the Aurora Project in the Main Zone South of the Hout River Shear Zone is added for Comparison (Venmyn-Rand, 2010).

	Average indicated grade PGE in g/t	Cu grade in % and tonnage in millions of tons	Ni grade in % and tonnage in millions of tons	Proportion of precious metals in %	Resources in millions of tons
Aurora	1.34	0.08 110,930	0.05 68,2000	Pt 30.7, Pd 49.2, Au 16.5, Rh + Ru + Ir 0.6, Ag 2.9	125
Waterberg T	3.88	0.16	0.08	Pt 29, Pd 49, Au 21, Rh 1	31.54
Waterberg F	3.49	0.07	0.16	Pt 30, Pd 64, Au 5, Rh 1	186.725

Data for the Waterberg project from PTM (October 2016)

4.8.1. Model for the formation of the Waterberg intrusion

Based on the much reduced total thickness of 1 km (Fig. 4.25) and the lateral variations in the occurrence of the ultramafic-mafic Waterberg succession, together with the mineralogical and geochemical contrasts (published elsewhere) with other limbs of the Bushveld Complex, we argue that the Waterberg intrusion represents a separate structurally controlled basin fed from a different subchamber rather than a marginal extension of the northern limb of the Bushveld Complex (Fig. 4.25).

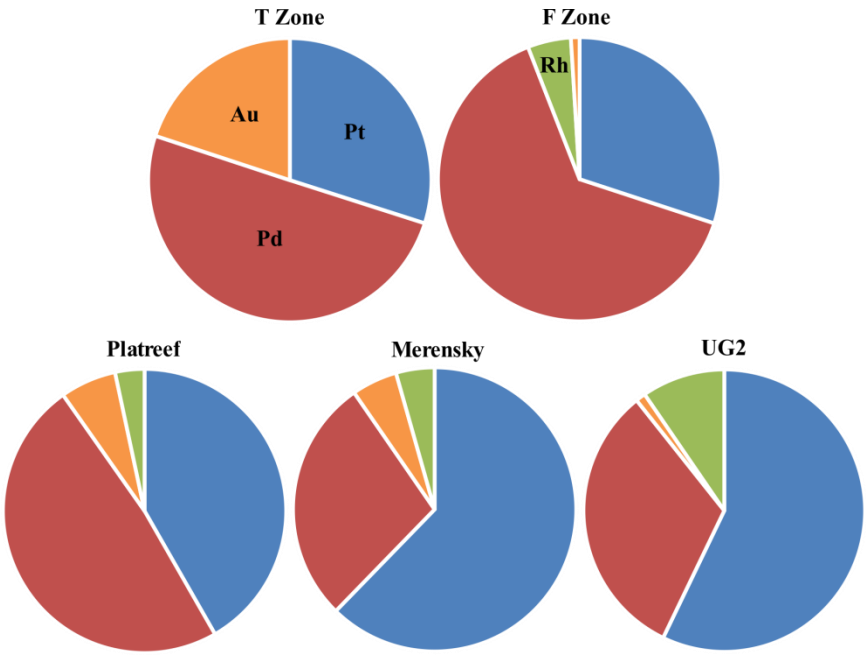

Figure 4.24: A comparison of the noble metal abundance of the Waterberg T and F mineralized zones compared to the Platreef, Merensky reef, and UG2, showing the predominance of palladium in the Waterberg deposit. Data for the Merensky reef and UG2 from Barker (2012), for the Platreef based on data for Sandsloot from the Anglo Platinum annual report (2011), and for Waterberg from PTM 43-101.

The first stage of magmatism was the emplacement of thin gabbroic and pyroxenitic sills of Marginal zone affinity that reacted with gneissic floor rocks to create the agmatites. The initial phase of the formation of the main body, we suggest, was probably by tube-like ultramafic chonolithic

intrusions whose distribution was controlled by basement floor topography. Lateral dilation, followed by the emplacement of sulfide-bearing ultramafic lithologies, resulted in the formation of mineralized orthopyroxenite and harzburgite of the Ultramafic sequence. This in turn was followed by a further intrusion that formed a sheet-like body of troctolites, later fractionating into gabbroic rocks. An influx of Upper zone magma mixed with the residual troctolite-gabbronorite-anorthosite sequence magma and formed the lithologically varied T zone. It is possible that the Pd, Au, and Cu enrichment may have been related to the timing of late-stage sulfide saturation in the magma as opposed to fractionation of the magma, which is consistent with magmatic S isotope values (McCreesh *et al*., 2015). The Au in this T zone was derived from a Main zone-type magma, which also produced Au-enriched PGE mineralization in Main zone rocks in the Aurora project farther south (McDonald *et al*., 2017). The lack of T zone in more than 100 holes may be due to non-deposition of this part of the succession or the T zone may have been assimilated by the later magma influx. Whatever the mechanism, there is considerable lateral variability of the lithologies partly due to structural control, basement floor topography, and partly to magmatic erosion. The position of both silicate rocks and mineralization may be controlled by its unique structural position north of the Hout River shear zone.

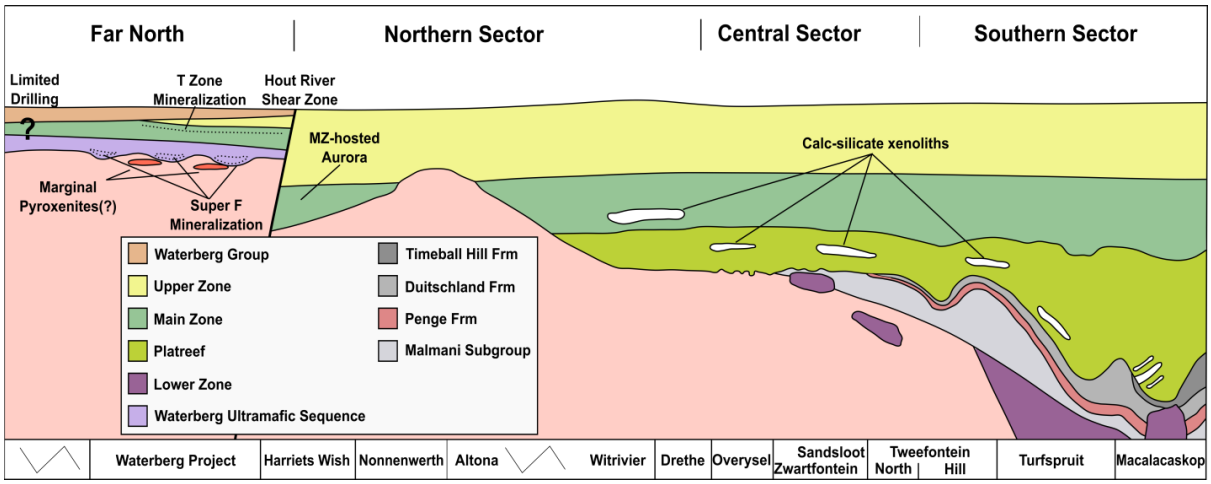

Figure 4.25: Schematic diagram showing the contrast in thickness between the Waterberg intrusive package in the far north of the northern limb of the Bushveld Complex and the intrusive sequence south of the Hout River shear zone. Modified from Kinnaird (2005).

Based on U-Pb age dating, the Waterberg sediments appear to have been deposited penecontemporaneously with the intrusion of the Bushveld Complex (U-Pb dating of zircon, Dorland et al., 2006; and a 2056 ± 6 Ma age of detrital zircons at the base of the Waterberg sediments, Huthmann *et al*., 2016). However, the identification of gibbsite in a siltstone layer at the top of the Bushveld stratigraphy in the Waterberg project indicates that a paleosol formed on weathered Bushveld rocks in a tropical climate before the deposition of the Waterberg sediments (Yudovskaya and Kinnaird, 2013; Yudovskaya *et al*., 2015). Thus the Setlaole and Makgabeng Formations were

deposited between ~2.05 and ~1.93 Ga after the intrusion of the Bushveld rocks and before the intrusion of a dolerite sill at ~1.88 Ma (Hanson *et al*., 2004; Dorland *et al*., 2006).

4.9. Conclusions

1. The ultramafic-mafic succession of the Waterberg project, north of the exposed part of the northern limb of the Bushveld layered intrusion, probably represents a separate compartment north of the Hout River shear zone. The northeast-oriented lobate arc extends 24 km from the previously known outcrop of Bushveld rocks. Dating has revealed an emplacement age of 2053 ± 5 Ma. A general dip of 34° to 38° westward is observed for the layered units.
2. The Bushveld succession comprises a basal ultramafic sequence, a troctolite-gabbronorite-anorthosite sequence, and an Upper zone with overlying Waterberg red beds that were deposited between ~2.05 and ~1.93 Ma
3. The basal Ultramafic zone is at a minimum depth of 180 m from the surface and is typically 100 m thick. It consists dominantly of feldspathic harzburgite and feldspathic pyroxenite. It has been divided into an upper harzburgite (HF) olivine-rich unit, and an underlying feldspathic orthopyroxenite (FP) unit layer <60 m thick that consists mainly of orthopyroxenite.
4. The troctolite-gabbronorite-anorthosite sequence is at a minimum depth of 130 m from the surface and is up to 850 m thick. It consists mainly of gabbronorites. The upper boundary with the Upper zone is defined by increased changes in magnetic susceptibility due to the formation of primary cumulus magnetite in the Upper zone.
5. The Upper zone of magnetite gabbro and gabbronorite varies between 0 and 500 m in thickness. In parts of the project area where the Upper zone is not developed, sedimentary rocks of the Waterberg Group rest on Main zone lithologies. There are two mineralized intervals, a lower F zone and an upper T zone that vary from 3 to 60 m in thickness. The F zone within the Ultramafic zone hosts disseminated sulfides with accessory chromite. PGM are dominated by sperrylite with lesser Pt-Pd bismuthotellurides, Au-Ag alloys, Pd arsenides, and Pt-Rh sulfoarsenide. The rocks have PGE grades of <7 g/t Pt + Pd + Au. PGE comprise 65% Pd, 30% Pt, and 5% Au with 0.07% Ni and 0.17% Cu. The T zone occurs close to the boundary between the gabbronorite-norite-anorthosite unit and the Upper zone. An upper and lower mineralized section may be separated by a barren middling. PGM are dominated by Pt-Pd bismuthotellurides with an overall PGE for the T zone of 49% Pd, 29% Pt, 21% Au with 0.16% Cu, and 0.08% Ni.

Chapter 5

Platinum-group minerals of the F and T zones, Waterberg Project, Far Northern Bushveld Complex: implication for the formation of the PGE mineralisation

This chapter contains the full text of the paper "Platinum-group minerals of the Waterberg deposit, Bushveld Complex: implication for the formation of the PGE mineralisation" by McCreesh, M. J. G., Yudovskaya, M., Kinnaird, J. A. and Reinke, C. as accepted and currently in press *Mineralogical Magazine*.

This publication provides a detailed account of the base metal sulphide, PGE and PGM mineralisation in the Waterberg Bushveld stratigraphy. We aimed to investigate the importance of magmatic and hydrothermal processes involved in the development of the mineralisation within the Waterberg ore zones. This publication also provides an in depth model on the emplacement of the Waterberg mineralisation and stratigraphy based on the findings.

5.1. Candidate's contribution:

- Marina Yudovskaya and the candidate were responsible for detailed logging and sample collection in the field
- The candidate was responsible for all figure production.
- Marina Yudovskaya was responsible for the heavy mineral separates
- Christian Reinke was responsible for the preparation and assistance with the microprobe analysis.
- Both Marina Yudovskaya and Judith Kinnaird were involved in the discussion and preparation of the paper.
- The candidate was responsible for the write up of the paper.
- The candidate contributed approximately 65 to 70% towards the publication.

5.2. Abstract

This study provides the first detailed mineralogical data on PGE mineralisation of the Waterberg project, in a previously unknown segment of the Bushveld Complex located in the Southern Marginal Zone of the Limpopo Belt. The lower ultramafic F zone is dominated by sperrylite (up to 82 area %) with minor Pt-Pd bismuthotellurides, Pd-Ni arsenides, Au-Ag alloy, Rh-Pt sulphoarsenides and rare Pt-Fe alloys. The upper felsic-richer gabbroic T zone is dominated by Pt-Pd bismuthotellurides (up to 90 area %), Pd tellurides and Au-Ag alloy with rare sperrylite, braggite, Pd stannides and antimonides. The platinum-group minerals (PGM) of the F zone are mainly associated with magmatic base metal sulphides (pyrrhotite, troilite, chalcopyrite and pentlandite), that have undergone alteration during significant serpentinisation, accompanied by the formation of the secondary sulphide assemblage. The T zone in a leucogabbroic sequence contains relics of magmatic sulphides and is characterised by the development of the indicative chalcopyrite-millerite-pyrite assemblage, which is associated with widespread hydrothermal quartz and hydrous silicates (amphiboles, phlogopite, epidote and chlorite). The fluid-induced style of PGM remobilisation, the high Au/PGE and the high proportion of native gold in the high-grade T zone ores in the magnetite-bearing leucogabbroic rocks are unique to the Bushveld Complex. The genesis of the T ores is interpreted as a result of primary PGE enrichment in the zone of interaction between the first influxes of the Upper Zone fertile melt and a resident gabbroic melt at the top of the Troctolite-Gabbronorite-Anorthosite (TGA) fractionated sequence with subsequent fluid remobilization. Whether the hydrothermal overprint facilitated the PGE sequestration in a favourable setting or dispersed the pre-existing magmatic concentrations along fluid pathways remains essentially unresolved at the current stage.

Keywords: Bushveld, Waterberg project, platinum-group minerals, sperrylite, Pt-Pd bismuthotellurides, gold, magmatic sulphides, hydrothermal remobilisation.

5.3. Introduction

The geology and mineralisation of the northern limb of the Bushveld Complex (BC) has been the topic of many studies, covered by a number of authors (i.e. Kinnaird, 2005; Kinnaird *et al*., 2005; Ashwal *et al*., 2005; Maier *et al*., 2008; McDonald and Holwell, 2011). Most of the attention has been paid to the world class PGE deposit of the Platreef but the discovery of mineralisation hosted in the upper stratigraphic units both in the far north (McDonald *et al*., 2017; Kinnaird *et al*., 2017) and south of the limb (Maier and Barnes, 2010; Holwell *et al*., 2013) fundamentally changed the exploration target concept. Some earlier studies proposed that the northern limb terminated at the Hout River Shear Zone (Grobler and Whitfield, 1970) and linked in an arc with the Villa Nora fragment, although van der Merwe (1976) suggested that the northern limb extends further north beneath cover. This was confirmed by exploration in 2010/2011 that led to the discovery of mineralised Bushveld rocks by Platinum Group Metals (PTM) beneath Waterberg Group sediments north of the Hout River Shear Zone. The Bushveld succession in the Waterberg project hosts two mineralised zones, a lower ultramafic F mineralised zone and an upper mineralised T zone in a gabbronorite-dominated package.

In this paper, we present for the first time detailed mineralogical characteristics of the sulphide and PGM mineralisation for both mineralised zones of the Waterberg project. The basal F zone is compared with the Platreef marginal style mineralisation whereas ore mineralogy and noble metal deportment of the T zone is somewhat unique in the Bushveld. To some extent the lithological heterogeneity of the host package resembles the diversity of the rocks hosting Platreef-style mineralisation further to the south, however, the stratigraphic position, felsic-rich host rocks, PGE, Au and base metal ratios of the T zone cannot be directly correlated with any known mineralisation in the BC. A model for the emplacement of the mineralised succession of the Waterberg project is based on our new PGE and PGM data and takes into account petrochemical constraints that suggest chonolith-like intrusions of the Ultramafic Sequence (Kinnaird *et al*., 2017: Huthmann *et al*., 2018).

5.3.1. Bushveld Complex Geology

The 2055.91±0.26 Ma (Zeh *et al*., 2015) BC is the largest layered intrusion on Earth and hosts the world's largest magmatic ore deposits (Fig. 5.1) (Lee, 1996). The BC was emplaced as five limbs with an estimated areal extent of approximately >90000 km^2 according to recent geophysical estimates (Finn *et al*., 2015) and results of the drilling underneath the cover of the Waterberg Group sediments (Kinnaird *et al*., 2017) north of the exposed northern limb.

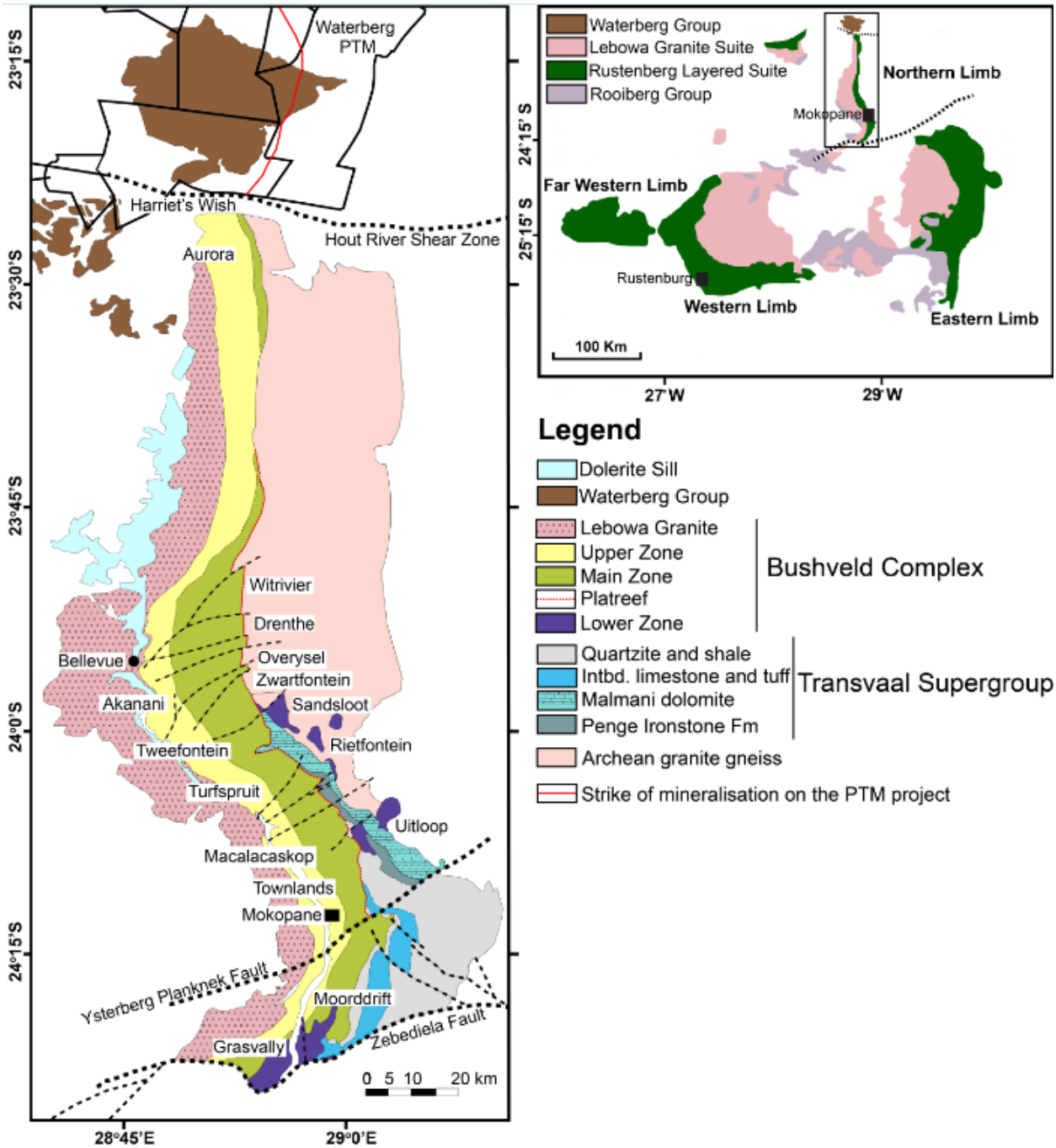

Figure 5.1: Schematic geological map of the Bushveld Complex and enlarged map of the northern limb including the extension of the Waterberg Project in the far north. Modified after 1:250 000 geological map of the northern limb (van der Merwe, 1976).

The BC is subdivided into the Rooiberg Group, the Rustenburg Layered Suite, the Rashoop Granophyre Suite and the Lebowa Granite Suite (Cawthorn *et al*., 2006). The 7-8 km thick Rustenburg Layered Suite is further subdivided into the Basal Ultramafic Sequence, Marginal, Lower, Critical, Main and Upper

Zones, comprising rock types ranging from dunite, chromitite, pyroxenite to norite, anorthosite and gabbronorite to gabbrodiorite (von Gruenewaldt *et al*., 1985; Wilson *et al*., 2015).

The northern limb is separated from other limbs of the BC by the long-lived Thabazimbi-Murchison Lineament (TML) and its connection with the western and eastern limbs (Fig. 5.1) remains debatable. The limb is exposed over a strike length of 110 km (Fig. 5.1) and extends from the Zebediela Fault, a branch of the TML in the south, to the Hout River Shear Zone (HRSZ) in the north. The northern limb succession overlies progressively older Paleoproterozoic Transvaal Supergroup metasediments in the south to Archean granite-gneisses in the far north (van der Merwe, 1976). North of the Ysterberg-Planknek Fault, the earliest intrusions were fine-grained noritic to pyroxenitic sills of the Marginal Zone which occur in contact with metamorphosed sediments beneath and above the Lower Zone. The Lower Zone north of the Ysterberg-Planknek Fault was emplaced into trough-like depressions forming chonolith-like intrusions within the Transvaal metasedimentary rocks and the Archean granite-gneisses (van der Merwe, 1976; Yudovskaya *et al*., 2013). Originally this Lower Zone was believed to be limited to satellite bodies cutting Archean Granite (van der Merwe, 1976), but is now known to form a sequence, up to 800 m thick, beneath the Platreef on Sandsloot and Turfspruit (Yudovskaya *et al*., 2013). The next unit holds the stratigraphic position of the Critical Zone and is called the Platreef. The Main Zone unconformably overlies the Platreef. It is approximately 2000 m thick and comprises gabbronorite and norite with minor anorthosite and pyroxenite layers and hosts a 100 m thick troctolitic horizon, 100 m above the base, which does not occur in the Main Zone in the rest of the BC (van der Merwe, 1976; Ashwal *et al*., 2005). The Main-Upper Zone boundary in the main BC was defined by the first occurrence of cumulus magnetite, which forms up to 20 magnetitite layers further up the sequence (SACS, 1980). However, Ashwal *et al*. (2005) defined the Main-Upper Zone boundary in the northern limb on the appearance of disseminated magnetite as detected by magnetic susceptibility measurements. This parameter placed the boundary ~50 m below the first cumulus magnetite in the Bellevue drill-core. These changes in magnetic susceptibility proved a useful correlation between borehole cores in the Waterberg project for definition of the Main-Upper Zone boundary area (Kinnaird *et al*., 2017).

5.3.2. The Platreef

The Platreef is developed north of the Ysterberg-Planknek Fault (Fig. 5.1) (Wagner, 1929; van der Merwe, 1976) as a series of mafic-ultramafic sills with incorporated interlayers of metasedimentary footwall rocks (Kinnaird *et al*., 2005). The Platreef carries Ni-Cu-PGE mineralisation of three different

types: massive sulphide bodies at the base, marginal or contact disseminated ore in hybrid rocks, and exoskarns as well as reef style mineralisation hosted by feldspathic pyroxenite and harzburgite at the top, near the boundary with the Main Zone (Yudovskaya *et al*., 2017). The variable footwall plays a controlling role in the PGM assemblage of the disseminated marginal style mineralisation along the Platreef strike (Holwell and McDonald, 2006; Nichol and Kinnaird, 2008). In the southern and northern sectors, where the footwall is unreactive quartzite and anhydrous gneiss, these floor rocks allow for limited fluid activity and the deposition of PGE was controlled by the presence of immiscible sulphide liquids (Holwell and McDonald, 2006; Maier *et al*., 2008). In the central sector, highly reactive footwall rocks such as dolomite and shale of the Malmani Subgroup and Duitschland Formation were dehydrated during metamorphism or assimilation and the fluid released remobilised PGE and BMS forming low temperature PGE mineralisation (Hutchison and Kinnaird, 2005). High-grade zones may locally occur within the disseminated sulphides in exoskarn, hybrid and magmatic rocks (Holwell *et al*., 2006; Klemd *et al*., 2016). Generally, contact style mineralisation and massive sulphides in the basal Platreef are typically characterised by a significantly lower tenor, a higher BMS abundance, lower Pt/Pd <1 and a higher Cu/Pd (Yudovskaya *et al*., 2017).

The reef style mineralisation occurs in uncontaminated pristine layers of feldspathic pyroxenite and harzburgite rimmed by persistent chromite seams at the top and the base (Yudovskaya *et al*., 2017). BMS abundance (<5%), Pt/Pd ratios (>1), sulphide tenor (as high as 600 ppm PGE) and PGM assemblages closely resemble that of the Merensky reef mineralisation: chromitites host predominant Pt-Pd sulphides grading into Pt-Fe alloy, whereas sperrylite and Pt-Pd bismuthotellurides become more abundant downwards.

The Platreef is not the only mineralised unit in the northern limb. To the south of the Ysterberg Planknek Fault, PGE mineralisation occurs in harzburgite and pyroxenites of the Lower Zone rocks on Grasvally (Hulbert and von Gruenewaldt, 1985) as well as on Moorddrift in more felsic gabbroic lithologies higher up in the stratigraphy (Maier and Barnes, 2010; Holwell *et al*., 2013). To the north, in the Main Zone, on the Harriet's Wish to Aurora sector, mineralisation is hosted in felsic gabbroic and anorthosite lithologies (Harmer *et al*., 2004; McDonald *et al*., 2017).

5.3.3. Waterberg Project Setting

The Waterberg Project is located 85 km north of Mokopane, north of the Hout River Shear Zone (HRSZ), within the Southern Marginal Zone of the Limpopo Belt, which is located between the Zimbabwe craton in the north and the Kaapvaal craton in the south. The Southern Marginal Zone is believed to represent

the metamorphosed and sheared section of the Kaapvaal craton thrusted upon the latter along the series of shear zones (van Reenen *et al*., 1992). A stage of long-lasting regional tectonism which temporarily coincided with, or slightly postdated the emplacement of the BC, resulted in significant uplift and erosion of the exposed parts of the complexes. The Waterberg Group sediments with a thickness from 3 to 7 km were deposited upon the weathered top of the Bushveld sequence between 1.9-2.0 Ga (Huthmann *et al*., 2016).

The intrusion in the Waterberg project area is a long lobe of Bushveld age (Huthmann *et al*., 2016; 2018) that forms a >24 km northern extension of the BC (Fig. 5.1) (Kinnaird *et al*., 2017). This extension to the northern limb generally strikes NE-SW and dips at 34-38° NW in contrast to the north-south strike of the northern limb south of the Hout River Shear Zone, although certain blocks may deviate due to structural and tectonic controls (PTM, 2016). The intrusive succession in the Waterberg project area has a thickness up to approximately 1200 m.

5.3.3. A. Waterberg Project Geology

The stratigraphy and geology of the Waterberg project is described in detail by Huthmann *et al*. (2016, 2018), McCreesh (2016) and Kinnaird *et al*. (2017), therefore only a brief overview of the stratigraphy and geology is given below.

The footwall rocks are Archean granite gneisses (Fig. 5.2), although most borehole cores intercept a mixing zone, formed by an interaction between the Waterberg Bushveld magma and the Archean granite-gneisses. This interfingering of alternating felsic-rich layers and pyroxenite-rich layers is locally known as a granofels (Kinnaird *et al*., 2017). The floor contains numerous thin bands of fine-grained mafic-ultramafic rocks from pyroxenite to lherzolite, gabbronorite and norite that may represent the first intrusive sills intruded into the basement granite-gneisses. The intercumulus assemblage may contain abundant quartz and quartz-feldspathic granophyric intergrowths indicating contamination and partial melting of the floor.

The basal Ultramafic Sequence (UmS) varies in thickness from 2.5 m to 100 m (McCreesh, 2016). It comprises a lower medium-grained olivine-pyroxenite, orthopyroxenite and feldspathic pyroxenite and an upper feldspathic harzburgite to mela-troctolite that generally shows extensive serpentinisation and chloritisation (Fig. 5.3). A mineralised horizon, called the F zone occurs within the UmS.

The boundary between the UmS and the overlying troctolite-gabbronorite-anorthosite (TGA) sequence is gradational and is interpreted to be the result of magmatic erosion and digestion of the ultramafic unit by surges of later troctolitic melts (Kinnaird *et al*., 2017). The TGA sequence is characterised by a

thick package of troctolite at the base, cyclically grading into medium- to coarse-grained olivine-gabbronorite and norite with minor feldspathic pyroxenite and anorthosite towards the top of the sequence. The TGA sequence ranges from 400 m to 850 m thick (McCreesh, 2016; Kinnaird *et al*., 2017). A mineralised horizon, called the T zone occurs at the contact between the TGA sequence and the Upper Zone (UZ), in a package of varying sulphide-bearing compositionally-varied rock types that include gabbronorite, mafic and ultramafic pegmatoids, anorthosite, feldspathic pyroxenite, feldspathic harzburgite and troctolite.

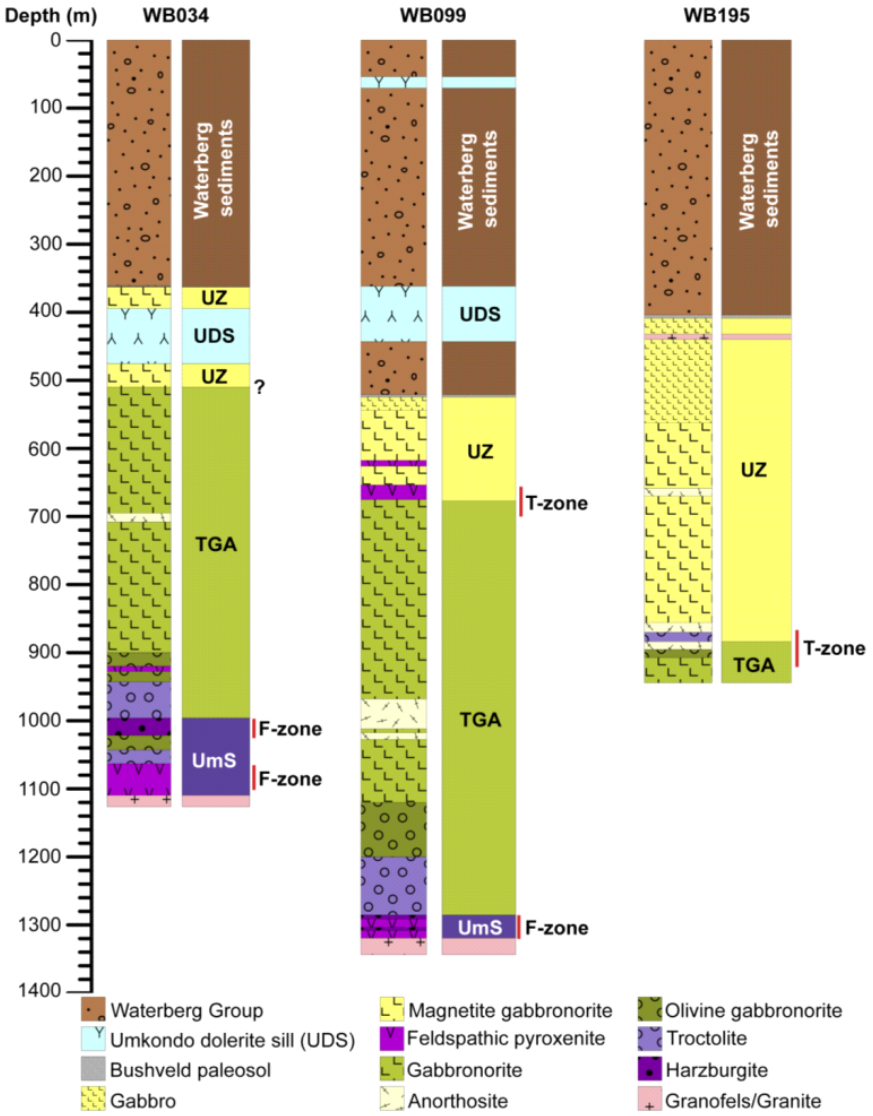

Figure 5.2: Schematic stratigraphic columns for WB034, WB099 and WB195 boreholes in the Waterberg exploration area. The first column shows the lithology, whereas the second column shows stratigraphic units: UmS – Ultramafic Sequence, TGA – Troctolite-Gabbronorite-Anorthosite sequence, T2 – lower mineralised sub-zone in the TGA, T1 – upper mineralised sub-zone in the TGA and UDS – Umkondo Dolerite sill.

The base of the UZ is determined by an increase in magnetic susceptibility. The UZ is dominantly magnetite gabbro and gabbronorite with minor anorthosite layers. The maximum thickness of the UZ reaches 500 m but thins northwards and is completely eroded in the centre and northern parts although preserved in the far northern part of the project area. Where the UZ is absent, either an attenuated TGA sequence or UmS are in contact with the overlying Waterberg sediments indicating that the variations of the UZ thickness are due to erosion prior to deposition of the Waterberg Group sediments.

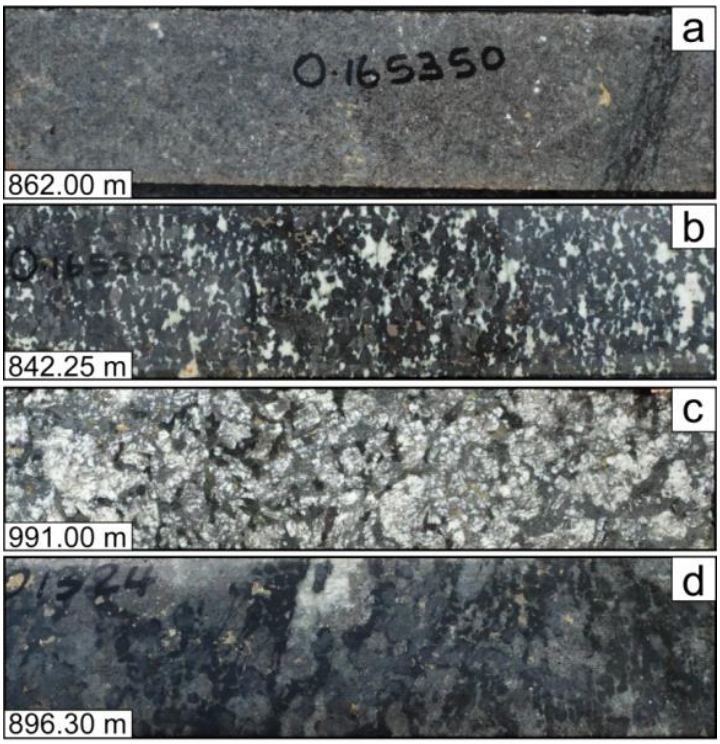

Figure 5.3: Typical lithologies of the mineralised zones from WB161D0 (F zone) and WB195D0 (T zone); (a) medium- to fine-grained feldspathic orthopyroxenite with disseminated sulphides within the F zone, (b) feldspathic harzburgite/mela-troctolite with disseminated sulphides within the F zone, (c) coarse-grained leucogabbro/anorthosite with interstitial chalcopyrite from the T2 subzone, (d) medium- to coarse-grained feldspathic harzburgite with disseminated sulphides from the T1 subzone. Photo of half-core cut samples 5 cm in diameter.

Towards the top of the Bushveld mafic succession, a highly altered zone, dominated by hematite and quartz is believed to be the weathered top of the intrusive rocks before the deposition of the overlying Waterberg Group sediments. The Setlaole and Makgabeng Formations of the Waterberg Group consist of arenites, sandstones and mudstones and pebbly conglomerates.

Dolerite sills or dykes with a maximum thickness of 200 m, but generally ~80 m thick intrude either the Waterberg sediments or the Bushveld mafic rocks although most typically they occur at the contact between the two. Age dating of a sill correlates with the 1.1 Ga Umkondo Igneous Province (Huthmann *et al*., 2016).

U/Pb dating of zircons from the mafic-ultramafic rocks of the Waterberg intrusive rocks have yielded ages of 2059±3 and 2053±5 Ma (Huthmann *et al*., 2016), indicating that the magmatic succession at the Waterberg project is coeval with the main BC (Zeh *et al*., 2015). The detrital zircons with the U-Pb isotope age of ~2045 Ma in the basal layer of the Setlaole Formation suggest that the roof and upper parts of the Bushveld sequence were removed within a short time span before the Waterberg Group sedimentation (Huthmann *et al*., 2016).

5.4. Methodology

Five boreholes, WB099 and WB195 (representative for upper T zone) and WB034, WB091 and WB165 (representative for a thick well developed basal ultramafic F zone with minor alteration) were selected for study based on company assay data and our logs of 10 boreholes. Results from continuous half core sampling assay by Platinum Group Metals (PTM) Ltd through the high-grade zones, from 602 m to 715 m in WB099 (upper T zone) and from 930 m to 1097 m in WB034 (lower F zone) are shown in Figures 4 and 5. Quarter-core samples were collected from the mineralised intervals.

The PGM assemblage was studied in 50 polished thin sections of ore samples and 10 heavy mineral concentrates (Table 5.1). The PGM concentrates were panned in tribromomethane from a manually crushed fraction <0.5 mm of the quarter-core samples weighing from 18 to 50 grams. The minerals were laid out using a needle and a tiny spatula in rows on carbon tape. Each row of PGMs was mapped using FEI200 and FEI400 field-emission scanning electron microscopes (SEM) in back-scattered electron (BSE) mode at the Microscopy and Microanalysis Unit (MMU) at the University of the Witwatersrand. The chemical compositions of each PGM were semi-quantitatively identified using a LINK energy-dispersive spectrometer (EDS). PGM sizes are shown in two-dimensional equivalent circle diameter (microns) and therefore, the PGM proportions are reported as percentage of sum of apparent grain diameters of the total in each sample (Table 5.1). This method is cost effective and provides more representative data on the proportion of PGMs compared to the analysis from polished thin sections because of higher volumes of material involved and preservation of micron-sized particles, which are commonly lost during polishing of heavy separate blocks. The polished sections were used for observation and photography of textures and intergrowths at the MMU as well as at IGEM RAS using a SEM JSM 5610 equipped with an EDS Two polished thin sections from the WB195-898.7 m sample of the T zone contain abundant tiny micron-sized disseminated PGM observed under SEM. Their duplicates were analysed by ALS Minerals using automated Mineral Liberation Analysis (MLA). The sections were analysed using the Sparse Phase Liberation Dual Zoom technique that is based on analysis of BSE images to locate PGMs and identify

their compositions using X-ray spectra. The SEM and MLA studies provided data on PGM associations (Table 5.2) as well as the PGM modal proportions and grain size distributions, which are obtained by analysis of the heavy mineral separates.

The quantitative electron-microprobe analysis of PGM (Tables 5.3 and 5.4) and sulphides (Supplementary Tables 5.5 and 5.6) was done on grains in polished sections using a Cameca SX100 wave-length microanalyser at the University of Johannesburg. Analyses were performed at 20 kV acceleration voltage and 40 nA sample current with 2 micron beam diameter. The following X-ray lines, spectrometer crystals, counting time for peak/background and standards (in brackets) were used: SKα, PET, 11/11, (FeS); FeKα, LLIF, 8/8, (Fe); CoKα, LLIF, 8/8, (Co); NiKα, LLIF, 8/8, (Ni); CuKα, LLIF, 8/8, (Cu); AsLα, TAP, 41/41, (As); SeLα, TAP, 35/35, (Se); OsMα, TAP, 44/44, (Os); RuLα, PET, 23/23, (Ru); RhLα, LPET, 21/21, (Rh); PdLα, LPET, 19/19, (Pd); AgLα, LPET, 19/19, (Ag); AgLα, LPET, 27/27, (AgS); SnLα, PET, 13/13, (Sn); SbLα, PET, 13/13, (Sb); TeLα, LPET, 12/12, (Te); IrLα, LLIF, 18/18, (Ir); PtLα, LLIF, 20/20, (Pt); AuLα, LLIF, 23/23, (Au); HgLα, LLIF, (HgS); PbMα, PET, 56/56, (PbS), BiMα, PET, 53/53, (Bi). Off-line corrections for interference were applied to avoid peak interferences for all elements according to a procedure described by Fialin *et al*., (1997). Secondary standard sample PGM1 of MINTEK (the Council for Mineral Technology, Johannesburg, South Africa) was analysed before analysis and reproducibility varied by less than 2%.

5.5. Results

5.5.1. Stratigraphy in boreholes WB034, WB099 and WB195

In WB034, the footwall rocks consist of quartz-rich granofels (Fig. 5.2). Overlying the basement rocks is the UmS which is ~110 m thick, composed of medium- to coarse-grained pegmatoidal feldspathic orthopyroxenite and harzburgite. The 557 m thick TGA sequence gradationally overlies the UmS and includes a ~81 m thick cross-cutting dolerite sill (Fig. 5.2). The TGA is dominated by medium- to coarse-grained “salt and pepper” textured troctolite at the base, cyclically grading upwards into olivine-bearing gabbronorite, gabbro and norite with minor anorthosite, feldspathic pyroxenite layers and pegmatoidal lenses. A 0.7 m thick palaeosol and haematised and mylonitised siltstone lies between the TGA and the overlying Setlaole Formation quartz-rich clast-supported conglomerate with sandstone and mudstone upwards.

WB099 is 1344 m long (Fig. 5.2). A ~25 m thick interval of granofels at the base of the borehole includes abundant quartz-feldspathic veinlets. The UmS is 179 m thick and consists of medium- to coarse-grained feldspathic pyroxenite at the base overlain by coarse-grained harzburgite and mela-troctolite with xenoliths of feldspathic pyroxenite. The TGA sequence has a gradational contact with the underlying

UmS. The TGA sequence from 1280 m to 602 m depth consists of basal barren troctolite grading into an olivine-bearing gabbronorite, gabbro and norite with minor anorthosite. The UZ is covered by a 3.5 m thick hematite-rich clay palaeosol along the erosional boundary with the overlying Waterberg matrix-supported conglomerate with quartz pebbles, and succession of intercalated sandstone and mudstone upwards.

Borehole WB195 is 944 m long (Fig. 5.2). It has a 60 m thick TGA package of medium- to coarse-grained gabbronorite, leucogabbro and anorthosite with minor olivine-rich intervals. The 475 m thick overlying UZ is marked by the appearance of titanomagnetite and consists of magnetite-bearing gabbronorite and leucogabbro with minor layers of anorthosite, olivine norite and leuco-troctolite. A 4.7 m thick palaeosol at the top of the UZ developed along the erosional boundary with the overlying Waterberg sediments mainly composed of medium- to coarse-grained sandstone with a basal quartz pebble conglomerate.

5.5.2. Stratigraphy of the mineralised zones

The F zone mineralisation is hosted in feldspathic pyroxenite that grades into feldspathic harzburgite upwards (Fig. 5.3a). Cumulus orthopyroxene (Mg# up to 84) and interstitial plagioclase (An# from 77 to 84 up to 88 according to Huthmann *et al*. (2018) are accompanied by lesser clinopyroxene; minor olivine relics (<15%) and occasional chromite grains. Fragments of granoblastic orthopyroxenite with well-defined contacts within the overlying feldspathic harzburgite are interpreted as xenoliths trapped by a later magma influx.

Feldspathic harzburgite typically has a poikilitic texture with coarser-grained orthopyroxene oikocrysts compared to smaller pyroxene grains in the pyroxenite. Olivine (Mg# up to 83-84) occurs as chadacrysts in orthopyroxene as well as rounded to amoeboid grains surrounded by interstitial plagioclase. Chromite commonly occurs as rare small euhedral and corroded grains forming, <1 vol. % of the rock, although may be accumulated into disseminated concentration in zones up to 20 cm thick. An increasing proportion of clinopyroxene results in the appearance of lherzolite with typical oikocrystic clinopyroxene and peritectic orthopyroxene rims around olivine grains. Phlogopite forms interstitial poikilitic grains and overgrowths on olivine and chromite. Magnetite is a secondary mineral accompanying pervasive serpentinisation and replacing chromite and sulphides.

The harzburgite has an irregular erosional or transitional contact with coarse-grained mela-troctolite, which is composed of cumulus olivine and plagioclase, and large oikocrysts of orthopyroxene (Fig. 5.3b). Olivine and pyroxenes in this unit are extremely altered to serpentine and chlorite with common relics of the pre-existing minerals remaining. Intervals with elongated harristic olivine up to 2-3 cm long with relics of corroded chromite (20-1000 µm) in interstitial plagioclase were observed. Above the

transitional poikilitic mela-troctolite a typical “salt and pepper” textured barren troctolite occurs, which eventually grades into an olivine-norite or gabbronorite, that represents the hanging wall to the F zone. Olivine has Mg# <77 in troctolite and between 64 and 73 in olivine norite. Its grains are significantly larger than those of plagioclase with the latter exhibiting both euhedral and interstitial habits.

The upper mineralised zone is subdivided into two subzones: the lower T2 and upper T1. It is separated from the underlying F mineralised zone by 100-600 m of a barren TGA. The T2 subzone (Fig. 5.3c) is hosted in medium- to coarse-grained gabbronorite, leucogabbronorite and leucogabbro to anorthosite. The T2 is characterised by distinctive elongated and rounded isometric milky-white plagioclase cores and crystals, which are saussuritised and filled with microinclusions of Fe-oxides. Whereas the T2 footwall gabbronorite is mostly composed of equigranular cumulus plagioclase, orthopyroxene (± inverted pigeonite) and clinopyroxene that is typical of the Main Zone in the rest of the BC, the T2 gabbro is characterised by a prevalence of cumulus plagioclase with both euhedral and oikocrystic subordinate pyroxenes. Euhedral (cumulus) titanomagnetite and ilmenite have the first appearance in the sequence, although, their sporadic coarse crystals occur in pegmatoidal lenses of the TGA rocks below. Another remarkable feature of the T2 subzone leucocratic rocks is the regular presence of quartz, amphiboles and chlorite as crusts around sulphides blebs.

The hanging wall to the T2 subzone is the Lower Pegmatoidal Anorthosite (LPA) with spotted and mottled textures of clinopyroxene oikocrysts. The appearance of olivine marks the boundary with the heterogeneous upper T1 subzone composed of intercalated thin layers and veins of feldspathic harzburgite and pyroxenite, olivine-bearing pyroxenite, troctolite and olivine norite as well as their pegmatoidal varieties (Fig. 5.3d). The discrete layers in the T1 subzone have an irregular distribution and varying thickness so the package resembles a zone of mingling between different magmas or crystal mushes. The upper contact with the Upper Pegmatoidal Anorthosite (UPA) is sharp although the latter may include thin vein-like injections of medium-grained olivine- and magnetite-bearing leucogabbro. The mottled and spotted texture of the UPA is composed of coarse plagioclase with large clinopyroxene and magnetite oikocrystic aggregates (2-3 cm). The magnetite content does not exceed 1-2 vol. %. The proportion of plagioclase in the UPA may locally decrease to 70 vol. % resulting in a pegmatoidal gabbro within the anorthositic unit.

5.5.3. Downhole PGE variations through the F and T zones

Variations in 2PGE+Au, base metal, S and Cr contents in core/sample WB034 (F zone) are shown in Fig. 5.4 based on exploration assay data of Platinum Group Metals (PTM). The F zone has S contents,

commonly > 0.02 wt. % S and up to 0.76 wt. % S, which decreases gradually downward to the base of the F zone. Above the F zone, still within the UmS, the S content decreases to below detection limits, although there are minor spikes up to 0.02 wt. % S within the thin harzburgite interlayers (Fig. 5.4). The S distribution correlates directly with Cu, Ni and PGE distribution at a 0.5 m sampling scale. Nickel has a perfect correlation with Cu and S in the high-grade zones, however, Ni shows elevated values in the intermediate ultramafic hanging wall, where Cu and S fall to background values. The mineralisation is mostly confined to orthopyroxenite, feldspathic harzburgite and mela-troctolite although in some cases can be associated with olivine-gabbronorite close to the base of the succession as seen in Fig. 5.4. The mineralised zone is characterised by an elevated Cr content (>0.1 wt. % Cr) compared to the hanging wall where the Cr content drops to <0.02-0.03 wt. % Cr (Fig. 5.4). The elevated Cr is mostly related to harzburgite and pyroxenite interlayers, whereas Cr minima in the ore zone characterise subordinate veins of low-Cr troctolite. The footwall of the F zone is also characterised by elevated but variable Cr content that reflects changing ultramafic and gabbroic lithologies. 2PGE+Au in the >25 m thick F zone of WB034 has an average of 5 g/t with a maximum peak of 10 g/t 2PGE+Au two meters above the Cr peak (0.33 wt. % Cr, Fig. 5.4).

The Cu/Pd value is a good indicator of sulphide melt enrichment due to a contrast in Cu and Pd partitioning coefficients into sulphide melt during exchange with silicate melts (Naldrett *et al*., 2009). The average Cu/Pd value in the Critical Zone of the BC is around 4000 and the lower Cu/Pd values indicate enhanced sulphide upgrading (Barnes and Maier, 2002; Naldrett *et al*., 2009). The Cu/Pd values in the F zone is around 500 (Fig. 5.4), similar to the ranges of the Merensky Reef (Naldrett *et al*., 2009) and the high-grade reefs at Turfspruit, Akanani and Sandsloot (Fig. 5.1) (Yudovskaya *et al*., 2017). The F mineralisation has a remarkably S-depleted character compared to the Merensky Reef and the Platreef, where S content ranges between 0.2-2.5 wt. % S at the same Cu/Pd values. Within the mineralised zone, the Pt/Pd ratio is fairly constant around 0.6 (Fig. 5.4) and the PGE comprise 65% Pd, 30% Pt with 5% Au (PTM, 2016).

Semi-massive sulphides occur in a few intersections at the base of the F zone, however, they have a much higher Cu/Pd ratio and are likely to represent marginal style mineralisation similar to the disseminated and massive PGE-Cu-Ni ore-bodies in the Platreef contaminated rocks.

The concentrations of metals and S, as well as metal ratios representative for the T zone, are plotted against stratigraphic height in core/sample WB099 (Fig. 5.5), where the T zone 2PGE + Au basket comprises 50% Pd, 30% Pt, and 20% Au on average (PTM, 2016). The almost 30-meter thick T2 subzone is hosted in gabbronorite to gabbro. The 2PGE+Au contents range between 2-7 g/t with a maximum of

12 g/t in this section. The base metals and S show good correlations with PGE+Au in the T2 subzone. The Au/Pt ratio of around 1 is remarkably high with the Au content reaching 4 g/t Au and the Au/Pt peaks up to 4. The Pt/Pd ratio in the T2 is fairly constant at 0.6 (Fig 5.5). Copper prevails over Ni with Cu content ranging from 0.01 to 0.73 wt. % Cu. The S content is similar to that in the F zone with the highest values not exceeding 0.2 wt. % S.

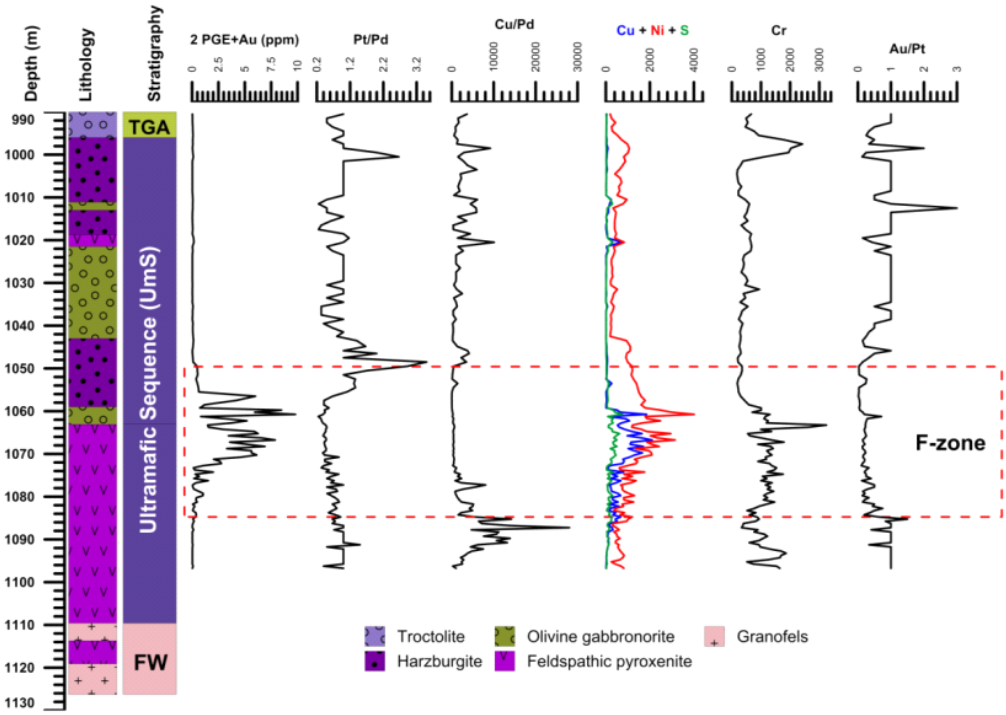

Figure 5.4: Variations of 2PGE+Au, Pt/Pd, Au, Cu, Ni, S, Cr and Au/Pt abundances through the WB034 section of the Ultramafic Sequence, F zone Data of 0.5 m sampling are shown by courtesy of Platinum Group Metals (PTM).

The overlying T1 subzone is mostly barren in WB099, which is a rather typical pattern. There is a minor increase in 2PGE+Au at the depth interval of 650-660 m within a thin layer of olivine-bearing feldspathic pyroxenite. The slightly elevated base metal contents at the base of the T1 are accompanied by elevated PGE tenors (Fig. 5.5).

Generally, the Cu content exceeds 0.6 wt. % Cu within the T zone and is higher than the Ni content. The higher Cu content results in an elevated Cu/Ni ratio, however, the latter does not necessarily correlate with a higher abundance of chalcopyrite or other Cu minerals rather it reflects the lower silicate Ni in the heterogeneous T zone compared to the ultramafic F zone. The whole T zone is also dominated by Pd, has the unusually high Au content and has significantly lower Cr values below 0.03 wt. % (Fig. 5.5) compared with the F zone (Fig. 5.4) and with other mineralised reefs of the BC. This is consistent with the gabbroic composition of host lithologies, the absence of chromite or Cr-spinels, and abundant

titanomagnetite and ilmenite in the T zone. The Cu/Pd ratio is <1000 in the high-grade intervals, although it drastically increases in the barren interlayers.

The Pegmatoidal Anorthosite carries sporadic elevated 2PGE+Au grades, although this unit is not always present.

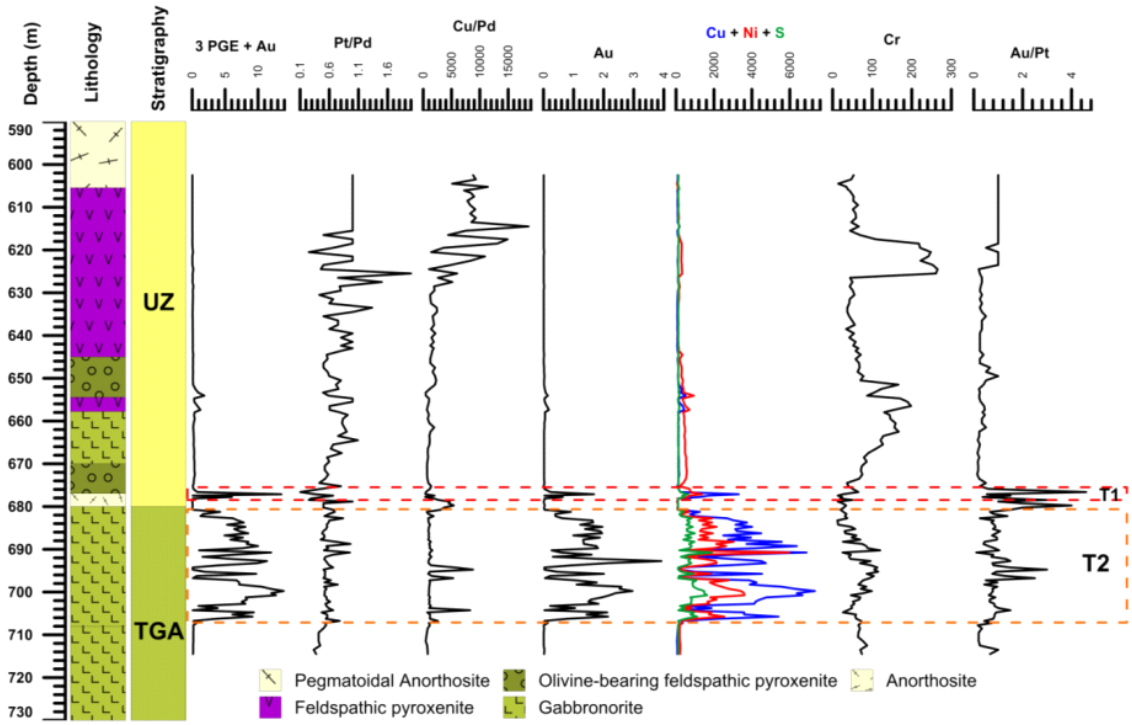

Figure 5.5: Variations of 2PGE+Au, Pt/Pd, Cu/Pd, Au, Cu, Ni, S, Cr and Au/Pt abundances through the WB099 section of the upper T zone. Data of 0.5 m sampling are shown by courtesy of Platinum Group Metals (PTM).

5.5.4. Sulphide Assemblages of the F zone

Base metal sulphides (BMS) commonly account for ~1-5 vol. % in the upper part of the zone, although they may form semi-massive ores with up to 25 vol. % sulphides at the base. Disseminated and blebby magmatic sulphides (pyrrhotite/troilite ~ 45%, chalcopyrite ~30%, pentlandite ~20% on average) are accompanied by minor pyrite, covellite, valleriite, cobaltite-gersdorfite and bornite. Typically, primary interstitial sulphides occur as a discontinuous network of blebs with a pyrrhotite core, and pentlandite and chalcopyrite closer to the margins (Figs. 5.6a, b, c). Similar textures in the Merensky Reef (Vermaak and Hendricks, 1976) and in the Platreef (Hutchinson and Kinnaird, 2005) have been interpreted to be a result of crystallisation of immiscible sulphide melts.

Troilite [FeS] and intermediate pyrrhotite [$Fe_{1-x}S$] (Suppl. Table 5.5) are recognised among Fe monosulphides in the F zone according to the criteria of Becker *et al*. (2010) for the Merensky Reef sulphides. These authors found that metal/S ratio and Ni content can be used to distinguish between troilite, intermediate and monoclinic pyrrhotite. Merensky Reef troilite is the most poor in Ni whereas

coexisting intermediate pyrrhotite is slightly richer up to 0.3 wt. % Ni and monoclinic pyrrhotite contains 0.44-1.3 wt. % (Becker *et al*., 2010). On the Waterberg project intermediate pyrrhotite contains up to 0.6 wt. % Ni and reveals rare flame-like pentlandite exsolutions. Troilite forms separate grains and lens-like exsolution lamellae in pyrrhotite. The Ni content in troilite is <0.09 wt. % (Suppl. Table 5.5). Troilite is not rare in the reefs of the BC and has been identified in a number of studies (Vermaak and Hendriks, 1976; Schouwstra *et al*., 2000; Cabri *et al*., 2008; Yudovskaya *et al*., 2017).

Several morphological varieties of pentlandite [$(Fe,Ni)_9S_8$] are found in polished sections. Coarse-grained fractured or brecciated pentlandite occurs mostly at the margins of interstitial sulphide blebs (Fig. 5.6a), and is also present within sulphide inclusions in coarse chromite (see Fig. 12d in Kinnaird *et al*., 2017). It contains 31-34 wt. % Ni and elevated, but variable amounts of Co (0.7-1.5 wt. %). Pentlandite exsolutions in pyrrhotite have the same major element chemistry as the coarse-grained variety, whereas pentlandite in irregular veinlets and disseminations among serpentinised silicates and secondary minerals is characterised by lower Ni (23-28 wt. % Ni) but the same elevated Co contents (Suppl. Table 5.5). Anhedral pentlandite associated with bornite (Fig. 5.6d) is Ni-rich with up to 42 wt. % Ni and is also Co-bearing (an. 2 in Suppl. Table 5.5). Both Ni-poor and Ni-rich pentlandite may be associated with native gold and PGM in intergrowths that imply their coeval deposition.

Chalcopyrite [$CuFeS_2$] is the most abundant Cu mineral, while cubanite [$CuFe_2S_3$] was only observed in sulphide inclusions in chromite. Rare bornite {Cu_5FeS_4] (Suppl. Table 5.5) and covellite [CuS] are secondary after primary chalcopyrite and may form emulsion-like intergrowths (Fig. 5.6d).

Primary pentlandite-chalcopyrite interstitial intergrowths are locally replaced by aggregates of newly formed Cu-Ni sulphides (Fig. 5.7a). The compositions of some secondary lamellar grains with persistent 24-27 wt. % Ni and 7.7-9.8 wt. % Cu and a nonstoichiometric formula [$Cu_{0.9\text{-}1.2}Fe_{4\text{-}4.3}Ni_{2.6\text{-}3.4}S_{7.6\text{-}7.7}$] are close to that of sugakiite [$CuFe_6Ni_2S_8$] or Cu-rich pentlandite [$(Fe,Ni,Cu)_9S_8$] (an. 12 and 36, Suppl. Table 5.5). The mineral is very similar to pentlandite under reflected light although its weak anisotropy indicates that it might be sugakiite. Exact identification would require X-ray study.

The intergrowths with this newly-formed sulphide (Fig. 5.7a) resemble the textures described by Kitakaze *et al*. (2011) for sulphides from the Horoman serpentinised peridotite, where sugakiite was first discovered. Tetragonal sugakiite from Horoman contains from 6 to 8 wt. % Cu (Kitakaze *et al*., 2011) and has a composition close to that of cubic Cu-rich pentlandite. Copper-rich pentlandite of secondary origin was described from mooihoekite-talnakhite-cubanite ores of the Noril'sk deposit to contain 7.5 wt. % Cu and has a formula [$(Fe_{5.52}Ni_2Cu_{0.88})_{8.4}S_8$] (Genkin *et al*., 1981).

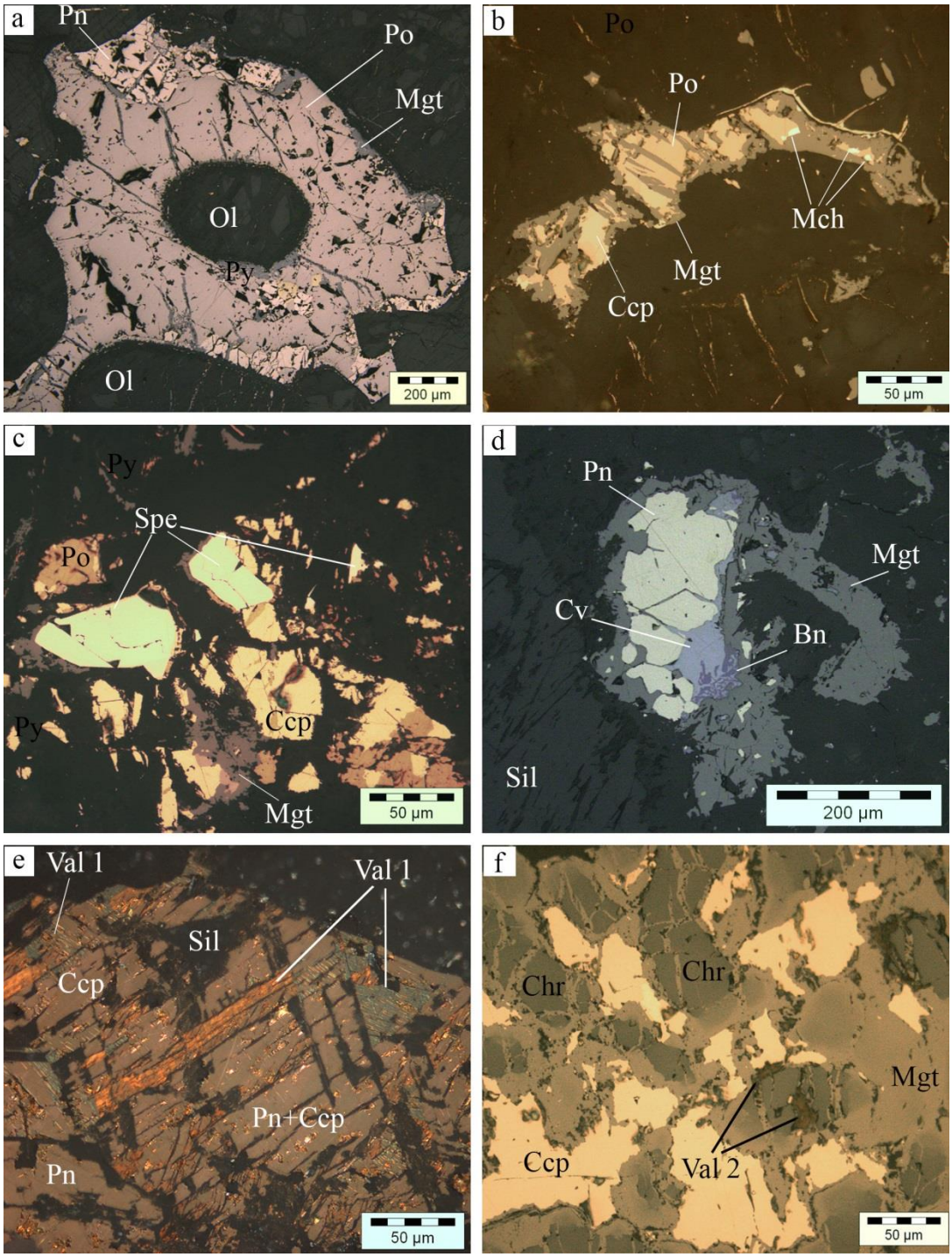

Figure 5.6: Photomicrographs of sulphides in the F zone under reflected light: (a) pyrrhotite (Po) and pentlandite (Pn) with minor chalcopyrite and magnetite (Mgt) rimming an altered olivine (Ol) grain (WB165–1118.1), (b) chalcopyrite and pyrrhotite (Ccp, Po) replaced by secondary magnetite (Mgt) with minor inclusions of moncheite (Mch), and pyrrhotite along the cleavage in silicates (WB034–1060.85), (c) euhedral crystals of sperrylite (Spe), surrounded by chalcopyrite and pyrrhotite (Ccp, Po), replaced by secondary magnetite (Mgt) in serpentinite (WB034-1060.85). (d) Ni-rich pentlandite (Pn) associated with covellite (Cv) and bornite (Bn) and rimmed by magnetite (Mgt) (WB165–1109.4), (e) chalcopyrite and pentlandite (Ccp, Pn) replaced by valleriite-like mineral 1 (Val 1) (WB034–1060.85), (f) Ni-rich chalcopyrite (Ccp) interstitial between chromite (Chr) grains, replaced by magnetite (Mgt). Valleriite-like mineral 2 (Val 2) is developed after phlogopite and serpentine in brecciated chromite (WB034–1060.85); (a-d and f) – plane polarised, (e) – cross-polarised light.

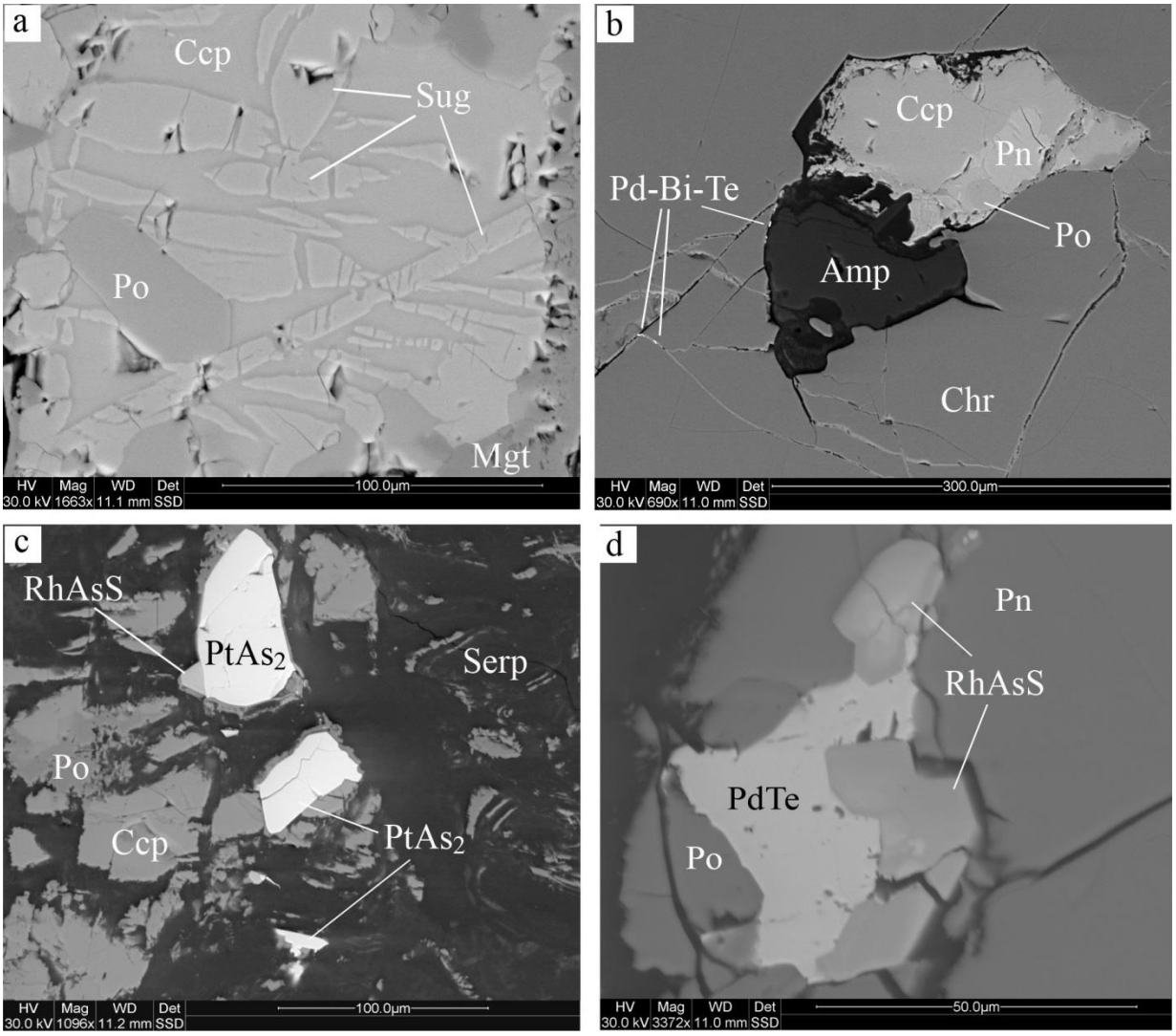

Figure 5.7: BSE images of PGM and sulphide assemblages of the F zone in polished sections in core WB034: (a) lenses and lamella of probable sugakiite (Sug, an 12 and 36, Suppl. Table 5) in association with chalcopyrite (Ccp, an. 13-14, Suppl. Table 5) and pyrrhotite (Po, an. 22-23, Suppl. Table 5) in sulphide bleb rimmed by magnetite (Mgt) (1060.85 m), (b) inclusion in chromite (Chr) composed of amphibole (Amp), chalcopyrite (Ccp), pentlandite (Pn) and pyrrhotite (Po). Tiny particles of Pd-Bi-Te mineral are located along fractures in chromite (1060.85 m), (c) brecciated sperrylite ($PtAs_2$, an. 1-6, Table 3) and hollingworthite (RhAsS, an. 8 and 9, Table 3) among pyrrhotite (Po) and chalcopyrite (Ccp) replaced by serpentine (Serp) (1060.85 m), (d) euhedral hollingworthite (RhAsS, an. 10-13 in Table 3) with Ir- and Pt-richer cores in association with kotulskite (PdTe), pyrrhotite (Po) and pentlandite (Pn) in feldspathic harzburgite (1060.93 m).

Two valleriite-like minerals (valleriite – [$4(Fe,Cu)S*3(Mg,Al)(OH)_2$]) are present in the F zone. One valleriite-like mineral is a dirty yellow in colour under reflected light, is bireflectant and strongly anisotropic from cyan-blue to bright orange (Fig. 5.6e) with an obvious cleavage and lamellar brittle structure similar to a variety of valleriite after chalcopyrite, described by Ramdohr (1969). Partial microprobe analysis of this valleriite-like mineral gives 1-3 wt. % Ni, 20-21 wt. % Fe, 19-22 wt. % Cu and 23-24 wt. % S with <70 wt. % total. Energy-dispersive and electron microscope analysis confirms an absence of other elements (such as Mg, Al and halogens) so the low totals are perhaps accounted for by

the presence of hydroxyl layers in a layered lattice of the valleriite-type. Magnesium-free valleriite is known from massive talnakhite ores of the Noril'sk deposit, whereas different varieties are abundant in other ore types (Genkin *et al*., 1981). While the lamellar texture of the Waterberg valleriite-like mineral 1 is similar to that of valleriite formed after chalcopyrite (Ramdohr, 1969) (Fig. 5.6e), both optical features and composition do not exactly fit the known mineral. The second type of valleriite-like mineral is developed both after phlogopite and serpentine, where they are associated with chalcopyrite (Fig. 5.6f). This mineral is distinguished by a brown colour and strong anisotropy and contains sets of both chalcophile (Cu, Fe, S) and siderophile elements (Mg, Al, Si, K, Cl and Cr) according to the EDS analysis. Both valleriite-like minerals reveal features of secondary origin and are found in serpentinised harrisitic troctolite in associations with chlorite, phlogopite, sulphides and altered chromite.

Primary sulphide blebs in the F zone are also replaced or rimmed by secondary Fe oxides as well as by late-stage and secondary silicates such as tremolite, phlogopite, serpentine and chlorite (Fig. 5.6e, f). In addition, a minor carbonate replacement accompanies serpentinisation. Secondary Ca-Mg-Fe carbonates, calcite and talc forms rare thin veinlets in the samples. However, disseminated chromite grains and their sporadic segregations may be selectively replaced by carbonates with a formation of stichtite [$Mg_6Cr_2CO_3$ (OH) 16x4H_2O]. As a rule, chromite replaced by carbonate is associated with a much more common replacement by magnetite and hercynite, therefore, complete psuedomorphs after chromite are eventually composed of Cr-Mg-carbonate, magnetite, hercynite and later hematite. Chromite replacement by secondary magnetite is related to both serpentinisation and exchange with BMS. In the latter case, chromite can be completely replaced with the blurred shadow of Cr-magnetite relics among massive magnetite indicating the earlier presence of chromite (Fig. 5.6f). Massive crystals of magnetite in troctolite, as opposed to disseminated serpentinisation-related magnetite, are most likely complete pseudomorphs after chromite.

The common and diverse replacement textures indicate a much higher initial abundance of chromite and sulphides in the F zone. It can be roughly estimated based on polished section observations that half of the magmatic S (with accompanying Cu and Ni) as well as more than half of the Cr were removed mostly due to major replacement by magnetite and subordinate carbonisation. The secondary sulphides are mostly formed within the limits of the pre-existing sulphide aggregates.

5.5.5. Sulphide Assemblages of the T zone

Sulphides account for ~ 1-2 vol. % in the T1 and ~ 5-7 vol. % up to 10 vol. % in the T2 subzone. Sulphides include chalcopyrite, pentlandite, pyrrhotite, arsenopyrite [FeAsS], secondary millerite [NiS], pyrite,

galena, sphalerite and bornite (Fig. 5.8). Two main sulphide assemblages occur in the ores: a primary magmatic assemblage (~ 40% pyrrhotite, ~30 % chalcopyrite, ~30 % pentlandite) (Fig. 5.8b) and a secondary assemblage (~40 % millerite, ~35% chalcopyrite, ~15% pyrite) (Fig. 5.8c). Minerals of the secondary assemblages are superimposed onto primary ones through the whole zone, although they are more widespread in more altered rocks and are predominant in gabbroic pegmatoids.

The textures of primary sulphides are blebby, interstitial and finely disseminated (Fig. 5.8), and can be ascribed to segregation and migration of immiscible sulphide melts. BMS tend to occur as irregular or rounded inclusions inside titanomagnetite (Fig. 5.8a). Pentlandite occurs as fractured granular crystals (an. 1-6, Suppl. Table 5.6) and as flames-like exsolutions in pyrrhotite (sees Fig. 17a in Kinnaird *et al*., 2017). Flame-like pentlandite may locally be recrystallised into skeletal herring-bone aggregates arranged along boundaries of deformational twins in pyrrhotite. Chalcopyrite (an.7-10, Suppl. Table 5.6) is found at the margins of aggregates with pentlandite and pyrrhotite and as separate vein-like segregations. Margins of sulphide aggregates are corroded and replaced by late magmatic amphiboles, chlorite and quartz. Pentlandite contains 35-37 wt. % Ni and up to 1.6 wt. % Co. Chalcopyrite is characterised by elevated Ni up to 0.5 wt. % Ni. Pyrrhotite is subordinate because of widespread conversion into pyrite.

Secondary sulphides replace primary magmatic sulphide blebs and interstitial aggregates and also form new crusts, pseudomorphs after silicates and titanomagnetite, or veinlets and disseminations.

Pyrite is a major mineral in the T zone and is predominant in the Upper and Lower Pegmatoidal Anorthosites in particular. Pyrite forms (i) euhedral crystals with sporadic chalcopyrite and pyrrhotite inclusions; (ii) symplectitic intergrowths with chalcopyrite and millerite (Fig. 5.8c); (iii) replacement after titanomagnetite; (iv) euhedral metacrysts in silicates rimmed by chlorite and quartz; (v) symplectitic intergrowths with magnetite (Fig. 5.8d) and gangue silicates; (vi) crusts and crusty veins around and across sulphide aggregates (Fig. 5.8e). Up to 1.4 wt. % Ni and 2.6 wt. % Co was measured in some pyrite grains (an. 11-14, Suppl. Table 5.6). A pyrite-millerite-chalcopyrite association is indicative of T mineralisation. Millerite occurs together with pyrite and chalcopyrite in the absence of pentlandite with the latter likely being replaced by millerite and pyrite (Fig. 5.8a, c, d). Euhedral magmatic titanomagnetite is common and associated with ilmenite grains and lamellae (Fig. 5.8a), whereas secondary magnetite replacement is not as widespread as in the F zone. Titanomagnetite is often replaced completely by silicates and pyrite, whereas remnants of ilmenite plates remain (Fig. 17b in Kinnaird *et al*., 2017).

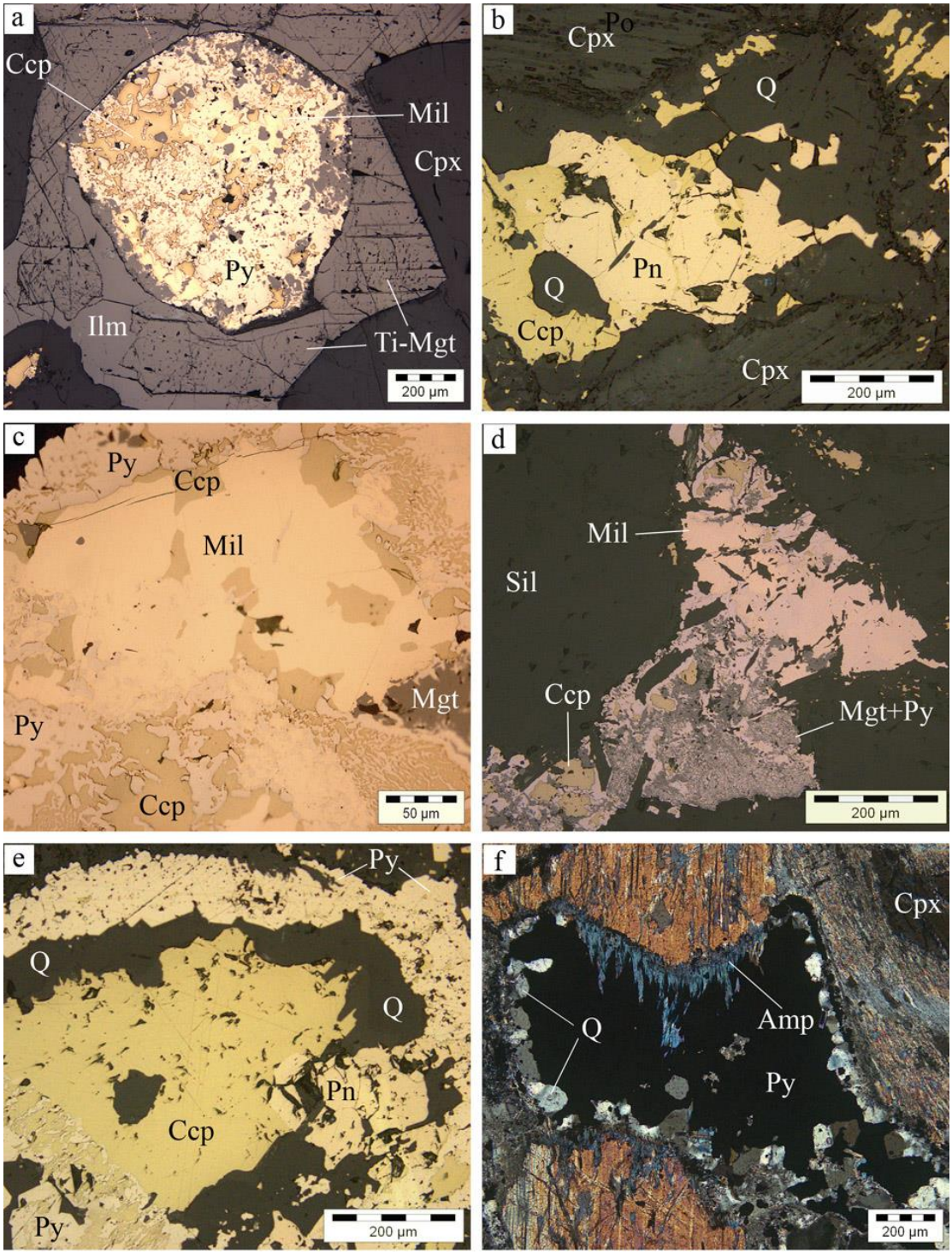

Figure 5.8: Photomicrographs of sulphide assemblages of the T zone: (a) millerite-chalcopyrite-pyrrhotite (Mil, Ccp and Py) association after a primary sulphide bleb inside a larger titanomagnetite-ilmenite intergrowth (Ti-Mgt and Ilm) in gabbronorite (Cpx – clinopyroxene) (WB165-493 m), (b) relics of primary interstitial pentlandite-chalcopyrite (Pn, Ccp) assemblage rimmed by quartz (Q) crust among cumulus clinopyroxene (Cpx) (WB195-902.3 m), (c) millerite (Mil) within pyrite-chalcopyrite (Py, Ccp) symplectitic intergrowths (WB165-493 m); (d) millerite (Mil) and chalcopyrite (Ccp) intergrowth with pyrite-magnetite (Py, Mgt) symplectite within silicates (Sil) (WB165-493 m), (e) chalcopyrite (Ccp) and chalcopyrite-pyrite symplectites rimmed by quartz (Q) and pyrite (Py) (WB195-902.3 m), (f) pyrite (Py) rimmed by quartz-amphibole (Q, Amp) crust interstitial to cumulus clinopyroxene (Cpx) (WB195-902.7 m); (a-e) reflected light, (f) cross-polarised transmitted light.

Quartz and chlorite are closely associated with secondary sulphide assemblages (Fig. 5.8f). Quartz rims, commonly 50-200 microns thick are associated with amphibole, chlorite and subordinate carbonate and epidote. Sulphides rimmed by quartz in most cases, are represented by secondary assemblages with relics of primary pentlandite and pyrrhotite. The amount of quartz is highly variable (0.5-5 vol. %) through the T zone and does not correlate with the stratigraphic height, changes in rock types, sulphide content or PGE grades.

5.5.6. Platinum-group minerals (PGM)

Overall, approximately 1000 grains of PGM and native gold were recovered in the 10 heavy separates from the F zone in WB034 and from the T zone in WB099 (Table 5.1). Almost 500 additional grains were found in the 5 polished sections from the thick T zone in WB195 under SEM with manual grain counting and measurements (Table 5.2). Two duplicates of WB195-898.7 m sections were repeatedly analysed by MLA in the ALS commercial laboratory and gave 325 PGM particles (Table 5.2). Size of PGM grains in sections and separates varies from <1 to 100 microns with a few bigger grains up to 150 microns.

All PGM were Pd, Pt and Rh minerals, with no Ru, Ir and Os minerals being identified. The PGM minerals were grouped into; (1) Pt-Pd bismuthotellurides; (2) sperrylite $PtAs_2$; (3) Pt-Rh sulpharsenides; (4) minerals of the system Pd-Ni-As; (5) Pt-Fe alloys; (6) Pt-Pd (± Ni) sulphides; (7) minerals of the system Pt-Pd-Sn, and (8) Au-Ag alloys. The relative abundance of different PGM types indicates that there are two very different dominant assemblages for the F and T mineralised zones in the Waterberg project (Table 5.1 and 5.2).

F mineralised zone

Sperrylite $PtAs_2$ is the dominant PGM that is indicative of the F zone and accounts for up to 82 % of the PGM assemblage (Table 5.1) although its proportion decreases downwards into the orthopyroxenite of the mineralised zone. Sperrylite occurs as intergrowths with other PGM (Figs. 5.9b, c and 5.7c), along the margins of BMS and as isolated crystals in secondary silicates where features indicate sulphide removal (Fig. 5.6c). It contains traces of Fe (up to 0.6 wt. %), Ir (up to 0.5wt. %) and lesser Ni and Cu (Table 5.3).

Twenty-eight grains of minerals from the system Pd-Ni-As (majakite PdNiAs and menshikovite $Pd_3Ni_2As_3$) and palladoarsenide Pd_2As were encountered in the heavy separates (Figs. 5.9a, d, f). They are mostly associated with other PGM and Au-Ag alloys, in which they form multiple inclusions up to 20-microns

long (Fig. 5.9d). Rare stibiopalladinite ($Pd_{5+x}(Sb, As)_{2+x}$) forms complex intergrowths with menshikovite ($Pd_3Ni_2As_3$) (Fig. 5.9*f*).

Table 5.1: Abundances and proportions (area %) of the PGM types in the heavy separates from the Waterberg deposit. The F zone is represented by mineralisation in feldspathic harzburgite to melatroctolite in the borehole WB034. The T zone is represented by mineralisation in gabbronorite and magnetite gabbro in the borehole WB099. D – apparent grain diameter in microns.

Chemical Composition	**Pt-Fe**		**Pd-Ni-As**		**Pd-Te**		**Pt-Pd-Bi-Te**		**$PtAs_2$**		**Au-Ag**		**(Rh,Pt)AsS**		**Total**	
depth Interval, m	# grains	% of total D	# grains	% of total D	# grains	% of total D	# grains	% of total D	# grains	% of total D	# grains	% of total D	# grains	% of total D	# grains	Apparent equiv D, microns
F zone in WB034																
1060.30-1060.45	-	-	11	15.2			12	12.2	**50**	**69.7**	2	1.9	7	1.1	77	1800
1060.85-1061	-	-	4	3.9			17	9.5	**118**	**76.4**	7	8.9	5	1.2	148	3300
1061.06-1061.20	-	-	2	7.3			2	9.4	**41**	**81.6**	-	-	1	1.7	46	1170
1061.45-1061.61	-	-	-	-			1	21.4	**4**	**78.6**	-	-	-	-	5	140
1061.61-1061.83	-	-	9	7.5			12	11.6	**60**	**63.8**	4	9	26	8.2	111	1945
1067.57-1067.70	2	0.7	2	1			67	32	**131**	**57.1**	11	6.8	11	2.5	224	6100
T zone in WB099																
698.67-698.84					11	24.1	**24**	**65**	1	0.9	6	10.3			42	1740
699.40-699.60					23	24.6	**110**	**63**	-	-	19	12			152	4585
700.00-700.37					10	11.9	**87**	**83**	-	-	7	4.7			104	3600
705.50-705.75					3	1.6	**132**	**91**	4	0.5	15	7.2			152	5145

Bismuthotellurides of Pt and Pd comprise michenerite PdBiTe (Fig. 5.8c), maslovite PtBiTe (Fig. 5.9b), moncheite $PtTe_2$ and kotulskite Pd(Bi, Te) (Fig. 5.7d) and account for 9-32 % of PGMs (Figs. 5.9c and 5.7b, d). They are mostly intergrown with pentlandite and rarely with chalcopyrite and pyrrhotite, form exsolutions inside sulphides as well as thin rims around sulphide aggregates (Fig, 5.6b). Bismuthotellurides may contain up to 4.6 wt. % Pb (Table 5.3).

Hollingworthite (Rh, Pt, Ir, Os)AsS is also a mineral indicative of the F zone; around 50 grains from 1 to 25 µm in size were recovered in the heavy separates (Table 5.1), while more were detected under SEM as overgrowths on the faces of larger euhedral sperrylite crystals (Figs. 5.9c and Fig. 5.7c), in association with Ni-Co sulpharsenides and Pd bismuthotellurides as well as zoned euhedral crystals intergrowing with other PGM (Fig. 5.7d). All analysed compositions belong to the Rh-dominant end-member of the hollingworthite-irarsite-platarsite series (Table 5.3).

Two grains, ~20 µm in diameter, composed of intimate fine intergrowths of a Pt-Fe alloy and pyrrhotite were identified in the heavy separates in WB034. The nonstoichiometric Pt-Fe alloys are represented by xenomorphic lumpy particles 0.1-2 microns in size (Fig. 5.10a); and are confined to or arranged along mircofractures in pyrrhotite, whose internal part is devoid of inclusions of Pt-Fe alloy. Euhedral isoferroplatinum and cooperite as well as symplectitic intergrowths of isoferroplatinum with BMS are typical for the reef-style mineralisation in chromitite seams of the BC (for example, Fig. 40-2 in Cabri, 2002; Yudovskaya *et al*. 2017). However, the morphology of alloys in the intergrowths observed here is different and may have resulted from later alteration of the primary magmatic assemblages.

Rare electrum (Au-Ag alloy) accounts for ~5% of the noble metal minerals (PGE + Au). It is preferentially associated with secondary silicates, other PGM (Fig. 9d) and rarely with sulphides and sulpharsenides (Fig. 5.9e). Based on results of microprobe (Table 5.3) and EDS analysis, alloys range in composition from Au_5Ag_5 to $Au_{75}Ag_{25}$.

In addition, two grains of atheneite $(Pd,Hg)_3As$ (Fig. 5.10b) and a grain of sopcheite $Ag_4Pd_3Te_4$ from 10 to 15 µm in size were found in the WB034 heavy separates.

Although we did not calculate weight percentage of PGE comprised in discrete PGM, a rough Pt/Pd values can be approximated from the PGM proportions in Table 5.1. The fairly constant whole rock Pt/Pd of 0.6 within the F zone is obviously inconsistent with the Pt/Pd ratio of ~3 to 6 calculated from the PGM proportions. This imbalance can be explained by an assumed Pd storage in pentlandite that is a typomorphic feature of the Bushveld reef style and low sulphide types of mineralisation (for example, Klemd *et al*., 2016).

Table 5.2: Proportions (area %) of the PGM types in the polished sections of poikilitic leucogabbronorite of the T2 subzone in core WB195 according to the MLA results and grain counting under the scanning electron microscope (SEM).

Chemical Composition	**Pt-Pd-Ni-S**		**Pt-Pd-Bi-Te**		**Pt-Pd-Sn**		**Au-Ag**		**Total**		**Association**	
Depth Interval (m)	# grains	% of total D	# grains	% of total D	# grains	% of total D	# grains	% of total D	# grains	Apparent equiv D, sq. microns	area % in silicates	area % in sulphides
896.3-SEM	-	-	**105**	**91.9**	1	1.9	8	6.6	114	663	80	20
897.15-SEM	-	-	**30**	**100**	-	-	-	-	30	294	80	20
898.7-SEM	-	-	**144**	**86.1**	33	6.9	14	7	191	1238	100	-
898.7-MLA	4	0.1	**183**	**86.8**	51	3.8	87	9.3	325	-	95	5
903.2-SEM	-	-	**49**	**94.1**	-	-	2	5.9	51	372	60	40
905.6-SEM	12	20.8	**83**	**70.9**	2	0.8	11	7.6	108	515	98	2

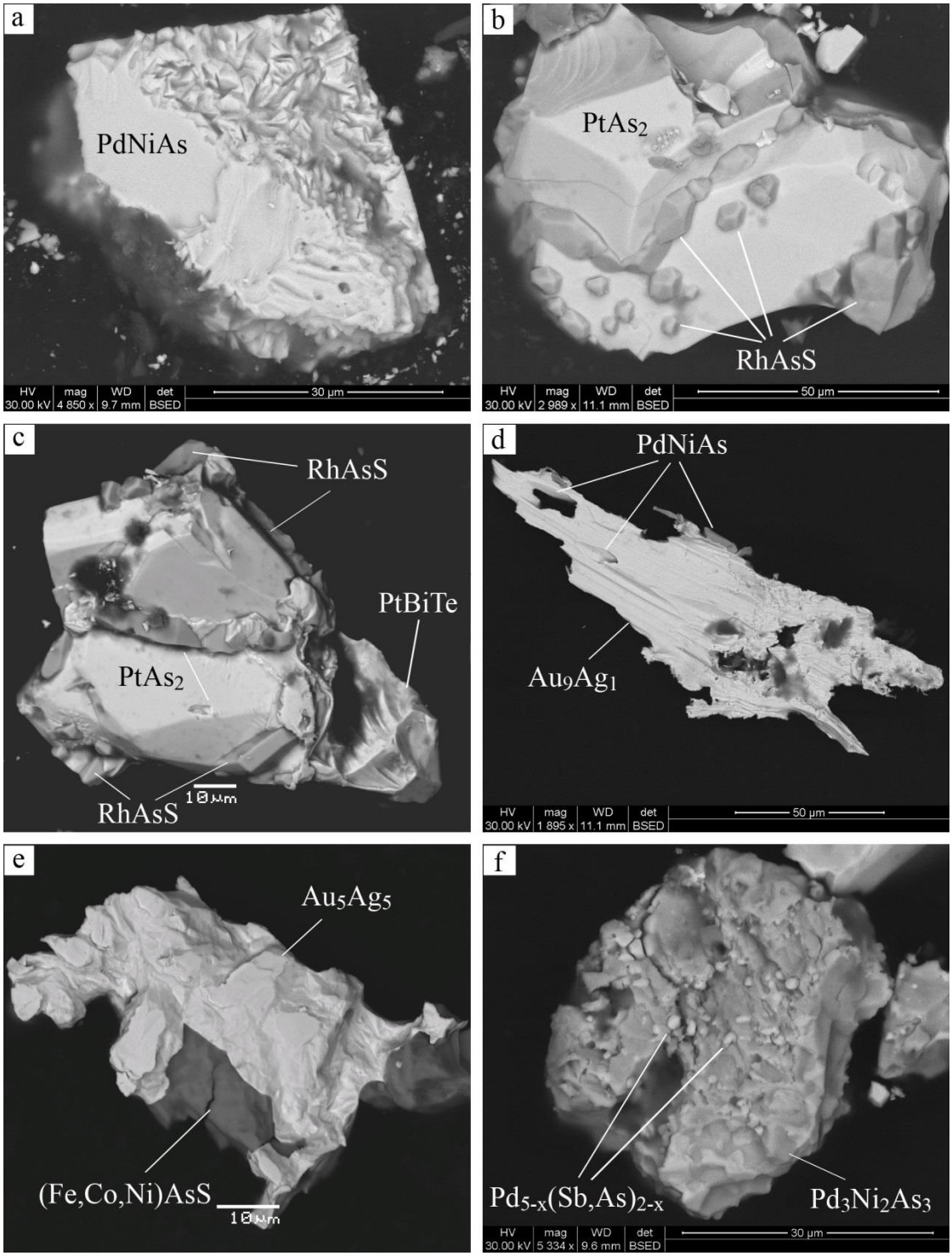

Figure 5.9: BSE images of typical PGM grains in heavy mineral separates of the F zone in core WB034: (a) majakite (PdNiAs) with prints of secondary silicates (1060.3 m), (b) euhedral sperrylite ($PtAs_2$) with epitaxitic hollingworthite (RhAsS) on its faces (1061.6 m), (c) an intergrowth of maslovite (PtBiTe) and sperrylite ($PtAs_2$) with epitaxitic hollingworthite (RhAsS) (1067 m), (d) native gold (Au_9Ag_1) with inclusions of majakite (PdNiAs) (1061.6 m), (e) Au-Ag alloy (Au_5Ag_5) with inclusions of cobaltite (Fe,Co,Ni)AsS (1018.00 m), (f) inclusions of stibiopalladinite ($Pd_{5+x}(Sb)_{2+x}$) in menshikovite ($Pd_3Ni_2As_3$) (1060.3 m).

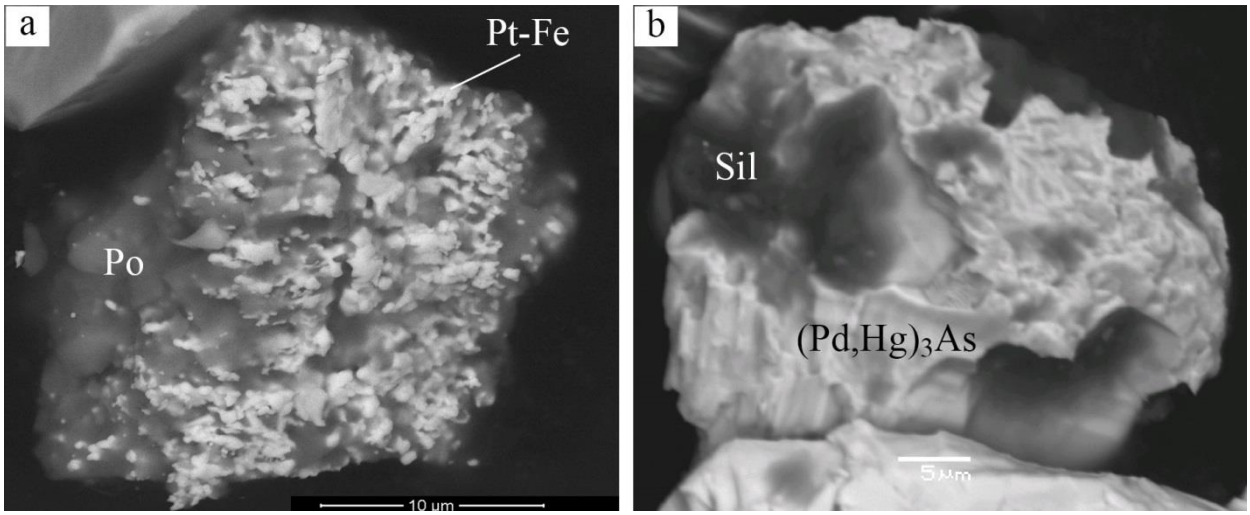

Figure 5.10: BSE images of rare PGM from the F zone in core WB034: (a) intergrowing Pt-Fe alloy and pyrrhotite on surface of a pyrrhotite (Po) particle (1067 m), (b) surface of atheneite $(Pd,Hg)_3As$ with ingrowths and prints of fine-grained hydrous silicates (1019 m).

T mineralised zone

The T2 subzone of WB099 is mainly dominated by Pt-Pd bismuthotellurides with no significant change through the mineralised package (Fig. 5.11a, b, Table 5.4). The uppermost sample (698 m) of the T2 hosts merenskyite ($PdTe_2$), kotulskite (PdTe), moncheite ($PtTe_2$), froodite ($PdBi_2$) and insizwaite ($PtBi_2$) associated with Au-Ag alloy and minor sperrylite. From 699 m depth downwards, the mineralisation is dominated by moncheite and Au-Ag alloys with inclusions of palarstannide. Merenskyite, moncheite and Au-Ag alloys are present 1 m below at a depth of 700 m. At the base of the T zone (705 m) mineralisation consists of merenskyite and moncheite, with Au-Ag alloys with inclusions of kotulskite. Sperrylite, mertieite I and palarstannide are rare.

Pt-Pd bismuthotellurides account for up to 100 vol. % through the T zone (Tables 5.1 and 5.2). Moncheite forms generally the largest layered crystals (Fig. 5.11a, b) up to 100 µm in size. Bismuthotellurides form rims at the margins of the BMS blebs (Fig. 5.12a), intergrowths with chalcopyrite and with each other (Fig. 5.11c). All tellurides are commonly associated with hydrous silicates (up to 100 % association, Table 5.2) where sulphides have been removed or replaced.

Sperrylite is very rare in the T zone with <1 vol. % (Table 5.1), as compared to the <82 vol. % in the lower F zone. Five euhedral crystals between 5 and 15 µm in size were found in the WB099 separates, whereas no sperrylite was found in the WB195 samples. The sperrylite crystals are associated with Au-Ag alloy (Fig. 5.10d) and hydrous silicates.

Table 5.3: Representative electron microprobe analyses of PGM (wt. %) in the F zone from the cores WB034 and WB091.

B.H.I.D	No.	Depth	Ag	As	Au	Bi	Co	Cu	Fe	Ir	Ni	Os	Pb	Pd	Pt	Rh	Ru	S	Te	Total
Sperrylite																				
WB034	1	1060.85	-	42.85	-	-	-	0.11	0.25	0.14	0.15	-	-	-	55.54	-	-	0.28	-	99.32
WB034	2	1060.85	-	43.02	-	-	-	-	0.11	0.50	0.08	0.05	-	-	55.65	-	-	0.21	-	99.62
WB034	3	1060.85	-	43.01	-	-	-	0.06	0.39	0.49	0.29	-	-	-	55.14	-	-	0.16	-	99.54
WB034	4	1060.85	-	43.22	-	-	0.04	0.20	0.63	0.54	0.36	-	-	-	54.70	-	-	0.26	-	99.95
WB034	5	1060.85	-	42.79	-	-	-	-	0.30	0.53	0.18	0.05	-	-	55.31	-	-	0.24	-	99.40
WB034	6	1060.85	-	43.18	-	-	-	0.13	0.42	-	0.26	-	-	-	55.32	0.09	-	0.32	-	99.72
WB091	7	474	-	42.93	-	-	-	0.10	0.60	0.53	-	-	-	-	55.59	-	0.05	0.23	-	100.03
WB091	8	474	-	43.73	-	-	-	0.39	0.60	0.19	-	0.05	-	-	55.16	0.09	-	0.19	-	100.40
WB091	9	474	-	43.94	-	-	0.04	0.07	2.13	0.14	1.42	-	-	-	54.68	0.10	-	0.46	-	102.98
Hollingworthite																				
WB034	10	1060.85	0.12	35.41	-	-	1.74	0.06	1.61	0.12	1.53	0.40	-	3.81	6.18	32.51	1.90	14.97	-	100.36
WB034	11	1060.85	-	35.91	-	-	2.00	0.16	1.89	-	1.55	0.24	-	3.70	5.07	33.44	1.80	15.15	-	100.91
WB034	12	1060.93	-	34.58	-	-	1.62	-	0.98	-	1.06	0.64	-	4.04	3.07	35.44	2.26	15.63	-	99.32
WB034	13	1060.93	-	35.61	-	-	2.26	-	1.39	0.14	2.01	0.73	-	6.76	1.90	30.07	3.25	15.38	-	99.50
WB034	14	1060.93	-	30.78	-	-	0.47	-	0.61	17.56	0.66	1.64	-	0.68	10.60	20.52	1.28	13.16	-	97.96
WB034	15	1060.93	-	31.36	-	-	0.46	-	1.03	17.76	1.23	1.71	-	0.67	12.42	19.81	1.39	12.69	-	100.53
WB091	16	474	0.05	35.29	-	-	0.29	0.28	2.07	-	0.09	-	-	-	6.94	43.16	0.32	14.71	-	103.20
WB091	17	474	-	43.94	-	-	0.04	0.07	2.13	0.14	1.42	-	-	-	54.68	0.10	-	0.46	-	102.98
WB091	18	474	0.06	34.40	-	0.42	0.45	0.89	1.29	0.42	0.20	0.09	0.13	0.34	11.33	37.32	0.54	14.10	0.67	102.65
Kotulskite																				
WB034	19	1060.93	0.21	-	-	17.47	-	-	0.10	-	0.11	-	0.19	40.80	-	-	-	0.03	41.49	100.40
WB091	20	474	-	-	-	14.49	-	0.06	0.71	-	-	-	4.55	42.47	0.25	-	-	0.03	39.51	102.07
WB091	21	474	-	-	-	9.34	-	-	0.87	-	0.35	-	3.91	42.84	-	-	-	-	45.03	102.34
Au-Ag alloys																				
WB091	22	474	28.33	-	72.25	-	-	1.06	0.51	-	0.07	-	-	0.14	-	-	-	0.07	-	102.56
WB091	23	474	22.00	-	76.56	-	-	0.66	0.96	-	0.07	-	-	0.20	-	-	-	0.07	-	100.52
Detection Limits			0.05 - 0.15	0.02	0.08 - 0.1	0.05 - 0.08	0.03	0.03	0.03	0.05 - 0.08	0.03	0.03	0.06 - 0.09	0.04 - 0.16	0.06 - 0.08	0.03 - 0.07	0.03 - 0.04	0.04	0.04 - 0.05	

The occurrence of Pt-Pd stannides, arsenides and antimonides is variable (Fig. 5.11d) accounting for 7 vol. % at a depth of 898.7 m of borehole WB195. Eighty-seven grains, mostly less than 1 to 5 micrometres in size were counted in the samples (Table 5.2). The microprobe analysis of the only coarse grain of Pt-Pd stannide (Fig. 5.12b), yields a composition corresponding to a formula [$Pd_{3.85-3.96}Pt_{0.18-0.23}Sn_{0.88-0.92}Te_{0.77-0.93}$] (an. 6 and 7, Table 5.4) calculated on the basis of 6 atoms as the simplest one. The unidentified potentially new mineral contains some Au (0.59-0.69 wt. %) and Ag (0.34-0.46 wt. %) (Table 5.4). The composition is markedly different to the known composition of kojonenite [$Pd_{7-x}SnTe_2$] from the system Pd-Sn-Te (Stanley and Vymazalová, 2015). However, it is close to the experimental ternary phase with compositions from $Pd_{72}Sn_{16}Te_{12}$ to $Pd_{73}Sn_{14}Te_{13}$ (Vymazalová and Drabek, 2010), which has not been described in nature yet. The coarse grain of the mineral is located in altered clinopyroxene and is surrounded by a halo of disseminated particles 0.5-5 microns in size of similar composition (Fig. 5.11b).

Sulphides of Pt-Pd and Pt alloys were not found in the heavy mineral separates. However, several grains of braggite [(Pt,Pd,Ni)S] were identified in the 898.7 and 905.6 samples of WB195 (an. 1-5, Table 5.4).

The occurrence at 898.7 m depth is composed of a single large xenomorphic grain 120 µm long within relic pentlandite and an accompanied trail of smaller particles jammed between secondary silicates and quartz (Fig. 5.12c). The braggite and adjacent pentlandite are corroded by secondary amphibole and quartz encrustations. The braggite grain contains tiny inclusions of quartz, amphibole, calcite and epidote as well as thin veinlets of a Pt-richer variety of braggite (an. 2 and 4, Table 5.4, Fig. 5.12c). The composition of braggite in the matrix corresponds to a formula [$Pt_{0.38-0.54}Pd_{0.27-0.36}Ni_{0.2-0.24}S_{0.92-1.03}$], whereas Pt-richer braggite veinlets have a composition of [$Pt_{0.63}Pd_{0.1}Ni_{0.23}S_{1.03}$] (Table 5.4). The braggite intergrowth suggests a secondary origin, although the chemistry of a precursor is difficult to constrain. It is known that cooperite is the highest-temperature Pt sulphide in the Bushveld reefs and it may be replaced or overgrown by later braggite at the late magmatic stage (Merkle and Verryn, 2003; Yudovskaya *et al*., 2017). The Ni-rich braggite and vysotskite (Pd, Ni)S are not widespread in the Bushveld reefs, rather they are known to be formed under postmagmatic hydrothermal conditions, for example, in massive sulphides ores of the Noril'sk deposit (Genkin *et al*., 1981).

Gold accounts for 25% of the budget of noble metal phases in the T zone (PTM, 2016), but the proportion of the detected Au-Ag alloys does not exceed ~10 vol. % in the studied samples (Tables 5.1 and 5.2). These minerals form euhedral, anhedral and platy crystals between 5 and 50 µm in size (Fig. 5.11). They commonly contain inclusions of PGM (Fig. 5.11c, e), and are intergrown with BMS, and with primary and secondary silicates. A euhedral crystal of electrum was found in small cavities at the centre of a pyrite rim (Fig. 5.12d) although no native gold was found enclosed in pyrite crystals.

The MLA study reveals the bimodal distribution of PGM grain size in the T zone sample at an 898.7 m depth (Fig. 5.13a). Half of all PGM found are within a size range of 0-6 µm disseminated as micrograins among silicates (Fig. 5.13b), whereas the other half are 70-80 µm in size. Only around 5 area % of the PGM in the T zone sample is associated with sulphides according to the MLA results (Table 5.2), whereas the proportion in the other samples varies from 0 to 40 area % according to the SEM manual grain counting and observations. It was shown that statistical data on polished sections tend to be biased towards finding considerably more fine-grained minerals compared to coarse particles (Cabri *et al*., 2008; Cabri, 2015). Nevertheless, the consistency of the average PGM grain size varying from 5 to 10 microns (Table 5.2) through the 10 m thick T zone in the WB195 by the different methods supports the validity of the MLA results.

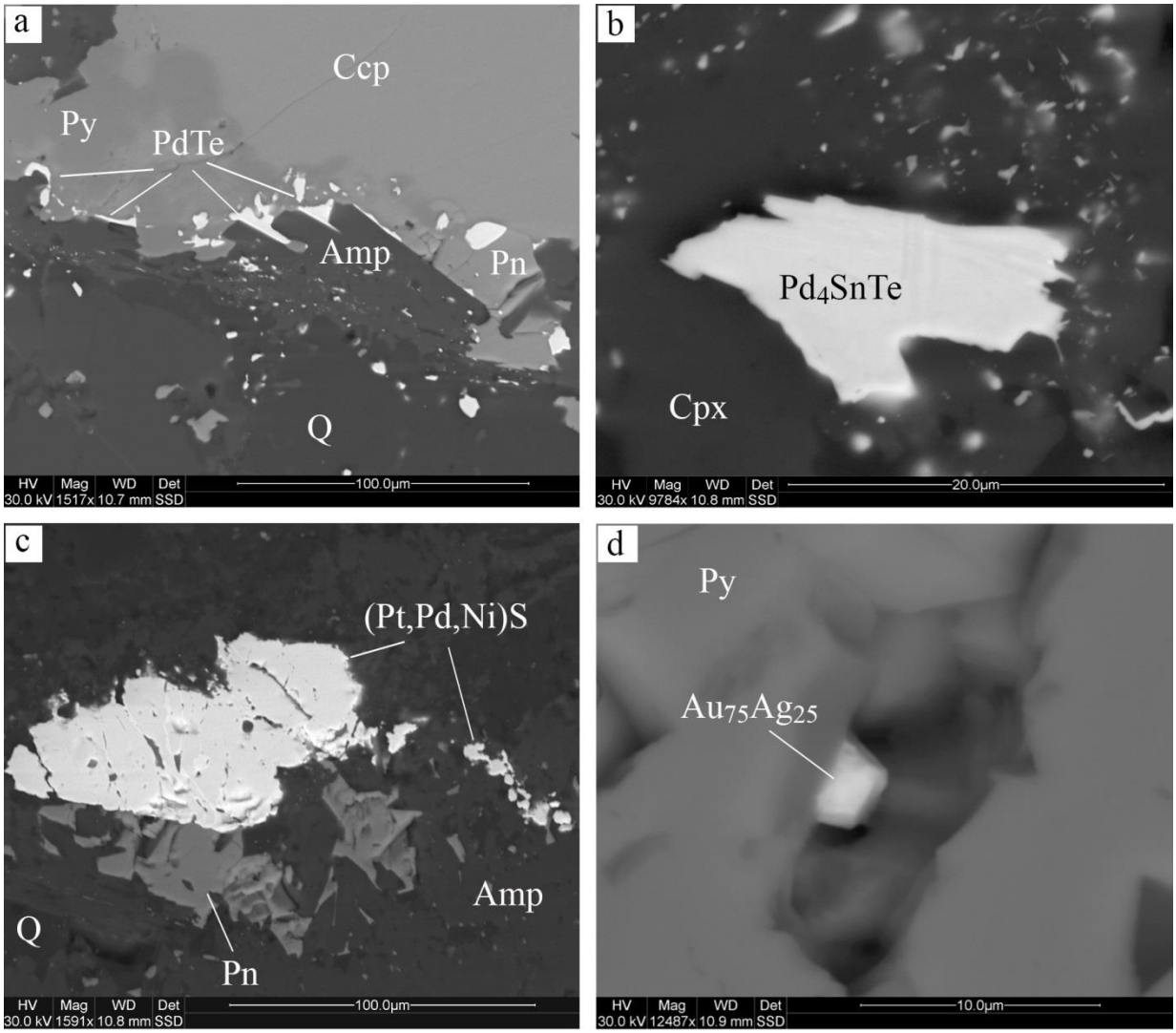

Figure 5.11: BSE images of typical PGM assemblages in the heavy separates of the T zone in core WB099: (a) merenskyite ($PdTe_2$) intergrown with chalcopyrite (Ccp) (700 m), (b) an euhedral layered crystal of moncheite $(Pd,Pt)Te_2$ (705 m), (c) an intergrowth between layered moncheite ($PtTe_2$) and native gold (Au_9Ag_1) with inclusions of kotulskite (PdTe) associated with chalcopyrite (Ccp) (705 m), (d) sperrylite ($PtAs_2$) and native gold (Au_9Ag_1) associated with chalcopyrite (Ccp) (705 m), (e) palarstannide $Pd_5(Sn,As)_2$ on native gold (Au_9Ag_1) with secondary silicates (705 m), (f) $Au_{75}Ag_{25}$ alloy associated with hydrous silicates (Sil) (705 m).

Table 5.4: Representative electron microprobe analyses of PGM (wt. %) in the T zone from the core WB195.

B.H.I.D	No.	Depth (m)	Ag	As	Au	Bi	Co	Cu	Fe	Ni	Pb	Pd	Pt	S	Sb	Sn	Te	Total
Braggite																		
WB195	1	905.6	-	-	-	-	-	-	0.16	7.06	-	17.37	57.63	19.91	-	-	-	102.13
WB195	2	905.6	-	-	-	-	-	0.12	0.11	7.65	-	6.49	68.89	18.80	-	-	-	102.06
WB195	3	905.6	-	-	-	-	-	-	0.14	8.34	-	24.87	48.18	21.08	-	-	-	102.64
WB195	4	905.6	-	-	-	-	-	-	0.48	7.65	-	16.72	56.52	15.87	-	-	-	97.27
WB195	5	905.6	-	-	-	-	0.04	0.14	0.15	7.77	-	6.08	69.04	18.62	-	-	-	101.84
Pd_4SnTe																		
WB195	6	898.7	0.34	-	0.59	-	-	0.08	0.24	-	-	60.33	6.52	-	0.08	16.07	17.47	101.72
WB195	7	898.7	0.46	1.31	0.69	-	-	0.06	0.28	-	-	62.82	5.12	0.03	0.91	15.64	14.67	101.99
Kotulskite																		
WB195	8	898.7	-	-	-	3.68	-	-	-	0.53	0.74	44.73	-	0.04	-	-	51.68	101.72
Detection Limits			0.05 - 0.15	0.02	0.08 - 0.1	0.05 - 0.08	0.03	0.03	0.03	0.03	0.06 - 0.09	0.04 - 0.16	0.06 - 0.08	0.04	0.05 - 0.06	0.04 - 0.05	0.04 - 0.05	

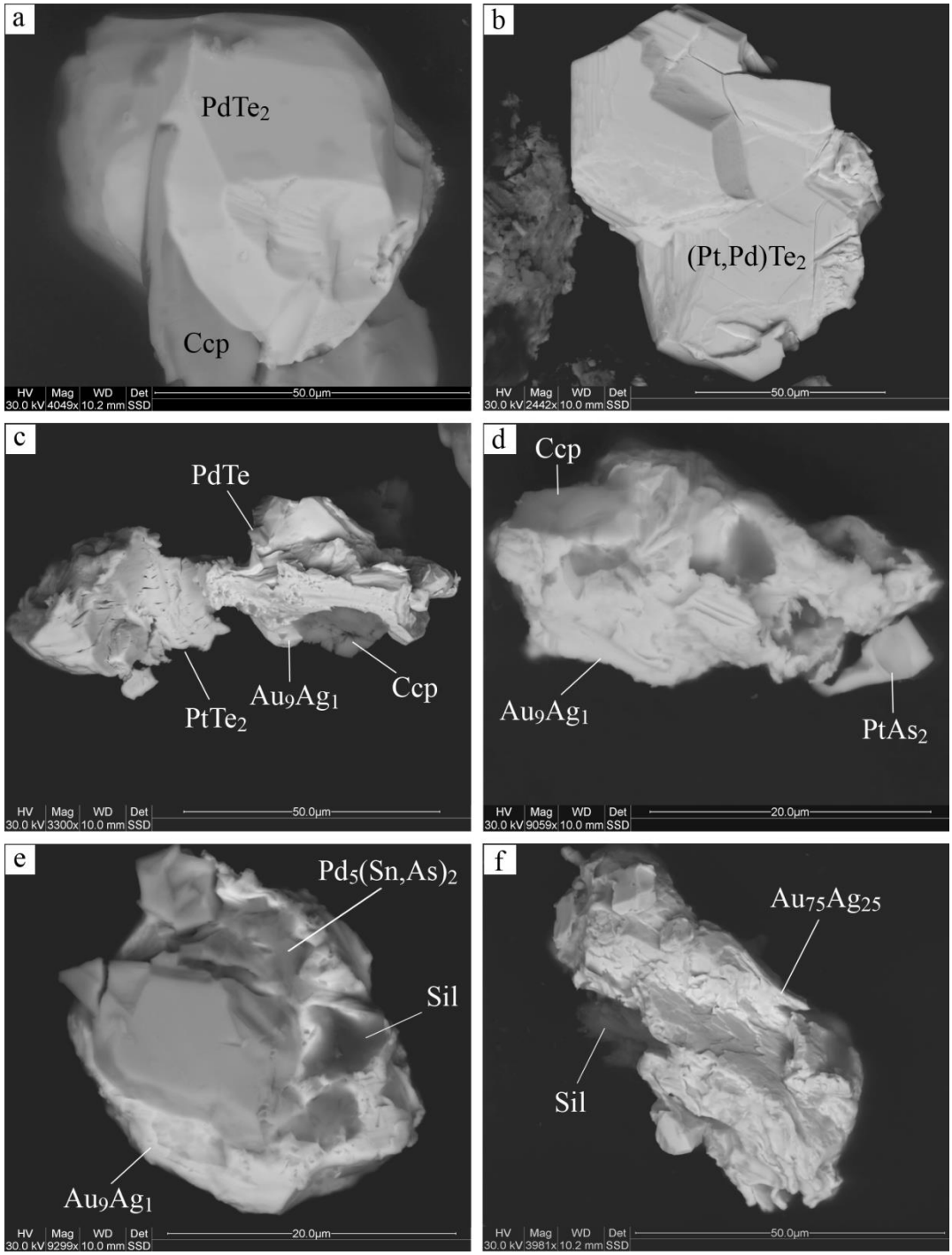

Figure 5.12: BSE images of PGM assemblages of the T zone in polished sections in core WB195: (a) disseminated kotulskite (PdTe) (an. 8, Table 4) on margins of chalcopyrite (Ccp) bleb with minor pentlandite (Pn) and pyrite (Py). PGM dissemination extends into neighbouring amphibole-quartz (Amp, Q) intergrowth (898.7 m), (b) an unidentified mineral (Pd_4SnTe) (an. 6-7, Table 4) within altered clinopyroxene (Cpx) and secondary silicates. An aureole of Pd-Sn dissemination in silicates surrounds the coarser particle (905.6 m), (c) heterogeneous grain of braggite (Pt,Pd,Ni)S (an. 1-5, Table 4) of variable composition in an intergrowth with pentlandite (Pn) within secondary amphibole (Amp). The grain is crosscut by micro- veinlets of Pt-rich braggite. Note a tail of disseminated braggite in secondary silicates (905.6 m), (d) euhedral crystal of Au-Ag alloy ($Au_{75}Ag_{25}$) in a hole encrusted by euhedral pyrite (Py) (898.7 m).

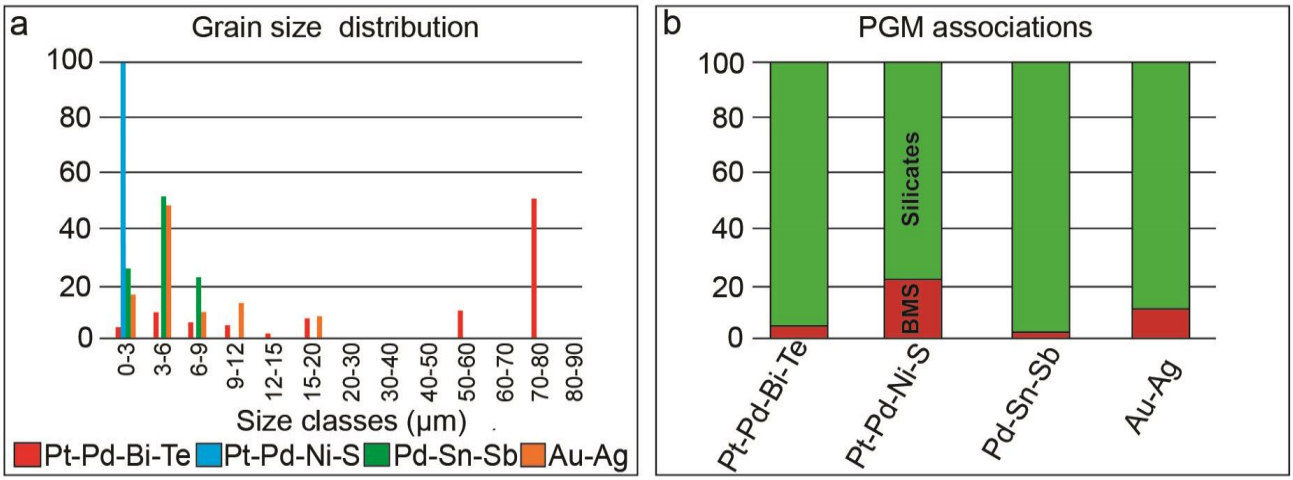

Figure 5.13: PGM statistics from the MLA study of the T zone core sample WB195-898.7: (a) grain size distribution, (b) PGM associations with silicates or base metal sulphides (BMS).

5.6. Discussion

5.6.1. Comparison of the F and T zones with other Bushveld mineralised intervals

The discovery of PGE mineralisation in the Waterberg project area north of the Hout River Shear Zone (HRSZ) has increased the interest in exploration of the upper stratigraphic zones of the northern limb. The initial studies of the intrusion in the Waterberg (McCreesh, 2016; Kinnaird *et al*., 2017) have pointed to significant similarities to the rest of the BC. However, the differences in the stratigraphy and mineralisation are notable compared to those of the western and eastern limbs and the northern limb south of the HRSZ.

South of the HRSZ, on the Harriet's Wish to Aurora section of the northern limb (Fig. 5.1) mineralisation is hosted in more felsic lithologies. McDonald *et al*. (2017), discussed the question as to whether the Aurora mineralisation is a continuation of the contact style Platreef deposits (Maier *et al*., 2008) or belongs to a Main Zone style of mineralisation defined earlier by Maier and Barnes, (2010). McDonald *et al*. (2017) argued for a possible correlation between the upper mineralised zone of the intrusion at the Waterberg project and the Aurora mineralisation. This contribution constrains possible correlations with the northern limb and the rest of the BC on the basis of the first detailed data on the mineralisation styles and the PGM assemblages of the F and T mineralisation.

The PGE mineralisation in the BC occurs in two distinct styles, (1) contact-style mineralisation along the footwall of the northern limb (Kinnaird *et al*., 2005; Maier *et al*., 2008; McDonald and Holwell, 2011), (2) laterally highly continuous stratiform reefs including the Merensky reef, the UG2 chromitite layer and the PGE reefs at the top of the Platreef (Scoon and Teigler, 1994; Barnes and Maier, 2002; Yudovskaya *et al*., 2017). These two styles of mineralisation occur exclusively in the Critical Zone and the correlative Platreef. A third style of PGE mineralisation in the gabbroic sequence higher up in the stratigraphy has

been described recently (Harmer *et al*., 2004; Maier and Barnes, 2010; Holwell *et al*., 2013; McDonald *et al*., 2017) while some sub-economic PGE grade has been reported in the Upper Zone long ago (von Gruenewaldt, 1976; Harney and von Gruenewaldt, 1995).

The Ultramafic Lithologies and the F mineralised zone

The Pt/Pd and Pt/Au ratios in the F zone are much lower than those in the Merensky Reef or UG2 chromitites, whereas these values are within the range of those known for the Platreef contact-style (Kinloch, 1982; McLaren and De Villiers, 1982). Both have 5% Au within the precious metal budget. The Platreef is characterised by significant variations in PGE values and ratios along strike and down dip related to changes in host lithologies and mineralisation styles (Kinnaird *et al*., 2005; McDonald and Holwell, 2011). The Platreef formed as coalescing multiple intrusions with the basal contaminated units hosting Pd-dominated contact-style mineralisation (Kinnaird, 2005; McDonald *et al*., 2005; Maier *et al*., 2008) and the top part carrying Pt-dominated reef-style mineralisation (Yudovskaya *et al*., 2017). Therefore, the PGE variations across the Platreef vertical section are related to the change of the mineralisation styles whereas the PGE proportions along the strike of the stratiform PGE reef are uniform. The reefs of the upper Platreef are characterised by perfect correlations between PGE and S, whereas a poor correlation exists between BMS and PGE in the contact style mineralisation of the lower contaminated Platreef on Turfspruit and Macalacaskop (Hutchinson and Kinnaird, 2005) (Fig. 5.1). The range of the Cu/Pd values (as low as 500) in the stratiform reefs of the Platreef (Yudovskaya *et al*., 2017) is similar to that in the F zone (Fig. 5.4) and is within the range for the Merensky Reef (Naldrett *et al*., 2009). The Cu/Pd values in the Platreef contact style mineralisation are generally much higher and variable, reflecting heterogeneous PGE distribution in contaminated magmatic rocks, skarns and hornfels (McDonald and Holwell, 2011).

The Pt-dominated reefs of the Platreef are interpreted to have formed as chonolith-like coalescing intrusions composed of feldspathic pyroxenite and harzburgite (Yudovskaya *et al*., 2017) and the same mode of intrusion is suggested for the ultramafic bodies hosting the F zone (Kinnaird *et al*., 2017; and this study).

The primary magmatic BMS assemblages of the F zone (Fig. 5.6) are typical of PGE deposits in ultramafic sequences including the deposits of the BC (McDonald and Holwell, 2011), and the secondary sulphide assemblage is also typical of serpentinised ultramafic economic or barren packages (Ramdohr, 1969; Kitakaze, 2008).

Disseminated chromite and chromitite seams within the Platreef package are generally enriched in PGE (Yudovskaya and Kinnaird, 2010). The chromitite seams bounding the stratiform sulphide reefs of the BC

are considered to mark the base of a cyclic unit and zone of mixing between a residual magma and a new melt influx (Naldrett *et al*., 2012). The F zone hosts irregularly distributed disseminated chromite, whereas chromitite seams 1-20 cm thick are rare. It may be related to the magmatic erosion at the top of the UmS by a surge of later troctolitic melt. Most of the TGA sequence is Cr-poor and chromite was not a liquidus phase in the TGA parental gabbroic melt. Disseminated chromite in troctolite is xenocrystic in nature suggesting it was derived from digested and consumed UmS harzburgite.

The Platreef contact style mineralisation shows a great variability of PGM assemblages (Viljoen and Schürmann, 1998) and these changes seem to be related to the change in footwall lithologies (McDonald *et al*., 2005; Nichol and Kinnaird, 2008; McDonald and Holwell, 2011). On the farms Rietfontein, Macalacaskop and Turfspruit (Fig. 5.1), the PGMs in the contaminated sequence are represented by Pd-dominated bismuthotellurides and antimonides that comprise up to 90% of the PGM basket, with minor sperrylite and a single grain of PGE sulphide (vysotskite PdS) identified (Armitage *et al*., 2002; Hutchinson and Kinnaird, 2005). From south to north the most abundant PGM identified are Pt-Pd bismuthotellurides at Tweefontein Hill, Pt-Pd sulphides, on Tweefontein North, Pt-Pd alloys and bismuthotellurides, on Sandsloot and Zwartfontein, Pt-Pd sulphides and tellurides on Overysel and Pt-Pd tellurides on Drenthe (Fig. 5.1) (Schneiderhöhn, 1929; Mostert, 1982; Kinloch, 1982; Viljoen and Schürmann, 1998; Armitage *et al*., 2002; Holwell *et al*., 2006). In these earlier studies, the reef style and the contact mineralisation were not distinguished and, therefore, the characteristics above reflect the bulk PGM proportions across the 100-600 m thick Platreef vertical section. The PGE-rich layers at the top of the Platreef are the thickest reefs in the BC (from 1 up to 90 m thick) but they are relatively thin compared to the much thicker zones of basal marginal mineralisation. Therefore, the contribution of PGM types from the reefs was inevitably subordinate in the whole balance.

The recent work by Yudovskaya *et al*. (2017) at Turfspruit has indicated that the PGM assemblage in the uncontaminated stratiform reefs is dominated by Pt sulphides and Pt-Fe alloys and has been interpreted to be mineralogically similar to the Merensky Reef in the rest of the BC. The association of sperrylite-hollingworthite-cobaltite-gersdorffite can be considered as indicative (Good *et al*., 2017) of both the Waterberg F zone and for the Akanani harzburgite reefs (Yudovskaya *et al*., 2011). In contrast, Pt sulphides and alloys indicative of the Merensky Reef style (Schouwstra *et al*., 2000; Prichard *et al*., 2004) are absent in the F zone supporting the idea that it is a zone (Kinnaird *et al*., 2017) and not a stratiform reef.

The Felsic-Rich Lithologies and the T mineralised zone

The recent discovery of high-grade PGE mineralisation within the Upper-Main Zone of the northern limb warrants the question whether these mineralised zones are continuous south of the HRSZ. The TGA sequence hosts the upper mineralisation at its very top, at the contact with the Upper Zone rocks. The first appearance of cumulus titanomagnetite, which is an indicative mineral of the Upper Zone sequence (Ashwal *et al*., 2005) is confined to the T zone. On this basis, T mineralisation may be assigned to the base of the Upper Zone rather than the top of the TGA. Below we compare characteristics of the T zone with other known mineralised intervals along the Main Zone strike in the northern limb, on the Moorddrift farm south of Mokopane and the Aurora project.

The highest PGE grades on Moorddrift farm are hosted by mottled anorthosite and gabbronorite which are associated with a pyroxenite layer (Holwell *et al*., 2013). Maier and Barnes (2010) suggested that the pyroxenite layer is correlative to the true 'Pyroxenite Marker' of the eastern and western limbs of the BC. Cawthorn (2012) and Holwell *et al*. (2013), however, argued that a variable number of thin pyroxenite layers occur elsewhere in the upper Main Zone of the northern limb, and that the Moorddrift layer may represent one of these layers. The mineralised interval at Moorddrift (Fig 5.1) is also associated with brecciated lithologies, where PGE have been remobilised during hydrothermal activities (Holwell *et al*., 2013). The sulphide assemblage comprises pyrrhotite-chalcopyrite-pentlandite with overprinting by pyrite. The $\delta^{34}S$ isotope signature for the PGE mineralised interval at Moorddrift ranged between 2.8‰ to 11.5‰ $\delta^{34}S$ indicating contamination by Transvaal sediments. The Moorddrift mineralisation is Pt-dominated with the PGM assemblages dominated by Pt arsenides up to 70 % (Maier and Barnes, 2010; Holwell *et al*., 2013). Therefore, the position of the Moorddrift mineralisation is not related to the Upper-Main Zone boundary as established for the Waterberg T zone. The elevated Pt/Pd, the Pt arsenide dominance, typically lower grades and the sulphur isotope $\delta^{34}S$ values which are indicative of crustal contamination do not support a genetic link between the southern Moorddrift and far northern Waterberg mineralisation.

South of the Hout River Shear Zone, mineralisation is hosted by gabbronorite to leucogabbronorite, minor troctolite and magnetite gabbro at the Aurora project (Fig. 5.1) (Harmer *et al*., 2004; Manyeruke, 2007; McDonald *et al*., 2017). These lithologies are similar to the T zone in our study area and are assigned to the Main Zone by McDonald *et al*. (2017) although the presence of magnetite gabbro is not consistent with the Main Zone stratigraphy anywhere else. McDonald *et al*. (2017) described inverted pigeonite in the mineralised intervals. In the BC the first pigeonite occurs at the top of the Critical Zone (de Klerk, 1992) whereas the cyclic reappearance of pigeonite further upwards in the Bushveld

stratigraphy serves as a basis for subdivision of the Main and Upper Zones into subzones (Nex *et al*., 1998). The T zone gabbro may contain sporadic occurrences of inverted pigeonite although pigeonite becomes more widespread in the overlying Upper Zone magnetite-bearing gabbro. McDonald *et al*. (2017) reported the presence of calc-silicates up to 2 m thick on the Aurora project whereas it is a rare feature in the Waterberg project sections. These authors highlighted that the Aurora mineralisation is Cr-poor with the Cr abundance <300 ppm Cr that is typical for Bushveld gabbroic rocks and a negative correlation between Cr and PGE. Similar Cr values and Cr-PGE relationship are noted in the Waterberg T zone (Fig. 5.5). Both areas are characterised by Pd dominant over Pt with Pt/Pd of approximately 0.6 although Cu/Pd of ~4000 in Aurora is remarkably higher than that of the higher-grade Waterberg project mineralisation. However, both are still within the range of mantle-derived magmatic sulphides (Naldrett *et al*., 2012). The Aurora sulphides have magmatic sulphur isotope signatures as the $\delta^{34}S$ values range from -0.8 ‰ to +5.24 ‰ with an average of 0.99 ‰ (Holwell *et al*., 2007; Manyeruke, 2007; McDonald *et al*., 2017) that is similar to the Waterberg project $\delta^{34}S$ values of around 0 ‰ (McCreesh *et al*., 2015). The most common PGM on Aurora include Pd tellurides (merenskyite and kotulskite) and Au-Ag alloys with subordinate Pt tellurides and arsenides and rare Pt-Pd sulphides (McDonald *et al*., 2017). The Aurora sulphide assemblage of pyrrhotite-chalcopyrite-pentlandite contains only minor secondary pyrite. The PGM association with primary sulphides and silicates on Aurora strongly contrasts to the hydrothermal quartz-chlorite and pyrite-millerite secondary assemblages seen in the T zone. However, given the significant similarities between the two adjacent project areas and the likelihood of a link between their host sequences, we suggest that the Aurora mineralised units may represent a southern distal facies of the T zone.

The Main Zone magma of the BC was not traditionally considered as a fertile PGE source (Naldrett *et al*., 2012) although some sporadic sulphides were identified in the upper part. Van der Merwe (1976) analysed gabbronorite samples from the upper Main Zone in the northern limb, and found anomalous enrichment in Cu and S values. Ashwal *et al*. (2005) reported an increase in opaque minerals in the upper Main Zone, although they did not indicate their composition. Barnes *et al*. (2004) noted relatively low Cu/Pd and elevated Cu content in the upper Main Zone from the Bellevue drill-core in the northern limb, similar to the ranges for the Waterberg project and Aurora mineralisation. Holwell *et al*. (2005) have established that the Main Zone in the northern limb unconformably overlies the Platreef and have interpreted that the Main Zone may hold a metal budget of its own. McDonald *et al*. (2017) speculated that this break between Platreef and Main Zone in the northern limb might explain the anomalous PGE budget of the Main Zone magma in the northern limb compared with the rest of the BC.

The upper Main Zone sequence of the western and eastern limbs also locally bears similar anomalies. Wilhelm *et al*. (1997) reported on the basis of soil and sediment geochemical data that Ni, Cu, PGE and Au anomalies associated with the upper Main Zone could be traced for more than 100 km along strike in the western limb of the BC. Sharpe (1985) and Wilhelm *et al*. (1997) have predicted the appearance of mineralisation associated with the Pyroxenite Marker or at the boundary between the Main and Upper Zones. Consequently, several studies on the Pyroxenite Marker have revealed a moderate PGE enrichment in a few samples, although, most PGE abundances were below analytical detection limits (Maier *et al*., 2001; Maier and Barnes, 1999). Therefore, the known sulphide mineralisation in the upper Main Zone and Upper Zone of the eastern and western limbs was confirmed to be uneconomic (Harney and Merkle, 1990; Harney and von Gruenewaldt, 1995).

5.6.2. Relationships between PGM, BMS and rock-forming minerals

Typical magmatic PGE concentrations in the Bushveld stratiform deposits are associated with chromite (Lee, 1996), which is a major index mineral of the Lower and Critical Zone melts. In this sense, the Waterberg project mineralisation is atypical for the BC as one of the ore zones is hosted in gabbroic and leucogabbroic Cr-poor magnetite-bearing rocks. Thus, the Critical Zone melts parental to all known Bushveld PGE deposits were not involved in the formation of the T zone mineralisation. The different composition of the parental melt does not markedly affect the patterns and compositions of BMS. The zonal sulphide blebs, pentlandite exsolution in pyrrhotite and troilite exsolution within hexagonal pyrrhotite are typical textures seen in the Merensky Reef, Platreef, Upper Zone and other magmatic sulphide deposits. The elevated Co content in the Waterberg pentlandite (Fig. 5.14) and pyrite is likely related to later hydrothermal modification as was suggested for Co-enriched pentlandite in the contaminated Platreef (Hutchinson and Kinnaird, 2005).

Naldrett and Duke (1980) described that a typical magmatic sulphide liquid immiscible with the co-existing silicate liquid scavenges base metals and PGE. As a result of the crystallisation of mss, iss and PGE-rich residue, PGM would commonly be found along the margins of BMS blebs (Naldrett *et al*., 1986). The magmatic PGM assemblages are composed of a variety of PGM, among which some of the PGM are considered to be indicative of contamination or hydrothermal remobilisation. For example, the abundance of sperrylite is often interpreted as a consequence of assimilation of As-rich sediments as the As concentrations in ultramafic melts are commonly too low to achieve saturation in arsenides (Hutchinson and Kinnaird, 2005; Holwell *et al*., 2006; Djon and Barnes, 2012; Holwell *et al*., 2013). The Archean granite-gneisses footwall of sperrylite-rich F mineralisation cannot be an effective source of As.

We believe that the F zone index assemblage of sperrylite+hollingworthite is of high-temperature magmatic origin.

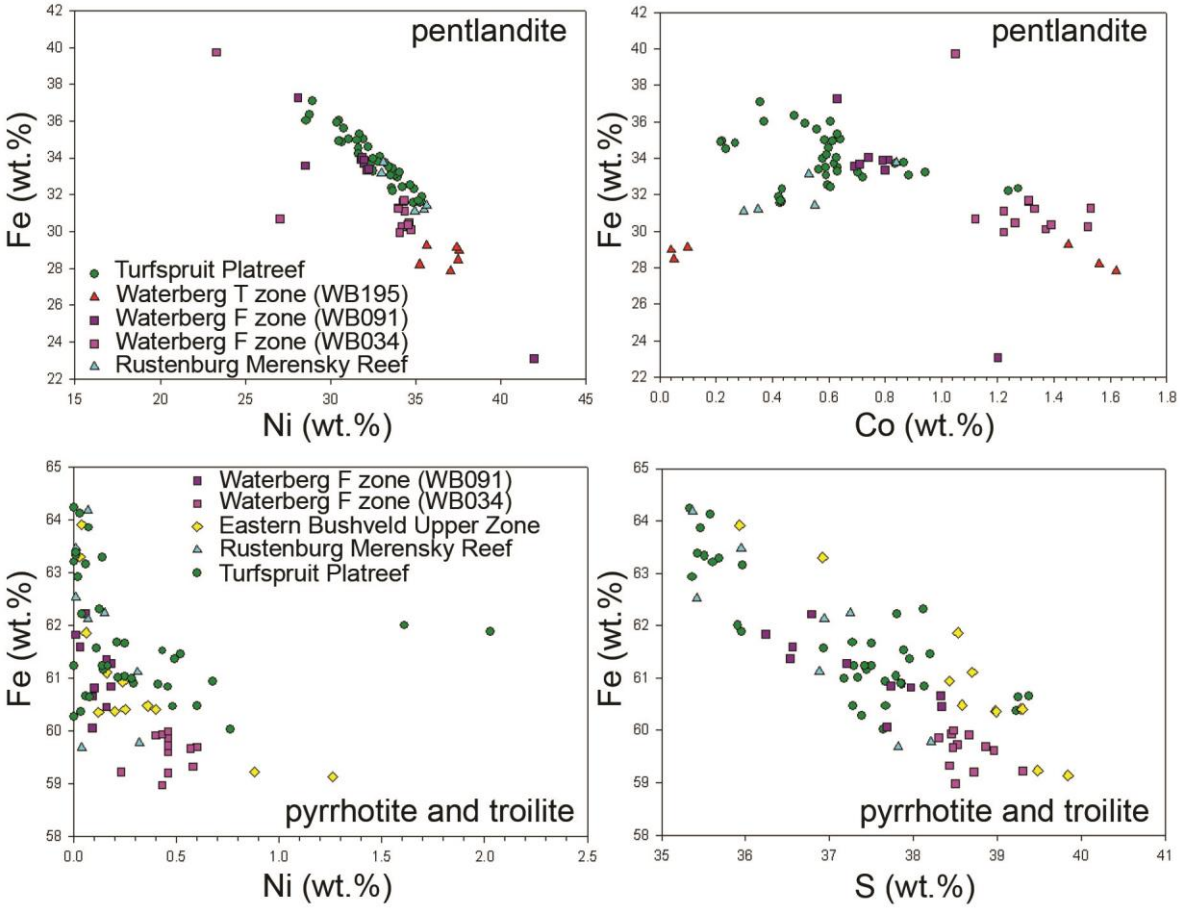

Figure 5.14: Chemical compositions (wt. %) of pentlandite (Ni and Co vs Fe), and pyrrhotite and troilite (Ni and S vs Fe) from the F and T zones at the Waterberg project. The data are compared with compositions from the Turfspruit reef in the Platreef (Yudovskaya *et al*., 2017), the Upper Zone in the eastern Bushveld (von Gruenewaldt, 1976) and the Merensky Reef at Rustenburg (Kawohl and Frimmel, 2016).

BMS have been altered along their margins and replaced by hydrous silicates (actinolite, phlogopite, tremolite, chlorite and epidote) and quartz. The PGMs occur as isolated crystals hosted by hydrous silicates due to removal and replacement of their host sulphides (Figs. 5.8 and 5.12). Similar textures are seen in the Platreef (Holwell *et al*., 2006), the Merensky Reef and UG-2 chromitite layer (Li *et al*., 2004). The latter authors suggested that the reaction involves the addition of Ca, Mg and Si from the assimilation of Malmani dolomites. Holwell *et al*. (2006) argued that a hydrous fluid reacted with the BMS forming a sulphuric acid which dissolved the margins of BMS, allowing the hydrous silicates to grow into voids along the regressed margins.

The crystallisation of primary PGM in both the F and T mineralised zones predates the alteration, as seen by the crosscutting relationships between the PGM and the secondary silicates (Figs. 5.8 and 5.12). Primary magmatic Pt-Pd bismuthotellurides and native gold are generally easily remobilised by hydrothermal fluids and can precipitate in associated hydrous silicates (Watkinson and Ohnenstetter, 1992; Li *et al*., 2004; Helmy *et al*., 2007). The euhedral gold crystals in the cavities among pyrite crusts (Fig. 5.12d) confirm the hydrothermal transport of gold.

However, the primary PGE enrichment was the main controlling factor of mineralisation. The pegmatoidal intervals in the middling of the T zone are PGE-poor despite of wide development of the hydrothermal assemblages with quartz-pyrite crusts and titanomagnetite replacement. Although the best PGE grade of the T zone is confined to the hydrothermally-reworked leucogabbro (as in the WB195 section), the variability of the T host lithologies from harzburgite to anorthosite suggests that T mineralisation does not belong to the stratiform reef type. It is generally controlled by the zone of intermingling and interaction of two different gabbroic melts with subordinate influxes of Cr-poor ultramafics. The intensive hydrothermal reworking did not change significantly PGE spatial distribution although did modify the PGM assemblage and may affect the primary geochemical characteristics such as Au/Pt value. Zotov *et al*. (2017) experimentally showed that Au/Pt in high-temperature chloride fluid in equilibrium with native Au, native Pt and Pt sulphide increases up to 1 order at increasing temperature from 550 to 700 ^{o}C. A decrease in pressure and an increase in sulfur fugacity towards pyrite predominance over pyrrhotite also lead to enrichment of the fluid in Au relative to Pt. Zotov *et al*. (2017) suggested that these coupled tendencies are related to a drop in the fluid density and exsolution of low density supercritical fluid at around 550 ^{o}C that may be a cause of high Au/Pt in pyrite-bearing mineralisation.

5.6.3. Model of the Waterberg Bushveld Succession

We suggest a provisional model for the origin of the PGE mineralisation and the emplacement of the Waterberg project succession on the basis of our data and as a development of earlier expressed ideas shared by Kinnaird *et al*. (2017) and Huthmann *et al*. (2018). The tectonic setting of the Limpopo Belt basement and its pre-existing anisotropies (fractures, faults, shear zones, foliations and lithological contacts) have played an important role during the initial stages of magmatism in the Waterberg project area. Structural controls of the emplacement of the earlier melts defined the observed sill-like and chonolith morphology of the separate units. The initial emplacement started at 2.05 Ma (Huthmann *et al*., 2016) with the intrusions of the Marginal orthopyroxenite, gabbronorite and norite sills into the Hout River gneiss basement (Fig. 5.15a). These intrusions melted Archean granite gneisses which

mingled with a pyroxenitic magma to form granofels, which is similar to the granofels at the contact of the Platreef with gneissic floor (Holwell and McDonald, 2006). Continuous influxes of ultramafic magma carved out channelised pathways under lateral dilation to form elongated chonolith-like bodies (Lister and Kerr, 1991) (Fig. 5.15a). The earlier ultramafic melts crystallised mineralised feldspathic orthopyroxenite at the base of the F zone (Fig. 5.15b). Then melts with olivine on the liquidus were transported along the heated channels to crystallise feldspathic harzburgite in the upper part of the F zone (Fig. 5.15b). High-Mg ultramafic magmas are generally enriched in PGE, which is related to a high degree of partial melting of the mantle source (Barnes *et al*., 2016). With the continuous flow of ultramafic magma through these elongated channels, thermo-mechanical erosion formed embayments within the footwall of the Hout River Gneiss (Fig. 5.15b). At the same time, this hot ultramafic magma used points of weakness to widen the conduit for progressive transport and assimilation of the resident orthopyroxene cumulates that were redeposited as xenoliths within the overlying harzburgite (Holwell and McDonald, 2006). The maximum heat and melt flow would be focused at the centre of the elongated bodies prohibiting crystallisation and allowing for a long-lasting sulphide-silicate exchange to form high-tenor magmatic sulphides (Campbell *et al*., 1983). In a recent study by Mungall and Brenan (2014), extremely high partition coefficients for PGE (from 10^5 to 10^6) between the sulphide and silicate melts were found. The calculations for the Merensky sulphides (Mungall and Brennan, 2014) confirm a possibility of formation of the high-tenor PGE sulphides mineralisation in situ in the resident chamber with no need for a pre-enrichment and an accumulation of a large pool of sulphide melt at depth in the staging chamber. The continuous propagation of magma through the chonoliths is an effective mechanism for the concentration of the sulphide-droplets during magma emplacement (Naldrett, 2010) and formation of thicker and higher grade ore zones (up to 5g/t PGE for 60 m interval), which then formed the Super F zone on the PTM exploration site. The PGE ores in the olivine-rich sequence are well known in the BC, although harzburgitic reefs (such as the Pseudo reef and the Turfspruit Main reef) are commonly located below the pyroxenite-hosted reef that assumes the earlier emplacement of the former. Otherwise, the observed stratigraphic order does not necessary reflect the order of emplacement as separate sills and chonoliths can transgress through layering and intrude out of sequence.

Following the ultramafic channelized melt flow, continuous pulses of troctolitic magma utilized pre-existing points of weakness or anisotropies to form more laterally extensive sheet-like bodies (Fig. 5.15c). The processes of roof uplift and floor depression (Cruden, 1998) may have played a crucial role for creating space for the voluminous pool of stagnant magma to fractionate. The initial influxes of the

troctolitic magma with a high proportion of phenocrysts at some point mixed with the earlier ultramafic melts either in the sub-chamber or in the feeder zone (Saper and Liang, 2014), to form mela-troctolite grading into troctolite, olivine gabbronorite, gabbronorite and anorthosite (Fig. 5.15d). The several regular occurrences of anorthosite at the top of gabbroic cycles within the TGA sequence testifies to multiple surges of magma that were similar compositionally to the Main Zone magmas elsewhere. The prolonged fractionation of the TGA sequence may be one of the key factors in producing the T zone at the top (Fig. 5.15e) (Keays and Tegner, 2016). During the fractionation of the TGA magma, the incompatible elements such as S, Cu, Pt, Pd and Au would have become enriched in the residual melt after deposition of the barren olivine-plagioclase cumulate (Andersen *et al*., 1998; Nielsen *et al*., 2005; Keays and Tegner, 2016). The T zone also marks the first appearance of cumulus magnetite that may indicate a decrease in temperature and fO_2 of the magma (Keays and Tegner, 2016) or may be an indication of a first influx of the Upper Zone melts into the resident chamber. Mixing between the TGA leucogabbroic residue and the Upper Zone melt with magnetite on liquidus, triggered sulphide saturation and exsolution of T2 sulphides. The heterogeneity of the overlying T1 package suggests that the entire T zone was formed as a result of consecutive mixing events. The appearance of T1 harzburgite above anorthosite testifies to an influx of an olivine-saturated magma, which transgress through the underlying T2 and initiated the crystallisation of pegmatoidal pods and lenses due to undercooling during protracted crystallisation. The T1 and T2 mineralisation subzones have the same metal basket but very different lithologies. The PGE grade in the T1, however, is not persistent and, in some cases, the T1 is completely barren as seen in WB099 (Fig. 5.5). The T1 may have thermally eroded the T2 and the overlying anorthositic interlayer.

The fractionation of the voluminous Upper Zone gabbroic magma may have been disturbed by new influxes of less evolved melts forming at least a 500 m thick Upper Zone of the Waterberg Bushveld succession, which may have included now eroded apatite-bearing rocks seen in the rest of the BC (Fig. 5.15f). Soon after the uplift and partial erosion of the Waterberg Bushveld succession and its possible volcanic roof, the Waterberg Group sediments were deposited upon the weathered surface (Fig. 5.15g).

The T zone package of the intercalated diverse lithologies served as favourable pathways for fluid migration at the late and post-magmatic stages. The late magmatic alteration involved the replacement of sulphides along the margins with secondary amphiboles and silicates, whereas hydrothermal activity resulted in the deposition of quartz, magnetite replacement, crystallisation of pyrite-millerite assemblages and remobilisation of PGM and BMS out of sulphide blebs into the silicate matrix. The F zone magmatic mineralisation underwent a superimposed alteration during the late magmatic stage and

later serpentinisation. The late magmatic processes resulted in the replacement of magmatic sulphides by secondary silicates, whereas serpentinisation induced a significant BMS and chromite dissolution with spatially restricted PGE remobilisation.

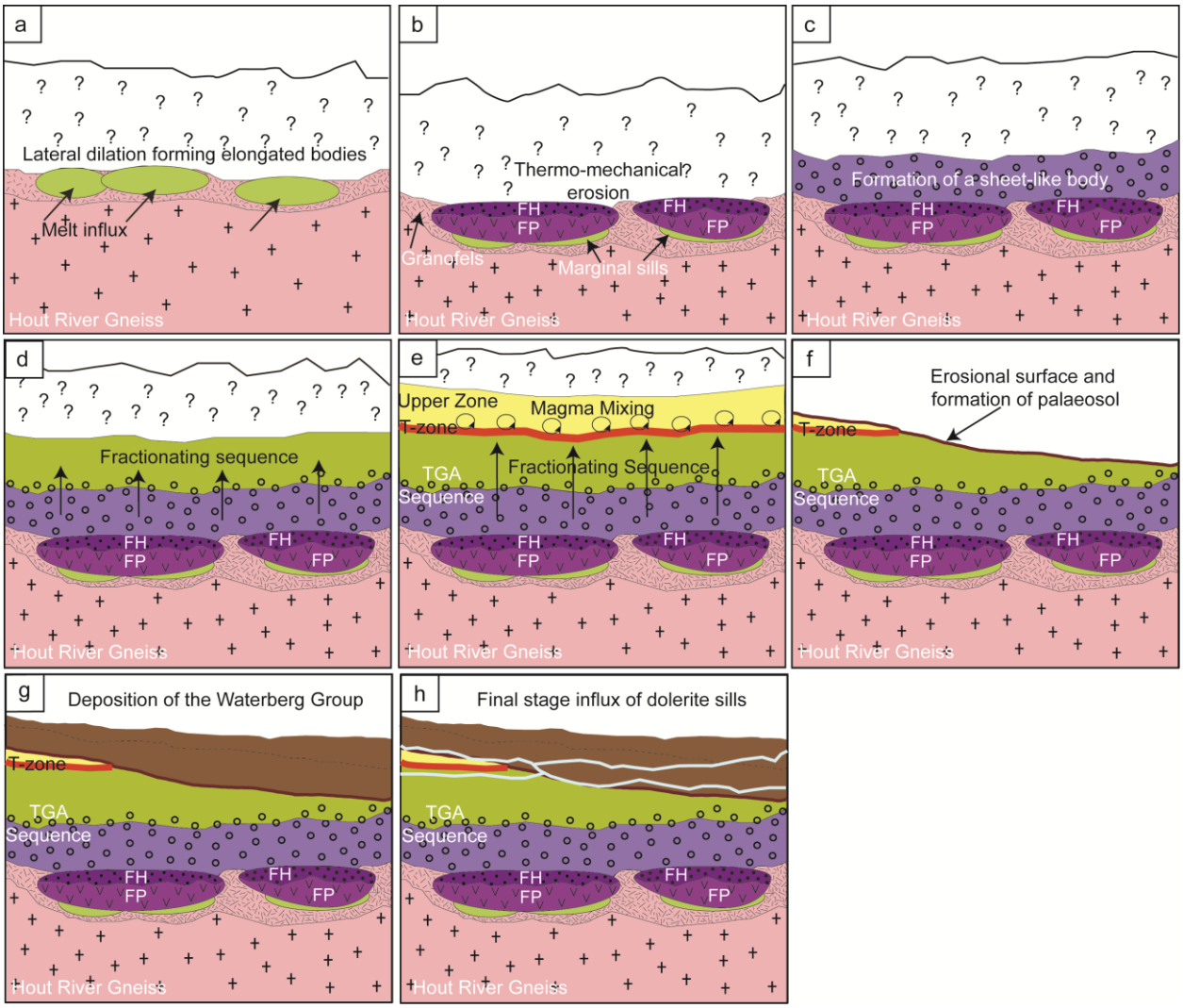

Figure 5.15: The conceptual model for the emplacement of the entire Waterberg magmatic succession and formation of the mineralised zones: (a) the initial influxes interact with the Archean basement to form marginal sills of fine-grained pyroxenite and gabbronorite, and granofels under lateral dilation, (b) the channelised emplacement of ultramafic melts to form feldspathic orthopyroxenite (FP) and overlying harzburgite (FH). Thermal-mechanical erosion creates embayments in the footwall whereas mixing initiates exsolution of sulphide-droplets, (c) emplacement of the troctolitic sheet-like bodies extending laterally due to roof uplift and floor depression, (d) magma mixing between resident ultramafics and gabbroic melts at the base of the TGA sequence, (e) prolonged fractionation of the TGA melt column resulting in a build-up of S, Cu, Ni and PGE+Au in the residual melt. The influx of fertile magma of the Upper Zone affinity, magma mixing and formation of the T zone, (f) the area experiences uplift and erosion. Palaeosol forms after weathered Bushveld rocks, (g) deposition of the Waterberg Group sediments, (h) intrusions of the Umkondo dolerite sills.

5.7. Conclusion

The two economic PGE zones in the Waterberg project succession do not have comparable analogues in the rest of the Bushveld Complex. The detailed PGM and sulphide mineralogy corroborates the earlier ideas (Huthmann *et al*., 2016; Kinnaird *et al*., 2017) of an independent development of the Waterberg project area as a separate magmatic basin within the Southern Marginal Zone of the Limpopo belt. Our data on PGM and PGE deportment allow the following conclusions regarding the formation of the mineralised zones:

(1) Sperrylite and Pt-Pd bismuthotellurides are the dominant PGM in the F zone in the ultramafic rocks, where sulpharsenides of PGE, Fe and Co are index minerals of this type of mineralisation. The widespread serpentinisation resulted in a significant sulphide and chromite removal and determined the composition of the secondary sulphide assemblages typical of altered ultramafic rocks. The F zone mineralisation is confined to the basal layers of the succession and is comparable to mineralisation in the Platreef ultramafic sills and chonoliths, assuming similar mechanism of sulphide enrichment in the channelised magmatic flows.

(2) The T zone is dominated by Pt-Pd bismuthotellurides, PGE-stannides and electrum. The stratigraphic position at the level of the first cumulus magnetite appearance suggests that Upper Zone melts were involved in the formation of the T ore-bearing package. The higher proportions of ultramafic and troctolitic lithologies distinguish the T zone from the mineralised zone on Aurora; perhaps the latter is hosted in the distal facies of the same succession. Widespread secondary silicates (tremolite, actinolite, epidote, serpentine and chlorite), crusty quartz, carbonates and associated pyrite-millerite assemblages indicate hydrothermal modification of PGM. The hydrothermal reworking was responsible for the observed bimodal PGM grain size distribution where the rare coarse grains are accompanied by haloes and trails of the numerous disseminated PGM in silicates.

Supplementary Tables:

Table 5.5. Sulphide composition within the F-mineralised zone (WB091)

				Content of elements, wt. %					
B.H.I.D.	**Depth (m)**	**Stratigraphy**	**Samples**	**Fe**	**S**	**Ni**	**Cu**	**Co**	**Total wt. %**
				Bornite					
WB091	474	F Z	1	11.31	26.03	0.06	62.61	0.02	100.03
WB091	474	F Z	2	11.49	24.72	0.07	60.11	0.01	96.40
				Pentlandite					
WB091	474	F Z	3	30.06	30.80	19.01	9.85	0.43	90.15
WB091	474	F Z	4	33.57	33.45	28.51	2.33	0.69	98.55
WB091	474	F Z	5	33.93	33.23	31.77	0.00	0.81	99.74

WB091	474	F Z	6	33.90	33.62	31.94	0.00	0.79	100.25
WB091	474	F Z	7	34.05	34.04	31.85	0.00	0.74	100.68
WB091	474	F Z	8	33.68	33.58	31.93	0.00	0.71	99.90
WB091	474	F Z	9	37.26	34.30	28.09	0.01	0.63	100.29
				Chalcopyrite					
WB091	474	F Z	10	29.68	34.16	0.14	33.45	0.00	97.43
WB091	474	F Z	11	30.17	34.97	0.00	34.14	0.02	99.30
				Troilite					
WB091	474	F Z	12	60.66	38.33	0.09	0.04	0.00	99.12
WB091	474	F Z	13	60.06	37.68	0.09	0.08	0.00	97.91
WB091	474	F Z	14	61.60	36.56	0.03	0.08	0.00	98.27
WB091	474	F Z	15	61.83	36.24	0.01	0.00	0.01	98.09
WB091	474	F Z	16	60.82	37.97	0.10	0.00	0.02	98.91
WB091	474	F Z	17	62.22	36.79	0.06	0.00	0.02	99.09
				Pyrrhotite					
WB091	474	F Z	18	61.28	37.21	0.18	0.02	0.01	98.70
WB091	474	F Z	19	61.37	36.53	0.16	0.00	0.01	98.07
WB091	474	F Z	20	60.85	37.73	0.18	0.01	0.00	98.77
WB091	474	F Z	21	60.46	38.34	0.16	0.00	0.02	98.98

F Z - F zone mineralisation

Table 5.6. Sulphide composition within the F-mineralised zone (WB034)

				Content of Elements, wt. %					
B.H.I.D.	**Depth (m)**	**Stratigraphy**	**Samples**	**Fe**	**S**	**Ni**	**Cu**	**Co**	**Total wt. %**
				Pentlandite					
WB034	1060.85	F Z	1	31.28	31.91	33.99	0.00	1.53	98.71
WB034	1060.85	F Z	2	30.25	33.13	34.21	0.52	1.52	99.63
WB034	1060.85	F Z	3	39.74	35.59	23.31	0.12	1.05	99.81
WB034	1060.93	F Z	4	30.36	32.41	34.55	0.00	1.39	98.71
WB034	1060.93	F Z	5	31.24	33.88	33.94	0.00	1.33	100.39
WB034	1060.93	F Z	6	31.61	33.22	34.26	0.00	1.31	100.40
WB034	1060.93	F Z	7	31.71	33.27	34.29	0.00	1.31	100.58
WB034	1060.93	F Z	8	29.96	33.48	34.05	0.00	1.22	98.71
WB034	1060.93	F Z	9	30.47	34.05	34.59	0.00	1.26	100.37
WB034	1060.93	F Z	10	31.11	33.50	34.34	0.00	1.22	100.17
WB034	1060.85	F Z	11	30.12	33.65	34.71	0.15	1.37	100.00
				Sugakiite					
WB034	1060.85	F Z	12	30.68	33.25	27.04	7.69	1.12	99.78
				Chalcopyrite					
WB034	1060.85	F Z	13	30.45	34.72	0.01	34.12	0.02	99.32
WB034	1060.85	F Z	14	29.85	34.54	0.11	33.81	0.02	98.33
WB034	1060.93	F Z	15	28.99	34.98	0.02	34.09	0.01	98.09
WB034	1060.93	F Z	16	29.51	35.13	0.02	34.22	0.00	98.88
WB034	1060.93	F Z	17	27.43	34.81	0.02	32.35	0.01	94.62
WB034	1060.93	F Z	18	28.99	34.98	0.02	34.09	0.01	98.09
WB034	1060.93	F Z	19	29.51	35.13	0.02	34.22	0.00	98.88
WB034	1060.93	F Z	20	27.43	34.81	0.02	32.35	0.01	94.62

WB034	1060.85	F Z	21	29.28	34.91	0.05	33.48	0.01	97.73
				Pyrrhotite					
WB034	1060.85	F Z	22	59.86	38.30	0.46	0.05	0.00	98.67
WB034	1060.85	F Z	23	58.98	38.50	0.43	0.13	0.00	98.04
WB034	1060.93	F Z	24	59.33	38.43	0.58	0.00	0.01	98.35
WB034	1060.93	F Z	25	59.70	38.86	0.60	0.03	0.02	99.21
WB034	1060.93	F Z	26	59.67	38.47	0.57	0.00	0.01	98.72
WB034	1060.93	F Z	27	59.92	38.66	0.40	0.00	0.00	98.98
WB034	1060.93	F Z	28	59.21	38.72	0.46	0.00	0.02	98.41
WB034	1060.93	F Z	29	59.62	38.96	0.46	0.04	0.01	99.09
WB034	1060.93	F Z	30	59.73	38.52	0.46	0.00	0.01	98.72
WB034	1060.93	F Z	31	59.94	38.45	0.43	0.00	0.01	98.83
WB034	1060.93	F Z	32	60.00	38.48	0.46	0.02	0.00	98.96
WB034	1060.85	F Z	33	59.23	39.30	0.23	0.03	0.00	98.79
				Mackinawite					
WB034	1060.85	F Z	36	30.2	34.18	24.04	9.84	0.8	99.06
WB034	1060.85	F Z	37	29.41	33.52	19.3	14.28	0.62	97.13
WB034	1060.85	F Z	39	27.51	32.35	12.16	19.76	0.4	92.18

F Z - F zone mineralisation

Table 5.7. Sulphide composition within the T-mineralised zone (WB195)

				Content of elements, wt. %					
B.H.I.D.	**Depth (m)**	**Stratigraphy**	**Samples**	**Fe**	**S**	**Ni**	**Cu**	**Co**	**Total wt. %**
				Pentlandite					
WB195	905.6	T Z	1	28.20	33.19	35.23	0.00	1.56	98.18
WB195	898.7	T Z	2	28.46	33.38	37.48	0.18	0.05	99.55
WB195	898.7	T Z	3	28.98	33.52	37.53	0.31	0.04	100.38
WB195	898.7	T Z	4	29.25	33.49	35.64	0.00	1.45	99.83
WB195	905.6	T Z	5	27.83	33.17	37.05	0.01	1.62	99.68
WB195	905.6	T Z	6	29.13	32.98	37.40	0.00	0.10	99.61
				Chalcopyrite					
WB195	898.7	T Z	7	29.93	34.88	0.06	34.21	0.01	99.09
WB195	905.6	T Z	8	29.92	34.94	0.00	34.56	0.02	99.44
WB195	905.6	T Z	9	29.89	35.10	0.36	34.05	0.04	99.44
WB195	905.6	T Z	10	31.70	37.73	0.46	30.39	0.37	100.65
				Pyrite					
WB195	898.7	T Z	11	45.37	53.63	1.39	0.07	0.00	100.46
WB195	898.7	T Z	12	46.33	53.84	0.52	0.38	0.02	101.09
WB195	905.6	T Z	13	46.44	53.50	0.09	0.00	0.01	100.04
WB195	905.6	T Z	14	44.00	53.65	0.13	0.09	2.60	100.47

T Z - T zone Mineralisation

Chapter 6

Whole rock geochemistry and mineral chemistry of the Waterberg PGE deposit, South Africa: implication for the Bushveld stratigraphy and the formation of the PGE mineralisation.

This chapter contains the full text of the paper "Whole rock geochemistry and mineral chemistry of the Waterberg PGE deposit, South Africa: implications for the Bushveld stratigraphy and the formation of the PGE mineralisation" by McCreesh, M. J. G., Yudovskaya, M. and Kinnaird, J. A. still in preparation.

This paper sets out to investigate the whole-rock and mineral chemistry of the Waterberg stratigraphy, with the intention of revealing the mechanisms involved in the formation or emplacement of the mineralisation. Geochemical comparisons are made with the rest of the Bushveld Complex and the known mineralisation which occurs in the northern limb south of the Waterberg project area.

6.1. Candidate's contribution:

- The candidate was responsible for detailed logging, sample collection and preparation for analysis, as well as petrology, mineral microprobe analyses, figure production, data interpretation and wrote the paper.
- The candidate contributed approximately 90% towards the publication.
- Marina Yudovskaya and Judith Kinnaird assisted with data interpretation and discussion during the preparation of the manuscript.

6.2. Abstract

The Waterberg Cu-Ni-PGE deposit is situated in the Southern Marginal Zone of the Limpopo Belt, north of the exposed northern limb. The Waterberg stratigraphy is subdivided into a basal Ultramafic Sequence (UmS), overlying Troctolite-Gabbronorite-Anorthosite (TGA) sequence and an Upper Zone (UZ) based on indicator minerals and magnetic susceptibility results. The whole-rock and mineral compositions suggest influxes of a more primitive magma and show upward fractionation trends, however, with numerous reversals and discontinuity in mineral compositions. The lower F zone mineralisation shows striking similarities in mineral and whole-rock chemistry, Pt/Pd ratios and Au enrichment to some Platreef localities, although it does have its own unique characteristic. The upper T zone situated at the boundary between the TGA sequence and UZ has sulphides and PGE mineralisation predominately hosted by felsic-rich lithologies with extremely low Cr (>300 ppm) concentrations and a more evolved chemistry compared with the lower F zone. The upper mineralisation on the Aurora project shows similarities in Cu, Pd and Au-rich mineralisation with an anti-correlation with Cr. However, differences are seen in the mineral chemistry and the stratigraphic position of the mineralised intervals. Although there are comparisons with the Bushveld succession elsewhere, significant differences in thickness and type of lithologies, geochemistry, and mineralisation of the Waterberg segment, compared to the rest of the Bushveld Complex, suggest that the Waterberg ultramafic-mafic body represents a structurally controlled separate compartment of the Bushveld Complex north of the Hout River shear zone.

6.3. Introduction

The northern limb of the Bushveld Complex includes one of the world's most important Ni-Cu-PGE deposits hosted by the Platreef (see reviews in Kinnaird *et al*., 2005; McDonald and Holwell, 2011; Kinnaird and Nex, 2015). Anglo Platinum has been exploiting the shallow Platreef since 2001 with open pit operations at the Mogalakwena complex. Recently, Ivan Plats started to sink a shaft on Turfspruit farm to mine what they call the Flatreef, a gently dipping portion of the Platreef at depth (Grobler *et al*., 2012; Grobler *et al*., 2018). In recent years the discovery of Cu-Ni-PGE deposits associated with the upper Main Zone of the northern limb stratigraphy have brought renewed interests to the northern limb (Harmer *et al*., 2004; Maier and Barnes, 2010). The discovery of the Waterberg Cu-Ni-PGE deposits by Platinum Group Metals (Ltd) (RSA), focuses on a >3.5 by 24 km lobate intrusion where two mineralised zones have been intercepted, a lower ultramafic mineralised F-zone and an upper felsic-rich mineralised T-zone. The purpose of this paper is to provide detailed descriptions of the stratigraphy, geochemistry and mineralogy of the Waterberg Cu-Ni-PGE deposits. This will allow comparison between the two mineralised intervals on the Waterberg deposit with mineralised zones in the northern limb such as the Platreef or the recently discovered mineralisation in the upper Main Zone on the Moorddrift farm south of the Planknek-Ysterberg fault or in the apparent Main Zone of the Aurora project in the northern portion of the northern limb.

Geology of the Northern limb

The northern limb is exposed over a strike length of 110 km and is 15 km wide (van der Merwe, 1976; Gain and Mostert, 1982). The northern limb extends from the Zebediela fault in the south to the Hout River Shear Zone in the north (Fig. 6.1) (van der Merwe, 1976; Good and de Wit, 1997). The footwall rocks from south of the Zebediela fault northwards are progressively older Transvaal Supergroup sediments until north of Zwartfontein the layered rocks rest on Archean granite gneisses (Fig. 6.1) (Hall, 1932; Eriksson *et al*., 2001). The Transvaal Supergroup sediments subdivided into a lower Chuniespoort Group and an upper Pretoria Group were deposited upon the Archean granite-gneisses during the period from 2670-2100 Ma (Eriksson *et al*., 2001). The magmatic succession in the northern limb is similar to the eastern and western limbs although detailed stratigraphy is significantly different and cannot be directly compared with the rest of the Bushveld Complex (McDonald and Holwell, 2011).

The Marginal Zone is poorly exposed although is interpreted as the earliest intrusion composed of fine-grained noritic and pyroxenitic sills which are associated with the footwall metasedimentary rocks beneath or above the Lower Zone (Yudovskaya *et al*., 2013).

North of the Ysterberg-Planknek fault the Lower Zone was believed to form satellite bodies cutting Archean granite-gneisses (Fig. 6.1) (van der Merwe, 1976). However, more recent drilling has revealed Lower Zone successions, up to 800 m thick on Sandsloot and Turfspruit (Yudovskaya *et al*., 2013). The ultramafic sequence was emplaced in trough-like depressions within the metasedimentary rocks and the Archean granite-gneisses (Yudovskaya *et al*., 2013). These Lower Zone successions are similar to the Grasvally section of the northern limb south of the Ysterberg-Planknek fault (Hulbert and von Gruenewaldt, 1982, 1985) and to the basal ultramafic sequence found in the Clapham section of the eastern limb (Wilson, 2012) but differ somewhat to the ultramafic sequence as described in the western limb (Teigler and Eales, 1996). These Lower Zone rocks of the northern limb are chemically primitive (Mg# up to 91), with the highest recorded Cr_2O_3 wt. % in chromitite layers and the presence of economic Ni-PGE sulphides (Hulbert and von Gruenewaldt, 1982, 1985; Yudovskaya *et al*., 2013).

The Platreef is developed north of the Ysterberg Planknek fault. It comprises a series of geochemically distinct mafic-ultramafic sills, dominated by feldspathic pyroxenite (Hutchinson and Kinnaird, 2005; Kinnaird *et al*. 2005). The Platreef is a complex PGE-, Cu- and Ni-bearing body situated between the footwall and Main Zone, which obtains a strike length of 30 km north of Mokopane (Van der Merwe, 1978; Armitage *et al*., 2002; Kinnaird *et al*., 2005; Kinnaird and McDonald, 2005). The Platreef is not a simple tabular deposit. The orientation varies from south to north, generally dipping at 45° to the west, and flattens with depth where it is then termed the Flatreef, dipping at 10° to 15° southwest (Grobler *et al*., 2012). Locally the Platreef is up to 500 m thick due to the incorporation of thick interlayers of metasedimentary rocks (Kinnaird *et al*., 2005). Further north where the Platreef rests on Archean granite gneisses it has a thickness of approximately 50 m (Kinnaird *et al*., 2005). The top of the Platreef is marked by a spotted anorthosite, however, northwards the hanging wall grades into a norite or gabbronorite (Kinnaird *et al*. 2005; Mitchell and Scoon 2012; Van der Merwe 2012).

The Main Zone unconformably overlies the Platreef and is host to a 100 m thick troctolitic horizon unqiue to the Main Zone of the northern limb (Van der Merwe, 1976; Ashwal *et al*., 2005). The Main Zone is approximately 2000 m thick and is composed of gabbronorite and norite with minor anorthosite and pyroxenite layers (van der Merwe, 1976; Ashwal *et al*., 2005; Roelofse and Ashwal, 2012). The Main-Upper Zone boundary is identified by the first appearance of cumulus magnetite, which forms up to 20

magnetitite layers further up the sequence (Eales and Cawthorn, 1996; Ashwal *et al*., 2005). In a detailed study of the Bellevue drill core, a magnetic susceptibility meter was used to determine the boundary between the Main and Upper Zones. The study revealed that the boundary is approximately ~50 m below the appearance of cumulus magnetite (Ashwal *et al*., 2005).

The UZ in the northern limb is approximately 1400 m thick (Ashwal *et al*., 2005). The Rustenburg layered Suite in the northern limb is covered by granophyres and Bushveld granites (Fig. 6.1). These roof rocks consist of the older Rooiberg Group felsites which predate the layered rocks, and the younger Lebowa Granite Suite (McNaughton *et al*., 1993).

PGE mineralisation is not restricted to the Platreef in the northern limb. South of the Ysterberg-Planknek fault PGE mineralisation is hosted in a pyroxenite layer in the upper Main Zone on Moorddrift farm (Fig. 6.1) (Maier and Barnes, 2010; Holwell *et al*., 2013). In the far north of the northern limb where the Main Zone rocks reappear and rest on Archean granite-gneisses on the Aurora project (Fig. 6.1), PGE mineralisation has been discovered within felsic-rich lithologies (Manyeruke, 2007; Maier *et al*., 2008; McDonald *et al*., 2017). In addition, the Waterberg mineralisation described in this paper has led to a surge of interest in atypical PGE mineralisation in Bushveld rocks.

The Waterberg PGE deposit

The Waterberg platinum project is focused on a >3.5 x 24 km lobate body north of the Hout River Shear Zone (Fig. 6.1) (Kinnaird *et al*. 2017). The project area lies 85 km north of Mokopane in the Seshego, Mokerong and Bochum districts of the Limpopo Province. The Waterberg PGE deposit, discovered by Platinum Group Metals (Ltd) (RSA) in 2011, has a NE-SW strike which contrasts with the north-south orientation of the exposed northern limb south of the Hout River Shear Zone. The Waterberg sector has a general dip of 34° - 38° towards the northwest although some blocks show different dip angles depending on structural and tectonic controls (Lomberg and Goldschmidt 2014). U/Pb zircon age dating of the layered succession gives intrusion ages of 2059±3 and 2053±5 Ma (Huthmann *et al*., 2016) indicating that the Waterberg Bushveld succession is coeval with the rest of the Bushveld Complex (Walraven and Hattingh, 1993; Zeh *et al*., 2015).

Geology of the Waterberg PGE deposit

The stratigraphy and geology of the Waterberg project is described in detail by McCreesh (2016), Huthmann *et al*. (2016) and Kinnaird *et al*. (2017), therefore only a short overview is described below.

The footwall is Archean Hout River Granite Gneiss, although most boreholes intercept a mixing zone between the basement granite-gneiss and the initial Bushveld magma, known as granofels (McCreesh and Kinnaird, 2014). Overlying the granofels footwall is an Ultramafic Sequence (UmS) which ranges from 100 to 2.5 m thick. The UmS comprises a basal medium-grained feldspathic orthopyroxenite and feldspathic pyroxenite and the overlying feldspathic harzburgite grading into a mela-troctolite which is generally altered (Kinnaird *et al*., 2017). The UmS hosts the basal mineralisation known as the F zone.

The boundary between the UmS and the overlying troctolite-gabbronorite-anorthosite (TGA) sequence is gradational and interpreted as a result of magmatic erosion during the surge of the troctolite magma emplacement (Kinnaird *et al*., 2017). The TGA sequence is characterised by a troctolite package at the base grading into olivine gabbronorite, gabbronorite and minor feldspathic pyroxenite and anorthosite layers towards the top of the succession. The TGA sequence is 400 m to 800 m thick (McCreesh, 2016; Kinnaird *et al*., 2017). The upper mineralised T zone occurs at the boundary between the TGA sequence and the UZ. This package of sulphide-bearing lithologies comprises gabbronorite, anorthosite, olivine feldspathic pyroxenite, troctolite and harzburgite.

The boundary between the Main Zone and UZ is determined by magnetic susceptibility as used on the Bellevue drillcore (Ashwal *et al*., 2005). The UZ is dominated by magnetite-bearing gabbronorite and ferro-gabbro and ranges from 0 m to 500 m thick (McCreesh, 2016). The UZ is not present throughout the deposit mostly due to ancient erosional processes prior to the deposition of the younger Waterberg sediments (Kinnaird *et al*., 2017). The UZ succession of the Waterberg project lacks the magnetitite layers which characterise the UZ south of the Hout River Shear Zone.

The overlying Waterberg Group is subdivided into the Setlaole and Makgabeng Formations (McCreesh, 2013; Engela, 2014). The Setlaole Formation consists of medium to coarse-grained granule-rich arenites, banded arkoses and fine-grained mudstone with a poorly sorted quartz-pebbly conglomerate at the basal unconformable contact (McCreesh, 2013). This formation has upward fining channels deposited in narrow braid plains of fluvial systems (Jansen, 1982), and has a maximum thickness of 450 m. The Makgabeng Formation gradationally overlies the Setlaole Formation and is composed of medium-grained sandstones. A dolerite sill with a maximum thickness of 200 m, but typically ~80 m thick, is intercepted in most boreholes (McCreesh 2016; Kinnaird. *et al*., 2017). It has distinctive thick chilled margins at both contacts. The sill forms part of the Umkondo Igneous Province with a baddeleyite age of 1125 ± 5 Ma (Huthmann *et al*., 2016).

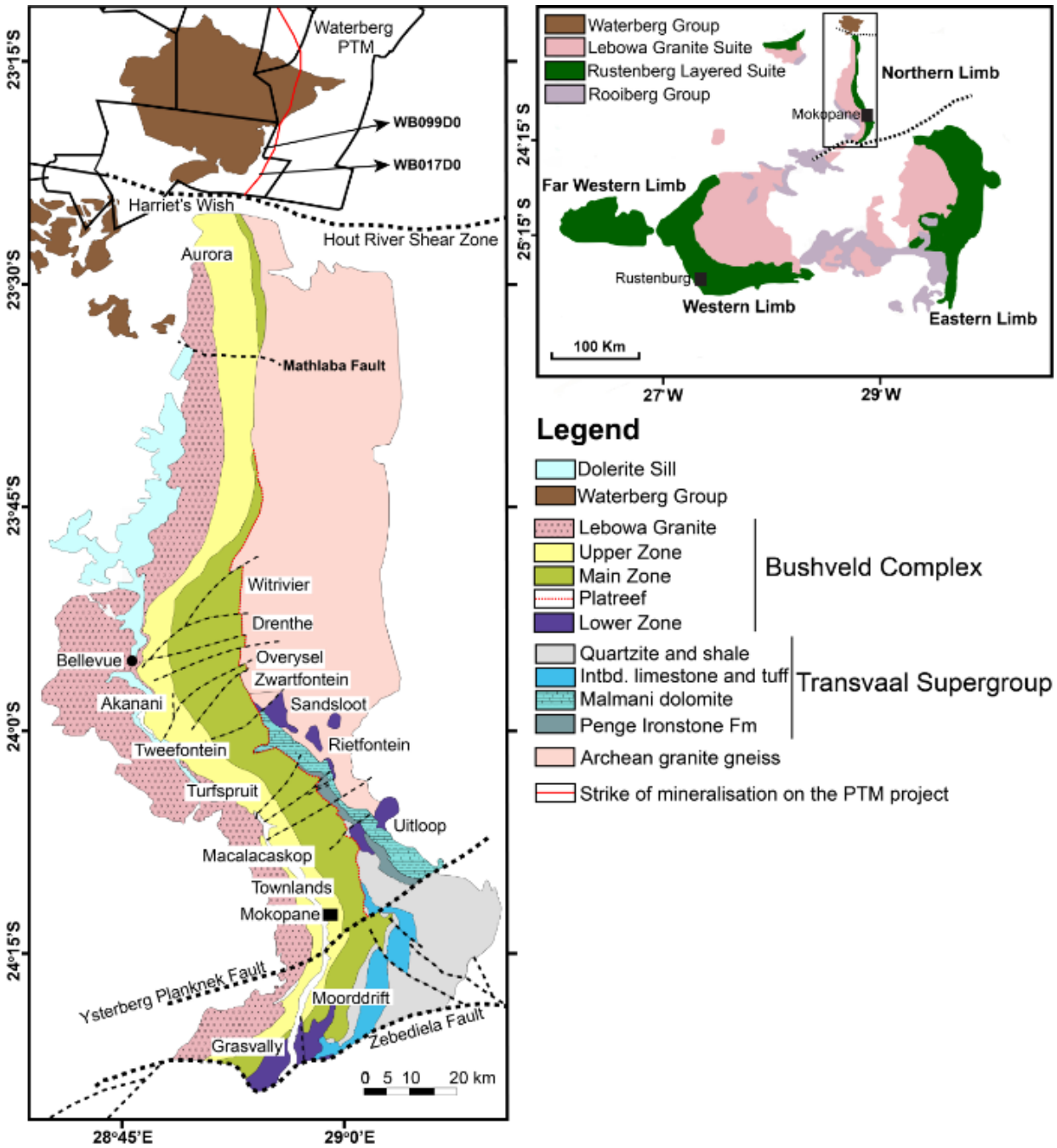

Figure 6.1: Schematic geological map of the Bushveld Complex and enlarged map of the northern limb including the extension of the Waterberg Project in the far north, as well as the location of boreholes WB017 and WB099. Modified after 1:250 000 geological map of the northern limb (van der Merwe, 1976). PTM: Platinum Group Metals Ltd; HRSZ: Hout River Shear Zone; YPF: Ysterberg-Planknek fault; TML: Thabazimbi-Murchison Lineament.

6.4. Sample material

Borehole WB017

Borehole WB017 is located in the south-west portion of the Platinum Group Metals Ltd (PTM) exploration site on the farm Ketting 368LR (Fig. 6.2) and extends 1094.23 m in depth. The footwall rocks are composed of granofels and pyroxenite, formed from the interaction between the Bushveld magma and the footwall Archean granite gneisses. Overlying is the Ultramafic Sequence (UmS) (Fig. 6.2), which has an apparent thickness of 75.74 m. The UmS is dominated by a harzburgite unit grading into a mela-troctolite unit and a thick basal feldspathic orthopyroxenite and pyroxenite unit. The harzburgite unit at the top of the UmS is 12.24 m thick. The mela-troctolite unit of the UmS is 5.60 m thick. The harzburgite and mela-troctolite units have gradational contacts. The basal feldspathic orthopyroxenite unit is 55.80 m thick with a pegmatoidal unit in the middle from 1047.00 m to 1054.00 m depth. The UmS has extensive alteration (chloritisation and serpentinisation), especially associated with the olivine-bearing rocks.

The UmS is gradationally overlain by the troctolite-gabbronorite-anorthosite (TGA) sequence, which is dominated by a troctolite package at the base that is approximately 23 m thick, which grades upwards into an olivine-bearing gabbronorite-norite. Olivine decreases upwards with gabbronorite, norite and minor anorthosite, towards the top of the TGA sequence (Fig. 6.2). The TGA sequence has an apparent thickness of 403.76 m. In the middle of the homogenous sequence is an anorthosite layer (693.20 m – 714.00 m depth) with sharp bottom and top contacts. Towards the top contact of the TGA sequence there is a zone composed of varied rock types that include a feldspar-rich pegmatoid, feldspathic pyroxenites, harzburgite and sulphide-bearing gabbronorite. This is the mineralised T zone, with a thickness of 43.89 m (642.50 m to 689.39 m). The T zone is subdivided into the T1 with is composed of feldspathic pyroxenite and harzburgite and the underlying T2 that is composed of sulphide-bearing gabbronorite.

The TGA sequence and UZ boundary is at a depth of 600 m in this core. The boundary was determined by magnetic susceptibility and the appearance of fine-grained, disseminated titanomagnetite (Fig. 6.2). The UZ has an apparent thickness of 421.37 m, dominated by magnetite-bearing gabbronorite and minor ferrogabbro units towards the top.

An angular unconformity marks the boundary between the Waterberg sediments (WB) (Fig. 6.2) and the underlying Bushveld lithologies, at a depth of 176.73 m. The Waterberg package is mainly composed of

banded arkose, sandstone and mudstone and at the base of the sedimentary sequence there is a poorly sorted quartz pebble conglomerate. Close to the base of the sediment package is a 27 m thick dolerite sill that crosscuts the core (142.66 m to 169.73 m).

Borehole WB099

Borehole WB099 from the northeastern portion of the farm Ketting 368LR (Fig. 6.2) is 1343.92 m long. The footwall agmatite at the base of the borehole (1319.32 m to 1343.92 m depth), has alternating felsic-rich and pyroxenite-rich bands. The pyroxenite-rich intervals are extensively chloritised and serpentinised. The overlying Ultramafic Sequence (UmS) (Fig. 6.2) has an apparent thickness of 49.32 m in this borehole. The UmS is dominated by feldspathic orthopyroxenite, minor troctolite and harzburgite. The troctolite unit sandwiched in the basal feldspathic orthopyroxenite is 5 m thick. The basal feldspathic orthopyroxenite overlying the troctolite is 13 m thick and the underlying feldspathic orthopyroxenite is 12 m thick. The feldspathic orthopyroxenite is medium-grained with disseminated chalcopyrite and pyrrhotite. There is only one feldspathic harzburgite layer in the UmS (1285.36 m to 1291.27 m depth), which is medium-grained with disseminated chalcopyrite and pyrrhotite. The UmS has extensive alteration (chloritisation and serpentinisation), particularly associated with the olivine-bearing rocks.

The troctolite package overlying the UmS has an apparent thickness of 77 m and is coarse-grained with melanocratic and leucocratic variations depending on the olivine content within the TGA sequence. The TGA sequence has an apparent thickness of 616.31 m (Fig. 6.2). The TGA sequence is composed of a troctolite package at the base grading into olivine-bearing gabbronorite-norite, which grades into typical Main Zone gabbronorite with minor anorthosite, pegmatoids, feldspathic pyroxenite and olivine-bearing pyroxenite towards the top of the sequence. The T zone has an apparent thickness of 50 m in this borehole, dominated by sulphide-bearing gabbronorite (T2) and olivine-bearing feldspathic pyroxenite (T1). The mineralised gabbronorite (T2) has fine-grained disseminated chalcopyrite and towards the base, coarse, blebby sulphides of pentlandite and pyrrhotite.

The UZ is marked by the appearance of fine-grained interstitial magnetite, the presence of which is supported by magnetic susceptibility results. The UZ has an apparent thickness of 129.17 m in this borehole (Fig. 6.2) and is predominately composed of magnetite-bearing gabbronorite with minor ferrogabbro towards the top.

The Waterberg (WB) sedimentary rocks have a sharp contact with the underlying Bushveld rocks and have an apparent thickness of 520.97 m (Fig. 6.2). The WB is mainly composed of banded arkose, coarse-grained sandstone, and fine-grained chocolate-coloured mudstone, including a poorly sorted quartz-rich pebble conglomerate at the base of the sedimentary sequence. There are two dolerite sills crosscutting the WB; the thicker of the two sills occurs from 361.59 m to 443.20 m in this borehole (Fig. 6.2) and the other, thinner sill close to the top of the borehole is 16.77 m thick. The dolerite sills have well-defined chilled margins on both their upper and lower contacts and are generally coarse-grained towards the centre, with extensive chloritisation and epidotisation.

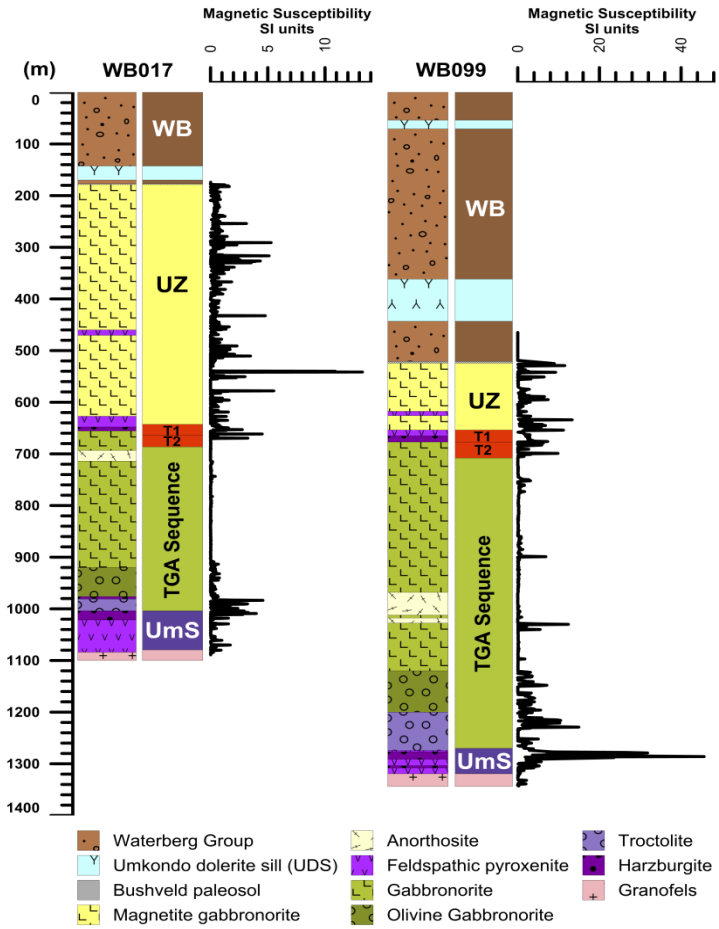

Figure 6.2: Lithological columns of boreholes (a) WB017 and (b) WB099 showing the stratigraphy and lithologies intercepted at depth on the Waterberg PGE deposit. WB, Waterberg Group; UZ, Upper Zone; T1 and T2, T zone; TGA sequence, troctolite-gabbronorite-anorthosite sequence; UmS, Ultramafic Sequence.

6.5. Analytical Methods

Magnetic susceptibility measurements were done along the lengths of WB017 and WB099 using a handheld magnetic susceptibility meter (Kappa-Meter KM-7). An average of 3 readings were recorded

every half meter (Fig. 6.3). This method has been used elsewhere in the northern limb to determine the boundary between the Main and Upper Zone (Ashwal *et al*., 2005).

Quarter-core sampling (15-30 cm in length) was undertaken through the stratigraphy of the borehole cores and representative samples selected for specific rock types. Samples were cut along the core axis and one-half was milled for geochemical analyses, and the other half was used for polished sections and mineral separation.

Samples were crushed, milled in a tungsten carbide mill, and analysed at the Earth laboratory, Bernard Price Building, University of the Witwatersrand. Whole-rock major elements were analysed by PANalytical PW2404 X-ray fluorescence (XRF) using the fused disk method. Trace elements content were also determined by the PANalytical PW2404 X-ray fluorescence (XRF) using pressed pellets and matrix-matched standards, and a detailed description of analytical procedure can be found in Wilson (2012). The Pt, Pd and Au data was provided by Platinum Group Metals Ltd RSA (PTM).

The remaining portion of the quarter-core samples were crushed, milled and sieved to an approximate size (250-100 µm). These samples were then cleaned with water and dried in an oven at 80°C. Mineral grains of orthopyroxene, clinopyroxene, plagioclase and olivine were picked under the microscope and placed on double-sided tapes in rows according to the sample. A circular mould is placed over the grains and an Epofix Resin is poured into the mould to make ore blocks. The ore blocks were carbon-coating prior to analysis.

Electron probe microanalysis data acquisition took place at Department of Geology, Rhodes University, utilising the Jeol JXA 8230 Superprobe, using four wavelength-dispersive spectrometers. The analytical conditions employed were: acceleration voltage of 15 kV, probe current 20 nA, counting time of 10 seconds on peak and 5 seconds on the background. Orthopyroxene and clinopyroxene grains were analysed with a beam spot of 1 µm in diameter. The standards used for quantifying the characteristic Kα radiations were natural minerals: albite standard (sd) for Na, orthoclase sd for K, kaersutite sd for Si, plagioclase (An 65) sd for Al and Ca, periclase sd for Mg, magnetite sd for Fe, rutile sd for Ti, pentlandite sd for Ni, rhodonite sd for Mn and chromite sd for Cr. The ZAF matrix correction method was used for quantification. EPMA analysis provides major element data to within 2% error, totals were between 98.5 % and 101.5%; results which did not fall within this error margin were omitted from the study.

6.6. Results

6.6.1. Magnetic Susceptibility

The magnetic susceptibility profiles are based on more than 8000 measurements through the two boreholes (Fig. 6.2). The granofels at the base of the stratigraphy has very low magnetic susceptibility values. The magnetic susceptibility values increase in the UmS due to the presence of pyrrhotite in the feldspathic orthopyroxenite and secondary magnetite formed by serpentinisation of olivine (Fig. 6.2). The magnetic susceptibility values range from 5.00 to >40.00 SI units associated with the UmS (Fig. 6.2). Through the TGA sequence the magnetic susceptibility measurements decrease upwards as the olivine content decreases. Above the olivine-bearing lithologies, the susceptibility values are very low (0.05 SI units), consistent with the Main Zone magnetic susceptibility values obtained in the Bellevue drillcore (Ashwal *et al*., 2005). Minor increased magnetic susceptibility values (5.00 SI units) within the TGA sequence are associated with thin olivine-rich intervals (Fig. 6.2). The magnetic susceptibility measurements increase slightly (0.01 to 3.00 SI units) towards the base of T2 due to the presence of pyrrhotite, which increase upwards into the T1, and have values between 1.00 and 12.00 SI units associated with olivine-rich lithologies and disseminated titanomagnetite (Fig. 6.2). Above the T-zone the magnetic susceptibility values (>5.00 SI units) increase dramatically, associated with incoming disseminated titanomagnetite of the UZ (Fig. 6.2). The position where there is a dramatic increase in the magnetic susceptibility values is where the boundary is placed between the TGA sequence and UZ, similar to the results obtained in the Bellevue drillcore study by Ashwal *et al*. (2005). The Ti and V content in the UZ are inversely proportional, although this has no effect on the magnetic susceptibility values (Klemn *et al*., 1985; Cawthorn and Molyneux, 1986; Clark and Emerson, 1991; Clark, 1997; Ashwal *et al*., 2005). The magnetic susceptibility values are dependent on the size of the titanomagnetite crystals with values ranging from 1.00 to 50.00 SI units (Clark and Emerson, 1991).

6.6.2. Petrology

In both cores, the footwall is represented by a banded granofels consisting of alternating felsic and mafic-rich units, similar to that seen in the northern limb where Bushveld lithologies overlie Achaean granite gneiss (Cawthorn *et al*., 1985). This interval is sometimes overlain by fine-grained gabbronorite, norite and pyroxenite interpreted as Marginal sills (Kinnaird *et al*., 2017). The major silicate minerals of the lower UmS within the feldspathic orthopyroxenite are subhedral cumulus orthopyroxene (60 to 75 modal %), with mostly subhedral to anhedral interstitial plagioclase (<10 modal %) and clinopyroxene (10 to 15 modal %) (Fig. 6.3a). Accessory minerals include olivine, sulphides, chromite and secondary

biotite, amphibole, sericite and epidote. This lower pyroxenite unit is fine- to medium-grained at the base and coarsens upwards and is homogenous in textural appearance. The overlying feldspathic harzburgite is predominantly composed of subrounded olivine (55 to 80%), cumulus and poikilitic orthopyroxene (15 to 25%) and minor interstitial subhedral to anhedral plagioclase (<10%), although plagioclase increases upwards (Fig. 6.3b). This unit is generally extremely altered with a high degree of serpentinisation and chloritisation. Accessory minerals include sulphides, chromite, and secondary biotite, sericite, magnetite and amphiboles. The chromite is generally disseminated, although in some cases form clusters with up to 70% chromite. There is a lack of chromitite stringers and layers in the Waterberg Bushveld succession.

The base of the TGA sequence is composed of subrounded olivine (45 to 65 modal %) and cumulus euhedral plagioclase (35 to 50 modal %) with large anhedral oikocrysts of orthopyroxene. This basal troctolite unit has disseminations and clusters of chromite up to 60% (Fig. 6.3c). Olivine decreases upwards and cumulus plagioclase, cumulus subhedral orthopyroxene and clinopyroxene (40 to 55 modal %) increases upwards within the gabbronorite package (Fig. 6.3d). The upper mineralised zone consists of varying rock types; the lower T2 is dominated by medium- to coarse-grained homogeneous gabbronorite composed of euhedral laths of plagioclase (50%) with cumulus clinopyroxene and orthopyroxene (45%) and in some cases the presence of inverted pigeonite (Fig. 6.3e). Accessory minerals include sulphides (5 to 10%), biotite, sericite and amphiboles. The upper T1 is identified by the presence of subrounded altered olivine grains ranging from 10 to 60%. The T1 is generally coarse-grained and composed of harzburgite, troctolite or olivine-feldspathic pyroxenite. The middling between the T2 and T1 as well as the hanging wall to the T1 is generally coarse-grained to pegmatoidal and composed of plagioclase (60 to 90 modal %) with anhedral oikocrysts of clinopyroxene and minor titanomagnetite. The middling and hanging wall may contain sulphides.

The presence of finely disseminated cumulus magnetite indicates the start of the UZ overlying the T zone. The UZ is composed of cumulus pyroxenes (35 to 55%) and euhedral plagioclase (50%). The magnetite forms complex intergrowths or symplectic textures with subhedral orthopyroxene grains (Fig. 6.3f). Subrounded olivine grains have been identified at the top of the Bushveld succession in WB017 indicating an olivine-gabbro unit, although this was not identified in WB099.

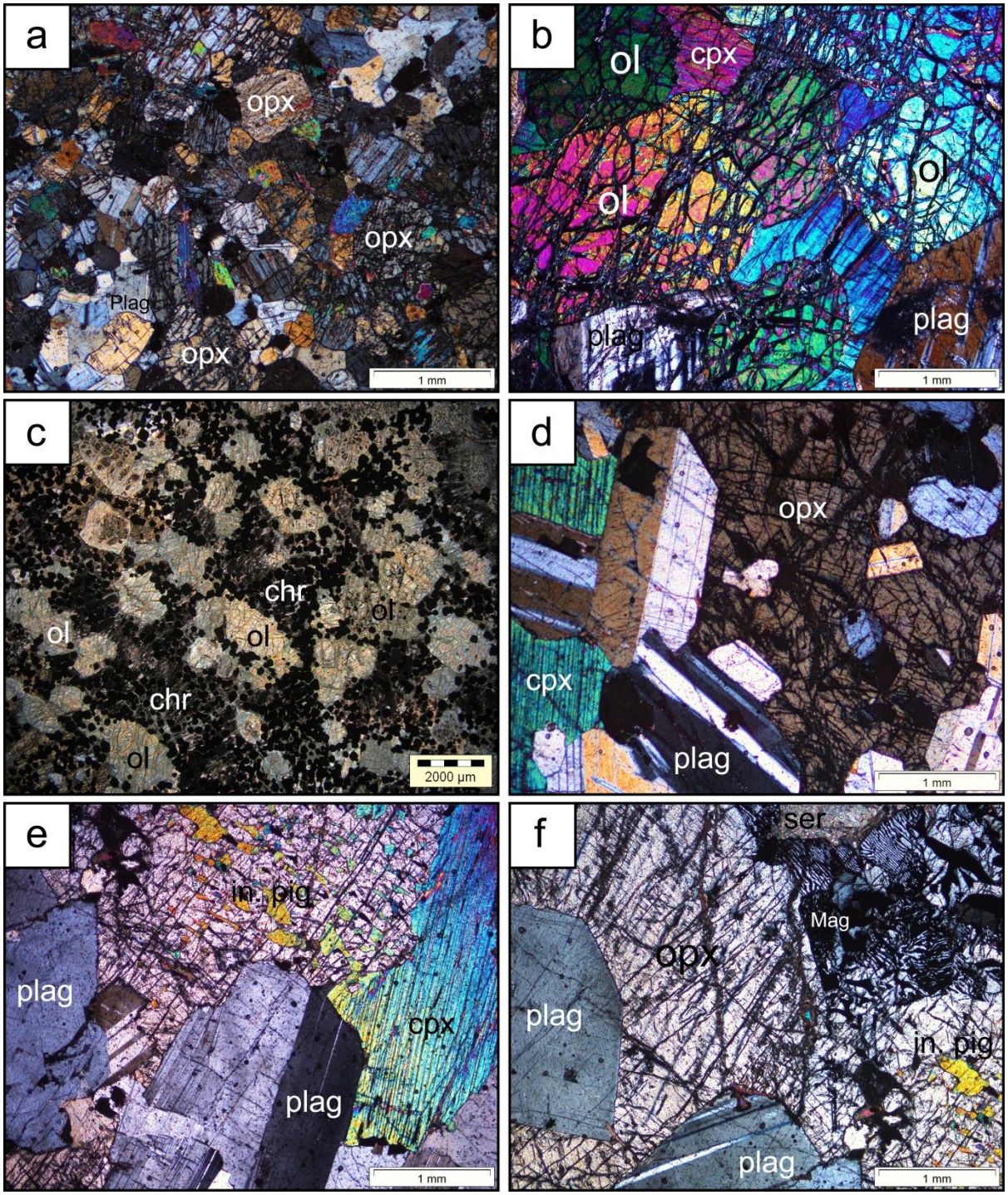

Figure 6.3: Photomicrographs of the different lithologies seen in the Waterberg Bushveld succession (a) fine- to medium-grained orthopyroxene with minor interstitial plagioclase (orthopyroxenite WB099 – 1315.77 m) (b) subrounded olivine associated with interstitial clinopyroxene and plagioclase (harzburgite WB099 – 1228.50 m) (c) (troctolite WB165 – 749.90 m) (d) euhedral plagioclase and subhedral clinopyroxene and orthopyroxene with an ophitic texture (gabbronorite WB099 – 1021.18) (e) euhedral plagioclase and exsolution between clinopyroxene and orthopyroxene (gabbronorite WB099 – 628.50 m) (f) euhedral plagioclase, symplectic texture associated with orthopyroxene and magnetite and inverted pigeonite (magnetite gabbronorite WB099 – 551.80 m). Images a-f are taken in cross polarised, transmitted light.

6.6.3. Mineral chemistry

Mineral chemistry data of orthopyroxene, clinopyroxene, olivine and plagioclase for borehole WB099 are presented in Figures 6.5, 6.6 and 6.7. The data are also shown on relevant classification diagrams in Fig. 6.4.

Orthopyroxene

The orthopyroxene are mainly enstatites and show a range of Mg# between 61 and 87 through the Waterberg Bushveld stratigraphy with the CaO being <2 wt. % (Fig. 6.4 and 6.5). The low-Ca pyroxenes in the UmS are Mg-rich (Mg# 76 to 87; average Mg# 82). These values are similar to both the feldspathic pyroxenite and feldspathic harzburgite lithologies found in the Platreef down dip on Akanani (Yudovskaya *et al*., 2011). The Cr concentration in low-Ca pyroxene within the UmS ranges from 700 to 4300 ppm (average ~2400 ppm), which mirrors the Mg# (Fig. 6.5). MnO (0.16 to 0.40 wt. %) shows an opposite trend to the Mg# and Cr values within the UmS. The Mg# of low-Ca pyroxene in the TGA sequence decreases gradually upwards, with the highest Mg# associated with the troctolite unit at the base of the sequence (Fig. 6.5).

The basal TGA sequence (1270.16 m to 952.00 m) has a high Cr concentration ranging from 700 to 5000 ppm (average ~3100 ppm) hosted by troctolite and olivine-gabbronorite. Above the olivine-bearing intervals at the base of the TGA sequence the Cr content decreases upwards to the base of the T2 (Fig. 6.5). The Mg# of low-Ca pyroxene in the T zone is fairly constant between 67 and 72, with a slight increase in the T1 associated with olivine-rich lithologies. The Cr concentration is fairly low in the T zone between 120 and 900 ppm (average ~500 ppm) which is significantly lower than UmS. The Mn content ranges from 2500 to 3800 ppm and shows an opposite trend to the Mg# (Fig. 6.5). The low-Ca pyroxene in the magnetite gabbronorite samples of the UZ are more Fe-rich and have an Mg# ranging from 63 to 77 (Fig. 6.5).

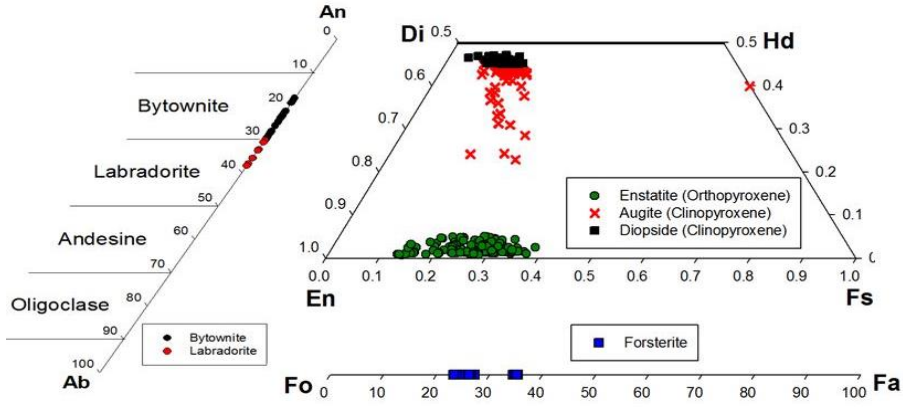

Figure 6.4: Variation in composition of pyroxene, plagioclase and olivine mineral separates in the Waterberg Bushveld stratigraphy.

Clinopyroxene

The clinopyroxenes are mainly augite and diopside, with Mg# between 71 and 93 and the CaO is >20 wt. % (Fig. 6.4 and 6.6). The UmS contains minor amounts of clinopyroxene as this stratigraphic unit is dominated by orthopyroxene. The clinopyroxene compositions obtained from the UmS sequence have an Mg# between 82 and 89 which are slightly higher than the low-Ca pyroxene values (Fig. 6.6). The Cr concentrations are high in the clinopyroxene within the UmS, ranging from 2400 to 9000 ppm (average ~6000 ppm). The MnO shows an opposite trend to the Mg# (Fig. 6.6). The Mg# of the clinopyroxene in the TGA sequence ranges from 77 to 93, with the highest values associated with olivine-bearing gabbronorite, and a slight decrease to the base of the T2.

The clinopyroxene Mg# in the T zone is lower than the two previous sequences, ranging from 73 to 81 (average 78). The Cr concentrations are very low compared with the UmS, the Cr ranges from 300 to 1500 ppm (average ~1000 ppm) (Fig. 6.6). The clinopyroxene grains are slightly more Fe-rich towards the top contact with the UZ lithologies. The Mn values are 1.2 x higher in the T zone compared with the UmS (Fig. 6.6). The Mg# associated with the magnetite gabbronorite of the UZ range from 75 to 83. Overall the clinopyroxene Mg# values are higher through the Waterberg Bushveld stratigraphy compared with the Mg# values obtained from the orthopyroxene samples (Fig. 6.5 and 6.6). Similar features are seen in the northern limb stratigraphy (Bellevue drillcore) and in the Aurora project stratigraphy (Ashwal *et al*. 2005; Roelofse and Ashwal 2012; Tanner *et al*. 2014; McDonald *et al*. 2017).

Plagioclase

The plagioclase is mainly labradorite and bytownite, which displays a variation in composition (An_{54-82}) through the Waterberg stratigraphy (Fig. 6.4). The plagioclase associated with the feldspathic pyroxenite and feldspathic harzburgite within the UmS are generally interstitial and their composition has a large range (An_{54-85}) (Fig. 6.7). Within the TGA sequence the plagioclase crystals are mainly cumulus and the composition has a more restricted range (An_{65-80}, average of An_{72}) (Fig. 6.7). The plagioclase in the T zone has compositions of An_{69-82}, although there are three samples within the mineralised package with more sodic compositions (An_{61-63}) associated with pegmatoidal units. The UZ rocks show the most restricted plagioclase compositions (An_{68-74}) (Fig. 6.7).

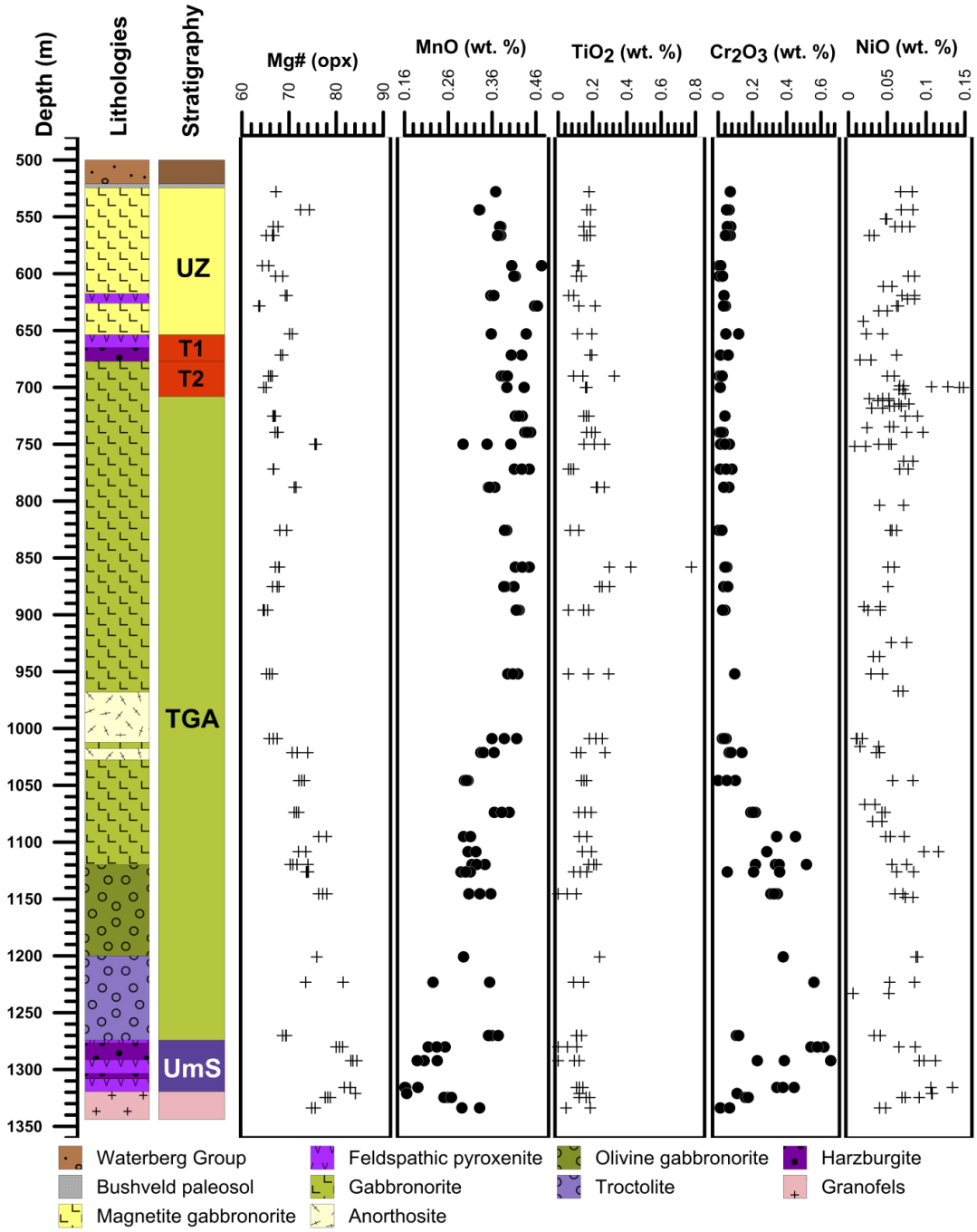

Figure 6.5: The compositional variations in orthopyroxene mineral separates through the stratigraphy of the Waterberg Bushveld succession from borehole WB099: Mg# (Opx), MnO (wt. %), TiO_2 (wt. %), Cr_2O_3 (wt. %) and NiO (wt. %).

Olivine

The olivine composition is dominated by forsterite which ranges from Fo_{61-89} within the olivine bearing units of the Waterberg Bushveld succession (Fig. 6.4). The olivine compositions are extremely high (Fo_{74-89}, average Fo_{82}) within the olivine-bearing UmS (Fig. 6.7). The overlying troctolite unit at the base of the

TGA sequence from 1270.16 m to 1208.00 m, has a restricted composition for olivine (Fo_{76-80}, average Fo_{77}, NiO wt. % 0.23 to 0.27) (Fig. 6.7). Olivine concentrations decrease upwards into an olivine-gabbronorite with a larger compositional range (Fo_{69-75}, average Fo_{72}, NiO wt. % 0.16 to 0.27). The T1 contains olivine with a restricted compositional range (Fo_{64-66}, NiO wt. % 0.18 to 0.21) associated with olivine-feldspathic pyroxenite and troctolite (Fig. 6.7).

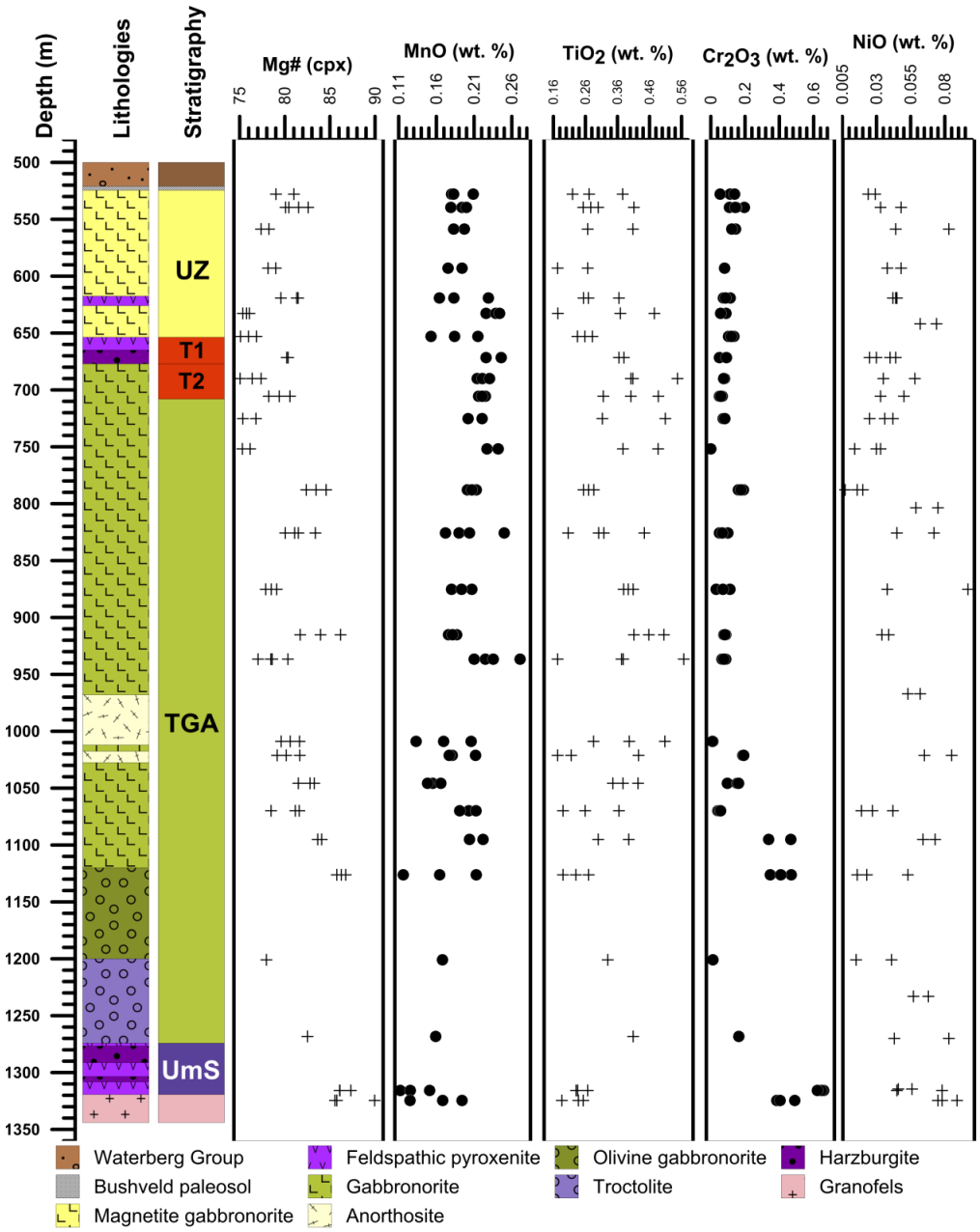

Figure 6.6: The compositional variations in clinopyroxene mineral separates through the stratigraphy of the Waterberg Bushveld succession from borehole WB099: Mg# (Opx), MnO (wt. %), TiO_2 (wt. %), Cr_2O_3 (wt. %) and NiO (wt. %).

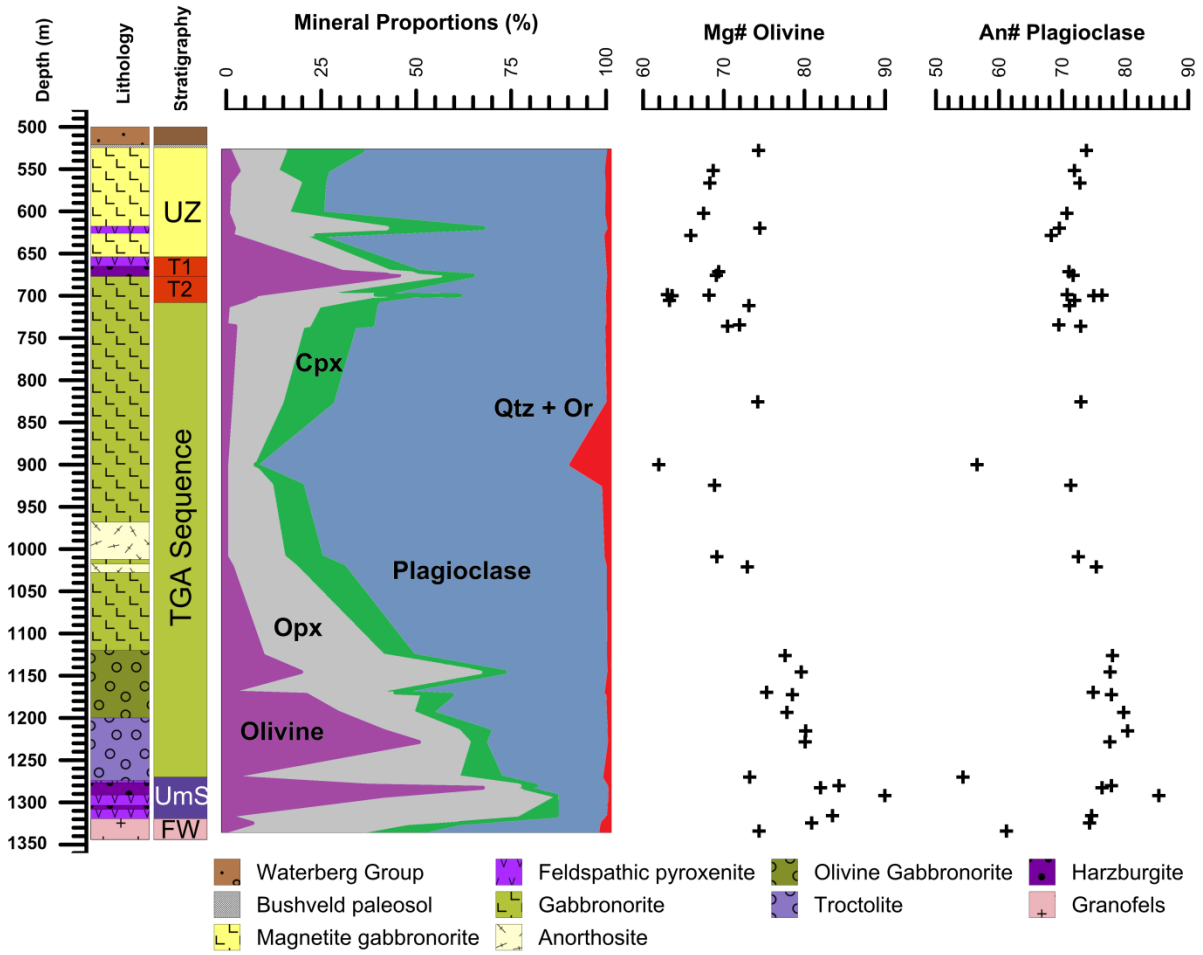

Figure 6.7: The proportions of olivine, orthopyroxene (Opx), clinopyroxene (Cpx), plagioclase and quartz (Qtz) and orthoclase (Or) through the stratigraphy of WB099. The olivine (Mg#) and plagioclase (An#) are also shown through the stratigraphy of borehole WB099.

6.6.4. Whole rock geochemistry

Whole rock geochemical data for borehole WB017 are presented in Figures 6.8 and 6.9. In these graphs the scale has been chosen to represent the data most clearly and to show the full stratigraphy of the Waterberg Bushveld succession. Therefore, some of the extremely altered lithologies, xenoliths or quartz-feldspathic veins are omitted on many diagrams either because of their very low or very high values. In order to determine whether the two mineralised zones in the Waterberg stratigraphy have any compositional similarities, various geochemical ratios and calculations have been chosen.

The Mg# ranges from 68 to 82 (Fig. 6.8h) within the UmS indicating a primitive magma source although the magma was crystallising feldspars. The overlying TGA sequence shows a differentiating sequence with an Mg# of 78 at the base decreasing upwards to 62 (Fig. 6.8h) at the base of the T zone. The Mg# of

the T zone ranges from 70 to 59. The overlying UZ lithologies have Mg# between 70 and 55 generally decreasing upwards (Fig. 6.8h).

The CaO/Al_2O_3 ratio is used to monitor contamination (Kinnaird, 2005). Pure plagioclase has a ratio of 0.6 and orthopyroxene contains minimal amounts of either element, therefore values above or below 0.6 suggest the presence of clinopyroxene or possible reactions with dolomite (Kinnaird, 2005). Most of the samples in the Waterberg succession have $CaO:Al_2O_3$ ratio around 0.6, although there are higher values within the TGA sequences and UZ which may reflect the presence of clinopyroxene (Fig. 6.8g).

According to Eales *et al*. (1986) the $Sr:Al_2O_3$ ratio is used to recognise different magmatic influxes. The UmS shows a large variation with the $Sr:Al_2O_3$ ratio through the feldspathic orthopyroxenite, harzburgite and mela-troctolite, ranging from 4 to 30 (Fig. 6.8f). There is a gradual increase in the $Sr:Al_2O_3$ ratio throughout the TGA sequence with a dramatic decrease associated with the anorthosite and gabbronorite samples directly below the T zone (Fig. 6.8f). At the base of the T2 there is an increase in the $Sr:Al_2O_3$ ratio that decreases gradually towards the top of the T1, with $Sr:Al_2O_3$ dropping from 18 to 10. The UZ samples show a range from 2 to 8 associated with the $Sr:Al_2O_3$ ratio. According to Kinnaird (2005) the Al_2O_3:FeO+MgO ratio varies with changing pyroxene to plagioclase proportions and sudden changes may indicate whether more than one magma was involved in forming the Bushveld succession. There is only one significant change in the Al_2O_3:FeO+MgO ratio at the contact between the UmS and TGA sequence in the Waterberg stratigraphy. The UmS has Al_2O_3:FeO+MgO ratio values < 0.6 and the TGA sequence has values > 1 (Fig. 6.8e). The $SiO_2:Al_2O_3$ shows fairly similar results throughout the Waterberg Bushveld succession although a few samples have slightly higher values (Fig. 6.8a).

The Fe_2O_3 values for the UmS, T zone and the UZ have large variations probably due to the Fe content within the ultramafic, sulphide-bearing and magnetite-bearing lithologies, whereas the TGA sequence has a fairly uniform amount of Fe_2O_3 (Fig. 6.4b). The TiO_2 contents in the UmS varies depending on the lithologies, the feldspathic orthopyroxenite samples have higher TiO_2 values (0.14 and 0.23 wt. %) and the TiO_2 contents ranges between 0.06 to 0.08 wt. % for the harzburgite and mela-troctolite samples. The TGA sequence has constant TiO_2 values with a slight increase within the T zone. The UZ shows a large variation in terms of the TiO_2 content (Fig. 6.8c). Both the UmS and the T zone show large variations in Sr values, whereas the TGA sequence and the UZ have constant values apart from a few anomalies (Fig. 6.8d).

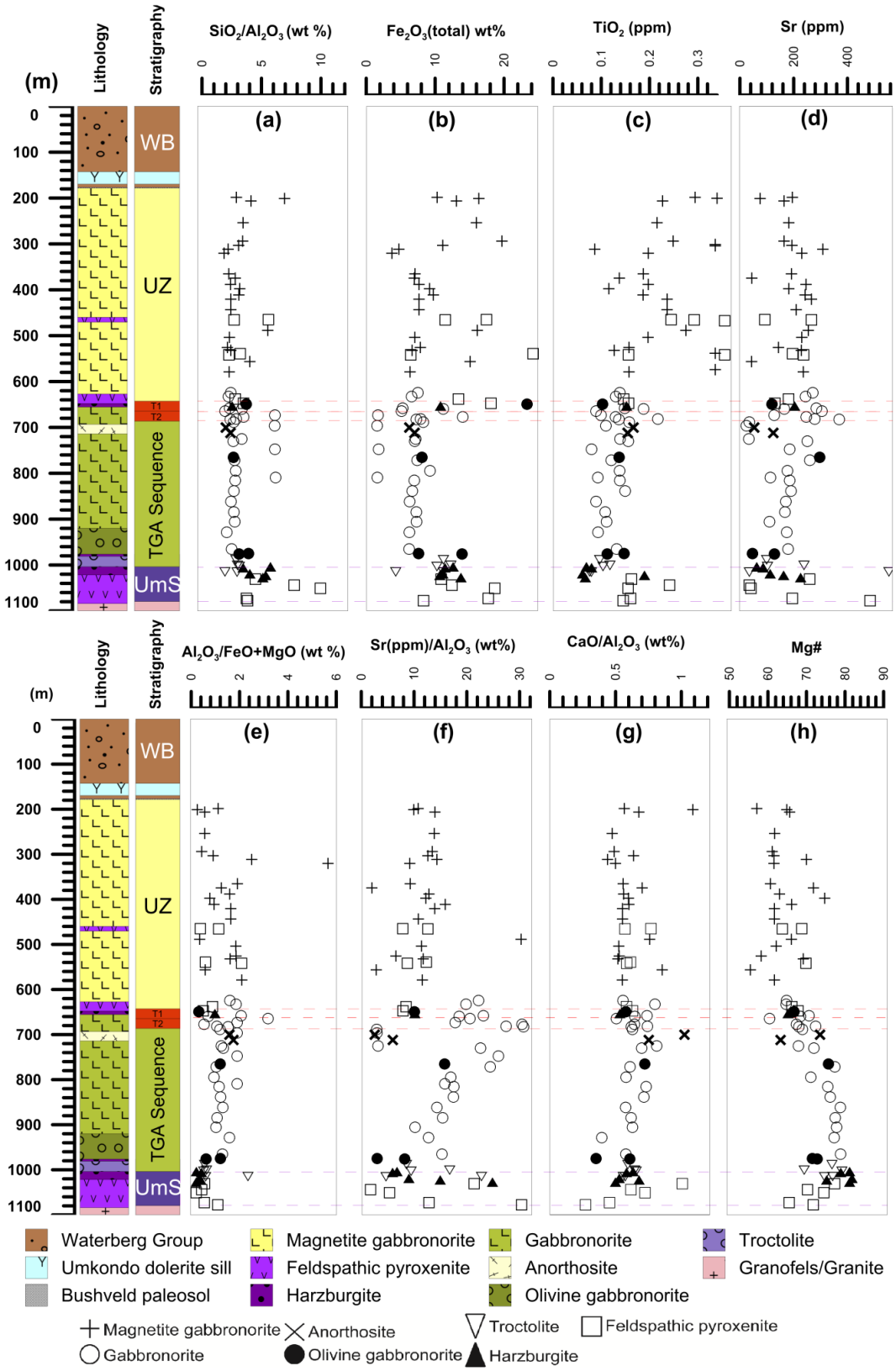

Figure 6.8: Whole-rock major and trace element geochemical variations with depth and lithology in borehole WB017. (a) SiO_2:Al_2O_3 (wt. %); (b) Fe_2O_3 (wt. %); (c) TiO_2 (wt. %); (d) Sr (ppm); (e) Al_2O_3/FeO+MgO; (f) Sr/Al_2O_3; (g) CaO/Al_2O_3 (wt. %); (h) Mg#. WB, Waterberg sediments; UZ, Upper Zone; T1 and T2, T zone; TGA sequence, troctolite-gabbronorite-anorthosite; UmS, Ultramafic Sequence.

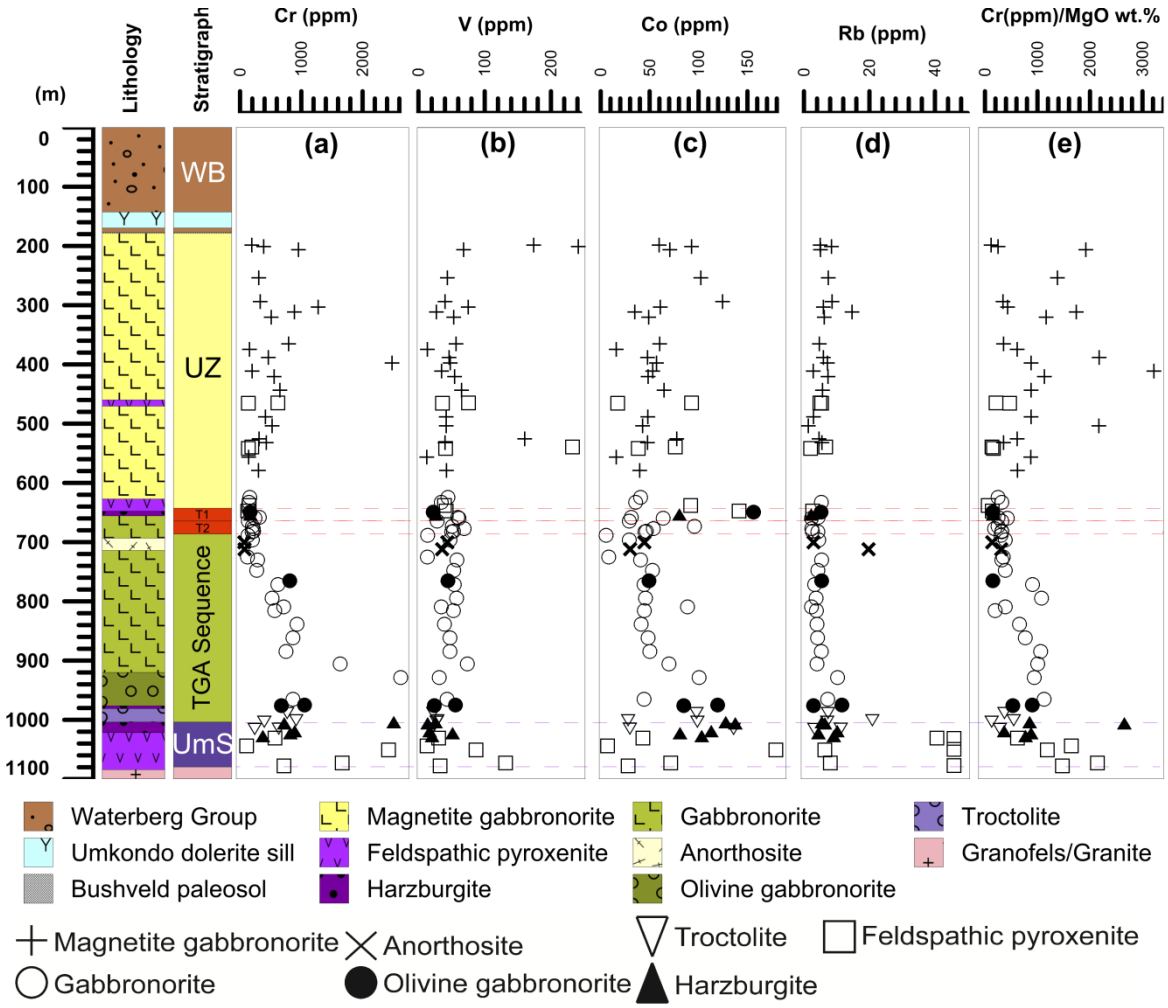

Figure 6.9: Whole-rock trace element geochemical variations with depth and lithology in borehole WB017. (a) Cr (ppm); (b) V (ppm); (c) Co (ppm); (d) Rb (ppm) and (e) Cr/MgO ratio. WB, Waterberg sediments; UZ, Upper Zone; T1 and T2, T zone; TGA sequence, troctolite-gabbronorite-anorthosite; UmS, Ultramafic Sequence.

The feldspathic orthopyroxenite samples within the basal part of the UmS have elevated Cr values (1500-2200 ppm) as do one of the overlying harzburgite samples 2200 ppm Cr (Fig. 6.9a).The rest of the samples in the UmS have a moderate Cr content between 200 and 600 ppm. The TGA sequence shows an upward decrease in Cr content (Fig. 6.9a). The T zone has the lowest Cr content <100 ppm. The overlying UZ has the largest variation in terms of Cr between 50 to 2400 ppm (Fig. 6.9a). The V content is constant through the Waterberg Bushveld stratigraphy with a few anomalies (Fig. 6.9b). There are elevated Co values for the UmS and the T1, which is consistent with the higher distribution coefficient for Co into olivine and pyroxene-rich lithologies compared with plagioclase-rich lithologies (Fig. 6.9c). The Rb values are low and constant with elevated values associated with the basal feldspathic orthopyroxenite and one anorthosite sample. There is a slight increase in the Rb values associated with the upper UZ samples (Fig. 6.9d). The Cr:MgO ratio shows elevated values for the basal feldspathic orthopyroxenite and one harzburgite sample, although there is a gradual decrease to the top of the

UmS. At the base of the TGA sequence there is a slight increase, although from 861.50 m there is a gradual decrease towards the top of the T zone. The UZ lithologies have a large variation associated with the Cr:MgO ratio (Fig. 6.9e).

6.6.5. Mineralisation

Variations in PGE+Au grades, base metals, S and Cr content in the WB017 F zone are shown in Fig. 6.10 based on the assay results obtained from Platinum Group Metals (PTM). The mineralised interval is approximately 50 m thick (1004.00 m to 1054.00 m) in WB017 with grades of Pt+Pd+Au ranging from <2 g/t to >10 g/t (Fig. 6.10).

The high grades are hosted by feldspathic orthopyroxenite at the base of the UmS and harzburgite and mela-troctolite towards the top (Fig. 6.10). The Pt/Pd ratio is 0.6 within the feldspathic orthopyroxenite unit, but increases towards the top of the feldspathic harzburgite up to 5 (Fig. 6.10). Although, the UmS contains high Cr values there is an anti-correlation between PGE+Au grade and Cr. Where there are grade maxima, these correspond with Cr minima (Fig. 6.10). There is high sulphur content within the UmS, although poor correlation between sulphur and PGE+Au grades. However the Ni and Cu content show excellent correlations with PGE+Au (Fig. 6.10). The Ni values are total Ni as no acid-soluble assays were done to distinguish between Ni in silicate and Ni within sulphides. There is generally a good correlation with visible chalcopyrite and pentlandite in core with high PGE+Au grades.

The Cu/Pd values are a good indicator of sulphide melt enrichment due to a contrast in Cu and Pd partitioning coefficient into sulphide melt during the exchange with silicate melts (Barnes and Maier 2002; Naldrett *et al*. 2009). The Cu/Pd values are between 250 and 600 associated with grades greater than 2 g/t of 2PGE+Au. The F mineralised zone hosts disseminated, blebby and semi-massive sulphides with accessory chromite, the PGE comprise 65% Pd, 30% Pt, and 5% Au with 0.07% Ni and 0.17% Cu (Table 6.1) (PTM 2016). The dominant PGM that occur in the F zone are sperrylite (up to 82%) and Pt-Pd bismuthotellurides (up to 32%) and there is a lack of PGE sulphides (McCreesh *et al*., 2018).

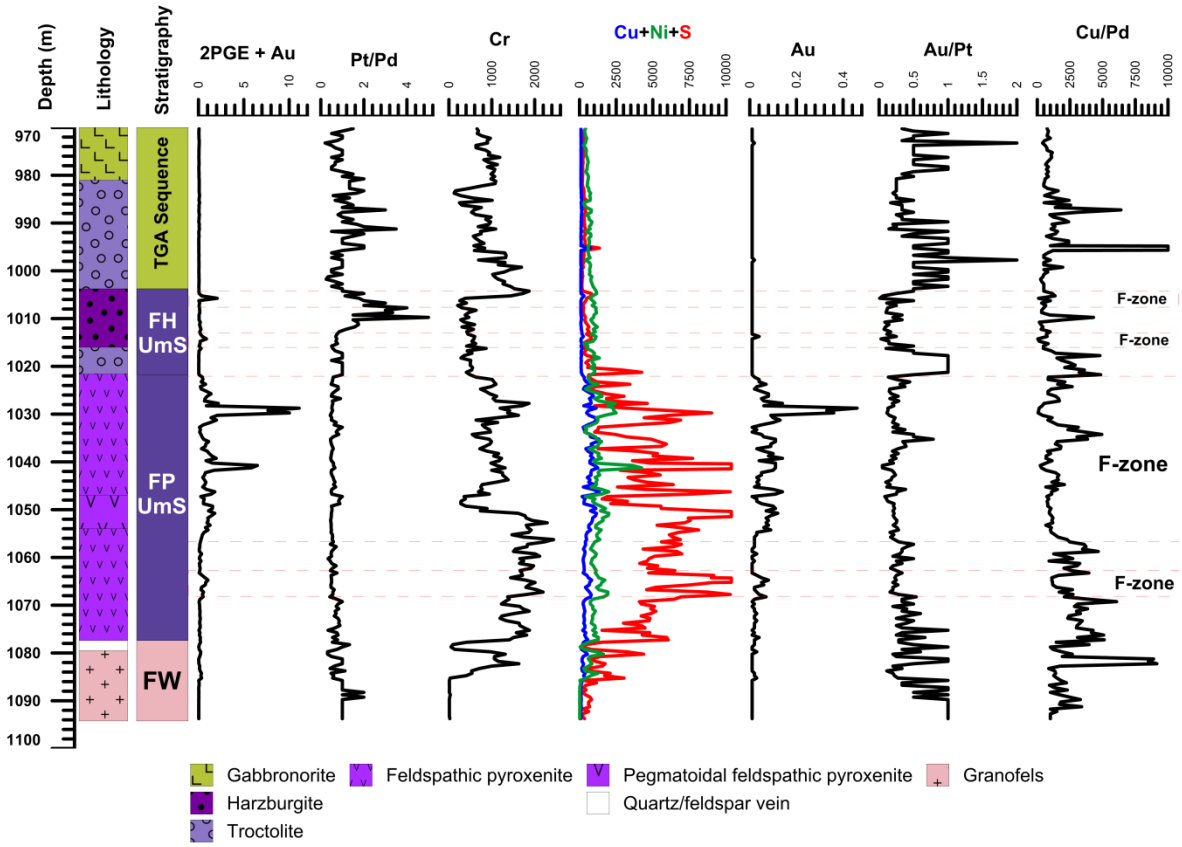

Figure 6.10: Variations of 2PGE+Au, Pt/Pd, Au, Cr, Cu, Ni, S, Au, Au/Pt and Cu/Pd ratios through the WB017 section of the Ultramafic Sequence. Data of 0.5 m sampling are shown by courtesy of Platinum Group Metals (PTM).

The concentration of PGE+Au, base metals, S and Cr are plotted against the stratigraphic height for the T zone for WB017 (Fig. 6.11) based on the assay results obtained from PTM. The T1 is poorly mineralised in WB017 with narrow intervals with <2 g/t. At the contact between the T1 and T2 which is defined by the absence of olivine, there is a dramatic increase in PGE+Au (Fig. 6.11). PGE+Au within the T2 range from <2 g/t to >7 g/t with a maximum of 19 g/t. The Pt/Pd ratio is ~0.4 within the T2 mineralised zone. The Cr content is extremely low (<300 ppm) and there is an anti-correlation with Cr and PGE+Au enrichment which is similar to the F zone (Fig. 6.11). The base metal sulphides and S have an excellent correlation with good PGE+Au grade and there are elevated Cu values associated with the T zone. The Cu/Pd ratio is between 550 and 1200 within this mineralised zone (Fig. 6.11). The PGE have an unusual mineralised basket comprising 49% Pd, 29% Pt, and 21% Au with 0.08% Ni and 0.16% Cu (Table 6.1) (PTM 2016). The PGM are dominated by Pt-Pd bismuthotellurides and Au alloys (McCreesh *et al*., 2018).

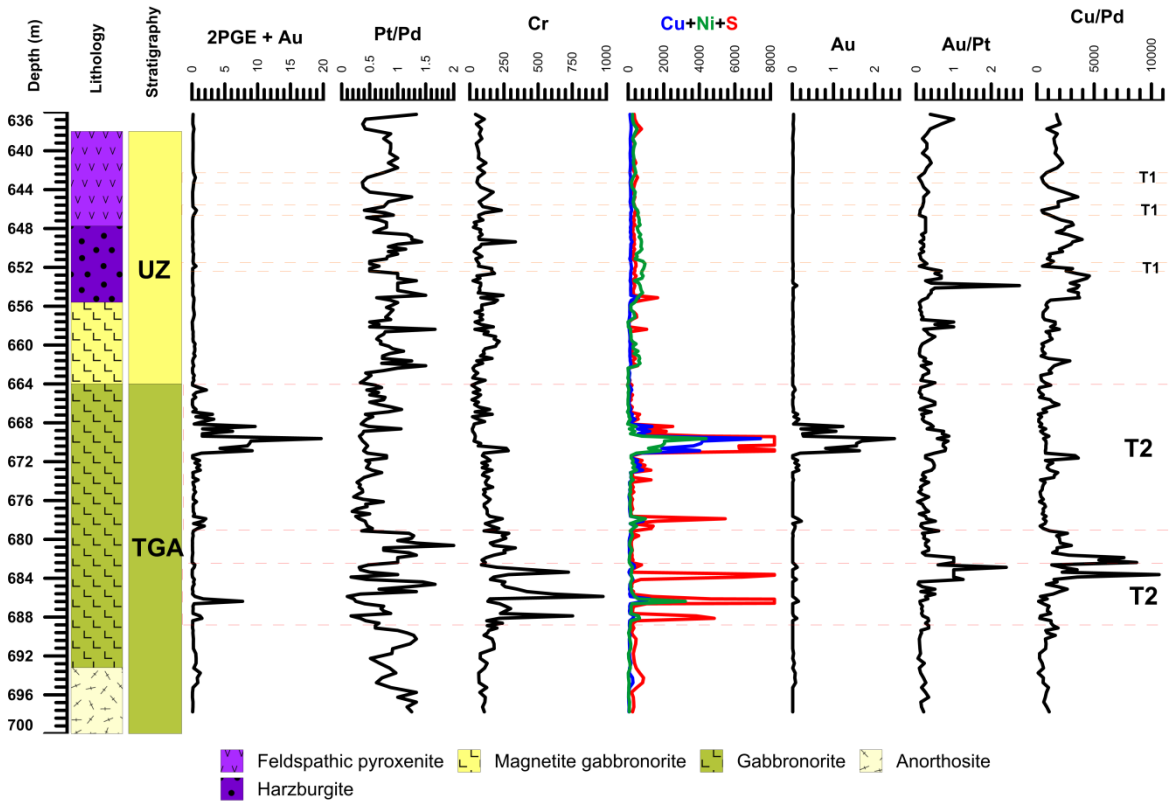

Figure 6.11: Variations of 2PGE+Au, Pt/Pd, Cr, Cu, Ni, S, Au, Au/Pt and Cu/Pd ratios through the WB017 section of the upper T zone. Data of 0.5 m sampling are shown by courtesy of Platinum Group Metals (PTM).

Table 6.1: Different Pt:Pd and Ni:Cu ratios from the two mineralised zone in the Waterberg project from WB017 and WB099; OV-FPYX – olivine-feldspathic pyroxenite; GN – gabbronorite; HARZ – harzburgite; FPYX – feldspathic pyroxenite. The location of these borehole cores are seen in Figure 6.2.

WB017	Lithology	Pt:Pd	Ni:Cu	WB099	Lithology	Pt:Pd	Ni:Cu
T1	OV-FPYX	0.71	0.77	T1	OV-FPYX	0.51	1.1
T2	GN	0.42	0.9	T2	GN	0.58	0.5
-	-	-	-	FH	HARZ	0.68	5
FP	FPYX	0.58	2.27	FP	FPYX	0.54	4.64

6.7. Discussion

The stratigraphy and mineralised zones within the Waterberg project are extremely variable along strike on both kilometre and meter scale. Whole-rock and mineral chemistry vary between the different stratigraphic units and the most notable differences are seen within the UmS at the base of the Waterberg succession. The two mineralised zones intercepted on the Waterberg project have different lithologies, whole-rock and mineral chemistry, which may indicate completely different formation processes.

Calc-silicates and carbonate assimilated rocks are absent through the whole Waterberg stratigraphy as implied by the $CaO:Al_2O_3$ ratio with an average of 0.6 (Kinnaird *et al*., 2005), which is different to the exposed northern limb stratigraphy. The initial intrusive magma is interpreted to be a fine-grained sill-like pyroxenite or in some cases fine-grained gabbronorite/norite (Kinnaird *et al*., 2017), similar to the Marginal Zone in the rest of the Bushveld Complex. These initial magmas interacted with the floor rocks to produce a granofels unit similar to the floor rocks on Overysel (Cawthorn *et al*., 1985; Holwell and McDonald, 2006). The overlying UmS is composed of orthopyroxenite and harzburgite. The feldspathic orthopyroxenites are primitive rocks with high Mg# values and Cr concentrations. The overlying harzburgite is the most primitive rock in the Waterberg succession where the whole-rock Mg# of 82 mirrors the Mg# of 82.5 for low-Ca pyroxenes and has the highest olivine Fo values (89). The uppermost harzburgite unit also has the highest Cr concentrations. The orthopyroxenite and harzburgite units form part of the F zone with Pt:Pd ratio of 0.6 and Ni:Cu ratio between 2.5 and 5. The mineralised orthopyroxenite and harzburgite have the highest Cr/MgO ratios in the Waterberg succession. The pyroxene increase in grain size upwards and is dominated by orthopyroxene, the harzburgite unit has xenoliths of feldspathic orthopyroxenite up to a few meters thick with sharp contacts. This indicates that the orthopyroxenite was semi-solid before the intrusion of the overlying harzburgite which ripped up fragments of the orthopyroxenite. Both the orthopyroxenite and harzburgite have the same precious metal basket, although distinctively different minerology.

The overlying TGA sequence has a primitive unmineralised troctolite package at the base. Olivine decrease upwards resulting in olivine-gabbronorite and olivine appears to be absent where cumulus orthopyroxene, clinopyroxene and plagioclase form varying leucocratic and melanocratic gabbronorite, norite and gabbro and finally anorthosite. The unmineralised troctolite package has whole-rock Mg# 74, which is similar to the Mg# of 73 for large oikocryst of orthopyroxene. The olivine grains within this troctolite package have a fairly high Fo_{78} with NiO 0.25 wt. %. The plagioclase An# content in the unmineralised troctolite have the lowest values in the TGA sequence of between 62 and 77.

There are differences between the Al_2O_3:FeO+MgO ratio between the harzburgite unit, the unmineralised troctolite package and the overlying gabbroic unit, which indicates more than one magma was involved in forming these units. We suggest that the troctolite package formed from magma mixing between a peridotite-rich magma and a gabbroic-rich magma. The $SiO_2:Al_2O_3$ and $Sr:Al_2O_3$ ratios for the orthopyroxenite, harzburgite and the overlying unmineralised troctolite also have different values which may suggest different influxes of magma.

The TGA sequence shows a fractionating sequence with the whole-rock Mg# and the Mg# of low-Ca pyroxenes decreasing towards the top of the succession. The upper mineralised T zone represents an evolved magma compared with the primitive basal ultramafic mineralisation. The T zone has a slightly lower Pt:Pd ratio of 0.55 and Ni:Cu ratio of 0.8. The olivine composition (Fo_{64-69}) is also low associated with the T1 zone. The Cr concentrations are extremely low in the T zone <200 ppm, although the Co concentration is similar to the basal F zone. The whole-rock geochemistry and mineral chemistry for the two mineralised zones in the Waterberg succession are fairly different and indicate different formation processes.

6.7.1. Correlation with the Mineralised Intervals of the Northern Limb

The northern limb of the Bushveld Complex hosts a significant Cu-Ni-PGE deposit that has sparked global interest in recent years for mining, exploration and academic works (Armitage *et al*., 2002; Ashwal *et al*., 2005; Kinnaird *et al*., 2005; Kinnaird, 2005; Maier *et al*., 2008; McDonald and Holwell, 2011; Yudovskaya *et al*. 2011; Holwell *et al*., 2013; Tanner *et al*., 2014; McDonald *et al*., 2017). Hence, it is important to determine whether the Waterberg mineralisation is related to the Platreef-style (Kinnaird, 2005; Maier *et al*., 2008) or the Main Zone type of mineralisation found on the Moorddrift farm (Maier and Barnes, 2010) or on the Aurora project (McDonald and Harmer, 2010; McDonald *et al*., 2017). The F-zone is hosted by ultramafic lithologies which will be compared with the Platreef (Kinnaird, 2005; Yudovskaya *et al*., 2011) and the Troctolite Horizon (Van der Merwe, 1976; Ashwal *et al*., 2005; Roelofse, 2010; Tanner *et al*., 2014), whereas the upper T-zone is generally hosted in more felsic-rich lithologies similar to the Aurora project (McDonald and Harmer, 2010; McDonald *et al*., 2017) and mineralisation in the upper Main Zone on the farm Moorddrift farm (Maier and Barnes, 2010; Holwell *et al*., 2013).

F zone

The F zone mineralisation is hosted by ultramafic lithologies and may represent contact-style mineralisation similar to the Platreef as the F zone rests against the Archean footwall. South of the Waterberg project on the Aurora project (Fig. 6.1), mineralisation is also hosted in a basal ultramafic unit termed Unit 1 by McDonald *et al*. (2017). This Unit 1 is composed of websterite, melagabbronorite and serpentinised peridotites (Manyeruke, 2007; McDonald *et al*., 2017), which may be similar to the orthopyroxenite sequence at the base of the UmS. However, Unit 1 on the Aurora project lacks the olivine-rich package and olivine is present only as a minor phase (<10 % modal proportion) in websterite (McDonald *et al*., 2017). Calc-silicate xenoliths are absent in the UmS apart from one located in borehole

WB027. The Unit 1 sequence on Aurora hosts a calc-silicate xenolith between 2 and 6 m thick (Manyeruke, 2007; Maier *et al*., 2008). Although both ultramafic sequences have Cr/MgO ratios >70, the low-Ca pyroxene in the F-zone are slightly more primitive (Mg# 78-86) (Fig. 6.12). The Cr content in the low-Ca pyroxenes is similar in the orthopyroxenite and websterite units (1200-2000 ppm) (McDonald *et al*., 2017), however, the Cr-content (2500-4300 ppm) of low-Ca pyroxene in the overlying harzburgite and mela-troctolite sequence of the F zone is much higher (Fig. 6.12). The Mn content of the low-Ca pyroxenes is significantly lower in the F zone (Mn; 1300-2200 ppm) compared with Unit 1 (Mn; 2900-3200 ppm) recorded by McDonald *et al*. (2017) (Fig. 6.12). On the Aurora project there is no record of disseminations, clusters or stringers of chromites associated with Unit 1, which differs from the F zone (Fig. 6.3c). Unit 1 is not strongly mineralised and the mineralisation is generally associated with more felsic-rich intrusive veins (Harmer *et al*., 2004; McDonald and Harmer, 2010) rather than the ultramafic lithologies as seen in the F zone. Even though there are significant differences between the two areas, the PGE mineralisation in both ultramafic packages show an anti-correlation with chromite (Fig. 6.13), which differs from the rest of the mineralised intervals of the Bushveld Complex (McDonald *et al*., 2017).

Recently McDonald *et al*., (2017) suggested that the F zone of the Waterberg project and the ultramafic Unit 1 on Aurora may be related to the troctolite horizon intercepted at a depth of 2745.11 m-2940 m in the Bellevue drillcore (Ashwal *et al*., 2005; Tanner *et al*., 2014). The troctolite horizon is composed of troctolite, olivine-norite and minor leucocratic varieties and pyroxenite. The average olivine content is 21.1 modal % (Ashwal *et al*., 2005), which is significantly lower than the olivine content of up to 65 modal % in the F-zone. The olivine (Fo_{74-79}) compositions are similar, although in some samples the olivine (up to Fo_{89}) compositions are more primitive in the F zone. The low-Ca pyroxenes of the troctolite horizon have a lower Mg# and Cr content compared with the F zone, and Mn content of low-Ca pyroxenes of the troctolite horizon show similarities to Unit 1 on the Aurora project (Fig. 6.12) (Ashwal *et al*., 2005; Tanner *et al*., 2014). The An content of plagioclase in the troctolite horizon and the F zone show similar irregular decreasing upward trends, although An values are slightly higher in the F zone. There is no record of sulphide mineralisation hosted in the troctolite horizon Ashwal *et al*. (2005). However, elevated Cr concentrations associated with pyroxenite layers above the troctolite horizon are thought to indicate influxes of new magma and may have potential for PGE exploration Tanner *et al*. (2014). Ashwal *et al*. (2005), Roelofse and Ashwal (2012) and Tanner *et al*. (2014) provided a detailed stratigraphy of the northern limb, although there is an estimated ~490 m of the lower troctolite horizon unaccounted for (Roelofse and Ashwal, 2012). This missing stratigraphy might show similarities to the UmS on the Waterberg project. Currently no published data on this portion of the troctolite horizon

exist. However, Unit 1 on the Aurora project and the troctolite horizon show similarities in terms of mineral chemistry as seen in Fig. 6.12. However, these two ultramafic sequences show significant differences in terms of mineralogy, geochemistry and mineralisation when compared to the ultramafic F zone.

The Platreef package of the northern limb is interpreted to represent a series of chemically different sills based on whole-rock and mineral chemistry as well as PGE ratios (Harris and Chaumba, 2001; Kinnaird, 2005; Manyeruke *et al*., 2005; McDonald *et al*., 2005; Holwell and McDonald, 2006; Maier *et al*., 2008). The ultramafic rocks at the base of the Waterberg stratigraphy also show chemical differences between the basal orthopyroxenite, the harzburgite and the overlying troctolite package at the base of the TGA sequence. However, caution must be exercised when comparing the UmS with the Platreef, as the Platreef has incorporated and assimilated various footwall lithologies along strike that may have influenced the geochemistry (Kinnaird, 2005; McDonald *et al*., 2005). The whole-rock geochemistry of the UmS is enriched with Mg ($Mg\#_{72-81}$), (MgO >12 wt. % and up to 28 wt. %) and the Cr content is between 500 to 2200 ppm which are all comparable to that of the Platreef (Seabrook *et al*., 2005, Kinnaird *et al*., 2005; McDonald and Holwell, 2011). The low-Ca pyroxene shows remarkable similarities to the Platreef, with the Mg# (72-87, average 82) of low-Ca pyroxenes for the UmS (Fig. 6.12) (Manyeruke *et al*., 2005; Yudovskaya *et al*., 2011; Roelofse and Ashwal, 2012). The MnO (wt. %) and Cr_2O_3 (wt. %) of low-Ca pyroxenes are also comparable to that of the low-Ca pyroxene in the Platreef (Fig. 6.12). Olivine is an important component of the UmS. Olivine associated with the mineralised feldspathic harzburgite has a range of Fo values from 73 to 85. In certain areas of the Platreef and Merensky Reef (western limb) olivine (Fo_{81-85} and Fo_{79-80}, respectively) forms feldspathic harzburgite (Van der Merwe, 1976; Vermaak and Hendriks, 1976; Kruger and Marsh, 1982; Maier and Eales, 1997; Yudovskaya *et al*., 2011).

Although there are remarkable similarities in the whole-rock and mineral chemistry between the UmS and the Platreef, there are noticeable differences as well. In parts of the Platreef there are chromitite seams up to 2 m thick (Yudovskaya *et al*., 2011; Mitchell and Scoon, 2012), and there is an anti-correlation between PGE and Cr in the F zone which contrasts remarkably with the Cr vs PGE relationship found in the Platreef (Fig. 6.13). The mineralisation of the UmS is dominated by palladium (Pt/Pd ratio of 0.6) (Fig. 6.10), in contrast to the platinum dominated Merensky Reef and UG2 (Pt/Pd 2.33) (Naldrett and von Gruenewaldt, 1989; Barnes and Maier, 2002; Cawthorn *et al*., 2002) and the Platreef with a Pt/Pd ratio of 0.91 (Ihlenfeld and Keays, 2011; Kinnaird and Nex, 2015). However,

according to Kinnaird *et al*. (2005), basal mineralised sills of the Platreef are dominated by palladium. The F zone also has a Ni/Cu ratio >2 and (Pt+Pd)/Au ratio >20 which is comparable with some localities in the Platreef (McDonald and Holwell, 2011). When comparing all the available data on the northern limb with the F zone, there are more similarities with the Platreef mineralisation, as compared with other ultramafic units in the northern limb. However, the F zone has some unique features, rather than indicating that this mineralised zone is directly related to the Platreef, we suggest that the F zone formed from a Critical Zone type melt (i.e. Platreef).

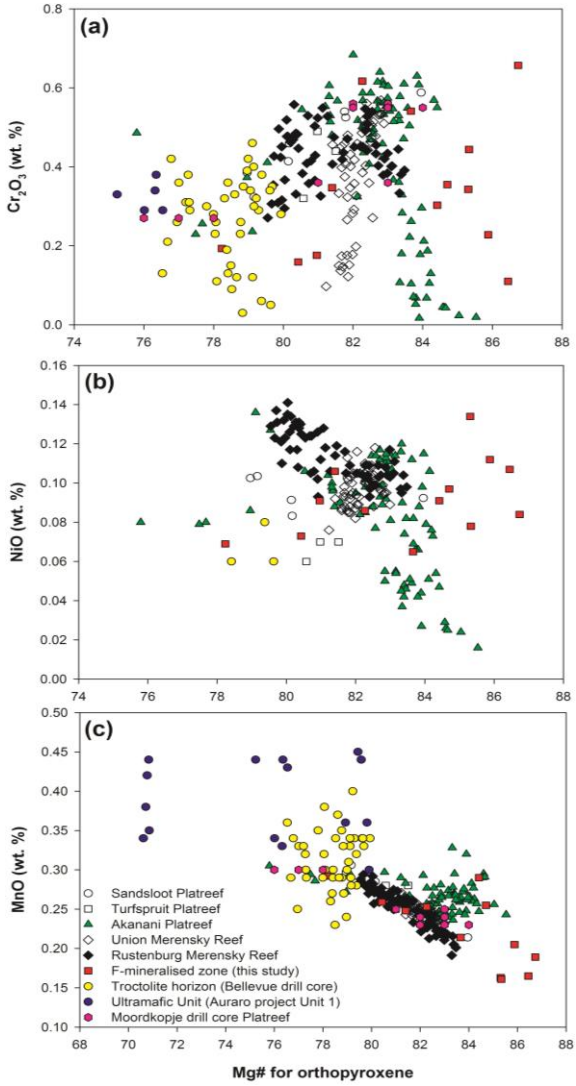

Figure 6.12: Binary variation diagrams for the ultramafic mineralised zones and the Troctolite Horizon of orthopyroxene mineral-chemistry from different Northern limb sites; Sandsloot Platreef, Turfspruit Platreef and Akanani down dip Platreef (data from Yudovskaya *et al*., 2011), Union Merensky Reef and Rustenburg Merensky Reef (data from Naldrett *et al*., 2009), Waterberg project F zone (this study), Bellevue drillcore (BV1) Troctolite Horizon (data from Ashwal *et al*., 2005), Moordkopje drillcore (MO1) Platreef (data from Roelofse and Ashwal, 2012), Aurora project Unit 1 (McDonald *et al*., 2017). The comparison of Mg# (opx) vs. Cr_2O_3 (wt. %), NiO (wt. %) and MnO (wt. %).

T zone

The T zone in the Waterberg project is associated with elevated Au values, which seems to be a common feature of mineralised zones associated with the upper stratigraphy of the northern limb, as seen in the Aurora project (Harmer *et al*., 2004; Maier *et al*., 2008; McDonald and Harmer, 2010; McDonald *et al*., 2017), and on Moorddrift (Maier and Barnes, 2010; Holwell *et al*., 2013). Although Yudovskaya *et al*. (2017) also recorded elevated Au values associated with the upper reef mineralisation of the Platreef on Turfspruit.

The geochemistry, mineralogy, sulphur isotopes and mineralisation on Moorddrift farm are described by Maier and Barnes (2010) and Holwell *et al*. (2013). The high grade PGE mineralisation is hosted by gabbronorite, anorthosite and pyroxenite. The sulphide mineralisation is composed of a primary assemblage of chalcopyrite, pentlandite and pyrrhotite and a secondary assemblage of millerite, chalcopyrite and pyrite similar to the sulphide assemblages recorded for the T-zone (McCreesh *et al*., 2018). The sulphur isotopic results of Moorddrift are significantly different from the magmatic derived sulphur isotope signature obtained for the T zone (Holwell *et al*., 2013; McCreesh *et al*., 2015). In addition, parameters such as whole-rock Mg#, MgO and Cr for the Moorddrift are slightly higher compared to the T zone (Maier and Barnes, 2010). The T zone is dominated by palladium up to 65 % of the metal basket, which is opposite to the Pt-rich mineralisation on Moorddrift (Holwell *et al*., 2013). Therefore, the absence of olivine-rich lithologies, the elevated Pt/Pd ratio, contaminated sulphur isotope results and the slight difference in whole-rock geochemistry makes the Moorddrift mineralisation incomparable with the Waterberg T zone.

The magnetic susceptibility results indicate that the T zone is situated at the boundary between the TGA sequence and the Upper Zone. The upper mineralised interval on the Aurora project is suggested to be situated in the upper Main Zone due to similar mineral chemistry comparable to the Bellevue drillcore (Ashwal *et al*., 2005; Tanner *et al*., 2014; McDonald *et al*., 2017). However, a magnetic susceptibility survey has not been conducted on the Aurora project as of yet. The upper mineralised zone on the Aurora project have been subdivided in Unit 2 and 3 which are associated with more felsic rich lithologies (Harmer *et al*., 2004; McDonald *et al*. 2017). The primary sulphide assemblage is the same for both areas and both show magmatic sulphur isotopic signatures (average close to 0‰) (Holwell *et al*., 2007; Manyeruke, 2007; McCreesh *et al*., 2015; McDonald *et al*., 2017). McDonald *et al*. (2017) showed the presence of abundant inverted pigeonite in Unit 3, which is slightly different to the sporadic nature of inverted pigeonite in T2. Unit 2 on Aurora has low Cr (<250 ppm) concentrations, comparable to the

values obtained for the T zone, although the Cr/MgO ratios (68-250) are significantly higher within the T zone (McDonald *et al*., 2017). The Mg# of 55-73 of low-Ca pyroxene is slightly lower than the values obtained for the T-zone (Mg# 66-77), which increase upwards associated with the olivine-rich lithologies in T1. The MnO content in low-Ca pyroxene is significantly higher in Unit 2 compared with the T zone, being 0.30-0.73 wt. % and 0.30-0.43 wt. %, respectively. The Cr content of low-Ca pyroxene also increase upwards in the T zone from 75 to 960 ppm, whereas the Cr content of low-Ca pyroxene associated with Unit 2 are mostly below detection limits. The olivine-rich lithologies within Unit 2 have forsterite values between 63 and 68 (McDonald *et al*., 2017) which are similar forsterite values for olivine-bearing lithologies in the T1 mineralised zone. The An# of plagioclase overlaps between Unit 2 and the T zone, being 60-79 and 66-82, respectively. Although the An content is slightly higher in the olivine-bearing lithologies of T1. Therefore, in terms of mineral chemistry between the two mineralised intervals there are slight differences in concentrations. The most remarkable similarities between the two areas are seen in the mineralisation. Both mineralised zones are Pd-rich and have elevated Au values. The PGE mineralisation has an anti-correlation with Cr (Fig. 6.13). PGE grade maxima correspond invariably with Cr minima (McDonald *et al*., 2017). Both mineralised zones are dominated by palladium-rich bismuthotellurides and tellurides (McDonald and Harmer, 2010; McCreesh *et al*., 2018). Both mineralised zones are Cu-rich (Cu/Ni ratio ~2) and Au-rich (Au/Pt+Pd ratio ~0.16) which are significantly higher than the ratios obtained for the Platreef (McDonald and Harmer, 2010). All the observations on the mineralisation hosted in more evolved rocks in the Waterberg succession and the Aurora project suggest the likelihood of a link. Although there are differences in mineral chemistry, the overall style of mineralisation seems to be the same.

6.7.2. Mineral Chemistry and Magnetic Susceptibility Stratigraphy Comparisons

The whole Waterberg Bushveld succession is approximately 1200 m thick, which is significantly thinner than the approximately 4000 m thick stratigraphy of the northern limb (Ashwal *et al*., 2005; Roelofse and Ashwal, 2012). The magnetic susceptibility results clearly reveal the boundary between the TGA sequence and the UZ. These results were established based on the outcome of the magnetic susceptibility results of the Bellevue drillcore (Ashwal *et al*., 2005). The T zone is located stratigraphically at the boundary been the TGA sequence and UZ. Major and trace elements of pyroxenes and plagioclase in the T zone are compared with data from the MZ-UZ boundary (1575.80 m depth) of the Bellevue drillcore (Ashwal *et al*., 2005; Tanner *et al*., 2014). Mg# values of pyroxenes and An# content of plagioclase are significantly more primitive as compared to the Bellevue drillcore associated with the

MZ-UZ boundary, although a similar trend is seen with values increasing upwards into the UZ (Ashwal *et al*., 2005; Tanner *et al*., 2014). The mineral chemistry of pyroxene and plagioclase is different at the two boundary locations, we suggest that the T zone is absent further south in the northern limb.

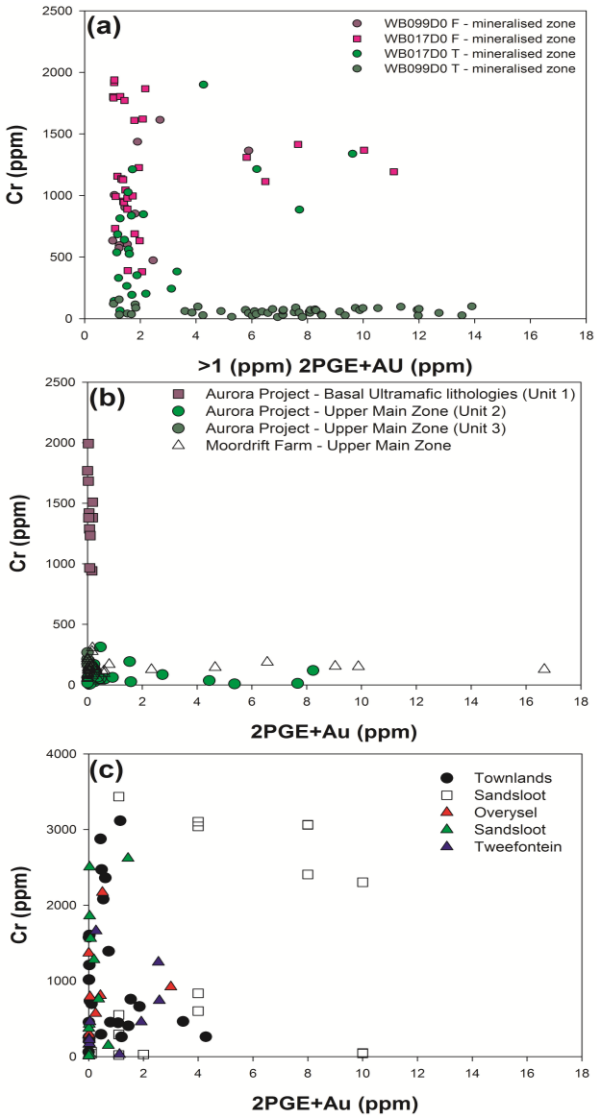

Figure 6.13: Binary variation diagram for mineralised intervals in the Northern limb, PGE+Au (ppm) grades versus Cr (ppm) concentrations (A) Waterberg Project (this study); (B) Aurora Project (both the ultramafic unit and the upper Main Zone mineralised zones) (McDonald *et al*., 2017) and the upper Main Zone mineralisation on the Moorddrift farm (Maier and Barnes, 2010); (C) Platreef Townlands (Manyeruke *et al*., 2005), Sandsloot (McDonald *et al*., 2005; Ihlenfeld and Keays, 2011), Overysel and Tweefontein (Ihlenfeld and Keays, 2011), diagram modified from McDonald *et al*., 2016.

McDonald *et al*. (2017) pointed to the importance of inverted pigeonite and orthopyroxene associated with leucogabbronorite in Unit 2 and 3 and compares this interval stratigraphically with the occurrence of inverted pigeonite in the Bellevue drillcore (2000-2200 m depth) (Ashwal *et al*., 2005; Tanner *et al*.,

2014). The presence of inverted pigeonite has been used to characterise different intervals in the Main Zone in the rest of the Bushveld Complex (Atkins, 1969; Eales and Cawthorn, 1996; Nex *et al*., 1998). The T2 hosts sporadic inverted pigeonite (Figs. 6.3e and f), although comparing mineral chemistry of pyroxenes and plagioclase with the interval between 2000 to 2200 m of the Bellevue drillcore, there are differences in the Mg# and An#, and the Ni and Mn content of low-Ca pyroxene (Ashwal *et al*., 2005; Tanner *et al*., 2014). Cumulus magnetite is an indicator mineral used to mark the boundary between the MZ-UZ (Molyneux, 1974). Magnetite is present in both the T zone and the upper mineralised interval on the Aurora project (McDonald *et al*., 2017), which indicates close approximation with the MZ-UZ boundary. However, the mineral chemistry for Unit 1 on Aurora project suggested that this unit is situated within the Main Zone, when comparing mineral chemistry to the Main Zone of the Bellevue drillcore (McDonald *et al*., 2017). Overall, the mineral chemistry of the Waterberg succession is slightly more primitive than the exposed northern limb south of the Hout River Shear Zone. This may be directly associated with the thickness of the Waterberg succession, not allowing for progressive fractionation to occur.

Genesis of the Waterberg mineralisation

When considering the emplacement of the Waterberg magma, any accounts need to include that the Waterberg succession is situated in the Southern Marginal Zone of the Limpopo Belt (van Reenen *et al*., 1987), unlike the northern limb situated on the stable Kaapvaal Craton (Eales and Cawthorn, 1996; Cawthorn, 2015). The Waterberg layered rocks also strike and dip in a completely different direction compared to the layered rocks south of the Hout River Shear Zone (Lomberg and Goldschmidt, 2014; Kinnaird *et al*., 2017). The tectonic setting of the Limpopo Belt may have played an important role during the emplacement of the Waterberg magmas, which probably used pre-existing structures and influenced the initial stages of magmatism in the Waterberg project area (Schaller *et al*., 1999; Clarke *et al*., 2009; Barnes *et al*., 2015).

The magmatic history of the Waterberg Bushveld succession is proposed to have started with fingers of marginal gabbroic and orthopyroxenite magmas intruding the basement Archean granite-gneisses and an overlying unknown roof lithology (Yudovskaya *et al*., 2015). The overlying mineralised feldspathic orthopyroxenite and feldspathic harzburgite probably were emplaced as sill-like or chonolithic bodies (Barnes *et al*., 2015; Kinnaird *et al*., 2017). These ultramafic lithologies were emplaced into embayments related to the topography of the Archean granite gneisses and other pre-existing structures (Kinnaird *et al*., 2017). Both the orthopyroxenite and the harzburgite have the same precious metal basket (65% Pd,

30% Pt, and 5% Au) indicating the same source. Field evidence shows that the feldspathic orthopyroxenite formed first, as there are xenoliths up to 6 m thick of feldspathic pyroxenite in the overlying harzburgite. The two ultramafic mineralised units are the most primitive packages of the Waterberg succession hosting PGE (dominated by Pd) and Au-poor (<5%) mineralisation with an uneven distribution of chromite observed as disseminations, clusters or seams, similar to locations within the Platreef (Kinnaird *et al*., 2005; McDonald and Holwell, 2011). Calc-silicates are absent and there is little evidence of assimilation of local S from secondary sedimentary sources as most of the sulphur isotopic results gave magmatic signatures (McCreesh *et al*., 2015) associated with the ultramafic F-zone. Ihlenfeld and Keays (2011) suggest that magma was contaminated by sulphur-rich crustal rock in the mid- to upper crust prior to emplacement of magma. The contaminated sulphur isotope signatures are erased during the interaction and exchange of assimilated S with mantle-derived sulphur in a dynamic Ni-Cu-PGE system characterised by a high R-factor (Ripley and Li, 2003). However, recent work by Mungall and Brenan (2014) indicates that the sulphide/silicate partitioning coefficients for PGE and Au are extremely high (10^5 to 10^6), indicating that large pools of sulphides at depth are not necessary to form PGE+Au rich zones (Mungall and Brenan, 2014).

The mapping work by Holwell *et al*. (2005) and Holwell and Jordaan (2006) suggested a hiatus between the Platreef and Main Zone, implying that the Main Zone magma has the potential to host PGE and Au that have not been scavenged (McDonald *et al*., 2017). The contact between the UmS and the unmineralised troctolite at the base of the TGA sequence is not a distinct contact seen in the boreholes, rather, it is a magmatic erosional contact which may represent a break in time between the two units. A better understanding of this contact will be revealed once underground mining operations begin. This contact may be a fundamental factor for the formation of the mineralisation in the upper TGA sequence.

The troctolite unit at the base of the TGA sequence represents an addition of primitive magma with high Cr content (Tanner *et al*., 2014). The troctolite unit forms more laterally extensive sheets, rather than the sill-like or chonolithic bodies as seen with the underlying UmS (Huthmann *et al*. in press). The troctolite unit formed from the intrusion of both a peridotitic-rich and gabbroic-rich melt with evidence of harrisitic-textures associated with the basal troctolite unit of the TGA sequence (Drouin *et al*., 2009; Reena and Tribuzio, 2011). Subsequently, fractionation of gabbroic magmas may have been disturbed by addition of more gabbroic liquid, leading to a fractionated TGA sequence upwards.

The upper T2 is characterised by low Cr concentration (<200 ppm), rejecting the notion of an influx of primitive magma (Maier, 2005; Tanner *et al*., 2014). Instead the sulphide saturation may have been

achieved from prolonged fractionation of the TGA sequence, which would explain the high concentrations of Cu and Au associated with BMS and felsic-rich lithologies (McDonald *et al*., 2017). Furthermore, interstitial disseminated magnetite is present in the upper T2, indicating a possible conversion of SO_4^{-2} in the magma to S^{-2} that contributed to sulphur saturation being attained (Keays and Tegner, 2015). The overlying T1 zone is hosted by more primitive olivine-rich lithologies and is interpreted to have been an influx of new magma as the Cr content can be as high as 1500 ppm (Fig. 6.13). The T1 and T2 have the same precious metal basket, however, the T1 is generally has lower grades compared to the T2. The magnetic susceptibility data indicate that the boundary between the TGA sequence and UZ also occurs in the upper T2. Therefore, the formation of the T1 zone may have resulted from magma mixing between the residual T2 mineralised melt and the incoming ultramafic T1 melt (Kinnaird *et al*., 2017). The Waterberg succession lacks the evolved uppermost UZ lithologies due to extensive erosion followed by uplift and deposition of the sedimentary Waterberg Group.

6.8. Conclusion

This study has highlighted similarities and differences of the Waterberg Bushveld succession and the northern limb of the Bushveld Complex. The mineralisation shares certain features with PGE deposits of the northern limb, although simultaneously exhibits unique characteristics.

(1) The UmS is the most primitive unit, and hosts the basal mineralised interval in the Waterberg succession. Characteristics of the mineralisation and overall geochemistry of the UmS are similar to certain localities in the Platreef and simultaneously show unique features. Hence the UmS and mineralised F zone may have formed from a Critical Zone type magma, and represent a north facies.

(2) The unmineralised troctolite package at the base of the TGA sequence is associated with cumulus plagioclase rather than the interstitial plagioclase within the UmS. The troctolite package is interpreted to have formed from an impulse of primitive olivine and Cr-rich melt that mixed with a gabbroic melt. Subsequently, in-situ fractionation of gabbroic magmas formed the upper portion of the TGA sequence.

(3) The T zone is located at the boundary between the TGA-sequence and UZ. Prolonged fractionation of the TGA sequence and influx of more primitive magmas are thought to be the main processes involved in the formation of the T2 and T1, respectively. Correlations in terms of mineralisation between the T zone and upper mineralisation on Aurora suggest the likelihood of

a link, although contradictions are met in terms of mineral chemistry and possibly stratigraphic positions.

(4) The UZ lacks the evolved rocks seen in the northern limb stratigraphy due to uplift and later subsidence leading to extensive erosion of the UZ before the deposition of the Waterberg Group sediments.

These comparisons imply that the Waterberg Bushveld succession has significant similarities, but also notable differences with the exposed northern limb immediately south of the Hout River Shear Zone.

Chapter 7

Sulphur Isotopes of the Waterberg PGE deposit, South Africa: implication for the formation of the PGE mineralisation

This chapter contains the full text of the paper "Sulphur Isotopes of the Waterberg PGE deposit, South Africa: implication for the formation of the PGE mineralisation" by McCreesh, M. J. G., Yudovskaya, M. and Kinnaird, J. A. as submitted to *South African Journal of Geology* and currently working on correction as suggested by the reviewers.

This publication investigates the sulphur isotopic signatures associated with the Waterberg mineralisation and has implications on the style of emplacement and formation of the mineralisation in the area.

7.1. Candidate's contribution:

- The candidate was responsible for detailed logging, sample collection and preparation for analysis, as well as petrology, figure production, data interpretation and wrote the paper.
- The candidate contributed approximately 90% towards the publication and the writing of the paper.
- Marina Yudovskaya and Judith Kinnaird were involved in discussions during the preparation of the manuscript.

7.2. Abstract

The Waterberg deposit is located in the Southern Marginal Zone of the Limpopo Belt and represents a new high-grade platinum-group element deposit of the Bushveld Complex. The Waterberg Bushveld succession differences in stratigraphy and mineralisation style to the northern limb south of the Hout River Shear Zone. The ultramafic mineralised zone at the base of the Waterberg succession has sulphur isotopic signatures which are within mantle range (average $\delta^{34}S$ = 1.18 ‰), although close to the footwall, there are a few samples with higher S isotope ratios thought to be related to remobilisation of sulphides during later hydrothermal processes (highest $\delta^{34}S$ = 3.17 ‰). The upper T mineralised zone has the most mantle-like sulphur isotope compositions ($\delta^{34}S$ between -0.48 and +0.16 ‰). Sulphur isotope ratios are consistent with the involvement of mantle S only in the mineralised zones. There is no evidence for contamination involving S-bearing sedimentary rocks; this is a unique characteristic compared with the rest of the northern limb. The data suggest that sulphide saturation in the magmas was not caused by external S addition, and that PGE enrichment was due to fractional crystallisation processes or influxes of PGE enriched magmas.

7.3. Introduction

Sulphur isotopic systematics have proven to be an important tool for evaluation of assimilation and source of sulphur in the formation of Cu-Ni-PGE deposits. Many authors have considered the presence of sulphur-bearing country rocks as one of the favourable factors in producing sulphide mineralisation, as an addition of external sulphur during transportation or emplacement is thought to be a key processes for the formation of many magmatic Cu-Ni-PGE deposit (Naldrett, 2004; Ripley and Li, 2013; Lesher *et al*., 2017). The reef-style PGE mineralisation in the Bushveld Complex such as the Merensky Reef, UG2 and the newly discovered reef-style mineralisation in the upper Platreef on Turfspruit and Sandsloot generally have sulphur isotopic signatures that are consistent with mantle derivation (Liebenberg 1968; Holwell *et al*., 2007; Penniston-Dorland *et al*., 2012; Yudovskaya *et al*., 2017). This differs from the contaminated contact-style PGE mineralisation of the Platreef, where sulphur isotope compositions have wider ranges depending on the composition of the Transvaal footwall lithologies as well as evidence of hydrothermal fluid transfer between the magmatic rocks and sedimentary floor rocks (Sharman-Harris et al., 2005; Sharman *et al*., 2013; Penniston-Dorland *et al*., 2008). Some authors suggested that sulphur saturation and formation of PGE mineralisation in the contact-style Platreef mineralisation was caused by addition of external sulphur during magma interaction with the local footwall (Buchanan *et al*., 1981; Gain and Mostert 1982; Sharman-Harris *et al*., 2005). Alternatively, a

number of researches argued that the Platreef magma was PGE enriched and sulphide-saturated prior to emplacement (Barton *et al*., 1986; Holwell *et al*., 2007; Maier *et al*., 2008; Penniston-Dorland *et al*., 2008). Regardless of local contamination, the parental magmas of the Bushveld Complex show clear evidence of progressive contamination by mid- to upper-continental crust (Kruger and Marsh, 1982; Maier *et al*., 2000) that occurs in a deep-staging chamber prior to transportation and emplacement (McDonald and Holwell, 2011; Naldrett *et al*., 2012; Roelofse and Ashwal, 2012). The crustal contaminated signatures can be masked or erased by sulphur isotope exchange during sulphide liquid enrichment through interaction with silicate melt that is essential to form high-grade and high-tenor PGE mineralisation (Ripley and Li, 2003; Ihlenfeld and Keays, 2011; Lesher *et al*., 2017). This study aims to determine whether external sulphur played a crucial role in the formation of the newly discovered PGE mineralised zones in ultramafic and gabbroic rocks of the Waterberg Project north of the Hout River Shear Zone (HRSZ). The relationship between the northern limb and the Waterberg segment, which is located within the Southern Marginal Zone of the Limpopo belt, is not well understood as the Platreef is believed to terminate south of the HRSZ with the Upper Zone rocks coming into immediate contact with the granitic floor. Our findings also shed a light on a style mineralisation in the Waterberg area when comparing with the rest of the mineralised zones associated with the Bushveld Complex.

7.4. Regional Geology

7.4.1. Transvaal Supergroup

The Neoarchean-Palaeoproterozoic Transvaal Supergroup was deposited between 2670 and 2100 Ma (Coetzee, 2001; Eriksson *et al*., 2001) within three separate structurally controlled basins, the Transvaal, Kanye and the Griqualand West Basins, preserved on the Kaapvaal craton (Eriksson and Reczko 1995; Eriksson *et al*., 2001). The up to 15 km thick Transvaal Supergroup succession overlies predominantly Archean granites, gneisses and greenstones, as well as the Witwatersrand and Ventersdorp Supergroups (Button, 1986). The Transvaal Supergroup is divided into the Wolkberg, Chuniespoort and Pretoria Groups (Eriksson *et al*., 2001). The Transvaal Supergroup forms much of the footwall to the Bushveld Complex. The magmatic sequence of the northern limb transgresses successively older Transvaal Supergroup lithologies northwards and eventually overlies the Archean granite-gneisses in the far north (Eriksson *et al*., 2001). In the southern sector the Platreef and the Lower Zone are the basal units that overlie quartzite of the Magaliesberg and Daspoort Formations. Successively northwards the Platreef crosscuts shales and dolomite of the Timeball Hill and Duitschland Formations, banded ironstone of the Penge Formation, and dolomite of the Malmani Subgroup (Kinnaird *et al*., 2005). North of Zwartfontein

the Platreef and northern limb overlies the Archean basement rocks (Fig. 7.1a) whereas further north transgressive intrusions of the Main and Upper Zone come into contact with the basement.

7.4.2. Bushveld Complex

The platinum-group element (PGE) resources of the Bushveld Complex are hosted by three of the largest PGE deposits; the UG2, the Merensky Reef and the Platreef (Eales and Cawthorn, 1996). The Bushveld Complex (Fig. 7.1) forms five major limbs; the western, far western, eastern and the northern limb all outcrop at surface, and the southern limb (Bethal limb) is buried beneath younger Karoo sediments (SACS, 1980). The complex is subdivided into four units; the Rooiberg Group, the Rustenburg Layered Suite, the Lebowa Granite Suite and the Rashoop Granophyre Suite (Eales and Cawthorn, 1996) that covers an area of > 90 000 km^2 (Kinnaird *et al*., 2017). The Rustenburg Layered Suite, which reaches a thickness of 7-9 km, is further subdivided into the Marginal, Lower, Critical, Main and Upper Zones based on lithologies and the appearance or disappearance of indicator minerals (von Gruenewaldt, 1973; Cawthorn *et al*., 2006).

7.4.3. Northern Limb

The northern limb (Fig. 7.1) of the Bushveld Complex has been reviewed in great detail by a number of authors (e.g. Kinnaird *et al*., 2005; Ashwal *et al*., 2005; Maier *et al*., 2008; McDonald and Holwell, 2011; Yudovskaya *et al*., 2017; McDonald *et al*., 2017). North of the Zebediela fault (Fig. 7.1) a branch of the Thabazimbi-Murchison Lineament (TML), the northern limb is exposed as a northwest striking sequence over 110 km in length and with a maximum width of 15 km (van der Merwe, 1976; Buchanan *et al*., 1981). The sequence of the northern limb has been correlated with the eastern and western limbs such that the Marginal, Lower, Main and Upper Zones are recognised. The Platreef in the northern limb is likely to be an equivalent to the Critical Zone in the rest of the complex (Kinnaird, 2005; Yudovskaya *et al*., 2017). The Lower Zone is separated from the Platreef by metasedimentary rocks of the Transvaal Supergroup in the south and forms satellite bodies within the Archean basement and overlying sediments in the central part of the limb (van der Merwe, 1976; Yudovskaya *et al*., 2013). The fine-grained rocks of the Marginal Zone intruded both the footwall and the metasedimentary rocks in between the Lower Zone and Platreef (Yudovskaya *et al*., 2013). The Platreef forms multiple mafic-ultramafic sill-like bodies, merged together or separated by intervals of metasedimentary xenoliths and autoliths (Kinnaird, 2005; Kinnaird *et al*., 2005). The Main Zone unconformably overlies the Platreef and includes a 110 m thick troctolite marker horizon which is unqiue to the Main Zone of the northern limb (van der Merwe, 1976; Holwell and Jordaan, 2006). The Upper Zone-Main Zone boundary is determined

by the first appearance of cumulus magnetite in the eastern and western limbs whereas Ashwal *et al*. (2005) and Kinnaird *et al*. (2017) defined the boundary between the Main and Upper Zone on the basis of a change in magnetic susceptibility.

The Platreef comprises mafic-ultramafic intrusions predominantly of pyroxenitic composition, and contains autoliths and xenoliths of floor material, with variable Cu-Ni-PGE mineralisation (van der Merwe, 1976; Kinnaird *et al*., 2005; Kinnaird and McDonald, 2005; McDonald *et al*., 2005).The Platreef occupies the stratigraphic position of the Critical Zone north of the Ysterberg-Planknek fault, whereas south of the Ysterberg-Planknek fault is another Critical Zone analogue, termed the gabbro-norite-pyroxenite-anorthosite (GNPA) member (Hulbert and von Gruenewaldt, 1985). Van der Merwe (2008) suggested that the GNPA sequence is the Critical Zone equivalent and grades into the Platreef north of the Ysterberg-Planknek fault. The Platreef's internal structures and lithologies are highly variable and mainly depend on the change in footwall lithologies (Gain and Mostert, 1982; Hutchison *et al*., 2004).

Recent studies found that down dip, where the Platreef gradually flattens referred to as the 'Flatreef', its sequence looks more like the typical Critical Zone with similar cyclicity, traceable chromitites and persistent PGE reefs at the top (Grobler *et al*., 2012; Yudovskaya *et al*., 2017). The reef-style mineralisation in the Platreef is characterised by the zonal distribution of platinum-group minerals (PGM) in the vertical section. The top chromitite seam carries indicative Pt sulphides and Pt alloys whereas mineralised silicate rocks contain predominantly Pt-Pd bismuthotellurides and sperrylite. The mineralogy of base metal sulphides, host rock composition and PGE geochemistry of the reefs resemble closely those of the Merensky Reef that gives more support to the correlation between the uncontaminated deep Platreef and the Upper Critical Zone.

Disseminated contact-style sulphide mineralisation in the contaminated part of the Platreef varies in style and texture and is mainly a combination of pyrrhotite, pentlandite, chalcopyrite and pyrite with subordinate bornite. Massive PGE-poor sulphides from net-textured to interstitial have been recorded up to several meters thick, dominated by pyrrhotite with minor chalcopyrite and pentlandite (Sharman-Harris *et al*., 2005; Holwell *et al*., 2007). Sulphides and PGE grades may occur within calcsilicate or hornfels, where higher proportions of pyrite occur with subordinate pyrrhotite (Gain and Mostert, 1982; Klemd *et al*., 2016).

The upper Main Zone of the northern limb has recently been a topic of discussion with regards to PGE mineralisation. It is known that the Main Zone of the eastern and western limbs is barren and depleted

both in PGE and Cr. McDonald and Harmer (2010) argued that the PGE budget of the Main Zone in the northern limb remains unreduced because of the break between the Platreef and the Main Zone intrusions established in some areas of the northern limb (Holwell and Jordaan, 2006). Thus, the Main Zone magma could later supply metals for deposits as on Aurora and Moorddrift, where mineralisation is hosted in leucocratic lithologies (Harmer *et al*., 2004; Manyeruke, 2007; Maier *et al*., 2008; McDonald and Harmer, 2010; McDonald *et al*., 2017). However, Maier and Barnes (2010) suggested that mineralisation at Moorddrift south of Mokopane is associated with the Pyroxenite Marker at the base of the upper Main Zone and is related to a major replenishment event. Earlier, Maier *et al*. (2008) speculated that the occurrence of contact style mineralisation (including that at Moorddrift and Nonnenwerth) is controlled by the marginal setting and rocks of both the upper Critical Zone and Main Zone lineage (and their mixtures) may have been mineralised where they abut against the margins of the intrusion.

7.4.4. Waterberg Project

The Waterberg platinum project is located north of the exposed northern limb of the Bushveld Complex, between the HRSZ and the Palala Shear Zone, within the Southern Marginal Zone of the Limpopo Belt (Fig. 7.1a). U/Pb zircon age dating of the Waterberg Bushveld succession gives intrusion ages of 2059 ± 3 and 2053 ± 5 Ma (Huthmann *et al*., 2016), indicating that the Waterberg intrusion is coeval with the intrusion of the Bushveld Complex (Walraven and Hattingh, 1993; Scoates and Friedman, 2008; Yudovskaya *et al*., 2013; Zeh *et al*., 2015). The Waterberg magmatic succession is up to 1200 m thick and unconformably overlain by Waterberg Group sediments (Kinnaird *et al*., 2017). The magmatic succession is subdivided into a basal Ultramafic Sequence (UmS) comprising feldspathic orthopyroxenite and harzburgite, unconformably overlain by a troctolite-gabbronorite-anorthosite (TGA) sequence and in some parts of the project area by Upper Zone (UZ), magnetite-bearing gabbro/gabbronorite (Fig. 7.1b). The absence of massive magnetitites in the Upper Zone, atypical lithologies in the equivalent of the Main Zone, the Cr-depleted signature of the ultramafic base and the homogenous Sr isotope composition of plagioclase through the sequence all favour a suggestion that the Waterberg segment was emplaced within a separate magmatic basin (Kinnaird *et al*., 2017; Huthmann *et al*., 2018). The stratigraphy and geology of the Waterberg project is described in detail by McCreesh (2016) and Kinnaird *et al*. (2017), thus, only a brief overview of the stratigraphy and geology is given here.

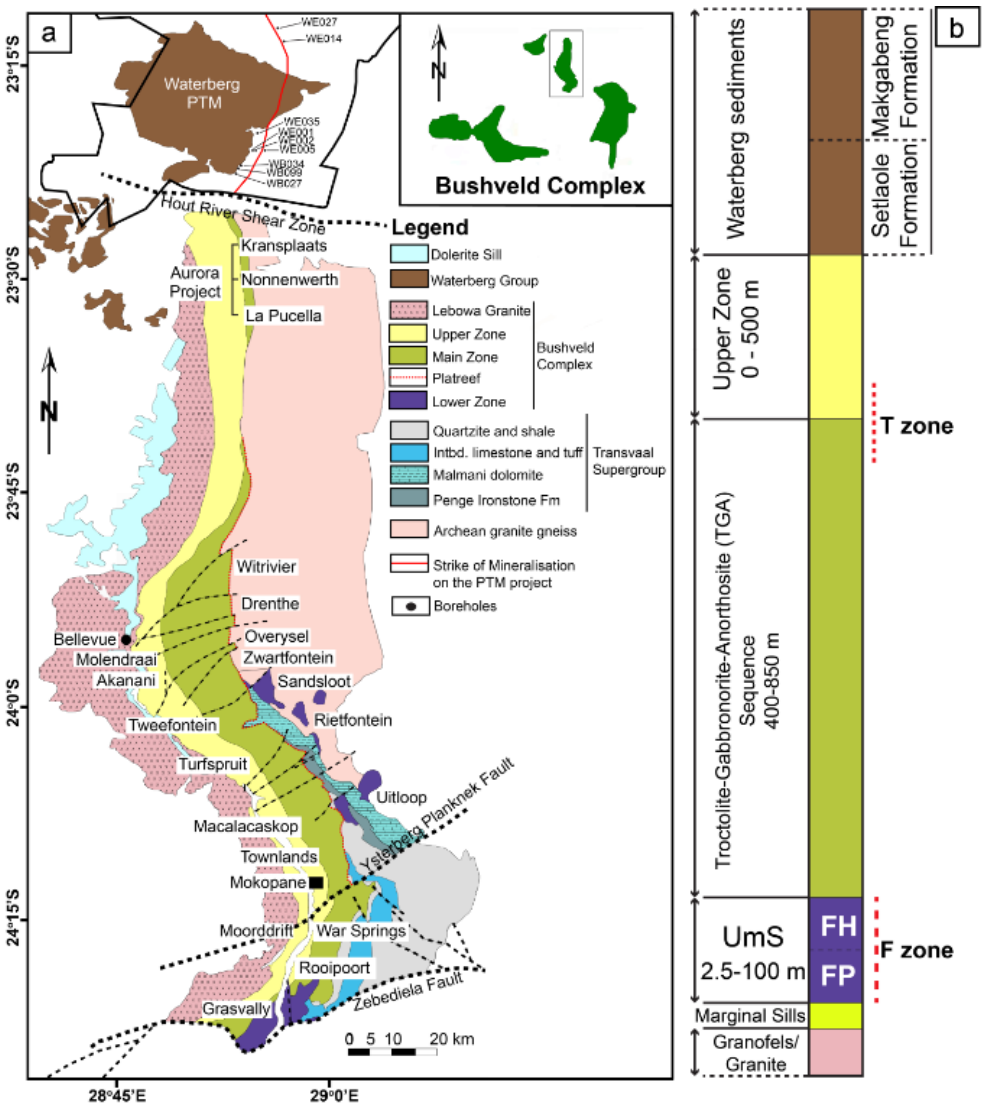

Figure 7.1: (a) Sketch geological map of the Bushveld Complex and enlarged map of the northern limb including the extension of the Waterberg Project in the far north and also the location of boreholes in the Waterberg segment. (b) Stratigraphy of the Waterberg project area.

The lowest part of the intrusion is generally comprises of fine-grained pyroxenitic to gabbroic rocks that partially melted the granite-gneisses footwall developing granofels (Fig. 7.1b). The pyroxenitic and gabbroic rocks are interpreted as the initial intrusive magma pulses in the area, and are attributed to Marginal Zone sills (Kinnaird *et al*., 2017). The overlying Ultramafic Sequence (UmS), intruded as chonolith-shaped bodies (i.e. elongated, irregular or tube-like bodies propagating as finger-like injections) (Huthmann *et al*., 2018). The base of the UmS is composed of feldspathic orthopyroxenite (FP) with subsequent intrusions of feldspathic harzburgite (FH), which incorporated xenoliths of underlying feldspathic orthopyroxenite. The FP and FH host the F mineralised zone, which carries interstitial sulphide assemblages of mainly pyrrhotite, chalcopyrite and pentlandite with associated PGM

and chromite. The UmS reaches a maximum thickness of 100 m (Fig. 7.1b) where the F zone within the UmS is traced along a strike of over 17 km (Kinnaird *et al*., 2017).

The troctolite-gabbronorite-anorthosite (TGA) sequence (Fig. 7.1b) overlies the UmS chonolithic bodies featuring magmatic mingling and erosion along the contact. The laterally extensive TGA sequence is differentiated upwards and reaches a maximum thickness of 850 m. A melatroctolitic unit at the base of the TGA sequence grades into troctolite to olivine-gabbronorite/norite and, finally, into a gabbro and anorthosite. The Upper Zone (UZ) is dominated by magnetite-gabbronorite, but lacks magnetitite layers which are typically seen in the rest of the UZ of the Bushveld Complex (Molyneux, 1974; Ashwal *et al*., 2005). The presence of finely disseminated magnetite in the UZ may be difficult to identify. Therefore, a magnetic susceptibility meter was used to determine the boundary between the TGA sequence and the UZ (Fig. 7.1b) (Kinnaird *et al*., 2017). At the top of the TGA sequence or at the base of the overlying Upper Zone the T mineralised zone occurs in the southwestern part of the exploration area.

There is a good correlation between visible sulphide mineralisation and PGE grades in both the F and T zones. The F mineralised package is typically <10 m thick, although it can be up to 60 m thick with grades of 2-4 g/t 3PGE+Au that is locally known as the Super F zone. The T zone can be as thick as >10 m that is known as the Super T zone with grades of 1-7 g/t 3PGE+Au and the Au is up to 21% of the metal basket. Both mineralised zones in the Waterberg deposit are dominated by Pd over Pt (Kinnaird *et al*., 2017).

The upper contact of the Bushveld succession is represented by an erosional angular unconformity overlain by sedimentary rocks of the Waterberg Group. The Setlaole Formation forms the base of the Waterberg Group in the study area and is composed primarily of coarse-to-medium grained arenite, to arkose and fine-grained mudstone. The sequence coarsens down to a poorly sorted quartz-rich pebble conglomerate (Callaghan *et al*., 1991; Kinnaird *et al*., 2017). The Setlaole Formation is gradationally overlain by the Makgabeng Formation.

It is interpreted that in the period between 1.95 and 2.045 Ga, the area between the HRSZ and the Palala Shear Zone underwent transpressive tectonic deformations coupled with a significant uplift followed by erosion, which removed at least 3-6 km of Bushveld roof rocks and the upper part of the Upper Zone (Huthmann *et al*., 2016). The fast erosion of the Limpopo Mountains resulted in the supply of unsorted molasses such as sediments of the Setlaole and Makgabeng Formations that were deposited slightly after 2.0 Ga upon the weathered Bushveld top. The unconformable top contact between the Bushveld rocks and the overlying Waterberg sediments is complex. There is often a sharp mylonitised

haematitic red siltstone layer or less commonly a prominent white-grey layer at the contact that are interpreted as facies of a paleosol (McCreesh, 2016; Kinnaird *et al*., 2017).

7.5. Previous Sulphur Isotope Work on the Northern Limb

There have been extensive sulphur isotope studies conducted on the northern limb of the Bushveld Complex (see data compilation in Fig. 7.2). Some of the first sulphur isotopic work was done by Liebenberg (1968) on the Zwartfontein farm, where mantle-like $\delta^{34}S$ values for sulphides from pegmatoidal norite (+0.7 ‰) and calcsilicate (+1.9 ‰) were obtained. Liebenberg (1968) also analysed sulphides from the Transvaal sediments that yielded $\delta^{34}S$ values between -11.6 to and +7.8 ‰ (Fig. 7.2).

Buchanan *et al*. (1981) and Buchanan and Rouse (1984) reported sulphur isotope values on sulphides from the Tweefontein and Turfspruit farm. Pyrrhotite hosted in pyroxenite from Tweefontein farm yielded $\delta^{34}S$ values of 2.7 to 6.3 ‰; the elevated values were attributed to contamination with anhydrite associated with the Malmani dolomite footwall. Sulphides from graphite layers on Turfspruit yielded values from -2.42 to +2.0 ‰ that are also within the conventional mantle-like range whereas the Pretoria Group shales had more variable sulphur isotope compositions of -11.6 and +7.8 ‰ $\delta^{34}S$ (Buchanan *et al*., 1981). Buchanan and Rouse (1984) also reported $\delta^{34}S$ values of +17 ‰ for anhydrite from the Duitschland Formation (Fig. 7.2).

Hulbert (1983) reported $\delta^{34}S$ values ranging from +0.96 to +7.54 ‰ in sulphides from the GNPA member (pyroxenite, chromitites and anorthosite) and Lower Zones (pyroxenite and chromitites) in the Grasvally area (Fig. 7.2). Hulbert (1983) also analysed Upper Zone sulphides from the Molendraai farm, which yielded $\delta^{34}S$ values of around +2 ‰. Hulbert (1983) concluded that most of the sulphides formed from S of mantle origin, whereas the elevated values were attributed to contamination with volatiles from sedimentary material. Maier *et al*. (2008) later reported a similar $\delta^{34}S$ range from +1.8 to +5.1 ‰ for 16 samples from the GNPA member.

Recently, Smith *et al*. (2016) conducted the most extensive sulphur isotopic study to date on the area south of the Ysterberg-Planknek fault. Smith *et al*. (2016) discriminated between two generations of sulphides in the GNPA member; the primary sulphide assemblage (pyrrhotite, chalcopyrite and pentlandite) showed $\delta^{34}S$ values between +1.6 to +4 ‰ whereas the secondary assemblage (pyrite and millerite) had $\delta^{34}S$ values ranging from +2.6 to 6.8 ‰. Sulphides from chromitites in the GNPA member have roughly the same sulphur isotopic composition of +2.8 to 7.1 ‰ $\delta^{34}S$ (Smith *et al*., 2016) (Fig. 7.2). Chalcopyrite and millerite hosted by the quartzite footwall exhibit $\delta^{34}S$ values from +3.6 to +5.6 ‰ that

were interpreted as a result of infiltration of magmatic sulphide liquid into the footwall. Metasedimentary pyrite hosted by the Magaliesburg Quartzite Formation is characterised by a $\delta^{34}S$ range from +3.5 to 10.5 ‰ revealing a strong crustal signature. Smith *et al*. (2016) argued that the positive $\delta^{34}S$ values of the primary sulphide assemblage provide evidence for the GNPA member having been crustally contaminated and sulphur saturated at the time of emplacement regardless of local contamination of the parental magma(s).

On the Townlands farm Manyeruke and Maier (2004) found that the Platreef sills are interlayered with three different hornfels rafts at different depths and on this basis divided the Platreef into the Upper, Middle and Lower units. The sulphur isotope values for sulphides from the Upper and Lower units ranges between +5.7 and +10.1 ‰ whereas the Middle unit sulphides show slightly lower $\delta^{34}S$ values between +2.6 and +5.3 ‰. Manyeruke *et al*. (2005) interpreted the elevated $\delta^{34}S$ values as evidence for assimilation of external sulphur, possibly, from the Timeball Hill shales, which were found to be characterised by highly positive $\delta^{34}S$ values from +14 to +17 ‰ (Fig. 7.2).

Sharman-Harris *et al*. (2005) performed a sulphur isotope study on Platreef rocks from the Rietfontein, Turfspruit, Macalacaskop and Drenthe farms, and also analysed samples from the different footwall lithologies of the Duitschland and Timeball Hill Formations and Malmani Subgroup. It was found that sulphides from the upper portion of the Platreef on Turfspruit have mantle-like signatures with $\delta^{34}S$ values ranging from +1.1 to +1.8 ‰. In contrast, the lower 180 m of the contaminated Platreef yielded values between +3 and +6 ‰, which was interpreted as evidence of an involvement of an external sulphur source. Sulphide samples from the different footwall lithologies had sulphur isotope compositions enriched in $\delta^{34}S$ from +2.9 to +20.2 ‰. Sulphides from hornfels and calcsilicate xenoliths were also reported to have heavy isotope compositions varying from +3.6 to 9.7 ‰ $\delta^{34}S$ (Fig. 7.2). However, on Drenthe, where the Platreef was intruded beneath a roof of Malmani dolomite, the upper Platreef was contaminated, with $\delta^{34}S$ values with an average of +6.4 ‰ while the lower Platreef, in contact with basement granite gneiss had mantle-like sulphur values with an average of +3.3 ‰.

Holwell *et al*. (2007), reported sulphur isotope values in sulphides from the Sandsloot, Zwartfontein, Overysel and Witrivier farms on the Anglo Platinum property. Sulphides from fresh feldspathic pyroxenite yielded magmatic $\delta^{34}S$ values between -0.6 and +2.6 ‰. The olivine-replaced reef sulphides on Sandsloot have compositions of +1.4 and +3.1 ‰ $\delta^{34}S$, whereas the olivine-replaced reef on Zwartfontein showed $\delta^{34}S$ values similar to those in feldspathic pyroxenite. The Main Zone mottled anorthosite hangingwall overlying the Platreef contains sulphides with $\delta^{34}S$ values ranging from +2.2 to

+3.2 ‰ (Fig. 7.2). Serpentinized calcsilicate xenoliths, quartz veins and intrusive norites are also characterised by positive $\delta^{34}S$ values. Further north on the Witrivier farm, sulphides from fresh feldspathic pyroxenite of the Platreef yielded $\delta^{34}S$ values between -0.7 and +2.2 ‰, whereas the hangingwall gabbronorite of the Main Zone has slightly higher $\delta^{34}S$ values from +2 to +4 ‰. Sulphides from Archean granite-gneisses on Overysel and Witrivier yielded $\delta^{34}S$ values of -1.2 ‰ similar to $\delta^{34}S$ values of -1.5 ‰ in PGE-rich sulphides from the granite footwall (Holwell *et al*., 2007) (Fig. 7.2).

Sharman *et al*. (2013) showed on the basis of an extensive dataset on the farms Turfspruit, Tweefontein, Rietfontein, Sandsloot, Overysel and Drenthe that there is regional variability in the sulphur isotope content, as the southern and northern sectors of the Platreef had lower $\delta^{34}S$ values as compared with the central sector. In their new study Sharman *et al*. (2013) revealed much broader ranges of $\delta^{34}S$ values in footwall rocks and xenoliths. Sulphides from calcsilicates in the northern and central sectors have $\delta^{34}S$ values ranging from +0.7 to +8.2 ‰, while in the southern sector the calcsilicates and dolomite footwall contains sulphides with $\delta^{34}S$ values between +14.7 to 28.7 ‰ (Sharman *et al*., 2013). The hornfels samples recorded the widest range (-20.9 to 18.1 ‰) and the only negative $\delta^{34}S$ values of sulphides observed in the study.

Interstitial sulphides from the most chemically primitive Lower Zone magmatic rocks (Mg# of olivine up to 92) on Turfspruit yielded highly positive $\delta^{34}S$ values ranging between +9 ‰ and +14.2 ‰ (Fig. 7.2) (Yudovskaya *et al*., 2017), which were interpreted to have resulted from the assimilation of anhydrite-rich sediments of the Duitschland Formation. Analyses of sulphides from the newly discovered reef-style mineralisation hosted by pyroxenite and harzburgite yielded $\delta^{34}S$ values ranging from +2.3 to +2.5 ‰ for the pyroxenite hosted reef and from +2.54 ‰ to +3.07 ‰ for the harzburgite hosted reef (Fig. 7.2). This data supports the earlier idea that the mantle-like sulphur isotope signature of the upper part of the Platreef is similar to that of the Merensky Reef and favours their correlation (Sharman-Harris *et al*., 2005; Holwell *et al*., 2007).

Sulphur isotope data are also available for mineralisation associated with the Main Zone in the northern limb. Holwell *et al*. (2007) sampled pyrite, chalcopyrite and millerite from granite-gneiss on the La Pucella farm and obtained $\delta^{34}S$ values ranging from -1.5 to 0.8 ‰. McDonald *et al*. (2017) sampled sulphides from the mineralised zone on La Pucella as well and obtained a narrow magmatic $\delta^{34}S$ range between -0.8 and +1.1 ‰ (Fig. 7.2). Data by Manyeruke (2007) also indicate mantle-like signatures (+0.73 to +1.87 ‰) for sulphides hosted in gabbronorite, norite, gabbro and anorthosite of the mineralised unit on the Nonnenwerth farm, although sulphides from an altered gabbronorite sample

an elevated $\delta^{34}S$ value of +5.24 ‰.

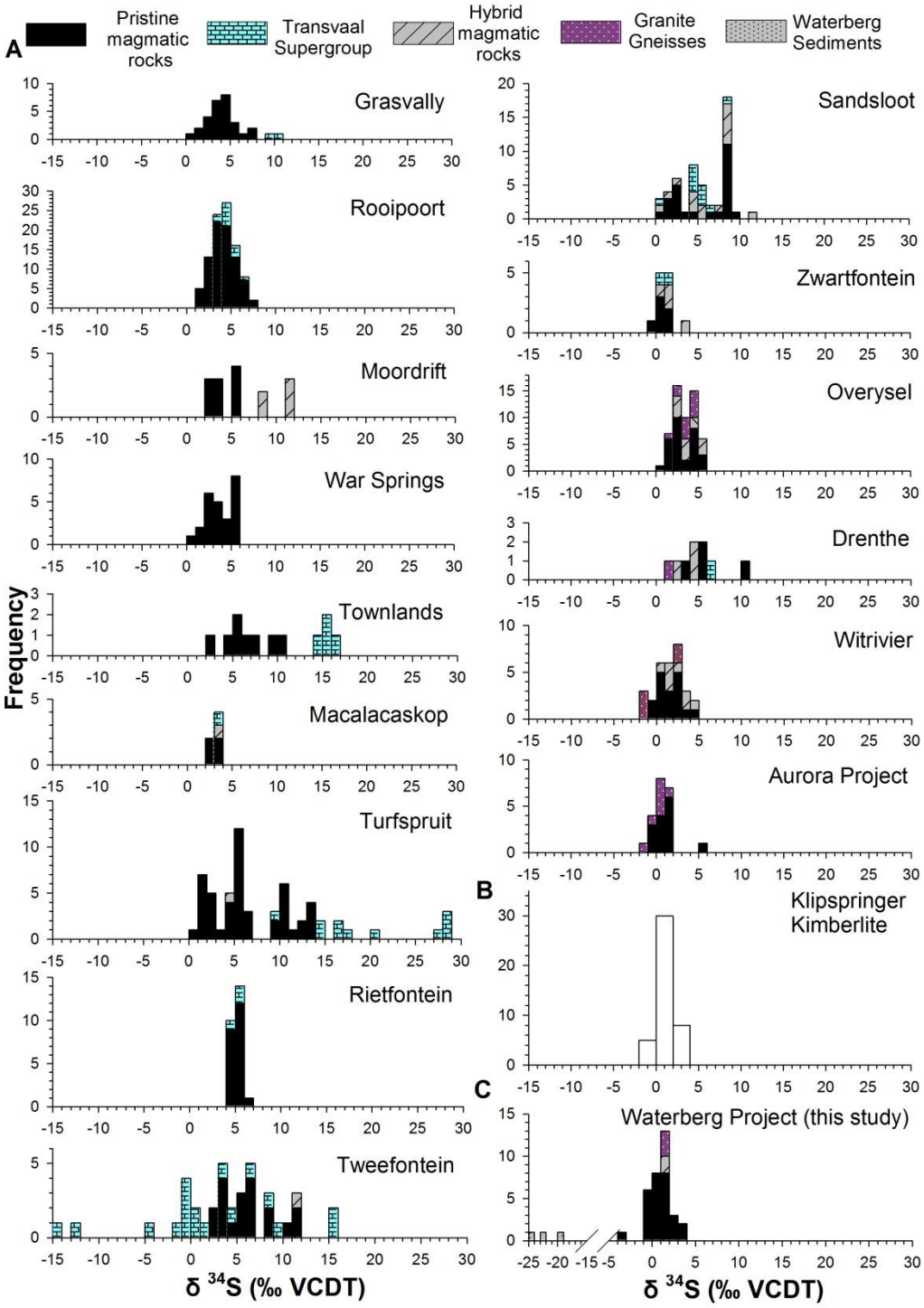

Figure 7.2: Sulphur isotope results for the northern limb (A) summary of previous sulphur isotope data on the northern limb (Liebenberg 1968; Buchanan *et al*., 1981; Hulbert, 1983; Buchanan and Rouse 1984; Manyeruke *et al*., 2005; Sharman-Harris *et al*., 2005; Holwell *et al*., 2007; Holwell *et al*., 2013; Sharman *et al*., 2013; Smith *et al*., 2016 McDonald *et al*., 2017; Yudovskaya *et al*., 2017). (B) Sulphur isotope data from the Klipspringer Kimberlite (Westerlund *et al*., 2004) and (C) the sulphur isotope results from the Waterberg Project in this study.

The mineralisation in the upper Main Zone on the Moorddrift farm south of Mokopane have $\delta^{34}S$ values ranging from +2.8 to +11.5 ‰ that indicate a significant contribution of crustal sulphur (Holwell *et al*., 2013). Primary sulphides hosted within gabbronorite and anorthosite yielded $\delta^{34}S$ values between +3.9 and +5.3 ‰ whereas secondary pyrite demonstrates lower $\delta^{34}S$ values between +2.8 to +3.5 ‰ (Holwell *et al*., 2013).

Sulphur isotope compositions have also been investigated in other parts of the Bushveld Complex. Liebenberg (1968) reported $\delta^{34}S$ values of +7.8 and +7.5 ‰ in sulphides from the Lower Zone harzburgite and pyroxenite in the western limb of the Bushveld Complex, respectively. Penniston-Dorland *et al*. (2012) reported $\delta^{34}S$ values between +1.1 ‰ and +2.2 ‰ for Merensky Reef whole rocks in the eastern and western limbs, where Liebenberg (1968) has earlier reported lower $\delta^{34}S$ value of -0.6 ‰ for the Merensky Reef sulphides. Sulphides from the UG2 chromitite layer in the eastern and western limbs have $\delta^{34}S$ values between +2.2 and +3.2 ‰ according to Penniston-Dorland *et al*. (2012) and between +0.3 and +3.5 ‰ according to the earlier study by Liebenberg (1968). The Main Zone whole-rock samples in the eastern and western limbs are characterised by a narrow range of +1.3 to +1.5 ‰ (Penniston-Dorland *et al*., 2012) whereas the Upper Zone diorites of the eastern limb showed a similar narrow range from +0.5 to +0.9 ‰ $\delta^{34}S$ (Liebenberg 1968).

Sulphur isotope of sulphides from basal gabbro and ore-bearing harzburgite of the satellite Uitkomst Complex within the Bushveld Large Igneous Province ranging from -0.9 to +2.6 ‰ and -7.1 to -2.6 ‰, respectively (Li *et al*., 2002). Gauert *et al*. (1996), however, found $\delta^{34}S$ values between -20 and +2 ‰ and suggested that the wide range reflects sulphur assimilation from wall rock dolomites or shales with the latter having $\delta^{34}S$ values of -16 to -11 ‰. Sulphides from the massive sulphide body showed a range of +0.7 to +1.1 ‰ $\delta^{34}S$ which were hosted in the Malmani dolomite (Gauert *et al*., 1996).

Cameron (1982) conducted sulphur isotope analyses for the Transvaal Supergroup floor rocks in the eastern Bushveld. The Timeball Hill Formation sulphides showed the most variable $\delta^{34}S$ values from -12 to +18 ‰, sulphides from the Penge Formation from -3 to -6 ‰, pyrite-bearing shales from the Malmani Subgroup contains sulphides with compositions from 0 to +8 ‰ $\delta^{34}S$ and pyrite from Black Reef quartzite yielded a $\delta^{34}S$ value of +3 ‰ (Cameron, 1982). Guo *et al*. (2009) investigated sulphur isotope signatures in the Duitschland Formation and found a major change in $\delta^{34}S$ values between the upper and lower parts of the formation divided by glacial diamictites. The lower parts have $\delta^{34}S$ values in sulphides ranging from +4.7 to +11.1 ‰, whereas the upper part contains isotopically much heavier sulphides with $\delta^{34}S$ values ranging from +11.8 ‰ to as high as +42.3 ‰ (Guo *et al*., 2009). These authors

interpreted the major change to be associated with the transition from an anoxic to an oxic atmosphere in the Paleoproterozoic.

7.6. Sampling and Methodology

Sulphide-bearing samples were collected throughout the stratigraphy of the Waterberg PGE deposit. Samples were chosen from selected borehole cores on the Waterberg Joint Venture Project (WB027, WB034 and WB099) and the New Waterberg Extension Project (WE001, WE002, WE005, WE014, WE027 and WE035).

Samples were crushed and then sieved to +90 µm in size. The sieved material was then washed and dried to remove the very fine material. Samples were then placed in the magnetic separator, to separate according to minerals magnetic properties (eg: magnetite and pyrrhotite). Sulphides were extracted manually under a zoom stereo microscope (Olympus SC30) and separated into different sulphides (chalcopyrite, pyrrhotite and pentlandite). Sulphides were then crushed to a powder. These samples were weighed and prepared to approximately 600 mg of sulphide plus 200 mg of V_2O_5 (BDH 98.5%) and placed into a small aluminium cap. Three standard samples were made per batch. Standards included; 600 mg of Ferrous Sulphide EP (FeS) and 200 mg of OGS 115 and were weighed and prepared in the small aluminium caps. The analyses were conducted at the Environmental Isotope Laboratory of the iThemba Laboratories in South Africa. Sulphur isotope samples were prepared using the Horstmann and Malinga (2004) method and the samples were analysed using a continuous-flow isotope ratio mass-spectrometer (GEO20-20). All sulphur isotope data are reported relative to Vienna-Canon Diablo Troilite (V-CDT).

7.7. Results

7.7.1. Sulphur Isotopes

Sulphide samples were analysed throughout the stratigraphy of the Waterberg area including the Archean granite footwall, the Marginal Sills, the basal Ultramafic Sequence including the F zone, the TGA sequence, the T zone, the Upper Zone and Waterberg sediments. All the sulphur isotope results are listed in Table 7.1. Sulphide samples from the Waterberg area exhibit various textures which include disseminated, blebby, net-textured, hosted in secondary veinlets and minor semi-massive occurrences associated with the basal contact between the granofels footwall and the UmS. Chalcopyrite, pyrrhotite and pentlandite were separated and gave a broad range of $\delta^{34}S$ values from -24.41 to +3.17 ‰.

Archean Granite-Gneisses: sulphides separated from three samples hosted by medium- to coarse-grained potassic granite from borehole WE005 was mainly chalcopyrite. The sulphur isotope composition of the Archean granite-gneisses samples is relatively uniform with an average $\delta^{34}S$ value of +1.25 ‰ (Fig. 7.3).

Transitional zone in granofels: the alternating bands of felsic-rich and mafic-rich lithologies may host semi-massive sulphides which are generally hosted within the orthopyroxene-rich bands. Two pyrrhotite samples were analysed from the granofels unit and yielded $\delta^{34}S$ values of +1.55 ‰ and +1.77 ‰ (Fig. 7.3).

Marginal Sill: three sulphide separate samples were analysed from fine-grained marginal pyroxenite and gabbronorite. The disseminated and blebby sulphides are mostly pyrrhotite, which yielded $\delta^{34}S$ values between +2.35 and +3.17 ‰ (Fig. 7.3).

F zone: the basal mineralised zone hosts a typical magmatic assemblage of pyrrhotite, chalcopyrite and pentlandite, which underwent significant replacement by secondary silicates and serpentinisation-related magnetite (McCreesh *et al*., 2018). The F zone samples are characterised by an average $\delta^{34}S$ of +1.18 ‰, however, there are a few anomalies seen within the F zone sulphur isotope compositions. Anomalous $\delta^{34}S$ values were obtained for the samples from the borehole WB034 that varies from -3.52 ‰ to +2.61 and +2.91 ‰ $\delta^{34}S$. These sulphides are associated with high-grade sperrylite-dominant mineralisation in heavily serpentinised harzburgite. The primary magmatic sulphides are replaced by secondary sulphides and magnetite that results in the removal of approximately half of their initial volume. The rest of the F-zone samples from this and the other boreholes plot within the mantle-like range between -1 to +2 ‰ (Fig. 7.3).

Troctolite-gabbronorite-anorthosite sequence: disseminated chalcopyrite was sampled from gabbronorite with ~50% plagioclase, ~30-35% orthopyroxene, ~10-15% clinopyroxene and minor alteration that is typical for the Main Zone in the rest of the Bushveld Complex. The two sulphide samples gave $\delta^{34}S$ values of +0.20 and +0.21 ‰. A sulphide sample from anorthosite yielded a $\delta^{34}S$ value of +0.30 ‰ (Fig. 7.3).

Table 7.1: Results of the conventional sulphur isotope analyses for the Waterberg Project performed at iThemba Laboratory. WB - Waterberg sediments, UZ - Upper Zone, TZ - T-mineralised zone, TGA - troctolite-gabbronorite-anorthosite sequence, FZ - F-mineralised zone, MnS - Marginal Sills, TRNZ - Transitional zone of granofels, BAS – Archean basement.

B.H.I.D	Depth (m)	Stratigraphy	Rock type	Sulphides	Sulphide Textures	δ^{34} S ‰
WE033	438.50	WB	Conglomerate	Chalcopyrite	Disseminated	-24.41
WE033	440.74	WB	Conglomerate	Chalcopyrite	Disseminated	-22.83
WE033	440.86	WB	Conglomerate	Chalcopyrite	Disseminated	-19.96
WE027	888.37	UZ	Magnetite gabbronorite	Chalcopyrite	Disseminated	0.80
WE027	888.70	UZ	Magnetite gabbronorite	Chalcopyrite	Disseminated	1.87
WB099	698.67	T Zone	Gabbronorite	Pyrrhotite	Blebs	-0.48
WB099	698.84	T Zone	Gabbronorite	Pyrrhotite	Blebs	-0.34
WB099	699.40	T Zone	Gabbronorite	Chalcopyrite	Disseminated	-0.30
WB099	699.60	T Zone	Gabbronorite	Chalcopyrite	Disseminated	-0.29
WB099	700.02	T Zone	Gabbronorite	Pentlandite	Disseminated	-0.23
WB099	700.37	T Zone	Gabbronorite	Pentlandite	Disseminated	-0.17
WB099	705.50	T Zone	Gabbronorite	Chalcopyrite	Disseminated	0.16
WB099	705.75	T Zone	Gabbronorite	Chalcopyrite	Disseminated	0.29
WB099	825.75	TGA	Gabbronorite	Chalcopyrite	Disseminated	0.20
WB099	825.88	TGA	Gabbronorite	Chalcopyrite	Disseminated	0.21
WB099	900.03	TGA	Anorthosite	Chalcopyrite	Disseminated	0.30
WB034	997.65	F Zone	Feldspathic Harzburgite	Chalcopyrite	Blebs	-3.52
WB034	1060.30	F Zone	Feldspathic Harzburgite	Pyrrhotite	Blebs	0.98
WB034	1060.85	F Zone	Feldspathic Harzburgite	Pyrrhotite	Blebs	1.16
WB034	1061.00	F Zone	Feldspathic Harzburgite	Chalcopyrite	Blebs	1.19
WB034	1061.20	F Zone	Feldspathic Harzburgite	Chalcopyrite	Blebs	1.28
WB034	1061.45	F Zone	Feldspathic Harzburgite	Chalcopyrite	Blebs	1.65
WB034	1061.61	F Zone	Feldspathic Harzburgite	Pentlandite	Blebs	1.82
WB034	1061.83	F Zone	Feldspathic Harzburgite	Pentlandite	Blebs	1.91
WB034	1067.70	F Zone	Feldspathic Harzburgite	Pentlandite	Blebs	1.98
WB034	1018.90	F Zone	Feldspathic Harzburgite	Chalcopyrite	Blebs	2.61
WB034	1019.10	F Zone	Feldspathic Harzburgite	Chalcopyrite	Blebs	2.94
WB035	630.20	F Zone	Orthopyroxenite	Chalcopyrite	Disseminated	0.58
WB035	630.50	F Zone	Orthopyroxenite	Chalcopyrite	Disseminated	0.77
WE014	873.00	MnS	Fine-grained pyroxenite	Pyrrhotite	Disseminated	2.35
WE014	894.47	MnS	Fine-grained pyroxenite	Pyrrhotite	Blebs	3.10
WE014	880.78	MnS	Fine-grained pyroxenite	Pyrrhotite	Disseminated	3.17
WE002	683.37	TRANZ	Granofels	Pyrrhotite	Semi-massive	1.54
WE002	677.75	TRANZ	Granofels	Pyrrhotite	Semi-massive	1.77
WE005	420.05	BAS	Granite-gneiss	Chalcopyrite	Blebs	1.13
WE005	421.83	BAS	Granite-gneiss	Chalcopyrite	Blebs	1.21
WE005	420.47	BAS	Granite-gneiss	Chalcopyrite	Disseminated	1.41

T zone: eight sulphide separates from medium- to coarse-grained gabbronorite and gabbro showed a narrow range of -0.48 to 0.29 ‰, which are the "purest" mantle-like signature within the Waterberg dataset (Fig. 7.3).

Upper Zone: two sulphide samples from the Upper Zone comprise mostly disseminated chalcopyrite in association with magnetite. These samples yielded $\delta^{34}S$ values of +0.80 and +1.87 ‰ (Fig. 7.3).

Waterberg Sediments: disseminated chalcopyrite was sampled near the contact between the Waterberg sediments and the Bushveld mafic rocks. Sulphides are not commonly seen in the Waterberg sediments in the project area. The range of $\delta^{34}S$ values is from -20 to -25 ‰ (Table 7.1).

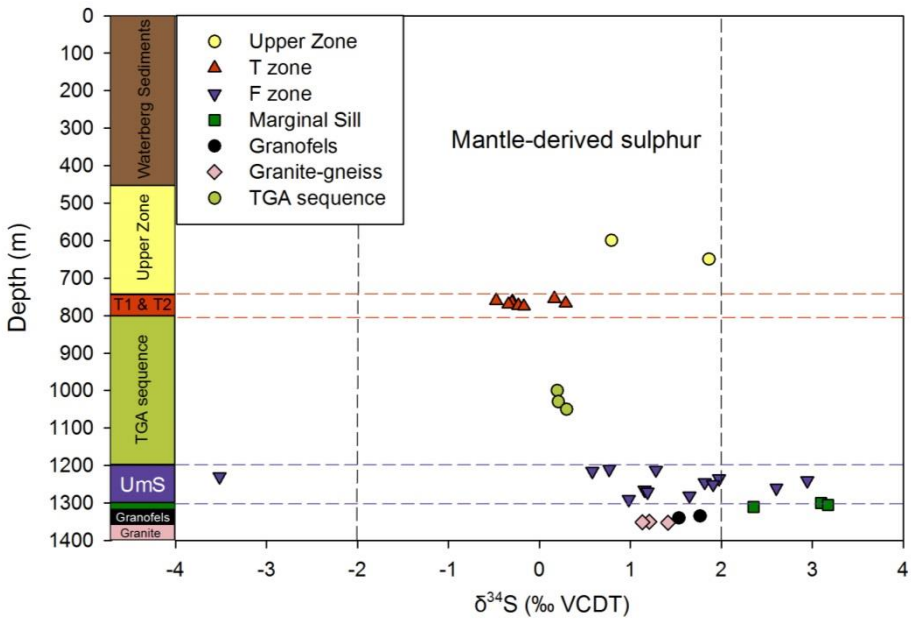

Figure 7.3: The sulphur isotope composition in ‰ $\delta^{34}S$ versus the stratigraphy of the Waterberg succession excluding the values obtained for the Waterberg sediments. The mantle-derived sulphur isotope ranges are adopted from Westerlund *et al*. (2004).

7.8. Discussion

Sulphur isotope signatures of the lithospheric mantle of the Kaapvaal Craton beneath the Bushveld Complex can be inferred from the isotope compositions of the sulphide inclusions in eclogites found in kimberlite pipes. Westerlund *et al*. (2004) analysed sulphide inclusions in diamonds hosted by eclogites from the Klipspringer kimberlite 25 km east of Mokopane, which yielded $\delta^{34}S$ values between -1.8 and +2.4 ‰ with a mean of +1.0 ‰ determined from 44 samples (Fig. 7.2). These data provide a range of $\delta^{34}S$ values for mantle-like sulphides for the northern limb and the Bushveld Complex as a whole.

Two mineralised zones were intercepted on the Waterberg project, the lower F zone and the upper T zone (Kinnaird *et al*., 2017). The F zone sulphides comprise primary magmatic pyrrhotite, chalcopyrite and pentlandite which have undergone later stage alteration forming a secondary sulphide assemblage (pyrite, Cu-Ni sulphides, covellite, valleriite and bornite) (McCreesh *et al*., 2018). Both sulphides and chromite in the F zone revealed significant resorption and replacement by secondary silicates and magnetite. The upper T zone hosts two sulphides assemblages: relics of a primary magmatic assemblage and a later stage hydrothermal assemblage of pyrite, millerite and chalcopyrite (McCreesh *et al*., 2018). The primary base metal sulphides in the T zone are also altered along the margins and replaced by hydrous silicates (amphiboles, phlogopite, chlorite and epidote). Hydrothermal quartz crustifications are abundant and associated with secondary sulphides. The platinum-group metals in the mineralised intervals are mostly isolated crystals at the edge of sulphide aggregates or within hydrous silicates due to the removal or replacement of sulphides (McCreesh *et al*., 2018).

The sulphides in the Waterberg succession all have mantle-like isotope signatures in consistency with the restricted range determined by Westerlund *et al*. (2004) (Figs. 7.2 and 7.3). This implies that the low-sulphide mineralisation on the Waterberg is formed from orthomagmatic processes and the main sulphur source for the mineralisation is of mantle origin (Ripley and Li, 2017). These sulphur isotope compositions are within the same range of $\delta^{34}S$ values reported for the Merensky Reef and UG2 and reef-style mineralisation of the upper Platreef (Liebenberg 1968; Penniston-Dorland *et al*., 2012; Yudovskaya *et al*., 2017), although it should be emphasized that we envisage the Waterberg mineralisation forming as mineralised zones rather than reef-style mineralisation. This interpretation of our data in good agreement with the conclusion of Lesher *et al*. (2017) who noticed that a mantle origin has to be imputed to sulphides with highly homogenous and restricted values close to 0 ‰ on the basis that mantle-derived magmas of a komatiitic lineage are produced at a relatively high degree of partial melting and should contain homogenous sulphur isotope composition. In this regard, any scattering of $\delta^{34}S$ values beyond the range 0 to ± 2 ‰ $\delta^{34}S$ should be carefully considered as probable evidence of a contribution of external sulphur.

The high PGE grades and high PGE tenors of sulphides in the PGE deposits of the Waterberg succession suggest that the immiscible sulphide liquid was exposed to an overwhelmingly larger volume of silicate liquid (Naldrett, 2010). The scale of the interaction can be expressed as an “R-factor” (Campbell and Naldrett, 1979), which represents the ratio of the mass of silicate liquid to the mass of sulphide liquid, and the higher the “R-factor” the higher the concentration of PGE (Naldrett, 2010). A recent

experimental study by Mungall and Brenan (2014) suggested that sulphide/silicate partition coefficients of PGE and Au are much higher, up to 10^6, compared to previously assumed lower values. This implies that an extremely high R-factor and large pools of sulphide liquid are not necessary to form high-grade PGE deposits as seen in the Waterberg succession and Bushveld reefs. Therefore, low-sulphide mineralisation with a narrow mantle range of sulphur isotope compositions may not require any addition of external sulphur. At the same time, Ripley and Li (2003) discussed the potential of sulphur isotope exchange between the assimilated crustal sulphur and the magmatic sulphur that masks or erases the isotopic evidence indicating possible contamination within dynamic Ni-Cu-PGE systems characterised by high R-factors. The similar PGE tenors in the Bushveld reefs and the Waterberg ore zones imply that their R-factor should be of the similar order. However, slightly heavier sulphur isotope compositions of sulphides coupled with higher sulphur content in the reef-style mineralisation at the top of the Platreef likely testify to an involvement of sedimentary derived sulphur within the mineralisation.

It is widely accepted that parental magmas of the Bushveld Complex were contaminated by material of the crust or the sub-continental lithospheric mantle that may result in sulphide saturation prior to emplacement (Richardson and Shirey, 2008; Naldrett *et al*., 2012). Ihlenfeld and Keays (2011) argued that there are two phases of sulphur assimilation responsible for the observed features of Platreef mineralisation: primary sulphur assimilation within the upper or mid crust prior to the emplacement of Platreef magma and a secondary sulphur assimilation associated with local floor rock contamination. The primary sulphur assimilation may produce a magmatic sulphur isotopic signature undistinguishably similar to the mantle. Barnes *et al*. (2009) suggested that the variations in S/Se ratio and Pd tenors may help to detect crustal sulphur assimilation and concluded that magma was saturated in sulphides at depth and may have been partly deposited during transportation. Therefore, although the assimilation of crustal material prior to emplacement is an acknowledged feature of the Bushveld primary melts, it is still highly debatable whether the putative sulphur contamination at depth was a positive or negative factor of sulphide mineralisation (Ihlenfeld and Keays, 2011; Naldrett *et al*., 2012).

The modest scattering of $\delta^{34}S$ values out of the mantle range in the Waterberg samples is interpreted to be a result of sulphide remobilisation by hydrothermal fluids. The high degree of hydrous silicate replacement including the complete removal of sulphides is associated with postmagmatic exsolved fluid activity as well as with serpentinisation (McCreesh *et al*., 2018). These processes are different from hydrothermal activity in the contaminated Platreef, as the Transvaal Supergroup footwall, xenoliths and autoliths provides fluids with external sulphur isotope characteristics (Sharman-Harris *et al*., 2005;

Holwell *et al*., 2007). The footwall rocks of the Waterberg area are composed of Archean granite-gneiss that is poor in sulphur and volatiles. No significant carbonate or calcsilicate xenoliths were found within the Waterberg magmatic-ultramafic sequence and the whole rock $CaO:Al_2O_3$ ratio of ~0.6 is typical for uncontaminated Bushveld igneous rocks (Kinnaird, 2005). Therefore, the hydrothermal fluid was predominantly of a late to postmagmatic origin that allowed the magmatic sulphides to preserve a mantle-derived sulphur isotopic signature as seen elsewhere in the northern limb where Archean basement forms the footwall (Holwell *et al*., 2007). According to Ohmoto (1972) the sulphur isotope composition of hydrothermal fluids is strongly controlled by the oxygen fugacity, pH levels and temperature. The observed shift in the $\delta^{34}S$ values can be attributed to isotopic fractionation under conditions of variable oxygen activity during the evolution of the hydrothermal fluid.

The highly negative $\delta^{34}S$ values from -24.41 to -19.96 ‰ in sulphides from the base of the Setlaole Formation are interpreted as a result of bacteria-involved redox reactions (Eldridge *et al*., 1988). The sulphur might be remobilised from the underlying magmatic Bushveld rocks due to fluid circulation along the contact zone or might be derived from dissolution of detritus during the deposition of the Waterberg Group sediments.

7.9. Conclusion

The Waterberg low-sulphide PGE mineralisation is characterised by a homogenous mantle-like sulphur signature and shows no signs of local sedimentary contamination to upgrade the sulphur budget. Contamination in a crustal chamber at depth cannot be excluded since the contaminated isotope characteristics may have been masked or erased by sulphur isotope exchange during the transportation of the magmas as suggested by Ihlenfeld and Keays (2011) and Ripley and Li (2013). The observed minor contaminated $\delta^{34}S$ values slightly beyond the mantle range are related to postmagmatic hydrothermal fluid circulation and serpentinisation. The Waterberg unaltered mineralisation shows a restricted range of sulphur isotopic variations as is seen elsewhere in the northern limb where the footwall is composed of Archean granite-gneisses. We suggest that only this narrow range should be considered as a valid indication of pristine magmatic origin of PGE mineralisation in the Bushveld Complex whereas any wider variations should raise questions to their causes

Chapter 8

Geochemistry and PGE of the lower mineralized zone of the Waterberg Project, South Africa

This section contains the full text of the paper "Geochemistry and PGE of the lower mineralized zone of the Waterberg Project, South Africa" by Huthmann, F.M., Yudovskaya, M.A., Kinnaird, J.A., McCreesh, M. and McDonald, I. It has been published in *Ore Geology Reviews*. The PDF document as published can be found in Appendix A2.

This publication provides a detailed account of the lower ultramafic mineralized zone and describes in detail a set of drill holes in the central part of PTM's exploration area and contains logging, petrographical and geochemical data

8.1. Candidate's contribution:

- The candidate assisted the first author with field work: core logging and collecting samples.
- The candidate was involved with the discussion during the preparation stages of the manuscript.
- The candidate contributed approximately 5 to 10% towards the publication.
- Florian Huthmann was responsible for the write up of the paper.

8.2. Abstract

The Waterberg deposit is located north of the Northern Lobe of the Bushveld Complex in South Africa and represents a large, high-grade, new Platinum-Group-Element (PGE) discovery. The first comprehensive study of the lower ultramafic section of the area has been completed, and whole-rock chemical analyses and PGE data are presented.

The section studied comprises mineralized harzburgite and marginal orthopyroxenite, overlain by troctolite grading into gabbroic rocks. Whole-rock analyses show geochemical variations typical of differentiated assemblages of cumulus olivine, plagioclase, and pyroxene. Normalized trace element data display HREE depletion, strong positive Eu and Sr anomalies and LREE enrichment. The negative anomalies for Th, Rb, Nb, and Ta are typical for rocks of the Bushveld Complex. Normalized PGE distributions are fractionated (Pd/Ir 177), Pd-enriched, and Au-poor.

Emplacement of the magmas is believed to have commenced with west-east trending, finger-like intrusions, followed by lateral dilation and emplacement of sulfide droplet-bearing, ultramafic magmas. This was followed by a second phase of intrusions, characterized by sheet-like bodies of troctolite. Fractionation of these magmas led to the development of gabbroic rocks that make up the top of the succession. The Waterberg Project is located in the Southern Marginal Zone of the Limpopo Belt. This position in a structurally active area may have facilitated the creation of space for initial magmas.

It is argued, that the mafic to ultramafic succession of the Waterberg Project does not represent a simple marginal extension of the Northern Lobe, nor does it directly correlate with the Platreef. It shares geological features but represents a separate magmatic basin.

8.3. Introduction

The Northern Lobe of the Bushveld Complex hosts the Platreef and its world-class ore bodies. The stratigraphy and mineralization of the Northern Lobe has been the topic of many studies in recent years. Most of them were made on the giant Mogalakwena mine that processes the shallow Platreef high-grade mineralization in contaminated sequences (McDonald and Holwell, 2011). A new underground project commenced at Turfspruit is focused on the reef-style mineralization at depth confirming unlimited perspectives westwards (Yudovskaya *et al*., 2017). In the light of the discovery of Main Zone-hosted mineralization in the far north and south of the lobe (Harmer *et al*., 2004; Maier and Barnes, 2010), the Main Zone of the Bushveld Complex is now also being explored. The Waterberg Project is located north of the Northern Lobe and represents a large, recent PGE discovery (Huthmann *et al*., 2016, 2017; Kinnaird *et al*., 2017).

The significant Waterberg Pd-Pt mineral system is a >3.5 by 24 km, mafic to ultramafic, lobate intrusion hosting an indicated resource of 24.9 million ounces 4E (Pt+Pd+Rh+Au; 2.5 g/t cut-off) in upper (T Zone) and lower (F Zone) mineralized zones. Its U/Pb ages of 2059±3 and 2053±5 Ma (Huthmann *et al*., 2016) overlap within error with the 2.06 Ga age (Scoates and Friedman, 2008; Scoates and Wall, 2015; Zeh *et al*., 2015) of the Bushveld Complex. Kinnaird *et al*. (2017) provide an extensive overview of the local geology, the relationship of the succession with its roof rocks, and details of the T and F mineralized zones. In this contribution, the stratigraphy of a small area, hosting the Super F mineralized zone is described in detail. The term Super F Zone is used by Platinum Group Metals to refer to intersected F zone mineralization tens of meters in thickness.

Drill data from >100 drill holes indicate the presence of discontinuous and variable lithologies in the study area. In this study, a range of drill holes has been logged in detail and whole-rock major and trace element geochemistry as well as PGE are compared to company assays. The data gathered for this study is used to present the first conceptual model for the evolution of the Waterberg Succession. Possible correlations with the sections of the Northern lobe (Harmer *et al*., 2004) immediately to the south are explored in detail in the discussion section.

8.4. Geology

The 2.06 Ga (Scoates and Friedman, 2008; Scoates and Wall, 2015; Zeh *et al*., 2015) Bushveld Complex is the largest layered intrusion on Earth and the world's largest repository of PGE, Cr and V (Lee, 1996). It is believed to consist of 5 lobes with an estimated areal extent of approximately 65,000 km^2 (Willemse, 1969). The intersected ultramafic-mafic rocks at the northern end of the Northern Lobe, and recent geo

physical studies, however, increase this total areal extent to >90,000 km^2 (Finn *et al*., 2015). Although the lobes were historically interpreted to be separate bodies, more recent interpretation of the gravity data allows for the possibility that the Eastern and Western Lobes connect at depth (Webb *et al*., 2004; Finn *et al*., 2015). Links between the Northern Lobe and the Eastern and Western Lobes are contentious (Cawthorn and Webb, 2001), and links between the Northern Lobe and the Waterberg Project remain to be established. The controversy also includes the gently south-dipping Villa Nora Segment (Fig. 8.1) and its relationship to both the Northern Lobe and the Waterberg Project. The Bushveld Complex comprises heterogeneous, predominantly felsic volcanics, a mafic to ultramafic suite of 7–8 km thickness, a granite as well as a granophyre suite (von Gruenewaldt *et al*., 1985). The mafic package, also known as the Rustenburg Layered Suite, is subdivided into the noritic Marginal Zone, the Lower Zone comprising pyroxenite and harzburgite, the cyclical Critical Zone of chromitite norite pyroxenite, the Main Zone comprised of gabbronorite and the Upper Zone of anorthosite, gabbro and magnetitite. Lateral facies variations are common and not all zones are always present (Eales and Cawthorn, 1996; Kruger, 2005; McDonald and Holwell, 2011).

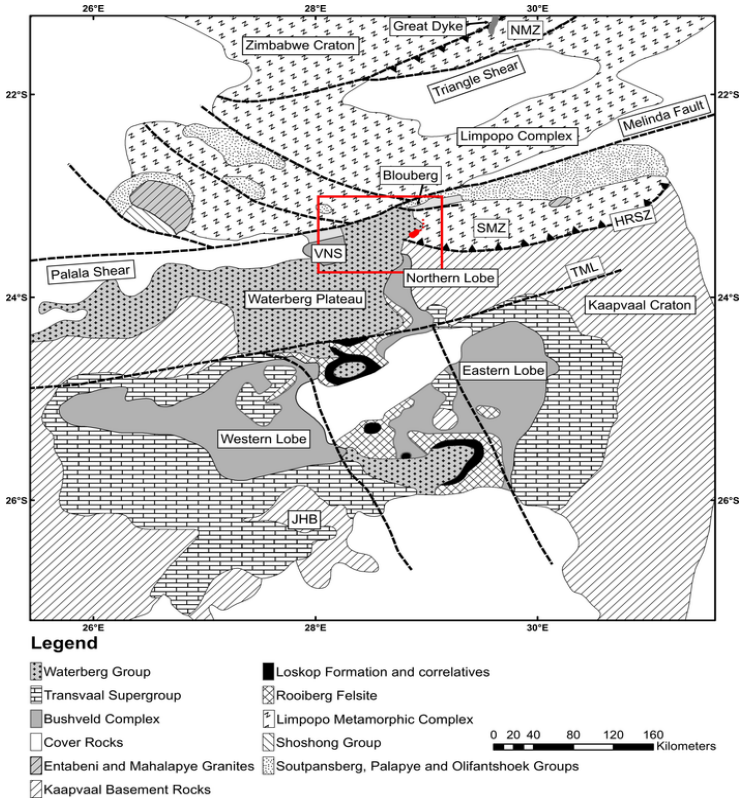

Figure 8.1: Map showing the distribution of major lithological units in northern South Africa. JHB Johannesburg; SMZ Southern Marginal Zone; NMZ Northern Marginal Zone; TML Thabazimbi-Murchison lineament; HSRZ Hout River Shear Zone VNS Villa Nora Segment. The small rectangle indicates the Waterberg area. Modified after Dorland *et al*. (2006).

8.4.1. The Northern Lobe and the Platreef

The geology of the Platreef and Northern Lobe are reviewed in great detail in van der Merwe (1976), Ashwal *et al*. (2005), Kinnaird *et al*. (2005), McDonald and Holwell (2011) and Kinnaird and Nex (2015). An overview of the geology relevant for the discussion of the Waterberg Project is provided by Kinnaird *et al*. (2017). The Northern Lobe is separated from the Bushveld by the Thabazimbi-Murchison-Lineament. The TML is a 500 km long and 25 km wide, ENE-WSW striking, long-lived and repeatedly reactivated craton-scale structure (Good and de Wit, 1997). Based on seismic anisotropy, the TML is interpreted to represent a fundamental crustal and possibly deep lithospheric mantle lineament within the Kaapvaal craton. It is thought to have influenced regional stresses and tectonically induced fluid flux during its re-active history between 2960 and 145 Ma (Good and de Wit, 1997). The stratigraphic correlation between the Northern Lobe to the north and Eastern and Western Lobes to the south of the TML remains contentious (van der Merwe, 1976; Ashwal *et al*., 2005; Kruger, 2005; McDonald *et al*., 2005; Kinnaird and Nex, 2015).

The succession of mafic to ultramafic rocks in the Northern Lobe differs from the Eastern and Western Lobes, but arguably all zones can be recognized. The Lower Zone was emplaced in trough-like depressions and is characterized by high-Mg rocks, chromitites and zones of Ni-PGE mineralization (Hulbert and von Gruenewaldt, 1982, 1985; Yudovskaya *et al*., 2013b, 2017). The Lower Zone is separated from the Platreef by older Transvaal sediments or granite gneisses. The main basal unit is the Platreef, a pyroxenite-dominated, lithologically variable unit irregularly mineralized with PGE and Ni and Cu sulfides. It onlaps northwards onto progressively older Transvaal metasedimentary units of oxide facies iron formations and dolomite and eventually onto Archean granites and gneisses (Kinnaird *et al*., 2005). The Platreef disappears approximately half-way along the Northern Lobe. Data from Turfspruit confirms a general westward dip of 30° to 60° close to surface, the dip however lessens with depth into a more regularly layered sequence (Grobler *et al*., 2012; Yudovskaya *et al*., 2017). The Platreef is considered to be the stratigraphic equivalent of the Critical Zone and unconformably overlain and intruded (Holwell *et al*., 2005; Holwell and Jordaan, 2006) by the <2000 m thick Main Zone. Overlying the Main Zone, the Upper Zone of the Northern Lobe is marked by the first occurrence of massive magnetitite (van der Merwe, 1976). The Upper Zone is transgressive and overlies Main Zone for most of the strike length of the Northern Lobe, although in the north it is in direct contact with a basement high (Fig. 8.2A). This basement high separates what might be a southern magmatic basin comprising the Platreef, and a northern magmatic basin comprising the Aurora mineralization (Kinnaird *et al*., 2005;

McDonald *et al*., 2017). In the Bellevue drill core (Fig. 8.2A), the Upper Zone comprises 1200 m of predominantly magnetite-rich olivine gabbro and olivine ferrodiorite (Ashwal *et al*., 2005).

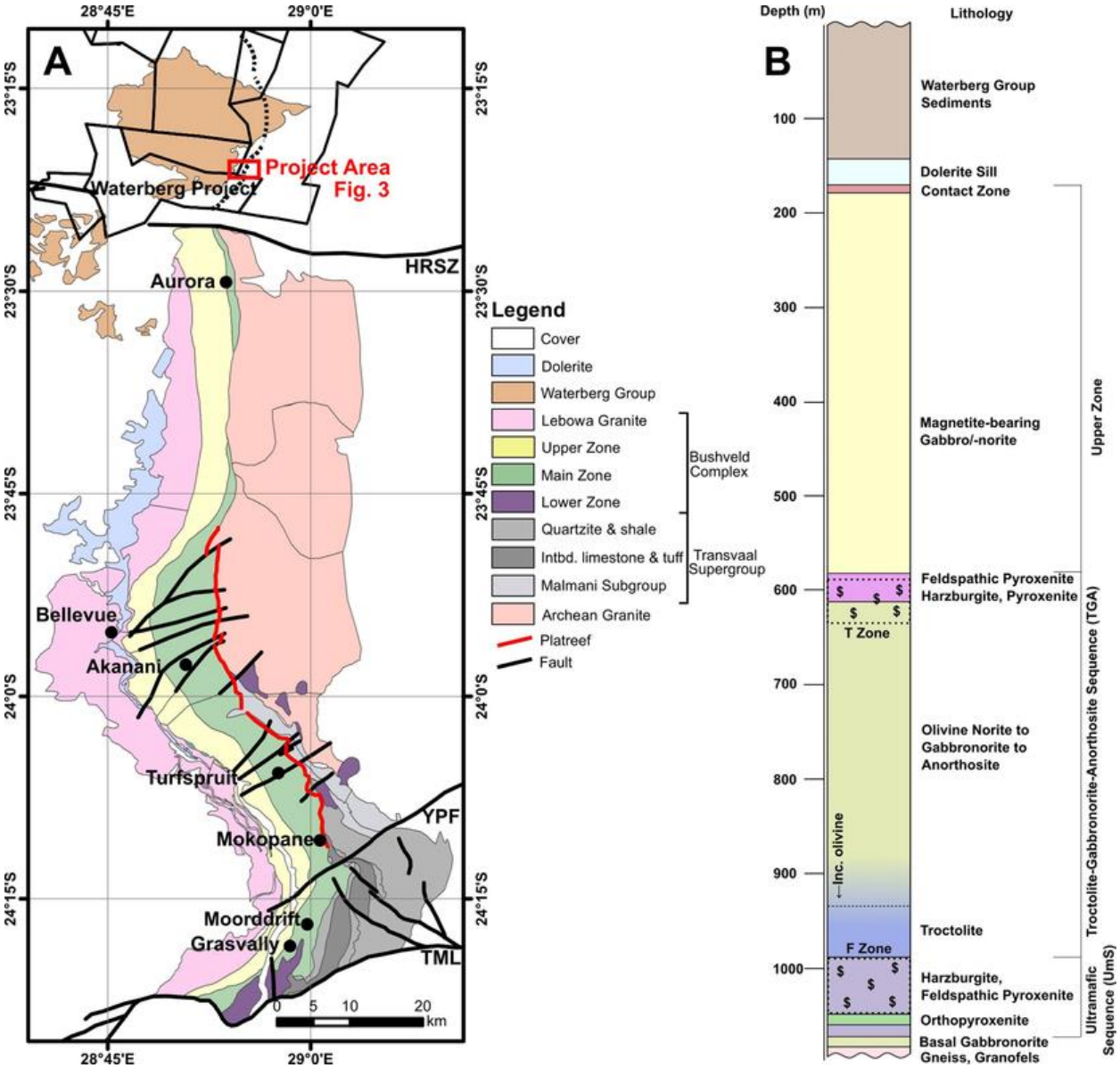

Figure 8.2: A: Geological map of the Northern Lobe of the Bushveld Complex showing the town of Mokopane and selected mining and exploration projects. HRSZ - Hout River Shear Zone; YPF - Ysterberg-Planknek fault; TML - Thabazimbi-Murchison lineament. Red Rectangle highlights the area of interest. B: Simplified stratigraphic column for the Waterberg succession. Both the marginal gabbronorite and the pyroxenite may not be present or occur at varying position and with varying thickness in the Ultramafic Sequence.

Correlations between the Eastern and Western Lobes and the Northern Lobe are complicated by the enigmatic Troctolite Marker, which is a ~110 m thick package of noritic troctolite located 1100 m above the base of the Main Zone along 35 km strike length in the central south of the Northern Lobe (van der Merwe, 1976). Very little olivine occurs in the Main Zones of the Eastern and Western Lobes (Eales and

Cawthorn, 1996). A Cr-rich pyroxenite zone at the top of the Troctolite Marker has been proposed as a new magma input and a potential PGE-rich zone by Tanner *et al*. (2014). The Main Zone of the Northern Lobe has an erosional contact at its base and is interpreted to significantly postdate the emplacement of the Platreef (Holwell *et al*., 2005; Holwell and Jordaan, 2006). On this basis, it was proposed that rather than being involved in the formation of the Platreef-equivalent Critical Zone deposits in the Eastern and Western Lobes, the Main Zone of the Northern Lobe may therefore have retained a PGE budget (Holwell *et al*., 2005; McDonald *et al*., 2017). Whereas most of the economic value of the Northern Lobe is concentrated in the Platreef, sub-economic mineralization has been intersected in rocks interpreted to belong to the Main Zone in the far north at Aurora and south at Moorddrift (Fig. 8.2A; Harmer *et al*., 2004; Manyeruke, 2007; Maier *et al*., 2008; Maier and Barnes, 2010; McDonald and Harmer, 2010; Holwell *et al*., 2013; McDonald *et al*., 2017).

The Platreef is one of the world's largest and most valuable mafic to ultramafic successions comprising platinum-group elements and associated significant Ni and Cu reserves (Naldrett, 2010). It differs from the UG2 and Merensky Reef deposits of the main Bushveld Complex. The Platreef carries Ni-Cu-PGE mineralization of three different types: massive sulfide bodies at the base, marginal or contact disseminated ore in hybrid rocks and exoskarns, and reef style mineralization hosted by feldspathic pyroxenite and harzburgite at the top, near the boundary with the Main Zone. It has lower average Pt/Pd ratios of approximately 1, and a lower grade of >4 g/t PGE, where mined (Kinnaird *et al*., 2005). These characteristics, however, depend on the type of mineralization investigated, and in detail the interpreted Merensky analogue has high Pt/Pd ratios. PGE and base metal sulfides are generally associated, however, in detail they may be decoupled, possibly due to hydrothermal alteration and local remobilization (Kinnaird *et al*., 2005; Holwell and McDonald, 2006). A recent age date for the Platreef of 2056±5Ma (Yudovskaya *et al*., 2013a) overlaps within error with precise 2056.88±0.41Ma and 2057.04±0.55Ma ages for the Merensky Reef (Scoates and Wall, 2015) and indicates that both deposits formed broadly contemporaneously. These ages are also in agreement with high-precision U-Pb dating that indicates crystallization of the Bushveld Complex over 1Ma (Zeh *et al*., 2015).

Mineralization south of Mokopane at Moorddrift (Maier and Barnes, 2010), the Aurora Project (Harmer *et al*., 2004; Manyeruke, 2007; Maier *et al*., 2008; McDonald and Harmer, 2010; McDonald *et al*., 2017) and the Waterberg Project (Kinnaird *et al*., 2014, 2017; Huthmann *et al*., 2016) is explicitly excluded from the Platreef (Kinnaird *et al*., 2005; McDonald and Holwell, 2011). The Aurora Project is interpreted to be an upper Main Zone-hosted Cu-Ni-PGE deposit (McDonald *et al*., 2017) located to the south of the Waterberg Project at the very northern end of the Northern Lobe (Fig. 8.2A). At Aurora, the

Main Zone reappears at surface and is in direct contact with Archean granite. Mineralization occurs in two main mineralized horizons and a thinner discontinuous horizon closer to the basal contact.

The Hout River Shear Zone (Fig. 8.2A) marks the boundary between the granulite- facies Southern Marginal Zone (SMZ) of the Limpopo Complex and the Archean Kaapvaal Craton. It is generally interpreted to represent a composite structure along which the Southern Marginal Zone was thrust southward during the Neoarchean (Smit *et al*., 1992; Barton *et al*., 2006). According to recent work by Nicoli *et al*. (2015), the SMZ consists of reworked Kaapvaal Craton basement gneisses, mafics, and clastic sedimentary rocks with ages between 3.3 and 2.7 Ga which are overlain by younger sedimentary rocks. There is still little consensus regarding some elements of the geodynamic history of the Limpopo orogeny (e.g. Treloar *et al*., 1992; Holzer *et al*., 1998; Barton *et al*., 2006; Nicoli *et al*., 2015), however, a N-S directed, long-lived tectonothermal activity of >700 Ma is well established (Kramers and Mouri, 2011). Several studies (Schaller *et al*., 1999; Barton *et al*., 2006; Clarke *et al*., 2009; Smirnov *et al*., 2013; Rajesh *et al*., 2014) proposed a Paleoproterozoic (and not Archean) collision of the Zimbabwe and Kaapvaal craton that may account for certain geological features observed in the project area (described below). Regardless of the timing of the Limpopo Belt orogeny, the location of the Waterberg Succession in the SMZ (not the Kaapvaal Craton) may expose it to a level of Paleoproterozoic tectonism that is not generally observed in the undeformed Bushveld Complex.

8.4.2. Local geology

In the area immediately north of the Hout River Shear Zone (Fig. 8.2A) Platinum Group Metals (PTM) has intersected a mafic to ultramafic succession subdivided into an Ultramafic Sequence (UmS) overlain by the Troctolite Gabbronorite Anorthosite Sequence (TGA) and an Upper Zone (UZ) of magnetite-bearing gabbroic rocks to ferrogabbros. The rocks rest on a footwall of Archean gneisses that is commonly interfingered with pyroxenite near the contact (Fig. 8.2B). Except for one drill hole in the very south of the prospect, calc-silicate xenoliths are absent in the Waterberg area. Early pyroxenitic magmas intruding the floor rocks caused melting and subsequent mingling of the pyroxenitic magma and granitic melt, leading to the formation of a granofels. The igneous package of rocks dips ~30° toward the west-northwest, with variations because of structural controls and/or thermo-mechanical erosion. Significant faults are indicated by variations in intersection depth of the sedimentary-igneous rock contact, however, due to vertical drilling these potential steeply-dipping structures are not typically intersected.

Recent geophysical modelling suggests a continuation of the mafic succession to the north and west of the drill intersections and a greatly increasing thickness towards the southwest (Finn *et al*., 2015). The subdivision of the stratigraphy has changed since the early years of exploration and the

ongoing work by company geologists and academics involved with this project has questioned some relationships (e.g. in Huthmann *et al*., 2016) and prompted a new subdivision to reflect interpreted petrogenetic relationships (Kinnaird *et al*., 2017).

The base of the succession sometimes comprises very fine- to fine-grained orthopyroxenites and/or gabbronorites. Orthopyroxenites occur as cm- to meter-sized fragments to sill-like bodies that have sharp to gradational contacts with their respective host rocks, and in places are almost completely assimilated by subsequent ultramafic rocks (see below). Gabbronorites generally appear less affected by their host and their relative age is uncertain. The pyroxenites are interpreted to be the crystallization product of initial magmas intruding the area, and based on drill intersects outside of the study area may intrude >100 m into the footwall granite-gneisses. Due to very limited drilling into the deep basement, their distribution is not certain. Based on the observed degree of assimilation and their distribution, they may also represent autoliths. The gabbronorites, on the other hand, are plagioclase-dominated rocks of varying grain-size (finer-grained towards the footwall) that resemble the gabbroic rocks observed higher up in the succession.

Harzburgite and feldspathic pyroxenite of the UmS are the primary basal unit of the succession. The UmS is discontinuous and where present it may exceed 80 m in thickness, hosts PGE and Au mineralization, and unevenly distributed chromite clusters and seams. Olivine-bearing units in the UmS are very strongly altered with relicts of primary minerals remaining, having been replaced primarily by serpentine and magnetite. The unit is very heterogeneous and comprises small amounts of juxtaposed pyroxenite, serpentinite, troctolite and dunite. Calc-silicate xenoliths are absent.

Overlying the UmS, the TGA Sequence is primarily composed of gabbronoritic rocks with minor anorthosite, grading into norite, olivine norite and troctolite at the base (Fig. 8.2B). The rocks appear to grade into the UZ at the top of the succession. Due to the fine-grained nature of the magnetite and similarity of rock types, no clear contacts can be observed. The enigmatic troctolite has a gradational, mingled or irregular contact with olivine gabbronorite upwards and a sharp, erosional (?) contact with harzburgite at the base (Fig. 8.3B). Further south, the top of the TGA Sequence is host to the T Zones, a set of 2–3 discontinuous, mineralized gabbronorite, pyroxenite to troctolite, horizons. In the area of focus for this study, the T Zones are either absent or extremely poorly developed, possibly related to non-deposition, structural controls, or erosion preceding the deposition of Waterberg Group sediments.

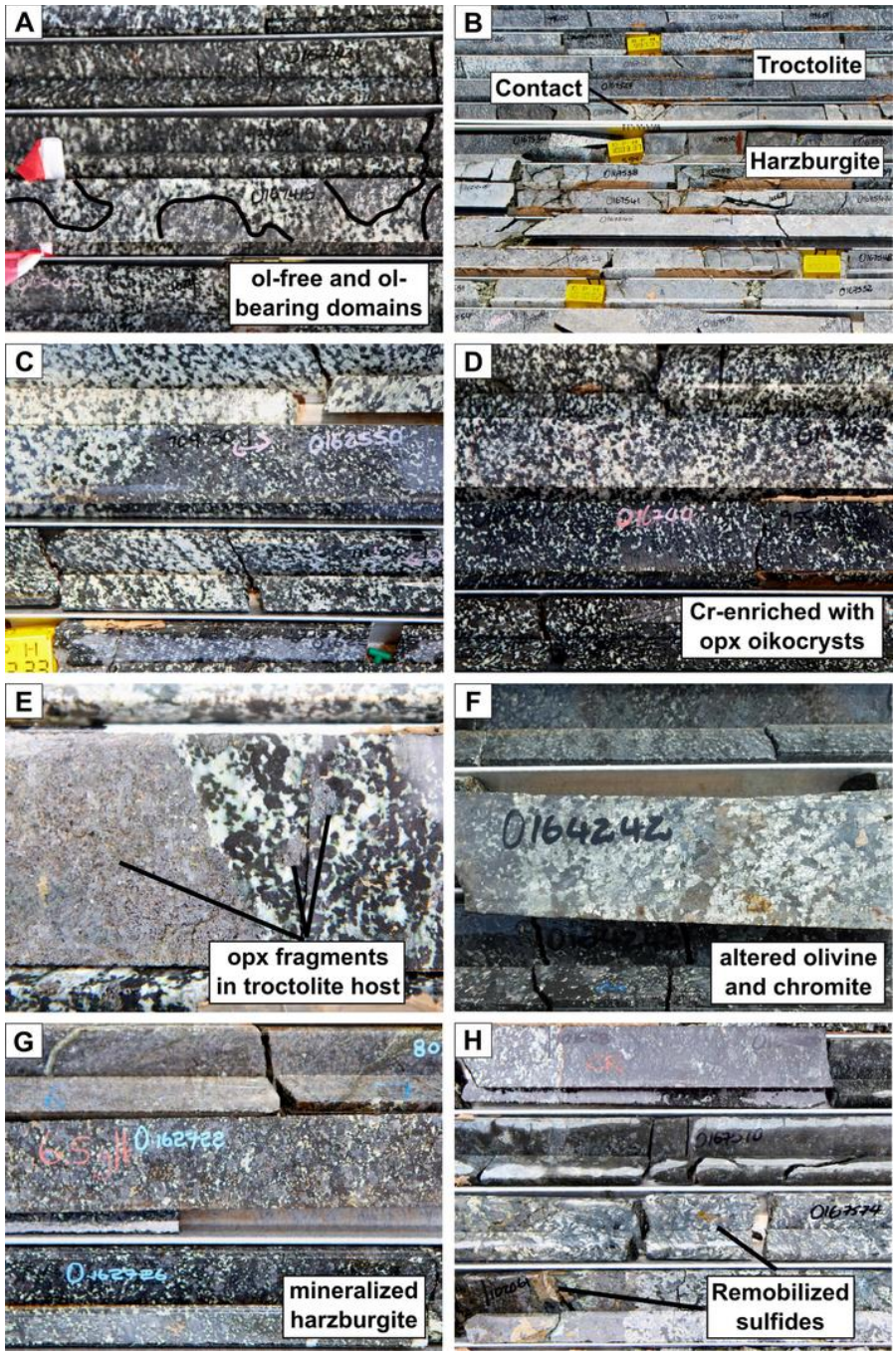

Figure 8.3: Textural relationships in examples of rock types from drill core in the Waterberg Project. A: Upper contact of the TGA Sequence troctolite showing discrete zones of gabbroic and troctolitic rocks interpreted to represent mingling of cumulates; B: Typical Ultramafic Sequence. In the top tray the sharp contact between overlying troctolite and harzburgite is visible; C: Variations in the troctolite zone showing leucotroctolite and zones of abundant orthopyroxene oikocrysts; D: Variations in olivine abundance in the troctolite zone. The oikocryst-rich melatroctolite is characterized by significant spikes in Cr content; E: Orthopyroxenite autolith in troctolite. Note the small pyroxenite fragments in the troctolite and the presence of possibly remobilized sulfides in both rocks; F: Chromite in TGA Sequence troctolite adjacent to an alteration halo and remobilized sulfides; G: Mildly altered mineralized zone with 6.5 g/t Pt+Pd+Au; H: Vari-textured zone of Cr-enriched serpentinite and sulfide remobilization.

The upper part of the succession on the Waterberg Prospect is composed of magnetite-bearing gabbronorite and gabbro that have varying ortho- and clinopyroxene content. It is tentatively correlated with the Upper Zone elsewhere in the Complex, even though it lacks the magnetitite layers that are characteristic for the Upper Zone else-where in the Bushveld Complex (e.g. Molyneux, 1974; Ashwal *et al*., 2005). Instead, magnetite in the Upper Zone at the Waterberg Project occurs as very fine-grained disseminations that in the field are most easily identified by the use of a magnetic susceptibility meter. The UZ thins in places and its exact distribution requires further research.

The top contact of the succession is a remarkable erosional unconformity overlain by Paleoproterozoic Waterberg Group sediments (Callaghan *et al*., 1991; Huthmann *et al*., 2016), typically starting with a coarse, poorly-sorted and polymict breccia. The top of the succession is complex and sometimes an up to 10 m wide and strongly altered, sheared, and tuffaceous contact zone is located between the sediments and igneous units. Detrital zircons of the basal breccia have recently been dated and encompass age clusters of 2045 to 3354 Ma, generally attributed to the Limpopo Belt (Corcoran *et al*., 2013; Huthmann *et al*., 2016).

Recently acquired age dates (2059±3 and 2053±5 Ma; Huthmann *et al*., 2016) from zircons extracted from mafic rocks of the succession are within error coeval with published ages for the Eastern and Western Lobe of the Bushveld Complex (Walraven and Hattingh, 1993; Walraven, 1997; Buick *et al*., 2001; Scoates and Friedman, 2008; Scoates and Wall, 2015; Zeh *et al*., 2015), and the Northern Lobe (Yudovskaya *et al*., 2013a). This indicates that the intrusions belong to the Bushveld Large Igneous Province and are therefore related.

Mineralization occurs in the T and F zones, located just below the Upper Zone and in the Ultramafic Sequence, respectively (Fig. 8.2B). The mineralized zones are 3 to >60 m thick and have so far been intersected along 17 km of strike (Kinnaird *et al*., 2014). T and F Zone refers to zones of elevated PGE grades which in detail are not strictly stratabound (Fig. 8.2B). The T Zone, in particular, occurs in two distinct stratigraphic levels with distinct mineralogy (Kinnaird *et al*., 2017). New mineral assemblages are still being discovered and will be the subject of upcoming publications. The mineralized F Zone closely follows the westerly trend of the harzburgite and may form Super F Zones with grades that can exceed 15 g/t 3E (Pt+Pd+Au) in individual assayed intervals (Kinnaird *et al*., 2017). These zones of high grade are separated by weakly to unmineralized troctolite of the TGA Sequence.

8.5. Methodology

For this study drill core from nine holes intersecting the center and periphery of one of the Super F (mineralized) Zones (Fig. 8.4) have been logged. The selected drill holes allow for an assessment of any

correlation of rock types, distribution of the mineralization and ultimately the generation of an emplacement model. This particular Super F Zone forms an elongated, SW-plunging mineralization envelope of >200 by >1000 m with anomalous PGE and Au of greater than 0.5 g/t over >120 m in core and economic grade of over 2.5 g/t over >60 m. Platinum Group Metal's assay database for the study area, consisting of approximately 9500 assays of Pt, Pd, Ni, Cr, Cu, Co, and S, was made available. Fire assay was used for Pt, Pd, Rh, and Au, and Cu, Ni, and S were determined by XRF analysis at Set Point Laboratory in Johannesburg.

Fifty-eight samples of approximately 25 cm long, NQ size quartered core were selected from the logged drill holes. Care was taken to avoid zones of veining, strong alteration and autoliths/xenoliths. Sample preparation was conducted at the University of the Witwatersrand following established methods (Wilson, 2012).

All samples were analyzed for major and trace elements and loss on ignition (LOI) at the University of the Witwatersrand analytical facilities. Major and selected trace elements were determined using a Panalytical PW2404 X-ray fluorescence (XRF) spectrometer with fused disks and the SuperQ program. Sulfur was determined for selected samples from pressed pellets employing the same instrument and the ProTrace program. All other trace elements were determined by inductively coupled plasma mass spectrometry (ICP-MS) employing a Perkin Elmer Elan instrument. All analytical procedures followed the methods described by Wilson (2012).

Platinum group elements and Au were determined for selected samples at Cardiff University from 15 g sample weight powders prepared at the University of the Witwatersrand. The analysis was carried out by Ni-sulfide fire assay followed by Te co-precipitation and ICP-MS (McDonald and Viljoen, 2006). Accuracy for all whole-rock geochemistry was constrained by the analysis of certified international reference materials and internal standards while the precision for fire assays was estimated by repeat analysis of several samples.

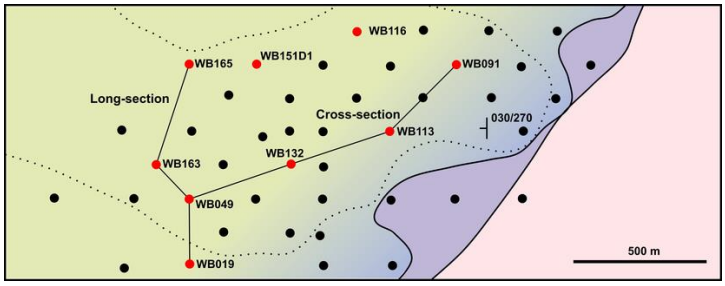

Figure 8.4: Subcrop map of the area shown in Fig. 2. Shown are the positions of the drill holes investigated in detail (red) and the cross- and long-section from Figs. 13 and 14. The stippled line marks the approximate outline of a 1 g/t 3E grade shell projected to surface. It has a 30° dip to the west. The sedimentary rocks overlying the succession are approximately 240 m thick in the east, and their thickness increases slightly to the west.

8.6. Results

8.6.1. Field relationships and petrography

Given the very heterogeneous and irregular nature of lithologies observed in drill core, we discuss suites of intrusives and zones of mineralization rather than individual lithologies (cf. McDonald and Holwell, 2011). It has to be emphasized, that although individual rock types are important, the amount of variation in mineralogy, alteration, chemistry, and mineralization makes lithological correlation between 200m-spaced drill holes difficult. The variation in mineralogy observed in the core may be related to mingling and mixing of crystal-rich liquids. The term mixing is used in situations where two or more magmas produce hybrid rocks with the identities of the parent magmas obscured, whereas mingling represents interactions in which the original magmas or cumulates retain their identity (Fig. 8.4; Wiebe, 1980).

In accordance with informal tradition amongst Bushveld Complex geologists, rock types are named based on their cumulus mineralogy, hence a rock consisting of cumulus olivine and plagioclase with significant intercumulus orthopyroxene is called a troctolite rather than an olivine norite. The term reef is avoided in favor of mineralized zone, as reef implies a lateral continuity that may not be present in the project area. Additionally, the mineralization may to a limited degree transgress boundaries between rock types.

The following section provides drill core and petrological observations for the four main lithologies of the study area, namely the marginal orthopyroxenite and gabbronorite, as well as the Ultramafic Sequence (UmS), and Troctolite-Gabbronorite- Anorthosite Sequence (TGA).

8.6.1. A. Marginal orthopyroxenite

The lowest sills of orthopyroxenite to gabbronorite and gabbro are defined here as marginal sills because of their position close to the contact with, or within the footwall. These types of sills in contact with, or within the sedimentary floor rocks were assigned to the Marginal Zone elsewhere in the Bushveld Complex (Vermaak, 1976), although recent studies show their common presence also within the overlying RLS units (Wilson, 2015).

Orthopyroxenite occurs as sill-like bodies and as autoliths throughout the Ultramafic Sequence and more rarely in the troctolite of the TGA Sequence. Outside the area investigated as part of this study, orthopyroxenites may intrude deep into the footwall, however, due to limited drilling into the basement, their detailed distribution is not well established. The autoliths are several centimeters to <6 m in size. Their contacts are generally well-recognizable, but particularly in harzburgite may be obscured

by alteration. The rocks consist of medium to very fine-grained orthopyroxene and may contain up to 15% olivine. Clinopyroxene and plagioclase are minor interstitial phases. Both orthopyroxene and olivine may host disseminated crystals of chromite which range in size from <50 µm to <10 µm. The smallest of those crystals may form trails in the host silicate.

The orthopyroxenites are barren, or, where their texture suggests sulfide remobilization into the rock, contain trace 3E (Pt+Pd+Au) levels. Inspection of the drill cores indicates, that intervals of orthopyroxenite often have highly anomalous Cr values (Figs. 8.13 and 8.14, see below). Core logging also indicates, that incorporation of these pyroxenites by younger olivine-bearing rocks may lead to zones of increased orthopyroxene oikocrysts or xenocrysts with chromitite clusters.

Near the granite-gneiss footwall contact, varying amounts of interaction between magmas can be observed and the drill core shows features ranging from discrete felsic and pyroxenitic patches to almost complete homogenization. Although the amount of pyroxenite preserved in the core is often limited to patches of cm-size, a generally decreasing crystal size up hole can be observed. The respective thin sections have small crystal size, triple-junction assemblages of orthopyroxene, and occurrences of quartz-feldspar granophyric intergrowths. Fragments of orthopyroxenite with fine- grained granoblastic texture can be found in ultramafic assemblages, indicating their assimilation by later melt in fluxes. Together, these observations indicate that the pyroxenite was the first unit to intrude the study area.

8.6.1. B. Marginal gabbronorite

The marginal gabbronorite is a very fine- to medium-grained rock, dark in color and when fine-grained resembles pyroxenites in hand specimen.

Thin sections show that the dark color is due to extensive cloudiness and spotty alteration of plagioclase. The basal rocks exhibit highly variable textures both within a single thin section, as well as between different drill cores. Modal mineralogy is dominated by plagioclase with varying amounts of clino- and orthopyroxene. Pyroxene may occur interstitially, as small cumulus crystals, or as large oikocrysts. Plagioclase is often altered by very fine-grained mineral aggregates. Overall, in thin section these rocks resemble gabbroic rocks higher up in the stratigraphy.

8.6.1. C. The ultramafic sequence

The mineralized Ultramafic Sequence (UmS) is a highly complex array of a variety of rock types that includes strongly to very strongly altered harzburgite, serpentinite, and feldspathic pyroxenite with very coarse-grained to pegmatitic crystal size. It varies in thickness between 60 and >80 m and generally comprises autoliths of orthopyroxenite which may or may not be altered and which do not contain primary sulfides. Alteration and remobilization appear to have at least some control over the high-grade

zones and may have affected low-grades zones as well (Fig. 8.3H). Chromite may occur as highly irregularly-distributed seams or clusters of chromite grains that cannot be correlated between the widely-spaced holes.

The UmS is the primary basal unit in the project area and can be recognized by its strong alteration and overall heterogeneous texture. Its texture is in sharp contrast to the overlying troctolite's salt and pepper appearance (Fig. 8.3B). The lower contact of the UmS may be either with the marginal units, with granofels, or, at the outer margins of the mineralized zone with barren, relatively unaltered meso- to melatroctolite (Figs. 8.13 and 8.14). The appearance of the unaltered texture of the troctolite invariably indicates barren zones (Fig. 8.13, WB113D0), however sulfide remobilization may lead to zones of highly irregular grade (Figs. 8.3H, 8.13, WB091D0). Due to this, base metal sulfides can be found highly concentrated and may comprise zones of >10 g/t 3E for individual samples (Fig. 8.3H bottom). This relationship is not consistent, however, and both base and precious metals may occur separately. Where drill cores suggest interactions of different magmas, base metal sulfides (and associated PGE) may be absent (Fig. 8.3H top).

The harzburgites are medium- to coarse-grained rocks consisting of about equal proportions of orthopyroxene and olivine. Plagioclase and clinopyroxene are subordinate interstitial components. Plagioclase may form leucocratic patches of generally finer grain size. Pyroxene and olivine, in particular, are very strongly altered and only the outline of former minerals remains in some cases. The dominant alteration is to serpentine and magnetite, however, chlorite and a range of other alteration minerals occur. Carbonates or carbonate overprint are not observed. Chromite forms rare small grains in amounts of less than 1 vol.%, although it can be found as chromite clusters (Fig. 8.5) or as irregular seams. Sulfide minerals observed as part of the F Zone mineralization include pentlandite, pyrrhotite and chalcopyrite, often associated with significant secondary magnetite due to the strong alteration of the harzburgites. Platinum group minerals in the T Zone are variable (Fig. 8.6). Sperrylite is dominant and subordinate Pt-Pd bismutho-tellurides, Au-Ag alloys, Pd arsenides and Pt-Rh sulphoarsenides can be found.

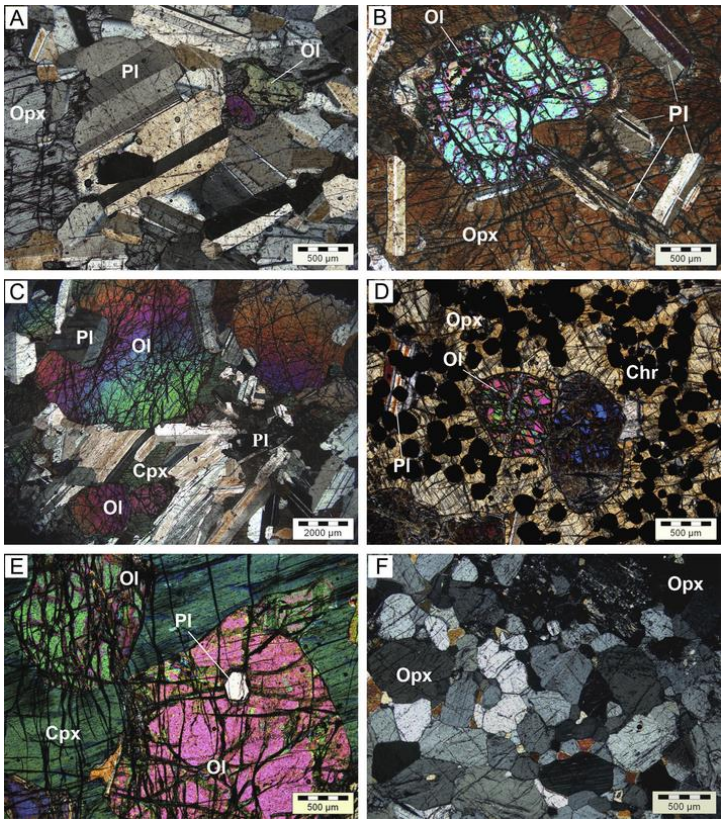

Figure 8.5: Rock textures of the Waterberg body under cross-polarized transmitted light. A: Small olivine crystals rimed by peritectic orthopyroxene in olivine-bearing leuconorite in the uppermost part of the TGA Sequence; B: Corroded olivine and euhedral plagioclase laths in orthopyroxene oikocryst in olivine norite; C: Coarse olivine and plagioclase of smaller size in troctolite; D: chadacrysts of olivine and chromite enclosed by orthopyroxene in poikilitic chromitite of the Ultramafic Sequence; E: Coarse grains of olivine with plagioclase inclusions among interstitial clinopyroxene in lherzolite of the Ultramafic Sequence; F: Recrystallized orthopyroxenite with triple junction texture of orthopyroxene grains.

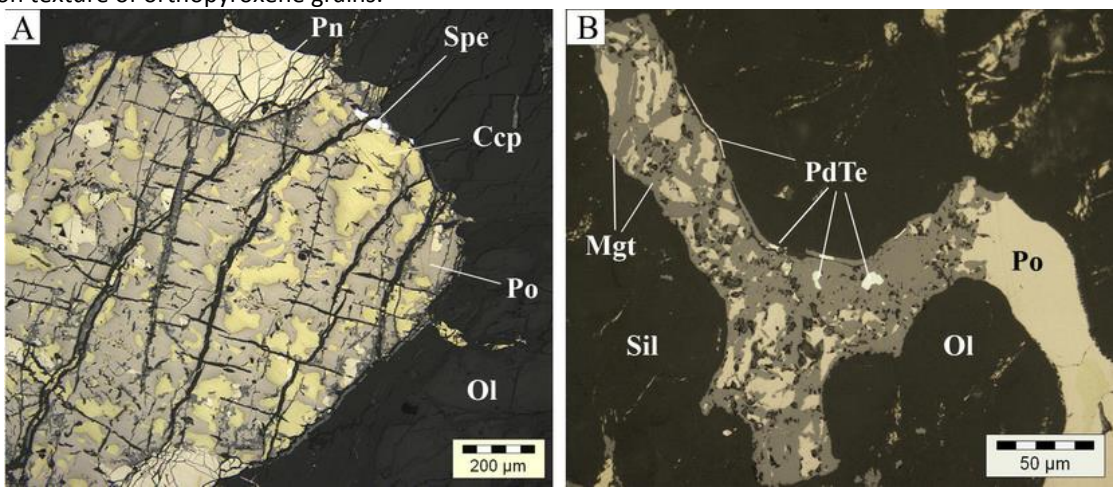

Figure 8.6: Sulfide assemblages of the F Zone under reflected light. A: Primary magmatic sulfide bleb composed of pentlandite (Pn), pyrrhotite (Po) and chalcopyrite (Ccp) in harzburgite. Sperrylite (Spe) occurs at the margin on contact with olivine (Ol); B: Interstitial pyrrhotite partly replaced by secondary magnetite (Mgt) in harzburgite. Kotulskite (PdTe) is located inside magnetite and remobilized along the contact between sulfides and silicates (Sil). Olivine is completely replaced by serpentine.

8.6.1. D. The Troctolite-Gabbronorite-Anorthosite Sequence

The troctolites in the lower part of the Troctolite-Gabbronorite-Anorthosite (TGA) Sequence form an unmineralized, 50 to 110 m thick package ranging in composition from leucotroctolite and olivine norite to melatroctolite, with rare plagiodunite towards the base. The troctolites have a cross-cutting and erosional relationship with underlying harzburgites of the UmS (Fig. 8.3B). Towards the lower contact, the troctolite typically gradually increases in olivine content, and its appearance is more homogeneous. Most of the sequence contains between 50 and 80% olivine, giving it a distinct salt and pepper appearance. Sharp breaks in composition may occur, leading to the juxtaposition of rocks of varying olivine content (Fig. 8.3C). Where developed, the more anorthite-rich phases appear to crosscut and postdate the olivine-rich zones. The sequence is coarse-grained with rare pegmatitic patches, typically with increased anorthite content. Most of the sequence contains up to 10% orthopyroxene in the form of up to several centimeter-sized oikocrysts. This may increase in the lower half of the sequence to >40%, usually at the expense of plagioclase. The upper 10–50% of the sequence may be very heterogeneous in composition, and discrete domains of troctolitic and gabbronoritic composition can be distinguished (Fig. 8.3A). This is interpreted to indicate the interaction of the respective differentiating crystal-rich liquids.

As with the harzburgite of the UmS, the troctolite is host to a number of pyroxenitic autoliths, ranging in size from a few centimeters to several meters. The autoliths are typically medium- to coarse-grained, dominated by orthopyroxene and with sharp, cuspate contacts. They may display a pronounced enrichment in Cr independent of their visible mineralogy (Fig. 8.3E). Where visible chromite crystals are absent, chromite can be found as inclusions in silicate phases. The intrusion and emplacement of hot, olivine-phyric silicate liquids into earlier orthopyroxenites is thought to have led to the thermo-mechanical erosion, transport, and incorporation of orthopyroxenite into younger melt fluxes, thereby leading to anomalous Cr contents.

In thin section, the troctolites are characterized by cumulate textured olivine and plagioclase and strong alteration of both minerals. Depending on the sampling location, the sample may contain significant amounts of oikocrystic orthopyroxene and very limited plagioclase (Fig. 8.5). All major mineral phases may host <50 µm crystals of chromite, often rimmed by magnetite.

Gabbronorites make up the largest part of the TGA Sequence. They form a unit of 100 to 300 m thickness, consisting of varying amounts of orthopyroxene, plagioclase, and clinopyroxene. Variations in pyroxene content may bring this unit close to a norite composition, while varying amounts of olivine may occur at the base where the rocks grade into troctolite. This transition usually involves an increase

in olivine content, with what appears to be a mingling of gabbroic and troctolitic material, often forming discrete areas in core. The unit is generally medium-grained, however, rare pegmatoidal patches of gabbroic composition occur. In the southern half of the area held by Platinum Group Metals (Fig. 8.2A), the upper TGA Sequence hosts a sometimes pegmatoidal, mineralized zone of anorthositic, pyroxenitic, noritic or troctolitic composition (the T Zone). In the study area, these rocks are absent or poorly developed, with PGE and Au only weakly elevated (Fig. 8.14, WB165D0). The controls on the deposition or emplacement of the mineralization are currently unresolved, and either non-deposition/emplacement or later erosion appear plausible.

In thin section, the gabbronorites are typical gabbroic cumulate rocks consisting of coarse plagioclase and varying amounts of clino- and orthopyroxene. The latter two may occur as oikocrysts. Upwards through the stratigraphy the amount of clinopyroxene is generally increasing and sporadic inverted pigeonite may be observed. Alteration throughout the whole sequence is minor.

In other parts of PTM's prospects, the TGA Sequence is overlain by magnetite-bearing gabbros and gabbronorites of the Upper Zone. In the study area, however, these rocks are poorly developed to absent. Due to the fine-grained, disseminated nature of the magnetite in the Upper Zone, the contact can be hard to identify in core and a sharp rise in magnetic susceptibility due to the appearance of magnetite is taken as the contact.

8.6.2. Geochemistry

8.6.2. A. Major and trace element variation diagrams

Data are displayed as bivariate plots with MgO as the differentiation index in Figs. 8.7 and 8.8. Variations in major element composition for the rocks analyzed reflect the proportion of olivine, pyroxene, and plagioclase present and clearly differentiate between the olivine + orthopyroxene-dominated Ultramafic Sequence and the plagioclase + clinopyroxene±olivine±orthopyroxene assemblages of the TGA Sequence and Upper Zone (Fig. 8.7; Table 8.1).

SiO_2 values range from 40 to 61 wt. % and decrease towards higher MgO. Three groups of samples can be distinguished: i) harzburgite and 2 feldspathic pyroxenite samples of the UmS form a high-Mg cluster of samples; ii) Marginal orthopyroxenites form a separate trend from other samples; iii) rocks of the TGA sequence and UZ, dominated by gabbronorite and troctolite, form a trend extending from high- to low-Mg rocks. The wide range of MgO and other major elements for some of the troctolites reflects their cumulus assemblage ranging from <90% olivine to leucotroctolite (Fig. 8.7).

The orthopyroxenites follow a trend of higher SiO_2 for a given MgO than the harzburgites. This elevated SiO_2 reflects the higher SiO_2 in orthopyroxene. Al_2O_3 follows a sharp, decreasing trend with

values between 4 and 27 wt. %. Fe_2O_3 (as total Fe) decreases with decreasing MgO for most samples, even though there are Mg-rich, orthopyroxenite outliers. Trend lines drawn for the troctolites and harzburgites show that the rock types follow slightly different trends (Fig. 8.7). Low Fe_2O_3 values correspond to the paucity of magnetite in the study area. CaO and Na_2O increase with decreasing MgO, reflecting the plagioclase and pyroxene assemblages of the Upper Zone and TGA Sequence. K_2O is generally low with values between 0.1 and 0.2 wt. %. P_2O_5 is less than 0.1 wt. % reflecting the absence of apatite even in the Upper Zone. TiO_2 values are low, corresponding to limited development of the Upper Zone.

Vanadium strongly fractionates into magnetite and hence values are higher for Upper Zone samples. NiO is enriched in troctolites, olivine-bearing pyroxenites and due to the presence of sulfides strongly anomalous in mineralized rocks. Chromium is strongly enriched in pyroxenites and troctolites that contain small chromite clusters. P_2O_5, Sr and Zr levels are low in general, with outliers for the marginal gabbronorite (Fig. 8.8).

8.6.2. B. Multi-element normalized plots

All samples analyzed show almost identical trends on primitive mantle normalized multi-element plots (Sun and McDonough, 1989). They display negative Th, Nb, Ta and sometimes mildly negative Rb and Ti anomalies while in most cases displaying strong positive Sr and Eu anomalies (Fig. 8.9). Gabbroic rocks display Rb<Ba, while the opposite is true for the harzburgites and marginal pyroxenites. Mean Rb/Ba_N for the troctolites is 1.

For most groups of samples MREE and HREE are depleted relative to primitive mantle values. Eu/Eu^* ranges from 1.1 to 2.1, HREE are generally not fractionated with mean Tb/Yb_N of close to 1. The marginal pyroxenite displays significant variation in and has a mean Tb/Yb_N of 1.6 (Fig. 8.10). LREE are enriched (Mean Ce/Sm_N=2) with mean Ce/Sm_N for the TGA Sequence and marginal gabbronorite at 2.7 and 2.2, respectively. Th is enriched relative to Sm, in particular in the troctolite and marginal pyroxenite (Mean Th/Sm_N=4.2 and 3.4, respectively). Although low Eu abundances are expected for the plagioclase-poor pyroxenite, there is some decoupling of plagioclase mode and Eu anomalies.

Samples of UZ, TGA Sequence gabbronorite and troctolite display a tight grouping of results with patterns that are almost identical. The marginal pyroxenite, mineralized harzburgite, and marginal gabbronorite display more within-group variation while still following the overall pattern. Maximum within-group variation is observed in the marginal rocks. Their proximity to the granitic footwall may account for some or all of the variation observed, however, some enrichment may also be attributed to trapped liquid (estimated following Maier and Barnes, 1999; McDonald *et al*., 2009). Regardless of

within-sample variation, a small but systematic increase of REE contents can be observed from the troctolite at the base of the succession to the gabbroic units at the top.

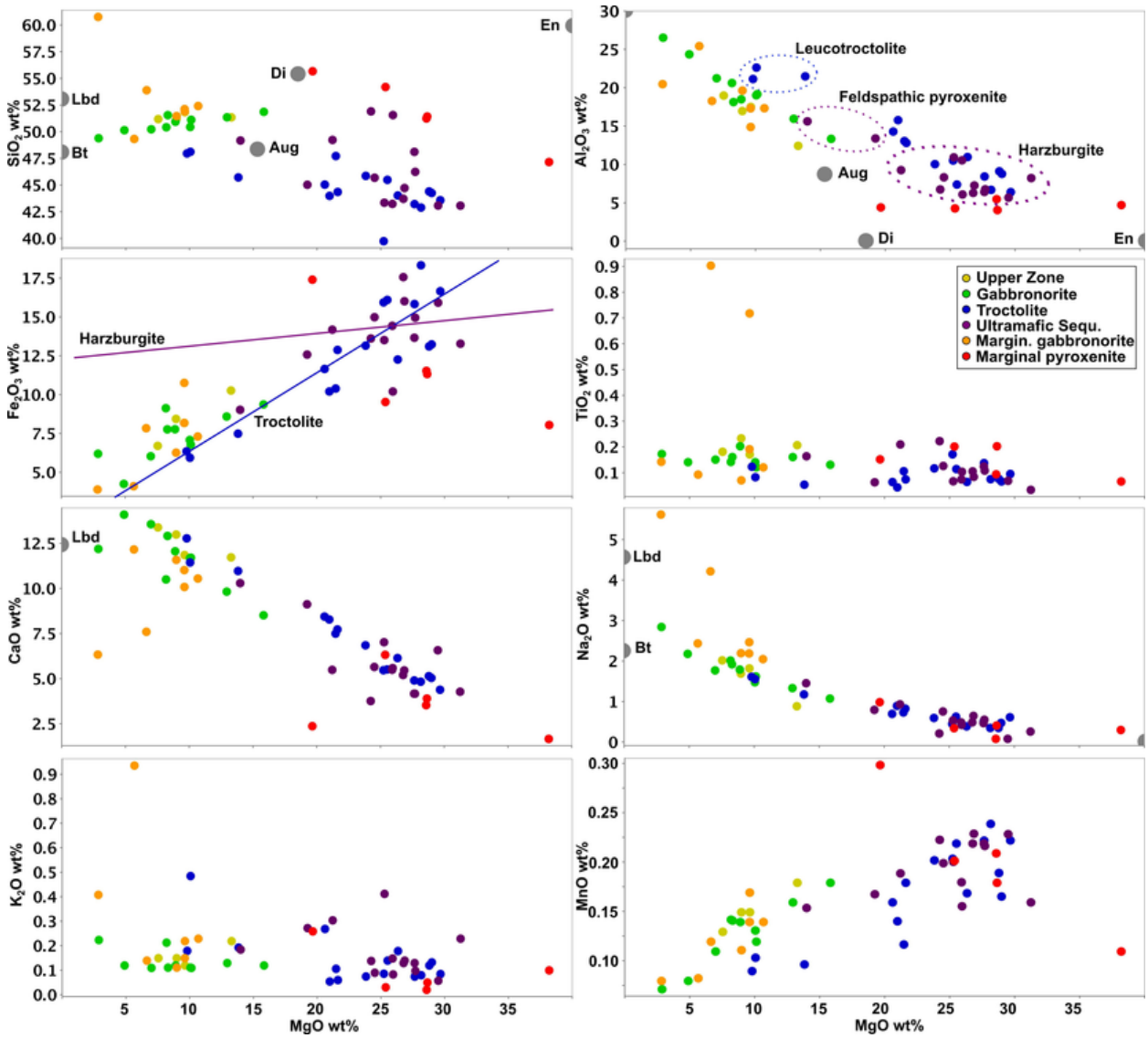

Figure 8.7: Binary variation diagrams of MgO vs major elements. Except for two samples of feldspathic pyroxenite, the UmS group of samples comprises only harzburgite. The lines in the SiO_2 vs. Fe_2O_3 plot demonstrate the different trends of troctolite and harzburgite (see text). Lbd Labradorite; Bt Bytownite; Aug Augite; Di Diopside; En Enstatite.

8.6.2. C. PGE and Au

For this study 28 samples from a range of lithologies were selected for fire assay and the results, normalized to chondrite values (Lodders, 2003), are plotted in Fig. 8.11. Results for total PGE range from 12 to 12,300 ppb with 1.1 to 1100 ppb Au.

Table 8.1: Representative geochemical results for rocks analyzed during this study.

Sample I.D	UZ1	UZ2	UZ3	UZ4	MZ1	MZ2	MZ3	MZ4	MZ5	MZ6	MZ7	MZ8	MZ9	MZ10	TR1	TR2	TR3	TR4	TR5
Rock Type	FEFG	FEFG	FEFG	FEFG	GN	GN	GN	GN	GN	GN	GN	GN	T Zone peg N	T Zone PYX	Opx TR	Peg TR	TR	TR	TR
Group	UZ	UZ	UZ	UZ	TGA	TGA	TGA	TGA	TGA	TGA	TGA	TGA	TGA	TGA	TGA	TGA	TGA	TGA	TGA
XRF wt. %																			
SiO_2	51.34	51.22	51.83	51.18	50.44	51.55	51.35	51.11	51.86	50.14	50.23	50.93	50.42	49.39	43.21	47.72	43.58	44.40	44.02
Al_2O_3	12.43	16.96	17.50	18.98	19.02	18.13	15.96	19.16	13.33	24.36	21.24	18.49	20.62	26.53	8.43	13.05	6.39	9.11	10.97
Fe_2O_3	10.26	8.44	8.17	6.70	7.08	7.76	8.59	6.78	9.37	4.25	6.03	7.77	9.13	6.19	15.83	10.39	16.66	13.10	12.26
MnO	0.18	0.15	0.15	0.13	0.13	0.14	0.16	0.01	0.18	0.08	0.11	0.14	0.14	0.07	0.22	0.12	0.22	0.19	0.17
MgO	13.28	8.98	9.63	7.55	10.06	8.30	12.94	10.13	15.83	4.89	7.00	8.90	8.18	2.87	27.65	21.48	29.67	28.79	26.34
CaO	11.72	12.98	11.85	13.38	11.68	12.91	9.82	11.70	8.51	14.09	13.56	12.06	10.50	12.19	4.90	7.49	4.39	5.14	6.14
Na_2O	0.88	1.69	1.82	2.02	1.48	1.92	1.33	1.62	1.07	2.18	1.77	1.79	2.01	2.84	0.51	0.73	0.61	0.35	0.39
K_2O	0.22	0.15	0.12	0.15	0.11	0.11	0.13	0.11	0.12	0.12	0.11	0.12	0.21	0.22	0.07	0.11	0.08	0.12	0.18
TiO_2	0.21	0.23	0.17	0.18	0.14	0.16	0.16	0.12	0.13	0.14	0.15	0.20	0.14	0.17	0.14	0.11	0.10	0.08	0.06
P_2O_5	0.02	0.02	0.02	0.02	0.02	0.02	0.02	0.02	0.02	0.02	0.02	0.02	0.02	0.10	0.02	0.02	0.02	0.02	0.02
Cr_2O_3	0.06	0.03	0.02	0.02	0.11	0.03	0.12	0.10	0.14	0.05	0.06	0.03	0.01	0.00	0.62	0.10	0.04	0.10	0.06
NiO	0.03	0.02	0.02	0.02	0.03	0.02	0.03	0.03	0.04	0.01	0.02	0.02	0.10	0.33	0.18	0.17	0.21	0.18	0.17
LOI	3.23	1.38	0.43	0.66	0.46	0.47	0.35	0.47	0.58	0.55	0.47	1.25	1.13	1.48	5.30	5.56	5.39	7.34	6.60
Total	99.72	100.12	100.57	99.73	99.66	100.37	999.84	100.38	99.75	99.93	99.75	99.78	100.66	100.34	100.34	100.55	100.49	100.40	99.67
S ppm XRF	196	361	NA	172	NA	NA	NA	41	39	95	NA	NA	2731	12786	466	1146	467	269	NA
ICP-MS ppm																			
Li	3.27	2.37	2.06	1.99	2.07	1.35	2.39	3.22	1.03	1.21	2.22	3.19	1.95	2.76	1.45	0.75	3.26	1.56	2.58
P	35.08	66.22	40.14	52.69	61.93	21.22	65.47	39.58	33.92	40.68	60.15	71.17	28.60	400.53	63.48	45.03	59.58	31.79	56.53
Sc	21.02	17.66	14.57	14.90	12.89	16.35	7.35	10.07	11.76	6.84	9.95	9.09	8.87	1.63	11.04	9.65	7.12	6.56	7.62
Ti	1177.14	1567.47	1095.39	1278.42	845.51	811.62	764.64	556.25	605.09	675.87	795.64	1242.24	665.33	804.89	785.45	452.36	402.58	253.98	269.05
V	162.31	163.79	133.68	135.28	93.66	129.91	90.92	87.00	94.35	77.85	109.44	110.57	74.13	37.53	94.56	48.63	41.93	35.40	32.09
Cr	297.94	167.72	59.75	94.37	632.59	612.41	495.62	632.01	646.01	225.39	301.40	129.36	68.15	7.47	3493.35	391.13	166.84	505.57	316.68
Co	60.06	46.99	70.40	55.73	39.81	54.61	57.20	47.39	69.00	24.23	35.94	67.12	65.63	75.55	193.28	114.69	157.70	130.69	135.57
NiO	203.37	162.84	175.56	125.56	183.63	501.27	225.06	238.08	228.36	96.46	120.75	163.50	680.41	1949.27	1136.85	1041.82	1372.40	1070.04	1023.52
Cu	62.70	34.16	69.73	36.97	30.83	48.11	24.37	33.59	26.73	22.48	23.98	33.82	808.71	3251.31	20.63	99.13	34.77	6.64	10.68
Zn	59.34	48.73	62.10	49.23	41.63	50.85	52.07	41.69	55.19	24.64	35.76	64.14	55.68	104.01	109.74	50.65	89.92	64.36	66.08
Ga	7.69	10.77	13.42	15.01	10.02	12.04	9.60	10.93	7.79	13.53	12.30	13.60	11.42	14.23	7.41	7.64	4.00	4.68	5.86
As	0.30	0.36	0.20	0.30	0.31	0.24	0.17	0.21	0.20	0.20	0.21	0.33	0.32	14.23	0.40	0.25	0.18	0.15	0.19
Rb	3.64	1.30	0.93	1.55	1.38	0.66	1.88	0.64	1.78	0.49	0.73	1.30	2.42	0.26	2.70	3.75	1.66	3.63	4.59
Sr	64.07	107.61	99.20	129.34	104.30	121.14	94.87	110.46	79.34	123.46	112.43	105.81	106.22	1.72	56.33	143.97	52.63	67.33	95.63
Y	4.22	4.16	2.97	2.93	2.43	3.22	1.36	1.77	1.56	1.39	2.10	1.85	1.69	85.03	2.03	2.05	1.52	1.24	1.36
Zr	8.28	13.05	10.61	14.04	10.31	5.60	6.09	5.51	4.22	6.02	7.90	12.69	6.71	1.34	12.51	8.82	3.64	4.47	3.87
Nb	0.27	0.64	0.38	0.49	1.14	0.14	0.26	0.19	0.16	0.20	0.20	0.73	0.20	8.49	0.35	0.26	0.15	0.19	0.19
Ba	36.63	32.30	32.55	38.13	26.29	28.24	29.16	28.64	36.80	23.42	23.56	31.40	38.90	0.66	26.24	36.72	26.03	38.80	40.18
Sn	0.24	1.14	0.64	3.34	0.41	0.43	0.27	0.38	0.16	0.25	0.32	0.60	0.33	18.27	0.59	0.26	0.19	0.15	0.22
Cs	0.17	0.07	0.05	0.05	0.07	0.03	0.06	0.07	0.11	0.02	0.03	0.05	0.21	0.54	0.22	0.45	0.26	0.31	0.68
La	1.45	1.82	1.14	1.28	1.19	0.95	1.20	0.87	0.95	0.91	1.28	1.50	0.91	0.15	1.07	1.26	1.01	0.97	1.08
Ce	3.09	4.69	2.39	3.19	2.57	2.71	2.50	2.26	1.85	2.48	2.83	3.05	2.81	1.20	1.64	2.31	1.56	1.57	1.68
Pr	0.39	0.49	0.28	0.30	0.25	0.25	0.22	0.18	0.18	0.20	0.26	0.29	0.20	4.18	0.25	0.27	0.18	0.17	0.19
Nd	1.86	2.26	1.30	1.40	1.12	1.24	0.91	0.81	0.77	0.88	1.15	1.22	0.88	0.33	1.05	1.17	0.81	0.73	0.81
Sm	0.53	0.59	0.37	0.39	0.29	0.37	0.20	0.22	0.19	0.22	0.29	0.28	0.22	1.44	0.25	0.29	0.21	0.18	0.19
Eu	0.22	0.23	0.16	0.17	0.15	0.16	0.14	0.13	0.12	0.14	0.15	0.17	0.15	0.30	0.13	0.14	0.11	0.11	0.11
Gd	0.63	0.68	0.46	0.48	0.34	0.46	0.22	0.26	0.22	0.26	0.34	0.35	0.26	0.09	0.28	0.30	0.23	0.18	0.21
Tb	0.11	0.11	0.08	0.08	0.06	0.08	0.03	0.05	0.04	0.04	0.05	0.05	0.04	0.34	0.05	0.05	0.04	0.03	0.03
Dy	0.79	0.77	0.57	0.54	0.42	0.58	0.25	0.32	0.27	0.27	0.38	0.35	0.30	0.05	0.34	0.35	0.27	0.21	0.23
Ho	0.17	0.16	0.13	0.12	0.09	0.13	0.05	0.07	0.06	0.06	0.08	0.07	0.07	0.29	0.07	0.08	0.06	0.05	0.05
Er	0.49	0.47	0.36	0.34	0.28	0.38	0.15	0.21	0.19	0.16	0.23	0.22	0.20	0.06	0.22	0.22	0.17	0.14	0.15
Tm	0.07	0.07	0.06	0.05	0.04	0.06	0.02	0.03	0.03	0.03	0.03	0.04	0.03	0.15	0.03	0.03	0.03	0.02	0.02
Yb	0.53	0.45	0.37	0.33	0.30	0.39	0.17	0.24	0.22	0.16	0.23	0.22	0.23	0.02	0.23	0.24	0.19	0.16	0.17
Lu	0.08	0.07	0.06	0.05	0.05	0.06	0.03	0.04	0.04	0.03	0.04	0.03	0.04	0.14	0.04	0.04	0.03	0.03	0.03
Hf	0.27	0.39	0.31	0.41	0.26	0.19	0.17	0.16	0.12	0.17	0.21	0.33	0.20	0.02	0.27	0.22	0.10	0.11	0.10
Ta	0.02	0.04	0.03	0.03	0.10	0.01	0.02	0.01	0.01	0.02	0.02	0.05	0.01	0.04	0.03	0.01	0.03	0.03	0.02
W	0.03	0.04	0.03	0.03	0.04	0.06	0.03	0.02	0.02	0.03	0.03	0.04	0.02	0.02	0.08	0.02	0.15	0.09	0.07
Pb	1.60	0.97	2.05	2.41	0.65	0.95	0.58	0.75	0.62	0.70	0.89	2.08	2.83	14.28	2.68	2.76	1.07	1.71	0.67
Th	0.11	0.22	0.13	0.18	0.13	0.07	0.13	0.10	0.11	0.08	0.10	0.16	0.15	0.21	0.16	1.15	0.07	0.08	0.14
U	0.04	0.08	0.08	0.10	0.05	0.03	0.06	0.05	0.04	0.04	0.04	0.11	0.06	0.12	0.07	0.12	0.03	0.06	0.04
PGE ppb																			
Os	0.29	0.13	NA	0.11	NA	NA	NA	0.07	0.21	0.06	NA	NA	29.70	1.59	0.05	0.23	0.24	0.09	NA
Ir	0.52	0.09	NA	0.10	NA	NA	NA	0.17	0.95	0.55	NA	NA	29.20	5.65	0.04	0.35	0.30	0.13	NA
Ru	0.35	0.21	NA	0.23	NA	NA	NA	0.49	1.08	0.39	NA	NA	115.00	11.30	0.20	1.11	0.91	0.53	NA
Rh	3.26	0.54	NA	0.53	NA	NA	NA	0.93	3.70	2.53	NA	NA	85.30	12.30	0.53	1.77	1.87	0.99	NA
Pt	20.50	38.70	NA	54.60	NA	NA	NA	20.80	26.00	10.20	NA	NA	5076	1804	10.70	28.80	9.86	7.00	NA
Pd	11.30	20.20	NA	38.60	NA	NA	NA	40.30	37.40	8.20	NA	NA	6951	2805	4.43	45.60	15.80	4.26	NA
Au	2.55	1.46	NA	2.38	NA	NA	NA	3.83	2.90	1.12	NA	NA	1095	365	2.43	4.33	2.61	1.77	NA

Abbreviations: FEFG = Fero-gabbronorite, GN = Gabbronorite, T Zone peg N = T Zone pegmatoidal norite, T Zone PYX = T Zone pyroxenite, Peg TR = Pegmatoidal troctolite, TR = Troctolite, UZ = Upper Zone, TGA = troctolite-gabbronorite-anorthosite sequence.

Table 8.1: Representative geochemical results for rocks analyzed during this study.

Sample I.D	TR6	TR7	TR8	TR9	TR10	TR11	TR12	HZ1	HZ2	HZ3	HZ4	HZ5	HZ6	HZ7	HZ8	HZ9	HZ10	HZ11	HZ12
Rock Type	TR	TR	TR	TR	TR	TR	TR	DUN/HZ	HZ-serp	HZ-serp	HZ-serp	HZ-serp	HZ-serp	HZ-serp	HZ-serp	HZ-serp	Serp	Serp	HZ
Group	TGA	TGA	TGA	TGA	TGA	TGA	TGA	UmS	UmS	UmS	UmS	UmS	UmS	UmS	UmS	UmS	UmS	UmS	UmS
XRF wt. %																			
SiO_2	42.89	45.04	44.35	39.74	45.86	44.25	45.71	44.72	43.71	46.24	48.11	51.56	49.17	49.23	51.90	43.90	45.03	43.08	45.69
Al_2O_3	6.68	14.29	12.81	10.51	10.03	8.77	21.48	7.26	6.28	6.76	6.41	6.08	15.62	9.26	6.74	10.92	13.39	5.67	8.32
Fe_2O_3	18.33	11.65	12.87	15.94	13.15	13.23	7.48	16.01	17.56	14.95	13.66	10.20	9.02	14.18	13.61	13.51	12.58	15.92	14.00
MnO	0.24	0.16	0.18	0.20	0.20	0.20	0.10	0.23	0.22	0.22	0.22	0.16	0.15	0.19	0.22	0.20	0.17	0.23	0.20
MgO	28.16	20.61	21.62	25.23	23.83	28.99	13.83	26.86	26.77	27.70	27.64	25.95	14.00	21.22	24.24	25.28	19.24	29.50	24.52
CaO	4.83	8.44	7.73	5.47	6.85	5.04	10.97	5.46	5.20	4.16	4.17	5.59	10.29	5.49	3.76	7.02	9.12	6.57	5.65
Na_2O	0.35	0.70	0.83	0.45	0.59	0.47	1.18	0.65	0.49	0.55	0.47	0.42	1.45	0.93	0.21	0.53	0.79	0.08	0.76
K_2O	0.08	0.27	0.06	0.09	0.07	0.12	0.19	0.14	0.13	0.10	0.13	0.08	0.18	0.30	0.14	0.41	0.27	0.06	0.09
TiO_2	0.07	0.06	0.07	0.17	0.12	0.07	0.05	0.08	0.11	0.11	0.12	0.10	0.16	0.21	0.22	0.07	0.06	0.07	0.13
P_2O_5	0.02	0.02	0.02	0.02	0.02	0.02	0.02	0.02	0.02	0.02	0.01	0.02	0.02	0.03	0.02	0.02	0.02	0.01	0.02
Cr_2O_3	0.03	0.09	0.08	2.41	0.52	0.13	0.02	0.06	0.08	0.10	0.32	0.28	0.10	0.09	0.30	0.04	0.07	0.09	0.07
NiO	0.22	0.12	0.14	0.17	0.15	0.19	0.10	0.23	0.62	0.31	0.19	0.39	0.46	0.28	0.14	0.23	0.43	0.32	0.37
LOI	6.46	5.93	5.45	6.47	5.83	9.14	6.47	4.62	4.91	7.51	3.22	3.33	2.26	4.51	5.61	10.13	4.39	12.39	4.80
Total	100.24	100.39	99.59	98.95	100.21	100.27	100.44	100.29	99.61	99.86	100.20	99.93	99.81	100.14	100.27	100.36	100.05	100.16	99.43
S ppm XRF	721	NA	NA	499	NA	NA	NA	NA	11935	2493	1248	6580	9928	8000	525	1044	9442	2036	6805
ICP-MS ppm																			
Li	2.66	2.22	1.84	2.01	1.92	0.91	7.92	3.28	1.38	2.16	1.37	3.88	5.71	4.72	3.79	4.86	2.18	1.96	0.90
P	29.83	24.60	31.13	30.67	13.53	30.21	20.90	26.87	62.32	50.58	32.88	21.54	46.99	83.19	59.74	20.43	15.59	21.40	26.38
Sc	7.93	8.62	10.77	9.44	13.00	7.03	1.70	9.00	9.43	11.46	12.85	15.44	9.35	15.38	19.11	7.53	7.63	9.82	12.24
Ti	252.65	284.68	346.79	437.16	638.26	310.53	262.86	513.37	535.98	557.96	612.95	467.20	733.83	1015.95	1352.20	274.05	245.32	279.65	508.05
V	36.62	41.77	49.20	79.38	82.32	32.86	16.44	53.82	63.97	49.45	70.05	67.29	72.66	74.88	101.64	36.37	44.24	45.69	60.69
Cr	91.64	351.49	462.63	5598.44	2606.25	580.25	50.59	238.54	318.08	370.93	1378.88	1241.13	500.13	416.92	1643.24	280.91	322.41	411.38	348.05
Co	148.71	103.73	117.47	108.67	144.09	173.25	104.44	188.62	191.68	195.57	99.23	110.82	97.48	112.33	102.20	115.95	135.46	103.26	143.36
NiO	1271.49	630.69	862.13	928.64	878.10	1052.88	661.21	1495.61	4062.16	1819.59	930.41	2498.85	2963.47	1839.36	796.96	1282.99	2616.62	1451.10	2112.82
Cu	60.70	45.65	44.66	23.45	39.55	7.11	49.81	184.85	2507.57	453.47	233.49	975.01	2114.10	1169.29	61.51	171.33	1157.92	103.80	791.92
Zn	109.24	61.50	62.54	63.46	95.41	86.37	50.99	115.65	102.36	96.91	61.12	69.04	48.77	75.61	113.88	81.89	61.30	46.68	75.12
Ga	4.02	6.87	6.87	5.53	8.04	5.58	10.08	5.49	3.82	5.77	4.10	4.09	8.22	7.22	7.63	5.20	6.39	2.65	5.75
As	0.17	0.21	0.21	0.16	0.28	0.35	0.32	0.35	0.17	0.32	0.18	0.32	0.36	0.30	1.47	0.69	0.18	1.11	0.19
Rb	2.17	4.32	0.80	2.52	2.50	6.29	4.93	4.41	2.78	4.92	3.64	3.46	3.00	22.50	8.50	12.68	4.68	2.92	1.79
Sr	66.29	93.99	87.83	64.01	64.30	61.58	228.31	57.50	54.94	63.24	46.20	62.86	270.68	101.47	24.73	118.38	142.52	57.72	61.39
Y	1.42	1.35	1.55	1.42	2.15	1.19	0.42	1.13	1.83	1.88	2.01	2.09	2.07	3.83	4.37	1.24	0.81	1.25	2.35
Zr	2.12	2.84	4.47	2.69	6.21	5.38	2.78	3.23	5.42	5.80	4.78	3.85	7.44	19.66	20.51	2.01	1.69	2.99	3.74
Nb	0.08	0.09	0.11	0.17	0.37	0.48	0.11	0.12	0.25	0.25	0.63	0.11	0.31	2.48	0.78	0.06	0.08	0.10	0.11
Ba	26.07	29.81	20.53	17.14	19.52	28.40	70.94	30.68	71.48	41.79	15.78	16.76	42.56	47.46	26.52	73.90	88.55	3.68	27.37
Sn	0.17	0.18	0.21	0.23	0.45	0.25	0.22	0.41	0.81	0.72	0.26	0.44	0.68	0.59	0.55	1.05	0.59	0.43	0.39
Cs	0.31	0.31	0.02	0.26	0.09	0.66	0.27	0.25	0.57	1.17	0.32	0.52	0.20	1.76	0.97	2.01	0.49	0.86	0.28
La	0.67	0.89	0.85	0.76	1.10	0.91	0.68	0.64	1.15	1.59	0.79	0.92	1.60	2.23	5.40	0.73	0.59	0.52	1.10
Ce	1.03	1.49	1.59	1.35	1.85	1.47	1.15	0.91	2.10	2.18	1.27	1.75	3.14	5.06	8.13	1.23	1.04	0.88	1.93
Pr	0.13	0.17	0.19	0.16	0.25	0.19	0.12	0.12	0.25	0.26	0.15	0.20	0.33	0.60	1.03	0.14	0.11	0.11	0.24
Nd	0.59	0.74	0.81	0.70	1.03	0.78	0.47	0.53	1.08	1.09	0.72	0.82	1.39	2.59	3.93	0.58	0.47	0.49	1.05
Sm	0.18	0.19	0.19	0.17	0.26	0.17	0.12	0.15	0.30	0.27	0.20	0.21	0.32	0.63	0.74	0.18	0.16	0.12	0.29
Eu	0.10	0.14	0.14	0.10	0.13	0.09	0.12	0.09	0.13	0.14	0.10	0.09	0.19	0.23	0.14	0.14	0.13	0.06	0.16
Gd	0.21	0.20	0.22	0.20	0.31	0.19	0.11	0.17	0.28	0.30	0.24	0.25	0.34	0.64	0.82	0.18	0.12	0.15	0.33
Tb	0.03	0.04	0.04	0.03	0.05	0.03	0.01	0.03	0.05	0.05	0.04	0.05	0.06	0.10	0.11	0.03	0.02	0.03	0.06
Dy	0.25	0.24	0.26	0.24	0.37	0.20	0.08	0.20	0.33	0.32	0.32	0.32	0.37	0.67	0.74	0.21	0.15	0.20	0.40
Ho	0.06	0.05	0.06	0.05	0.08	0.04	0.02	0.04	0.07	0.07	0.08	0.08	0.08	0.15	0.16	0.05	0.03	0.05	0.09
Er	0.16	0.16	0.17	0.16	0.23	0.13	0.05	0.13	0.19	0.21	0.23	0.23	0.23	0.42	0.49	0.14	0.09	0.14	0.27
Tm	0.02	0.02	0.03	0.02	0.04	0.02	0.01	0.02	0.03	0.03	0.04	0.03	0.03	0.06	0.08	0.02	0.01	0.02	0.04
Yb	0.18	0.16	0.18	0.17	0.25	0.14	0.05	0.13	0.19	0.22	0.25	0.27	0.25	0.44	0.52	0.16	0.10	0.17	0.29
Lu	0.03	0.03	0.03	0.03	0.04	0.02	0.01	0.02	0.03	0.04	0.04	0.04	0.04	0.07	0.09	0.03	0.02	0.03	0.05
Hf	0.07	0.08	0.11	0.09	0.18	0.14	0.07	0.10	0.16	0.16	0.14	0.12	0.21	0.60	0.54	0.06	0.05	0.07	0.11
Ta	0.00	0.02	0.02	0.01	0.03	0.04	0.01	0.01	0.02	0.04	0.05	0.01	0.02	0.17	0.05	0.00	0.00	0.05	0.01
W	0.11	0.02	0.03	0.00	0.03	0.09	0.01	0.11	0.41	0.12	0.02	0.08	0.07	0.18	0.21	0.10	0.08	0.09	0.03
Pb	1.59	0.39	0.38	0.92	1.07	2.34	1.13	5.50	9.92	9.67	0.85	2.00	2.67	5.18	1.83	1.02	5.46	1.95	2.68
Th	0.04	0.12	0.06	0.06	0.31	0.25	0.05	0.04	0.14	0.11	0.07	0.07	0.15	1.30	0.36	0.04	0.03	0.03	0.08
U	0.02	0.04	0.02	0.02	0.09	0.16	0.02	0.03	0.06	0.05	0.02	0.03	0.06	0.69	0.23	0.02	0.02	0.01	0.03
PGE ppb																			
Os	0.35	NA	NA	22.60	NA	NA	NA	NA	11.20	14.44	1.33	4.32	11.80	4.35	0.53	13.51	11.38	10.10	8.45
Ir	0.68	NA	NA	40.70	NA	NA	NA	NA	18.00	12.16	1.92	11.60	23.10	6.48	1	14.49	18.50	14.30	14.36
Ru	1.87	NA	NA	102	NA	NA	NA	NA	41.50	45.89	5.87	24.80	53.50	16.80	2.41	50.91	47.81	41.60	36.78
Rh	2.86	NA	NA	322	NA	NA	NA	NA	81.20	49.12	7.73	73.30	146	38.40	3.61	61.86	96.51	75.10	63.93
Pt	15.90	NA	NA	3594	NA	NA	NA	NA	1955	617.74	71.70	1108	2125	470	46.34	534.64	1309.31	1020	1045.98
Pd	10.33	NA	NA	2675	NA	NA	NA	NA	2993	1548.93	241	3141	5178	1695	113.25	840.29	3482.22	2902	2077.50
Au	2.71	NA	NA	9.69	NA	NA	NA	NA	224	103.58	16.60	150	307	123	11.55	32.77	162.53	158	168.53

Abbreviations: TR = Troctolite, DUN/HZ = Dunite/harzburgite, HZ-serp = Serpentinised harzburgite, Serp = Serpentinite, TGA = troctolite-gabbronorite-anorthosite sequence, UmS = Ultramafic Sequence.

Table 8.1: Representative geochemical results for rocks analyzed during this study.

Sample I.D	MGN1	MGN2	MGN3	MGN4	MGN5	MGN6	MGN7	MPX1	MPX2	MPX3	MPX4	MPX5
Rock Type	AN/marginal N	Marginal GN	AN	Marginal GN	Marginal GN	GN	PYX AN (LN)	Chr PYX	ol (fsp) PYX	ol OPX	ol OPX	ol OPX
Group	Marginal GN	Marginal GN	Marginal GN	Marginal GN	Marginal GN	Marginal GN	Marginal GN	Marginal PYX	Marginal PYX	Marginal PYX	Marginal PYX	Marginal PYX
XRF wt. %												
SiO_2	60.76	49.32	53.89	51.92	51.46	52.41	52.12	51.24	55.67	51.42	47.16	54.19
Al_2O_3	20.47	25.43	18.27	14.88	19.63	17.33	17.31	5.47	4.39	4.05	4.70	4.27
Fe_2O_3	3.89	4.10	7.84	10.75	6.26	7.30	8.17	11.53	17.40	11.32	8.04	9.52
MnO	0.08	0.08	0.12	0.17	0.11	0.14	0.14	0.21	0.30	0.18	0.11	0.20
MgO	2.83	5.66	6.64	9.62	8.99	10.68	9.61	28.58	19.66	28.64	38.20	25.37
CaO	6.33	12.16	7.60	10.08	11.58	10.55	11.02	3.53	2.37	3.90	1.66	6.32
Na_2O	5.62	2.44	4.22	2.47	2.19	2.05	2.19	0.08	0.98	0.41	0.30	0.34
K_2O	0.41	0.94	0.14	0.22	0.11	0.23	0.15	0.02	0.26	0.05	0.10	0.03
TiO_2	0.14	0.09	0.90	0.72	0.07	0.12	0.19	0.09	0.15	0.20	0.07	0.20
P_2O_5	0.12	0.02	0.70	0.03	0.01	0.01	0.02	0.01	0.07	0.01	0.02	0.01
Cr_2O_3	0.02	0.02	0.04	0.08	0.04	0.05	0.06	0.46	0.12	0.50	0.43	0.34
NiO	0.01	0.03	0.01	0.02	0.09	0.04	0.05	0.15	0.11	0.22	0.24	0.14
LOI	1.54	2.71	0.34	1.09	0.63	0.56	0.55	3.91	1.12	1.24	9.04	0.64
Total	100.33	99.91	99.67	100.00	99.99	100.25	100.29	100.34	99.89	99.88	100.30	100.06
S ppm XRF	NA	NA	NA	NA	1586.00	NA	NA	NA	NA	NA	415	542
ICP-MS ppm												
Li	9.98	17.18	3.11	7.37	2.61	7.87	5.07	3.41	1.95	0.54	0.68	1.22
P	494.88	49.00	3053.13	88.84	5.92	20.86	40.51	15.24	279.71	20.74	46.31	38.77
Sc	2.70	3.77	4.87	20.58	7.49	13.81	12.54	12.22	27.21	12.50	5.36	16.09
Ti	761.40	497.20	4600.15	3763.27	419.44	640.96	958.40	397.05	685.38	936.37	247.78	1158.50
V	25.11	42.69	79.39	205.75	65.96	88.08	111.84	68.77	101.80	85.02	34.68	77.78
Cr	58.49	63.82	188.22	516.51	181.96	269.96	322.48	2165.51	731.82	2302.85	1642.61	1631.25
Co	14.35	38.02	30.98	51.46	77.81	51.54	54.52	93.25	114.16	95.92	72.57	93.35
NiO	36.09	197.21	70.01	172.12	620.61	271.44	297.95	763.23	618.28	1205.41	1326.61	916.00
Cu	9.91	22.30	24.73	53.06	329.66	58.76	256.35	65.67	250.92	695.22	58.77	119.74
Zn	47.29	36.38	71.48	88.32	47.96	46.24	50.90	64.50	162.81	70.08	32.78	115.86
Ga	19.47	16.38	15.54	14.57	14.31	11.10	11.13	3.04	7.54	3.51	2.80	4.67
As	0.17	0.03	0.23	0.46	0.30	0.22	0.20	0.17	0.53	0.13	0.25	0.24
Rb	4.79	26.87	0.40	2.31	1.58	3.36	1.40	0.85	24.92	1.32	2.88	1.77
Sr	395.40	451.43	429.09	216.27	144.25	150.52	118.98	11.23	63.75	32.54	26.95	64.63
Y	1.36	0.68	2.03	8.07	0.69	1.88	2.47	0.89	8.89	2.51	1.00	4.35
Zr	20.98	5.69	5.06	12.65	1.47	6.39	8.52	1.65	23.36	4.27	6.44	6.49
Nb	0.96	0.36	1.39	0.09	0.03	0.19	0.22	0.05	2.28	0.18	0.42	0.14
Ba	177.67	203.28	159.87	149.39	28.91	67.69	40.58	3.55	37.22	9.24	39.30	11.96
Sn	0.39	0.31	0.21	0.91	0.32	2.49	0.39	0.42	0.73	0.55	0.32	1.18
Cs	0.36	0.63	0.03	0.31	0.11	0.14	0.09	0.36	2.55	0.09	0.45	0.28
La	6.45	0.88	4.65	2.03	0.37	0.96	1.09	1.19	3.88	0.90	1.92	0.82
Ce	13.24	1.57	10.15	1.89	0.62	2.63	3.55	0.55	7.31	1.41	3.13	1.43
Pr	1.19	0.13	1.24	0.66	0.06	0.21	0.28	0.06	0.85	0.17	0.34	0.26
Nd	4.73	0.53	6.03	3.60	0.26	0.97	1.30	0.23	3.54	0.83	1.27	1.34
Sm	0.84	0.21	1.22	1.22	0.09	0.27	0.35	0.07	0.93	0.24	0.24	0.45
Eu	0.50	0.18	0.72	0.61	0.10	0.15	0.16	0.05	0.14	0.10	0.09	0.15
Gd	0.71	0.14	1.07	1.33	0.10	0.30	0.42	0.09	1.07	0.32	0.22	0.56
Tb	0.07	0.02	0.11	0.23	0.02	0.05	0.07	0.02	0.20	0.06	0.03	0.10
Dy	0.31	0.12	0.49	1.57	0.13	0.35	0.45	0.13	1.41	0.44	0.18	0.73
Ho	0.05	0.03	0.08	0.33	0.03	0.08	0.10	0.03	0.32	0.10	0.04	0.16
Er	0.15	0.08	0.19	0.89	0.08	0.22	0.29	0.11	1.02	0.29	0.11	0.46
Tm	0.02	0.01	0.02	0.13	0.01	0.04	0.04	0.02	0.17	0.05	0.02	0.07
Yb	0.54	0.08	0.12	0.91	0.10	0.24	0.29	0.14	1.33	0.32	0.13	0.44
Lu	0.08	0.01	0.02	0.14	0.01	0.04	0.05	0.02	0.21	0.05	0.02	0.07
Hf	0.04	0.16	0.14	0.57	0.05	0.19	0.25	0.06	0.70	0.14	0.17	0.25
Ta	0.08	0.04	0.13	0.02	0.03	0.02	0.02	0.00	0.22	0.02	0.04	0.01
W	0.04	0.04	0.01	0.11	0.01	0.05	0.04	0.07	0.50	0.04	0.44	0.03
Pb	3.50	6.26	0.93	3.14	2.05	0.77	1.61	1.15	5.72	1.49	1.09	5.52
Th	0.39	0.10	0.03	0.01	0.01	0.07	0.10	0.03	1.32	0.07	0.23	0.05
U	0.16	0.06	0.01	0.01	0.01	0.03	0.04	0.01	1.02	0.03	0.12	0.03
PGE ppb												
Os	NA	NA	NA	NA	1.95	NA	NA	NA	NA	NA	NA	0.34
Ir	NA	NA	NA	NA	2.60	NA	NA	NA	NA	NA	NA	0.44
Ru	NA	NA	NA	NA	8.14	NA	NA	NA	NA	NA	NA	1.45
Rh	NA	NA	NA	NA	12.80	NA	NA	NA	NA	NA	NA	0.48
Pt	NA	NA	NA	NA	151	NA	NA	NA	NA	NA	NA	4
Pd	NA	NA	NA	NA	467	NA	NA	NA	NA	NA	NA	5
Au	NA	NA	NA	NA	27.70	NA	NA	NA	NA	NA	NA	1

Abbreviations: AN = Anorthosite, Chr PYX = Chromite-bearing pyroxenite, Marginal N = Marginal Norite, Marginal GN = Marginal gabbronorite, Marginal PYX = Marginal pyroxenite, ol (fsp) PYX = Olivine-bearing feldspathic pyroxenite, ol OPX = Olivine-bearing orthopyroxenite.

Upper Zone and TGA Sequence gabbroic rocks display mildly fractionated profiles across the IPGE and after a moderate increase of concentration a flat profile across the PPGE and Au. Samples of the troctolite are mostly characterized by mildly sloping IPGE and except for a mineralized sample have flat PPGE distributions.

The serpentinized harzburgite exhibits strong fractionation with Pd/ Ir of 177. The rocks are enriched in Pd relative to Pt, and Au is depleted relative to Pd. This pattern is identical for that of the mineralized troctolite. A sample of the marginal pyroxenite is characterized by unfractionated PGE (Fig. 8.11).

Fig. 8.11 displays variation diagrams of S versus Cu, Pt and Pt. It can be seen, that Cu and S exhibit an excellent correlation, whereas the correlation of S and Pt or Pd is significantly poorer. Sulfur levels are overall very low, with a maximum of approx. 12000 ppm. These levels and correlations are identical to commercial assays provided courtesy of Platinum Group Metals.

8.6.2. D. PGE and Cr assay data provided by Platinum Group Metals

Assay data provided by PTM can be used to assess the validity of the results that were presented above. The available assay data for >100 drill holes from the study area were extracted and are shown in the diagrams below.

Fig. 8.12A-C show binary variation diagrams of S vs Cu, Pt, and Pd. It can be seen, that Cu and S show excellent correlation, whereas there is only a weak correlation of S with Pt and Pd, respectively. Pt and Pd exhibit a good correlation (Table 8.2). Fig. 8.12D shows a ternary plot of Pt, Pd, and Au. It can be seen, that the majority of assays are dominated by Pd with Pd/Pt approx. 0.6 and only low Au content. This is in contrast to Pt/Pd observed in the Merensky Reef, and closer to the Pt/Pd observed in some sectors of the Platreef (Kinnaird, 2005). Low Au is typical of the F Zone, whereas in the T Zone and the Aurora Project Au makes up approximately 20% of the precious metals budget. Fig. 12D highlights, that the anti-correlation of Cr and PGE also applies for the rest of the assays in the area. It can be seen, that a large number of samples plot in between the low-PGE/high-Cr and high-Cr/low-PGE trends. This is due to Cr-rich orthopyroxene autoliths and mingled orthopyroxenitic lithologies that cannot be avoided during sampling. This data also experiences a sampling bias towards mineralized samples (the purpose of the company's sampling program), and Cr-rich, unmineralized samples are therefore not well-represented.

8.6.3. Lateral variation in lithology and mineralization

Typical cross and long sections through the study area (Fig. 8.4) are shown in Figs. 8.13 and 8.14. Both sections show the dominant lithology and PTM's assay values for 3E (Pt+Pd+Au) and Cr as well as Pt/Pd and Cu/Pd.

Fig. 8.13 shows a typical sequence of gabbronorite dominated upper TGA Sequence overlying olivine-bearing rocks. The base of the TGA Sequence is characterized by heterogeneous and patchy gabbronorite, norite, and troctolite, and textures observed in core range from incompletely blended olivine- or pyroxene-dominant patches to discrete autoliths and xenoliths (Fig. 8.3A, B). Downwards this zone grades into salt and pepper textured leuco- to melatroctolite.

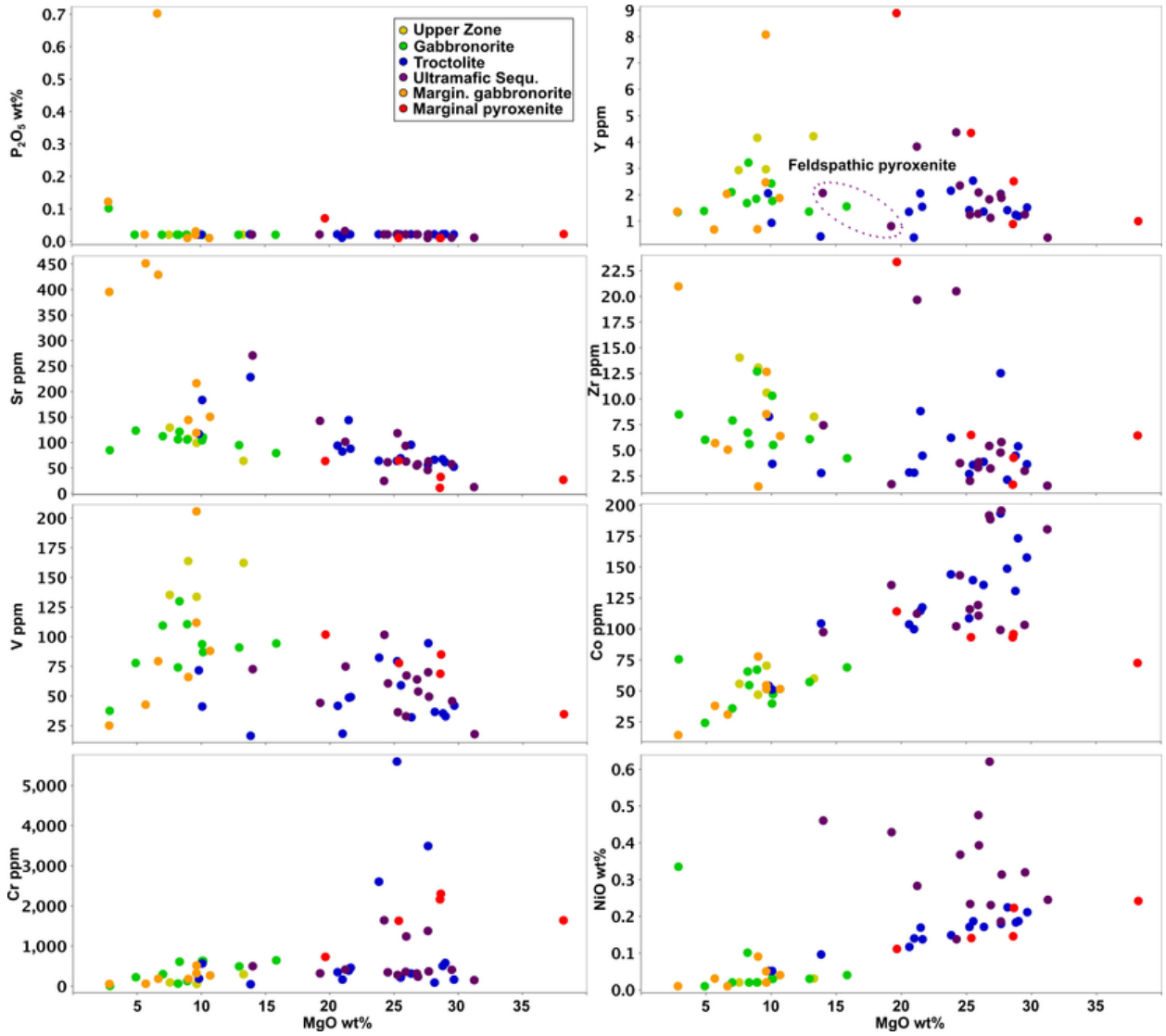

Figure 8.8: Binary variation diagrams of MgO vs trace elements.

Below the troctolite, strongly altered harzburgite hosts the bulk of the mineralization. Orthopyroxenite autoliths occur throughout this part of the succession, and where abundant are schematically indicated in the section. These rocks are typically enriched in Cr, and their abundance correlates with the Cr concentration shown. Below the harzburgite may be more orthopyroxenite, marginal gabbronorite, or more troctolite toward the eastern side of the section (drill hole WB091). The sequence of rocks continues up dip, until on the eastern side (not shown) the harzburgite is directly overlain by sedimentary rocks. In zones of mineralization, the Pt/Pd ratio is fairly constant around 0.6 with a Cu/Pd ratio at approximately 530. As shown above, the mineralization is dominated by Pd with little Au in the metal budget.

The four holes in the long-section (Fig. 8.14) are located at the western edge of PTM's drilling in this sector (Fig. 8.4) and mineralization is hosted by strongly altered, ultramafic rocks of varying mineralogy and texture. Holes WB163 and WB049 are located at or around the center of the mineralized zone, while holes WB165 and WB019 are located at its northern and southern edge, respectively. It can be seen, that all four holes share a very similar stratigraphy with Cr-enriched intervals that appear to correlate between the holes. Mineralization (shown as Pt+Pd+Au) is most strongly developed in the central section, and is poorly developed or absent at the northern and southern sections. The long section also shows well-developed troctolite regardless of the thickness and 3E grade of the harzburgite. This suggests, that the intrusion of both suites of rocks is independent of each other. Pt/Pd and Cu/Pd are again fairly consistent in the mineralized segments.

In summary, the sections show a SW to NE-oriented, tube-shaped and slightly flattened, mineralized zone of up to 80m thickness that is dominantly confined to ultramafic rocks. Although most mineralization is confined to harzburgite and feldspathic pyroxenite, in detail the UmS is a highly heterogeneous zone with signs of magma mingling, mixing, fluid flow and sulfide remobilization. Grade drops off towards the northern and southern edges before increasing in the next high-grade, high-thickness harzburgitic zone (not shown in the sections). Grade is also lower in areas of abundant orthopyroxenite and an anti-correlation of Cr and 3E can be seen.

To visualize this area of the Waterberg Project, a Leapfrog 3D model using the logging data from >100 drill holes has been created. Due to the nature of company drill logs, some assumptions and generalizations of logging codes had to be made. This includes grouping various logged rocks into broader categories, but also the assumption that all logged serpentinite is secondary and the product of harzburgite alteration. Additionally, given the nature of the ultramafic rocks, the model uses a >1 g/t 3E grade shell rather than lithology to demonstrate the approximate outline of the UmS. Fig. 8.15A shows

the granite-gneiss basement and the up to 80 m thick grade shell. It follows what appears to be a basement depression in a northeasterly direction. To its north, a less-well developed area of PGE mineralization follows the same trend.

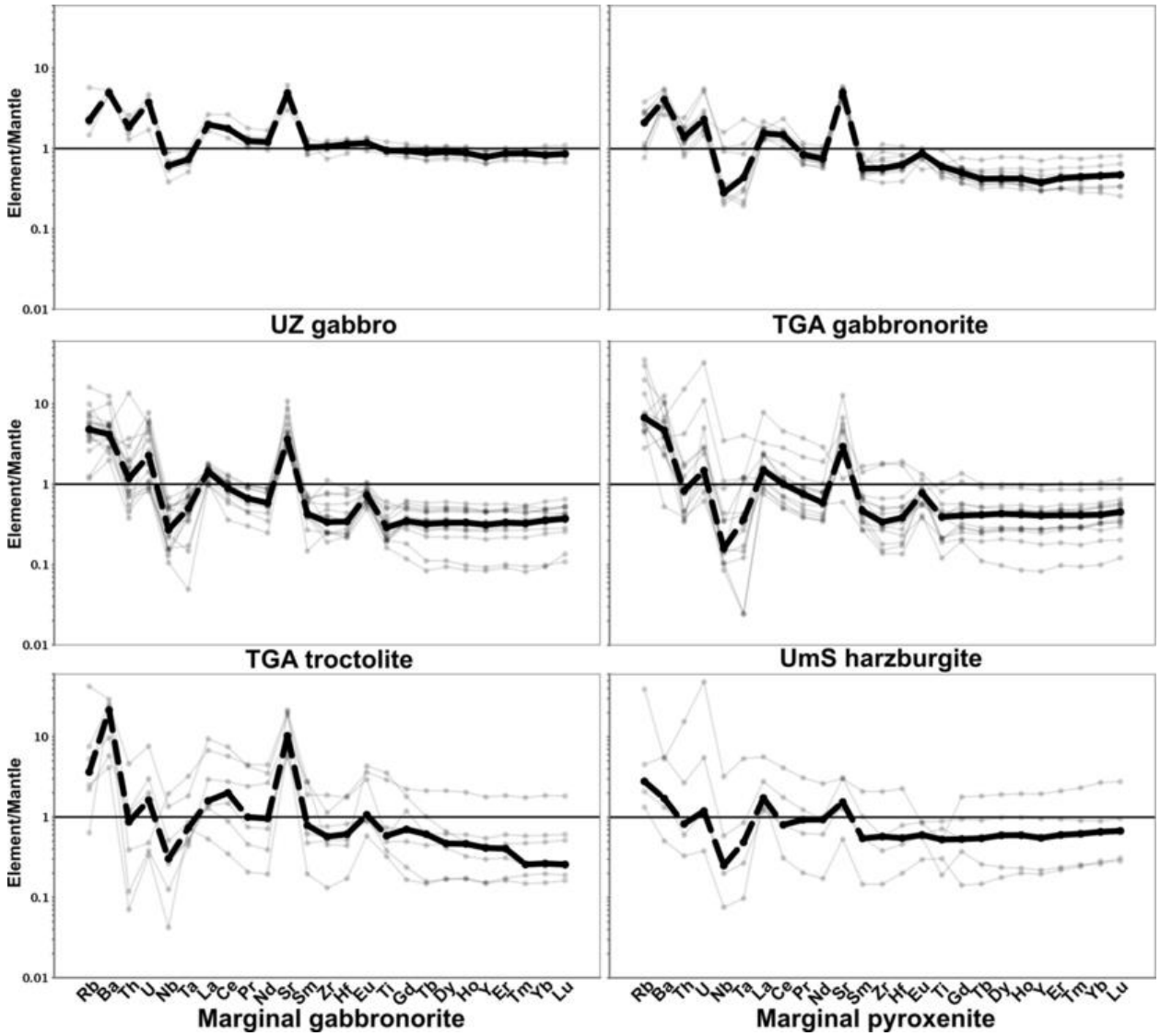

Figure 8.9: Primitive mantle normalized (Sun and McDonough, 1989) multi-element plots for all six groups of rocks with thick lines showing the average for each group of samples. It can be seen that except for a stratigraphic increase in absolute concentrations the patterns are almost identical. Variations in marginal gabbronorites and pyroxenites are believed to result from contamination by assimilation.

These depressions may represent a primary feature controlling magma flow, or alternatively, represent zones of highest heat and fluid flux and the associated thermo-mechanical erosion. Among researchers associated with this project, the tubular intrusions are referred to as chonoliths (e.g. Kinnaird *et al*., 2017). It is important to stress, that this grade shell was not developed by Platinum Group Metals to indicate resources, but rather models our understanding of PGE distribution. In Fig. 8.15B, the olivine-

bearing lithologies of the lower TGA and Ultramafic Sequence have been added, and the erosional unconformity of the Waterberg Group sediments and dolerite sills are shown. The vertical offset in the dolerite dikes may indicate some fault control. The open area between the upper contact of the olivine-bearing rocks and the base of the sediments is occupied by gabbroic rocks of the TGA Sequence.

8.7. Discussion

8.7.1. Discussion of the data presented

The correlation of the Platreef and the Northern Lobe's northernmost, mineralized lithologies at Aurora has recently received some attention (Harmer *et al*., 2004; Manyeruke, 2007; Maier *et al*., 2008; McDonald and Harmer, 2010; McDonald *et al*., 2017). McDonald *et al*. (2017) describe several key factors that make it unlikely that the Aurora Project is a simple strike extension of the Platreef and instead suggest, that it represents a marginal facies of the Main Zone above the Troctolite Marker (which is located 1100 m above the base of the Main Zone). Considering the location of the Waterberg succession less than 20 km north of the Aurora Project, it is appealing to simply link the two zones as a northern magmatic basin. Some of the similarities between the upper Main Zone-hosted Aurora mineralization and the Waterberg T Zone are provided by McDonald *et al*. (2017) and this contribution will expand on their work.

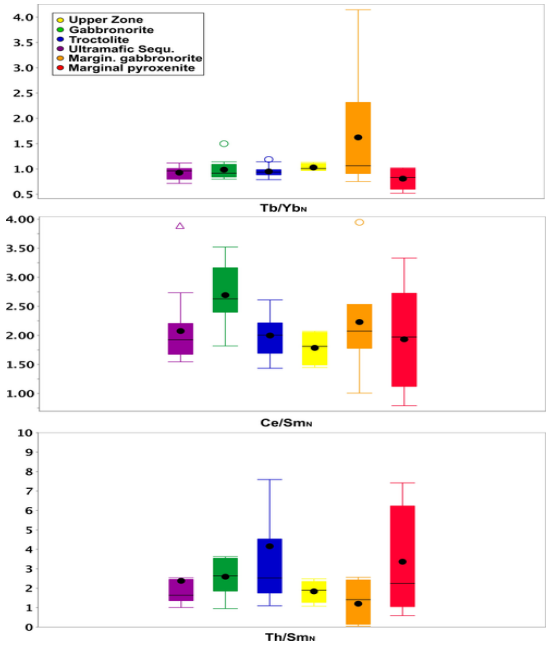

Figure 8.10: Box plots displaying Tb/Yb_N, Ce/Sm_N and Th/Sm_N values for groups of samples. Color scheme as in Fig. 8.7. Most variation is exhibited by marginal gabbronorites and pyroxenites, which is interpreted to represent contamination by assimilation. The box represents the inter quartile range with the median represented as horizontal line and the mean as a black circle.

Both the Platreef and the Waterberg Succession exhibit variations in rock type and mineralization along their strike, although compared to the Platreef the Waterberg Succession is small with approximately 15 km strike length. Dynamic emplacement environments with multiple, channelized magma injections along a westerly to northwesterly direction (rather than a north to south magma flow) have been proposed for the Platreef (Yudovskaya *et al*., 2017; cf. Barnes *et al*., 2016), and may together with floor rock control (Kinnaird *et al*., 2005) be used to explain clear differences along strike. The existing similarities between individual sectors (such as Aurora and the Waterberg Project, Fig. 8.2A) may be attributed to the fact, that all of them are related to the Bushveld Large Igneous Province, and hence share the same melting event.

In an initial study, laser-ablation U/Pb dating by Huthmann *et al*. (2016) demonstrated that zircons from mafic rocks of the succession have an age that is within error identical to ages published for the Bushveld Complex. This study also showed, that the sedimentary rocks unconformably overlying the coarse-grained mafic to ultramafic rocks have a maximum depositional age of 2045 Ma, with what is interpreted to be an ash-rich paleosol in-between (Yudovskaya *et al*., 2015). Given the absence of more evolved mafic rocks, i.e. apatite-bearing UZ or similar, and the absence of any sort of felsic roof rocks, then several kilometers of material must have been removed between c. 2056 and 2045 Ma. The Waterberg Project is characterized by significant erosion, a unique stratigraphy of harzburgites and troctolites, a relatively small size and limited thickness, and a position wedged in between the Palala Shear Zone in the North and the Hout River Shear Zone in the South (Fig. 8.1). These place the succession in a unique situation compared to the rest of the Bushveld Complex. The structural position, in particular, may have created transtensional spaces and crustal anisotropies along which initial magmas could ascend (Lightfoot and Evans-Lamswood, 2015). Further fault movement until 1.97Ga brought the succession closer to surface and to a mineable depth (Schaller *et al*., 1999).

As shown by logging and geochemical data, all samples represent ultramafic to gabbroic cumulate rocks dominated by varying proportions of olivine, plagioclase, clino- and orthopyroxene. Clinopyroxene becomes the dominant pyroxene towards the top of the succession. Pigeonite may be found towards the top of the succession, however, its appearance is erratic. The lower part of the succession comprises strongly altered harzburgites and feldspathic pyroxenites hosting the F Zone mineralization, and is overlain by troctolite. Contrary to what has been described at the nearby Aurora prospect (Manyeruke, 2007; McDonald *et al*., 2017), no significant carbonate xenoliths or carbonate alteration has been found in the project area.

In contrast to what is published on the Troctolite Marker in the Northern Lobe (an olivine-bearing gabbroic rock, van der Merwe, 1976), the troctolite of the Waterberg area is a true troctolite comprising cumulus olivine and plagioclase. The sharp lower contact and the gradational contact with the overlying gabbroic rocks has been shown in drill core (Fig. 8.3). The Waterberg troctolite is interpreted to be the result of magma mingling and mixing, and is part of a fractionating sequence eroding the earlier harzburgite. Consequently, based on available data, it is not believed to be the direct lateral equivalent of the Troctolite Marker in the Northern Lobe, which itself is interpreted to be at least partly an influx of primitive magma into a pre-existing Main Zone (Tanner *et al*., 2014). The PGE-undepleted Troctolite Marker and the cryptic pyroxenite intrusions described by these workers highlight the significant lateral and vertical variations in the Northern Lobe. Furthermore, although the work of Ashwal *et al*. (2005) and Roelofse and Ashwal (2012) provides a detailed stratigraphy for most of the Northern Lobe, about 490m of stratigraphy are unaccounted for. Most crucially, the missing segment is at the base of the troctolite marker where ultramafic rocks might be expected.

Above the olivine-bearing rocks is a package of noritic to gabbronoritic rocks, grading into magnetite-bearing gabbros/gabbronorites. The gabbroic rocks are typically taken to be the equivalent of the Northern Lobe's Main and Upper Zone given their mineralogy. While this may be the case, gabbroic rocks are typical of evolving layered mafic intrusions and their occurrence does not necessitate a connection of magma conduits between the Northern Lobe and the project area.

The lower part of the succession hosts autoliths of Cr-enriched, olivine-bearing orthopyroxenite (which are therefore older). The exact lateral distribution of these rocks is currently poorly understood, and some may represent either rafts or perhaps simultaneously intruded sills. Where these rocks have been assimilated by younger intrusive phases, the resulting drill core sections are characterized by increased Cr levels (Figs. 8.13 and 8.14). Additionally, given their unmineralized nature, a commensurate drop in PGE levels can be observed in the assay intervals including these autoliths (Figs. 8.13 and 8.14). Highest PGE grade intervals are often found in zones of intense alteration of primary silicates and may contain sulfide stringers and veins. Both features suggest some remobilization of initial sulfides, leading to a decoupling of sulfides and to a more limited degree of Pt and Pd. This process can be observed in the company assay data presented earlier, where Pd is remobilized preferentially over Pt (Barnes and Liu, 2012). Whether this process has an effect on the overall Pt/Pd ratio is currently undetermined.

Major element whole-rock geochemistry places the rocks in three distinct groups, representing the Cr-enriched marginal orthopyroxenite, the harzburgite of the Ultramafic Sequence, and the Troctolite-Gabbronorite-Anorthosite Sequence and Upper Zone. Rocks of the TGA Sequence form a

continuous trend from high-Mg, olivine-rich troctolite to the magnetite-bearing gabbroic rocks of the Upper Zone. This trend may indicate that the TGA Sequence and the Upper Zone of the Waterberg Succession form a continuum and should be grouped together. The marginal gabbroic rocks resemble the TGA rocks in chemistry and mineralogy, and may represent downward injections into older units. Outliers in troctolite composition may be related to variable amounts of oikocrystic orthopyroxene and contamination by the underlying harzburgite and orthopyroxenite. Trends of harzburgite and troctolite differ, suggesting the crystallization of harzburgite from a more Mg-rich liquid and consequently the crystallization of more Mg-rich olivine.

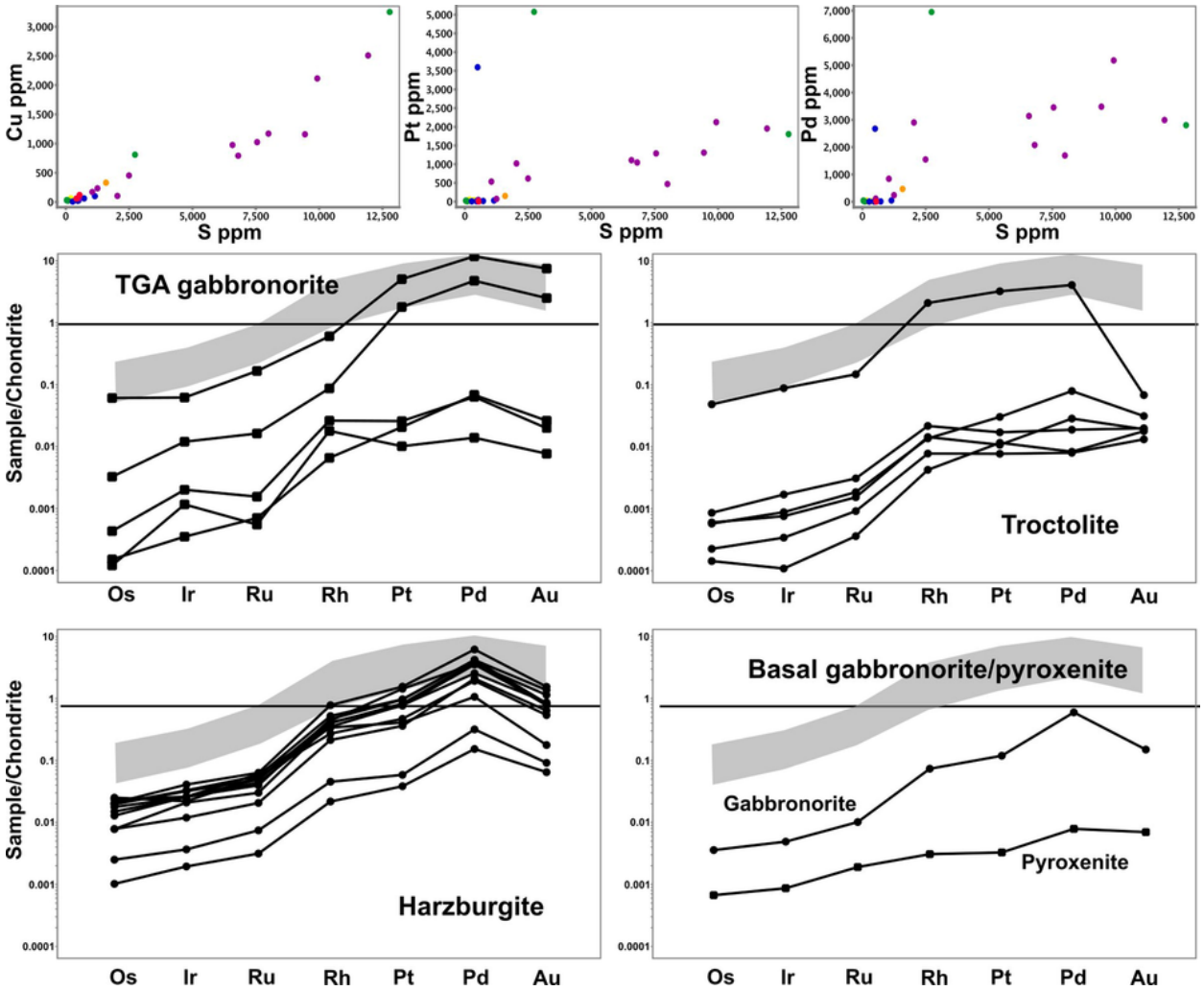

Figure 8.11: Top: Binary variation diagrams of S vs Cu, Pt and Pd. S vs Cu show an excellent correlation, however the correlation between S and Pt and Pd is weak; Bottom: Chondrite normalized PGE plots for the samples analyzed in this study. Light grey represents PGE distribution from the Turfspruit and Sandsloot high-grade reef-style mineralization in the Northern Lobe (from Yudovskaya *et al*., 2017).

Normalized REE patterns show near uniformity (e.g. fairly consistent Ce/Yb, Th/Nd) with a minor stratigraphic increase in abundances. Except for Eu, all REE are incompatible in the cumulus phases of

the Waterberg succession (olivine, orthopyroxene, plagioclase, clinopyroxene) which is reflected in the primitive mantle-normalized diagrams. Accessory phases (other than zircon) that would concentrate LREE have not been observed, and hence the REE budget is controlled by intercumulus liquid (Maier and Barnes, 1998). Normalized REE values below one are interpreted to reflect the fact that the rocks of the Waterberg Succession are crystal cumulates. The incompatible element budget of the parental magma was either retained in a staging chamber, or lost with migrating interstitial liquid. The variations in incompatible elements and REE contents and the associated extreme outliers, particularly in the basal rocks, are interpreted to represent wall rock contamination. Gabbroic rocks are characterized by $Rb_N < Ba_N$, while the opposite is true for ultramafic rocks. Troctolite Rb/Ba_N are approx. 1, again suggesting contamination of troctolite by underlying harzburgites. Estimates of trapped liquids using La or Zr (not shown; Maier and Barnes, 1999; McDonald *et al*., 2009) exhibit a good correlation with peaks in incompatible element abundances. Given the interaction of pyroxenites and granite-gneisses observed in drill core, the validity of these calculations, however, is questionable for the project area. The slight upward stratigraphic increase in LREE observed is interpreted to be related to the increased proportions of clinopyroxene in the rocks. Troughs for the elements Th, Rb, Nb, and Ta are fairly typical for Bushveld rocks, and generally interpreted to represent contamination by lower-mid continental crust (Barnes and Maier, 2002).

8.7.2. Correlation with the Aurora Project

McDonald *et al*. (2017) recently presented data for the Aurora Project south of the Waterberg Project. The data presented in their work may be used to create a simplified and continuous emplacement model. At this point, most areas of the Northern Lobe are, however, not nearly as well-researched as the well-exposed open cut mines at Sandsloot. Caution and reliance on published data is therefore needed when correlating individual prospects.

McDonald *et al*. (2017) describe the Aurora Project as consisting of three main units, namely Unit 1 with peridotites and melagabbronorites, Unit 2 with gabbronorites and leucogabbronorites and Unit 3 comprising pigeonite gabbronorites. Additionally, Aurora comprises zones of sometimes pegmatitic magnetite gabbros and olivine-bearing gabbroic rocks. Mineralization is hosted predominantly by felsic rocks. The mineralogical details and geochemical data provided in their work suggests the following correlation:

Unit 1 at Aurora is characterized by orthopyroxenite, enrichment in Cr and consequently high Cr/MgO ratios. These features suggest that Unit 1 might correlate with the Cr-rich marginal orthopyroxenites described for the Waterberg Succession. This interpretation is supported by

mineralogy and similar trends and positions on bivariate major and trace element plots and close to identical trace element ratios.

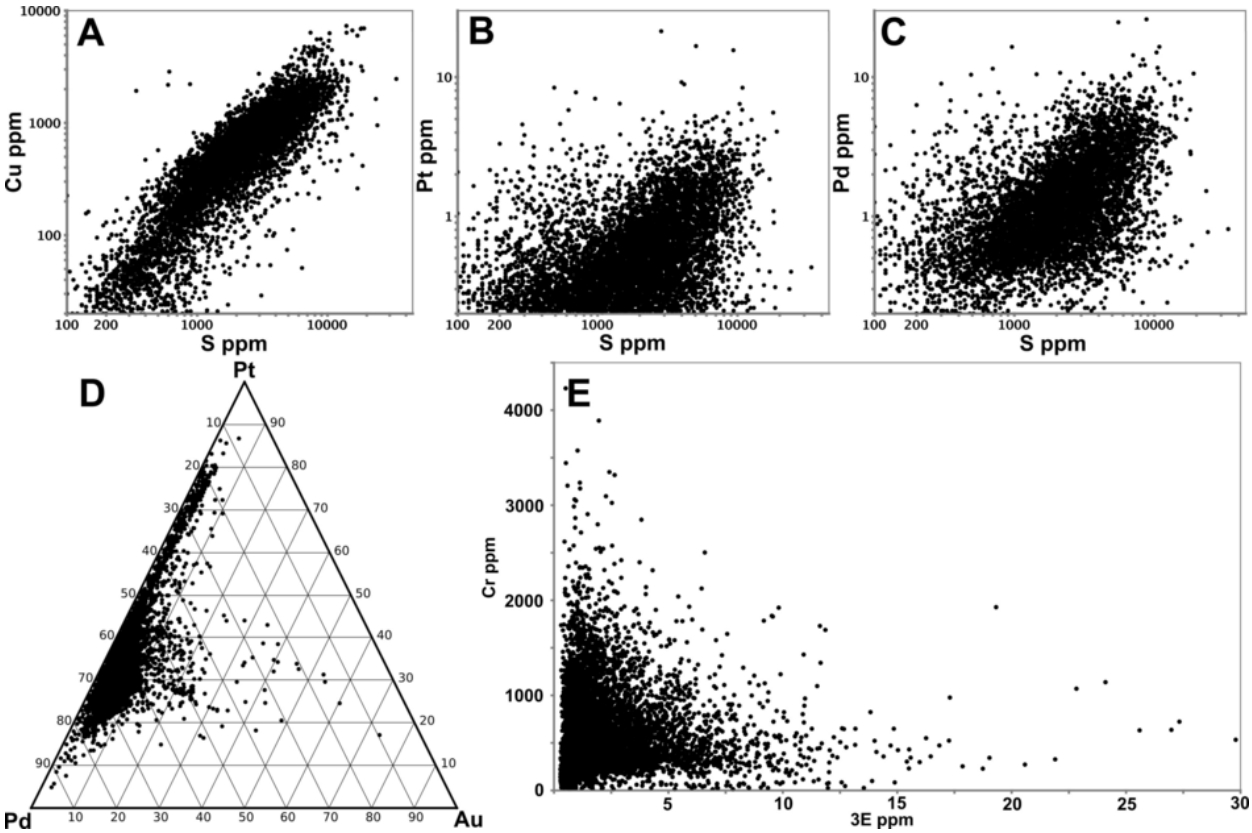

Figure 8.12: A-C: Binary variation diagrams of chalcophile elements vs sulfur. There is an excellent correlation between Cu and S and a very weak correlation between S and Pt/Pd. D: Ternary diagram showing the relative proportions of Pt, Pd and Au for the assays for the project area. E) Pt+Pd+Au vs Cr diagram highlighting the anti-correlation of precious metals and Cr-rich lithologies. Data filtered for Pt and Pd >0.1ppm, c. 9500 assays. Sulfide-bearing zones were preferentially sampled by PTM geologists.

Table 8.2

Correlation	Pt	Pd	Rh	Au	Cu	Ni	S
Pt	1	0.85	0.71	0.58	0.52	0.56	0.38
Pd	0.85	1	0.72	0.62	0.62	0.66	0.47
Rh	0.71	0.72	1	0.19	0.13	0.34	0.1
Au	0.58	0.62	0.19	1	0.74	0.45	0.45
Cu	0.52	0.62	0.13	0.74	1	0.66	0.74
Ni	0.56	0.66	0.34	0.45	0.66	1	0.62
S	0.38	0.47	0.1	0.45	0.74	0.62	1

Both Unit 2 and 3 at Aurora are more evolved gabbroic rocks interpreted to correlate with the upper TGA Sequence of the project area. This interpretation is again supported by both mineralogical and geochemical features. Where developed, the upper TGA Sequence in the Waterberg Succession hosts two mineralized zones, often with a middling in between. It features olivine-bearing rocks, the

appearance of pegmatites, and pigeonite. This is comparable to the variable nature of rocks in the Aurora Project, also characterized by several mineralized zones. Geochemically, available data for the upper TGA Sequence again shares similar positions on bivariate plots and almost identical trace element ratios with the Aurora Project.

The main geochemical difference between the two deposits exists in Rb/Ba_N ratios, with generally lower values for Aurora. McDonald *et al*. (2017) report a carbonate overprint and carbonate assimilation for the Aurora project. No significant carbonate has been found at the Waterberg, indicating purely granite-gneiss host rocks. The differing Rb/Ba_N ratios may therefore be the result of different host rocks.

In terms of precious metals, the Aurora Project is characterized by approximately 20% Au in its precious metals budget (Fig. 8.16). This also holds true for the T Zone of the Waterberg Project. It is worth noting, however, that elevated Au/PGE ratios have not only been recorded at Aurora, the T Zone and Moorddrift (Harmer *et al*., 2004; Maier *et al*., 2008; McDonald and Harmer, 2010; Maier and Barnes, 2010; Holwell *et al*., 2013; McDonald *et al*., 2017), but also for the Upper Reef at Turfspruit (Yudovskaya *et al*., 2017) and for other offset-reefs from around the world (e.g. Skaergaard, Rincón del Tigre). Hence, elevated Au may be a feature associated with higher stratigraphic position in the mafic sequence, given no previous metal depletion. Considering the weak grade at Aurora compared to the Waterberg Project, Aurora might represent a southern extension of the Waterberg Succession rather than the other way around.

This possible correlation between T Zone mineralization and the Aurora Project does not account for the economically significant F mineralized Zone, which is located stratigraphically below the T Zone. Following the argument of Aurora being located in the upper Main Zone (McDonald *et al*., 2017), the F Zone would have to represent a highly unusual, richly-mineralized lower Main Zone of olivine-bearing rocks, i.e. the Troctolite Marker, or a marginal, very northern expression of the Critical Zone, i.e. the Platreef.

It is crucial to note, that on the farm Harriet's Wish in the far north of the Northern Lobe (Fig. 8.2A) the igneous units exhibit a pronounced change in strike direction from NNW to NNE when crossing the Hout River Shear Zone. The shear zone itself has, as far as the authors are aware, not been intersected in drill core. Despite the mineralogical and geochemical similarities described above, the exact nature of the relationship of Waterberg Project and Aurora Project therefore still needs to be established.

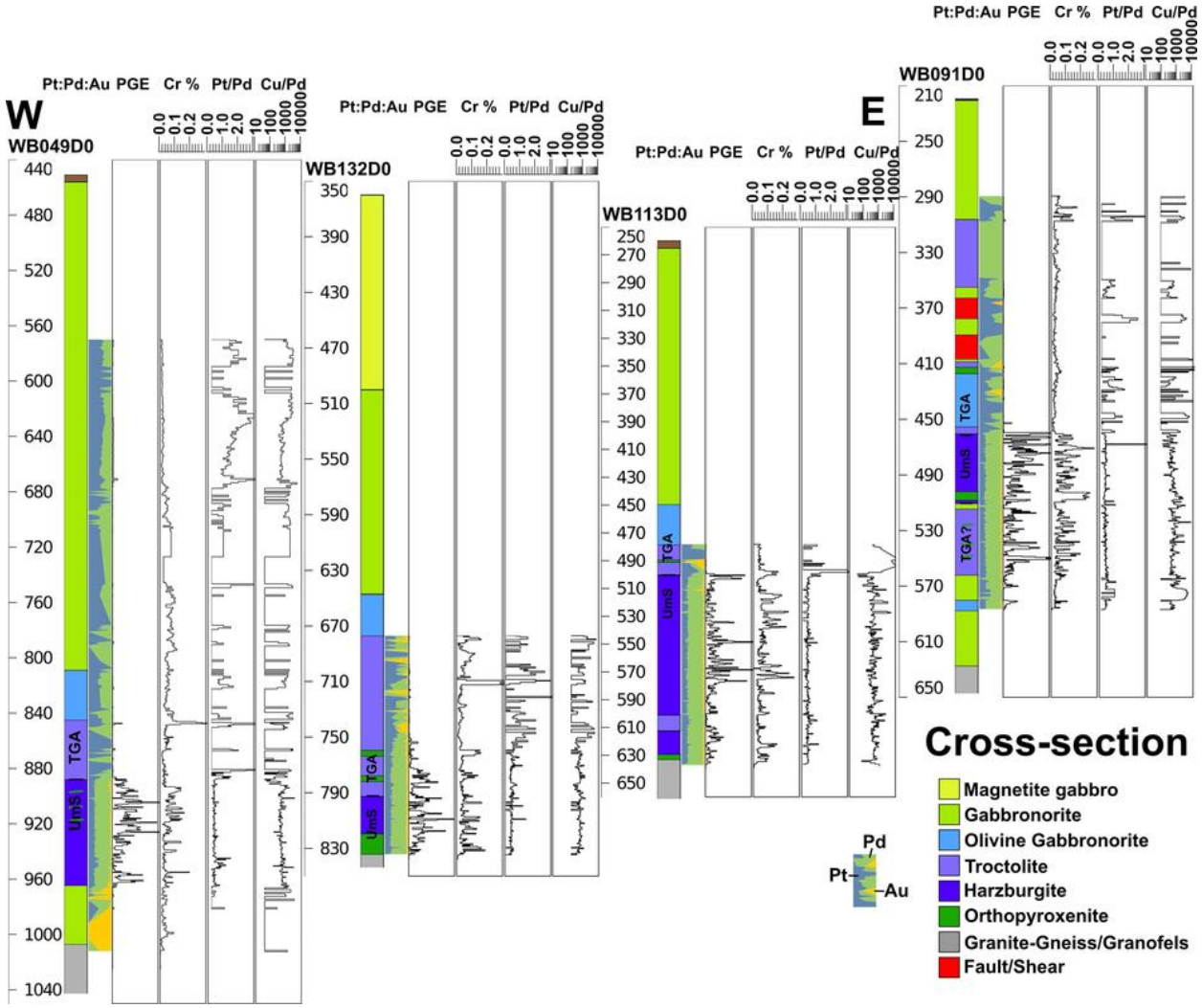

Figure 8.13: Cross section through the study area as shown in Fig. 8.4. Columns presented show dominant lithology, the grade of Pt+Pd+Au, Cr%, Pt/Pd and Cu/Pd extracted from PTM's database. PGE units have been omitted.

8.7.3 Correlation with the Platreef

Given that the Aurora Project does not represent a satisfactory correlative for the F Zone, the data presented can be compared with the Platreef in the south of the Northern Lobe. Mineralization in the F Zone of the Waterberg Succession is characterized by its anti-correlation with Cr, a Pt/Pd ratio of 0.6 and approximately 5% Au in the metal budget (Fig. 8.16). Ni/Cu is significantly higher than other Northern Lobe mines at 6–8. Chondrite-normalized PGE patterns show mildly fractionated IPGE and significantly enriched and also mildly fractionated PPGE.

The PGE patterns and ratios resemble those observed at various Platreef projects (Maier *et al*., 2008 and references therein, Yudovskaya *et al*., 2017) and what is typical for ultramafic hosts in the Bushveld Complex (Naldrett *et al*., 2011). The slightly higher fractionation observed between IPGE and PPGE may be related to IPGE (and chromite) retardation somewhere at depth. The low Pt/Pd ratios are

typical for those recorded for the lower Platreef (e.g. Kinnaird, 2005), while the (Pt+Pd)/Au and Ni/Cu place the F Zone in a field with Platreef exploration and mining projects (Fig. 4 in McDonald *et al*., 2017; our data would need adjustment due to its harzburgite host). The absence of a correlation between PGE and S is typical for disseminated mineralization at the base of the Platreef (Hutchinson and Kinnaird, 2005). The poor correlation between the PGE and S is ascribed to the remobilization and partial removal of sulfides after emplacement, thereby selectively remobilizing Pd over Pt. Cr/MgO ratios are consistently low and dissimilar to the Platreef unit (McDonald and Holwell, 2011). Detailed comparisons of the F Zone with the lower part of the Troctolite Marker are hampered by the lack of published and peer-reviewed descriptions and data.

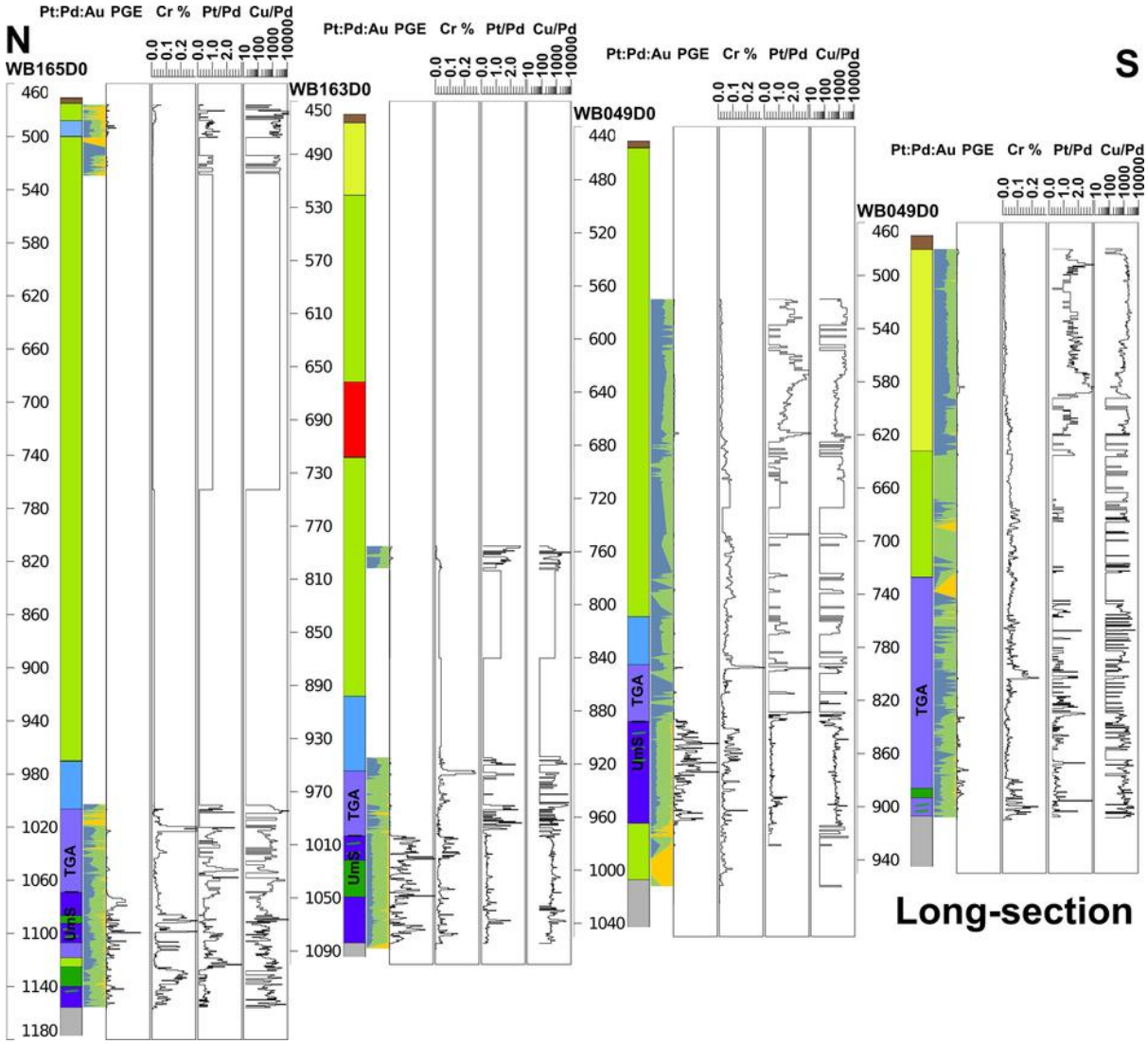

Figure 8.14: Long section through the study area as shown in Fig. 8.4. Color scheme as in Fig. 8.13. Columns presented show dominant lithology, the grade of Pt+Pd+Au, Cr%, Pt/Pd and Cu/ Pd extracted from PTM's database. In contrast to the previous section, harzburgite thickness and associated PGE grade decreases towards the N and S. PGE units have been omitted.

Analogously to the Platreef, the mineralized harzburgites and feldspathic pyroxenites are interpreted to have been emplaced as sill- or chonolith-like bodies. Cross- and long sections as well as a 3D representation of one of the Super F Zones have been presented in Figs. 8.13, 8.14 and 8.15, respectively. In these figures, it can be seen that where these lithologies are absent, their space is taken up by the otherwise overlying TGA Sequence. This is particularly apparent in Fig. 8.15, where grade is sparse above the basement high in the center of the figure, and increases both to the north and south.

In summary, the lower mineralized zone of the Waterberg Project has been shown to have similarities with the Platreef, however, there are clear differences. Consequently, the Waterberg Project does not simply represent a northern Platreef.

8.7.4. A preliminary model

Any model for the Waterberg Succession must account for the following observations (Kinnaird *et al*., 2014, 2017; Huthmann *et al*., 2016):

- The Waterberg Succession contains a magnetite-bearing gabbroic Upper Zone, a mineralized Troctolite-Gabbronorite-Anorthosite Sequence and a lower, mineralized Ultramafic Sequence of harzburgite and feldspathic pyroxenite.
- The troctolite of the Waterberg Succession is a true plagioclase and olivine cumulate unconformably overlying ultramafic rocks. It is characterized by significant thickness, high-Mg, and the fractionation into olivine norite and later gabbronorite.
- The overall thickness of the Waterberg Succession is approximately 25% of the Northern Lobe, however due to an erosional unconformity an unknown amount of material (several km?) as well as roof rocks of unknown nature have as of yet not been intercepted in drill core.
- The mineralization of the Waterberg T Zone contains approximately 20% Au in the metal budget.
- Based on chemistry, the Aurora Project may represent the southern margin of the Waterberg Succession.
- Despite being hosted by harzburgites rather than pyroxenites, the F Zone mineralization shares certain characteristics with the Platreef. It is Pd-dominated and Au-poor, however, Cr/MgO are dissimilar to the Platreef. The Waterberg's F Zone does not form reefs and mineralization occurs along high-aspect ratio elongated bodies or chonoliths.
- Geochemical results presented show Bushveld-type cumulate signatures.

A simplified model for the evolution of the Waterberg Succession is presented in Fig. 8.17. The magmatic history of the area is believed to have started with finger-like intrusions of marginal

orthopyroxenites intruding into a host rock of granite-gneiss and perhaps overlying sedimentary rocks. Unlike the Northern Lobe, the Waterberg Succession is situated in the Southern Marginal Zone of the Limpopo Belt (van Reenen *et al*., 1987), wedged in between the Hout River and Palala Shear Zones. Given the tectonic setting of the Limpopo Belt, this initial emplacement may have been facilitated either by pre-existing anisotropies related to faulting or perhaps ongoing faulting during the time of emplacement (Schaller *et al*., 1999; Clarke *et al*., 2009; Lightfoot and Evans-Lamswood, 2015). Fig. 8.17 displays the initial stages near a possible basement - cover sequence contact. Whether this is indeed the case is unknown, and depth of emplacement may instead be the depth of neutral buoyancy of the ascending magma.

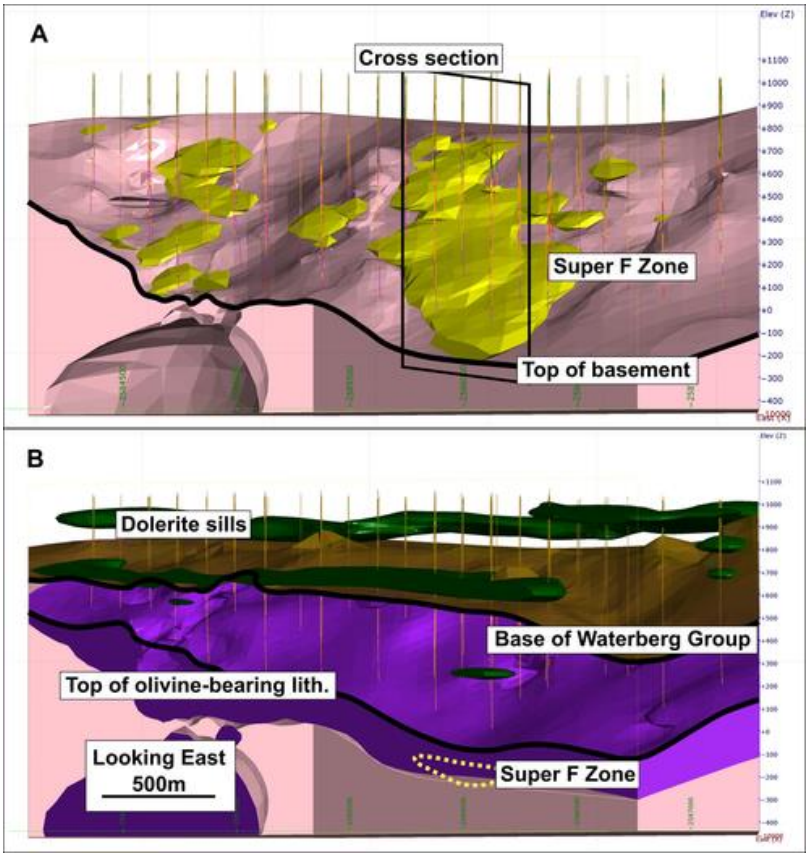

Figure 8.15: Simplified 3D model of the project area. A: Shown is the geometry of the basement and in yellow a >1g/t 3E (Pt+Pd+Au) grade shell. The mineralization envelope has a chonolith-shape and is trending in a NE direction. Also shown is the position of holes studied (Fig. 8.13). B: This panel shows the distribution of the olivine-bearing rocks of the Ultramafic and lower TGA Sequence as logged in PTM's database. The erosional unconformity bringing Waterberg Group sediment in contact with mafic rocks and the dolerite sills are also shown. Note the vertical offset between the two dolerite sheets, perhaps indicating fault control. (For interpretation of the references to color in this figure legend, the reader is referred to the web version of this article).

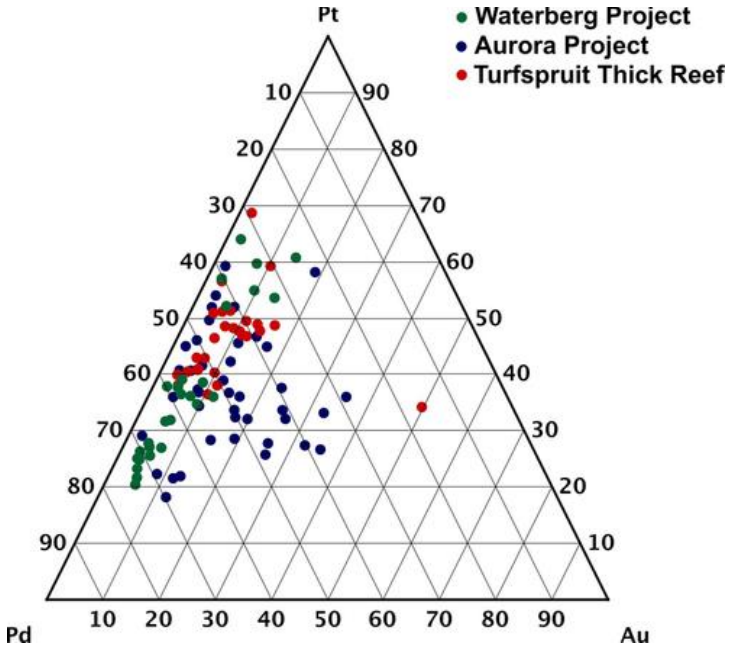

Figure 8.16: Ternary diagram for Pt, Pd and Au displaying data for the Waterberg Project, the Aurora Project (McDonald *et al*., 2017) and Turfspruit (Yudovskaya *et al*., 2017). It can be seen, that Aurora rocks are relatively Au-rich whereas F Zone rocks from the Waterberg Project are Pd-rich.

Given the age and location of the Waterberg Succession (Huthmann *et al*., 2016), the magmas are of course ultimately related to the Bushveld Large Igneous Province.

With increasing magma flux, the magma conduits would experience lateral dilation until eventually forming larger elongated lobes. Maximum liquid flux would be focused on their respective cores, where the crystallization is suppressed due to the high heat flux (Hon *et al*., 1994). These heated zones of weakness could then be utilized by subsequent intrusion of parental crystal-rich liquids for the harzburgites, in the process widening the conduit while assimilating and transporting earlier rocks (Robertson *et al*., 2015). The harzburgites are thought to have acted as the transport medium for sulfide droplets, perhaps remobilizing dense sulfide from some initial staging zone (McDonald *et al*., 2009). Given the tube-like shape of the grade shells and the fairly even distribution of grade throughout the shell, a slumping of sulfides along the basement is not considered viable. Mungall and Brenan (2014) recently demonstrated extremely high partition coefficients of 10^5 to 10^6 for PGE. This means, that the kinetics of the interaction between sulfide liquid and magma and the architecture of the emplacement zone may be more important than large pools of sulfide liquid at depth. The geometry of the emplacement zone, in particular, may be responsible for the substantial thickness and grade of the Super F Zones. The position of the mineralized zones and the distribution of sulfides therein again appears to suggest, that the UmS represents zones of crystallization of the respective carrier liquids, and not a basal accumulation of sulfides. Constant Cu/Pd ratios observed in PTM's assay data suggest one

common PGE reservoir for this particular Super F Zone. The Waterberg Succession has an indicated resource of > 24 million ounces 4E (Pt+Pd+Au+Rh). The deposit is still open at depth.

The reasons for sulfide saturation are only speculative at present. Possible options may be the assimilation of Cr-rich orthopyroxenites or mixing of successive melt fluxes. Given the granite-gneiss basement and the extreme scarcity of xenoliths, sulfide saturation due to sulfur-rich host-rock assimilations appears unlikely and the sulfur source is under investigation. Detailed petrographic analysis of a wide range of thin sections confirms the remobilization of sulfides observed in core and suspected from geochemical data, and hence the original distribution and mineralogy of the ore minerals is uncertain.

Following the emplacement of mineralized harzburgitic lithologies, any subsequent intrusion could utilize the extensive pre-heating of country rocks to form a more laterally extensive sheet of troctolites by thermo-mechanical erosion. This was perhaps assisted by pre-existing anisotropies along a basement sedimentary rock interface. At this point in time, the succession was moving from a stage of finger- like liquid flow and lateral dilation to a stage of sheet-like lobes with sufficient thickness to allow for in-situ fractionation. This ultimately led to the formation of a sequence of troctolites-gabbronorites-magnetite-bearing gabbros and to a transition from heterogeneous to homogeneous flow. It is envisioned, that the formation of troctolitic units was related to the mixing of gabbroic and peridotitic crystal-rich magmas in the feeder zone of the succession (Renna and Tribuzio, 2011; Saper and Liang, 2014). The subsequent in-situ fractionation of gabbroic magmas may have been disturbed by new cryptic influxes of more gabbroic liquids (cf. Tanner *et al*., 2014). Fractionation may have led to rocks comparable to what can be seen in the Upper Zone of the Northern Lobe (Ashwal *et al*., 2005), however, in the Waterberg Project this zone has been eroded. Mineralized harzburgite cores at the base of the troctolite were preserved, and the extensive alteration and sulfide remobilization in the harzburgite may be a sign of continuing heat and fluid flux in the system. The occasional pegmatoidal and vari-textured rocks throughout the succession perhaps attest to this continuing interaction of heat with the footwall.

The exact nature of the connection between Waterberg Project and the aforementioned Aurora Project can only be estimated. Taking into account the occurrence of early orthopyroxenites and later gabbroic lithologies, perhaps both areas were connected intermittently with assimilation of dolomite being locally important at Aurora. Correlation of the two projects might indicate that both of them form a northern, partially or intermittently connected magmatic basin. This basin is internally subdivided by the Hout River and other small shear zones and separated from the south by a basement high south of Aurora (van der Merwe, 1976, 1978, Fig. 2A). The occurrence of magnetitites on the farm Harriet's Wish (but

not found in the project area) and recent Sr isotopic results (Huthmann *et al*., 2017) complicate the situation and require further study.

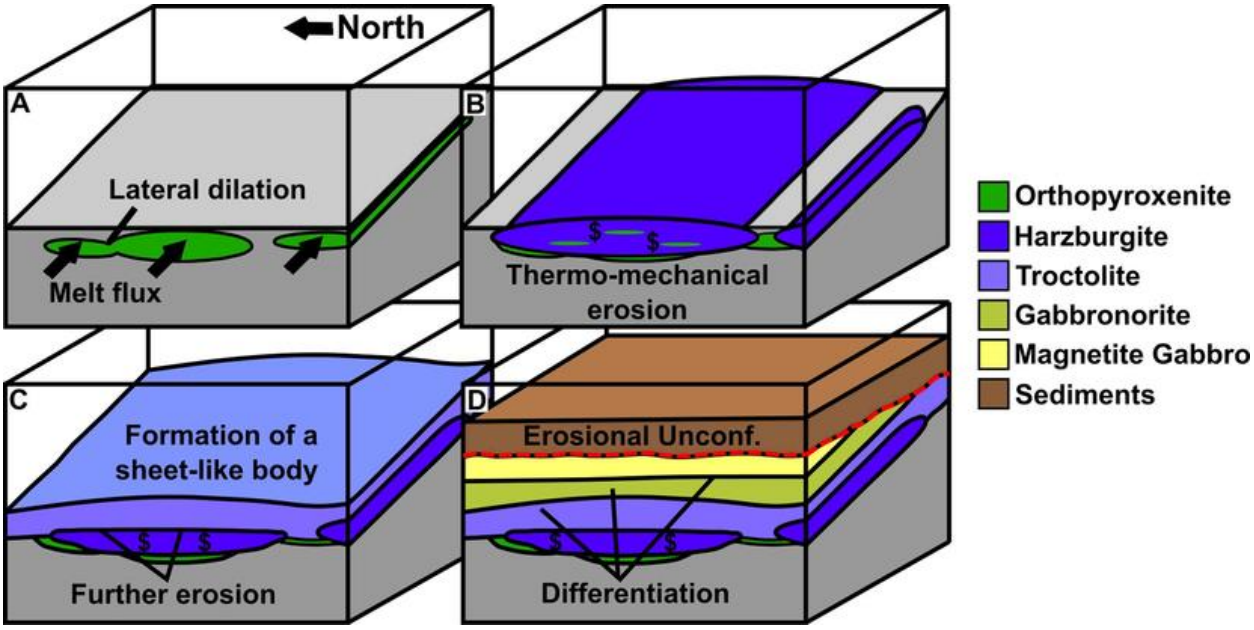

Figure 8.17: Conceptual model for the emplacement of the lower part (excluding the T Zone mineralization) of the Waterberg Succession. A: Emplacement of marginal orthopyroxenites as finger-like elongated bodies. Lateral dilation with continuing magma flow. B: Emplacement of harzburgitic magma and sulfides by thermo- mechanical erosion of earlier intrusive phases and the host rock. C: Emplacement of troctolitic magma, marking the departure from a finger-like geometry and the formation of magma sheets. D: After the emplacement and fractionation of more magma, the area experienced extensive uplift and the deposition of Waterberg Group Sediments on an erosional unconformity.

As a final step, uplift and later subsidence led to an erosional unconformity and the deposition of Waterberg Group Sediments on top of the succession. This step is crucial, as without significant uplift and erosion the succession might have been covered by several kilometers of evolved rocks.

The model presented above requires the intrusion of two distinct magmas during the course of the formation of the Waterberg Succession, one being peridotitic and one gabbroic in character. Given the similarities of the Ultramafic Sequence with the Platreef, it is envisioned that it may have crystallized from a Critical Zone-type magma. How a presumably Cr-rich Critical Zone magma crystallized the overall Cr-poor rocks is not resolved in detail. This does not imply a direct connection of the Waterberg area with either the main Bushveld Complex or the Northern Lobe, but rather refers to the fact that all intrusions belong to the same large igneous province.

8.8. Conclusion

The Waterberg Succession is a truly outstanding and exciting new PGE discovery. It shares features with mining and exploration prospects to the south, while simultaneously exhibiting unique characteristics.

The combination of rock types, type and distribution of the mineralization, and tectonic setting is unique and presented here for the first time. Based on observations and geochemical results, the project area may be linked with the Aurora Project to the south, with both projects possibly representing a separate basin rather than a marginal extension of the Northern Lobe. A first conceptual model for the area has been presented and shows how recent advances in our understanding of partition coefficients, fluid dynamics, and the continued work of colleagues in other parts of the Bushveld lead to a better understanding of this magmatic system.

The conclusion that the Waterberg Succession does not represent a simple strike extension of the Northern Lobe is excellent news for explorers of the Bushveld Complex. It demonstrates, that cooperation of industry and academia can lead to significant discoveries in well-explored terrains. Rather than obstructing deposit formation, structural features and sedimentary sequences may aid by concentrating melt and facilitating later uplift.

Chapter 9

Discussion and Conclusion

9.1. Introduction

This thesis has presented extensive new petrographic, mineralogical and geochemical data for the Waterberg project, an extension of the Bushveld Complex north of the Hout River Shear Zone. These include detailed studies of whole-rock geochemistry, mineral chemistry, platinum-group minerals analyses and sulphur isotope data. The results of the study make important contributions to three main fields of research (i) they have led to improved characterisation and knowledge of the stratigraphy of the Waterberg project and its correlation to the rest of the Bushveld Complex, (ii) they have provided insight and constraints to the emplacement of the magmas and crystallisation history of the Waterberg Bushveld stratigraphy, and (iii) they have provided an insight into the formation/emplacement of the mineralisation associated with the Waterberg Bushveld succession and have shed light on the mantle source of magmatism and mineralisation.

This chapter aims to summarise the findings of the foregoing chapters and to put them into context of the overall study on the Waterberg project area and to develop a genetic model that integrates all the available data.

9.2. Stratigraphic Correlations of the Waterberg Project

The discovery of mineralisation hosted by ultramafic/mafic lithologies in the Waterberg project (Fig. 3.1), initially begged the question as to whether these mineralised rocks were of Bushveld age (Zeh *et al*., 2015), or related to the Great Dyke in Zimbabwe (2575 Ma) (Oberthür *et al*., 2002), or to other Paleoproterozoic intrusions in the Limpopo Mobile Belt such as the Bandelierkop Complex (Kramers *et al*., 2006). Having established that the age of the Waterberg ultramafic/mafic intrusive rocks is coeval with the rest of the Bushveld Complex (Huthmann *et al*., 2016), the challenge was to compare the stratigraphy and mineralisation of the Waterberg project succession with the known stratigraphy of the eastern, western and northern limbs of the Bushveld Complex. There are significant similarities, but also notable differences in terms of stratigraphy, petrology, mineralogy, geochemistry and mineralisation, even with the adjacent northern limb immediately south of the Hout River Shear Zone.

Footwall

The Waterberg project is located north of the Hout River Shear Zone which marks the boundary between the Southern Marginal Zone of the Limpopo Belt and the stable Archean Kaapvaal craton (Smit *et al*., 1992; van Reenen *et al*., 1992). The Southern Marginal Zone is composed of granulite facies granitic gneiss, amphibolitic gneiss and minor quartzite (Goudplaats-Hout River Gneiss) (van Reenen *et al*., 1987; Smit and van Reenen, 1997). Van Reenen *et al*. (1990) interpreted the Southern Marginal Zone to be the high grade metamorphic equivalent to the adjacent granitoid-greenstone assemblage associated with the northern portion of the Kaapvaal Craton. Although, >90 % of the boreholes drilled on the Waterberg project have intercepted an intermingling zone, where the initial Bushveld magmas interacted with the granitic gneiss footwall locally termed a granofels (Fig. 4.6) and <10% of the boreholes go directly into granite-gneisses of the Southern Marginal Zone. These lithologies comprise pyroxenitic/gabbroic fragments within a granitic matrix. Similar lithologies have been intercepted on the farms Overysel and Drenthe where the Platreef magma interacts with the Archean basement (Cawthorn *et al*., 1985; Barton *et al*., 1986; Holwell and McDonald, 2006). Similar rock types have also been identified on Sandsloot and Overysel and can be distinguished visually from granofels by sharp contacts between mafic and felsic rich layers (Manenzhe, 2006).

Ultramafic Sequence (UmS)

The UmS overlies the granofels and Marginal sills and is dominated by orthopyroxenite and harzburgite (Fig. 4.7). These ultramafic lithologies are typical constituents of the Basal Ultramafic sequence (Wilson, 2015) of the Lower and Critical Zone elsewhere in the Bushveld Complex (Cameron, 1978; Teigler, 1990; Teigler and Eales, 1996). Interstitial plagioclase in the UmS commonly exceeds 10 to 15 vol. %, which is higher than the average plagioclase proportions associated with the Basal Ultramafic Sequence in the Clapham section in the eastern Bushveld Complex (2 - 10 vol. %, Wilson, 2015), and the Lower Zone (2 - 6 vol. %, Cameron, 1978; Lee and Tredoux, 1986; Teigler, 1990). The proportions of plagioclase are more comparable with the Critical Zone and the Platreef. The harzburgite units associated with the UmS commonly have a poikilitic texture, which differs from the granular harzburgite of the Lower Zone at Grasvally (Hulbert and von Gruenewaldt, 1985), at Clapham (Wilson, 2012) and at Turfspruit (Yudovskaya *et al*., 2013). Intervals with elongated harristic olivine up to 2-3 cm long with relics of corroded chromite (20-1000 µm) in interstitial plagioclase were observed in parts of the harzburgite/mela-troctolite units of the UmS. Similar features are seen in the Basal Ultramafic Sequence in the Clapham section of the eastern Bushveld Complex (Wilson, 2012) and in other layered ultramafic/mafic intrusions e.g. the Rum and Muskox intrusions (Brown, 1956; Wager and Brown, 1968; Irvine, 1970). Kink bands and chromite-pyroxenite lamellae are a common feature of the Lower Zone (Wilson, 2012; Yudovskaya *et al*., 2013), which

were not observed in the olivine-rich units of the UmS. The multi-element chondrite-normalised plots of the UmS lithologies show similar trends as the Lower Zone pyroxenites beneath the Platreef on Turfspruit which show a negative Nb-Ta anomaly, a variable negative Ti anomaly and a gently sloped Y and HREE pattern (Fig. 4.21). The Mg# of olivine associated with the Lower Zone lithologies in Turfspruit, Grasvally and Clapham section have some of the highest values (Mg# 84-91 olivine) ever recorded in the Bushveld Complex (Hulbert, 1983; Wilson, 2012; Yudovskaya *et al*., 2013), these values are also significantly higher than the UmS with an average forsterite value of Fo_{82}.

The laminar fabric of preferred elongated orthopyroxene that is considered to be a typomorphic feature of the Lower Zone pyroxenite (Boorman *et al*., 2004) is not observed in the pyroxenites of the UmS. The Mg# of orthopyroxene is generally higher (Mg# 78-91 of orthopyroxene) in the Lower Zone lithologies of Sandsloot and Turfspruit (Yudovskaya *et al*., 2013), which is similar to the values obtained in the Grasvally and Clapham section (Hulbert, 1983; Wilson, 2012). These orthopyroxene values are also more primitive than values elsewhere in the Lower Zone of the eastern and western limbs of the Bushveld Complex. The orthopyroxene hosted in the UmS have Mg# of between 76 and 87 with an average of 82 which are lower than the Lower Zone values. The Lower Zone on the farms Sandsloot, Grasvally and Clapham section hosts regular chromitite seams with sharp boundaries (Hulbert and von Gruenewaldt, 1985; Wilson, 2015; Yudovskaya *et al*., 2013) and the chromite in the Lower Zone generally makes up <1 modal % elsewhere in the Bushveld Complex (Maier *et al*., 2013). Chromitites are a rare occurrence in the UmS of the Waterberg project. Furthermore, the Lower Zone is not known for high grade PGE mineralisation apart from at Grasvally (Hulbert and von Gruenewaldt, 1982), whereas the UmS in the Waterberg project hosts a thick package of PGE mineralisation (F zone). Therefore, it is highly unlikely that the UmS of the Waterberg project is an equivalent of the Lower Zone seen in the rest of the Bushveld Complex.

When comparing the UmS with the upper Critical Zone and the Platreef there are some significant similarities. The upper Critical Zone is known for its spectacular layering which is not observed in the UmS of the Waterberg project which is more similar to the Platreef. The Critical Zone in the eastern and western limbs of the Bushveld Complex hosts several chromitite layers (Hatton and von Gruenewaldt, 1987; Eales and Cawthorn, 1996). However, the chromite in the UmS concentrates into bands of disseminated grains (up to 75% chromite) with irregular diffuse outlines similar to the Platreef chromitites in the northern limb of the Bushveld Complex as described by Yudovskaya and Kinnaird (2010). Chromite grains are found throughout the UmS, although generally the highest concentrations are associated with the harzburgite units and the orthopyroxenite xenolith hosted in the harzburgite units. The chemical compositions of the most primitive olivine and chromite

analysed are consistent with the Critical Zone lineage as Fo in olivine varies from 74 to 89 and the Cr_2O_3 content in chromite has a maximum of 0.49 wt. %, although generally less than 0.32 wt. %.

The lower Critical Zone of the eastern and western limb is predominantly orthopyroxenite, up to 89% (Teigler and Eales, 1996), which is similar to the basal orthopyroxenite of the UmS. Harzburgitic rocks also occur in the lower Critical Zone (Cameron, 1982). However, numerous chromitite layers occur in the lower Critical Zone (Cousins and Feringa, 1964; Teigler *et al*., 1992; Crowson, 2001) which are not observed in the UmS of the Waterberg project. The upper Critical Zone is composed of layers of orthopyroxenite (70%), norite (25%) and anorthosite (5%) with a number of chromitite layers (Teigler and Eales, 1996; Maier *et al*., 2005). These lithologies are very different from those observed in the UmS. The Critical Zone is stratigraphically in the middle of the Rustenburg Layered Suite (Eales and Cawthorn, 1996), whereas the UmS is in contact with the footwall lithologies on the Waterberg project.

The Platreef is the basal part of the Rustenburg Layered Suite in the northern limb in contact with different footwall lithologies along strike (van der Merwe, 1976). Although in recent years thick succession of ultramafic lithologies have been discovered beneath the Platreef in certain localities, they have been correlated with the Lower Zone (Yudovskaya *et al*., 2013). The Platreef is dominated by feldspathic pyroxenite (Armitage *et al*., 2002; Kinnaird *et al*., 2005; Nex *et al*., 2006; Holwell and McDonald, 2006), and down dip of the Platreef, more olivine-rich lithologies have been intercepted on the farms Akanani, Sandsloot and Turfspruit (Fig. 3.1), where the Platreef is composed of feldspathic pyroxenite, pyroxenite, feldspathic harzburgite, harzburgite and minor norite and gabbronorite (Yudovskaya *et al*., 2011; Mitchell and Scoon, 2012). Yudovskaya *et al*. (2011) indicate that the feldspathic pyroxenite consists of cumulus orthopyroxene, with up to 90 modal %, and the harzburgite has a poikilitic texture and may be plagioclase free, as well as been highly serpentinised, which are similar features seen in the UmS.

The orthopyroxene compositions associated with the UmS, show similarities to the orthopyroxenes analysed for the Platreef and the Critical Zone of the eastern and western limbs of the Bushveld Complex. The Mg# of orthopyroxenes for the UmS is between 78 and 86 which are similar to Mg# values obtained for certain localities in the Platreef and the Critical Zone (Table 9.1). The Cr content in the orthopyroxene of the UmS is highest associated with the harzburgite units (up to 4300 ppm), which are similar to the Cr values in orthopyroxene on the farms Akanani, Sandsloot and Turfspruit, associated with harzburgitic rocks of the down dip Platreef (Yudovskaya *et al*., 2011; 2013). More commonly, the Cr content in orthopyroxene is on average 2400 ppm, which is similar to the Critical Zone and the Platreef (Table 9.1). The MnO content of orthopyroxene associated with the UmS is

lower than the other ultramafic/mafic intervals in the northern limb (Aurora Unit 1 and the Troctolite Horizon), although is comparable with the Platreef and Critical Zone (Table 9.1). In terms of mineral chemistry the UmS shows some significant similarities with the Platreef.

Table 9.1: Compilation of available orthopyroxene compositional data from the ultramafic/mafic intervals including the Platreef in the northern limb and the Critical Zone of the eastern and western limbs of the Bushveld Complex.

Location	Mg# (opx)	Cr (ppm) (opx)	MnO (wt. %)	Source of Data
Waterberg project UmS	78-86	1200-4300	0.13-0.22	This Study
Aurora project Unit 1	70-79	1980-2600	0.30-0.44	McDonald *et al*., 2017
Troctolite Horizon BV	76-79	205-3200	0.23-0.40	Ashwal *et al*., 2005
Platreef				
Townland	68-82	700-2000	0.18-0.32	Manyeruke *et al*., 2005
Turfspruit	66-76	-	-	Mothetha, 2006
	64-83	-	-	Haufiku, 2005
	80-81	2100-3000	0.25-0.28	Yudovskaya *et al*., 2013
Tweefontein Hill	73-81	-	-	Nyama *et al*., 2005
	74-78	680-3200	0.23-0.29	Buchanan *et al*., 1981
Sandsloot	76-83	3000-3700	0.22-0.28	Harris and Chaumba, 2001
	74-78	-	-	Holwell *et al*., 2005
	76-80	-	-	McDonald *et al*., 2005
	72-83	-	-	Pronost *et al*., 2008
	78-86	2100-4000	0.20-0.31	Yudovskaya *et al*., 2013
Akanani (down dip Platreef)	77-86	110-4680	0.22-0.32	Yudovskaya *et al*., 2011
Overysel	71-77	200-1800	0.21-0.34	Cawthorn *et al*., 1985
Drenthe	60-74	-	-	Gain and Mostert, 1982
Moordkopje (MO-1)	77-83	1800-3800	0.23-0.30	Roelofse and Ashwal, 2012
GNPA member	63-83	270-3100	0.20-0.43	Smith, 2014
MANO unit	63-74	270-2800	0.27-0.43	Smith, 2014
LMF unit	66-83	820-3100	0.20-.40	Smith, 2014
Eastern Limb				
Lower Critical Zone	81-85	-	-	Cameron, 1980; 1982
Upper Critical Zone	77	-	-	Cameron, 1980; 1963
Upper Critical Zone	75-83	-	-	Teigler and Eales, 1996
Western Limb				
Upper Critical Zone	74-77	350-1800	0.18-0.33	Maier and Teigler, 1995
Upper Critical Zone	71-81	1400-3100	-	Maier and Eales, 1997

Immediately south of the Hout River Shear Zone on the Harriet's wish and Aurora section (Fig. 3.1) of the northern limb, an ultramafic/mafic succession was discovered at the base of the intrusion in contact with the granitic footwall or fine-grained norite and gabbronorite (Manyeruke, 2007; McDonald *et al*., 2017). Notably, this occurs in a similar setting to the UmS on the Waterberg project just north of the Hout River Shear Zone. This ultramafic/mafic succession on the Aurora project was termed Unit 1 by McDonald *et al*. (2017) and is composed of orthopyroxenite, websterite and melagabbronorite, which is similar to the basal orthopyroxenite interval of the UmS. However, according to McDonald *et al*. (2017), olivine is a minor phase (<10 modal %) in Unit 1 which is

significantly different to the olivine-rich intervals of the UmS of the Waterberg project. Both the UmS on the Waterberg project and Unit 1 on Aurora project host PGE mineralisation.

McDonald *et al*. (2017) proposed that Unit 1 and the UmS may form part of a northern extension of the Troctolite Horizon in the northern limb first described by van der Merwe, (1978). Based on orthopyroxene compositions, Unit 1 and the Troctolite Horizon show significant similarities in terms of Mg#, Cr (ppm) and MnO (wt. %) contents (Ashwal *et al*., 2005; Tanner *et al*., 2014; McDonald *et al*., 2017) (Table 9.1). However, the orthopyroxene compositions of the UmS are more primitive and the Cr contents are significantly higher, the MnO (wt. %) is much lower, than the values obtained for Unit 1 and the Troctolite Horizon. Ashwal *et al*. (2005) and Tanner *et al*. (2014) didn't mention any sulphide or PGE mineralisation associated with the Troctolite Horizon in the Bellevue drill-core, although Tanner *et al*. (2014) indicated the potential for PGE mineralisation based on elevated Cr concentrations associated with pyroxenite layers directly above the Troctolite Horizon.

A major difference between the UmS of the Waterberg project and other ultramafic/mafic successions in the northern limb is the absence of calc-silicate or hornfels xenoliths and dolomitic rafts in the UmS. In the southern sector of the Platreef, fine-grained hornfels xenoliths are common (Kinnaird and Nex, 2015), and in the central sector calc-silicate, anhydrite and parapyroxenites are common hybrid rocks (Wagner, 1929; Nex *et al*., 2006; King, 2009). In the northern sector there are granitic xenoliths and dolomitic rafts (Kinnaird and Nex, 2015). In the far north on the Aurora project, McDonald *et al*. (2017) report calc-silicates up to 6 m thick in the ultramafic/mafic rocks of Unit 1. Thus far only one calc-silicate (<1 m thick) has been identified in borehole WB027 within the basal Marginal sills below the UmS on the Waterberg project.

In summary, the UmS in the Waterberg project area shares some similarities with mafic/ultramafic rock units in other parts of the Bushveld Complex, however, the general set-up and mineral-chemical details of the UmS are distinctly different from comparable units elsewhere in the Bushveld Complex.

Troctolite-Gabbronorite-Anorthosite (TGA) sequence

The TGA sequence is composed of an unmineralised troctolite at the base, grading upwards into olivine-bearing norite or gabbronorite. Upwards the sequence grades into a thick succession of gabbronorite and gabbro with minor anorthosite layers in the middle and at the top of the TGA sequence (Fig. 4.8). Originally the basal troctolite unit of the TGA sequence on the Waterberg project was thought to represent the troctolite in the Main Zone of the northern limb, identified by van der Merwe (1976) and observed in the Bellevue drill core (Ashwal *et al*., 2005; Tanner *et al*., 2014). Both

have high magnetic susceptibility values, a result of the presence of secondary magnetite which formed from the alteration of olivine (Figs. 4.10 and 6.2). However, there are differences in the chondrite-normalised multi-element signatures (Table 9.2), and some lithologic, mineralogical and geochemical contrasts. According to Ashwal *et al*. (2005), the troctolite horizon is mainly composed of olivine-norite, gabbro, and gabbronorite with minor leucocratic varieties and pyroxenite layers, rather than being a true troctolite. The troctolite horizon in the Bellevue drill core has an average modal abundance of 21.1 % olivine which decrease irregularly upwards (Ashwal *et al*., 2005). In contrast, the troctolite unit in the Waterberg stratigraphy is composed of cumulus feldspar (35 to 55 modal %) and olivine (25 to 65 modal %), with interlayers or xenoliths of medium-grained pyroxenite or feldspathic pyroxenite (cumulus orthopyroxene and clinopyroxene with minor interstitial plagioclase). In the troctolite unit at the base of the TGA sequence, olivine decreases irregularly in Fo content upwards from ~Fo_{78-80} in true troctolite to ~Fo_{75-76} in more olivine-noritic rocks and the NiO content in olivine also decreases upwards from 0.27 to 0.23 wt.%. Similar features are observed in the troctolite horizon of the Bellevue drill-core (Ashwal *et al*., 2005), although the values are more primitive associated with the troctolite unit in the Waterberg stratigraphy. The orthopyroxene compositions in the troctolite unit of the TGA are similar to the Troctolite Horizon although more primitive values occur at the contact between the UmS and TGA sequence on the Waterberg project. The Cr content of orthopyroxene associated with the troctolite unit in the TGA is much higher that the values obtained for the Troctolite Horizon (Ashwal *et al*., 2005). The average Cr content of orthopyroxene is ~3100 ppm, whereas the Cr content ranges between 200 and 2800 ppm for the Troctolite Horizon in the Bellevue drill-core (Ashwal *et al*., 2005; Tanner *et al*., 2014).

Table 9.2: Compositional comparisons and contrasts between the mantle normalised multi-element variations of the Waterberg TGA sequence (troctolite), the Troctolite Horizon in the Bellevue drill core and the Platreef on Sandsloot, Zwartfontein and Overysel (data from Jones, 2013; Kinnaird *et al*., 2015).

Waterberg TGA sequence troctolite and pyroxenite	**Troctolite Horizon (Main Zone) Bellevue drill-core**	**Platreef Sandsloot to Overysel**
Little to no Nb-Ta anomaly	Nb-Ta anomaly	Little to no Nb-Ta anomaly
Absence of Ti anomaly	Negavite Ti anomaly	Absence of Ti anomaly
Strongly upward sloped of Y and HREE	Generally flat Y and HREE	Generally flat Y and HREE

Above the troctolite unit, the TGA sequence of the Waterberg stratigraphy is dominated by medium- to coarse-grained gabbronorite, norite and gabbro with minor layers of anorthosite, feldspathic pyroxenite, pyroxenite and pegmatoidal units. This sequence of mainly gabbroic rocks is characterised by higher Al, Sr, and low Cr concentrations compared to the underlying UmS and troctolite unit. There are also sporadic occurrences of inverted pigeonite and an overlying magnetite-bearing zone, as well as Cr/MgO ratios of less than 80 (Fig. 4.15). There is also a general

fractionating trend upwards (Fig 6.8). All these parameter are characteristic of the Main Zone rocks elsewhere in the Bushveld Complex (Nex *et al*., 1998; Nex *et al*., 2002; Seabrook *et al*., 2005). However, notable contrasts do also exist. The Main Zone in the western limb of the Bushveld Complex is ~2200 m thick (Mitchell, 1990), reaches ~3940 m in the eastern limb (von Gruenewaldt, 1973), and it is ~3110 m thick in the northern limb (Ashwal *et al*., 2005; Roelofse and Ashwal, 2012). The maximum thickness of the TGA sequence in the Waterberg area is ~850 m (Fig. 9.1). The mineral chemistry is also significantly more primitive in the TGA sequence ($Mg\#_{opx}$ 83-67 decreasing irregularly upwards) compared to the Main Zone in the Bellevue drill-core ($Mg\#_{opx}$ 77-53 decreasing upwards), although this may be directly associated with the thickness of the package as there would be less prolonged fractionation.

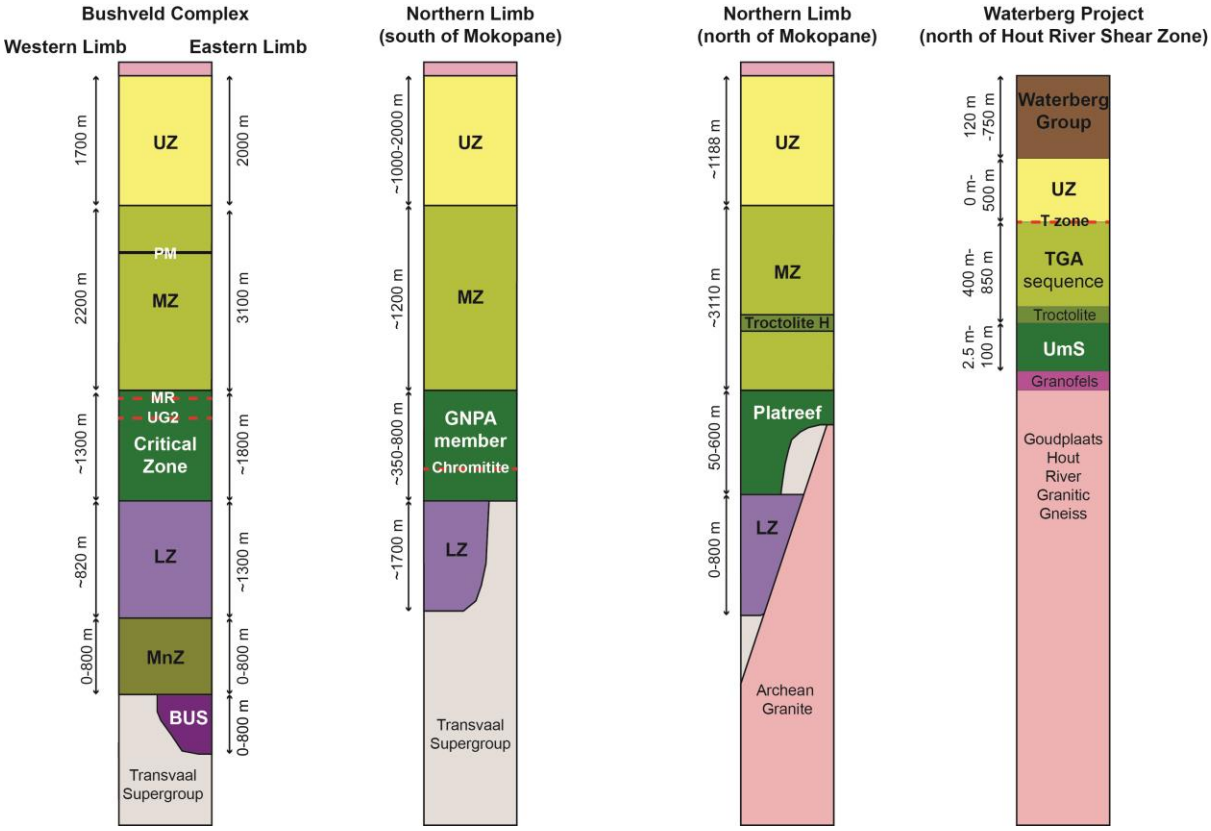

Figure 9.1: A schematic diagram of the differences and similarities in the magmatic stratigraphy across the Bushveld Complex. (Data from von Gruenewaldt, 1973; Molyneux, 1974; Cameron, 1978; Hulbert, 1983; Hulbert and von Gruenewaldt, 1985; Mitchell, 1990; Teigler *et al*., 1992; Eales and Cawthorn, 1996; Ashwal *et al*., 2005; Kinnaird *et al*., 2005; Cawthorn *et al*., 2006; Maier and Barnes, 2010; Yudovskaya *et al*., 2011; Roelofse and Ashwal, 2012; Smith, 2014; Wilson, 2015).

Within the Main Zone of the eastern and western limbs of the Bushveld Complex, a distinctive Pyroxenite Marker subdivides the Main Zone into the upper and lower Main Zone (von Gruenewaldt, 1973; Klemm *et al*., 1985; Cawthorn *et al*., 1991; Nex *et al*., 2002; Ashwal *et al*., 2005). Kruger (1990; 1994) proposed that the Pyroxenite Marker marks the first influx of Upper Zone magma based on isotopic grounds, although most authors take the boundary between the Main and Upper Zone at

the first appearance of cumulus magnetite (SACS, 1980; Eales and Cawthorn, 1996). The Main Zone of the Bellevue drill-core hosts two distinct pyroxenite-rich layers (Knoper and von Gruenewaldt, 1992; Ashwal *et al*., 2005). One of these pyroxenite layers occurs at the same stratigraphic position as the Pyroxenite Marker described by Cawthorn *et al*. (1991) in the eastern and western limbs of the Bushveld Complex, although Ashwal *et al*. (2005) did not equate this pyroxenite layer to the Pyroxenite Marker based on mineralogical contrasts (inverted pigeonite 80 modal %) and the lack of a significant Mg# reversal (von Gruenewaldt, 1973; Klemm *et al*., 1985; Cawthorn *et al*., 1991; Kruger, 1990; Nex *et al*., 2002; Ashwal *et al*., 2005). There are no significant pyroxenite layers in the TGA sequence (only thin layers that are discontinuous) and they are not observed in all borehole cores of the Waterberg project. A major difference between the Main Zone of the northern limb and the rest of the complex, compared with the TGA sequence, is the presence of a mineralised interval at the top of the succession in contact with the Upper Zone, which will be discussed in more detail below.

The boundary between the Main and Upper Zone of the eastern and western limbs of the Bushveld Complex is based on different approaches. Mineralogically, the boundary is defined by the first appearance of cumulus magnetite and is generally the most accepted boundary (Molyneux, 1974; SASC, 1980). Kruger (1990; 1994) places the boundary at the orthopyroxene-bearing Pyroxenite Marker due to the results of initial Sr isotope ratios, which is interpreted as a major influx of new magma. In the western Bushveld, in the Marikana area, the boundary may be positioned where there is a new magma influx ~100 m below the Pyroxenite Marker based on whole-rock major element and mineral data (Nex *et al*., 2002). However, the trace element data suggests a new influx of magma occurs ~130 to ~150 m below the Pyroxenite Marker depending on the trace element used (Nex *et al*., 2002). In the eastern limb south of Roosenekal, Klemm *et al*. (1985) also suggested that the influx of new magma was below the Pyroxenite Marker.

In the northern limb, Ashwal *et al*. (2005) defined the boundary between the Main and Upper Zone in the Bellevue drill core based on changes in magnetic susceptibility. Through the Main Zone cumulate sequence, magnetic susceptibility values are generally low between 0.02 and 0.05 SI units, whereas the Upper Zone has higher values up to 5.00 SI units (Ashwal *et al*., 2005). The boundary between the TGA sequence and Upper Zone in the Waterberg cores is determined by the appearance of fine-grained cumulus magnetite equivalent to the rest of the Main – Upper Zone boundaries in the Bushveld Complex (SASC, 1980). The magnetite is fine-grained and not easily identified in core and therefore, the boundary is identified based on magnetic susceptibility (Figs.

4.10 and 6.2) adopted from the work of Ashwal *et al*. (2005) on the Bellevue drill-core. The boundary between the TGA sequence and the Upper Zone in the Waterberg stratigraphy occurs within the upper T mineralised zone, where disseminated cumulus magnetite is responsible for the high values obtained in the magnetic susceptibility measurements. At this boundary also marks a change in geochemistry, interpreted to represent a new influx of magma with magnetite on the liquidus mixing with the evolved resident magma of the TGA sequence (Figs. 6.5, 6.6 and 6.8).

Upper Zone

The Upper Zone of the Waterberg stratigraphy is dominated by magnetite gabbro and gabbronorite with rare ferrogabbro at the top (Fig. 4.9a) and ranges from 0 to 500 m thick (Fig. 9.1). The Upper Zone in the Bellevue drill core is ~1188 m thick and is composed of magnetite gabbro (41.1%), olivine ferrodiorite (21.4%), and minor gabbronorite, magnetite-bearing plagioclase cumulus rocks and pyroxenites with 32 magnetitite layers (Ashwal *et al*., 2005). The Upper Zone in the eastern and western limbs is approximately 2000 m thick and contains 26 magnetitite layers (Molyneux, 1970; 1974; von Gruenewaldt *et al*., 1985; von Gruenewaldt, 1993; Cawthorn *et al*., 2006; Tegner *et al*., 2006; Fischer *et al*., 2016).

The Upper Zone in the Waterberg stratigraphy lacks the typical magnetitite layers found in the rest of the Upper Zone succession of the Bushveld Complex. Only one borehole (WB001) in the far south of the project area intercepted a 2.5 m thick magnetite layer (Fig. 4.9b), however, this borehole is located south of the Hout River Shear Zone. All boreholes drilled north of the Hout River Shear Zone have no magnetite layers. The widespread occurrence of disseminated cumulus magnetite has led to equating this unit with the Upper Zone in the rest of the Bushveld Complex.

The Upper Zone of the Bellevue drill-core shows plagioclase compositions from An_{69} to An_{36} with a general decreasing upward trend (Ashwal *et al*., 2005; Cawthorn and Ashwal, 2009). Similar trends are seen in the Upper Zone of the eastern and western limbs where plagioclase compositions range from An_{70} to An_{40} (von Gruenewaldt, 1973; Molyneux, 1974; Eales and Cawthorn, 1996). The plagioclase compositions are more primitive within the Upper Zone of the Waterberg stratigraphy, with values ranging from An_{78} to An_{67} with no uniform or regular tend (Fig. 6.7) (Huthmann *et al*., in press). Another significant difference is the absence of anorthosite layers in the Upper Zone of the Waterberg stratigraphy compared with the Upper Zone elsewhere (Ashwal *et al*., 2005; von Gruenewaldt, 1973; Molyneux, 1974; Eales and Cawthorn, 1996). The orthopyroxene compositions within the Upper Zone of the Bellevue drill-core show a similar upward fractionation trend from Mg_{72} to Mg_{26} (Ashwal *et al*., 2005), while the Mg# values of orthopyroxene in the Upper Zone of the

Waterberg stratigraphy range from Mg_{63} to Mg_{77} with no uniform trend. The primitive mineral chemistry of the Upper Zone in the Waterberg stratigraphy is probably related to the thickness of the package as prolonged fractionation was limited and the lack of magnetite layers, in spite of the occurrence of abundant disseminated cumulus magnetite, may be related to the dynamic magma movement so that magnetite could not settle to form magnetite layers as seen in the rest of the Bushveld Complex.

A borehole (NP1) drilled on the farm non-Parella (350LR) within the Seshego District, north-west of the Waterberg project, also north of the Hout River Shear Zone, intercepted a thick (>1100 m) succession of Upper Zone lithologies beneath the Waterberg sediments. Here the Upper Zone also lacks magnetitite layers, although magnetite occurs as fine-grained disseminated cumulus grains or veinlets. The Upper Zone in NP1 is composed of fine- to medium-grained gabbro, olivine gabbro and gabbronorite with minor anorthosite layers. This succession of Upper Zone lithologies shows some similar features to the Upper Zone is the Waterberg stratigraphy, although NP1 also has differences such as the thickness, anorthosite layers and abundance of olivine-bearing lithologies.

The Upper Zone in the eastern and western limbs of the Bushveld Complex is subdivided into three subzones based on the appearance of indicator minerals (magnetite - subzone A; olivine – subzone B; apatite – subzone C) (Wager and Brown, 1968; SASC, 1980), each subzone also has several magnetitite layers. These subzones have also been recognised in the northern and southern limbs of the complex (van der Merwe, 1976; Buchanan, 1975; Ashwal *et al*., 2005). Only one subzone has been recognised in the Upper Zone of the Waterberg stratigraphy, which is based on the appearance of cumulus magnetite, although it lacks the magnetitite layers. Two boreholes (WB017 and WB125) have intercepted olivine-rich intervals at the top of the Upper Zone. The Upper Zone in the rest of the Bushveld Complex hosts the most evolved rocks at the top of the sequence such as quartz monzonite with up to 65 wt.% SiO_2 (Cawthorn, 2013). Such evolved rocks are absent from the Waterberg stratigraphy. The relatively unevolved chemical composition and coarse-grained texture of the Upper Zone magnetite-gabbro in the Waterberg stratigraphy suggests that significant erosion of the Upper Zone may have occurred with at least 1 km of roof rocks and Upper Zone removed before the deposition of the overlying Waterberg sediments.

Hanging wall

Towards the top of the ultramafic/mafic Waterberg succession, the gabbroic rocks are completely or partially altered and mainly composed of epidote, chlorite and hematite. The hematite concentrations increase upwards. The top contact of the ultramafic/mafic succession is complex. While often very sharp and mylonitised, it is commonly marked by a hematite-rich siltstone or less commonly by a prominent fine-grained white-grey tuffaceous layer at the contact (Fig. 4.5). The contact between the haematised siltstone layer and the overlying Waterberg sediments is represented by a sharp angular unconformity (Fig. 4.5). The hematitised siltstone is generally <10 m thick and composed mainly of up to 70% hematite with a fine-grained matrix composed mostly of silica and phengite (K dominant) particles with subordinate chlorite and gibbsite (Yudovskaya *et al*., 2015). Numerous relics of the mafic minerals, replaced by secondary assemblages, indicate that the lower part of the hematitised siltstone may represent a paleosol that developed on the weathered Bushveld gabbros. In some cores, the upper part of this layer is white-grey in colour and lacks the mafic silicate pseudomorphs and hosts multiple fractured quartz clasts. This layer is richer in silica (up to 72 wt. % SiO_2) and potassium compared with the underlying paleosol. The mineral composition of the matrix is similar to that of the hematitised paleosol, although hematite and ilmenite are less abundant and accessory fluorite, apatite, monazite, dumortierite, Al-Si chlorides and fluorides are more common (Yudovskaya *et al*., 2015). The fractured quartz porphyroclasts, K-dominant mica compositions, coarse zircon intergrown with quartz and low Ti content are different when compared with the gabbroic paleosol origin. This discontinuous layer has been interpreted as pyroclastic or tuffaceous in origin which may likely represent the original roof rocks into which the Waterberg igneous rocks were intruded.

In the Waterberg project area, the Waterberg group sedimentary sequence unconformably caps the eroded Bushveld rocks whereas south of the Hout River Shear Zone there is a thick differentiated granite sheet capping the Upper Zone lithologies (van der Mewer, 1978; Ashwal *et al*., 2005). The oldest formations of the Waterberg Group are confined to the central Bushveld Complex, which preserved the granitic roof rocks of the central Bushveld. Further deposition of sediments migrated northwards over time (Dorland *et al*., 2006). If we accept the argument by Dorland *et al*. (2006) that the preserved felsic rocks below the lower Swaershoek Formation of the Waterberg Group in the central Bushveld have not experienced much erosion and deformation, then serval kilometres of roof rock and Upper Zone have been eroded north of the Hout River Shear Zone (Schweitzer *et al*., 1995; Lenhardt and Eriksson, 2012; Yudovskaya *et al*., 2015; Huthmann *et al*., 2016).

The Setlaole Formation forms the base on the Waterberg Group in the Waterberg project area, which generally unconformably overlies eroded Upper Zone lithologies. However, in parts of the project area, the sedimentary rocks may unconformably overlie eroded TGA sequence or UmS depending of the level of erosion. The Setlaole Formation is interpreted to be the third sequence within the sedimentary Waterberg Group (Martini, 1998; Dorland *et al*., 2006). This formation consists of medium- to coarse-grained granule-rich red bed arenite, medium-grained dark brown, banded arkose, very fine-grained chocolate-brown mudstone and purple shales, with a poorly sorted coarse-grained pebble conglomerate at the base (Fig. 4.3). Thus far, no Bushveld igneous fragments have been found in the lithic clasts.

The Setlaole Formation shows a number of upward-fining channels in the succession, and reaches a maximum thickness of 450 m in the project area. This formation is interpreted to have formed as a proximal fluvial facies deposited on a narrow braid plain (Jansen, 1976; 1982; Callaghan *et al*, 1991), with evidence of channel flows and cross-trough bedding in drill core. Zircons found in the basal conglomerate of the Setlaole Formation gave a maximum age of deposition of ca. 2045 Ma (Huthmann *et al*., 2016). The abundance of zircons of Archean age in the samples may indicate that the Limpopo belt to the north was the source for some of the early sediments, which is consistent with the paleocurrent directions (Barker *et al*., 2006), while the Paleoproterozoic zircon ages are interpreted to have derived from the now eroded roof rocks of the Waterberg intrusion.

The Setlaole Formation is unconformably overlain by the Makgabeng Formation in the project area. This Formation is composed of fine- to medium-grained pale-red banded sandstones that are generally horizontal (Fig. 4.3d). There is evidence of a former fluvial system at the base of the Formation, although dunes occur higher up in the formation and desiccation cracks indicate interdune and localised playa lake deposits (Eriksson *et al*., 2000).

Dolerite sill

A major dolerite sill, up to 200 m (WE027) but typically ~80 m thick, occurs in most drill cores of the Waterberg project. It has distinctive chilled margins on both contacts. The dolerite sill is the youngest unit in the Waterberg stratigraphy which cross-cuts the cores at different levels although it is usually intercepted within the lower sedimentary units. U-Pb age dating of baddeleyite extracted from the dolerite sill within the Mogalakwena Formation yielded ages of 1.92 – 1.87 Ga (Hanson *et al*., 2004). A recent U-Pb age of baddeleyite extracted from the dolerite sill on the Waterberg project is 1125 ± 5 Ma (Huthmann *et al*., 2016). The latter age indicates that the dolerite sill is related to the Umkondo Igneous Province (Munyanyiwa, 1999; Hanson *et al*., 2004; Bullen *et al*., 2012).

Dorland *et al*. (2006) determined U-Pb zircon ages of 2054 ± 4 Ma and 2051 ± 8 Ma from lavas close to the base of the Waterberg Group in the Rust de Winter area and suggested that the Waterberg sediments were deposited immediately or even concurrently with the Rustenburg Layered Suite emplacement. Huthmann *et al*. (2016) obtained a 2056 ± 6 Ma age from detrital zircons at the base of the Waterberg sediments in the Waterberg project area. However, based on the identification of gibbsite in the upper hematite-rich siltstone layer in the Waterberg project area, it is interpreted that a paleosol formed on weathered Bushveld rocks in a tropical climate before the deposition of the Waterberg sediments (Yudovskaya and Kinnaird, 2013; Yudovskaya *et al*., 2015). Therefore, the Setlaole and Makgabeng Formations were deposited between ~2.05 and ~1.93 Ga after the intrusion of the Bushveld rocks and after extensive erosion occurred, and before the intrusion of the dolerite sill at ~1.88 Ma (Hanson *et al*., 2004; Dorland *et al*., 2006; Huthmann *et al*., 2016).

9.3. Waterberg Mineralisation

The PGE mineralisation in the Bushveld Complex mainly occurs in two distinct styles, (1) contact-style mineralisation along the footwall of the northern limb (Kinnaird *et al*., 2005; Maier *et al*., 2008; McDonald and Holwell, 2011), and (2) laterally highly continuous stratiform reefs which include the Merensky reef, the UG2 and other (LG; MG; UG) chromitite layers and the PGE reefs at the top of the Platreef (Scoon and Teigler, 1994; Barnes and Maier, 2002; Yudovskaya *et al*., 2017). These two styles of mineralisation are restricted to the Critical Zone of the eastern and western limbs as well as the Platreef in the northern limb of the Bushveld Complex. A third style of mineralisation of PGE occurrences in the gabbroic sequence higher in the stratigraphy has been described recently (Harmer *et al*., 2004; Maier and Barnes, 2010; Holwell *et al*., 2013; McDonald *et al*., 2017) although some sub-economic PGE grade had been reported in the Upper Zone earlier (von Gruenewaldt, 1976; Harney and von Gruenewaldt, 1995). Two mineralised intervals have been intercepted in the Waterberg stratigraphy, namely a basal F mineralised zone and an upper T mineralised zone. The mineralisation in the Waterberg project shows similar characteristics to mineralised intervals found elsewhere in the Bushveld Complex, although it simultaneously shows unique features.

F zone

The F mineralised zone forms part of the Ultramafic Sequence near the base of the Waterberg stratigraphy, where mineralisation is generally confined to feldspathic orthopyroxenite and harzburgite. These lithologies resemble some of the lithologies which host mineralisation in the rest of the complex, and the mineral chemistry of the F zone lithologies also show similarities to the Platreef and Critical Zone of the Bushveld Complex as mentioned above. The F zone mineralisation is dominated by palladium over platinum which is atypical of the mineralisation in the eastern and

western limbs of the Bushveld Complex (Kinloch, 1982; McLaren and De Villiers, 1982; Kinloch and Peyerl, 1990; Barnes and Maier, 2002; Cawthorn *et al*., 2002). The Platreef in the northern limb is also palladium dominated with a Pd/Pt ratio of 2:1 in the basal sill of the Platreef, and palladium is slightly higher than platinum for the overall Platreef. Both the Platreef and F zone share a similar Pt/Au ratios, with both having 5% Au in their metal budget (Kinnaird, 2005; McDonald and Holwell, 2011).

The grades of 3PGE+Au for the F zone (Fig. 4.14, 5.2 and 6.3) on the Waterberg project are compared with grades of 4.9 to 5.9 g/t (3PGE+Au) for the Merensky Reef in the eastern limb, and 5.6 to 9.2 g/t (3PGE+Au) in the western limb (Cawthorn *et al*., 2002; Barker, 2012; Cawthorn, 2015), as well as with the UG2 grades of 4.39 g/t in the eastern limb and 5.1 g/t in the western limb (Barker, 2012). The precious metal distribution of the F zone is completely different to that of the Merensky Reef and UG2 in the eastern and western limbs of the Bushveld Complex, however, there are similarities in terms of Pd dominance and Au proportions to the Platreef of the northern limb (Fig. 4.23). The Merensky Reef is generally 30 to 90 cm thick, although it can be up to 7 m thick in some localities (Cawthorn, 2015), and is bounded by two chromitite layers/stringers forming a stratiform reef. The chromitite seams bound the stratiform, generally pegmatoidal, feldspathic pyroxenite/pyroxenite sulphide reef of the Merensky Reef, and are considered to mark the base of the cyclic units and the zone of mixing between the residual magma and a new melt influx (Cawthorn *et al*., 2004; Cawthorn, 2011; Naldrett *et al*., 2012; Naldrett *et al*., 2015). Initially, there was no consensus on the correlation of the Platreef in the northern limb to the upper Critical Zone in the rest of the Bushveld Complex, based on significant differences in geochemistry and mineralogy (White, 1994; McDonald *et al*., 2005), although a number of authors identified features in the GNPA member and the Platreef and regarded these features to be equivalent to the upper Critical Zone (Hulbert, 1983; Maier *et al*., 2008; Naldrett *et al*., 2008; van der Merwe, 2008). Recent down dip drilling on the farms Turfspruit, Akanani and Sandsloot have intercepted Pt-rich stratiform reef-style mineralisation in the upper part of the Platreef, which has a remarkable resemblance to the upper Critical Zone and Merensky Reef (Dunnett *et al*., 2012; Grobler *et al*., 2012; Kekana, 2015; Nodder *et al*., 2015; Yudovskaya *et al*., 2017). Furthermore, a stratiform-style reef at the top of the Platreef shares a similar stratigraphic position, whole-rock geochemistry and isotopic characteristics as well as the regular appearance of chromitite seams (cyclic units) to that of the upper Critical Zone and the Merensky Reef (Yudovskaya *et al*., 2017, Fig. 3 in this paper). In addition to the stratiform reef-style mineralisation at the top of the Platreef, the Platreef also contains disseminated mineralisation associated with both magmatic igneous rocks as well as hybrid footwall rocks as seen in the shallow up dip sections of the Platreef (Yudovskaya *et al*., 2017).

The F zone mineralisation is hosted by similar ultramafic lithologies (feldspathic pyroxenite and harzburgite) as the stratiform reef-style in the Platreef, and both mineralised intervals are interpreted to have formed as chonolith-like coalescing intrusions (Yudovskaya *et al*., 2017). However, the F zone mineralisation lacks the stratiform reef style mineralisation of the Platreef and distinct cyclic units seen in the upper Critical Zone (Eales and Cawthorn, 1996; Grobler *et al*., 2012). The F zone is a stratabound deposit similar to the shallow Platreef which overlies the footwall lithologies rather than a stratiform reef-style mineralised interval. The F zone also lacks anorthosite layers and plagioclase generally occurs interstitially to orthopyroxene and olivine. One of the most notable differences is the lack of chromitite layers in the F zone. Only two chromitite stringers (<2 cm thick) have been identified in two boreholes within the F zone. More commonly, disseminated chromite is irregularly distributed through the F zone. The lack of chromitite layers may be related to the magmatic erosion at the top of the UmS by a surge of later troctolitic melt. However, most of the TGA sequence is Cr-poor and apparently, chromite was not a liquidus phase in the TGA parental gabbroic melt. Disseminated chromite in troctolite is xenocrystic in nature suggesting it was derived from digested and consumed UmS harzburgite.

Initially, the mineralisation in the F zone was thought to have an anti-correlation with chromite as evidenced by the assay data provided by Platinum Group Metals (Fig. 4.14, 5.2 and 6.3), although on further investigation with petrology and microprobe analysis the mineralisation does show some correlation with chromite (Fig. 5.6f and 5.9b). The nature of chromite in the F zone resembles the description of rare and discontinuous chromitite layers in the shallow Platreef by Yudovskaya and Kinnaird (2010). Although the shallow Platreef shows extensive contamination and the formation of a number of different hybrid rocks depending of the footwall lithologies (Kinnaird *et al*., 2005; Kinnaird and Nex, 2015), the F zone has little to no contamination and there are no hybrid rocks identified in the Waterberg stratigraphy.

The primary magmatic base metal sulphide assemblages of the F zone (pyrrhotite > chalcopyrite > pentlandite) (Fig. 5.6) are typical of PGE deposits hosted by ultramafic lithologies including the deposits of the Bushveld Complex (McDonald and Holwell, 2011). The secondary sulphide assemblages are also typical of hydrothermally altered economic or barren ores in ultramafic sequences (Fig. 5.6) (Ramdohr, 1969; Kitakaze, 2008). The primary sulphide mineralisation in the F zone is generally disseminated and blebby, although may form semi-massive aggregates (up to 45 vol. %) towards the base of the F zone. Similar sulphide textures have been identified in certain localities of the Platreef (Sharman-Harris *et al*., 2005; Holwell *et al*., 2007).

The PGE in the F zone generally show a good correlation with base metal sulphides. The Cu/Pd value is a good indicator of sulphide melt enrichment due to a contrast in Cu and Pd partition coefficients into sulphide melt during exchange with silicate melts (Naldrett *et al*., 2009). The average Cu/Pd value in the Critical Zone of the Bushveld Complex is around 4000 and any lower Cu/Pd values indicate enhanced sulphide upgrading (Barnes and Maier, 2002; Naldrett *et al*., 2009). The Cu/Pd values in the F zone is around 500 (Fig. 5.5), similar to the ranges of the Merensky Reef (Naldrett *et al*., 2009) and the high-grade reefs at Turfspruit, Akanani and Sandsloot (Yudovskaya *et al*., 2017). The F mineralisation has a remarkable sulphur depleted character compared to the Merensky Reef and the Platreef.

The PGM assemblages of the F zone show significant differences to the other mineralised intervals of the Bushveld Complex. The Platreef contact style mineralisation shows a great variability of PGM assemblages (Schneiderhöhn, 1929; Mostert, 1982; Kinloch, 1982; Viljoen and Schürmann, 1998; Armitage *et al*., 2002; Hutchinson *et al*., 2004; Hutchinson and Kinnaird, 2005; Holwell *et al*., 2006) and these changes seem to correlate with the change in footwall lithologies (McDonald *et al*., 2005; Nichol and Kinnaird, 2008; McDonald and Holwell, 2011). The recent work by Yudovskaya *et al*. (2017) on the stratiform reef-style mineralisation of the upper Platreef found on Turfspruit shows that it is dominated by Pt sulphides and Pt-Fe alloys and has been interpreted to be mineralogically similar to the Merensky Reef in the eastern and western limbs of the Bushveld Complex. Similar conclusions were made for the reef sections on Sandsloot and Akanani (Yudovskaya *et al*., 2011), whereas the bulk PGM in the whole Platreef are dominated by Pt-Pd bismuthotellurides with minor isoferroplatinum and sperrylite (Viljoen *et al*., 2015). The association of sperrylite-hollingworthite-cobaltite-gersdorfite can be considered as indicative for both the Waterberg F zone and for the Akanani harzburgite reefs (Yudovskaya *et al*., 2011). In contrast, the indicative assemblage of the Merensky Reef style includes Pt sulphides and alloys (Prichard *et al*., 2004).

F zone compared with other mineralised intrusions:

Stillwater J-M reef

The F zone and J-M reef of the Stillwater Complex both represent mineralisation associated with olivine-bearing lithologies (Table 9.3). The J-M reef occurs in the lower portion of the Banded Zone, some 400 to 450 m above the Ultramafic Zone of the Stillwater layered intrusion (McCallum *et al*., 1980; Todd *et al*., 1982; Barnes and Naldrett, 1985). The J-M reef is composed of harzburgite, troctolite, pyroxenite, olivine-bearing norite and anorthosite and these are similar lithologies to

those that host the mineralisation in the F zone, although there are no cumulus plagioclase-rich lithologies associated with the ultramafic F-zone.

The J-M reef is a 1 to 3 m thick stratiform deposit that is semi continuous over the ~47 km strike length of the Stillwater Complex (Todd *et al*., 1982; Barnes and Naldrett, 1985). According to Turner *et al*. (1985) the J-M reef in the east is olivine-rich and towards the west becomes more pyroxene-rich. Both mineralised intervals are dominated by palladium (McCallum *et al*., 1980). The PGE in the deposits have a strong correlation with the Ni, Cu and base-metal sulphides (Barnes and Naldrett, 1985). Both mineralised intervals are associated with disseminated chromite rather than chromitite layers. The PGM assemblage of the J-M reef is dominated by moncheite, cooperite, braggite, Pt-Fe alloys and kotulskite (Todd *et al*., 1982), which is very different from the sperrylite and Pt-Pd bismuthotelluride assemblage of the F-zone.

The Rum Eastern Layered Suite

The mineralisation of the Rum intrusion in Scotland is very different from that in the F zone (Table 9.3). Although the intrusion is composed of olivine-rich lithologies such as feldspathic peridotites, harzburgite, troctolite and olivine-bearing norite, the mineralisation is mainly concentrated within ~2 mm thin chromitite stringers (Brown, 1956; Emeleus *et al*., 1996; Power *et al*., 2000; Latypov *et al*., 2013; O'Driscoll *et al*., 2014). The Rum intrusion is composed of 16 cyclic units where the base of each unit is marked by a chromitite stringer (Power *et al*., 2000). The sulphide assemblage is that of a typical mineralised ultramafic succession. These sulphides are small (<100 µm) and are generally associated with the chromitite stringers and show a good correlation with the PGE (O'Driscoll *et al*., 2014).

Table 9.3: A summary of the difference between the J-M reef of the Stillwater Complex, The Rum Intrusion of NW Scotland and the F zone mineralisation associated with the Bushveld Complex (Data from Brown, 1956; McCallum *et al*., 1980; Todd *et al*., 1982; Barnes and Naldrett, 1985; Turner *et al*., 1985; Emeleus *et al*., 1996; Power *et al*., 2000; Latypov *et al*., 2013; O'Driscoll *et al*., 2014).

Features	**Waterberg F zone Bushveld Complex**	**J-M reef Stillwater Complex, Montana**	**The Rum Eastern Layered Suite NW Scotland**
Type of deposit	Stratabound	Stratiform	Stratiform
Host Rocks	Feldspathic orthopyroxnite, harzburgite, mela-troctolite	Harzburigite, troctolite, feldspathic pyroxenite, olivine-norite and anorthosite	Feldspathic peridotite, troctolite, olivine-gabbro and chromitite layers
Thickness	2.5 m to 60 m thick	1 m to 3 m thick, up to 5 m thick locally	~2 mm thick PGE bearing chromitites
PGE	Pd-dominant	Pd-dominant	Pt-dominant
Sulphides	Pyrrhotite>chalcopyrite>pentlandite	Chalcopyrite>pyrrhotite>pentlandite	Pyrrhotite>pentlandite>chalcopyrite
PGM	Sperrylite, michenerite, maslovite, mocheite, kotulskite and hollingworthite and minor majakite and menshikovite	Mocheite, cooperite, braggite, Pt-Fe alloys, kotulskite, vysotskite, telluropalladinite and stillwaterite	Pd-Cu alloys, Pt-Fe alloys, native Pt, laurite, moncheite, sperrylite, cooperite, braggite and isomerteite

Both the J-M reef of the Stillwater Complex and the mineralisation of the Rum intrusion show significant differences to the mineralisation of the F zone in the Waterberg area (Table 9.3). These stratiform reef-style mineralised intervals have more in common with the Merensky Reef, UG2 and

the stratiform reef-style of the Platreef (Barnes and Maier, 2002; Cawthorn *et al*., 2002; Yudovskaya *et al*., 2017).

T zone

The recent discoveries of PGE mineralisation within the upper portions of the Waterberg stratigraphy associated with the TGA sequence and Upper Zone boundary north of the Hout River Shear Zone warrants the question as to whether these mineralised zones are continuous south in the rest of the northern limb of the Bushveld Complex. The TGA sequence hosts the upper mineralisation at its very top, at the contact with the Upper Zone rocks. This TGA sequence is composed of a thick package of troctolite - olivine norite (>100 m thick) overlain by gabbroic rocks with typical Main Zone characteristics. The first appearance of cumulus titanomagnetite, which is an indicative mineral of the Upper Zone sequence (SACS, 1980; Ashwal *et al*., 2005), is confined to the T zone. On this basis, T mineralisation may be assigned to the base of the Upper Zone rather than the top of the TGA.

Platinum-group element mineralisation in the northern limb south of the Hout River Shear Zone is not restricted to the Platreef. South of the Ysterberg Planknek Fault PGE mineralisation was first identified in 1971 with the highest grades of 6.67 ppm PGE on the Moorddrift farm (Fig. 3.1) hosted by mottled anorthosite and gabbronorite which is also associated with a pyroxenite layer within the upper Main Zone (Maier and Barnes, 2010; Holwell *et al*., 2013). The upper Main Zone mineralisation on the Moorddrift farm can be traced along a strike length of ~1 km (Maier and Barnes, 2010). According to Holwell *et al*. (2013) the mineralisation is “reef style” and up to 10 m thick, although the package of mineralisation is extensively “disturbed” forming a mega breccia where mineralisation is locally distributed over an interval of more than 300 m. Maier and Barnes (2010) suggested that the pyroxenite layer is a correlative to the true ‘Pyroxenite Marker’ of the eastern and western limbs of the Bushveld Complex. Cawthorn (2012) and Holwell *et al*. (2013), however, argued that a variable number of thin pyroxenite layers occur elsewhere in the upper Main Zone of the northern limb, and that the Moorddrift layer may represent one of these layers.

The Moorddrift Main Zone mineralised interval contains 1 to 5 modal % of disseminated pyrrhotite, chalcopyrite and pentlandite that is heavily overprinted by secondary pyrite and millerite (Barnes and Maier, 2010; Holwell *et al*., 2013). The sulphides tend to be associated with secondary alteration minerals such as actinolite, tremolite, chlorite and quartz, which form halos around sulphides. The PGM are generally associated within alteration phases of the sulphides (Barnes and Maier, 2010; Holwell *et al*., 2013), and these features are very similar to the T mineralised zone in the Waterberg area. The PGM assemblage is dominated by Pt-Pd tellurides, sperrylite (up to 97%) and minor

stibiopalladinite in the “reef-style” interval, with an increase in antimonides associated with the brecciated intervals (Holwell *et al*., 2013).

The sulphur isotopic signatures of the sulphides in the mineralised interval on Moorddrift farm all show a crustal signature ($\delta^{34}S$ +2.8 to +5.3‰) (Holwell *et al*., 2013). These sulphur isotopic values are significantly different from the mantle derived sulphur $\delta^{34}S$ obtained for the T mineralised zone. In addition, the whole-rock geochemistry values (Mg#, MgO, Cr) for the Moorddrift farm are slightly higher than for the T zone (Maier and Barnes, 2010) and the PGE mineralisation is dominated by Pt on the Moorddrift, whereas the T zone is dominated by up to 65 % Pd. Therefore, based on stratigraphic position, whole-rock geochemistry, sulphur isotopic signatures and Pt dominated (sperrylite) mineralisation a genetic link between the Moorddrift upper Main Zone mineralisation and the T zone of the Waterberg project is unlikely.

North of Overysel, the Main Zone thins progressively until Upper Zone lithologies rest directly on basement granitic gneiss, where the basement high occurs (Fig. 9.3). On the northern side of the basement high, the Main Zone reappears on the surface directly in contact with the Archean granites (van der Mewer, 1976). At the far northern end of the exposed part of the northern limb, the Aurora project (Fig. 3.1) is situated just south of the Waterberg project, separated by the Hout River Shear Zone. The upper PGE-Cu-Ni mineralisation on Aurora is hosted by leucogabbro, gabbronorite, anorthosite and minor troctolite (Manyeruke, 2007; Maier *et al*., 2008; McDonald and Harmer, 2010; McDonald *et al*., 2017). Based on the appearance of inverted pigeonite and mineral chemistry comparable with the upper Main Zone of the Bellevue drill core, McDonald *et al*. (2017) places the mineralisation into the upper Main Zone. However, recent logging and a magnetic susceptibility survey down borehole LAP 30 (Fig. 9.2) indicates that the mineralisation on the Aurora project may be hosted in the Upper Zone of the Bushveld Complex.

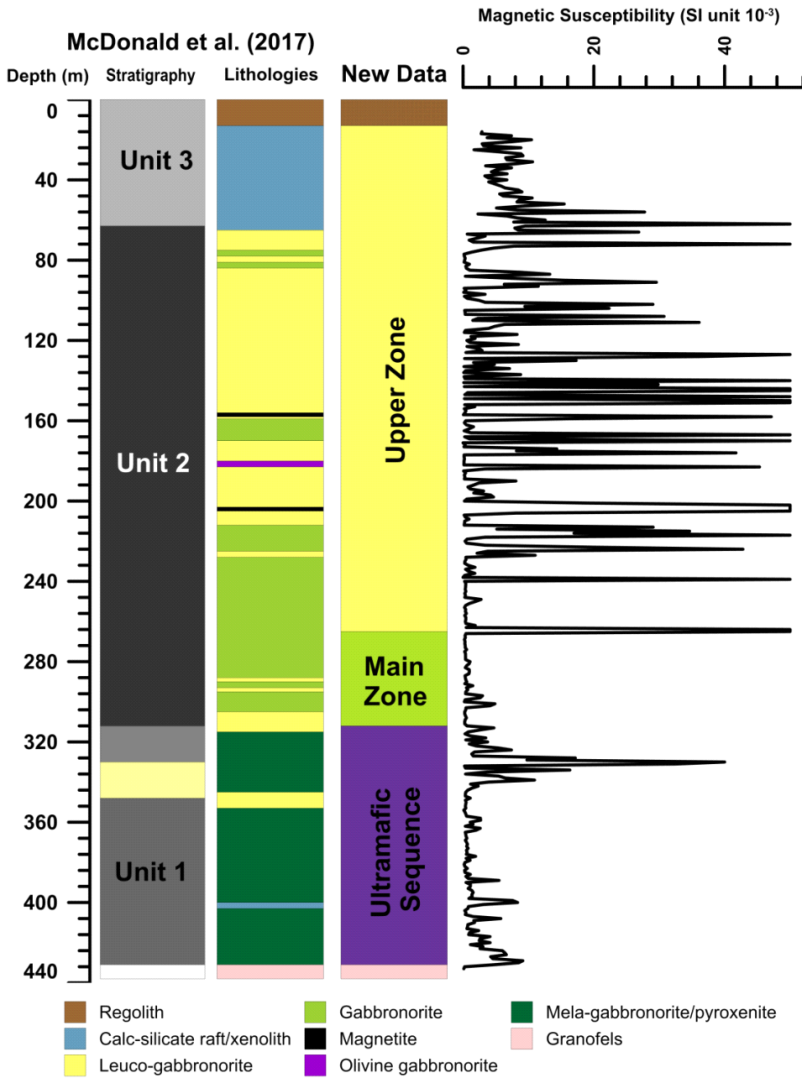

Figure 9.2: The magnetic susceptibility results of borehole LAP 30 from the Aurora project indicate that the upper mineralisation is associated with the Upper Zone (the first and second column-stratigraphy and lithology was taken from McDonald *et al*., 2017, the third and fourth columns were produced based on the magnetic susceptibility results obtained in this study).

Despite the different stratigraphic position of the mineralisation of both areas, there are some significant similarities although there are also a number of contrasts. McDonald *et al*. (2017) highlighted that the Aurora mineralisation is Cr-poor with typically <300 ppm Cr and a negative correlation between Cr and PGE. Similar Cr values and Cr-PGE relationships are noted in the Waterberg T zone (Fig. 5.5) (McDonald *et al*., 2017). Both areas are characterised by Pd dominant over Pt with Pt/Pd of approximately 0.6 although the Cu/Pd ratio of around 4000 in Aurora is remarkably higher than that of the higher-grade Waterberg mineralisation although both are still within the range of mantle-derived magmatic sulphides (Naldrett *et al*., 2012). McDonald *et al*. (2017) reported the presence of calc-silicates up to 6 m thick on the Aurora project whereas there are rare in the Waterberg sections. The mineral chemistry of pyroxenes, plagioclase and olivine are overall slightly more primitive in the T zone in the Waterberg area compared with that of the upper

mineralisation zone on Aurora (McDonald *et al*., 2017). The Aurora sulphide assemblage of pyrrhotite-chalcopyrite-pentlandite with minor secondary pyrite, does not show widespread hydrothermal sulphides, as seen in the T zone. The Aurora sulphides have mantle-like sulphur isotope signatures with the $\delta^{34}S$ values ranging from -0.8 ‰ to +5.24 ‰ with an average of 0.99 ‰ (Holwell *et al*., 2007; Manyeruke, 2007; McDonald *et al*., 2017). These values are similar to the Waterberg sulphur isotope $\delta^{34}S$ values of around 0 ‰ reported by McCreesh *et al*. (2015) (Fig. 7.2). The most common PGM on Aurora include Pd tellurides (merenskyite and kotulskite) and Au-Ag alloys with subordinate Pt tellurides and arsenides and rare Pt-Pd sulphides (McDonald and Harmer, 2010). The PGM association with primary sulphides and silicates on Aurora strongly contrasts to the hydrothermal quartz-chlorite and pyrite-millerite secondary assemblage seen in the T zone. However, given the similarities between the two adjacent project areas and the likelihood of a link between their host sequences, it is suggested here that the Aurora mineralised units may represent a southern distal facies of the T zone.

Table 9.4: A summary of the differences and similarities of the upper mineralised intervals between the Moorddrift farm, the Aurora project and the Waterberg project (Harmer *et al*., 2004; Manyeruke, 2007; Maier *et al*., 2008; Harmer and McDonald, 2010; Barnes and Maier, 2010; McDonald *et al*., 2017).

Features	Moorddrift farm	Aurora Project	Waterberg Project
stratigraphic position	upper Main Zone	Upper Zone (this study) upper Main Zone (McDonald et al., 2017)	TGA sequence-Upper Zone boundary
Host Rocks	Gabbronorite, gabbro, norite, anorthosite, minor pyroxenite	leucogabbro, gabbronorite, magnetite-gabbro and minor troctolite	T1 - Feldspathic pyroxenite, troctolite, harzburgite, olivine-gabbronorite T2 - gabbronorite and gabbro
Sulphides	Chalcopyrite, pyrrhotite, pyrite, pentlandite and millerite	Chalcopyrite, pyrrhotite, pentlandite and pyrite	Chalcopyrite, pyrrhotite, pentlandite, pyrite, millerite, bornite and galena.
Sulphur Isotopes ($\delta^{34}S$)	2.8 to 11.5 ‰	0.1 to 5.24 ‰	0.48 (negative) to 0.29 ‰
PGE	Pt - dominant	Pd - dominant	Pd - dominant
Highest avaible grades	6.67 g/t	~9 g/t	>30 g/t
PGM	Pt-Pd tellurides, sperrylite, antimonides and minor stibiopaladinite	Merenskyite, kotulskite, electrum and minor moncheite, sperrylite, platarsite. rare braggite and vysotskite	Merenskyite, koluskite, moncheite, froodite, insizwaite and electrum, rare braggite
Cr content	<300 ppm	<300 ppm	T1 - 500 to 910 ppm T2 - 120 to <300 ppm

The Main Zone magma of the Bushveld Complex was not traditionally considered as a fertile PGE source (Naldrett *et al*., 2012) although sporadic sulphides were identified in the upper part of the northern limb. Van der Merwe (1976) analysed gabbronorite samples from the upper Main Zone in the northern limb, and found anomalous enrichment in Cu and S values. Ashwal *et al*. (2005) reported an increase in opaque minerals in the upper Main Zone, although they did not indicate their composition. Barnes *et al*. (2004) noted relatively low Cu/Pd ratios and an elevated Cu content in the upper Main Zone from the Bellevue drill-core in the northern limb, similar to the ranges for the Waterberg and Aurora mineralisation. Holwell *et al*. (2005) and Holwell and Jordaan (2006) have established that the Main Zone in the northern limb unconformably overlies the Platreef and have interpreted that the Main Zone may hold a metal budget of its own. McDonald *et al*. (2017)

suggested that this break between Platreef and Main Zone in the northern limb may explain why the Main Zone or Upper Zone magma in the northern limb, retained its own PGE budget compared with the rest of the Bushveld Complex.

The upper Main Zone sequence of the western and eastern limbs also locally bears similar anomalies. Wilhelm *et al*. (1997) reported on the basis of soil and sediment geochemical data that Ni, Cu, PGE and Au anomalies associated with the upper Main Zone could be traced for more than 100 km along strike in the western limb of the Bushveld Complex. Sharpe (1985*a,b*) and Wilhelm *et al*. (1997) predicted the appearance of mineralisation associated with the Pyroxenite Marker or at the boundary between the Main and Upper Zones. Consequently, several studies on the Pyroxenite Marker have revealed a moderate PGE enrichment in a few samples (Maier *et al*., 2001; Maier and Barnes, 1999). Therefore, the known sulphide mineralisation in the upper Main Zone and Upper Zone of the eastern and western limbs was confirmed to be uneconomic (Harney and Merkle, 1990; Harney and von Gruenewaldt, 1995).

T zone compared with other mineralised intrusion

Platinova Reef Skaergaard Intrusion

The Platinova Reef is situated in the Triple Group (Wager and Deer, 1939; Wager and Brown, 1968) a 100 m thick unit at the top of the Middle Zone of the Skaergaard intrusion in Greenland. The mineralisation is hosted in mela- to leuco-gabbro rocks (Bird *et al*., 1991). The Middle Zone differs from the overlying Upper Zone due to the presence of cumulus olivine (Bird *et al*., 1991; Anderson *et al*., 1998). There are several Pd-rich layers (up to 5 enriched layers), the basal layer is regarded as the main Pd-rich layer, and the top layer is a gold rich layer with minor Pd (Anderson *et al*., 1998).

There are significant differences between the Platinova Reef and the T zone, fundamental similarities can be seen with the interpretation of the formation of the Pd and Au-rich mineralisation hosted by most felsic-rich lithologies, and their stratigraphic position at the upper part of the layered intrusions. A major factor responsible for the formation of the Pd+Au-rich layers in the Platinova Reef is prolonged fractionation of the magma, causing the build-up of S, Cu, Ni, Pd, Pt and Au in the residual liquid (Bird *et al*., 1991; Anderson *et al*., 1998; Holwell and Keays, 2014; Keays and Tegner, 2016). The rapid increase in precious and base metals coincides precisely with the appearance of cumulus magnetite, in both the T zone and the Platinova Reef. The cumulus magnetite occurs in the upper T2 due to the influx of the new Upper Zone melt with magnetite on its liquidus. Important factors that could have formed the T zone mineralisation are changes in oxygen fugacity (fO_2) and temperature due to presence of magnetite from the influx of the new Upper Zone melt (Keays and Tegner, 2015). The crystallisation of magnetite decreases the oxygen fugacity (fO_2) of the magma

and the conversion of SO_4^{-2} in the magma to S^{-2} for sulphur saturation (Keays and Tegner, 2015). These are factors that have been interpreted to have formed the Platinova Reef (Pd, Cu and Au mineralised interval) in the upper portion of the Skaergaard intrusion (Keays and Tegner, 2015; Holwell *et al*., 2015).

Table 9.5: A summary of differences and similarities between the Waterberg T zone (Bushveld Complex) and the Platinova Reef (Skaergaard Intrusion) (Wager and Deer, 1939; Wager and Brown, 1968; Bird *et al*., 1991; Anderson *et al*., 1998; Nielsen *et al*., 2005; Holwell and Keays, 2014; Keays and Tegner, 2015; Holwell *et al*., 2015; Keays and Tegner, 2016).

Features	**Waterberg T zone** **Bushveld Complex**	**Platinova Reef** **Skaergaard Intrusion**
Stratigraphic position	Boundary between the TGA sequence and Upper Zone Strata-bound deposits	Middle Zone associated with the Triple Group Strata-bound deposits
Subzones	Two subzones T1 and T2 based on lithologies	Five Pd-rich layers (Pd 5-1) and an overlying Au-rich layer
Host Rocks	T1 - Harzburgite, troctolite, pyroxenite olivine-gabbronorite T2 - Gabbronorite and gabbro	Mela/leuco gabbro
PGE	Pd - dominant and Au-rich	Pd - dominant and Au-rich
Sulphides	Chalcopyrite, pentlandite, pyrrhotite, pyrite millerite, bornite and minor galena	Microdroplets of bornite, digenite and chalcocite
Cumulus Magnetite	upper portion of the T2	throughout the Platinova Reef
PGM	Merenskyite, kotulskite, moncheite, froodite, insizwaite and electrum, rare braggite	Pd-rich zone - skaergaardite (PdCu), nielsenite ($PdCu_3$), braggite and vysotskite Au-rich zone - tetraauricupride (AuCu)

In terms of precious metals, the T zone mineralisation is characterised by up to 21% Au within the precious metal basket, similar to the upper mineralisation on the Aurora project and on the Moorddrift farm (Harmer *et al*., 2004; Maier *et al*., 2008; McDonald and Harmer, 2010; Maier and Barnes, 2010; Holwell *et al*., 2013; McDonald *et al*., 2017). In addition, Yudovskaya *et al*. (2017) report elevated Au/PGE ratios associated with the upper reef-style mineralisation of the Platreef on Turfspruit. High Au concentrations have also been noted for the Platinova Reef in the Skaergaard Intrusion (Bird *et al*., 1991; Anderson *et al*., 1998; Nielsen *et al*., 2005). Hence, elevated Au concentrations may be a feature associated with mineralised intervals higher in the stratigraphy of mafic sequences, given that there is no previous metal depletion.

Table 9.6: A summary of the differences between the F and T mineralised intervals in the Waterberg stratigraphy.

Features	F Zone	T Zone
Stratigraphic position	Base of the Waterberg Stratigraphy.	Boundary between the TGA sequence and the Upper Zone.
Lithologies	Feldspathic orthopyroxenite, harzburgite and melatroctolite.	T1 - Feldspathic pyroxenite, troctolite, harzburgite, olivine-gabbronorite T2 - gabbronorite and gabbro
Thickness (m)	2.5 to 30 m thick Super F zone >60 m thick	T1 - 2.40 m to 3.00 m thick T2 - 3.80 m to 5.00 m thick up to >10 m thick Super T zone
Cumulus phase	Orthopyroxene, olivine and minor plagioclase, clinopyroxene and disseminated chromite	T1 - Orthopyroxene, olivine, plagioclase, clinopyroxene and minor magnetite. T2 - Orthopyroxene, clinopyroxene, plagioclase and minor magnetite towards the top.
Sulphides	Pyrrhotite, troilite, chalcopyrite, pentlandite, pyrite, covellite, valleriite, cobaltite-gersdorffite and bornite.	Chalcopyrite, pentlandite, pyrrhotite, arsenopyrite, millerite, pyrite, galena, sphalerite and bornite.
PGM	Sperrylite ($PtAs_2$) dominant up to 82% and Bismuthotellurides 9-34%.	Pt-Pd Bismuthotellurides up to 100%.
PGE+Au proportions and base metals	64% Pd, 30% Pt, 5% Au and 1% Rh 0.07% Ni and 0.16% Cu	49% Pd, 29% Pt, 21% Au and 1% Rh 0.08% Ni and 0.16% Cu
Mineral Chemistry Orthopyroxene Clinopyroxene Plagioclase Olivine	 Mg# (76-89); Cr (1300-4300 ppm) Mg# (82-89) An# (54-85) Fo (74-89) NiO wt.% (0.23-0.27)	 Mg# (65-72); Cr (120-500 ppm) Mg# (76-82) An# (69-82) Fo (64-66) NiO wt.% (0.18-0.21)

9.4. Magma Emplacement

No consensus exists on the positive identification of feeders of the Bushveld Complex, although a number of authors consider the Thabazimbi-Murchison Lineament (TML) to be a likely linear feeder (Kinloch and Peyerl, 1990; Friese, 2004; Kruger, 2005). The most convincing feeder is at the site of an enormous gravity anomaly just west of Mokopane close to the Ysterberg-Planknek Fault, a branch of the TML, which van der Merwe (1976) interpreted as the feeder for the northern limb of the Bushveld Complex. Naldrett *et al*., (2008) suggested a "pudding basin" model for the emplacement of marginal mineralisation in the Bushveld Complex. An alternative feeder has been suggested by McDonald *et al*. (2009) and Yudovskaya *et al*. (2010) located downdip of Akanani, west of the central sector of the Platreef. This suggestion was based on mineral chemistry (highest Mg#), olivine-rich lithologies, high temperature PGM and high PGE tenors. Cawthorn *et al*. (2002) suggested the Steelpoort Fault to have been a linear feeder based on the stratigraphic differences seen on either side of the fault (Hatton and von Gruenewaldt, 1987), which has been interpreted as differential flow of magma to either side of the feeder zone (Cawthorn *et al*., 2002).

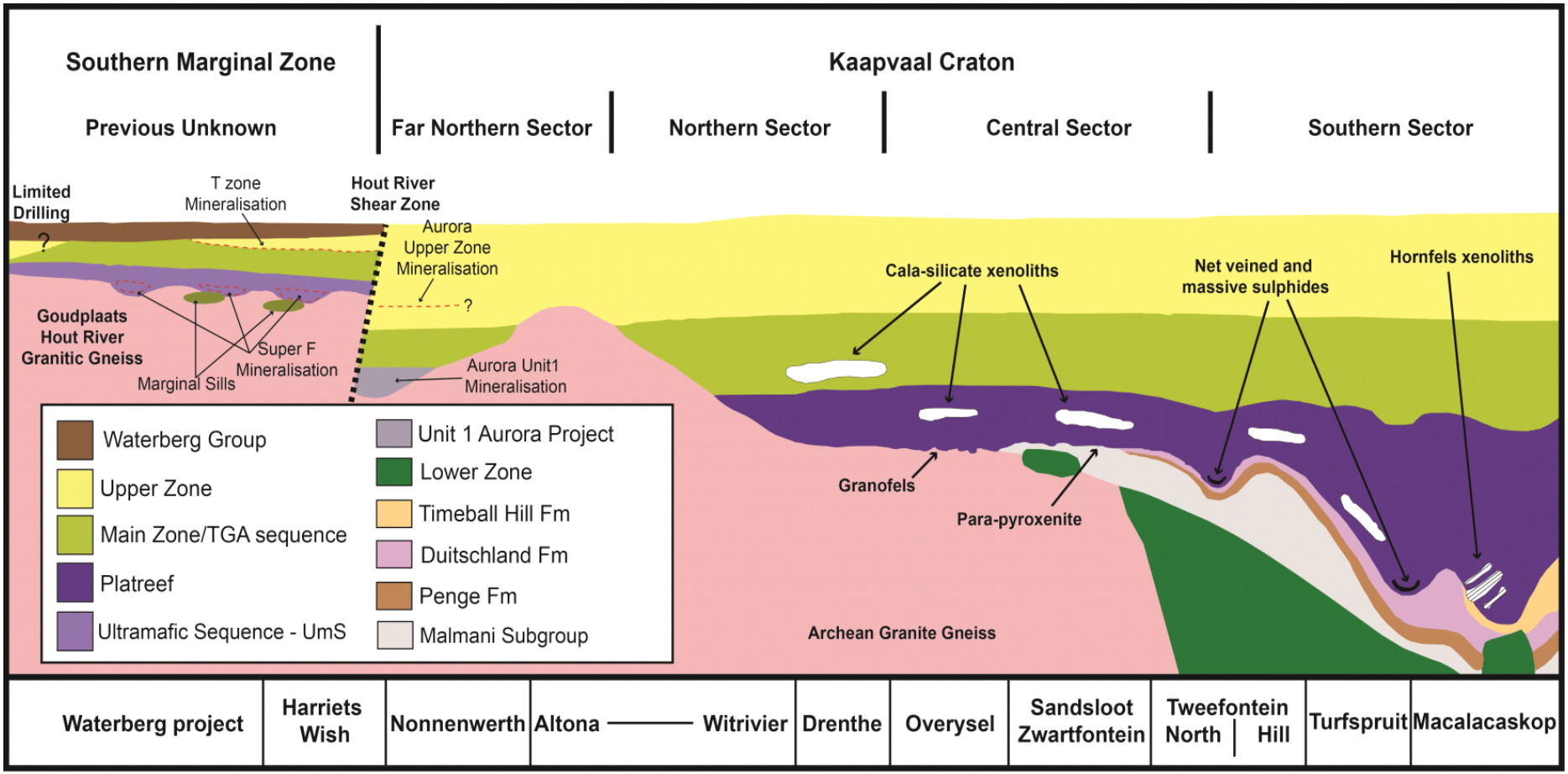

Figure 9.3 (above): Schematic diagram showing the contrast between the Waterberg intrusive package in comparison with the exposed northern limb of the Bushveld Complex south of the Hout River Shear Zone (Modified from Kinnaird, 2005; Kinnaird *et al*., 2017).

We propose a possible feeder zone associated with the Hout River Shear Zone based on the much reduced total Bushveld stratigraphy (<1.2 km thick), primitive mineral and whole-rock chemistry, high-grade PGE mineralisation compared to surrounding areas and significant differences in stratigraphy compared to the northern limb immediately south of the Hout River Shear Zone. The Waterberg Bushveld stratigraphy wedged between the Palala Shear Zone to the north and the Hout River Shear Zone to the south, has a southwest to northeast strike direction and the ultramafic/mafic lithologies dip to the northeast which may directly be controlled by the Southern Marginal Zone footwall topography. This differs from the south-north strike direction and westward dip of the northern limb south of the Hout River Shear Zone (van der Merwe, 1976). We propose that the Waterberg intrusive lithologies represent a separate, structurally controlled basin fed from a different subchamber associated with either the Hout River Shear Zone or the Palala Shear Zone, rather than being a marginal extension of the northern limb of the Bushveld Complex (Fig. 9.3).

9.4.1. Model of Waterberg Stratigraphy

The tectonic setting of the Limpopo Belt basement and its pre-existing anisotropies (fractures, faults, shear zones, foliations and lithological contacts) have played an important role during the initial stages of Waterberg project magmatism. Structural controls of the emplacement of the earlier melts defined the observed sill-like and chonolith morphology of the intrusion. The initial emplacement started at 2.05 Ma (Huthmann *et al*., 2016).

- *Marginal Sills*: The initial intrusions of the Marginal pyroxenite, gabbronorite and norite sills into the Hout River gneiss basement. These intrusions melted Archean granite gneisses which mingled with a pyroxenitic magma to form granofels (Fig. 5.15).

- *Ultramafic Sequence (UmS) and F zone*: Continuous influxes of ultramafic magma carved out channelised pathways under lateral dilation to form elongated chonolith-like bodies (Lister and Kerr, 1991; Barnicoat, 2008). The earlier ultramafic melts crystallised mineralised feldspathic orthopyroxenite at the base of the F zone. Then melts with olivine on the liquidus, were transported along the heated channels to crystallise feldspathic harzburgite in the upper part of the F zone. High-Mg ultramafic magmas are generally enriched in PGE, due to a high degree of partial melting of the mantle source (Barnes *et al*., 2016). With the continuous flow of ultramafic magma through these elongated channels, thermo-mechanical erosion formed embayments within the footwall of the Hout River Gneiss. At the same time, this hot ultramafic magma used points of weakness widening the conduit for progressive transport and assimilation of the resident orthopyroxene cumulates that were redeposited as xenoliths within the overlying harzburgite (Holwell and McDonald, 2006; Robertson *et al*.,

2015). The maximum heat and melt flow would be focused at the centre of the elongated bodies prohibiting crystallisation and allowing for a long-lasting sulphide-silicate exchange to form high-tenor magmatic sulphides (Campbell *et al*., 1983; Hon *et al*., 1994). Mungall and Brenan (2014) found extremely high partition coefficients for PGE (from 10^5 to 10^6) between the sulphide and silicate melts, which also obtained a PGE tenor from a reasonable R-factor. The calculations for the Merensky sulphides (Mungall and Brennan, 2014) confirm a possibility of formation of the high-tenor PGE sulphide mineralisation in situ in the resident chamber with no need for a pre-enrichment or an accumulation of a large pool of sulphide melt at a depth in the staging chamber as with the model of Holwell and McDonald, (2006). The continuous propagation of magma through the chonoliths is an effective mechanism for the concentration of the sulphide-droplets during magma emplacement (Naldrett, 2010) and formation of thicker and higher grade ore zones (up to 5g/t PGE for 60 m interval), termed the Super F zone on the PTM exploration site (Fig. 5.15 and Fig. 9.3).

- *Troctolite-Gabbronorite-Anorthosite (TGA) sequence*: Following the ultramafic channelised melt flow, continuous pulses of troctolitic magma utilised pre-existing points of weakness or anisotropies to form more laterally extensive sheet-like bodies. Processes like roof uplift and floor depression (Cruden, 1998) may have played a crucial role in creating space for the voluminous pool of stagnant magma to fractionate. The initial influxes of the troctolitic magma with a high proportion of phenocrysts at some point mixed with the earlier ultramafic melts either in the sub-chamber or in the feeder zone (Renna and Tribuzio, 2011; Saper and Liang, 2014) to form mela-troctolite grading into troctolite, olivine gabbronorite, gabbronorite and anorthosite. The several regular occurrences of anorthosite at the top of gabbroic cycles within the TGA sequence testify to multiple surges of magma that was similar compositionally to the Main Zone magmas elsewhere (Fig. 5.15).

- *T zone*: The T mineralisation occurs in the uppermost parts of the TGA sequence. The prolonged fractionation of the TGA sequence may be one of the key factors in producing the T zone at the top (Keays and Tegner, 2016). During the fractionation of the TGA magma, incompatible elements such as S, Cu, Pt, Pd and Au would have become enriched in the residual melt after deposition of the olivine-plagioclase cumulate (Tuner, 1986; Andersen *et al*., 1998; Nielsen *et al*., 2005; Wohlgemuth-Ueberwasser *et al*., 2013; Keays and Tegner, 2016). The T zone is a site of the first appearance of cumulus magnetite that may mark a decrease in temperature and fO_2 of the magma (Keays and Tegner, 2016) or may be an indication of a first influx of the Upper Zone melts into the resident chamber. Mixing

between the TGA leucogabbroic residue and the Upper Zone melt with magnetite on the liquidus triggered sulphide saturation and exsolution of T2 sulphides. The heterogeneity of the overlying T1 package suggests that the entire T zone was formed as a result of consecutive mixing events. The appearance of T1 harzburgite above anorthosite testifies to an influx of a later olivine-saturated magma, which transgressed through the underlying T2 and initiated the crystallisation of pegmatoidal pods and lenses due to undercooling during protracted crystallisation. The T1 and T2 mineralisation subzones have the same metal ratios but are hosted in very different lithologies. The PGE grade in the T1, however, is not persistent and in some cases, the T1 is completely barren. The T1 may have thermally eroded the T2 and the overlying anorthositic interlayer.

- *Upper Zone (UZ)*:The fractionation of the voluminous Upper Zone gabbroic magma may have been disturbed by new influxes of less evolved melts (Tanner *et al*., 2014), forming at least 500 m thick Upper Zone of the Waterberg Bushveld succession, which may have included now eroded apatite-bearing UZ rocks present in the rest of the Bushveld Complex. Soon after the uplift and erosion of the Waterberg Bushveld succession and its possible volcanic roof (Yudovskaya *et al*., 2015) the Waterberg Group sediments were deposited upon a weathered surface (Fig. 5.15).

9.4.2. Hydrothermal Activity and Redistribution of PGE

The F zone magmatic mineralisation underwent alteration during the late magmatic stage and later serpentinisation. The late magmatic processes resulted in the replacement of magmatic sulphides (pyrrhotite>chalcopyrite>pentlandite) by secondary silicates (actinolite, tremolite and chlorite), whereas serpentinisation induced significant BMS and chromite dissolution with spatially restricted PGE remobilisation. PGM such as sperrylite and Pt-Pd bismuthotellurides and tellurides are common in the F mineralisation which resembles a ‘primary’ mineralisation style (Fig. 5.9). These features are different from the Platreef, where hydrothermal activities associated with different footwall lithologies affected the assemblages and distribution of PGM (Armitage *et al*., 2002; Hutchison and Kinnaird, 2005). Although, where the Platreef rests on Archean basement, the hydrothermal remobilisation appears to be minor and the magmatic signature of the mineralisation is retained (Holwell, 2006; Kinnaird and Nex, 2015), which may be similar for the F zone mineralisation.

The T mineralised package composed of intercalated diverse lithologies served as favourable pathways for fluid migration at the late and post-magmatic stages. The late magmatic alteration involved the replacement of sulphides along the margins with secondary amphiboles and silicates, whereas hydrothermal activity resulted in the deposition of quartz, magnetite replacement,

crystallisation of pyrite-millerite-chalcopyrite assemblages and remobilisation of PGM and BMS out of sulphide blebs into the silicate matrix (Fig. 5.12 and 5.8). The hydrothermal reworking was responsible for the observed bimodal PGM grain size distribution (Fig. 5.13) where the rare coarse grains are accompanied by haloes and trails of numerous disseminated PGM in silicates. The pyrite-millerite-chalcopyrite assemblage associated with the T zone may represent a low temperature (~150-200°C) hydrothermal assemblage, which has also been recently described for the GNPA member by Holwell *et al*. (2017). The secondary assemblage involved a progressive change in mineralogy, element deportment and mobilisation, alongside a significant mass loss. Base and precious metals may have concentrated in the hydrothermal fluid (Ni, Cu and Pd) and be deposited elsewhere (Holwell *et al*., 2017). Similar features observed in the T1 mineralised zone are possibly responsible for the general poor PGE grades and extensively altered.

9.4.3. Contamination

The sulphur isotope study in this thesis has revealed that in both the F and T zone, there has been no contamination associated with the mineralisation. The sulphur isotope signatures of the Waterberg mineralisation represent mantle-derived sulphides (Table 7.1). The only sulphides that represent slight contamination are associated with the Marginal Sill composed of fine-grained pyroxenite or gabbronorite/norite. These lithologies are in direct contact with the granitic gneiss floor rocks, although sulphides from the granitic gneiss show mantle-derived signatures (Table 7.1). The Waterberg F and T zone data are significantly different from the sulphur isotope of the Platreef that show local evidence of crustal contamination where the floor, roof or assimilated xenoliths are dolomite or hornfels (Liebenberg, 1968; 1970; Sharman-Harris *et al*., 2005; Holwell *et al*., 2007). Although ~150 to 180 m above the Transvaal Supergroup footwall lithologies, magmatic sulphur isotope signatures are obtained for the primary magmatic Platreef (Sharman-Harris *et al*., 2005). Furthermore, there has only one calc-silicate xenolith identified in the Waterberg project area and no other kind of sedimentary xenoliths have been reported. This feature is unique as most of the northern limb south of the Hout River Shear Zone hosts xenoliths within the stratigraphy (Nex *et al*., 2006; King, 2009; Kinnaird and Nex, 2015; McDonald *et al*., 2017).

9.5. Conclusion

The ultramafic-mafic succession of the Waterberg project, north of the exposed northern limb of the Bushveld layered intrusion, is proposed to be a structurally controlled separate compartment wedge between the Hout River Shear Zone to the south and the Palala Shear Zone to the north. The north-east-oriented Waterberg lobate arc extends 24 km from the previously known outcrop of the northern limb Bushveld rocks. Zircon age dating gave an emplacement age of 2053 ± 5 Ma

(Huthmann *et al*., 2016), coeval with the Rustenburg Layered Suite. The Waterberg Bushveld stratigraphy comprises basal Marginal Sills, an Ultramafic Sequence, a troctolite-gabbronorite-anorthosite sequence and an Upper Zone, which is overlain by Waterberg Group sediments that were deposited between ~2.05 and ~1.93 Ma, after the extensive erosion of roof rocks and the Upper Zone and before the intrusion a dolerite sill of the ~1.1 Ga Umkondo Igneous Province.

- The basal Ultramafic Sequence is interpreted to have formed as chonolitic-like intrusions and is dominated by a basal orthopyroxenite, overlain by harzburgite that is typically 100 m thick. The Ultramafic Sequence hosts the lower F zone mineralisation. This succession of ultramafic lithologies is akin to the Platreef and upper Critical Zone based on mineral chemistry, mineralogy and mineralisation. Despite that, the succession displays unique characteristics and is interpreted to have formed from a Platreef/upper Critical Zone type melt which, however, not directly equated to the Platreef or upper Critical Zone of the Bushveld Complex south of the Hout River Shear Zone.

- The troctolite-gabbronorite-anorthosite (TGA) sequence hosts a barren troctolite unit at the base grading into gabbronorite and gabbro with minor anorthosite layers with sporadic occurrences of inverted pigeonite and typically resembles an upward fractionating sequence. These characteristics are typical of the Main Zone of the northern limb of the Bushveld Complex. The TGA sequence is ~850 m thick and the mineral chemistry is significantly more primitive than that of the Main Zone elsewhere, probably reflecting the relative thinness of the TGA sequence. In addition, at the top contact where the upper T zone mineralisation occurs, is unqiue to the Waterberg stratigraphy.

- The Upper Zone is identified by the appearance of cumulus magnetite as defined elsewhere in the Bushveld Complex. However, the Upper Zone in the Waterberg stratigraphy only reaches a maximum thickness of 500 m and is completely absent in certain areas of the Waterberg project due to extensive erosion. In addition, the Upper Zone lacks magnetitite layers and the mineral chemistry is also significantly more primitive in contrast to Upper Zone rocks immediately south of the Hout River Shear Zone.

- Overall it has been demonstrated within the foregoing chapters that magmatic and hydrothermal processes were instrumental in the development of the lower and upper mineralised zones, associated with base metal sulphides and PGE mineralisation of the Waterberg succession. Contamination, however, was insignificant in the formation of the

mineralisation as the sulphur isotopic signatures suggest that the mineralisation is mantle-derived.

- The lower F zone PGM mineralisation is dominated by sperrylite and Pt-Pd bismuthotellurides, where sulpharsenides of PGE, Fe and Co are index minerals of this type of mineralisation. Pervasive serpentinisation caused a significant sulphide and chromite removal and determined the composition of the secondary sulphide assemblages typical of altered ultramafic rocks.

- The upper T zone is dominated by Pt-Pd bismuthotellurides, stannides and electrum. The stratigraphic position at the level of the first cumulus magnetite appearance suggests that the Upper Zone melts were involved in the formation of the T zone mineralisation. Widespread secondary silicates (tremolite, actinolite, epidote, serpentine and chlorite), crusty quartz, carbonates and associated pyrite-millerite assemblages indicate low temperature hydrothermal modification of PGM.

The conclusion that the Waterberg Bushveld succession does not represent a simple strike extension of the northern limb is exciting and excellent news for the future of exploration in the Bushveld Complex.

9.6. Recommendation

A structural study needs to be undertaken focussing on the timing, movement and displacement of the faults and shear zones associated with the Waterberg intrusion especially that of the Hout River Shear Zone in the south and the Palala Shear Zone to the north of the project. An investigation based of the structures of the Hout River Shear Zone which masks the field relationship between the Waterberg stratigraphy and the northern limb stratigraphy to the south could be useful. This could provide a better understanding of the lateral relationship between the Waterberg project and the northern limb and whether the proposed hypothesis that the Waterberg intruded into a separate, structural controlled basin north of the Hout River Shear Zone. A regional study on the fault and shear zone movement within the far northern limb and the Waterberg project could also provide constraints on the location of a feeder source, whether certain phase of the faulting or shearing facilitated or prevented magma movement, and the control these structures may have had on the magmatic stratigraphy in the Waterberg project area.

References

Andersen, J. C. Ø., Rasmussen, H., Nielsen, T. F. D. and Ronsbo, J. C. (1998). The Triple Group and the Platinova gold and palladium reefs in the Skaergaard Intrusion: stratigraphic and petrographic relations. *Economic Geology*, **93**:488-509.

Armitage, P. E. B. (2011). Development of the Platreef in the northern limb of the Bushveld Complex at Sandsloot, Mokopane District, South Africa. Ph. D. thesis, the University of Greenwich, 283 pp.

Armitage, P. E. B., McDonald, I. and Tredoux, M. (2007). A geological investigation of the Waterberg hydrothermal platinum deposit, Mookgophong, Limpopo Province, South Africa. *Appl. Earth Sci. (Trans. Inst. Min. Metall. B)*, **116**:B113-129.

Armitage, P. E. B., McDonald, I. Edwards, S. J. and Manby, G. M. (2005). An introduction to mineralisation in the northern limb of the Bushveld Complex. *Transactions, Institute of Mining and Metallurgy*, **114**:194-198.

Armitage, P. E. B., McDonald, I., Edwards, S. J. and Manby, G. M. (2002). Platinum=group element mineralisation in the Platreef and calc-silicate footwall at Sandsloot, Potgietersrus District, South Africa. *The Institution of Mining and Metallurgy*, **111**:36-45.

Arndt, N. T., Lesher, C. M. and Czamanske, G. K. (2005). Mantle-derived magma and magmatic Ni-Cu-(PGE) deposits. *Economic Geology*, **100**:5-23.

Ashwal, L. D., Webb, S. J. and Knoper, M. W. (2005). Magmatic stratigraphy in the Bushveld northern lobe: continuous geophysical and mineralogical data from the 2950 m Bellevue drill core. *South African Journal of Geology*, **108**:199-232.

Atkins, F. B. (1969). Pyroxenes of the Bushveld Intrusion, South Africa. *Journal of Petrology*, **10**:222-249.

Azbel, I. Y. A., Tolstikhin, I. N., Kramers, D., Pechernikova, V. and Vityazev, A. V. (1993). Core growth and siderophile element depletion of the mantle during homogeneous Earth accretion. *Geochim. Cosmochim. Acta*., **57**:2889-2892.

Ballhaus, C. and Sylvester, P. (2000). Noble metal enrichment processes in the Merensky Reef, Bushveld Complex. *Journal of Petrology*, **41**:545-561.

Barker, O.B., 2012, Barker's platinum map of southern Africa [4th ed.]: Johannesburg, Books on the Wall Publishing CC.

Barker, O. B., Brandl, G., Callaghan, C. C., Eriksson, P. G. and von der Neut, M. (2006). The Soutpansberg and Waterberg Group and the Blouberg Formation. In: Johnson, M. R., Anhaeusser, C. R. and Thomas, R. J. (eds.), The Geology of South Africa: Geological Society and Council of Geosciences, South Africa, 301-318.

Barnes, S. –J. and Maier, W. D. (2002). Platinum-group element distribution in the Rustenburg Layered Suite of the Bushveld Complex, South Africa. In: Cabri, L. J. (ed.), The Geology, Geochemistry, Mineralogy and Mineral Beneficiation of Platinum-Group Elements. *Special Volume, Canadian, Institute of Mining, Metallurgy and Petroleum*, **54**:431-458.

Barnes, S.-J. and Maier, W.D. (2002). Platinum-group elements and microstructures of normal Merensky reef from Impala Platinum Mines, Bushveld Complex. *Journal of Petrology,* **43**: 109-128.

Barnes, S. J. and Naldrett, A. J. (1985). Geochemistry of the J-M Reef of the Stillwater Complex, Minneapolis Adit Area II. Silicate mineral chemistry and petrogenesis. *Journal of Petrology*, **27**:791-825.

Barnes, S. J., Cruden, A. R., Arndt, N. and Saumur, B. M. (2016). The mineral system approach applied to magmatic Ni-Cu-PGE sulphide deposits. *Ore Geology Reviews*, **76**:236-316.

Barnes, S. -J., Maier, W. D. and Ashwal, L. D. (2004). Platinum-group element distribution in the Main Zone and Upper Zone of the Bushveld Complex, South Africa. *Chemical Geology*, **28**:293-317.

Barnes, S. –J., Maier, W. D. and Curl, E. A. (2010). Composition of the Marginal Rocks and Sills of the Rustenburg Layered Suite, Bushveld Complex, South Africa: Implications for the formation of the platinum-group elements deposits. *Economic Geology*, **105**:1491-1511.

Barnes, S. –J., Naldrett, A. J. and Gorton, M. P. (1985). The origin of the fractionation of platinum-group elements in terrestrial magmas. *Chemical Geology*, **53**(3-4):303-323.

Barnes, S. –J., Savard, D., Bedard, L. P. and Maier, W. D., (2009). Selenium and sulfur concentrations in the Bushveld Complex of South Africa and implications for formation of the platinum-group element deposits. *Mineralium Deposita*, **44**(6): 647.

Barnes, S.J., Liu, W. (2012). Pt and Pd mobility in hydrothermal fluids: evidence from komatiites and from thermodynamic modelling. *Ore Geology Reviews*, **44**: 49–58.

Barnicoat, A. C. (2008). The mineral system approach of the pmd* CRC. Record. *Geoscience Australiapp*., 1-6.

Barton, J. M. Jr., Cawthorn, R. G. and White, J. A. (1986). The role of contamination in the evolution of the Platreef of the Bushveld Complex. *Economic Geology*, **81**:1096-1104.

Barton, J. M., Klemd, R. and Zeh, A. (2006). The Limpopo belt: A result of Archean to Proterozoic, Turkic-type orogenesis? *Geological Society of America Special Paper*, **405**:315-332.

Becker, M., De Villiers, J. and Bradshaw, D. (2010). The mineralogy and crystallography of pyrrhotite from selected nickel and PGE ore deposits. *Economic Geology*, **105**: 1025-1037.

Berger, M., Kramers, J. D. and Nägler, T. F. (1995). Geochemistry and geochronology of charno-enderbites in the Northern Marginal Zone of the Limpopo Belt, southern Africa and genetic models. *Schweiz. Mineral. Petrogr. Mitt*., **75**:17-42.

Berlincourt, L. E., Hummell, H. H. and Skinner, B. J. (1981). Phases and phase relations of the platinum-group elements. In: Cabri, L. J. (ed.), Platinum-group elements: Mineralogy, Geology, Recovery. Can. Inst. Mining Metall. Spec., **23**:19-45.

Bird, D. K., Brooks, C. K., Gannicott, R. A. and Turner, P. A. (1991). A gold bearing horizon in the Skaergaard Intrusion, East Greenland. *Economic Geology*, **86**:1083-1092.

Blenkinsop, T. G., Kröner, A. and Chiwara, V. (2004). Single stage, late Archaean exhumation of granulites in the Northern Marginal Zone, Limpopo Belt, Zimbabwe and relevance to gold mineralisation at Renco Mine. *South African Journal of Geology*, **107**:377-396.

Boorman, S., Boudreau, A. and Kruger, F. J. (2004). The Lower Zone – Critical Zone transition of the Bushveld Complex: A quantitative textural study. *Journal of Petrology*, **45**:1209-1235.

Borisov, A., Palme, H. and Spettel, B. (1994). Solubility of palladium in silicate melts: Implications for core formation in the Earth. *Geochim. Cosmochim. Acta*., **58**:705-716.

Boudreau, A. E. and Meurer, W. P. (1999). Chromatographic separation of the platinum-group elements, gold, base-metals and sulfur during degassing of a compacting and solidifying crystal pile. *Contributions to Mineralogy and Petrology*, **134**:174-185.

Brown, G. M. (1956). The Layered Ultrabasic Rocks of Rum Inner Hebrides. *Philosophical Transaction of the Royal Society of London*, **240**(668):1-53.

Buchanan, D. L. (1975). The petrography of the Bushveld Complex intersected by boreholes in the Bethal area. *Transaction of the Geological Society of South Africa*, **78**:335-348.

Buchanan, D. L. (1977). Cryptic variation in minerals from the Bushveld Complex of the Bethal area. *Transactions, Geological Society of South Africa*, **80**:49-52.

Buchanan, D. L. (1988). Platinum-group element exploration. Elsevier: Amsterdam, 185 pp.

Buchanan, D. L. and Nolan, J. (1979). Solubility of sulfur and sulfide immiscibility in synthetic tholeiitic melts and their relevance to Bushveld Complex rocks. *Can. Miner*., **17**:483-494.

Buchanan, D. L. and Rouse, J. E. (1984). Role of contamination in the precipitation of sulphides in the Platreef of the Bushveld Complex. In: Buchanan, D. L. and Jones, M. J. (eds.), Sulphides Deposits in Mafic and Ultramafic Rocks. *Transactions, Institute of Mining and Metallurgy*, 141-146.

Buchanan, D. L., Nolan, J., Suddaby, P., Rouse, J. E., Viljoen, M. J. and Davenport, J. W. J. (1981). The genesis of sulphide mineralisation in a portion of the Potgietersrus limb of the Bushveld Complex. *Economic Geology*, **76**:568-578.

Buchanan, P. C. (2006). The Rooiberg Group. In: Johnson, M. R., Anhaeusser, C. R. and Thomas, R. J. (eds.), The Geology of South Africa. Geological Society of South Africa, Johannesburg/Council for Geoscience, Pretoria, 283-289.

Buchanan, P. C., Reimold, W. U., Koeberl, C. and Kruger, F. J. (2002). Geochemistry of the intermediated to siliceous volcanic rocks of the Rooiberg Group Bushveld Magmatic Province, South Africa. *Contribution to Mineralogy and Petrology*, **144**:131-143.

Buick, I. S., Mass, R. and Gibson, R. (2001). Precise U-Pb titanite age constraints on the emplacement of the Bushveld Complex, South Africa. *Journal of the Geological Society of London*, **158**:3-6.

Bullen, D. S., Hall, R. P. and Hanson, R. E. (2012). Geochemistry and petrogenesis of mafic sill in the 1.1 Ga Umkondo Large Igneous Province, Southern Africa. *Lithos*, **142-143**:116-129.

Button, A. (1986). The Transvaal sub-basin of the Transvaal Sequence. In: Anhaeusser, C. R. and Maske, S. (eds.), Mineral Deposits of Southern Africa. Geological Society of South Africa, Johannesburg, 811-817.

Bye, A. R. (2001). Mining the Platreef. *Appl. Earth Sci. (Trans. Inst. Min. Metall. B)*, **110**:B209-210.

Bye, A. R. and Bell, F. G. (2001). Stability and slope design at Sandsloot open pit, South Africa. *Int. J. Rock Mech. Min*., **38**:449-466.

Cabri, L. J. (1972). The mineralogy of the platinum-group elements. *Mineral Science and Engineering*, **4**(3):3-29.

Callaghan, C. C., Eriksson, P. G. and Snyman, C. P. (1991). The sedimentology of the Waterberg Group in the Transvaal, South Africa: A overview. *Journal of African Earth Sciences*, **13**:121-139.

Cameron, E. N. (1963). Structure and rock sequence of the Critical Zone of the Eastern Bushveld Complex. *Min. Soc. Am. Spec. Pap*., **1**:93-107.

Cameron, E. N. (1978). The Lower Zone of the eastern Bushveld Complex in the Olifants River trough. *Journal of Petrology*, **19**:437-462.

Cameron, E. N. (1980). Evolution of the lower Critical Zone, central sector, eastern Bushveld Complex, and its chromite deposits. *Economic Geology*, **75**:845-871.

Cameron, E. N. (1982). The upper Critical Zone of the eastern Bushveld Complex; precursor of the Merensky Reef. *Economic Geology*, **77**:1307-1327.

Cameron, E. N. (1982). Sulphate and sulphate reduction in early Precambrian oceans. *Nature*, **296**: 145-148.

Campbell, I. H. and Naldrett, A. J. (1979). The influence of silicate: sulfide ratios on the geochemistry of magmatic sulfides. *Economic Geology*, **74**:1503-1505.

Campbell, I. H., Naldrett, A. J. and Barnes, S. J. (1983). A model for the origin of the platinum-rich sulphides horizons in the Bushveld and Stillwater Complexes. *Journal of Petrology*, **24**:133-165.

Campos-Alvarez, N.O., Samson, I.M. and Fryer, B.J. (2012). The role of magmatic and hydrothermal processes in PGE mineralisation, Ferguson Lake deposit, Nunavut, Canada. *Mineralium Deposita*, **47**(4): 441-465.

Carlson, R. W., Pearson, D. G., Boyd, S. B., Shirey, S. B., Irvine, G., Menzies, A. H. and Gurney, J. J. (1999). Re-Os systematics of lithospheric peridotites: implications for lithosphere formation and preservation. In: Gurney, J. J., Gurney, J. L., Pascoe, M. D. and Richardson, S. H. (eds.), Proceedings of the 7th International Kimberlite Conference. Red Roof Design, Cape Town, South Africa, 99-108.

Cawthorn, G. (2012). Lower Main Zone and Pyroxenite Marker in the Northern Limb: FACT vs FICTION. 5th Platreef Workshop, Mokopane, South Africa, 9-11th November, 2012.

Cawthorn, G. (2015). A review of the Bushveld Complex and its mineralisation. In: Hammond, N. Q. and Hatton, C. (eds.), Platinum-group element (PGE) mineralisation and resources of the Bushveld Complex, South Africa. Mineral Resources Series Number 2, Council for Geoscience, Pretoria, **5**:19-90.

Cawthorn, R. G. (1999). The platinum and palladium resources of the Bushveld Complex. *S. Afr. J. Sci*., **95**:481-489.

Cawthorn, R. G. (2002). The role of magmatic mixing in the genesis of PGE mineralisation in the Bushveld Complex: Thermodynamic calculations and new interpretations – a discussion. *Economic Geology*, **97**:663-666.

Cawthorn, R. G. (2005). Stratiform platinum-group element deposits in layered intrusions. In: Mungall, J. E. (ed.), Exploration for Platinum-Group Element Deposits. Short Course Series, mineralogical Association of Canada, **35**(3):57-73.

Cawthorn, R. G. (2007). The centenary of the discovery of platinum in the Bushveld Complex (10th November 1906). *Journal of the South African Institute of Mining and Metallurgy*, **107**:1-4.

Cawthorn, R. G. (2011). Geological interpretations from PGE distribution in the Bushveld Merensky and UG2 chromitite reefs. *Journal of the Southern African Institute of Mining and Metallurgy*, **11**:68-79.

Cawthorn, R. G. (2013). The residual of roof zone of the Bushveld Complex, South Africa. *Journal of Petrology*, **54**:1875-1900.

Cawthorn, R. G. and Ashwal, L. D. (2009). Origin of anorthosite and magnetitite layers in the Bushveld Complex: Constrained by major element compositions of plagioclase. *Journal of Petrology*, **50**:1607-1637.

Cawthorn, R. G. and McCarthy, T. S. (1981). Bottom crystallisation and diffusion control in layered complexes: evidence from Cr distribution in magnetite from the Bushveld Complex. *Transactions, Geological Society of South Africa*, **84**:41-50.

Cawthorn, R. G. and Molyneux, T. G. (1986). The vanadiferous magnetite deposits of the Bushveld Complex. In: Anhaeusser, C. R. and Maske, S. (eds.), Mineral Deposits of Southern Africa. Geological Society of South Africa, Johannesburg, II, 1251-1266.

Cawthorn, R. G. and Walraven, F. (1998). Emplacement and crystallization time for Bushveld Complex. *Journal of Petrology*, **39**:1669-1687.

Cawthorn, R. G. and Webb, S. J. (2001). Connectivity between the western and eastern Limbs of the Bushveld Complex. *Tectonophysics Elsevier*, **330**:195-209.

Cawthorn, R. G., Barton, J. M. Jr. and Viljoen, M. J. (1985). Interaction of floor rocks with the Platreef on Overysel, Potgietersrus, northern Transvaal. *Economic Geology*, **80**:988-1006.

Cawthorn, R. G., Eales, H. V., Walraven, F., Uken, R. and Watkeys, M. K. (2006). The Bushveld Complex. In: Johnson, M. R., Anhaeusser, C. R. and Thomas, R. J. (eds.), The Geology of South Africa. Geological Society of South Africa, Johannesburg/Council for Geoscience, Pretoria, 261-281.

Cawthorn, R. G., Lee, C. A., Schouwstra, R. P., and Mellowship, P. (2002). Relationship between PGE and PGM in the Bushveld Complex. *Canadian Mineralogist*, **40**:311-328.

Cawthorn, R. G., Merkle, R. K. and Viljoen, M. J. (2002). Platinum-group element deposits in the Bushveld Complex, South Africa. In: Cabri, L. J. (ed.), The Geology, Geochemistry, Mineralogy and

Mineral Beneficiation of Platinum-Group Elements. *Special Volume, Canadian Institute of Mining, Metallurgy and Petroleum*, **54**:431-458.

Cawthorn, R. G., Meyer, P. S. and Kruger, J. (1991). Major addition of magma at the Pyroxenite Marker in the western Bushveld Complex, South Africa. *Journal of Petrology*, **32**:739-763.

Cawthorn, R. G., Slabbert, M. and van der Merwe, J. (2004). The Full Merensky – its lithologies and genesis. Abstract Volume, Geoscience Africa, Johannesburg, 114-115.

Clark, D. A. (1997). Magnetic petrophysics and magnetic petrology: Aids to geological interpretation of magnetic surveys. *Journal of Australian Geology and Geophysics*, **17**: 83–103.

Clark, D. A. and Emerson, D.W. (1991). Notes on rock magnetization characteristics in applied geophysical studies. *Exploration Geophysics*, **22**: 547–555.

Clarke, B., Uken, R., Reinhardt, J. (2009). Structural and compositional constraints on the emplacement of the Bushveld Complex, South Africa. *Lithos*, **111** (1–2): 21–36.

Coertze, F.J., Jansen, H., and Walraven, F. (1977). The transition from the Transvaal sequence to the Waterberg Group. *South African Journal of Geology*, **80**: 145–156.

Coetzee, J. and Twist, D. (1989). Disseminated tin mineralisation in the roof of the Bushveld granite pluton at the Zaaiplaats Mine, with implications for the genesis of magmatic hydrothermal tin system. *Economic Geology*, **84**:1817-1834

Coetzee, L. L. (2001). Genetic stratigraphy of the Paleoproterozoic Pretoria Group in the Western Transvaal. Unpublished MSc thesis, Rand Afrikaans University, Johannesburg, South Africa, pp. 1-212.

Cornell, D. H., Armstrong, R. A. and Walraven, F. (1998). Geochronology of the Proterozoic Hartley Basalt Formation, South Africa: constraints on the Kheis tectogenesis and the Kaapvaal Craton's earliest Wilson Cycle. *Journal of African Earth Science*, **26**:5-27.

Corcoran, P.L., Bumby, A.J., Davis, D.W. (2013). The Paleoproterozoic Waterberg Group, South Africa: provenance and its relation to the timing of the Limpopo orogeny. *Precambrian Research*, **230**: 45–60.

Cousins, C. A. (1959). The structure of the mafic portion of the Bushveld Igneous Complex. *Transactions of the Geological Society of South Africa*, **62**:174-189.

Cousins, C. A. and Feringa, G. (1964). The chromite deposits of the western belt of the Bushveld Complex. *The geology of some ore deposits in Southern Africa*, **2**:183-202.

Cowley, A. (2014). Platinum 2013. Interim Review, Johnson Matthey, 40 pp.

Crocker, I. T. (1986). The Zaaiplaats tinfield, Potgietersrus district. In: Anhaeusser, C. R. and Maske, S. (eds.), Mineral Deposits of southern Africa. Vols I and II: *Geological Society of South Africa*, 1287-1299.

Crocket, J. H. (1981). Geochemistry of the platinum-group elements. In: Cabri, L. J. (ed.), Platinum-Group Elements: Mineralogy, Geology, Recovery. *Can. Inst. Mining and Metall. Spec*., **23**:47-64.

Crocket, J. H. (2002). Platinum-group element geochemistry of mafic and ultramafic rocks. In: Cabri, L. J. (ed.), the geology, geochemistry, mineralogy and mineral beneficiation of platinum-group elements. *Can. Inst. Mining and Metall. Spec*., **54**:177-210.

Crocket, J. H., Teruta, Y. and Garth, J. (1976). The relative importance of sulphides, spinels and platinoid minerals as carriers of Pt, Pd, Ir and Au in the Merensky Reef at Western Platinum Limited, near Marikana, South Africa. *Economic Geology*, **71**:1308-1323.

Crowson, P. (2001). Mineral handbook 2000-2001. Mining Journal Books, Eden Bridge, p. 486.

Cruden, A. R. (1998). On the emplacement of tabular granites. Journal of the Geological Society, London, **155**(5):853-862.

Davies, G. and Tredoux, M. (1985). The platinum-group elements and gold contents of the marginal rocks and sills of the Bushveld Complex. *Economic Geology*, **80**(4):838-848.

De Beer, J. H., Meyer, R. and Hattingh, P. J. (1987). Geoelectrical and Palaeomagnetic studies of the Bushveld Complex. In: Kröner, A. (ed.)., Proterozoic Lithospheric Evolution. *American Geophysical Union Geodynamics Series*, **17**:191-205.

De Klerk, W.J. (1992). Petrogenesis of the Upper Critical Zone in the western Bushveld Complex, with emphasis on the UG1 footwall and Bastard units.

De Klerk, L. (2005). Bushveld stratigraphy on Rooipoort, Potgietersrus limb. 2nd Platreef Workshop, Mokopane, South Africa, 28-30th October, 2005.

De Villiers, J. S. (1967). The geology of the area south of Potgietersrus, with special reference to the chromite deposits. Ph.D. thesis, University of the Witwatersrand, 124 pp.

De Villiers, J. S. (1970). The structure and petrology of the mafic rocks of the Bushveld Complex south of Potgietersrus. In: Visser, D. J. L. and von Gruenewaldt, G. (eds.), Symposium on the Bushveld Complex and other layered intrusions. Geological Society of South Africa, Johannesburg, 23-35.

De Waal, S. A. (1975). The mineralogy, chemistry and certain aspects of reactivity of chromite from the Bushveld Igneous Complex. National Institute for Metallurgy, Johannesburg, South Africa, Report No. 1709, pp. 80.

De Wit, M. J., Roering, C., Hart, R. J., Armstrong, R. A., De Ronde, C. E. J., Green, R. W. E., Tredoux, M., Peberdy, E. and Hart, R. A. (1992). Formation of an Archaean continent. *Nature*, **357**:553-563.

Djon, M.L.N. and Barnes, S.-J. (2012). Changes in sulfides and platinum-group minerals with the degree of alteration in the Roby, Twilight, and High Grade Zone of the Lac des Iles Complex, Ontario, Canada. *Mineralium Deposita,* **47**: 875-896.

Dorland, H. C., Beukes, N. J., Gutzmer, J., Evans, D. A. D. and Armstrong, R. A. (2006). Precise SHRIMP U-Pb zircon age constraints on the lower Waterberg and Soutpansberg Group, South Africa. *South African Journal of Geology*, **109**:139-156.

Drouin, M., Godard, M., Ildefonse, B., Bruguier, O. and Garrido, C. J. (2009). Geochemical and petrographic evidence for magmatic impregnation in the oceanic lithosphere at Atlantis Massif, Mid-Atlantic Ridge (IODP Hole UI309D, 30° N). *Chemical Geology*, **264**:71-88.

Du Plessis, C.P. (1987). New perspectives on early Waterberg Group sedimentation from the Gatkop area, northwestern Transvaal. *South African Journal of Geology*, **90**: 395–408.

Du Plessis, A. and Kleywegt, R. J. (1987). A dipping sheet model for the mafic lobes of the Bushveld Complex. *S. Afr. J. Geol*., **90**:1-6.

Du Plessis, C. P. and Walraven, F. (1990). The tectonic setting of the Bushveld Complex in southern Africa, Part 1: Structural deformation and distribution. *Tectonophysics*, **179**:305-319.

Du Toit, A. L. (1926). The Bushveld Igneous Complex and the associated rocks. London: Oliver and Boyd, pp. 136-150.

Du Toit, M. C., van Reenen, D. D. and Roering, C. (1983). Some aspects of the geology, structure and metamorphic of the Southern Marginal Zone of the Limpopo metamorphic complex. *Geological Society of South Africa, Special Publications*, **8**:121-142.

Dunnett, T., Grobler, D. F., Simmonotti, N. M. E. M. and Mapeka, J. M. (2012). Lithological variations within upper Critical Zone stratigraphy, Turfspruit 241KR, Northern Limb, Bushveld Complex. In: Abstract, 5th Platreef Workshop, Mokopane, South Africa 9th-11th November, 2012.

Eales, H. V. (1987). Upper Critical Zone chromitite layers at R. P. M. Union Section Mine, western Bushveld Complex. In: Stowe, C. W. (ed.), Evolution of Chromium Ore Fields. Van Nostrand Reinhold, New York, 109-143.

Eales, H. V. (2000). Implications of the chromium budget of the Western limb of the Bushveld Complex. *South African Journal of Geology*, **103**:141-150.

Eales, H. V. and Cawthorn, R. G. (1996). The Bushveld Complex. In: Cawthorn, R. G. (ed.), Layered Intrusions. Elsevier, Amsterdam, p. 181-230.

Eales, H. V. and Costin, G. (2012). Crustally contaminated Komatiite: primary source of the chromitites and Marginal, Lower and Critical Zone magma in a staging chamber beneath the Bushveld Complex. *Economic Geology*, **107**:645-665.

Eales, H. V., de Klerk, W. J. and Teigler, B. (1990). Evidence for magma mixing processes within the Critical and Lower Zones of the Northwestern Bushveld Complex, South Africa. *Chemical Geology*, **88**:261-278.

Eales, H. V., Marsh, J. S., Mitchell, A. A., de Klerk, W. j., Kruger, F. J. and Field, M. (1986). Some geochemical constraints upon models for the crystallization of the upper Critical Zone-Main Zone interval, northwestern Bushveld Complex. *Mineralogical Magazine*, **50**:567-582.

Eldridge, S. C., Compston, W., Williams, I. S., Both, R. A., Walshe, J. L. and Ohmoto, H. (1988). Sulfur isotope variability in sediment-hosted massive sulfide deposits as determine using the ion-microprobe, SHRIMP: I. An example from the Rammelsberg orebody. *Economic Geology*, **83**: 443-449.

Emeleus, C. H., Cheadle, M. J., Hunter, R. H., Upton, B. G. I. and Wadsworth, W. J. (1996). The Rum Layered Suite. In: Cawthorn, R. G. (ed.), Layered Igneous Rocks. Developments in petrology, v. 15, Elsevier Science BV, Amsterdam, p. 403-440.

Engela, A. (2014). An evaluation of the contact between the Bushveld Igneous Complex and the Waterberg Sedimentary Sequence in the Waterberg project. BSc thesis, University of the Witwatersrand, (unpublished). 78pp.

Engelbrecht, J. P. (1985). The chromites of the Bushveld Complex in the Nietverdiend area. *Economic Geology*, **80**:896-910.

Eriksson, P.G., and Reczko, B.F.F. (1995). The sedimentary and tectonic setting of the Transvaal Supergroup floor rocks to the Bushveld Complex. *Journal of African Earth Sciences*, **21**: 487–504.

Eriksson, P. G., Altermann, W., Catuneanu, O., Van der Merwe, R. and Bumby, A. J. (2001). Major influences on the evolution of the 2.67-2.1 Ga Transvaal Basin, Kaapvaal Craton. *Sedimentary Geology*, **141-142**:205-231.

Eriksson, P. G., Simpson, E. L., Eriksson, K. A., Bumby, A. J., Steyn, G. L. and Sarkar, S. (2000). Muddy roll-up structures in siliciclastic interdune beds of the 1.8 Ga Waterberg Group, South Africa. *Palaios*, **15**:177-183.

Fialin, M., Outrequin, M. and Staub, P.-F. (1997). A new tool to treat peak overlaps in electron-probe microanalysis of rare earth-element L-series X-rays. *European Journal of Mineralogy*, **9**: 965-968.

Finn, C. A., Bedrosain, P. A., Cole, J. C., Khoza, T. D. and Webb, S. J. (2015). Mapping the 3D extent of the Northern Lobe of the Bushveld Layered mafic intrusion from geophysical data. *Precambrian Research*, **268**:279-294.

Fischer, L. A., Wang, M., Charier, B., Namur, O., Robert, R. J., Veksler, I. V., Cawthorn, R. G. and Holtz, F. (2016). Immiscible iron- and silica-rich liquids in the Upper Zone of the Bushveld Complex. *Earth and Planetary Science Letters*, **443**:108-117.

Friese, A. E. W. (2004). Geology and tectono-magmatic evolution of the PPL concession area, Villa Nora – Potgietersrus Limb, Bushveld Complex. Geological Visitor Guide, Potgietersrus Platinum's Limited, 57pp.

Gain, S. B. (1985). The geological setting of the platiniferous UG2 chromitite layer on the farm Maandagshoek, eastern Bushveld Complex. *Economic Geology*, **77**:1395-1404.

Gain, S. B. and Mostert, A. B. (1982). The geological setting of the platinoid and base metal sulfide mineralisation in the Platreef of the Bushveld Complex on Drenthe, north of Potgietersrus. *Economic Geology*, **77**:1395-1404.

Gauert, C. D. K., de Waal, S. A. and Wallmach, T. (1996). Isotopic constraints on the source of sulphur for the base metal sulphides of the Uitkomst Complex, Badplaas, South Africa. *South African Journal of Geology*, **99**(1): 41-50.

Genkin, A. D , Distler, V. V., Gladyshev, G. D., Filimonova, A. A., Evstigneeva, T. L, Kovalenker, V. A., Laputina, I. P., Smirnov, A. V. and Grokhovskaya, T. L. (1981). Sulphide copper-nickel ores of the Noril'sk deposits. Nauka, Moscow (in Russian).

Godel, B., Barnes, S. J. and Maier, W. D. (2006). 3-D distribution of sulphide minerals in the Merensky Reef (Bushveld Complex, South Africa) and the JM Reef (Stillwater Complex, USA) and their

relationship to microstructures using X-ray computed tomography. *Journal of Petrology*, **47**(9):1853-1872.

Good, D. J., Cabri, J. J. and Ames, D. E. (2017). PGM facies variations for Cu-PGE deposits in the Coldwell Alkaline Complex, Ontario, Canada. Ore Geology Reviews. http://dx.doi.org/10.1016/j.oregeorev.2017.04.028.

Good, N., and de Wit, M. J. (1997). Thabazimbi-Murchison Lineament of the Kaapvaal craton, South Africa: 2700 Ma of episodic deformation. *Journal of the Geological Society, London*, **154**:93-97.

Grobler, N. J., and Whitfield, G. G. (1970). The olivine-apatite magnetitites and related rocks in the Villa Nora occurrence of the Bushveld Igneous Complex. *Geological Society of South Africa Special Publication* **1**: 208–227.

Grobler, D. F., Nielsen, S. A. and Broughton, D. W. (2012). Upper Critical Zone (Merensky Reef – UG2) correlates within the Platreef on Turfspruit 241KR, Northern Limb, Bushveld Complex. In: Abstract, 5th Platreef Workshop, Mokopane, South Africa, 9th – 11th November, 2012.

Grobler, D.F., Brits, J.A.N., Maier, W.D. and Crossingham, A., 2018. Litho-and chemostratigraphy of the Flatreef PGE deposit, northern Bushveld Complex. *Mineralium Deposita*, 1-26.

Guo, Q., Strauss, H., Kaufman, A. J., Schröder, S., Gutzmer, J., Wing, B., Baker, M. A., Bekker, A., Jin, Q., Kim, S.T. and Farquhar, J. (2009). Reconstructing Earth's surface oxidation across the Archean-Proterozoic transition. *Geology*, **37**(5): 399-402.

Hall, A. L. (1932). The Bushveld Igneous Complex of the central Transvaal. *Memoir. Geological Survey of South Africa*, **28**, 560pp.

Hanson, R. E., Gose, W. A., Crowley, J. L., Ramezoni, J., Bowring, S. A., Bullen, D. S., Hall, R. P., Pancake, J. A. and Mukwakwami, J. (2004). Paleoproterozoic intraplate magmatism and basin development on the Kaapvaal craton, age, paleomagnetism and geochemistry of ~1.93 to ~1.87 Ga post Waterberg dolerites. *South African Journal of Geology*, **107**:233-254.

Harmer, R. E. (2004). The Aurora project – Main Zone hosted PGE – base metal mineralisation at the northern outcrop limit of the Bushveld northern limb, north of Mokopane. Abstract Volume, Geoscience Africa, July 2004, University of the Witwatersrand, South Africa.

Harmer, R. E. (2005). The Aurora project. Extended Abstract Volume, Platinum Exploration and Exploitation in Africa, GSSA Directorate of Professional Programmes, 14th October, 2005.

Harmer, R. E. and Sharpe, M. R. (1985). Field relations and strontium isotope systematics of the marginal rocks of the eastern Bushveld Complex. *Economic Geology*, **80**(4):813-837.

Harmer, R. E. and von Gruenewaldt, G. (1991). A review of magmatism associated with the Transvaal Basin – implications for its tectonic settings. *South African Journal of Geology*, **94**:104-122.

Harmer, R. E., Pillay, N. and Davies, P. G. (2004). The Aurora project – Main Zone hosted PGE-base metal mineralisation at the northern outcrop of the Bushveld northern limb, north of Mokopane. Abstract, 1st Platreef Workshop Field Guide, Mokopane, 16-19 July 2004, Geoscience Africa, university of the Witwatersrand.

Harmer, R. E., Pillay, N. and Davies, P. G. (2004). The Aurora Project – Main Zone hosted PGE-base metal mineralisation at the northern outcrop limit of the Bushveld northern limb, north of Mokopane. In: Abstract, 1st Platreef Workshop, Mokopane, South Africa, July 16th-19th, 2004.

Harney, D. M. W. and Merkle, R. K. W. (1990). Pt-Pd minerals from the Upper Zone of the eastern Bushveld Complex, South Africa. *Canadian Mineralogist*, **28**:619-628.

Harney, D. M. W. and von Gruenewaldt, G. (1995). Ore forming processes in the upper part of the Bushveld Complex, South Africa. *Journal of African Earth Sciences*, **20**(2):77-89.

Harris, C. and Chaumba, J. B. (2001). Crustal contamination and fluid-rock interaction during the formation of the Platreef, northern limb of the Bushveld Complex, South Africa. *Journal of Petrology*, **42**:1321-1347.

Hatch, F. H. and Corstorphine, G. S. (1905). The geology of South Africa. Macmillan, London, 348 pp.

Hattingh, P. J. (1995). Palaeomagnetic constraints on the emplacement of the Bushveld Complex. *Journal of Africa Earth Sciences*, **21**:549-551.

Hattingh, P. J. and Pauls, N. D. (1994). New Palaeomagnetic results from the northern Bushveld Complex of South Africa. *Precambrian Research*, **69**:229-240.

Hatton, C. J. (1995). Mantle plume origin for the Bushveld and Ventersdorp magmatic provinces. *Journal of African Earth Sciences*, **21**:571-577.

Hatton, C. J. (1995). The Bushveld Complex, a product of interaction among magma derived from a mantle plume. Communs. *Geol. Surv. Namibia*, **10**:93-98.

Hatton, C. J. and Schweiter, J. K. (1995). Evidence for syn-chronous extrusive and intrusive Bushveld magmatism. *Journal of African Earth Sciences*, **21**:579-594.

Hatton, C. J. and Schweitzer, J. K. (1995). Evidence for synchronous extrusive and intrusive Bushveld magmatism. *Journal of African Earth Sciences*, **21**(4):579-594.

Hatton, C. J. and von Gruenewaldt, G. (1987). The geological setting and Petrogenesis of the Bushveld chromitite layers. Van Nostrand Reinhold Company, New York, p. 109-143.

Haufiku, M. N. (2005). Compositional variation in Core ATS057 through the southern Platreef. B.Sc. Honours dissertation, University of the Witwatersrand (Unpublished).

Haughton, D. R., Roeder, P. L. and Skinner, B. J. (1974). The solubility of sulfur in mafic magmas. *Economic Geology*, **69**:451-462.

Helmy, H.M., Ballhaus, C., Berndt, J., Bockrath, C. and Wohlgemuth-Ueberwasser, C. (2007). Formation of Pt, Pd and Ni tellurides: experiment in sulfide-telluride systems. *Contributions to Mineralogy and Petrology*, **153**: 577-465.

Hickman, M. H. (1978). Isotopic evidence for crustal reworking in the Rhodesian Craton, southern Africa. *Geology*, **6**:214-216.

Hiemstra, S. A. (1979). The role of collectors in the formation of platinum deposits in the Bushveld. *Canadian Mineralogist*, **17**:469-482.

Hiemstra, S. A. (1985). The distribution of some platinum-group elements in the UG2 chromitite layer of the Bushveld Complex. *Economic Geology*, **80**:944-957.

Hiemstra, S. A. (1986). The distribution of chalcophile and platinum-group elements in the UG2 chromitite layer of the Bushveld Complex. *Economic Geology*, **81**:1080-1086.

Holwell, D. A. (2006). The roles of magmatism, contamination and hydrothermal processes in the development of the Platreef mineralisation, Bushveld Complex, South Africa. Ph. D. Cardiff University, 299 pp.

Holwell, D. A. and Jordaan, A. (2006). Three-dimensional mapping of the Platreef at the Zwartfontein South Mine: implications for the timing of magmatic events in the northern limb of the Bushveld Complex. *Transaction, Institute of Mining and Metallurgy*, **115**:41-48.

Holwell, D. A. and Keays, R. R. (2014). The formation of low-volume, high-tenor magmatic PGE-Au sulfide mineralisation in closed systems: evidence from precious and base metal geochemistry of the Platinova Reef, Skaergaard Intrusion, East Greenland. *Economic Geology*, **109**:387-406.

Holwell, D. A. and McDonald, I. (2005). Variations in platinum-group element mineralisation within the Platreef, northern Bushveld Complex, South Africa. In: Törmanen, T. O. and Alapieti, T. T. (eds.), 10th International Platinum Symposium, University of Oulu, Extended Abstract, p. 110-113.

Holwell, D. A. and McDonald, I. (2006). Petrology, geochemistry and the mechanisms determining the distribution of platinum-group element and base metal sulphide mineralisation in the Platreef at Overysel, northern Bushveld Complex, South Africa. *Mineralium Deposita*, **41**:575-598.

Holwell, D. A., Adeyemi, Z., Ward, L. A., Smith, D. J., Graham, S. D., McDonald, I. and Smith, J. W. (2017). Low temperature alteration of magmatic Ni-Cu-PGE sulfides as a source for hydrothermal Ni and PGE ores: A quantitative approach using automated mineralogy. Ore Geology Reviews, http://dx.doi.org/10.1016/j.oregeorev.2017.08.025.

Holwell, D. A., Armitage, P. E. B. and McDonald, I. (2005). Observations on the relationship between the Platreef and its hanging wall. *Transaction, Institute of Mining and Metallurgy B*, **114**:199-207.

Holwell, D. A., Boyce, A. J. and McDonald, I. (2007). Sulfur isotope variations within the Platreef Ni-Cu-PGE deposit: genetic implications for the origin of sulphide mineralisation. *Economic Geology*, **102**:1001-1110.

Holwell, D. A., Jones, A., Smith, J. W. and Boyce, A. J. (2013). New mineralogical and isotopic constraints on Main Zone-hosted PGE mineralisation at Moordrift, northern Bushveld Complex. *Mineralium Deposita*, **48**:675-686.

Holwell, D. A., McDonald, I. and Armitage, P. E. B. (2006). Platinum-group mineral assemblages in the Platreef at the Sandsloot Mine, northern Bushveld Complex, South Africa. *Mineralogical Magazine*, **70**:83-101.

Holwell, D. A., Smith, J. W. and McDonald, I. (2015). GNPA-hosted PGE mineralisation south of Mokopane: Platreef, Merensky Reef, or neither. 6th Platreef Workshop, Mokopane, South Africa, 8-10th May, 2015, p. 18-21.

Holwell, D., Prasser, R., Barnes, S., Le Vaillant, M., Fisher, L. and Keays, R. (2015). 3D textural evidence for the formation of ultra-high tenor PGE and Au-bearing sulfide Microdroplets in the Platinova Reef, Skaergaard Intrusion, Greenland. In: Abstract, SGA – Magmatic (Ni-Cu-PGE) mineral systems; ore forming processes and geodynamic setting, p. 947-950.

Holzer, L., Frei, R., Barton, J. M., Jr., and Kramers, J. D. (1998). Unravelling the record of successive high grade events in the Central zone of the Limpopo belt using Pb single phase dating of metamorphic minerals. Precambrian Research, **87**: 87–115.

Hon, K., Kauahikaua, J., Denlinger, R. and Mackay, K. (1994). Emplacement and inflation of pahoehoe sheet flows: observations and measurements of active lava flows on Kilauea Volcano, Hawaii. *Geol. Soc. Am. Bull*., **106**:351-370.

Horstmann, U. E. and Malinga, O. (2003). Sulphur isotope analysis on a PDZ ANCA/GEO 20-20 continuous flow isotope ratio mass spectrometer. Part I – Hardware. Report Sable Isotope Lab 2003-06 (South Africa, Council for Geoscience).

Hulbert, L. J. (1983). A petrological investigation of the Rustenburg Layered Suite and associated mineralisation south of Potgietersrus. D. Sc. Thesis, University of Pretoria, 511 pp. (Unpublished).

Hulbert, L. J. and von Gruenewaldt, G. (1982). Nickel, copper and platinum mineralisation in the Lower Zone of the Bushveld Complex, south of Potgietersrus. *Economic Geology*, **77**:1296-1306.

Hulbert, L. J. and von Gruenewaldt, G. (1985). Textural and compositional features of chromite in the Lower and Critical Zones of the Bushveld Complex, south of Potgietersrus. *Economic Geology*, **80**:827-895.

Hulbert, L. J. and von Gruenewaldt, G. (1986). The structure of the upper and lower chromitite layers on the farms Grasvally and Zoetveld, south of Potgietersrus. In: Anheausser, C. R. and Maske, S. (eds.), Mineral Deposits of Southern Africa. Geological Society of South Africa, Johannesburg, v. 2, p. 1237-1249.

Hunter, R. H. (1996). Texture development in cumulate rocks. In: Cawthorn, R. G. (Ed), Layered Intrusions. Elsevier, Amsterdam, pp. 77-101.

Hutchinson, D. and Kinnaird, J. A. (2005). Complex multistage genesis for the Ni-Cu-PGE mineralisation in the southern region of the Platreef, Bushveld Complex, South Africa. *Transactions, Institute of Mining and Metallurgy*, **114**:208-224.

Hutchinson, D. and McDonald, I. (2008). Laser ablation ICP-MS study of platinum-group elements in sulphides from the Platreef at Turfspruit, northern limb of the Bushveld Complex, South Africa. *Mineralium Deposita*, **40**:576-597.

Hutchinson, D., Kinnaird, J. A. and Schurmann, L. W. (2004). Complex multi-stage mineralisation history in the southern sector of the Platreef, Bushveld Complex, RSA. Geoscience Africa, University of the Witwatersrand, 12-16th July, 2004.

Huthmann, F. M., Yudovskaya, M. A., Frei, D. and Kinnaird, J. A. (2016). Geochronological evidence for an extension of the northern lobe of the Bushveld Complex, Limpopo Province, South Africa. *Precambrian Research*, **280**:61-75.

Huthmann, F., Yudovskaya, M., Kinnaird, K., McCreesh, M. and McDonald, I. (2018). Petrogenesis and PGE of the Lower mineralised zone of the Waterberg Project, South Africa. *Ore Geology Reviews*, **92**:161-185.

Huthmann, F. M., Yudovskaya, M. A., Elburg, M. A., Kinnaird, J. A. (2017). The Sr isotopic stratigraphy of the far northern Bushveld Complex. *South African Journal of Geology*, **120**, in press

Ihlenfeld, C. and Keays, R. R. (2011). Crustal contamination and PGE mineralisation in the Platreef, Bushveld Complex, South Africa: evidence for multiple contamination events and transport of magmatic sulfides. *Mineralium Deposita*, **46**: 813-832.

Irvine, T. N. (1970). Crystallisation sequence in the Muskox intrusion and other layered intrusions. I. olivine-pyroxene-plagioclase relations. In: Visser, D. J. L. and von Gruenewaldt, G. (eds.), Symposium on the Bushveld igneous complex and other layered intrusions. *Geological Society of South Africa, Special Publication*, **1**:441-476.

Irvine, T. N. (1975). Crystallization sequence in the Muskox intrusion and other layered intrusions – II. Origin of chromitite layers and similar deposits of other magmatic ores. *Geochim. Cosmochim. Acta*., **39**:991-1020.

Irvine, T. N. (1977). Origin of chromitite layers in the Muskox intrusion and other stratiform intrusion: a new interpretation. *Geology*, **5**:273-277.

Irvine, T. N. (1979). Rocks whose composition is determined by crystal accumulation and sorting. In: Yoder, H. S. (ed)., The Evolution of the Igneous Rocks. Princeton University, Press, p. 245-306.

Irvine, T. N. and Sharpe, M. R. (1986). Magma mixing and the origin of stratiform oxide ore zones in the Bushveld and Stillwater Complex. In: Gallagher, M. G., Lxer, R. A., Neary, C. R. et al. (eds.), Metallogeny of Basic and Ultramafic Rocks. *Institute of Mining Metal, London*, p. 183-198.

Irvine, T. N., Keith, D. W. and Todd, S. G. (1983). The J-M platinum-palladium reef of the Stillwater Complex, Montana II. Origin by double-diffusive convective magma mixing and implications for the Bushveld Complex. *Economic Geology*, **78**:1287-1334.

Jansen, H. (1976). The Waterberg and Soutpansberg Groups in the Blouberg Area, Northern Transvaal. *Transactions of the Geological Society of South Africa*, **79**:281-291.

Jansen, H. (1982). The geology of the Waterberg basin in the Transvaal, Republic of South Africa. *Memoir of the Geological Survey of South Africa*, **71**:98pp.

Jones, R. E. (2013). Petrological and geochemical study of Platreef chromitites, northern Bushveld, South Africa. Ph.D. thesis, Cardiff University, 290pp. (Unpublished).

Jonson Matthey, (2011). Platinum Today. http://www.platinum.matthey.com

Kawohl, A. and Frimmel, H. E. (2016). Isoferroplatinum-pyrrhotite-troilite intergrowth as evidence of desulfurization in the Merensky Reef at Rustenburg (western Bushveld Complex, South Africa). *Mineralogical Magazine*, **80**(6): 1041-1053.

Keays, R. R. and Tegner, C. (2015). Magma chamber processes in the formation of the low-sulphide magmatic Au-PGE mineralisation of the Platinova Reef in the Skaergaard Intrusion, East Greenland. In: Abstract, SGA – Magmatic (Ni-Cu-PGE) mineral systems; ore forming processes and geodynamic setting, p. 959-961.

Keays, R. R. and Tegner, C. (2016). Magma chamber processes in the formation of the low-sulphide magmatic Au-PGE mineralisation of the Platinova Reef in the Skaergaard Intrusion, East Greenland. *Journal of Petrology*, **56**(12):2319-2340.

Kekana, S. M. (2015). Geochemical, mineralogical and tenor variations in the upper section of the Platreef, northern limb, Bushveld Complex and correlation with the Merensky Reef. In: Abstract, 6th Platreef Workshop, Mokopane, South Africa, 8th – 10th May, 2015.

Kennedy, B., McDonald, I. and Longridge, L. (2015). Platinum-group element mineralisation in the troctolite marker in the Main Zone, northern Bushveld Complex. In: Abstract, 6th Platreef Workshop, Mokopane, South Africa, 8th – 10th May, 2015, 28-29.

Kerr, A. and Leitch, A. M. (2005). Self-destructive sulfide segregation systems and the formation of high-grade magmatic ore deposits. *Economic Geology*, **100**:311-332.

King, A. (2009). Petrological and geochemical classification of Platreef alteration lithologies, Sandsloot Mine, South Africa. M.Sc. thesis, Camborne School of Mines, U.K. (Unpublished).

Kinloch, E. D. (1982). Regional trends in the platinum-group mineralogy of the Critical Zone of the Bushveld Complex, South Africa. *Economic Geology*, **77**:1328-1347.

Kinloch, E. D. and Peyerl, W. (1990). Platinum-group minerals in various rock types of the Merensky Reef: genetic implications. *Economic Geology*, **85**:537-555.

Kinnaird, J. A. (2004). What are the questions we need to ask about the Platreef? Extended Abstract Volume, 1st Platreef Workshop, Mokopane, South Africa, 16-19th July, 2004.

Kinnaird, J. A. (2005). Geochemistry evidence for multiphase emplacement in the southern Platreef. *Transactions, Institute of Mining and Metallurgy*, **114**:225-242.

Kinnaird, J. A. (2008). Have we answered the questions about the Platreef? Extended Abstract Volume, 3rd Platreef Workshop, Mokopane, South Africa, 11-13th July, 2008.

Kinnaird, J. A. and McDonald, I. (2005). An introduction to mineralisation in the northern limb of the Bushveld Complex. *Transaction, Institute of Mining and Metallurgy*, **114**:194-198.

Kinnaird, J. A. and Nex, P. A. M. (2003). Mechanisms of marginal mineralisation in the Bushveld Complex. *Appl. Earth Sci. (Trans. Inst. Min. Metall. B)*, **112**:B206-208.

Kinnaird, J. A. and Nex, P. A. M. (2015). An overview of the Platreef: Council for Geosciences, Mineral Resources Series 2, p. 193-342.

Kinnaird, J. A., Hutchinson, D., Schurmann, L., Nex, P. A. M. and de Lange, R. (2005). Petrology and mineralisation of the southern Platreef: Northern limb of the Bushveld Complex, South Africa. *Mineralium Deposita*, **40**:576-597.

Kinnaird, J. A., Kruger, F. J. and Cawthorn, R. G. (2004). Rb-Sr and Nd-Sm isotopes in fluorite related to the granites of the Bushveld Complex. *South African Journal of Geology*, **107**(3):413-430.

Kinnaird, J. A., Kruger, F. J., Nex, P. A. M. and Cawthorn, R. G. (2002). Chromitites of the Bushveld Complex – Process of formation and PGE enrichment. Economic Geology Research Institute, Huge Allsopp Laboratory. *Information Circular*, **369**:1-28.

Kinnaird, J. A., Kruger, F. J., Nex, P. A. M. and Cawthorn, R. G. (2002). Chromitite formation – a key to understanding processes of platinum enrichment. *The Institution of Mining and Metallurgy*, 23-35.

Kinnaird, J. A., Yudovskaya, M., McCreesh, M., Huthmann, F. and Botha, T. J. (2017). The Waterberg platinum-group element deposit: Atypical mineralisation in mafic-ultramafic rocks of the Bushveld Complex, South Africa. *Economic Geology*, **112**:1367-1394.

Kinnaird, J. A., Yudovskaya, M., Nichol, S., Naldrett, A. J., and Nex, P. A. M. (2010). Along strike and down-dip variations in multiphase sills of the Platreef, Bushveld Complex [abs.]: Platinum Symposium, 11th, Sudbury, Ontario, June 21–24, 2010, Abstracts.

Kinnaird, J. A., Yudovskaya, M. A., Botha, M. J. (2014). The Waterberg Extension to the Bushveld Complex. In: 11th International Platinum Symposium. Yekaterinburg, Russia.

Kitakaze, A. (2008). Sugakiite, $Cu(Fe,Ni)_8S_8$, a new mineral species from Hokkaido, Japan. *The Canadian Mineralogist*, **46**:263-267.

Kitakaze, A., Sugaki, A., Itoh, H. and Komatsu, R. (2011). A revision of phase relations in the system Fe-Ni-S from 650° to 450° C. *The Canadian Mineralogist*, **49**: 1687-1710.

Kleeman, G. J. (1985). The geochemistry and petrology of the roof rocks of the Bushveld Complex, east of Groblersdal. M.Sc. thesis, University of Pretoria, South Africa, p. 178.

Kleeman, G. J. and Twist, D. (1989). The compositionally zoned sheet-like granite pluton of the Bushveld Complex: Evidence bearing on the nature of A-type magmatism. *Journal of Petrology*, **30**:1383-1414.

Klemd, R., Junge, M., Oberthür, T., Herderich, T., Schouwstra, R. and Roberts, J. (2016). Platinum-group element concentrations in base-metal sulphides from the Platreef, Mogalakwena Platinum Mine, Bushveld Complex, South Africa. *South Africa Journal of Geology*, **119**:623-638.

Klemm, D. D., Henckel, J., Dehm, R. and von Gruenewaldt, G. (1985). The geochemistry of titanomagnetite in magnetitite layers and their host rocks of the eastern Bushveld Complex. *Economic Geology*, **80**:1075-1088.

Klemm, D. D., Ketterer, S., Reichardt, F., Steindl, J., and Weber-Diefenbach, K. (1985). Implication of vertical and lateral compositional variations across the Pyroxene Marker and its associated rocks in the upper part of the Main zone in the eastern Bushveld. *Economic Geology*, **80**: 1007–1015.

Knoper, M. W. and von Gruenewaldt, G. (1996). The Bellevue (BV-1) borehole core log: 2.9 km of Bushveld Complex stratigraphy (northern limb), Potgietersrus, South Africa. Available online at http://www.geocities.com/mwk.geo/bic.htm.

Kramers, J. D., McCourt, S. and van Reenen, D. D. (2006). The Limpopo Belt. In: Johnson, M. R., Anhaeusser, C. R. and Thomas, R. J. (eds.), The Geology of South Africa. Geological Society of South Africa, Johannesburg/Council for Geoscience, Pretoria, p. 57-94.

Kramers, J. D., Mouri, H. (2011). The geochronology of the Limpopo Complex: A controversy solved. In: van Reenen, D. D., Kramers, J. D., McCourt, S., Perchuk, L. L. (Eds.), Origin and Evolution of Precambrian High-grade Gneiss Terranes, with Special Emphasis on the Limpopo Complex of Southern Africa. *Geological Society of America Memoir*, pp. 85-106.

Kruger, F. J. (1990). The stratigraphy of the Bushveld Complex: a reappraisal and relocation of the Main Zone boundaries. *South African Journal of Geology*, **93**(2):376-381.

Kruger, F. J. (1994). The Sr-isotopic stratigraphy of the western Bushveld Complex. *South African Journal of Geology*, **97**:393-398.

Kruger, F. J. (2005). Filling the Bushveld Complex magma chamber: lateral expansion, roof and floor interaction, magmatic unconformities and the formation of giant chromitite, PGE and Ti-V-magnetitite deposits. *Mineralium Deposita*, **40**:451-472.

Kruger, F. J. and Marsh, J. S. (1982). Significance of $^{87}Sr/^{86}Sr$ ratios in the Merensky Cyclic Unit of the Bushveld Complex. *Nature*, **298**:53-55.

Kruger, F. J., Cawthorn, R. G., Meyer, P. S. and Walsh, K. L. (1986). Sr-isotopic, chemical and mineralogical variations across the pyroxenite marker and in the Upper Zone of the western Bushveld Complex. In: Geo-congress '86, Johannesburg: *Geological Society of South Africa*, 609-612.

Lana, C., Reimold, W. U., Gibson, R. L., Koeberl, C., and Siegesmund, S. (2004). Nature of the Archean midcrust in the core of the Vredefort dome, Central Kaapvaal craton, South Africa. *Geochimica et Cosmochimica Acta*, **68**: 623–642.

Latypov, R. M. and Egorova, V. (2012). Plagioclase composition give evidence for in situ crystallization under horizontal flow conditions in mafic sills. *Geology*, **40**:883-886.

Latypov, R., Chistyakova, S., Page, A. and Hornsey, R. (2016). Field evidence for the in-situ crystallisation of the Merensky Reef. *Journal of Petrology*, **56**(12):2341-2372.

Latypov, R., O'Driscoll, B. and Lavrenchuk, A. (2013). Towards a model for the in situ origin of PGE reefs in layered intrusions: insight from chromitite seams of the Rum Eastern Layered Intrusion, Scotland. *Contrib. Mineral Petrol*., **166**:309-327.

Latypov, R., Chistyakova, S., Barnes, S. J. and Hunt, E. J. (2017a). Origin of platinum deposits in layered intrusions by In situ crystallisation: Evidence from undercutting Merensky Reef of the Bushveld Complex. *Journal of Petrology*, **58**(4):715-762.

Latypov, R., Chistyakova, S. and Mukherjee, R. (2017b). A novel hypothesis for origin of massive chromitites in the Bushveld Igneous Complex. *Journal of Petrology*, 1-41; doi: 10.1093/petrology/egx077

Lee, C. A. (1983). Trace and platinum-group elements geochemistry and the development of the Merensky Reef of the Bushveld Complex. *Mineralium Deposita*, **18**:173-180.

Lee, C. A. (1996). A review of mineralisation in the Bushveld Complex and some other layered mafic intrusions. In: Cawthorn, R. G. (ed.), Layered Intrusions, Elsevier Science, 103-146.

Lee, C. A. and Parry, S. J. (1988). Platinum-group element geochemistry of the Lower and Middle Group chromitites of the eastern Bushveld Complex, *Economic Geology*, **83**:1127-1139.

Lee, C. A. and Tredoux, M. (1986). Platinum-group element abundances in the Lower and the lower Critical Zones of the eastern Bushveld Complex. *Economic Geology*, **81**:1087-1095.

Leeb-Du Toit, A. (1986). The Impala Platinum Mines. In: Anheausser, C. R. and Maske, S. (eds.), Mineral Deposits of Southern Africa. Geological Society of South Africa, Johannesburg, II, 1091-1106.

Lenhardt, N. and Eriksson, P. G. (2012). Volcanism of the Palaeoproterozoic Bushveld Large Igneous Province: the Rooiberg Group, Kaapvaal Craton, South Africa. *Precambrian Research*, **214-215**:82-94.

Lenthall, D. H. (1973). A proposed nomenclature system for the granophyres associated with the Bushveld Complex. *Transaction, Geological Society of South Africa*, **76**:75-76.

Li, C. and Naldrett, A. J. (1993). Sulfide capacity of magma: A quantitative model and its application to the formation of the sulfide ores at Sudbury. *Economic Geology*, **88**:1253-1260.

Li, C., Ripley, E. M., Merino, E. and Maier, W. D. (2004). Replacement of base metal sulphides by actinolite, epidote, calcite and magnetite in the UG-2 and Merensky Reef of the Bushveld Complex, South Africa. *Economic Geology*, **99**: 173-184.

Li, C. and Ripley, E. M. (2005). Empirical equations to predict the sulfur content of mafic magmas at sulfides saturation and applications to magmatic sulfide deposits. *Mineralium Deposita*, **40**:218-230.

Li, C. and Ripley, E. M. (2009). Sulphur contents at sulphide – liquid or anhydrite saturation in silicate melts: Empirical equations and example applications. *Economic Geology*, **104**:405-412.

Li, C., Maier, W. D. and de Waal, S. A. (2001). The role of magma mixing in the genesis of PGE mineralisation in the Bushveld Complex: Thermodynamic calculations and new interpretations. *Economic Geology*, **96**:653-662.

Li, C., Ripley, E. M., Maier, W. D. and Gomme, T. E. S. (2002). Olivine and sulphur isotopic compositions of the Uitkomst Ni-Cu sulfide ore bearing complex, South Africa: evidence for sulfur contamination and multiple magma emplacement. *Chemical Geology*,**188**: 149-159.

Liebenberg, L. (1968). The sulphides in the layered sequence of the Bushveld Igneous Complex. DSc thesis, University of Pretoria, South Africa, (Unpublished).

Liebenberg, L. (1970). The sulfides in the layered sequence of the Bushveld Igneous Complex. *Geological Society of South Africa, Special Publication*, **1**:108-208.

Lightfoot, P. C., Evans-Lamswood, D. (2015). Structural controls on the primary distribution of mafic-ultramafic intrusions containing Ni-Cu-Co (PGE) sulfide mineralization in the roots of large igneous provinces. *Ore Geology Reviews*, **64**: 354–386.

Lister, J. R. and Kerr, R. C. (1991). Fluid-mechanical models of crack propagation and their application to magma transport in dykes. *Journal of Geophysical Research*, **96**:10049-10077.

Lodders, K. (2003). Solar system abundances and condensation temperatures of the elements. *Astrophys. Journal*, **591** (2): 1220–1247.

Lomberg, K. and Goldschmidt, A. (2014). Technical report for the update on exploration drilling at the Waterberg Joint Venture and Waterberg Extension Project, South Africa (Latitude 23°14'11''S, Longitude 28°54'42''E). Platinum Group Metals Ltd (Internal Report).

Longridge, L. (2015). Magnetite layers of the Upper zone in the Northern limb—their formation and mineralisation potential [abs.]: Platreef Workshop, 6th, Mokopane, South Africa, May 8–10, 2015, Abstracts.

MacCaskie, D. R. (1983). Differentiation of the Nebo granite (Main Bushveld Granite), South Africa. Unpublished PhD thesis, University of Oregon, U.S.A.

Maier, W. D. (2002). Pt, Pd, Cu and sulfur contents of the Platreef on the farm Townlands, northern Bushveld Complex. In: Boudreau, A. (ed.), 9th International Platinum Symposium, extended abstract, 21-25th July, 2002, Billings, Montana, USA.

Maier, W. D. (2005). Platinum-group elements (PGE) deposits and occurrences: mineralisation styles, genetic concepts, and exploration criteria. *Journal of African Earth Sciences*, **41**:165-191.

Maier, W. D. and Barnes, S. –J. (1998). Concentration of rare-earth elements in silicate rocks of the Lower, Critical and Main Zones of the Bushveld Complex. *Chemical Geology*, **150**:85-103.

Maier, W. D. and Barnes, S. –J. (1999). Platinum-group elements in silicate rocks of the Lower, Critical and Main Zones at Union Section, Western Bushveld Complex. *Journal of Petrology*, **40**(11):1647-1671.

Maier, W. D. and Barnes, S. –J. (2010). The Petrogenesis of platinum-group element reefs in the upper Main Zone of the Northern Lobe of the Bushveld Complex on the farm Moorddrift, South Africa. *Economic Geology*, **105**:841-854.

Maier, W. D. and Eales, H. V. (1997). Correlation within the UG2-Merensky Reef interval of the Western Bushveld Complex, based on geochemical, mineralogical and petrological data. *Geol. Surv. S. Afr. Bull*., **120**:56pp.

Maier, W. D. and Teigler, B. (1995). A facies model for the western Bushveld Complex. *Economic Geology*, **90**:2343-2349.

Maier, W. D., Barnes, S. –J. and Groves, D. I. (2013). The Bushveld Complex, South Africa: formation of platinum- palladium-, chrome- and vanadium-rich layers via hydrodynamic sorting of a mobilised cumulate slurry in a large, relatively slowly cooling, subsiding magma chamber. *Mineralium Deposita*, **48**:1-56.

Maier, W. D., Barnes, S. –J. and Marsh, J. S. (2003). The concentrations of the noble metals in Southern Africa flood-type basalts and MORB: implication for Petrogenesis and sulphide exploration. *Cont. Miner. Petrol*., **146**:44-61.

Maier, W. D., Barnes, S. –J. and van der Merwe, M. J. (2001). The concentrations of PGE in the Pyroxenite Marker, Bushveld Complex: Implications for the formation of the Main Zone. *South African Journal of Geology*, **104**:335-342.

Maier, W. D., de Klerk, L., Blaine, J., Manyeruke, T., Barnes, S. –J., Stevens, M. V. A. and Mavrogenes, J. A. (2008). Petrogenesis of contact-style PGE mineralisation in the northern lobe of the Bushveld Complex: comparison of data from the farms Rooipoort, Townlands, Drenthe and Nonnenwerth. *Mineralium Deposita*, **43**:255-280.

Maier, W. D., Barnes, S. -J., and de Waal, S. A. (2001). Platinum-group elements in the Pyroxenite Marker, Bushveld Complex: Implications for the formation of the Main zone. *South African Journal of Geology*, **104**: 301–308.

Maier, W. D., Arndt, N. T. and Curl, E. A. (2000). Progressive crustal contamination of the Bushveld Complex: evidence from Nd isotopic analyses of the cumulate rocks. *Contributions to Mineralogy and Petrology*, **140**(3): 316-327.

Manenzhe, H. (2006). Investigation of the granofels and agmatitic breccia's of the Platreef. B.Sc. Honours thesis, University of the Witwatersrand, 56 pp. (Unpublished).

Mangwegape, M., Roelofse, F. Mock, T., and Carlson, R. W. (2016). The Sr-isotopic stratigraphy of the Northern Limb of the Bushveld Complex, South Africa. Journal of African Earth Sciences, **113**(1): 95-100.

Manyeruke, T. D. (2007). Composition and lithological variation of the Platreef on the farm Nonnenwerth, northern lobe of the Bushveld Complex: implications for the origin of the platinum-group element (PGE) mineralisation. Ph.D. thesis, University of Pretoria, 235pp. (Unpublished).

Manyeruke, T. D., Maier, W. D. and Barnes, S. –J. (2005). Major and trace element geochemistry of the Platreef on the farm Townlands, northern Bushveld Complex, South Africa. *Journal of Geology*, **108**:381-396.

Martini, J. E. J. (1998). The Loskop Formation and its relationship to the Bushveld Complex, South Africa. *Journal of Africa Earth Science*, **27**(2):193-222.

Mathez, E. A. and Mey, J. L. (2005). Character of the UG2 chromitite and host rocks and Petrogenesis of its pegmatoidal footwall, northeastern Bushveld Complex. *Economic Geology*, **100**(8):1617-1630.

Mavrogenes, J. A. and O'Neil, H. S. C. (1999). The relative effects of pressure, temperature and oxygen fugacity on the solubility of sulfide in mafic magma. *Geochimica et Cosmochimica Acta*, **63**:1173-1180.

McCallum, I. S., Ruedeke, L. D. and Mathez, E. A. (1980). Investigations of the Stillwater Complex: Part I. Stratigraphy and structure of the Banded Zone. *American Journal of Science*, **280-A**:59-87.

McCreesh, M. J. G. (2013). A study of the Main zone-Upper zone boundary beneath a thick succession of Waterberg sediments in the far north of the Northern limb of the Bushveld Complex. B.Sc. thesis, University of the Witwatersrand, 148 p.

McCreesh, M. J. G. (2016). An investigation of the mineralisation in the Waterberg PGE deposit, South Africa. M.Sc. thesis University of the Witwatersrand, 489 p.

McCreesh, M. J. G. and Kinnaird, J. A. (2014). Petrographic study of the sill and footwall from the boreholes of the Waterberg Project. (Internal report) p 1-4.

McCreesh, M. J. G., Kinnaird, J. A. and Yudovskaya, M. (2015). A comparison of the two unique mineralised packages associated with Main Zone rocks in the Waterberg Extension Project of the northern limb, Bushveld Complex. In: Abstract, 6th Platreef Workshop, Mokopane, South Africa, 8th – 10th May, 2015, 36-39.

McCreesh, M. J. G., Yudovskaya, M. A., Kinnaird, J. A. and Christian, R., (2018). Platinum-group minerals of the F and T zones, Waterberg Project, Far Northern Bushveld Complex: implication for the formation of the PGE mineralisation. *Mineralogical Magazine*, **82**(3):1-37.

McCutcheon, S. (2012). Platinum-group mineral assemblages in the Platreef on Tweefontein, northern Bushveld Complex, South Africa. M.Sc. thesis University of the Witwatersrand, 128p.

McDonald, I. and Armitage, P. E. B. (2003). The Platreef of the Northern Bushveld, South Africa – is it equivalent to the Merensky Reef? *Appl. Earth Sci. (Trans. Inst. Min. Metall. B)*, **112**:212-213.

McDonald, I. and Harmer, R. E. (2010). The nature of PGE mineralisation in the Aurora Project area, northern Bushveld Complex, South Africa. Abstract, 11th International Platinum Symposium, 21st – 24th June 2010, Sudbury, Ontario. In: Jugo, P. J., Lesher, C. M. and Mungall, J. E. (eds.), Ontario Geological Survey, Miscellaneous Release Data – 269 pp.

McDonald, I. and Holwell, D. A. (2011). Geology of the northern Bushveld Complex and the setting and genesis of the Platreef Ni-Cu-PGE deposit. *Reviews in Economic Geology*, **17**:297-327.

McDonald, I. and Viljoen K.S. (2006). Platinum-group element geochemistry of mantle eclogites: A reconnaissance study of xenoliths from the Orapa kimberlite, Botswana. *Applied Earth Science*, **115**(3): 81–93.

McDonald, I., Vaughan, D.J., and Tredoux, M. (1995). Platinum mineralization in quartz veins near Naboomspruit, central Transvaal. *South African Journal of Geology*, p. 168–175.

McDonald, I. and Holwell, D. A. and Armitage, P. E. B. (2005). Stratigraphy and platinum-group element mineralisation in the northern lobe of the Bushveld Complex, South Africa. In: Törmanen, T. D. and Alapieti, T. T. (eds.), 10th International Platinum Symposium, University of Oulu, Ext. Abstract, p. 193-196.

McDonald, I., Harmer, R. E., Holwell, D. A., Hughes, H. S. R. and Boyce, A. J. (2017). Cu-Ni-PGE mineralisation at the Aurora Project and potential for a new PGE province in the Northern Bushveld Main Zone. *Ore Geology Reviews*, **80**:1135-1159.

McDonald, I., Holwell, D. A. and Armitage, P. E. B. (2005). Geochemistry and mineralogy of the Platreef and Critical Zone of the northern limb of the Bushveld Complex, South Africa. *Mineralium Deposita*, **40**:526-549.

McDonald, I., Holwell, D. A. and Wesley, B. (2009). Assessing the potential involvement of an early magma staging chamber in the generation of the Platreef Ni-Cu-PGE deposit in the northern limb of the Bushveld Complex: a pilot study of the Lower Zone Complex at Zwartfontein. *Transactions, Institute of Mining and Metallurgy*, **118**:5-20.

McDonald, I., Ohnenstetter, D., Rowe, J. P., Tredoux, M., Pattrick, R. A. D. and Vaughan, D. J. (1999). Platinum precipitation in the Waterberg deposit, Naboomspruit, South Africa. *South African Journal of Geology*, **102**:184-191.

McDonough, W. F. and Sun, S. –S. (1995). The composition of the Earth. *Chem. Geology*, **120**:223-253.

McLaren, C. H. and De Villiers, J. P. R. (1982). The platinum-group chemistry and mineralogy of the UG2 chromitite layers of the Bushveld Complex. *Economic Geology*, **77**:1348-1366.

McNaughton, N. J., Pollard, P. J., Groves, D. I, and Taylor, R. G. (1993). A long-lived hydrothermal system in Bushveld Granites at the Zaaiplaats Tin Mine: Lead Isotope Evidence. *Economic Geology*, **88**:27-43.

Merensky, H. (1925). The platinum occurrence on the properties of Potgietersrus Platinum Limited. Report for Potgietersrus Platinum Limited.

Merkle, R. K. W. (1992). Platinum-group element minerals in the middle group of chromitite layers at Marikana, western Bushveld Complex. *Canadian Journal of Earth Sciences*, **29**:209-221.

Meyer, R. and de Beer, J. H. (1987). Structure of the Bushveld Complex from resistivity measurements. *Nature*, **325**(6105):610-612.

Merkle, R.K. and Verryn, S.M. (2003). Cooperite and braggite from the Bushveld Complex: implications for the miscibility gap and identification. *Mineralium Deposita*, **38**(3): 381-388.

Miller, J. D. Jr. and Anderson, J. C. O. (2002). Attributes of Skaergaard-type reefs. In: Boudreau, A. (ed.), Extended Abstracts, 9th International Platinum Symposium, Billings, Montana, 305-308.

Mills-Davies, J. E. (1925). The geology of the Transvaal platinum deposits. *S. Afr. Min. Eng*., **36**:63-66.

Misra, K. C. (2000). Understanding mineral deposits. Kluwer Academic Publishers, Dordrecht, pp. 845.

Mitchell, A. A. (1990). The stratigraphy, petrography and mineralogy of the Main Zone of the northwestern Bushveld Complex. *South African Journal of Geology*, **93**:818-831.

Mitchell, A. A. and Manthree, R. (2002). The Giant Mottled Anorthosite: a transition sequence at the top of the upper Critical Zone of the Bushveld Complex. *South Africa Journal of Geology*, **105**:15-24.

Mitchell, A. A. and Scoon, R. N. (2007). The Merensky Reef at Winnaarshoek, Eastern Bushveld Complex: A primary magmatic hypothesis based on a wide reef facies. *Economic Geology*, **102**:971-1009.

Mitchell, A. A. and Scoon, R. N. (2012). The Platreef of the Bushveld Complex, South Africa: A new hypothesis of multiple, non-sequential magma replenishment based on observation at the Akanani Project, north-west of Mokopane. *South African Journal of Geology*, **115.4**:535-550.

Molyneux, T. G. (1970). A geological investigation of the Bushveld Complex in Sekhukhuneland and part of the Steelpoort Valley, eastern Transvaal, with particular reference to the oxide minerals. D. Sc. Thesis, University of Pretoria.

Molyneux, T. G. (1970). The geology of the area in the vicinity of Magnet Heights, eastern Transvaal, with special reference to the magnetic iron ore. *Geological Society of South Africa Johannesburg Special Publication*, **1**: 228–241.

Molyneux, T. G. (1974). A geological investigation of the Bushveld Complex in Sekhukhuneland and part of the Steelpoort Valley. *Transactions, Geological Society of South Africa*, **77**:329-338.

Molyneux, T. G. and Klinkert, P. S. (1978). A structural interpretation of part of the eastern mafic lobe of the Bushveld Complex and its surroundings. *Transaction of the Geological Society of South Africa*, **81**:359-368.

Mondal, S. K. and Mathez, E. A. (2007). Origin of the UG2 chromitite layer, Bushveld Complex. *Journal of Petrology*, **48**:495-510.

Mostert, A. B. (1982). The mineralogy, petrology and sulphide mineralisation of the Platreef north-west of Potgietersrus, Transvaal, Republic of South Africa. *Bulletin, Geological Survey of South Africa*, **72**:48.

Mothetha, M. V. (2006). Petrology and geochemistry of the southern sector of the Platreef, Bushveld Complex. M.Sc. thesis, University of the Witwatersrand, 243 pp. (Unpublished).

Mukherjee, R., Latypov, R. and Balakrishna, A. (2017). An intrusive origin of some UG1 chromitite layers in the Bushveld Igneous Complex, South Africa: Insights form field relationships. *Ore Geology Reviews* (in press).

Mungall, J. E. and Brenan, J. M. (2014). Partitioning of platinum-group elements and Au between sulfide liquid and basalt and the origins of mantle-crust fractionation of the chalcophile elements. *Geochimica et Cosmochimica Acta*, **125**:265-289.

Mungall, J. E. and Naldrett, A. J. (2008). Ore deposits of the platinum-group elements. *Elements*, **4**(4):253-258.

Mungall, J. E., Ames, D. A. and Hanley, J. J. (2004). Geochemical evidence from the Sudbury structure for crustal redistribution by large bolide impacts. *Nature*, **429**:546-548.

Mungall, J. E., Kamo, S. L. and McQuade, S. (2016). U–Pb geochronology documents out-of-sequence emplacement of ultramafic layers in the Bushveld Igneous Complex of South Africa: *Nature Communications*, **7**: 13385, doi: 10.1038/ncomms13385

Munyanyiwa, H. (1999). Geochemical of the Umkondo dolerites and lavas in the Chimanimani and Chipinge Districts (eastern Zimbabwe) and their regional implications. *Journal of African Earth Sciences*, **28**(2):349-365.

Naldrett, A. J. (2004). Magmatic sulfide deposits: Geology, geochemistry and exploration. Springer Verlag, Heidelberg, 728 pp.

Naldrett, A. J. (2005). The Platreef: Death at Drenthe; Resurrection at Aurora. Extended Abstract Volume, 2nd Platreef Workshop, Mokopane, South Africa, 28-30th October, 2005.

Naldrett, A. J. (2010). From the mantle to the bank: the life of a Ni-Cu-(PGE) sulfide deposit. *South African Journal of Geology*, **113**(1):1-32.

Naldrett, A. J. (2010). Secular variation of magmatic sulfide deposits and their source magma. *Economic Geology*, **105**: 669-688.

Naldrett, A. J. (2011). Fundamentals of magmatic sulfide deposits. *Reviews in Economic Geology*, **17**:1-50.

Naldrett, A. J. and von Gruenewaldt, G. (1989). Association of platinum-group elements with chromitite in layered intrusions and ophiolite complexes. *Economic Geology*, **84**:180-187.

Naldrett, A.J. and Duke, J.M. (1980). Platinum metals magmatic sulfide ores. *Science*, **208**(4451):1417-1424.

Naldrett, A.J., Gasparrini, E.C., Barnes, S.J., Von Gruenewaldt, G. and Sharpe, M.R. (1986). The Upper Critical Zone of the Bushveld Complex and the origin of Merensky-type ores. *Economic Geology*, **81**(5): 1105-1117.

Naldrett, A. J., Kinnaird, J., Wilson, A. and Chunnett, G. (2008). Concentration of PGE in the Earth's Crust with special reference to the Bushveld Complex. *Earth Science Frontiers*, **15**(5):264-297.

Naldrett, A. J., Kinnaird, J. A., Wilson, A., and Chunnett, G. (2008). Links between the Platreef and the Upper Critical zone of the Bushveld Complex [ext. abs.]: Platreef Workshop, 3rd, Mokopane, South Africa, July 11–13, 2008, Extended Abstract Volume.

Naldrett, A. J., Lightfoot, P. C., Fedorenko, V. A., Gorbachev, N. S. and Doherty, W. (1992). Geology and geochemistry of intrusions and flood basalts of the Noril'sk region, USSR with implications for the origin of the Ni-Cu ores. *Economic Geology*, **87**:975-1004.

Naldrett, A. J., Wilson, A., Kinnaird, J. and Chunnett, G. (2009). PGE tenor and metal ratios within and below the Merensky Reef, Bushveld Complex: Implications for its genesis. *Journal of Petrology*, **50**:625-659.

Naldrett, A., Kinnaird, J.A., Wilson, A.H., Yudovskaya, M.A., Chunnett, G. (2011). Genesis of the PGE-enriched Merensky Reef and chromitite seams of the Bushveld Complex. In: *Reviews in Economic Geology* v. **17**. Society of Economic Geologists, pp. 235–296.

Naldrett, A. J., Wilson, A., Kinnaird, J., Yudovskaya, M. and Chunnett, G. (2012). The origin of chromitites and related PGE mineralisation in the Bushveld Complex: new mineralogical and petrological constraints. *Mineralium Deposita*, **47**:209-232.

Naldrett, A. J., Wilson, A., Kinnaird, J., Yudovskaya, M. and Chunnett, G. (2012). The application of MELTS to the formation of chromitites and related PGE mineralization in the Bushveld Complex and elsewhere. *Mineralium Deposita,* **47**, 209-232.

Naldrett, A., Kinnaird, J., Wilson, A., Chunnett, G. and Yudovskaya, M. (2015). Platinum-group elements in the Critical Zone of the Bushveld Complex. Council for Geosciences, Mineral Resources Series 2, 93-191.

Nell, J. (1985). The Bushveld metamorphic aureole in the Potgietersrus area: evidence for a two-stage metamorphic event. *Economic Geology*, **80**:1129-1152.

Nex, P. A. M. (2005). The structural setting of mineralisation on Tweefontein Hill, northern limb of the Bushveld Complex, South Africa. *Transaction of the Institute of Mining and Metallurgy*, **114**:243-251.

Nex, P. A. M. and Kinnaird, J. A. (2004). The Platreef: It's not as simple as A, B, C. Abstract Volume, Geoscience Africa 2004, University of the Witwatersrand, Johannesburg, South Africa, 494-495.

Nex, P. A. M., Cawthorn, R.G. and Kinnaird, J. A. (2002). Geochemical effects of magma addition: compositional reversal and decoupling of trends in the Main Zone of the western Bushveld Complex. *Mineralogical Magazine*, **66**(6):833-856.

Nex, P. A. M., Kinnaird, J. A., Jones, B. and Colloty, A. (2006). Platreef rock type definitions and descriptions. Anglo Platinum Report, 80 pp.

Nex, P. A., Kinnaird, J. A., Ingle, L. J., van der Vyver, B. A. and Cawthorn, R. G. (1998). A new stratigraphy for the Main Zone of the Bushveld Complex, in the Rustenburg area. *South Africa Journal of Geology*, **101**(3):215-223.

Nichol, S. and Kinnaird, J. A. (2008). Platinum-group mineral assemblages in the Platreef at Tweefontein North. Extended Abstract Volume, 3rd Platreef Workshop, Mokopane, South Africa, 11-13th July, 2008.

Nicoli, G., Stevens, G., Moyen, J. –F. and Frei, D. (2015). Rapid evolution from sediment to analectic granulite in an Archean continental collision zone: the example of the Bandelierkop Formation metapelites, South Marginal Zone, Limpopo Belt, South Africa. *Journal of Metamorphic Geology*, **33**:177-202.

Nielsen, T. F. D., Andersen, J. C. Ø. and Brooks, C. K. (2005). The Platinova Reef of the Skaergaard Intrusion. In: Mungall, J. E (ed.), Exploration for Platinum Group Element Deposits. *Mineralogical Association of Canada Short Course Series*, **35**:431-455.

Nodder, S., McDonald, I. and Grobler, D. (2015). Correlating the northern limb with the western and eastern limbs: A geochemical and petrological study of Turfspruit core. In: Abstract, 6th Platreef Workshop, Mokopane, South Africa, 8th – 10th May, 2015.

Nyama, N., Nex, P. and Yao, Y. (2005). Preliminary petrological studies of the Platreef on Tweefontein Hill, Bushveld Igneous Complex, South Africa. Extended Abstract, 10th International Platinum Symposium, Oulu, Finland, 8-11th August, 2005.

Nyama, N., Nex, P. and Yao, Y. (2006). Mineralisation and petrology studies of the Platreef on Tweefontein Hill, Bushveld Igneous Complex, South Africa. SEG Conference, Wealth Creation in the Minerals Industry, Keystone, Colorado.

O'Driscoll, B., Butcher, A. R. and Latypov, R. (2014). New insights into precious metal enrichment on the Isle of Rum, Scotland. The Geologist's Association and The Geological Society of London, *Geology Today*, **30**(4):133-139.

Oberthür, T., Davies, D. W., Blenkinsop, T. G. and Höhndorf, A. (2002). Precise U-Pb mineral, ages, Rb-Sr and Sm-Nd systematics for the Great Dyke, Zimbabwe – constraints on late Archean events in the Zimbabwe craton and Limpopo. *Precambrian Research*, **113**:293-305.

Ohmoto, H. (1972). Systematics of sulfur and carbon isotopes in hydrothermal ore deposits. *Economic Geology*, **67**: 551-578.

Onovwiona, H. and Uqursal, V. I. (2006). Residential cogeneration systems: review of the current technology. *Renewable and Sustainable Energy Reviews*, **10**:389-431.

Pebane, M. and Latypov, R. (2017). The significance of magmatic erosion for bifurcation of UG1 chromite layers in the Bushveld Complex. *Ore Geology Reviews*, (in press).

Penniston-Dorland, S. C., Mathez, E. A., Wing, B. A., Farquhar, J. and Kinnaird, J. A. (2012). Multiple sulfur isotope evidence for surface-derived sulfur in the Bushveld Complex. *Earth and Planetary Science Letters*, **337-338**: 236-242.

Penniston-Dorland, S. C., Wing, B. A., Nex, P. A., Kinnaird, J. A., Farquhar, J., Brown, M. and Sharman, E. R. (2008). Multiple sulfur isotopes reveal a magmatic origin for the Platreef platinum-group element deposit, Bushveld Complex, South Africa. *Geology*, **36**(12): 979-982.

Platinum Group Metals, (2016). Independent technical report on the Waterberg project including mineral resource update and pre-feasibility study: Johannesburg, South Africa, Platinum Group Metals, Consultancy Report, October 16th, 2016.

Power, M. R., Pirrie, D., Anderson, J. C. Ø. and Butcher, A. R. (2000). Stratigraphical distribution of platinum-groups minerals in the Eastern Layered Series, Rum, Scotland. *Mineralium Deposita*, **35**:762-775.

Prichard, H. M., Barnes, S. J., Maier, W. D. and Fisher, P. C. (2004). Variations in the nature of the platinum-group minerals in a cross-section through the Merensky Reef at Impala Platinum: implications for the mode of formation of the reef. *The Canadian Mineralogist*, **42**(2):423-437.

Pringle, I. C. (1986). The Zwartkloof fluorite deposits, Warmbad District. In: Anhaeusser, C. R. and Maske, S. (eds.), Mineral Deposits of Southern Africa. Geological Society of South Africa, Johannesburg, **2**:1343-1349.

Pronost, J., Harris, C. and Pin, C. (2008). Relationship between footwall composition, crustal contamination, and fluid-rock interaction in the Platreef, Bushveld Complex, South Africa. *Mineralium Deposita*, **43**:825-848.

Rajesh, H. M., Santosh, M., Wan, Y., Lui, D., Liu, S. J. and Belyanin, G. A. (2014). Ultrahigh temperature granulite and magnesian charnockites: Evidence for Neoarchean accretion along the northern margin of the Kaapvaal craton. *Precambrian Research*, **24**:150-159.

Ramdohr, P. (1969). The ore minerals and their intergrowths. International Series of Monographs on Earth Sciences.

Renna, M. R. and Tribuzio, R. (2011). Olivine-rich troctolite from Ligurian Ophiolites (Italy): Evidence for impregnation of replacive mantle conduits by MORB-type melts. *Journal of Petrology*, **52**(9):1763-1790.

Reynolds, I. M. (1985). Contrasted mineralogy and textural relations in the upper most Ti-magnetite layers of the Bushveld Complex in the Bierkraal area north of Rustenburg. *Economic Geology*, **80**:1027-1048.

Richardson, S. H. and Shirey, S. B. (2008). Continental mantle signature of Bushveld magmas and coeval diamonds. *Nature*, **453**:910-913.

Righter, K. (2003). Mantle-silicate partitioning of siderophile elements and core formation in the early Earth. *Annu. Rev. Earth Pl. Sci*., **32**:135-174.

Ripley, E. M. and Li, C. (2003). Sulfur isotope exchange and metal enrichment in the formation of magmatic Cu-Ni-(PGE) deposits. *Economic Geology*, **98**: 635-641.

Ripley, E. M. and Li, C. (2013). Sulfide saturation in mafic magmas: Is external sulfur required for magmatic Ni-Cu-(PGE) ore genesis? *Economic Geology*, **108**: 45-58.

Robb, L. J., Brandl, G., Anhaeusser, C. R. and Poujol, M. (2006). Archaean granitoid intrusions. In: Johnson, M. R., Anhaeusser, C. R. and Thomas, R. J. (eds.), The Geology of South Africa. Geological Society of South Africa, Johannesburg/Council for Geoscience, Pretoria, 57-94.

Roberts, M. D., Reid, D. L., Miller, J. A., Bassoon, I. J., Roberts, M. and Smith, D. (2007). The significance of the footwall reconstitution within normal to regional pothole reef types in the Bushveld Complex. *Mineralium Deposita*, **42**:271-292.

Robertson, J. C., Ripley, E. M., Barnes, S. –J. and Li, C. (2015). Sulfur liberation from country rocks and incorporation in mafic magma. *Economic Geology*, **110**:1111-1123

Roelofse, F. and Ashwal, L. D. (2012). The lower Main Zone in the Northern Limb of the Bushveld Complex – a >1.3 km thick sequence of intruded and variably contaminated crystal mushs. *Journal of Petrology*, **53**(7):1449-1476.

Roelofse, F., Ashwal, L. D., Pineda-Vargas, C. A. and Przybylowicz, W. J. (2009). Enigmatic texture developed along plagioclase-augite grain boundaries at the base of the Main Zone, Northern limb, Bushveld Complex – evidence for late stage melt infiltration into a nearly solidified crystal mush. *South African Journal of Geology*, **112**:39-46.

Roering, C., van Reenen, D. D., de Wit, M., Smit, C. A., de Beer, J. and van Schalkwyk, J. F. (1992). Structural, geological and metamorphic significance of the Kaapvaal craton – Limpopo belt contact. *Precambrian Research*, **55**:69-80.

Ruiz, J., Barra, F., Ashwal, L. D. and Le Grange, M. (2004). Re-Os systematic on sulfides from the Platreef, Bushveld Complex. Geoscience Africa, University of the Witwatersrand, 12-16th July, 2004.

SACS (South African Committee for Stratigraphy), (1980). Stratigraphy of South Africa. Part 1: Lithostratigraphy of the Republic of South Africa, South West Africa/Namibia, and Republics of Bophuthatswana, Transkei and Venda (L. E. Kent, Comp.). Handbook, Geological Survey of South Africa, Pretoria, v. 8, pp. 690.

Sampson, E. (1932). Magmatic chromite deposits in southern Africa. *Economic Geology*, **27**(2):113-144.

Saper, L. and Liang, Y. (2014). Formation of plagioclase-bearing peridotite and plagioclase-bearing wehrlite and gabbro suite through reactive crystallisation: an experimental study. *Contribution to Mineralogy and Petrology*, **167**:985pp.

Schaller, M., Steiner, O., Studer, I., Holzer, L. and Herwegh, M. (1999). Exhumation of Limpopo Central Zone granulites and dextral continent-scale transcurrent movement at 2.0 Ga along the Palala shear zone, Northern province, South Africa. *Precambrian Research*, **96**:263-288.

Schneiderhöhn, H. (1929). The mineragraphy and spectrography of the sulphidic platinum ores of the Bushveld Complex. *The Platinum Deposits of South Africa*, 206-246.

Schouwstra, R. P., Kinloch, E. D., & Lee, C. A. (2000). A Short Geological Review of the Bushveld Complex. *Platinum Metals Review*, **44**(1):33-39.

Schurmann, L. W., Grabe, P. –J. and Steenkamp, C. J. (1998). Chromium. In: Wilson, M. G. C. and Anhaeusser, C. R. (eds.), The mineral resources of South Africa, Handbook, Council for Geoscience, Pretoria, **16**:90-105.

Schweitzer, J. K., Hatton, C. J. and De Waal, S. A. (1995). Regional lithochemical stratigraphy of the Rooiberg Group, upper Transvaal Supergroup: a proposed new subdivisions. *South African Journal of Geology*, **3**:245-255.

Scoates, J. S. and Friedman, R. M. (2008). Precise age of the platiniferous Merensky Reef, Bushveld Complex, South Africa, by the U-Pb zircon chemical abrasion ID-TIMS technique. *Economic Geology*, **103**:465-471.

Scoates, J. S., Wall, C. J. (2015). Geochronology of Layered Intrusions. In: Charlier, B., Namur, O., Latypov, R., Tegner, C. (eds.), Layered Intrusions. Springer, Netherlands, Dordrecht, pp. 3–74.

Scoon, R. N. and Mitchell, A. A. (2004). Petrogenesis of discordant magnesian dunites from the Central Sector of the eastern Bushveld Complex with emphasis on the Winnaarshoek pipe and disruption of the Merensky Reef. *Economic Geology*, **99**:517-541.

Scoon, R. N. and Teigler, B. (1994). Platinum-group element mineralisation in the Critical Zone of the Western Bushveld Complex: I sulfide-poor chromitites below the UG2. *Economic Geology*, **89**:1094-1121.

Scoon, R. N. and Mitchell, A. A. (2011). The principal geological features of the Mooihoek platiniferous dunite pipe, eastern limb of the Bushveld Complex, and similarities with replaced Merensky Reef at the Amandelbult Mine, South Africa. *South African Journal of Geology*, **114**: 15-40.

Seabrook, C. L., Cawthorn, R. G. and Kruger, F. J. (2005). The Merensky Reef, Bushveld Complex: mixing of minerals not mixing of magmas. *Economic Geology*, **100**:1191-1206.

Sharman Harris, E. R., Kinnaird, J. A., Harris, C. and Horstmann, U. E. (2005). A new look at sulphides mineralisation of the northern limb, Bushveld Complex: a stable isotope study. Special Issue, *Transactions, Institute of Mining and Metallurgy*, **114**:252-263.

Sharman, E. R., Penniston-Dorland, S. C., Kinnaird, J. A., Nex, P. A. M., Brown, M. and Wing, B. A. (2013). Primary origin of marginal Ni-Cu-(PGE) mineralisation in layered intrusions: $\delta^{33}S$ evidence from the Platreef, Bushveld, South Africa. *Society of Economic Geologists*, **108**: 365-377.

Sharpe, M. R. (1981). The chronology of magma influxes to the eastern compartment of the Bushveld Complex as exemplified by its marginal border groups. *Journal of the Geological Society*, **138**(3):307-326.

Sharpe, M. R. (1985a). Strontium isotope evidence for preserved density stratification in the Main Zone of the Bushveld Complex. *Nature*, **316**:119-126.

Sharpe, M. R. (1985b). Where is the Bushveld's missing platinum. *Canadian Mineralogist*, **23**: 330.

Sharpe, M. R. and Hulbert, L. J. (1985). Ultramafic sill beneath the eastern Bushveld Complex; mobilized suspensions of early Lower Zone cumulates in a parental magma with boninitic affinities. *Economic Geology*, **80**(4):849-871.

Sharpe, M. R., Bahat, D. and von Gruenewaldt, G. (1981). The concentric elliptical structure of feeder sites to the Bushveld Complex and possible economic implications. *Trans. Geol. Soc. S. Afr*., **84**:239-244.

Shima, H. and Naldrett, A. J. (1975). Solubility of sulfur in an ultramafic melt and the relevance of the system Fe-S-O. *Economic Geology*, **70**:960-967.

Silver, P. G., Fouch, M. J., Gao, S. S. and Schmitz, M. (2004). Seismic anisotropy, mantle fabric, and the magmatic evolution of Precambrian southern Africa. *South African Journal of Geology*, **107**(1-2):45-58.

Smirnov, A. V., Evans, D. A. D., Ernst, R. E., Söderlund, U. and Li, Z. –X. (2013). Trading partners: Tectonic ancestry of southern Africa and Western Australia, in Archaean supercratons Vaalbara and Zimgarn. *Precambrian Research*, **224**:11-22.

Smit, C. A. and van Reenen, D. D. (1997). Deep crustal shear zone high-grade tectonites and associated alteration in the Limpopo Belt, South Africa: implication for deep crustal processes. *Journal of Geology*, **105**:37-57.

Smit, C. A., Roering, C. and van Reenen, D. D. (1992). The structural framework of the southern margin of the Limpopo Belt, South Africa. In: van Reenen, D. D., Roering, C., Ashwal, L. D. and de Wit, M. J. (eds.), The Archean Limpopo Granulite Belt: Tectonics and Deep Crustal Processes. *Precambrian Research*, 51-67.

Smith, D. S., Basson, I. J. and Reid, D. L. (2004). Normal reef subfacies of the Merensky Reef at Northam platinum mine, Zwartklip facies, western Bushveld Complex, South Africa. *The Canadian Mineralogist*, **42**(2):243-260.

Smith, J. W. (2014). The nature and origin of PGE mineralisation in the Rooipoort area, northern Bushveld Complex, South Africa. Ph. D. thesis, University of Leicester, 302 pp.

Smith, J. W., Holwell, D. A. and McDonald, I. (2014). Precious and base-metal geochemistry and mineralogy of the Grasvally-Norite-Pyroxenite-Anorthosite (GNPA) member, northern Bushveld Complex, South Africa: implication for a multistage emplacement. *Mineralium Deposita*, **49**:667-692.

Smith, J. W., Holwell, D. A., McDonald, I. and Boyce, A. J. (2016). The application of S isotopes and S/Se ratios in determining ore-forming processes of magmatic Ni-Cu-PGE sulfide deposits: A cautionary case study from the northern Bushveld Complex. *Ore Geology Reviews*, **73**: 148-174.

Strauss, C. A. (1954). The geology and mineral deposits of the Potgietersrust tin-fields. *South African Geol. Survey Mem*., **46**:241pp

Stanley, C. J. and Vymazalová, A. (2015). Kojonenite, a new palladium tin telluride mineral from the Stillwater Layered Igneous Intrusion, Montana, USA. *American Mineralogist*, **100**(2-3): 447-450.

Sun, S. S., and McDonough, W. F. (1989). Chemical and isotopic systematics of oceanic basalts: Implications for mantle composition and processes. *Geological Society, London, Special Publication,* **42**: 313–345.

Sylvania Platinum Ltd. Report 2010. http://www.sylvania-platinum.com/b/files/appendix/competent-persons-report-volspruit-complex.pdf.

Tanner, D., Mavrogenes, J. A., Arculus, R. J. and Jenner, F. E. (2014). Trace element stratigraphy of the Bellevue Core, Northern Bushveld: Multiple magma injections obscured by diffusive processes. *Journal of Petrology*, **55**(5):859-882.

Tegner, C., Cawthorn, R. G. and Kruger, F. J. (2006). Cyclicity in the Main and Upper Zone of the Bushveld Complex, South Africa: crystallisation from a zoned magma sheet. *Journal of Petrology*, **47**:2257-2279.

Teigler, B. (1990), Mineralogy, petrology and geochemistry of the Lower and lower Critical Zone, northwestern Bushveld Complex. Ph. D. thesis, Rhodes University, Grahamstown.

Teigler, B. and Eales, H. V. (1996). The Lower and Critical Zones of the western limb of the Bushveld Complex, as indicated by the Nooitgedacht boreholes. *Geological Survey of South Africa Bulletin*, **111**:126.

Teigler, B., Eales, H. V. and Scoon, R. N. (1992). The cumulate succession in the Critical Zone of the Rustenburg Layered Suite at Brits, western Bushveld Complex. *South African Journal of Geology*, **95**:17-28.

Todd, S. G., Keith, D. W., Le Roy, L. W., Schissel, D. J., Mann, E. L. and Irvine, T. N. (1982). The J-M platinum-palladium reef of the Stillwater Complex, Montana: I. Stratigraphy and Petrology. *Economic Geology*, **77**:1454-1480.

Tredoux, M., Lindsay, N. M., Davies, G. and McDonald, I. (1995). The fractionation of platinum-group elements in magmatic systems, with the suggestion of a novel causal mechanism. *South Africa Journal of Geology*, **98**:157-167.

Treloar, P. J., Coward, M. P. and Harris, N. B. W. (1992). Himalayan-Tibetan analogies for the evolution of the Zimbabwe craton and Limpopo belt. *Precambrian Research*, **55**:571-587.

Truter, F. C. (1947). A remarkable transcurrent fault near Potgietersrus Transvaal. *Trans. Geol. Soc. S. Afr.*, **50**:1-15.

Turner, A. R., Wolfgram, D. and Barnes, S. J. (1985). Geology of the Stillwater County Sector of the J-M Reef, including the Minneapolis Adit. In: Czamanske, G. K. and Zientek, M. L. (eds.), The Stillwater Complex, Montana, Geology and Guide. *Montana Bureau of Mine and Geology, Special Publication*, **92**:210-230.

Turner, P. A. (1986). The sulfide mineralogy and the behaviour of S and certain trace elements in the Skaergaard Intrusion, East Greenland. M.Sc. thesis, Dartmouth College, Hanover, New Hampshire, 79pp.

Twist, D. and French, B. M. (1983). Voluminous acid volcanism in the Bushveld Complex: a review of the Rooiberg felsite. *Bull. Volcanol.*, **46**:225-242.

Van der Merwe, F., Viljoen, F. and Knoper, M. (2012). The mineralogy and mineral associations of platinum-group elements and gold in the Platreef at Zwartfontein, Akanani Project, Northern Bushveld Complex, South Africa. *Mineralogy and Petrology*, **106**(1):25-38.

Van der Merwe, M. J. (1976). The layered sequence of the Potgietersrus limb of the Bushveld Complex. Ph. D. thesis, University of the Witwatersrand, 176 pp. (Unpublished).

Van der Merwe, M. J. (1978). The geology of the basic and ultramafic rocks of the Potgietersrus limb of the Bushveld Complex. Ph.D. thesis, University of the Witwatersrand, 176pp. (Unpublished).

Van der Merwe, M. J. (2008). The geology and structure of the Rustenburg Layered Suite in the Potgietersrus/Mokopane area of the Bushveld Complex, South Africa. *Mineralium Deposita*, **43**:405-419.

Van der Merwe, F., Viljoen, F. and Knoper, M. (2012). The mineralogy and mineral associated of platinum-group elements and gold in the Platreef at Zwartfontein, Akanani Project, Northern Bushveld Complex, South Africa. Miner. Petrol., **106**:25-38.

Van Reenen, D. D. (1986). Hydration of cordierite and hypersthene and a description of the retrograde orthoamphibole isograd in the Limpopo Belt, South Africa. *Am. Mineral.*, **71**:900-915.

Van Reenen, D. D., Barton, J. M., Jr., Roering, C., Smit, C. A. and van Schalkwyk, J. F. (1987). Deep crustal response to continental collision: the Limpopo Belt of southern Africa. *Geology*, **15**:11-14.

Van Reenen, D. D., Roering, C., Ashwal, L. D. and de Wit, M. J. (1992). The Archean Limpopo granulites belt: Tectonics and deep crustal processes. *Precambrian Research*, **55**:587.

Van Reenen, D. D., Roering, C., Brandl, G., Smith, C. A. and Barton, J. M. (1990). The granulite facies rocks of the Limpopo Belt southern Africa. In: Vielzeuf, D. and Vidal, P. (eds.), Granulite and Crustal Evolution. Kluwer, Dordrecht, 257-289.

Van Rooyen, D. P. (1954). Die geologie van ‘n gedeelte van gedied 7 (Potgietersrus). Report Geol. Survey S. Afr., Pretoria, 116 pp.

Van Tongeren, J. A. and Mathez, E. A. (2012). Large-scale liquid immiscibility at the top of the Bushveld Complex, South Africa. *Geology*, 40:491-494.

Vermaak, C. F. (1976). The Merensky Reef – thoughts on its environment and genesis. *Economic Geology*, **71**:1270-1298.

Vermaak, C. F., and von Gruenewaldt, G. (1986). Introduction to the Bushveld Complex, *in* Anhaeusser, C.R., and Maske, S. (eds.), Mineral deposits of southern Africa. *Geological Society of South Africa*, **2**: 1021–1029.

Vermaak, C. F. and Hendricks, L. P. (1976). A review of the mineralogy of the Merensky reef, with specific reference to new data on the precious metal mineralogy. *Economic Geology*, **71**: 1244-1260.

Venmyn-Rand, (2010). Independent technical experts report on the mineral assets of Sylvania Resources Limited—in the form of a competent persons report by Venmyn-Rand (Pty.) Limited: 151 p.

Viljoen, F., Ramakoloi, N., Rose, D. and Reinke, C. (2015). Mineral chemistry of (Pt-Pd)-bismuthotelluride minerals in the Platreef at Zwartfontein, Akanani Project, northern Bushveld Complex, South Africa. *The Canadian Mineralogist*, **53**:1109-1127.

Viljoen, M. C. and Scoon, R. N. (1985). The distribution and main geologic features of discordant bodies of Fe rich ultramafic pegmatite in the Bushveld Complex. *Economic Geology*, **80**:1109-1128.

Viljoen, M. J. (1994). A review of regional variations in facies and grade distribution of the Merensky Reef, western Bushveld Complex, with some mining implications. Proceeding, XVth CMMI Congress, South Africa Institute of Mining and Metallurgy, Johannesburg, v. 3, p. 183-194.

Viljoen, M. J. (1999). The nature and origin of the Merensky Reef of the western Bushveld Complex based on geological facies and geophysical data. *South Africa Journal of Geology*, **102**:221-239.

Viljoen, M. J. and Hieber, R. (1986). The Rustenburg Section of Rustenburg Platinum Mines Limited. In: Anhaeusser, C. R. and Maske, S. (eds.), Mineral Deposits of Southern Africa, Geological Society of South Africa, Johannesburg, II, 1107-1134.

Viljoen, M. J. and Schurmann, L. W. (1998). Platinum-group metals. In: Wilson, M. G. C. and Anhauesser, C. R. (eds.), The mineral resources of Southern Africa, Council for Geoscience, 532-568.

Viljoen, M. J., De Klerk, W. J., Coetzer, P. M., Hatch, N. P., Kinloch, E. and Peyerl, W. (1986). The union section of Rustenburg platinum mines limited with reference to the Merensky Reef. *Mineral deposits of southern Africa*, **2**:1061-1090.

Viljoen, M. J., Theron, J., Underwood, B., Walters, B. M., Weaver, J. and Peyerl, W. (1986). The Amandelbult section of Rustenburg Platinum Mines Limited, with reference to the Merensky reef. *Mineral Deposits of Southern Africa. Geological Society of South Africa*, pp.1041-1060.

Viljoen, M. (2016). The Bushveld Complex: host to the world's largest platinum, chromium and vanadium resources. Abstract In: Wilson, M. G. C. and Viljoen, R. P. (Eds) The Great Mineral Fields of Africa, Journal of International Geoscience, Special Issue for the 35th IGC, Cape Town 27th August – 4th September 2016, *Episodes*, **39**(2):239-268.

Viring, R. G. and Cowell, M. W. (1999). The Merensky Reef on Northam Platinum Limited. *South African Journal of Geology*, **102**:192-208.

von Gruenewald, G. (1970). On the phase-change orthopyroxene-pigeonite and the resulting textures in the Main and Upper zones of the Bushveld Complex in the eastern Transvaal. Symposium on the Bushveld igneous complex and other layered intrusions. *Geological Society of South Africa Special Publication*, **1**: 67–73.

von Gruenewaldt, G. (1971). A petrographical and mineralogical investigation of the rocks of the Bushveld Igneous Complex in the Tauteshoogte-Roossenekal area of the eastern Transvaal. Ph. D. thesis, University of Pretoria, 228 pp.

von Gruenewaldt, G. (1973). The Main and Upper Zones of the Bushveld Complex in the Roossenekal area, eastern Transvaal. *Transactions, Geological Society of South Africa*, **76**:207-227.

von Gruenewaldt, G. (1976). Sulfides in the Upper Zone of the eastern Bushveld Complex. *Economic Geology*, **71**:1324-1336.

von Gruenewaldt, G. (1993). Ilmenite – apatite enrichment in the Upper Zone of the Bushveld Complex: a major titanium-rock phosphate resource. *International Geology Review*, **35**:987-1000.

von Gruenewaldt, G., Hulbert, L. J. and Naldrett, A. J. (1989). Contrasting platinum-group element concentration patterns in cumulates of the Bushveld Complex. *Mineralium Deposita*, **24**:219-229.

von Gruenewaldt, G., Klemm, D. D., Henckel, J. and Dehm, R. M. (1985). Exsolution features in titanomagnetites from massive magnetite layers and their host rocks in the Upper Zone, eastern Bushveld Complex. *Economic Geology*, **80**:1049-1061.

von Gruenewaldt, G., Sharpe, M. R. and Hatton, C. J. (1985). The Bushveld Complex, introduction and review. *Economic Geology*, **80**(4): 803-812.

Voordouw, R. J., Gutzmer, J. and Beukes, N. J. (2010). Zoning of platinum group mineral assemblages in the UG2 chromitite determined through in situ SEM-EDS-based image analysis. *Mineralium Deposita*, **45**(2):147-159.

Vymazalová, A. and Drábek, M. (2010). The system Pd–Sn–Te at 400 C and mineralogical implications. I. The binary phases. *The Canadian Mineralogist*, **48**(5): 1041-1050.

Wager, L. R. and Brown, G. M. (1968). Layered Igneous Rocks. Oliver and Boyd, Edinburg, 588 pp.

Wager, L. R. and Deer, W. A. (1939). Geological investigations in East Greenland, Part III. The petrology of the Skaergaard Intrusion, Kangerdlugssuaq, East Greenland. *Meddeleser om Grønland*, **105**:1-352.

Wager, L. R., Brown, G. M. and Wadsworth, W. J. (1960). Types of igneous cumulates. *Journal of Petrology*, **1**:73-85.

Wagner, P. A. (1929). The platinum deposits and mines of South Africa. Oliver and Boyd, Edinburgh, 326 pp.

Walraven, F. (1985). Genetic aspects of the granophyric rocks of the Bushveld Complex. *Economic Geology*, **80**:1166-1180.

Walraven, F. (1986). A note on the stratigraphic terminology of the Bushveld Complex, *in* Anhaeusser, C.R., and Maske, S., eds., Mineral deposits of southern Africa. *Geological Society of South Africa*, **2**: 1039–1040.

Walraven, F. (1988). Notes of the age and genetic relationships of the Makhutso Granite, Bushveld Complex, South Africa. Chemical Geology, v. 72, p. 17-28.

Walraven, F. (1997). Geochronology of the Rooiberg Group, Transvaal Supergroup, South Africa. Economic Geology Research Unit Information Circular, University of the Witwatersrand, Johannesburg, v. 316, pp. 21.

Walraven, F., and Hattingh, E. (1993). Geochronology of the Nebo Granite, Bushveld Complex: *South African Journal of Geology*, **96**: 31–41.

Walraven, F., Armstrong, R. A. and Kruger, F. J. (1990). A chronostratigraphic framework for the north-central Kaapvaal Craton, the Bushveld Complex and Vredefort structure. *Tectonophysics*, **171**:23-48.

Watkinson, D. H. and Ohnenstetter, D. (1992). Hydrothermal origin of platinum-group mineralisation in the Two Duck Lake Intrusion, Coldwell Complex, northwestern Ontario. *Canadian Mineralogist*, **30**: 121-136.

Webb, S. J., Cawthorn, R. G., Nguuri, T. and James, D. (2004). Gravity model of the Bushveld Complex connectivity supported by Southern African seismic experiment results. *South African Journal of Geology*, **107**:207-218.

Weise, S. (2010). Characterisation of the Main Zone – Platreef contact in the northern limb of the Bushveld Complex. M. Sc. Thesis, University of the Witwatersrand, (Unpublished).

Westland, A. D. (1981). Inorganic chemistry of the platinum-group elements. Canadian Institute of Mining and Metallurgy, Special Volume 23, p. 5-18.

Westerlund, K. J., Gurney, J. J., Carlson, R. W., Shirey, S. B., Hauri, E. H. and Richardson, S. H. (2004). A metasomatic origin for late Archean eclogites diamonds: Implications from internal morphology of diamonds and Re-Os and S isotope characteristics of their sulfide inclusions from the Late Jurassic Klipspringer kimberlite. *South African Journal of Geology*, **107**: 199-130.

White, J. A. (1994). The Potgietersrus Prospect – geology and exploration history: XVth CMMI congress, Johannesburg, SAIMM, **3**:173-181.

Wiebe, R. A. (1980). Commingling of contrasted magmas in the plutonic environment: examples from the Nain anorthositic complex. *Journal of Geology*, **88** (2): 197–209.

Wilhelm, H. J., Zhang, H., Chen, F. L., Elsenbroek, J. H., Lombard, M. and de Bruin, D. (1997). Geochemical exploration for platinum-group elements in the Bushveld Complex, South Africa. *Mineralium Deposita*, **32**:349-361.

Willemse, J. (1969). The geology of the Bushveld Igneous Complex, the largest repository of magmatic ore deposits in the world. In: Magmatic Ore Deposits – A symposium, p. 1-22.

Wilmore, C. C., Boudreau, A. E. and Kruger, F. J. (2000). The halogen geochemistry of the Bushveld Complex, Republic of South Africa: Implications for chalcophile element distribution in the Lower and Critical Zones. *Journal of Petrology*, **41**:1517-1539.

Wilson, A. H. (2012). A chill sequence to the Bushveld Complex: Insight into the first stage of emplacement and implication for the parental magmas. *Journal of Petrology*, 1-46.

Wilson, A. H. (2015). The earliest stage of emplacement of the Eastern Bushveld Complex: Development of the Lower Zone, Marginal Zone and Basal Ultramafic Sequence. *Journal of Petrology*, **56**(2):347-388.

Wilson, A. H. and Chunnett, G. (2006). Trace element and platinum-group element distributions and the genesis of the Merensky Reef, western Bushveld Complex. *South African Journal of Petrology*, **47**:2369-2403.

Wilson, A. H. and Zeh, A. (2015). Emplacement and magma compositions of the lowest succession of the Bushveld Complex. Abstract: 6th Platreef Workshop, Mokopane, 8th - 10th of May 2015, p. 57-58.

Wilson, A. H., Lee, C. A. and Brown, R. T. (1999). Geochemistry of the Merensky reef, Rustenburg Section, Bushveld Complex: controls on the silicate framework and distribution of trace elements. *Mineralium Deposita*, **34**(7):657-672.

Wilson, A. H., Lee, C. and Brown, R. T. (1990). Geochemistry of the Merensky Reef, Rustenburg section, Bushveld Complex: controls on the silicate framework and distribution of trace metals. *Mineralium Deposita*, **34**:657-672.

Wilson, J., Ferre, E.C. and Lespinasse, P. (2000). Repeated tabular injection of high-level alkaline granites in the eastern Bushveld, South Africa. *Journal of the Geological Society*, **157**(5):1077-1088.

Wohlgemuth-Ueberwasser, C. C., Fonseca, R. O., Ballhaus, C. and Berndt, J. (2013). Sulfide oxidation as a process for the formation of copper-rich magmatic sulfides. *Mineralium Deposita*, **48**:115-127.

Woods, T. (2012). Nature and origin of mineralisation within the Main Zone beyond the North End of the Northern Limb of the Bushveld Complex (unpublished). Honours Research, University of the Witwatersrand, 142pp.

Yudovskaya, M. A. and Kinnaird, J. A. (2013). The updates on the Waterberg site (PTM). Unpublished, the University of the Witwatersrand, Johannesburg, South Africa (Internal Report).

Yudovskaya, M. A., Kinnaird, J. A., Grobler, D., Costin, G., Abramova, V. D., Dunnett, T. and Barnes, S. –J. (2017). Zonation of Merensky-style platinum mineralisation in Turfspruit thick reef facies (northern limb of the Bushveld Complex). *Economic Geology*, (in press).

Yudovskaya, M. A., Kinnaird, J. A., Sobolev, A. V., Kuzmin, D. V., McDonald, I. and Wilson, A. H. (2013). Petrogenesis of the Lower Zone olivine-rich cumulates beneath the Platreef and their correlation with recognized occurrences in Bushveld Complex. *Economic Geology*, **108**:1923-1952.

Yudovskaya, M. and Kinnaird, J. A. (2010). Chromite in the Platreef (Bushveld Complex, South Africa): occurrence and evolution of its chemical composition. *Mineralium Deposita*, **45**:369-391.

Yudovskaya, M. and Kinnaird, J. A. (2013). An update on the Waterberg site (PTM). Unpublished, The University of the Witwatersrand, Johannesburg, South Africa.

Yudovskaya, M., Belousova, E., Kinnaird, J., Dubinina, E., Grobler, D. F. and Pearson, N. (2017). Re-Os and S isotope evidence for the origin of Platreef mineralisation (Bushveld Complex). *Geochimica et Cosmochimica Acta*, **214**:282-307.

Yudovskaya, M., Kinnaird, J. A., Naldrett, A. J., Rodionov, N., Antonov, A., Simakin, S. and Kuzmin, D. (2013). Trace element study and age dating of zircon from chromitites of the Bushveld Complex (South Africa). *Mineralogy and Petrology*, **107**(9):915-942.

Yudovskaya, M., Kinnaird, J., McCreesh, M. and Frei, D. (2015). The lithology at the contact between the Bushveld mafic-ultramafic sequence and over laying Waterberg sediments on Waterberg. In: Abstract, 6th Platreef Workshop, Mokopane, 8th – 10th May, 2015, p. 59-61.

Yudovskaya, M., Kinnaird, J., Naldrett, A. J., Mokhov, A. V., McDonald, I. and Reinke, C. (2011). Facies variation in PGE mineralisation in the central Platreef of the Bushveld Complex, South Africa. *The Canadian Mineralogist*, **49**:1349-1384.

Yudovskaya, M., Kinnaird, J., Naldrett, A. J., Mokhov, A., Kuznetsova, M. and McDonald, I. (2010). Facies variation in PGE mineralisation in the central Platreef of the Bushveld Complex, South Africa. *The Canadian Mineralogy*, **49**:1349-1384.

Yudovskaya, M. A., Kinnaird, J. A., Udachina, L. V., Distler, V. V. and Kuz'min, D. V. (2014). Role of magmatic and fluid concentrating in formation of platinum mineralisation in the Lower Zone and Platreef as follow from composition of phlogopite, cumulus silicates and sulfide melt, the northern limb of the Bushveld Complex. *Geology of Ore Deposits*, **56**(6):451-478.

Zeh, A., Ovtcharova, M., Wilson, A. H. and Schaltegger, U. (2015). The Bushveld Complex was emplaced and cooled in less than one million years – results of zirconology, and geotectonic implications. *Earth and Planetary Science Letters*, **418**:103-114.

Appendix A

Publications

A1

The Waterberg Platinum Group Element Deposit: Atypical Mineralization in Mafic-Ultramafic Rocks of the Bushveld Complex, South Africa

Judith A Kinnaird, Marina Yudovskaya, Matthew McCreesh, Florian Huthmann, and Thys J. Botha

A2

Geochemistry and PGE of the lower mineralized zone of the Waterberg Project, South Africa

Florian Huthmann, Marina Yudovskaya, Judith A Kinnaird, Matthew McCreesh, Iain McDonald

©2017 Society of Economic Geologists, Inc.
Economic Geology, v. 112, pp. 1367–1394

The Waterberg Platinum Group Element Deposit: Atypical Mineralization in Mafic-Ultramafic Rocks of the Bushveld Complex, South Africa

Judith A Kinnaird,[1,2,†] Marina Yudovskaya,[1,2,3] Matthew McCreesh,[1,2] Florian Huthmann,[1,2] and Thys J. Botha[4]

[1] *Economic Geology Research Institute, University of the Witwatersrand, 2050 Wits, South Africa*

[2] *Centre of Excellence for Integrated Mineral and Energy Resource Analysis, The National Research Foundation/ Department of Science and Technology Centre of Excellence, University of the Witwatersrand, 2050 Wits, South Africa*

[3] *Institute of Geology of Ore Deposits, Petrography, Mineralogy and Geochemistry, Russian Academy of Science, 35, Staromonetny, Moscow 119017, Russia*

[4] *PTM, Platinum House, 24, Sturdee Avenue, Rosebank, Johannesburg*

Abstract

The exposed northern limb of the Bushveld Complex forms the eastern part of a much larger basin, ~160 × –125 km in size based on geophysical data. Within this basin, the recently discovered ultramafic-mafic succession that extends 24 km northeast from the Hout River shear zone has been shown to have a Bushveld intrusion age of 2.06 Ga. The succession is typically 1 km thick, dips west at 34° to 38°, and comprises a basal Ultramafic sequence, a troctolite-gabbronorite-anorthosite sequence, and an Upper zone. Overlying Waterberg red beds were deposited between ~2.05 and ~1.93 Ma. The basal Ultramafic sequence comprises a lower orthopyroxenite <60 m thick overlying Archean granite gneisses with an intervening agmatite, which is interpreted to be remobilized footwall gneiss interfingered with pyroxenite. The upper portion of the Ultramafic sequence is composed of serpentinized harzburgite. The troctolite-gabbronorite-anorthosite sequence is <850 m thick and is dominated by gabbronorites with minor anorthosites at the top and thick troctolite layers <50 m thick, which are locally pegmatoidal, toward the base. The boundary with the Upper zone is defined by increased magnetic susceptibility due to increased cumulus magnetite. The Upper zone of ferrogabbro and magnetite gabbronorite varies between 0 and 500 m in thickness. Disseminated magnetite is ubiquitous but magnetitite layers that are characteristic of the Upper zone elsewhere in the Bushveld Complex are lacking, except in one core from the extreme south of the project.

There are two PGE-Cu-Ni-Au mineralized intervals, a lower F zone and an upper T zone that vary from 3 to 60 m in thickness. The T zone is restricted to the southern portion of the project, whereas the F zone extends 17 km along strike. In both there is a correlation between visible chalcopyrite and pentlandite abundance and grade of PGE. The F zone of the Ultramafic sequence hosts disseminated sulfides with accessory chromite. Platinum group minerals (PGM), based on more than 1,000 grains recovered, are dominated by sperrylite with lesser Pt-Pd bismuthotellurides, Au-Ag alloys, Pd arsenides, and Pt-Rh sulfoarsenide with a grade of <7 g/t Pt + Pd + Au. The precious metal budget comprises 64% Pd, 30% Pt, 1% Rh, and 5% Au with 0.16% Ni and 0.07% Cu. Mineralization occurs over an interval of ~10 m although in the central portion of the northeasterly oriented body, the "Super F zone" thickens to 60 m, with grades of 3 g/t over this interval. The T zone occurs in a lithologically variable sequence close to the boundary between the troctolite-gabbronorite-anorthosite sequence and the Upper zone. In the south, the T zone is ~30 m thick but increases northward to >50 m thick. An upper T1 and lower T2 are separated by a barren middling that is sometimes absent. Grade in both T1 and T2 is indicated as 3.88 g/t Pt + Pd + Rh + Au, although locally with up to 14 g/t. PGM are less varied than in the F zone and are dominated by Pt-Pd bismuthotellurides. Both T1 and T2 zones have a consistent and unusually gold-enriched metal ratio of ~49% Pd, ~29% Pt, 1% Rh, and 21% Au with 0.08% Ni and 0.16% Cu. Neither the T nor F mineralized zones has direct correlatives in other limbs of the Bushveld Complex.

Although there are comparisons with the Bushveld succession elsewhere, significant differences in thickness and type of lithologies, geochemistry, and mineralization of this arcuate intrusion of the Waterberg segment, compared to the eastern, western, and northern limbs of the Bushveld Complex, suggest that the Waterberg ultramafic-mafic body may represent a structurally controlled separate compartment north of the Hout River shear zone.

Introduction

The exposed northern limb of the Paleoproterozoic Bushveld Complex (Fig. 1) has a N-S-oriented sinuous outcrop that is up to 15 km in width with exposure extending 100 km from the Zebediela fault in the south, to the Hout River shear zone in the north (Fig. 1). The limb has been regarded as forming part of a much larger lobe of the Bushveld Complex, up to 160 × 125 km in size as suggested by aeromagnetic and gravity data (Kinnaird et al., 2005; Finn et al., 2015). Many previous workers believed that the limb terminated at the Hout River shear zone (HRS zone, Fig. 1) and linked in an arcuate form with the Villa Nora fragment of the exposed Upper zone, which is truncated in the north by the Abbottspoort fault, part of the Zoutfontein-Palala shear zone (Grobler and Whitfield, 1970). However, papers in the 1980s (e.g., Vermaak and von Gruenewald, 1986) suggested that the northern limb of the Bushveld extended undercover, north of known outcrops, and the discovery in 2011 by Platinum Group Metals Ltd. of a

† Corresponding author: e-mail, Judith.Kinnaird@wits.ac.za

doi: 10.5382/econgeo.2017.4513
0361-0128/17/1367-28

Submitted: May 31, 2016
Accepted: March 15, 2017

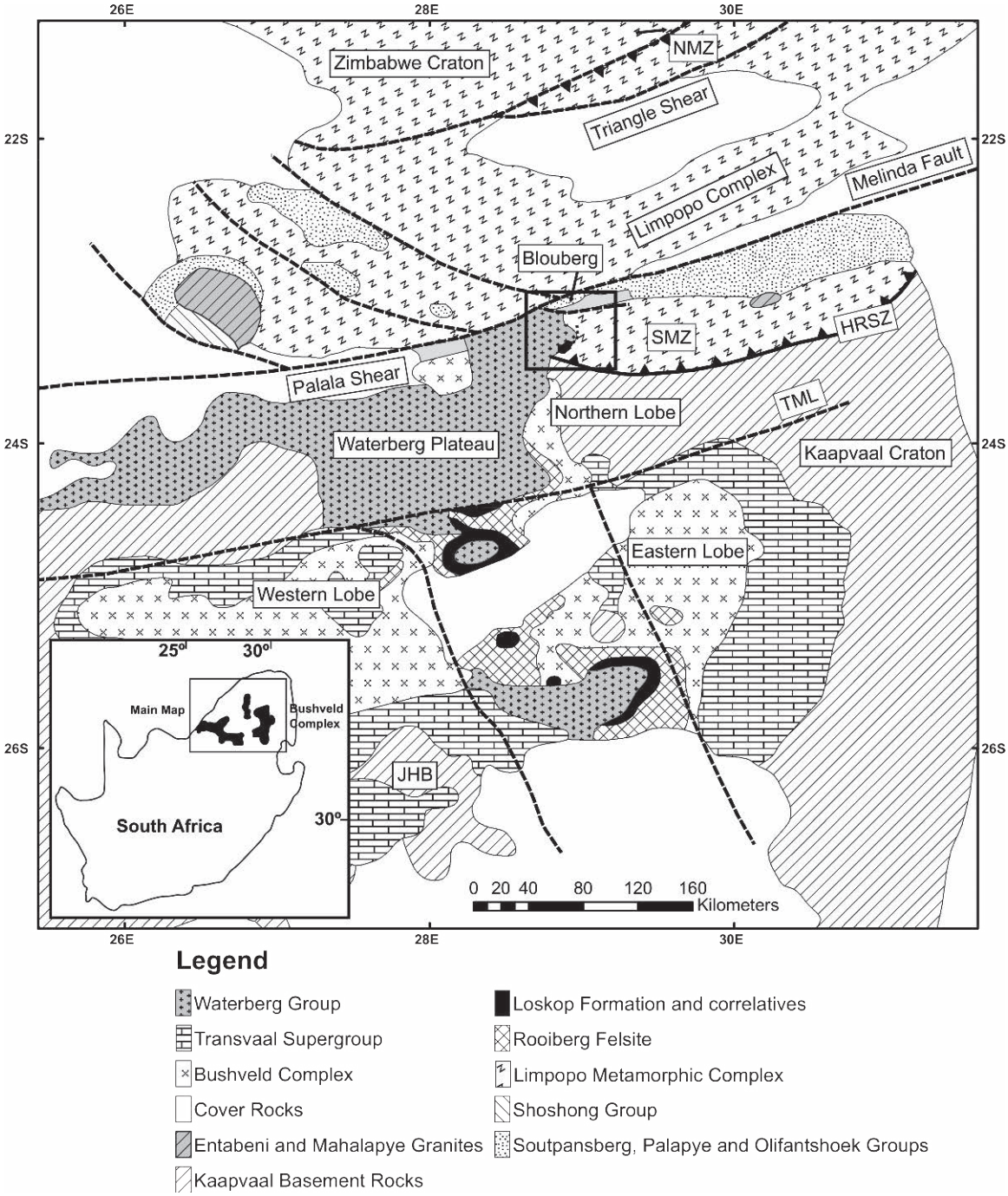

Fig. 1. Map showing the distribution of major lithologic units in northern South Africa. Abbreviations: HRSZ =Hout River shear zone, JHB = Johannesburg, NMZ = Northern mginal zone, SMZ = Southern marginal zone, TML = Thabazimbi-Murchison lineament. The small box indicates the Waterberg area. After Dorland et al. (2006).

buried mineralized ultramafic-mafic succession north of the Hout River shear zone in the Waterberg project has confirmed some of these earlier interpretations. The Waterberg PGM deposit was found by Platinum Group Metals Ltd. following a new generative geologic model and geophysics to target drilling through the Waterberg sedimentary succession. The succession shows a number of contrasts with Bushveld stratigraphy elsewhere, not least because economic grades of PGE mineralization occur in a gabbronorite-dominated sequence that could be correlated with Main zone rocks, or because a sedimentary succession directly overlies weathered mafic Bushveld rocks. In addition, geophysical studies by Finn et al. (2015) have confirmed that mafic Bushveld rocks continue under the Waterberg and Karoo sedimentary units as far north as the Palala shear zone and west to the Lebowa granite north of the Thabazimbi-Murchison lineament, confirming

the suggestion by van der Merwe (1976), Kinnaird et al. (2005), and others of the extent of the northern limb. This would increase the total areal extent of the Bushveld Complex to >90,000 km². Our paper aims to summarize the current knowledge of this new platinum deposit, one of the most globally significant PGE discoveries of recent times. It is meant to be a general overview of the regional geology, and a series of papers will follow giving more specific details on mineralogy, geochemistry, isotopic characteristics, and mineralization.

Geology of the Northern Limb

The Archean basement consists of tonalitic gneiss intruded by heterogeneous potassic granites. The <12-km-thick Transvaal Supergroup sediments were deposited on the Archean basement between 2670 to 2100 Ma (Eriksson et al., 2001) and comprise a thin basal clastic unit (Black Reef Formation) followed by a sequence of dolomites, ironstones, and minor shales (Malmani Subgroup, Penge Formation, Duitschland Formation). These are overlain disconformably by the Pretoria Group (Timeball Hill Formation), which is dominantly a clastic succession with minor volcanics.

North of the Planknek-Ysterberg fault (PYF, Fig. 2), one of the faults in the Thabazimbi-Murchison lineament array, the Bushveld Complex intruded Transvaal Supergroup metasediments and Archean basement (Fig. 2A). The Thabazimbi-Murchison lineament, which extends east-northeast–west-southwest for more than 500 km, has been active since 2960 Ma (Good and de Wit, 1997) to the present day. The sequence which strikes north-northwest has correlates with the eastern and western limbs, such that the Marginal, Lower, Main, and Upper zone units are widely recognized zones elsewhere in the Bushveld Complex (e.g., Kinnaird, 2005; McDonald et al., 2005). The Platreef, which occurs between the Lower and Main zones, is the stratigraphic equivalent of

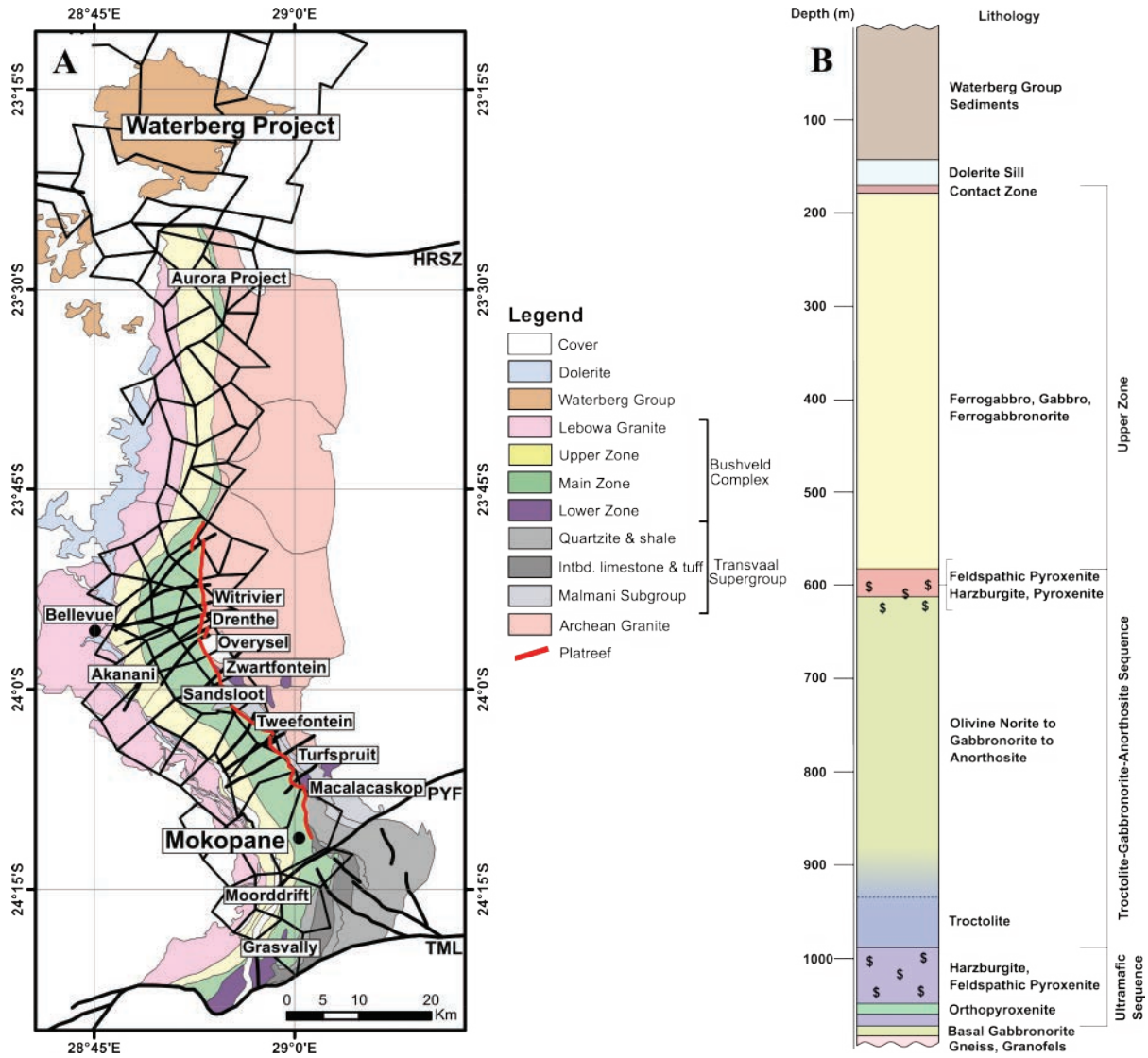

Fig. 2. Geology of the northern limb of the Bushveld Complex (A) map, showing locations that are mentioned in the text. HRSZ = Hout River shear zone, PYF = Planknek-Ysterberg fault, TML = Thabazimbi-Murchison lineament (B) stratigraphy of the Waterberg project area.

the Critical zone. South of the Planknek-Ysterberg fault, a series of ~400 m of intercalated gabbronorites, norites, pyroxenites and anorthosites (the GNPA member) equated with the upper Critical zone by Hulbert (1983), overlie the Lower zone ultramafic cumulates in Grasvally. The layered sequence strikes northeast and dips 15° to 27° W and rests on quartzites of the Magaliesburg Formation, near the top of the Transvaal Supergroup.

The Lower zone of the northern limb was believed to be limited to satellite bodies cutting Archean granite (van der Merwe, 1976) as shown in Figure 2A. However, a Lower zone sequence, up to 800 m thick, was confirmed by drilling beneath the Platreef on Sandsloot and Turfspruit (Fig. 2A; Yudovskaya et al., 2013a). The ultramafic sequence is composed of dunite-harzburgite-pyroxenite cycles with sporadic chromite seams and contains one of the most magnesian rich olivine compositions identified in the whole Bushveld Complex with a Mg number [Mg/(Mg + Fe) up to 91 and a Ni content that varies from <0.4 wt % NiO in Turfspruit to 0.66 wt % NiO in Sandsloot. These Lower zone sequences are more similar to the Grasvally section of the northern limb (Hulbert and von Gruenewaldt, 1985) and the Clapham section of the eastern limb (Wilson, 2012) than to the earlier described sections of the western limb (Teigler and Eales, 1996).

The Platreef is a composite body of geochemically distinct mafic-ultramafic sills (Hutchinson and Kinnaird, 2005; Kinnaird, 2005; Manyeryuke et al, 2005), dominantly of feldspathic pyroxenites that are variably mineralized in PGE, Ni, and Cu between the footwall and the Main zone (Van der Merwe 1978; Armitage et al., 2002; Kinnaird et al., 2005; Manyeruke et al., 2005; Kinnaird and McDonald, 2005; McDonald et al., 2005). The Platreef may be more than 500 m thick locally, in part due to the incorporation of thick interlayers of metasedimentary rocks. Where Lower zone rocks do not form the footwall to the Platreef, it overlies successively older Transvaal metasedimentary rocks northward. In the south the Platreef rests on shales, banded ironstones, calc-silicates, siltstones, and quartzite of the Chuniespoort Group, in the central sector the footwall is of Malmani dolomite, while to the north, the Platreef rests on a footwall of Archean granite-gneiss. Just above the top of the Platreef there is often a spotted anorthosite, overlain by a 300-m-thick succession of intercalated noritic rocks and pyroxenite layers that grade upward into the gabbronorites of the Main zone. Zircons from the upper Platreef give a concordant age of 2056.2 ± 4.4 Ma (MSWD = 0.05; Yudovskaya et al., 2013b), which is indistinguishable within error of a SHRIMP zircon age of 2053.7 ± 3.2 Ma for a granite dike crosscutting the Platreef (Hutchinson et al., 2004). New data from Turfspruit confirms that while the Platreef generally dips westward between 30° to 60° close to surface, the dip gradually lessens with depth downplunge into a more regularly layered sequence, termed the Flatreef, that looks more like the typical Critical zone (Grobler et al., 2012).

Mineralization is a combination of PGE and/or sulfide enrichment that varies within each of the individual sills and not all of the sills are well mineralized (Kinnaird, 2005; Manyeruke et al., 2005; Yudovskaya et al., 2011). Typically, mineralization is bottom-loaded in the south and top-loaded in the central and northern sectors, although this is an oversimplification (Kinnaird and Nex, 2015). The main PGE-bearing reef with PGE grade and tenor identical to those of the Merensky reef (Naldrett et al., 2008, 2012) is located close to the Main zone boundary in the same stratigraphic position as the Merensky reef. However, the thickness of the PGE reefs at Sandsloot and Turfspruit in the northern limb is much greater and may locally reach 90 m. Whereas there is a floor rock control on PGM mineralogy in contaminated parts of the Platreef, the mineralization in the upper sill carries predominantly Pt alloy and sulfides typical of the Merensky reef (Yudovskaya et al., 2017). Chromitite seams occur as discontinuous lenses at a constant stratigraphic level in the shallow Platreef (Yudovskaya and Kinnaird, 2010), but they become persistent and more numerous with depth. The Platreef is becoming a major world focus for platinum group element (PGE) production as current open pits are expanded and new underground operations are developed. Overviews of the recent work on the Platreef are given in Kinnaird (2005), Kinnaird et al. (2005), McDonald and Holwell (2011), and Kinnaird and Nex (2015).

The Main zone, which is <2,000 m thick in the northern limb, overlies the Platreef. It is dominated by gabbronorites, with lesser norites, especially toward the base, pyroxenites, and anorthosites. The distinctive >100-m-thick sequence of olivine-bearing norites and gabbronorites, 1,100 m from the base, which is unique to the northern limb, was mapped as a troctolite for about 35 km along strike by van der Merwe (1978).

The Upper zone is transgressive, resting on the Main zone in the south but on Archean footwall in the far north of the exposed northern limb (Fig. 2A). It is distinguished from the Main zone by the appearance of magnetite and apatite. In the Bellevue drill core (Fig. 2A), it is ~1,188 m thick and is dominated by magnetite-rich olivine gabbro and olivine ferrodiorite, with minor gabbronorite, plagioclase-magnetite cumulates, magnetitite, pyroxenite, and anorthosite (Ashwal et al., 2005). Magnetitite layers are characteristic with 32 discrete layers in the Bellevue core (Fig. 2A), ranging in thickness between 7 cm and 13 m (Ashwal et al., 2005). Commercial prospecting of these layers has identified at least 18 individual vanadiferous titanomagnetite layers elsewhere in the northern limb, ranging in thickness from a few centimeters to 10s of meters, with a number of zones with heavily disseminated (but not massive) magnetite (Longridge, 2015).

PGE mineralization in the northern limb is not restricted to the Platreef. South of the Planknek-Ysterberg fault, mineralization at Moorddrift (Fig. 2A) has been noted close to a pyroxenitic layer in the Main zone (Maier and Barnes, 2010; Holwell et al., 2013). North of Overysel (Fig. 2A) the Main zone thins progressively until Upper zone cumulates rest directly on basement gneiss (Fig. 2A), then northward the Main zone reappears at surface directly in contact with Archean granite. Here mineralization occurs in two main horizons, each generally between 5 and 25 m thick, with a thinner discontinuous deeper horizon close to the basal contact with Archean granite gneiss (Manyeruke, 2007; Maier et al., 2008; McDonald et al., 2017).

The felsic rocks that overlie the Upper zone include the older Rooiberg felsites, which predate the mafic rocks, and the younger Lebowa Granite Suite.

Regional Geology of the Waterberg Project

The Hout River shear zone marks the boundary between the southern Marginal zone of the Limpopo belt and the stable Archean craton. It has been regarded as representing a composite structure along which the southern Marginal zone of the Limpopo belt was thrust southward during a Paleoproterozoic collision between the Zimbabwean and Kaapvaal cratons (Schaller et al., 1999; Barton et al., 2006; Smirnov et al., 2013; Rajesh et al., 2014), although there is still little consensus regarding aspects of the timing of the Limpopo orogeny (e.g., Treloar et al., 1992; Holzer et al., 1998; Barton et al., 2006). Long-lived tectonothermal activity over more than 700 Ma has been suggested (Good and de Wit, 1997; Kramers and Mouri, 2011). The southern Marginal zone is comprised of granulite facies granitic gneiss, amphibolitic gneiss, and minor quartzite. Within the southern Marginal zone there are several major shear zones that trend parallel to the Hout River shear zone (van Reenen et al., 1992) through the Waterberg project area (Fig. 1).

The term Waterberg relates to a geographic area so the term is used to describe a number of different geologic features of very different ages. In this paper, we use the term Waterberg project to refer to studies on the mineralized intrusion of Bushveld age north of the Hout River shear zone. The sedimentary term, the Waterberg Group, refers to a sedimentary succession which began deposition around ~2,050 Ma, while the Waterberg platinum veins of Bushveld age (e.g., McDonald et al, 1995) occur near Naboomspruit. The Karoo-aged Waterberg coalfield west of Lephalale is completely unrelated to any of the other geologic uses of the term.

The Waterberg platinum project is focused on a >3.5- × 24-km lobate intrusion north of the Hout River shear zone (Figs. 1, 2A). The Waterberg PGM deposit was found by Platinum Group Metals Ltd., following a new generative geologic model and geophysics to target drilling through Waterberg sediments. The intrusion consists of a layered package of troctolites, gabbros, gabbronorites, norites, and anorthosites with harzburgite, dunites, and orthopyroxenites toward the base (Fig 2B). U/Pb zircon age dating of the ultramafic-mafic succession gives intrusion ages of 2059 ± 3 and 2053 ± 5 Ma (Huthmann et al., 2016), indicating that the Waterberg intrusion is coeval with the intrusion of the Bushveld Complex (Walraven and Hattingh, 1993; Walraven, 1997; Buick et al., 2001; Scoates and Friedman, 2008; Zeh et al., 2015). The igneous rocks are covered by up to 750 m of sedimentary rocks of the Waterberg Group, a Paleoproterozoic red-bed succession of coarse siliciclastic rocks developed in a continental fault-bound basin that covers large parts of the Archean Kaapvaal craton and the Limpopo belt (Callaghan et al., 1991; Barker et al., 2006).

The development of the Transvaal basin from ~2670 Ma (Eriksson and Reczko, 1995; Eriksson, et al., 2001) and the Waterberg basin from ~2050 Ma (Dorland et al., 2006) evolved from relatively small protobasins, to large basins with a massive sedimentary infill, to shrinking basins. The two major cycles were not necessarily separated by the intrusion of the Bushveld Complex, as Coertze et al. (1977) described sedimentation continuing throughout Bushveld magmatism on a local scale, especially in the Ootse basin in Botswana. The main Waterberg basin evolved as a continental fault-bounded basin, possibly extending far beyond its present fault-bounded margins (Barker et al., 2006). The total thickness of the Waterberg Group is variously estimated to be between 2,700 and 7000 m (Barker et al., 2006) although ~5 km is generally accepted (du Plessis, 1987; Callaghan et al., 1991; Dorland et al., 2006). A volcanic quartz porphyry in the oldest formation has yielded zircon SHRIMP ages of 2054 ± 4 and 2051 ± 2 Ma (Dorland et al., 2006), which are synchronous with Bushveld granite magmatism. Coertze et al. (1977) suggested that the quartz porphyry lavas were an extrusive equivalent of the Nebo granite of the Bushveld Complex.

The oldest formations of the Waterberg Group are confined to the central Bushveld Complex and deposition of sediments migrated northward over time, with the Setlaole Formation overlying the project area. This formation (Fig. 3) consists of medium- to coarse-grained granule-rich red-bed arenites with alteration (chloritization/epidotization); medium-grained, dark-brown, banded arkose; very fine grained chocolate-brown mudstone and purple shales with upward-fining channels, and a coarsening down sequence to a basal poorly sorted coarse-grained pebble conglomerate composed of quartz pebbles 0.1 to 5 cm in size with minor amounts of detrital mica, hematite, apatite, and zircon. The amount of detrital hematite grains, 1 to 10 mm in size, is variable and may reach 50 to 70 vol %, forming discrete layers of hematite sandstone up to 1 m thick. It is notable that there are no Bushveld igneous lithologies in the lithic clasts. The Setlaole Formation, which reaches a maximum thickness of 450 m in the area, shows evidence of channel flows and cross-trough bedding in drill core and is interpreted to have formed as a proximal fluvial facies, deposited on a narrow braid-plain (Jansen, 1976, 1982; Callaghan et al., 1991). Zircons from the basal conglomerate of the Setlaole Formation gave a maximum age of deposition of ca. 2045 Ma (Huthmann et al., 2016). Abundant zircons of Archean age in the sample may indicate that the Limpopo belt to the north was the source for some of the sediments, which is consistent with the paleocurrent directions (Barker et al., 2006), while Paleoproterozoic zircons are interpreted to have been derived from the now-eroded roof rocks of the Waterberg intrusion.

The Makgabeng Formation overlies the Setlaole Formation. The Makgabeng Formation is composed of fine- to medium-grained pale-red banded sandstones that are generally horizontal. It is exposed in the mountain cliffs in the western part of the project area. There is evidence of a former fluvial system at the base, although dunes occur higher up in the formation. Ripple marks, interference ripple marks, adhesion warts, and desiccation cracks indicate interdune and localized playa lake deposits (Eriksson et al., 2000). The hematitic coloration to the sands and gravels reflect an oxygenated atmosphere at this time.

A major dolerite sill, which is up to 200 m but typically ~80 m thick, occurs in most drill cores of the project area. It may be hosted within the Waterberg sediments, or within the Bushveld intrusion, but commonly occurs at the contact between the mafic igneous rocks and the Waterberg sedimentary succession. It has distinctive thick chilled margins on both contacts. The sill has been confirmed to belong to the Umkondo igneous province with a U/Pb baddeleyite age of 1125 ± 5 Ma (Huthmann et al., 2016). There is a cover

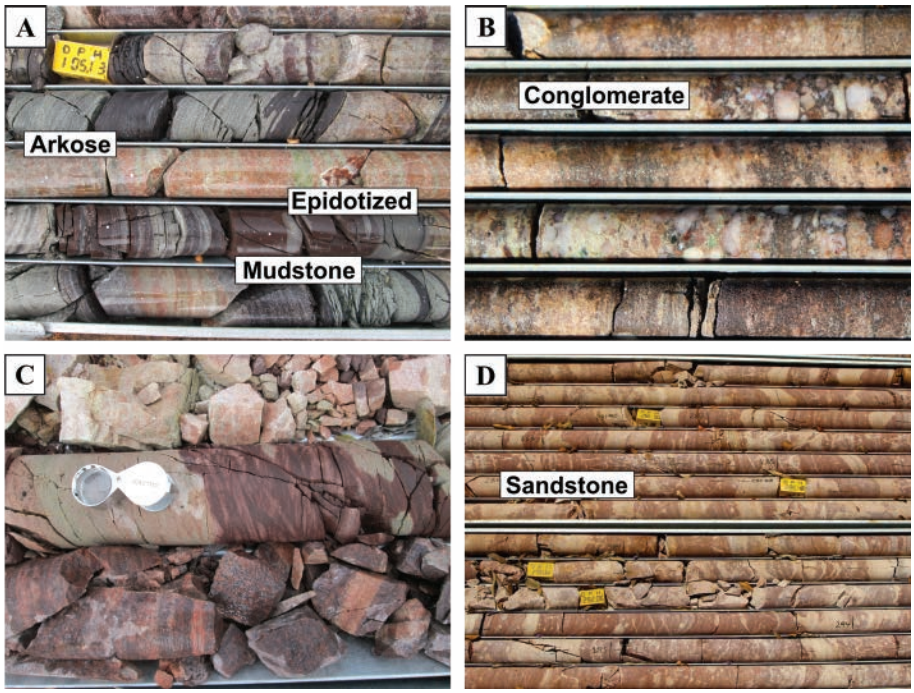

Fig. 3. Selected photographs of cores showing different lithologies of the Waterberg sediments. (A). Medium- to coarse-grained red-bed sandstone interbedded with purple brown banded arkose and light-green epidotized zones and a very fine grained chocolate-brown mudstone (WB017). (B). Coarse-grained conglomerate containing quartz pebbles and various types of lithic fragments (WB047). (C). Cross trough-bedded and hummocky cross-stratification in variably colored fine-grained sandstone (WB027). (D). Typical variably colored sandstone of the Setlaole Formation of the Waterberg Group (WB096).

of unconsolidated soils, weathered sediments, and younger Karoo sediments which are usually only a couple of meters thick.

Methodology

The study is based on detailed logging and sampling during 2011 to 2016. Data in this paper are based on 15 boreholes as shown in Figure 4, although many additional boreholes were checked for exact lithologic boundaries and potential mineralization. A Kappa-Meter KM-7 pocket meter was used to determine the magnetic susceptibility prior to documentation and sampling. An average of three readings was recorded at 1-m intervals. This method was found to be indispensable for determining the change from Main to Upper zone lithologies elsewhere in the northern limb (Ashwal et al., 2005) and has since been used on a regular basis by the exploration team. Quarter-core sampling (20–30 cm in length) was undertaken through the entire borehole core and representative samples selected for specific rock types. Samples were cut along the core axis and one-half was milled for geochemical analyses, and the other half was used for polished sections and mineral separation.

Samples were crushed, milled in a tungsten carbide mill, and analyzed at the School of Geosciences, University of the Witwatersrand. Whole-rock major elements, Co, Ni, Cu, and Cr were analyzed by X-ray fluorescence (XRF) using pressed pellets and matrix-matched standards. Trace element contents were determined by ICP-MS and a detailed description of analytical procedure can be found in Wilson (2012). A set of 28 representative samples was analyzed for major and trace elements at Cardiff University, UK. The analysis of 250 mg powder was carried out using a JY Horiba Ultima 2 inductively coupled plasma-optical emission spectrometer (ICP-OES) and Thermo X7 series ICP-MS (McDonald and Viljoen, 2006). The accuracy of the analysis was assessed by analysis of the certified reference materials (CRM) JB1a, JP1, and BIR-1. Platinum group elements, Au, and S in core samples from WB003 were analyzed by Genalysis (Perth, Western Australia), using collection by means of the standard Ni-S fire assay method and determination by ICP-MS with an Elan Sciex 6100 system. International reference material AMIS0278 was analyzed to ensure the accuracy of the PGE data. Detection limits for PGE were better than 1 ppb for all PGE and 2 ppb for Au. Sulfur was analyzed by infrared spectrometry after melting in an induction furnace with a detection limit of 0.01 wt % S. The PGE distribution in all other boreholes as shown in plots and columns is provided from the exploration assay database courtesy of Platinum Group Metals. Half-core samples were analyzed every half-meter in high-grade intervals and every meter in weakly mineralized interval. Fire assay was used for Pt, Pd, Rh, and Au, and Cu, Ni, and S were determined by XRF analysis at Set Point Laboratory in Johannesburg. The compositions of olivine, orthopyroxene, and sulfides were analyzed on a Jeol JXA 8200 microprobe at IGEM RAS (Moscow) with a measurement precision of 2 to 3% based on measurements of secondary standards. Petrography and mineralogy were studied in more than 150 polished thin sections and 12 heavy mineral concentrates. Platinum group minerals and zircon were separated in tribromomethane from a fraction <0.5 mm and laid out as rows on carbon

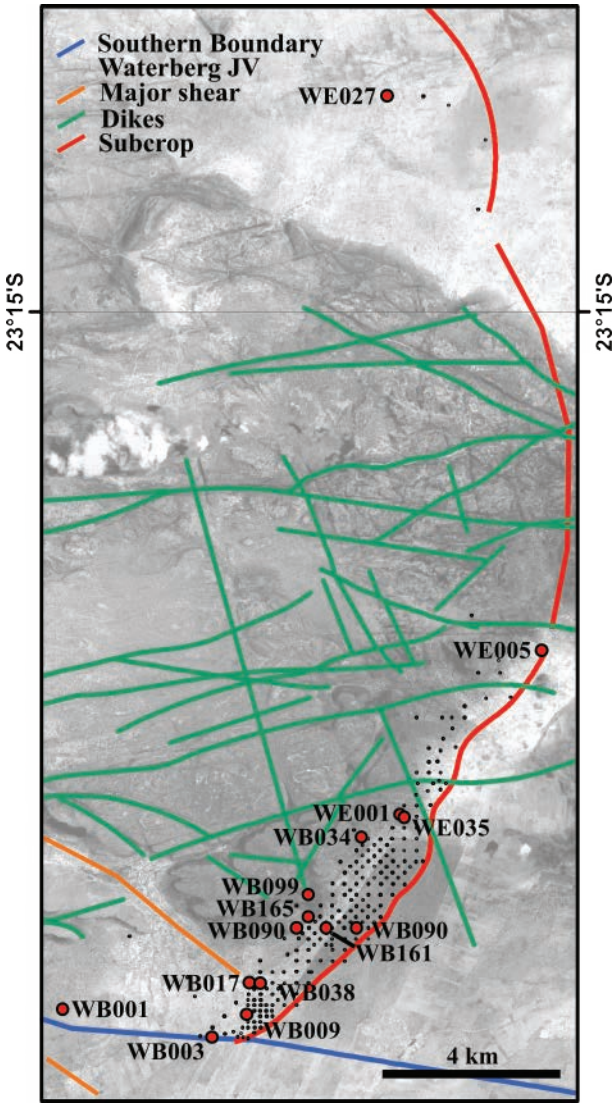

Fig. 4. Schematic map showing the location of the boreholes discussed together with major shear zones and dikes within the project area.

tape. More than 1,000 PGM have been recovered. Chemical compositions of PGM and sulfides in the polished sections and grains in the separates were semiquantitatively identified with a LINK EDS spectrometer attached to a FEI200 scanning electron microscope at the Microscopy and Microanalysis Unit of the University of the Witwatersrand. Images of minerals were obtained in a back scattered electron (BSE) mode with the same instrument.

Project Geology

The Waterberg platinum project lies 85 km north of Mokopane in the Limpopo province (Fig. 2A) centered at 23°22'01" south and 28°49'42" east. The magmatic succession comprises a basal Ultramafic sequence, comprising harzburgite and feldspathic pyroxenite, overlain by a troctolite-gabbronorite-anorthosite, and in some areas by Upper zone ferrogabbro and magnetite gabbronorite with overlying Waterberg red beds (Fig. 2B). A general westward dip of 34° to 38° occurs although some blocks may be tilted at different angles depending on structural and/or tectonic controls. The top contact of the Bushveld Complex is complex and while often very sharp and mylonitized is commonly marked by a red siltstone (Fig. 5) or less commonly by a prominent fine-grained white-gray tuffaceous layer at the contact.

The red aluminous- and hematite-rich siltstone is <10 m thick. It is strongly altered and sheared between the Upper zone and the overlying sediments (Yudovskaya et al., 2015). It comprises <70% hematite with a fine-grained matrix composed mostly of silica and phengite particles with subordinate chlorite and gibbsite. Silica is dispersed as colloform chalcedony, although it locally recrystallized into coarser aggregates of particles 5 to 100 μm in size. Phengite composition is mostly K dominant, although subordinate separate domains of Na-dominant mica (paragonite) occur in intergrowths (Yudovskaya et al., 2015). Hematite, with ilmenite exsolution lamellae, occurs as anhedral interstitial grains formed after magnetite, as coarse-grained margins to decomposed mineral and rock fragments and also as disseminations in the matrix. Numerous relics of mafic minerals, replaced by secondary assemblages, indicate that the lower part of the siltstone is a

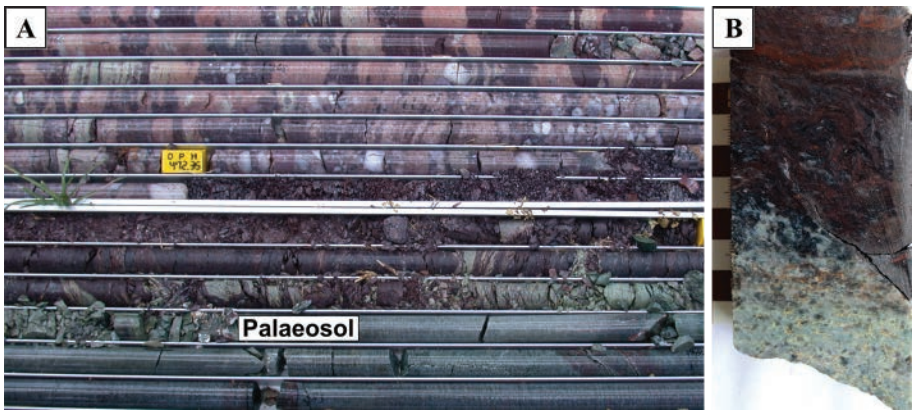

Fig. 5. Contact between Bushveld gabbro and the overlying Waterberg sediments. (A), Coarse Waterberg conglomerate overlying altered and weathered Bushveld lithologies with remnants of a paleosol (WB004). (B). Sharp contact of altered light-greenish gabbro with relics of decomposed silicates and overlying foliated hematitized siltstone, which may represent the original volcanic roof rocks into which the Waterberg igneous rocks were intruded (WB038) (Yudovskaya et al., 2015).

paleosol that developed on weathered Bushveld gabbros. In some cores, the upper part is white-gray in color, lacks the mafic silicate pseudomorphs, and instead contains multiple fractured quartz clasts <5 mm in size. This layer is richer in silica (<72 wt % SiO_2) and potassium with respect to the underlying paleosol. The mineral composition of the matrix is similar to that of hematitized paleosol, but hematite and ilmenite are not so abundant whereas accessory fluorite, apatite, monazite, dumortierite, Al-Si chlorides, and fluorides are common (Yudovskaya et al., 2015). The fractured quartz porphyroclasts, K-dominant mica compositions, occurrence of coarse zircon intergrown with quartz, and low Ti content are not consistent with a gabbroic paleosol origin. We interpret this discontinuous layer between weathered Bushveld and overlying Waterberg conglomerate as of pyroclastic or tuffaceous origin that is likely to represent the original roof rocks into which the Waterberg igneous rocks were intruded.

The footwall to the intrusive sequence is an Archean granite or granite gneiss. Commonly however, a banded agmatite formed from the interaction between Bushveld magma and the footwall has developed between the intrusive sequence and the floor rocks (Fig. 6). Often the agmatite shows well-defined banding of alternating felsic- and pyroxenite-rich layers. Rare chalcopyrite and pyrrhotite occur within both granite gneiss and agmatite. In a few boreholes there are xenoliths of calc-silicate in the pyroxenite at the base of the intrusive package, suggesting that at least locally a dolomite formed the footwall.

For the nomenclature of igneous rocks in subsequent sections, we follow the convention of Bushveld geologists and distinguish between cumulus and intercumulus minerals, thus for example, when plagioclase and orthopyroxene are cumulus, we use the term norite, whereas when orthopyroxene is cumulus and the plagioclase is intercumulus, the rock is classified as feldspathic pyroxenite.

The basal Ultramafic sequence, which is <100 m thick, trends northeast from the Hout River shear zone and dips moderately to the northwest. There are two components, a lower feldspathic orthopyroxenite (FP) unit that is <60 m thick, and an overlying harzburgite (FH) unit (Fig. 2B). The pyroxenites, which are interpreted as the initial magma to intrude the area, are interfingered with what are interpreted as Marginal zone fine-grained equigranular gabbronorite sills such that in some cores, gabbronorite forms the basal lithology (Fig. 2B). The pyroxenites are generally medium grained, dominated by up to 90% cumulus orthopyroxene with a high Mg number of up to 84, 10 to 15% clinopyroxene, and 2 to 5% chalcopyrite, pentlandite, and pyrrhotite in the upper part, but with up to 15% where semimassive sulfides occur. Rare chromitite stringers have been identified in a few cores.

The harzburgite sequence in the Ultramafic sequence is 80 to 100 m thick and locally pegmatoidal toward the base, with lesser olivine-bearing gabbronorite, olivine-bearing norite, pyroxenite, feldspathic pyroxenite, and serpentinized units that have been extensively chloritized and serpentinized (Fig. 7). It is possible that some of these units such as the olivine-bearing gabbronorite or feldspathic pyroxenite may be younger intrusive sills. The harzburgites have <65% olivine with orthopyroxene and lesser interstitial plagioclase and clinopyroxene. There is generally a high degree of alteration (Fig. 7B) with fractures in olivine filled with secondary magnetite and serpentine. Clinopyroxene occurs as small intercumulus

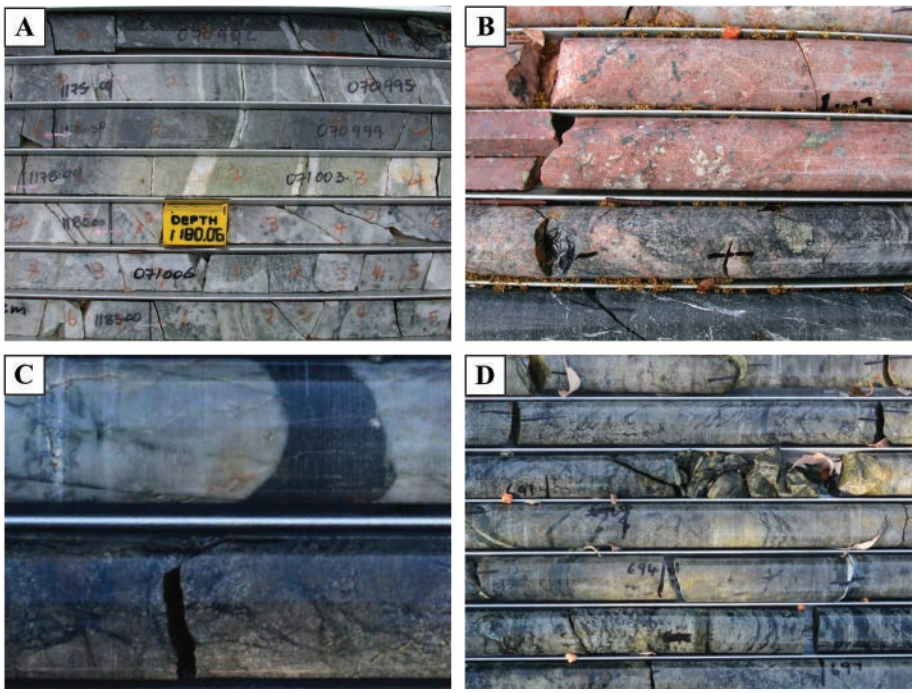

Fig. 6. Selected photos of footwall rocks. (A). Banded agmatite formed from the interaction between Bushveld magma and the footwall granite gneiss (WB017). (B). Granite gneiss with rare chalcopyrite and pyrrhotite (WE005D0). (C). Agmatite with well-defined banding of felsic- and pyroxenite-rich layers (WE035). (D). Highly altered agmatite (WE035). From McCreesh 2016.

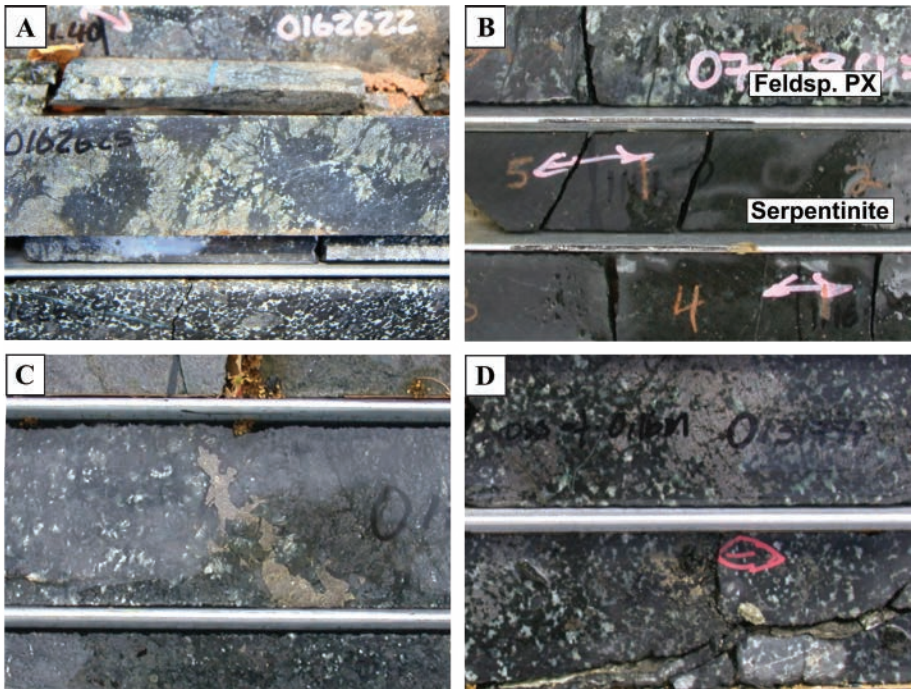

Fig. 7. Selected images showing the variation in the ultramafic lithologies. (A). Strongly serpentinized harzburgite from WB132. (B). Feldspathic pyroxenite (Feldsp. PX) at the top and a unit that has been completely serpentinized below (WB027). (C). Feldspathic pyroxenite with blebs of pyrrhotite and chalcopyrite and veinlets of serpentine (WE035). (D). Harzburgite/feldspathic harzburgite with large oikocrysts of orthopyroxene (WB017). From McCreesh (2016).

grains, whereas orthopyroxene forms large oikocrysts and in some samples rims of orthopyroxene partially or completely surround olivine crystals. Medium-grained feldspathic pyroxenites have <30% interstitial plagioclase and <45% cumulus orthopyroxene 5 mm in size, although some samples contain up to 50% clinopyroxene that varies from 1 to 5 mm in size. Chalcopyrite, pentlandite, and pyrrhotite (2–5%) within the unit are associated with PGE mineralization (Fig. 7C).

The troctolite-gabbronorite-anorthosite sequence (TGA, Fig. 2B) is a lithologically varied unit that reaches a maximum of 850 m in thickness. The troctolite unit at the base of the troctolite-gabbronorite-anorthosite sequence ranges in thickness from 40 to 100 m and varies in composition from melatroctolite and rare dunite to olivine norite and leucotroctolite, all with a medium- to coarse-grained equigranular texture intercalated with lenses of pyroxenite ranging up to a meter in size (Fig. 8). Most of the sequence comprises 50 to 80% olivine. In thin section, altered olivines are usually subrounded and range from 3 to 7 mm in size. Sericitized plagioclase, 2 to 5 mm in size, forms <40%, while orthopyroxene (up to 10%) is either intercumulus surrounding or rimming olivine or forming occasional centimeter-sized oikocrysts. Both olivine and pyroxene may host chromite crystals up to 50 μm in size. The upper portion of the troctolite is heterogeneous and grades upward into olivine-bearing gabbroic rocks. The gabbronorites are medium- to coarse-grained (melanocratic, leucocratic, and altered) with varying proportions of orthopyroxene, subordinate clinopyroxene, inverted pigeonite, and <50% plagioclase of labradorite-bytownite composition. Grain size varies from 0.5 to 5 mm with minor pegmatoidal patches. Orthopyroxenes are generally subhedral and range from 0.5 to 4 mm and may form <50% of the mineralogy locally becoming a norite or olivine-bearing norite. Selected chemical analyses of the gabbronorites are shown in Table 1.

Toward the top of the troctolite-gabbronorite-anorthosite sequence in the southern part of the project area, a mineralized zone (the T zone) occurs within a variable package of pyroxenite, feldspathic pyroxenites, troctolite/harzburgite, norite to anorthosite that is locally pegmatoidal. In the north of the project area the zone is either poorly developed or missing. The anorthosite is generally medium-grained sometimes becoming pegmatitic. It is often a light greenish-gray to milky-white color due to alteration of the plagioclase, with <10% oikocrysts of orthopyroxene forming a mottled and spotted texture locally.

The Upper zone is dominated by magnetite gabbro and gabbronorite (Fig. 9) with ferrogabbro at the top in some borehole cores. In the southwest close to the Hout River shear zone the unit may be as thick as 350 m, but northward it thins and is completely absent in the north-central project area, but it reappears in the far north where it can be 70 to 500 m thick. In core, the gabbro shows an inequigranular texture with large plagioclases, ranging from 2 to 5 mm in size, within a finer grained groundmass of orthopyroxene, clinopyroxene, and magnetite (0.5–5 mm) that may comprise up to 20% of the groundmass. However, magnetite is also intergrown with pyroxene crystals. The olivine-bearing gabbronorite has a similar composition to the magnetite-bearing gabbronorite apart from the presence of added olivine, although the former tends to have higher degrees of alteration. The uppermost portions of the Upper zone are characterized by brick-red alteration and a highly sheared contact zone. Geochemical analyses of

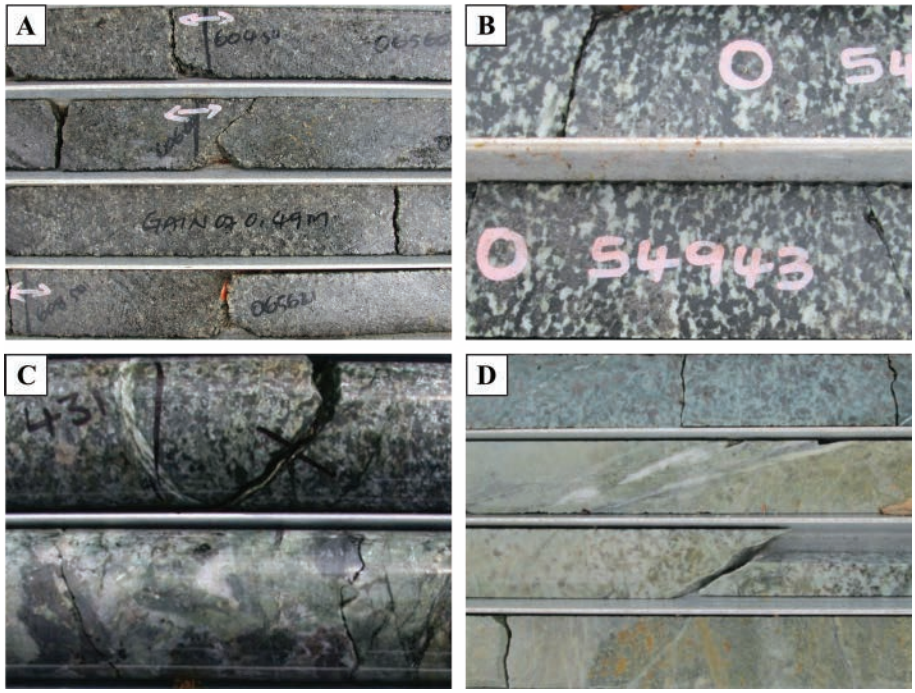

Fig. 8. Lithologic variation in the troctolite-norite-anorthosite sequence. (A). Gabbronorite (WB0170). (B). Troctolite (WB163). (C). Pegmatoidal unit (WE001). (D). Anorthosite (WB017). From McCreesh (2016).

typical magnetite-bearing gabbronorite and ferrogabbro are shown in Table 1. Where the Upper zone is missing, either the troctolite-gabbronorite-anorthosite sequence troctolite or pyroxenite of the Ultramafic sequence is in contact with the overlying Waterberg Group. Where this occurs, the troctolite-gabbronorite-anorthosite sequence rocks at the contact show similar alteration to that of the Upper zone rocks elsewhere.

The Upper zone is overlain by the relatively flat-lying Waterberg sedimentary package that varies from 120 to 760 m thick, with dip angles ranging from to 2° to 5°.

Magnetic susceptibility variations

Magnetic susceptibility profiles based on more than 15,000 measurements through six cores were created in order to distinguish between the different stratigraphic units. In the Ultramafic sequence, magnetic susceptibility measurements (Fig. 10) highlight pyrrhotite in feldspathic pyroxenite and secondary magnetite formed from the serpentinization of olivine. The magnetic susceptibility values range from 1.00 to 10.00 SI units with a maximum of >40.00 SI units associated with harzburgite intervals. Through the troctolite-gabbronorite-anorthosite sequence, magnetic susceptibility values decrease upward from olivine-bearing to olivine-free lithologies, such that the majority of the troctolite-gabbronorite-anorthosite sequence has susceptibility values that are very low. These low values continue into the lower part of the T zone where susceptibility values range from 0.01 to 3.00 SI units. Upward in the T1 zone, values are from 0.01 to 5.00 with maximum values of <12.00 SI units associated with olivine-rich intervals. Upward in the succession the magnetic susceptibility becomes consistently higher, reflecting the incoming of magnetite as a primary mineral crystallizing from an Upper zone magma influx. The

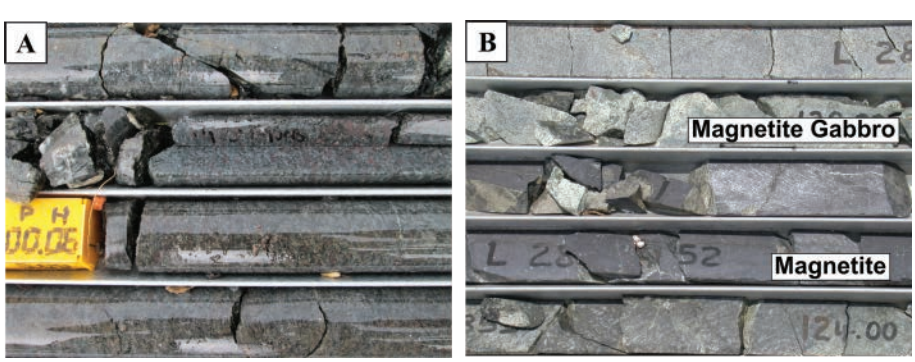

Fig. 9. Upper zone lithologies from different cores. (A). Weakly altered ferrogabbro with pinkish altered olivine (WB017). (B). A 2-m-thick magnetite layer (in core tray slots 3 and 4 from the top) only seen in borehole WB001. From McCreesh (2016).

Table 1. Geochemical Analytical Data for Selected Samples from Waterberg

Units	FW	UmS	UmS	UmS	UmS	UmS	TGA	TGA	TGA	TGA	TGA	TGA	TGA	UZ	UZ	UZ	UZ
Rock type	GG	FPYX	FPYX	FPYX	FPYX	HZ	TOC	TOC	TOC	GN	GN	GN	GN	MGN	MGN	FG	FG
(wt %)																	
SiO_2	64.24	51.65	49.97	48.67	54.86	44.10	45.70	48.48	46.79	50.61	51.37	51.04	49.90	51.88	48.64	52.48	52.37
Al_2O_3	21.70	5.18	13.46	4.61	4.26	10.27	15.75	24.66	14.68	17.02	24.58	21.91	21.54	12.94	14.47	18.12	7.54
Fe_2O_3	0.08	1.69	1.60	0.91	1.16	1.53	1.11	0.42	0.99	1.10	0.46	0.65	0.50	1.31	1.59	1.03	1.64
FeO	0.63	13.65	12.96	7.37	9.42	12.35	8.99	3.38	8.02	8.94	3.72	5.31	4.02	10.57	12.87	8.37	13.25
MnO	0.01	0.24	0.18	0.14	0.20	0.18	0.14	0.07	0.16	0.18	0.07	0.11	0.10	0.22	0.21	0.12	0.28
MgO	0.28	22.50	14.07	35.51	25.33	22.63	17.86	6.78	17.41	8.85	5.32	7.35	5.45	12.45	12.83	6.94	15.27
CaO	6.09	3.75	6.09	2.60	4.59	6.70	9.25	13.64	10.73	10.81	10.78	11.33	15.86	8.73	6.86	10.25	8.20
Na_2O	6.06	0.42	1.10	0.22	0.37	0.34	1.00	2.03	0.94	1.92	2.89	2.07	2.23	1.55	1.62	2.24	0.88
K_2O	0.38	0.05	0.11	0.04	0.06	0.24	0.15	0.31	0.23	0.14	0.54	0.16	0.13	0.13	0.17	0.26	0.22
TiO_2	0.07	0.15	0.15	0.11	0.13	0.08	0.10	0.08	0.10	0.37	0.09	0.13	0.15	0.23	0.22	0.29	0.36
P_2O_5	0.04	0.02	0.01	0.02	0.02	0.02	0.02	0.02	0.01	0.02	0.02	0.02	0.01	0.02	0.02	0.02	0.02
Cr_2O_3	0.00	0.31	0.22	0.39	0.31	0.04	0.12	0.09	0.18	0.06	0.04	0.02	0.04	0.05	0.01	0.04	0.07
NiO	0.00	0.36	0.12	0.25	0.12	0.45	0.10	0.02	0.10	0.02	0.01	0.02	0.01	0.03	0.06	0.02	0.04
(ppm)																	
Sc	2.28	38.01	37.33	15.73	27.93	14.68	20.55	18.02	25.41	34.88	18.08	20.39	41.07	38.10	23.43	33.93	53.69
V	8.82	208.55	333.70	62.96	102.64	53.60	44.80	48.53	79.27	170.87	41.87	76.56	127.05	151.98	86.01	173.77	241.08
Cr	19.41	2,118.90	1,431.24	2,388.51	2,001.94	219.42	627.74	757.96	1,052.97	383.81	252.24	97.40	202.95	275.18	56.75	190.73	383.94
Co	0.55	175.26	67.98	99.20	80.76	135.63	29.59	97.47	88.48	57.03	25.69	41.53	28.88	69.24	107.55	59.85	92.87
Ni	6.89	2,819.35	881.34	1,899.45	936.99	2,840.78	157.20	793.96	776.19	170.97	96.30	140.62	113.64	194.64	464.59	150.58	260.11
Cu	9.42	1,282.28	208.00	58.18	63.95	1,242.38	28.70	37.03	50.26	58.42	51.92	71.09	40.94	63.78	60.53	81.80	71.50
Zn	10.35	88.87	103.92	59.81	96.64	82.76	23.40	62.83	56.56	61.39	29.14	38.89	27.62	77.46	89.16	46.40	99.29
Ga	21.82	5.44	12.28	3.79	5.13	7.16	13.36	9.17	9.79	12.18	15.86	16.49	14.34	11.63	11.88	16.07	9.22
Rb	8.60	5.39	7.24	3.62	4.63	10.59	9.91	5.95	7.43	5.00	13.96	4.56	2.34	4.07	6.55	4.94	8.41
Sr	1,692.94	36.94	189.36	32.46	29.49	67.46	556.18	132.49	141.82	186.21	306.05	222.37	278.55	156.51	174.67	194.84	74.99
Y	2.29	3.34	2.02	0.78	2.38	1.78	0.88	1.34	3.16	6.29	2.09	4.96	6.68	7.16	3.73	6.79	11.42
Zr	81.79	6.83	5.44	7.40	4.37	2.88	6.54	5.19	4.91	14.61	16.28	10.77	8.58	11.86	15.57	13.84	23.93
Nb	1.69	2.01	0.79	1.08	0.65	0.45	1.15	1.46	0.61	3.01	1.59	1.71	1.37	3.47	3.74	2.36	3.45
Mo	0.51	0.86	0.79	0.39	d.l.	0.04	0.20	1.13	0.85	0.13	0.21	0.00	0.03	0.20	0.90	0.37	1.31
Ba	292.24	21.07	60.76	24.44	17.19	42.66	112.54	37.65	45.61	66.32	186.59	58.09	40.42	78.14	78.34	100.20	80.62
Pb	10.26	8.29	6.23	6.30	5.82	6.47	2.52	0.97	4.44	4.01	4.31	5.53	3.93	3.52	4.52	3.22	2.51

Abbreviations: FG = ferro-gabbro, FH = F-zone harzburgite, FP = F-zone pyroxenite, FPYZ = feldspathic pyroxenite, FW = footwall, GG = granite/granofels, GN = gabbronorite, HZ - harzburgite, MGN = magnetite-bearing gabbronorite, MZ = Main zone, TROC = troctolite, UZ = Upper zone

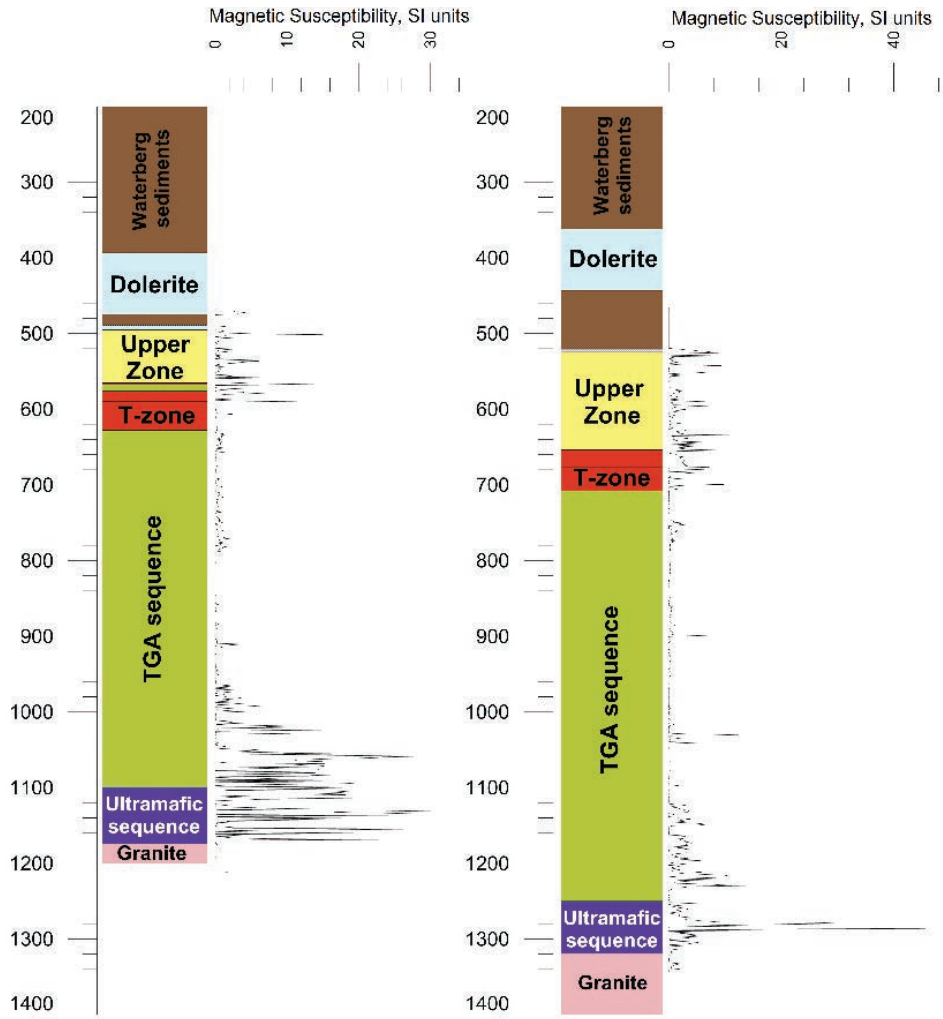

Fig. 10. The magnetic susceptibility values (SI units) plotted against the depth for WB027 (left) and WB099 (right). The high magnetic susceptibility in the Ultramafic sequence is due to secondary magnetite formed from the serpentinization of olivine. Olivine persists upward at the base of the troctolite-gabbronorite-anorthosite sequence. The increase in magnetic susceptibility values in the T zone is where the boundary is drawn between the troctolite-gabbronorite-anorthosite sequence and the Upper zone, even though there may be no notable lithologic change. From McCreesh (2016).

position of the sustained increase in magnetic susceptibility value is where the boundary is now drawn between the troctolite-gabbronorite-anorthosite sequence and the Upper zone. Distinct chemical changes support this rationale, even though there may be no notable lithologic change. Although the Ti and V content of magnetite varies through the Upper zone, there is little or no change in the magnetic susceptibility values (Klemm et al., 1985; Cawthorn and Molyneux, 1986; Clark and Emerson, 1991; Clark, 1997; Ashwal et al., 2005). According to Clark and Emerson (1991) titanomagnetite ranges from 1 to 50 SI units, depending on the size of the titanomagnetite crystal. This magnetic susceptibility technique is now used as a routine method by PTM as it provides a reliable technique that can be applied readily and cheaply to identify a boundary that can be correlated across all the borehole cores.

Mineralization

There are two mineralized intervals, a lower F zone and an upper T zone (Fig. 11). These mineralized zones are 3.0 to 60 m thick. The T zone outlined so far is restricted to the southern portion of the project area, whereas the F zone has been intersected along a strike length of 17 km. From the Hout River shear zone the succession thickens northward with greater separation between the two mineralized zones. There is a correlation between visible chalcopyrite and pentlandite abundance and the grade of PGE in both the T and F zones.

F zone: The F mineralized zone occurs in the Ultramafic sequence pyroxenite and harzburgite. In the southern portion, the F zone is typically <10 m thick but in the central portion, the "Super F zone" thickens to 60 m in true thickness, with grades of 2 to 4 g/t 2PGE + Au over this interval. The basal pyroxenite has variable grade: when the PGE grade is good in the pyroxenite then grade is also high in the harzburgite unit above. The mineralization generally comprises blebs, net-textured to disseminated pyrrhotite, chalcopyrite and pentlandite with accessory chromite, chalcocite, and pyrite (Fig. 12). Chromite crystals are often enclosed in silicates, while chromite itself may host sulfide inclusions (Fig. 12D) and rare

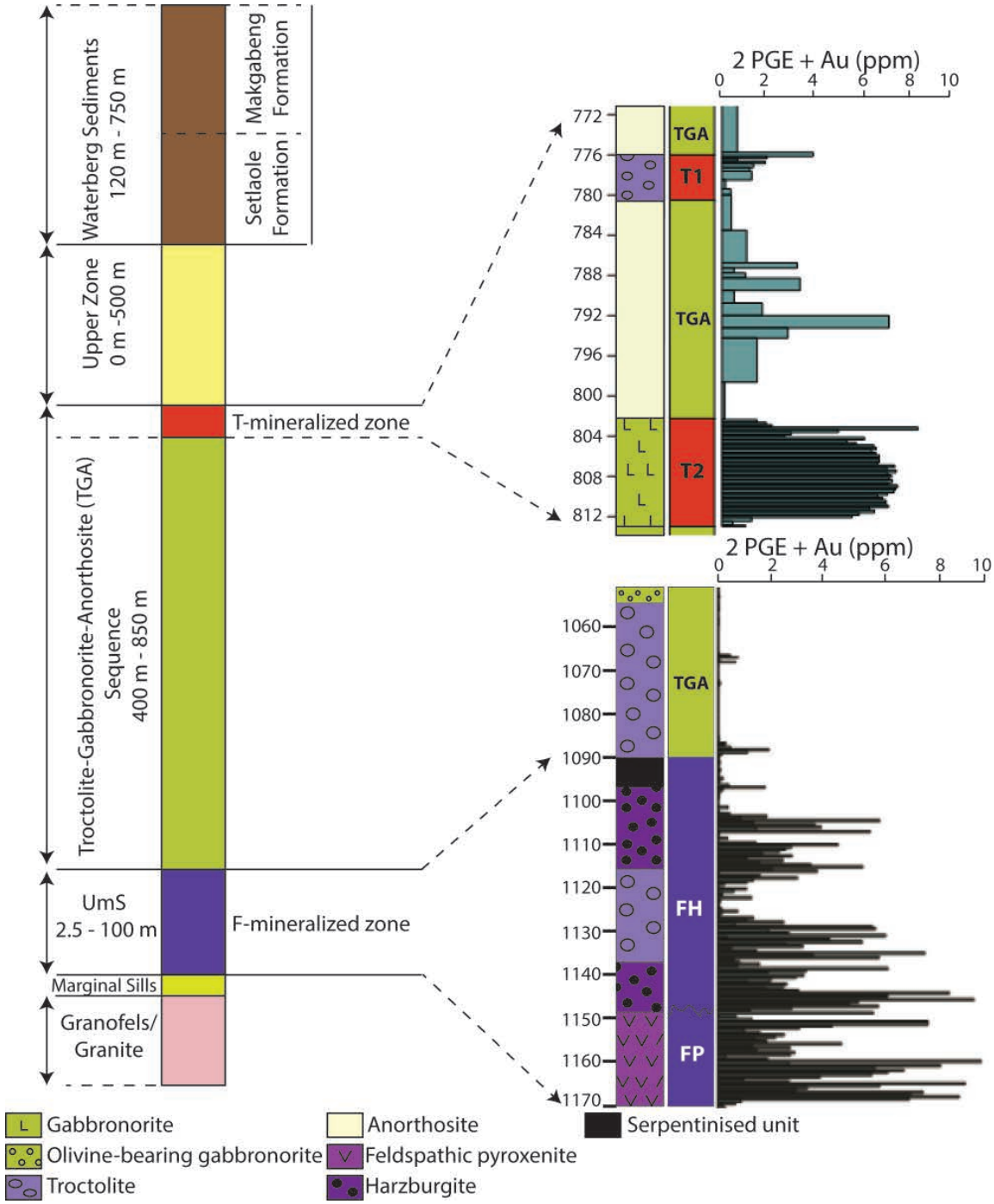

Fig. 11. Schematic idealized section through the Bushveld intrusive rocks of the Waterberg project, showing the location of the mineralized F and T zones within the stratigraphy. The variability in Pt + Pd + Au grade is shown for both zones and the histograms reflect PGE grades that are typically up to 7 g/t.

chromitite stringers have been identified in two boreholes. Magnetite has often replaced sulfides and chromite. More than 600 PGM grains have been recovered for study. PGM (Fig. 13) are variable with dominant sperrylite and subordinate Pt-Pd bismuthotellurides, Au-Ag alloys, Pd arsenides, and Pt-Rh sulfarsenides. More textural details will be described in a subsequent paper. Variations in Cr, Ni, Cu, and PGE in one of the borehole cores are shown in Figure 14. The overall grade is given in Table 2. There is an anticorrelation between the Cr and PGE grade, with the highest PGE values coincident with the lowest Cr values. The changes in MgO%, Mg number, and Cr/MgO across the interface of the F zone and the troctolite-gabbronorite-anorthosite sequence are shown in Figure 15. Selected chemical analyses are shown in Table 1.

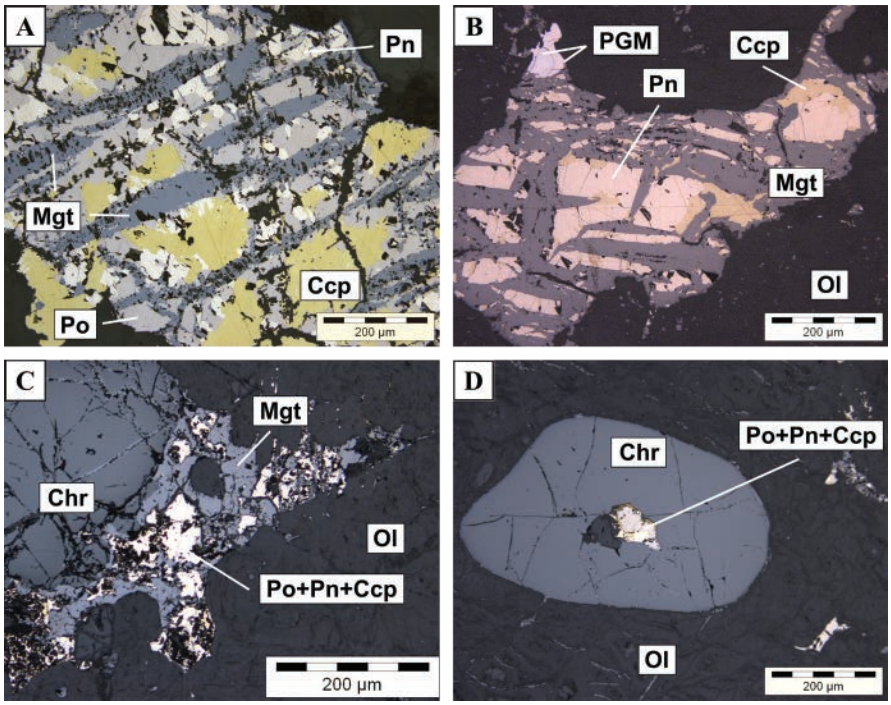

Fig. 12. Photomicrographs of sulfide mineralization in the F zone. (A). Magnetite replacement of sulfides. (B). Chalcopyrite, pentlandite, magnetite, and platinum group minerals in olivine. (C). Magnetite replaces chromite and sulfides. (D). Chromite with sulfide inclusion. Abbreviations: Ccp = chalcopyrite, Chr = chromite, Mgt = magnetite, Ol = olivine, Pn = pentlandite, PGM = platinum group minerals, Po = pyrrhotite.

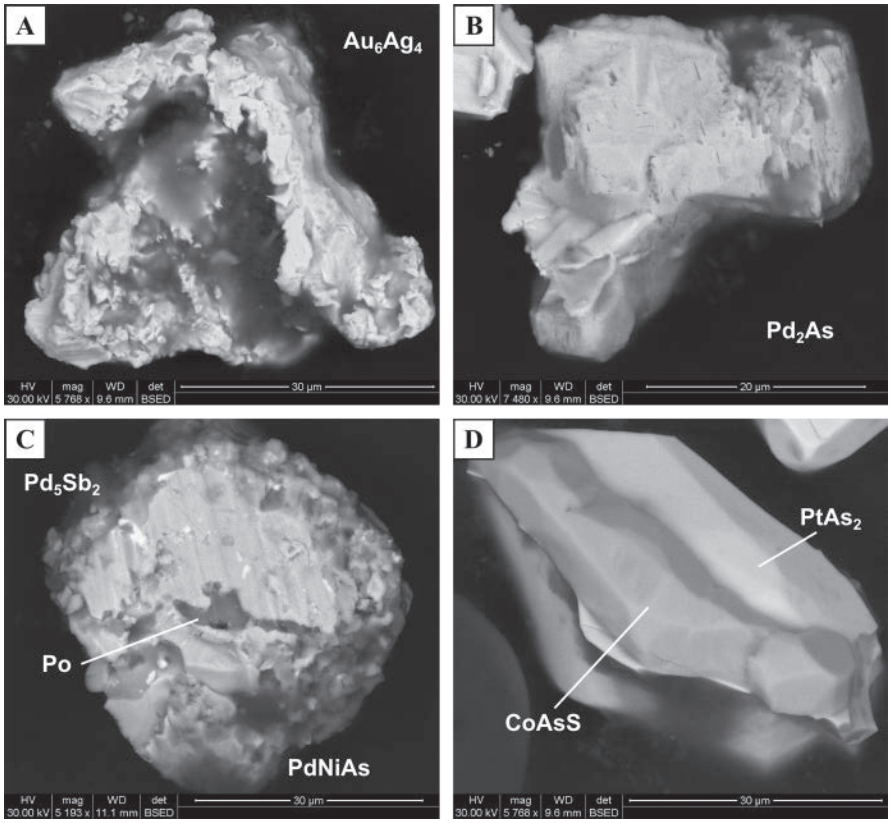

Fig. 13. Noble metal minerals from the F zone in core sample WB034 (A). Electrum Au_6Ag_4 = 1,060.3-m depth. (B) Palladioarsenide Pd_2As = 1,060.3-m depth. (C). Majakite PdNiAs + stibiopalladinite, bright (Pd_5Sb_2) + pyrrhotite - 1061 m. (D). Sperrylite ($PtAs_2$) and cobaltite CoAsS = 1,018-m depth. Scale bars are 30 μm in length.

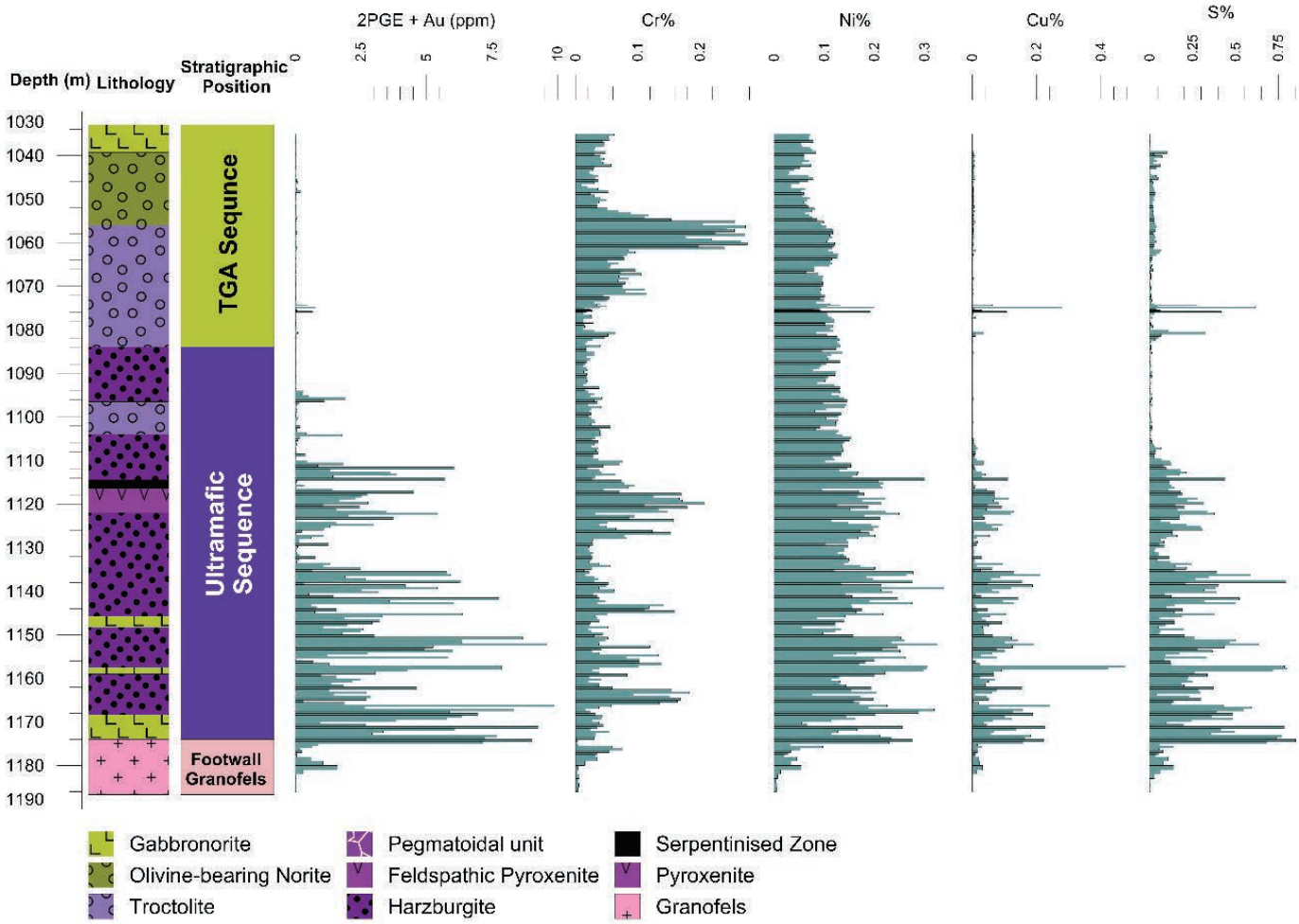

Fig. 14. The F zone showing the 2 PGE + Au (ppm) grade and abundances for Cr, Ni, Cu, and S in core WB027. From McCreesh (2015).

T zone: The T zone (Fig. 11) occurs at the top of the troctolite-gabbronorite-anorthosite sequence just beneath the contact of the overlying Upper zone and at its shallowest is at 130 m in depth, subcropping against the Waterberg sedimentary rocks. In core sample WB003 in the south of the project area, the T zone is ~30 m thick but thickens northward to <50 m thick. The zone is characterized by its lithologic variability and includes anorthosite, pegmatoidal gabbros, pyroxenite, troctolite, harzburgite, gabbronorite, and norite. The T mineralized zone is subdivided into two mineralized zones the lower T2 unit and the upper T1 layer (Fig. 16). These units can be traced for several kilometers along strike.

T2 mineralization is hosted in homogeneous gabbronorite/gabbro that is locally pegmatoidal and is characterized by distinctive, elongated milky-white plagioclase <1 cm in size. It may grade into a feldspathic pyroxenite (Fig. 16). The T2 ranges from 2 to 15 m thick with disseminated and blebby pyrrhotite, pentlandite, chalcopyrite, and pyrite with minor millerite, sphalerite, and bornite. PGM are less varied than in the F zone and are dominated by Pt-Pd bismuthotellurides. Both T zones have a consistent and unusual metal ratio with 21% Au in the precious metals (Table 2). T2 grades downward into an unmineralized gabbronorite/norite unit.

Grade values for precious and base metals in the F and T zones are given in Table 2. Grade values given are derived from a total of 298,538 m of diamond drilling in 231 drill holes and 373 deflections. (PTM, October 2016). The indicated mineral resources in millions of tons have been based on a cut-off grade of 2.5 g/t and a depth of 1,250 m, although both the T and F zones continue below this depth.

Table 2. Grade Values for Precious and Base Metals in the F and T Zones

	Pt	Pd	Au	Rh	Cu (%)	Ni (%)	Proportion of precious metals (%)	Indicated resources (Mt)	Inferred resource (Mt)
T zone	1.13	1.90	0.81	0.04	0.16	0.08	Pt 29, Pd 49, Au 21, Rh 1	31.540	19.917
F zone	1.05	2.23	0.17	0.04	0.07	0.16	Pt 30, Pd 64, Au 5, Rh 1	186.725	77.295

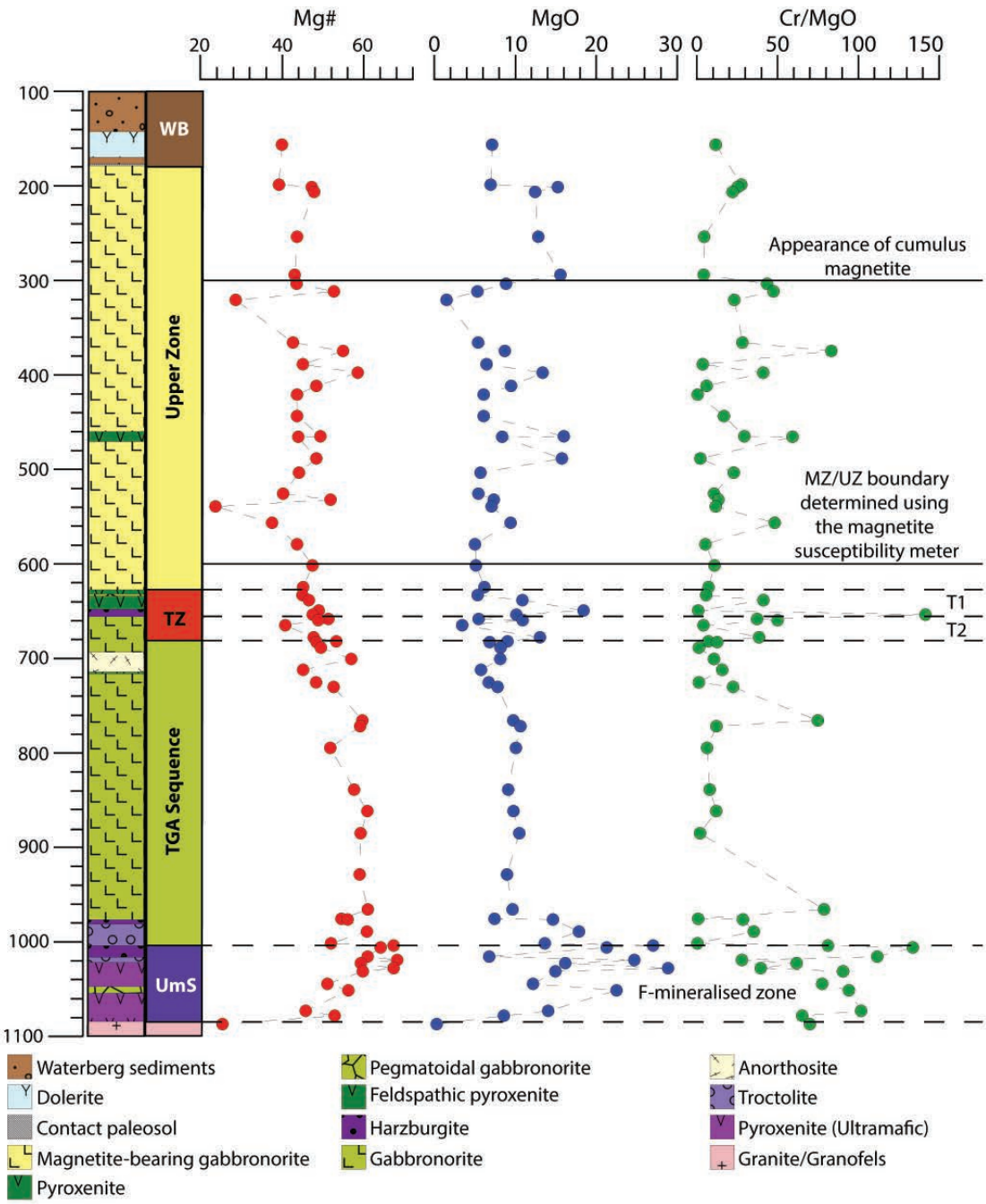

Fig. 15. Compositional variation of MgO (wt %), Mg number, and Cr/MgO (ratio) through core WB017. Dashed lines indicate the mineralized units. TGA sequence = troctolite-gabbronorite-anorthosite, T zone = T mineralized zone, UmS = Ultramafic zone, WB = Waterberg sedimentary sequence. McCreesh et al. (2015).

The middling between the T2 and T1 is not always present. Where it occurs it varies in thickness from ~20 cm to 35 m and comprises pegmatoidal leucogabbro or a varitextured pegmatoidal anorthosite that is compositionally similar to the pegmatoidal anorthosite in the T1 hanging wall (Fig. 16). This hanging wall can range from 0 to 20 m in thickness. The middling and hanging-wall units only locally have good grade.

The T1 mineralized zone is hosted in a variety of rock types, including troctolite (Fig. 16), which may grade into a feldspathic harzburgite or sometimes to an olivine-bearing feldspathic pyroxenite. All show minor chloritization and serpentinization in olivine-bearing intervals. The thickness of T1 varies from 3.5 to 5 m. Sulfides are common (Fig. 17) as blebby to net-textured chalcopyrite and pentlandite, with minor disseminated pyrrhotite, as flame-textured pentlandite in pyrrhotite and pyrite, as pyrite replacing magnetite and pyrrhotite, or rimming earlier sulfides. The limited variations in MgO%, Mg number, and Cr/MgO within the troctolite-gabbronorite-anorthosite sequence are shown in Figure 15, while the variations in Cr, Ni, Cu, and PGE in one of the borehole

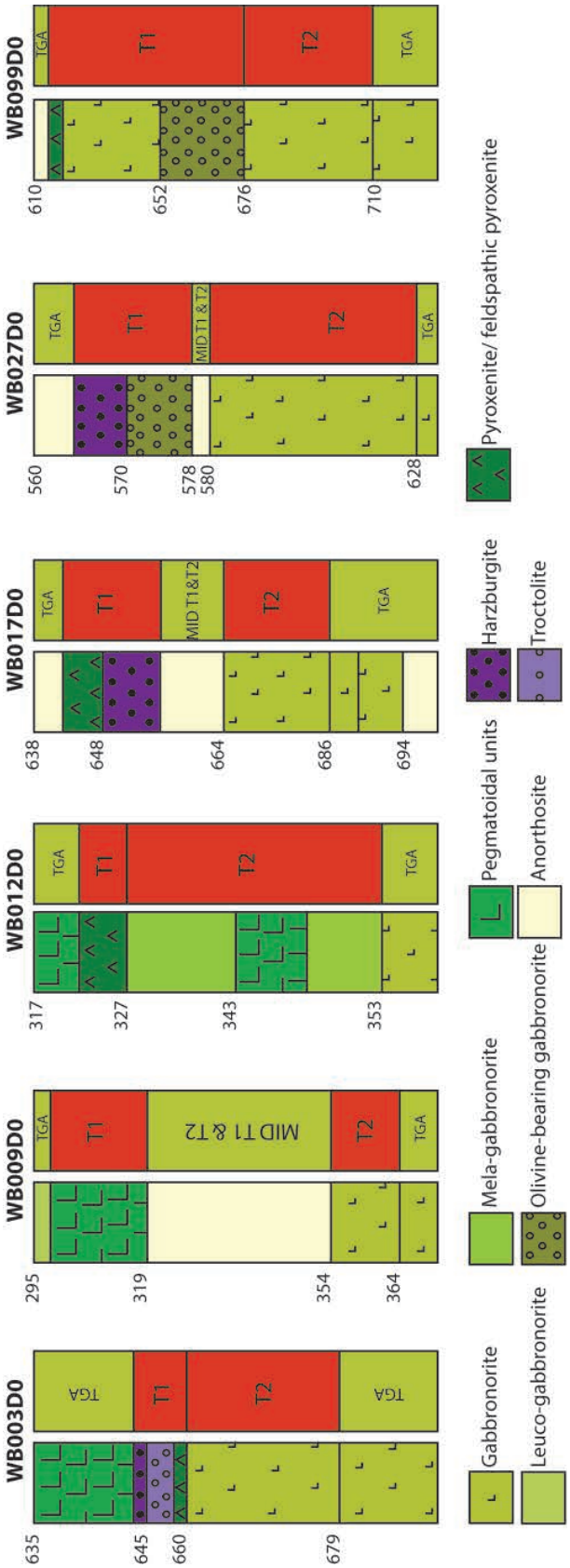

Fig. 16. Schematic section through the T zone, showing the variability of the rock types and the host rocks of the mineralization in the T1 and T2 layers. The column to the left shows the lithology, while the column to the right for each borehole shows the stratigraphic affiliation of the various units.

cores are shown in Figure 18. The Pt + Pd + Rh + Au grade is typically 1 to 7 g/t (Table 2). Selected chemical analyses are shown in Table 1.

The hanging wall to T1 is generally a pegmatoidal anorthosite or coarse-grained leucogabbronorite that varies in thickness from 2 to <100 m although it is absent in a few cores (Fig. 16). This unit may host PGE mineralization together with chalcopyrite, pentlandite, and pyrrhotite.

Discussion

When the PGE mineralization was discovered at the Waterberg project, a significant question was whether the intrusion was of Bushveld age, related to the Great Dyke (2575 Ma; Oberthür et al, 2002) or to other Paleoproterozoic intrusions in the Limpopo belt. Having established that the intrusion on the Waterberg project is of similar age to the Bushveld Complex (Huthmann et al., 2016), the challenge is to compare and contrast the project stratigraphy and mineralization with that of the eastern, western, and northern limbs of the complex. It is apparent that there are significant similarities, but also notable differences, even with the northern limb immediately to the south of the Hout River shear zone. In the Waterberg platinum project, a Waterberg sedimentary sequence caps the eroded Bushveld rocks, whereas south of the Hout River shear zone, thick differentiated granite sheets cap the Upper zone.

Ultramafic sequence: Harzburgite and orthopyroxenite are typical constituents of both the Lower and Critical zones elsewhere in the Bushveld Complex. The amount of interstitial plagioclase in the Waterberg ultramafic rocks commonly exceeds 10 to 15 vol %, which is higher than the plagioclase proportions in the Lower zone rocks (2–6 vol % according to definition of Cameron, 1978) and is more comparable with the proportions in the Critical zone and the Platreef. The most common texture of the Waterberg harzburgite is poikilitic, whereas granular harzburgite transitional into dunite as in the Lower zone at Grasvally (Hulbert and von Gruenewaldt 1985), Clapham (Wilson, 2012), and Turfspruit (Yudovskaya et al., 2013a) was not observed in the Waterberg rocks. Kink bands and chromite-pyroxene lamella, which were described in Lower zone olivine (Wilson et al., 2012; Yudovskaya et al., 2013a), were not found in olivine from Waterberg harzburgite. The laminar fabric of preferred elongated orthopyroxene that is considered to be a typomorphic feature of the Lower zone pyroxenite (Boorman et al., 2004) was also not observed in Waterberg. The regular chromite seams with sharp boundaries common in the Lower Critical and in the Lower zones on Grasvally and Clapham are absent at Waterberg. Instead, chromite concentrates into bands of disseminated grains with irregular diffuse outlines resembling the appearance of Platreef chromitite in the northern limb of the Complex as described by Yudovskaya and Kinnaird (2010). Chemical compositions of the most primitive olivine and chromite analyzed so far are also more consistent with the Critical zone lineage as Fo in olivine varies from 77 to 83 and Cr_2O_3 content in chromite does not exceed 32 wt %. Furthermore, apart from at Grasvally there is no PGE or Cr mineralization known in the Lower zone anywhere else in the Bushveld Complex.

Troctolite-gabbronorite-anorthosite sequence: Originally the troctolite unit in the Waterberg project was thought to

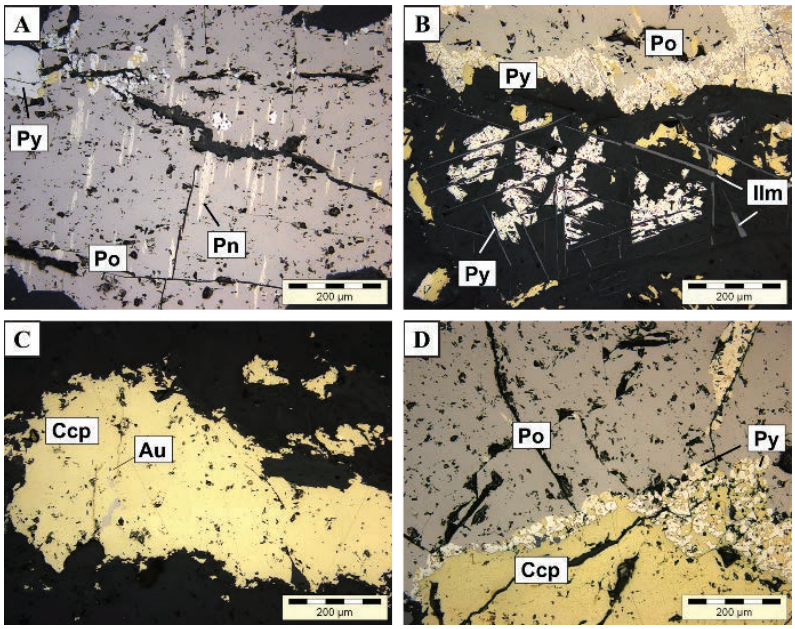

Fig. 17. Photomicrographs of sulfide mineralization in the T zone. (A). Flame-textured pentlandite in pyrrhotite and pyrite. (B). Pyrite after magnetite and pyrrhotite. (C). Au and pyrrhotite in chalcopyrite. (D). Pyrite growing along the boundary of pyrrhotite and chalcopyrite. All images in reflected light. Abbreviations: Ccp = chalcopyrite, Ilm = ilmenite, Pn = pentlandite, Po = pyrrhotite, Py = pyrite.

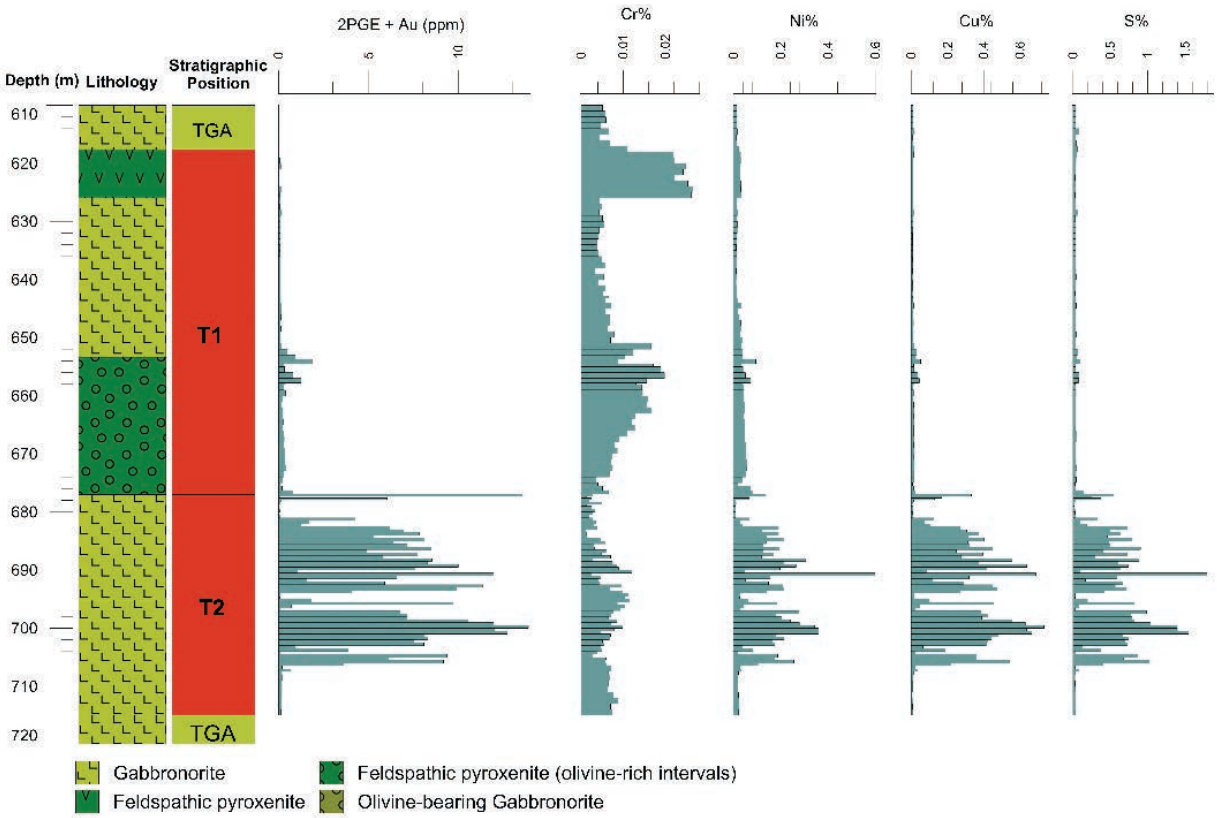

Fig. 18. The mineralized T zone showing the distribution of 2 PGE + Au (ppm) grade within T1 and T2. Variations in the Cr, Ni, Cu, and S % in core WB099 are also shown. Note how the high PGE do not correlate with zones of high Cr %. Samples were analyzed for Pt, Pd, and Au (all ppm) by standard 25-g lead fire-assay using a silver collector. Rh was assayed using the same method but with a palladium collector. After preconcentration by fire assay the resulting solutions were analyzed using ICP-OES for copper, nickel, cobalt, and chromium. This technique results in "almost" total digestion. Data by courtesy of PTM in McCreesh (2015).

correlate with the troctolite in the Main zone of the northern limb, identified by van der Merwe (1976) and observed in the Bellevue drill core (Ashwal et al., 2005). Both have high magnetic susceptibility signatures, which resulted from the formation of secondary magnetite during the alteration of olivine, and there is an overall similarity in chondrite-normalized multielement signatures. However, there are lithologic and mineralogical contrasts. According to Ashwal et al. (2005) the troctolite package in the Bellevue drill core is mainly composed of olivine-norite, gabbro, and gabbronorite with minor leucocratic varieties and pyroxenite horizons, rather than being a true troctolite, with the average modal abundance of olivine in the olivine-bearing sequence of 21.1% and decreasing irregularly upward. In contrast, the troctolite unit in the Waterberg stratigraphy is composed of cumulus feldspar and 25 to 65% olivine, with interlayers of pyroxenite or feldspathic pyroxenite (cumulus orthopyroxene and clinopyroxene with minor interstitial feldspars).

Above the troctolite, the troctolite-gabbronorite-anorthosite sequence of the Waterberg project is dominated by medium- to coarse-grained gabbronorite and norite, with minor anorthosite, feldspathic pyroxenite, pyroxenite, and pegmatoidal units. The sequence is characterized by higher Al, Sr, and low Cr concentrations compared to the Ultramafic sequence, the occurrence of inverted pigeonite in parts of the succession, an overlying magnetite-bearing zone, and a Cr/MgO ratio of less than 80 (Fig. 15) a parameter which Seabrook et al. (2005) believe to be characteristic of Main zone rocks. However, there are also notable contrasts. The Main zone in the western limb of the Complex is ~2,200 m thick (Mitchell, 1990), up to 3,940 m thick in the Roossenekal area of the eastern limb (von Gruenewaldt, 1973), and ~1,370 m thick in the Bellevue core south of the Hout River shear zone (Ashwal et al., 2005). In contrast the maximum thickness of the troctolite-gabbronorite-anorthosite sequence in the Waterberg area is 850 m (core sample WB099).

The subzones of the Main zone of the eastern and western limbs of the Complex are determined by the occurrence or absence of primary orthopyroxene, clinopyroxene/augite, and inverted pigeonite in the western limb. Nex et al. (1998) identified five subzones (Fig. 19). The occurrence of inverted pigeonite in the basal troctolite-gabbronorite-anorthosite sequence of the Waterberg project suggests a potential correlation with the Hexrivier unit of subzone C (Fig. 19) as both are characterized by up to 10% olivine, although subzone C is not fully developed in the Waterberg stratigraphy. Upward, the homogeneous equigranular gabbronorite with primary orthopyroxene, which lacks inverted pigeonite, could be correlated with subzone D of Nex et al. (1998). The upper troctolite-gabbronorite-anorthosite sequence of the Waterberg project, which is characterized by the reappearance of inverted pigeonite oikocrysts, with plagioclase and augite, could be correlated with subzone E (Nex et al., 1998; McCreesh, 2013), although this subzone is not always present in the Waterberg project.

Within the Main zone of the eastern and western limbs of the Bushveld Complex, a distinctive pyroxenite marker is noted (von Gruenewaldt, 1973; Klemm et al., 1985; Cawthorn et al., 1991: Nex et al., 2002; Ashwal et al., 2005), as shown in Figure 20. This marker horizon is where Kruger (1994) regarded the influx of the Upper zone magma to have occurred, although SACS (1980) regard the boundary as marked by the appearance of cumulus magnetite, shown in Figure 20 as the horizon of "magnetite-in." For the Main

Subzones	Units	Cumulus mineralogy	Textures	Waterberg features
E		plagioclase, augite and inverted pigeonite no primary opx.	similar to subzone C with occasional interstitial magnetite. Reticulated framework of inverted pigeonite on weathered surfaces	plagioclase, augite and inverted pigeonite
D		plagioclase, augite, primary opx no inverted pigeonite	slightly oikocrystic primary opx otherwise generally equigranular. In outcrop, large euhedral primary opx and prominent needles of augite at the base	homogeneous equigranular gabbronorite with primary opx
			microgabbronorite	
	Hexrivier			
C		plagioclase, augite, inverted pigeonite no primary augite	cumulus plagioclase with oikocrystic inverted pigeonite and minor interstitial and subgranular augite. Frequent myrmekite. Reticulated framework of pigeonite on weathered surface	inverted pigeonite at the base, with <10% olivine
	Springbok			
		3 pyroxenes	rhythmically layered	
	Zebra			
B		plagioclase, augite, primary opx	cumulus plagioclase with discrete primary opx, usually large crystals. In outcrop, distinctive large euhedral grains of primary opx	
A		plagioclase and primary opx		

Fig. 19. Classification of the Main zone rocks in the Western Bushveld (Nex et al., 1998). Waterberg features indicate comparative mineralogy and tentative correlation on the Waterberg project Main zone rocks; opx = orthopyroxene.

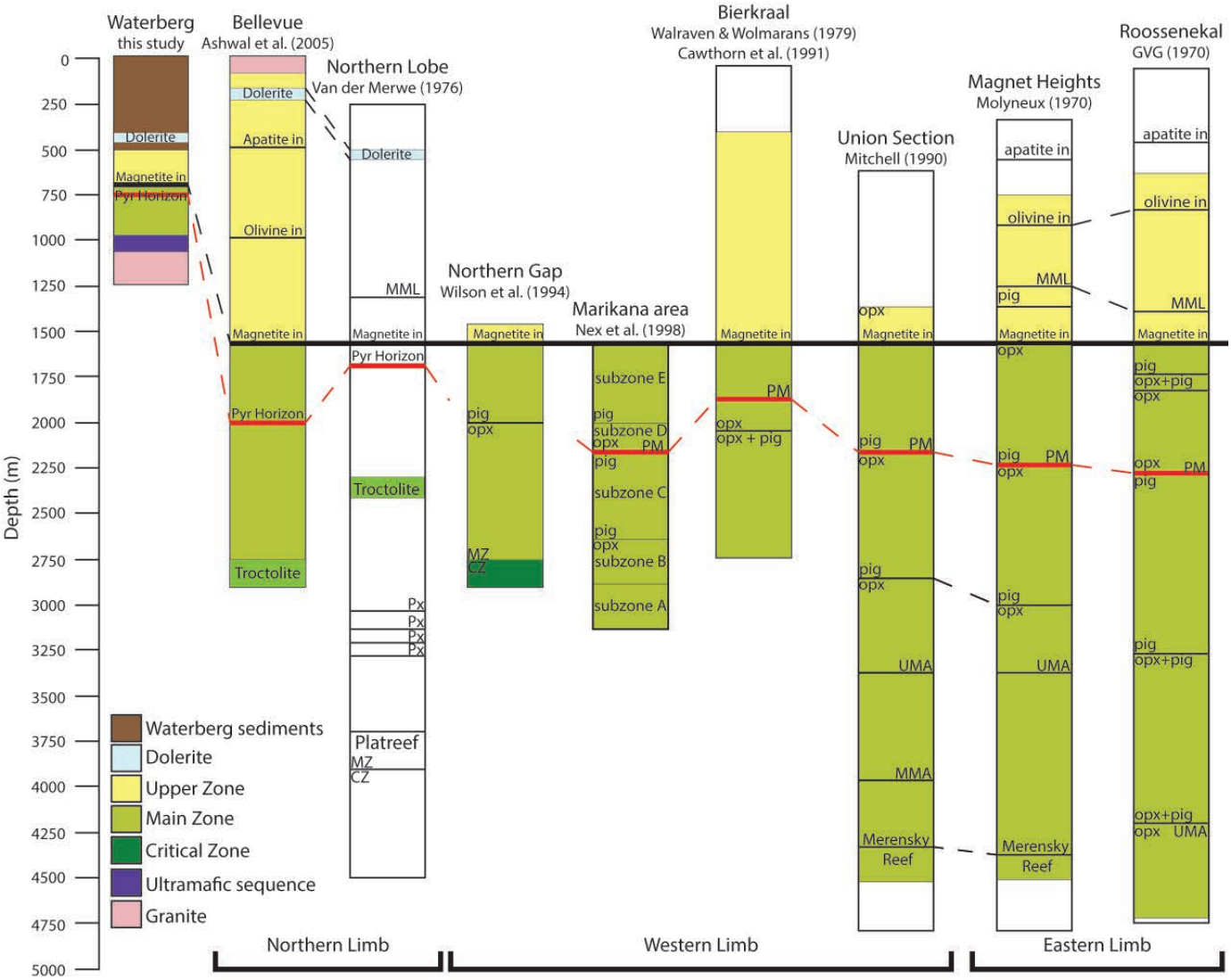

Fig. 20. Profiles through the Main zone-Upper zone boundary in various parts of the Bushveld Complex, showing the position of a pyroxenitic layer that may be ortho- or clinopyroxene dominated, relative to where cumulus magnetite is recognized. Modified from Ashwal et al. (2005). GVG 1970 = von Gruenewaldt (1970).

zone of the Bellevue core there are two distinct pyroxene-rich horizons, the lower one is at a depth of 2,806.80 m (2.3 m thick) and an upper one at 1,971.80-m depth that is 1.88 m thick (Ashwal et al., 2005). The upper clinopyroxene-rich horizon in the Bellevue drill core occurs at the same stratigraphic position as the T1 zone in the Waterberg exploration area and both are dominated by clinopyroxene (McCreesh, 2013). This latter pyroxenite horizon is also at the appropriate stratigraphic position of the Pyroxenite Marker described by Cawthorn et al. (1991) in the eastern and western limbs of the Bushveld Complex (Fig. 20), although Ashwal et al. (2005) did not equate the pyroxenite layer 380 m below the Marginal-Upper zone boundary with the Pyroxenite Marker because the Pyroxenite Marker elsewhere in the Bushveld Complex is dominated by orthopyroxene (von Gruenewaldt, 1973; Cawthorn et al., 1991: Nex et al., 2002; Ashwal et al., 2005). Nevertheless, these distinctive clino- or orthopyroxenite horizons all seem to mark the position of an influx of new Upper zone magma around the Bushveld Complex at approximately the same stratigraphic level (Fig. 20).

Upper zone: Although fine-grained cumulus magnetite occurs in the Upper zone of the Waterberg project, as observed in core samples and identified based on magnetic susceptibility, typical magnetitite layers are lacking except in one borehole in the far south of the project property where a 2.5-m-thick magnetite layer occurs in core sample WB001, a borehole core from south of the Hout River shear zone. The widespread occurrence of disseminated magnetite has led to the recognition of this unit as the equivalent of the Upper zone.

In the Waterberg area the Upper zone, which is dominated by magnetite gabbro and gabbronorite (Fig. 9) with occasional ferrogabbro at the top, varies between 0 and 500 m in thickness (WE027), whereas south of the Hout River shear zone, the Upper zone in the Bellevue drill core is <1,188 m thick and is composed mainly of magnetite gabbro (41.1%),

olivine ferrodiorite (21.4%), and minor gabbronorite, magnetite-bearing plagioclase cumulate rocks, and pyroxenites with 32 magnetitite layers or magnetite-rich rocks (Ashwal et al., 2005). The Upper zone in the eastern and western limbs is approximately 2,000 m thick and contains 26 magnetitite layers (Molyneux; 1970, 1974; Cawthorn et al., 2006; Tegner et al., 2006). The lack of magnetitite layers in the Waterberg project, in spite of the occurrence of abundant magnetite, may possibly relate to dynamic magma movement so that magnetite layers couldn't form, or because the smaller volume of the Upper zone magma was not capable of coalescing magnetite to form distinctive layers.

In the Upper zone of the Bushveld Complex, the most evolved rocks are quartz monzonite with up to 65 wt % SiO_2 (Cawthorn, 2013) but these are not found in the Waterberg area. The relatively unevolved chemical composition and coarse-grained texture of Upper zone gabbro in the Waterberg project suggest that significant erosion of the Upper zone may have occurred with at least 1 km of roof rocks and Upper zone removed before sedimentation in this part of the Waterberg basin began. Geochemical analyses of typical magnetite-bearing gabbronorite and ferrogabbro are shown in Table 1.

Geochemical comparisons with other Bushveld mafic-ultramafic rocks: The mantle-normalized trace element patterns of Waterberg rocks (Fig. 21) are remarkably similar to the profiles of other mafic-ultramafic rocks in the Bushveld. The patterns are identical in shape to the profile of the Archean midcrustal rocks of the Kaapvaal craton (Lana et al., 2004) that emphasizes an overwhelming crustal contamination of Bushveld melts. The abundances of incompatible elements in ultramafic rocks are determined by their concentrations in the cumulus minerals (which are commonly not high) but mostly by the proportion of intercumulus liquid and products of its crystallization. On this basis, feldspathic harzburgite and pyroxenite are characterized by the highest and most variable proportion of intercumulus assemblages as expressed in the wide ranges of element variations in the profile (Fig. 21). Troctolite and olivine gabbronorite are predominantly adcumulates with a low concentration or absence of mesostasis that results in a relative depletion in incompatible elements.

Boundary between the Main and Upper zones: The recognition of exactly where the boundary lies between the Main and Upper zones in the eastern and western limbs of the Bushveld Complex is debatable. Based on the initial Sr isotope ratios, the boundary is at the orthopyroxene-bearing Pyroxenite Marker (Kruger; 1990, 1994). Mineralogically, the boundary defined by Molyneux, (1974) and SACS, (1980) at the first sustained occurrence of cumulus magnetite is well above the isotopic boundary. In the western Bushveld in the Marikana area, the position of the new magma influx is ~100 m below a Pyroxenite Marker based on whole-rock major element and mineral data (Nex et al., 2002). However, using trace element data the new magma influx is 135 to 150 m below the pyroxenite horizon, depending on which trace element is used (Nex et al., 2002). For the eastern limb south of Roosenekal, Klemm et al (1985) also suggests the influx of a new magma prior to the formation of the Pyroxenite Marker.

Ashwal et al. (2005) defined the boundary between the Main and Upper zones in drill core from the Bellevue borehole in the northern limb on the basis of a change in magnetic susceptibility. Through the Main zone cumulates, magnetic susceptibility values are between 0.02 and 0.05 SI units, while the Upper zone generally has higher values up to 5.00 SI units, although anorthositic horizons have very low magnetic susceptibility (Ashwal et al., 2005). In the Waterberg project, there is a significant change in magnetic susceptibility at the T zone, with disseminated magnetite responsible for the significant increase in susceptibility values, even though magnetite only becomes apparent as a cumulus phase in visual inspection of core ~100 m higher in the stratigraphy. Geochemical profiles suggest that mineralization in the T zone of the

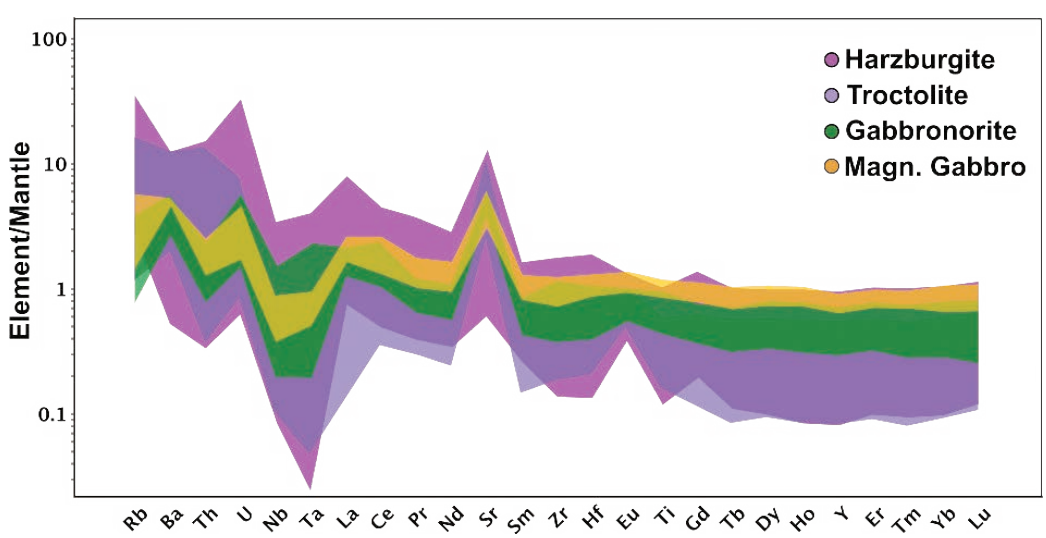

Fig. 21. Multielement chondrite-normalized plot for mafic-ultramafic rocks, showing the overall similarity of the different rock sequences in the Waterberg project area. There is a similarity to all Bushveld lithologies from the eastern and western limbs with a negative Nb-Ta and a positive Sr anomaly. Lower zone pyroxenites beneath the Platreef on Turfspruit also show a negative Nb-Ta anomaly, a variable negative Ti anomaly, and gently sloped Y and HREE. Data shown are from unpublished data of one of the authors (54 samples, Huthmann et al., unpub. data). Chondrite values from Sun and McDonough (1989).

Waterberg project occurs at a level where there was a new influx of magma mixing with the evolving resident magma (Figs. 15, 22). The boundary between the troctolite-gabbronorite-anorthosite sequence and Upper zone in the Waterberg stratigraphy has therefore been drawn on the changes in magnetic susceptibility and this position is in agreement with the noted geochemical changes.

Mineralization: In the Waterberg project, the dominance of Pd over Pt is atypical for mineralization of the eastern and western limbs of the Complex, although the Platreef overall is also Pd dominated with a Pd/Pt ratio of 2/1 in the basal Platreef and Pd slightly higher than Pt for the overall Platreef (Kinnaird, 2005; McDonald and Holwell, 2011). The PGE grade in the T zone in the Waterberg project is unusual as elsewhere in the Bushveld Complex, the Main zone has generally lower grade PGE with Pt and Pd in the 1- to 20-ppb level (Maier et al, 2013), although localized PGE enrichment has been noted both in the northern and western limbs with reported grades lower than in the current prospect (Maier and Barnes, 2010; Kinnaird and Nex, 2015; McDonald et al.,

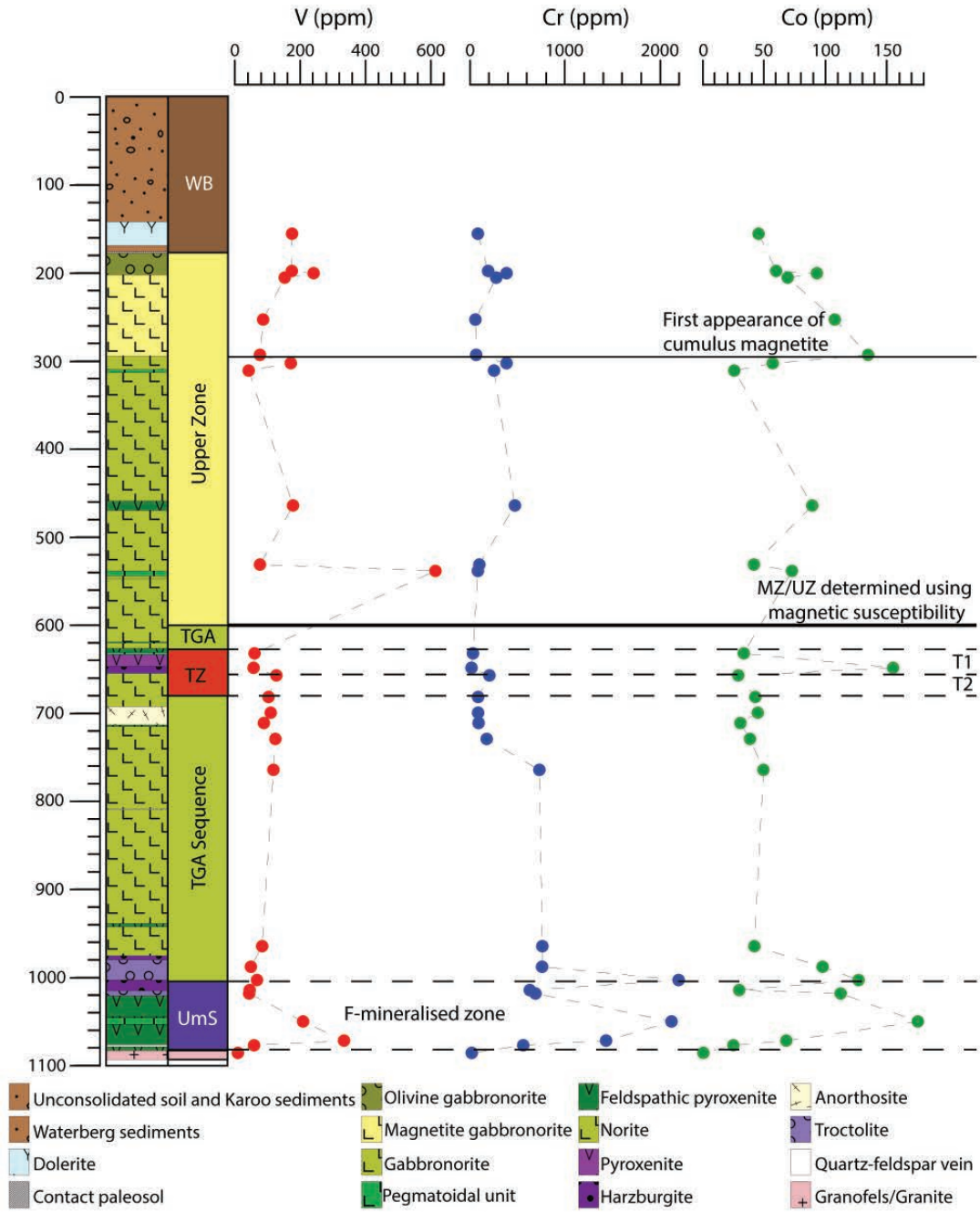

Fig. 22. Variations in the V, Cr, and Co (ppm) of borehole WB017. The solid black line represents the Main-Upper zone boundary determined using the magnetic susceptibility results. The black dashed lines represent the F and T zones. From McCreesh et al. (2015).

2017). There is no mineralization reported in the clinopyroxenite horizon of the Bellevue core, which is in the same stratigraphic position as the T zone of the Waterberg project (Fig. 20). In the western limb of the Complex, stream-sediment samples showed enhanced Pt + Pd + Au concentrated toward the top of the Marginal zone that could be traced for more than 100 km (Wilhelm et al., 1997). Nine Pyroxenite Marker samples from the western limb averaged 23 ppb Pt, 10 ppb Pd, and 1.27 ppb Au according to Maier et al. (2001) so they concluded that while the Pyroxenite Marker may locally contain elevated sulfide and PGE contents, the layer is a poor target for PGE.

Platinum group element mineralization in the northern limb south of the Hout River shear zone is not restricted to the Platreef. PGE mineralization was identified in 1971 in Main zone anorthosite, gabbronorite, and pyroxenite layers in Moorddrift, south of the Planknek-Ysterberg fault, with grades of <6.67-ppm PGE (Maier and Barnes, 2010). Later drilling found PGE enrichment along a strike length of ~1 km. Highest grades were 3.21-ppm PGE over 4.6 m, with seven PGE-enriched zones in a thickness of ~400 m associated with the Pyroxenite Marker, with the most important "reef" (0.5–~4.3 m thick) in and just below the main pyroxenite. This unit contains 1 to 5% modal disseminated pyrite, chalcopyrite a,nd pyrrhotite with accessory millerite and pentlandite (Maier and Barnes, 2010). This could be similar to the Waterberg mineralization in the T1 zone, although the PGE in Moorddrift are Pt rather than Pd dominant. However, according to Cawthorn (2012), the Pyroxenite Marker described by Maier and Barnes (2010) is not equivalent to the Pyroxenite Marker in the eastern and western limbs of the Bushveld Complex based on the chemical variations of Cr/MgO, MgO, and Mg number. The position of the mineralization in Moorddrift relative to the pyroxenite horizon is shown in Figure 23.

North of Overysel (Fig. 2A), the Main zone thins progressively until Upper zone cumulates rest directly on basement gneiss (Fig. 2A); then northward the Main zone reappears at surface directly in contact with Archean granite (van der Merwe, 1976). At the northern end of the exposed part of the northern limb, the Aurora project (Fig. 2A), which comprises seven farms just south of the Waterberg project boundary, has PGE-Cu-Ni mineralization in leucogabbro, anorthosite, and minor troctolite units (Manyeruke, 2007; Maier et al., 2008; McDonald and Harmer, 2010; McDonald et al., 2017). However, according to McDonald et al. (2017) this mineralization occurs above the pyroxenite/melagabbronorite unit (Fig. 23), although the pyroxenite horizon is also dominated by clinopyroxene, similar to both the Bellevue drill core and the Waterberg site. Mineralization in the Aurora project is associated with more felsic rocks than the Platreef and highest PGE grades occur where Cr is lowest (McDonald et al., 2017) so it cannot be linked to the Platreef, and links to the Pyroxenite Marker are also debatable.

Mineralization in Aurora was initially identified from geochemical soil anomalies between 1974 and 1992 by the Union Corporation and 43 boreholes were drilled by Genmin on the farm Nonnenwerth to verify the occurrence (Venmyn-Rand, 2010). Pan Palladium subsequently defined an inferred resource based on a further 92 boreholes across 18 km of strike during the period 2002 to 2010 (Table 3). The mineralization in Aurora has been suggested to be correlative of the T zone mineralization on the Waterberg project to the north as it is also gold rich and palladium dominated (e.g., McDonald et al., 2017), although the overall PGE grade is much lower (Table 4).

The average grades for the F and T zones of the Waterberg project compare with the grade of 4.09 g/t for the Merensky reef in the eastern limb, 6.07 g/t in the western limb (Barker, 2012), and the UG2 grades of 4.39 g/t in the eastern limb, and

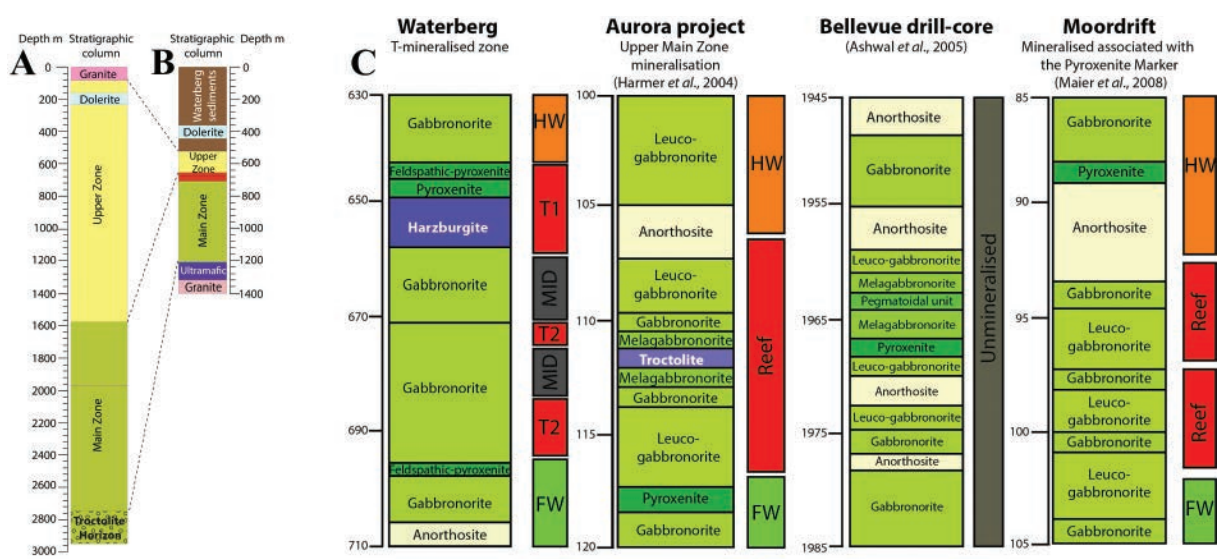

Fig. 23. A schematic diagram comparing the stratigraphy in Waterberg cores with that for other areas of the northern limb, showing the distinctive lithologic differences between the different areas in the upper Main zone. (A). Bellevue core (Ashwal et al., 2005). (B). Waterberg stratigraphy showing how the thickness of the succession varies between the Waterberg and the Bellevue cores. (C). Sections through the Main zone in other areas, showing the position of mineralization. From McCreesh (2016).

Table 3. Potential Correlation of Upper Zone Rocks in the Waterberg Project with Those in the Eastern and Western Limbs of the Complex (subzones of the eastern and western limbs from Eales and Cawthorn, 1996)

Subzones	Lithology	Waterberg features
Apatite Upper zone C	Olivine-apatite diorite	NA
Olivine Upper zone B	Ferrogabbronorite, olivine-magnetite, gabbronorite	Ferrogabbro, olivine-magnetite-gabbro
Magnetite Upper zone A	Magnetite-bearing gabbronorite, magnetite layers	Magnetite-bearing gabbronorite, magnetite layers (very south)

Table 4. JORC-Compliant Data for the Aurora Project in the Main Zone South of the Hout River Shear Zone is Added for Comparison (Venmyn-Rand, 2010)[1]

	Average indicated grade PGE in g/t	Cu grade in % and tonnage in millions of tons	Ni grade in % and tonnage in millions of tons	Proportion of precious metals in %	Resources in millions of tons
Aurora	1.34	0.08 110,930	0.05 68,2000	Pt 30.7, Pd 49.2, Au 16.5, Rh + Ru + Ir 0.6, Ag 2.9	125
Waterberg T	3.88	0.16	0.08	Pt 29, Pd 49, Au 21, Rh 1	31.540
Waterberg F	3.49	0.07	0.16	Pt 30, Pd 64, Au 5, Rh 1	186.725

[1] Data for the Waterberg project from PTM (October 2016)

5.1 g/t in the western limb (Barker, 2012). However, as Figure 24 shows both the T and F zone mineralization on the Waterberg project are very Pd dominated and compare more closely with the lower part of the Platreef than with the Merensky reef or UG2. The thick Super F zone in the Waterberg mineralization may have resulted from variations in basement topography with the formation of higher grade and thicknesses where embayments or large-scale changes in magma-flow direction facilitated the accumulation of magmatic sulfides.

Model for the formation of the Waterberg intrusion

Based on the much reduced total thickness of 1 km (Fig. 25) and the lateral variations in the occurrence of the ultramafic-mafic Waterberg succession, together with the mineralogical and geochemical contrasts (published elsewhere) with other limbs of the Bushveld Complex, we argue that the Waterberg intrusion represents a separate structurally controlled basin fed from a different subchamber rather than

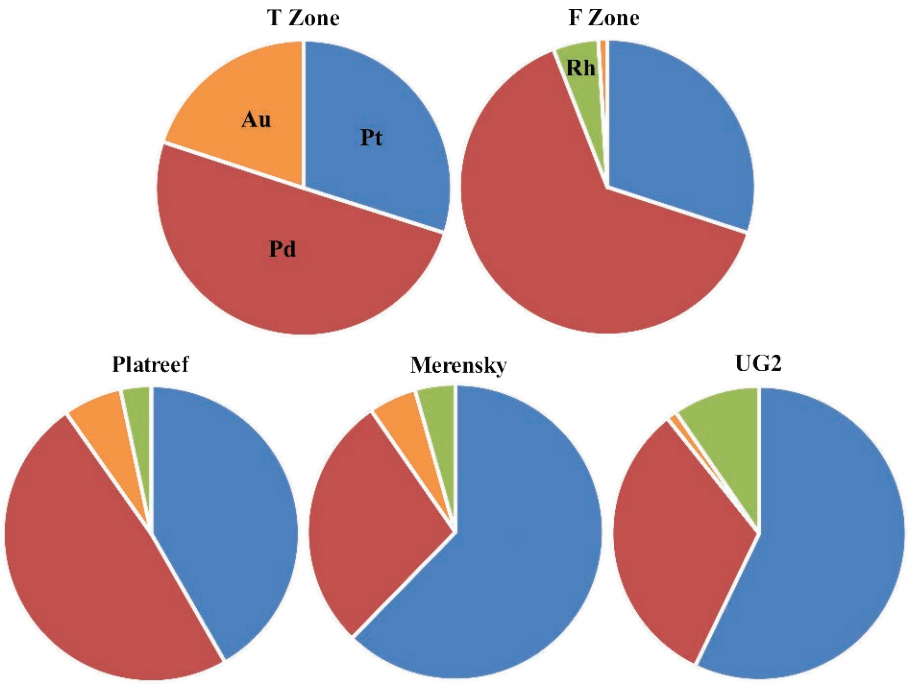

Fig. 24. A comparison of the noble metal abundance of the Waterberg T and F mineralized zones compared to the Platreef, Merensky reef, and UG2, showing the predominance of palladium in the Waterberg deposit. Data for the Merensky reef and UG2 from Barker (2012), for the Platreef based on data for Sandsloot from the Anglo Platinum annual report (2011), and for Waterberg from PTM 43-101.

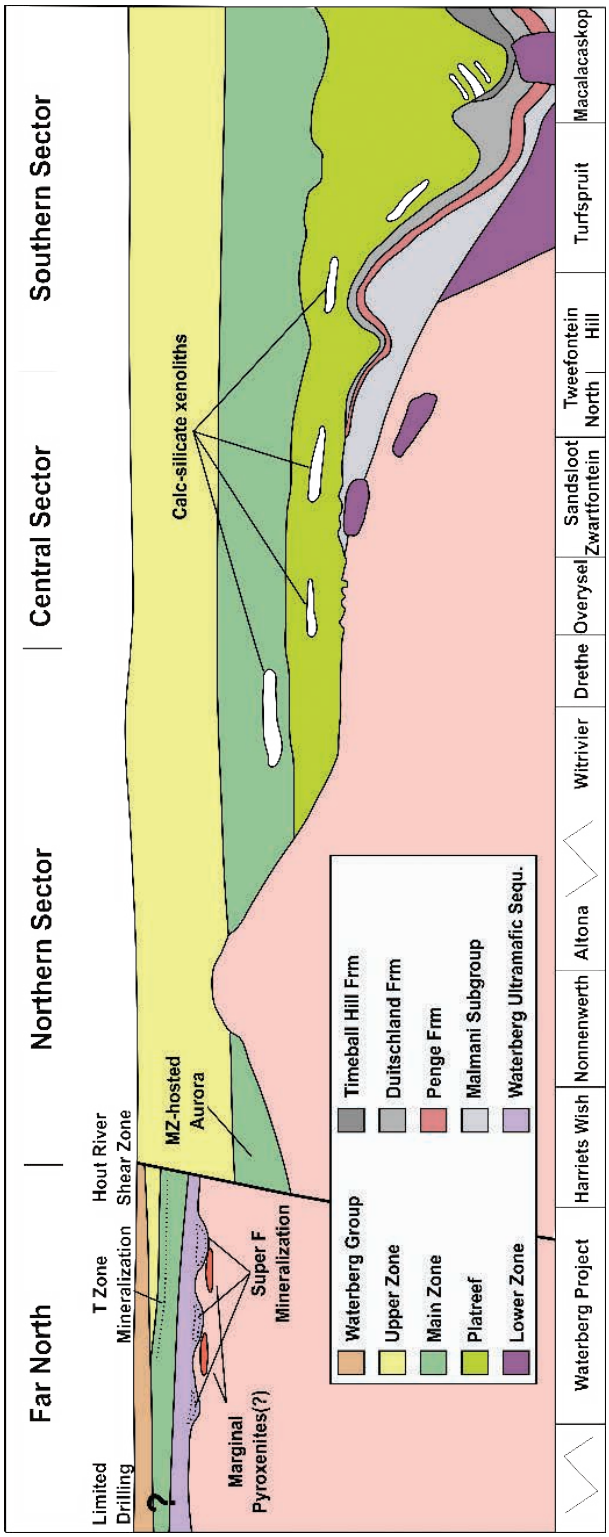

Fig. 25. Schematic diagram showing the contrast in thickness between the Waterberg intrusive package in the far north of the northern limb of the Bushveld Complex and the intrusive sequence south of the Hout River shear zone. Modified from Kinnaird (2005).

a marginal extension of the northern limb of the Bushveld Complex (Fig. 25).

The first stage of magmatism was the emplacement of thin gabbroic and pyroxenitic sills of Marginal zone affinity that reacted with gneissic floor rocks to create the agmatites. The initial phase of the formation of the main body, we suggest, was probably by tube-like ultramafic chonolithic intrusions whose distribution was controlled by basement floor topography. Lateral dilation, followed by the emplacement of sulfide-bearing ultramafic lithologies, resulted in the formation of mineralized orthopyroxenite and harzburgite of the Ultramafic sequence. This in turn was followed by a further intrusion that formed a sheet-like body of troctolites, later fractionating into gabbroic rocks. An influx of Upper zone magma mixed with the residual troctolite-gabbronorite-anorthosite sequence magma and formed the lithologically varied T zone. It is possible that the Pd, Au, and Cu enrichment may have been related to the timing of late-stage sulfide saturation in the magma as opposed to fractionation of the magma, which is consistent with magmatic S isotope values (McCreesh et al., 2015). The Au in this T zone was derived from a Main zone-type magma, which also produced Au-enriched PGE mineralization in Main zone rocks in the Aurora project farther south (McDonald et al., 2017). The lack of T zone in more than 100 holes may be due to nondeposition of this part of the succession or the T zone may have been assimilated by the later magma influx. Whatever the mechanism, there is considerable lateral variability of the lithologies partly due to structural control, basement floor topography, and partly to magmatic erosion. The position of both silicate rocks and mineralization may be controlled by its unique structural position north of the Hout River shear zone.

Based on U-Pb age dating, the Waterberg sediments appear to have been deposited penecontemporaneously with the intrusion of the Bushveld Complex (U-Pb dating of zircon, Dorland et al., 2006; and a 2056 ± 6 Ma age of detrital zircons at the base of the Waterberg sediments, Huthmann et al., 2016). However, the identification of gibbsite in a siltstone layer at the top of the Bushveld stratigraphy in the Waterberg project indicates that a paleosol formed on weathered Bushveld rocks in a tropical climate before the deposition of the Waterberg sediments (Yudovskaya and Kinnaird, 2013; Yudovskaya et al., 2015). Thus the Setlaole and Makgabeng Formations were deposited between ~2.05 and ~1.93 Ga after the intrusion of the Bushveld rocks and before the intrusion of a dolerite sill at ~1.88 Ma (Hanson et al., 2004; Dorland et al., 2006).

Conclusions

1. The ultramafic-mafic succession of the Waterberg project, north of the exposed part of the northern limb of the Bushveld layered intrusion, may represent a separate compartment north of the Hout River shear zone. The northeast-oriented lobate arc extends 24 km from the previously known outcrop of Bushveld rocks. Dating has revealed an emplacement age of 2053 ± 5 Ma. A general dip of 34° to 38° westward is observed for the layered units.
2. The Bushveld succession comprises a basal ultramafic sequence, a troctolite-gabbronorite-anorthosite sequence, and an Upper zone with overlying Waterberg red beds that were deposited between ~2.05 and ~1.93 Ma.

3. The basal Ultramafic zone is at a minimum depth of 180 m from the surface and is typically 100 m thick. It consists dominantly of feldspathic harzburgite and feldspathic pyroxenite. It has been divided into an upper harzburgite (HF) olivine-rich unit, and an underlying feldspathic orthopyroxenite (FP) unit layer <60 m thick that consists mainly of orthopyroxenite.
4. The troctolite-gabbronorite-anorthosite sequence is at a minimum depth of 130 m from the surface and is up to 850 m thick. It consists mainly of gabbronorites. The upper boundary with the Upper zone is defined by increased changes in magnetic susceptibility due to the formation of primary cumulus magnetite in the Upper zone.
5. The Upper zone of magnetite gabbro and gabbronorite varies between 0 and 500 m in thickness. In parts of the project area where the Upper zone is not developed, sedimentary rocks of the Waterberg Group rest on Main zone lithologies. There are two mineralized intervals, a lower F zone and an upper T zone that vary from 3 to 60 m in thickness. The F zone within the Ultramafic zone hosts disseminated sulfides with accessory chromite. PGM are dominated by sperrylite with lesser Pt-Pd bismuthotellurides, Au-Ag alloys, Pd arsenides, and Pt-Rh sulfoarsenide. The rocks have PGE grades of <7 g/t Pt + Pd + Au. PGE comprise 65% Pd, 30% Pt, and 5% Au with 0.07% Ni and 0.17% Cu. The T zone occurs close to the boundary between the gabbronorite-norite-anorthosite unit and the Upper zone. An upper and lower mineralized section may be separated by a barren middling. PGM are dominated by Pt-Pd bismuthotellurides with an overall PGE for the T zone of 49% Pd, 29% Pt, 21% Au with 0.16% Cu, and 0.08% Ni.

Acknowledgments

We would like to acknowledge the support of R. Michael Jones, Rob van Egmond, Gordon Chunnett, Sibusiso Sithole, and Aleck Mkhabela and funding for this project from PTM. We thank Tony Naldrett, Paul Nex, and Iain McDonald for useful discussions. CIMERA is also thanked for promoting interuniversity access to equipment. The study at IGEM RAS was supported by the Russian Science Foundation (grant 14-17-00693). The authors would also like to thank Steve Barnes and David Holwell for comments on the manuscript.

REFERENCES

Armitage, P.E.B., McDonald, I., Edwards, S.J., and Manby, G.M., 2002, Platinum-group element mineralisation in the Platreef and calc-silicate footwall at Sandsloot, Potgietersrus district, South Africa: Transactions of the Institution of Mining and Metallurgy, v. 111, p. 36–45.

Ashwal, L.D., Webb, S.J., and Knoper, M.W., 2005, Magmatic stratigraphy in the Bushveld northern lobe: Continuous geophysical and mineralogical data from the 2950 m Bellevue drill core: South African Journal of Geology, v. 108, p. 199–232.

Barker, O.B., 2012, Barker's platinum map of southern Africa [4th ed.]: Johannesburg, Books on the Wall Publishing CC.

Barker, O.B., Brandl, G., Callaghan, C.C., Eriksson, P.G. and von der Neut, M., 2006, The Soutpansberg and Waterberg Groups and the Blouberg Formation, *in* Johnson, M.R., Anhaeusser, C.R., and Thomas R.J., eds., The geology of South Africa: South Africa, Geological Society and Council of Geosciences, p. 301–318.

Barton, J.M., Klemd, R., and Zeh, A., 2006, The Limpopo belt: A result of Archean to Proterozoic, Turkic-type orogenesis?: Geological Society of America Special Paper, v. 405, p. 315–332.

Boorman, S., Boudreau, A., and Kruger, F.J., 2004, The Lower zone-Critical zone transition of the Bushveld Complex: A quantitative textural study: Journal of Petrology, v. 45, p. 1209–1235

Buick, I.S., Maas, R., and Gibson, R., 2001, Precise U-Pb titanite age constraints on the emplacement of the Bushveld Complex, South Africa: Journal of the Geological Society, London, v. 158, p. 3–6.

Callaghan, C.C., Eriksson, P.G., and Snyman, C.P., 1991, The sedimentology of the Waterberg Group in the Transvaal, South Africa: An overview: Journal of African Earth Sciences, v. 13, p. 121–139.

Cameron, E.N., 1978, The Lower zone of the eastern Bushveld Complex in the Olifants River trough: Journal of Petrology, v. 19, p. 437–462.

Cawthorn, R.G., 2012, Lower Main zone and Pyroxenite Marker in the Northern limb: Fact vs. fiction [abs.]: Platreef Workshop, 5th, Mokopane, South Africa, 9th–11th November, 2012, Abstracts.

——2013, The residual or roof zone of the Bushveld Complex, South Africa, Journal of Petrology, v. 54, p. 1875–1900.

Cawthorn, R.G., and Molyneux, T.G., 1986, Vanadiferous magnetite deposits of the Bushveld Complex, *in* Anhaeusser, C.R., and Maske, S., eds., Mineral deposits of South Africa: Geological Society of South Africa, v. 2, p. 1251–1266.

Cawthorn, R.G., Meyer, S.P., and Kruger, F.J., 1991, Major addition of magma at the Pyroxenite Marker in the western Bushveld Complex, South Africa: Journal of Petrology, v. 32, p. 739–763.

Cawthorn, R.G., Eales, H.V., Walraven, F., Uken, R., and Watkeys, M.K., 2006, The Bushveld Complex, *in* Johnson, M.R., Anhaeusser, C.R., and Thomas R.J., eds., The geology of South Africa: South Africa, Geological Society and Council of Geosciences, p. 261–281.

Clark, D.A., 1997, Magnetic petrophysics and magnetic petrology: Aids to geological interpretation of magnetic surveys: Journal of Australian Geology and Geophysics, v. 17, p. 83–103.

Clark, D.A., and Emerson, D.W., 1991, Notes on rock magnetization characteristics in applied geophysical studies: Exploration Geophysics, v. 22. p. 547–555.

Coertze, F.J., Jansen, H., and Walraven, F., 1977, The transition from the Transvaal sequence to the Waterberg Group: South African Journal of Geology, v. 80, p. 145–156.

Dorland, H.C., Beukes, N.J., Gutzmer, J., Evans, D.A.D., and Armstrong, R.A., 2006, Precise SHRIMP U-Pb zircon age constraints on the lower Waterberg and Soutpansberg Groups, South Africa: South African Journal of Geology, v. 109, p. 139–156.

du Plessis, C.P., 1987, New perspectives on early Waterberg Group sedimentation from the Gatkop area, northwestern Transvaal: South African Journal of Geology, v. 90, p. 395–408.

Eales, H.V., and Cawthorn, R.G., 1996, The Bushveld Complex, *in* Cawthorn, R.G., ed., Layered intrusions: Amsterdam, Elsevier, p. 181–222.

Eriksson, P.G., and Reczko, B.F.F., 1995, The sedimentary and tectonic setting of the Transvaal Supergroup floor rocks to the Bushveld Complex: Journal of African Earth Sciences, v. 21, p. 487–504.

Eriksson, P.G., Simpson, E.L., Eriksson, K.A., Bumby, A.J., Steyn, G.L., and Sarkar, S., 2000, Muddy roll-up structures in siliciclastic interdune beds of the 1.8 Ga Waterberg Group, South Africa: Palaios, v. 15. p. 177–183.

Eriksson, P.G., Altermann, W., Catuneanu, O., van der Merwe, R., and Bumby, A.J., 2001, Major influences on the evolution of the 2.67–2.1 Ga Transvaal basin, Kaapvaal craton: Sedimentary Geology, v. 141–142, p. 205–231.

Finn, C.A., Bedrosia, P.A., Cole, J.C, Khoza, T.D, Webb, S.J., 2015, Mapping the 3D extent of the Northern lobe of the Bushveld layered mafic intrusion from geophysical data: Precambrian Research, v. 268, p. 279–294.

Good, N., and de Wit, M.J., 1997, The Thabazimbi-Murchison lineament of the Kaapvaal craton, South Africa: 2700 Ma of episodic deformation: Journal of the Geological Society, London, v. 154, p. 93–97.

Grobler, N.J., and Whitfield, G.G., 1970, The olivine-apatite magnetitites and related rocks in the Villa Nora occurrence of the Bushveld Igneous Complex: Geological Society of South Africa Special Publication 1, p. 208–227.

Grobler, D.F., Nielsen, S.A., and Broughton, D.W., 2012, Upper Critical zone (Merensky reef-UG2) correlates within the Platreef on Turspruit Farm, northern limb, Bushveld Complex [ext. abs.]: Platreef Workshop, 5th, Mokopane, South Africa, July 16–19, 2012, Extended Abstract Volume.

Hanson, R.E., Gose, W.A., Crowley, J.L., Ramezoni, J., Bowring, S.A., Bullen, D.S., Hall, R.P., Pancake, J.A., and Mukwakwami, J., 2004, Paleoproterozoic intraplate magmatism and basin development on the Kaapvaal craton: Age, paleomagnetism and geochemistry of ~1.93 to ~ 1.87 Ga post Waterberg dolerites: South African Journal of Geology, v. 107, p. 233–254.

Harmer, R.E., Pillay, N., and Davies, P.G., 2004, The Aurora project—Main zone hosted PGE-base metal mineralisation at the northern outcrop limit of the Bushveld Northern limb, north of Mokopane [abs.]: Platreef Workshop, 1st, Mokopane, South Africa, July 16–19, 2004, Abstracts.

Holwell, D.A., Jones, A., Smith, J.W., and Boyce, A.J., 2013. New mineralogical and isotopic constraints on Main zone-hosted PGE mineralization at Moorddrift, northern Bushveld Complex: Mineralium Deposita, v. 48, p. 675–686.

Holzer, L., Frei, R., Barton, J.M., Jr., and Kramers, J.D., 1998, Unravelling the record of successive high grade events in the Central zone of the Limpopo belt using Pb single phase dating of metamorphic minerals: Precambrian Research, v. 87, p. 87–115.

Hulbert, L.J., 1983, A petrological investigation of the Rustenburg Layered Suite and associated mineralization south of Potgietersrus: DSc. thesis, South Africa, University of Pretoria, 511 p.

Hulbert, L.J., and von Gruenewaldt, G., 1985, Textural and compositional features of chromite in the Lower and Critical zones of the Bushveld Complex south of Potgietersrus: Economic Geology, v. 80, p. 872–895.

Hutchinson, D., and Kinnaird, J.A., 2005, Complex multistage genesis for the Ni-Cu-PGE mineralisation in the southern region of the Platreef, Bushveld Complex, South Africa: Transactions of the Institution of Mining and Metallurgy, v. 114, p. 208–224.

Hutchinson, D., Kinnaird, J.A., and Schürmann, L.W., 2004, Complex multistage mineralisation history in the southern sector of the Platreef, Bushveld Complex, South Africa [abs.]: Platreef Workshop, 1st, Mokopane, South Africa, July 16–19, 2004, Abstracts.

Huthmann, F.M., Yudovskaya, M.A., Frei, D., and Kinnaird, J.A., 2016, Geochronological evidence for an extension of the Northern lobe of the Bushveld Complex, LimpopopProvince, South Africa: Precambrian Research, v. 280, p. 61–75.

Jansen, H., 1976, The Waterberg and Soutpansberg Groups in the Blouberg Area, Northern Transvaal: Transactions of the Geological Society of South Africa, v. 79, p. 281–91.

——1982, The Geology of the Waterberg basin in the Transvaal, Republic of South Africa: Memoir of the Geological Survey of South Africa, v. 71, 98 p.

Kinnaird, J.A., 2005, Geochemical evidence for multiphase emplacement in the southern Platreef: Transactions of the Institution of Mining and Metallurgy, v. 114, p. 225–242.

Kinnaird, J.A., and McDonald, I., 2005, An introduction to mineralisation in the northern limb of the Bushveld Complex: Transactions of the Institution of Mining and Metallurgy, v. 114, p. 194–198.

Kinnaird, J.A., and Nex, P., 2015, An overview of the Platreef: Council for Geosciences, Mineral Resources Series 2, p. 193–342.

Kinnaird, J.A., Hutchinson, D., Schurmann, L., Nex, P.A.M., and de Lange, R., 2005, Petrology and mineralisation of the southern Platreef: Northern limb of the Bushveld Complex, South Africa: Mineralium Deposita, v. 40, p. 576–597.

Kinnaird, J.A., Yudovskaya, M., Nichol, S., Naldrett, A.J., and Nex, P.A.M., 2010, Along strike and down-dip variations in multiphase sills of the Platreef, Bushveld Complex [abs.]: Platinum Symposium, 11th, Sudbury, Ontario, June 21–24, 2010, Abstracts.

Klemm, D.D., Ketterer, S., Reichardt, F., Steindl, J., and Weber-Diefenbach, K., 1985, Implication of vertical and lateral compositional variations across the Pyroxene Marker and its associated rocks in the upper part of the Main zone in the eastern Bushveld: Economic Geology, v. 80, p. 1007–1015.

Kramers, J.D., and Mouri, H., 2011, The geochronology of the Limpopo Complex: A controversy solved: Geological Society of America Memoir 207, p. 85–106.

Kruger, F.J., 1990, The stratigraphy of the Bushveld Complex: A reappraisal and relocation of the Main zone boundaries: South Africa Journal of Geology, v. 93, p. 376–381.

——1994, The Sr-isotopic stratigraphy of the western Bushveld Complex: South African Journal of Geology, v. 97, p. 393–398.

Lana, C., Reimold, W.U., Gibson, R.L., Koeberl, C., and Siegesmund, S., 2004, Nature of the Archean midcrust in the core of the Vredefort dome, Central Kaapvaal craton, South Africa: Geochimica et Cosmochimica Acta, v. 68, p. 623–642.

Longridge, L., 2015, Magnetite layers of the Upper zone in the Northern limb—their formation and mineralisation potential [abs.]: Platreef Workshop, 6th, Mokopane, South Africa, May 8–10, 2015, Abstracts.

Maier, W.D., and Barnes, S.-J., 2010, The petrogenesis of platinum-group element reefs in the upper Main zone of the Northern lobe of the Bushveld Complex on the farm Moorddrift, South Africa: Economic Geology, v. 105, p. 841–854.

Maier, W.D., Barnes, S.-J., and de Waal, S.A., 2001, Platinum-group elements in the Pyroxenite Marker, Bushveld Complex: Implications for the formation of the Main zone: South African Journal of Geology, v. 104, p. 301–308.

Maier, W.D., de Klerk, L., Blaine, J., Manyeruke, T., Barnes, S-J., Stevens, M.V.A., and Mavrogenes, J.A., 2008, Petrogenesis of contact-style PGE mineralization in the northern lobe of the Bushveld Complex: Comparison of data from the farms Rooipoort, Townlands, Drenthe and Nonnenwerth: Mineralium Deposita, v. 43, p. 255–280.

Maier, W.D., Barnes, S.-J., and Groves, D.I., 2013, The Bushveld Complex, South Africa: Formation of platinum-palladium, chrome and vanadium-rich layers via hydrodynamic sorting of a mobilized cumulate slurry in a large, relatively slowly cooling, subsiding magma chamber: Mineralium Deposita, v. 48, p. 1–56.

Manyeruke, T.D. 2007, Compositional and lithological variation of the Platreef on the farm Nonnenwerth, northern lobe of the Bushveld Complex: Implications for the origin of the PGE mineralisation: Ph.D. thesis, South Africa, University of Pretoria, Pretoria, 235 p.

Manyeruke, T.D., Maier, W.D., and Barnes, S-J., 2005, Major and trace element geochemistry of the Platreef on the farm Townlands, northern Bushveld Complex: South African Journal of Geology, v. 108, p. 381–396.

McCreesh, M.J.G., 2013, A study of the Main zone-Upper zone boundary beneath a thick succession of Waterberg sediments in the far north of the Northern limb of the Bushveld Complex: B.Sc. thesis, University of the Witwatersrand, 148 p.

——2016, An investigation of the mineralisation in the Waterberg PGE deposit, South Africa: M.Sc. thesis University of the Witwatersrand, 489 p.

McCreesh, M.J.G., Kinnaird, J.A., and Yudovskaya, M., 2015, A comparison of the two unique mineralised packages associated with Main zone rocks in the Waterberg Extension Project of the northern limb, Bushveld Complex [ext. abs.]: Platreef Workshop, 6th, Mokopane, South Africa, May 8–10, 2015, Extended Abstract Volume, p. 36–39.

McDonald, I., and Harmer, R.E., 2010, The nature of PGE mineralisation in the Aurora project area, northern Bushveld Complex, South Africa: International Platinum Symposium, 11th, Ontario Geological Survey of Canada.

McDonald, I., and Howell, D.A., 2011, Geology of the northern Bushveld Complex and the setting and genesis of the Platreef Ni-Cu-PGE deposit: Reviews in Economic Geology, v. 17, p. 297–328.

McDonald, I. and Viljoen K.S. 2006, Platinum-group element geochemistry of mantle eclogites: A reconnaissance study of xenoliths from the Orapa kimberlite, Botswana: Applied Earth Science, v. 115, is. 3, p. 81–93.

McDonald, I., Vaughan, D.J., and Tredoux, M., 1995. Platinum mineralization in quartz veins near Naboomspruit, central Transvaal: South African Journal of Geology, p. 168–175.

McDonald, I., Howell, D.A., and Armitage, P.E.B., 2005, Geochemistry and mineralogy of the Platreef and "Critical zone" of the northern limb of the Bushveld Complex, South Africa: Mineralium Deposita, v. 40, p. 526–549.

McDonald, I., Harmer, R. E. Holwell, D.A., Hughes, H.S.R. and Boyce, A.J., 2017, Cu-Ni-PGE mineralisation at the Aurora project and potential for a new PGE province in the northern Bushveld Main zone: Ore Geology Reviews, v. 80, p. 1135–1159.

Mitchell, A.A., 1990, The stratigraphy, petrography and mineralogy of the Main zone of the northwestern Bushveld Complex: South African Journal of Geology, v. 93, p. 818–831.

Molyneux, T.G., 1970, The geology of the area in the vicinity of Magnet Heights, eastern Transvaal, with special reference to the magnetic iron ore: Geological Society of South Africa Johannesburg Special Publication 1, p. 228–241.

——1974, A geological investigation of the Bushveld Complex in Sekhukhuneland and part of the Steelport Valley: Transactions of the Geological Society of South Africa, v. 77, p. 329–338.

Naldrett, A.J., Kinnaird, J.A., Wilson, A., and Chunnett, G., 2008, Links between the Platreef and the Upper Critical zone of the Bushveld Complex [ext. abs.]: Platreef Workshop, 3rd, Mokopane, South Africa, July 11–13, 2008, Extended Abstract Volume.

Naldrett A.J., Wilson A., Kinnaird. J.A., Yudovskaya, M., and Chunnett G.C., 2012, The origin of chromitites and related PGE mineralization in the Bushveld Complex: New mineralogical and petrological constraints: Mineralium Deposita, v. 45, p. 369–391.

Nex, P.A.M., Kinnaird, J.A., van der Vyver, B.A., Ingle, L.J., and Cawthorn R.G., 1998, A new stratigraphy for the Main zone of the Bushveld Complex, in the Rustenburg area: South African Journal of Geology, v. 101, p. 215–223.

Nex, P.A.M., Cawthorn, R.G., and Kinnaird, J.A., 2002, Geochemical effects of magma addition: Compositional reversals and decoupling of trends in the Main zone of the western Bushveld Complex: Mineralogical Magazine v. 66, p. 833–856.

Oberthür, T., Davis, D.W., Blenkinsop, T.G., and Hohndorf, A., 2002, Precise U-Pb mineral, ages, Rb-Sr and Sm-Nd systematics for the Great Dyke, Zimbabwe—constraints on late Archaean events in the Zimbabwe craton and Limpopo belt: Precambrian Research, v. 113, p. 293–305.

Platinum Group Metals, 2016, Independent technical report on the Waterberg project including mineral resource update and pre-feasibility study: Johannesburg, South Africa, Platinum Group Metals, Consultancy Report, October 16th, 2016.

Rajesh, H.M., Santosh, M., Wan, Y., Liu, D., Liu, S. J., and Belyanin, G.A., 2014, Ultrahigh temperature granulites and magnesian charnockites: Evidence for Neoarchean accretion along the northern margin of the Kaapvaal craton: Precambrian Research, v. 24, p. 150–159.

SACS (South African Committee for Stratigraphy) 1980, Stratigraphy of South Africa. Part 1, *in* Kent, L.E., comp., Lithostratigraphy of the Republic of South Africa, South West Africa/Namibia and the Republic of Bophuthatswana, Transkei and Venda: Geological Survey South Africa Handbook, v. 8, 690 p.

Schaller, M., Steiner, O., Studer, I., Holzer, L., and Herwegh, M., 1999, Exhumation of Limpopo Central zone granulites and dextral continent-scale transcurrent movement at 2.0 Ga along the Palala shear zone, Northern province, South Africa: Precambrian Research, v. 96. p. 263–288.

Scoates, J.S., and Friedman, R.M., 2008, Precise age of the platiniferous Merensky reef, Bushveld Complex, South Africa, by the U-Pb zircon chemical abrasion ID-TIMS technique: Economic Geology, v. 103, p. 465–471.

Seabrook, C.L., Cawthorn, R.G., and Kruger, F.J., 2005, The Merensky reef, Bushveld Complex: Mixing of minerals not mixing of magmas: Economic Geology, v. 100, p. 1191–1206.

Smirnov, A.V., Evans, D.A.D., Ernst, R.E., Söderlund, U., and Li, Z.-X., 2013. Trading partners: Tectonic ancestry of southern Africa and Western Australia, in Archean supercratons Vaalbara and Zimgarn: Precambrian Research, v. 224, p. 11–22.

Sun, S.S., and McDonough, W.F., 1989, Chemical and isotopic systematics of oceanic basalts: Implications for mantle composition and processes: Geological Society, London, Special Publication 42, p. 313–345.

Tegner, C., Cawthorn, R.G., and Kruger, F.J., 2006, Cyclicity in the Main and Upper zone of the Bushveld Complex, South Africa: Crystallization from a zoned magma sheet: Journal of Petrology, v. 47, p. 2257–2279.

Teigler, B., and Eales, H.V., 1996, The Lower and Critical zones of the western limb of the Bushveld Complex as intersected by the Nooitgedacht boreholes: Geological Survey of South Africa Bulletin 111, p. 1–126.

Treloar, P.J., Coward, M.P., and Harris, N.B.W., 1992, Himalayan-Tibetan analogies for the evolution of the Zimbabwe craton and Limpopo belt: Precambrian Research, v. 55, p. 571–587.

van der Merwe, M.J., 1976, The layered sequence of the Potgietersrus limb of the Bushveld Complex: Economic Geology, v. 71, p. 1337–1351.

——1978, The geology of the basic and ultramafic rocks of the Potgietersrus limb of the Bushveld Complex: Ph.D. thesis South Africa, University of the Witwatersrand, 176 p.

van Reenen, D.D., Roering, C., Ashwal, L.D., and De Wit, M.J., 1992, The Archaean Limpopo granulite belt: Tectonics and deep crustal processes: Precambrian Research, v. 55, 587 p.

Venmyn-Rand, 2010, Independent technical experts report on the mineral assets of Sylvania Resources Limited—in the form of a competent persons report by Venmyn-Rand (Pty.) Limited: 151 p.

Vermaak, C.F., and von Gruenewaldt, G., 1986, Introduction to the Bushveld Complex, *in* Anhaeusser, C.R., and Maske, S., eds., Mineral deposits of southern Africa: Geological Society of South Africa, v. 2, p. 1021–1029.

von Gruenewald, G., 1970, On the phase-change orthopyroxene-pigeonite and the resulting textures in the Main and Upper zones of the Bushveld Complex in the eastern Transvaal. Symposium on the Bushveld igneous complex and other layered intrusions: Geological Society of South Africa Special Publication 1, p. 67–73.

——1973, The Main and Upper zones of the Bushveld Complex in the Roossenekal area eastern Transvaal: Geological Society South Africa Transactions, v. 76, p. 207–227.

Wager, L.R., and Brown, G.M., 1968, Layered igneous rocks: Edinburgh, Oliver and Boyd, 588 p.

Walraven, F., 1986, A note on the stratigraphic terminology of the Bushveld Complex, *in* Anhaeusser, C.R., and Maske, S., eds., Mineral deposits of southern Africa: Geological Society of South Africa, v. 2, p. 1039–1040.

——1997, Geochronology of the Rooiberg Group, Transvaal Supergroup, South Africa: Economic Geology Research Institute, University of the Witwatersrand, Information Circular 316, 25 p.

Walraven, F., and Hattingh, E., 1993, Geochronology of the Nebo Granite, Bushveld Complex: South African Journal of Geology, v. 96, p. 31–41.

Wilhem, H.J., Zhang, H., Chen, F.L., Elsenbrock, J.H., Lombard, M., and de Bruin, D., 1997, Geochemical exploration for platinum-group elements in the Bushveld Complex, South Africa: Mineralium Deposita, v. 32, p. 349–361.

Wilson, A.H., 2012, A chill sequence to the Bushveld Complex: Insight into the first stage of emplacement and implications for the parental magmas: Journal of Petrology, v. 53, p. 1123–1168.

Yudovskaya, M.A., and Kinnaird, J.A., 2010, Chromite in the Platreef (Bushveld Complex, South Africa): Occurrence and evolution of its chemical composition: Mineralium Deposita, v. 45, p. 369–391.

——2013, An update on the Waterberg site (PTM). Unpublished, The University of the Witwatersrand, Johannesburg, South Africa.

Yudovskaya, M., Kinnaird J., Naldrett A.J., Mokhov A., McDonald I., and Reinke C., 2011, Facies variation in PGE mineralization in the Central Platreef, Bushveld Complex: Canadian Mineralogist, v. 49, p. 1349–1384.

Yudovskaya, M.A., Kinnaird J.A., Sobolev A.V., Kuzmin D.V., McDonald I., and Wilson A.H., 2013a, Petrogenesis of the Lower zone olivine-rich cumulates beneath the Platreef and their correlation with recognized occurrences in the Bushveld Complex: Economic Geology, v. 108, p. 1923–1952.

Yudovskaya, M., Kinnaird, J.A., Naldrett, A.J., Rodionov, N., Antonov, A., Simakin, S., and Kuzmin, D., 2013b, Trace-element study and age dating of zircon from chromitites of the Bushveld Complex (South Africa): Mineralogy and Petrology, v. 107, p. 915–942.

Yudovskaya, M., Kinnaird, J.A., McCreesh, M.J.G., and Frei, D. 2015, The lithology at the contact between the Bushveld Mafic-Ultramafic sequence and overlying Waterberg sediments on the Waterberg [ext. ab.]: Platreef Workshop, 6th, Mokopane, South Africa, 8th–10th May, 59–61, Extended Abstract Volume.

Yudovskaya, M.A., Kinnaird, J.A., Grobler, D.F., Costin, G., Abramova, V.D., Dunnett, T., and Barnes, S.-J., 2017, Zonation of Merensky-style platinum mineralization in Turfspruit thick reef facies (northern limb of the Bushveld Complex): Economic Geology, v. 112, p. 1333–1365.

Zeh, A., Ovtcharova, M., Wilson, A.H., and Schaltegger, U., 2015, The Bushveld Complex was emplaced and cooled in less than one million years—results of zirconology, and geotectonic implications: Earth and Planetary Science Letters, v. 418, p. 103–114.

Ore Geology Reviews 92 (2018) 161–185

Contents lists available at ScienceDirect

Ore Geology Reviews

journal homepage: www.elsevier.com/locate/oregeorev

Geochemistry and PGE of the lower mineralized Zone of the Waterberg Project, South Africa

Florian M. Huthmann[a,*], Marina A. Yudovskaya[a,b], Judith A. Kinnaird[a], Matthew McCreesh[a], Iain McDonald[c]

[a] School of Geosciences, University of the Witwatersrand, Private Bag 3, Wits 2050, Johannesburg, South Africa
[b] Institute of Geology of Ore Deposits, Mineralogy, Petrography and Geochemistry RAS, Staromonetny 35, Moscow 119017, Russia
[c] School of Earth & Ocean Sciences, Cardiff University, Main Building, Park Place, Cardiff CF10 3YE, UK

ARTICLE INFO

Keywords:
Bushveld Complex
Northern Limb
Mafic succession
PGE mineralization

ABSTRACT

The Waterberg deposit is located north of the Northern Lobe of the Bushveld Complex in South Africa and represents a large, high-grade, new Platinum-Group-Element (PGE) discovery. The first comprehensive study of the lower ultramafic section of the area has been completed, and whole-rock chemical analyses and PGE data are presented.

The section studied comprises mineralized harzburgite and marginal orthopyroxenite, overlain by troctolite grading into gabbroic rocks. Whole-rock analyses show geochemical variations typical of differentiated assemblages of cumulus olivine, plagioclase, and pyroxene. Normalized trace element data display HREE depletion, strong positive Eu and Sr anomalies and LREE enrichment. The negative anomalies for Th, Rb, Nb, and Ta are typical for rocks of the Bushveld Complex. Normalized PGE distributions are fractionated (Pd/Ir 177), Pd-enriched, and Au-poor.

Emplacement of the magmas is believed to have commenced with west-east trending, finger-like intrusions, followed by lateral dilation and emplacement of sulfide droplet-bearing, ultramafic magmas. This was followed by a second phase of intrusions, characterized by sheet-like bodies of troctolite. Fractionation of these magmas led to the development of gabbroic rocks that make up the top of the succession. The Waterberg Project is located in the Southern Marginal Zone of the Limpopo Belt. This position in a structurally active area may have facilitated the creation of space for initial magmas.

It is argued, that the mafic to ultramafic succession of the Waterberg Project does not represent a simple marginal extension of the Northern Lobe, nor does it directly correlate with the Platreef. It shares geological features but represents a separate magmatic basin.

1. Introduction

The Northern Lobe of the Bushveld Complex hosts the Platreef and its world-class ore bodies. The stratigraphy and mineralization of the Northern Lobe has been the topic of many studies in recent years. Most of them were made on the giant Mogalakwena mine that processes the shallow Platreef high-grade mineralization in contaminated sequences (McDonald and Holwell, 2011). A new underground project commenced at Turfspruit is focused on the reef-style mineralization at depth confirming unlimited perspectives westwards (Yudovskaya et al., 2017). In the light of the discovery of Main Zone-hosted mineralization in the far north and south of the lobe (Harmer et al., 2004; Maier and Barnes, 2010), the Main Zone of the Bushveld Complex is now also being explored. The Waterberg Project is located north of the Northern Lobe and represents a large, recent PGE discovery (Huthmann et al., 2016, 2017; Kinnaird et al., 2017).

The significant Waterberg Pd-Pt mineral system is a > 3.5 by 24 km, mafic to ultramafic, lobate intrusion hosting an indicated resource of 24.9 million ounces 4E (Pt + Pd + Rh + Au; 2.5 g/t cut-off) in upper (T Zone) and lower (F Zone) mineralized zones. Its U/Pb ages of 2059 ± 3 and 2053 ± 5 Ma (Huthmann et al., 2016) overlap within error with the 2.06 Ga age (Scoates and Friedman, 2008; Scoates and Wall, 2015; Zeh et al., 2015) of the Bushveld Complex. Kinnaird et al. (2017) provide an extensive overview of the local geology, the relationship of the succession with its roof rocks, and details of the T and F mineralized zones. In this contribution, the stratigraphy of a small

* Corresponding author.
E-mail addresses: f.huthmann@fugro.com (F.M. Huthmann), marina.yudovskaya@wits.ac.za (M.A. Yudovskaya), judith.kinnaird@wits.ac.za (J.A. Kinnaird), matthew.mccreesh@wits.ac.za (M. McCreesh), mcdonaldi1@cardiff.ac.uk (I. McDonald).

https://doi.org/10.1016/j.oregeorev.2017.10.023
Received 1 February 2017; Received in revised form 13 October 2017; Accepted 25 October 2017
Available online 23 November 2017
0169-1368/ © 2017 Elsevier B.V. All rights reserved.

area, hosting the Super F mineralized zone is described in detail. The term Super F Zone is used by Platinum Group Metals to refer to intersected F zone mineralization tens of meters in thickness.

Drill data from > 100 drill holes indicate the presence of discontinuous and variable lithologies in the study area. In this study, a range of drill holes has been logged in detail and whole-rock major and trace element geochemistry as well as PGE are compared to company assays. The data gathered for this study is used to present the first conceptual model for the evolution of the Waterberg Succession. Possible correlations with the sections of the Northern lobe (Harmer et al., 2004) immediately to the south are explored in detail in the discussion section.

2. Geology

The 2.06 Ga (Scoates and Friedman, 2008; Scoates and Wall, 2015; Zeh et al., 2015) Bushveld Complex is the largest layered intrusion on Earth and the world's largest repository of PGE, Cr and V (Lee, 1996). It is believed to consist of 5 lobes with an estimated areal extent of approximately 65,000 km^2 (Willemse, 1969). The intersected ultramafic-mafic rocks at the northern end of the Northern Lobe, and recent geophysical studies, however, increase this total areal extent to > 90,000 km^2 (Finn et al., 2015). Although the lobes were historically interpreted to be separate bodies, more recent interpretation of the gravity data allows for the possibility that the Eastern and Western Lobes connect at depth (Webb et al., 2004; Finn et al., 2015). Links between the Northern Lobe and the Eastern and Western Lobes are contentious (Cawthorn and Webb, 2001), and links between the Northern Lobe and the Waterberg Project remain to be established. The controversy also includes the gently south-dipping Villa Nora Segment (Fig. 1) and its relationship to both the Northern Lobe and the Waterberg Project.

The Bushveld Complex comprises heterogeneous, predominantly felsic volcanics, a mafic to ultramafic suite of 7–8 km thickness, a granite as well as a granophyre suite (von Gruenewaldt et al., 1985). The mafic package, also known as the Rustenburg Layered Suite, is subdivided into the noritic Marginal Zone, the Lower Zone comprising pyroxenite and harzburgite, the cyclical Critical Zone of chromitite norite pyroxenite, the Main Zone comprised of gabbronorite and the Upper Zone of anorthosite, gabbro and magnetitite. Lateral facies variations are common and not all zones are always present (Eales and Cawthorn, 1996; Kruger, 2005; McDonald and Holwell, 2011).

2.1. The Northern Lobe and the Platreef

The geology of the Platreef and Northern Lobe are reviewed in great detail in van der Merwe (1976), Ashwal et al. (2005), Kinnaird et al. (2005), McDonald and Holwell (2011) and Kinnaird and Nex (2015). An overview of the geology relevant for the discussion of the Waterberg Project is provided by Kinnaird et al. (2017). The Northern Lobe is separated from the Bushveld by the Thabazimbi-Murchison-Lineament. The TML is a 500 km long and 25 km wide, ENE-WSW striking, long-lived and repeatedly reactivated craton-scale structure (Good and de Wit, 1997). Based on seismic anisotropy, the TML is interpreted to represent a fundamental crustal and possibly deep lithospheric mantle lineament within the Kaapvaal craton. It is thought to have influenced regional stresses and tectonically induced fluid flux during its reactive history between 2960 and 145 Ma (Good and de Wit, 1997). The stratigraphic correlation between the Northern Lobe to the north and Eastern and Western Lobes to the south of the TML remains contentious (van der Merwe, 1976; Ashwal et al., 2005; Kruger, 2005; McDonald et al., 2005; Kinnaird and Nex, 2015).

The succession of mafic to ultramafic rocks in the Northern Lobe differs from the Eastern and Western Lobes, but arguably all zones can be recognized. The Lower Zone was emplaced in trough-like depressions and is characterized by high-Mg rocks, chromitites and zones of Ni-PGE mineralization (Hulbert and von Gruenewaldt, 1982, 1985; Yudovskaya et al., 2013b, 2017). The Lower Zone is separated from the Platreef by older Transvaal sediments or granite gneisses. The main basal unit is the Platreef, a pyroxenite-dominated, lithologically variable unit irregularly mineralized with PGE and Ni and Cu sulfides. It onlaps northwards onto progressively older Transvaal metasedimentary units of oxide facies iron formations and dolomite and eventually onto Archean granites and gneisses (Kinnaird et al., 2005). The Platreef disappears approximately half-way along the Northern Lobe. Data from Turfspruit confirms a general westward dip of 30° to 60° close to surface, the dip however lessens with depth into a more regularly layered sequence (Grobler et al., 2012; Yudovskaya et al., 2017). The Platreef is considered to be the stratigraphic equivalent of the Critical Zone and unconformably overlain and intruded (Holwell et al., 2005; Holwell and Jordaan, 2006) by the < 2000 m thick Main Zone. Overlying the Main Zone, the Upper Zone of the Northern Lobe is marked by the first occurrence of massive magnetitite (van der Merwe, 1976). The Upper Zone is transgressive and overlies Main Zone for most of the strike length of the Northern Lobe, although in the north it is in direct contact with a basement high (Fig. 2A). This basement high separates what might be a southern magmatic basin comprising the Platreef, and a northern magmatic basin comprising the Aurora mineralization (Kinnaird et al., 2005; McDonald et al., 2017). In the Bellevue drill core (Fig. 2A), the Upper Zone comprises 1200 m of predominantly magnetite-rich olivine gabbro and olivine ferrodiorite (Ashwal et al., 2005).

Correlations between the Eastern and Western Lobes and the Northern Lobe are complicated by the enigmatic Troctolite Marker, which is a ~110 m thick package of noritic troctolite located 1100 m above the base of the Main Zone along 35 km strike length in the central south of the Northern Lobe (van der Merwe, 1976). Very little olivine occurs in the Main Zones of the Eastern and Western Lobes (Eales and Cawthorn, 1996). A Cr-rich pyroxenite zone at the top of the Troctolite Marker has been proposed as a new magma input and a potential PGE-rich zone by (Tanner et al., 2014). The Main Zone of the Northern Lobe has an erosional contact at its base and is interpreted to significantly postdate the emplacement of the Platreef (Holwell et al., 2005; Holwell and Jordaan, 2006). On this basis, it was proposed that rather than being involved in the formation of the Platreef-equivalent Critical Zone deposits in the Eastern and Western Lobes, the Main Zone of the Northern Lobe may therefore have retained a PGE budget (Holwell et al., 2005; McDonald et al., 2017). Whereas most of the economic value of the Northern Lobe is concentrated in the Platreef, sub-economic mineralization has been intersected in rocks interpreted to belong to the Main Zone in the far north at Aurora and south at Moorddrift (Fig. 2A; Harmer et al., 2004; Manyeruke, 2007; Maier et al., 2008; Maier and Barnes, 2010; McDonald and Harmer, 2010; Holwell et al., 2013; McDonald et al., 2017).

The Platreef is one of the world's largest and most valuable mafic to ultramafic successions comprising platinum-group elements and associated significant Ni and Cu reserves (Naldrett, 2010). It differs from the UG2 and Merensky Reef deposits of the main Bushveld Complex. The Platreef carries Ni-Cu-PGE mineralization of three different types: massive sulfide bodies at the base, marginal or contact disseminated ore in hybrid rocks and exoskarns, and reef style mineralization hosted by feldspathic pyroxenite and harzburgite at the top, near the boundary with the Main Zone It has lower average Pt/Pd ratios of approximately 1, and a lower grade of > 4 g/t PGE, where mined (Kinnaird et al., 2005). These characteristics, however, depend on the type of mineralization investigated, and in detail the interpreted Merensky analogue has high Pt/Pd ratios. PGE and base metal sulfides are generally associated, however, in detail they may be decoupled, possibly due to hydrothermal alteration and local remobilization (Kinnaird et al., 2005; Holwell and McDonald, 2006). A recent age date for the Platreef of 2056 ± 5 Ma (Yudovskaya et al., 2013a) overlaps within error with precise 2056.88 ± 0.41 Ma and 2057.04 ± 0.55 Ma ages for the Merensky Reef (Scoates and Wall, 2015) and indicates that both deposits formed broadly contemporaneously. These ages are also in

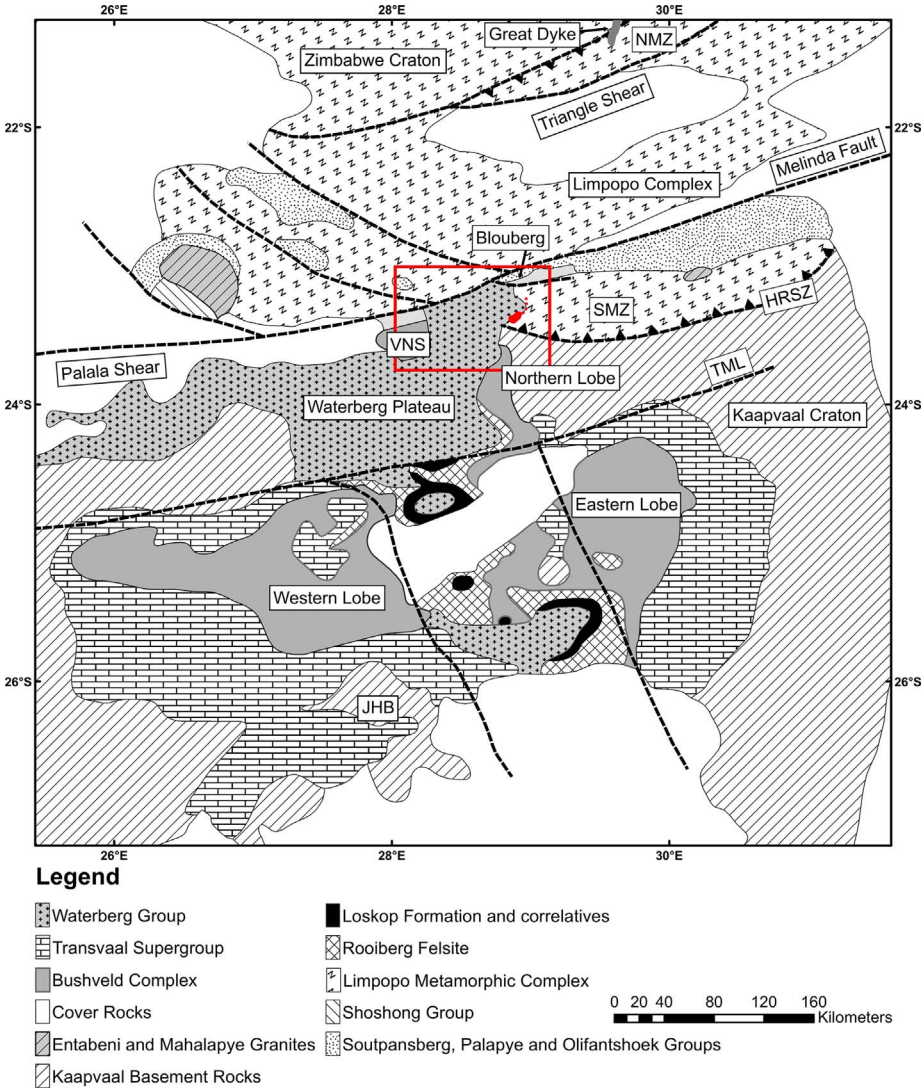

Fig. 1. Map showing the distribution of major lithological units in northern South Africa. JHB Johannesburg; SMZ Southern Marginal Zone; NMZ Northern Marginal Zone; TML Thabazimbi-Murchison lineament; HSRZ Hout River Shear Zone VNS Villa Nora Segment. The small rectangle indicates the Waterberg area. Modified after Dorland et al. (2006).

agreement with high-precision U-Pb dating that indicates crystallization of the Bushveld Complex over 1 Ma (Zeh et al., 2015).

Mineralization south of Mokopane at Moorddrift (Maier and Barnes, 2010), the Aurora Project (Harmer et al., 2004; Manyeruke, 2007; Maier et al., 2008; McDonald and Harmer, 2010; McDonald et al., 2017) and the Waterberg Project (Kinnaird et al., 2014, 2017; Huthmann et al., 2016) is explicitly excluded from the Platreef (Kinnaird et al., 2005; McDonald and Holwell, 2011). The Aurora Project is interpreted to be an upper Main Zone-hosted Cu-Ni-PGE deposit (McDonald et al., 2017) located to the south of the Waterberg Project at the very northern end of the Northern Lobe (Fig. 2A). At Aurora, the Main Zone reappears at surface and is in direct contact with Archean granite. Mineralization occurs in two main mineralized horizons and a thinner discontinuous horizon closer to the basal contact.

The Hout River Shear Zone (Fig. 2A) marks the boundary between the granulite- facies Southern Marginal Zone (SMZ) of the Limpopo Complex and the Archean Kaapvaal Craton. It is generally interpreted to represent a composite structure along which the Southern Marginal Zone was thrust southward during the Neoarchean (Smit et al., 1992; Barton et al., 2006). According to recent work by Nicoli et al. (2015), the SMZ consists of reworked Kaapvaal Craton basement gneisses, mafics, and clastic sedimentary rocks with ages between 3.3 and 2.7 Ga which are overlain by younger sedimentary rocks. There is still little consensus regarding some elements of the geodynamic history of the Limpopo orogeny (e.g. Treloar et al., 1992; Holzer et al., 1998; Barton et al., 2006; Nicoli et al., 2015), however, a N–S directed long-lived tectonothermal activity of > 700 Ma is well established (Kramers and Mouri, 2011). Several studies (Schaller et al., 1999; Barton et al., 2006; Clarke et al., 2009; Smirnov et al., 2013; Rajesh et al., 2014) proposed a Paleoproterozoic (and not Archean) collision of the Zimbabwe and Kaapvaal craton that may account for certain geological features observed in the project area (described below). Regardless of the timing of the Limpopo Belt orogeny, the location of the Waterberg Succession in the SMZ (not the Kaapvaal Craton) may expose it to a level of Paleoproterozoic tectonism that is not generally observed in the undeformed Bushveld Complex.

2.2. Local geology

In the area immediately north of the Hout River Shear Zone (Fig. 2A) Platinum Group Metals (PTM) has intersected a mafic to ultramafic succession subdivided into an Ultramafic Sequence (UmS) overlain by the Troctolite Gabbronorite Anorthosite Sequence (TGA) and an Upper Zone (UZ) of magnetite-bearing gabbroic rocks to ferrogabbros. The rocks rest on a footwall of Archean gneisses that is commonly interfingered with pyroxenite near the contact (Fig. 2B). Except for one drill hole in the very south of the prospect, calc-silicate xenoliths are absent in the Waterberg area. Early pyroxenitic magmas intruding the floor rocks caused melting and subsequent mingling of the pyroxenitic magma and granitic melt, leading to the formation of a

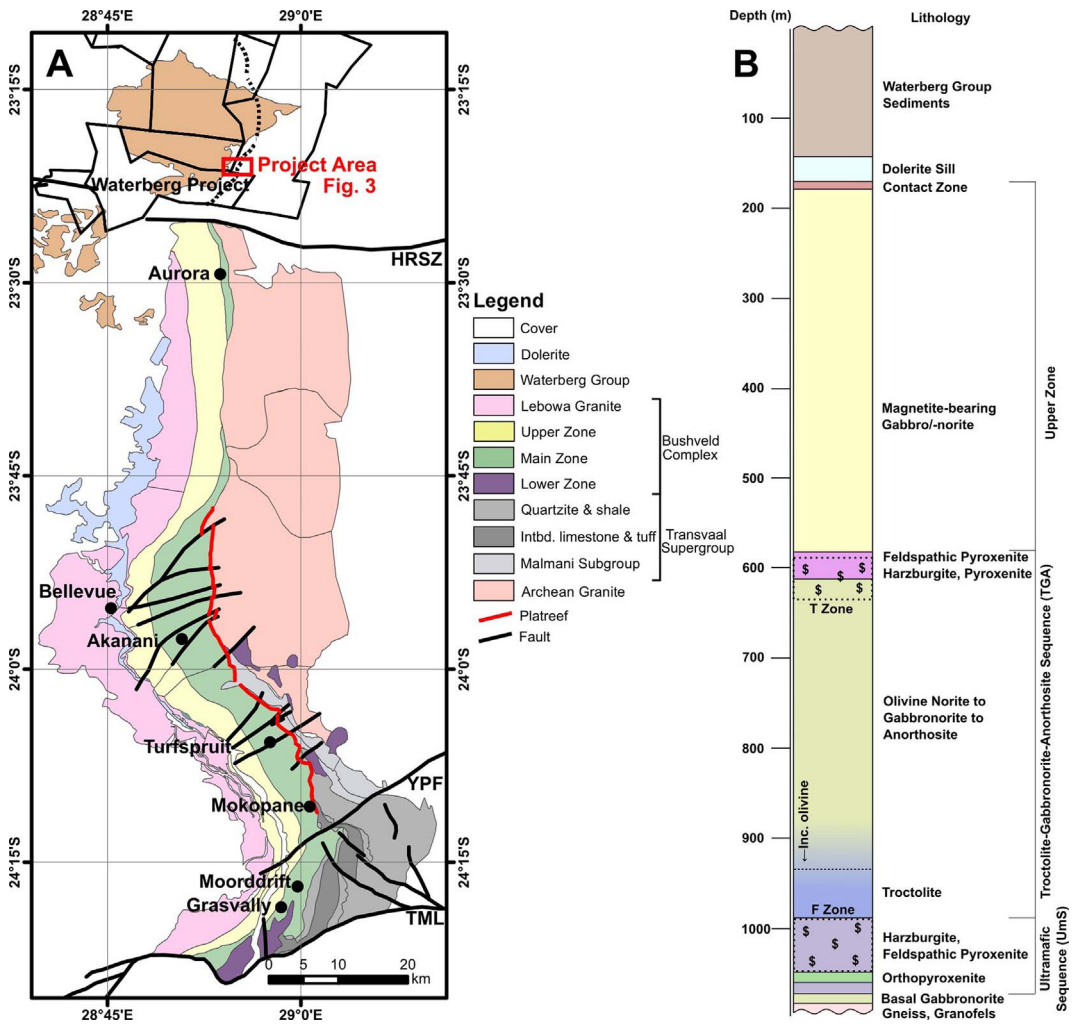

Fig. 2. A: Geological map of the Northern Lobe of the Bushveld Complex showing the town of Mokopane and selected mining and exploration projects. HRSZ Hout River Shear Zone; YPF Ysterberg-Planknek Fault; TML Thabazimbi-Murchison lineament. Red Rectangle highlights the area of interest. B: Simplified stratigraphic column for the Waterberg succession. Both the marginal gabbronorite and the pyroxenite may not be present or occur at varying position and with varying thickness in the Ultramafic Sequence.

granofels. The igneous package of rocks dips ~30° toward the west-northwest, with variations because of structural controls and/or thermo-mechanical erosion. Significant faults are indicated by variations in intersection depth of the sedimentary-igneous rock contact, however, due to vertical drilling these potential steeply-dipping structures are not typically intersected.

Recent geophysical modeling suggests a continuation of the mafic succession to the north and west of the drill intersections and a greatly increasing thickness towards the southwest (Finn et al., 2015). The subdivision of the stratigraphy has changed since the early years of exploration and the ongoing work by company geologists and academics involved with this project has questioned some relationships (e.g. in Huthmann et al., 2016) and prompted a new subdivision to reflect interpreted petrogenetic relationships (Kinnaird et al., 2017).

The base of the succession sometimes comprises very fine- to fine-grained orthopyroxenites and/or gabbronorites. Orthopyroxenites occur as cm- to meter-sized fragments to sill-like bodies that have sharp to gradational contacts with their respective host rocks, and in places are almost completely assimilated by subsequent ultramafic rocks (see below). Gabbronorites generally appear less affected by their host and their relative age is uncertain. The pyroxenites are interpreted to be the crystallization product of initial magmas intruding the area, and based on drill intersects outside of the study area may intrude > 100 m into the footwall granite-gneisses. Due to very limited drilling into the deep basement, their distribution is not certain. Based on the observed degree of assimilation and their distribution, they may also represent autoliths. The gabbronorites, on the other hand, are plagioclase-dominated rocks of varying grain-size (finer-grained towards the footwall) that resemble the gabbroic rocks observed higher up in the succession.

Harzburgite and feldspathic pyroxenite of the UmS are the primary basal unit of the succession. The UmS is discontinuous and where present it may exceed 80 m in thickness, hosts PGE and Au mineralization, and unevenly distributed chromite clusters and seams. Olivine-bearing units in the UmS are very strongly altered with relicts of primary minerals remaining, having been replaced primarily by serpentine and magnetite. The unit is very heterogeneous and comprises small amounts of juxtaposed pyroxenite, serpentinite, troctolite and dunite. Calc-silicates xenoliths are absent.

Overlying the UmS, the TGA Sequence is primarily composed of gabbronoritic rocks with minor anorthosite, grading into norite, olivine norite and troctolite at the base (Fig. 2B). The rocks appear to grade into the UZ at the top of the succession. Due to the fine-grained nature of the magnetite and similarity of rock types, no clear contacts can be observed. The enigmatic troctolite have a gradational, mingled or irregular contact with olivine gabbronorite upwards and a sharp, erosional(?) contact with harzburgite at the base (Fig. 4B). Further south, the top of the TGA Sequence is host to the T Zones, a set of 2–3 discontinuous, mineralized gabbronorite, pyroxenite to troctolite, horizons. In the area of focus for this study, the T Zones are either absent or extremely poorly developed, possibly related to non-deposition,

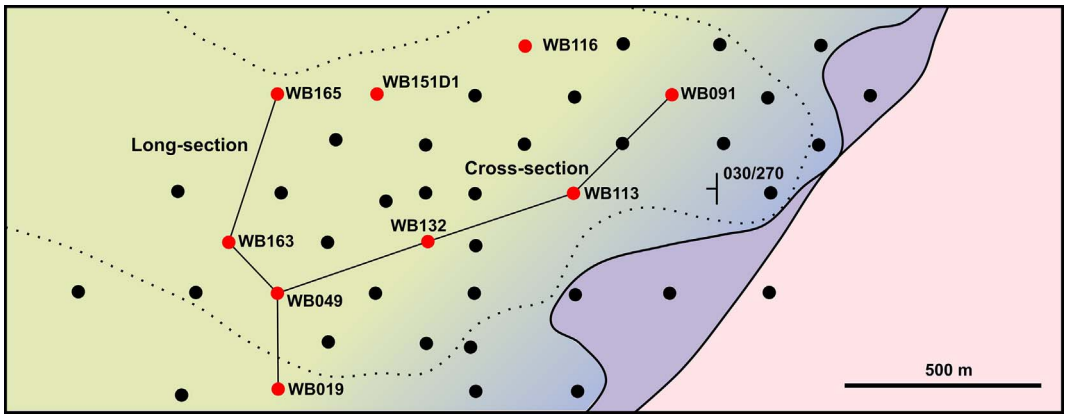

Fig. 3. Subcrop map of the area shown in Fig. 2. Shown are the positions of the drill holes investigated in detail (red) and the cross- and long-section from Figs. 13 and 14. The stippled line marks the approximate outline of a 1 g/t 3E grade shell projected to surface. It has a 30 dip to the west. The sedimentary rocks overlying the succession are approximately 240 m thick in the east, and their thickness increases slightly to the west.

structural controls, or erosion preceding the deposition of Waterberg Group sediments.

The upper part of the succession on the Waterberg Prospect is composed of magnetite-bearing gabbronorite and gabbro that have varying ortho- and clinopyroxene content. It is tentatively correlated with the Upper Zone elsewhere in the Complex, even though it lacks the magnetitite layers that are characteristic for the Upper Zone elsewhere in the Bushveld Complex (e.g. Molyneux, 1974; Ashwal et al., 2005). Instead, magnetite in the Upper Zone at the Waterberg Project occurs as very fine-grained disseminations that in the field are most easily identified by the use of a magnetic susceptibility meter. The UZ thins in places and its exact distribution requires further research.

The top contact of the succession is a remarkably flat erosional unconformity overlain by Paleoproterozoic Waterberg Group sediments (Callaghan et al., 1991; Huthmann et al., 2016), typically starting with a coarse, poorly-sorted and polymict breccia. The top of the succession is complex and sometimes an up to 10 m wide and strongly altered, sheared, and tuffaceous contact zone is located between the sediments and igneous units. Detrital zircons of the basal breccia have recently been dated and encompass age clusters of 2045 to 3354 Ma, generally attributed to the Limpopo Belt (Corcoran et al., 2013; Huthmann et al., 2016).

Recently acquired age dates (2059 ± 3 and 2053 ± 5 Ma; Huthmann et al., 2016) from zircons extracted from mafic rocks of the succession are within error coeval with published ages for the Eastern and Western Lobe of the Bushveld Complex (Walraven and Hattingh, 1993; Walraven, 1997; Buick et al., 2001; Scoates and Friedman, 2008; Scoates and Wall, 2015; Zeh et al., 2015), and the Northern Lobe (Yudovskaya et al., 2013a). This indicates that the intrusions belong to the Bushveld Large Igneous Province and are related.

Mineralization occurs in the T and F zones, located just below the Upper Zone and in the Ultramafic Sequence, respectively (Fig. 2B). The mineralized zones are 3 to > 60 m thick and have so far been intersected along 17 km of strike (Kinnaird et al., 2014). T and F Zone refers to zones of elevated PGE grades which in detail are not strictly stratabound (Fig. 2B). The T Zone, in particular, occurs in two distinct stratigraphic levels with distinct mineralogy (Kinnaird et al., 2017). New mineral assemblages are still being discovered and will be subject of upcoming publications. The mineralized F Zone closely follows the westerly trend of the harzburgite and may form Super F Zones with grades that can exceed 15 g/t 3E (Pt + Pd + Au) in individual assayed intervals (Kinnaird et al., 2017). These zones of high grade are separated by weakly to unmineralized troctolite of the TGA Sequence.

3. Methodology

For this study drill core from nine holes intersecting the center and periphery of one of the Super F (mineralized) Zones (Fig. 3) have been logged. The selected drill holes allow for an assessment of any correlation of rock types, distribution of the mineralization and ultimately the generation of an emplacement model. This particular Super F Zone forms an elongated, SW-plunging mineralization envelope of > 200 by > 1000 m with anomalous PGE and Au of greater 0.5 g/t over > 120 m in core and economic grade of over 2.5 g/t over > 60 m. Platinum Group Metal's assay database for the study area, consisting of approximately 9500 assays of Pt, Pd, Ni, Cr, Cu, Co, and S, was made available. Fire assay was used for Pt, Pd, Rh, and Au, and Cu, Ni, and S were determined by XRF analysis at Set Point Laboratory in Johannesburg.

Fifty-eight samples of approximately 25 cm long, NQ size quarter-core were selected from the logged drill holes. Care was taken to avoid zones of veining, strong alteration and autoliths/xenoliths. Sample preparation was conducted at the University of Witwatersrand following established methods (Wilson, 2012).

All samples were analyzed for major and trace elements and loss on ignition (LOI) at the University of the Witwatersrand analytical facilities. Major and selected trace elements were determined using a Panalytical PW2404 X-ray fluorescence (XRF) spectrometer with fused disks and the SuperQ program. Sulphur was determined for selected samples from pressed pellets employing the same instrument and the ProTrace program. All other trace elements were determined by inductively coupled plasma mass spectrometry (ICP-MS) employing a Perkin Elmer Elan instrument. All analytical procedures followed the methods described by Wilson (2012).

Platinum group elements and Au were determined for selected samples at Cardiff University from 15 g sample weight powders prepared at the University of the Witwatersrand. The analysis was carried out by Ni-sulfide fire assay followed by Te co-precipitation and ICP-MS (McDonald and Viljoen, 2006). Accuracy for all whole- rock geochemistry was constrained by the analysis of certified international reference materials and internal standards while the precision for fire assays was estimated by repeat analysis of several samples.

4. Results

4.1. Field relationships and petrography

Given the very heterogeneous and irregular nature of lithologies observed in drill core, we discuss suites of intrusives and zones of mineralization rather than individual lithologies (cf. McDonald and

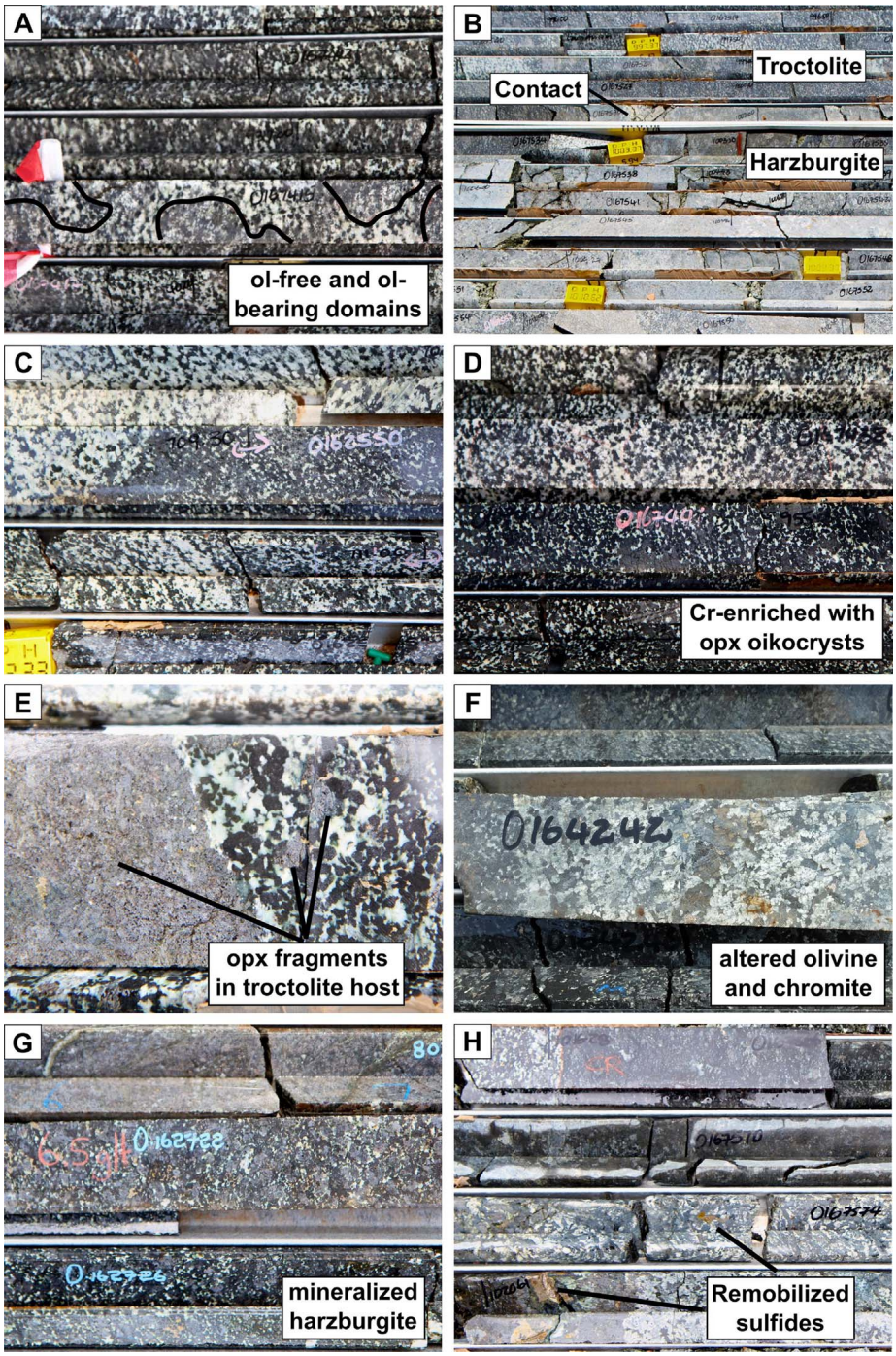

Fig. 4. Textural relationships in examples of rock types from drill core in the Waterberg Project. A: Upper contact of the TGA Sequence troctolite showing discrete zones of gabbroic and troctolitic rocks interpreted to represent mingling of cumulates; B: Typical Ultramafic Sequence. In the top tray the sharp contact between overlying troctolite and harzburgite is visible; C: Variations in the troctolite zone showing leucotroctolite and zones of abundant orthopyroxene oikocrysts; D: Variations in olivine abundance in the troctolite zone. The oikocryst-rich melatroctolite is characterized by significant spikes in Cr content; E: Orthopyroxenite autolith in troctolite. Note the small pyroxenite fragments in the troctolite and the presence of possibly remobilized sulfides in both rocks; F: Chromite in TGA Sequence troctolite adjacent to an alteration halo and remobilized sulfides; G: Mildly altered mineralized zone with 6.5 g/t Pt + Pd + Au; H: Vari-textured zone of Cr-enriched serpentinite and sulfide remobilization.

Holwell, 2011). It has to be emphasized, that although individual rock types are important, the amount of variation in mineralogy, alteration, chemistry, and mineralization makes lithological correlation between 200 m-spaced drill holes difficult. The variation in mineralogy observed in the core may be related to mingling and mixing of crystal-rich liquids. The term mixing is used in situations where two or more magmas produce hybrid rocks with the identities of the parent magmas obscured, whereas mingling represents interactions in which the original magmas or cumulates retain their identity (Fig. 4; Wiebe, 1980).

In accordance with informal tradition amongst Bushveld Complex geologists, rock types are named based on their cumulus mineralogy, hence a rock consisting of cumulus olivine and plagioclase with significant intercumulus orthopyroxene is called a troctolite rather than an olivine norite. The term reef is avoided in favor of mineralized zone, as reef implies a lateral continuity that may not be present in the project area. Additionally, the mineralization may to a limited degree transgress boundaries between rock types.

The following section provides drill core and petrological observations for the four main lithologies of the study area, namely the marginal orthopyroxenite and gabbronorite, as well as the Ultramafic Sequence (UmS), and Troctolite-Gabbronorite- Anorthosite Sequence (TGA).

4.1.1. *Marginal orthopyroxenite*

The lowest sills of orthopyroxenite to gabbronorite and gabbro are defined here as marginal sills because of their position close to the contact with, or within the footwall. These types of sills in contact with, or within the sedimentary floor rocks were assigned to the Marginal

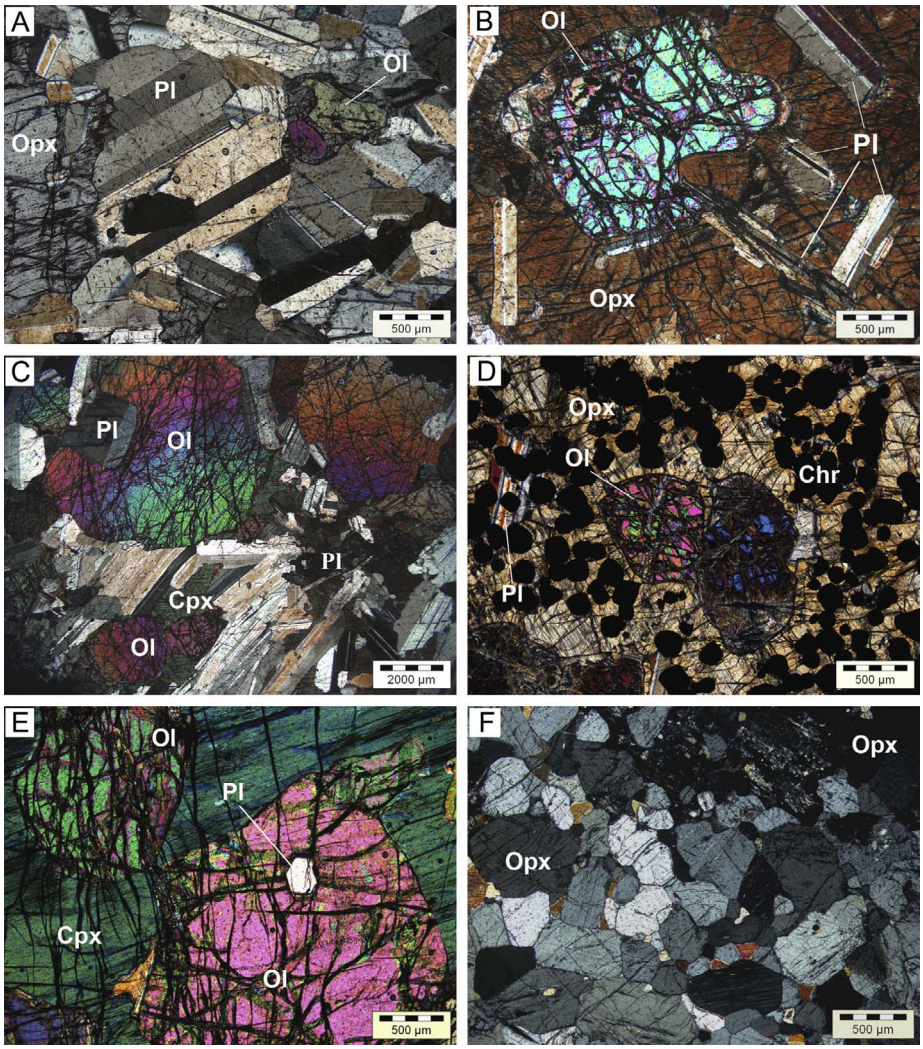

Fig. 5. Rock textures of the Waterberg body under cross-polarized transmitted light. A: Small olivine crystals rimed by peritectic orthopyroxene in olivine-bearing leuconorite in the uppermost part of the TGA Sequence; B: Corroded olivine and euhedral plagioclase laths in orthopyroxene oikocryst in olivine norite; C: Coarse olivine and plagioclase of smaller size in troctolite; D: chadacrysts of olivine and chromite enclosed by orthopyroxene in poikilitic chromitite of the Ultramafic Sequence; E: Coarse grains of olivine with plagioclase inclusions among interstitial clinopyroxene in lherzolite of the Ultramafic Sequence; F: Recrystallized orthopyroxenite with triple junction texture of orthopyroxene grains.

Zone elsewhere in the Bushveld Complex (Vermaak, 1976), although recent studies show their common presence also within the overlying RLS units (Wilson, 2015).

Orthopyroxenite occurs as sill-like bodies and as autoliths throughout the Ultramafic Sequence and more rarely in the troctolite of the TGA Sequence. Outside the area investigated as part of this study, orthopyroxenites may intrude deep into the footwall, however, due to limited drilling into the basement, their detailed distribution is not well established. The autoliths are several centimeters to < 6 m in size. Their contacts are generally well-recognizable, but particularly in harzburgite may be obscured by alteration. The rocks consist of medium to very fine-grained orthopyroxene and may contain up to 15% olivine. Clinopyroxene and plagioclase are minor interstitial phases. Both orthopyroxene and olivine may host disseminated crystals of chromite which range in size from < 50 µm to < 10 µm. The smallest of those crystals may form trails in the host silicate.

The orthopyroxenites are barren, or, where their texture suggests sulfide remobilization into the rock, contain trace 3E (Pt + Pd + Au) levels. Inspection of the drill cores indicates, that intervals of orthopyroxenite often have highly anomalous Cr values (Figs. 13 and 14, see below). Core logging also indicates, that incorporation of these pyroxenites by younger olivine-bearing rocks may lead to zones of increased orthopyroxene oikocrysts or xenocrysts with chromitite clusters.

Near the granite-gneiss footwall contact, varying amounts of interaction between magmas can be observed and the drill core shows features ranging from discrete felsic and pyroxenitic patches to almost complete homogenization. Although the amount of pyroxenite preserved in the core is often limited to patches of cm-size, a generally decreasing crystal size up hole can be observed. The respective thin sections have small crystal size, triple-junction assemblages of orthopyroxene, and occurrences of quartz-feldspar granophyric intergrowths. Fragments of orthopyroxenite with fine- grained granoblastic texture can be found in ultramafic assemblages, indicating their assimilation by later melt in fluxes. Together, these observations indicate that the pyroxenite was the first unit to intrude the study area.

4.1.2. Marginal gabbronorite

The marginal gabbronorite is a very fine- to medium-grained rock, dark in color and when fine-grained resembles pyroxenites in hand specimen.

Thin sections show that the dark color is due to extensive cloudiness and spotty alteration of plagioclase. The basal rocks exhibit highly variable textures both within a single thin section, as well as between different drill cores. Modal mineralogy is dominated by plagioclase with varying amounts of clino- and orthopyroxene. Pyroxene may occur interstitial, as small cumulus crystals, or as large oikocrysts. Plagioclase is often altered by very ne-grained mineral aggregates. Overall, in thin section these rocks resemble gabbroic rocks higher up in the stratigraphy.

4.1.3. The Ultramafic Sequence

The mineralized Ultramafic Sequence (UmS) is a highly complex

array of a variety of rock types that includes strongly to very strongly altered harzburgite, serpentinite, and feldspathic pyroxenite with very fine to pegmatitic crystal size. It varies in thickness between 60 and > 80 m and generally comprises autoliths of orthopyroxenite which may or may not be altered, and which do not contain primary sulfides. Alteration and remobilization appear to have at least some control over the high-grade zones and may have affected low-grades zones as well (Fig. 4H). Chromite may occur as highly irregularly-distributed seams or clusters of chromite grains that cannot be correlated between the widely-spaced holes.

The UmS is the primary basal unit in the project area and can be recognized by its strong alteration and overall heterogeneous texture. Its texture is in sharp contrast to the overlying troctolite's salt and pepper appearance (Fig. 4B). The lower contact of the UmS may be either with the marginal units, with granofels, or, at the outer margins of the mineralized zone with barren, relatively unaltered meso- to melatroctolite (Figs. 13 and 14). The appearance of the unaltered texture of the troctolite invariably indicates barren zones (Fig. 13, WB113D0), however, sulfide remobilization may lead to zones of highly irregular grade (Figs. 4H, 13, WB091D0). Due to this, base metal sulfides can be found highly concentrated and may comprise zones of > 10 g/t 3E for individual samples (Fig. 4H bottom). This relationship is not consistent, however, and both base and precious metals may occur separately. Where drill cores suggest interactions of different magmas, base metal sulfides (and associated PGE) may be absent (Fig. 4H top).

The harzburgites are medium- to coarse-grained rocks consisting of about equal proportions of orthopyroxene and olivine. Plagioclase and clinopyroxene are subordinate interstitial components. Plagioclase may form leucocratic patches of generally finer grain size. Pyroxene and olivine, in particular, are very strongly altered and only the outline of former minerals remains in some cases. The dominant alteration is to serpentine and magnetite, however, chlorite and a range of other alteration minerals occur. Carbonates or carbonate overprint are not observed. Chromite forms rare small grains in amounts of less than 1 vol %, although it can be found as chromite clusters (Fig. 5) or as irregular seams. Sulfide minerals observed as part of the F Zone mineralization include pentlandite, pyrrhotite and chalcopyrite, often associated with significant secondary magnetite due to the strong alteration of the harzburgites. Platinum group minerals in the T Zone are variable (Fig. 6). Sperrylite is dominant and subordinate Pt-Pd bismutho-tellurides, Au-Ag alloys, Pd arsenides and Pt-Rh sulpharsenides can be found.

4.1.4. The Troctolite-Gabbronorite-Anorthosite Sequence

The troctolites in the lower part of the Troctolite-Gabbronorite-Anorthosite (TGA) Sequence form an unmineralized, 50 to 110 m thick package ranging in composition from leucotroctolite and olivine norite to melatroctolite, with rare plagiodunite towards the base. The troctolites have a cross-cutting and erosional relationship with underlying harzburgites of the UmS (Fig. 4B). Towards the lower contact, the troctolite typically gradually increases in olivine content, and its appearance is more homogeneous. Most of the sequence contains between 50 and 80% olivine, giving it a distinct salt and pepper appearance. Sharp breaks in composition may occur, leading to the juxtaposition of rocks of varying olivine content (Fig. 4C). Where developed, the more anorthite-rich phases appear to crosscut and postdate the olivine-rich zones. The sequence is coarse-grained with rare pegmatitic patches, typically with increased anorthite content. Most of the sequence contains up to 10% orthopyroxene in the form of up to several centimeter-sized oikocrysts. This may increase in the lower half of the sequence to > 40%, usually at the expense of plagioclase. The upper 10–50% of the sequence may be very heterogeneous in composition, and discrete domains of troctolitic and gabbronoritic composition can be distinguished (Fig. 4A). This is interpreted to indicate the interaction of the respective differentiating crystal-rich liquids.

As with the harzburgite of the UmS, the troctolite is host to a number of pyroxenitic autoliths, ranging in size from a few centimeters to several meters. The autoliths are typically medium- to coarse-grained, dominated by orthopyroxene and with sharp, cuspate contacts. They may display a pronounced enrichment in Cr independent of their visible mineralogy (Fig. 4E, see below). Where visible chromite crystals are absent, chromite can be found as inclusions in silicate phases. The intrusion and emplacement of hot, olivine-phyric silicate liquids into earlier orthopyroxenites is thought to have led to the thermo-mechanical erosion, transport, and incorporation of orthopyroxenite into younger melt fluxes, thereby leading to anomalous Cr contents.

In thin section, the troctolites are characterized by cumulate textured olivine and plagioclase and strong alteration of both minerals. Depending on the sampling location, the sample may contain significant amounts of oikocrystic orthopyroxene and very limited plagioclase (Fig. 5). All major mineral phases may host < 50 µm crystals of chromite, often rimmed by magnetite.

Gabbronorites make up the largest part of the TGA Sequence. They form a unit of 100 to 300 m thickness, consisting of varying amounts of orthopyroxene, plagioclase, and clinopyroxene. Variations in pyroxene content may bring this unit close to a norite composition, while varying amounts of olivine may occur at the base where the rocks grade into troctolite. This transition usually involves an increase in olivine content, with what appears to be a mingling of gabbroic and troctolitic material, often forming discrete areas in core. The unit is generally

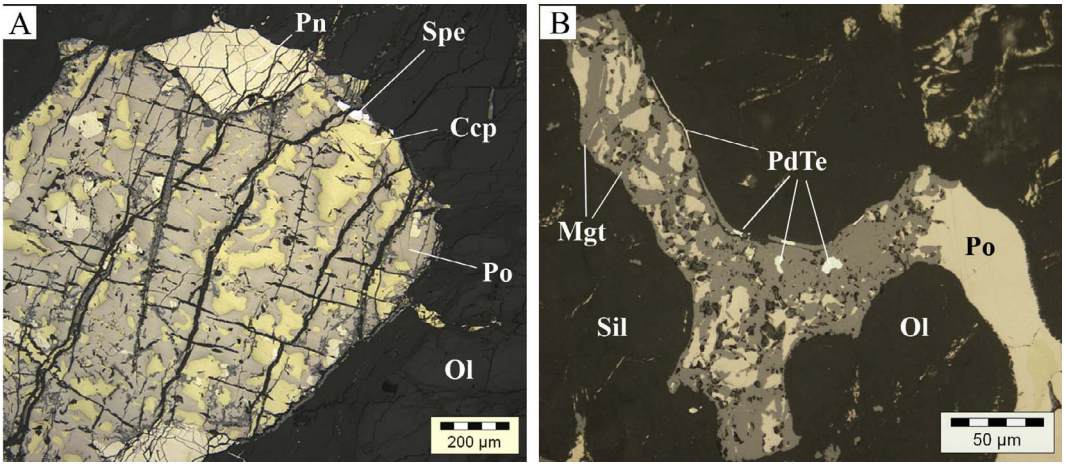

Fig. 6. Sulfide assemblages of the F Zone under reflected light. A: Primary magmatic sulfide bleb composed of pentlandite (Pn), pyrrhotite (Po) and chalcopyrite (Ccp) in harzburgite. Sperrylite (Spe) occurs at the margin on contact with olivine (Ol); B: Interstitial pyrrhotite partly replaced by secondary magnetite (Mgt) in harzburgite. Kotulskite (PdTe) is located inside magnetite and remobilized along the contact between sulfides and silicates (Sil). Olivine is completely replaced by serpentine.

medium-grained, however, rare pegmatoidal patches of gabbroic composition occur. In the southern half of the area held by Platinum Group Metals (Fig. 2A), the upper TGA Sequence hosts a sometimes pegmatoidal, mineralized zone of anorthositic, pyroxenitic, noritic or troctolitic composition (the T Zone). In the study area, these rocks are absent or poorly developed, with PGE and Au only weakly elevated (Fig. 14, WB165D0). The controls on the deposition or emplacement of the mineralization are currently unresolved, and either non-deposition/emplacement or later erosion appear plausible.

In thin section, the gabbronorites are typical gabbroic cumulate rocks consisting of coarse plagioclase and varying amounts of clino- and orthopyroxene. The latter two may occur as oikocrysts. Upwards through the stratigraphy, the amount of clinopyroxene is generally increasing and sporadic inverted pigeonite may be observed. Alteration throughout the whole sequence is minor.

In other parts of PTM's prospects, the TGA Sequence is overlain by magnetite-bearing gabbros and gabbronorites of the Upper Zone. In the study area, however, these rocks are poorly developed to absent. Due to the fine-grained, disseminated nature of the magnetite in the Upper Zone, the contact can be hard to identify in core and a sharp rise in magnetic susceptibility due to the appearance of magnetite is taken as the contact.

4.2. Geochemistry

4.2.1. Major and trace element variation diagrams

Data are displayed as bivariate plots with MgO as the differentiation index in Figs. 7 and 8. Variations in major element composition for the rocks analyzed reflect the proportion of olivine, pyroxene, and plagioclase present and clearly differentiate between the olivine + orthopyroxene-dominated Ultramafic Sequence and the plagioclase + clinopyroxene ± olivine ± orthopyroxene assemblages of the TGA Sequence and Upper Zone (Fig. 7; Table 1).

SiO_2 values range from 40 to 61 wt% and decrease towards higher MgO. Three groups of samples can be distinguished: i) harzburgite and 2 feldspathic pyroxenite samples of the UmS form a high-Mg cluster of samples; ii) Marginal orthopyroxenites form a separate trend from other samples; iii) rocks of the TGA sequence and UZ, dominated by gabbronorite and troctolite, form a trend extending from high- to low-Mg rocks. The wide range of MgO and other major elements for some of the troctolites reflects their cumulus assemblage ranging from < 90% olivine to leucotroctolite (Fig. 7).

The orthopyroxenites follow a trend of higher SiO_2 for a given MgO than the harzburgites. This reflects the higher SiO_2 in orthopyroxene. Al_2O_3 follows a sharp, decreasing trend with values between 4 and 27 wt%. Fe_2O_3 (as total Fe) decreases with decreasing MgO for most samples, even though there are Mg-rich, orthopyroxenite outliers. Trend lines drawn for the troctolites and harzburgites show that the rocks types follow slightly different trends (Fig. 7). Low Fe_2O_3 values correspond to the paucity of magnetite in the study area. CaO and Na_2O increase with decreasing MgO, reflecting the plagioclase and pyroxene assemblages of the Upper Zone and TGA Sequence. K_2O is generally low with values between 0.1 and 0.2 wt%. P_2O_5 is less than 0.1 wt%, reflecting the absence of apatite even in the Upper Zone. TiO_2 values are low, corresponding to limited development of the Upper Zone.

Vanadium strongly fractionates into magnetite and hence values are

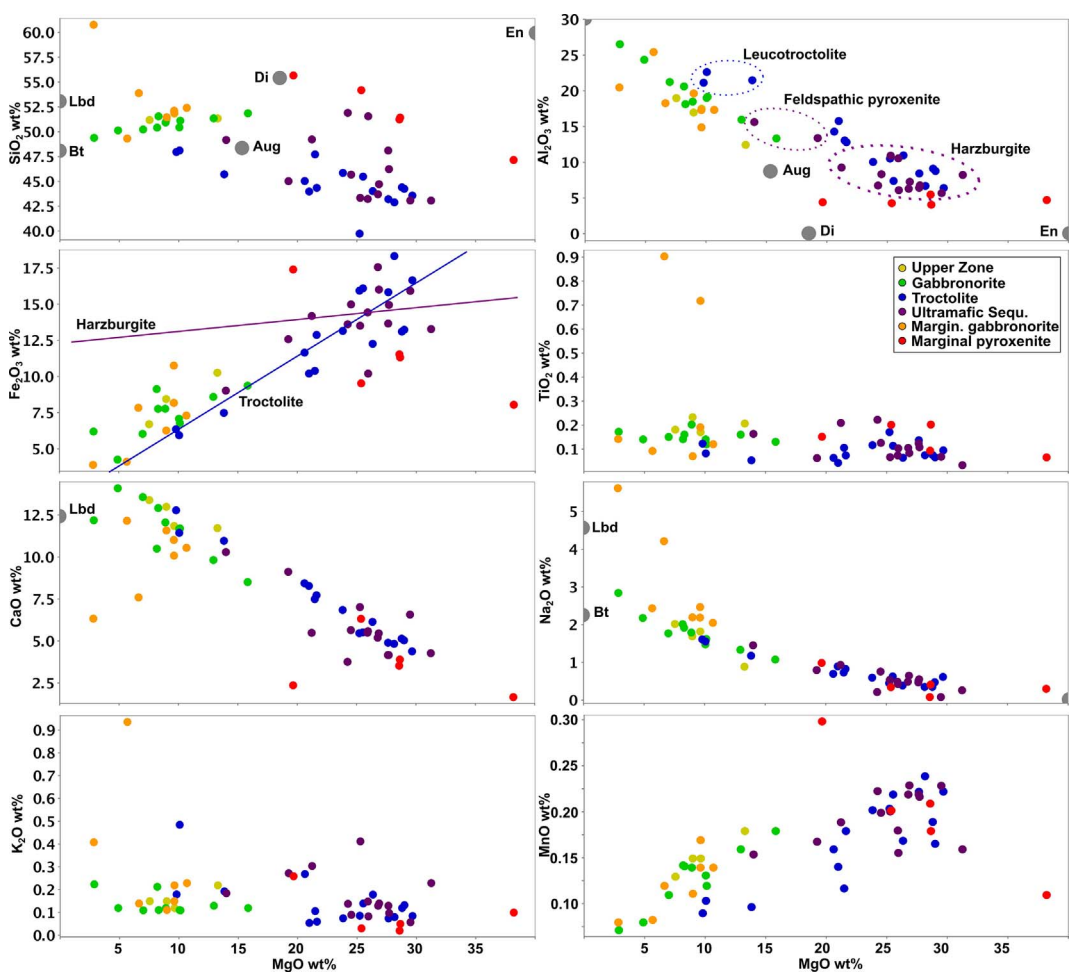

Fig. 7. Binary variation diagrams of MgO vs major elements. Except for two samples of feldspathic pyroxenite, the UmS group of samples comprises only harzburgite. The lines in the SiO_2 vs. Fe_2O_3 plot demonstrate the different trends of troctolite and harzburgite (see text). Lbd Labradorite; Bt Bytownite; Aug Augite; Di Diopside; En Enstatite.

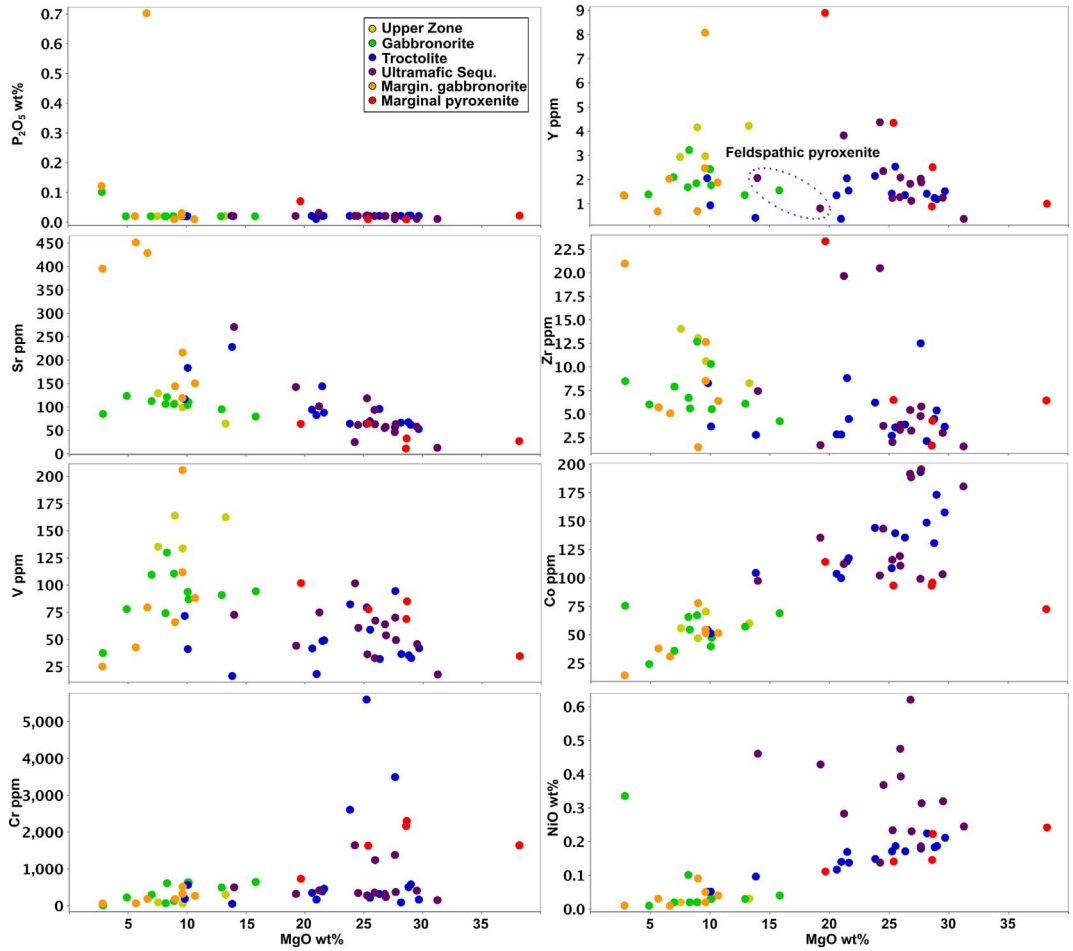

Fig. 8. Binary variation diagrams of MgO vs trace elements.

higher for Upper Zone samples. NiO is enriched in troctolites, olivine-bearing pyroxenites and due to the presence of sulfides strongly anomalous in mineralized rocks. Chromium is strongly enriched in pyroxenites and troctolites that contain small chromite clusters. P_2O_5, Sr and Zr levels are low in general, with outliers for the marginal gabbronorite (Fig. 8).

4.2.2. Multi-element normalized plots

All samples analyzed show almost identical trends on primitive mantle normalized multi-element plots (Sun and McDonough, 1989). They display negative Th, Nb, Ta and sometimes mildly negative Rb and Ti anomalies while in most cases displaying strong positive Sr and Eu anomalies (Fig. 9). Gabbroic rocks display Rb < Ba, while the opposite is true for the harzburgites and marginal pyroxenites. Mean Rb/Ba_N for the troctolites is 1.

For most groups of samples MREE and HREE are depleted relative to primitive mantle values. Eu/Eu^* ranges from 1.1 to 2.1, HREE are generally not fractionated with mean Tb/Yb_N of close to 1. The marginal pyroxenite displays significant variation in and has a mean Tb/Yb_N of 1.6 (Fig. 10). LREE are enriched (Mean $Ce/Sm_N = 2$) with mean Ce/Sm_N for the TGA Sequence and marginal gabbronorite at 2.7 and 2.2 respectively. Th is enriched relative to Sm, in particular in the troctolite and marginal pyroxenite (Mean $Th/Sm_N = 4.2$ and 3.4, respectively). Although low Eu abundances are expected for the plagioclase-poor pyroxenite, there is some decoupling of plagioclase mode and Eu anomalies.

Samples of UZ, TGA Sequence gabbronorite and troctolite display a tight grouping of results with patterns that are almost identical. The marginal pyroxenite, mineralized harzburgite, and marginal gabbronorite display more within-group variation while still following the overall pattern. Maximum within-group variation is observed in the marginal rocks. Their proximity to the granitic footwall may account for some or all of the variation observed, however, some enrichment may also be attributed to trapped liquid (estimated following Maier and Barnes, 1999; McDonald et al., 2009). Regardless of within-sample variation, a small but systematic increase of REE contents can be observed from the troctolite at the base of the succession to the gabbroic units at the top.

4.2.3. PGE and Au

For this study 28 samples from a range of lithologies were selected for fire assay and the results, normalized to chondrite values (Lodders, 2003), are plotted in Fig. 11. Results for total PGE range from 12 to 12,300 ppb with 1.1 to 1100 ppb Au.

Upper Zone and TGA Sequence gabbroic rocks display mildly fractionated profiles across the IPGE and after a moderate increase of concentration a flat profile across the PPGE and Au. Samples of the troctolite are mostly characterized by mildly sloping IPGE and except for a mineralized sample have flat PPGE distributions.

The serpentinized harzburgite exhibits strong fractionation with Pd/Ir of 177. The rocks are enriched in Pd relative to Pt, and Au is depleted relative to Pd. This pattern is identical for that of the mineralized troctolite. A sample of the marginal pyroxenite is characterized by unfractionated PGE (Fig. 11).

Fig. 11 displays variation diagrams of S versus Cu, Pt, and Pt. It can be seen, that Cu and S exhibit an excellent correlation, whereas the correlation of S and Pt or Pd is significantly poorer. Sulfur levels are overall very low, with a maximum of approx. 12000 ppm. These levels

Table 1

Sample ID	UZ1	UZ2	UZ3	UZ4	MZ1	MZ2	MZ3	MZ4	MZ5	MZ6	MZ7	MZ8	MZ9
Rock Type	FEGB	FEGB	FEGB	FEGN	GN	GN	GN	GN	GN	GN	GN	GN	T Zone peg N
Group	UZ	UZ	UZ	UZ	TGA	TGA	TGA	TGA	TGA	TGA	TGA	TGA	TGA
XRF %													
SiO_2	51.34	51.22	51.83	51.18	50.44	51.55	51.35	51.11	51.86	50.14	50.23	50.93	50.42
Al_2O_3	12.43	16.96	17.50	18.98	19.02	18.13	15.96	19.16	13.33	24.36	21.24	18.49	20.62
$Fe_2O=$	10.26	8.44	8.17	6.70	7.08	7.76	8.59	6.78	9.37	4.25	6.03	7.77	9.13
MnO	0.18	0.15	0.15	0.13	0.13	0.14	0.16	0.12	0.18	0.08	0.11	0.14	0.14
MgO	13.28	8.98	9.63	7.55	10.06	8.30	12.94	10.13	15.83	4.89	7.00	8.90	8.18
CaO	11.72	12.98	11.85	13.38	11.68	12.91	9.82	11.70	8.51	14.09	13.56	12.06	10.50
Na_2O	0.88	1.69	1.82	2.02	1.48	1.92	1.33	1.62	1.07	2.18	1.77	1.79	2.01
K_2O	0.22	0.15	0.12	0.15	0.11	0.11	0.13	0.11	0.12	0.12	0.11	0.12	0.21
TiO_2	0.21	0.23	0.17	0.18	0.14	0.16	0.16	0.12	0.13	0.14	0.15	0.20	0.14
P_2O_5	0.02	0.02	0.02	0.02	0.02	0.02	0.02	0.02	0.02	0.02	0.02	0.02	0.02
Cr_2O_3	0.06	0.03	0.02	0.02	0.11	0.03	0.12	0.10	0.14	0.05	0.06	0.03	0.01
NiO	0.03	0.02	0.02	0.02	0.03	0.02	0.03	0.03	0.04	0.01	0.02	0.02	0.10
LOI	3.23	1.38	0.43	0.66	0.46	0.47	0.35	0.47	0.58	0.55	0.47	1.25	1.13
Total	99.72	100.12	100.57	99.73	99.66	100.37	99.84	100.38	99.75	99.93	99.75	99.78	100.66
S ppm XRF	196	361	NA	172	NA	NA	NA	41	39	95	NA	NA	2731
ICP-MS ppm													
Li	3.27	2.37	2.06	1.99	2.07	1.35	2.39	3.22	1.03	1.21	2.22	3.19	1.95
P	35.08	66.22	40.14	52.69	61.93	21.22	65.47	39.58	33.92	40.68	60.15	71.17	28.60
Sc	21.02	17.66	14.57	14.90	12.89	16.35	7.35	10.07	11.76	6.84	9.95	9.09	8.87
Ti	1177.14	1567.47	1095.39	1278.42	845.51	811.62	764.64	556.25	605.09	675.87	795.64	1242.24	665.33
V	162.31	163.79	133.68	135.28	93.66	129.91	90.92	87.00	94.35	77.85	109.44	110.57	74.13
Cr	297.94	162.72	59.75	94.37	632.59	612.41	495.62	632.01	646.01	225.39	301.40	129.36	68.15
Co	60.06	46.99	70.40	55.73	39.81	54.61	57.20	47.39	69.00	24.23	35.94	67.12	65.63
Ni	203.37	162.84	175.56	125.56	183.63	501.27	225.06	238.08	228.36	96.46	120.75	163.50	680.41
Cu	62.70	34.16	69.73	36.97	30.83	48.11	24.37	33.59	26.73	22.48	23.98	33.82	808.77
Zn	59.34	48.73	62.10	49.23	41.63	50.85	52.07	41.69	55.19	24.64	35.76	64.14	55.68
Ga	7.69	10.77	13.42	15.01	10.02	12.04	9.60	10.93	7.79	13.53	12.30	13.60	11.42
As	0.30	0.36	0.20	0.30	0.31	0.24	0.17	0.21	0.20	0.20	0.21	0.33	0.32
Rb	3.64	1.30	0.93	1.55	1.38	0.66	1.88	0.64	1.78	0.49	0.73	1.30	2.42
Sr	64.07	107.61	99.20	129.34	104.30	121.14	94.87	110.46	79.34	123.46	112.43	105.81	106.22
Y	4.22	4.16	2.97	2.93	2.43	3.22	1.36	1.77	1.56	1.39	2.10	1.85	1.69
Zr	8.28	13.05	10.61	14.04	10.31	5.60	6.09	5.51	4.22	6.02	7.90	12.69	6.71
Nb	0.27	0.64	0.38	0.49	1.14	0.14	0.26	0.19	0.16	0.20	0.20	0.73	0.20
Ba	36.63	32.30	32.55	38.13	26.29	28.24	29.16	28.64	36.80	23.42	23.56	31.40	38.90
Sn	0.24	1.14	0.64	3.34	0.41	0.43	0.27	0.38	0.16	0.25	0.32	0.60	0.33
Cs	0.17	0.07	0.05	0.05	0.07	0.03	0.06	0.07	0.11	0.02	0.03	0.05	0.21
La	1.45	1.82	1.14	1.28	1.19	0.95	1.20	0.87	0.95	0.91	1.28	1.50	0.91
Ce	3.09	4.69	2.39	3.19	2.57	2.71	2.50	2.26	1.85	2.48	2.83	3.05	2.81
Pr	0.39	0.49	0.28	0.30	0.25	0.25	0.22	0.18	0.18	0.20	0.26	0.29	0.20
Nd	1.86	2.26	1.30	1.40	1.12	1.24	0.91	0.81	0.77	0.88	1.15	1.22	0.88
Sm	0.53	0.59	0.37	0.39	0.29	0.37	0.20	0.22	0.19	0.22	0.29	0.28	0.22
Eu	0.22	0.23	0.16	0.17	0.15	0.16	0.14	0.13	0.12	0.14	0.15	0.17	0.15
Gd	0.63	0.68	0.46	0.48	0.34	0.46	0.22	0.26	0.22	0.26	0.34	0.35	0.26
Tb	0.11	0.11	0.08	0.08	0.06	0.08	0.03	0.05	0.04	0.04	0.05	0.05	0.04
Dy	0.79	0.77	0.57	0.54	0.42	0.58	0.25	0.32	0.27	0.27	0.38	0.35	0.30
Ho	0.17	0.16	0.13	0.12	0.09	0.13	0.05	0.07	0.06	0.06	0.08	0.07	0.07
Er	0.49	0.47	0.36	0.34	0.28	0.38	0.15	0.21	0.19	0.16	0.23	0.22	0.20
Tm	0.07	0.07	0.06	0.05	0.04	0.06	0.02	0.03	0.03	0.03	0.03	0.04	0.03
Yb	0.53	0.45	0.37	0.33	0.30	0.39	0.17	0.24	0.22	0.16	0.23	0.22	0.23
Lu	0.08	0.07	0.06	0.05	0.05	0.06	0.03	0.04	0.04	0.03	0.04	0.03	0.04
Hf	0.27	0.39	0.31	0.41	0.26	0.19	0.17	0.16	0.12	0.17	0.21	0.33	0.20
Ta	0.02	0.04	0.03	0.03	0.10	0.01	0.02	0.01	0.01	0.02	0.02	0.05	0.01
W	0.03	0.04	0.03	0.03	0.04	0.06	0.03	0.02	0.02	0.03	0.03	0.04	0.02

Table 1 *(continued)*

Pb	1.60	0.97	2.05	2.41	0.65	0.95	0.58	0.75	0.62	0.70	0.89	2.08	2.83
Th	0.11	0.22	0.13	0.18	0.13	0.07	0.13	0.10	0.11	0.08	0.10	0.16	0.15
U	0.04	0.08	0.08	0.10	0.05	0.03	0.06	0.05	0.04	0.04	0.04	0.11	0.06
PGE ppb													
Os	0.29	0.13	NA	0.11	NA	NA	NA	0.07	0.21	0.06	NA	NA	29.7
Ir	0.52	0.09	NA	0.10	NA	NA	NA	0.17	0.95	0.55	NA	NA	29.2
Ru	0.35	0.21	NA	0.23	NA	NA	NA	0.49	1.08	0.38	NA	NA	115
Rh	3.26	0.54	NA	0.53	NA	NA	NA	0.93	3.70	2.53	NA	NA	85.3
Pt	20.5	38.7	NA	54.6	NA	NA	NA	20.8	26.0	10.2	NA	NA	5076
Pd	11.3	20.2	NA	38.6	NA	NA	NA	40.3	37.4	8.20	NA	NA	6951
Au	2.55	1.46	NA	2.38	NA	NA	NA	3.83	2.90	1.12	NA	NA	1095

Sample ID	MZ10	TR1	TR2	TR3	TR4	TR5	TR6	TR7	TR8	TR9	TR10	TR11	TR12
Rock Type	T Zone PX	opx TR	peg TR	TR	TR	TR	TR	TR	TR	TR	TR	TR	TR
Group	TGA	TGA	TGA	TGA	TGA	TGA	TGA	TGA	TGA	TGA	TGA	TGA	TGA
XRF %													
SiO_2	49.39	43.21	47.72	43.58	44.40	44.02	42.89	45.04	44.35	39.74	45.86	44.25	45.71
Al_2O_3	26.53	8.43	13.05	6.39	9.11	10.97	6.68	14.29	12.81	10.51	10.03	8.77	21.48
$Fe_2O=$	6.19	15.83	10.39	16.66	13.10	12.26	18.33	11.65	12.87	15.94	13.15	13.23	7.48
MnO	0.07	0.22	0.12	0.22	0.19	0.17	0.24	0.16	0.18	0.20	0.20	0.17	0.10
MgO	2.87	27.65	21.48	29.67	28.79	26.34	28.16	20.61	21.62	25.23	23.83	28.99	13.83
CaO	12.19	4.90	7.49	4.39	5.14	6.14	4.83	8.44	7.73	5.47	6.85	5.04	10.97
Na_2O	2.84	0.51	0.73	0.61	0.35	0.39	0.35	0.70	0.83	0.45	0.59	0.47	1.18
K_2O	0.22	0.07	0.11	0.08	0.12	0.18	0.08	0.27	0.06	0.09	0.07	0.13	0.19
TiO_2	0.17	0.14	0.11	0.10	0.08	0.06	0.07	0.06	0.07	0.17	0.12	0.07	0.05
P_2O_5	0.10	0.02	0.02	0.02	0.02	0.02	0.02	0.02	0.02	0.02	0.02	0.02	0.02
Cr_2O_3	0.00	0.62	0.10	0.04	0.10	0.06	0.03	0.09	0.08	2.41	0.52	0.13	0.02
NiO	0.33	0.18	0.17	0.21	0.18	0.17	0.22	0.12	0.14	0.17	0.15	0.19	0.10
LOI	1.48	5.30	5.56	5.39	7.34	6.60	6.46	5.93	5.45	6.47	5.83	9.14	6.47
Total	100.34	100.34	100.55	100.49	100.40	99.67	100.24	100.39	99.59	98.95	100.21	100.27	100.44
S ppm XRF	12786	466	1146	467	269	NA	721	NA	NA	499	NA	NA	NA
ICP-MS ppm													
Li	2.76	1.45	0.75	3.26	1.56	2.58	2.66	2.22	1.84	2.01	1.92	0.91	7.92
P	400.53	63.48	45.03	59.58	31.79	56.53	29.83	24.60	31.13	30.67	13.53	30.21	20.90
Sc	1.63	11.04	9.65	7.12	6.56	7.62	7.93	8.62	10.77	9.44	13.00	7.03	1.70
Ti	804.89	785.45	452.36	402.58	253.98	269.05	252.65	284.68	346.79	437.16	638.26	310.53	262.86
V	37.53	94.56	48.63	41.93	35.40	32.09	36.62	41.77	49.20	79.38	82.32	32.86	16.44
Cr	7.47	3493.35	391.13	166.84	505.57	316.68	91.64	351.49	462.63	5598.44	2606.25	580.25	50.59
Co	75.55	193.28	114.69	157.70	130.69	135.57	148.71	103.73	117.47	108.67	144.09	173.25	104.44
Ni	1949.27	1136.85	1041.82	1372.40	1070.04	1023.52	1271.49	630.69	862.13	928.64	878.10	1052.88	661.21
Cu	3251.31	20.63	99.13	37.77	6.64	10.68	60.70	45.65	44.66	23.45	39.55	7.11	49.81
Zn	104.01	109.74	50.65	89.92	64.36	66.08	109.24	61.50	62.54	63.46	95.41	86.37	50.99
Ga	14.23	7.41	7.64	4.00	4.68	5.86	4.02	6.87	6.87	5.53	8.04	5.58	10.08
As	0.26	0.40	0.25	0.18	0.15	0.19	0.17	0.21	0.21	0.16	0.28	0.35	0.32
Rb	1.72	2.70	3.75	1.66	3.63	4.59	2.17	4.32	0.80	2.52	2.50	6.29	4.93
Sr	85.03	56.33	143.97	52.63	67.33	95.63	66.29	93.99	87.83	64.01	64.30	61.58	228.31
Y	1.34	2.03	2.05	1.52	1.24	1.36	1.42	1.35	1.55	1.42	2.15	1.19	0.42
Zr	8.49	12.51	8.82	3.64	4.47	3.87	2.12	2.84	4.47	2.69	6.21	5.38	2.78
Nb	0.66	0.35	0.26	0.15	0.19	0.19	0.08	0.09	0.11	0.17	0.37	0.48	0.11
Ba	18.27	26.24	36.72	26.03	38.80	40.18	26.07	29.81	20.53	17.14	19.52	28.40	70.94
Sn	0.54	0.59	0.26	0.19	0.15	0.22	0.17	0.18	0.21	0.23	0.45	0.25	0.22
Cs	0.15	0.22	0.45	0.26	0.31	0.68	0.31	0.31	0.02	0.26	0.09	0.66	0.27
La	1.20	1.07	1.26	1.01	0.97	1.08	0.67	0.89	0.85	0.76	1.10	0.91	0.68
Ce	4.18	1.64	2.31	1.56	1.57	1.68	1.03	1.49	1.59	1.35	1.85	1.47	1.15
Pr	0.33	0.25	0.27	0.18	0.17	0.19	0.13	0.17	0.19	0.16	0.25	0.19	0.12
Nd	1.44	1.05	1.17	0.81	0.73	0.81	0.59	0.74	0.81	0.70	1.03	0.78	0.47

Table 1 *(continued)*

Sm	0.30	0.25	0.29	0.21	0.18	0.19	0.18	0.19	0.19	0.17	0.26	0.17	0.12
Eu	0.09	0.13	0.14	0.11	0.11	0.11	0.10	0.14	0.14	0.10	0.13	0.09	0.12
Gd	0.34	0.28	0.30	0.23	0.18	0.21	0.21	0.20	0.22	0.20	0.31	0.19	0.11
Tb	0.05	0.05	0.05	0.04	0.03	0.03	0.03	0.04	0.04	0.03	0.05	0.03	0.01
Dy	0.29	0.34	0.35	0.27	0.21	0.23	0.25	0.24	0.26	0.24	0.37	0.20	0.08
Ho	0.06	0.07	0.08	0.06	0.05	0.05	0.06	0.05	0.06	0.05	0.08	0.04	0.02
Er	0.15	0.22	0.22	0.17	0.14	0.15	0.16	0.16	0.17	0.16	0.23	0.13	0.05
Tm	0.02	0.03	0.03	0.03	0.02	0.02	0.02	0.02	0.03	0.02	0.04	0.02	0.01
Yb	0.14	0.23	0.24	0.19	0.16	0.17	0.18	0.16	0.18	0.17	0.25	0.14	0.05
Lu	0.02	0.04	0.04	0.03	0.03	0.03	0.03	0.03	0.03	0.03	0.04	0.02	0.01
Hf	0.25	0.27	0.22	0.10	0.11	0.10	0.07	0.08	0.11	0.09	0.18	0.14	0.07
Ta	0.04	0.03	0.01	0.03	0.03	0.02	0.00	0.02	0.02	0.01	0.03	0.04	0.01
W	0.02	0.08	0.02	0.15	0.09	0.07	0.11	0.02	0.03	0.00	0.03	0.09	0.01
Pb	14.28	2.68	2.76	1.07	1.71	0.67	1.59	0.39	0.38	0.92	1.07	2.34	1.13
Th	0.21	0.16	1.15	0.07	0.08	0.14	0.04	0.12	0.06	0.06	0.31	0.25	0.05
U	0.12	0.07	0.12	0.03	0.06	0.04	0.02	0.04	0.02	0.02	0.09	0.16	0.02
PGE ppb													
Os	1.59	0.05	0.23	0.24	0.09	NA	0.35	NA	NA	22.6	NA	NA	NA
Ir	5.65	0.04	0.35	0.30	0.13	NA	0.68	NA	NA	40.7	NA	NA	NA
Ru	11.3	0.20	1.11	0.91	0.53	NA	1.87	NA	NA	102	NA	NA	NA
Rh	12.3	0.53	1.77	1.87	0.99	NA	2.86	NA	NA	322	NA	NA	NA
Pt	1804	10.7	28.8	9.86	7.00	NA	15.9	NA	NA	3594	NA	NA	NA
Pd	2805	4.43	45.6	15.8	4.26	NA	10.33	NA	NA	2675	NA	NA	NA
Au	365	2.43	4.33	2.61	1.77	NA	2.71	NA	NA	9.69	NA	NA	NA

Sample ID	HZ1	HZ2	HZ3	HZ4	HZ5	HZ6	HZ7	HZ8	HZ9	HZ10	HZ11	HZ12
Rock Type	DUN/HZ	HZ- serp	HZ- serp	HZ- serp	HZ- serp	HZ- serp	HZ- serp	HZ- serp	HZ- serp	Serp	Serp	HZ
Group	UmS	UmS	UmS	UmS	UmS	UmS	UmS	UmS	UmS	UmS	UmS	UmS
XRF %												
SiO_2	44.72	43.71	46.24	48.11	51.56	49.17	49.23	51.90	43.35	45.03	43.08	45.69
Al_2O_3	7.26	6.28	6.76	6.41	6.08	15.62	9.26	6.74	10.92	13.39	5.67	8.32
Fe_2O_3	16.01	17.56	14.95	13.66	10.20	9.02	14.18	13.61	13.51	12.58	15.92	14.98
MnO	0.23	0.22	0.22	0.22	0.16	0.15	0.19	0.22	0.20	0.17	0.23	0.20
MgO	26.86	26.77	27.70	27.64	25.95	14.00	21.22	24.24	25.28	19.24	29.50	24.52
CaO	5.46	5.20	4.16	4.17	5.59	10.29	5.49	3.76	7.02	9.12	6.57	5.65
Na_2O	0.65	0.49	0.55	0.47	0.42	1.45	0.93	0.21	0.53	0.79	0.08	0.76
K_2O	0.14	0.13	0.10	0.13	0.08	0.18	0.30	0.14	0.41	0.27	0.06	0.09
TiO_2	0.08	0.11	0.11	0.12	0.10	0.16	0.21	0.22	0.07	0.06	0.07	0.13
P_2O_5	0.02	0.02	0.02	0.01	0.02	0.02	0.03	0.02	0.02	0.02	0.01	0.02
Cr_2O_3	0.06	0.08	0.10	0.32	0.28	0.10	0.09	0.30	0.04	0.07	0.09	0.07
NiO	0.23	0.62	0.31	0.19	0.39	0.46	0.28	0.14	0.23	0.43	0.32	0.37
LOI	4.62	4.91	7.51	3.22	3.33	2.26	4.51	5.61	10.13	4.39	12.39	4.80
Total	100.29	99.61	99.86	100.20	99.93	99.81	100.14	100.27	100.36	100.05	100.16	99.43
S ppm XRF	NA	11935	2493	1248	6580	9928	8000	525	1044	9442	2036	6805
ICP-MS ppm												
Li	3.28	1.38	2.16	1.37	3.88	5.71	4.72	3.79	4.86	2.18	1.96	0.90
P	26.87	62.32	50.58	32.88	21.54	46.99	83.19	59.74	20.43	15.59	21.40	26.38
Sc	9.00	9.43	11.46	12.85	15.44	9.35	15.38	19.11	7.53	7.63	9.82	12.24
Ti	513.37	535.98	557.96	612.95	467.20	733.83	1051.95	1352.20	274.05	245.32	279.65	508.05
V	53.82	63.97	49.45	70.05	67.29	72.66	74.88	101.64	36.37	44.24	45.69	60.69
Cr	238.54	318.08	370.93	1378.88	1241.13	500.13	416.92	1643.24	280.91	322.41	411.38	348.05
Co	188.62	191.68	195.57	99.23	110.82	97.48	112.33	102.20	115.95	135.46	103.26	143.36
Ni	1495.61	4062.16	1819.59	930.41	2498.85	2963.47	1839.36	796.96	1282.99	2616.62	1451.10	2112.82
Cu	184.85	2507.57	453.47	233.49	975.01	2114.10	1169.29	61.51	171.33	1157.92	103.80	791.92
Zn	115.65	102.36	96.91	61.12	69.04	48.77	75.61	113.88	81.89	61.30	46.68	75.12
Ga	5.49	3.82	5.77	4.10	4.09	8.22	7.22	7.63	5.20	6.39	2.65	5.75

Table 1 *(continued)*

As	0.35	0.17	0.32	0.18	0.32	0.36	0.30	1.47	0.69	0.18	1.11	0.19
Rb	4.41	2.78	4.92	3.64	3.46	3.00	22.50	8.50	12.68	4.68	2.92	1.79
Sr	57.50	54.94	63.24	46.20	62.86	270.68	101.47	24.73	118.38	142.52	57.72	61.39
Y	1.13	1.83	1.88	2.01	2.09	2.07	3.83	4.37	1.24	0.81	1.25	2.35
Zr	3.23	5.42	5.80	4.78	3.85	7.44	19.66	20.51	2.01	1.69	2.99	3.74
Nb	0.12	0.25	0.25	0.63	0.11	0.31	2.48	0.78	0.06	0.08	0.10	0.11
Ba	30.68	71.48	41.79	15.78	16.76	42.56	47.46	26.52	73.90	88.55	3.68	27.37
Sn	0.41	0.81	0.72	0.26	0.44	0.68	0.59	0.55	1.05	0.59	0.43	0.39
Cs	0.25	0.57	1.17	0.32	0.52	0.20	1.76	0.97	2.01	0.49	0.86	0.28
La	0.64	1.15	1.59	0.79	0.92	1.60	2.23	5.40	0.73	0.59	0.52	1.10
Ce	0.91	2.10	2.18	1.27	1.75	3.14	5.06	8.13	1.23	1.04	0.88	1.93
Pr	0.12	0.25	0.26	0.15	0.20	0.33	0.60	1.03	0.14	0.11	0.11	0.24
Nd	0.53	1.08	1.09	0.72	0.82	1.39	2.59	3.93	0.58	0.47	0.49	1.05
Sm	0.15	0.30	0.27	0.20	0.21	0.32	0.63	0.74	0.18	0.16	0.12	0.29
Eu	0.09	0.13	0.14	0.10	0.09	0.19	0.23	0.14	0.14	0.13	0.06	0.16
Gd	0.17	0.28	0.30	0.24	0.25	0.34	0.64	0.82	0.18	0.12	0.15	0.33
Tb	0.03	0.05	0.05	0.04	0.05	0.06	0.10	0.11	0.03	0.02	0.03	0.06
Dy	0.20	0.33	0.32	0.32	0.32	0.37	0.67	0.74	0.21	0.15	0.20	0.40
Ho	0.04	0.07	0.07	0.08	0.08	0.08	0.15	0.16	0.05	0.03	0.05	0.09
Er	0.13	0.19	0.21	0.23	0.23	0.23	0.42	0.49	0.14	0.09	0.14	0.27
Tm	0.02	0.03	0.03	0.04	0.03	0.03	0.06	0.08	0.02	0.01	0.02	0.04
Yb	0.13	0.19	0.22	0.25	0.27	0.25	0.44	0.52	0.16	0.10	0.17	0.29
Lu	0.02	0.03	0.04	0.04	0.04	0.04	0.07	0.09	0.03	0.02	0.03	0.05
Hf	0.10	0.16	0.16	0.14	0.12	0.21	0.60	0.54	0.06	0.05	0.07	0.11
Ta	0.01	0.02	0.04	0.05	0.01	0.02	0.17	0.05	0.00	0.00	0.05	0.01
W	0.11	0.41	0.12	0.02	0.08	0.07	0.18	0.21	0.10	0.08	0.09	0.03
Pb	5.50	9.92	9.67	0.85	2.00	2.67	5.18	1.83	1.02	5.46	1.95	2.68
Th	0.04	0.14	0.11	0.07	0.07	0.15	1.30	0.36	0.04	0.03	0.03	0.08
U	0.03	0.06	0.05	0.02	0.03	0.06	0.69	0.23	0.02	0.02	0.01	0.03
PGE ppb												
Os	NA	11.2	14.44	1.33	4.32	11.8	4.35	0.53	13.51	11.38	10.1	8.45
Ir	NA	18.0	12.16	1.92	11.6	23.1	6.48	1.00	14.49	18.50	14.3	14.36
Ru	NA	41.5	45.89	5.87	24.8	53.5	16.8	2.41	50.91	47.81	41.6	36.78
Rh	NA	81.2	49.12	7.73	73.3	146	38.4	3.61	61.86	96.51	75.7	63.93
Pt	NA	1955	617.74	71.7	1108	2125	470	46.34	534.64	1309.31	1020	1045.98
Pd	NA	2993	1548.93	241	3141	5178	1695	113.25	840.29	3482.22	2902	2077.50
Au	NA	224	103.58	16.6	150	307	123	11.55	32.77	162.53	158	168.53

Sample ID	MGN1	MGN2	MGN3	MGN4	MGN5	MGN6	MGN7	MPX1	MPX2	MPX3	MPX4	MPX5
Rock Type	AN/basal N	basal GN	AN	basal GN	basal GN	GN	px AN (LN)	chr PX	ol (fsp) PX	ol OPX	ol OPX	OPX
Group	Marginal GN	Marginal GN	Marginal GN	Marginal GN	Marginal GN	Marginal GN	Marginal GN	Marginal PX	Marginal PX	Marginal PX	Marginal PX	Marginal PX
XRF %												
SiO_2	60.76	49.32	53.89	51.92	51.46	52.41	52.12	51.24	55.67	51.42	47.16	54.19
Al_2O_3	20.47	25.43	18.27	14.88	19.63	17.33	17.31	5.47	4.39	4.05	4.70	4.27
Fe_2O_3	3.89	4.10	7.84	10.75	6.26	7.30	8.17	11.53	17.40	11.32	8.04	9.52
MnO	0.08	0.08	0.12	0.17	0.11	0.14	0.14	0.21	0.30	0.18	0.11	0.20
MgO	2.83	5.66	6.64	9.62	8.99	10.68	9.61	28.58	19.66	28.64	38.20	25.37
CaO	6.33	12.16	7.60	10.08	11.58	10.55	11.02	3.53	2.37	3.90	1.66	6.32
Na_2O	5.62	2.44	4.22	2.47	2.19	2.05	2.19	0.08	0.98	0.41	0.30	0.34
K_2O	0.41	0.94	0.14	0.22	0.11	0.23	0.15	0.02	0.26	0.05	0.10	0.03
TiO_2	0.14	0.09	0.90	0.72	0.07	0.12	0.19	0.09	0.15	0.20	0.07	0.20
P_2O_5	0.12	0.02	0.70	0.03	0.01	0.01	0.02	0.01	0.07	0.01	0.02	0.01
Cr_2O_3	0.02	0.02	0.04	0.08	0.04	0.05	0.06	0.46	0.12	0.50	0.43	0.34
NiO	0.01	0.03	0.01	0.02	0.09	0.04	0.05	0.15	0.11	0.22	0.24	0.14
LOI	1.54	2.71	0.34	1.09	0.63	0.56	0.55	3.91	1.12	1.24	9.04	0.64
Total	100.33	99.91	99.67	100.00	99.99	100.25	100.29	100.34	99.89	99.88	100.30	100.06

Table 1 *(continued)*

S ppm XRF	NA	NA	NA	NA	1586	NA	NA	NA	NA	NA	415	542
ICP-MS ppm												
Li	9.98	17.18	3.11	7.37	2.61	7.87	5.07	3.41	1.95	0.54	0.68	1.22
P	494.88	49.42	3053.13	88.84	5.92	20.86	40.51	15.24	279.71	20.74	46.31	38.77
Sc	2.70	3.77	4.87	20.58	7.49	13.81	12.54	12.22	27.21	12.50	5.36	16.09
Ti	761.40	497.20	4600.15	3763.27	419.44	640.96	958.40	397.05	685.38	936.37	247.78	1158.50
V	25.11	42.69	79.39	205.75	65.96	88.08	111.84	68.77	101.80	85.02	34.68	77.78
Cr	58.49	63.82	188.22	516.51	181.96	269.96	322.48	2165.51	731.82	2302.85	1642.61	1631.25
Co	14.35	38.02	30.98	51.46	77.81	51.54	54.52	93.25	114.16	95.92	72.57	93.35
Ni	36.09	197.21	70.01	172.12	620.61	271.44	297.95	763.23	618.28	1205.41	1326.61	916.00
Cu	9.91	22.30	24.73	53.06	329.66	58.76	256.35	65.67	250.92	695.22	58.77	119.74
Zn	47.29	36.38	71.48	88.32	47.96	46.24	50.90	64.50	162.81	70.08	32.78	115.86
Ga	19.47	16.38	15.54	14.57	14.31	11.10	11.13	3.04	7.54	3.51	2.80	4.67
As	0.17	0.34	0.23	0.46	0.30	0.22	0.20	0.17	0.53	0.13	0.25	0.24
Rb	4.79	26.87	0.40	2.31	1.58	3.36	1.40	0.85	24.92	1.32	2.88	1.77
Sr	395.40	451.43	429.09	216.27	144.25	150.52	118.98	11.23	63.75	32.54	26.95	64.63
Y	1.36	0.68	2.03	8.07	0.69	1.88	2.47	0.89	8.89	2.51	1.00	4.35
Zr	20.98	5.69	5.06	12.65	1.47	6.39	8.52	1.65	23.36	4.27	6.44	6.49
Nb	0.96	0.36	1.39	0.09	0.03	0.19	0.22	0.05	2.28	0.18	0.42	0.14
Ba	177.67	203.28	159.87	149.39	28.91	67.69	40.58	3.55	37.22	9.24	39.30	11.96
Sn	0.39	0.31	0.21	0.91	0.32	2.49	0.39	0.42	0.73	0.55	0.32	1.18
Cs	0.36	0.63	0.03	0.31	0.11	0.14	0.09	0.36	2.55	0.09	0.45	0.28
La	6.45	0.88	4.65	2.03	0.37	0.96	1.09	1.19	3.88	0.90	1.92	0.82
Ce	13.24	1.57	10.15	4.89	0.62	2.63	3.55	0.55	7.31	1.41	3.13	1.43
Pr	1.19	0.13	1.24	0.66	0.06	0.21	0.28	0.06	0.85	0.17	0.34	0.26
Nd	4.73	0.53	6.03	3.60	0.26	0.97	1.30	0.23	3.54	0.83	1.27	1.34
Sm	0.84	0.21	1.22	1.22	0.09	0.27	0.35	0.07	0.93	0.24	0.24	0.45
Eu	0.50	0.18	0.72	0.61	0.10	0.15	0.16	0.05	0.14	0.10	0.09	0.15
Gd	0.71	0.14	1.07	1.33	0.10	0.30	0.42	0.09	1.07	0.32	0.22	0.56
Tb	0.07	0.02	0.11	0.23	0.02	0.05	0.07	0.02	0.20	0.06	0.03	0.10
Dy	0.31	0.12	0.49	1.57	0.13	0.35	0.45	0.13	1.41	0.44	0.18	0.73
Ho	0.05	0.03	0.08	0.33	0.03	0.08	0.10	0.03	0.32	0.10	0.04	0.16
Er	0.15	0.08	0.19	0.89	0.08	0.22	0.29	0.11	1.02	0.29	0.11	0.46
Tm	0.02	0.01	0.02	0.13	0.01	0.04	0.04	0.02	0.17	0.05	0.02	0.07
Yb	0.13	0.08	0.12	0.91	0.10	0.24	0.29	0.14	1.33	0.32	0.13	0.44
Lu	0.02	0.01	0.02	0.14	0.01	0.04	0.05	0.02	0.21	0.05	0.02	0.07
Hf	0.54	0.16	0.14	0.57	0.05	0.19	0.25	0.06	0.70	0.14	0.17	0.25
Ta	0.08	0.04	0.13	0.02	0.03	0.02	0.02	0.00	0.22	0.02	0.04	0.01
W	0.04	0.04	0.01	0.11	0.01	0.05	0.04	0.07	0.50	0.04	0.44	0.03
Pb	3.50	6.26	0.93	3.14	2.05	0.77	1.61	1.15	5.72	1.49	1.09	2.52
Th	0.39	0.10	0.03	0.01	0.01	0.07	0.10	0.03	1.32	0.07	0.23	0.05
U	0.16	0.06	0.01	0.01	0.01	0.03	0.04	0.01	1.02	0.03	0.12	0.03
PGE ppb												
Os	NA	NA	NA	NA	1.95	NA	NA	NA	NA	NA	NA	0.34
Ir	NA	NA	NA	NA	2.60	NA	NA	NA	NA	NA	NA	0.44
Ru	NA	NA	NA	NA	8.14	NA	NA	NA	NA	NA	NA	1.45
Rh	NA	NA	NA	NA	12.8	NA	NA	NA	NA	NA	NA	0.48
Pt	NA	NA	NA	NA	151	NA	NA	NA	NA	NA	NA	3.67
Pd	NA	NA	NA	NA	467	NA	NA	NA	NA	NA	NA	5.32
Au	NA	NA	NA	NA	27.7	NA	NA	NA	NA	NA	NA	1.17

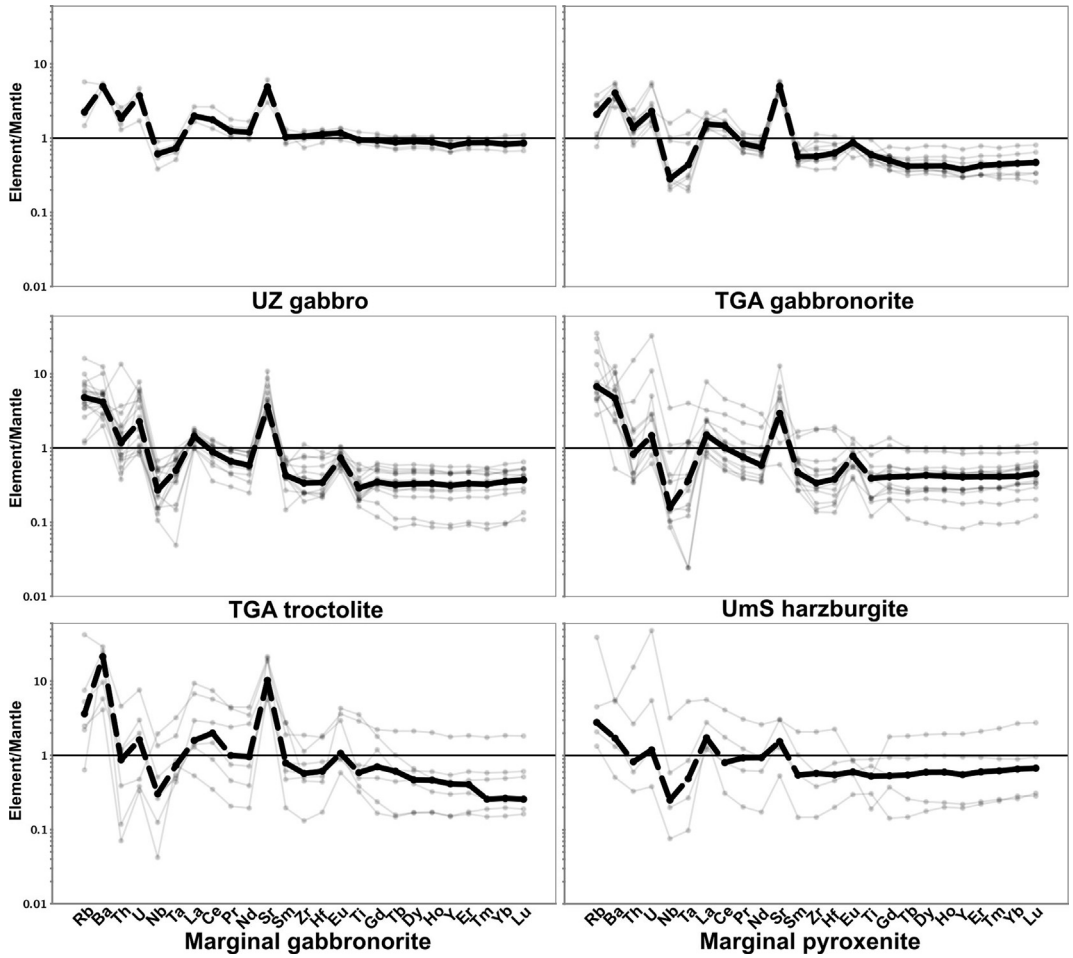

Fig. 9. Primitive mantle normalized (Sun and McDonough, 1989) multi-element plots for all six groups of rocks with thick lines showing the average for each group of samples. It can be seen that except for a stratigraphic increase in absolute concentrations the patterns are almost identical. Variations in marginal gabbronorites and pyroxenites are believed to result from contamination by assimilation.

and correlations are identical to commercial assays provided courtesy of Platinum Group Metals.

4.2.4. PGE and Cr assay data provided by Platinum Group Metals

Assay data provided by PTM can be used to assess validity of the results that were presented above. The available assay data for > 100 drill holes from the study area were extracted and are shown in the diagrams below.

Fig. 12A-C show binary variation diagrams of S vs Cu, Pt, and Pd. It can be seen, that Cu and S show excellent correlation, whereas there is only a weak correlation of S with Pt and Pd, respectively. Pt and Pd exhibit a good correlation (Table 2). Fig. 12D shows a ternary plot of Pt, Pd, and Au. It can be seen, that the majority of assays are dominated by Pd with Pd/Pt approx. 0.6 and only low Au content. This is in contrast to Pt/Pd observed in the Merensky Reef, and closer to the Pt/Pd observed in some sectors of the Platreef (Kinnaird, 2005). Low Au is typical of the F Zone, whereas in the T Zone and the Aurora Project Au makes up approximately 20% of the precious metals budget. Fig. 12D highlights, that the anti-correlation of Cr and PGE also applies for the rest of the assays in the area. It can be seen, that a large number of samples plot in between the low-PGE/high-Cr and high-Cr/low-PGE trends. This is due to Cr-rich orthopyroxene autoliths and mingled orthopyroxenitic lithologies that cannot be avoided during sampling. This data also experiences a sampling bias towards mineralized samples (the purpose of the company's sampling program), and Cr-rich, unmineralized samples are therefore not well-represented.

4.3. Lateral variation in lithology and mineralization

Typical cross and long sections through the study area (Fig. 3) are shown in Figs. 13 and 14. Both sections show the dominant lithology and PTM's assay values for 3E (Pt + Pd + Au) and Cr as well as Pt/Pd and Cu/Pd.

Fig. 13 shows a typical sequence of gabbronorite dominated upper TGA Sequence overlying olivine-bearing rocks. The base of the TGA Sequence is characterized by heterogeneous and patchy gabbronorite, norite, and troctolite, and textures observed in core range from incompletely blended olivine- or pyroxene-dominant patches to discrete autoliths and xenoliths (Fig. 4A, B). Downwards this zone grades into salt and pepper textured leuco- to melatroctolite.

Below the troctolite, strongly altered harzburgite hosts the bulk of the mineralization. Orthopyroxenite autoliths occur throughout this part of the succession, and where abundant are schematically indicated in the section. These rocks are typically enriched in Cr, and their abundance correlates with the Cr concentration shown. Below the harzburgite may be more orthopyroxenite, marginal gabbronorite, or more troctolite toward the eastern side of the section (drill hole WB091). The sequence of rocks continues up dip, until on the eastern side (not shown) the harzburgite is directly overlain by sedimentary rocks. In zones of mineralization, the Pt/Pd ratio is fairly constant around 0.6 with a Cu/Pd ratio at approximately 530. As shown above, the mineralization is dominated by Pd with little Au in the metal budget.

The four holes in the long-section (Fig. 14) are located at the western edge of PTM's drilling in this sector (Fig. 3) and mineralization is

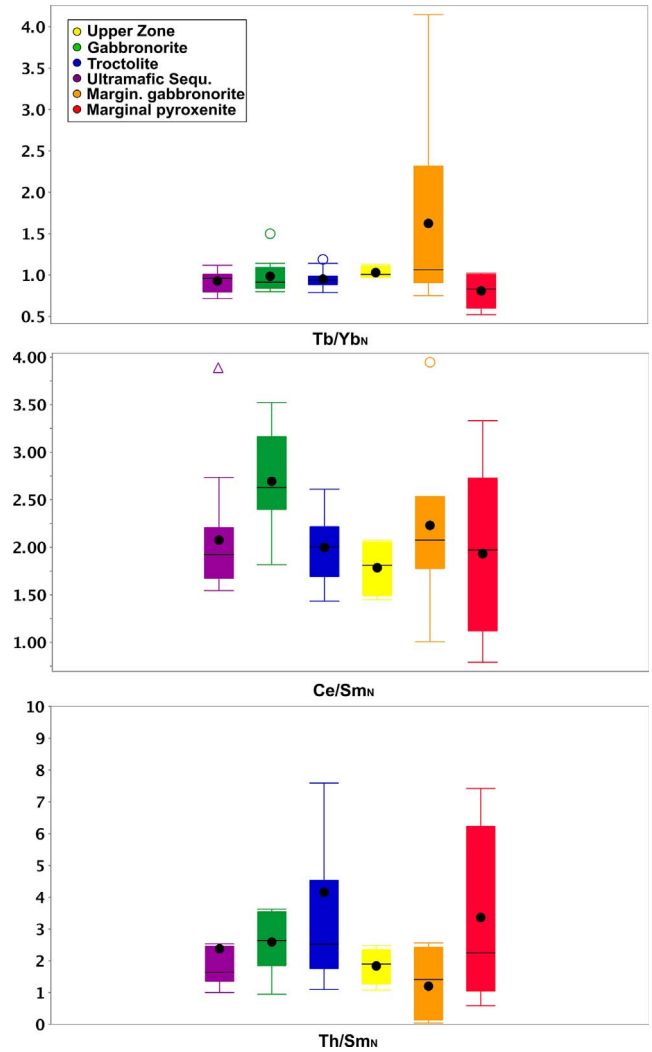

Fig. 10. Box plots displaying Tb/Yb_N, Ce/Sm_N and Th/Sm_N values for groups of samples. Color scheme as in Fig. 7. Most variation is exhibited by marginal gabbronorites and pyroxenites, which is interpreted to represent contamination by assimilation. The box represents the inter quartile range with the median represented as horizontal line and the mean as a black circle.

hosted by strongly altered, ultramafic rocks of varying mineralogy and texture. Holes WB163 and WB049 are located at or around the center of the mineralized zone, while holes WB165 and WB019 are located at its northern and southern edge, respectively. It can be seen, that all four holes share a very similar stratigraphy with Cr-enriched intervals that appear to correlate between the holes. Mineralization (shown as Pt + Pd + Au) is most strongly developed in the central section, and is poorly developed or absent at the northern and southern sections. The long section also shows well-developed troctolite regardless of the thickness and 3E grade of the harzburgite. This suggests, that the intrusion of both suites of rocks is independent of each other. Pt/Pd and Cu/Pd are again fairly consistent in the mineralized segments.

In summary, the sections how an SW to NE-oriented, tube-shaped and slightly flattened, mineralized zone of up to 80 m thickness that is dominantly confined to ultramafic rocks. Although most mineralization is confined to harzburgite and feldspathic pyroxenite, in detail the UmS is a highly heterogeneous zone with signs of magma mingling, mixing, fluid flow and sulfide remobilization. Grade drops off towards the northern and southern edges before increasing in the next high-grade, high-thickness harzburgitic zone (not shown in the sections). Grade is also lower in areas of abundant orthopyroxenite and an anti-correlation of Cr and 3E can be seen.

To visualize this area of the Waterberg Project, a Leapfrog 3D model using the logging data from > 100 drill holes has been created. Due to the nature of company drill logs, some assumptions and generalizations of logging codes had to be made. This includes grouping various logged rocks into broader categories, but also the assumption that all logged serpentinite is secondary and the product of harzburgite alteration. Additionally, given the nature of the ultramafic rocks, the model uses a > 1 g/t 3E grade shell rather than lithology to demonstrate the approximate outline of the UmS. Fig. 15A shows the granite-gneiss basement and the up to 80 m thick grade shell. It follows what appears to be a basement depression in a northeasterly direction. To its north, a less-well developed area of PGE mineralization follows the same trend.

These depressions may represent a primary feature controlling magma flow, or alternatively, represent zones of highest heat and fluid flux and the associated thermo-mechanical erosion. Among researchers associated with this project, the tubular intrusions are referred to as chonoliths (e.g. Kinnaird et al., 2017). It is important to stress, that this grade shell was not developed by Platinum Group Metals to indicate resources and resources, but rather models our understanding of PGE distribution. In Fig. 15B, the olivine-bearing lithologies of the lower TGA and Ultramafic Sequence have been added, and the erosional unconformity of the Waterberg Group sediments and dolerite sills are shown. The vertical offset in the dolerite dikes may indicate some fault control. The open area between the upper contact of the olivine-bearing rocks and the base of the sediments is occupied by gabbroic rocks of the TGA Sequence.

5. Discussion

5.1. Discussion of the data presented

The correlation of the Platreef and the Northern Lobe's northernmost, mineralized lithologies at Aurora has recently received some attention (Harmer et al., 2004; Manyeruke, 2007; Maier et al., 2008; McDonald and Harmer, 2010; McDonald et al., 2017). McDonald et al. (2017) describe several key factors that make it unlikely that the Aurora Project is a simple strike extension of the Platreef and instead suggest, that it represents a marginal facies of the Main Zone above the Troctolite Marker (which is located 1100 m above the base of the Main Zone). Considering the location of the Waterberg succession less than 20 km north of the Aurora Project, it is appealing to simply link the two zones as a northern magmatic basin. Some of the similarities between the upper Main Zone-hosted Aurora mineralization and the Waterberg T Zone are provided by McDonald et al. (2017), and this contribution will expand on their work.

Both the Platreef and the Waterberg Succession exhibit variations in rock type and mineralization along their strike, although compared to the Platreef the succession in the project area is small with approximately 15 km strike length. Dynamic emplacement environments with multiple, channelized magma injections along a westerly to northwesterly direction (rather than a north to south magma flow) have been proposed for the Platreef (Yudovskaya et al., 2017; cf. Barnes et al., 2016), and may together with floor rock control (Kinnaird et al., 2005) be used to explain clear differences along strike. The existing similarities between individual sectors (such as Aurora and the Waterberg Project, Fig. 2A) may be attributed to the fact, that all of them are related to the Bushveld Large Igneous Province, and hence share the same melting event.

In an initial study, laser-ablation U/Pb dating by Huthmann et al. (2016) demonstrated that zircons from mafic rocks of the succession have an age that is within error identical to ages published for the Bushveld Complex. This study also showed, that the sedimentary rocks unconformably overlying the coarse-grained mafic to ultramafic rocks have a maximum depositional age of 2045 Ma, with what is interpreted to be an ash-rich paleosoil in-between (Yudovskaya et al., 2015). Given

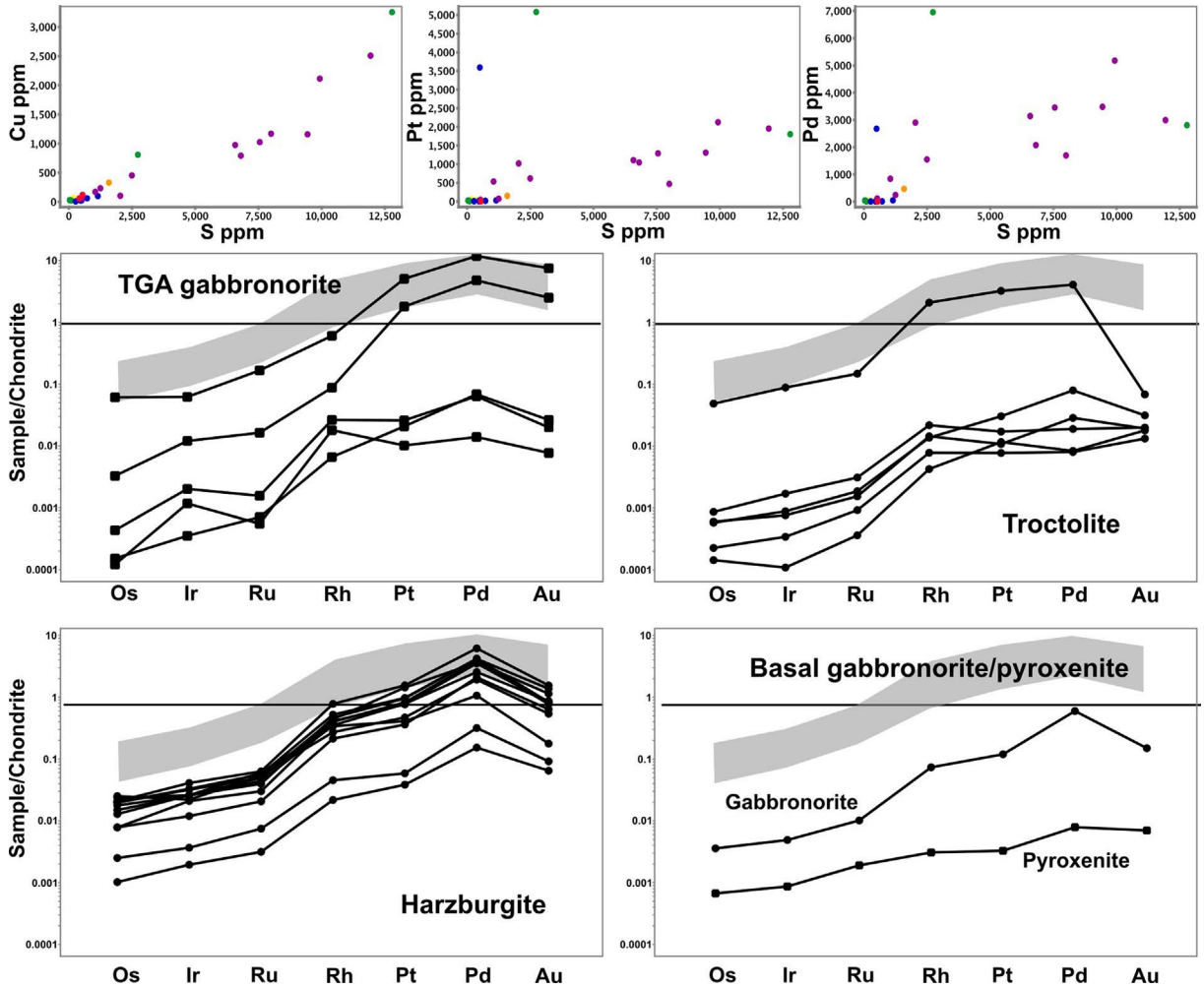

Fig. 11. Top: Binary variation diagrams of S vs Cu, Pt and Pd. S vs Cu show an excellent correlation, however the correlation between S and Pt and Pd is weak; Bottom: Chondrite normalized PGE plots for the samples analyzed in this study. Light grey represents PGE distribution from the Turfspruit and Sandsloot high-grade reef-style mineralization in the Northern Lobe (from Yudovskaya et al., 2017).

the absence of more evolved mafic rocks, i.e. apatite-bearing UZ or similar, and the absence of any sort of felsic roof rocks, then several kilometers of material must have been removed between c. 2056 and 2045 Ma. The Waterberg Project is characterized by significant erosion, a unique stratigraphy of harzburgites and troctolites, a relatively small size and limited thickness, and a position wedged in between the Palala Shear Zone in the North and the Hout River Shear Zone in the South (Fig. 1). This places the succession in a unique situation compared to the rest of the Bushveld Complex. The structural position, in particular, may have created transtensional spaces and crustal anisotropies along which initial magmas could ascend (Lightfoot and Evans-Lamswood, 2015). Further fault movement until 1.97 Ga brought the succession closer to surface and to a mineable depth (Schaller et al., 1999).

As shown by logging and geochemical data, all samples represent ultramafic to gabbroic cumulate rocks dominated by varying proportions of olivine, plagioclase, clino- and orthopyroxene. Clinopyroxene becomes the dominant pyroxene towards the top of the succession. Pigeonite may be found towards the top of the succession, however, its appearance is erratic. The lower part of the succession comprises strongly altered harzburgites and feldspathic pyroxenites hosting the F Zone mineralization, and is overlain by troctolite. Contrary what has been described at the nearby Aurora prospect (Manyeruke, 2007; McDonald et al., 2017), no significant carbonate xenoliths or carbonate alteration has been found in the project area.

In contrast to what is published on the Troctolite Marker in the Northern Lobe (an olivine-bearing gabbroic rock, van der Merwe, 1976), the troctolite of the Waterberg area is a true troctolite comprising cumulus olivine and plagioclase. The sharp lower contact and the gradational contact with the overlying gabbroic rocks has been shown in drill core (Fig. 4). The Waterberg troctolite is interpreted to be the result of magma mingling and mixing, and is part of a fractionating sequence eroding the earlier harzburgite. Consequently, based on available data, it is not believed to be the direct lateral equivalent of the Troctolite Marker in the Northern Lobe, which itself is interpreted to be at least partly an influx of primitive magma into a pre-existing Main Zone (Tanner et al., 2014). The PGE-undepleted Troctolite Marker and the cryptic pyroxenite intrusions described by these workers highlight the significant lateral and vertical variations in the Northern Lobe. Furthermore, although the work of Ashwal et al. (2005) and Roelofse and Ashwal (2012) provides a detailed stratigraphy for most of the Northern Lobe, about 490 m of stratigraphy are unaccounted for. Most crucially, the missing segment is at the base of the troctolite marker where ultramafic rocks might be expected.

Above the olivine-bearing rocks is a package of noritic to gabbronoritic rocks, grading into magnetite-bearing gabbro/gabbronorite. The gabbroic rocks are typically taken to be the equivalent of the Northern Lobe's Main and Upper Zone given their mineralogy. While this may be the case, gabbroic rocks are typical of evolving layered mafic intrusions and their occurrence does not necessitate a connection of magma conduits between the Northern Lobe and the project area.

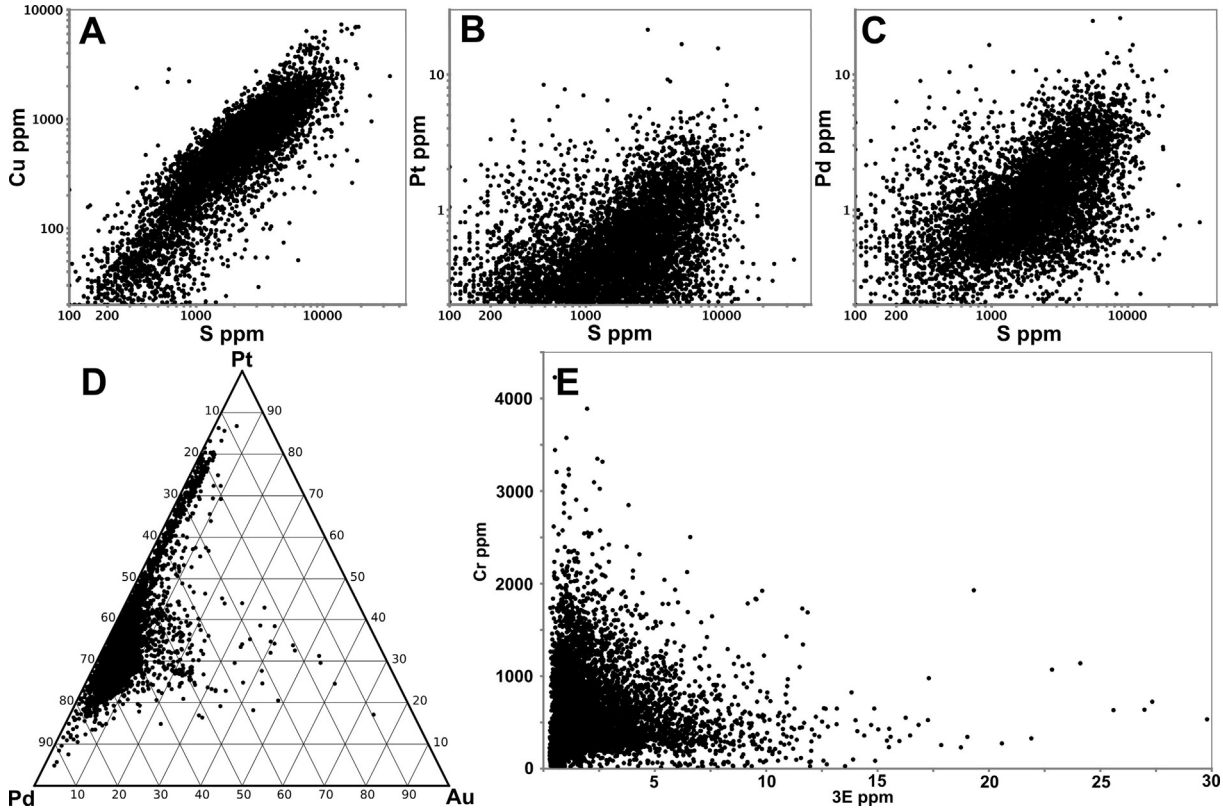

Fig. 12. A-C: Binary variation diagrams of chalcophile elements vs sulfur. There is an excellent correlation between Cu and S and a very weak correlation between S and Pt/Pd. D: Ternary diagram showing the relative proportions of Pt, Pd, and Au for the assays for the project area. E) Pt + Pd + Au vs Cr diagram highlighting the anti-correlation of precious metals and Cr-rich lithologies. Data filtered for Pt and Pd > 0.1 ppm, c. 9500 assays. Sulfide-bearing zones were preferentially sampled by PTM geologists.

Table 2

Correlation	Pt	Pd	Rh	Au	Cu	Ni	S
Pt	1	0.85	0.71	0.58	0.52	0.56	0.38
Pd	0.85	1	0.72	0.62	0.62	0.66	0.47
Rh	0.71	0.72	1	0.19	0.13	0.34	0.1
Au	0.58	0.62	0.19	1	0.74	0.45	0.45
Cu	0.52	0.62	0.13	0.74	1	0.66	0.74
Ni	0.56	0.66	0.34	0.45	0.66	1	0.62
S	0.38	0.47	0.1	0.45	0.74	0.62	1

The lower part of the succession hosts autoliths of Cr-enriched, olivine-bearing orthopyroxenite (which are therefore older). The exact lateral distribution of these rocks is currently poorly understood, and some may represent either rafts or perhaps simultaneously intruded sills. Where these rocks have been assimilated by younger intrusive phases, the resulting drill core sections are characterized by increased Cr levels (Figs. 13 and 14). Additionally, given their unmineralized nature, a commensurate drop in PGE levels can be observed in the assay intervals including these autoliths (Figs. 13 and 14).

Highest PGE grade intervals are often found in zones of intense alteration of primary silicates and may contain sulfide stringers and veins. Both features suggest some remobilization of initial sulfides, leading to a decoupling of sulfides and to a more limited degree of Pt and Pd. This process can be observed in the company assay data presented earlier, where Pd is remobilized preferentially over Pt (Barnes and Liu, 2012). Whether this process has an effect on the overall Pt/Pd ratio is currently undetermined.

Major element whole-rock geochemistry places the rocks in three distinct groups, representing the Cr-enriched marginal orthopyroxenite, the harzburgite of the Ultramafic Sequence, and the Troctolite-Gabbronorite-Anorthosite Sequence and Upper Zone. Rocks of the TGA Sequence form a continuous trend from high-Mg, olivine-rich troctolite to the magnetite-bearing gabbroic rocks of the Upper Zone. This trend may indicate that the TGA Sequence and the Upper Zone of the Waterberg Succession form a continuum and should be grouped together. The marginal gabbroic rocks resemble the TGA rocks in chemistry and mineralogy, and may represent downward injections into older units. Outliers in troctolite composition may be related to variable amounts of oikocrystic orthopyroxene and contamination by the underlying harzburgite and orthopyroxenite. Trends of harzburgite and troctolite differ, suggesting the crystallization of harzburgite from a more Mg-rich liquid and consequently the crystallization of more Mg-rich olivine.

Normalized REE pattern show near uniformity (e.g. fairly consistent Ce/Yb, Th/Nd) with a minor stratigraphic increase in abundances. Except for Eu, all REE are incompatible in the cumulus phases of the succession (olivine, orthopyroxene, plagioclase, clinopyroxene), which is reflected in the primitive mantle-normalized diagrams. Accessory phases (other than zircon) that would concentrate LREE have not been observed, and hence the REE budget is controlled by intercumulus liquid (Maier and Barnes, 1998). Normalized REE values below one are interpreted to reflect the fact that the rocks of the succession are crystal cumulates. The incompatible element budget of the parental magma was either retained in a staging chamber, or lost with migrating interstitial liquid. The variations in incompatible elements and REE contents and the associated extreme outliers, particularly in the basal rocks, are interpreted to represent wall rock contamination. Gabbroic rocks are characterized by $Rb_N < Ba_N$, while the opposite is true for ultramafic rocks. Troctolite Rb/Ba_N are approx. 1, again suggesting contamination of troctolite by underlying harzburgites. Estimates of trapped liquids using La or Zr (not shown; Maier and Barnes, 1999; McDonald et al.,

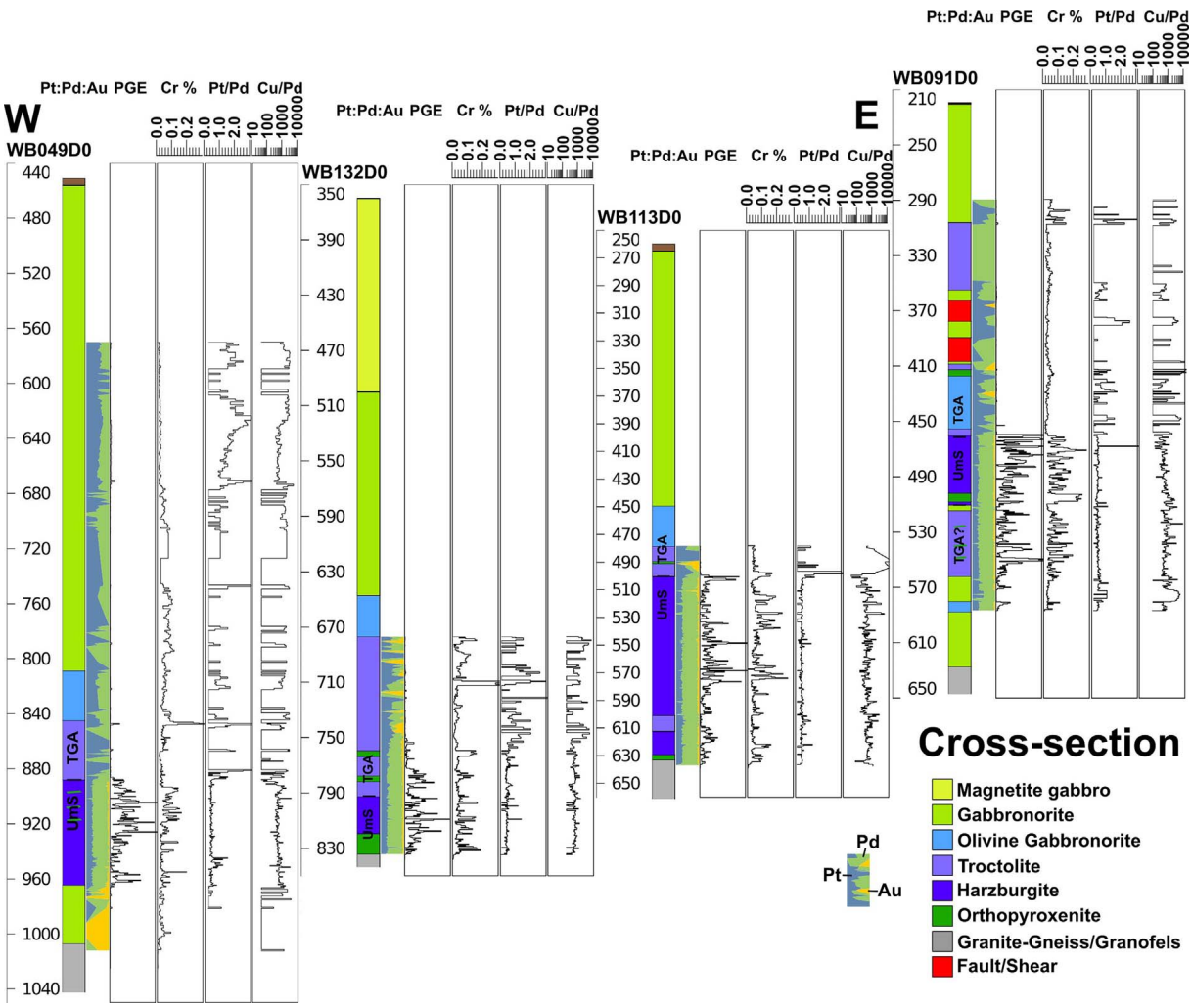

Fig. 13. Cross section through the study area as shown in Fig. 3. Columns presented show dominant lithology, the grade of Pt + Pd + Au, Cr%, Pt/Pd, and Cu/Pd extracted from PTM's database. PGE units have been omitted.

2009) exhibit a good correlation with peaks in incompatible element abundances. Given the interaction of pyroxenites and granite-gneisses observed in drill core, the validity of these calculations, however, is questionable for the project area. The slight upward stratigraphic increase in LREE observed is interpreted to be related to the increased proportions of clinopyroxene in the rocks. Troughs for the elements Th, Rb, Nb, and Ta are fairly typical for Bushveld rocks, and generally interpreted to represent contamination by lower-mid continental crust (Barnes and Maier, 2002).

5.2. Correlation with the Aurora Project

McDonald et al. (2017) recently presented data for the Aurora Project south of the Waterberg Project. The data presented in their work may be used to create a simplified and continuous emplacement model. At this point, most areas of the Northern Lobe are, however, not nearly as well-researched as the well-exposed open cut mines at Sandsloot. Caution and reliance on published data is therefore needed when correlating individual prospects.

McDonald et al. (2017) describe the Aurora Project as consisting of three main units, namely Unit 1 with peridotites and melagabbronorites, Unit 2 with gabbronorites and leucogabbronorites and Unit 3 comprising pigeonite gabbronorites. Additionally, Aurora comprises zones of sometimes pegmatitic magnetite gabbros and olivine-bearing gabbroic rocks. Mineralization is hosted predominantly by felsic rocks. The mineralogical details and geochemical data provided in their work suggests the following correlation:

Unit 1 at Aurora is characterized by orthopyroxenite, enrichment in Cr and consequently high Cr/MgO ratios. These features suggest that Unit 1 might correlate with the Cr-rich marginal orthopyroxenites described for the succession in the project area. This interpretation is supported by mineralogy and similar trends and positions on bivariate major and trace element plots and close to identical trace element ratios.

Both Unit 2 and 3 at Aurora are more evolved gabbroic rocks interpreted to correlate with the upper TGA Sequence of the project area. This interpretation is again supported by both mineralogical and geochemical features. Where developed, the upper TGA Sequence in the Waterberg Succession hosts two mineralized zones, often with a middling in between. It features olivine-bearing rocks, the appearance of pegmatites, and pigeonite. This is comparable to the variable nature of rocks in the Aurora Project, also characterized by several mineralized zones. Geochemically, available data for the upper TGA Sequence again shares similar positions on bivariate plots and almost identical trace element ratios with the Aurora Project.

The main geochemical difference between the two deposits exists in Rb/Ba_N ratios, with generally lower values for Aurora. McDonald et al. (2017) report a carbonate overprint and carbonate assimilation for the Aurora project. No significant carbonate has been found at the Waterberg, indicating purely granite-gneiss host rocks. The differing Rb/Ba_N ratios may therefore be the result of different host rocks.

In terms of precious metals, the Aurora Project is characterized by

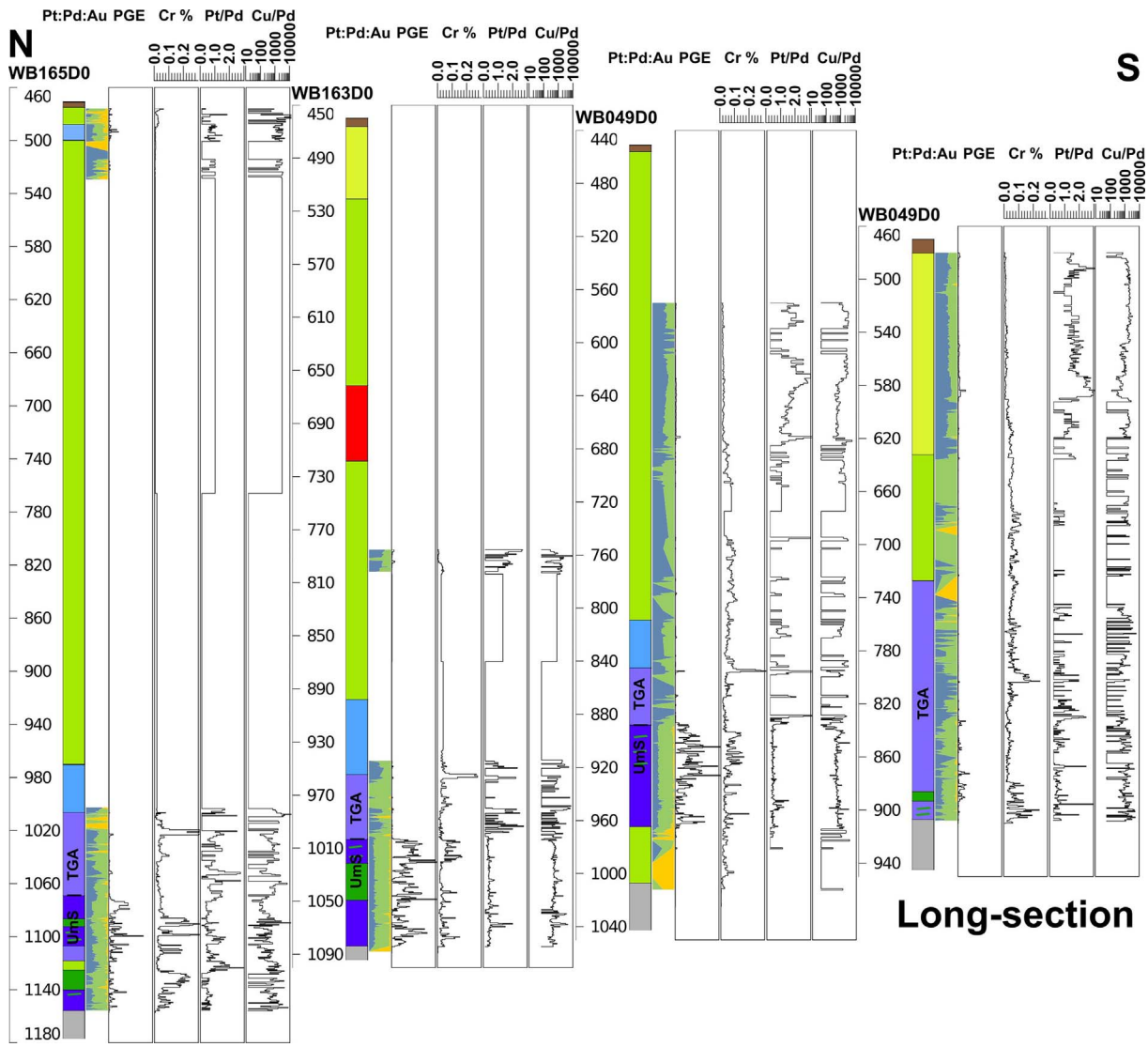

Fig. 14. Long section through the study area as shown in Fig. 3. Color scheme as in Fig. 13. Columns presented show dominant lithology, the grade of Pt + Pd + Au, Cr%, Pt/Pd, and Cu/Pd extracted from PTM's database. In contrast to the previous section, harzburgite thickness and associated PGE grade decreases towards the N and S. PGE units have been omitted.

approximately 20% Au in its precious metals budget (Fig. 16). This also holds true for the T Zone of the Waterberg Project. It is worth noting, however, that elevated Au/PGE ratios have not only been recorded at Aurora, the T Zone and Moorddrift (Harmer et al., 2004; Maier et al., 2008; McDonald and Harmer, 2010; Maier and Barnes, 2010; Holwell et al., 2013; McDonald et al., 2017), but also for the Upper Reef at Turfspruit (Yudovskaya et al., 2017) and for other offset-reefs from around the world (e.g. Skaergaard, Rincón del Tigre). Hence, elevated Au may be a feature associated with higher stratigraphic position in the mafic sequence, given no previous metal depletion. Considering the weak grade at Aurora compared to the Waterberg Project, Aurora might represent a southern extension of the Waterberg Succession rather than the other way around.

This possible correlation between T Zone mineralization and the Aurora Project does not account for the economically significant F mineralized Zone, which is located stratigraphically below the T Zone. Following the argument of Aurora being located in the upper Main Zone (McDonald et al., 2017), the F Zone would have to represent a highly unusual, richly-mineralized lower Main Zone of olivine-bearing rocks, i.e. the Troctolite Marker, or a marginal, very northern expression of the Critical Zone, i.e. the Platreef.

It is crucial to note, that on the farm Harriet's Wish in the far north of the Northern Lobe (Fig. 2A) the igneous units exhibit a pronounced change in strike direction from NNW to NNE when crossing the Hout River Shear Zone. The shear zone itself has, as far as the authors are aware, not been intersected in drill core. Despite the mineralogical and geochemical similarities described above, the exact nature of the relationship of Waterberg Project and Aurora Project therefore still needs to be established.

5.3. Correlation with the Platreef

Given that the Aurora Project does not represent a satisfactory correlative for the F Zone, the data presented can be compared with the Platreef in the south of the Northern Lobe. Mineralization in the F Zone of the Waterberg Succession is characterized by its anti-correlation with Cr, a Pt/Pd ratio of 0.6 and approximately 5% Au in the metal budget (Fig. 16). Ni/Cu is significantly higher than other Northern Lobe mines at 6–8. Chondrite-normalized PGE patterns show mildly fractionated IPGE and significantly enriched and also mildly fractionated PPGE.

The PGE patterns and ratios resemble those observed at various Platreef projects (Maier et al., 2008 and references therein, Yudovskaya et al., 2017) and what is typical for ultramafic hosts in the Bushveld Complex (Naldrett et al., 2011). The slightly higher fractionation

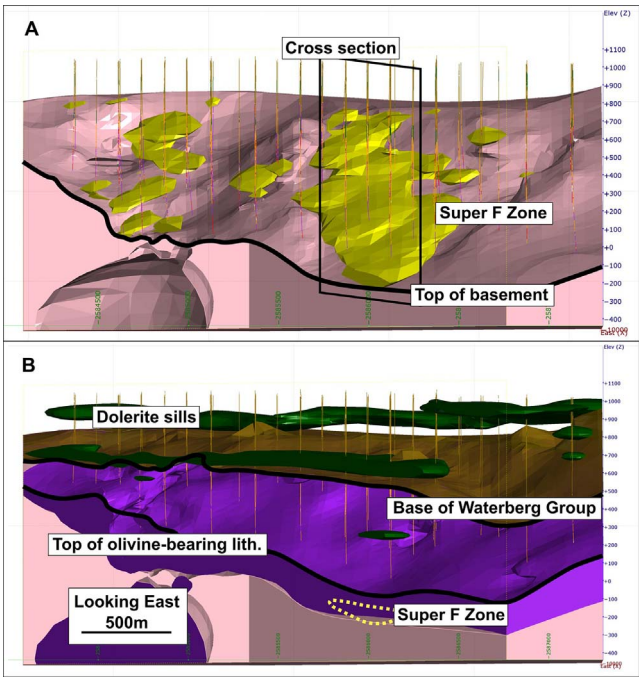

Fig. 15. Simplified 3D model of the project area. A: Shown is the geometry of the basement and in yellow a > 1 g/t 3E (Pt + Pd + Au) grade shell. The mineralization envelope has a chonolith-shape and is trending in a NE direction. Also shown is the position of holes studied (Fig. 13). B: This panel shows the distribution of the olivine-bearing rocks of the Ultramafic and lower TGA Sequence as logged in PTM's database. The erosional unconformity bringing Waterberg Group sediment in contact with mafic rocks and the dolerite sills are also shown. Note the vertical offset between the two dolerite sheets, perhaps indicating fault control. (For interpretation of the references to color in this figure legend, the reader is referred to the web version of this article.)

observed between IPGE and PPGE may be related to IPGE (and chromite) retardation somewhere at depth. The low Pt/Pd ratios are typical for those recorded for the lower Platreef (e.g. Kinnaird, 2005), while the (Pt + Pd)/Au and Ni/Cu place the F Zone in a field with Platreef exploration and mining projects (Fig. 4 in McDonald et al., 2017; our data would need adjustment due to its harzburgite host). The absence of a correlation between PGE and S is typical for disseminated mineralization at the base of the Platreef (Hutchinson and Kinnaird, 2005). The poor correlation between the PGE and S is ascribed to the remobilization and partial removal of sulfides after emplacement, thereby selectively remobilizing Pd over Pt. Cr/MgO ratios are consistently low and dissimilar to the Platreef unit (McDonald and Holwell, 2011). Detailed comparisons of the F Zone with the lower part of the Troctolite Marker are hampered by the lack of published and peer-reviewed descriptions and data.

Analogously to the Platreef, the mineralized harzburgites and feldspathic pyroxenites are interpreted to have been emplaced as sill- or chonolith-like bodies. Cross- and long-sections as well as a 3D representation of one of the Super F Zones have been presented in Figs. 13, 14 and 15, respectively. In these figures, it can be seen that where the these lithologies are absent, their space it taken up by the otherwise overlying TGA Sequence. This is particularly apparent in Fig. 15, where grade is sparse above the basement high in the center of the figure, and increases both to the north and south.

In summary, the lower mineralized zone of the Waterberg Project has been shown to have similarities with the Platreef, however, there are clear differences. Consequently, the Waterberg Project does not simply represent a northern Platreef.

5.4. A preliminary model

Any model for the Waterberg Succession must account for the following observations (Kinnaird et al., 2014, 2017; Huthmann et al., 2016):

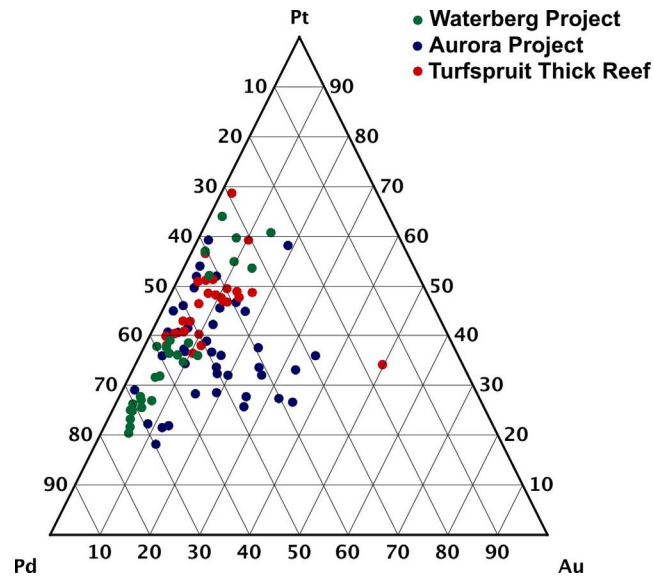

Fig. 16. Ternary diagram for Pt, Pd and Au displaying data for the Waterberg Project, the Aurora Project (McDonald et al., 2017) and Turfspruit (Yudovskaya et al., 2017). It can be seen, that Aurora rocks are relatively Au-rich whereas F Zone rocks from the Waterberg Project are Pd-rich.

- The Waterberg Succession contains a magnetite-bearing gabbroic Upper Zone, a mineralized Troctolite-Gabbronorite-Anorthosite Sequence and a lower, mineralized Ultramafic Sequence of harzburgite and feldspathic pyroxenite.
- The troctolite of the Waterberg Succession is a true plagioclase and olivine cumulate unconformably overlying ultramafic rocks. It is characterized by significant thickness, high-Mg, and the fractionation into olivine norite and later gabbronorite.
- The overall thickness of the Waterberg Succession is approximately 25% of the Northern Lobe, however, due to an erosional unconformity an unknown amount of material (several km?) is missing, and roof rocks of unknown nature have as of yet not been intercepted in drill core.
- The mineralization of the Waterberg T Zone contains approximately 20% Au in the metal budget.
- Based on chemistry, the Aurora Project may represent the southern margin of the Waterberg Project.
- Despite being hosted by harzburgites rather than pyroxenites, the F Zone mineralization shares certain characteristics with the Platreef. It is Pd-dominated and Au-poor, however, Cr/MgO are dissimilar from the Platreef. The Waterberg's F Zone does not form reefs and mineralization occurs along high-aspect ratio elongated bodies or chonoliths.
- Geochemical results presented show Bushveld-type cumulate signatures.

A simplified model for the evolution of the Waterberg Succession is presented in Fig. 17. The magmatic history of the area is believed to have started with finger-like intrusions of marginal orthopyroxenites intruding into a host rock of granite-gneiss and perhaps overlying sedimentary rocks. Unlike the Northern Lobe, the Waterberg Succession is situated in the Southern Marginal Zone of the Limpopo Belt (van Reenen et al., 1987), wedged in between the Hout River and Palala Shear Zones. Given the tectonic setting of the Limpopo Belt, this initial emplacement may have been facilitated either by pre-existing anisotropies related to faulting or perhaps ongoing faulting during the time of emplacement (Schaller et al., 1999; Clarke et al., 2009; Lightfoot and

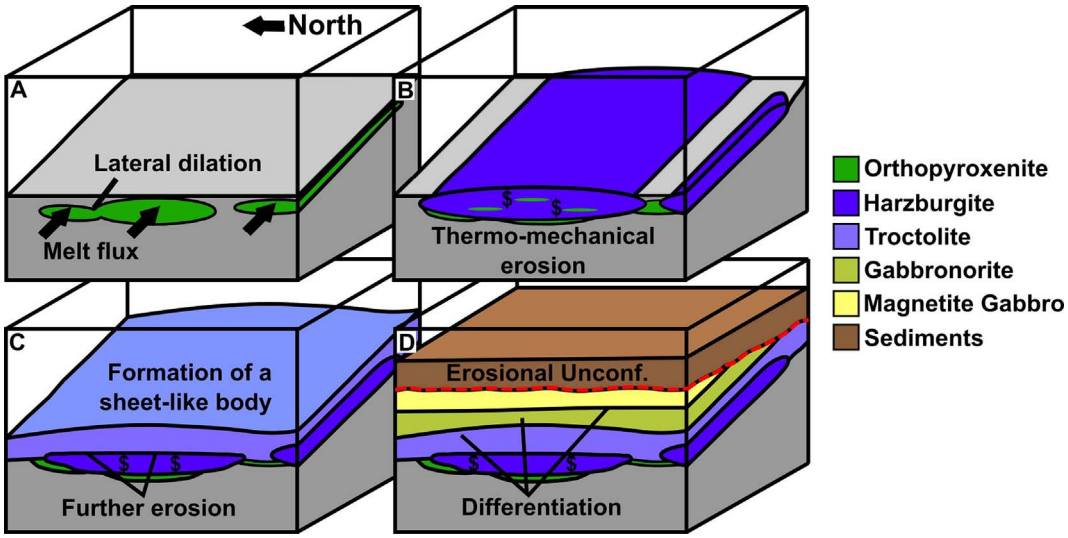

Fig. 17. Conceptual model for the emplacement of the lower part (excluding the T Zone mineralization) of the Waterberg Succession. A: Emplacement of marginal orthopyroxenites as finger-like elongated bodies. Lateral dilation with continuing magma flow. B: Emplacement of harzburgitic magma and sulfides by thermo- mechanical erosion of earlier intrusive phases and the host rock. C: Emplacement of troctolitic magma, marking the departure from a finger-like geometry and the formation of magma sheets. D: After the emplacement and fractionation of more magma, the area experienced extensive uplift and the deposition of Waterberg Group Sediments on an erosional unconformity.

Evans-Lamswood, 2015). Fig. 17 displays the initial stages near a possible basement - cover sequence contact. Whether this is indeed the case is unknown, and depth of emplacement may instead be the depth of neutral buoyancy of the ascending magma. Given the age and location of the Waterberg Succession (Huthmann et al., 2016), the magmas are of course ultimately related to the Bushveld Large Igneous Province.

With increasing magma flux, the magma conduits would experience lateral dilation until eventually forming larger elongated lobes. Maximum liquid flux would be focused on their respective cores, where the crystallization is suppressed due to the high heat flux (Hon et al., 1994). These heated zones of weakness could then be utilized by subsequent intrusion of parental crystal-rich liquids for the harzburgites, in the process widening the conduit while assimilating and transporting earlier rocks (Robertson et al., 2015). The harzburgites are thought to have acted as the transport medium for sulfide droplets, perhaps remobilizing dense sulfide from some initial staging zone (McDonald et al., 2009). Given the tube-like shape of the grade shells and the fairly even distribution of grade throughout the shell, a slumping of sulfides along the basement is not considered viable. Mungall and Brenan (2014) recently demonstrated extremely high partition coefficients of 10^5 to 10^6 for PGE. This means, that the kinetics of the interaction between sulfide liquid and magma and the architecture of the emplacement zone may be more important than large pools of sulfide liquid at depth. The geometry of the emplacement zone, in particular, may be responsible for the substantial thickness and grade of the Super F Zones. The position of the mineralized zones and the distribution of sulfides therein again appears to suggest, that the UmS represents zones of crystallization of the respective carrier liquids, and not a basal accumulation of sulfides. Constant Cu/Pd ratios observed in PTM's assay data suggest one common PGE reservoir for this particular Super F Zone. The Waterberg Succession has an indicated resource of > 24 million ounces 4E (Pt + Pd + Au + Rh). The deposit is still open at depth.

The reasons for sulfide saturation are only speculative at present. Possible options may be the assimilation of Cr-rich orthopyroxenites or mixing of successive melt fluxes. Given the granite-gneiss basement and the extreme scarcity of xenoliths, sulfide saturation due to sulfur-rich host-rock assimilations appears unlikely and the sulfur source is under investigation. Detailed petrographic analysis of a wide range of thin sections confirms the remobilization of sulfides observed in core and suspected from geochemical data, and hence the original distribution and mineralogy of the ore minerals is uncertain.

Following the emplacement of mineralized harzburgitic lithologies, any subsequent intrusion could utilize the extensive pre-heating of country rocks to form a more laterally extensive sheet of troctolites by thermo-mechanical erosion. This was perhaps assisted by pre-existing anisotropies along a basement sedimentary rock interface. At this point in time, the succession was moving from a stage of finger- like liquid flow and lateral dilation to a stage of sheet-like lobes with sufficient thickness to allow for in-situ fractionation. This ultimately led to the formation of a sequence of troctolites-gabbronorites-magnetite-bearing gabbros and to a transition from heterogeneous to homogeneous flow. It is envisioned, that the formation of troctolitic units was related to the mixing of gabbroic and peridotitic crystal-rich magmas in the feeder zone of the succession (Renna and Tribuzio, 2011; Saper and Liang, 2014). The subsequent in-situ fractionation of gabbroic magmas may have been disturbed by new cryptic influxes of more gabbroic liquids (cf. Tanner et al., 2014). Fractionation may have led to rocks comparable to what can be seen in the Upper Zone of the Northern Lobe (Ashwal et al., 2005), however, in the Waterberg Project this zone has been eroded. Mineralized harzburgite cores at the base of the troctolite were preserved, and the extensive alteration and sulfide remobilization in the harzburgite may be a sign of continuing heat and fluid flux in the system. The occasional pegmatoidal and vari-textured rocks throughout the succession perhaps attest to this continuing interaction of heat with the footwall.

The exact nature of the connection between Waterberg Project and the aforementioned Aurora Project can only be estimated. Taking into account the occurrence of early orthopyroxenites and later gabbroic lithologies, perhaps both areas were connected intermittently with assimilation of dolomite being locally important at Aurora. Correlation of the two projects might indicate that both of them form a northern magmatic basin. This basin is internally subdivided by the Hout River and other small shear zones and separated from the south by a basement high south of Aurora (van der Merwe, 1976, 1978, Fig. 2A). The occurrence of magnetitites on the farm Harriet's Wish (but not found in the project area) and recent Sr isotopic results (Huthmann et al., 2017) complicate the situation and require further study.

As a final step, uplift and later subsidence led to an erosional unconformity and the deposition of Waterberg Group Sediments on top of the succession. This step is crucial, as without significant uplift and erosion the succession might have been covered by several kilometers

of evolved rocks.

The model presented above requires the intrusion of two distinct magmas during the course of the formation of the succession, one being peridotitic and one gabbroic in character. Given the similarities of the Ultramafic Sequence with the Platreef, it is envisioned that it may have crystallized from a Critical Zone-type magma. How a presumably Cr-rich Critical Zone magma crystallized the overall Cr-poor rocks is not resolved in detail. This does not imply a direct connection of the Waterberg area with either the main Bushveld Complex or the Northern Lobe, but rather refers to the fact that all intrusions belong to the same large igneous province.

6. Conclusion

The Waterberg Succession is a truly outstanding and exciting new PGE discovery. It shares features with mining and exploration prospects to the south, while simultaneously exhibiting unique characteristics. The combination of rock types, type and distribution of the mineralization, and tectonic setting is unique and presented here for the first time. Based on observations and geochemical results, the project area may be linked with the Aurora Project to the south, with both projects possibly representing a separate basin rather than a marginal extension of the Northern Lobe. A first conceptual model for the area has been presented and shows how recent advances in our understanding of partition coefficients, fluid dynamics, and the continued work of colleagues in other parts of the Bushveld lead to a better understanding of this magmatic system.

The conclusion that the Waterberg Succession does not represent a simple strike extension of the Northern Lobe is excellent news for explorers of the Bushveld Complex. It demonstrates, that cooperation of industry and academia can lead to significant discoveries in well-explored terrains. Rather than obstructing deposit formation, structural features and sedimentary sequences may aid by concentrating melt ow and facilitating later uplift.

Acknowledgements

We would like to acknowledge the support and funding received from Platinum Group Metals. We would also like to acknowledge CIMERA. The work at IGEM RAS was supported by the Russian Foundation for Basic Research (grant 17-05-00456). The manuscript greatly benefited from the detailed comments by P. Lightfoot and W. Maier. We thank the editor F. Pirajno for his assistance.

Appendix A. Supplementary data

Supplementary data associated with this article can be found, in the online version, at http://dx.doi.org/10.1016/j.oregeorev.2017.10.023.

References

Ashwal, L.D., Webb, S.J., Knoper, M.W., 2005. Magmatic stratigraphy in the Bushveld Northern Lobe: continuous geophysical and mineralogical data from the 2950 m Bellevue drillcore. S. Afr. J. Geol. 108 (2), 199–232.
Barnes, S.J., Cruden, A.R., Arndt, N., Saumur, B.M., 2016. The mineral system approach applied to magmatic Ni Cu PGE sulphide deposits. Ore Geol. Rev. 76 (C), 296–316.
Barnes, S.J., Liu, W., 2012. Pt and Pd mobility in hydrothermal fluids: evidence from komatiites and from thermodynamic modelling. Ore Geol. Rev. 44 (C), 49–58.
Barnes, S.-J., Maier, W.D., 2002. Platinum-Group Element Distributions in the Rustenburg Layered Suite of the Bushveld Complex, South Africa. In: Cabri, L. J. (Ed.), The Geology, Geochemistry, Mineralogy and Mineral Beneficiation of Platinum-Group Elements. Canadian Institute of Mining, Metallurgy and Petroleum Special Volume 54, pp. 431–458.
Barton, J.M., Klemd, R., Zeh, A., 2006. The Limpopo belt: a result of Archean to Proterozoic, Turkic-type orogenesis? Geol. Soc. Am. Spec. Pap. 405, 315–332.
Buick, I.S., Maas, R., Gibson, R.L., 2001. Precise U-Pb titanite age constraints on the emplacement of the Bushveld Complex, South Africa. J. Geolog. Soc. 158 (1), 3–6.
Callaghan, C.C., Eriksson, P.G., Snyman, C.P., 1991. The sedimentology of the Waterberg Group in the Transvaal, South Africa: an overview. J. Afr. Earth Sc. 13 (1), 121–139.
Cawthorn, R.G., Webb, S.J., 2001. Connectivity between the western and eastern limbs of the Bushveld Complex. Tectonophysics 330 (3–4), 195–209.
Clarke, B., Uken, R., Reinhardt, J., 2009. Structural and compositional constraints on the emplacement of the Bushveld Complex, South Africa. Lithos 111 (1–2), 21–36.
Corcoran, P.L., Bumby, A.J., Davis, D.W., 2013. The Paleoproterozoic Waterberg Group, South Africa: provenance and its relation to the timing of the Limpopo orogeny. Precambr. Res. 230, 45–60.
Dorland, H.C., Beukes, N.J., Gutzmer, J., Evans, D.A.D., Armstrong, R.A., 2006. Precise SHRIMP U-Pb zircon age constraints on the lower Waterberg and Soutpansberg Groups, South Africa. S. Afr. J. Geol. 109 (1–2), 139–156.
Eales, H.V., Cawthorn, R.G., 1996. The bushveld complex. In: Layered Intrusions Elsevier, pp. 181–229.
Finn, C.A., Bedrosian, P.A., Cole, J.C., Khoza, T.D., Webb, S.J., 2015. Mapping the 3D extent of the Northern Lobe of the Bushveld layered mafic intrusion from geophysical data. Precambr. Res. 268, 279–294.
Good, N., de Wit, M.J., 1997. The Thabazimbi-Murchison lineament of the Kaapvaal Craton, South Africa: 2700 Ma of episodic deformation. J. Geolog. Soc. 154 (1), 93–97.
Grobler, D. F., Nielsen, S. A., Broughton, D., 2012. Upper Critical Zone (Merensky Reef-UG2) correlates within the Platreef on Turspruit Farm, northern limb, Bushveld Complex. In: 6th Platreef Workshop 8th–10th May 2015.
Harmer, R. E., Pillay, N., Davis, P. G., 2004. The Aurora Project - Main Zone hosted PGE-base metal mineralisation at the northern outcrop limit of the Bushveld Northern Limb, north of Mokopane. In: 1st Platreef Workshop, 16–19 July.
Holwell, D.A., Armitage, P.E.B., McDonald, I., 2005. Observations on the relationship between the Platreef and its hangingwall. Appl. Earth Sci. 114 (4), 199–207.
Holwell, D.A., Jones, A., Smith, J.W., Boyce, A.J., 2013. New mineralogical and isotopic constraints on Main Zone-hosted PGE mineralisation at Moorddrift, northern Bushveld Complex. Miner. Deposita 48 (6), 675–686.
Holwell, D.A., Jordaan, A., 2006. Three-dimensional mapping of the Platreef at the Zwartfontein South mine: implications for the timing of magmatic events in the northern limb of the Bushveld Complex, South Africa. Appl. Earth Sci. 115 (2), 41–48.
Holwell, D.A., McDonald, I., 2006. Petrology, geochemistry and the mechanisms determining the distribution of platinum-group element and base metal sulphide mineralisation in the Platreef at Overysel, northern Bushveld Complex, South Africa. Mineralium Deposita 41 (6), 575–598.
Holzer, L., Frei, R., Barton Jr., J.M., Kramers, J.D., 1998. Unraveling the record of successive high grade events in the Central Zone of the Limpopo Belt using Pb single phase dating of metamorphic minerals. Precambr. Res. 87 (1–2), 87–115.
Hon, K., Kauahikaua, J., Denlinger, R., Mackay, K., 1994. Emplacement and inflation of pahoehoe sheet flows: Observations and measurements of active lava flows on Kilauea Volcano, Hawaii. Geolog. Soc. Am. Bull. 106 (3), 351–370.
Hulbert, L.J., von Gruenewaldt, G., 1982. Nickel, copper, and platinum mineralization in the lower zone of the Bushveld Complex, south of Potgietersrus. Econ. Geol. 77 (6), 1296–1306.
Hulbert, L.J., von Gruenewaldt, G., 1985. Textural and compositional features of chromite in the lower and critical zones of the Bushveld Complex south of Potgietersrus. Econ. Geol. 80 (4), 872–895.
Hutchinson, D., Kinnaird, J.A., 2005. Complex multistage genesis for the Ni Cu PGE mineralisation in the southern region of the Platreef, Bushveld Complex, South Africa. Appl. Earth Sci. 114 (4), 208–224.
Huthmann, F.M., Yudovskaya, M.A., Elburg, M.A., Kinnaird, J.A., 2017. The Sr isotopic stratigraphy of the far northern Bushveld Complex. S. Afr. J. Geol. 120 (4) (in press).
Huthmann, F.M., Yudovskaya, M.A., Frei, D., Kinnaird, J.A., 2016. Geochronological evidence for an extension of the Northern Lobe of the Bushveld Complex, Limpopo Province, South Africa. Precambr. Res. 280, 61–75.
Kinnaird, J.A., 2005. Geochemical evidence for multiphase emplacement in the southern Platreef. Appl. Earth Sci. 114 (4), 225–242.
Kinnaird, J.A., Hutchinson, D., Schurmann, L., Nex, P.A.M., de Lange, R., 2005. Petrology and mineralisation of the southern Platreef: northern limb of the Bushveld Complex, South Africa. Mineralium Deposita 40 (5), 576–597.
Kinnaird, J.A., Nex, P.A.M., 2015. An Overview of the Platreef. In: Platinum- group element (PGE) mineralisation and resources of the Bushveld Complex, South Africa. An Overview of the Platreef. Council for Geoscience, South Africa, pp. 193–342.
Kinnaird, J.A., Yudovskaya, M.A., Botha, M.J., 2014. The Waterberg Extension to the Bushveld Complex. In: 11th International Platinum Symposium. Yekaterinburg, Russia.
Kinnaird, J.A., Yudovskaya, M.A., McCreesh, M.J.G., Huthmann, F.M., Botha, T.J., 2017. The Waterberg PGE Deposit – A typical mineralization in mafic-ultramafic rocks of the Bushveld Complex, South Africa. Econ. Geol. 112, 1367–1394.
Kramers, J.D., Mouri, H., 2011. The geochronology of the Limpopo Complex: A controversy solved. In: van Reenen, D.D., Kramers, J.D., McCourt, S., Perchuk, L.L. (Eds.), Origin and Evolution of Precambrian High-grade Gneiss Terranes, with Special Emphasis on the Limpopo Complex of Southern Africa. Geological Society of America Memoir, pp. 85–106.
Kruger, F.J., 2005. Filling the Bushveld Complex magma chamber: lateral expansion, roof and floor interaction, magmatic unconformities, and the formation of giant chromitite, PGE and Ti-V-magnetitite deposits. Mineralium Deposita 40 (5), 451–472.
Lee, C.A., 1996. A review of mineralization in the Bushveld Complex and some other layered intrusions. In: Layered Intrusions Elsevier, pp. 103–145.
Lightfoot, P.C., Evans-Lamswood, D., 2015. Structural controls on the primary distribution of mafic-ultramafic intrusions containing Ni-Cu-Co (PGE) sulfide mineralization in the roots of large igneous provinces. Ore Geol. Rev. 64 (C), 354–386.
Lodders, K., 2003. Solar system abundances and condensation temperatures of the elements. Astrophys. J. 591 (2), 1220–1247.
Maier, W.D., Barnes, S.-J., 1998. Concentrations of rare earth elements in silicate rocks of

the Lower, Critical and Main Zones of the Bushveld Complex. Chem. Geol. 150 (1–2), 85–103.
Maier, W.D., Barnes, S.-J., 1999. Platinum-Group Elements in Silicate Rocks of the Lower, Critical and Main Zones at Union Section, Western Bushveld Complex. J. Petrol. 40 (11), 1647–1671.
Maier, W.D., Barnes, S.-J., 2010. The petrogenesis of platinum-group element reefs in the Upper Main Zone of the Northern Lobe of the Bushveld Complex on the farm Moorddrift, South Africa. Econ. Geol. 105, 841–854.
Maier, W.D., De Klerk, L., Blaine, J., Manyeruke, T., Barnes, S.-J., Stevens, M.V.A., Mavrogenes, J.A., 2008. Petrogenesis of contact-style PGE mineralization in the northern lobe of the Bushveld Complex: comparison of data from the farms Rooipoort, Townlands, Drenthe and Nonnenwerth. Mineralium Deposita 43 (3), 255–280.
Manyeruke, T.D., 2007. Compositional and lithological variation of the Platreef on the farm Nonnenwerth, northern lobe of the Bushveld Complex: Implications for the origin of Platinum-group elements (PGE) mineralization. University of Pretoria (Ph.D. thesis).
McDonald, I., Harmer, R., Holwell, D.A., Hughes, H.S.R., Boyce, A.J., 2017. Cu-Ni-PGE mineralisation at the Aurora Project and potential for a new PGE province in the Northern Bushveld Main Zone. Ore Geol. Rev. 80, 1135–1159.
McDonald, I., Harmer, R.E., 2010. The Nature of PGE mineralization in the Aurora Project Area, Northern Bushveld Complex, South Africa. In: Jugo, P.J., Lesher, C.M., Mungall, J.E. (Eds.), 11th International Platinum Symposium.
McDonald, I., Holwell, D.A., 2011. Geology of the northern Bushveld Complex and the setting and genesis of the Platreef Ni-Cu-PGE deposit. In: Reviews in Economic Geology v. 17. Reviews in Economic Geology, pp. 297–327.
McDonald, I., Holwell, D.A., Armitage, P.E.B., 2005. Geochemistry and mineralogy of the Platreef and Critical Zone of the northern lobe of the Bushveld Complex, South Africa: implications for Bushveld stratigraphy and the development of PGE mineralisation. Miner. Deposita 40 (5), 526–549.
McDonald, I., Holwell, D.A., Wesley, B., 2009. Assessing the potential involvement of an early magma staging chamber in the generation of the Platreef Ni Cu PGE deposit in the northern limb of the Bushveld Complex: a pilot study of the Lower Zone Complex at Zwartfontein. Appl. Earth Sci. 118 (1), 5–20.
McDonald, I., Viljoen, K.S., 2006. Platinum-group element geochemistry of mantle eclogites: a reconnaissance study of xenoliths from the Orapa kimberlite, Botswana. Appl. Earth Sci. 115 (3), 81–93.
Molyneux, T.G., 1974. A geological investigation of the Bushveld Complex in Sekhukhuneland and part of the Steelpoort valley. Trans. Geolog. Soc. South Africa 329–338.
Mungall, J.E., Brenan, J.M., 2014. Partitioning of platinum-group elements and Au between sulfide liquid and basalt and the origins of mantle-crust fractionation of the chalcophile elements. Geochimica et Cosmochimica Acta 125 (C), 265–289.
Naldrett, A., Kinnaird, J.A., Wilson, A.H., Yudovskaya, M.A., Chunnett, G., 2011. Genesis of the PGE-enriched Merensky Reef and chromitite seams of the Bushveld Complex. In: Reviews in Economic Geology v. 17. Society of Economic Geologists, pp. 235–296.
Naldrett, A.J., 2010. Secular Variation of Magmatic Sulfide Deposits and Their Source Magmas. Econ. Geol. 105 (3), 669–688.
Nicoli, G., Stevens, G., Moyen, J.F., Frei, D., 2015. Rapid evolution from sediment to anatectic granulite in an Archean continental collision zone: the example of the Bandelierkop Formation metapelites, South Marginal Zone, Limpopo Belt, South Africa. J. Metamorph. Geol. 33 (2), 177–202.
Rajesh, H.M., Santosh, M., Wan, Y., Liu, D., Liu, S.J., Belyanin, G.A., 2014. Ultrahigh temperature granulites and magnesian charnockites: Evidence for Neoarchean accretion along the northern margin of the Kaapvaal Craton. Precambr. Res. 246, 150–159.
Renna, M.R., Tribuzio, R., 2011. Olivine-rich Troctolites from Ligurian Ophiolites (Italy): Evidence for Impregnation of Replacive Mantle Conduits by MORB- type Melts. J. Petrol. 52 (9), 1763–1790.
Robertson, J., Ripley, E.M., Barnes, S.J., Li, C., 2015. Sulfur Liberation from Country Rocks and Incorporation in Mafic Magmas. Econ. Geol. 110 (4), 1111–1123.
Roelofse, F., Ashwal, L.D., 2012. The Lower Main Zone in the Northern Limb of the Bushveld Complex a > 1.3 km Thick Sequence of Intruded and Variably Contaminated Crystal Mushes. J. Petrol. 53 (7), 1449–1476.
Saper, L., Liang, Y., 2014. Formation of plagioclase-bearing peridotite and plagioclase-bearing wehrlite and gabbro suite through reactive crystallization: an experimental study. Contrib. Miner. Petrol. 167, 985.
Schaller, M., Steiner, O., Studer, I., Holzer, L., Herwegh, M., 1999. Exhumation of Limpopo Central Zone granulites and dextral continent-scale transcurrent movement at 2.0 Ga along the Palala Shear Zone, Northern Province, South Africa. Precambr. Res. 96, 263–288.
Scoates, J.S., Friedman, R.M., 2008. Precise Age of the Platiniferous Merensky Reef, Bushveld Complex, South Africa, by the U-Pb Zircon Chemical Abrasion ID-TIMS Technique. Econ. Geol. 103 (3), 465–471.
Scoates, J.S., Wall, C.J., 2015. Geochronology of Layered Intrusions. In: Charlier, B., Namur, O., Latypov, R., Tegner, C. (Eds.), Layered Intrusions. Springer, Netherlands, Dordrecht, pp. 3–74.
Smirnov, A.V., Evans, D.A.D., Ernst, R.E., Söderlund, U., Li, Z.-X., 2013. Trading partners: Tectonic ancestry of southern Africa and western Australia, in Archean supercratons Vaalbara and Zimgarn. Precambr. Res. 224, 11–22.
Smit, C.A., Roering, C., van Reenen, D.D., 1992. The structural framework of the southern margin of the Limpopo Belt, South Africa. In: van Reenen, D.D., Roering, C., Ashwal, L.D., de Wit, M. J. (Eds.), The Archean Limpopo Granulite Belt: Tectonics and Deep Crustal Processes. Precambrian Research, pp. 51–67.
Sun, S.S., McDonough, W.F., 1989. Chemical and isotopic systematics of oceanic basalts: implications for mantle composition and processes. Geolog. Soc., London, Special Publ. 42 (1), 313–345.
Tanner, D., Mavrogenes, J.A., Arculus, R.J., Jenner, F.E., 2014. Trace Element Stratigraphy of the Bellevue Core, Northern Bushveld: Multiple Magma Injections Obscured by Diffusive Processes. J. Petrol. 55 (5), 859–882.
Treloar, P.J., Coward, M.P., Harris, N.B.W., 1992. Himalayan-Tibetan analogies for the evolution of the Zimbabwe Craton and Limpopo Belt. Precambr. Res. 55 (1–4), 571–587.
van der Merwe, M.J., 1976. The layered sequence of the Potgietersrus Limb of the Bushveld Complex. Econ. Geol. 71 (7), 1337–1351.
van der Merwe, M.J., 1978. The Geology of the Basic and Ultramafic Rocks of the Potgietersrus Limb of the Bushveld Complex (Ph.D. thesis).
van Reenen, D.D., Barton, J.M., Roering, C., Smith, C.A., Van Schalkwyk, J.F., 1987. Deep crystal response to continental collision: the Limpopo belt of southern Africa. Geology 15 (1), 11–14.
Vermaak, C.F., 1976. The Merensky Reef; thoughts on its environment and genesis. Econ. Geol. 71, 1270–1298.
von Gruenewaldt, G., Sharpe, M.R., Hatton, C.J., 1985. The Bushveld Complex; introduction and review. Econ. Geol. 80 (4), 803–812.
Walraven, F., 1997. Geochronology of the Rooiberg Group, Transvaal Supergroup, South Africa. Information Circular No. 316, Economic Geology Research Unit, University of the Witwatersrand.
Walraven, F., Hattingh, E., 1993. Geochronology of the Nebo Granite, Bushveld Complex. S. Afr. J. Geol. 96 (1/2), 31–41.
Webb, S.J., Cawthorn, R.G., Nguuri, T., James, D., 2004. Gravity modeling of Bushveld Complex connectivity supported by Southern African Seismic Experiment results. S. Afr. J. Geol. 107 (1–2), 207–218.
Wiebe, R.A., 1980. Commingling of contrasted magmas in the plutonic environment: examples from the Nain anorthositic complex. J. Geol. 88 (2), 197–209.
Willemse, J., 1969. The geology of the Bushveld Igneous Complex, the largest repository of magmatic ore deposits in the world. In: Magmatic Ore Deposits – A Symposium. pp. 1–22.
Wilson, A.H., 2012. A Chill Sequence to the Bushveld Complex: Insight into the First Stage of Emplacement and Implications for the Parental Magmas. J. Petrol. 53 (6), 1123–1168.
Wilson, A.H., 2015. The Earliest Stages of Emplacement of the Eastern Bushveld Complex: Development of the Lower Zone, Marginal Zone and Basal Ultramafic Sequence. J. Petrol. 56 (2), 347–388.
Yudovskaya, M.A., Kinnaird, J.A., Grobler, D.F., Costin, G., Abramova, V.D., Dunnett, T., Barnes, S.-J., 2017. Zonation of Merensky-Style Platinum-Group Element Mineralization in Turfspruit Thick Reef Facies (Northern Limb of the Bushveld Complex). Econ. Geol. 112 (6), 1333–1365.
Yudovskaya, M.A., Kinnaird, J.A., McCreesh, M.J.G., Frei, D., 2015. The lithology at the contact between the Bushveld Mafic Ultramafic sequence and overlying Waterberg sediments on the Waterberg. In: 6th Platreef Workshop 8th–10th May 2015. pp. 59–61.
Yudovskaya, M.A., Kinnaird, J.A., Naldrett, A.J., Rodionov, N., Antonov, A., Simakin, S., Kuzmin, D., 2013a. Trace-element study and age dating of zircon from chromitites of the Bushveld Complex (South Africa). Mineral. Petrol. 107 (6), 915–942.
Yudovskaya, M.A., Kinnaird, J.A., Sobolev, A.V., Kuzmin, D.V., McDonald, I., Wilson, A.H., 2013b. Petrogenesis of the Lower Zone olivine-rich cumulates beneath the Platreef and their correlation with recognized occurrences in the Bushveld Complex. Econ. Geol. 108, 1923–1952.
Zeh, A., Ovtcharova, M., Wilson, A.H., Schaltegger, U., 2015. The Bushveld Complex was emplaced and cooled in less than one million years results of zirconology, and geotectonic implications. Earth Planet. Sci. Lett. 418, 103–114.

Appendix B

Complete Detailed Core Logs

WB017D0

WB027D0

WB034D0

WB090D0

WB099D0

WB161D0

WB195D0

WE001D0

WE027D0

WE035D0

Appendix B: Core log WB017D0

Core-Log of Borehole WB017D0								
From (m)	**To (m)**	**Grain Size**	**Bottom Contact**	**Texture**	**Modal Proportions**	**Alteration**	**BMS**	**Rock Name**
0.00	1.96	M	Gradational	Poorly sorted	>90% quartz	-	-	Sandstone and mudstone
1.96	142.66	F-M-C	Sharp	Interlayered	>90% quartz	-	-	Sandstone, mudstone and siltstone
142.66	169.73	M-C	Sharp	Homogeneous	cpx>quartz> feldspar	Epidote	-	Dolerite sill
169.73	176.73	F-M-C	Gradational	Interlayered	>90% quartz	-	-	Sandstone, mudstone and siltstone
176.73	178.63	F-M	Gradational	Altered	>70% hematite	Hematite	-	Contact paleosol/Shale
178.63	202.90	M-C	Gradational	Equigranular	opx>plag>cpx>ol> mgt	Oxides	-	Ferro Gabbro
202.90	295.50	M-C	Gradational	Equigranular	opx> plag>cpx> mgt >10%	Chlorite	-	Magnetite gabbronorite
295.50	310.65	M-C	Sharp	Equigranular	opx>cpx>plag>mgt	Chlorite	-	Gabbronorite
310.65	314.00	PEG	Sharp	Pegmatoidal	opx>plag>cpx	Chlorite	-	Gabbronorite
314.00	459.90	M	Gradational	Equigranular	opx>cpx> in.pig> plag	Chlorite	-	Gabbronorite
459.90	470.50	M	Sharp	Homogeneous	opx>cpx>plag(interstitial)	Chlorite	>3%	Pyroxenite
470.50	539.20	M-C	Sharp	Equigranular	plag>opx>cpx	Chlorite	-	Leuco-gabbronorite
539.20	545.00	PEG	Sharp	Pegmatoidal	opx>plag>cpx	Chlorite	>2%	Gabbronorite
545.00	548.00	M	Sharp	Inequigranular	opx>plag>cpx>clay minerals	Chlorite	-	Altered Gabbronorite
548.00	620.10	M-C	Sharp	Equigranular	plag>opx>cpx	Chlorite	-	Leuco-gabbronorite
620.10	621.40	PEG	Sharp	Pegmatoidal	opx>plag>cpx	Chlorite	-	Gabbronorite
621.40	627.10	M-C	Gradational	Equigranular	opx>plag>cpx	Chlorite	-	Gabbronorite
627.10	631.70	M	Sharp	Homogeneous	opx>cpx>plag (interstitial)	-	-	Pyroxenite
631.70	634.00	PEG	Sharp	Pegmatoidal	opx>cpx>plag	Chlorite	-	Gabbronorite
634.00	647.75	M-C	Sharp	Homogeneous	opx>cpx>plag (interstitial)	-	<2%	Feldspathic pyroxenite
647.75	655.60	C	Gradational	Inequigranular	ol>opx	Serp/Chl	<3%	Harzburgite
655.60	693.20	M-C	Sharp	Equigranular	plag>opx>cpx	Chlorite	>5%	Leuco-gabbronorite
693.20	714.00	M-C	Sharp	Mottled	plag, cpx+mgt(oikocrysts)	Chlorite	-	Anorthosite
714.00	716.00	M	Sharp	Homogeneous	opx>cpx>plag (interstitial)	Chlorite	-	Pyroxenite
716.00	809.25	C	Sharp	Equigranular	opx>cpx>plag	-	-	Gabbronorite
809.25	810.36	C	Sharp	Mottled	plag, cpx(oikocrysts)	Chlorite	-	Anorthosite
810.36	939.64	M	Gradational	Equigranular	plag>opx>cpx>in.pig	Chlorite	-	Leuco-gabbronorite
939.64	943.43	M	Sharp	Homogeneous	opx>cpx>in.pig>plag	Chlorite	-	Pyroxenite
943.43	976.30	C	Gradational	Equigranular	opx>plag>cpx	Chlorite	-	Gabbronorite
976.30	1003.76	C	Gradational	Poikilitic	ol>plag>opx(oikocrysts)	Serp/Chl	-	Troctolite
1003.76	1016.00	M-C	Gradational	Inequigranular	ol>opx	Serp/Chl	>5%	Harzburgite
1016.00	1021.60	C	Gradational	Poikilitic	ol>plag(<20%)>opx(oikocryst	Serp/Chl	>5%	Mela-Troctolite
1021.60	1045.00	M	Gradational	Homogeneous	opx>cpx>plag (interstitial)	Chlorite	>7%	Feldspathic pyroxenite
1045.00	1047.00	M	Sharp	Homogeneous	opx>cpx>plag (interstitial)	Chlorite	>3%	Feldspathic pyroxenite
1047.00	1054.00	PEG	Sharp	Pegmatoidal	opx>cpx>plag (interstitial)	Chlorite	>10%	Feldspathic pyroxenite
1054.00	1077.40	M	Sharp	Homogeneous	opx>cpx>plag (interstitial)	Chlorite	>10%	Feldspathic pyroxenite
1077.40	1079.50	F-M	Sharp	Inequigranular	quartz>feldspar>phlogopite	Chlorite	-	Quartz-feldspar vein
1079.50	1084.00	M	Gradational	Homogeneous	opx>cpx>plag (interstitial)	Chlorite	>3%	Feldspathic pyroxenite
1084.00	1094.23	F-M	EOH	Inequigranular	quartz>feldspar>opx>cpx	Serp/Chl	-	Granofels

Appendix B: Core Log WB017D0

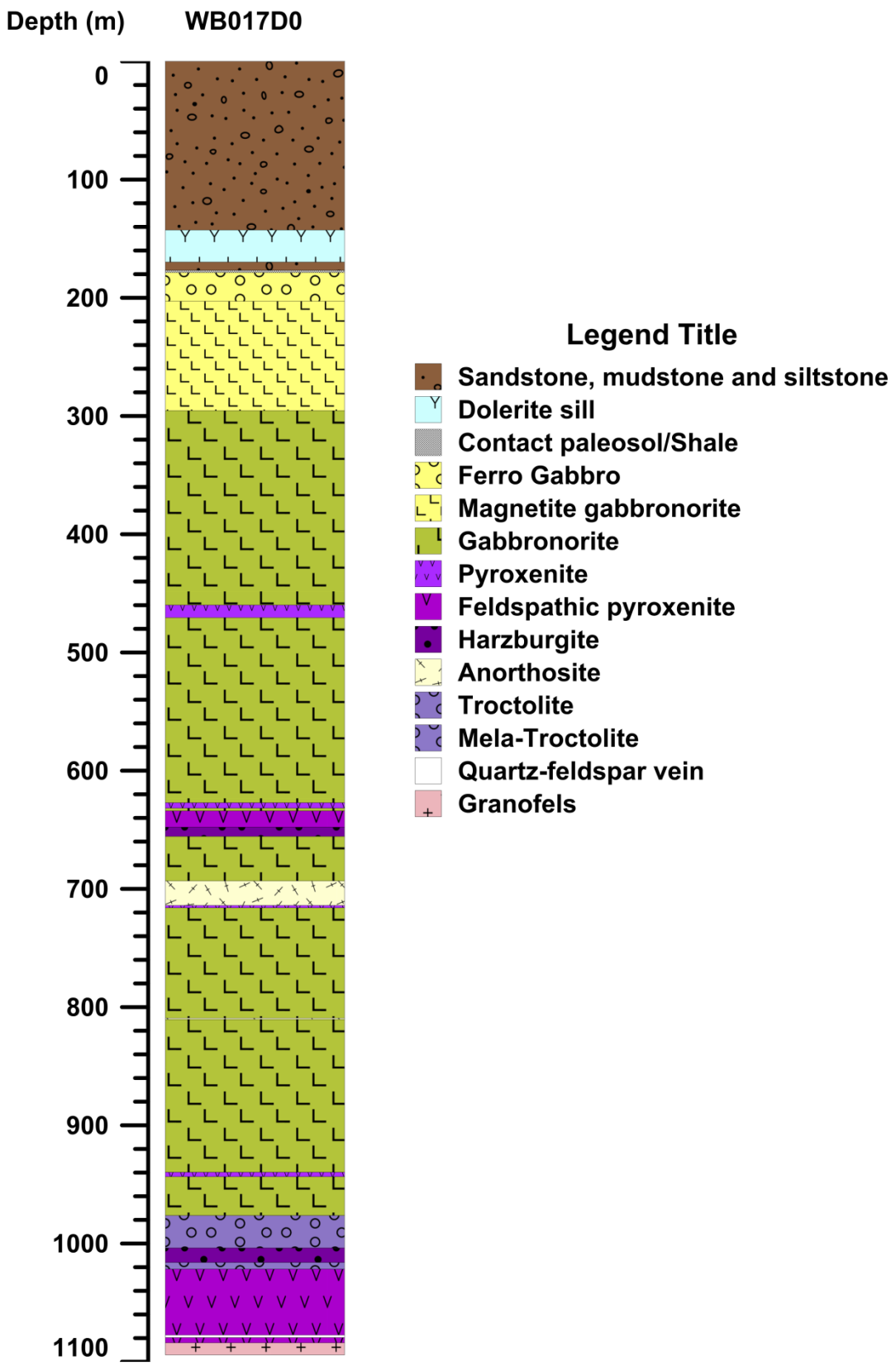

Appendix B: Core Log WB027D0

Core-Log Borehole WB027D0								
From (m)	**To (m)**	**Grain Size**	**Bottom Contact**	**Texture**	**Modal Proportions**	**Alteration**	**BMS**	**Rock Name**
0.00	10.50	M	Gradational	Poorly sorted	>90% quartz	-	-	Sandstone and mudstone
10.50	393.50	F-M-C	Sharp	Interlayered	>90% quartz	Epidote	-	Sandstone, mudstone and siltstone
393.50	474.95	M-C	Sharp	Inequigranular	cpx>quartz>feldspar	Epidote/Chl	-	Dolerite sill
474.95	488.20	F-M-C	Gradational	Interlayered	>90% quartz	Epidote	-	Sandstone, mudstone and siltstone
488.20	489.40	F-M	Sharp	Heterogeneous	>70% hematite	Hematite	-	Contact paleosol/Shale
489.40	495.10	M-C	Sharp	Inequigranular	cpx>quartz>feldspar	Epidote/Chl	-	Dolerite sill
495.10	495.20	F-M	Gradational	Heterogeneous	>70% hematite	Hematite	-	Contact paleosol/Shale
495.20	519.90	M-C	Sharp	Inequigranular	opx>plag>cpx	Epidote	-	Gabbronorite
519.90	521.50	PEG	Sharp	Pegmatoidal	opx>plag>cpx>mgt	Chlorite	-	Pegmatoidal Unit
521.50	555.50	M-C	Sharp	Equigranular	opx>plag>cpx>mgt	Chlorite	<1%	Mela-gabbronorite
555.50	555.60	PEG	Sharp	Pegmatoidal	cpx>plag>mgt	Chlorite	3%	Gabbro
555.60	565.20	M-C	Gradational	Equigranular	opx>plag>cpx	Chlorite	-	Gabbronorite
565.20	567.80	M-C	Gradational	Equigranular	opx>plag>cpx>mgt	Epidote/Chl	-	Altered Gabbronorite
567.80	576.00	C	Gradational	Inequigranular	plag>opx>cpx>ol	Serp/Chl	<3%	Olivine-bearing leuco-gabbronorite
576.00	581.00	M-C	Gradational	Inequigranular	ol>opx>plag (interstitial)	Serp/Chl	7%	Harzburgite
581.00	622.70	M-C	Gradational	Equigranular	opx>plag>cpx>mgt	Chlorite	5-10%	Gabbronorite
622.70	622.80	PEG	Sharp	Pegmatoidal	opx>plag>cpx	Chlorite	-	Mela-gabbronorite
622.80	625.00	M-C	Sharp	Equigranular	opx>plag>cpx>in.pig	Chlorite	-	Gabbronorite
625.00	625.10	PEG	Sharp	Pegmatoidal	opx>plag>cpx	-	-	Pegmatoidal Unit
625.10	648.00	M-C	Sharp	Equigranular	plag>opx>cpx	Chlorite	-	Leuco-gabbronorite
648.00	651.00	M	Sharp	Homogeneous	opx>cpx>plag (interstitial	-	3%	Feldspathic pyroxenite
651.00	797.00	M-C	Sharp	Equigranular	opx>plag>cpx	Chlorite	-	Gabbronorite
797.00	797.20	M-C	Sharp	Mottled	plag>cpx (oikocrysts)	Chlorite	-	Anorthosite
797.20	812.00	C	Sharp	Equigranular	plag>opx>cpx	Chlorite	-	Leuco-gabbronorite
812.00	817.55	M-C	Sharp	Mottled	plag>cpx (oikocrysts)	Chlorite	-	Anorthosite
817.55	888.50	M-C	Sharp	Equigranular	opx>plag>cpx	-	-	Gabbronorite
888.50	888.60	M-C	Sharp	Mottled	plag>cpx (oikocrysts)	Chlorite	-	Anorthosite
888.60	902.70	M-C	Gradational	Equigranular	opx>plag>cpx	Chlorite	-	Gabbronorite
902.70	904.30	M	Gradational	Homogeneous	opx>cpx>plag (interstitial	-	2%	Feldspathic pyroxenite
904.30	912.50	M-C	Gradational	Equigranular	opx>plag>cpx	Chlorite	-	Gabbronorite
912.50	912.60	PEG	Gradational	Pegmatoidal	opx>plag>cpx	Chlorite	-	Gabbronorite
912.60	919.60	M-C	Gradational	Equigranular	opx>plag>cpx	-	-	Gabbronorite
919.60	937.50	M-C	Sharp	Equigranular	opx>plag	-	-	Norite
937.50	939.75	M-C	Sharp	Mottled	plag>cpx (oikocrysts)	Chlorite	-	Anorthosite
939.75	971.20	M-C	Gradational	Equigranular	opx>plag	-	-	Norite
971.20	1015.20	M-C	Sharp	Equigranular	opx>plag>cpx	Chlorite	-	Gabbronorite
1015.20	1017.80	C-PEG	Sharp	Pegmatoidal	opx>cpx>plag (interstitial	-	-	Pyroxenite
1017.80	1039.30	M-C	Gradational	Equigranular	opx>plag>cpx	Chlorite	-	Gabbronorite
1039.30	1056.00	M-C	Gradational	Mottled	opx>plag>ol	Serp/Chl	-	Olivine-bearing Norite
1056.00	1074.40	M	Sharp	Poikilitic	ol>plag>opx (oikocrysts)	Serp/Chl	-	Troctolite
1074.40	1076.00	PEG	Sharp	Pegmatoidal	ol>plag>opx (oikocrysts)	Serp/Chl	10%	Pegmatoidal Unit
1076.00	1080.40	M-C	Sharp	Poikilitic	ol>plag>opx (oikocrysts)	Serp/Chl	-	Troctolite
1080.40	1081.30	M	Sharp	Homogeneous	opx>cpx>plag (interstitial	-	5%	Pyroxenite
1081.30	1083.90	M-C	Gradational	Poikilitic	ol>plag>opx (oikocrysts)	Serp/Chl	1%	Mela-troctolite
1083.90	1096.50	M-C	Gradational	Inequigranular	ol>opx>plag (interstitial)	Serp/Chl	3%	Harzburgite
1096.50	1104.00	M-C	Gradational	Poikilitic	ol>plag>opx (oikocrysts)	Serp/Chl	1%	Mela-troctolite
1104.00	1114.50	M-C	Gradational	Inequigranular	ol>opx>plag (interstitial)	Serp/Chl	1%	Harzburgite
1114.50	1116.50	F-M	Sharp	Homogeneous	serpentinite	Serp	2%	Serpentinised unit
1116.50	1122.00	C-PEG	Gradational	Pegmatoidal	opx>cpx>plag (interstitial	-	1%	Pyroxenite
1122.00	1145.80	C	Sharp	Inequigranular	ol>opx>plag (interstitial)	Serp/Chl	3%	Harzburgite
1145.80	1148.30	M-C	Sharp	Equigranular	opx>plag	-	1%	Norite
1148.30	1157.50	C	Sharp	Inequigranular	ol>opx>plag (interstitial)	Serp/Chl	10%	Harzburgite
1157.50	1159.00	M-C	Sharp	Equigranular	opx>plag	-	-	Norite
1159.00	1168.35	C	Sharp	Inequigranular	ol>opx>plag (interstitial)	Serp	3%	Harzburgite
1168.35	1174.00	M-C	Gradational	Equigranular	opx>plag	-	-	Norite
1174.00	1186.70	F-M	EOH	Inequigranular	quartz>feldspar>opx	Serp	-	Granofels

Appendix B: Core Log WB027D0

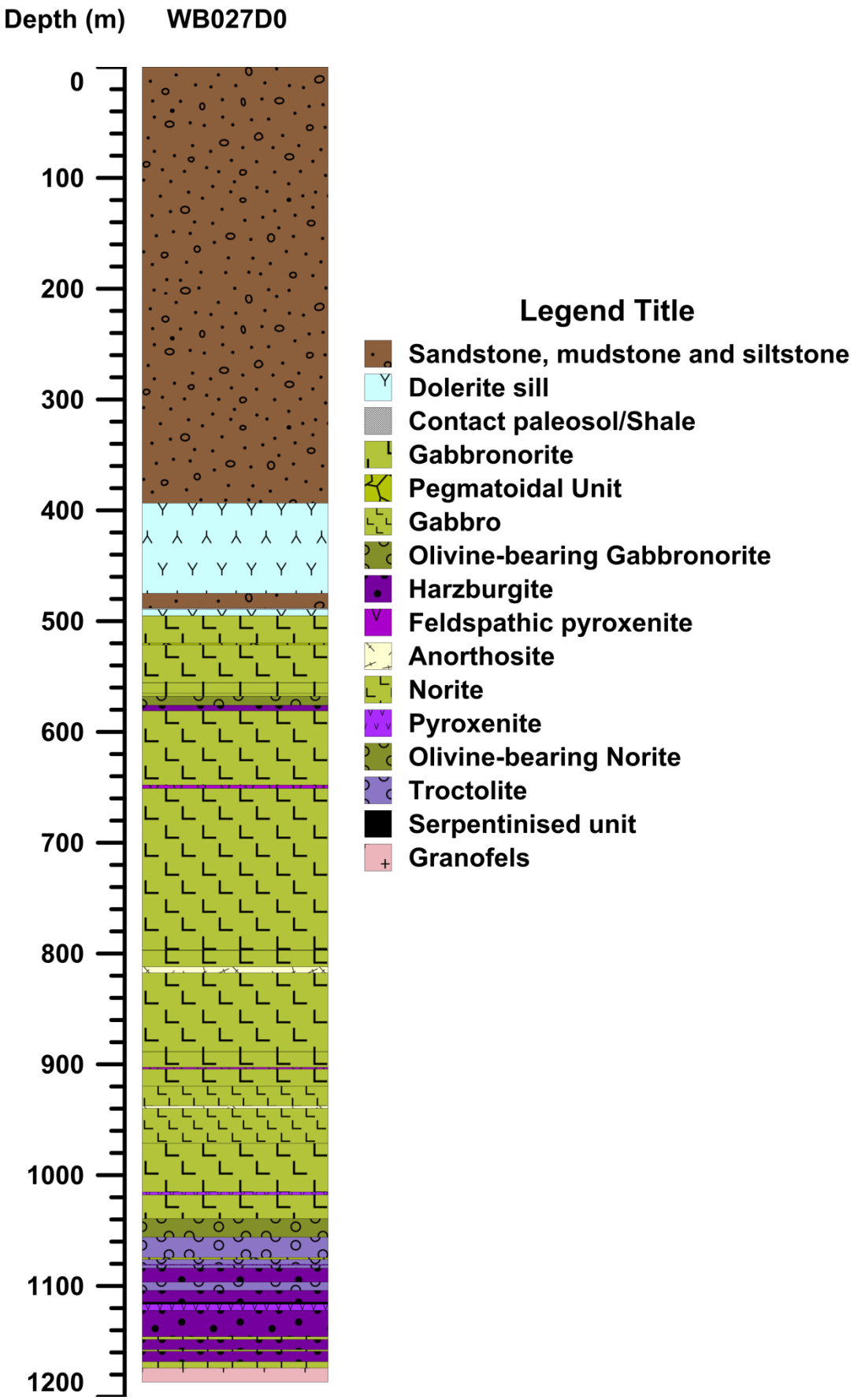

Appendix B: Core Log WB034D0

Core-Log of Borehole WB034D0								
From (m)	**To (m)**	**Grain Size**	**Bottom Contact**	**Texture**	**Modal Proportions**	**Alteration**	**BMS**	**Rock Name**
0.00	360.60	F-M-C	Sharp	Laminated/pebbly	>90% quartz	Epidote	-	Sandstone, mudstone and conglomerate
360.60	361.20	M-C	Sharp	Inequigranular	cpx>quartz>feldspar	Epidote	-	Dolerite
361.20	362.30	F-M-C	Sharp	Laminated/pebbly	>90% quartz	Epidote	-	Sandstone, mudstone and conglomerate
362.30	363.00	F-M	Gradational	Sheared	>70% hematite	Hematite	-	Bushveld paleosol/Shale
363.00	394.46	M-C	Sharp	Equigranular	opx>plag>cpx	Epidote/Chl	-	Gabbronorite
394.46	475.40	M-C	Sharp	Inequigranular	cpx>quartz>feldspar	Epidote	-	Dolerite
475.40	664.25	M	Gradational	Equigranular	opx>plag>cpx	Chlorite	-	Gabbronorite
664.25	672.00	M-C	Gradational	Equigranular	plag>opx>cpx	Chlorite	-	Leuco-gabbronorite
673.30	702.00	C	Gradational	Inequigranular	plag>opx>cpx	Chlorite	-	Leuco-gabbronorite
702.00	708.00	C-PEG	Gradational	Mottled	plag>cpx (oikocyrsts)	Chlorite	-	Anorthosite
708.00	830.70	M	Sharp	Equigranular	opx>plag>cpx	Chlorite	-	Gabbronorite
830.70	833.50	M	Sharp	Homogeneous	opx>cpx>plag (interstitial)	-	-	Feldspathic pyroxenite
833.50	892.20	M-C	Sharp	Equigranular	opx>plag>cpx	Chlorite	-	Gabbronorite
892.20	895.10	M	Sharp	Homogeneous	opx>cpx>plag (interstitial)	-	-	Feldspathic pyroxenite
895.10	896.80	M-C	Sharp	Equigranular	opx>plag>cpx	Chlorite	-	Gabbronorite
896.80	897.20	M	Sharp	Homogeneous	opx>cpx>plag (interstitial)	-	-	Feldspathic pyroxenite
897.20	905.20	M-C	Sharp	Equigranular	opx>plag>cpx	Chlorite	-	Gabbronorite
905.20	906.20	M	Sharp	Homogeneous	opx>cpx>plag (interstitial)	-	-	Feldspathic pyroxenite
906.20	923.00	M-C	Sharp	Equigranular	opx>plag>cpx	Chlorite	-	Gabbronorite
923.00	927.60	M	Sharp	Homogeneous	opx>cpx>plag (interstitial)	-	-	Feldspathic pyroxenite
927.60	932.00	M-C	Gradational	Equigranular	opx>plag>cpx	Chlorite	-	Gabbronorite
932.00	943.00	M-C	Gradational	Inequigranular	opx>plag>ol>cpx	Serp/Chl	-	Olivine-bearing gabbronorite
943.00	958.00	M-C	Gradational	Poikilitic	ol>plag>opx (oikocrysts)	Serp/Chl	-	Troctolite
958.00	968.00	M-C	Sharp	Inequigranular	opx>plag>ol>cpx	Serp/Chl	-	Olivine-bearing gabbronorite
968.00	972.00	C-PEG	Sharp	Mottled	plag>cpx (oikocyrsts)	Chlorite	-	Mottled Anorthosite
972.00	972.90	M-C	Gradational	Equigranular	opx>plag	-	-	Norite
972.90	974.00	M-C	Gradational	Inequigranular	opx>plag>ol	Serp/Chl	-	Olivine-bearing norite
974.00	981.00	M-C	Gradational	Inequigranular	ol>opx>plag (interstitial)	Serp/Chl	3%	Harzburgite
981.00	996.00	M-C	Gradational	Inequigranular	opx>plag>cpx>ol	Serp/Chl	1%	Olivine-bearing gabbronorite
996.00	1010.40	M-C	Gradational	Inequigranular	ol>opx>plag (interstitial)	Serp/Chl	5%	Harzburgite
1010.40	1010.90	M-C	Gradational	Inequigranular	opx>cpx>ol>plag (interstitial)	Serp/Chl	5%	Olivine-bearing feldspathic pyroxenite
1010.90	1011.10	M	Sharp	Homogeneous	opx>cpx>plag (interstitial)	-	2%	Feldspathic pyroxenite
1011.10	1013.00	M-C	Sharp	Equigranular	opx>plag	-	1%	Norite
1013.00	1018.75	M-C	Sharp	Inequigranular	ol>opx>plag (interstitial)	Serp/Chl	5%	Harzburgite
1018.75	1021.50	M	Sharp	Homogeneous	opx>cpx>plag (interstitial)	-	3%	Feldspathic pyroxenite
1021.50	1022.10	M-C	Sharp	Equigranular	opx>plag	-	-	Norite
1022.10	1023.15	M	Sharp	Homogeneous	opx>cpx>plag (interstitial)	-	1%	Feldspathic pyroxenite
1023.15	1043.00	M-C	Sharp	Equigranular	opx>plag>cpx	Chlorite	-	Gabbronorite
1043.00	1059.00	M-C	Sharp	Poikilitic	ol>plag>opx (oikocrysts)	Serp/Chl	1%	Troctolite
1059.00	1063.10	M-C	Gradational	Equigranular	opx>plag	-	1%	Norite
1063.10	1067.00	M	Gradational	Homogeneous	opx>cpx>plag (interstitial)	-	3%	Feldspathic pyroxenite
1067.00	1109.60	M	Gradational	Homogeneous	opx>cpx	-	-	Pyroxenite
1109.60	1113.70	F-M	Gradational	Inequigranular	opx>quartz>feldspar	Serp	-	Granofels
1113.70	1119.10	F	Gradational	Homogeneous	opx>cpx>plag (interstitial)	-	-	Feldspathic pyroxenite
1119.10	1126.30	F-M	EOH	Inequigranular	opx>quartz>feldspar	Serp	-	Granofels

Appendix B: Core Log WB034D0

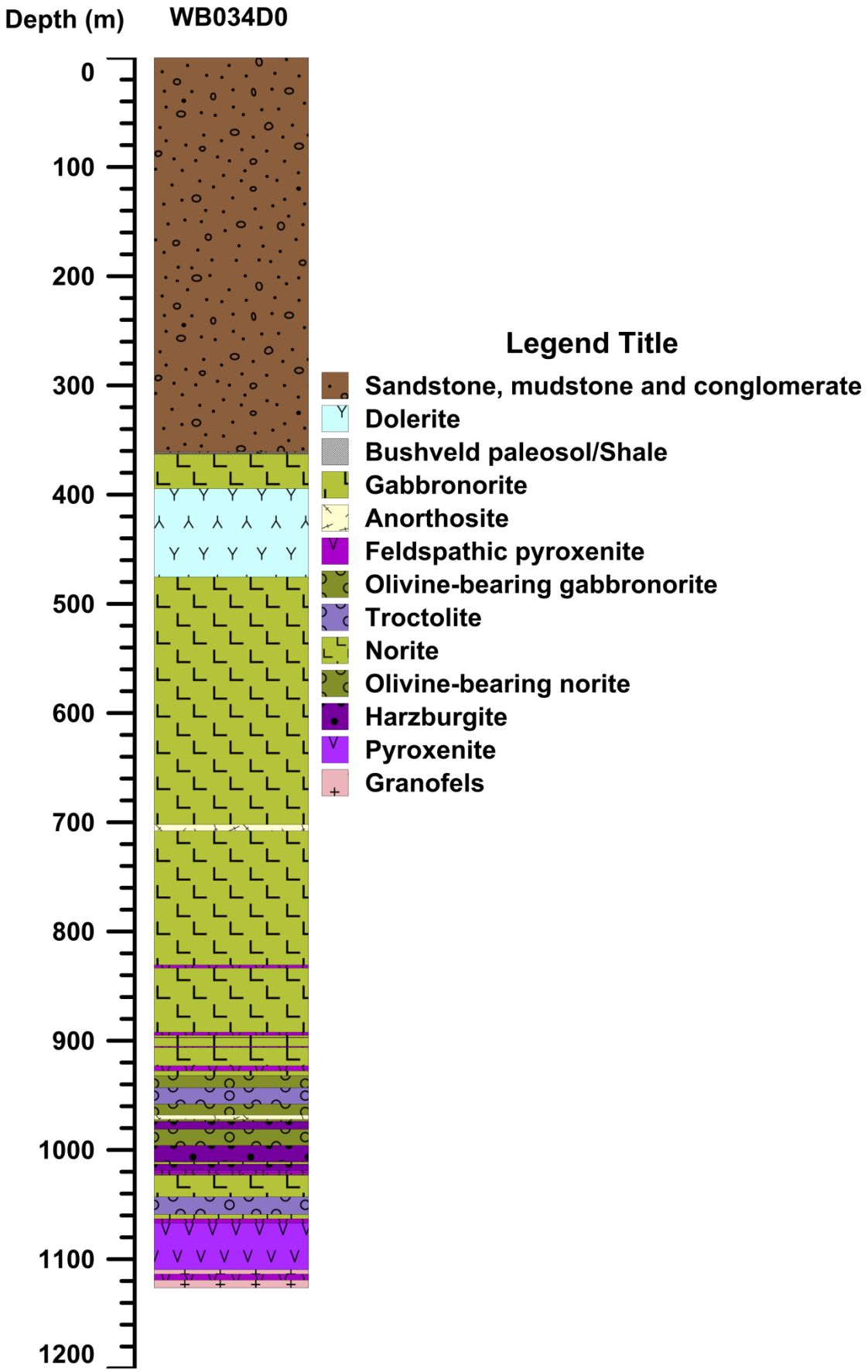

Appendix B: Core Log WB090D0

Core-Log of Borehole WB090D0								
From (m)	**To (m)**	**Grain Size**	**Bottom Contact**	**Texture**	**Modal Proportions**	**Alteration**	**BMS**	**Rock Name**
0.00	3.94	F-M	Gradational	Poorly sorted	>90% quartz	Oxidised	-	Sanstone and mudstone
3.94	95.90	F-M-C	Sharp	Laminated	>90% quartz	Epidote	-	Sanstone, mudstone and siltstone
95.90	135.15	M-C	Sharp	Inequigranular	cpx>quartz>feldspar	Epidote/Chl	-	Dorlerite
135.15	238.80	F-M-C	Gradational	Pebbly/Laminated	>90% quartz	Epidote	-	Sanstone, mudstone and conglomerate
238.80	240.30	F-M	Gradational	Sheared	>70% hematite	Hematite	-	Bushveld Palaeosol/Shale
240.30	241.00	M-C	Sharp	Inequigranular	Hematite>cpx>plag	Hematite/Epi	-	Altered gabbro
241.00	269.34	M-C	Sharp	Inequigranular	Hematite>cpx>plag	Hematite/Chl	-	Altered gabbro
269.34	279.00	M-C	Sharp	Equigranular	cpx>plag	Chlorite	-	Gabbro
279.00	281.00	M-C	Sharp	Equigranular	opx>plag>cpx	Chlorite	-	Gabbronorite
281.00	286.40	M-C	Gradational	Equigranular	cpx>plag	Chlorite	-	Gabbro
286.40	299.37	M-C	Gradational	Inequigranular	opx>plag>cpx>ol	Serp/Chl	1%	Olivine-bearing gabbronorite
299.37	317.90	C	Gradational	Poikilitic	ol>plag>opx (oikocrysts)	Serp/Chl	2%	Mela-troctolite
317.90	386.00	F	Sharp	Inequigranular	ol>opx>plag (interstitial)	Serp/Chl	1%	Feldspathic harzburgite
386.00	390.10	C	Sharp	Homogeneous	opx>plag (interst)>ol (relics	Serp/Chl	1%	Orthopyroxenite
390.10	395.70	C	Sharp	Inequigranular	ol>opx>plag (interstitial)	Serp/Chl	2%	Feldspathic harzburgite
395.70	472.00	F	Gradational	Homogeneous	opx>plag (interst)>ol (relics	Serp/Chl	5%	Orthopyroxenite
472.00	485.50	F-M	Gradational	Inequigranular	opx>quartz>feldspar>ol	Serp	1%	Granofels
485.50	527.83	F-M	EOH	Inequigranular	opx>quartz>feldspar>ol	Serp	-	Granofels

Appendix B: Core Log WB090D0

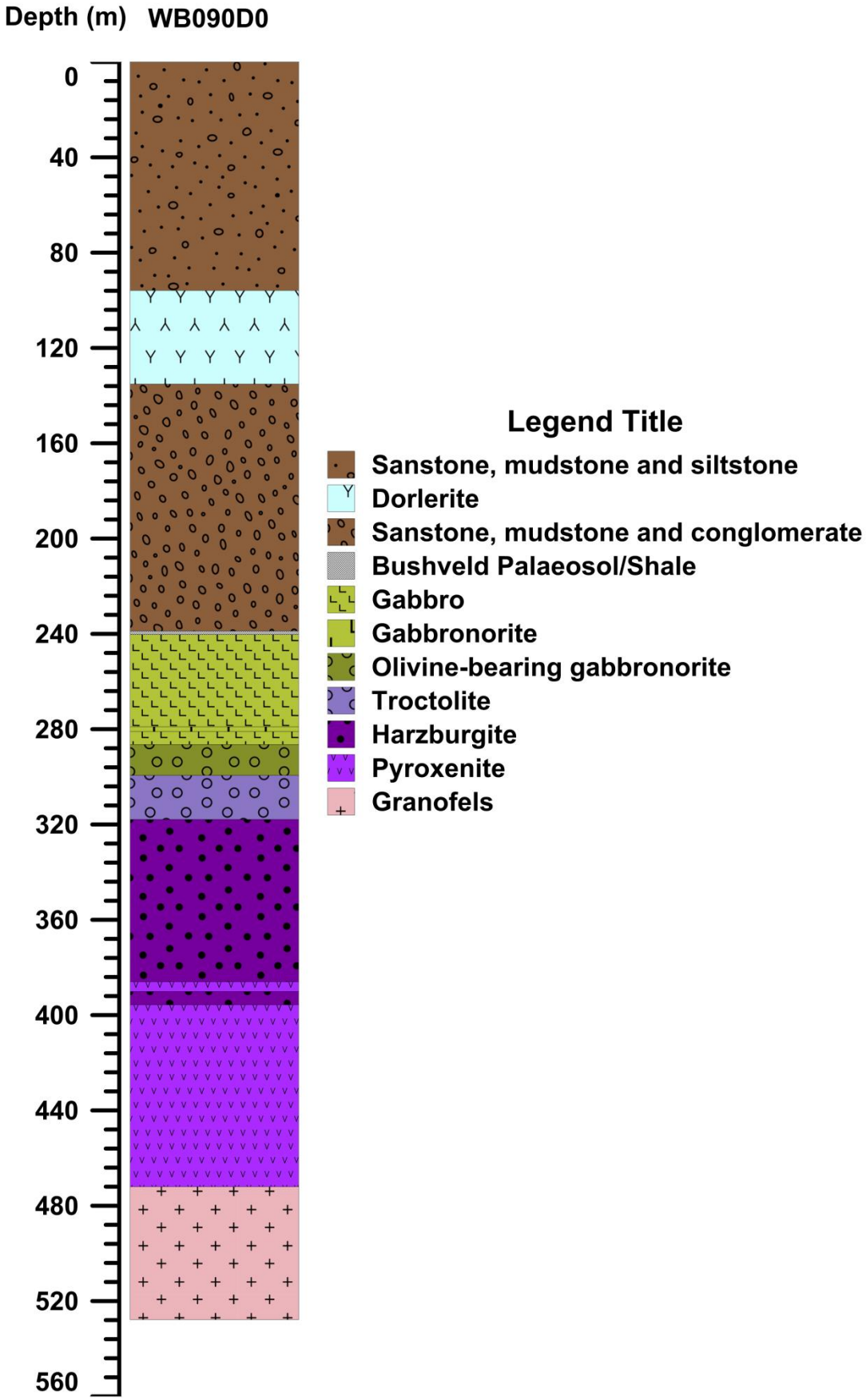

Appendix B: Core Log WB099D0

Core-Log of Borehole WB099D0								
From (m)	**To (m)**	**Grain Size**	**Bottom Contact**	**Texture**	**Modal Proportions**	**Alteration**	**BMS**	**Rock Name**
0.00	10.36	F-M-C	Gradational	Interlayered	>90% quartz	-	-	Sandstone, mudstone and siltstone
10.36	13.36	M	Gradational	Poorly sorted	>90% quartz	-	-	Sandstone and mudstone
13.36	34.74	F-M-C	Gradational	Interlayered	>90% quartz	-	-	Sandstone, mudstone and siltstone
34.74	53.90	M	Sharp	Poorly sorted	>90% quartz	Epidote	-	Sandstone and mudstone
53.90	70.67	M-C	Sharp	Ineqigranular	cpx>quartz>feldspar	Epidote	-	Dolerite sill
70.67	100.47	F-M-C	Sharp	Interlayered	>90% quartz	-	-	Sandstone, mudstone and siltstone
100.47	101.00	M-C	Sharp	Ineqigranular	cpx>quartz>feldspar	Epidote	-	Dolerite sill
101.00	361.59	F-M-C	Sharp	Laminated	>90% quartz	-	-	Sandstone, mudstone and siltstone
361.59	443.20	M-C	Sharp	Ineqigranular	cpx>quartz>feldspar	Epidote	-	Dolerite sill
443.20	520.97	C	Sharp	Pebbly	>90% quartz	Epidote	-	Sandstone and conglomerate
520.97	524.52	F-M	Gradational	Sheared	>70% hematite	Hematite	-	Contact paleosol/Shale
524.52	536.05	M-C	Gradational	Ineqigranular	opx>plag>cpx	Epidote	-	Gabbronorite
536.05	537.10	M-C	Gradational	Ineqigranular	opx>plag>cpx>ol	Oxide	-	Olivine Gabbronorite
537.10	601.98	M-C	Gradational	Equigranular	opx>plag>cpx>mgt	Chlorite	-	Magnetite Gabbronorite
601.98	605.45	M-C	Sharp	Equigranular	opx>plag>cpx	Chlorite	-	Gabbronorite
605.45	609.50	M-C	Sharp	Mottled	plag>cpx+mgt (oikocrysts)	Chlorite	1%	Anorthosite
609.50	617.57	M-C	Sharp	Equigranular	plag>opx>cpx>mgt	Chlorite	1%	Leuco-gabbronorite
617.57	626.00	M	Sharp	Homogeneous	opx>cpx>plag (interstitial)	-	2%	Feldspathic pyroxenite
626.00	653.69	M-C	Sharp	Equigranular	plag>opx>cpx	Chlorite	-	Leuco-gabbronorite
653.69	675.00	M-C	Gradational	Ineqigranular	opx>cpx>plag>ol	Serp/Chl	1%	Olivine-bearing feldspathic pyroxenite
675.00	677.05	M-C	Gradational	Ineqigranular	opx>plag>cpx>ol	Serp/Chl	2%	Olivine-bearing gabbronorite
677.05	753.66	M-C	Gradational	Equigranular	opx>plag>cpx	Chlorite	5%	Gabbronorite
753.66	757.14	M-C	Gradational	Ineqigranular	opx>plag>cpx>mgt	Chlorite	-	Altered gabbronorite
757.14	824.00	M-C	Gradational	Equigranular	opx>plag>cpx	Chlorite	-	Gabbronorite
824.00	828.20	M-C	Gradational	Equigranular	opx>plag	-	-	Norite
828.20	898.30	M-C	sharp	Equigranular	opx>plag>cpx	Chlorite	-	Gabbronorite
898.30	899.90	PEG	Sharp	Pegmatoidal	opx>plag>cpx	Chlorite	-	Pegmatoidal Unit
899.90	912.05	M-C	Gradational	Equigranular	plag>opx>cpx	Chlorite	-	Leuco-gabbronorite
912.05	927.10	M-C	Gradational	Equigranular	opx>plag	-	-	Norite
927.10	968.03	M-C	Sharp	Ineqigranular	opx>plag>cpx>ol	Serp/Chl	-	Altered gabbronorite
968.03	1012.15	C	Sharp	Mottled	plag>cpx (oikocrysts)	Chlorite	-	Anorthosite
1012.15	1017.60	M-C	Sharp	Ineqigranular	opx>plag>cpx>ol	Serp/Chl	-	Oivine-bearing gabbronorite
1017.60	1027.60	C	Sharp	Mottled	plag>cpx (oikocrysts)	Chlorite	-	Anorthosite
1027.60	1064.60	M-C	Gradational	Ineqigranular	opx>plag>cpx>ol	Serp/Chl	-	Olivine-bearing gabbronorite
1064.60	1070.70	M-C	Gradational	Ineqigranular	opx>plag>ol	Serp/Chl	-	Olivine-bearing norite
1070.70	1082.60	M-C	Gradational	Ineqigranular	opx>plag>cpx>ol	Serp/Chl	-	Olivine-bearing gabbronorite
1082.60	1121.48	M-C	Gradational	Ineqigranular	opx>plag>ol	Serp/Chl	-	Olivine-bearing norite
1121.48	1124.26	M	Sharp	Homogeneous	opx>cpx>plag (interstitial)	-	-	Feldspathic pyroxenite
1124.26	1149.15	M-C	Gradational	Ineqigranular	opx>plag>cpx>ol	Serp/Chl	-	Olivine-bearing gabbronorite
1149.15	1162.83	M-C	Gradational	Ineqigranular	opx>plag>ol	Serp/Chl	-	Olivine-bearing norite
1162.83	1176.53	M-C	Gradational	Ineqigranular	opx>plag>cpx>ol	Serp/Chl	-	Olivine-bearing gabbronorite
1176.53	1208.00	M-C	Gradational	Ineqigranular	opx>plag>ol	Serp/Chl	-	Olivine-bearing norite
1208.00	1274.20	M-C	Sharp	Poikilitic	ol>plag>opx (oikicrysts)	Serp	-	Troctolite
1274.20	1276.63	M	Sharp	Homogeneous	opx>cpx>plag (interstitial)	-	5%	Feldspathic pyroxenite
1276.63	1285.36	M-C	Gradational	Poikilitic	ol>plag>opx (oikicrysts)	Serp/Chl	3%	Mela-troctolite
1285.36	1291.27	M	Sharp	Ineqigranular	ol>opx>plag (interstitial)	Serp/Chl	5%	Harzburgite
1291.27	1303.50	M	Sharp	Homogeneous	opx>cpx>plag (interstitial)	-	5%	Feldspathic pyroxenite
1303.50	1308.15	M-C	Sharp	Poikilitic	ol>plag>opx (oikicrysts)	Serp/Chl	3%	Mela-troctolite
1308.15	1319.32	M	Gradational	Homogeneous	opx>cpx>plag (interstitial)	-	5%	Feldspathic pyroxenite
1319.32	1343.92	F-M	EOH	Ineqigranular	opx>quartz>feldspar	Serp	1%	Granofels

Appendix B: Core Log WB099D0

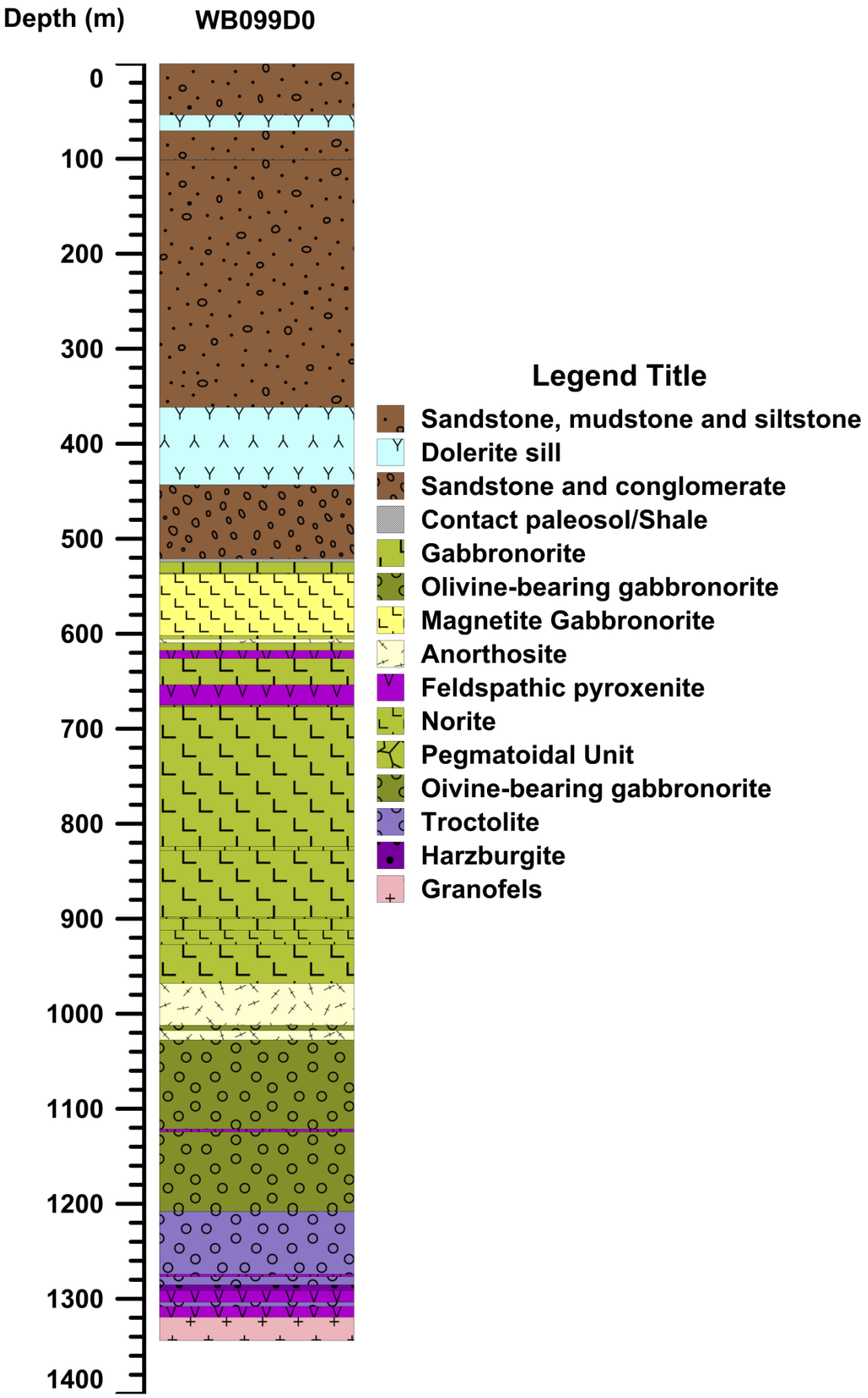

Appendix B: Core Log WB161D0

Core-Log of Borehole WB161D0								
From (m)	**To (m)**	**Grain Size**	**Bottom Contact**	**Texture**	**Modal Proportions**	**Alteration**	**BMS**	**Rock Name**
0.00	336.30	F-M-C	Sharp	Pebbly/laminated	>90% quartz	Epidote	-	Sandstone, mudstone, siltstone and conglomerates
336.30	415.40	M-C	Sharp	Inequigranular	cpx>quartz>feldspar	Epidote/Chl	-	Dolerite
415.40	421.87	M-C	Gradational	Inequigranular	plag>cpx>hematite	Hematite	-	Altered leuco-gabbro
421.87	426.40	C-PEG	Gradational	Equigranular	plag>opx>cpx	Epidote/Chl	-	Leuco-gabbronorite
426.40	427.90	C	Sharp	Spotted/Mottled	plag>cpx (oikocrysts)	Chlorite	-	Anorthosite
427.90	439.85	M-C	Sharp	Equigranular	plag>opx>cpx	Chlorite	-	Leuco-gabbronorite
439.85	441.00	C	Gradational	Spotted	plag>cpx+mgt (oikocrysts)	Chlorite	-	Anorthosite
441.00	441.60	M-C	Gradational	Equigranular	plag>opx>cpx	Chlorite	-	Leuco-gabbronorite
441.60	441.90	C	Sharp	Mottled	plag>cpx+mgt (oikocrysts)	Chlorite	-	Anorthosite
441.90	443.60	M-C	Sharp	Equigranular	opx+cpx=plag	Chlorite	-	Gabbronorite
443.60	444.40	C	Sharp	Spotted	plag>cpx+mgt (oikocrysts)	Chlorite	-	Anorthosite
444.40	446.85	M-C	Sharp	Equigranular	plag>opx>cpx	Chlorite	-	Leuco-gabbronorite
446.85	447.50	C	Sharp	Mottled	plag>cpx+mgt (oikocrysts)	Chlorite	-	Anorthosite
447.50	466.20	M-C	Gradational	Inequigranular	opx>plag>cpx	Bleached	-	Gabbronorite
466.20	477.70	M-C	Sharp	Equigranular	opx>plag>cpx	Chlorite	-	Gabbronorite
477.70	478.50	C	Sharp	Mottled	plag>cpx+mgt (oikocrysts)	Chlorite	-	Anorthosite
478.50	482.80	M-C	Sharp	Equigranular	opx>plag>cpx	Chlorite	-	Gabbronorite
482.80	483.50	C	Sharp	Mottled	plag>cpx+mgt (oikocrysts)	Chlorite	-	Anorthosite
483.50	493.38	M-C	Gradational	Equigranular	plag>cpx	-	-	Leuco-gabbro
493.38	516.00	M-C	Gradational	Inequigranular	plag>cpx	Chlorite	-	Leuco-gabbro
516.00	522.80	M-C	Gradational	Equigranular	cpx>plag>opx(<10%)	Chlorite	-	Gabbro
522.80	529.00	M-C	Gradational	Equigranular	cpx>plag>opx(<10%)	Chlorite	-	Gabbro
529.00	579.90	M-C	Gradational	Equigranular	opx>plag>cpx	Chlorite	-	Gabbronorite
579.90	582.20	M-C	Gradational	Inequigranular	plag>opx>cpx	Chlorite	-	Leuco-gabbronorite
582.20	583.69	M-C	Sharp	Equigranular	opx>plag>cpx	Chlorite	-	Gabbronorite
583.69	584.30	C-PEG	Sharp	Pegmatoidal	ol>opx>plag (interstitial)	Serp/Chl	2%	Feldspathic harzburgite
584.30	585.50	M-C	Gradational	Homogeneous	opx>cpx>plag (interstitial)	-	1%	Feldspathic pyroxenite
585.50	590.00	M-C	Gradational	Equigranular	opx>cpx>plag (minor)	Chlorite	-	Melagabbronorite
590.00	599.30	M-C	Gradational	Equigranular	opx>plag>cpx	Chlorite	-	Gabbronorite
599.30	601.80	M-C	Gradational	Equigranular	plag>cpx	Chlorite	-	Leuco-gabbro
601.80	606.00	C-PEG	Gradational	Pegmatoidal	plag>opx>cpx	Chlorite	-	Leuco-gabbronorite
606.00	616.40	M-C	Sharp	Equigranular	opx>plag>cpx	Chlorite	-	Gabbronorite
616.40	617.36	PEG	Sharp	Pegmatoidal	opx>plag>cpx>mgt	Chlorite	-	Gabbronorite
617.36	618.40	C	Sharp	Mottled	plag>cpx (oikocrysts)	Chlorite	-	Anorthosite
618.40	653.50	C	Sharp	Equigranular	opx>plag>cpx	Chlorite	-	Gabbronorite
653.50	655.00	M-C	Sharp	Equigranular	opx>cpx>plag	Chlorite	-	Melagabbronorite
655.00	656.30	M-C	Sharp	Inequigranular	opx>plag>cpx>ol	Serp/Chl	-	Olivine-bearing gabbronorite
656.30	657.00	M-C	Gradational	Equigranular	cpx>plag>opx(<10%)	Chlorite	-	Gabbro
657.00	658.00	C	Sharp	Mottled	plag>cpx (oikocrysts)	Chlorite	-	Anorthosite
658.00	666.50	M-C	Gradational	Inequigranular	opx>plag>ol	Serp/Chl	-	Olivine-bearing norite
666.50	716.00	M-C	Gradational	Inequigranular	cpx>opx>plag>ol	Serp/Chl	-	Olivine-bearing gabbronorite
716.00	718.90	M-C	Sharp	Inequigranular	opx>plag>ol	Serp/Chl	-	Olivine-bearing norite
718.90	720.35	PEG	Sharp	Pegmatoidal	opx>plag>ol	Serp/Chl	-	Olivine-bearing norite
720.35	721.50	M-C	Gradational	Inequigranular	opx>plag>ol	Serp/Chl	-	Olivine-bearing norite
721.50	770.65	M-C	Gradational	Poikilitic	ol>plag>opx (oikocrysts)>chr	Serp/Chl	3%	Troctolite
770.65	776.40	C	Gradational	Inequigranular	ol>opx>plag (interstitial)	Serp/Chl	7%	Feldspathic harzburgite
776.40	783.00	M-C	Gradational	Inequigranular	opx>plag>ol	Phlogopite	5%	Olivine-bearing norite
783.00	806.56	M-C	Gradational	Inequigranular	ol>opx>plag (interstitial)	Serp/Chl	5%	Feldspathic harzburgite
806.56	820.90	M-C	Sharp	Inequigranular	opx>ol>plag	Serp	7%	Olivine-bearing norite
820.90	846.00	M-C	Sharp	Poikilitic	ol>plag>opx (oikocrysts)>chr	Serp/Chl	3%	Troctolite
846.00	858.60	M-C	Sharp	Inequigranular	opx>plag>ol	Serp/Chl	1%	Olivine-bearing norite
858.60	864.15	F	Gradational	Homogeneous	opx>cpx>plag (interstitial)	-	3%	Feldspathic pyroxenite
864.15	882.50	F-M	EOH	Inequigranular	opx>quartz>feldspar	Serp	-	Granofels

Appendix B: Core Log WB161D0

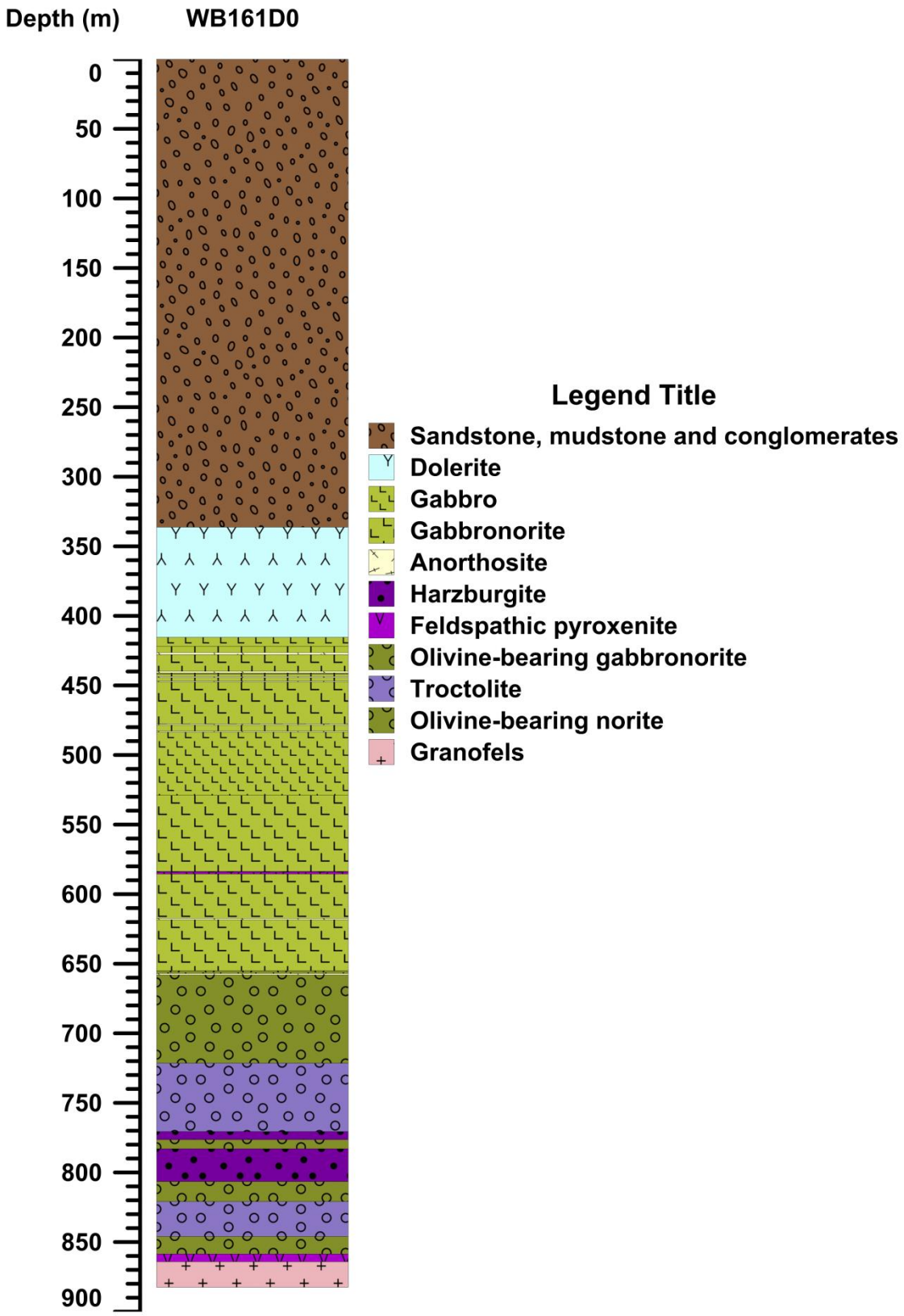

Appendix B: Core Log WB195D0

Core-Log of Borehole WB195D0								
From (m)	**To (m)**	**Grain Size**	**Bottom Contact**	**Texture**	**Modal Proportions**	**Alteration**	**BMS**	**Rock Name**
0.00	404.00	F-M-C	Sharp	Laminated	>90% quartz	Epidote	-	Sandstone, mudstone and conglomerate
404.00	408.70	F-M	Gradational	Sheared	>70% hematite	hematite	-	Bushveld paleosol
408.70	432.00	M-C	Sharp	Inequigranular	cpx>plag	Epidote/Chl	-	Gabbro
432.00	436.80	M-C	Sharp	Equigranular	quartz>feldspar>hrbl	Chlorite	-	Granitic veinlet
436.80	498.40	M-C	Sharp	Equigranular	plag>cpx>opx (<10%)	Chlorite	-	Leuco-gabbro
498.40	501.45	PEG	Sharp	Pegmatoidal	cpx>plg>mgt>phlg	Chlorite	2%	Gabbro
501.45	561.00	M-C	Sharp	Equigranular	cpx>plag	Chlorite	-	Gabbro
561.00	562.60	PEG	Sharp	Pegmatoidal	cpx>plag>mgt	Chlorite	2%	Gabbro
562.60	636.50	M-C	Gradational	Equigranular	opx>plag>cpx>mgt	Chlorite	-	Magnetite-gabbronorite
636.50	639.00	M-C	Gradational	Equigranular	plag>opx>cpx>mgt	Chlorite	-	Leuco-gabbronorite
639.00	643.40	C	Sharp	Equigranular	plag>cpx	Chlorite	-	Leuco-gabbro
643.40	658.50	M-C	Gradational	Equigranular	opx>plag>cpx	Chlorite	-	Gabbronorite
658.50	664.60	C	Sharp	Equigranular	opx>plag>cpx>mgt	Chlorite	-	Magnetite-gabbronorite
664.60	698.80	M	Sharp	Homogeneous	opx>plag>cpx>mgt	Chlorite	-	Magnetite-gabbronorite
698.80	701.00	M-C	Gradational	Inequigranular	plag>opx>cpx>mgt>ol	Chlorite	-	Leuco-gabbronorite
701.00	708.00	M	Gradational	Homogeneous	opx>plag>cpx	Chlorite	-	Gabbronorite
708.00	709.80	C	Gradational	Inequigranular	plag>opx>cpx>mgt>ol	Chlorite	-	Leuco-gabbronorite
709.80	781.40	M-C	Gradational	Inequigranular	opx>plag>ol>cpx	Serp/Chl	-	Olivine-bearing gabbronorite
781.40	837.98	M	Gradational	Equigranular	opx>plag>cpx>mgt	Chlorite	-	Magnetite-gabbronorite
837.98	855.71	M-C	Sharp	Equigranular	opx>plag>cpx>ol	Chlorite	3%	Gabbronorite
855.71	870.05	PEG	Sharp	Pegmatoidal/Motted	plag>cpx+mgt (oikocryst	Chlorite	2%	Anorthosite
870.05	883.76	M-C	Sharp	Inequigranular	opx>plag>ol (10%)	Serp/Chl	-	Olivne-bearing norite
883.76	895.50	PEG	Sharp	Pegmatoidal	plag>cpx+mgt (oikocryst	Chlorite	2%	Anorthosite
895.50	897.50	C	Sharp	Poikilitic	plag>ol>opx (oikocrysts)	Serp/Chl	3%	Leuco-troctolite
897.50	907.30	M-C	Gradational	Inequigranular	plag>cpx>ol	Serp/Chl	7%	Olivine-bearing leuco-gabbro
907.30	931.00	M-C	Sharp	Equigranular	plag>cpx	Chlorite	-	Leuco-gabbro
931.00	933.90	PEG	Sharp	Pegmatoidal	plag>cpx>phlg>mgt	Chlorite	-	Leuco-gabbro
933.90	944.29	M-C	EOH	Equigranular	cpx>plag>opx (<10%)	Chlorite	-	Mela-gabbro

Appendix B: Core Log WB195D0

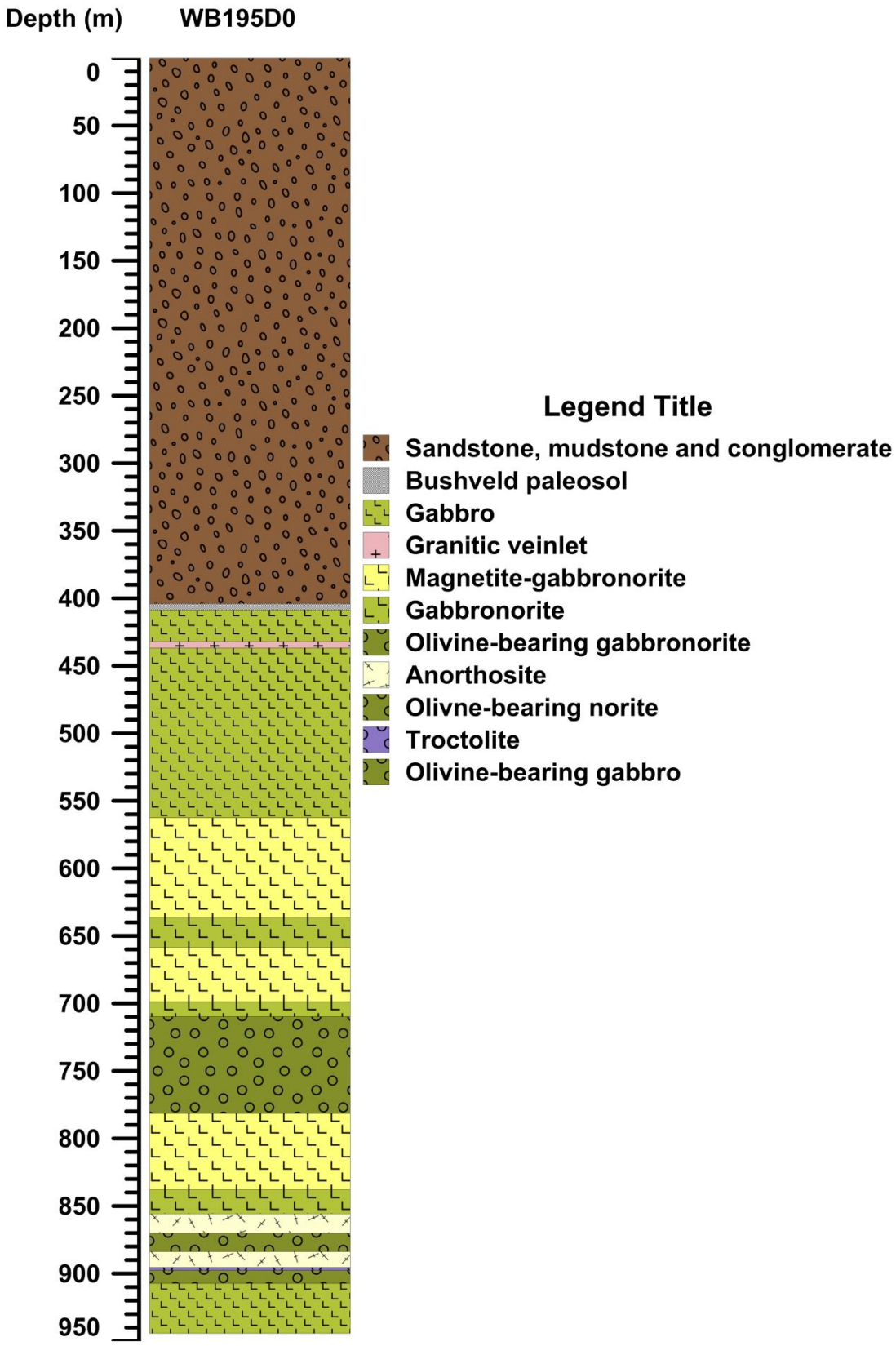

Appendix B: Core Log WE001D0

Core-Log of Borehole WE001D0								
From (m)	**To (m)**	**Grain Size**	**Bottom Contact**	**Texture**	**Modal Proportions**	**Alteration**	**BMS**	**Rock Name**
0.00	21.20	F-M	Gradational	Poorly Sorted	>90% quartz	-	-	Sandstone and Mudstone
21.20	301.16	F-M-C	Sharp	Laminated	>90% quartz	Epidote	-	Sandstone, mudstone and siltstone
301.16	340.22	M-C	Sharp	Inequigranular	cpx>quartz>feldspar	Epidote/Chl	-	Dolerite sill
340.22	371.05	F-M-C	Sharp	Laminated	>90% quartz	Epidote	-	Sandstone, mudstone and Conglomerate
371.05	377.60	F-M	Gradational	Sheared	>70% hematite	Hematite	-	Contact paleosol/Shale
377.60	626.40	M-C	Gradational	Equigranular	opx>plag>cpx	Epidote/Chl	-	Gabbronorite
626.40	640.00	M-C	Gradational	Inequigranular	opx>plag>cpx>ol	Serp/Chl	-	Olivine-bearing gabbronorite
640.00	695.00	M-C	Sharp	Poikilitic	ol>plag>opx (oikocrysts)	Serp/Chl	5%	Troctolite
695.00	665.16	PEG	Sharp	Pegmatoidal	ol>plag>opx (oikocrysts)	Serp/Chl	3%	Troctolite
665.16	701.00	M-C	Sharp	Poikilitic	ol>plag>opx (oikocrysts)	Serp/Chl	3%	Troctolite
701.00	704.50	M	Sharp	Homogeneous	opx>cpx>plag (interstitial)	-	3%	Feldspathic pyroxenite
704.50	705.30	M-C	Gradational	Poikilitic	ol>plag>opx (oikocrysts)	Serp/Chl	-	Troctolite
705.30	721.00	M-C	Gradational	Inequigranular	ol>opx>plag (interstitial)	Serp/Chl	5%	Harzburgite
721.00	723.85	M	Gradational	Poikilitic	ol>plag>opx (oikocrysts)	Serp/Chl	5%	Mela-troctolite
723.85	738.05	M-C	Gradational	Inequigranular	ol>opx>plag (interstitial)	Serp/Chl	5%	Harzburgite
738.05	744.20	M-C	Gradational	Poikilitic	ol>plag>opx (oikocrysts)	Serp/Chl	3%	Troctolite
744.20	751.50	M-C	Gradational	Inequigranular	ol>opx>plag (interstitial)	Serp/Chl	5%	Harzburgite
751.50	775.95	M-C	Gradational	Inequigranular	opx>cpx>ol	Serp	-	Olivine-bearing pyroxenite
775.95	777.22	M	Gradational	Homogeneous	opx>cpx>plag (interstitial)	-	3%	Feldspathic pyroxenite
777.22	785.88	M	Gradational	Inequigranular	opx>cpx>ol	Serp/phlog	5%	Olivine-bearing pyroxenite
785.88	792.70	M-C	Sharp	Equigranular	opx>plag>cpx	Chlorite	5%	Gabbronorite
792.70	794.58	M	Sharp	Homogeneous	opx>cpx>plag (interstitial)	-	3%	Feldspathic Pyroxenite
794.58	795.50	M-C	Sharp	Inequigranular	ol>opx>plag (interstitial)	Serp/Chl	3%	Harzburgite
795.50	803.00	M	Sharp	Homogeneous	opx>cpx>plag (interstitial)	-	2%	Feldspathic Pyroxenite
803.00	815.28	F-M	Gradational	Equigranular	opx>plag>cpx	Chlorite	7%	Gabbronorite
815.28	813.90	F-M	Gradational	Inequigranular	opx>quartz>feldspar	Serp	-	Granofels
813.90	837.30	F-M	Gradational	Inequigranular	opx	Serp	-	Orthopyroxenite
837.30	850.50	F-M	EOH	Inequigranular	quartz>feldspar>opx	-	-	Granofels

Appendix B: Core Log WE001D0

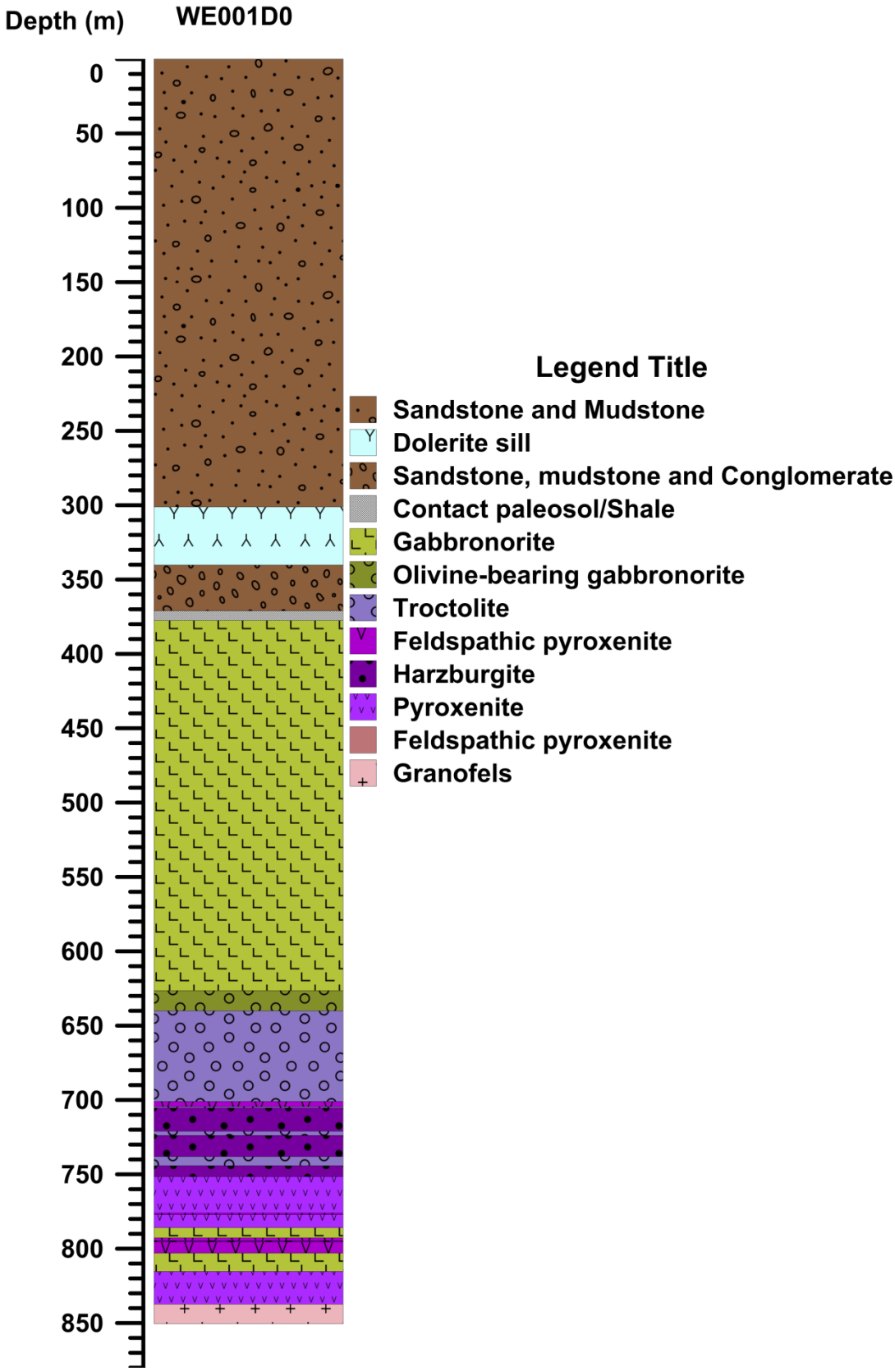

Appendix B: Core Log WE027D0

Core-Log of Borehole WE027D0								
From (m)	**To (m)**	**Grain Size**	**Bottom Contact**	**Texture**	**Modal Proportions**	**Alteration**	**BMS**	**Rock Name**
0.00	14.89	F-M	Gradational	Poorly sorted	>90% quartz	-	-	Sandstone and mudstone
14.89	410.35	F-M-C	Sharp	Laminated	>90% quartz	Epidote	-	Waterberg sediments
410.35	506.40	M-C	Sharp	Inequigranular	cpx>quartz>feldspar	Epidote/Chl	-	Dolerite
506.40	556.35	F-M-C	Sharp	Pebbly/laminated	>90% quartz	Epidote	-	Sandstone, mudstone and conglomerate
556.35	557.47	F-M	Gradational	Sheared	>70% hematite	Hematite/Epi	-	Bushveld paleosol/Shale
557.47	572.05	M-C	Gradational	Inequigranular	opx>plag>cpx	Epidote/Chl	-	Altered Gabbronorite
572.05	617.05	M-C	Sharp	Equigranular	opx>plag>cpx>mgt (10%)	Chlorite	-	Magnetite gabbronorite
617.05	625.57	PEG	Sharp	Pegmatoidal	opx>plag>cpx>mgt (10%)	Chlorite	-	Recrystalised magnetite gabbronorite
625.57	644.30	M-C	Gradational	Equigranular	opx>plag>cpx>mgt (5%)	Chlorite	-	Magnetite gabbronorite
644.30	653.70	M-C	Gradational	Equigranular	opx>plag>cpx	Chlorite	-	Gabbronorite
653.70	680.20	M-C	Gradational	Equigranular	opx>plag>cpx>ol>mgt (5%)	Chlorite	5%	Magnetite gabbronorite
680.20	716.63	M-C	Gradational	Equigranular	opx>plag>cpx	Chlorite	-	Gabbronorite
716.63	720.88	M-C	Sharp	Inequigranular	opx>plag>ol>cpx	Serp/Chl	-	Olivine-bearing gabbronorite
720.88	735.39	C-PEG	Sharp	Mottled	plag>cpx+mgt (oikocrysts)	Chlorite	-	Anorthosite
735.39	791.41	M-C	Sharp	Equigranular	opx>plag>cpx>ol (10%)	Chlorite	-	Mela-gabbronorite
791.41	806.10	M-C	Sharp	Inequigranular	cpx>quartz>feldspar	Epidote/Chl	-	Dolerite
806.10	810.31	M-C	Sharp	Equigranular	plag>opx>cpx	Chlorite	-	Leuco-gabbronorite
810.31	848.05	M-C	Sharp	Inequigranular	cpx>quartz>feldspar	Epidote/Chl	-	Dolerite
848.05	889.84	M-C	Sharp	Equigranular	opx>plag>cpx>mgt (5%)	Chlorite	10%	Magnetite gabbronorite
889.84	892.54	PEG	Sharp	Pegmatoidal	opx>plag>cpx>mgt (5%)	Chlorite	-	Recrystalised magnetite gabbronorite
892.54	980.95	M-C	Sharp	Equigranular	opx>plag>cpx>mgt (5%)	Chlorite	-	Magnetite gabbronorite
980.95	991.00	C	Sharp	Mottled	plag>cpx+mgt (oikocrysts)	Chlorite	-	Anorthosite
991.00	994.48	PEG	Sharp	Pegmatoidal/Mottled	opx>plag>cpx>mgt (5%)	Chlorite	-	Anorthosite
994.48	1241.47	M-C	Sharp	Inequigranular	cpx>quartz>feldspar	Epidote/Chl	-	Dolerite
1241.47	1242.46	M-C	Sharp	Equigranular	plag>opx>cpx>ol (5%)	Chlorite	-	Leuco-gabbronorite
1242.46	1251.70	M-C	Sharp	Inequigranular	cpx>quartz>feldspar	Epidote/Chl	-	Dolerite
1251.70	1256.50	M-C	Sharp	Equigranular	opx>plag>cpx	Chlorite	-	Gabbronorite
1256.50	1256.70	M-C	Sharp	Inequigranular	cpx>quartz>feldspar	Epidote/Chl	3%	Dolerite
1256.70	1274.74	M-C	Gradational	Equigranular	plag>opx>cpx	Chlorite	-	Leuco-gabbronorite
1274.74	1280.69	M-C	Gradational	Equigranular	opx>plag	-	-	Norite
1280.69	1380.22	M-C	Gradational	Equigranular	opx>plag>cpx>ol (5%)	Serp/Chl	-	Olivine-bearing gabbronorite
1380.22	1386.60	C	Gradational	Inequigranular	ol>opx>plag (interstitial)	Serp/Chl	5%	Harzburgite
1386.60	1422.20	M-C	Gradational	Inequigranular	opx>quartz>feldspar	Serp	3%	Granofels
1422.20	1427.00	F-M	Sharp	Homogeneous	opx>plag (interstitial)	Serp	-	orthopyroxenite
1427.00	1464.42	F-M	Sharp	Inequigranular	opx>quartz>feldspar	Serp	-	Granofels
1464.42	1465.95	F-M	Sharp	Homogeneous	opx>plag (interstitial)	Serp	-	orthopyroxenite
1465.95	1467.80	F-M	Sharp	Inequigranular	opx>quartz>feldspar	Serp	-	Granofels
1467.80	1470.20	F-M	Sharp	Homogeneous	opx>plag (interstitial)	Serp	-	Orthopyroxenite
1470.20	1477.39	F-M	EOH	Inequigranular	opx>quartz>feldspar	Serp	-	Granofels

Appendix B: Core Log WE027D0

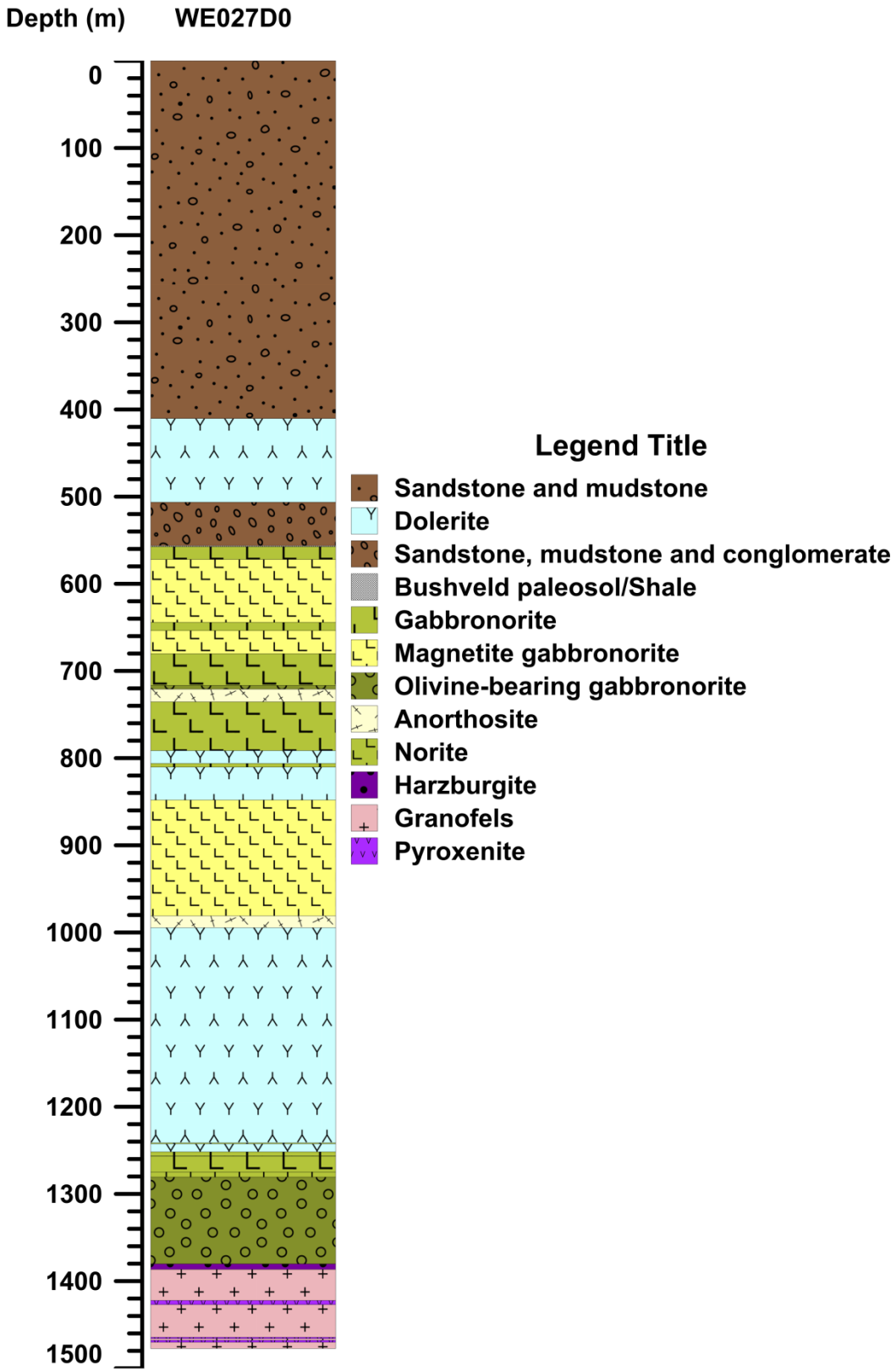

Appendix B: Core Log WE035D0

Core-Log of Borehole WE035D0								
From (m)	**To (m)**	**Grain Size**	**Bottom Contact**	**Texture**	**Modal Proportions**	**Alteration**	**BMS**	**Rock Name**
0.00	22.87	M-C	Gradational	Poorly Sorted	>90% quartz	-	-	Sandstone and mudstone
22.87	29.00	M-C	Gradational	Poorly Sorted	>90% quartz	Epidote	-	Sandstone and mudstone
29.00	275.03	F-M-C	Sharp	Laminated	>90% quartz	Epidote	-	Sandstone, mudstone and siltstone
275.03	344.39	M-C	Sharp	Ineqigranular	cpx>quartz>feldspar	Epidote/Chl	-	Dolerite
344.39	368.61	F-M-C	Sharp	Pebbly/laminated	>90% quartz	Epidote	-	Sandstone, mudstone and conglomerate
368.61	373.57	F-M	Gradational	Sheared	>70% hematite	Hematite	-	Bushveld paleosol/Shale
373.57	393.70	M-C	Sharp	Equigranular	opx>plag>cpx	Epidote/Chl	-	Gabbronorite
393.70	394.23	PEG	Sharp	Pegmatoidal	opx>plag>cpx	Chlorite	-	Recrystalised gabbronorite
394.23	495.55	M-C	Sharp	Inequigranular	opx>plag>cpx>ol	Serp/Chl	-	Olivine-bearing gabbronorite
495.55	499.51	M	Sharp	Homogeneous	opx>cpx>plag (interstitial)	-	-	Feldspathic pyroxenite
499.51	509.74	M-C	Sharp	Inequigranular	opx>plag>cpx>ol	Serp/Chl	-	Olivine-bearing gabbronorite
509.74	511.08	M	Sharp	Homogeneous	opx>cpx>plag (interstitial)	-	-	Feldspathic pyroxenite
511.08	519.30	M-C	Sharp	Ineqigranular	opx>plag>ol	Serp	-	Olivine Norite
519.30	520.30	M	Sharp	Homogeneous	opx>cpx>plag (interstitial)	-	-	Feldspathic pyroxenite
520.30	527.10	M-C	Gradational	Ineqigranular	opx>plag>ol	Serp/Chl	-	Olivine Norite
527.10	542.10	M-C	Gradational	Poikilitic	ol>plag>opx (oikocrysts)	Serp/Chl	-	Troctolite
542.10	546.20	M-C	Gradational	Spotted	opx>plag	Chlorite	-	Altered Norite
546.20	572.03	M-C	Sharp	Inequigranular	opx>plag>ol	Serp/Chl	-	Olivine Norite
572.03	602.10	M-C	Sharp	Homogeneous	opx>cpx>plag (interstitial)	-	-	Feldspathic pyroxenite
602.10	604.22	M-C	Gradational	Poikilitic	ol>plag>opx (oikocrysts)	Serp/Chl	3%	Troctolite
604.22	614.50	M-C	Gradational	Homogeneous	opx>cpx>plag (interstitial)	-	5%	Feldspathic Harzburgite
614.50	618.96	M-C	Gradational	Homogeneous	opx>cpx>plag (interstitial)	-	5%	Feldspathic pyroxenite
618.96	621.32	M-C	Sharp	Inequigranular	opx>plag>ol	Serp	1%	Olivine Norite
621.32	621.90	M	Sharp	Homogeneous	opx>cpx>plag (interstitial)	-	3%	Pyroxenite
621.90	630.02	M	Gradational	Homogeneous	opx>cpx>plag (interstitial)	-	5%	Feldspathic pyroxenite
630.02	645.05	M	Gradational	Homogeneous	opx>cpx>plag (interstitial)	-	3%	Pyroxenite
645.05	660.45	F-M	Gradational	Inequigranular	opx>quartz>feldspar	Serp	-	Granofels
660.45	666.95	F-M	Gradational	Inequigranular	quartz>feldspar	-	-	Granofels (felsic-rich)
666.95	730.47	F-M	EOH	Inequigranular	opx>quartz>feldspar	Serp	-	Granofels

Appendix B: Core Log WE035D0

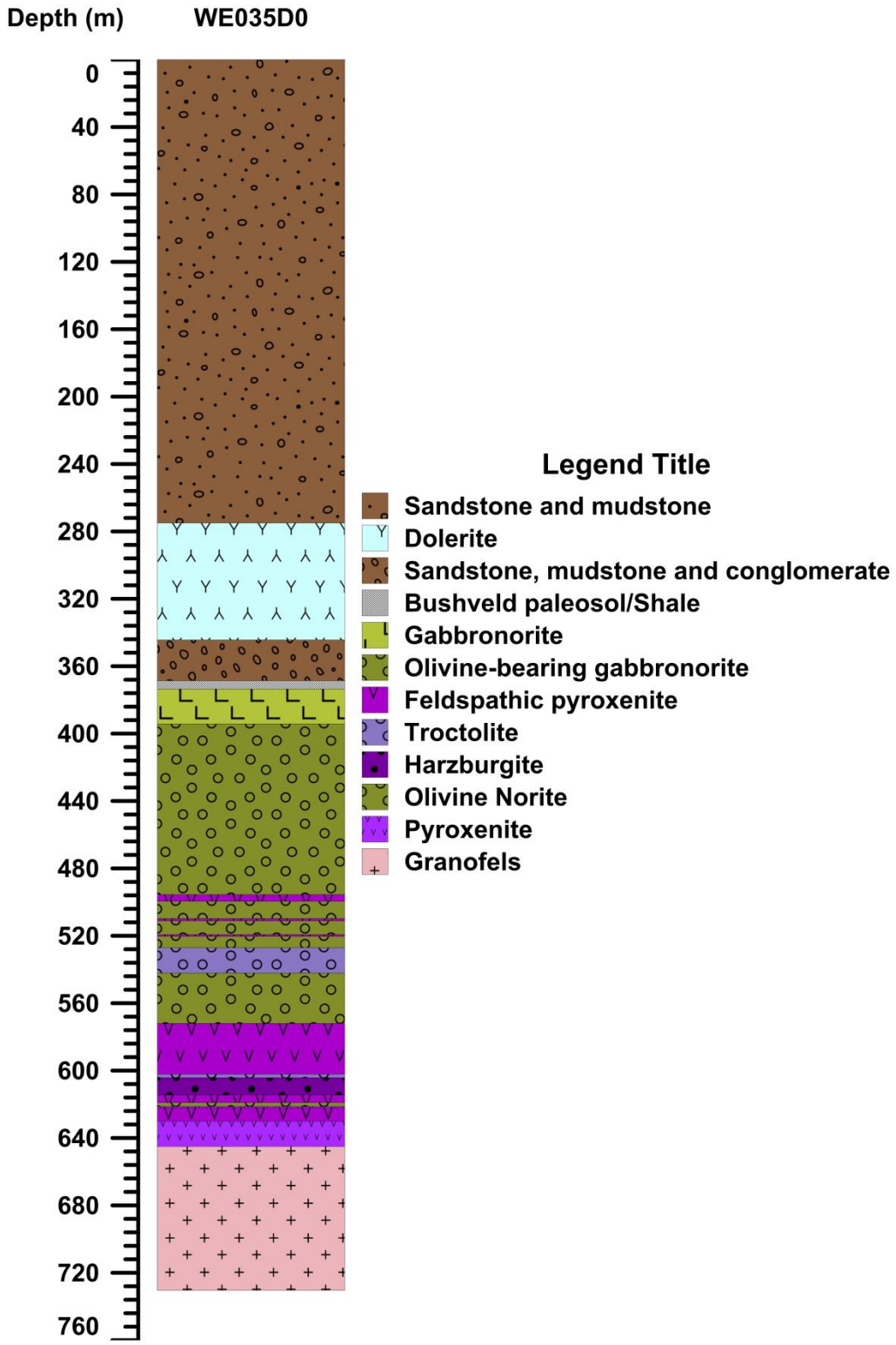

Appendix C

Hand-Sample Descriptions

(WB017 D0)

(WB027 D0)

(WB099 D0)

(WE001 D0)

(WE027 D0)

(WE035 D0)

WE001 D0 – Footwall samples

WE002 D0 – Footwall samples

WE003 D0 – Sill samples

WE005 D0 – Footwall samples

WE027 D0 – Footwall samples

Hand samples from sulphur isotope study

Appendix C:
Table 1: Hand Sample Description WB017

Sample Number (meter interval)	Major Minerals	Minor Minerals	Colour, Textures and features	Grain Size	Model Abundance	Rock Name	Sample Picture
(30.80 m - 31.00 m)	Quartz, clay minerals and lithic fragments	Unknown dark brown/black mineral	Alternating layers of pinkish white and purple brown	0.5-1.0 mm Fine-grained	Quartz 80%, Clay minerals and opaques 15% , lithic fragments 5%	**Sandstone**	
(93.78 m - 93.96 m)	Quartz, clay minerals and lithic fragments	Unknown black mineral Possible magnetite	Alternating bands of white which pinkish fragments, dark brown	0.7-1.2 mm medium-grained with 4 mm pink euhedral grains	Quartz 70%, clay minerals and opaques 20%, lithic fragments 10%	**Banded Arkose**	
(141.23 m - 141.64 m)	Quartz, clay minerals, lithic fragments	Unknown Black mineral	Light brown matrix, with light to transparent pebble casts	Matrix fine-grained less 1.0 mm, pebble casts 1.0-3.0 cm	Quartz 60%, clay minerals and opaques 30%, lithic fragments 10%	**Pebble Conglomerate**	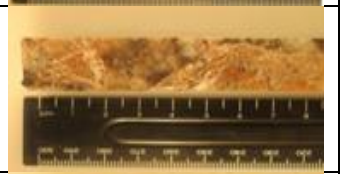
(156.36 m - 156.54 m)	Plagioclase, quartz, biotite	Unknown fine-grained black mineral	Black and white with orange/brown crystals	0.2-4.00 mm Coarse-grained	Plagioclase 70%, Quartz 15%, biotite 3%, unknown black mineral 2%	**Dolerite (sill)**	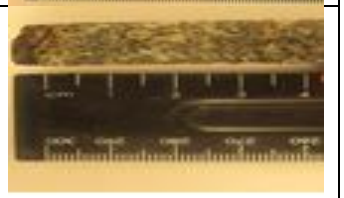
(198.55 m - 198.81 m)	Plagioclase, pyroxenes (Cpx and Opx), magnetite	Sulphides	Dark grey Opx + magnetite and pinkish Cpx, light grey plagioclase	1.0-4.0 mm	Cpx 15%, Opx 25%, plagioclase 45%, biotite 2%, Apatite 3%, magnetite 10%	**Ferro Gabbro**	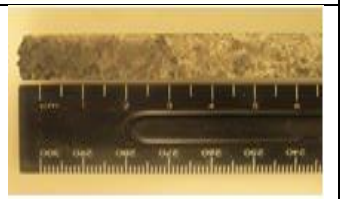
(201.20 m - 201.42 m)	Plagioclase, pyroxenes (Opx, Cpx) and magnetite	Sulphides	Dark grey Opx, black magnetite, pinkish grey Cpx, light grey plagioclase	1.0-5.0 mm	Opx 25%, Cpx 20%, plagioclase 40%, magnetite 10%, apatite 5%	**Ferro Gabbro**	

Appendix C:
Table 1: Hand Sample Description WB017

Sample Number (meter interval)	Major Minerals	Minor Minerals	Colour, Textures and features	Grain Size	Model Abundance	Rock Name	Sample Picture
(206.29 m - 206.57 m)	Plagioclase, pyroxenes (Opx + Cpx) magnetite	None	Light grey plagioclase and Cpx, Dark grey Opx and magnetite	1.0-5.0 mm	Plagioclase 45%, Cpx 15%, Opx 30%, magnetite 10%	**Magnetite Gabbronorite**	
(253.66 m - 253.86 m)	Plagioclase, pyroxenes (Opx, Cpx), magnetite	None	Light grey plagioclase and Cpx, Dark grey Opx and magnetite	1.0-7.0 mm	Plagioclase 40%, Cpx 20%, Opx 25%, magnetite 15%	**Magnetite Gabbronorite**	
(294 m - 294.21 m)	Plagioclase, pyroxenes (Opx, Cpx), magnetite	None	Light grey plagioclase and Cpx, Dark grey Opx and magnetite	1.0-5.0 mm	Plagioclase 45%, Cpx 25%, Opx 20%, magnetite 10%	**Magnetite Gabbronorite**	
(303.43 m - 303.70 m)	Plagioclase, pyroxenes (Opx, Cpx)	Magnetite	Light grey plagioclase and Cpx, Dark grey Opx and magnetite	1.0-4.0 mm	Plagioclase 50%, Cpx 15%, Opx 30%, magnetite 5%	**Gabbronorite**	
(311.16 m - 311.40 m)	Plagioclase, pyroxenes (Opx, Cpx)	None	Light grey plagioclase and Cpx, Dark grey Opx. Alteration (chloritisation)	1.0-2.0 mm	Plagioclase 65%, Cpx 15%, Opx 20%	**Leuco-Gabbronorite**	
(465.00 m - 465.20 m)	Pyroxenes (Cpx + Opx), plagioclase	None	Light grey plagioclase and Cpx, Dark grey Opx	2.0-5.0 mm	Plagioclase 15%, Cpx 35%, Opx 50%	**Pyroxenite**	

Appendix C:
Table 1: Hand Sample Description WB017

Sample Number (meter interval)	Major Minerals	Minor Minerals	Colour, Textures and features	Grain Size	Model Abundance	Rock Name	Sample Picture
(532.00 m - 532.30 m)	Plagioclase, pyroxenes (Opx, Cpx)	Inverted pigeonite	Light grey plagioclase and Cpx, Dark grey Opx	2.0-8.0 mm	Plagioclase 40%, Cpx 30%, Opx 30%	**Gabbronorite**	
(539.20 m - 539.45 m)	Plagioclase, pyroxenes (Opx, Cpx), magnetite	Inverted pigeonite and plagioclase	Light grey plagioclase and Cpx, Dark grey Opx, black magnetite	1.0-2.5 cm Coarse-grained	Plagioclase 40%, Cpx 15%, Opx 35%, magnetite 10%	**Feldspathic pyroxenite**	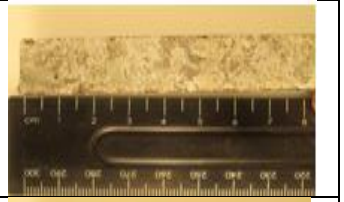
(633.00 m - 633.21 m)	Plagioclase	Pyroxene	Plagioclase light grey to white and pyroxenes greenish grey,	0.5-2.5 cm coarse-grained	Plagioclase 80%, pyroxenes 20%	**Pegmatoid**	
(649.25 m - 649.50 m)	Plagioclase, pyroxenes (Opx, Cpx),	None	Plagioclase and Cpx light grey, dark grey Opx, olivine rims Opx	0.5-1.0 cm	Plagioclase 30%, Opx 40%, Cpx 20%, Olivine 10%	**Gabbronorite**	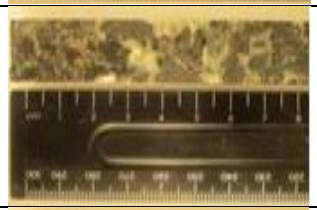
(658.00 m - 658.25 m)	Plagioclase, pyroxenes (Opx, Cpx)	None	Plagioclase and Cpx light grey, dark grey Opx,	0.6-1.5 cm	Plagioclase 60%, Opx 20%, Cpx 20%	**Pegmatoid/ Leuco-Gabbronorite**	
(682.50 m - 682.71 m)	Plagioclase, pyroxenes (Opx, Cpx),	None	Plagioclase and Cpx light grey, dark grey Opx	2.0-5.0 mm	Plagioclase 65%, Opx 15%, Cpx 20%	**Leuco-Gabbronorite**	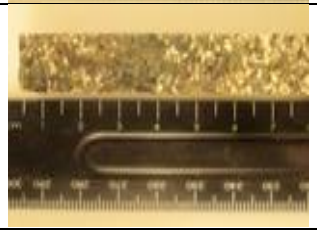

Appendix C:
Table 1: Hand Sample Description WB017

Sample Number (meter interval)	Major Minerals	Minor Minerals	Colour, Textures and features	Grain Size	Model Abundance	Rock Name	Sample Picture
(700.28 m - 700.52 m)	Plagioclase	Pyroxenes	Light grey to green, mottle texture	1.0-3.0 mm	Plagioclase 95%, Altered pyroxenes 5%	**Anorthosite**	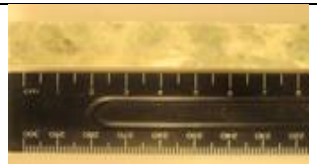
(711.88 m - 712.10 m)	Plagioclase	Pyroxene (brozonite)	Light grey, and light brown brozonite	0.5-1.0 cm	Plagioclase 90%, Altered pyroxenes (brozonite) 10%	**Anorthosite**	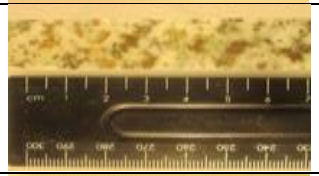
(730.26 m - 730.65 m)	Plagioclase, pyroxenes (Opx, Cpx)	None	Plagioclase light grey to white, Cpx light grey, dark grey Opx	3.0-8.0 mm	Plagioclase 65%, Opx 15%, Cpx 20%	**Leuco-Gabbronorite**	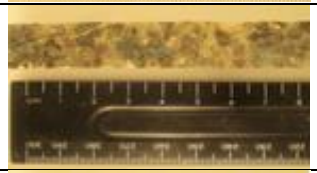
(765.27 m - 765.64 m)	Plagioclase, pyroxenes (Opx, Cpx)	Inverted pigeonite	Plagioclase light grey to white, Cpx light grey, dark grey Opx	1.0-5.0 mm	Plagioclase 60%, Opx 20%, Cpx 20%	**Leuco-Gabbronorite**	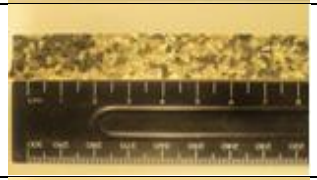
(842.74 m - 842.53 m)	Plagioclase, pyroxenes (Opx, Cpx)	None	Plagioclase light grey to white, Cpx light grey, dark grey Opx	3.0-5.0 mm	Plagioclase 55%, Opx 20%, Cpx 25%	**Leuco-Gabbronorite**	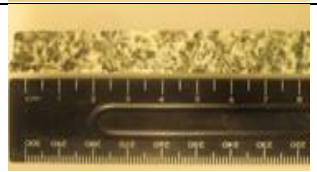
(965.52 m - 965.70 m)	Plagioclase, pyroxenes (Opx, Cpx)	Sulphides	Plagioclase light grey to white, Cpx light grey, dark grey Opx. Alteration	3.0-5.0 mm	Plagioclase 60%, Opx 20%, Cpx 20%	**Leuco-Gabbronorite**	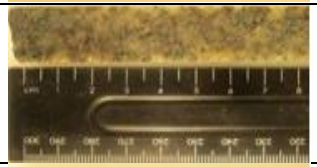
(988.74 m - 988.94 m)	Plagioclase, pyroxene (Cpx + Cpx), olivine	Inverted pigeonite	White plagioclase, dark grey green olivine and Opx	3.0-5.0 mm	Plagioclase 35%, olivine 30%, pyroxenes 20%	**Troctolite**	

Appendix C:
Table 1: Hand Sample Description WB017

Sample Number (meter interval)	Major Minerals	Minor Minerals	Colour, Textures and features	Grain Size	Model Abundance	Rock Name	Sample Picture
(1003.74 m - 1003.95 m)	Plagioclase, pyroxene (Cpx + Cpx), olivine	Sulphides	Dark blackish green circler olivine, Opx light grey and plagioclase greenish white. Alteration	0.2-1.0 cm	Plagioclase 15%, olivine 40%, pyroxenes 45%	**Harzburgite**	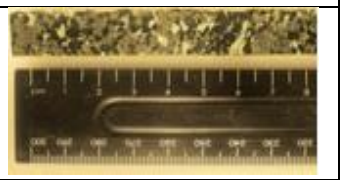
(1015.29 m - 1015.50 m)	Plagioclase, pyroxene (Cpx + Cpx)	None	White plagioclase, light grey pyroxenes. Alteration (chloritisation)	0.1-1.0 mm	Plagioclase 65%, pyroxenes 35%	**Leuco-Gabbronorite**	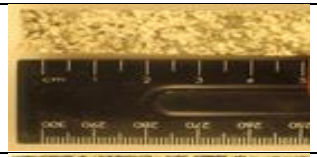
(1019.50 m - 1019.26 m)	Plagioclase, pyroxene (Cpx + Cpx), olivine	Sulphides	Whitish green plagioclase, dark grey green olivine and Opx	2.0-6.0 mm	Plagioclase 20%, olivine 40%, pyroxenes 30%	**Harzburgite**	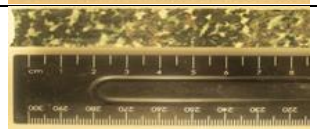
(1051.00 m - 1051.21 m)	Pyroxenes (Opx + Cpx), Plagioclase	Sulphides	Light grey plagioclase, Darker grey pyroxenes. Alteration (Serpentinisation)	2.0-5.0 mm	Plagioclase 15%, Cpx 35%, Opx 45%, Sulphides 5%	**Pyroxenites**	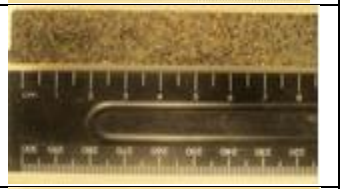
(1072.80 m - 1073.00 m)	Pyroxenes (Opx + Cpx), Plagioclase	Sulphides	Light grey plagioclase, Darker grey pyroxenes. Alteration (Serpentinisation)	2.0-5.0 mm	Plagioclase 15%, Cpx 35%, Opx 45%, Sulphides 5%	**Pyroxenites**	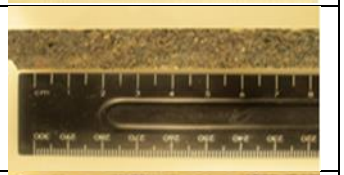
(1077.90 m - 1078.10 m)	Plagioclase, pyroxenes (Cpx)	Micas : phlogopite	Light grey plagioclase and Cpx. Light brown micas	1.0-0.5 mm	Plagioclase 85%, Cpx 10%, micas (phlogopite) 5%	**Plagioclase vein**	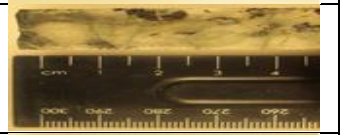
(1086.70 m - 1086.90 m)	Quartz	None	Light grey, veins and fractures	0.1-0.2 mm very fine-grained	Quartz 95%	**Quartzite**	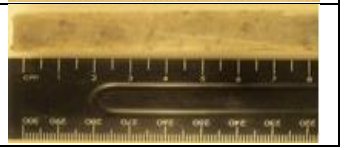

Appendix C:
Table 2: Hand Sample Description WB027

Sample Number WB027 (Meter Interval)	**Major Minerals**	**Minor Minerals**	**Colour Texture and Features**	**Grain Size**	**Other Features**	**Modal Abundance & Rock Name**	**Hand Sample Picture**
488.00 m – 488.10 m	Feldspars (plagioclase), Large quartz pebbles and hematite (extremely altered pyroxenes).	Magnetite	Shale unit, extremely altered gabbronorite and a gabbro texture. Large milky white quartz pebbles with sub-rounded shape.	3.00-9.00 mm	Alteration; epidotisation and hematisation. Hematite has completely altered the pyroxene grains.	Feldspars (plagioclase) 40%, Quartz pebbles 20%, extremely altered pyroxenes (hematisation) 38% and magnetite 3% locally. **Extremely Altered Gabbronorite**	
490.60 m – 490.80 m	Feldspars (plagioclase) and hematite (extremely altered pyroxenes).	Chlorite	Extremely altered gabbronorite and a gabbro texture. Most of the pyroxenes have been altered to hematite (reddish rusty material).	3.00-5.00 mm	Alteration; epidotisation and hematisation. Hematite has completely altered the pyroxene grains.	Feldspars (plagioclase) 45%, extremely altered pyroxenes (hematisation) 50% and Chlorite 5%. **Extremely Altered Gabbronorite**	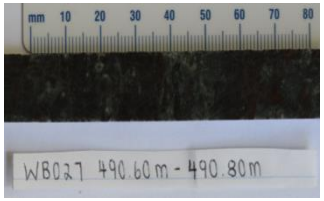
520.63 m – 520.80 m	Pyroxenes (Opx and Cpx) and Feldspars (plagioclase)	Magnetite and Chlorite	Large crystals of pyroxenes with interstitial plagioclase and magnetite.	1.00-2.50 cm	Veinlets filled with secondary minerals; Chlorite (altered). Large cumulus grains of magnetite.	Pyroxenes: Opx 25%, Cpx 25%, plagioclase 40%, Magnetite 7% locally and chlorite 3%. **Recrystalised gabbronorite, Pegmatoidal unit**.	
537.64 m – 537.85 m	Pyroxenes (Opx and Cpx) and Feldspars (plagioclase)	Magnetite, sulphides (chalcopyrite) and Chlorite	Opx, Cpx, plagioclase, magnetite are cumulus. Cpx and Opx are different shades of grey. Plagioclase is transparent. Magnetite is lustre	3.00-9.00 mm	Sulphides are disseminated 1% locally. The greenish tint seen is due to alteration (chloritisation).	Pyroxenes: Opx 20%, Cpx 26%, plagioclase 40%, Magnetite 10% locally, chlorite 3% and sulphides 1%. **Magnetite bearing Gabbronorite**	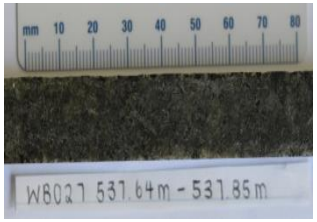

Appendix C:
Table 2: Hand Sample Description WB027

Sample Number WB027 (Meter Interval)	**Major Minerals**	**Minor Minerals**	**Colour Texture and Features**	**Grain Size**	**Other Features**	**Modal Abundance & Rock Name**	**Hand Sample Picture**
606.00 m – 606.20 m	Pyroxenes (Opx and Cpx) and Feldspars (plagioclase)	Magnetite, sulphides (chalcopyrite and pyrrhotite) and Chlorite	Opx, Cpx and plagioclase are cumulus. Cpx and Opx are different shades of grey. Plagioclase is transparent. Magnetite is lustre	3.00-5.00 mm	Sulphides are disseminated 3% locally. The greenish tint seen is due to alteration (chloritisation).	Pyroxenes: Opx 20%, Cpx 27%, plagioclase 40%, Magnetite 10% locally, chlorite 3% and sulphides 3% locally. **Magnetite bearing Gabbronorite**	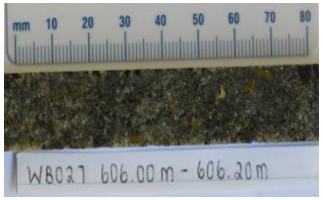
622.00 m – 622.20 m	Feldspars (plagioclase) and pyroxenes (Opx and Cpx)	Chlorite and inverted pigeonite.	The plagioclase is dominated with both a milky white and transparent colour. Cpx is pinkish grey.	2.00-5.00 mm	The greenish tint seen is due to alteration (chloritisation).	Pyroxenes: Opx 15%, Cpx 25%, plagioclase 55% and chlorite 5% **Altered gabbronorite**	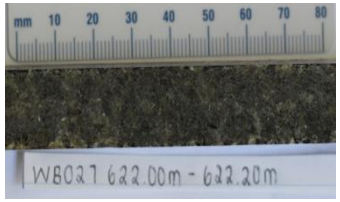
649.20 m – 649.40 m	Pyroxenes (Opx and Cpx).	Plagioclase, sulphides (chalcopyrite) and inverted pigeonite.	Pyroxenes are grey (Cpx with a pinkish tint). The plagioclase is interstitial.	3.00-6.00 mm	The greenish tint seen is due to alteration (chloritisation).	Pyroxenes: Opx 35%, Cpx 40%, plagioclase 10%, inverted pigeonite 3%. chlorite 5% and sulphides 2% **Pyroxenite**	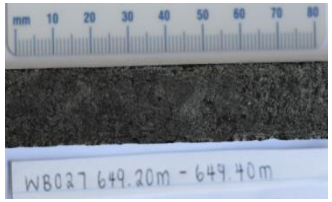
815.20 m – 815.30 m	Feldspars (plagioclase) and pyroxenes (Opx).	chlorite	Plagioclase is the dominate mineral with a milky white colour and a green tint due to alteration. Pyroxenes are cumulus.	3.00-5.00 mm	Veinlets and fracture are filled with secondary minerals (chlorite)	Feldspars (plagioclase) 65%, Pyroxenes (Opx) 30% and chlorite 5%. **Slight altered Norite**	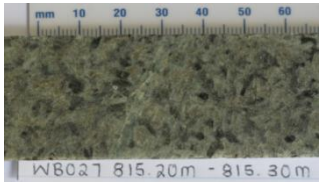

Appendix C:
Table 2: Hand Sample Description WB027

Sample Number WB027 (Meter Interval)	**Major Minerals**	**Minor Minerals**	**Colour Texture and Features**	**Grain Size**	**Other Features**	**Modal Abundance & Rock Name**	**Hand Sample Picture**
881.00 m – 881.25 m	Feldspars (plagioclase) and pyroxenes (Opx and Cpx)	Chlorite and inverted pigeonite.	The plagioclase is dominated with both a milky white and transparent colour. Cpx is pinkish grey.	3.00-7.00 mm	The greenish tint seen is due to alteration (chloritisation).	Pyroxenes: Opx 25%, Cpx 30%, plagioclase 40% and chlorite 5% **Gabbronorite**	
889.00 m – 889.10 m	Feldspars (plagioclase).	Pyroxenes (altered) and chlorite.	Plagioclase is the dominate minerals with a milky white colour and a sugary texture.	1.00-5.00 mm	Alteration; Chloritisation.	Plagioclase 80-90%, altered pyroxenes (Opx and Cpx) 5-10% and Chlorite 5% **Altered Anorthosite**	
928.48 m – 928.70 m	Feldspars (plagioclase) and Pyroxene (Opx).	Cpx and Chlorite	Dominate pyroxene is Opx grey colour with interlocking crystals. Plagioclase is either white are transparent.	3.00-7.00 mm	Alteration; Chloritisation seen in the plagioclase as a greenish tint and seen rimming some of the pyroxene crystals.	Plagioclase 50%, pyroxenes; Opx 40%, Cpx 5% and chlorite 5%. **Norite**	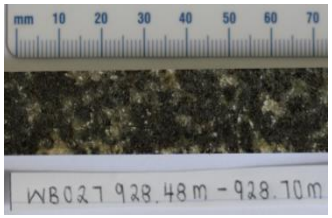
939.50 m – 939.70 m	Feldspars (plagioclase) and Pyroxene (Opx).	Cpx, Chlorite and inverted pigeonite.	Large oikocrysts of Opx (greenish grey), dominate mineral is plagioclase pinkish white.	7.00-2.00 mm	Mottle texture. Alteration; Chloritisation	Plagioclase 50%, pyroxenes; Opx 35%, inverted pigeonite 10%, Cpx 3% and chlorite 2%. **Mottle Norite**	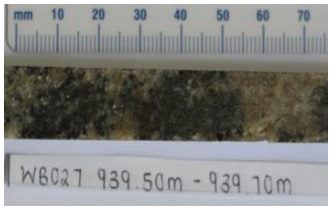

Appendix C:
Table 2: Hand Sample Description WB027

Sample Number WB027 (Meter Interval)	**Major Minerals**	**Minor Minerals**	**Colour Texture and Features**	**Grain Size**	**Other Features**	**Modal Abundance & Rock Name**	**Hand Sample Picture**
1060.50 m – 1060.70 m	Olivine, pyroxenes: Opx and Cpx and Feldspars (plagioclase).	Chlorite, sulphides (chalcopyrite) and inverted pigeonite.	Large oikocrysts of Opx (greenish grey). Olivine round, greenish black crystals. Plagioclase is greenish white and interstitial.	2.00-5.00 mm	Alteration; Chloritisation.	Olivine 40%,Plagioclase 15%, pyroxenes; Opx 35%, inverted pigeonite 10%, Cpx 3%, chlorite 2% and sulphides (chalcopyrite) 1% locally **Troctolite.**	
1090.70 m – 1090.90 m	Altered olivine, Plagioclase and Pyroxenes.	Chlorite and serpentine	Olivine round, greenish yellow in colour. Olivine rimming by chlorite and some grains have been completely altered. Plagioclase is both cumulus and intercumulus.	2.00-5.00 mm	Veinlets and fracture filled with secondary minerals (Feldspars). The plagioclase is a milky white colour.	Altered Olivine 55%, plagioclase 20%, Altered Opx 15% and 10% chlorite. **Extremely Altered Harzburgite.**	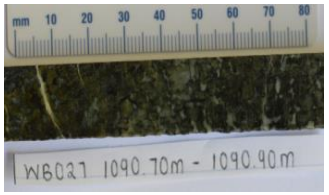
1092.00 m – 1092.20 m	Pyroxenes; Opx, feldspars (plagioclase) and olivine	Inverted pigeonite, chlorite and serpentine	White cumulus plagioclase. Round, greenish black olivine. Large interlocking crystals of Opx. Troctolite texture.	4.00-7.00 mm	Interlocking crystals of inverted pigeonite with a lustre colour when held at the right angle in the light. Greenish tint is alteration; Chloritisation	Olivine 15%, plagioclase 45%, Altered Opx 30%, Inverted pigeonite 7% and chlorite 3%. **Olivine bearing Norite.**	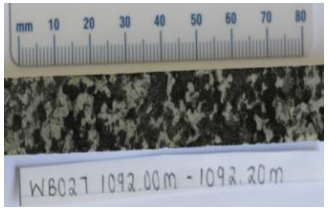
1116.10 m – 1116.22 m	Serpentine	Sulphides (chalcopyrite) and plagioclase.	The sample is completely black and fine-grained.	1.00-2.00 mm	Veinlets and fracture filled with feldspars (plagioclase). Altered serpentinisation.	Serpentine 95%, plagioclase 5% and sulphides (chalcopyrite) 1% locally. **Extremely altered unit (serpentinised unit).**	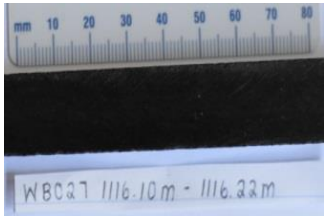

Appendix C:
Table 2: Hand Sample Description WB027

Sample Number WB027 (Meter Interval)	**Major Minerals**	**Minor Minerals**	**Colour Texture and Features**	**Grain Size**	**Other Features**	**Modal Abundance & Rock Name**	**Hand Sample Picture**
1152.20 m – 1152.40 m	Altered olivine, Plagioclase and Pyroxenes (Opx).	Chlorite, serpentine and sulphides (chalcopyrite and pyrrhotite).	Olivine round, greenish yellow in colour. Olivine rimming by chlorite and some grains have been completely altered. Plagioclase is both cumulus and intercumulus.	2.00-7.00 mm	Veinlets and fracture filled with secondary minerals (Feldspars). The plagioclase is a milky white colour.	Altered Olivine 55%, plagioclase 15%, Altered Opx 20%, sulphides (chalcopyrite and pyrrhotite) 3% locally and 5% chlorite. **Altered Harzburgite.**	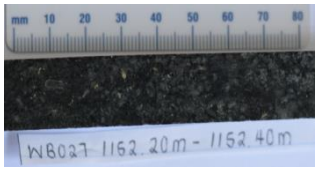
1174.70 m – 1174.80 m	Feldspars (plagioclase), Quartz and pyroxenes (Cpx and Opx)	Sulphides (chalcopyrite and pyrrhotite).	Feldspars (plagioclase) and quartz is milky white and large interlocking crystals. Pyroxenes grey to black.	3.00-8.00 mm	The sulphides are disseminated and are associated with the pyroxenes. Alternating units of feldspars and pyroxenes. Fractures and veinlets filled with secondary minerals.	Feldspars (plagioclase) 35%, Quartz 15%, pyroxenes 45% and sulphides 5% locally. **Granofels**	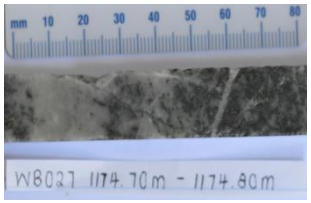
1178.10 m – 1178.20 m	Feldspars (plagioclase) and Quartz.	Pyroxenes and Epidote	Quartz white and coarse-grained. Small amounts of pyroxenes greenish black.	2.00 mm- 1.2 cm	Feldspars extremely altered epidotisation lime-green colour and yellow colour of alteration. Veinlet 2.00 cm thick filled with plagioclase and quartz.	Feldspars (plagioclase) 45%, Quartz 20%, pyroxenes 5% and epidotisation 30%. **Altered Granofels** (feldspars unit)	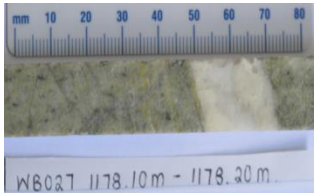

Appendix C:
Table 3: Hand Sample Description WB099

Sample Number WB099 (Meter Interval)	**Major Minerals**	**Minor Minerals**	**Colour and Textures**	**Grain Size**	**Other Features**	**Modal Abundance & Rock Name**	**Hand Sample Picture**
527.58 m-528.06 m	Pyroxenes (Opx and Cpx) and Feldspar (plag).	Sulphides (chalcopyrite and pyrrhotite) and magnetite.	Cumulates of both Pyroxenes (Opx and Cpx) and feldspars. Pyroxenes pinkish/greenish grey and feldspars with a milky white or transparent colour. Interlocking and equigranular texture. Phaneritic texture.	5.00-8.00 mm (Coarse-grained)	Sulphides (chalcopyrite) are disseminated. The magnetite is cumulus locally. Inverted pigeonite (Exsolution with both the pyroxenes) locally.	Pyroxenes (Opx and Cpx); 50-55% and Feldspars (plag) 45-50%, sulphides 1-2% locally and magnetite 5-10% locally. **Magnetite-Gabbronorite**	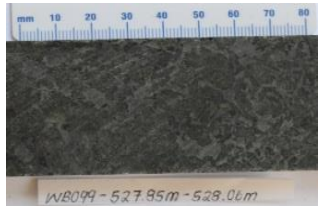
551.80 m-552.00 m	Pyroxenes (Opx and Cpx) and Feldspar (plag).	Sulphides (chalcopyrite and pyrrhotite) and magnetite.	Cumulates of both Pyroxenes (Opx and Cpx) and feldspars. Pyroxenes pinkish/greenish grey and feldspars with a milky white or transparent colour. Interlocking and equigranular texture. Phaneritic texture.	4.00-7.00 mm (Medium-Coarse-grained)	Sulphides (chalcopyrite) are disseminated. The magnetite is cumulus locally. Inverted pigeonite (Exsolution with both the pyroxenes) locally.	Pyroxenes (Opx and Cpx); 50-55% and Feldspars (plag) 45-50%, sulphides 1-3% locally and magnetite 5-10% locally. **Magnetite-Gabbronorite**	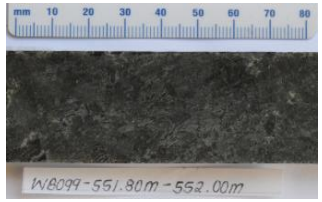
566.48 m-566.66 m	Pyroxenes (Opx and Cpx) and Feldspar (plag).	Sulphides (chalcopyrite) and magnetite.	Cumulates of both Pyroxenes (Opx and Cpx) and feldspars. Pyroxenes pinkish/greenish grey and feldspars with a milky white or transparent colour. Interlocking and equigranular texture. Phaneritic texture.	4.00-6.00 mm (Medium-Coarse-grained)	Sulphides (chalcopyrite) are disseminated. Inverted pigeonite (Exsolution with both the pyroxenes) locally.	Pyroxenes (Opx and Cpx); 50-55% and Feldspars (plag) 45-50%, sulphides 1-3% locally and magnetite 2-5% locally. **Magnetite-Gabbronorite**	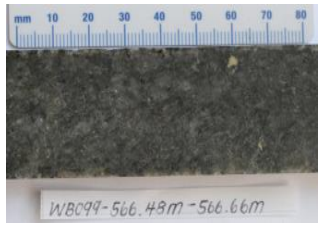

Appendix C:
Table 3: Hand Sample Description WB099

Sample Number WB099 (Meter Interval)	**Major Minerals**	**Minor Minerals**	**Colour and Textures**	**Grain Size**	**Other Features**	**Modal Abundance & Rock Name**	**Hand Sample Picture**
602.26 m-602.43m	Pyroxenes (Opx and Cpx) and Feldspar (plag).	Sulphides (chalcopyrite) and magnetite.	Cumulates of both Pyroxenes (Opx and Cpx) and feldspars. Pyroxenes pinkish/greenish grey and feldspars with a milky white or transparent colour. Interlocking and equigranular texture. Phaneritic texture.	4.00-7.00 mm (Medium-Coarse-grained)	Sulphides (chalcopyrite) are disseminated.	Pyroxenes (Opx and Cpx); 50-55% and Feldspars (plag) 45-50%, sulphides 2% locally and magnetite 2-5% locally. **Magnetite-Gabbronorite (T-reef)**	
619.80 m-620.00 m	Pyroxenes (Opx and Cpx).	Feldspars (plag).	Pyroxenes have a cumulus texture, pinkish and greenish grey. Feldspars (plag) intercumulus and cumulus, milky white or transparent colour. Inequigranular and phaneritic texture, with interlocking crystals.	3.00-7.00 mm (medium-Coarse-grained)	None.	Pyroxenes: Opx and Cpx; 75% and Feldspars: plag; 25%. **Feldspathic Pyroxenite unit (T-reef)**	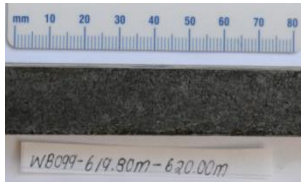
628.50 m-628.68 m	Pyroxenes (Opx and Cpx) and Feldspar (plag).	Sulphides (chalcopyrite) and magnetite	Cumulates of both Pyroxenes (Opx and Cpx) and feldspars. Pyroxenes pinkish/greenish grey and feldspars with a milky white or transparent colour. Interlocking and equigranular texture. Phaneritic texture.	4.00-8.00 mm (Medium-Coarse-grained)	Sulphides (chalcopyrite) are disseminated.	Pyroxenes (Opx and Cpx); 50-55% and Feldspars (plag) 45-50%, sulphides 2% locally and magnetite 2-5% locally. **Magnetite-Gabbronorite (T-reef)**	
671.57 m-671.74 m	Pyroxenes (Opx and Cpx).	Feldspars (plag), sulphides (pyrrhotite and chalcopyrite) and magnetite.	Pyroxenes have a cumulus texture, pinkish and greenish grey. Feldspars (plag) intercumulus and cumulus, milky white colour. Inequigranular and phaneritic texture, with interlocking crystals.	3.00-5.00 mm (medium-grained)	Sulphides (chalcopyrite, pyrrhotite and pentlandite) are disseminated. Disseminated magnetite.	Pyroxenes: Opx and Cpx; 75%, Feldspars: plag; 25% and sulphides (chalcopyrite) 1% locally. **Feldspathic Pyroxenite unit (T-reef)**	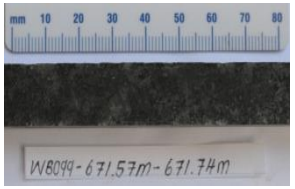

Appendix C:
Table 3: Hand Sample Description WB099

Sample Number WB099 (Meter Interval)	**Major Minerals**	**Minor Minerals**	**Colour and Textures**	**Grain Size**	**Other Features**	**Modal Abundance & Rock Name**	**Hand Sample Picture**
675.84 m-676.04 m	Pyroxenes (Opx and Cpx) and Feldspar (plag).	Sulphides (chalcopyrite and pyrrhotite). Biotite and chlorite.	Cumulates of both Pyroxenes (Opx and Cpx) and feldspars. Pyroxenes pinkish/greenish grey and feldspars with a milky white or transparent colour. Interlocking and equigranular texture. Phaneritic texture.	4.00-8.00 mm (Medium-Coarse-grained)	Sulphides (chalcopyrite and pentlandite) are disseminated.	Pyroxenes (Opx and Cpx); 50-55% and Feldspars (plag) 45-50% and sulphides 2-5% locally. **Gabbronorite (T-reef)**	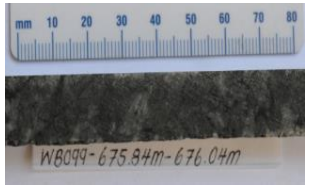
698.67 m-698.84 m	Pyroxenes (Opx and Cpx) and Feldspar (plag).	Sulphides (chalcopyrite, pyrrhotite and pentlandite).	Cumulates of both Pyroxenes (Opx and Cpx) and feldspars. Pyroxenes pinkish/greenish grey and feldspars with a milky white or transparent colour. Interlocking and equigranular texture.	4.00-6.00 mm (Medium-Coarse-grained)	Sulphides (chalcopyrite, pyrrhotite and pentlandite) are disseminated.	Pyroxenes (Opx and Cpx); 50-55% and Feldspars (plag) 45-50% and sulphides 10% locally. **Gabbronorite (T-reef)**	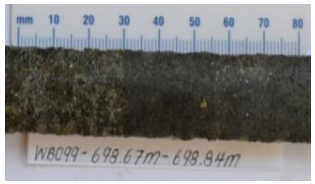
699.40 m-699.60 m	Pyroxenes (Opx and Cpx).	Feldspars (plag), and sulphides (pyrrhotite and chalcopyrite)	Pyroxenes have a cumulus texture, pinkish and greenish grey. Feldspars (plag) intercumulus and cumulus, milky white colour. Inequigranular and phaneritic texture, with interlocking crystals.	3.00-5.00 mm (medium-grained)	Sulphides (chalcopyrite, pyrrhotite and pentlandite) are disseminated. Inverted pigeonite (Exsolution with both the pyroxenes) locally.	Pyroxenes: Opx and Cpx; 75%, Feldspars: plag; 25% and sulphides (chalcopyrite) 5% locally. **Feldspathic Pyroxenite unit (T-reef)**	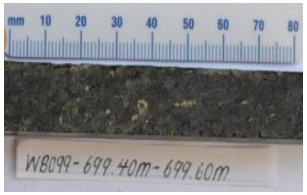
700.02 m-700.37 m	Pyroxenes (Opx and Cpx) and Feldspar (plag).	Sulphides (chalcopyrite, pyrrhotite and pentlandite).	Cumulates of both Pyroxenes (Opx and Cpx) and feldspars. Pyroxenes pinkish/greenish grey and feldspars with a milky white or transparent colour. Interlocking and equigranular texture. Phaneritic texture.	4.00-6.00 mm (Medium-Coarse-grained)	Inverted pigeonite (Exsolution of both pyroxenes). Sulphides (chalcopyrite, pyrrhotite and pentlandite) are disseminated.	Pyroxenes (Opx and Cpx); 50-55% and Feldspars (plag) 45-50% and sulphides 10% locally. **Gabbronorite (T-reef)**	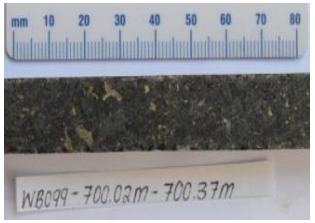

Appendix C:
Table 3: Hand Sample Description WB099

Sample Number WB099 (Meter Interval)	**Major Minerals**	**Minor Minerals**	**Colour and Textures**	**Grain Size**	**Other Features**	**Modal Abundance & Rock Name**	**Hand Sample Picture**
705.50 m-705.75 m	Pyroxenes (Opx and Cpx).	Feldspars (plag), and sulphides (pyrrhotite and chalcopyrite)	Pyroxenes have a cumulus texture, pinkish and greenish grey. Feldspars (plag) intercumulus and cumulus, milky white colour. Inequigranular and phaneritic texture, with interlocking crystals.	3.00-5.00 mm (medium-grained)	Sulphides (chalcopyrite, pyrrhotite and pentlandite) are disseminated. Inverted pigeonite (Exsolution with both the pyroxenes) locally.	Pyroxenes: Opx and Cpx; 75%, Feldspars: plag; 25% and sulphides (chalcopyrite) 5% locally. **Feldspathic Pyroxenite unit (T-reef)**	
711.80 m-711.96 m	Pyroxenes (Opx and Cpx) and Feldspar (plag).	None.	Cumulates of both Pyroxenes (Opx and Cpx) and feldspars. Pyroxenes pinkish/greenish grey and feldspars with a milky white or transparent colour. Interlocking and equigranular texture. Phaneritic texture.	4.00-6.00 mm (Medium-Coarse-grained)	Inverted pigeonite (Exsolution of both pyroxenes).	Pyroxenes (Opx and Cpx); 50-55% and Feldspars (plag) 45-50%. **Gabbronorite (T-reef)**	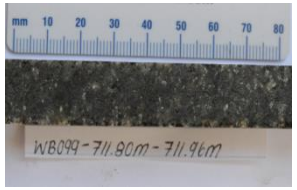
734.58 m-734.79 m	Pyroxenes (Opx and Cpx) and Feldspar (plag).	None.	Cumulates of both Pyroxenes (Opx and Cpx) and feldspars. Pyroxenes pinkish/greenish grey and feldspars with a milky white or transparent colour. Interlocking and equigranular texture.	4.00-6.00 mm (Medium-Coarse-grained)	Inverted pigeonite (Exsolution of both pyroxenes).	Pyroxenes (Opx and Cpx); 50-55% and Feldspars (plag) 45-50%. **Gabbronorite**	
763.00 m-763.22 m	Pyroxenes (Opx and Cpx) and Feldspar (plag).	Chlorite (Chloritisation) and sulphides (Chalcopyrite).	Cumulates of both Pyroxenes (Opx and Cpx) and feldspars. Pyroxenes pinkish grey and feldspars with a milky white or transparent colour. Interlocking and equigranular texture. Phaneritic texture.	4.00-7.00 mm (Coarse-grained)	Veinlets filled with secondary minerals; chlorite and feldspars. Alteration; chloritisation (milky green colour). Inverted pigeonite.	Pyroxenes (Opx and Cpx); 50-55%, Feldspars (plag) 45-50% and sulphides (chalcopyrite) 1% locally. **Gabbronorite**	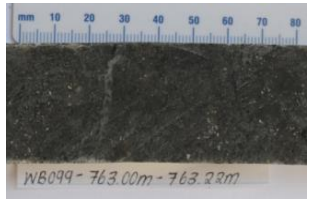

Appendix C:
Table 3: Hand Sample Description WB099

Sample Number WB099 (Meter Interval)	**Major Minerals**	**Minor Minerals**	**Colour and Textures**	**Grain Size**	**Other Features**	**Modal Abundance & Rock Name**	**Hand Sample Picture**
825.73 m-825.88 m	Pyroxenes (Opx and Cpx) and Feldspar (plag).	None.	Cumulates of both Pyroxenes (Opx and Cpx) and feldspars. Pyroxenes pinkish grey and feldspars with a milky white or transparent colour. Interlocking and equigranular texture. Phaneritic texture.	3.00-5.00 mm (medium-grained)	None	Pyroxenes (Opx and Cpx); 40% and Feldspars (plag) 60-65% **Leuco-gabbronorite**	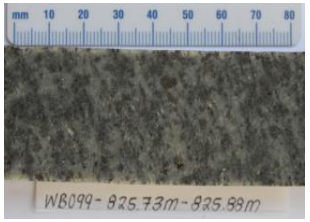
900.03 m-900.18 m	Feldspars (plag) and large oikocrysts of Opx.	Chlorite (Chloritisation) and sulphides (chalcopyrite).	Oikocrysts of Pyroxene (Opx) greenish grey and feldspars with a milky white or greenish white. Mottled texture and inequigranular texture. Phaneritic texture.	3.00-5.00 mm & oikocrysts are 1.00-1.50 cm	The large pyroxenes (oikocrysts) of Opx have chalcopyrite. Alteration; Chloritisation (greenish colour)	Feldspar (plag); 85%, oikocrysts of Opx; 10-15% and sulphides (chalcopyrite) 1% locally. **Mottled Anorthosite**	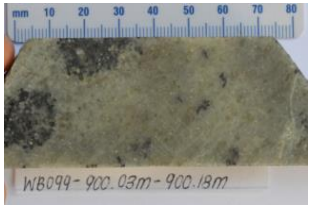
924.40 m-924.60 m	Pyroxenes (Opx) and Feldspar (plag).	None.	Cumulate Pyroxene (Opx) and feldspars. Pyroxenes pinkish grey and feldspars with a milky white or transparent colour. Inequigranular texture. Phaneritic texture.	3.00-10.00 mm (Coarse-grained)	Feldspars (plag) are coarse-grained and have an interlocking texture.	Pyroxenes (Opx); 35% and Feldspars (plag) 60-65% **Norite**	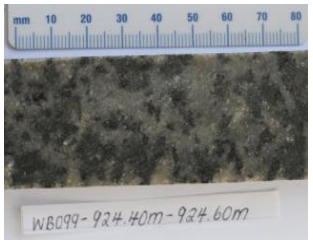

Appendix C:
Table 3: Hand Sample Description WB099

Sample Number WB099 (Meter Interval)	**Major Minerals**	**Minor Minerals**	**Colour and Textures**	**Grain Size**	**Other Features**	**Modal Abundance & Rock Name**	**Hand Sample Picture**
1009.00 m-1009.17 m	Pyroxenes (Opx and Cpx) and Feldspar (plag).	None.	Cumulates of both Pyroxenes (Opx and Cpx) and feldspars. Pyroxenes pinkish grey and feldspars with a milky white or transparent colour. Interlocking and equigranular texture. Phaneritic texture.	4.00-7.00 mm (coarse-grained)	None	Pyroxenes (Opx and Cpx); 40% and Feldspars (plag) 60-65% **Leuco-gabbronorite**	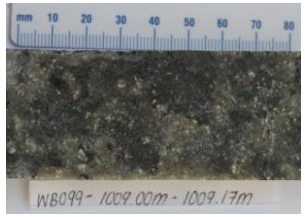
1021.18 m-1021.32 m	Pyroxenes (Opx and Cpx) and Feldspar (plag).	Sulphides (chalcopyrite).	Cumulates of both Pyroxenes (Opx and Cpx) and feldspars. Pyroxenes pinkish grey and feldspars with a milky white or transparent colour. Interlocking and equigranular texture. Phaneritic texture.	3.00-7.00 mm (medium-coarse-grained)	Sulphides (chalcopyrite) disseminated.	Pyroxenes (Opx and Cpx); 50%, Feldspars (plag) 50% and sulphides (chalcopyrite) 1% locally. **Gabbronorite**	
1069.70 m-1069.90 m	Pyroxenes (Opx and Cpx) and Feldspar (plag).	Chlorite (Chloritisation).	Cumulates of both Pyroxenes (Opx and Cpx) and feldspars. Pyroxenes pinkish grey and feldspars with a whitish or transparent colour. Interlocking and equigranular texture. Phaneritic texture.	3.00-5.00 mm (medium-coarse-grained)	Veinlets are filled with chlorite. Alteration; chloritisation. The pyroxenes are subhedral (rounded shape).	Pyroxenes (Opx and Cpx); 50% and Feldspars (plag) 50%. **Leuco-gabbronorite**	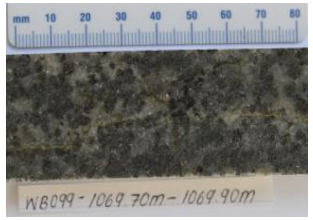

Appendix C:
Table 3: Hand Sample Description WB099

Sample Number WB099 (Meter Interval)	**Major Minerals**	**Minor Minerals**	**Colour and Textures**	**Grain Size**	**Other Features**	**Modal Abundance & Rock Name**	**Hand Sample Picture**
1126.18 m-1126.38 m	Pyroxenes (Opx and Cpx).	Feldspars (plag) and Olivine. Secondary magnetite and serpentine (serpentinisation)	Olivine, subrounded, greenish black grains. Pyroxene (Opx), greenish grey cumulates. The pyroxenes grains have an interlocking and equigranular texture. Phaneritic texture.	3.00-6.00 mm (medium-coarse-grained)	Olivine grains have been completely altered to magnetite and serpentine.	Pyroxenes: Opx and Cpx; 85%, and Olivine 10-15% locally. **Olivine bearing Pyroxenite**	
1145.51 m-1145.83 m	Olivine, feldspars (plag) and pyroxenes (Opx and Cpx).	Secondary magnetite and serpentine (serpentinisation)	Olivine, subrounded, greenish black grains. Pyroxene (Opx), greenish grey cumulates. Feldspar (plag) milky white, cumulates (euhedral).	3.00-7.00 mm (medium-coarse-grained)	Olivine grains have been completely altered to magnetite and serpentine.	Pyroxenes: Opx and Cpx; 75%, Feldspars: plag; 25% and Olivine 10-15% locally. **Olivine bearing Feldspathic Pyroxenite (F-zone)**	
1172.62 m-1172.86 m	Olivine, feldspars (plag) and pyroxenes (Opx).	Serpentine (Serpentinisation)	Olivine, subrounded, greenish black grains. Pyroxene (Opx), greenish grey cumulates (oikocrysts). Feldspar (plag) milky white, cumulates (euhedral). Poikilitic texture (Opx).	2.00-6.00 mm (medium-coarse-grained)	Veinlets filled with secondary minerals of serpentine. Olivine grains are both interlocking and individual grains Alteration; serpentinisation	Olivine; 35%, Feldspar; 30% and oikocrysts of Opx; 20-35%. **Poikilitic Troctolite (F-zone)**	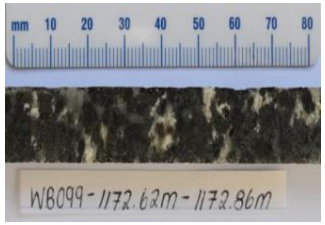

Appendix C:
Table 3: Hand Sample Description WB099

Sample Number WB099 (Meter Interval)	**Major Minerals**	**Minor Minerals**	**Colour and Textures**	**Grain Size**	**Other Features**	**Modal Abundance & Rock Name**	**Hand Sample Picture**
1193.50 m-1193.77 m	Olivine, feldspars (plag) and pyroxenes (Opx).	Serpentine (Serpentinisation)	Olivine, subrounded, greenish black grains. Pyroxene (Opx), greenish grey cumulates (oikocrysts). Feldspar (plag) milky white, cumulates (euhedral). Poikilitic texture (Opx).	2.00-6.00 mm (medium-coarse-grained)	Veinlets filled with secondary minerals of serpentine. Olivine grains are both interlocking and individual grains Alteration; serpentinisation	Olivine; 45%, Feldspar; 40% and oikocrysts of Opx; 15-20%. **Poikilitic Troctolite (F-zone)**	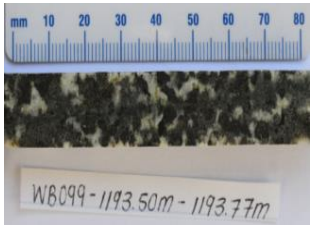
1215.48 m-1215.80 m	Olivine, feldspars (plag) and pyroxenes (Opx).	Serpentine (Serpentinisation) and chlorite (chloritisation).	Olivine, subrounded, greenish black grains. Pyroxene (Opx), greenish grey cumulates (oikocrysts). Feldspar (plag) milky white, cumulates (euhedral). Poikilitic texture (Opx).	2.00-6.00 mm (medium-coarse-grained)	Veinlets filled with secondary minerals of serpentine. Olivine grains are both interlocking and individual grains Alteration; serpentinisation	Olivine; 45%, Feldspar; 40% and oikocrysts of Opx; 15-20%. **Poikilitic Troctolite (F-zone)**	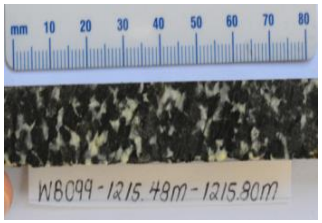
1228.50 m-1228.77 m	Olivine, feldspars (plag) and pyroxenes (Opx).	Serpentine (Serpentinisation).	Olivine, subrounded, greenish black grains. Pyroxene (Opx), greenish grey cumulates (oikocrysts). Feldspar (plag) milky white, cumulates (euhedral). Poikilitic texture (Opx).	2.00-6.00 mm (medium-coarse-grained)	Veinlets filled with secondary minerals of serpentine. Olivine grains are both interlocking and individual grains Alteration; serpentinisation	Olivine; 45%, Feldspar; 40% and oikocrysts of Opx; 15-20%. **Poikilitic Troctolite (F-zone)**	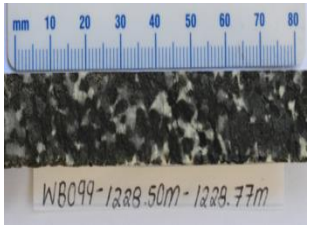

Appendix C:
Table 3: Hand Sample Description WB099

Sample Number WB099 (Meter Interval)	**Major Minerals**	**Minor Minerals**	**Colour and Textures**	**Grain Size**	**Other Features**	**Modal Abundance & Rock Name**	**Hand Sample Picture**
1270.16 m-1270.41 m	Pyroxenes (Opx and Cpx).	Feldspars (plag), and sulphides (pyrrhotite and chalcopyrite)	Pyroxenes have a cumulus texture, pinkish and greenish grey. Feldspars (plag) intercumulus and cumulus, milky white colour. Inequigranular and phaneritic texture, with interlocking crystals.	3.00-7.00 mm (medium-coarse-grained)	Veinlets filled with secondary minerals of chlorite and serpentine. Alteration; Chloritisation and serpentinisation.	Pyroxenes: Opx and Cpx; 75%, Feldspars: plag; 25%. **Feldspathic Pyroxenite unit (F-zone)**	
1280.17 m-1280.51 m	Pyroxenes (Opx and Cpx).	Feldspars (plag), olivine and serpentine.	Pyroxenes have a cumulus texture and the feldspar are intercumulus (interstitial) and some grains of feldspar are cumulus. Inequigranular and phaneritic texture.	3.00-5.00 mm (medium-grained)	Veinlets filled with serpentine and chlorite. Alteration; serpentinisation. Olivine interval has a rusty colour from the alteration of the secondary Fe-minerals.	Pyroxenes: Opx and Cpx; 75%, Feldspars: plag; 25% and Olivine 5-10% locally. **Olivine bearing Feldspathic Pyroxenite unit (F-zone)** (Serpentine veinlets)	
1282.67 m-1283.01 m	Olivine, Pyroxene (Opx) and Feldspars (plag).	Chlorite	Olivine, subrounded, greenish black grains. Pyroxene (Opx), greenish grey cumulates. Feldspar (plag) milky white, cumulates and intercumulus.	2.00-4.00 mm (medium-grained)	Olivine grains are both interlocking and individual subrounded grains. Phaneritic and equigranular texture. Minor chloritisation and serpentinisation.	Olivine; 35%, Pyroxene (Opx); 35 and Feldspars 30%. **Feldspathic Harzburgite (F-Zone)**	

Appendix C:
Table 3: Hand Sample Description WB099

Sample Number WB099 (Meter Interval)	**Major Minerals**	**Minor Minerals**	**Colour and Textures**	**Grain Size**	**Other Features**	**Modal Abundance & Rock Name**	**Hand Sample Picture**
1292.13 m-1292.43 m	Pyroxenes (Opx and Cpx).	Feldspars (plag), chlorite and serpentine.	Pyroxenes have a cumulus texture and the feldspar are intercumulus (interstitial) and some grains of feldspar are cumulus. Inequigranular and phaneritic texture.	3.00-5.00 mm (medium-grained)	Veinlets filled with serpentine and chlorite. Alteration chloritisation and serpentinisation.	Pyroxenes: Opx and Cpx; 75%, Feldspars: plag; 25%. **Feldspathic Pyroxenite unit (F-zone)** (Serpentine veinlets)	
1315.77 m-1316.00 m	Pyroxenes (Opx and Cpx).	Feldspars (plag).	Pyroxenes have a cumulus texture and the feldspar are intercumulus (interstitial). Equigranular and phaneritic texture.	1.00-3.00 mm (Medium-fine-grained)	Pyroxene rich unit in contact with a more feldspar and quartz rich interval.	Pyroxenes: Opx and Cpx; 75%, Feldspars: plag; 25%. **Pyroxenite unit (F-zone)** (contact with more felsic material)	
1324.53 m-1324.74 m	Pyroxenes (Opx and Cpx) and Feldspars (plag).	Sulphides (pyrrhotite and chalcopyrite) Chlorite.	Feldspars are milky white, pyroxenes; Opx- greenish grey and Cpx- pinkish grey. Inequigranular texture and phaneritic.	5.00-7.00 mm (Coarse-grained)	Large interlocking crystals of pyroxenes and feldspar, with minor disseminated sulphides	Pyroxenes: Opx; 30%, Cpx; 27%, Feldspars: plag; 47%, sulphides; 1% locally **Pegmatoidal unit (F-zone)** (pyroxene rich unit)	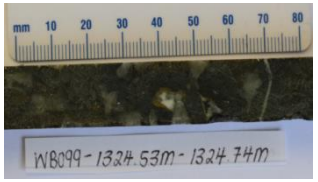
1333.85 m-1334.09 m	Pyroxenes (Opx and Cpx) and Feldspars (plag).	Sulphides (pyrrhotite and chalcopyrite) Chlorite and amphiboles. (biotite/ phlogopite).	Feldspars are milky white, pyroxenes; Opx- greenish grey and Cpx- pinkish grey. Inequigranular texture and phaneritic.	2.00-5.00 mm (Medium-grained)	Sulphides are disseminated and from around grains of pyroxenes. Minor Chlorite	Pyroxenes: Opx; 30%, Cpx; 25%, Feldspars: plag; 45%, sulphides; 3% locally and amphiboles: biotite/phlogopite 2%. **Granofels** (pyroxene rich unit)	

Appendix C:
Table 4: Hand Sample Description WE001

Sample Number WE001 (Meter Interval)	**Major Minerals**	**Minor Minerals**	**Colour Texture and Features**	**Grain Size**	**Other Features**	**Modal Abundance & Rock Name**	**Hand Sample Picture**
367.19 m – 367.35 m	Quartz, orthoclase and feldspars	Magnetite and epidote	Alternating bands of sandstone (purple or pinkish brown). Medium to coarse-grained. Large sub-rounded quartz pebbles	2.00 mm-2.5 cm	Sharp contacts between the alternating bands. Upward fining successions.	Quartz 70%, feldspars 25%, magnetite 3% and epidote. **Sandstone:** with large quartz pebbles in areas	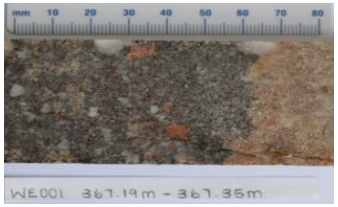
378.64 m – 378.75 m	Plagioclase and altered Pyroxenes to hematite.	Chlorite and epidote.	Plagioclase white, interstitial and cumulus in areas. Hematite reddish rusty colour, dominate in the sample that has altered the pyroxenes.	3.00-6.00 mm	Rusty minerals are secondary and have a streaky texture. Gabbronorite texture.	Plagioclase 35%, Altered Pyroxenes (hematite) 55%, chlorite 5% and epidote 5%. **Extremely altered Gabbronorite and Hematite unit**	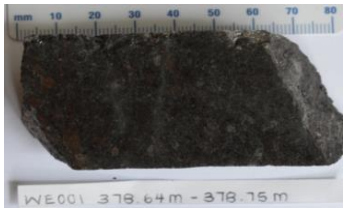
432.14 m – 432.19 m	Pyroxenes (Opx and Cpx), Feldspars (plagioclase).	Chlorite and Phlogopite.	Interlocking texture. Cpx dominate pyroxene, pinkish yellow. Euhedral and elongated plagioclase with milky white colour.	2.00-4.00 mm and at the contact with the pegmatoidal unit 2 cm grain size	Plagioclase has a greenish colour due to alteration: chloritisation	Pyroxenes; Cpx 30%, Opx 27%, plagioclase 35%, chlorite 5% and phlogopite 3%. **Gabbronorite**	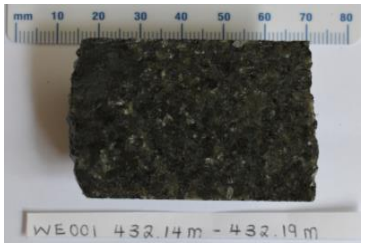
432.58 m – 432.69 m	Pyroxenes (Opx and Cpx), feldspars (plagioclase) and magnetite	Chlorite, phlogopite and sulphides (chalcopyrite)	Extremely large crystals with interlocking texture. Euhedral crystals. Feldspars milky white with rusty reddish colour.	2.00-5.00 cm	Veinlets and fractures filled with secondary minerals. Recrystalised gabbronorite.	Pyroxenes; Cpx 25%, Opx 20%, Feldspars (plagioclase) 40%, magnetite 10%, phlogopite 3%, chlorite 5% and sulphides 2%. **Pegmatoidal unit.**	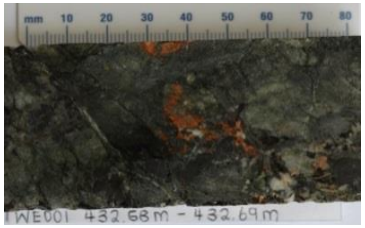

Appendix C:
Table 4: Hand Sample Description WE001

Sample Number WE001 (Meter Interval)	**Major Minerals**	**Minor Minerals**	**Colour Texture and Features**	**Grain Size**	**Other Features**	**Modal Abundance & Rock Name**	**Hand Sample Picture**
603.23 m – 603.43 m	Pyroxenes; Opx and Cpx, Feldspars (plagioclase).	Chlorite and olivine	Interlocking crystals. Opx grey, subhedral. Cpx pinkish grey, subhedral. Plagioclase cumulus, milky white	3.00-6.00 mm	Veinlets and fracture filled with secondary minerals; chlorite	Pyroxenes; Cpx 25%, Opx 25%, plagioclase 42%, chlorite 5% and olivine 3%. **Gabbronorite**	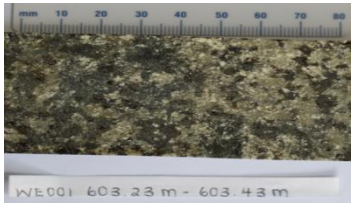
636.22 m – 636.32 m	Pyroxenes: Opx and Cpx, Feldspars (plagioclase) and Olivine	Chlorite	Plagioclase milky white, interstitial and cumulus. Olivine rounded, greenish black rimmed by serpentine. Opx large cumulus grains, greyish.	1.00-4.00 mm	Veinlets and fracture filled with secondary minerals; chlorite	Pyroxenes; Opx 30%, Cpx 10%, Feldspars (plagioclase) 45%, Olivine 10% and chlorite 5%. **Olivine-bearing gabbronorite**	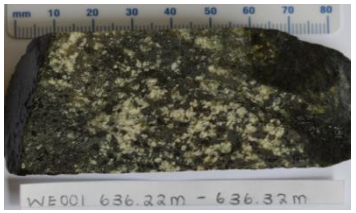
642.00 m – 642.08 m	Olivine, pyroxenes (Opx and Cpx) and feldspars (plagioclase).	Chlorite	Plagioclase milky white, cumulus (euhedral). Olivine rounded, greenish black rimmed by serpentine. Large amounts of serpentinisation.	3.00-5.00 mm	Veinlets and fracture filled with secondary minerals; chlorite. Interlocking texture.	Pyroxenes 25%, Olivine 35%, Plagioclase 20% and chlorite 5% and serpentine 15%. **Extremely altered troctolite**	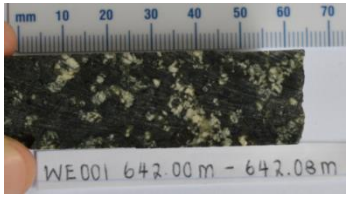
644.40 m – 644.60 m	Pyroxenes; Cpx and Opx and Plagioclase.	Olivine	Feldspars (plagioclase) milky white or greenish transparent colour. Pyroxenes greyish and the olivine grains are small rounded, greenish black.	3.00-5.00 mm	Alteration; chloritisation	Pyroxenes: Opx 25%, Cpx 25%, Feldspars (plagioclase) 40% and olivine 10%. **Olivine bearing gabbronorite.**	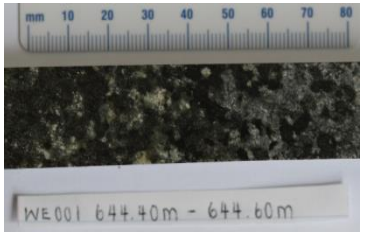

Appendix C:
Table 4: Hand Sample Description WE001

Sample Number WE001 (Meter Interval)	**Major Minerals**	**Minor Minerals**	**Colour Texture and Features**	**Grain Size**	**Other Features**	**Modal Abundance & Rock Name**	**Hand Sample Picture**
675.00 m – 675.10 m	Olivine, Plagioclase and Opx.	Serpentine and chlorite.	Olivine grains are completely altered with serpentine rims, olivine grains are rounded and greenish black, plagioclase euhedral grains milky white.	2.00-4.00 mm	The sample is extremely altered, Opx is interstitial and chlorite rimming the feldspars (plagioclase). Coarse-grained sample	Olivine (altered) 35%, plagioclase 20%, Opx 25%, serpentine 15%, chlorite 5%. **Altered troctolite**	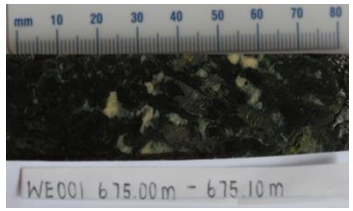
699.97 m – 700.17 m	Olivine, Plagioclase and Opx.	Cpx and serpentine	Olivine grains are rounded, greenish black and are interlocking. Large oikocrysts of Opx greyish. Plagioclase is interstitial and milky white.	2.00mm-2.00 cm	Slight green tint to the plagioclase due to alteration: chloritisation.	Olivine 40%, Opx 35%, plagioclase 10%, Cpx 5%, Serpentine 5% and Chlorite 5%. **Harzburgite**	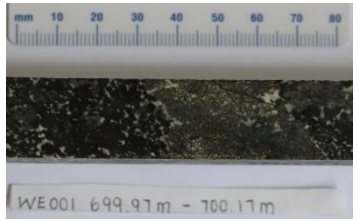
730.75 m – 730.90 m	Olivine, Plagioclase and Opx.	Cpx and serpentine	Olivine grains are rounded, greenish black and are interlocking. Large oikocrysts of Opx greyish. Plagioclase is interstitial and milky white.	3.00-6.00 mm	Slight green tint to the plagioclase due to alteration: chloritisation.	Olivine 40%, Opx 30%, plagioclase 15%, Cpx 5%, Serpentine 5% and Chlorite 5%. **Harzburgite**	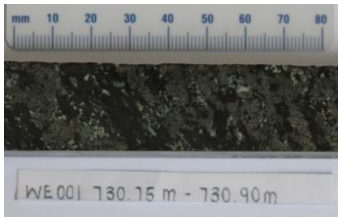
752.99 m – 753.25 m	Pyroxenes (Opx and Cpx), Feldspars (plagioclase).	Sulphides (chalcopyrite and pyrrhotite), olivine and chlorite.	Interlocking crystals. Opx grey, subhedral. Cpx pinkish grey, subhedral. Plagioclase cumulus, milky white	4.00-6.00mm	Sulphides interstitial and disseminated. Plagioclase has a greenish tint due to alteration; chlorite	Pyroxenes; Cpx 25%, Opx 25%, plagioclase 42%, chlorite 5% and olivine 3%. **Gabbronorite**	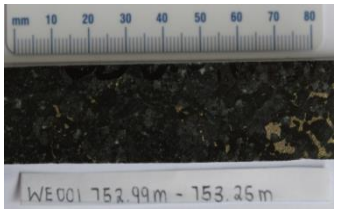

Appendix C:
Table 4: Hand Sample Description WE001

Sample Number WE001 (Meter Interval)	**Major Minerals**	**Minor Minerals**	**Colour Texture and Features**	**Grain Size**	**Other Features**	**Modal Abundance & Rock Name**	**Hand Sample Picture**
754.95 m – 755.10 m	Pyroxenes; Opx and Cpx, altered olivine	Plagioclase and serpentine	Extremely altered olivine completely serpentinised. Pyroxenes interlocking and have a streaky texture	2.00-3.00 mm	Veinlets and fracture filled with serpentine.	Pyroxenes; Opx 40%, Cpx 20%, plagioclase 15% and Olivine 5% and serpentine 20%. **Altered olivine bearing pyroxenite**	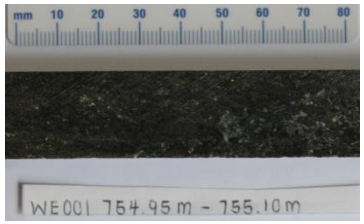
784.10 m – 784.20 m	Olivine, Plagioclase and Opx.	Cpx and sulphides (chalcopyrite and pyrrhotite).	Olivine grains are rounded, greenish black. Plagioclase interstitial, milky white. Pyroxene grey and pinkish.	2.00-4.00 mm	Sulphides interstitial and disseminated. Small amounts of alteration; chloritisation. Medium-grained samples.	Olivine 35%, plagioclase 15%, Opx 25%, Cpx 20% and sulphides 5%. **Troctolite**	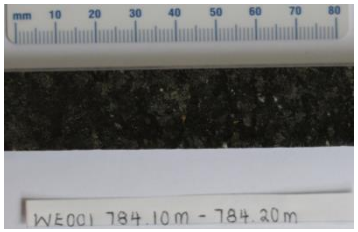
787.80 m – 787.95 m	Olivine, Plagioclase and Opx.	Cpx, sulphides (chalcopyrite and pyrrhotite), Chlorite and serpentine.	Olivine grains are rounded, greenish black. Plagioclase interstitial, milky white. Pyroxene grey and pinkish. Serpentine is black.	3.00-5.00 mm	Sulphides interstitial and disseminated. Plagioclase has a greenish tint due to alteration; chlorite	Olivine 40%, plagioclase 15%, Opx 30%, Cpx 10% and sulphides 5%. **Harzburgite**	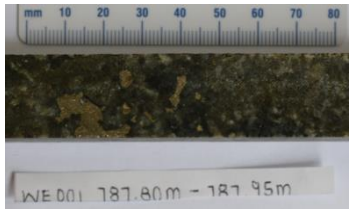
827.05 m – 827.20 m	Feldspars (plagioclase) and Quartz.	Pyroxenes, micas or phlogopite and chlorite.	Feldspars (plagioclase) are milky white. Quartz is transparent. Biotite is brownish. The crystals have an interlocking texture.	3.00-5.00 mm	Veinlets and fractures filled with secondary chlorite. Quartz crystals have a subhedral shape.	Feldspars (plagioclase) 45%, Quartz 45%, Pyroxenes 4% or less, chlorite 3% and biotite/phlogopite 3%. **Granofels** (more plag+qtz rich unit)	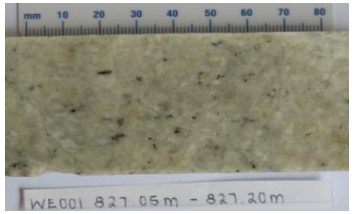

Appendix C:
Table 4: Hand Sample Description WE001

Sample Number WE001 (Meter Interval)	**Major Minerals**	**Minor Minerals**	**Colour Texture and Features**	**Grain Size**	**Other Features**	**Modal Abundance & Rock Name**	**Hand Sample Picture**
845.65 m – 845.84 m	Pyroxenes (Opx and Cpx), Feldspars (plagioclase) and serpentine.	Chlorite and magnetite.	Large sub-rounded oikocrysts of Opx and pinkish yellow Cpx. Interstitial feldspar that are milky white. Serpentine is a secondary mineral and is black.	3.00-6.00 mm and large oikocrysts of Opx up to 3.00 cm	Veinlets and fracture filled by secondary minerals (serpentine). Greenish colour is an alteration to form chlorite.	Pyroxenes; Opx 35% and Cpx 25%, feldspars (plagioclase) 25%, serpentine 10% and chlorite 5%. **Granofels** (more pyroxenite rich unit)	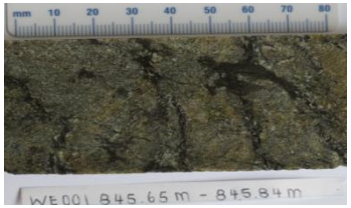

Appendix C

Table 5: Hand Sample Description WE027

Sample Number WE027 (Meter Interval)	**Major Minerals**	**Minor Minerals**	**Colour Texture and Features**	**Grain Size**	**Other Features**	**Modal Abundance & Rock Name**	**Hand Sample Picture**
553.96 m-554.17 m	Quartz, orthoclase and feldspars.	Magnetite, lithic fragments and epidote	Channel with an upward fining sequence. Medium to coarse-grained. Large sub-rounded quartz pebbles with a milky white/ transparent colour.	2.00 mm-2.00 cm (medium-coarse-grained)	Sharp contacts between the alternating bands. Upward fining successions. The veinlets and fractures are filled with quartz/ feldspar.	Quartz 70%, feldspars 25%, magnetite 3% and epidote. **Conglomerate**	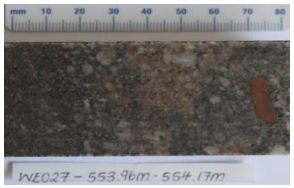
556.35 m-556.64 m	Plagioclase and altered Pyroxenes to hematite.	Chlorite and epidote.	Plagioclase white, interstitial and cumulus in areas. Hematite reddish rusty colour, dominate in the sample that has altered the pyroxenes.	1.00-6.00 mm (medium-coarse-grained)	Rusty minerals are secondary and have a streaky texture. Gabbronorite texture. Veinlets and fractures filled with feldspars and quartz.	Plagioclase 45-50%, Altered Pyroxenes (hematite) 35%, chlorite 5% and epidote 5%. **Paleosol Extremely altered Gabbronorite and Hematite unit**	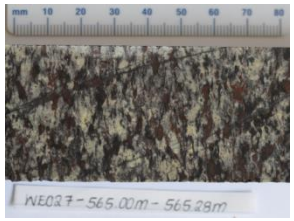
565.00 m-565.28 m	Pyroxenes (Opx and Cpx) and feldspars (plag).	Chlorite (chloritisation), biotite (biotitization) and sulphides (chalcopyrite).	Cumulates of pyroxenes (Opx and Cpx) greenish grey and feldspars (plag) milky white colour. Interlocking, inequigranular and phaneritic texture.	3.00-7.00 mm (medium-coarse-grained)	Alteration: Chloritisation and Biotitization.	Pyroxenes (Opx and Cpx): 45-50%, feldspars (plag): 45-50%. **Gabbronorite**	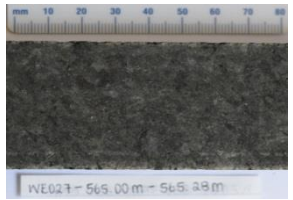
570.56 m-570.73 m	Pyroxenes (Opx and Cpx) and feldspars (plag).	Chlorite (chloritisation).	Cumulates of pyroxenes (Opx and Cpx) greenish grey and feldspars (plag) milky white colour. Interlocking, inequigranular and phaneritic texture.	3.00-7.00 mm (medium-coarse-grained)	Veinlets and fracture filled with secondary material (quartz/ feldspars/ chlorite).	Pyroxenes (Opx and Cpx): 35-40%, feldspars (plag): 60-65%. **Altered Leuco-gabbronorite**	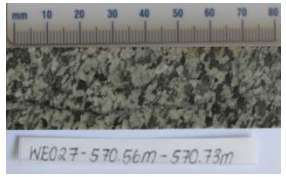

Appendix C

Table 5: Hand Sample Description WE027

Sample Number WE027 (Meter Interval)	**Major Minerals**	**Minor Minerals**	**Colour Texture and Features**	**Grain Size**	**Other Features**	**Modal Abundance & Rock Name**	**Hand Sample Picture**
578.27 m-578.27 m	Pyroxenes (Opx and Cpx) and feldspars (plag).	Chlorite (chloritisation), magnetite and biotite and phlogopite.	Cumulates of pyroxenes (Opx and Cpx) greenish grey and feldspars (plag) milky white. Biotite/ phlogopite secondary mineral with a brown colour. Equigranular and phaneritic texture.	2.00-6.00 mm (medium-coarse-grained)	Magnetite is disseminated. Magnetite rimming the pyroxenes. Inverted pigeonite (Exsolution of pyroxenes). Biotitization and chloritisation.	Pyroxenes (Opx and Opx): 55%, feldspars (plag): 35-40%, magnetite: 5-7%, and biotite and phlogopite 5%. **Magnetite Gabbronorite**	
580.59 m-580.84 m	Pyroxenes (Opx and Cpx) and feldspars (plag).	Chlorite (chloritisation), magnetite, sulphides (Chalcopyrite and pyrrhotite) and biotite and phlogopite.	Cumulates of pyroxenes (Opx and Cpx) greenish grey and feldspars (plag) milky white. Biotite/ phlogopite secondary mineral with a brown colour. Equigranular and phaneritic texture.	2.00-6.00 mm (medium-coarse-grained)	Sulphides and magnetite are disseminated. Magnetite rimming the pyroxenes. Inverted pigeonite (Exsolution of pyroxenes). Biotitization and chloritisation.	Pyroxenes (Opx and Opx): 55%, feldspars (plag): 35-40%, magnetite: 5-7%, sulphides (chalcopyrite and pyrrhotite): 3% locally and biotite and phlogopite 5%. **Magnetite Gabbronorite**	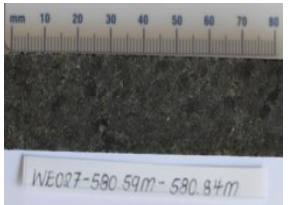
586.00 m-586.21 m	Pyroxenes (Opx and Cpx) and feldspars (plag).	Chlorite (chloritisation), magnetite, sulphides (Chalcopyrite and pyrrhotite) and biotite/ phlogopite.	Cumulates of pyroxenes (Opx and Cpx) greenish grey and feldspars (plag) milky white. Biotite secondary mineral with a brown colour. Equigranular and phaneritic texture.	2.00-6.00 mm (medium-coarse-grained)	Magnetite is disseminated and associated with pyroxene grains (rim). Sulphides are disseminated. Inverted pigeonite (Exsolution of pyroxenes)	Pyroxenes (Opx and Opx): 55-60%, feldspars (plag): 35-40%, magnetite: 5% and sulphides (chalcopyrite and pyrrhotite): 1% locally. **Magnetite Gabbronorite**	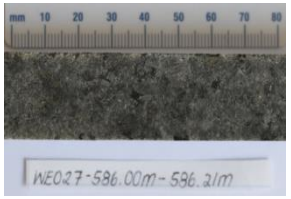
588.78 m-589.00 m	Pyroxenes (Opx and Cpx) and feldspars (plag).	Chlorite (chloritisation).	Cumulates of pyroxenes (Opx and Cpx) greenish grey and feldspars (plag) milky white colour. Interlocking, inequigranular and phaneritic texture.	3.00-7.00 mm (medium-coarse-grained)	Veinlets and fracture filled with secondary material (quartz/ feldspars/ chlorite).	Pyroxenes (Opx and Cpx): 35-40%, feldspars (plag): 60-65%. **Altered Leuco-gabbronorite**	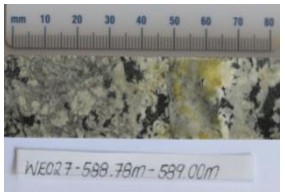

Appendix C

Table 5: Hand Sample Description WE027

Sample Number WE027 (Meter Interval)	**Major Minerals**	**Minor Minerals**	**Colour Texture and Features**	**Grain Size**	**Other Features**	**Modal Abundance & Rock Name**	**Hand Sample Picture**
594.58 m-594.80 m	Pyroxenes (Opx and Cpx) and feldspars (plag).	Chlorite (chloritisation), magnetite and biotite/ phlogopite.	Cumulates of pyroxenes (Opx and Cpx) greenish grey and feldspars (plag) milky white. Biotite secondary mineral with a brown colour. Equigranular and phaneritic texture.	2.00-6.00 mm (medium-coarse-grained)	Magnetite is disseminated and associated with pyroxene grains (rim). Inverted pigeonite (Exsolution of pyroxenes)	Pyroxenes (Opx and Opx): 55-60%, feldspars (plag): 35-40% and magnetite: 3% **Magnetite Gabbronorite**	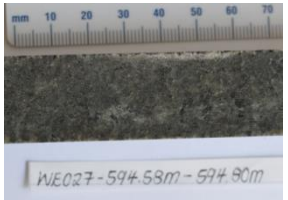
602.36 m-602.60 m	Pyroxenes (Opx and Cpx) and feldspars (plag).	Chlorite (chloritisation), magnetite and biotite/ phlogopite.	Cumulates of pyroxenes (Opx and Cpx) greenish grey and feldspars (plag) milky white. Biotite secondary mineral with a brown colour. Equigranular and phaneritic texture.	2.00-6.00 mm (medium-coarse-grained)	Magnetite is disseminated and associated with pyroxene grains (rim). Inverted pigeonite (Exsolution of pyroxenes)	Pyroxenes (Opx and Opx): 55-60%, feldspars (plag): 35-40% and magnetite: 3-5% **Magnetite Gabbronorite**	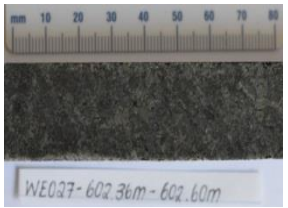
622.20 m-622.45 m	Pyroxenes (Opx and Cpx) and feldspars (plag).	Chlorite (chloritisation), sulphides (chalcopyrite and pyrrhotite) and biotite/ phlogopite.	Cumulates of pyroxenes (Opx and Cpx) greenish grey and feldspars (plag) milky white. Biotite secondary mineral with a brown colour. Equigranular and phaneritic texture.	1.00-1.50 cm (very coarse-grained)	Veinlets and fractures filled with secondary material (feldspars/ quartz/ chlorite). Sulphides are disseminated. Inverted pigeonite (Exsolution of pyroxenes)	Pyroxenes (Opx and Opx): 45-50% and feldspars (plag): 45-50% **Gabbronorite**	
631.16 m-631.43 m	Feldspars (plag) and Pyroxenes (Opx and Cpx).	Chlorite (chloritisation) and biotite and phlogopite.	Cumulates of pyroxenes (Opx and Cpx) greenish grey and feldspars (plag) green white. Interlocking crystals of plagioclase. Equigranular and phaneritic texture.	2.00-6.00 (medium-coarse-grained)	Greenish colouration due to alteration of chlorite (chloritisation). Veinlets and fractures filled with secondary material (feldspars/ quartz/ chlorite/ Calc-silicate).	Feldspars (plag): 60-65% and pyroxenes (Opx and Cpx) 30-35%. **Leuco-gabbronorite/ Anorthosite**	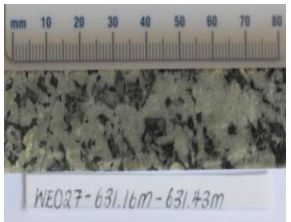

Appendix C

Table 5: Hand Sample Description WE027

Sample Number WE027 (Meter Interval)	**Major Minerals**	**Minor Minerals**	**Colour Texture and Features**	**Grain Size**	**Other Features**	**Modal Abundance & Rock Name**	**Hand Sample Picture**
635.40 m-635.61 m	Pyroxenes (Opx and Cpx) and feldspars (plag).	Chlorite (chloritisation), sulphides (chalcopyrite and pyrrhotite), magnetite and biotite/ phlogopite.	Cumulates of pyroxenes (Opx and Cpx) greenish grey and feldspars (plag) milky white. Biotite secondary mineral with a brown colour. Equigranular and phaneritic texture.	2.00-7.00 mm (medium-coarse-grained)	Veinlets and fractures filled with secondary material (feldspars/ quartz/ chlorite). Magnetite and sulphides are disseminated.	Pyroxenes (Opx and Opx): 45-50% and feldspars (plag): 45-50% **Gabbronorite**	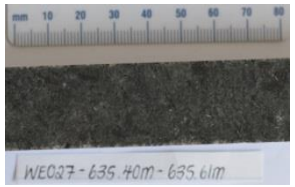
658.08 m-658.30 m	Pyroxenes (Opx and Cpx) and feldspars (plag).	Chlorite (chloritisation), magnetite and biotite/ phlogopite.	Cumulates of pyroxenes (Opx and Cpx) greenish grey and feldspars (plag) milky white. Biotite secondary mineral with a brown colour. Equigranular and phaneritic texture.	2.00-7.00 mm (medium-coarse-grained)	Greenish colouration due to alteration of chlorite (chloritisation). Veinlets and fractures filled with secondary material (feldspars/ quartz/ chlorite).	Pyroxenes (Opx and Opx): 45-50% and feldspars (plag): 45-50% **Gabbronorite**	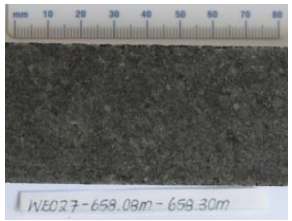
693.21 m-693.52 m	Pyroxenes (Opx and Cpx) and feldspars (plag).	Olivine, chlorite (chloritisation), sulphides (chalcopyrite and pyrrhotite) and biotite/ phlogopite.	Cumulates of pyroxenes (Opx and Cpx) greenish grey and feldspars (plag) milky white. Olivine (minor) subrounded, greenish black grains associated with veinlets. Equigranular and phaneritic texture.	3.00-10.00 mm (medium-coarse-grained)	Greenish colouration due to alteration of chlorite (chloritisation). Inverted pigeonite. Veinlets and fractures filled with secondary material (feldspars/ quartz/ chlorite).	Pyroxenes (Opx and Opx): 45-50% and feldspars (plag): 45-50% **Gabbronorite**	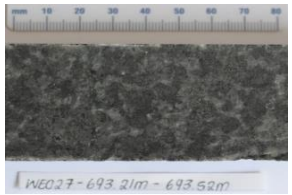
724.80 m-725.13 m	Pyroxenes (Opx and Cpx) and feldspars (plag).	Chlorite (chloritisation).	Cumulates of pyroxenes (Opx and Cpx) greenish grey and feldspars (plag) green/ milky white. Interlocking, Inequigranular and phaneritic texture.	1.00-3-.50 cm (very coarse-grained)	Veinlets and fractures filled with secondary material (feldspars/ quartz/ chlorite). Recrystallised gabbronorite.	Pyroxenes (Opx and Opx): 40-45% and feldspars (plag): 45-50% **Pegmatoidal Gabbronorite**	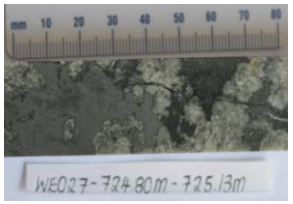

Appendix C

Table 5: Hand Sample Description WE027

Sample Number WE027 (Meter Interval)	**Major Minerals**	**Minor Minerals**	**Colour Texture and Features**	**Grain Size**	**Other Features**	**Modal Abundance & Rock Name**	**Hand Sample Picture**
748.42 m-748.75 m	Pyroxenes (Opx and Cpx) and feldspars (plag).	Magnetite, chlorite (chloritisation) and biotite/ phlogopite.	Cumulates of pyroxenes (Opx and Cpx) greenish grey and feldspars (plag) milky white. Equigranular and phaneritic texture.	1.00-7.00 mm (medium-coarse-grained)	Greenish colouration due to alteration of chlorite (chloritisation). Inverted pigeonite. Interstitial and disseminated magnetite.	Pyroxenes (Opx and Opx): 45-50%, feldspars (plag): 45-50% and magnetite 2% locally. **Gabbronorite**	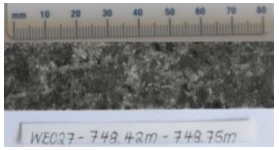
785.20 m-785.50 m	Pyroxenes (Opx and Cpx) and feldspars (plag).	Magnetite, chlorite (chloritisation) and biotite/ phlogopite.	Cumulates of pyroxenes (Opx and Cpx) greenish grey and feldspars (plag) milky white. Equigranular and phaneritic texture.	1.00-5.00 mm (medium-grained)	Greenish colouration due to alteration of chlorite (chloritisation). Inverted pigeonite. Interstitial and disseminated magnetite.	Pyroxenes (Opx and Opx): 45-50%, feldspars (plag): 45-50% and magnetite 2-3% locally. **Magnetite Gabbronorite**	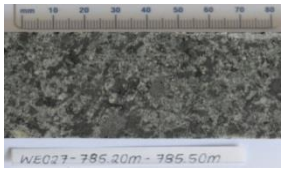
808.34 m-808.57 m	Feldspars (plag) and Pyroxenes (Opx and Cpx).	Chlorite (chloritisation).	Cumulates of pyroxenes (Opx and Cpx) greenish grey and feldspars (plag) green white. Interlocking crystals of plagioclase. Equigranular and phaneritic texture.	2.00-6.00 (medium-coarse-grained)	Greenish colouration due to alteration of chlorite (chloritisation). Inverted pigeonite. Veinlets and fractures filled with secondary material (chlorite).	Feldspars (plag): 60-65% and pyroxenes (Opx and Cpx) 30-35%. **Leuco-gabbronorite/ Anorthosite**	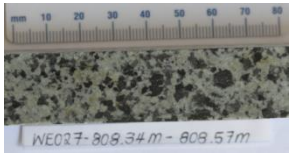
849.60 m-849.80 m	Pyroxenes (Opx and Cpx) and feldspars (plag).	Magnetite and chlorite (chloritisation).	Cumulates of pyroxenes (Opx and Cpx) greenish grey and feldspars (plag) milky white. Interlocking, Equigranular and phaneritic texture.	2.00-6.00 mm (medium-coarse-grained)	Magnetite interstitial or cumulus and disseminated. Veinlets and fractures filled with secondary materials (chlorite).	Pyroxenes (Opx and Opx): 40-45%, feldspars (plag): 45-50% and magnetite 2-3% locally. **Magnetite Gabbronorite**	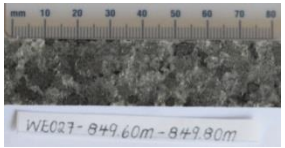
888.37 m-888.70 m	Pyroxenes (Opx and Cpx) and feldspars (plag).	Magnetite and Sulphides (Chalcopyrite and pyrrhotite), chlorite (chloritisation).	Cumulates of pyroxenes (Opx and Cpx) greenish grey and feldspars (plag) milky white. Interlocking, Equigranular and phaneritic texture.	1.00-7.00 mm (medium-coarse-grained)	Large abundance of magnetite, interstitial or cumulus and disseminated. Veinlets and fractures filled with secondary materials (chlorite).	Pyroxenes (Opx and Opx): 40-45%, feldspars (plag): 45-50%, magnetite 30% locally and sulphides 2% locally. **Magnetite Gabbronorite**	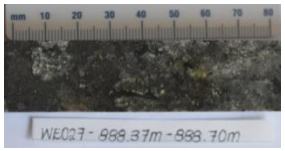

Appendix C

Table 5: Hand Sample Description WE027

Sample Number WE027 (Meter Interval)	**Major Minerals**	**Minor Minerals**	**Colour Texture and Features**	**Grain Size**	**Other Features**	**Modal Abundance & Rock Name**	**Hand Sample Picture**
891.52 m-891.78 m	Pyroxenes (Opx and Cpx) and feldspars (plag).	Magnetite, sulphides (chalcopyrite), biotite and chlorite (chloritisation).	Cumulates of pyroxenes (Opx and Cpx) greenish grey and feldspars (plag) green white. Interlocking, Equigranular and phaneritic texture.	1.00-3-.50 cm (very coarse-grained)	Magnetite interstitial or cumulus and disseminated. Veinlets and fractures filled with secondary material (chlorite). Recrystallised magnetite gabbronorite.	Pyroxenes (Opx and Opx): 40-45%, feldspars (plag): 45-50% and magnetite 5-7% locally. **Pegmatoidal Magnetite Gabbronorite**	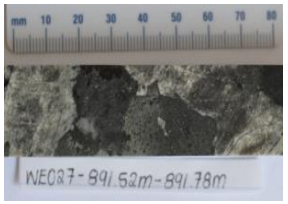
929.57 m-929.87 m	Pyroxenes (Opx and Cpx) and feldspars (plag).	Magnetite and Sulphides (Chalcopyrite and pyrrhotite), chlorite (chloritisation).	Cumulates of pyroxenes (Opx and Cpx) greenish grey and feldspars (plag) milky white. Interlocking, Equigranular and phaneritic texture.	1.00-7.00 mm (medium-coarse-grained)	Magnetite interstitial or cumulus and disseminated.	Pyroxenes (Opx and Opx): 40-45%, feldspars (plag): 45-50%, magnetite 5% locally and sulphides 2% locally. **Magnetite Gabbronorite**	
962.39 m-962.71 m	Pyroxenes (Opx and Cpx) and feldspars (plag).	Sulphides (Chalcopyrite and pyrrhotite), magnetite and chlorite (chloritisation).	Cumulates of pyroxenes (Opx and Cpx) greenish grey and feldspars (plag) milky white. Interlocking, Equigranular and phaneritic texture.	0.50-1.00 cm (coarse-grained)	Magnetite and sulphides are interstitial and disseminated.	Pyroxenes (Opx and Opx): 40-45%, feldspars (plag): 45-50%, magnetite 3-5% and sulphides 2-3% locally. **Magnetite Gabbronorite**	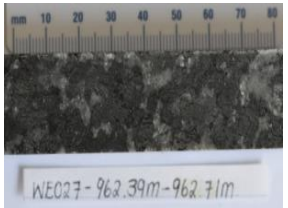
987.21 m-987.43 m	Feldspars (plag) and Pyroxenes (Opx and Cpx).	Chlorite (chloritisation).	Cumulates of pyroxenes (Opx and Cpx) greenish grey and feldspars (plag) green white. Interlocking crystals of plagioclase. Equigranular and phaneritic texture.	1.00-1.5 cm (coarse-grained)	Greenish colouration due to alteration of chlorite (chloritisation). Recrystallised anorthosite.	Feldspars (plag): 65-70% and pyroxenes (Opx and Cpx) 30-35%. **Anorthosite**	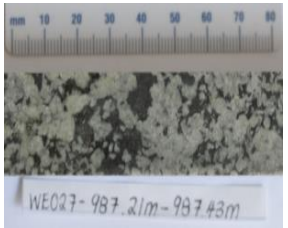

Appendix C

Table 5: Hand Sample Description WE027

Sample Number WE027 (Meter Interval)	**Major Minerals**	**Minor Minerals**	**Colour Texture and Features**	**Grain Size**	**Other Features**	**Modal Abundance & Rock Name**	**Hand Sample Picture**
994.04 m-994.23 m	Feldspars (plag) and Pyroxenes (Opx and Cpx).	Chlorite (chloritisation).	Cumulates of pyroxenes (Opx and Cpx) greenish grey and feldspars (plag) green white. Equigranular and phaneritic texture.	1.00-3.50 cm (very coarse-grained)	Greenish colouration due to alteration of chlorite (chloritisation). Recrystallised anorthosite.	Feldspars (plag): 65-70% and pyroxenes (Opx and Cpx) 30-35%. **Pegmatoidal Anorthosite**	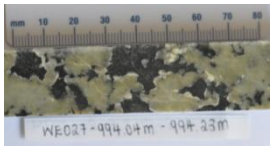
1252.15 m-1252.36 m	Pyroxenes (Opx and Cpx) and feldspars (plag).	Olivine and Chlorite (chloritisation).	Cumulates of pyroxenes (Opx and Cpx) pinkish/greenish grey, feldspars (plag) milky white/ transparent. Olivine subrounded greenish black grains. Equigranular and phaneritic texture.	3.00-5.00 mm (medium-grained)	Veinlets and fractures filled with secondary material (chlorite). Alteration: chloritisation and Exsolution of pyroxenes (inverted pigeonite).	Pyroxenes (Opx and Opx): 40%, feldspars (plag): 45% and olivine: 10-15%. **Olivine Gabbronorite**	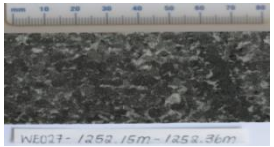
1282.94 m-1283.12 m	Pyroxenes (Opx and Cpx) and feldspars (plag).	Chlorite (chloritisation).	Cumulates of pyroxenes (Opx and Cpx) pinkish/greenish grey, feldspars (plag) milky white/ transparent. Equigranular and phaneritic texture.	3.00-5.00 mm (medium-grained)	Veinlets and fractures filled with secondary material (chlorite). Alteration: chloritisation and Exsolution of pyroxenes (inverted pigeonite).	Pyroxenes (Opx and Opx): 40-45% and feldspars (plag): 50-55%. **Gabbronorite**	
1345.20 m-1345.43 m	Pyroxenes (Opx and Cpx) and feldspars (plag).	Chlorite (chloritisation).	Cumulates of pyroxenes (Opx and Cpx) pinkish/greenish grey, feldspars (plag) milky white/ transparent. Equigranular and phaneritic texture.	3.00-7.00 mm (medium-coarse-grained)	Veinlets and fractures filled with secondary material (chlorite). Alteration: chloritisation and Exsolution of pyroxenes (inverted pigeonite).	Pyroxenes (Opx and Opx): 40-45% and feldspars (plag): 50-55%. **Gabbronorite**	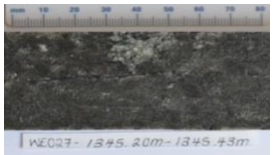
1381.20 m-1381.46 m	Pyroxenes (Opx and Cpx) and olivine.	Feldspars (plag), sulphides (chalcopyrite), Chlorite (chloritisation) and serpentine (serpentinisation).	Cumulates of pyroxenes (Opx and Cpx) pinkish/ greenish grey, Olivine subrounded, greenish black grains. Inequigranular and phaneritic texture.	2.00-6.00 mm (medium-coarse-grained)	Inverted pigeonite (Exsolution of pyroxenes). Veinlets filled with serpentine (serpentinisation). Sulphides (chalcopyrite) interstitial and disseminated.	Olivine: 20-25%, Pyroxenes (Opx and Cpx): 40-45%, feldspars (plag): 10-15% and sulphides (chalcopyrite): 1% locally. **Olivine-bearing pyroxenite**	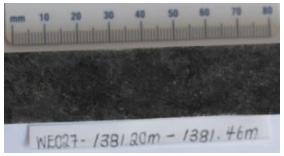

Appendix C

Table 5: Hand Sample Description WE027

Sample Number WE027 (Meter Interval)	**Major Minerals**	**Minor Minerals**	**Colour Texture and Features**	**Grain Size**	**Other Features**	**Modal Abundance & Rock Name**	**Hand Sample Picture**
1385.60 m-1385.41 m	Olivine, Pyroxene (Opx) and Feldspars (plag).	Chlorite (chloritisation) and serpentine (serpentinisation).	Cumulates of olivine subrounded, greenish black and feldspars (plag) milky white/ transparent. Oikocrysts of Opx pinkish grey. Inequigranular and phaneritic texture. Veinlets and fractures filled with secondary material.	1.00-6.00 mm (medium-coarse-grained)	The olivine grains are interlocking and individual grains. Olivine grains are rimmed with serpentine (serpentinisation). Pyroxenes (Opx) large oikocrysts (1.5 cm), Poikilitic texture.	Olivine: 40-45%, feldspars (plag): 10-15% and pyroxene (Opx oikocrysts): 25-30%. **Poikilitic feldspathic Harzburgite.**	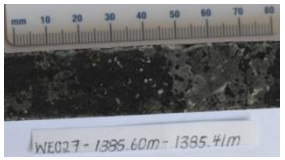
1386.66 m-1386.86 m	Olivine, Pyroxene (Opx) and Feldspars (plag).	Chlorite (chloritisation) and serpentine (serpentinisation).	Cumulates of olivine subrounded, greenish black and feldspars (plag) milky white/ transparent. Oikocrysts of Opx pinkish grey. Inequigranular and phaneritic texture.	1.00-7.00 mm (medium-coarse-grained)	The olivine grains are interlocking and individual grains. Olivine grains are rimmed with serpentine (serpentinisation). Pyroxenes (Opx) large oikocrysts (2 cm), Poikilitic texture.	Olivine: 40-45%, feldspars (plag): 20-25% and pyroxene (Opx oikocrysts): 25-30%. **Poikilitic feldspathic Harzburgite.**	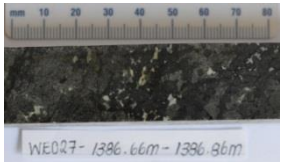
1393.60 m-1393.81 m	Pyroxenes (Opx and Cpx) and Feldspars (plag).	Sulphides (chalcopyrite and pyrrhotite) and chlorite (chloritisation).	Cumulates of pyroxenes (Opx and Cpx) pinkish/ greenish grey and feldspars (plag) milky white. Equigranular and Phaneritic texture.	1.00-3.00 mm (medium-grained)	Sulphides are interstitial and disseminated. Alteration: chloritisation.	Pyroxenes (Opx and Cpx): 55-60%, feldspars (plag): 30-35%, and sulphides: 3-5%. **Feldspathic Pyroxenite (Granofels).**	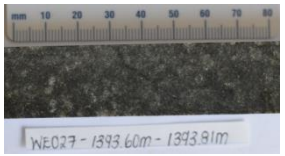
1403.92 m-1404.20 m	Pyroxenes (Opx and Cpx) and Feldspars (plag).	Olivine, sulphides (chalcopyrite and pyrrhotite) and chlorite (chloritisation).	Cumulates of pyroxenes (Opx and Cpx) pinkish/ greenish grey and feldspars (plag) milky white. Equigranular and Phaneritic texture.	1.00-4.00 mm (medium-grained)	Minor olivine with a subrounded, greenish black colour. Sulphides are interstitial and disseminated. Alteration: chloritisation.	Pyroxenes (Opx and Cpx): 50-55%, feldspars (plag): 30-35%, olivine: 10-15% and sulphides: 3-5%. **Feldspathic Pyroxenite (Granofels).**	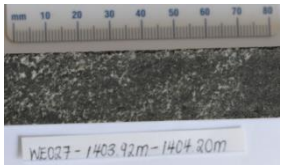

Appendix C:
Table 6: Hand Sample Description WE035

Sample Number WE035 (Meter Interval)	**Major Minerals**	**Minor Minerals**	**Colour Texture and Features**	**Grain Size**	**Other Features**	**Modal Abundance & Rock Name**	**Hand Sample Picture**
368.55 m-368.76 m	Quartz, orthoclase and feldspars.	Magnetite, lithic fragments and epidote	Channel with an upward fining sequence. Medium to coarse-grained. Large sub-rounded quartz pebbles with a milky white/ transparent colour.	2.00 mm-1.2 cm (medium-coarse-grained)	Sharp contacts between the alternating bands. Upward fining successions. The veinlets and fractures are filled with quartz/ feldspar.	Quartz 70%, feldspars 25%, magnetite 3% and epidote. **Conglomerate/ mudstone**	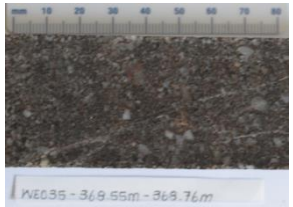
369.90 m-370.00 m	Plagioclase and altered Pyroxenes to hematite.	Chlorite and epidote.	Plagioclase white, interstitial and cumulus in areas. Hematite reddish rusty colour, dominate in the sample that has altered the pyroxenes.	3.00-6.00 mm (medium-coarse-grained)	Rusty minerals are secondary and have a streaky texture. Gabbronorite texture.	Plagioclase 35%, Altered Pyroxenes (hematite) 55%, chlorite 5% and epidote 5%. **Paleosol Extremely altered Gabbronorite and Hematite unit**	
377.53 m-377.76 m	Pyroxenes (Opx and Cpx) and Feldspars (plag).	Chlorite (Chloritisation), epidote (epidotisation) and olivine.	Cumulates of pyroxenes (Opx and Cpx), Feldspars (plag) and olivine. Pyroxenes greenish grey, feldspar greenish white/ milky white. Olivines are subrounded and greenish black. Equigranular and phaneritic texture.	2.00-5.00 mm (medium-grained)	Veinlets and fractures filled with feldspars/quartz. Alteration of chloritisation (greenish white colour) and a lime green colour of epidote. Invented pigeonite (Exsolution of pyroxenes).	Pyroxenes (Opx and Cpx): 40-45% and feldspar (plag): 50-55% and olivine 5-10% locally **Olivine Gabbronorite**	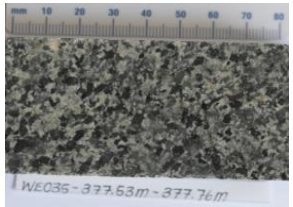
393.80 m-394.15 m	Pyroxenes (Opx and Cpx) and Feldspars (plag).	Chlorite (Chloritisation), biotite and magnetite.	Cumulates of pyroxenes (Opx and Cpx) and Feldspars (plag). Pyroxenes greenish grey, feldspar greenish white. Inequigranular and phaneritic texture.	7.00-15.00 mm (vey coarse-grained)	Veinlets and fractures filled with feldspars/quartz. Alteration of chloritisation (greenish white colour). Magnetite interstitial and disseminated.	Pyroxenes (Opx and Cpx): 40-45%, feldspar (plag): 50-55% and magnetite 3-5% locally. **Gabbronorite (pegmatitic)**	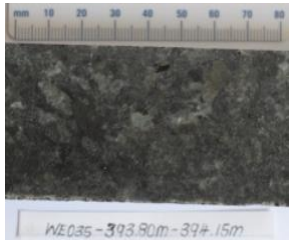

Appendix C:
Table 6: Hand Sample Description WE035

Sample Number WE035 (Meter Interval)	**Major Minerals**	**Minor Minerals**	**Colour Texture and Features**	**Grain Size**	**Other Features**	**Modal Abundance & Rock Name**	**Hand Sample Picture**
399.70 m-399.91 m	Pyroxenes (Opx and Cpx) and Feldspars (plag).	Chlorite (Chloritisation) and olivine.	Cumulates of pyroxenes (Opx and Cpx), Feldspars (plag) and olivine. Pyroxenes greenish grey, feldspar greenish white/ milky white. Olivines are subrounded and greenish black. Equigranular and phaneritic texture.	2.00-5.00 mm (medium-grained)	Veinlets and fractures filled with feldspars/quartz. Alteration of chloritisation (greenish white colour). Invented pigeonite (Exsolution of pyroxenes).	Pyroxenes (Opx and Cpx): 40-45% and feldspar (plag): 50-55% and olivine 5-10% locally **Olivine Gabbronorite**	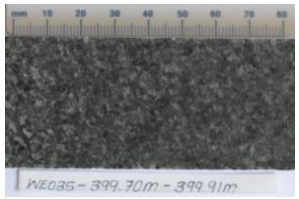
457.65 m-457.79 m	Pyroxenes (Opx and Cpx) and Feldspars (plag).	Chlorite (Chloritisation), olivine and sulphides (chalcopyrite).	Cumulates of pyroxenes (Opx and Cpx), Feldspars (plag) and olivine. Pyroxenes greenish grey, feldspar greenish white. Olivines are subrounded and greenish black. Equigranular and phaneritic texture.	4.00-6.00 mm (coarse-grained)	Veinlets and fractures filled with feldspars/quartz. Alteration of chloritisation (greenish white colour). Veinlets filled with serpentine (serpentinisation). Invented pigeonite (Exsolution of pyroxenes).	Pyroxenes (Opx and Cpx): 40-45% and feldspar (plag): 50-55%, olivine 5-10% locally and sulphides (chalcopyrite) 1% Locally) **Olivine Gabbronorite**	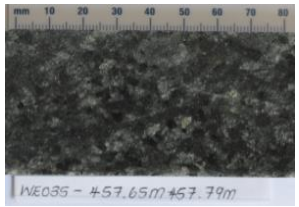
488.30 m-488.55 m	Pyroxenes (Opx and Cpx) and Feldspars (plag).	Chlorite (Chloritisation).	Cumulates of pyroxenes (Opx and Cpx) and Feldspars (plag). Pyroxenes greenish grey, feldspar greenish white. Inequigranular and phaneritic texture.	3.00-6.00 mm (medium-coarse-grained)	Veinlets and fractures filled with feldspars/quartz. Alteration of chloritisation (greenish white colour).	Pyroxenes (Opx and Cpx): 40-45% and feldspar (plag): 50-55%. **Leuco-Gabbronorite (altered)**	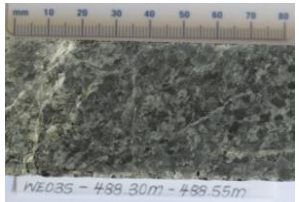
505.10 m-505.20 m	Pyroxene (Opx) and Feldspars (plag).	Inverted pigeonite, Olivine and Chlorite (Chloritisation).	Cumulates of pyroxene (Opx) and Feldspars (plag). Pyroxenes greenish grey, feldspar greenish white. Olivine subrounded, greenish black grains. Inequigranular and phaneritic texture.	3.00-6.00 mm (medium-coarse-grained)	Veinlets and fractures filled with feldspars/quartz. Alteration of chloritisation (greenish white colour). Inverted pigeonite (Exsolution of pyroxenes).	Pyroxenes (Opx): 30-40%, olivine: 5-10% and feldspar (plag): 35-40% **Olivine-Norite**	

Appendix C:
Table 6: Hand Sample Description WE035

Sample Number WE035 (Meter Interval)	**Major Minerals**	**Minor Minerals**	**Colour Texture and Features**	**Grain Size**	**Other Features**	**Modal Abundance & Rock Name**	**Hand Sample Picture**
515.30 m-515.46 m	Olivine, Pyroxene (Opx) and Feldspars (plag).	Sulphides (Chalcopyrite), inverted pigeonite and Chlorite (Chloritisation).	Cumulates of pyroxene (Opx) and Feldspars (plag). Pyroxenes greenish grey, feldspar greenish white. Olivine subrounded, greenish black grains. Inequigranular and phaneritic texture.	3.00-6.00 mm (medium-coarse-grained)	Veinlets and fractures filled with feldspars/quartz. Alteration of chloritisation (greenish white colour). Inverted pigeonite (Exsolution of pyroxenes).	Pyroxenes (Opx): 30%, olivine: 30%, feldspar (plag): 35-40% and sulphides (chalcopyrite) 1% locally. **Olivine-Norite**	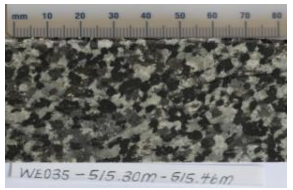
523.30 m-523.55 m	Feldspars (plag), pyroxenes (Opx and Cpx) and olivine.	Chlorite (chloritisation).	Cumulates of feldspars (plag) milky white, pyroxenes (Opx) greenish grey, olivine greenish black, subrounded.	3.00-6.00 mm (medium-coarse-grained)	Veinlets and fractures filled with secondary material (quartz/ feldspars). Greenish colour due to chloritisation. Inverted pigeonite (Exsolution of pyroxenes).	Feldspars (plag): 55-60%, pyroxenes (Opx and Cpx): 25-30% and olivine: 10-15% **Altered Leuco-gabbronorite**	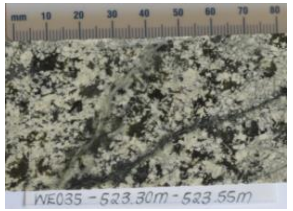
529.15 m-529.39 m	Olivine, feldspars (plag) and pyroxene (Opx).	Chlorite, serpentine, biotite and inverted pigeonite.	Olivine, subrounded to rounded, greenish black grains. Pyroxene (Opx), greenish grey cumulates (oikocrysts). Feldspar (plag) milky white, cumulates (euhedral). Poikilitic texture (Opx).	2.00-8.00 mm (medium-coarse-grained)	Veinlets filled with secondary minerals of serpentine and chloritisation. Olivine grains are both interlocking and individual grains. Inverted pigeonite.	Olivine; 30%, Feldspar; 35-40% and oikocrysts of Opx; 15-20%. **Poikilitic Troctolite (F-zone)**	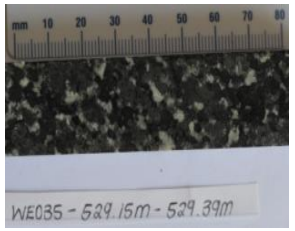
536.46 m-536.68 m	Olivine, feldspars (plag) and pyroxene (Opx).	Chlorite, serpentine and inverted pigeonite.	Olivine, subrounded to rounded, greenish black grains. Pyroxene (Opx), greenish grey cumulates (oikocrysts). Feldspar (plag) milky white, cumulates (euhedral). Poikilitic texture (Opx).	2.00-7.00 mm (medium-coarse-grained)	Veinlets filled with secondary minerals of serpentine and chloritisation. Olivine grains are both interlocking and individual grains. Inverted pigeonite.	Olivine; 30%, Feldspar; 35-40% and oikocrysts of Opx; 15-20%. **(Leuco) Poikilitic Troctolite (F-zone)**	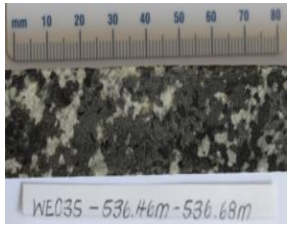

Appendix C:
Table 6: Hand Sample Description WE035

Sample Number WE035 (Meter Interval)	**Major Minerals**	**Minor Minerals**	**Colour Texture and Features**	**Grain Size**	**Other Features**	**Modal Abundance & Rock Name**	**Hand Sample Picture**
544.67 m-544.92 m	Olivine, feldspars (plag) and pyroxene (Opx).	Inverted pigeonite.	Olivine, subrounded to rounded, greenish black grains. Pyroxene (Opx), greenish grey cumulates (oikocrysts). Feldspar (plag) milky white, cumulates (euhedral). Poikilitic texture (Opx).	2.00-7.00 mm (medium-coarse-grained)	Veinlets filled with secondary minerals of serpentine and chloritisation. Olivine grains are both interlocking and individual grains. Inverted pigeonite.	Olivine; 30%, Feldspar; 35-40% and oikocrysts of Opx; 15-20%. **(Leuco) Poikilitic Troctolite (F-zone)**	
545.40 m-545.60 m	Feldspars (plag), pyroxenes (Opx and Cpx) and olivine.	Chlorite (chloritisation).	Cumulates of feldspars (plag) milky white, pyroxenes (Opx) greenish grey, olivine greenish black, subrounded.	3.00-6.00 mm (medium-coarse-grained)	Veinlets and fractures filled with secondary material (quartz/ feldspars). Greenish colour due to chloritisation. Inverted pigeonite (Exsolution of pyroxenes).	Feldspars (plag): 55-60%, pyroxenes (Opx and Cpx): 25-30% and olivine: 10-15% **Altered Leuco-gabbronorite**	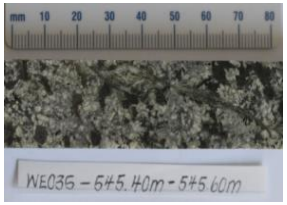
561.26 m-561.48 m	Olivine, feldspars (plag) and pyroxene (Opx).	Chlorite (chloritisation) and serpentine (serpentinisation).	Olivine, subrounded to rounded, greenish black grains. Pyroxene (Opx), greenish grey cumulates (oikocrysts). Feldspar (plag) milky white, cumulates (euhedral). Poikilitic texture (Opx).	2.00-6.00 mm (medium-coarse-grained)	Veinlets filled with secondary minerals of serpentine and chloritisation. Olivine grains are both interlocking and individual grains Alteration; serpentinisation and chloritisation. Inverted pigeonite.	Olivine; 30%, Feldspar; 35-40% and oikocrysts of Opx; 20%. **(Leuco) Poikilitic Troctolite (F-zone)**	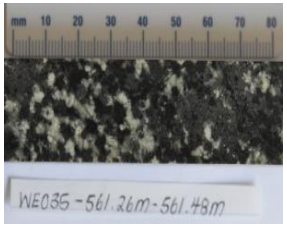
572.41 m-572.74 m	Olivine, feldspars (plag) and pyroxene (Opx).	Chlorite (chloritisation), serpentine (serpentinisation) and phlogopite.	Olivine, subrounded to rounded, greenish black grains. Pyroxene (Opx), greenish grey cumulates (oikocrysts). Feldspar (plag) milky white, cumulates (euhedral). Poikilitic texture (Opx).	2.00-6.00 mm (medium-coarse-grained)	Veinlets filled with secondary minerals of serpentine and chloritisation. Olivine grains are both interlocking and individual grains Alteration; serpentinisation and chloritisation.	Olivine; 35%, Feldspar; 30% and oikocrysts of Opx; 20-35%. **Poikilitic Troctolite (F-zone)**	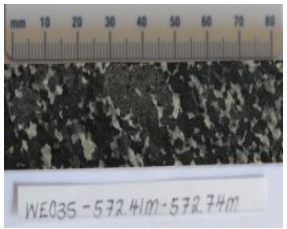

Appendix C:
Table 6: Hand Sample Description WE035

Sample Number WE035 (Meter Interval)	**Major Minerals**	**Minor Minerals**	**Colour Texture and Features**	**Grain Size**	**Other Features**	**Modal Abundance & Rock Name**	**Hand Sample Picture**
596.73 m-596.96 m	Olivine, feldspars (plag) and pyroxene (Opx).	Chlorite (chloritisation), serpentine (serpentinisation) and phlogopite.	Olivine, subrounded to rounded, greenish black grains. Pyroxene (Opx), greenish grey cumulates (oikocrysts). Feldspar (plag) milky white, cumulates (euhedral). Poikilitic texture (Opx).	2.00-6.00 mm (medium-coarse-grained)	Veinlets filled with secondary minerals of serpentine and chloritisation. Olivine grains are both interlocking and individual grains Alteration; serpentinisation and chloritisation. Inverted pigeonite.	Olivine; 35%, Feldspar; 30% and oikocrysts of Opx; 20-35%. **Poikilitic Troctolite (F-zone)**	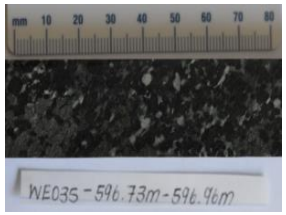
603.70 m-603.94 m	Olivine and feldspars (plag).	Pyroxenes (Opx) Chlorite (chloritisation) and serpentine (serpentinisation).	Olivine, subrounded to rounded, greenish black grains. Pyroxene (Opx), greenish grey cumulates (oikocrysts). Feldspar (plag) milky white, cumulates (euhedral). Poikilitic texture (Opx).	2.00-5.00 mm (medium-grained)	Veinlets filled with secondary minerals of chloritisation. Olivine grains are both interlocking and individual grains Alteration; chloritisation.	Olivine; 35-40%, Feldspar; 35-45% and oikocrysts of Opx; 5-10%. **(Leuco) Poikilitic Troctolite (F-zone)**	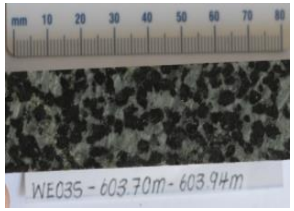
604.60 m-604.80 m	Olivine, feldspars (plag) and pyroxene (Opx).	Chlorite (chloritisation) and serpentine (serpentinisation).	Olivine, subrounded to rounded, greenish black grains. Pyroxene (Opx), greenish grey cumulates (oikocrysts). Feldspar (plag) milky white, cumulates (euhedral). Poikilitic texture (Opx).	7.00-7.00 mm (medium-coarse-grained)	Veinlets filled with secondary minerals of serpentine and chloritisation. Olivine grains are both interlocking and individual grains Alteration; serpentinisation and chloritisation.	Olivine; 40-45%, Feldspar; 30% and oikocrysts of Opx; 20%. **Poikilitic Troctolite (F-zone)**	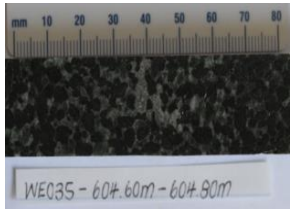
606.40 m-606.60 m	Olivine, feldspars (plag) and pyroxene (Opx).	Serpentine (serpentinisation).	Olivine, subrounded to rounded, greenish black grains. Olivine grains are altered. Feldspar (plag) milky white, cumulates (euhedral). Interlocking olivine grains.	6.00-15.00 mm (coarse-grains)	Veinlets filled with secondary minerals of serpentine and chloritisation.	Olivine: 55-65%, feldspars (plag): 20-20% and pyroxenes (Opx): 10-15% **Altered Harzburgite**	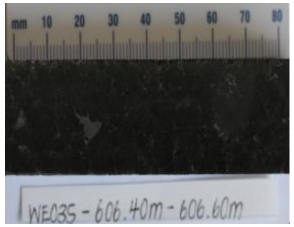

Appendix C:
Table 6: Hand Sample Description WE035

Sample Number WE035 (Meter Interval)	**Major Minerals**	**Minor Minerals**	**Colour Texture and Features**	**Grain Size**	**Other Features**	**Modal Abundance & Rock Name**	**Hand Sample Picture**
609.90 m-610.15 m	Olivine, feldspars (plag) and pyroxene (Opx).	Serpentine (serpentinisation) and sulphides (chalcopyrite and pyrrhotite).	Olivine, subrounded to rounded, greenish black grains. Olivine grains are altered. Feldspar (plag) milky white, cumulates (euhedral). Interlocking olivine grains.	5.00-9.00 mm (coarse-grains)	Sulphides (chalcopyrite and pyrrhotite) found within the olivine grains.	Olivine: 50-55%, feldspars (plag): 20-25%, pyroxenes (Opx): 10-15% and sulphides (chalcopyrite and pyrrhotite): 2-5% locally. **Altered Feldspathic Harzburgite**	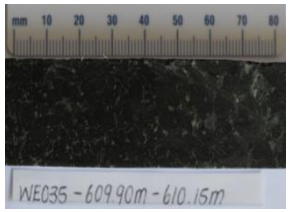
613.40 m-613.60 m	Olivine, feldspars (plag) and pyroxene (Opx).	Chlorite (chloritisation), serpentine (serpentinisation) and sulphides (chalcopyrite and pyrrhotite).	Olivine, subrounded to rounded, greenish black grains. Pyroxene (Opx), greenish grey cumulates (oikocrysts). Feldspar (plag) milky white, cumulates (euhedral). Interlocking olivine grains.	2.00-6.00 mm (medium-coarse-grained)	Veinlets filled with secondary minerals of serpentine and chloritisation. Olivine grains are both interlocking and individual grains Alteration; serpentinisation and chloritisation. Inverted pigeonite.	Olivine; 35-40%, Feldspar; 30-35%, Opx; 20% and sulphides (chalcopyrite and pyrrhotite) 1% locally. **Troctolite (F-zone)**	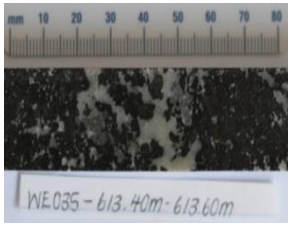
616.68 m-616.90 m	Pyroxenes (Opx and Cpx) and Feldspars (plag).	Olivine.	Pyroxenes have a cumulus texture and the feldspars (plag) are intercumulus (interstitial) and some grains of feldspar are cumulus. Inequigranular and phaneritic texture.	2.00-6.00 mm (medium-coarse-grained)	Small amounts of veinlets and fracture filled with secondary minerals of serpentine and chlorite (serpentinisation and chloritisation). Olivine grains are subrounded, greenish black colour. Inverted pigeonite.	Pyroxenes: Opx and Cpx; 65%, Feldspars: plag; 25-30%, olivine 10%. **Olivine bearing Feldspathic Pyroxenite (F-zone)**	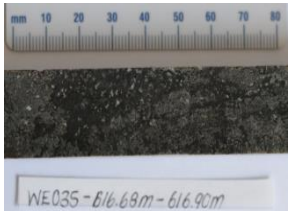
630.20 m-630.50 m	Pyroxenes (Opx and Cpx) and Feldspars (plag).	Olivine and sulphides (chalcopyrite and pyrrhotite).	Pyroxenes have a cumulus texture and the feldspars (plag) are intercumulus (interstitial) and some grains of feldspar are cumulus. Inequigranular and phaneritic texture.	3.00-6.00 mm (medium-coarse-grained)	Small amounts of veinlets and fracture filled with secondary minerals of serpentine and chlorite (serpentinisation and chloritisation). Olivine grains are subrounded, greenish black colour.	Pyroxenes: Opx and Cpx; 65%, Feldspars: plag; 25-30%, olivine 10% sulphides 5% locally. **Olivine bearing Feldspathic Pyroxenite (F-zone)**	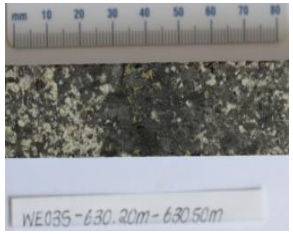

Appendix C:
Table 6: Hand Sample Description WE035

Sample Number WE035 (Meter Interval)	**Major Minerals**	**Minor Minerals**	**Colour Texture and Features**	**Grain Size**	**Other Features**	**Modal Abundance & Rock Name**	**Hand Sample Picture**
641.06 m-641.32 m	Pyroxenes (Opx and Cpx).	Feldspars (plag).	Pyroxenes have a cumulus texture and the feldspars (plag) are intercumulus (interstitial) and some grains of feldspar are cumulus. Inequigranular and phaneritic texture.	3.00-7.00 mm (medium-coarse-grained)	Small amounts of veinlets and fracture filled with secondary minerals of serpentine and chlorite (serpentinisation and chloritisation).	Pyroxenes: Opx and Cpx; 75%, Feldspars: plag; 25%. **Feldspathic Pyroxenite (F-zone)**	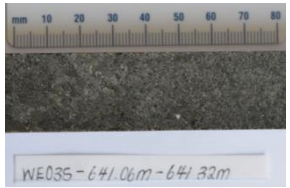
650.62 m-650.82 m	Olivine, pyroxenes (Opx and Cpx), feldspars and quartz.	Chlorite (chloritisation), serpentine (serpentinisation) biotite/ phlogopite and sulphides (chalcopyrite and pyrrhotite).	Feldspars are milky white, pyroxenes; Opx-greenish grey and Cpx-pinkish grey, quartz white or transparent colour. Olivine subrounded, greenish black grains Inequigranular texture and phaneritic.	2.00-5.00 mm (Medium-grained)	Sulphides are disseminated and from around grains of pyroxenes. Minor Chlorite (chloritisation). Veinlets and fractures filled with serpentine and chlorite.	Pyroxenes: Opx; 30%, Cpx; 25%, Feldspars: plag; 25-30%, Quartz: 10-15% and olivine: 10%. **Serpentinised Granofels** (pyroxene rich unit)	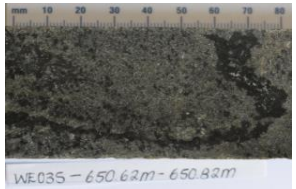
678.40 m-678.65 m	Pyroxenes (Opx and Cpx), feldspars and quartz.	Chlorite (chloritisation), biotite/ phlogopite and sulphides (chalcopyrite and pyrrhotite).	Feldspars are milky white, pyroxenes; Opx-greenish grey and Cpx-pinkish grey, quartz white or transparent colour. Inequigranular texture and phaneritic.	2.00-5.00 mm (Medium-grained)	Sulphides are disseminated and from around grains of pyroxenes. Minor Chlorite (chloritisation).	Pyroxenes: Opx; 30%, Cpx; 25%, Feldspars: plag; 35-40%, Quartz: 10-15% sulphides; 1% locally and amphiboles: biotite/phlogopite 1%. **Granofels** (pyroxene rich unit)	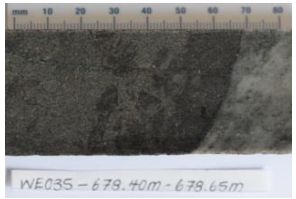

Appendix C: The Footwall and Sill
Table 7: WE001 Hand Sample Descriptions

Sample Number WE001 (Meter Interval)	**Major Minerals**	**Minor Minerals**	**Colour Texture and Features**	**Grain Size**	**Modal Abundance**	**Rock Name**	**Hand Sample Picture**
301.30 m - 301.35 m. **Chill Margin**	Feldspars (Plagioclase), Pyroxenes (Cpx and Opx).	None	The sample is mainly a light grey colour, with some rusty colour feldspar crystals.	Less than 1.0mm, extremely fine grained.	The Grain size is too small to determine the different individual grains.	**Chill margin at the top of the Dolerite (sill)**	
318.10 m – 318.30 m	Feldspars (Plagioclase and K-feldspar), Pyroxenes (Cpx and Opx).	Biotite and magnetite	Light Grey-white plagioclase crystals, dark green black pyroxene crystals. Euhedral plagioclase crystals, interlocking texture. Rusty colour from K-feldspar or altered of Al in minerals.	2.0 – 3.0 mm	Plagioclase 55%, pyroxenes (Cpx and Opx) 40% and magnetite 5%.	**Dolerite (sill)**	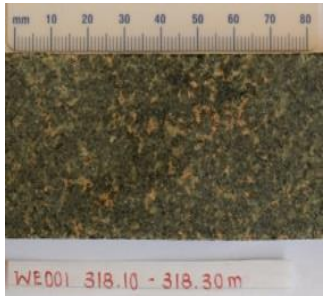
332.20 m - 332.34 m	Feldspars (Plagioclase), Pyroxenes (Cpx and Opx).	Biotite.	Light Grey-white plagioclase crystals, dark green black pyroxene crystals. Euhedral plagioclase crystals, interlocking texture. Altered light greenish colour possible chloritisation.	2.0 – 3.0 mm	Plagioclase 55% and pyroxenes (Cpx and Opx) 45%.	**Dolerite (sill)**	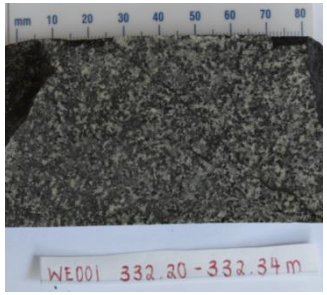

Appendix C: The Footwall and Sill
Table 7: WE001 Hand Sample Descriptions

Sample Number WE001 (Meter Interval)	**Major Minerals**	**Minor Minerals**	**Colour Texture and Features**	**Grain Size**	**Modal Abundance**	**Rock Name**	**Hand Sample Picture**
816.80 m - 817.00 m	Quartz and Feldspar (plagioclase).	Pyroxenes (Cpx and Opx).	Large euhedral grains of light grey quartz and dark green smaller grains of pyroxene (minor). Altered light greenish colour possible Chloritisation.	2.0 – 6.0 mm	Quartz 75%, Feldspar (plagioclase) 15%, Pyroxenes (Cpx and Opx) 10%.	**Granofels**	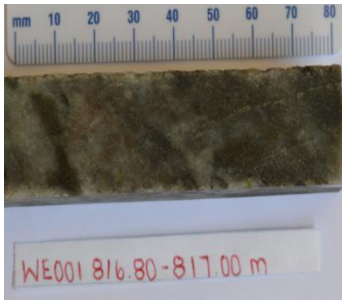
830.90 m	Pyroxenes (Opx and Cpx)	feldspars (plagioclase)	Fine grained with a grey colour. Veinlets of plagioclase. Slight greenish colour in the veinlet possibly chloritisation alteration.	Less than 1.0mm, extremely fine grained.	Pyroxene (Cpx and Opx) 85%, and feldspar (plagioclase) 15%.	**Pyroxenite**	
835.05 m - 835.15 m	Feldspar (plagioclase) and Quartz.	Pyroxenes (Cpx and Opx).	White or transparent Feldspar, (plagioclase) subhedral grains. Large subhedral quartz grains with smoky white-grey colour. Pyroxenes (Cpx and Opx) dark greenish colour.	1.0 – 5.0 mm	Quartz 40%, Feldspars (plagioclase) 45% and Pyroxene (Opx and Cpx) 15%.	**Granofels**	

Appendix C: The Footwall
Table 8: WE002 Hand Samples Descriptions

Sample Number WE002 (Meter Interval)	**Major Minerals**	**Minor Minerals**	**Colour Texture and Features**	**Grain Size**	**Modal Abundance**	**Rock Name**	**Hand Sample Picture**
677.75 m - 678.05 m	Plagioclase and pyroxene (Cpx and Opx)	Sulphides (Chalcopyrite, Pyrite and Pyrrhotite)	Light to dark grey pyroxene (Opx and Cpx), plagioclase interstitial with a milky white colour.	1.0 – 2.0 mm	Plagioclase 30%, Pyroxene (Cpx and Opx) 65% and sulphides 5%.	**Pyroxenite**	
685.14 m - 685.52 m	Plagioclase, pyroxene (Cpx and Opx) and Sulphides (Chalcopyrite, Pyrite and Pyrrhotite)	None	Euhedral light to dark grey pyroxene (Opx and Cpx), plagioclase interstitial with a milky white colour. Sulphides are massive on one side or the sample and disseminated on the other side. Mainly Pyrrhotite.	2.0 – 7.0 mm	Plagioclase 20%, Pyroxene (Cpx and Opx) 25% and sulphides 55%.	**Granofels**	
701.15 m - 701.30 m	Plagioclase, pyroxene (Cpx and Opx).	Sulphides (Chalcopyrite and Pyrrhotite	The contact where a rich pyroxenite unit meets a very quartz and feldspar rich unit. The pyroxenite unit is dominating in Cpx and other mafic minerals.	1.0 – 2.0 mm	Plagioclase 48%, Pyroxene (Cpx and Opx) 50% and sulphides 2%.	**Granofels**	

Appendix C: The Sill
Table 9: WE003 Hand Samples Descriptions

Sample Number WE003 (Meter Interval)	**Major Minerals**	**Minor Minerals**	**Colour Texture and Features**	**Grain Size**	**Modal Abundance**	**Rock Name**	**Hand Sample Picture**
294.00 m – 294.10 m. **Sample from the top of the Sill.**	Feldspars (Plagioclase and K-feldspar), Quartz, Pyroxenes (Cpx and Opx).	Magnetite	Light Grey-white plagioclase crystals, dark green black pyroxene crystals. Euhedral plagioclase crystals, interlocking texture. Rusty colour from K-feldspar or altered of Al in minerals.	2.0 – 3.0 mm	Plagioclase 45%, pyroxenes (Cpx and Opx) 40%, Quartz 10% and magnetite 5%.	**Dolerite (sill)**	
300.70 m – 300.80 m. **Transition to pink facies**	Feldspars (Plagioclase and K-feldspar), Quartz, Pyroxenes (Cpx and Opx).	Magnetite	Light Grey-white plagioclase crystals, dark green black pyroxene crystals. Interstitial plagioclase crystals, interlocking texture. Rusty colour from K-feldspar or altered of Al in minerals.	2.0 – 3.0 mm	Plagioclase 35%, pyroxenes (Cpx and Opx) 55%, Quartz 8% and magnetite 2%.	**Dolerite (sill)**	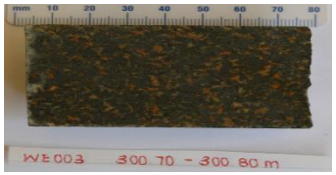
308.40 m – 308.55 m. **Coarse-grained pink facies**	Feldspar (plagioclase and K-feldspar) and pyroxene (Cpx and Opx)	Chlorite and Quartz	Large subhedral feldspar grains with a rusty colour. Veinlets filled with secondary minerals (chloritisation). Dark greenish black grains of pyroxenes.	2.0 – 7.0 mm	Feldspars (Plagioclase and K-feldspar) 55%, pyroxenes (Cpx and Opx) 35%, Quartz 5% and chlorite 5%.	**Dolerite (sill)**	
326.00 m – 326.10 m.	Feldspars (Plagioclase and K-feldspar), Quartz, Pyroxenes (Cpx and Opx).	None	Light Grey-white plagioclase crystals, dark green black pyroxene crystals. Euhedral plagioclase crystals, interlocking texture. Rusty colour from K-feldspar or altered of Al in minerals.	2.0 – 3.0 mm	Feldspars (Plagioclase and K-feldspar) 35%, pyroxenes (Cpx and Opx) 60% and Quartz 5%.	**Dolerite (sill)**	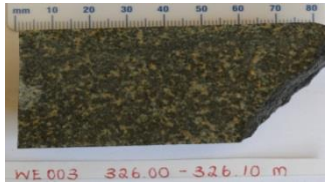

Appendix C: The Footwall
Table 10: WE005 Hand Sample Descriptions

Sample Number WE005 (Meter Interval)	**Major Minerals**	**Minor Minerals**	**Colour Texture and Features**	**Grain Size**	**Modal Abundance**	**Rock Name**	**Hand Sample Picture**
328.55 m	Pyroxenes (Cpx and Opx) and Feldspars (plagioclase).	None	Greyish to black colour – pyroxenes and the milky white colour is plagioclase. The greenish colour could be alteration of minerals to form chlorite (chloritisation).	1.0 – 3.0 mm	Pyroxenes (Cpx and Opx) 65 %, Feldspars (plagioclase) 30% and chlorite 5%.	**Pyroxenite or an pyroxene rich interval in the Granofels.**	
330.83 m	K-Feldspar, plagioclase and Quartz.	Black micas	Subhedral feldspars (plagioclase, k-feldspar and orthoclase) and surround by interstitial quartz which has a whitish transparent colour.	2.0 – 4.0 mm	Quartz 40%, K-feldspar 10%, plagioclase or orthoclase 45% and black mica minerals 5%.	**Granite**	
375.12 m	K-Feldspar, plagioclase and Quartz.	Biotite and dark black mica minerals.	Euhedral, whitish-transparent quartz crystals, milky white plagioclase or orthoclase and reddish K-feldspar crystals.	3.0 – 8.0 mm	Quartz 35%, K-feldspar 45%, plagioclase or orthoclase 15% and 5% of the biotite or black mica minerals.	**Granite**	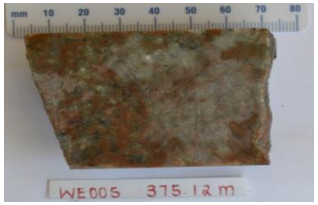
420.05 m	K-Feldspar, plagioclase and Quartz.	Biotite, dark black mica minerals and sulphides (chalcopyrite, pyrite and pyrrhotite).	Euhedral, whitish-transparent quartz crystals, milky white plagioclase or orthoclase and reddish K-feldspar crystals. Sulphides are disseminated.	2.0 – 8.0 mm	Quartz 25%, K-feldspar 35%, plagioclase or orthoclase 30%, 5% of the biotite or black mica minerals and sulphides 5%.	**Granite**	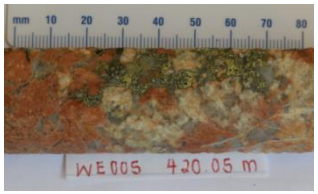

Appendix C: The Footwall
Table 11: WE027 Hand Sample Descriptions

Sample Number WE027 (Meter Interval)	**Major Minerals**	**Minor Minerals**	**Colour Texture and Features**	**Grain Size**	**Modal Abundance**	**Rock Name**	**Hand Sample Picture**
1171.10 m – 1171.30 m	Feldspars (plagioclase) and pyroxenes (Cpx and Opx).	Sulphides (Chalcopyrite and pyrrhotite).	Plagioclase crystals have a white milky colour, plagioclase is interstitial. Pyroxene crystals are light grey and are subhedral in shape.	2.0 – 5.0 mm	Feldspars (plagioclase) 45%, Pyroxenes (Cpx and Opx) 50% and sulphides (chalcopyrite and pyrrhotite) 5%.	**Granofels**	
1171.90 m – 1172.15 m	Feldspars (plagioclase) and pyroxenes (Cpx and Opx).	Chlorite and Sulphides (Chalcopyrite and pyrrhotite).	Plagioclase has subhedral shaped crystals with a whitish colour. The plagioclase also has a since greenish colour due to alteration of chloritisation. The pyroxene grains are grey in colour.	3.0 – 6.0 mm	Feldspars (plagioclase) 45%, Pyroxenes (Cpx and Opx) 45%, chlorite 5% and sulphides (chalcopyrite and pyrrhotite) 5%.	**Granofels**	
1173.10 m – 1173.40 m	Feldspar (plagioclase) and pyroxenes (Cpx and Opx).	Sulphides (Chalcopyrite and pyrrhotite).	Milky white, interstitial plagioclase. Disseminated sulphides and grey pyroxene.	1.0 – 2.0 mm	Feldspars (plagioclase) 45%, Pyroxenes (Cpx and Opx) 45%, chlorite 5% and sulphides (chalcopyrite and pyrrhotite) 5%.	**Granofels**	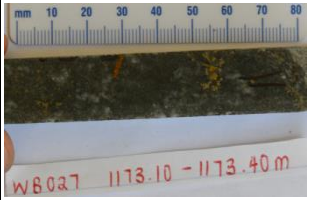
1180.40 m – 1180.48 m	Feldspar (plagioclase) and pyroxenes (Cpx and Opx).	Sulphides (Chalcopyrite and pyrrhotite).	Milky white, interstitial plagioclase. Disseminated sulphides (chalcopyrite and pyrrhotite) and grey pyroxene.	2.0 – 5.0 mm	Feldspars (plagioclase) 60%, Pyroxenes (Cpx and Opx) 30%, chlorite 5% and sulphides (chalcopyrite and pyrrhotite) 5%.	**Granofels**	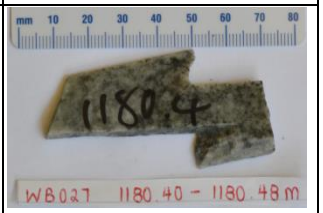

Appendix C: The Footwall
Table 11: WE027 Hand Sample Descriptions

Sample Number WE027 (Meter Interval)	**Major Minerals**	**Minor Minerals**	**Colour Texture and Features**	**Grain Size**	**Modal Abundance**	**Rock Name**	**Hand Sample Picture**
1180.60 m – 1180.70 m	Feldspar (plagioclase) and pyroxenes (Cpx and Opx).	Chlorite	Plagioclase has subhedral shaped crystals with a whitish colour. The plagioclase also has a since greenish colour due to alteration of chloritisation. The pyroxene grains are grey in colour.	2.0 – 7.0 mm	Feldspars (plagioclase) 60%, Pyroxenes (Cpx and Opx) 35% and chlorite 5%.	**Granofels**	

Appendix C:

Table 12: Hand Sample Descriptions for Sulphur Isotope samples

Sample Number & Borehole I.D (Meter Interval)	**Major Minerals**	**Minor Minerals**	**Colour Texture and Features**	**Grain Size**	**Other Features**	**Modal Abundance & Rock Name**	**Hand Sample Picture**
WE020; 416.35-416.62	Pyroxenes (Cpx and Opx) and feldspars.	Sulphides (pyrrhotite and chalcopyrite), hematite and speculerite.	Extremely fine-grained, difficult to identify individual minerals in hand sample.	Extremely fine-grained	Fractures and veinlets filled with secondary minerals	Pyroxenes (Cpx and Opx) 60%, feldspars 30%, sulphides 5% and hematite 5%. **Dolerite (sill)**	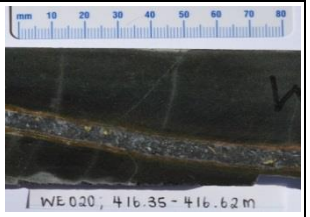
WE033; 434.76-434.97 m	Quartz, orthoclase and feldspars.	Sulphides (pyrrhotite) and epidote	Large angular-subrounded, milky white quartz. Coarse-grained.	2.00 mm – 2.5 cm	Clusters of quartz pebbles, purple colour, finer sediments in the matrix. Greenish colour is epidote (alteration)	Quartz 70%, feldspars 15%, orthoclase 10%, sulphides 3% and epidote 2%. **Sandstone/ Conglomerate:** with large quartz pebbles in areas	
WE033; 438.5-438.62 m	Quartz, orthoclase and feldspar	Sulphides (pyrrhotite and chalcopyrite) and epidote.	Medium-grained with milky white quartz. Feldspars creamy greenish colour.	1.00-4.00 mm	Greenish colour is due to alteration (epidotisation). Light colour compared with normal Waterberg sediments	Quartz 70%, feldspars 10%, orthoclase 10%, epidote 7%, and sulphides 3%. **Sandstone**	
WE033; 438.96-438.99 m	Quartz, orthoclase and feldspar	Sulphides (pyrrhotite and chalcopyrite) and epidote.	Medium-grained with milky white quartz. Feldspars creamy greenish colour.	1.00-4.00 mm	Greenish colour is due to alteration (epidotisation). Light colour compared with normal Waterberg sediments	Quartz 65%, feldspars 15%, orthoclase 5%, epidote 5%, and sulphides 10%. **Sandstone**	

Appendix C:

Table 12: Hand Sample Descriptions for Sulphur Isotope samples

Sample Number & Borehole I.D (Meter Interval)	**Major Minerals**	**Minor Minerals**	**Colour Texture and Features**	**Grain Size**	**Other Features**	**Modal Abundance & Rock Name**	**Hand Sample Picture**
WE033; 440.63 m	Quartz and feldspars	Sulphides (pyrrhotite and Chalcopyrite) and pyroxenes.	Large angular-subrounded, milky quartz. Coarse-grained.	3.00 mm-1.00 cm	Large Fractures and veinlets filled with secondary material. Greenish colour is alteration (epidote).	Quartz 70%, feldspars 10%, orthoclase 10%, epidote 5%, and sulphides 5%. **Sandstone**	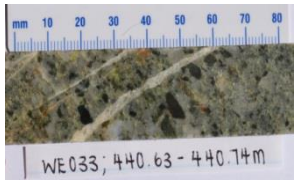
WE033; 440.74 m	Quartz and feldspars	Sulphides (pyrrhotite and Chalcopyrite) and pyroxenes.	Large angular-subrounded, milky quartz. Coarse-grained.	3.00 mm-1.50 cm	Large greenish pebbles, altered quartz grains (epidotisation)	Quartz 70%, feldspars 10%, orthoclase 10%, epidote 5%, and sulphides 5%. **Sandstone/ Conglomerate**	
WE033; 440.86 m	Quartz and feldspars	Sulphides (pyrrhotite and Chalcopyrite) and pyroxenes.	Large angular-subrounded, milky quartz. Coarse-grained.	3.00 mm-4.00 cm	Fractures and veinlets filled with secondary material. Greenish colour is alteration (epidote).	Quartz 70%, feldspars 10%, orthoclase 10%, epidote 5%, and sulphides 5%. **Sandstone/ Conglomerate**	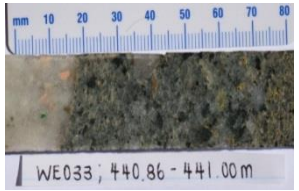
WE038; 441.30-441.55 m	Quartz, orthoclase and feldspars.	Sulphides (pyrrhotite and chalcopyrite) and epidote	Large angular-subrounded, milky white quartz. Fine-grained material in the matrix. Coarse-grained.	2.00 mm – 1.00 cm	Clusters of quartz pebbles, purple colour, finer sediments in the matrix. Greenish colour is epidote (alteration)	Quartz 70%, feldspars 15%, orthoclase 10%, sulphides 3% and epidote 2%. **Sandstone:**	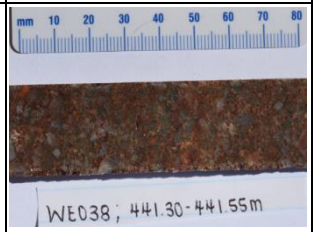

Appendix C:

Table 12: Hand Sample Descriptions for Sulphur Isotope samples

Sample Number & Borehole I.D (Meter Interval)	**Major Minerals**	**Minor Minerals**	**Colour Texture and Features**	**Grain Size**	**Other Features**	**Modal Abundance & Rock Name**	**Hand Sample Picture**
WE038; 442.24-442.45 m	Quartz, orthoclase and feldspars.	Sulphides (pyrrhotite), epidote and Magnetite	Large, angular, milky white quartz. Matrix is finer sediments. Coarse-grained.	2.00 mm-1.00 cm	Cluster of quartz, greenish colour due to alteration (epidotisation).	Quartz 70%, feldspars 10%, orthoclase 10%, epidote 5%, magnetite 2% and sulphides 3%. **Sandstone/ Conglomerate**	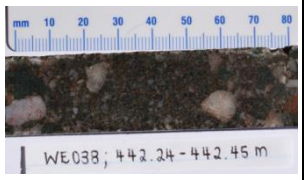

Appendix D

Polished Thin Section Description

(WB017 D0)

(WB027 D0)

(WB099 D0)

(WE001 D0)

(WE027 D0)

(WE035 D0)

WB027 D0 – Footwall samples

WE001 D0 – Footwall and Sill samples

WE002 D0 – Footwall samples

WE003 D0 – Sill samples

WE005 D0 – Footwall samples

Appendix D:
Table 1: WB017 Polished Thin Section Descriptions

Sample Number (Interval in meters)	Major Minerals	Minor Minerals	Textures	Alteration and Degree of Alteration	% of Alteration	Reflected light observations	Other Features	Modal Abundance (%) & Rock Name.	Thin Section Picture
(30.80 m - 31.00 m)	Quartz, clay minerals & lithic fragments	Magnetite & minor chlorite	Sub-angular quartz grains & brownish clay minerals & opaque minerals	Minor Chloritisation	2%	Magnetite: 70%, Pyrite: 10% & Pyrrhotite: 20%. Reddish colour surrounding the magnetite grains. Grains are angular to rounded.	Thin magnetite vein & the quartz is fractured and has undulose extinction	Quartz: 55%, Clay minerals and opaques: 30%, Lithic fragments: 15%. **Arkose**	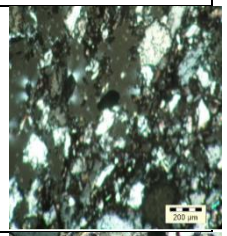
(93.78 m - 93.96 m)	Quartz, clay minerals & lithic fragments	Magnetite & minor chlorite	Alternating layers of sub-angular quartz grains & angular opaque minerals & brownish clay minerals.	Minor chloritisation	2%	Magnetite: 75%, Pyrite: 15% & Pyrrhotite: 10%. Minor rounded grains of magnetite, pyrite within pyrrhotite.	Thin magnetite veins & the quartz is fractured and has undulose extinction	Quartz: 65%, Clay minerals and opaques: 30%, Lithic fragments: 5%. **Banded Arkose**	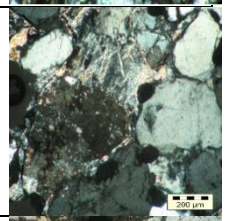
(141.23 m - 141.64 m)	Quartz, clay minerals & lithic fragments	Minor Magnetite & calcite in the matrix	Large Sub-rounded quartz grains, clay and lithic fragments in the matrix	Minor chloritisation	Minor chloritisation between the grains in the matrix 2%	Magnetite: 65% & pyrrhotite: 35%. Subrounded magnetite grains, small disseminated pyrrhotite.	Angular magnetite & the quartz is fractured and has undulose extinction, grain >5mm	Quartz: 65%, Clay & calcite minerals and opaques: 30%, Lithic fragments: 5%. **Pebble-Conglomerate**	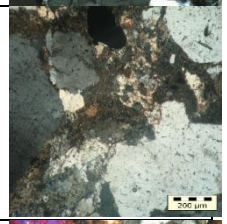
(156.36 m - 156.54 m)	OPX, CPX & Plagioclase	Biotite, hornblende & magnetite	Graphic texture or Perthitic texture, twinning in the plag, euhedral grains of plag & CPX. Interstitial OPX, biotite.	Alteration of OPX to biotite & chlorite greenish brown grains. Serpentinisation & sericitisation.	45%	Magnetite: 55%, Pyrite: 10%, Pyrrhotite: 30% & Chalcopyrite 5%. Angular shaped.	Hornblende is an igneous mineral and not due to alteration	Clinopyroxene: 25%, Plagioclase: 45%, Orthopyroxene: 10%, Biotite: 5%, hornblende: 5%, Magnetite: 5% **Dolerite (sill)**	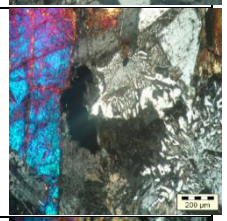
(198.55 m - 198.81 m)	OPX, CPX & Plagioclase	Biotite, tremolite & magnetite	Twinning in the plag, euhedral grains of plag & CPX. Interstitial OPX, biotite.	Alteration of OPX to biotite & chlorite greenish brown grains. Serpentinisation & sericitisation.	20%	Magnetite: 55%, Pyrite: 5%, Pyrrhotite: 25% & Chalcopyrite 15%. Disseminated droplets & veinlets between silicates	Exsolution in the CPX & OPX. Most the OPX is altered.	Clinopyroxene: 25%, Plagioclase: 45%, Orthopyroxene: 5%, Biotite: 5%, Chlorite, 5%, Olivine; 10%, Magnetite: 5%. **Ferro Gabbro**	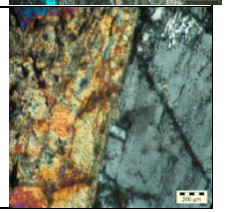

Appendix D:
Table 1: WB017 Polished Thin Section Descriptions

Sample Number (Interval in meters)	Major Minerals	Minor Minerals	Textures	Alteration and Degree of Alteration	% of Alteration	Reflected light observations	Other Features	Modal Abundance (%) & Rock Name.	Thin Section Picture
(201.20 m - 201.42 m)	OPX, CPX, Olivine & Plagioclase	Biotite, Chlorite & magnetite	Euhedral plag & CPX. Twinning in the Plag grains. Interstitial OPX, Biotite & chlorite.	Alteration of OPX to chlorite greenish brown grains. Serpentinisation & sericitisation.	10%	Magnetite: 35%, Pyrite: 12%, Pyrrhotite: 35% & Chalcopyrite 18%. Disseminated droplets & veinlets between silicates	Exsolution in the CPX & OPX.	Clinopyroxene: 10%, Plagioclase: 40%, Orthopyroxene: 27%, Olivine: 15%, Chlorite 3%, Magnetite: 5%. **Ferro Gabbro**	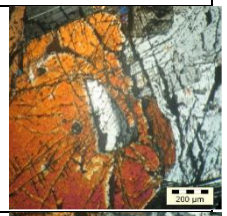
(206.29 m - 206.57 m)	OPX, CPX, Olivine & Plagioclase	Biotite, Chlorite & magnetite (minor)	Euhedral plag grains. Angular OPX grains. Biotite around OPX grains. Olivine grains are highly fractured and altered, with rounded shape.	Alteration of OPX to chlorite greenish brown grains. Sericitisation with most plag grains.	30%	Magnetite: 10%, Pyrrhotite: 40% & Chalcopyrite 50%. Disseminated droplets and grains are angular shaped.	Exsolution in the CPX & OPX. Chlorite veins and chloritisation.	Clinopyroxene: 13%, Plagioclase: 45%, Orthopyroxene: 15%, Olivine: 17%, Chlorite: 5%, Magnetite: 5%. **Gabbronorite**	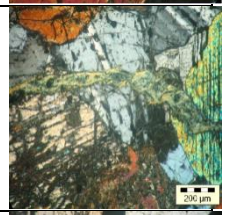
(253.66 m - 253.86 m)	OPX, CPX, Olivine, Magnetite & Plagioclase	Chlorite & Biotite.	Euhedral plag grains. Chlorite rimming plag.	Alteration of OPX to biotite then chlorite greenish brown grains. Sericitisation.	10%	Magnetite: 80%, Pyrrhotite: 15% & Chalcopyrite 5%. Magnetite is in between silicate minerals, in veinlets and disseminated.	Exsolution in the CPX & OPX. Magnetite intergrowth in the OPX.	Clinopyroxene: 10%, Plagioclase: 38%, Orthopyroxene: 15%, Olivine: 20 Chlorite 2%, Magnetite: 15%. **Magnetite Gabbronorite**	
(294 m - 294.21 m)	OPX, CPX, Olivine & Plagioclase	Chlorite & tremolite	Euhedral plag grains.	Minor chloritisation	5%	Magnetite: 50%, Pyrite: 5%, Pyrrhotite: 15% & Chalcopyrite 30%. Disseminated droplets & veinlets between silicates	Inclusions of CPX & plag in OPX.	Clinopyroxene: 10%, Plagioclase: 40%, Orthopyroxene: 17%, Olivine: 30%, Chlorite 3%. **Olivine-bearing Gabbronorite**	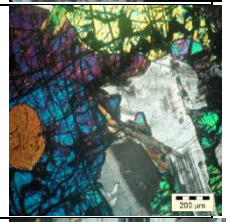
(303.43 m - 303.70 m	OPX, CPX & Plagioclase	Chlorite & biotite.	Chloritisation with the OPX & CPX grains.	Minor, Sericitisation & chloritisation.	3%	Magnetite: 60% &, Chalcopyrite 40%. Disseminated and some grains are rounded in shape.	Exsolution in the CPX & OPX.	Clinopyroxene: 25%, Plagioclase: 50%, Orthopyroxene: 20%, Chlorite 5%. **Gabbronorite**	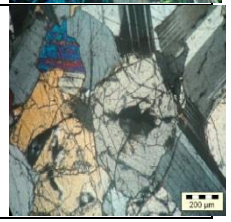

Appendix D:
Table 1: WB017 Polished Thin Section Descriptions

Sample Number (Interval in meters)	Major Minerals	Minor Minerals	Textures	Alteration and Degree of Alteration	% of Alteration	Reflected light observations	Other Features	Modal Abundance (%) & Rock Name.	Thin Section Picture
(311.16 m - 311.40 m)	Plagioclase	Chlorite, biotite & opaques.	Euhedral plag grains. The chlorite and biotite are alteration minerals.	Sericitisation, chloritisation & clay minerals.	65%	Magnetite: 35%, Pyrite: 15%, Pyrrhotite: 20% & Chalcopyrite 30%. Magnetite rims.	CPX & OPX all altered.	Plagioclase: 70%, Biotite: 7%, Chlorite: 18% & Opaques (sulphides): 5%. **Pegmatoid**	
(465.00 m - 465.20 m)	OPX, CPX, Olivine & Plagioclase	Chlorite & biotite.	Euhedral plag grains. The olivine grains are fractured and rounded in shape.	Chloritisation along grain boundaries and veins filled with chlorite material. Interstitial OPX and CPX.	30%	Pyrite: 15%, Pyrrhotite: 70% & Chalcopyrite 15%. Disseminated found in between silicate minerals.	Exsolution in the CPX (inverted pigeonite)	Clinopyroxene: 15%, Plagioclase: 50%, Orthopyroxene: 10%, Olivine: 15% Chlorite 5%, Biotite: 5%.**Gabbronorite**	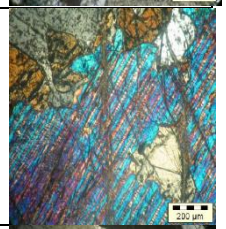
(532.00 m - 532.30 m)	OPX, CPX & Plagioclase	Chlorite, talc & biotite.	Euhedral plag grains. Interfingering texture of CPX.	Chloritisation along grain boundaries. Sericitisation & clay minerals replacement of plag.	45%	Pyrrhotite: 70% & Chalcopyrite 30% Disseminated found in between silicate minerals.	Exsolution in the CPX (inverted pigeonite)	Clinopyroxene: 20%, Plagioclase: 60%, Orthopyroxene: 12%, Chlorite 5%, Biotite: 3%.**Gabbronorite**	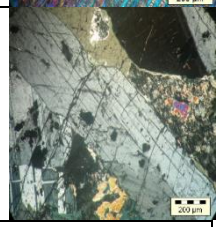
(539.20 m - 539.45 m)	Plagioclase	CPX, Chlorite, biotite & sulphides.	Euhedral plag grains. Interfingering texture of CPX	Chloritisation along grain boundaries. Sericitisation & clay minerals replacement of plag.	60%	Pyrrhotite: 85% & Chalcopyrite 15% Disseminated found in between silicate minerals.	The OPX & CPX have mostly been altered to secondary minerals like biotite and chlorite.	Clinopyroxene: 17%, Plagioclase: 55%, Orthopyroxene: 10%, Chlorite 10%, Biotite: 5% & sulphides 3%. **Altered Gabbronorite**	

Appendix D:
Table 1: WB017 Polished Thin Section Descriptions

Sample Number (Interval in meters)	Major Minerals	Minor Minerals	Textures	Alteration and Degree of Alteration	% of Alteration	Reflected light observations	Other Features	Modal Abundance (%) & Rock Name.	Thin Section Picture
(633.00 m - 633.21 m)	Plagioclase	CPX, Chlorite. Absence of OPX.	Small euhedral grains of CPX and Plag. Large grains of recrystallized material.	Sericitisation & clay minerals replacement of plag.	85%	Minor sulphides as droplets around silicate grains, sulphide % too small for composition estimate	Veins filled with serpentine and Plag and CPX overgrowth.	Clinopyroxene: 15%, Plagioclase: 65%, Clay minerals 15%, Chlorite 5%. **Pegmatoid**	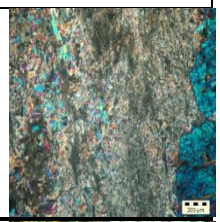
(649.25 m - 649.50 m)	Plagioclase, olivine, OPX.	CPX, biotite & chlorite.	Olivine grains are altered and has rims of CPX and the plagioclase in interstitial.	Sericitisation & clay minerals replacement of plag. Chloritisation and Serpentinisation.	22%	Pyrrhotite: 60%, Pyrite: 25% Chalcopyrite 15% Disseminated and veinlets found in between silicate minerals.	Fractures in the olivine grains are perpendicular to the cleavage.	Olivine: 38%, Orthopyroxene: 25%, Plagioclase: 25%, Clinopyroxene: 5% biotite: 5% & chlorite 3%. **Harzburgite**	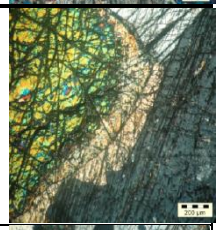
(658.00 m - 658.25 m)	OPX, CPX & Plagioclase	Biotite & chlorite.	Euhedral plag grains. Interstitial OPX & CPX.	Sericitisation & Serpentinisation.	45%	Minor sulphides as droplets around silicate grains, sulphide % too small for composition estimate	Exsolution in the CPX (inverted pigeonite)	Clinopyroxene: 15%, Plagioclase: 55%, Inverted pigeonite: 20%, Orthopyroxene: 5%, Chlorite 2%, Biotite: 3%. **Gabbronorite**	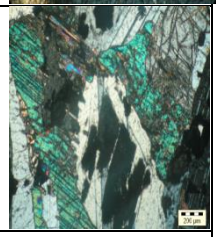
(682.50 m - 682.71 m)	Plagioclase & inverted pigeonite.	OPX & CPX	Euhedral plag grains. Interstitial inverted pigeonite.	Sericitisation & Chloritisation.	25%	Pyrrhotite: 5%, Pyrite: 70% Chalcopyrite 25%	Exsolution in the CPX (inverted pigeonite)	Clinopyroxene: 30%, Plagioclase: 50%, Inverted pigeonite: 5%, opaques: 7%, biotite: 3%, chlorite, 5%. **Gabbronorite**	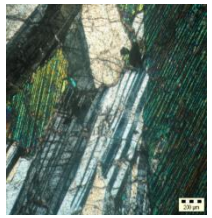

Appendix D:
Table 1: WB017 Polished Thin Section Descriptions

Sample Number (Interval in meters)	Major Minerals	Minor Minerals	Textures	Alteration and Degree of Alteration	% of Alteration	Reflected light observations	Other Features	Modal Abundance (%) & Rock Name.	Thin Section Picture
(700.28 m - 700.52 m)	Plagioclase	CPX	Extremely fine grained and difficult to distinguish individual grains.	Large amounts of sericitisation and clay minerals.	55%	Pyrrhotite: 40%, Pyrite: 10% Chalcopyrite 50%	Extremely altered & may have been replaced into calcite.	Plagioclase: 75%, Calcite, clay minerals and other alteration minerals: 25%. **Altered Anorthosite**	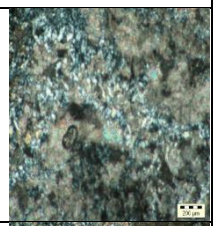
(711.88 m - 712.10 m)	Plagioclase and calcite	CPX	Extremely fine grained and difficult to distinguish individual grains.	Large amounts of sericitisation and clay minerals. Most of the sample has been altered.	60%	Pyrrhotite: 35%, Pyrite: 5% Chalcopyrite 60%	Extremely altered & may have been replaced into calcite. Veins are filled with calcite mineral.	Plagioclase: 70%, Calcite, clay minerals and other alteration minerals: 30%. **Altered Anorthosite**	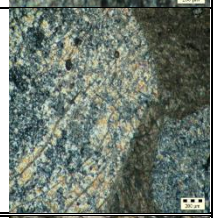
(730.26 m - 730.65 m)	OPX, CPX, Plagioclase & inverted pigeonite.	Biotite & chlorite.	Euhedral plag grains.	Sericitisation & chloritisation, clay minerals replacement of the plag grains.	20%	Pyrrhotite: 30%, Pyrite: 25% Chalcopyrite 45% Disseminated and veinlets found in between silicate minerals.	Exsolution in the CPX (inverted pigeonite)	Clinopyroxene: 20%, Plagioclase: 45%, Orthopyroxene: 15%, Chlorite 3%, Olivine: 15%, & Biotite: 2%. **Olivine-bearing Gabbronorite**	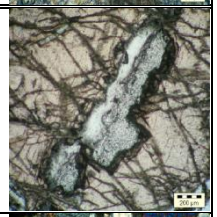
(765.27 m - 765.64 m)	Plagioclase, Olivine, OPX & CPX	Inverted pigeonite, chlorite and biotite	Large grains of CPX, interstitial plag, euhedral in shape.	Sericitisation & chloritisation, clay minerals replacement of the plag grains.	15%	Pyrrhotite: 10%, Pyrite: 55% Chalcopyrite 35% Disseminated and veinlets found in between silicate minerals.	Exsolution in the CPX (inverted pigeonite). No OPX present due all of it been altered.	Clinopyroxene: 20%, Plagioclase: 40%, Orthopyroxene: 15%, Olivine: 20%, Chlorite 3% & Biotite: 2%. **Olivine-bearing Gabbronorite**	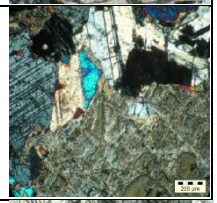
(842.74 m - 842.53 m)	OPX, CPX & Plagioclase.	Biotite.	Large grains of OPX, interstitial plag, euhedral in shape.	Sericitisation, clay minerals replacement of plag & Serpentinisation.	10%	Minor sulphides as droplets around silicate grains, sulphide % too small for composition estimate.	The large grains are extremely fractured and the veins are filled with serpentine material.	Clinopyroxene: 15%, Plagioclase: 50%, Orthopyroxene: 28%, opaques: 5% & Biotite: 2%. **Gabbronorite**	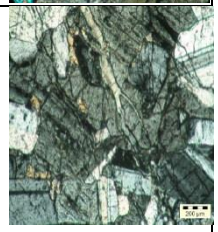

Appendix D:
Table 1: WB017 Polished Thin Section Descriptions

Sample Number (Interval in meters)	Major Minerals	Minor Minerals	Textures	Alteration and Degree of Alteration	% of Alteration	Reflected light observations	Other Features	Modal Abundance (%) & Rock Name.	Thin Section Picture
(965.52 m - 965.70 m)	OPX, CPX & Plagioclase.	Biotite, talc & chlorite.	Euhedral plag grains. Interstitial OPX & CPX. Inclusion of plag grains in large OPX grains.	Sericitisation, clay minerals replacement of plag & chloritisation.	10%	Pyrrhotite: 5%, Pyrite: 75% Chalcopyrite 20%. Disseminated.	Exsolution in the CPX (inverted pigeonite)	Clinopyroxene: 15%, Plagioclase: 52%, Orthopyroxene: 25%, Biotite: 5% & chlorite: 3%. **Gabbronorite**	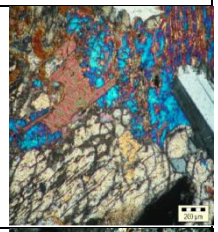
(988.74 m - 988.94 m)	Plagioclase, olivine, CPX & OPX.	Biotite & chlorite.	Large euhedral grains of plag. Olivine grains are fractured and highly altered.	Sericitisation, clay minerals replacement of plag, chloritisation & Serpentinisation.	40%	Pyrrhotite: 50%, Pyrite: 10% Chalcopyrite 40% Disseminated and veinlets found in between silicate minerals.	Exsolution in the CPX (inverted pigeonite)	Clinopyroxene: 10%, Plagioclase: 30%, Olivine: 30% Orthopyroxene: 25%, Biotite: 3% & chlorite: 2%. **Harzburgite**	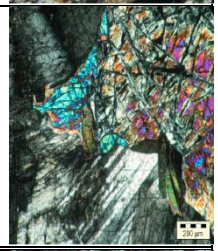
(1003.74 m - 1003.95 m	Olivine, plagioclase & OPX	Opaques & CPX	Large grains of olivine, subrounded grains.	Sericitisation, clay minerals replacement of plag & Serpentinisation.	55%	Pyrrhotite: 5 %, Pyrite: 80 % Chalcopyrite: 15%. Veinlets found in between silicate minerals.	Highly altered with veins filled with serpentine materials.	Clinopyroxene: 5%, Plagioclase: 20%, Olivine: 38% Orthopyroxene: 30%, Biotite: 4% & opaques: 3%. **Harzburgite**	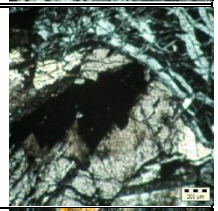
(1015.29 m - 1015.50 m)	Plagioclase, Olivine, OPX & CPX.	Opaques, chlorite & biotite.	Large, euhedral grains of plagioclase, with interstitial OPX & CPX.	Sericitisation, clay minerals replacement of plag & the OPX in some cases is extremely altered.	40%	Minor sulphides as droplets around silicate grains, sulphide % too small for composition estimate.	Highly altered with veins filled with serpentine materials. Exsolution in the CPX (inverted pigeonite).	Clinopyroxene: 5%, Plagioclase: 30%, Orthopyroxene: 38%, Olivine: 15% Biotite: 5%, Chlorite: 2% & opaques: 5%. **Harzburgite**	

Appendix D:
Table 1: WB017 Polished Thin Section Descriptions

Sample Number (Interval in meters)	Major Minerals	Minor Minerals	Textures	Alteration and Degree of Alteration	% of Alteration	Reflected light observations	Other Features	Modal Abundance (%) & Rock Name.	Thin Section Picture
(1019.50 m - 1019.26 m)	Olivine, plagioclase & OPX	Opaques, CPX & chlorite.	Large euhedral grains of plag. Olivine grains are fractured and highly altered.	Sericitisation, clay minerals replacement of plag, chloritisation & Serpentinisation	35%	Pyrrhotite: 60%, Pyrite: 15% Chalcopyrite 25% Disseminated and veinlets found in between silicate minerals.	Highly altered with veins filled with serpentine materials. CPX rimming altered olivine.	Clinopyroxene: 2%, Plagioclase: 45%, Olivine: 38% Orthopyroxene: 10% & chlorite: 5%. **Troctolite**	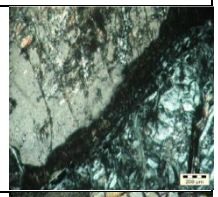
(1051.00 m - 1051.21 m)	Plagioclase, OPX & CPX.	Opaques, chlorite & biotite.	Large sub-angular grains of CPX & OPX. Interstitial plag	Sericitisation, clay minerals replacement of plag, chloritisation & Serpentinisation	10%	Pyrrhotite: 35%, Pyrite: 15% Chalcopyrite 50% Disseminated and anhedral droplets of sulphides in between silicate minerals.	Exsolution in the CPX (inverted pigeonite)	Clinopyroxene: 35%, Plagioclase: 20%, Orthopyroxene: 35% & chlorite: 2% biotite: 3%, sulphides 5%. **Pyroxenite**	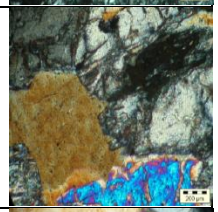
(1072.80 m - 1073.00 m)	Plagioclase, OPX & CPX.	Opaques, chlorite & biotite.	Large sub-angular grains of CPX & OPX. Interstitial plag	Sericitisation, clay minerals replacement of plag, chloritisation & Serpentinisation	10%	Pyrrhotite: 35%, Pyrite: 15% Chalcopyrite 50%. Droplets of sulphides in between silicate minerals.	Exsolution in the CPX (inverted pigeonite)	Clinopyroxene: 35%, Plagioclase: 20%, Orthopyroxene: 35% & chlorite: 2% biotite: 3%, sulphides 5%. **Pyroxenite**	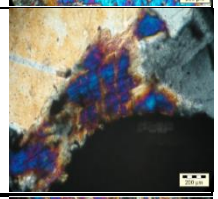
(1077.90 m - 1078.10 m)	Plagioclase, CPX, Chlorite, biotite & phlogopite.	Quartz	Large euhedral grains of plag, small rounded quartz grains.	Sericitisation, clay minerals replacement of plag, chloritisation.	20%	No sulphides presence.	Large amounts of secondary minerals due to alteration.	Clinopyroxene: 10%, Plagioclase: 70%, Chlorite: 5% biotite: 15%. **Plagioclase vein**	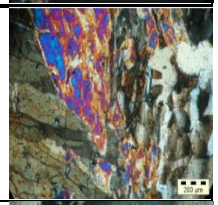
(1086.70 m - 1086.90 m)	Quartz & plagioclase	Biotite	Fine-grained euhedral plagioclase grains and subrounded quartz grains with undulose extinction.	Sericitisation, clay minerals replacement of plagioclase.	3%	Minor sulphides as droplets around silicate grains, sulphide % too small for composition estimate.		Quartz: 85%, Plagioclase: 13% & biotite: 2%. **Granofels (Felsic unit)**	

Appendix D:
Table 2: WB027 Polished Thin Section Descriptions

Sample Number (Interval in meters)	Major Minerals	Minor Minerals	Textures	Alteration and Degree of Alteration	% of Alteration	Reflected light observations	Other Features	Modal Abundance (%) & Rock Name.	Thin Section Picture
488.00 – 488.10 m	Quartz, feldspars, sericite and hematite (opaque minerals)	Calcite	Quartz grains are anhedral and have undulose extinction. Most of the feldspars have been altered to sericite. Inequigranular and aphanitic textures.	Hematisation and sericitisation.	70%	Hematite and magnetite.	Iron staining from the hematite and magnetite grains.	Quartz; 20%, feldspars (altered to sericite); 50%, calcite; 10% and hematite; 20%. **Altered Volcanic Clastic Rock.**	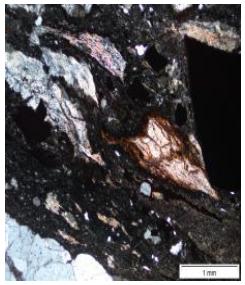
490.60 – 490.80 m	Quartz, feldspars, sericite and hematite (opaque minerals)	Calcite	Quartz grains are anhedral and have undulose extinction. Most of the feldspars have been altered to sericite. Inequigranular and aphanitic textures.	Hematisation and sericitisation.	90%	Hematite and magnetite.	Iron staining from the hematite and magnetite grains. Hematite has a wavely and string like-texture.	Quartz; 5%, feldspars (altered to sericite); 65%, calcite; 10% and hematite; 20%. **Palaesol (Contact between Waterberg sediments and Bushveld rocks)**	
520.63 – 520.80 m	Feldspars (plagioclase) and pyroxenes (Opx and Cpx).	Chlorite, biotite and magnetite	Plagioclase shows albite twinning and is euhedral in shape. Opx is grey with subhedral shape and regular fractures. Cpx is interstitial and seen as inclusions in Opx (exsolution).	Chloritisation, biotitization and sericitisation. Cpx is altering to chlorite and biotite. Opx is rimming by biotite and chlorite. The plagioclase is slightly altered to sericite.	10%	Large grain of magnetite and sulphides (chalcopyrite and pyrrhotite are seen on the magnetite grain boundary. Other sulphides are disseminated, droplets or along grain boundaries.	Veinlets and fractures are filled with secondary material (chlorite, sericite and biotite). Ophitic, equigranular and phaneritic textures.	Plagioclase; 45%, Opx; 30%, Cpx 20%, chlorite and biotite; 2%, and magnetite 3% locally. **Pegmatoidal unit (recrystallised gabbronorite)**	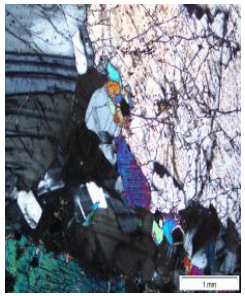

Appendix D:
Table 2: WB027 Polished Thin Section Descriptions

Sample Number (Interval in meters)	Major Minerals	Minor Minerals	Textures	Alteration and Degree of Alteration	% of Alteration	Reflected light observations	Other Features	Modal Abundance (%) & Rock Name.	Thin Section Picture
537.64 – 537.85 m	Plagioclase and pyroxenes (Opx and Cpx)	Chlorite and biotite.	Plagioclase grains show albite twinning and are euhedral. Pyroxenes grains are interstitial with exsolution textures.	Chloritisation, biotitization and sericitisation. Pyroxene grains altering to chlorite and biotite.	5%	Minor disseminated sulphides (chalcopyrite and pyrrhotite). Located as inclusion in silicate minerals and along grain boundaries.	Equigranular, poikilitic and phaneritic textures. The pyroxenes have exsolution texture showing lamination on grains (inverted pigeonite).	Plagioclase; 55%, Cpx; 25%, Opx; 5%, inverted pigeonite; 10%, chlorite and biotite; 5%. **Gabbronorite**	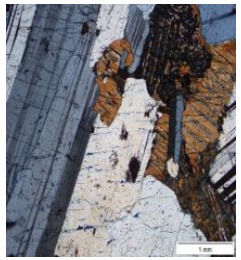
606.00 – 606.20 m	Plagioclase, sulphides and pyroxenes (Opx and Cpx).	Chlorite and biotite	Plagioclase shows albite twinning and euhedral shape. Cpx is mainly interstitial and altered. Opx is grey-yellow with regular fractures.	Chloritisation, biotitization and sericitisation. Pyroxene grains altering to chlorite and biotite.	5%	Sulphides (chalcopyrite, pentlandite and pyrrhotite), are droplets, inclusions with pyroxene grains or along grain boundaries. Sulphides are clustered and associated magnetite	Inequigranular and phaneritic texture. Veinlets and fractures are filled with secondary minerals.	Plagioclase; 55%, Opx; 15%, Cpx (altered); 10%, sulphides and magnetite; 15%, sericite, biotite and chlorite; 5%. **Gabbronorite**	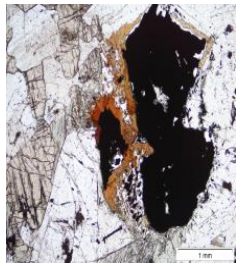
622.00 – 622.20 m	Olivine, feldspars (plagioclase), pyroxenes (Opx and Cpx).	Chlorite, biotite and inverted pigeonite.	Olivine grains are subrounded and altered. Plagioclase shows albite twinning and is euhedral. Pyroxene grains are interlocking and some have exsolution to inverted pigeonite.	Chloritisation, sericitisation and biotitization. Biotite and chlorite alteration from the pyroxenes and some are rimming the pyroxenes.	15%	Disseminated sulphides (chalcopyrite and pentlandite). Minor magnetite associated with sulphides.	Ophitic textures large Opx grains with inclusion of plagioclase. Inequigranular and phaneritic textures. Interlocking texture.	Olivine; 7%, Opx; 20%, Cpx; 25%, plagioclase; 40%, chlorite 3%, biotite; 3%, magnetite and sulphides; 2% **Gabbronorite**	

Appendix D:
Table 2: WB027 Polished Thin Section Descriptions

Sample Number (Interval in meters)	Major Minerals	Minor Minerals	Textures	Alteration and Degree of Alteration	% of Alteration	Reflected light observations	Other Features	Modal Abundance (%) & Rock Name.	Thin Section Picture
649.20 – 649.40 m	Olivine, pyroxenes (Opx and Cpx) and plagioclase	Chlorite, biotite, sericite and inverted pigeonite.	Olivine grains are subrounded and highly fractured. Pyroxene are anhedral, Opx has regular fractures and grey. Plagioclase shows albite twinning and euhedral shaped. Interlocking grains.	Chloritisation, sericitisation and biotitization. Biotite and chlorite alteration from the pyroxenes and some are rimming the pyroxenes.	15%	Minor sulphides (chalcopyrite and pyrrhotite).	Inequigranular and phaneritic textures. The pyroxene grains show exsolution (inverted pigeonite).	Olivine; 25%, Opx; 25%, Cpx; 30%, plagioclase 15% and chlorite, biotite and sericite; 5%. **Olivine-bearing Pyroxenite**	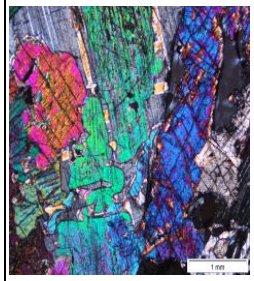
815.20 – 815.30 m	Plagioclase and pyroxenes (Opx and Cpx).	Olivine, Sericite, chlorite, biotite, serpentine.	Olivine is highly fractured and mostly altered. Plagioclase albite twinning with euhedral shape and some grains are slightly altered to sericite. Pyroxenes are grey and mostly altered.	Chloritisation, sericitisation and serpentinisation.	25%	Minor sulphides (chalcopyrite and pyrrhotite) associated with magnetite, found along grain boundaries mainly of Cpx.	Equigranular, phaneritic textures. The Pyroxenes are mainly altering to chlorite and biotite. Veinlets and fractures are filled with secondary minerals.	Plagioclase; 42%, Opx; 10%, Cpx; 25%, olivine (altered); 5%, sericite; 10%, chlorite and biotite; 5%, sulphides (chalcopyrite and pyrrhotite) and magnetite: 3% locally. **Altered Gabbronorite**	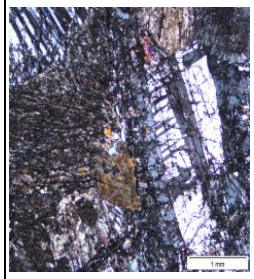
881.00 – 881.25 m	Plagioclase and pyroxenes (Opx and Cpx)	Chlorite, biotite and sericite.	Plagioclase grains show albite twinning and have a euhedral shape. The pyroxenes are anhedral and some grains are interstitial. The pyroxenes are also altering to biotite and chlorite. Interlocking grains.	Chloritisation, biotitization and sericitisation. Pyroxene grains altering to chlorite and biotite.	5%	Minor disseminated sulphides (chalcopyrite and pyrrhotite). Droplets or in fractures of grains or along grain boundaries.	Equigranular and phaneritic texture. Cpx rims a few of the plagioclase grains. Plagioclase grains meet at 120° triple junction.	Plagioclase; 55%, Opx; 15%, Cpx; 20%, Chlorite, biotite and sericite; 8% and sulphides (chalcopyrite and pyrrhotite); 2% locally. **Gabbronorite**	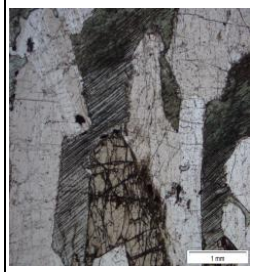

Appendix D:
Table 2: WB027 Polished Thin Section Descriptions

Sample Number (Interval in meters)	Major Minerals	Minor Minerals	Textures	Alteration and Degree of Alteration	% of Alteration	Reflected light observations	Other Features	Modal Abundance (%) & Rock Name.	Thin Section Picture
889.00 – 889.10 m	Feldspars (plagioclase and orthoclase) and sericite.	Quartz, epidote, calcite, chlorite and biotite.	Feldspar is mainly altered to sericite and epidote. Quartz grains are found filling veins and fractures.	Chloritisation and sericitisation.	70%	None	Inequigranular and aphanitic texture.	Feldspars (altered) to sericite; 75%, Quartz; 10%, epidote, calcite, chlorite and biotite; 15%. **Altered Anorthosite**	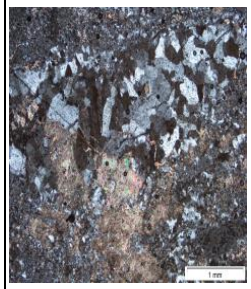
928.48 – 928.70 m	Feldspars (plagioclase) and pyroxene (Opx and Cpx)	Chlorite, biotite and inverted pigeonite	Subhedral to euhedral feldspars with albite twinning (plag) and Carlsbad twinning (orthoclase). Opx and Cpx have subhedral to anhedral grains.	Chloritisation, biotitization and seritization	7%	Minor sulphides (pentlandite and chalcopyrite) as droplets, inclusion within silicate minerals and along grain boundaries. The sulphides are disseminated.	Exsolution between pyroxene grains showing laminated inverted pigeonite. Ophitic textures and fractures filled with sericite seen in pyroxene grains.	Opx; 25%, Cpx; 20%, plagioclase; 45%, biotite 3%, Chlorite; 5% and sulphides (chalcopyrite and pentlandite); 1%. **Gabbronorite**	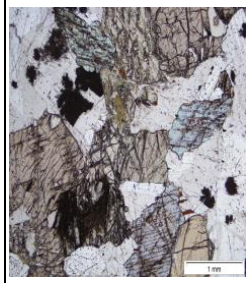
939.50 – 939.70 m	Feldspars (plagioclase) and pyroxene (Opx).	Sericite and Chlorite	Plagioclase is euhedral with albite twinning and orthoclase with Carlsbad twinning. Plagioclase has interlocking crystal boundaries. Opx is grey with fracture. Inequigranular and phaneritic texture.	Alteration of plagioclase to sericite and minor chloritisation.	5%	Minor disseminated sulphides (chalcopyrite) along grain boundaries.	Perthitic Exsolution seen in the albite plagioclase. Poikilitic (intergrowth) texture with Opx and plagioclase.	Plagioclase; 55%, orthoclase; 15%, Opx; 20%, sericite; 5%, chlorite; 3% and sulphides (chalcopyrite and pentlandite); 2%. **Mottle Norite**	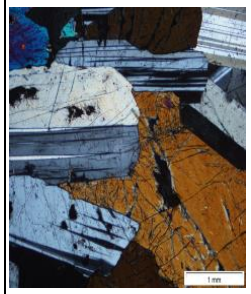

Appendix D:
Table 2: WB027 Polished Thin Section Descriptions

Sample Number (Interval in meters)	Major Minerals	Minor Minerals	Textures	Alteration and Degree of Alteration	% of Alteration	Reflected light observations	Other Features	Modal Abundance (%) & Rock Name.	Thin Section Picture
1060.50 – 1060.70 m	Olivine, pyroxene; Cpx and Opx and sericite.	Plagioclase, chlorite, biotite, serpentine and opaque minerals	Olivine grains are subrounded and have irregular fracture, most are completely altered. Pyroxenes are interstitial and some grains have been altered completely to biotite and chlorite. Plagioclase showing albite twinning.	Alteration of plagioclase to sericite. Pyroxenes altered to biotite and chlorite and olivine altered to serpentine. Chloritisation, biotitization, sericitisation and serpentinisation.	55%	Veinlets and fractures filled with secondary magnetite associated with the olivine grains. Disseminated sulphides (chalcopyrite and pyrrhotite).	Plagioclase is interstitial and is altered to sericite. Olivine grains are highly fractured. Inequigranular and phaneritic texture.	Olivine; 45%, Opx; 15%, Cpx; 20%, plagioclase; 5%, Chlorite, biotite and serpentine; 10% and sulphides (chalcopyrite and pyrrhotite); 1%. **Harzburgite**	
1090.70 – 1090.90 m	Olivine (altered), serpentine, calcite, sericite.	Biotite and chlorite.	Olivine altered has subrounded grains and highly fractured. The sample is almost completely altered to serpentine, sericite and calcite.	Chloritisation, biotitization, sericitisation and serpentinisation.	90%	Veinlets and fractures filled with secondary magnetite associated with the olivine grains. Disseminated sulphides (chalcopyrite and pyrrhotite).	Veinlets and fractures filled with secondary minerals (magnetite and serpentine). Boundaries of olivine grains visible however the grains are completely altered.	Olivine (altered); 55%, serpentine; 20%, sericite and calcite; 20% and magnetite; 5%. **Altered Harzburgite (xenolith)**	
1092.00 – 1092.20 m	Olivine, pyroxenes (Opx and Cpx) and feldspars (plag).	Chlorite, biotite and serpentine.	Olivine grains are subrounded and completely altered. Plagioclase shows albite twinning and is euhedral, also altering to sericite. Pyroxenes are subhedral to anhedral, Opx is grey and fractured. Inequigranular and phaneritic texture	Chloritisation, biotitization, serpentinisation and seritization	55%	Minor sulphides (pentlandite and chalcopyrite) as droplets, inclusion within silicate minerals and along grain boundaries. The sulphides are disseminated.	Olivine completely altered, with fractures filled with serpentine and magnetite. Veinlets and fractures filled with secondary minerals (Chlorite and serpentine). Cpx rimming Opx.	Olivine; 25%, Opx: 25%, Cpx; 15%, Plagioclase; 20%, sericite 10%, serpentine and magnetite; 5% and sulphides (Chalcopyrite and pentlandite) 1% **Altered Troctolite**	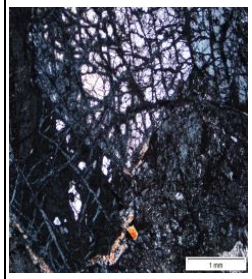

Appendix D:
Table 2: WB027 Polished Thin Section Descriptions

Sample Number (Interval in meters)	Major Minerals	Minor Minerals	Textures	Alteration and Degree of Alteration	% of Alteration	Reflected light observations	Other Features	Modal Abundance (%) & Rock Name.	Thin Section Picture
1116.10 – 1116.22 m	Serpentine and sericite	Chlorite and epidote.	Completely altered olivine to serpentine.	Chloritisation and serpentinisation.	99%	Disseminated magnetite and sulphides (chalcopyrite and pyrrhotite). Magnetite also associated with veins.	Olivine grains can be seen however they are completely altered to serpentine.	Serpentine; 80%, sericite; 10% and chlorite and epidote; 10% **Altered Harzburgite**	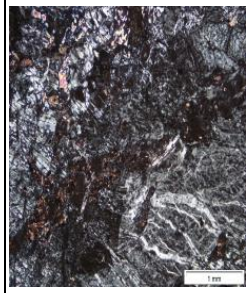
1152.20 – 1152.40 m	Olivine, pyroxene (Opx and Cpx) and sericite and serpentine	Chlorite, biotite and epidote	Olivine grains are subrounded and highly fracture, most olivine grains are altered. Pyroxenes are interstitial and altering to biotite and chlorite. Plagioclase (albite twinning) is almost completely altered to sericite.	Serpentinisation and chloritisation.	70%	Disseminated sulphides (chalcopyrite, pentlandite and pyrrhotite) inclusion, droplets or along grain boundaries, associated with magnetite.	Abundance of magnetite and serpentine rich veins. Abundance of secondary overgrowth and rimming on grains. Inequigranular and phaneritic texture.	Olivine; 20%, Cpx; 10%, Opx; 10% and plagioclase; 10%, sericite; 20%, serpentine and magnetite; 15%, chlorite and epidote; 5% and sulphides 1% **Serpentinised unit (Altered Harzburgite)**	
1174.70 – 1174.80 m	Quartz, feldspars (plagioclase and orthoclase) and sericite.	Chlorite, Sulphides (chalcopyrite and pyrrhotite), serpentine and biotite.	Quartz grains are anhedral with undulose extinction. Plagioclase shows albite twinning and subhedral shape.	Serpentinisation and chloritisation.	10%	Disseminated sulphides (chalcopyrite, pyrrhotite and pentlandite)	Veinlets and fractures filled with secondary material (serpentine and calcite). Inequigranular and aphanitic.	Quartz; 60%, plagioclase; 25%, orthoclase; 5%, sulphides (chalcopyrite and pyrrhotite); 5% and sericite, biotite and chlorite; 5%. **Granofels**	

Appendix D:
Table 2: WB027 Polished Thin Section Descriptions

Sample Number (Interval in meters)	Major Minerals	Minor Minerals	Textures	Alteration and Degree of Alteration	% of Alteration	Reflected light observations	Other Features	Modal Abundance (%) & Rock Name.	Thin Section Picture
1178.10 – 1178.20 m	Quartz, feldspars (plagioclase and orthoclase) and sericite.	Chlorite, epidote, serpentine and biotite.	Quartz grains are anhedral with undulose extinction. Most of the plagioclase and orthoclase has been altered to sericite.	Seritisation and serpentinisation.	70%	Minor disseminated sulphides (chalcopyrite and pyrrhotite).	Veinlets and fractures filled with secondary material (serpentine and calcite). Inequigranular and aphanitic.	Quartz; 25%, sericite; 45%, serpentine; 25%, chlorite; 2%, biotite; 2% and sulphides (chalcopyrite and pyrrhotite); 1% **Granofels**	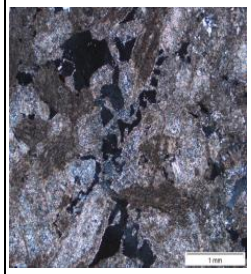

Appendix D:
Table 3: WB099 Polished Thin Section Descriptions

Sample Number WB099 (Interval in meters)	Major Minerals	Minor Minerals	Textures	Alteration and Degree of Alteration	% of Alteration	Reflected light observations	Other Features	Modal Abundance (%) & Rock Name.	Thin Section Picture
527.58 m-528.06 m	Feldspars (plagioclase) and pyroxenes (Opx and Cpx).	Biotite and chlorite.	Plagioclase shows albite twinning and euhedral shape. Cpx is mainly interstitial with an altered rim of chlorite and biotite. Opx is grey and cumulus. Equigranular texture.	Chloritisation and biotitization.	5%	Minor sulphides (chalcopyrite and pyrrhotite) disseminated and within silicate minerals. Minor secondary magnetite.	Inclusions of Opx in the Cpx grains and plagioclase rimmed by cpx.	Feldspars (plagioclase): 55% and pyroxenes: Opx: 15% and Cpx: 30%. **Gabbronorite**	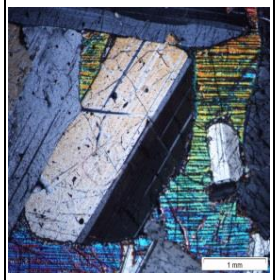
551.80 m-552.00 m	Feldspars (plagioclase) and pyroxenes (Opx and Cpx).	Magnetite, sericite, inverted pigeonite biotite and chlorite.	Plagioclase shows albite twinning and euhedral shape. Opx and Cpx are both intercumulus and cumulus, Opx has a grey colour. Equigranular texture.	Chloritisation, biotitization and sericitisation.	15%	Minor sulphides (chalcopyrite and pyrrhotite), sulphides associated with magnetite. Magnetite overgrowth and replacement of silicate minerals.	Magnetite overgrowth with Opx grains. Feldspars completely altered to sericite. Exsolution of pyroxenes (inverted pigeonite).	Feldspars (plagioclase): 50%, Pyroxenes: Opx: 20%, Cpx: 25% and magnetite and sericite 5%. **Magnetite Gabbronorite**	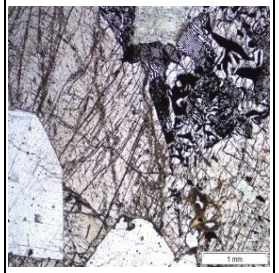
566.48 m-566.66 m	Feldspars (plagioclase) and pyroxenes (Opx and Cpx).	Olivine, magnetite sericite, inverted pigeonite biotite and chlorite.	Plagioclase shows albite twinning and is subhedral to euhedral in shape. Opx and Cpx are both intercumulus and cumulus. Equigranular texture.	Chloritisation, biotitization and sericitisation.	10%	Minor sulphides (chalcopyrite and pyrrhotite), disseminated and sulphides associated with magnetite. Magnetite overgrowth and replacement of silicate minerals.	Cpx and Opx altering to biotite and chlorite. Cpx has rims of chlorite.	Feldspars (plagioclase): 50%, Pyroxenes: Opx: 20%, Cpx: 25% and magnetite, chlorite, biotite and sericite 5%. **Magnetite Gabbronorite**	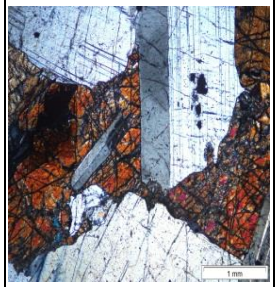

Appendix D:
Table 3: WB099 Polished Thin Section Descriptions

Sample Number WB099 (Interval in meters)	Major Minerals	Minor Minerals	Textures	Alteration and Degree of Alteration	% of Alteration	Reflected light observations	Other Features	Modal Abundance (%) & Rock Name.	Thin Section Picture
602.26 m-602.43m	Feldspars (plagioclase) and pyroxenes (Opx and Cpx).	Magnetite, sericite, inverted pigeonite biotite and chlorite.	Plagioclase shows albite twinning euhedral shape. Opx and Cpx are both intercumulus and cumulus. Cpx is rimmed with chlorite and the pyroxenes also show exsolution textures.	Chloritisation and sericitisation	15%	Sulphides (chalcopyrite and pyrrhotite), disseminated. Sulphides are associated with magnetite. Sulphides are droplets, along grain boundaries or within silicate grains.	Veinlets and fractures filled with secondary minerals (chlorite). Interlocking grains and inclusions of Cpx and plag in Opx.	Feldspars (plagioclase): 50%, Pyroxenes: Opx: 15%, Cpx: 30% and magnetite, chlorite: 5%. **Magnetite Gabbronorite**	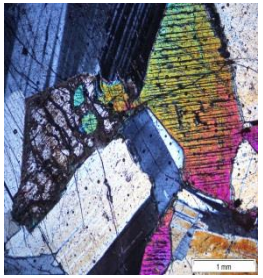
619.80 m-620.00 m	Olivine, pyroxenes (Opx and Cpx) and feldspars (plagioclase).	Chlorite, biotite and inverted pigeonite.	Olivine grains are subrounded to rounded with irregular fractures. Pyroxenes show exsolution textures with subhedral shape. Plagioclase is mainly interstitial and show albite twinning.	Chloritisation, biotitization and serpentinisation.	10%	Minor sulphides (chalcopyrite and pyrrhotite) disseminated, along grain boundaries and within grains.	Veinlets and fractures filled with secondary minerals (chlorite and serpentine). Olivine altering to serpentine and magnetite.	Olivine: 15%, pyroxenes: Opx: 30% and Cpx: 25%, feldspars (plagioclase): 25% and chlorite, serpentine and inverted pigeonite: 5% **Olivine-bearing feldspathic pyroxenite**	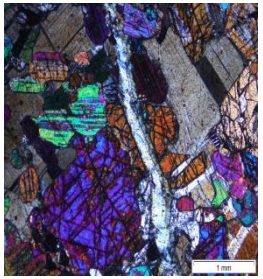
628.50 m-628.68 m	Feldspars (plagioclase) and pyroxenes (Opx and Cpx).	Chlorite, biotite, magnetite, inverted pigeonite and sericite.	Plagioclase show albite twinning and is euhedral in shape. Pyroxenes are showing exsolution and have a subhedral shape. Equigranular texture.	Chloritisation and biotitization.	15%	Minor sulphides (chalcopyrite and pyrrhotite), disseminated and associated with magnetite.	Grains completely altered to sericite and overgrowth of magnetite. Pyroxenes rimmed with chlorite and fractures filled with secondary veinlets.	Feldspars (plagioclase): 50%, pyroxenes: Opx: 20% and Cpx: 25%, magnetite, sericite and chlorite: 5%. **Magnetite Gabbronorite**	

Appendix D:
Table 3: WB099 Polished Thin Section Descriptions

Sample Number WB099 (Interval in meters)	Major Minerals	Minor Minerals	Textures	Alteration and Degree of Alteration	% of Alteration	Reflected light observations	Other Features	Modal Abundance (%) & Rock Name.	Thin Section Picture
671.57 m-671.74 m	Olivine, pyroxenes (Opx and Cpx) and feldspars (plagioclase)	Chlorite, biotite and serpentine.	Plagioclase shows albite twinning and has euhedral shape. Olivine is subrounded to rounded with irregular fractures. Pyroxenes are subhedral. Inequigranular texture.	Chloritisation, biotitization and serpentinisation.	20%	Minor sulphides (chalcopyrite and pyrrhotite) disseminated and associated with magnetite. Magnetite within olivine grains, secondary mineral (alteration).	Olivine rimmed by Opx and biotite and Cpx rimmed by chlorite. Veinlets and fractures filled with secondary minerals (magnetite and serpentine).	Feldspars (plagioclase): 40%, Olivine: 20% and pyroxenes: Opx: 10%, Cpx: 25%, chlorite, serpentine and biotite: 5%. **Olivine-bearing Gabbronorite**	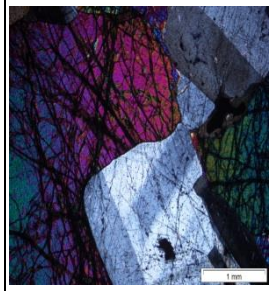
675.84 m-676.04 m	Olivine, Feldspars (plagioclase) and pyroxenes (Opx and Cpx).	Chlorite, biotite, sericite and serpentine.	Olivine grains subrounded in shape with irregular fractures. Plagioclase shows albite twinning and has euhedral shape. Pyroxenes are mainly altered or completely replaced.	Chloritisation, biotitization and serpentinisation.	25%	Minor sulphides (chalcopyrite and pyrrhotite) disseminated and associated with magnetite. Magnetite within olivine grains, secondary mineral (alteration).	Olivine grains are rimmed by Opx, chlorite and biotite. Cpx has been completely replaced by biotite. Inclusions of plagioclase within olivine grains.	Olivine: 25%, Pyroxenes: Opx: 15% and Cpx (altered): 15%, feldspars (plagioclase): 40%, biotite: 2% Chlorite and serpentine: 3% **Olivine-bearing Gabbronorite**	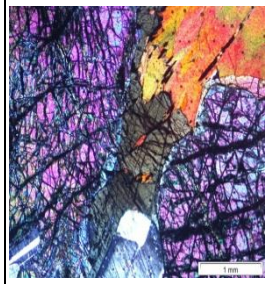
698.67 m-698.84 m	Feldspars (plagioclase and orthoclase) and pyroxenes (Opx and Cpx).	Olivine, chlorite, biotite, sericite, sulphides (chalcopyrite and pyrrhotite) and serpentine.	Feldspars show albite and carlsbad twinning and interlocking grains. Pyroxenes are subhedral, Cpx mostly interstitial. Olivine with surrounded and irregular fractures.	Chloritisation and biotitization.	15%	Sulphides (chalcopyrite and pyrrhotite), disseminated, along grain boundaries and included within grains. Small amounts of magnetite within fractures and veinlets.	Inclusions of Plagioclase within Opx (Ophitic texture).Cpx rimmed and replaced by biotite.	Feldspars (plagioclase and orthoclase): 45%, Pyroxenes: Opx: 15% and Cpx: 20%, Olivine: 5%, sulphides, Chlorite and biotite: 5%. **Gabbronorite**	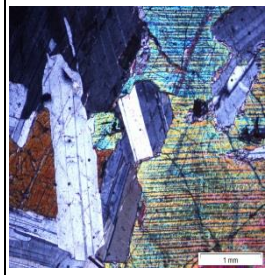

Appendix D:
Table 3: WB099 Polished Thin Section Descriptions

Sample Number WB099 (Interval in meters)	Major Minerals	Minor Minerals	Textures	Alteration and Degree of Alteration	% of Alteration	Reflected light observations	Other Features	Modal Abundance (%) & Rock Name.	Thin Section Picture
699.40 m-699.60 m	Feldspars (plagioclase), pyroxenes (Opx and Cpx) and sulphides (chalcopyrite and pyrrhotite).	Olivine, chlorite and biotite.	Plagioclase shows albite twinning and euhedral interlocking grains. Pyroxenes are subhedral, Opx is grey and Cpx is altering to sericite and chlorite.	Chloritisation, biotitization and sericitisation.	25%	Sulphides (Chalcopyrite, pyrrhotite and pentlandite). Disseminated, along grain boundaries, inclusion and interstitial or droplets.	Inclusions of Plagioclase within Opx (Ophitic texture).Cpx rimmed and replaced by biotite. Exsolution between Cpx and Opx.	Feldspars (plagioclase): 45%, pyroxenes: Opx: 25% and Cpx: 20%, Sulphides (chalcopyrite and pyrrhotite): 5%, Chlorite and biotite: 5%. **Gabbronorite**	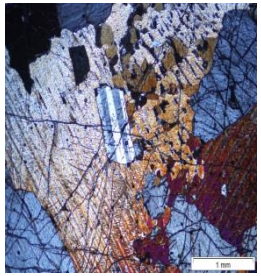
700.02 m-700.37 m	Feldspars (plagioclase and orthoclase), pyroxenes (Opx and Cpx) and sulphides (chalcopyrite and pyrrhotite).	Chlorite, serpentine, sericite and biotite.	Plagioclase and orthoclase show albite and carlsbad twinning, euhedral, interlocking grains. Pyroxenes are subhedral and altering.	Chloritisation, biotitization, serpentinisation and sericitisation.	20%	Sulphides (Chalcopyrite, pyrrhotite and pentlandite). Disseminated, along grain boundaries, inclusion and interstitial or droplets.	Veinlets and fractures filled with secondary minerals (serpentine and chlorite). Plagioclase is altering to sericite.	Feldspars (plagioclase): 45%, pyroxenes: Opx: 25% and Cpx: 20%, Sulphides (chalcopyrite and pyrrhotite): 5%, Chlorite and biotite: 5%. **Gabbronorite**	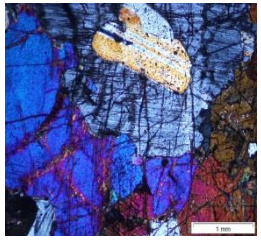
705.50 m-705.75 m	Feldspars (plagioclase and orthoclase), pyroxenes (Opx and Cpx), olivine and sulphides	Chlorite, biotite, epidote and sericite.	Feldspars show albite and carlsbad twinning, euhedral and interlocking grains. Olivine subrounded with irregular fractures. Pyroxene grains are subhedral to anhedral.	Chloritisation, biotitization, serpentinisation and sericitisation.	15%	Sulphides (chalcopyrite, pyrrhotite and pentlandite), associated with magnetite and chromite grains. Sulphides are within veinlets, droplets, inclusions or along grain boundaries.	Veinlets and fractures filled with secondary minerals. Inclusions of plagioclase in olivine and Opx grains (Ophitic texture). Exsolution textures seen in the pyroxenes.	Feldspars: (plagioclase and orthoclase) 45%, pyroxenes: Opx: 20%, Cpx: 15%, olivine: 5%, chlorite, biotite: 5% and sulphides: 5%. **Olivine-bearing Gabbronorite**	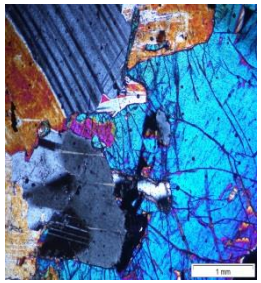

Appendix D:
Table 3: WB099 Polished Thin Section Descriptions

Sample Number WB099 (Interval in meters)	Major Minerals	Minor Minerals	Textures	Alteration and Degree of Alteration	% of Alteration	Reflected light observations	Other Features	Modal Abundance (%) & Rock Name.	Thin Section Picture
711.80 m-711.96 m	Feldspars (plagioclase and orthoclase) and pyroxenes (Opx and Cpx).	Chlorite, biotite and sericite.	Feldspars show albite and carlsbad twinning, euhedral and interlocking grains. Pyroxenes anhedral and are both intercumulus and cumulus.	Chloritisation, biotitization, and sericitisation.	15%	Minor sulphides (chalcopyrite, pentlandite and pyrrhotite), disseminated, droplets, along grain boundaries or inclusions. In some cases associated with magnetite.	Exsolution with the pyroxene grains (inverted pigeonite). Cpx mainly intercumulus and rimming plagioclase and inclusions of Cpx seen in plagioclase.	Feldspars: plagioclase: 35% and orthoclase: 15%, pyroxenes: Opx: 20% and Cpx: 25%, chlorite, biotite and sericite: 5%. **Gabbronorite**	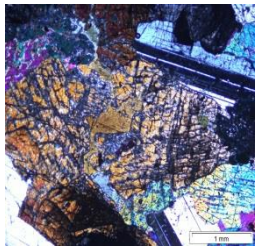
734.58 m-734.79 m	Olivine, feldspars (plagioclase and orthoclase) and pyroxenes (Opx and Cpx).	Chlorite, biotite, inverted pigeonite and sericite.	Olivine is subrounded with irregular fractures. Feldspars show albite and carlsbad twinning, grains are cumulus and euhedral. Pyroxenes are anhedral and Cpx is mainly intercumulus.	Chloritisation, biotitization, and sericitisation.	10%	Minor sulphides (chalcopyrite, pentlandite and pyrrhotite), disseminated, droplets, along grain boundaries or inclusions. In some cases associated with magnetite.	Cpx altering to chlorite and biotite. Pyroxenes have exsolution textures (inverted pigeonite). Inclusion of Cpx and plagioclase in olivine grains.	Feldspars: plagioclase: 35% and orthoclase: 10%, pyroxenes: Opx: 20% and Cpx: 25%, olivine: 5%, chlorite, biotite and sericite: 5%. **Olivine-bearing Gabbronorite**	
763.00 m-763.22 m	Feldspars (plagioclase and orthoclase) and pyroxenes (Opx and Cpx).	Chlorite, biotite, sericite and serpentine.	Feldspars show albite and carlsbad twinning, euhedral and interlocking grains. Pyroxenes are subhedral to anhedral and are both intercumulus and cumulus.	Chloritisation, biotitization, serpentinisation and sericitisation.	35%	Minor sulphides (chalcopyrite, pentlandite and pyrrhotite), disseminated. Magnetite secondary alteration minerals replacing or filling fractures within grains.	Pyroxenes in some cases are completely altered to chlorite, biotite or sericite. Pyroxenes also show exsolution textures. Ophitic texture (plag inclusions in Opx).	Feldspars: plagioclase: 35% and orthoclase: 15%, pyroxenes (altered): Opx: 20% and Cpx: 25%, chlorite, biotite and sericite: 5%. **Gabbronorite**	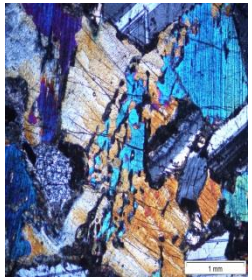

Appendix D:
Table 3: WB099 Polished Thin Section Descriptions

Sample Number WB099 (Interval in meters)	Major Minerals	Minor Minerals	Textures	Alteration and Degree of Alteration	% of Alteration	Reflected light observations	Other Features	Modal Abundance (%) & Rock Name.	Thin Section Picture
825.73 m-825.88 m	Feldspars (orthoclase and plagioclase) and pyroxenes (Opx and Cpx).	Chlorite and sericite.	Plagioclase and orthoclase shows albite and carlsbad twinning, grains are euhedral and interlocking textures. Pyroxenes are subhedral to anhedral, Opx is cumulus and Cpx is mainly intercumulus.	Chloritisation, biotitization, and sericitisation.	5%	Minor sulphides (chalcopyrite, pentlandite and pyrrhotite), disseminated.	Inclusion of plagioclase within Opx (ophitic texture). Exsolution texture seen in the Cpx grains.	Feldspars: plagioclase: 40% and orthoclase: 20%, pyroxenes: Opx: 20% and Cpx: 15%, chlorite, biotite and sericite: 5%. **Leuco- Gabbronorite**	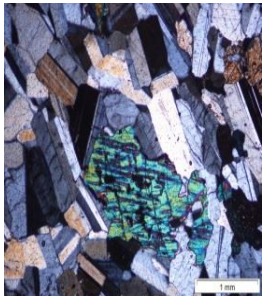
900.03 m-900.18 m	Feldspars (plagioclase and orthoclase).	Pyroxenes (Opx and Cpx), chlorite and sericite.	Plagioclase and orthoclase shows albite and carlsbad twinning, grains are euhedral and interlocking textures.	Chloritisation and sericitisation.	10%	Minor sulphides (chalcopyrite and pyrrhotite), disseminated.	Feldspars are altering to sericite and the pyroxenes- Cpx is intercumulus and the Opx form oikocrysts. The pyroxenes are also mainly altered.	Feldspars: plagioclase: 65% and orthoclase: 20%, sericite: 5% and pyroxenes: both Cpx and Opx: 10%. **Anorthosite**	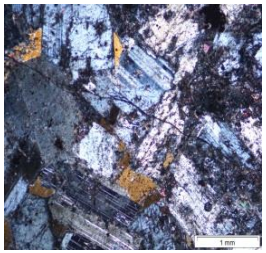
924.40 m-924.60 m	Feldspars (plagioclase and orthoclase) and pyroxenes (Opx and Cpx).	Chlorite, biotite and sericite.	Feldspars show albite and carlsbad twinning, euhedral and interlocking crystals. Pyroxenes- Cpx mainly intercumulus and Opx is cumulus, subhedral to anhedral.	Chloritisation, biotitization, and sericitisation.	10%	Minor sulphides (chalcopyrite and pyrrhotite), disseminated. Magnetite seen within the fractures and cleavage of grains.	Inclusions of plagioclase and orthoclase in Opx grains (ophitic texture). Grains of Cpx completely been replaced as chlorite and biotite.	Feldspars: plagioclase: 45% and orthoclase: 15%, pyroxenes: Opx: 15% and Cpx (altered): 20%, Chlorite and biotite: 5% **Leuco- Gabbronorite**	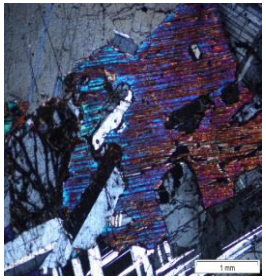

Appendix D:
Table 3: WB099 Polished Thin Section Descriptions

Sample Number WB099 (Interval in meters)	Major Minerals	Minor Minerals	Textures	Alteration and Degree of Alteration	% of Alteration	Reflected light observations	Other Features	Modal Abundance (%) & Rock Name.	Thin Section Picture
1009.00 m-1009.17 m	Feldspars (plagioclase and orthoclase) and pyroxenes (Opx and Cpx).	Chlorite, biotite, epidote, serpentine and sericite.	Plagioclase and orthoclase show albite and carlsbad twinning, euhedral and interlocking grains. Pyroxenes are mainly altered and are intercumulus.	Chloritisation, biotitization, serpentinisation, epidotisation and sericitisation.	40%	Minor sulphides (chalcopyrite and pyrrhotite), disseminated.	Fractures and veinlets filled with secondary minerals (chlorite, biotite, serpentine and epidote). Pyroxenes in some case completely altered to chlorite and biotite.	Feldspars: plagioclase: 45% and orthoclase: 15%, pyroxenes: Opx: 10% and Cpx (altered): 20%, Chlorite, sericite and biotite: 10% **Altered Leuco-Gabbronorite**	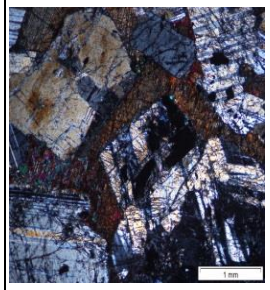
1021.18 m-1021.32 m	Feldspars (plagioclase and orthoclase) and pyroxenes (Opx and Cpx).	Chlorite, biotite, epidote, serpentine and sericite.	Plagioclase and orthoclase show albite and carlsbad twinning, euhedral and interlocking grains. Altered pyroxene, Opx cumulus and Cpx mainly intercumulus.	Chloritisation, biotitization, serpentinisation, epidotisation and sericitisation.	35%	Sulphides (Chalcopyrite and pyrrhotite), disseminated, droplets, inclusions and along grain boundaries. Minor Magnetite associated with sulphides.	Fractures and veinlets filled with secondary minerals (chlorite, biotite, serpentine and epidote). Inclusion of plagioclase within Opx (Ophitic texture).	Feldspars: plagioclase: 40% and orthoclase: 5%, pyroxenes: Opx: 20% and Cpx (altered): 25%, Chlorite, sericite and biotite: 10% **Gabbronorite**	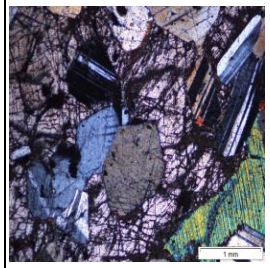
1069.70 m-1069.90 m	Olivine, Feldspars (plagioclase and orthoclase) and pyroxenes (Cpx and Opx).	Chlorite, biotite, epidote, serpentine and sericite.	Olivine grains are subrounded with irregular fractures. Feldspars show albite and carlsbad twinning, euhedral and interlocking grains. Pyroxenes are mainly altered.	Chloritisation, biotitization, serpentinisation, epidotisation and sericitisation.	30%	Sulphides (Chalcopyrite and pyrrhotite), disseminated, droplets, inclusions and along grain boundaries. Minor Magnetite associated with sulphides.	Fractures and veinlets filled with secondary minerals (chlorite, biotite, serpentine and epidote). Olivine is altering to magnetite and serpentine.	Feldspars: plagioclase: 35% and orthoclase: 5%, pyroxenes: Opx: 20% and Cpx: 20%, Olivine: 10%, chlorite, biotite, serpentine and sericite: 10% **Olivine-bearing Gabbronorite**	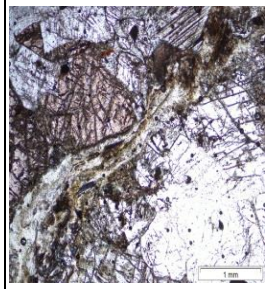

Appendix D:
Table 3: WB099 Polished Thin Section Descriptions

Sample Number WB099 (Interval in meters)	Major Minerals	Minor Minerals	Textures	Alteration and Degree of Alteration	% of Alteration	Reflected light observations	Other Features	Modal Abundance (%) & Rock Name.	Thin Section Picture
1126.18 m-1126.38 m	Olivine, Feldspars (plagioclase and orthoclase) and pyroxenes (Cpx and Opx).	Chlorite, biotite, epidote, serpentine and sericite	Olivine grains are subrounded with irregular fractures and altering to serpentine. Feldspars show albite and carlsbad twinning, euhedral shape and interlocking grains. Pyroxenes are intercumulus.	Chloritisation, biotitization, serpentinisation, epidotisation and sericitisation.	35%	Sulphides (Chalcopyrite and pyrrhotite), disseminated and droplets. Magnetite seen in the fractures within the olivine grains.	Fractures and veinlets filled with secondary minerals (chlorite, biotite, serpentine and epidote). Inclusion of plagioclase grains in olivine and Opx.	Feldspars: plagioclase: 30%, pyroxenes: Opx: 20% and Cpx: 20%, Olivine: 20%, chlorite, biotite, serpentine and sericite: 10% **Olivine-bearing Gabbronorite**	
1145.51 m-1145.83 m	Olivine, Feldspars (plagioclase and orthoclase) and pyroxenes (Cpx and Opx).	Chlorite, biotite, serpentine and sericite.	Olivine subrounded, irregular fractures. Opx is subhedral to anhedral. Cpx is intercumulus. Feldspars are both intercumulus and cumulus.	Chloritisation, biotitization, serpentinisation, and sericitisation.	25%	Sulphides (Chalcopyrite and pyrrhotite), disseminated and droplets. Magnetite seen in the fractures within the olivine grains.	Fractures and veinlets filled with secondary minerals (chlorite, biotite and serpentine). Inclusion of plagioclase grains in olivine and Opx.	Feldspars: plagioclase: 25%, pyroxenes: Opx: 20% and Cpx: 10%, Olivine: 35%, chlorite, biotite, serpentine and sericite: 10%. **Poikilitic Troctolite**	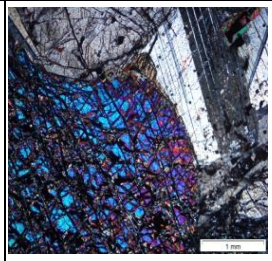
1172.62 m-1172.86 m	Olivine, Feldspars (plagioclase and orthoclase) and pyroxenes (Cpx and Opx).	Chlorite, biotite, serpentine and sericite.	Olivine subrounded, irregular fractures. Plagioclase is intercumulus or cumulus, euhedral grains. Opx and Cpx are intercumulus. Inequigranular texture.	Chloritisation, biotitization, serpentinisation, and sericitisation.	30%	Sulphides (Chalcopyrite and pyrrhotite), disseminated, droplets and along grain boundaries. Magnetite seen in the fractures within the olivine grains.	Fractures and veinlets filled with secondary minerals (chlorite and serpentine). The irregular fractures of olivine are filled with secondary magnetite and chlorite. (Ophitic texture).	Feldspars: plagioclase: 20%, pyroxenes: Opx: 25% and Cpx: 15%, Olivine: 30%, chlorite, biotite, serpentine and sericite: 10%. **Poikilitic Troctolite**	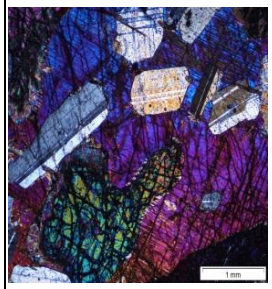

Appendix D:
Table 3: WB099 Polished Thin Section Descriptions

Sample Number WB099 (Interval in meters)	Major Minerals	Minor Minerals	Textures	Alteration and Degree of Alteration	% of Alteration	Reflected light observations	Other Features	Modal Abundance (%) & Rock Name.	Thin Section Picture
1193.50 m-1193.77 m	Olivine, Feldspars (plagioclase and orthoclase) and pyroxene (Opx).	Pyroxene (Cpx), feldspars (orthoclase), Chlorite, Biotite, serpentine and sericite.	Olivine subrounded, irregular fractures (altered). Plagioclase shows albite twinning, euhedral. Pyroxenes- Opx large intercumulus, subhedral to anhedral grains.	Chloritisation, biotitization, serpentinisation, and sericitisation.	45%	Sulphides (Chalcopyrite and pyrrhotite), disseminated, droplets, fractures and along grain boundaries. Magnetite seen in the fractures within the olivine grains.	Fractures and veinlets filled with chlorite and serpentine. Cpx grains mainly completely altered to chlorite and biotite. Inclusion of plagioclase in Opx (Ophitic texture).	Feldspars: plagioclase: 20%, pyroxenes: Opx: 30% and Cpx: 5%, Olivine: 35%, chlorite, biotite, serpentine and sericite: 10%. **Poikilitic Troctolite**	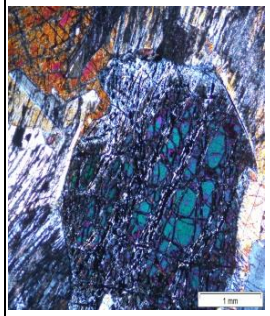
1215.48 m-1215.80 m	Olivine, Feldspars (plagioclase and orthoclase) and pyroxene (Opx).	Pyroxene (Cpx), feldspars (orthoclase), Chlorite, Biotite, serpentine and sericite.	Pyroxenes- Opx large intercumulus grains. Olivine grains are subrounded with irregular fractures. Plagioclase small euhedral, intercumulus grains that show albite twinning.	Chloritisation, biotitization, serpentinisation, and sericitisation.	35%	Sulphides (Chalcopyrite and pyrrhotite), disseminated, droplets, fractures and along grain boundaries. Magnetite seen in the fractures within the olivine grains.	The subrounded olivine grains are rimmed by Opx and in some case been completely altered to serpentine and magnetite. (Ophitic texture).	Olivine: 40%, feldspars (plagioclase): 25%, Pyroxenes (Opx): 25%, chlorite, biotite, sericite and serpentine: 10%. **Poikilitic Troctolite**	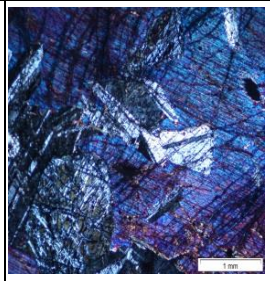
1228.50 m-1228.77 m	Olivine, Feldspars (plagioclase and orthoclase) and pyroxene (Opx).	Pyroxene (Cpx), feldspars (orthoclase), Chlorite, Biotite, serpentine and sericite.	Pyroxenes- Opx large intercumulus grains. Olivine grains are subrounded with irregular fractures. Plagioclase small euhedral, intercumulus show albite twinning.	Chloritisation, biotitization, serpentinisation, and sericitisation.	40%	Sulphides (Chalcopyrite and pyrrhotite), disseminated, droplets, fractures and along grain boundaries. Magnetite (secondary) fills the fractures in the olivine grains.	Olivine grains are rimmed by Opx, and most are altered to serpentine and magnetite. Plagioclase is altering to sericite. Plagioclase inclusion with in Opx (ophitic texture).	Olivine: 50%, feldspars (plagioclase): 25%, Pyroxenes (Opx): 15%, chlorite, biotite, sericite and serpentine: 10%. **Poikilitic Troctolite**	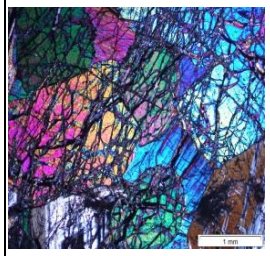

Appendix D:
Table 3: WB099 Polished Thin Section Descriptions

Sample Number WB099 (Interval in meters)	Major Minerals	Minor Minerals	Textures	Alteration and Degree of Alteration	% of Alteration	Reflected light observations	Other Features	Modal Abundance (%) & Rock Name.	Thin Section Picture
1270.16 m-1270.41 m	Pyroxenes (Opx and Cpx).	Feldspars (plagioclase and orthoclase), olivine, chlorite, sericite and biotite.	Feldspars show albite and carlsbad twinning, mainly intercumulus grains. Minor olivine, subrounded and irregular fractures within the grains. Pyroxenes are mainly Opx with both intercumulus and cumulus phases.	Chloritisation, biotitization, serpentinisation, and sericitisation.	30%	Sulphides (Chalcopyrite, pentlandite and pyrrhotite), disseminated, droplets, fractures and along grain boundaries. Magnetite associated with sulphides. Magnetite is found within fractures and along grain boundaries.	Olivine and Opx grains have interlocking textures. Feldspars are altering to sericite. Fractures and veinlets filled with secondary minerals (chlorite and sericite).	Pyroxenes: Opx: 50% and Cpx: 20%, Olivine: 10%, feldspars: plagioclase and orthoclase: 10%, chlorite, biotite and sericite: 10%. **Feldspathic Pyroxenite**	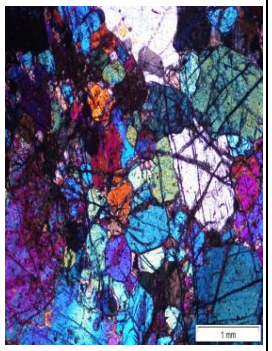
1280.17 m-1280.51 m	Olivine and Pyroxene (Opx).	Feldspars (plagioclase and orthoclase), pyroxenes (Cpx), chlorite and biotite.	Olivine is subrounded with irregular fractures. Feldspars (plagioclase and orthoclase) showing albite and carlsbad twinning, mainly intercumulus. Pyroxene; (Opx) is grey, subhedral to anhedral and Cpx is intercumulus and altered.	Chloritisation, biotitization, serpentinisation, and sericitisation.	35%	Minor sulphides (chalcopyrite and pyrrhotite), disseminated. Chromite grains subrounded and associated with olivine and Opx grains.	Fractures and veinlets filled with chlorite and serpentine. Cpx grains mainly completely altered to chlorite and biotite. Inclusion of plagioclase in Opx (Ophitic texture).	Pyroxenes: Opx: 35% and Cpx: 10%, Olivine: 45%, Feldspars: plagioclase and orthoclase: 10%. **Harzburgite**	

Appendix D:
Table 3: WB099 Polished Thin Section Descriptions

Sample Number WB099 (Interval in meters)	Major Minerals	Minor Minerals	Textures	Alteration and Degree of Alteration	% of Alteration	Reflected light observations	Other Features	Modal Abundance (%) & Rock Name.	Thin Section Picture
1282.67 m-1283.01 m	Olivine and pyroxene (Opx).	Feldspars (plagioclase and orthoclase), pyroxene (Cpx), chlorite, biotite, serpentine and sericite.	Olivine subrounded grains with irregular fracture. Pyroxene (Opx) is grey both intercumulus and cumulus, (Cpx) mainly intercumulus.	Chloritisation, biotitization, serpentinisation, and sericitisation.	35%	Minor sulphides (chalcopyrite and pyrrhotite), disseminated. Chromite grains subrounded and associated with olivine and Opx grains. The chromite grains are been replace by magnetite.	Plagioclase and orthoclase are found as inclusion in the olivine and Opx grains (Ophitic textures). Fractures are filled with serpentine and magnetite.	Pyroxenes: Opx: 35% and Cpx: 5%, Olivine: 45%, Feldspars: plagioclase and orthoclase: 10%, sericite, serpentine, chlorite and biotite: 5%. **Harzburgite**	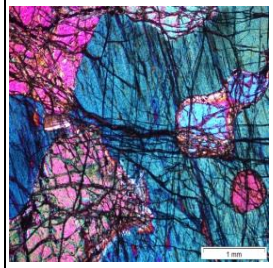
1292.13 m-1292.43 m	Olivine and pyroxene (Opx).	Feldspars (plagioclase and orthoclase), pyroxene (Cpx), chlorite, biotite, serpentine and sericite.	Olivine grains are subrounded, with irregular fractures and mainly altered (serpentine). Feldspars are mainly intercumulus with albite twinning. Opx is both cumulus and intercumulus and altered.	Chloritisation, biotitization, serpentinisation, and sericitisation.	45%	Minor sulphides (chalcopyrite and pyrrhotite), disseminated. Chromite grains subrounded and associated with olivine and Opx grains. The chromite grains are been replace by magnetite.	Large veinlet or fracture filled with secondary minerals (sericite, serpentine and magnetite). Most of the grains are altered.	Pyroxenes: Opx: 30%, Olivine: 50%, Feldspars: plagioclase and orthoclase: 5%, sericite, serpentine, chlorite and biotite: 15%. **Harzburgite**	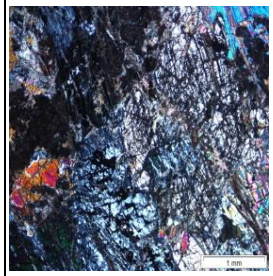

Appendix D:
Table 3: WB099 Polished Thin Section Descriptions

Sample Number WB099 (Interval in meters)	Major Minerals	Minor Minerals	Textures	Alteration and Degree of Alteration	% of Alteration	Reflected light observations	Other Features	Modal Abundance (%) & Rock Name.	Thin Section Picture
1324.53 m-1324.74 m	Pyroxenes (Opx and Cpx) and feldspars (plagioclase and orthoclase).	Chlorite, sericite and biotite.	Feldspars (plagioclase and orthoclase) showing albite and carlsbad twinning and euhedral shape. Pyroxenes Opx is mainly cumulus and Cpx mainly intercumulus and show exsolution textures.	Chloritisation, biotitization, and sericitisation.	20%	Minor sulphides (chalcopyrite and pyrrhotite), disseminated and along grain boundaries. Minor magnetite associated with sulphides.	Inclusions of plagioclase in Opx (ophitic texture). Cpx rimmed by biotite and chlorite. Fractures and veinlets filled with secondary minerals.	Pyroxenes: Opx: 40% and Cpx: 25%, feldspars: 25%, chlorite, biotite and sericite: 10%. **Feldspathic Pyroxenite**	
1333.85 m-1334.09 m	Pyroxenes (Opx and Cpx), feldspars (plagioclase and orthoclase) and sericite.	Olivine, chlorite, biotite, sulphides (chalcopyrite and pyrrhotite) and serpentine.	Feldspars (plagioclase and orthoclase) showing albite and carlsbad twinning, euhedral grains, however most grains have altered to sericite. Pyroxenes are altered and are both cumulus and intercumulus. Olivine is subrounded with irregular fractures.	Chloritisation, biotitization, serpentinisation, and sericitisation.	70%	Sulphides (Chalcopyrite, pentlandite and pyrrhotite), disseminated, droplets, fractures and along grain boundaries.	Fractures and veinlets filled with secondary minerals (chlorite, sericite, biotite and serpentine).	Feldspars (plagioclase): 25%, pyroxenes: Opx: 15% and Cpx: 15%, sericite: 40%, biotite and chlorite: 5% **Altered Olivine-bearing Pyroxenite**	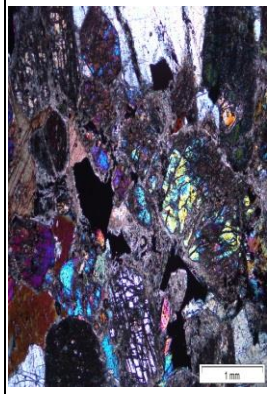

Appendix D:
Table 4: WE001 Polished Thin Section Descriptions

Sample Number (Interval in meters)	Major Minerals	Minor Minerals	Textures	Alteration and Degree of Alteration	% of Alteration	Reflected light observations	Other Features	Modal Abundance (%) & Rock Name.	Thin Section Picture
367.19 – 367.35 m	Quartz, clay minerals and lithic fragments.	Magnetite (opaque mineral), feldspars and minor chlorite	Sub-angular, white-yellow quartz with undulose extinction.	Exsolution between quartz and feldspars (pathetic texture) intergrowth of quartz and feldspars.	15%	Magnetite	Fine-grained matrix with clay minerals and lithic fragments. Sericitisation.	Quartz: 70%, Clay minerals: 15%. Feldspars: 5%, opaques: 5%, Lithic fragments: 5%. **Sandstone**	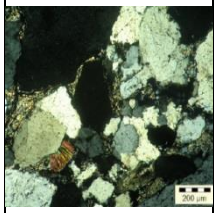
378.64 – 378.75 m	Completely altered Plagioclase, Quartz and sericite	Silica and phengite (sample is extremely altered and difficult to distinguish individual minerals).	Sample is extremely altered and difficult to distinguish individual minerals.	Sericitisation, chloritisation and hematitisation.	75%	None	Fractured quartz and feldspar phenocrysts. Groundmass extremely fine-grained with silica and phengite.	Quartz; 5%, feldspars (altered to sericite); 65%, calcite; 10% and hematite; 20%. **Palaesol (Contact between Waterberg sediments and Bushveld rocks)**	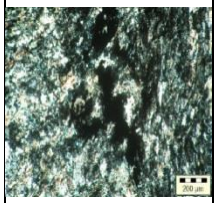
432.58 – 432.69 m	Magnetite, Plagioclase, Biotite, Cpx and Opx	Olivine (altered),Chlorite, serpentine and sulphides (chalcopyrite)	Plagioclase with albite twinning and euhedral to subhedral shape. Cpx altered to biotite and chlorite, Olivine completely altered to magnetite and serpentine.	Sericitisation. Olivine altered to magnetite (intergrowth or overgrowth texture). Chloritisation, biotitization, serpentinisation.	10%	Sulphides (chalcopyrite and pyrrhotite), droplets, veinlets or within silicate minerals magnetite is associated sulphides.	Veinlets and fractures filled with secondary minerals (chlorite and serpentine).	Plagioclase: 30%, Pyroxenes (Opx and Cpx (altered)): 25%, Magnetite 25%, chlorite: 7%, biotite: 8%, serpentine: 3% and sulphides: 2%. **Magnetite-bearing Gabbronorite.**	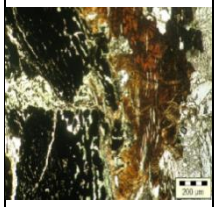
603.23 – 603.43 m	Pyroxenes (Opx and Cpx) and Plagioclase.	Olivine, Biotite and Chlorite.	Cumulus Opx and Plagioclase, with interstitial Cpx. Plagioclase with typical albite twinning and Opx & Cpx with good cleavage.	Cpx altering to chlorite and biotite. Plagioclase been altered completely to sericite.	15%	Minor sulphides (Chalcopyrite 1%) with magnetite, sulphides located along grain boundaries.	Inclusions of Cpx in altered Opx. Altered olivine grains with inclusions of Cpx and are rimmed by Opx and secondary minerals (biotite and Chlorite)	Opx: 30%, Cpx: 15%, Plagioclase: 35%, chlorite: 7%, biotite: 5%, olivine (altered): 5%, Magnetite and Sulphides 3%. **Gabbronorite**	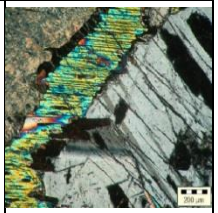

Appendix D:
Table 4: WE001 Polished Thin Section Descriptions

Sample Number (Interval in meters)	Major Minerals	Minor Minerals	Textures	Alteration and Degree of Alteration	% of Alteration	Reflected light observations	Other Features	Modal Abundance (%) & Rock Name.	Thin Section Picture
636.22 – 636.32 m	Plagioclase, Pyroxenes (Opx and Cpx).	Olivine (altered) Chlorite and biotite	Cumulus grains of all major minerals. Plagioclase with albite twinning and pyroxenes with good cleavage.	Cpx is mostly altered with rims of chlorite and biotite. Overgrowth of Cpx and Opx. Plagioclase altered to sericite. Olivine completely altered. Sericitisation and Chloritisation.	15%	Minor sulphides (chalcopyrite 1%), located within the altered olivine grains and between grain boundaries.	Plagioclase rimmed by sericite or completely altered to sericite. Cpx rims Opx grains. Interlocking texture between grains. Ophitic texture present. Veins and fractures filled with sericite.	Opx: 35%, Cpx: 15%, Plagioclase (sericite): 35%, Olivine: 10%, Sulphides: (Chalcopyrite <1%), Chlorite 3% and Biotite 2%. **Olivine-bearing Gabbronorite**	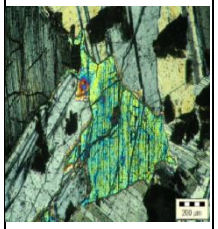
642.00 – 642.08 m	Plagioclase and Cpx	Olivine (altered), Chlorite and biotite	Cpx extremely altered with anhedral shape, Cpx is altering to chlorite and Biotite. Plagioclase is completely altered to sericite.	Sericitisation and Chloritisation	45%	Minor sulphides (chalcopyrite <1%)	Elongated, needle-like Cpx grains (intergranular texture). Olivine grains are completely altered only the shape and fractures can be seen in PPL.	Plagioclase (sericite): 50%, Cpx: 35%, Olivine: 5%, Chlorite: 7% Biotite 3% and sulphides: <1%. **Altered Troctolite**	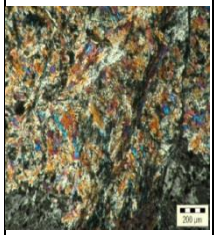
644.40 – 644.60 m	Altered olivine, Opx, altered Cpx and Plagioclase	Chlorite, biotite and serpentine.	Olivine grains are highly fractured and altered; fractures are filled with serpentine, magnetite and chlorite. Plagioclase grains are mostly altered sericite.	Chloritisation, serpentinisation, uralitization (pyroxene replaced by amphibole) and Sericitisation	20%	Minor sulphides (chalcopyrite, pentlandite and pyrrhotite) associated with magnetite. Sulphides are droplets.	Olivine grains are rimmed by sericite and chlorite. Olivine grains have been completely serpentinised.	Olivine: 25%, pyroxenes (Opx and Cpx): 15%, plagioclase: 40%, serpentine: 5%, chlorite: 10% and sulphides + magnetite 5%. **Altered poikilitic Troctolite**	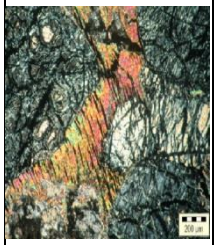

Appendix D:
Table 4: WE001 Polished Thin Section Descriptions

Sample Number (Interval in meters)	Major Minerals	Minor Minerals	Textures	Alteration and Degree of Alteration	% of Alteration	Reflected light observations	Other Features	Modal Abundance (%) & Rock Name.	Thin Section Picture
675.00 – 675.10 m	Altered: plagioclase, olivine and Opx	Magnetite, biotite, chlorite and sulphides (Chalcopyrite and pyrrhotite)	Sub-rounded olivine grains highly fractured and extremely altered, seen only in PPL. Plagioclase altered completely to sericite and Opx large grains seen in PPL with good cleavage.	Sericitisation and Chloritisation. Round elongated olivine grains completely altered.	65%	Sulphides (chalcopyrite and pyrrhotite), within grains as droplets, veinlets and in between silicate grains.	Olivine grains are fractured and are filled by secondary minerals (magnetite and chlorite).	Olivine: 30%, Opx: 25%, plagioclase (sericite) 30%, sulphides: 5%, magnetite: 5, Chlorite: 3% and biotite: 2%. **Altered Poikilitic Troctolite**	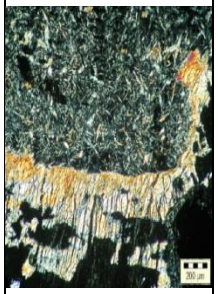
699.97 – 700.17 m	Olivine, Opx, plagioclase	Magnetite, Cpx, biotite, chlorite, sulphides (Chalcopyrite)	Sub-rounded olivine highly fractured. Opx and Cpx angular shaped	Chloritisation fractures within the olivine grains have been filled with secondary minerals (chlorite and magnetite).	55%	Minor sulphides (chalcopyrite) as droplets and veinlets. Sulphides are inclusion within other silicate grains	Olivine rimed by Cpx and chlorite. Inclusions of olivine in Cpx and Opx. Sericitisation of most plagioclase grains	Olivine: 50%, Opx: 10%, Cpx: 15% sericite (plag): 17%, magnetite 5% and sulphides 2%. **Altered Harzburgite**	
730.75 – 730.90 m	Altered Olivine, serpentine and Opx	Chlorite, biotite, Cpx and plagioclase	Sub-rounded altered olivine grains. Opx anhedral, good cleavage. Plagioclase show albite twinning and is interstitial.	Chloritisation fractures within the olivine grains have been filled with secondary minerals (chlorite and magnetite. Sericitisation and uralitisation.	40%	Sulphides (chalcopyrite, pyrrhotite and pentlandite). Droplets, veinlets and between grain boundaries.	Veinlets and fractures filled with secondary minerals (chlorite and serpentine	Olivine: 45%, Opx: 25%, Plagioclase: 10%, serpentine: 12%, Chlorite: 5%, biotite: 3%. **Altered Harzburgite**	

Appendix D:
Table 4: WE001 Polished Thin Section Descriptions

Sample Number (Interval in meters)	Major Minerals	Minor Minerals	Textures	Alteration and Degree of Alteration	% of Alteration	Reflected light observations	Other Features	Modal Abundance (%) & Rock Name.	Thin Section Picture
752.99 – 753.25 m	Olivine, Opx and Plagioclase.	Chlorite, serpentine and biotite	Sub-rounded olivine grains, highly fractured. Opx subhedral grains. Plagioclase subhedral to euhedral with sericite alteration.	Chloritisation, fractures within the olivine grains have been filled with secondary minerals (chlorite, serpentine and magnetite). Sericitisation and serpentinisation.	45%	Minor sulphides (chalcopyrite) as droplets and veinlets. Sulphides are inclusion within other silicate grains.	Olivine rimed by Cpx and chlorite. Inclusions of olivine in Cpx and Opx. Sericitisation of most plagioclase grains.	Olivine: 40%, Opx: 15%, Cpx: 4% sericite plagioclase: 25%, Chlorite and biotite: 10% magnetite 2% and sulphides 2%. **Altered Poikilitic Harzburgite**	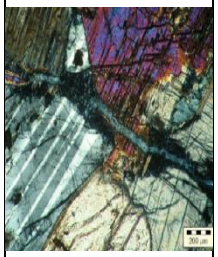
754.95 – 755.10 m	Olivine (altered), Opx and Plagioclase (interstitial)	Chlorite, biotite and serpentine.	Sub-rounded olivine, most completely altered to serpentine. Opx is anhedral with good cleavage, Cpx is interstitial.	Chloritisation, serpentinisation and Sericitisation. Olivine grains are fracture and filled with secondary minerals.	30%	Minor sulphides (chalcopyrite), droplets within silicate minerals. Magnetite associated with the sulphides.	Plagioclase is both anhedral and a few euhedral grains main interstitial. Veinlets and fractures filled with secondary minerals (magnetite).	Olivine: 45%, Opx: 25%, Plagioclase: 10%, serpentine: 12%, Chlorite: 5%, biotite: 3%. **Altered Poikilitic Harzburgite**	
784.10 – 784.20 m	Olivine, Opx and Plagioclase	Chlorite, serpentine and biotite	Sub-rounded olivine grains, highly fractured. Opx anhedral grains. Plagioclase subhedral to euhedral with sericite alteration.	Chloritisation fractures within the olivine grains have been filled with secondary minerals (chlorite, serpentine and magnetite). Sericitisation and serpentinisation.	40%	Minor sulphides (chalcopyrite) as droplets and veinlets. Sulphides are inclusion within other silicate grains.	Plagioclase is altered to sericite and some plagioclase grains show clear albite twinning (euhedral shaped). Olivine highly fractures and filled with secondary minerals (chlorite).	Olivine: 45%, Opx: 20%, sericite plagioclase: 20%, Chlorite and biotite: 10% magnetite 2% and sulphides 3%. **Poikilitic Troctolite**	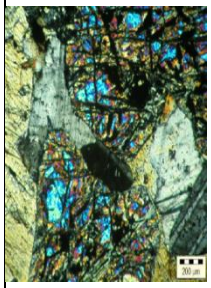

Appendix D:
Table 4: WE001 Polished Thin Section Descriptions

Sample Number (Interval in meters)	Major Minerals	Minor Minerals	Textures	Alteration and Degree of Alteration	% of Alteration	Reflected light observations	Other Features	Modal Abundance (%) & Rock Name.	Thin Section Picture
787.80 – 787.95 m	Pyroxenes (Opx and Cpx) and plagioclase	Biotite and chlorite	Opx grains are euhedral and anhedral shape, good cleavage. Plagioclase show albite twinning and mostly euhedral shaped.	Sericitisation, chloritisation and uralitisation. Plagioclase is altered to sericite and pyroxenes show Exsolution textures.	10%	Sulphides (chalcopyrite). Droplets, within veinlets and along grain boundaries, sulphides are associated with magnetite.	Interlocking textures. Cpx found on the rims of Opx grains. Ophitic texture (large Opx grains with inclusions of plagioclase.	Opx: 35%, Cpx: 10%, plagioclase: 40%, sericite: 8%, chlorite: 3% and biotite: 2% and sulphides and magnetite: 2%. **Altered Gabbronorite**	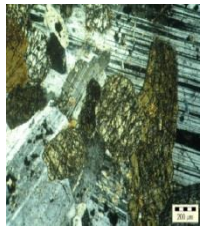
827.05 – 827.20 m	K-feldspar, plagioclase and quartz.	None	Quartz has undulose extinction; plagioclase shows albite twinning and k-feldspar anhedral grains.	Sericitisation	10%	One sulphides droplet was found in the sample (chalcopyrite)	Perthite texture between the feldspars. The grains are equigranular and anhedral.	K-feldspar: 50%, plagioclase: 30% and quartz: 20%. **Granofels (felsic unit)**	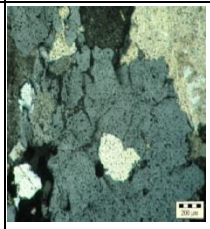
845.65 – 845.84 m	Opx and serpentine	Plagioclase and biotite	Opx grains have good cleavage, grey brown colour, with subhedral to anhedral grains. Serpentine is found in the fracture and veins.	Chloritisation, serpentinisation and sericitisation.	15%	Minor sulphides (chalcopyrite) droplets in silicate minerals.	Opx has interlocking texture and equigranular texture. Plagioclase show albite twinning and is interstitial with sericite alteration.	Orthopyroxene: 75%, serpentine: 15%, plagioclase: 5%, biotite: 3% and sulphides + magnetite 2%. **Granofels (pyroxenite-rich unit)**	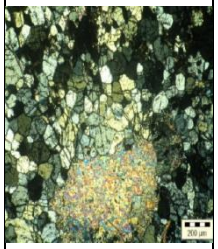

Appendix D:
Table 5: WE027 Polished Thin Section Descriptions

Sample Number WE027 (Interval in meters)	Major Minerals	Minor Minerals	Textures	Alteration and Degree of Alteration	% of Alteration	Reflected light observations	Other Features	Modal Abundance (%) & Rock Name.	Thin Section Picture
553.96 m-554.17 m	Quartz, magnetite and hematite	Epidote	Quartz is subhedral to euhedral with undulose extinction. Magnetite is subrounded. The matrix is fine-grained with some epidote elongated grains.	Sericitisation, epidotisation and minor chlorite and biotite.	10%	Magnetite grains are seen. Hematite has a wavely texture.	Magnetite and hematite show wave textures and some grains are subrounded.	Quartz: 70%, Fine-grained matrix: 15%, magnetite: 7%, epidote: 3%, chlorite and biotite: 2%. **Sandstone**	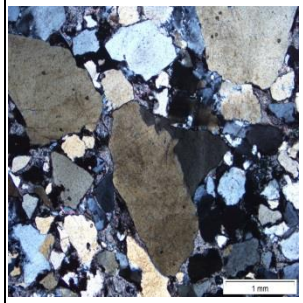
556.35 m-556.64 m	Sericite, magnetite and hematite	Serpentine and chlorite/ epidote	Magnetite subrounded grains. The rest of the material is extremely altered, completely altered to sericite.	Sericitisation, chloritisation and hematitisation.	99%	Magnetite grains are seen. Hematite has a wavely texture.	Veinlets and fractures filled with chlorite and serpentine.	Quartz: 20%, feldspars altered to sericite: 60%, magnetite: 10%, hematite: 5%, chlorite and epidote: 5%. **Palaesol**	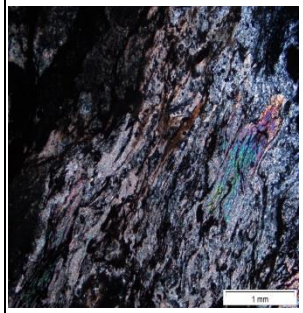
565.00 m-565.28 m	Feldspars (plagioclase) and pyroxenes (Opx and Cpx).	Biotite, chlorite, sericite and sulphides (chalcopyrite and pyrrhotite).	Plagioclase and orthoclase show albite and carlsbad twinning. Feldspars are euhedral and interlocking grains. Pyroxenes are mainly subhedral.	Sericitisation, chloritisation and biotitization.	10%	Minor disseminated sulphides (chalcopyrite and pyrrhotite). Magnetite seen as cumulus and intercumulus, seen along grain boundaries, within grains as inclusions	Pyroxenes especially Cpx are rimmed by chlorite and biotite. Cpx is also been completely replaced by chlorite and biotite in certain grains. Feldspar are also rimmed by Cpx	Feldspars (plagioclase and orthoclase): 60%, pyroxenes (Opx and Cpx): 30%, olivine: 3%, biotite: 3%, chlorite: 2% and Magnetite: 2%. **Magnetite Gabbronorite**	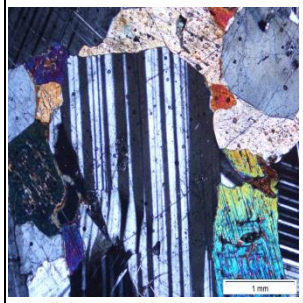

Appendix D:
Table 5: WE027 Polished Thin Section Descriptions

Sample Number WE027 (Interval in meters)	Major Minerals	Minor Minerals	Textures	Alteration and Degree of Alteration	% of Alteration	Reflected light observations	Other Features	Modal Abundance (%) & Rock Name.	Thin Section Picture
570.56 m-570.73 m	Sericite (altered feldspars), olivine and pyroxenes (Cpx and Opx).	Biotite, chlorite, sulphides (chalcopyrite and pyrrhotite) and serpentine.	Plagioclase show albite twinning, however most feldspars are completely altered to sericite. Pyroxenes and olivine are also extremely altered to chlorite, biotite and serpentine.	Sericitisation, biotitization, chloritisation, epidotisation and serpentinisation.	80%	Sulphides (chalcopyrite and pyrrhotite). Mainly seen within silicates with a skeletal texture. Sulphides also seen as sulphides droplets.	Pyroxenes (Cpx) is rimming both Opx and olivine however grains are extremely altered. Fractures and veinlets are filled with secondary.	Feldspars (plagioclase, orthoclase and sericite): 55%, pyroxenes (Opx and Cpx):20%, olivine: 10%, epidote: 5%, biotite: 3%, chlorite: 2% and sulphides (chalcopyrite): 5%. **Altered olivine-bearing Gabbronorite**	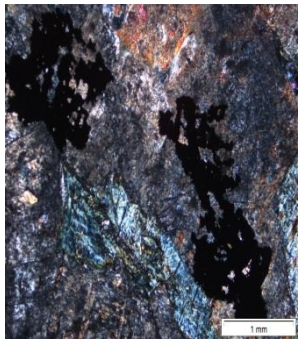
578.27 m-578.27 m	Feldspars (plagioclase and orthoclase) and pyroxenes (Opx).	Pyroxenes (Cpx), biotite, chlorite and sericite.	Plagioclase and orthoclase show albite and carlsbad twinning. Feldspars are euhedral and interlocking grains. Minor pyroxenes are mainly subhedral or interstitial.	Sericitisation, chloritisation and biotitization.	5%	Minor disseminated magnetite.	Pyroxenes are slightly altered with chlorite, epidote and biotite rims. Feldspars have small patches of sericite but are mainly fresh grains of feldspars.	Feldspars (plagioclase and orthoclase): 83%, Pyroxenes (Opx and Cpx) 15%, chlorite and biotite: 2%. **Leuco-Gabbronorite.**	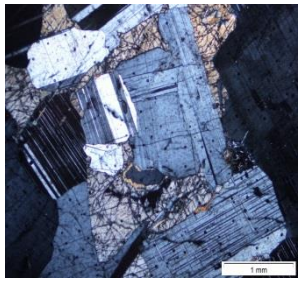
580.59 m-580.84 m	Feldspars (plagioclase and orthoclase) and pyroxenes (Opx and Cpx)	Sericite, biotite and chlorite.	Plagioclase and orthoclase show albite and carlsbad twinning. Feldspars are euhedral and interlocking. Pyroxenes are mainly subhedral and Cpx seen to be interstitial and highly altered.	Sericitisation, chloritisation and biotitization.	25%	Sulphides (chalcopyrite and pyrrhotite) are within fractures and veinlets and also seen between grain boundaries or as sulphide droplets.	Cpx in most cases is completely replaced by chlorite and biotite and the rest of the Cpx is rimmed by chlorite or biotite.	Feldspars (plagioclase and orthoclase): 65%, Pyroxenes (Opx and Cpx) 25%, Olivine: 6%, chlorite and biotite: 3% and sulphides (chalcopyrite): 1%. **Leuco gabbronorite**	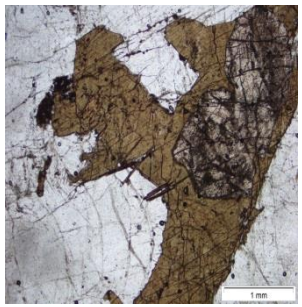

Appendix D:
Table 5: WE027 Polished Thin Section Descriptions

Sample Number WE027 (Interval in meters)	Major Minerals	Minor Minerals	Textures	Alteration and Degree of Alteration	% of Alteration	Reflected light observations	Other Features	Modal Abundance (%) & Rock Name.	Thin Section Picture
586.00 m-586.21 m	Feldspars (plagioclase and orthoclase) and pyroxenes (Opx and Cpx).	Chlorite, biotite, magnetite, sulphides (chalcopyrite and pyrrhotite), sericite and inverted pigeonite.	Plagioclase and orthoclase shows albite and carlsbad twinning, feldspars are euhedral and interlocking. Pyroxenes Opx is subhedral to euhedral, and Cpx is mainly interstitial. Minor subrounded olivine with irregular fractures.	Sericitisation, chloritisation and biotitization.	7%	Minor disseminated sulphides (chalcopyrite). Magnetite both cumulus and intercumulus.	Pyroxenes especially Cpx is rimmed with biotite and chlorite. Olivine is also rimmed by chlorite. Inclusion of feldspars in pyroxenes (ophitic texture). Feldspars have patches of alteration (sericite).	Feldspars (plagioclase and orthoclase): 65%, Pyroxenes (Opx and Cpx) 30%, chlorite and biotite: 3% and magnetite: 2%. **Magnetite gabbronorite**	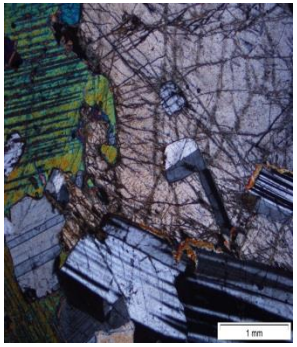
588.78 m-589.00 m	Chlorite, biotite, pyroxenes (Opx and Cpx) and feldspar (plagioclase).	Epidote and sericite.	Plagioclase and orthoclase shows albite and carlsbad twinning, feldspars are euhedral and interlocking. Pyroxenes grains are mainly completely altered.	Sericitisation, biotitization, chloritisation and serpentinisation.	55%	Minor amounts of magnetite.	Feldspars are mostly altered to sericite. Pyroxenes are altered or replaced by biotite and chlorite. Fractures and veinlets are filled with secondary minerals.	Feldspars (plagioclase, orthoclase and sericite): 75%, Pyroxene (Cpx) 15%, epidote, serpentine, chlorite and biotite: 10 %. **Altered Leuco-Gabbronorite**	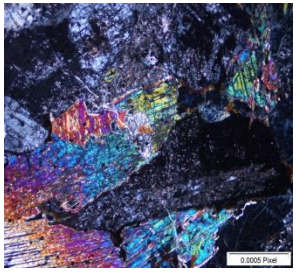
594.58 m-594.80 m	Feldspars (plagioclase and orthoclase), olivine and pyroxenes (Opx and Cpx).	Biotite, chlorite, sericite, magnetite, serpentine and inverted pigeonite.	Plagioclase and orthoclase both show albite and carlsbad twinning. Feldspars are mainly euhedral and interlocking. Pyroxenes are mainly subhedral with cleavage.	Sericitisation, chloritisation and biotitization.	10%	Minor sulphides (chalcopyrite and pyrrhotite) within grains or along grain boundaries.	Pyroxenes especially Cpx is rimmed by both biotite and chlorite. Opx has inclusions of plagioclase (ophitic texture).	Feldspars (plagioclase and orthoclase): 65%, Pyroxenes (Opx and Cpx) 35%, chlorite and biotite: 5%. **Gabbronorite**	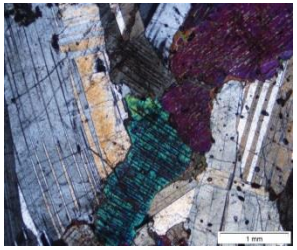

Appendix D:
Table 5: WE027 Polished Thin Section Descriptions

Sample Number WE027 (Interval in meters)	Major Minerals	Minor Minerals	Textures	Alteration and Degree of Alteration	% of Alteration	Reflected light observations	Other Features	Modal Abundance (%) & Rock Name.	Thin Section Picture
602.36 m-602.60 m	Feldspars (plagioclase and orthoclase) and pyroxenes (Opx and Cpx).	Chlorite, biotite, sericite, serpentine, inverted pigeonite magnetite and sulphides - chalcopyrite	Plagioclase and orthoclase both show albite and carlsbad twinning. Feldspars are mainly euhedral and interlocking. Pyroxenes are mainly subhedral and in some cases have exsolution textures.	Sericitisation, chloritisation and biotitization.	20%	Interstitial magnetite and minor sulphides (chalcopyrite and pyrrhotite) within grains or along grain boundaries.	Pyroxenes especially Cpx is rimmed by both biotite and chlorite. Opx has inclusions of plagioclase (ophitic texture).	Feldspars (plagioclase and orthoclase): 55%, Pyroxenes (Opx and Cpx) 35%, Olivine: 5% chlorite and biotite: 2% and magnetite: 3%. **Magnetite Gabbronorite**	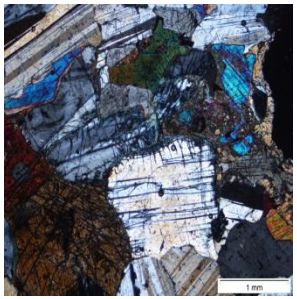
622.20 m-622.45 m	Feldspars (plagioclase and orthoclase) and pyroxenes (Opx and altered Cpx).	Magnetite, chlorite, biotite and sericite.	Plagioclase and orthoclase both show albite and carlsbad twinning. Feldspars are mainly euhedral and interlocking. Pyroxenes are mainly subhedral and in some cases have exsolution textures.	Sericitisation, chloritisation, epidotisation and biotitization.	10%	Cumulus magnetite grain on the boundary of a plagioclase (silicate) grain.	Pyroxenes especially Cpx is rimmed by both biotite and chlorite. Cpx also rimming Opx. Opx has inclusions of plagioclase (ophitic texture).	Feldspars (plagioclase and orthoclase): 65%, Pyroxenes (Opx and Cpx) 30%, chlorite and biotite: 5% **Leuco-Gabbronorite**	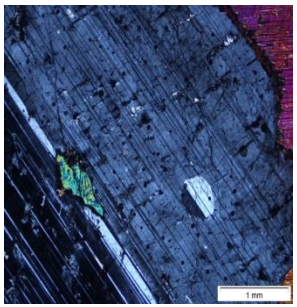
631.16 m-631.43 m	Sericite (altered feldspars), serpentine and pyroxenes (altered Opx and Cpx)	Chlorite, biotite, epidote and sulphides (chalcopyrite)	Sericite (white micas) feldspars are completely altered. Olivine and pyroxenes are also completely altered to serpentine, chlorite and biotite.	Sericitisation, biotitization, chloritisation, epidotisation and serpentinisation.	85%	Minor disseminated sulphides (chalcopyrite and pyrrhotite) and cumulus magnetite and magnetite along grain boundaries.	Veinlets and fractures are filled with secondary material (epidote and serpentine). Some feldspars show slight albite twinning, but mostly altered.	Feldspars (plagioclase, orthoclase and sericite): 60%, Pyroxenes (Opx and Cpx) 20%, Olivine: 10% serpentine, chlorite and biotite: 9% and magnetite: 1%. **Altered olivine-bearing Gabbronorite**	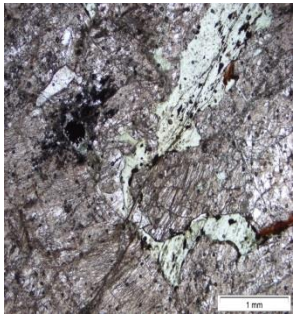

Appendix D:
Table 5: WE027 Polished Thin Section Descriptions

Sample Number WE027 (Interval in meters)	Major Minerals	Minor Minerals	Textures	Alteration and Degree of Alteration	% of Alteration	Reflected light observations	Other Features	Modal Abundance (%) & Rock Name.	Thin Section Picture
635.40 m-635.61 m	Feldspars (plagioclase and orthoclase) and pyroxenes (Opx and Cpx)	Sericite, biotite, chlorite, epidote, olivine, magnetite and sulphides (chalcopyrite and pyrrhotite).	Feldspars show albite and carlsbad twinning. Feldspars are euhedral and interlocking. Pyroxenes are subhedral to euhedral. Olivine (minor) is subrounded with irregular fractures.	Sericitisation, biotitization, chloritisation, epidotisation and serpentinisation.	15%	Sulphides (chalcopyrite and pyrrhotite) have a skeletal texture and form as sulphide droplets. Magnetite is seen mainly between grain boundaries and along grain boundaries.	Pyroxenes are rimmed by biotite and chlorite and in some cases the Cpx has been completely replaced by chlorite and biotite.	Feldspars (plagioclase, orthoclase and sericite): 58%, Pyroxenes (Opx and Cpx) 30%, Olivine: 2% chlorite and biotite: 6% and magnetite: 4%. **Magnetite Gabbronorite**	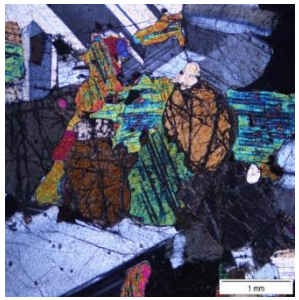
658.08 m-658.30 m	Olivine, Pyroxenes (Opx and Cpx) and feldspars (plagioclase).	Sericite, chlorite, biotite, serpentine, magnetite and sulphides (chalcopyrite and pyrrhotite).	Feldspars show albite and carlsbad twinning, euhedral and interlocking. Olivine subrounded with irregular fractures. Pyroxenes are mainly subhedral, some show exsolution texture.	Sericitisation, chloritisation and biotitization.	10%	Minor disseminated sulphides (chalcopyrite and pyrrhotite). Magnetite shows an intergrowth or replaced texture with silicates (olivine and Opx).	Large plagioclase grain inclosing small Opx grains (subophitic texture or poikilitic texture). Pyroxenes are rimmed or been replaced by chlorite or biotite.	Feldspars (plagioclase, orthoclase and sericite): 50%, Pyroxenes (Opx and Cpx) 40%, Olivine: 5% chlorite and biotite: 3% and magnetite: 2%. **Magnetite Gabbronorite**	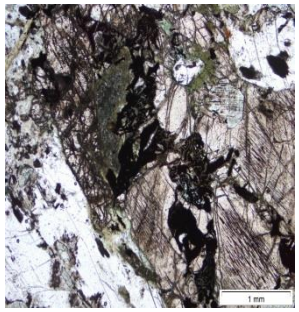
693.21 m-693.52 m	Feldspars (plagioclase and orthoclase), olivine and pyroxenes (Opx and Cpx).	Chlorite, biotite, sericite and magnetite and sulphides (chalcopyrite and pyrrhotite).	Feldspars show albite and carlsbad twinning, feldspars are mainly euhedral and interlocking. Olivine is subrounded with irregular fractures. Pyroxenes mainly Cpx are interstitial>	Sericitisation, biotitization, chloritisation and epidotisation.	10%	Minor disseminated sulphides (chalcopyrite) seen along grain boundaries, within grains as inclusion and as sulphide droplets.	Inclusion of plagioclase within pyroxenes (Ophitic texture). Pyroxenes and olivine are rimmed by chlorite, biotite and epidote.	Feldspars (plagioclase, orthoclase and sericite): 55%, Pyroxenes (Opx and Cpx) 25%, Olivine: 15% chlorite and biotite: 3% and magnetite: 2%. **Olivine-bearing Gabbronorite**	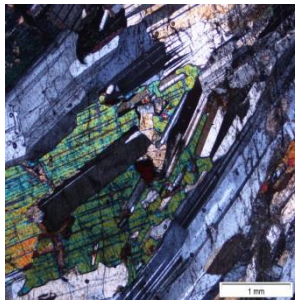

Appendix D:
Table 5: WE027 Polished Thin Section Descriptions

Sample Number WE027 (Interval in meters)	Major Minerals	Minor Minerals	Textures	Alteration and Degree of Alteration	% of Alteration	Reflected light observations	Other Features	Modal Abundance (%) & Rock Name.	Thin Section Picture
724.80 m-725.13 m	Feldspars (plagioclase and orthoclase) and pyroxenes (altered Opx and Cpx).	Sericite, epidote, biotite and chlorite.	Plagioclase and orthoclase show albite and carlsbad twinning, feldspars are interlocking. Pyroxenes are mainly altered especially Cpx and replaced by chlorite and biotite.	Sericitisation, biotitization, chloritisation and epidotisation.	65%	Minor sulphides and extremely disseminated.	Pyroxenes are rimmed by biotite, chlorite and epidote. Ophitic texture where plagioclase is completely surrounded by Cpx.	Feldspars (plagioclase, orthoclase and sericite): 65%, Pyroxenes (Opx and Cpx) 25%, Olivine: 5% chlorite and biotite: 5%. **Gabbronorite**	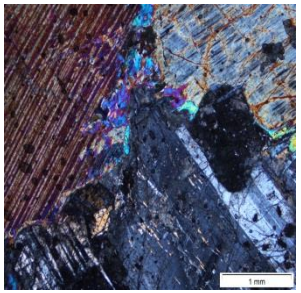
748.42 m-748.75 m	Feldspars (plagioclase and orthoclase) and pyroxene (Opx)	Pyroxene (altered Cpx), chlorite, biotite, sericite, magnetite and epidote.	Plagioclase and orthoclase show albite and carlsbad twinning, euhedral and interlocking grains. Pyroxenes: Opx large subhedral grain with greyish-brown colour and cleavage. Cpx is mainly subhedral or interstitial.	Sericitisation, chloritisation and biotitization.	10%	Large amounts of secondary magnetite (intergrowth or replacement) within the silicate minerals. Minor sulphides (chalcopyrite) along silicate grain boundaries and as sulphide droplets.	Feldspars have patches of altered (sericite). Pyroxenes are rimmed or replaced by chlorite and biotite. Inclusions of feldspars in pyroxenes (ophitic texture).	Feldspars (plagioclase, orthoclase and sericite): 65%, Pyroxenes (Opx and Cpx) 30%, Olivine: 3% chlorite and biotite: 3% and magnetite: 4%. **Magnetite Gabbronorite**	
785.20 m-785.50 m	Feldspars (plagioclase) and Pyroxenes (Opx and Cpx).	Orthoclase, Biotite, chlorite and sericite.	Plagioclase and orthoclase show albite and carlsbad twinning. Pyroxenes are anhedral and altered. Cpx is mainly altered with chlorite and biotite rims.	Sericitisation and chloritisation.	30%	None	Plagioclase and orthoclase are altering to sericite.	Feldspars (plagioclase, orthoclase and sericite): 65%, Pyroxenes (Opx and Cpx) 25%, Olivine: 5% chlorite and biotite: 5% **Olivine-bearing Gabbronorite**	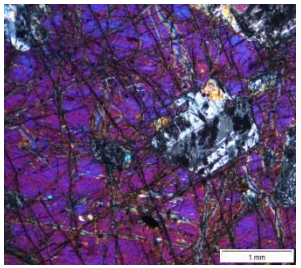

Appendix D:
Table 5: WE027 Polished Thin Section Descriptions

Sample Number WE027 (Interval in meters)	Major Minerals	Minor Minerals	Textures	Alteration and Degree of Alteration	% of Alteration	Reflected light observations	Other Features	Modal Abundance (%) & Rock Name.	Thin Section Picture
808.34 m-808.57 m	Sericite (altered feldspars), pyroxenes (altered Opx and Cpx).	Chlorite, biotite, serpentine, magnetite and sulphides (chalcopyrite)	Feldspars are mainly altered to sericite. Pyroxenes are also mainly altered to biotite and chlorite.	Sericitisation, chloritisation and biotitization.	70%	Minor disseminated magnetite and sulphides (chalcopyrite and pyrrhotite).	Pyroxenes mainly Cpx are rimmed by chlorite and biotite and most samples are completely replaced.	Feldspars (plagioclase, orthoclase and sericite): 70%, Pyroxenes (Opx and Cpx) 20%, Olivine: 5% chlorite and biotite: 5%. **Altered Leuco-Gabbronorite**	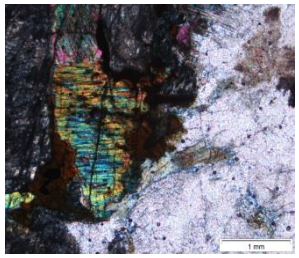
849.60 m-849.80 m	Feldspars (plagioclase), olivine and pyroxene (Opx).	Pyroxenes (altered Cpx), sericite, biotite, chlorite, serpentine, magnetite and sulphides (chalcopyrite).	Feldspars show albite and carlsbad twinning, feldspars are euhedral and interlocking. Olivine grains are subrounded and have irregular fractures. Pyroxenes are subhedral and some grain show exsolution textures.	Sericitisation, biotitization, chloritisation and serpentinisation.	15%	Disseminated sulphides associated with magnetite. Sulphides and magnetite seen along grain boundaries, as inclusion and are sulphide droplets. Secondary magnetite has intergrowth texture.	Pyroxenes especially Cpx is been altered and replaced by chlorite and biotite. Opx and Cpx rim olivine grains. Olivine also has sericite, chlorite, serpentine and biotite rims. Feldspars have patches of sericite in certain grains.	Feldspars (plagioclase and orthoclase): 50%, Pyroxenes (Opx and Cpx) 25%, Olivine: 15% chlorite and biotite: 5%, magnetite 5%. **Olivine-Gabbronorite**	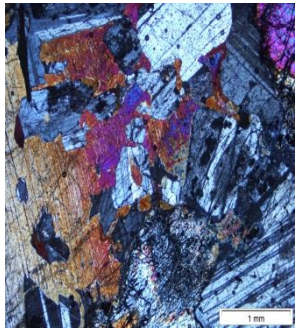
888.37 m-888.70 m	Magnetite, feldspars (plagioclase), pyroxene (altered Cpx).	Biotite, chlorite, serpentine and sulphides (chalcopyrite and pyrrhotite).	Magnetite (opaque mineral) cumulus and intercumulus. Feldspars show albite and carlsbad twinning. Pyroxenes are completely altered to chlorite, epidote and biotite.	Sericitisation, biotitization, chloritisation, serpentinisation and epidotisation.	15%	Sulphides mainly associated with magnetite. Sulphides rimming, inclusions within magnetite. Sulphides disseminated along silicate grain boundaries and as sulphide droplets.	Veinlets and fractures are filled with secondary material (serpentine chlorite and epidote). Quartz with undulose extinction also seen in the fracture and veinlets.	Feldspars (plagioclase and orthoclase): 50%, Pyroxenes (Opx and Cpx) 10%, Olivine: 10% chlorite and biotite: 3% sulphides (chalcopyrite): 2% and, magnetite 25%. **Magnetite Gabbronorite**	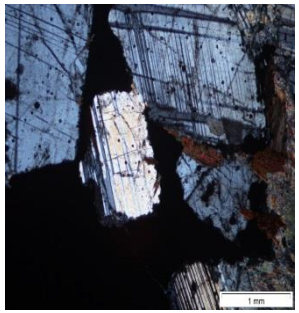

Appendix D:
Table 5: WE027 Polished Thin Section Descriptions

Sample Number WE027 (Interval in meters)	Major Minerals	Minor Minerals	Textures	Alteration and Degree of Alteration	% of Alteration	Reflected light observations	Other Features	Modal Abundance (%) & Rock Name.	Thin Section Picture
891.52 m-891.78 m	Feldspars (plagioclase) and pyroxene (altered Cpx).	Biotite, chlorite, sericite and sulphides (chalcopyrite and pyrrhotite).	Plagioclase and orthoclase show albite and carlsbad twinning. Feldspars are slight altered to sericite. Pyroxenes are altered to chlorite and biotite (replaced).	Sericitisation, biotitization, chloritisation and epidotisation.	40%	Minor disseminated magnetite.	Inclusions of feldspars in pyroxenes (ophitic texture). Pyroxenes rimmed by biotite and chlorite.	Feldspars (plagioclase and orthoclase): 45%, Pyroxenes (Opx and Cpx) 45%, chlorite and biotite: 8% and sulphides (chalcopyrite): 2% **Pegmatoidal unit (recrystallised Gabbronorite)**	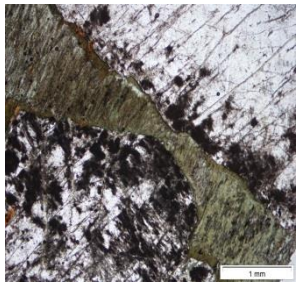
929.57 m-929.87 m	Feldspars (plagioclase and orthoclase) and pyroxenes (Opx and Cpx).	Sericite, olivine, magnetite, biotite and chlorite.	Plagioclase and orthoclase shows albite and carlsbad. Feldspars euhedral and interlocking. Pyroxenes are subhedral. Minor olivine subrounded with irregular fractures.	Sericitisation, biotitization, chloritisation, epidotisation and serpentinisation.	20%	Large amounts of secondary magnetite (intergrowth or replacement) within the silicate minerals.	Pyroxenes are altered, rimmed or replaced by chlorite and biotite. Feldspars altered to sericite. Inclusions of feldspars in olivine and Opx (ophitic texture).	Feldspars (plagioclase and orthoclase): 55%, Pyroxenes (Opx and Cpx) 30%, Olivine: 5% chlorite and biotite: 7% and, magnetite 3%. **Magnetite Gabbronorite**	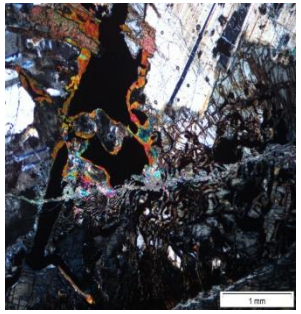
962.39 m-962.71 m	Feldspars (plagioclase and orthoclase), pyroxenes (Opx and Cpx) and olivine.	Sericite, biotite, chlorite, serpentine and sulphides (chalcopyrite and pyrrhotite).	Olivine subrounded with irregular fractures. Plagioclase and orthoclase has albite and carlsbad twinning, feldspars are mainly interstitial. Pyroxenes are subhedral.	Sericitisation, biotitization, chloritisation and serpentinisation.	15%	Minor disseminated sulphides (chalcopyrite) and magnetite, along grains boundaries and as sulphide droplets.	Pyroxenes are altering, rimmed and been replace by chlorite and biotite. Olivines also have alteration rims. Inclusions of plagioclase in pyroxenes (ophitic texture).	Feldspars (plagioclase and orthoclase): 40%, Pyroxene (Opx) 25%, Olivine: 30% chlorite and biotite: 5% **Poikilitic Troctolite**	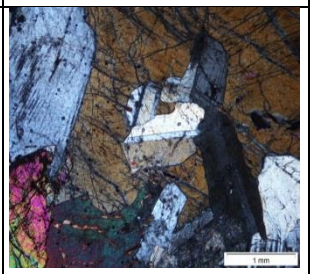

Appendix D:
Table 5: WE027 Polished Thin Section Descriptions

Sample Number WE027 (Interval in meters)	**Major Minerals**	**Minor Minerals**	**Textures**	**Alteration and Degree of Alteration**	**% of Alteration**	**Reflected light observations**	**Other Features**	**Modal Abundance (%) & Rock Name.**	**Thin Section Picture**
987.21 m-987.43 m	Sericite (altered feldspars) and pyroxenes (altered Opx and Cpx).	Biotite, chlorite, serpentine and epidote.	Plagioclase and orthoclase have been completely altered to sericite. Pyroxenes have been altered to both biotite and chlorite.	Sericitisation, chloritisation, epidotisation and biotitization.	85%	Minor disseminated sulphides (chalcopyrite)	Veinlets and fractures are filled with chlorite, biotite, epidote and sericite.	Feldspars (plagioclase, orthoclase and sericite): 75%, Pyroxene (Opx and Cpx) 20%, Olivine: 2% chlorite and biotite: 3% **Altered Anorthosite/ leuco-Gabbronorite**	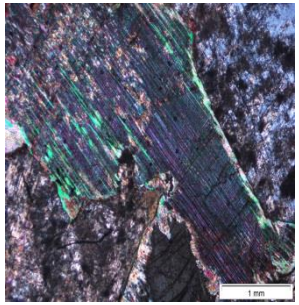
994.04 m-994.23 m	Sericite (altered feldspars), chlorite and biotite (altered pyroxenes).	Epidote, serpentine and sulphides (chalcopyrite)	Plagioclase and orthoclase have been completely altered to sericite. Pyroxenes have been altered to both biotite and chlorite.	Sericitisation, chloritisation and biotitization.	95%	Sulphides (chalcopyrite and pyrrhotite) are seen as inclusions within altered feldspars, within fractures and as sulphide droplets.	Veinlets and fractures are filled with serpentine and epidote.	Feldspars (plagioclase, orthoclase and sericite): 85%, Pyroxene (Opx and Cpx) 10%, Olivine: 2% chlorite and biotite: 3% **Altered Anorthosite**	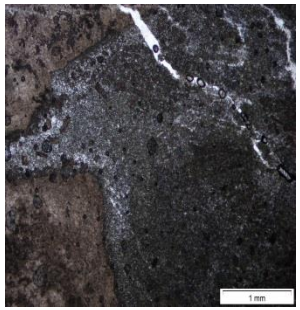
1252.15 m-1252.36 m	Feldspars (plagioclase and orthoclase), olivine and pyroxene (Opx).	Biotite, chlorite, sericite, serpentine and magnetite.	Plagioclase and orthoclase show albite and carlsbad twinning and are mainly interstitial. Olivine subrounded with irregular fractures. Pyroxenes are subhedral.	Sericitisation, biotitization and chloritisation.	15%	Minor disseminated sulphides (chalcopyrite) and magnetite, along grains boundaries.	Inclusions of feldspars in pyroxenes (ophitic texture). Pyroxenes rimmed by biotite and chlorite.	Feldspars (plagioclase and orthoclase): 35%, Pyroxenes (Opx and Cpx) 40%, Olivine: 20% chlorite and biotite: 5%. **Olivine-bearing Gabbronorite**	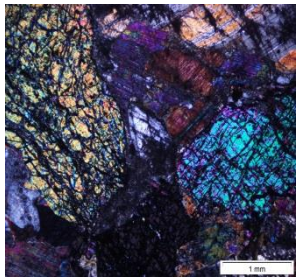

Appendix D:
Table 5: WE027 Polished Thin Section Descriptions

Sample Number WE027 (Interval in meters)	Major Minerals	Minor Minerals	Textures	Alteration and Degree of Alteration	% of Alteration	Reflected light observations	Other Features	Modal Abundance (%) & Rock Name.	Thin Section Picture
1282.94 m-1283.12 m	Feldspars (plagioclase and orthoclase) and pyroxenes (Opx and Cpx).	Chlorite, biotite, sericite and inverted pigeonite.	Minor olivine subrounded with irregular fractures. Plagioclase and orthoclase with albite and carlsbad twinning, feldspars are interlocking. Pyroxenes are mainly subhedral.	Sericitisation, biotitization, chloritisation, epidotisation and serpentinisation.	10%	Minor sulphides (chalcopyrite and pyrrhotite), with skeletal texture and other as sulphide droplets.	Inclusions of plagioclase within pyroxenes (ophitic texture). Pyroxenes and olivine rimmed by biotite and chlorite.	Feldspars (plagioclase and orthoclase): 50%, Pyroxenes (Opx and Cpx) 45%, chlorite and biotite: 5% **Gabbronorite**	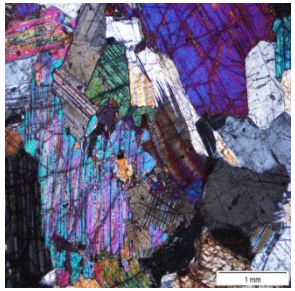
1345.20 m-1345.43 m	Feldspars (plagioclase and orthoclase) and pyroxenes (Opx and altered Cpx).	Biotite, chlorite, sericite and inverted pigeonite.	Plagioclase and orthoclase shows albite and carlsbad. Feldspars euhedral and interlocking. Pyroxenes are subhedral.	Sericitisation, biotitization and chloritisation.	15%	None	Inclusions of plagioclase within pyroxenes (ophitic texture). Pyroxenes and olivine rimmed by biotite and chlorite.	Feldspars (plagioclase and orthoclase): 65%, Pyroxenes (Opx and Cpx) 30%, chlorite and biotite: 5% **Leuco-Gabbronorite**	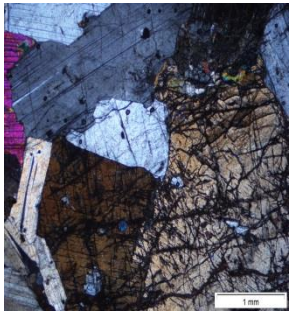
1381.20 m-1381.46 m	Olivine (altered), pyroxenes (extremely altered Opx and Cpx) and sericite (altered feldspars).	Epidote, chlorite, biotite, serpentine, tremolite, sulphides (chalcopyrite and pyrrhotite) and magnetite.	Feldspars are completely altered to sericite. Olivine subrounded with irregular fractures, however mainly altered grains. Pyroxenes are extremely altered to chlorite, biotite and sericite.	Sericitisation, biotitization, chloritisation, epidotisation and serpentinisation.	85%	Minor sulphides (chalcopyrite). Large amounts of secondary magnetite (intergrowth or replacement) within the silicate minerals.	Veinlets and fractures are filled with secondary material (serpentine, sericite, biotite, epidote and chlorite). Epidote showing needle like texture.	Feldspars (plagioclase, orthoclase and sericite): 30%, Pyroxene (Opx) 27%, Olivine: 30%, epidote:10%, chlorite and biotite: 3% **Altered Poikilitic Troctolite**	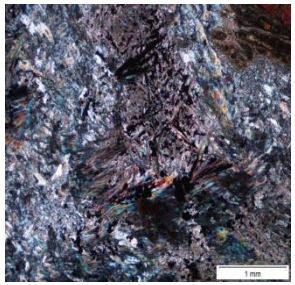

Appendix D:
Table 5: WE027 Polished Thin Section Descriptions

Sample Number WE027 (Interval in meters)	Major Minerals	Minor Minerals	Textures	Alteration and Degree of Alteration	% of Alteration	Reflected light observations	Other Features	Modal Abundance (%) & Rock Name.	Thin Section Picture
1385.60 m-1385.41 m	Olivine (altered), pyroxene (altered olivine), magnetite and serpentine.	Sericite, epidote, chlorite and biotite.	Plagioclase shows albite twinning, interstitial and mainly altered to sericite. Olivine grains are subrounded with irregular fractures.	Sericitisation, biotitization, chloritisation, epidotisation and serpentinisation.	55%	Minor sulphides (chalcopyrite). Large amounts of secondary magnetite (intergrowth or replacement) within the silicate minerals (within the fractures of olivine grains).	Large interstitial Opx grain (poikilitic texture). Olivine grains are rimmed or been replaced by serpentine.	Feldspars (plagioclase, orthoclase and sericite): 20%, Pyroxene (Opx) 20%, Olivine: 50%, epidote and serpentine:7%, chlorite and biotite: 3% **Altered Harzburgite**	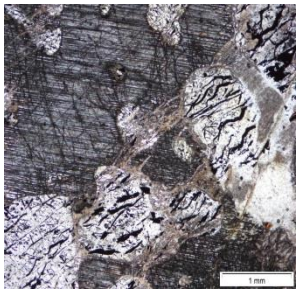
1386.66 m-1386.86 m	Olivine (altered) and sericite (altered feldspars)	Pyroxene (Opx altered), chlorite, biotite, epidote, serpentine, sulphides (chalcopyrite) and magnetite	Minor feldspars, completely altered to sericite. Olivine are subrounded with irregular fracture and mainly altered to serpentine and magnetite. Pyroxenes are altered to biotite and chlorite and are mainly interstitial.	Sericitisation, biotitization, chloritisation, epidotisation and serpentinisation.	60%	Minor disseminated sulphides (chalcopyrite) within olivine grains. Secondary magnetite seen in the irregular fractures of olivine grains.	Pyroxenes are mainly altered and have rims of biotite and epidote. Veinlets and fractures are filled with secondary minerals (epidote, serpentine and magnetite).	Feldspars (plagioclase, orthoclase and sericite): 15%, Pyroxene (Opx) 25%, Olivine: 50%, epidote and serpentine:7%, chlorite and biotite: 3% **Altered Harzburgite**	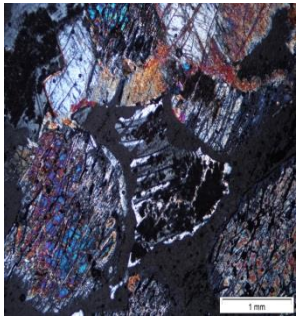
1393.60 m-1393.81 m	Feldspars (plagioclase and orthoclase) and pyroxenes (Opx and Cpx)	Quartz, sericite, magnetite, sulphides (chalcopyrite and pyrrhotite), biotite and chlorite.	Feldspars are mainly altered to sericite, some show albite and carlsbad twinning. Feldspars are interstitial. Olivine subrounded with irregular fractures. Pyroxenes are subhedral.	Sericitisation, biotitization, epidotisation and minor chloritisation.	15%	Disseminated sulphides (chalcopyrite) and. secondary magnetite.	Pyroxene (Opx) is altered and replaced by biotite and epidote. Minor quartz with undulose extinction.	Feldspars (plagioclase and, orthoclase): 30%, Pyroxene (Opx and cpx) 65%, Quartz: 2%, chlorite and biotite: 3% **Granofels (feldspathic pyroxenite unit)**	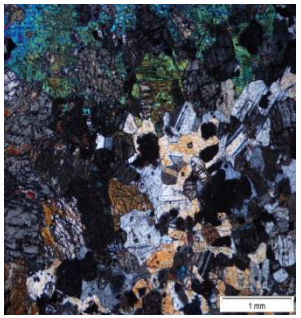

Appendix D:
Table 5: WE027 Polished Thin Section Descriptions

Sample Number WE027 (Interval in meters)	Major Minerals	Minor Minerals	Textures	Alteration and Degree of Alteration	% of Alteration	Reflected light observations	Other Features	Modal Abundance (%) & Rock Name.	Thin Section Picture
1403.92 m-1404.20 m	Olivine and pyroxenes (Opx and Cpx).	Sericite, feldspars (altered plagioclase), Quartz, biotite, chlorite, epidote and serpentine.	Plagioclase and orthoclase are mainly altered to sericite, some feldspars show albite and carlsbad twinning. Feldspars are interstitial. Olivine subrounded with irregular fractures. Pyroxenes mainly Opx are subhedral.	Sericitisation, biotitization, epidotisation and minor chloritisation.	20%	Disseminated sulphides (chalcopyrite and pyrrhotite) are seen as inclusions within altered feldspars, within fractures and veinlets, as well as sulphide droplets.	Pyroxene (Opx) is altered and replaced by biotite and epidote. Minor quartz with undulose extinction.	Feldspars (plagioclase and, orthoclase): 35%, Pyroxene (Opx and cpx) 60%, Quartz: 2%, chlorite and biotite: 3% **Granofels (feldspathic pyroxenite unit)**	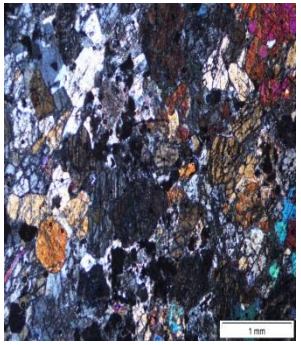

Appendix D:
Table 6: WE035 Polished Thin Section Descriptions

Sample Number WE035 (Interval in meters)	Major Minerals	Minor Minerals	Textures	Alteration and Degree of Alteration	% of Alteration	Reflected light observations	Other Features	Modal Abundance (%) & Rock Name.	Thin Section Picture
368.55m-368.76m	Quartz, hematite and magnetite.	Epidote and very fine-grained matrix.	Quartz with an angular shape and undulose extinction. Matrix is very fine-grained with epidote.	Sericitisation and epidotisation.	5%	Minor magnetite seen along grain boundaries and as inclusion in grains.		Quartz: 70%, Fine-grained matrix: 15%, magnetite: 7%, epidote: 3%, chlorite and biotite: 2%. **Sandstone**	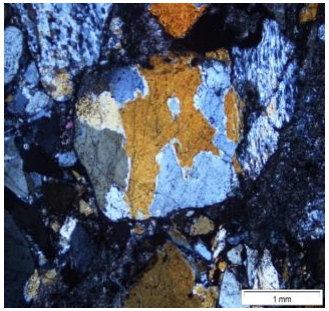
369.90m-370.00m	Sericite, magnetite and hematite.	Quartz, epidote and very fine-grained matrix.	Magnetite subrounded grains. The rest of the material is extremely altered, completely altered to sericite. Quartz grains are angular and have undulose extinction.	Sericitisation, chloritisation and hematitisation.	99%	Magnetite grains are seen. Hematite has a wavely texture.	Veinlets and fractures filled with chlorite and serpentine.	Quartz: 20%, feldspars altered to sericite: 60%, magnetite: 10%, hematite: 5%, chlorite and epidote: 5%. **Palaesol**	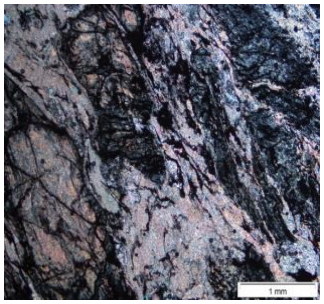
377.53m-377.76m	Feldspars (plagioclase and orthoclase altered) and pyroxenes (Opx and Cpx).	Sericite, epidote, chlorite and biotite.	Feldspars are completely altered to sericite. Pyroxenes are also altered or been replace by chlorite and biotite.	Chloritisation, sericitisation, and biotitization.	70%	Minor disseminated sulphides (Chalcopyrite).	Pyroxenes especially Cpx have been completely replaced by epidote and most of these grains are rimmed by biotite.	Feldspars (plagioclase, orthoclase and sericite): 50%, pyroxenes (Opx and Cpx): 45%, biotite: 3%, chlorite: 2%. **Gabbronorite**	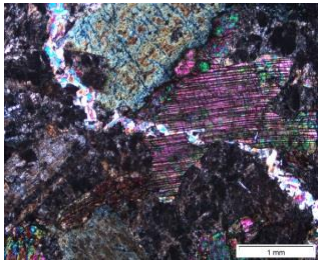

Appendix D:
Table 6: WE035 Polished Thin Section Descriptions

Sample Number WE035 (Interval in meters)	Major Minerals	Minor Minerals	Textures	Alteration and Degree of Alteration	% of Alteration	Reflected light observations	Other Features	Modal Abundance (%) & Rock Name.	Thin Section Picture
393.80m-394.15m	Olivine, pyroxenes (Opx and Cpx) and feldspars (plagioclase and orthoclase).	Sericite, inverted pigeonite, magnetite, sulphides, chlorite and biotite.	Plagioclase and orthoclase show albite and carlsbad twinning, feldspars are euhedral and interlocking. Pyroxenes are subhedral. Olivine subrounded with irregular fractures.	Chloritisation, sericitisation, epidotisation, and biotitization.	25%	Minor disseminated sulphides (Chalcopyrite) and minor magnetite.	Cpx grains are mainly altered or been replaced by epidote, chlorite or biotite. Pyroxenes show exsolution textures (inverted pigeonite).	Feldspars (plagioclase, orthoclase and sericite): 50%, pyroxenes (Opx and Cpx): 45%, biotite: 3%, chlorite: 2%. **Gabbronorite**	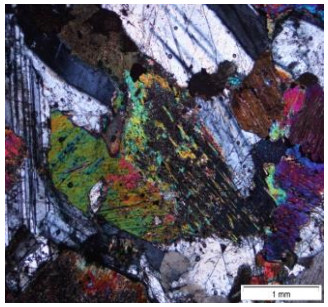
399.70m-399.91m	Feldspars (plagioclase and orthoclase) and pyroxenes (Opx and Cpx).	Sericite, epidote, chlorite and biotite.	Plagioclase and orthoclase show albite and carlsbad twinning, feldspars are euhedral and interlocking. Pyroxenes subhedral with cleavage,	Chloritisation, sericitisation, and biotitization.	40%	Minor disseminated sulphides (Chalcopyrite) and minor magnetite.	Pyroxenes altered or been replaced by epidote, chlorite or biotite. Fractures and veinlets are filled with secondary material (chlorite and sericite).	Feldspars (plagioclase, orthoclase and sericite): 60%, pyroxenes (Opx and Cpx): 30%, Olivine: 5%, biotite: 3%, chlorite: 2%. **Olivine-bearing Gabbronorite**	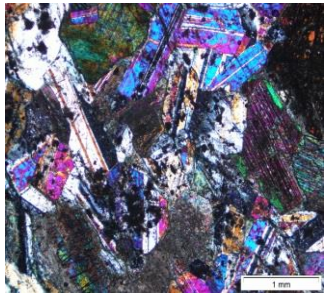
457.65m-457.79m	Feldspars (plagioclase and orthoclase) and pyroxenes (Opx and Cpx).	Chlorite, biotite, sericite and serpentine.	Plagioclase and orthoclase show albite and carlsbad twinning, feldspars are euhedral and interlocking. Pyroxenes subhedral with cleavage,	Chloritisation, sericitisation, and biotitization.	45%	Minor disseminated sulphides (Chalcopyrite).	Pyroxenes are altered or been replaced by epidote, chlorite or biotite. Fractures and veinlets are filled with secondary material (chlorite and sericite).	Feldspars (plagioclase, orthoclase and sericite): 55%, pyroxenes (Opx and Cpx): 45%, biotite: 3%, chlorite: 2%. **Gabbronorite**	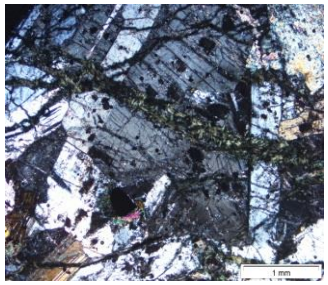

Appendix D:
Table 6: WE035 Polished Thin Section Descriptions

Sample Number WE035 (Interval in meters)	Major Minerals	Minor Minerals	Textures	Alteration and Degree of Alteration	% of Alteration	Reflected light observations	Other Features	Modal Abundance (%) & Rock Name.	Thin Section Picture
488.30m-488.55m	Feldspars (plagioclase) and pyroxenes (Opx and Cpx altered).	Sericite, epidote, chlorite and biotite.	Feldspars are completely altered to sericite. Pyroxenes are also altered or been replace by chlorite and biotite.	Chloritisation, sericitisation, and biotitization.	70%	Minor disseminated sulphides (Chalcopyrite).	Pyroxenes especially Cpx have been completely replaced by epidote and most of these grains are rimmed by biotite.	Feldspars (plagioclase, orthoclase and sericite): 55%, pyroxenes (Opx and Cpx): 40%, biotite: 5%, chlorite: 5%. **Altered Gabbronorite**	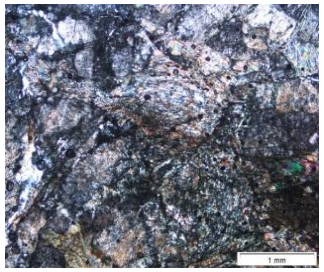
505.10m-505.20m	Feldspars (plagioclase and orthoclase), altered olivine and pyroxenes (Opx and Cpx).	Inverted pigeonite, chlorite, biotite and sericite.	Plagioclase and orthoclase show albite and carlsbad twinning, feldspars are euhedral and interlocking. Pyroxenes mainly Opx subhedral. Highly altered olivine grains are subrounded	Chloritisation, sericitisation, and biotitization.	25%	None	Olivine grains are rimmed with Opx. Feldspars are altered to sericite. Inclusions of plag within Opx and olivine (ophitic texture). Pyroxenes exsolution textures	Feldspars (plagioclase and orthoclase): 50%, pyroxenes (Opx and Cpx): 45%, biotite and chlorite: 5%. **Gabbronorite**	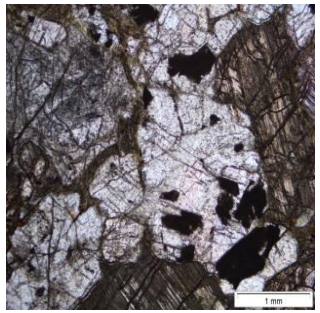
515.30m-515.46m	Altered olivine, pyroxene (Opx) and sericite.	Feldspars (plagioclase), chlorite, biotite, epidote, serpentine and magnetite.	Feldspars are completely altered to sericite. Pyroxenes altered or replace by chlorite and biotite. Olivine subrounded with irregular fractures. Ophitic texture present.	Chloritisation, sericitisation, epidotisation, serpentinisation and biotitization.	55%	Minor disseminated sulphides (chalcopyrite and pyrrhotite) and minor secondary magnetite associated with silicates (olivine).	Olivine grains are rimmed with Opx and epidote. The fracture within the olivine grains are filled with serpentine, chlorite and secondary magnetite.	Feldspars (plagioclase, orthoclase and sericite): 40%, pyroxenes (Opx and Cpx): 35%, Olivine: 15%, biotite: 3%, chlorite: 2% and serpentine and magnetite: 5%. **Olivine-bearing Gabbronorite**	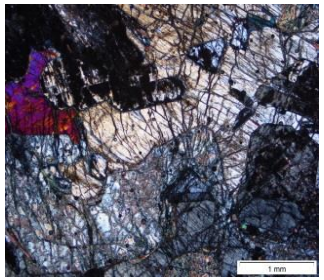

Appendix D:
Table 6: WE035 Polished Thin Section Descriptions

Sample Number WE035 (Interval in meters)	Major Minerals	Minor Minerals	Textures	Alteration and Degree of Alteration	% of Alteration	Reflected light observations	Other Features	Modal Abundance (%) & Rock Name.	Thin Section Picture
523.30m-523.55m	Pyroxenes (Opx and Cpx altered) and sericite.	Epidote, chlorite, biotite, and olivine.	Feldspars are completely altered to sericite. Pyroxenes are also altered or been replace by chlorite and biotite.	Chloritisation, sericitisation, epidotisation and biotitization.	85%	None	Pyroxenes especially Cpx have been completely replaced by epidote and most of these grains are rimmed by biotite.	Feldspars (plagioclase, orthoclase and sericite): 60%, pyroxenes (Opx and Cpx): 25%, Olivine: 10%, biotite: 3%, chlorite: 2% **Alerted Olivine-bearing Gabbronorite**	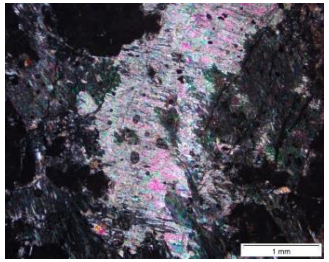
529.15m-529.39m	Feldspars (plagioclase and orthoclase), Olivine and pyroxene (Opx and Cpx).	Epidote, chlorite, biotite, magnetite, serpentine and sericite.	Plagioclase and orthoclase show albite and carlsbad twinning, feldspars are euhedral and interlocking. Olivine subrounded with irregular fractures. Pyroxenes are anhedral/ interstitial	Chloritisation, sericitisation, epidotisation and biotitization.	20%	Minor disseminated magnetite.	Pyroxenes are rimmed or replaced by chlorite or biotite. Inclusions of plagioclase within Opx and olivine (ophitic texture).	Feldspars (plagioclase, orthoclase and sericite): 50%, pyroxenes (Opx and Cpx): 20%, Olivine: 25%, biotite: 3%, chlorite: 2% **Poikilitic Troctolite**	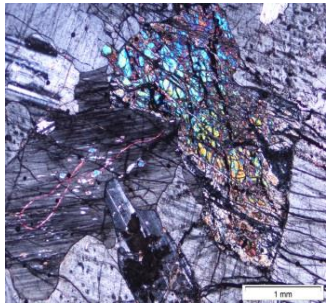
536.46m-536.68m	Feldspars (plagioclase and orthoclase), Olivine and pyroxene (Opx and Cpx).	Chlorite, biotite, magnetite, serpentine and sericite.	Plagioclase and orthoclase shows albite and carlsbad twinning, feldspars are euhedral and interlocking. Olivine subrounded with irregular fractures. Pyroxenes are interstitial.	Chloritisation, sericitisation, epidotisation, serpentinisation and biotitization.	35%	Minor disseminated sulphides (chalcopyrite and pyrrhotite) and minor secondary magnetite.	Pyroxenes are rimmed or replaced by chlorite, epidote and biotite. Pyroxenes are mainly interstitial and from a poikilitic texture.	Feldspars (plagioclase, orthoclase and sericite): 40%, pyroxenes (Opx and Cpx): 25%, Olivine: 20%, biotite: 3%, chlorite: 2% **Olivine-bearing Gabbronorite**	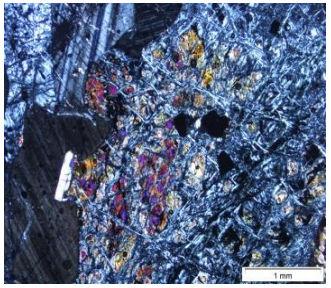

Appendix D:
Table 6: WE035 Polished Thin Section Descriptions

Sample Number WE035 (Interval in meters)	Major Minerals	Minor Minerals	Textures	Alteration and Degree of Alteration	% of Alteration	Reflected light observations	Other Features	Modal Abundance (%) & Rock Name.	Thin Section Picture
544.67m-544.92m	Altered olivine, pyroxene (Opx), sericite, serpentine and chlorite.	Feldspars (plagioclase and orthoclase), magnetite, biotite and pyroxene (Cpx).	Plagioclase and orthoclase shows albite and carlsbad twinning, feldspars are altering to sericite. Olivine subrounded with irregular fractures. Pyroxenes are interstitial.	Chloritisation, sericitisation, epidotisation, serpentinisation and biotitization.	30%	Minor Secondary magnetite.	Pyroxenes are rimmed or replaced by chlorite, epidote and biotite. Pyroxenes are mainly interstitial and from a poikilitic texture.	Feldspars (plagioclase, orthoclase and sericite): 35%, pyroxenes (Opx and Cpx): 30%, Olivine: 30%, biotite: 3%, chlorite: 2% **Poikilitic Troctolite**	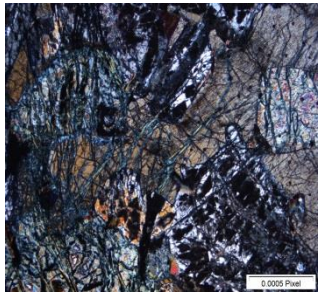
545.40m-545.60m	Altered olivine, sericite and pyroxenes (Opx and Cpx altered).	Epidote, chlorite, biotite, feldspars (plagioclase), quartz and serpentine.	Plagioclase and orthoclase shows albite and carlsbad twinning, feldspars are altering to sericite. Pyroxenes are subhedral and interstitial, show cleavage.	Chloritisation, sericitisation, epidotisation, serpentinisation and biotitization.	45%	None	Pyroxenes are been replaced by biotite and chlorite. Fractures and veinlets are filled with secondary material (quartz with undulose extinction).	Feldspars (plagioclase, orthoclase and sericite): 65%, pyroxenes (Opx and Cpx): 25%, biotite and chlorite: 10%. **Altered Leuco-Gabbronorite**	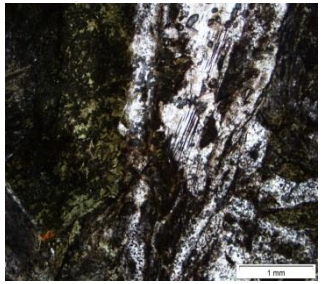
561.26m-561.48m	Feldspars (plagioclase and orthoclase), Olivine and pyroxene (Opx).	Epidote, chlorite, biotite, magnetite, serpentine and sericite.	Plagioclase and orthoclase shows albite and carlsbad twinning, feldspars are euhedral and interlocking. Olivine subrounded with irregular fractures. Pyroxenes are interstitial.	Chloritisation, sericitisation, epidotisation, serpentinisation and biotitization.	35%	Secondary magnetite rimming and filling fractures with altered silicates (olivine).	Pyroxenes are been replaced by biotite and chlorite. Pyroxenes are interstitial and from a poikilitic textures. Fractures and veinlets are filled with secondary material.	Feldspars (plagioclase, orthoclase and sericite): 40%, pyroxenes (Opx and Cpx): 25%, Olivine: 25%, biotite: 3%, chlorite: 2% and epidote and serpentine: 5%. **Poikilitic Troctolite**	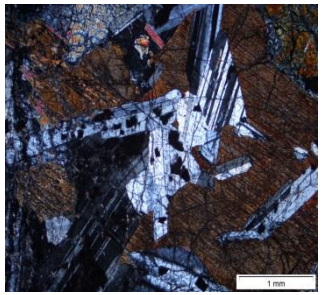

Appendix D:
Table 6: WE035 Polished Thin Section Descriptions

Sample Number WE035 (Interval in meters)	Major Minerals	Minor Minerals	Textures	Alteration and Degree of Alteration	% of Alteration	Reflected light observations	Other Features	Modal Abundance (%) & Rock Name.	Thin Section Picture
572.41m-572.74m	Altered olivine, sericite and pyroxene (Opx).	Epidote, chlorite, biotite, feldspars (plagioclase and orthoclase) and serpentine.	Altered Olivine subrounded with irregular fractures filled with chlorite and serpentine. Feldspars are mainly altered to sericite. Interstitial Opx (poikilitic texture).	Chloritisation, sericitisation, epidotisation, serpentinisation and biotitization.	50%	Secondary magnetite rimming and filling fractures with altered silicates (olivine).	Fractures and veinlets are filled with secondary material (epidote, chlorite and sericite). Pyroxenes are been replaced by biotite and chlorite.	Feldspars (plagioclase, orthoclase and sericite): 30%, pyroxenes (Opx and Cpx): 25%, Olivine: 35%, biotite: 3%, chlorite: 2% and epidote and serpentine: 5%. **Poikilitic Troctolite**	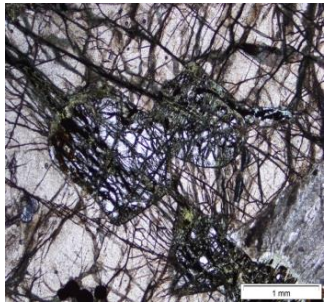
596.73m-596.96m	Altered olivine, sericite, serpentine and pyroxene (Opx).	Chlorite, epidote, biotite, quartz and magnetite	Altered Olivine subrounded with irregular fractures filled with chlorite and serpentine. Feldspars are mainly altered to sericite. Interstitial Opx (poikilitic texture).	Chloritisation, sericitisation, epidotisation, serpentinisation and biotitization.	85%	Minor secondary disseminated magnetite. Minor disseminated sulphides (chalcopyrite and pyrrhotite).	Fractures and veinlets are filled with secondary material (quartz with undulose extinction). Pyroxenes are been replaced by biotite and chlorite.	Feldspars (plagioclase, orthoclase and sericite): 25%, pyroxenes (Opx and Cpx): 25%, Olivine: 45%, biotite and, chlorite: 2% and epidote and serpentine: 3%. **Poikilitic Troctolite**	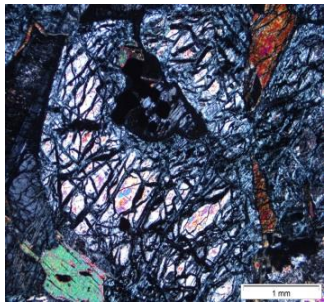
603.70m-603.94m	Altered olivine, sericite and epidote	Chlorite, biotite, magnetite, serpentine, quartz, pyroxenes (Opx and Cpx) and sericite.	Altered Olivine subrounded with irregular fractures filled with chlorite and serpentine. Feldspars are mainly altered to sericite.	Chloritisation, sericitisation, epidotisation, serpentinisation and biotitization.	90%	Minor secondary disseminated magnetite.	Minor pyroxenes mainly interstitial and altered to chlorite and biotite. Fractures and veinlets are filled with secondary material (epidote and sericite).	Feldspars (plagioclase, orthoclase and sericite): 40%, pyroxenes (Opx and Cpx): 15%, Olivine: 40%, biotite and, chlorite: 2% and epidote and serpentine: 3%. **Altered Poikilitic Troctolite**	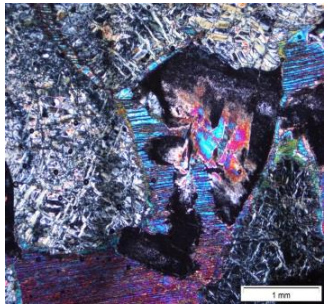

Appendix D:
Table 6: WE035 Polished Thin Section Descriptions

Sample Number WE035 (Interval in meters)	Major Minerals	Minor Minerals	Textures	Alteration and Degree of Alteration	% of Alteration	Reflected light observations	Other Features	Modal Abundance (%) & Rock Name.	Thin Section Picture
604.60m-604.80m	Altered olivine, pyroxenes (Opx and Cpx altered), epidote and serpentine.	Sericite (feldspars completely altered), chlorite and biotite.	Altered olivine subrounded shape with irregular fractures. Pyroxenes are mainly altered to chlorite and epidote, a few grains have subhedral shape and show cleavage.	Chloritisation, sericitisation, epidotisation, and biotitization.	55%	Minor disseminated sulphides (chalcopyrite and pyrrhotite).	Pyroxenes are rimmed or completely replace by chlorite, epidote or biotite. Fractures and veinlets are filled with secondary material (serpentine, chlorite and epidote).	Feldspars (plagioclase, orthoclase and sericite): 20%, pyroxenes (Opx and Cpx): 25%, Olivine: 48%, biotite and, chlorite: 2% and epidote and serpentine: 5%. **Altered Poikilitic Troctolite**	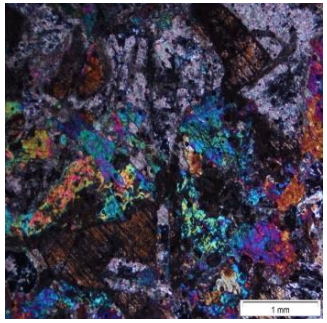
606.40m-606.60m	Altered olivine, serpentine and sericite.	Chlorite, biotite and pyroxenes (Opx and Cpx).	Altered olivine subrounded with irregular fractures is completely altered to magnetite and serpentine, only the shape remains. Feldspars and pyroxenes are mainly altered	Chloritisation, sericitisation, epidotisation, serpentinisation and biotitization.	90%	Secondary magnetite rimming and filling fractures with altered silicates (olivine).	Fractures and veinlets are filled with secondary material (serpentine, chlorite and epidote).	Feldspars (plagioclase, orthoclase and sericite): 10%, pyroxenes (Opx and Cpx): 30%, Olivine: 53%, biotite and, chlorite: 2% and epidote and serpentine: 5%. **Altered harzburgite**	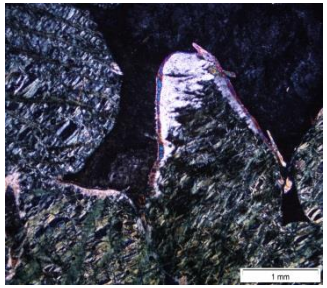
609.90m-610.15m	Altered olivine and sericite.	Chlorite, biotite, epidote, serpentine and secondary magnetite.	Altered olivine subrounded with irregular fractures is completely altered to magnetite and serpentine, only the shape remains. Feldspars and pyroxenes are mainly altered	Chloritisation, sericitisation, epidotisation, serpentinisation and biotitization.	95%	Minor disseminated sulphides (chalcopyrite and pyrrhotite). Secondary magnetite rimming and filling fractures with altered silicates (olivine).	Fractures and veinlets are filled with secondary material (serpentine, chlorite and epidote).	Feldspars (plagioclase, orthoclase and sericite): 20%, pyroxenes: 35%, Olivine: 40%, biotite and, chlorite: 2% and epidote and serpentine: 3%. **Altered harzburgite**	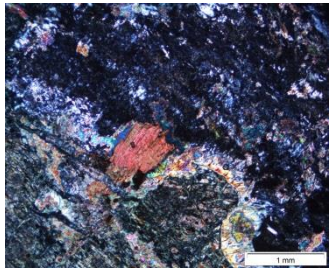

Appendix D:
Table 6: WE035 Polished Thin Section Descriptions

Sample Number WE035 (Interval in meters)	Major Minerals	Minor Minerals	Textures	Alteration and Degree of Alteration	% of Alteration	Reflected light observations	Other Features	Modal Abundance (%) & Rock Name.	Thin Section Picture
613.40m-613.60m	Altered olivine, pyroxenes (Opx and Cpx altered) and feldspars (plagioclase mainly altered to sericite).	Secondary magnetite, sericite, chlorite, biotite, epidote and serpentine.	Altered olivine with subrounded shape and irregular fractures. Feldspars and pyroxenes are mainly altered to sericite, chlorite and epidote.	Chloritisation, sericitisation, epidotisation, serpentinisation and biotitization.	55%	Disseminated sulphides (chalcopyrite and pyrrhotite) along grain boundaries and as inclusion, and are mainly associated with magnetite. Secondary magnetite.	Olivine grains are altering to serpentine and magnetite, fractures within the olivine grains are filled with secondary minerals from the alteration of the olivine.	Feldspars (plagioclase, orthoclase and sericite): 20%, pyroxenes (Opx and Cpx): 25%, Olivine: 50%, biotite and, chlorite: 2% and epidote and serpentine: 3%. **Altered harzburgite**	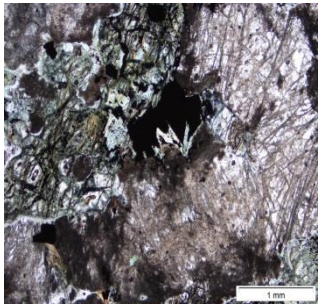
616.68m-616.90m	Olivine and Pyroxenes (Opx and Cpx)	Feldspars (plagioclase and orthoclase), epidote, biotite, chlorite, serpentine, sericite and magnetite.	Minor feldspars show albite and carlsbad twinning, mainly interstitial. Olivine subrounded with irregular fractures. Pyroxenes mainly Opx with subhedral shape.	Chloritisation, sericitisation, epidotisation, serpentinisation and biotitization.	20%	Minor disseminated sulphides (chalcopyrite and pyrrhotite). Secondary magnetite associated with altered silicates (olivine).	Intergrowth between Opx and olivine grains. Inclusion of smaller olivine grains within Opx. Fractures and veinlets filled with secondary material.	Feldspars (plagioclase and orthoclase): 25%, pyroxenes (Opx and Cpx): 65%, Olivine: 5%, biotite and, chlorite: 3% **Feldspathic Pyroxenite.**	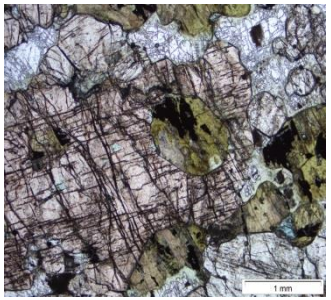
630.20m-630.50m	Feldspars (plagioclase and orthoclase), pyroxenes (Opx and Cpx), Epidote and chlorite.	Sericite, biotite and sulphides (chalcopyrite and pyrrhotite).	Plagioclase and orthoclase show albite and carlsbad twinning. Feldspars are mainly euhedral and interlocking. Pyroxenes are subhedral and have cleavage	Chloritisation, sericitisation, epidotisation and biotitization	45%	Sulphides (chalcopyrite and pyrrhotite) are seen along grain boundaries, as inclusions and as sulphides droplets.	Feldspars have patches of sericite. Pyroxenes especially Cpx are rimmed or replaced by chlorite, biotite and epidote.	Feldspars (plagioclase and orthoclase): 50%, pyroxenes (Opx and Cpx): 40%, biotite and, chlorite: 5% and sulphides (chalcopyrite and pyrrhotite): 5% **Gabbronorite**	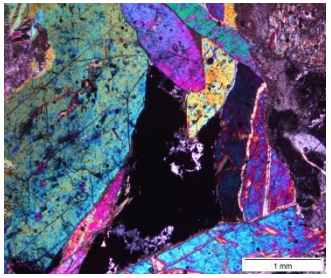

Appendix D:
Table 6: WE035 Polished Thin Section Descriptions

Sample Number WE035 (Interval in meters)	Major Minerals	Minor Minerals	Textures	Alteration and Degree of Alteration	% of Alteration	Reflected light observations	Other Features	Modal Abundance (%) & Rock Name.	Thin Section Picture
641.06m-641.32m	Olivine and Pyroxenes (Opx and Cpx)	Feldspars (plagioclase and orthoclase), epidote, biotite, chlorite and sericite.	Olivine is subrounded with irregular fractures. Pyroxenes are mainly Opx subhedral with good cleavage. Plagioclase shows albite twinning and is mainly interstitial.	Chloritisation, sericitisation, epidotisation and biotitization.	10%	Minor disseminated magnetite.	Inclusion of plagioclase in pyroxenes (ophitic texture). Cpx rims Opx and Cpx is also rimmed or replaced by chlorite and epidote.	Feldspars (plagioclase and orthoclase): 15%, pyroxenes (Opx and Cpx): 75%, Olivine: 5%, biotite and, chlorite: 5% **Feldspathic Pyroxenite.**	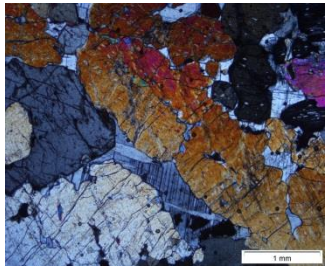
650.62m-650.82m	Pyroxenes (Opx and Cpx) and Olivine.	Chlorite, biotite, epidote, quartz and sericite.	Altered olivine subrounded with irregular fractures mainly filled with chlorite and epidote. Feldspars are completely altered sericite. Opx is rims olivine and is mainly subhedral or interstitial.	Chloritisation, sericitisation, serpentinisation, epidotisation and biotitization.	80%	Minor disseminated sulphides (chalcopyrite and pyrrhotite).	Veinlets and fractures filled with secondary material (sericite, serpentine and secondary magnetite). Pyroxenes are rimmed or replaced by chlorite or biotite.	Feldspars (plagioclase and, orthoclase): 15%, Pyroxene (Opx and cpx) 65%, Olivine: 15%, Quartz: 2%, chlorite and biotite: 3% **Granofels (feldspathic pyroxenite unit)**	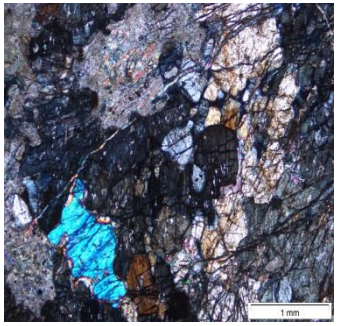
678.40m-678.65m	Pyroxenes (Opx and Cpx) and Olivine.	Chlorite, biotite, epidote, feldspars (plagioclase), quartz and sericite.	Olivine subrounded with irregular fractures. Pyroxenes are subhedral and have cleavage. Plagioclase show albite twinning and is mainly interstitial.	Chloritisation, sericitisation and biotitization.	15%	Minor disseminated magnetite seen along the boundaries of silicate minerals.	Veinlets and fractures filled with secondary material (sericite and secondary magnetite). Quartz is interstitial with undulose extinction.	Feldspars: 15%, Pyroxene (Opx and cpx) 75%, Quartz: 5%, chlorite and biotite: 5% **Granofels (feldspathic pyroxenite unit)**	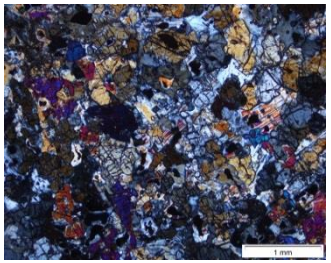

Appendix D: The Footwall
Table 7: WB027 Polished Thin Section Descriptions

Sample Number WB027 (Meter Intervals)	**Major Minerals**	**Minor Minerals**	**Texture**	**Alteration and Degree of Alteration**	**% of Alteration**	**Other Features**	**Modal Abundance (%) and Rock Name**	**Polished Thin Section Picture**
1171.10 m – 1171.30 m	Altered Cpx and Plagioclase.	Chlorite, Biotite and Sulphides.	Euhedral plagioclase and Cpx. Plagioclase showing normal twinning and Carlsbad twinning. Interlocking crystals.	Chloritisation and Seritization.	30%	Veinlets filled with secondary minerals (chlorite). Mostly minerals are extremely altered.	Plagioclase 45%, Cpx 40%, Chlorite 10%, Biotite 3% and Sulphides 2%. **Granofels**	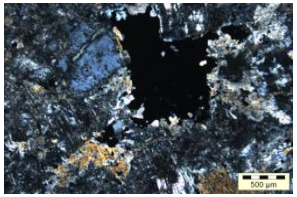
1171.90 m – 1172.15 m	Altered Cpx and Plagioclase.	Chlorite and Sulphides.	Euhedral plagioclase and Cpx, some Cpx crystals are interstitial. The Cpx is mostly altered. Plagioclase showing Carlsbad and normal twinning.	Chloritisation and Seritization. Chlorite is rimming the Altered Cpx crystals.	40%	Veinlets filled with secondary minerals (chlorite). Mostly minerals are extremely altered.	Plagioclase 45%, Cpx 40%, Chlorite 10% and Sulphides 5%. **Granofels**	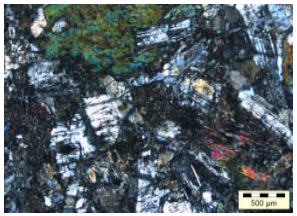
1173.10 m – 1173.40 m	Altered Cpx, Quartz and Plagioclase.	Chlorite and Sulphides.	Euhedral plagioclase and Cpx, some Cpx crystals are interstitial. The Cpx is mostly altered. Plagioclase showing Carlsbad and normal twinning.	Chloritisation and Seritization. Mostly of the Cpx crystals have been altered to sericite.	20%	The Quartz crystals have undulose extinction and are interlocking crystals.	Plagioclase 35%, Quartz 25%, Cpx 33%, Chlorite 5% and Sulphides 2%. **Granofels**	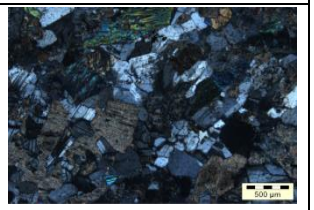
1180.40 m – 1180.48 m	Plagioclase, Quartz and Cpx.	Chlorite, biotite and Sulphides	Euhedral plagioclase crystals with interlocking quartz crystals. The Cpx are smaller euhedral crystals.	Chloritisation and Minor Seritization compared with other samples.	5%	The Quartz crystals have undulose extinction. Inclusion of sulphides in the plagioclase or on the grain boundaries.	Plagioclase 55%, Quartz 15%, Cpx 25%, Chlorite 2% and Sulphides 3%. **Granofels**	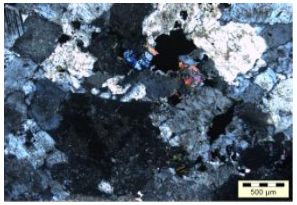

Appendix D: The Footwall

Table 7: WB027 Polished Thin Section Descriptions

Sample Number WE027 (Meter intervals)	**Major Minerals**	**Minor Minerals**	**Texture**	**Alteration and Degree of Alteration**	**% of Alteration**	**Other Features**	**Modal Abundance (%) and Rock Name**	**Polished Thin Section Picture**
1180.60 m – 1180.70 m	Plagioclase, Quartz and Cpx.	Chlorite, biotite and Sulphides	Euhedral Plagioclase crystals and interstitial quartz, with smaller euhedral Cpx crystal along the boundaries of the plagioclase. Interlocking texture between the crystals.	Chloritisation and minor Seritization	5%	The Quartz crystals have undulose extinction. Inclusion of sulphides in the plagioclase or on the grain boundaries.	Plagioclase 55%, Quartz 15%, Cpx 25%, Chlorite 2% and Sulphides 3%. **Granofels**	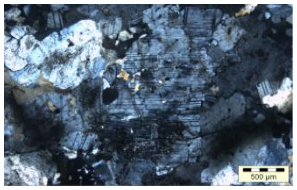

Appendix D: The Footwall and Sill

Table 8: WE001 Polished Thin Section Descriptions

Sample Number WE001 (Meter Intervals)	**Major Minerals**	**Minor Minerals**	**Texture**	**Alteration & Degree of Alteration**	**% of Alteration**	**Other Features**	**Modal Abundance (%) & Rock Name**	**Polished Thin Section Picture**
318.10 m - 318.30 m	Plagioclase and Cpx	Quartz, magnetite, biotite and chlorite	Interlocking crystals of plagioclase and Cpx. Euhedral crystals of plagioclase and Cpx.	Chloritisation, Serpentinisation and Seritization	20%	Interlocking Crystals. Chlorite rimming the altered Cpx crystals.	Plagioclase 40%, Cpx 35%, Quartz 10%, Biotite 3%, Chlorite 10%, and magnetite 2%. **Dolerite**	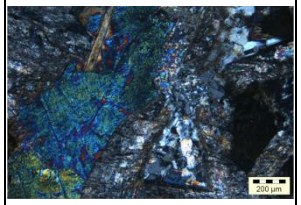
332.20 m - 332.34 m	Plagioclase, Opx, Cpx	Quartz, magnetite chlorite and biotite	Interlocking crystals of plagioclase in Cpx (ophitic texture). Euhedral plagioclase and Cpx crystals. Myrmekite texture.	Chloritisation, Serpentinisation and Seritization.	10%	Veinlets filled with secondary minerals (chlorite). Plagioclase with normal and Carlsbad twinning. Cpx rimmed by secondary minerals.	Plagioclase 40%, Cpx 30%, Opx 15%, Quartz 5%, Biotite 3%, Chlorite 5%, and magnetite 2%. **Dolerite**	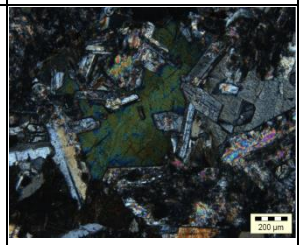
816.80 m - 817.00 m	Quartz, Cpx, Clay minerals & lithic fragments.	Magnetite and chlorite.	Interlocking crystals of Quartz and Cpx. Euhedral Cpx and Quartz crystals	Minor Chloritisation and Seritization.	10%	Veinlets filled with crystals of Cpx and Quartz, Chill margin and surrounding fine grained minerals	Quartz 25%, Cpx 25%, Clay minerals 15%, lithic fragments 15% and Chlorite 10%. Extremely fine grained minerals. **Granofels**	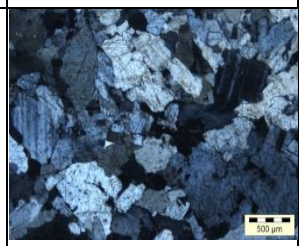
830.90 m	Plagioclase, Quartz, Cpx, Opx, Clay minerals & lithic fragments	Sulphides and chlorite	Interlocking crystals of plagioclase, quartz and pyroxenes. Equigranular with larger Opx grains. Foliated texture.	Minor Chloritisation and Seritization	10%	Veinlets filled with secondary minerals (chlorite). Interlocking crystals. Plagioclase showing normal twinning.	Plagioclase 40%, Cpx 25%, Opx 15%, Quartz 15%, chlorite 3% and sulphides 2%. **Granofels**	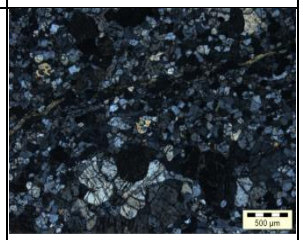

Appendix D: The Footwall and Sill

Table 8: WE001 Polished Thin Section Descriptions

Sample Number WE001 (Meter Intervals)	**Major Minerals**	**Minor Minerals**	**Texture**	**Alteration & Degree of Alteration**	**% of Alteration**	**Other Features**	**Modal Abundance (%) & Rock Name**	**Polished Thin Section Picture**
835.05 m - 835.15 m	Quartz and Plagioclase	Chlorite	Euhedral plag and quartz crystals, with interlocking texture.	Minor Chloritisation and Seritization	5%	Undulose extinction quartz crystals and veinlets cross cutting different minerals	Quartz 30%, Plagioclase 25%, Sericite 35% and Chlorite 5%. **Quartzite**	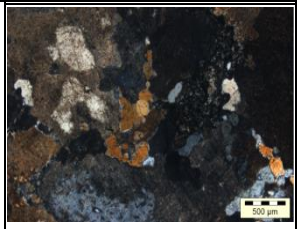

Appendix D: The Footwall

Table 9: WE002 Polished thin Section Descriptions

Sample Number WE002 (Meter interval)	**Major minerals**	**Minor Minerals**	**Textures**	**Alteration and Degree of Alteration**	**% of Alteration**	**Other Features**	**Modal Abundance (%) and Rock Name**	**Thin Section Picture**
677.75 m - 678.05 m	Olivine, Cpx and plagioclase	Chlorite, Biotite, and Sulphides	Subrounded olivine crystals, Euhedral Cpx and plag. Plag is also interstitial. The Olivine crystals show randomly orientated cracks.	Chloritisation and Seritization	30%	Inclusion of sulphides in the olivine crystals. Veinlet filled with secondary minerals (chlorite & biotite).	Olivine 22%, Plagioclase 30%, Cpx 30%, Biotite 5%, Chlorite 10% and sulphides 3%. **Olivine bearing Gabbro**	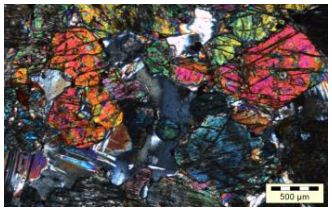
685.14 m - 685.52 m	Quartz, Cpx, Opx Plagioclase and microcline	Chlorite and Sulphides	Euhedral Plagioclase Cpx and Opx crystals, interstitial Quartz.	Minor Seritization	5%	Sulphides and Quartz crystals interstitial, Quartz with undulose extinction and some quartz crystals are euhedral with an interlocking texture with other crystals	Cpx 25%, Opx 30%, Plagioclase 25%, microcline 5%, Quartz 12% and Sulphides 3%. **Granofels**	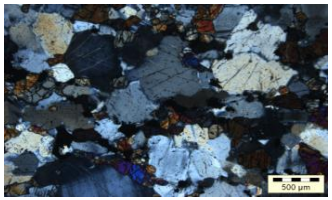
701.15 m - 701.30 m	Plagioclase, Cpx and Quartz	Sericite	Euhedral Plagioclase crystals with twinning. Cpx is extremely altered with poikilitic texture.	Minor Seritization	5%	Interstitial Quartz with undulose extinction. The crystals are interlocking.	Plagioclase 50%, Cpx 30%, Quartz 15% and 5% sericite. **Granofels**	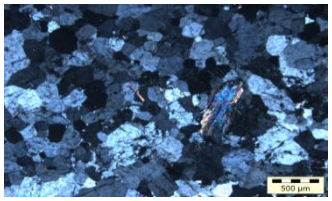

Appendix D: The Sill

Table 10: WE003 Polished Thin Section Descriptions

Sample Number WE003 (Meter intervals)	**Major Minerals**	**Minor Minerals**	**Textures**	**Alteration and degree of alteration**	**% of Alteration**	**Other Features**	**Modal Abundance (%) and Rock Name**	**Polished Thin Section Picture**
294.00 m – 294.10 m. Sample from the top of the Sill.	Plagioclase, Quartz and Cpx.	Chlorite, magnetite, and biotite.	Elongate, euhedral (needle-like) plagioclase crystals, Myrmekite texture plag & Quartz. Quartz with undulose extinction. Cpx extremely altered. Ophitic texture.	Minor Biotite, Chloritisation and Seritization	20%	Veinlets filled with secondary minerals (chlorite and biotite).	Plagioclase 40%, Altered Cpx 35%, Quartz 10%, Chlorite 10% and Biotite 5%. **Dolerite**	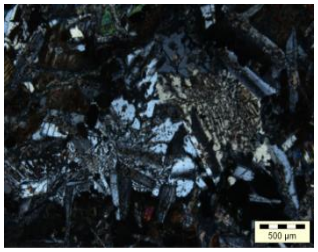
300.70 m – 300.80 m. Transition to pink facies	Plagioclase, Quartz and Cpx.	Chlorite, magnetite and biotite.	Euhedral plagioclase crystals, interstitial quartz, intergrowth Myrmekite texture (graphic texture). Quartz undulose extinction and the Cpx is mostly altered	Minor Biotite, Chloritisation and Seritization.	30%	Veinlets filled with secondary minerals (chlorite and biotite). The secondary minerals also rim the Cpx crystals	Plagioclase 40%, Altered Cpx 30%, Quartz 5%, Chlorite 15% and Biotite 10%. **Dolerite**	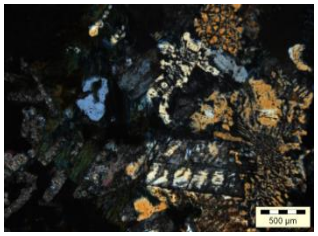
308.40 m – 308.55 m. Coarse-grained pink facies	Plagioclase, Quartz and Cpx.	Chlorite and biotite.	Euhedral plagioclase crystals with Carlsbad twinning, interstitial quartz, intergrowth Myrmekite texture. Quartz undulose extinction and the Cpx is mostly altered	Minor Biotite, Chloritisation and Seritization.	25%	Veinlets filled with secondary minerals (chlorite and biotite). The secondary minerals also rim the Cpx crystals	Plagioclase 45%, Altered Cpx 35%, Quartz 5%, Chlorite 8% and Biotite 7%. **Dolerite**	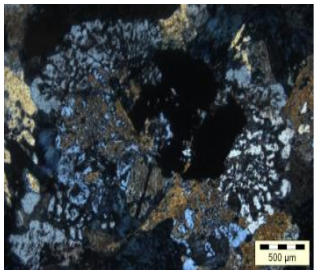

Appendix D: The Sill

Table 10: WE003 Polished Thin Section Descriptions

326.00 m – 326.10 m.	Plagioclase, Quartz and Cpx.	Chlorite, magnetite and biotite.	Euhedral plagioclase and Cpx crystals. Myrmekite texture. Elongated plagioclase crystals.	Minor Biotite, Chloritisation and Seritization.	20%	Most of the Cpx crystals have been altered and there is chlorite rimming most of the Cpx crystals.	Plagioclase 50%, Cpx 30%, Quartz 10%, Chlorite 5%, Biotite 3% and magnetite 2%. **Dolerite**	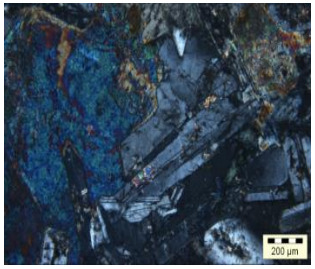

Appendix D: The Footwall

Table 11: WE005 Polished Thin Section Descriptions

Sample Number WE005 (Meter Interval).	**Major Minerals.**	**Minor Minerals.**	**Texture.**	**Alteration and Degree of Alteration.**	**% of Alteration**	**Other Features.**	**Modal Abundance (%) and Rock Name.**	**Polished Thin section Pictures.**
328.55 m	Quartz, Lithic Fragments and Clay Minerals.	Chlorite, Magnetite and Altered Cpx Fragments	Phenocrysts of Quartz, surrounded by an extremely fine-grained groundmass (porphyritic texture).	Seritization and most of the groundmass is too small to identify	10%	Quartz has undulose extinction. Magnetite is secondary rims the altered Cpx.	Quartz 35%, Lithic Fragments and Groundmass 45%, Magnetite 10%, Chlorite 5%, Clay Minerals 5% . **Granofels**	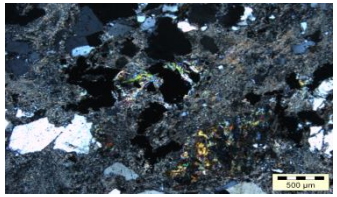
330.83 m	Quartz, Lithic Fragments and Clay Minerals.	Chlorite and sericite.	Large phenocrysts of Quartz interlocking with other Quartz crystals.	Seritization and most of the groundmass is too small to identify	15%	Quartz has undulose extinction. Veinlets filled with secondary minerals (sericite and chlorite). Chlorite rimming some extremely altered minerals.	Quartz 40%, Lithic Fragments and Groundmass 54%, Chlorite 3% and Clay Minerals 3%. **Granofels**	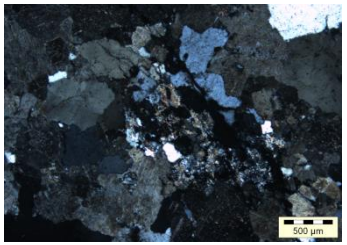
375.12 m	Quartz, plagioclase, Lithic fragments	Chlorite, tremolite and sericite	Large euhedral plagioclase and quartz interlocking crystals.	Seritization and Chloritisation	5%	Quartz has undulose extinction. Veinlets filled with secondary minerals (sericite and chlorite).	Quartz 35%, plagioclase 35%, Lithic Fragments and Groundmass 17%, Chlorite 5%, Sulphides 3% and Tremolite 5%. **Granite**	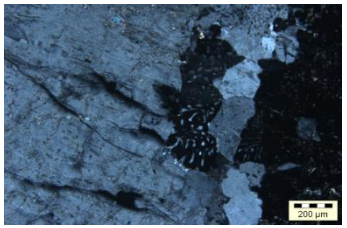

Appendix D: The Footwall

Table 11: WE005 Polished Thin Section Descriptions

420.05 m	Quartz, Plagioclase and Lithic Fragments	Chlorite, tremolite and Sulphides	Graphic texture. Large phenocrysts of quartz and plagioclase surrounded by a fine-grained groundmass.	Seritization and most of the groundmass is too small to identify, most of the plagioclase is altered but in area normal twinning is visible.	10%	Veinlets filled with secondary minerals (sericite). Inclusions of sulphides in the interlocking Quartz crystals.	Quartz 35%, plagioclase 25%, Lithic Fragments and Groundmass 30%, Chlorite 5%, Sulphides 3% and Tremolite 2%. **Granite**	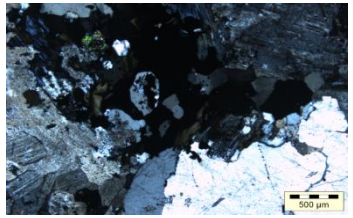

Appendix E

Magnetic Susceptibility

WB017D0

WB027D0

WB099D0

WE001D0

WE027D0

WE035D0

LAP 31 Aurora Project

Appendix E: Magnetic Susceptibility
Table 1: Borehole WB017D0

Depth (m)	Av. 3 Values	Depth (m)	Av. 3 Values	Depth (m)	Av. 3 Values	Depth (m)	Av. 3 Values	Depth (m)	Av. 3 Values	Depth (m)	Av. 3 Values	Depth (m)	Av. 3 Values
174.0	0.01	190.0	0.32	206.0	0.20	222.0	0.78	238.0	0.80	254.0	3.13	270.0	0.60
174.5	0.01	190.5	0.40	206.5	0.36	222.5	0.49	238.5	1.09	254.5	0.28	270.5	0.78
175.0	0.01	191.0	0.54	207.0	0.24	223.0	0.44	239.0	0.21	255.0	0.44	271.0	0.30
175.5	0.01	191.5	0.25	207.5	0.85	223.5	0.49	239.5	0.59	255.5	0.54	271.5	0.64
176.0	0.01	192.0	0.51	208.0	0.60	224.0	0.30	240.0	1.25	256.0	0.45	272.0	0.00
176.5	0.00	192.5	0.48	208.5	0.45	224.5	0.67	240.5	0.29	256.5	0.19	272.5	0.78
177.0	0.00	193.0	0.84	209.0	0.00	225.0	0.37	241.0	0.48	257.0	0.41	273.0	0.52
177.5	0.00	193.5	0.35	209.5	0.00	225.5	0.43	241.5	0.39	257.5	0.33	273.5	0.57
178.0	0.00	194.0	0.00	210.0	0.28	226.0	0.59	242.0	0.77	258.0	0.52	274.0	0.27
178.5	0.24	194.5	0.00	210.5	0.24	226.5	0.53	242.5	0.31	258.5	0.58	274.5	0.51
179.0	1.23	195.0	0.60	211.0	0.49	227.0	0.35	243.0	0.57	259.0	0.55	275.0	0.31
179.5	0.90	195.5	0.47	211.5	0.29	227.5	0.52	243.5	0.36	259.5	0.50	275.5	0.60
180.0	0.76	196.0	0.46	212.0	0.44	228.0	0.31	244.0	0.66	260.0	0.71	276.0	0.50
180.5	1.29	196.5	0.40	212.5	0.30	228.5	0.32	244.5	0.24	260.5	0.20	276.5	0.35
181.0	1.55	197.0	0.33	213.0	0.38	229.0	0.56	245.0	0.41	261.0	0.36	277.0	0.55
181.5	1.51	197.5	0.44	213.5	0.62	229.5	0.51	245.5	0.34	261.5	0.36	277.5	0.60
182.0	1.29	198.0	0.47	214.0	0.57	230.0	0.60	246.0	0.32	262.0	0.19	278.0	0.01
182.5	1.63	198.5	0.67	214.5	0.37	230.5	0.34	246.5	0.08	262.5	0.27	278.5	0.74
183.0	0.00	199.0	0.57	215.0	0.37	231.0	0.53	247.0	0.42	263.0	0.16	279.0	1.45
183.5	0.00	199.5	0.70	215.5	0.35	231.5	0.32	247.5	0.31	263.5	0.36	279.5	0.51
184.0	0.49	200.0	0.56	216.0	0.42	232.0	0.53	248.0	0.47	264.0	0.19	280.0	0.74
184.5	0.52	200.5	0.05	216.5	0.39	232.5	0.39	248.5	0.46	264.5	0.10	280.5	0.06
185.0	0.37	201.0	0.45	217.0	0.37	233.0	0.27	249.0	0.68	265.0	0.82	281.0	0.81
185.5	0.40	201.5	0.39	217.5	0.67	233.5	0.43	249.5	0.50	265.5	0.71	281.5	0.50
186.0	0.64	202.0	0.34	218.0	0.72	234.0	0.37	250.0	0.82	266.0	0.56	282.0	0.28
186.5	0.50	202.5	0.74	218.5	0.54	234.5	0.40	250.5	0.37	266.5	0.88	282.5	0.47
187.0	0.45	203.0	0.62	219.0	0.69	235.0	0.37	251.0	0.42	267.0	0.90	283.0	1.14
187.5	0.33	203.5	0.45	219.5	0.56	235.5	0.49	251.5	0.28	267.5	0.53	283.5	0.96
188.0	0.25	204.0	0.47	220.0	0.64	236.0	0.30	252.0	0.19	268.0	0.45	284.0	0.70
188.5	0.28	204.5	0.37	220.5	0.37	236.5	0.24	252.5	0.27	268.5	1.04	284.5	0.78
189.0	0.00	205.0	0.21	221.0	0.68	237.0	0.19	253.0	0.30	269.0	0.56	285.0	1.18
189.5	0.00	205.5	0.44	221.5	0.72	237.5	0.41	253.5	0.50	269.5	0.53	285.5	0.92

Appendix E: Magnetic Susceptibility
Table 1: Borehole WB017D0

Depth (m)	Av. 3 Values	Depth (m)	Av. 3 Values	Depth (m)	Av. 3 Values	Depth (m)	Av. 3 Values	Depth (m)	Av. 3 Values	Depth (m)	Av. 3 Values	Depth (m)	Av. 3 Values
286.0	0.53	302.0	0.60	318.0	0.20	334.0	0.51	350.0	0.56	366.0	0.68	382.0	0.33
286.5	0.32	302.5	0.54	318.5	0.78	334.5	0.19	350.5	0.28	366.5	0.39	382.5	0.50
287.0	0.40	303.0	0.77	319.0	1.31	335.0	0.51	351.0	1.20	367.0	1.84	383.0	0.28
287.5	0.01	303.5	0.47	319.5	0.68	335.5	1.11	351.5	0.47	367.5	0.20	383.5	0.49
288.0	0.00	304.0	0.20	320.0	0.33	336.0	0.15	352.0	0.27	368.0	0.31	384.0	0.57
288.5	0.01	304.5	0.28	320.5	0.02	336.5	0.30	352.5	0.27	368.5	0.50	384.5	0.50
289.0	0.00	305.0	0.28	321.0	2.12	337.0	0.05	353.0	0.26	369.0	0.30	385.0	0.54
289.5	0.00	305.5	0.24	321.5	0.56	337.5	1.18	353.5	0.01	369.5	0.29	385.5	0.24
290.0	0.00	306.0	0.10	322.0	2.42	338.0	0.04	354.0	0.01	370.0	0.13	386.0	0.74
290.5	0.02	306.5	0.02	322.5	0.33	338.5	2.06	354.5	0.22	370.5	0.39	386.5	0.47
291.0	5.29	307.0	0.22	323.0	0.03	339.0	0.54	355.0	0.11	371.0	0.67	387.0	0.29
291.5	0.07	307.5	0.31	323.5	0.20	339.5	0.16	355.5	0.36	371.5	0.80	387.5	0.04
292.0	0.03	308.0	0.46	324.0	0.02	340.0	0.76	356.0	0.48	372.0	0.85	388.0	0.13
292.5	0.89	308.5	0.30	324.5	2.58	340.5	1.02	356.5	0.53	372.5	0.90	388.5	0.21
293.0	0.07	309.0	0.22	325.0	0.37	341.0	1.07	357.0	0.32	373.0	0.45	389.0	0.90
293.5	0.48	309.5	0.32	325.5	0.03	341.5	0.36	357.5	0.08	373.5	0.80	389.5	0.45
294.0	1.22	310.0	0.23	326.0	0.01	342.0	0.17	358.0	0.00	374.0	0.28	390.0	0.84
294.5	0.25	310.5	0.38	326.5	4.34	342.5	0.50	358.5	0.61	374.5	0.47	390.5	1.07
295.0	0.02	311.0	0.01	327.0	1.67	343.0	1.58	359.0	0.74	375.0	0.20	391.0	0.03
295.5	2.29	311.5	0.01	327.5	3.91	343.5	0.20	359.5	0.30	375.5	0.33	391.5	0.08
296.0	0.39	312.0	0.01	328.0	0.21	344.0	0.96	360.0	0.25	376.0	0.55	392.0	0.03
296.5	0.33	312.5	0.14	328.5	0.00	344.5	0.19	360.5	0.23	376.5	0.48	392.5	0.22
297.0	0.31	313.0	0.00	329.0	0.03	345.0	1.13	361.0	0.24	377.0	0.35	393.0	0.38
297.5	0.78	313.5	0.21	329.5	1.79	345.5	0.09	361.5	0.17	377.5	0.21	393.5	0.16
298.0	0.78	314.0	0.48	330.0	3.55	346.0	0.48	362.0	0.17	378.0	0.18	394.0	0.17
298.5	0.56	314.5	1.07	330.5	0.26	346.5	0.41	362.5	0.21	378.5	0.55	394.5	0.09
299.0	0.22	315.0	0.25	331.0	0.33	347.0	0.18	363.0	0.13	379.0	0.13	395.0	0.05
299.5	1.16	315.5	0.28	331.5	0.05	347.5	0.68	363.5	0.36	379.5	0.07	395.5	0.05
300.0	0.63	316.0	2.42	332.0	0.02	348.0	0.71	364.0	0.31	380.0	0.00	396.0	0.03
300.5	1.11	316.5	5.11	332.5	0.00	348.5	0.37	364.5	0.25	380.5	0.32	396.5	0.02
301.0	0.82	317.0	0.05	333.0	0.70	349.0	0.71	365.0	0.08	381.0	0.51	397.0	0.06
301.5	0.92	317.5	0.25	333.5	0.33	349.5	1.10	365.5	0.15	381.5	1.29	397.5	0.02

Appendix E: Magnetic Susceptibility
Table 1: Borehole WB017D0

Depth (m)	Av. 3 Values	Depth (m)	Av. 3 Values	Depth (m)	Av. 3 Values	Depth (m)	Av. 3 Values	Depth (m)	Av. 3 Values	Depth (m)	Av. 3 Values	Depth (m)	Av. 3 Values
398.0	0.03	414.0	0.00	430.0	0.21	446.0	0.37	462.0	0.15	478.0	0.96	494.0	1.04
398.5	0.04	414.5	0.29	430.5	0.49	446.5	0.16	462.5	0.08	478.5	0.71	494.5	0.00
399.0	0.03	415.0	0.34	431.0	0.41	447.0	0.00	463.0	0.15	479.0	0.09	495.0	0.76
399.5	0.00	415.5	0.46	431.5	0.18	447.5	0.54	463.5	0.21	479.5	0.00	495.5	1.65
400.0	0.00	416.0	0.20	432.0	0.16	448.0	0.72	464.0	0.04	480.0	0.05	496.0	0.59
400.5	0.00	416.5	0.69	432.5	4.78	448.5	0.32	464.5	0.27	480.5	0.56	496.5	0.71
401.0	0.00	417.0	0.46	433.0	0.15	449.0	0.43	465.0	0.33	481.0	0.00	497.0	0.87
401.5	0.08	417.5	0.09	433.5	0.03	449.5	0.78	465.5	0.26	481.5	0.17	497.5	1.13
402.0	0.05	418.0	0.12	434.0	0.08	450.0	0.44	466.0	0.46	482.0	0.21	498.0	1.70
402.5	0.24	418.5	0.16	434.5	0.15	450.5	0.73	466.5	0.47	482.5	0.32	498.5	0.57
403.0	0.18	419.0	0.29	435.0	0.37	451.0	0.45	467.0	0.10	483.0	0.12	499.0	1.09
403.5	0.76	419.5	0.13	435.5	0.02	451.5	0.24	467.5	0.12	483.5	0.08	499.5	0.00
404.0	0.18	420.0	0.15	436.0	0.08	452.0	0.21	468.0	0.50	484.0	0.16	500.0	0.88
404.5	0.53	420.5	0.42	436.5	0.41	452.5	0.00	468.5	0.11	484.5	0.80	500.5	1.42
405.0	0.19	421.0	0.13	437.0	0.22	453.0	0.27	469.0	0.67	485.0	0.00	501.0	0.59
405.5	0.14	421.5	0.10	437.5	0.24	453.5	0.43	469.5	0.01	485.5	0.18	501.5	0.48
406.0	0.46	422.0	0.03	438.0	0.04	454.0	1.62	470.0	0.04	486.0	0.13	502.0	1.40
406.5	0.47	422.5	0.26	438.5	0.05	454.5	1.06	470.5	0.01	486.5	0.13	502.5	0.30
407.0	0.28	423.0	0.01	439.0	0.02	455.0	0.51	471.0	0.00	487.0	0.27	503.0	0.18
407.5	0.36	423.5	0.03	439.5	0.02	455.5	0.49	471.5	0.00	487.5	0.00	503.5	0.03
408.0	0.34	424.0	0.52	440.0	0.25	456.0	0.42	472.0	0.00	488.0	0.36	504.0	1.19
408.5	0.68	424.5	0.58	440.5	0.13	456.5	0.71	472.5	0.00	488.5	0.16	504.5	0.12
409.0	0.08	425.0	0.52	441.0	0.08	457.0	0.07	473.0	0.00	489.0	0.00	505.0	0.00
409.5	0.13	425.5	0.12	441.5	0.38	457.5	0.00	473.5	0.00	489.5	0.00	505.5	1.40
410.0	0.00	426.0	0.14	442.0	0.48	458.0	1.00	474.0	0.00	490.0	0.00	506.0	0.77
410.5	0.30	426.5	0.54	442.5	0.18	458.5	1.35	474.5	0.02	490.5	0.36	506.5	1.35
411.0	0.44	427.0	0.15	443.0	0.01	459.0	0.42	475.0	0.11	491.0	2.31	507.0	2.09
411.5	0.03	427.5	0.17	443.5	0.53	459.5	0.96	475.5	0.00	491.5	0.00	507.5	0.00
412.0	0.00	428.0	0.40	444.0	0.30	460.0	0.46	476.0	0.28	492.0	0.00	508.0	1.07
412.5	0.00	428.5	0.36	444.5	0.21	460.5	0.26	476.5	0.21	492.5	0.00	508.5	0.18
413.0	0.00	429.0	0.33	445.0	0.74	461.0	0.29	477.0	0.03	493.0	0.00	509.0	0.00
413.5	0.00	429.5	0.32	445.5	0.56	461.5	0.25	477.5	0.08	493.5	0.00	509.5	0.00

Appendix E: Magnetic Susceptibility
Table 1: Borehole WB017D0

Depth (m)	Av. 3 Values	Depth (m)	Av. 3 Values	Depth (m)	Av. 3 Values	Depth (m)	Av. 3 Values	Depth (m)	Av. 3 Values	Depth (m)	Av. 3 Values	Depth (m)	Av. 3 Values
510.0	0.17	526.0	0.00	542.0	0.26	558.0	0.00	574.0	0.00	590.0	0.00	606.0	0.05
510.5	3.49	526.5	0.03	542.5	0.01	558.5	0.00	574.5	0.00	590.5	0.00	606.5	0.03
511.0	0.03	527.0	0.20	543.0	0.00	559.0	0.00	575.0	0.00	591.0	0.00	607.0	0.06
511.5	0.00	527.5	0.08	543.5	0.24	559.5	0.00	575.5	0.00	591.5	0.07	607.5	0.04
512.0	0.09	528.0	0.04	544.0	0.00	560.0	0.00	576.0	0.00	592.0	1.03	608.0	0.08
512.5	0.06	528.5	0.00	544.5	0.00	560.5	0.00	576.5	0.00	592.5	0.68	608.5	0.67
513.0	0.03	529.0	0.00	545.0	0.00	561.0	0.00	577.0	0.01	593.0	0.20	609.0	0.01
513.5	0.00	529.5	0.00	545.5	0.00	561.5	0.00	577.5	0.41	593.5	0.00	609.5	0.02
514.0	1.06	530.0	0.22	546.0	0.18	562.0	0.00	578.0	5.52	594.0	0.00	610.0	0.00
514.5	0.00	530.5	0.00	546.5	0.00	562.5	0.00	578.5	0.40	594.5	0.00	610.5	0.00
515.0	0.08	531.0	0.02	547.0	0.19	563.0	0.00	579.0	1.55	595.0	0.00	611.0	0.00
515.5	0.02	531.5	0.01	547.5	0.10	563.5	0.00	579.5	0.00	595.5	1.33	611.5	0.04
516.0	0.04	532.0	0.03	548.0	0.00	564.0	0.00	580.0	0.00	596.0	1.62	612.0	0.02
516.5	0.01	532.5	0.00	548.5	1.16	564.5	0.00	580.5	0.12	596.5	0.00	612.5	0.01
517.0	0.00	533.0	0.02	549.0	0.00	565.0	0.00	581.0	0.52	597.0	0.00	613.0	0.03
517.5	0.07	533.5	0.02	549.5	0.00	565.5	0.00	581.5	0.29	597.5	0.04	613.5	0.01
518.0	0.00	534.0	0.01	550.0	0.38	566.0	0.00	582.0	0.35	598.0	0.14	614.0	0.00
518.5	0.02	534.5	0.00	550.5	3.01	566.5	0.00	582.5	0.88	598.5	0.97	614.5	0.00
519.0	0.41	535.0	0.00	551.0	0.65	567.0	0.00	583.0	0.00	599.0	0.17	615.0	0.04
519.5	0.01	535.5	0.00	551.5	0.32	567.5	0.00	583.5	0.00	599.5	0.15	615.5	0.67
520.0	0.00	536.0	0.00	552.0	1.61	568.0	0.00	584.0	0.02	600.0	0.03	616.0	0.01
520.5	0.00	536.5	0.00	552.5	2.24	568.5	0.00	584.5	0.04	600.5	0.02	616.5	0.03
521.0	0.06	537.0	0.02	553.0	0.10	569.0	0.00	585.0	0.00	601.0	0.40	617.0	0.02
521.5	0.00	537.5	0.00	553.5	0.31	569.5	0.00	585.5	0.05	601.5	0.00	617.5	0.02
522.0	0.31	538.0	0.00	554.0	0.07	570.0	0.00	586.0	0.05	602.0	0.00	618.0	0.27
522.5	0.00	538.5	0.00	554.5	0.26	570.5	0.00	586.5	0.05	602.5	0.07	618.5	0.00
523.0	0.01	539.0	0.00	555.0	0.59	571.0	0.00	587.0	0.06	603.0	0.10	619.0	1.55
523.5	0.25	539.5	0.56	555.5	0.02	571.5	0.00	587.5	0.18	603.5	0.00	619.5	0.07
524.0	0.06	540.0	10.90	556.0	0.00	572.0	0.00	588.0	0.08	604.0	0.06	620.0	0.02
524.5	0.00	540.5	0.03	556.5	0.00	572.5	0.00	588.5	0.14	604.5	0.05	620.5	0.30
525.0	0.17	541.0	0.45	557.0	0.00	573.0	0.00	589.0	0.03	605.0	0.31	621.0	0.00
525.5	0.09	541.5	13.27	557.5	0.00	573.5	0.00	589.5	0.08	605.5	0.53	621.5	0.20

Appendix E: Magnetic Susceptibility
Table 1: Borehole WB017D0

Depth (m)	Av. 3 Values	Depth (m)	Av. 3 Values	Depth (m)	Av. 3 Values	Depth (m)	Av. 3 Values	Depth (m)	Av. 3 Values	Depth (m)	Av. 3 Values	Depth (m)	Av. 3 Values
622.0	0.00	638.0	0.03	654.0	0.47	670.0	0.79	686.0	0.02	702.0	0.00	718.0	0.07
622.5	0.00	638.5	0.00	654.5	1.36	670.5	0.01	686.5	0.01	702.5	0.00	718.5	0.12
623.0	0.00	639.0	0.26	655.0	0.53	671.0	0.01	687.0	0.00	703.0	0.00	719.0	0.11
623.5	0.00	639.5	0.45	655.5	0.14	671.5	0.00	687.5	0.01	703.5	0.00	719.5	0.05
624.0	0.00	640.0	0.45	656.0	0.00	672.0	0.01	688.0	0.01	704.0	0.00	720.0	0.02
624.5	0.00	640.5	0.30	656.5	0.00	672.5	0.00	688.5	0.01	704.5	0.00	720.5	0.03
625.0	0.02	641.0	0.14	657.0	0.00	673.0	0.00	689.0	0.01	705.0	0.00	721.0	0.03
625.5	0.01	641.5	0.00	657.5	0.00	673.5	0.01	689.5	0.00	705.5	0.00	721.5	0.04
626.0	0.00	642.0	0.45	658.0	0.00	674.0	0.00	690.0	0.01	706.0	0.00	722.0	0.02
626.5	0.00	642.5	0.39	658.5	0.00	674.5	0.00	690.5	0.04	706.5	0.00	722.5	0.01
627.0	0.00	643.0	0.14	659.0	0.00	675.0	0.01	691.0	0.01	707.0	0.00	723.0	0.01
627.5	1.37	643.5	0.68	659.5	0.00	675.5	0.01	691.5	0.00	707.5	0.00	723.5	0.01
628.0	0.00	644.0	0.54	660.0	0.00	676.0	0.01	692.0	0.00	708.0	0.00	724.0	0.03
628.5	0.22	644.5	0.44	660.5	0.00	676.5	0.01	692.5	0.00	708.5	0.00	724.5	0.00
629.0	0.37	645.0	0.78	661.0	0.02	677.0	0.01	693.0	0.00	709.0	0.00	725.0	0.01
629.5	0.35	645.5	0.15	661.5	4.51	677.5	0.01	693.5	0.01	709.5	0.00	725.5	0.01
630.0	0.29	646.0	0.44	662.0	0.86	678.0	0.00	694.0	0.00	710.0	0.00	726.0	0.00
630.5	0.22	646.5	0.32	662.5	0.00	678.5	0.03	694.5	0.00	710.5	0.00	726.5	0.03
631.0	0.32	647.0	0.38	663.0	0.00	679.0	0.01	695.0	0.00	711.0	0.00	727.0	0.01
631.5	0.39	647.5	0.53	663.5	0.00	679.5	0.02	695.5	0.00	711.5	0.00	727.5	0.01
632.0	0.00	648.0	0.97	664.0	0.64	680.0	0.02	696.0	0.00	712.0	0.00	728.0	0.01
632.5	0.00	648.5	0.52	664.5	0.00	680.5	0.01	696.5	0.00	712.5	0.00	728.5	0.01
633.0	0.00	649.0	1.16	665.0	0.00	681.0	0.02	697.0	0.00	713.0	0.00	729.0	0.01
633.5	0.01	649.5	1.54	665.5	0.00	681.5	0.01	697.5	0.00	713.5	0.00	729.5	0.06
634.0	0.52	650.0	1.09	666.0	0.00	682.0	0.01	698.0	0.00	714.0	0.01	730.0	0.05
634.5	0.76	650.5	0.63	666.5	0.00	682.5	0.01	698.5	0.00	714.5	0.07	730.5	0.03
635.0	1.48	651.0	0.59	667.0	0.00	683.0	0.01	699.0	0.00	715.0	0.17	731.0	0.02
635.5	0.08	651.5	0.85	667.5	0.00	683.5	0.01	699.5	0.00	715.5	0.14	731.5	0.03
636.0	0.00	652.0	1.56	668.0	0.00	684.0	0.02	700.0	0.00	716.0	0.13	732.0	0.01
636.5	0.63	652.5	0.91	668.5	0.00	684.5	0.01	700.5	0.00	716.5	0.11	732.5	0.08
637.0	0.47	653.0	2.76	669.0	0.00	685.0	0.00	701.0	0.00	717.0	0.14	733.0	0.02
637.5	0.01	653.5	0.22	669.5	3.25	685.5	0.00	701.5	0.00	717.5	0.07	733.5	0.03

Appendix E: Magnetic Susceptibility
Table 1: Borehole WB017D0

Depth (m)	Av. 3 Values	Depth (m)	Av. 3 Values	Depth (m)	Av. 3 Values	Depth (m)	Av. 3 Values	Depth (m)	Av. 3 Values	Depth (m)	Av. 3 Values	Depth (m)	Av. 3 Values
734.0	0.03	750.0	0.02	766.0	0.00	782.0	0.02	798.0	0.03	814.0	0.02	830.0	0.00
734.5	0.07	750.5	0.02	766.5	0.01	782.5	0.15	798.5	0.04	814.5	0.01	830.5	0.01
735.0	0.03	751.0	0.04	767.0	0.01	783.0	0.02	799.0	0.04	815.0	0.02	831.0	0.01
735.5	0.02	751.5	0.01	767.5	0.03	783.5	0.03	799.5	0.04	815.5	0.01	831.5	0.00
736.0	0.02	752.0	0.01	768.0	0.02	784.0	0.02	800.0	0.01	816.0	0.01	832.0	0.00
736.5	0.02	752.5	0.01	768.5	0.00	784.5	0.01	800.5	0.02	816.5	0.01	832.5	0.01
737.0	0.04	753.0	0.03	769.0	0.00	785.0	0.00	801.0	0.01	817.0	0.01	833.0	0.01
737.5	0.04	753.5	0.03	769.5	0.01	785.5	0.01	801.5	0.04	817.5	0.02	833.5	0.03
738.0	0.04	754.0	0.09	770.0	0.01	786.0	0.00	802.0	0.06	818.0	0.01	834.0	0.00
738.5	0.04	754.5	0.04	770.5	0.01	786.5	0.02	802.5	0.02	818.5	0.01	834.5	0.01
739.0	0.07	755.0	0.05	771.0	0.01	787.0	0.03	803.0	0.01	819.0	0.01	835.0	0.01
739.5	0.04	755.5	0.04	771.5	0.02	787.5	0.01	803.5	0.01	819.5	0.01	835.5	0.01
740.0	0.05	756.0	0.03	772.0	0.01	788.0	0.01	804.0	0.02	820.0	0.02	836.0	0.01
740.5	0.03	756.5	0.03	772.5	0.03	788.5	0.01	804.5	0.01	820.5	0.02	836.5	0.00
741.0	0.06	757.0	0.04	773.0	0.00	789.0	0.01	805.0	0.02	821.0	0.01	837.0	0.00
741.5	0.07	757.5	0.02	773.5	0.01	789.5	0.03	805.5	0.01	821.5	0.01	837.5	0.00
742.0	0.05	758.0	0.02	774.0	0.01	790.0	0.07	806.0	0.01	822.0	0.00	838.0	0.00
742.5	0.04	758.5	0.02	774.5	0.01	790.5	0.04	806.5	0.00	822.5	0.01	838.5	0.00
743.0	0.06	759.0	0.02	775.0	0.01	791.0	0.06	807.0	0.00	823.0	0.01	839.0	0.00
743.5	0.41	759.5	0.03	775.5	0.02	791.5	0.07	807.5	0.00	823.5	0.01	839.5	0.00
744.0	0.00	760.0	0.02	776.0	0.01	792.0	0.06	808.0	0.01	824.0	0.01	840.0	0.00
744.5	0.02	760.5	0.02	776.5	0.01	792.5	0.05	808.5	0.01	824.5	0.01	840.5	0.00
745.0	0.02	761.0	0.01	777.0	0.01	793.0	0.02	809.0	0.02	825.0	0.01	841.0	0.00
745.5	0.05	761.5	0.00	777.5	0.01	793.5	0.05	809.5	0.00	825.5	0.01	841.5	0.00
746.0	0.03	762.0	0.01	778.0	0.00	794.0	0.07	810.0	0.00	826.0	0.01	842.0	0.00
746.5	0.01	762.5	0.01	778.5	0.02	794.5	0.02	810.5	0.01	826.5	0.01	842.5	0.00
747.0	0.01	763.0	0.01	779.0	0.01	795.0	0.04	811.0	0.01	827.0	0.01	843.0	0.00
747.5	0.03	763.5	0.00	779.5	0.01	795.5	0.03	811.5	0.02	827.5	0.01	843.5	0.00
748.0	0.01	764.0	0.01	780.0	0.02	796.0	0.08	812.0	0.02	828.0	0.02	844.0	0.00
748.5	0.12	764.5	0.00	780.5	0.02	796.5	0.03	812.5	0.00	828.5	0.00	844.5	0.00
749.0	0.01	765.0	0.00	781.0	0.01	797.0	0.01	813.0	0.01	829.0	0.00	845.0	0.00
749.5	0.02	765.5	0.00	781.5	0.02	797.5	0.04	813.5	0.02	829.5	0.06	845.5	0.00

Appendix E: Magnetic Susceptibility
Table 1: Borehole WB017D0

Depth (m)	Av. 3 Values	Depth (m)	Av. 3 Values	Depth (m)	Av. 3 Values	Depth (m)	Av. 3 Values	Depth (m)	Av. 3 Values	Depth (m)	Av. 3 Values	Depth (m)	Av. 3 Values
846.0	0.01	862.0	0.02	878.0	0.02	894.0	0.01	910.0	0.04	926.0	0.27	942.0	0.18
846.5	0.01	862.5	0.02	878.5	0.02	894.5	0.01	910.5	0.00	926.5	0.25	942.5	0.04
847.0	0.00	863.0	0.02	879.0	0.02	895.0	0.01	911.0	0.00	927.0	0.17	943.0	0.18
847.5	0.01	863.5	0.01	879.5	0.02	895.5	0.01	911.5	0.00	927.5	0.46	943.5	0.02
848.0	0.01	864.0	0.01	880.0	0.01	896.0	0.02	912.0	0.05	928.0	0.30	944.0	0.02
848.5	0.01	864.5	0.01	880.5	0.01	896.5	0.01	912.5	0.02	928.5	0.25	944.5	0.68
849.0	0.01	865.0	0.01	881.0	0.01	897.0	0.01	913.0	0.03	929.0	0.33	945.0	0.07
849.5	0.01	865.5	0.01	881.5	0.01	897.5	0.01	913.5	0.67	929.5	0.39	945.5	0.01
850.0	0.00	866.0	0.04	882.0	0.02	898.0	0.01	914.0	0.46	930.0	0.33	946.0	0.01
850.5	0.01	866.5	0.01	882.5	0.01	898.5	0.01	914.5	0.32	930.5	0.37	946.5	0.01
851.0	0.01	867.0	0.02	883.0	0.01	899.0	0.01	915.0	0.23	931.0	0.24	947.0	0.02
851.5	0.01	867.5	0.03	883.5	0.01	899.5	0.01	915.5	0.02	931.5	0.37	947.5	0.06
852.0	0.01	868.0	0.02	884.0	0.01	900.0	0.02	916.0	0.10	932.0	0.77	948.0	0.01
852.5	0.01	868.5	0.03	884.5	0.02	900.5	0.02	916.5	0.26	932.5	0.50	948.5	0.01
853.0	0.01	869.0	0.02	885.0	0.02	901.0	0.00	917.0	0.18	933.0	0.37	949.0	0.01
853.5	0.01	869.5	0.03	885.5	0.02	901.5	0.00	917.5	0.39	933.5	0.08	949.5	0.06
854.0	0.01	870.0	0.02	886.0	0.02	902.0	0.00	918.0	0.34	934.0	0.11	950.0	0.06
854.5	0.02	870.5	0.02	886.5	0.01	902.5	0.00	918.5	0.23	934.5	0.24	950.5	0.11
855.0	0.01	871.0	0.01	887.0	0.03	903.0	0.00	919.0	0.18	935.0	0.03	951.0	0.15
855.5	0.01	871.5	0.01	887.5	0.01	903.5	0.01	919.5	0.23	935.5	0.08	951.5	0.01
856.0	0.01	872.0	0.01	888.0	0.01	904.0	0.01	920.0	0.33	936.0	0.29	952.0	0.08
856.5	0.01	872.5	0.02	888.5	0.02	904.5	0.01	920.5	0.30	936.5	0.04	952.5	0.13
857.0	0.01	873.0	0.01	889.0	0.00	905.0	0.02	921.0	0.02	937.0	0.03	953.0	0.01
857.5	0.00	873.5	0.02	889.5	0.00	905.5	0.02	921.5	0.16	937.5	0.03	953.5	0.03
858.0	0.01	874.0	0.02	890.0	0.00	906.0	0.02	922.0	0.24	938.0	0.03	954.0	0.15
858.5	0.01	874.5	0.02	890.5	0.00	906.5	0.03	922.5	0.42	938.5	0.02	954.5	0.25
859.0	0.01	875.0	0.04	891.0	0.00	907.0	0.03	923.0	0.00	939.0	0.03	955.0	0.01
859.5	0.01	875.5	0.01	891.5	0.01	907.5	0.12	923.5	0.00	939.5	0.01	955.5	0.00
860.0	0.01	876.0	0.02	892.0	0.00	908.0	0.03	924.0	0.00	940.0	0.76	956.0	0.07
860.5	0.02	876.5	0.01	892.5	0.01	908.5	0.06	924.5	0.00	940.5	0.21	956.5	0.36
861.0	0.02	877.0	0.02	893.0	0.01	909.0	0.29	925.0	0.42	941.0	0.12	957.0	0.25
861.5	0.03	877.5	0.02	893.5	0.01	909.5	0.11	925.5	0.32	941.5	0.30	957.5	0.05

Appendix E: Magnetic Susceptibility
Table 1: Borehole WB017D0

Depth (m)	Av. 3 Values	Depth (m)	Av. 3 Values	Depth (m)	Av. 3 Values	Depth (m)	Av. 3 Values	Depth (m)	Av. 3 Values	Depth (m)	Av. 3 Values	Depth (m)	Av. 3 Values
958.0	0.24	974.0	0.14	990.0	2.71	1006.0	0.02	1022.0	0.02	1038.0	0.51	1054.0	0.40
958.5	0.28	974.5	0.61	990.5	3.22	1006.5	0.85	1022.5	0.01	1038.5	0.31	1054.5	0.15
959.0	0.10	975.0	0.40	991.0	2.90	1007.0	3.28	1023.0	0.01	1039.0	0.02	1055.0	0.18
959.5	0.00	975.5	0.55	991.5	0.00	1007.5	0.96	1023.5	0.00	1039.5	0.02	1055.5	0.05
960.0	0.39	976.0	0.16	992.0	0.03	1008.0	1.68	1024.0	0.01	1040.0	0.02	1056.0	0.09
960.5	0.14	976.5	0.65	992.5	0.06	1008.5	1.34	1024.5	0.02	1040.5	0.02	1056.5	0.04
961.0	0.02	977.0	0.55	993.0	1.75	1009.0	3.99	1025.0	0.03	1041.0	0.00	1057.0	0.16
961.5	0.00	977.5	0.42	993.5	0.52	1009.5	1.66	1025.5	0.02	1041.5	0.04	1057.5	0.11
962.0	0.45	978.0	0.41	994.0	0.16	1010.0	0.00	1026.0	0.01	1042.0	0.03	1058.0	0.38
962.5	0.24	978.5	0.34	994.5	1.15	1010.5	1.55	1026.5	0.03	1042.5	0.03	1058.5	0.44
963.0	0.34	979.0	0.35	995.0	0.59	1011.0	2.80	1027.0	0.01	1043.0	0.05	1059.0	0.46
963.5	0.02	979.5	0.22	995.5	1.45	1011.5	0.63	1027.5	0.00	1043.5	0.03	1059.5	0.28
964.0	0.02	980.0	0.28	996.0	0.81	1012.0	0.04	1028.0	0.50	1044.0	0.03	1060.0	0.28
964.5	0.00	980.5	0.46	996.5	0.08	1012.5	0.02	1028.5	0.35	1044.5	0.03	1060.5	0.52
965.0	0.01	981.0	0.34	997.0	0.00	1013.0	0.02	1029.0	1.56	1045.0	0.01	1061.0	0.98
965.5	0.00	981.5	0.35	997.5	0.02	1013.5	0.01	1029.5	1.07	1045.5	0.01	1061.5	0.36
966.0	0.00	982.0	0.31	998.0	0.17	1014.0	0.01	1030.0	0.01	1046.0	0.01	1062.0	0.31
966.5	0.01	982.5	0.62	998.5	1.06	1014.5	0.02	1030.5	0.07	1046.5	0.02	1062.5	0.02
967.0	0.19	983.0	1.92	999.0	2.38	1015.0	0.01	1031.0	0.02	1047.0	0.01	1063.0	0.02
967.5	0.01	983.5	4.57	999.5	0.04	1015.5	0.01	1031.5	0.02	1047.5	0.01	1063.5	0.01
968.0	0.00	984.0	2.56	1000.0	0.28	1016.0	0.01	1032.0	0.40	1048.0	0.01	1064.0	0.01
968.5	0.01	984.5	1.89	1000.5	1.05	1016.5	0.02	1032.5	0.06	1048.5	0.01	1064.5	0.01
969.0	0.21	985.0	0.21	1001.0	2.11	1017.0	0.01	1033.0	0.01	1049.0	0.02	1065.0	0.01
969.5	0.20	985.5	0.00	1001.5	1.17	1017.5	0.00	1033.5	0.00	1049.5	0.04	1065.5	0.02
970.0	0.05	986.0	0.02	1002.0	2.26	1018.0	1.55	1034.0	0.01	1050.0	0.02	1066.0	0.02
970.5	0.38	986.5	0.02	1002.5	2.10	1018.5	1.06	1034.5	0.01	1050.5	0.02	1066.5	0.02
971.0	0.21	987.0	1.73	1003.0	2.17	1019.0	0.00	1035.0	0.01	1051.0	0.04	1067.0	0.04
971.5	0.24	987.5	0.95	1003.5	1.59	1019.5	0.00	1035.5	0.01	1051.5	0.01	1067.5	0.04
972.0	0.31	988.0	0.02	1004.0	2.93	1020.0	0.01	1036.0	0.04	1052.0	0.11	1068.0	0.08
972.5	0.27	988.5	0.97	1004.5	0.53	1020.5	0.14	1036.5	0.05	1052.5	0.01	1068.5	0.05
973.0	0.24	989.0	0.47	1005.0	0.22	1021.0	0.16	1037.0	0.03	1053.0	0.26	1069.0	0.15
973.5	0.04	989.5	2.41	1005.5	0.06	1021.5	0.21	1037.5	0.02	1053.5	0.40	1069.5	0.11

Appendix E: Magnetic Susceptibility
Table 1: Borehole WB017D0

Depth (m)	Av. 3 Values	Depth (m)	Av. 3 Values	Depth (m)	Av. 3 Values	Depth (m)	Av. 3 Values	Depth (m)	Av. 3 Values	Depth (m)	Av. 3 Values	Depth (m)	Av. 3 Values
1070.0	1.72	1073.5	0.46	1077.0	0.15	1080.5	0.50	1084.0	0.25	1087.5	0.01		
1070.5	1.02	1074.0	0.50	1077.5	0.06	1081.0	0.08	1084.5	0.21	1088.0	0.01		
1071.0	0.18	1074.5	0.01	1078.0	0.06	1081.5	0.07	1085.0	0.06	1088.5	0.01		
1071.5	0.20	1075.0	0.18	1078.5	0.01	1082.0	0.17	1085.5	0.00	1089.0	0.01		
1072.0	0.09	1075.5	0.02	1079.0	0.00	1082.5	0.12	1086.0	0.00				
1072.5	0.07	1076.0	0.14	1079.5	0.00	1083.0	0.04	1086.5	0.01				
1073.0	0.11	1076.5	0.10	1080.0	0.91	1083.5	0.02	1087.0	0.01				

Appendix E: Magnetic Susceptibility Interpretation
Figure 1: WB017D0

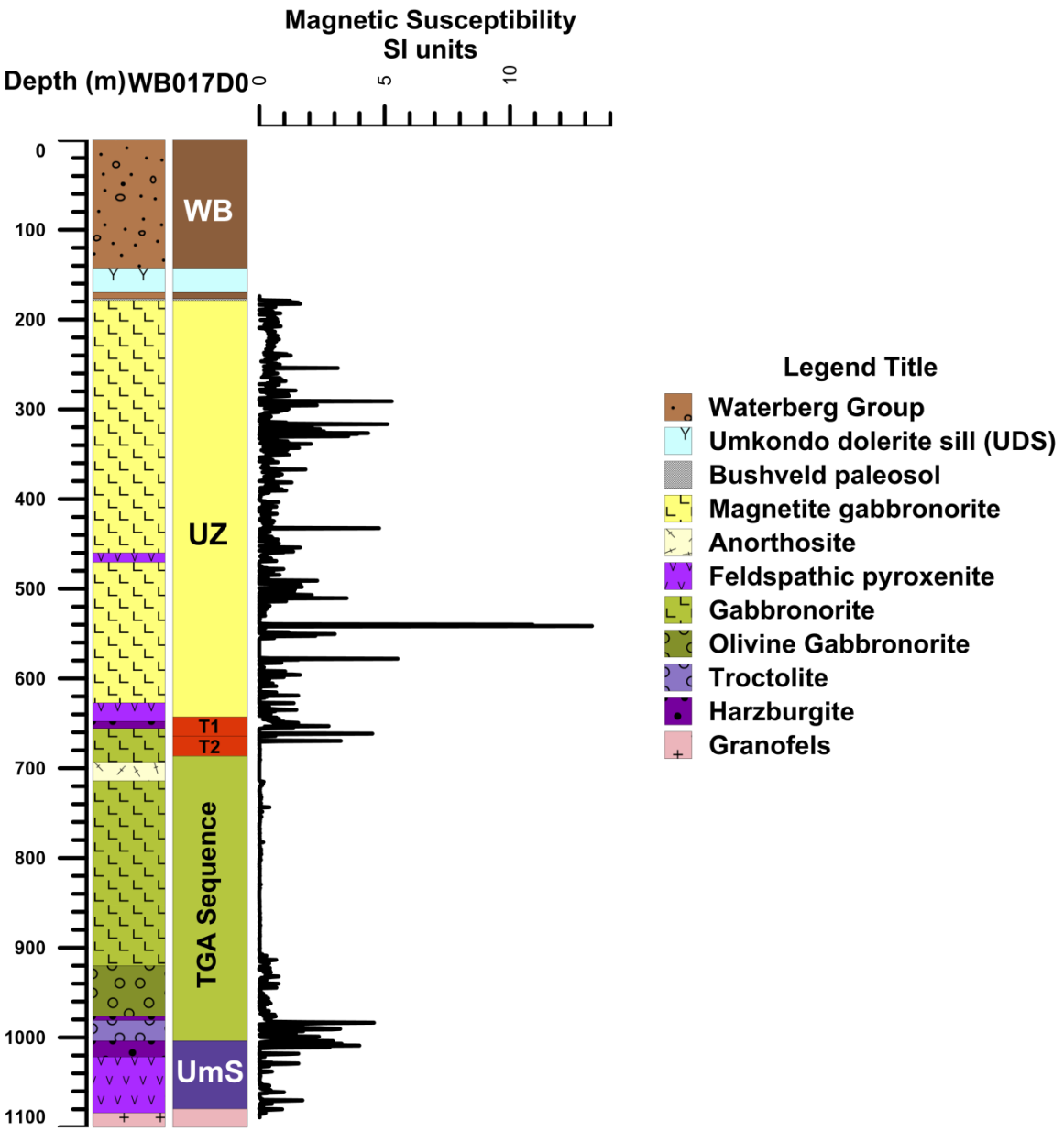

Appendix E: Magnetic Susceptibility
Table 2: Borehole WB027D0

Depth (m)	Av. 3 Values	Depth (m)	Av. 3 Values	Depth (m)	Av. 3 Values	Depth (m)	Av. 3 Values	Depth (m)	Av. 3 Values	Depth (m)	Av. 3 Values	Depth (m)	Av. 3 Values
470.00	2.61	502.00	1.60	534.00	5.65	566.00	6.60	598.00	0.05	630.00	0.13	662.00	0.10
471.00	2.78	503.00	1.20	535.00	0.08	567.00	15.99	599.00	0.05	631.00	0.10	663.00	0.07
472.00	4.16	504.00	0.07	536.00	6.16	568.00	0.01	600.00	0.12	632.00	1.10	664.00	0.10
473.00	3.00	505.00	2.96	537.00	2.98	569.00	0.01	601.00	0.08	633.00	0.76	665.00	0.05
474.00	3.24	506.00	0.03	538.00	4.77	570.00	0.02	602.00	0.10	634.00	1.48	666.00	0.07
475.00	0.03	507.00	0.05	539.00	2.05	571.00	0.03	603.00	0.16	635.00	0.88	667.00	0.13
476.00	0.00	508.00	0.03	540.00	0.89	572.00	0.97	604.00	0.15	636.00	0.88	668.00	0.12
477.00	0.00	509.00	0.00	541.00	0.08	573.00	4.28	605.00	0.32	637.00	0.91	669.00	0.17
478.00	0.00	510.00	0.47	542.00	0.10	574.00	0.92	606.00	2.43	638.00	0.57	670.00	0.40
479.00	0.00	511.00	0.00	543.00	1.59	575.00	0.02	607.00	0.14	639.00	0.00	671.00	0.15
480.00	0.02	512.00	0.22	544.00	0.25	576.00	0.18	608.00	0.15	640.00	0.99	672.00	0.17
481.00	0.00	513.00	0.25	545.00	0.49	577.00	4.08	609.00	0.13	641.00	0.51	673.00	0.21
482.00	0.00	514.00	0.31	546.00	0.89	578.00	3.70	610.00	0.11	642.00	1.00	674.00	0.21
483.00	0.00	515.00	0.32	547.00	0.59	579.00	7.12	611.00	0.09	643.00	0.80	675.00	0.29
484.00	0.00	516.00	0.14	548.00	0.41	580.00	1.53	612.00	0.17	644.00	0.78	676.00	0.15
485.00	0.01	517.00	0.18	549.00	0.17	581.00	0.03	613.00	0.16	645.00	0.65	677.00	0.19
486.00	0.00	518.00	0.13	550.00	0.63	582.00	0.00	614.00	0.18	646.00	0.82	678.00	0.17
487.00	0.00	519.00	0.02	551.00	0.15	583.00	0.00	615.00	0.17	647.00	0.23	679.00	0.12
488.00	0.02	520.00	3.19	552.00	0.04	584.00	0.01	616.00	0.15	648.00	0.64	680.00	0.14
489.00	0.00	521.00	1.00	553.00	0.01	585.00	0.00	617.00	0.24	649.00	0.69	681.00	0.13
490.00	1.52	522.00	0.50	554.00	0.02	586.00	0.06	618.00	0.23	650.00	0.32	682.00	0.10
491.00	0.00	523.00	0.14	555.00	3.16	587.00	3.89	619.00	0.13	651.00	1.70	683.00	0.06
492.00	0.00	524.00	1.83	556.00	1.63	588.00	0.06	620.00	0.16	652.00	0.20	684.00	0.08
493.00	0.00	525.00	0.03	557.00	0.07	589.00	11.41	621.00	0.19	653.00	0.42	685.00	0.06
494.00	0.02	526.00	0.01	558.00	9.87	590.00	0.03	622.00	0.17	654.00	0.13	686.00	0.01
495.00	0.06	527.00	0.17	559.00	0.06	591.00	0.05	623.00	0.32	655.00	0.06	687.00	0.02
496.00	1.27	528.00	0.03	560.00	0.00	592.00	0.06	624.00	0.24	656.00	1.45	688.00	0.12
497.00	0.58	529.00	1.25	561.00	0.02	593.00	0.08	625.00	0.26	657.00	0.15	689.00	0.28
498.00	0.45	530.00	0.20	562.00	0.00	594.00	0.04	626.00	0.24	658.00	0.17	690.00	0.36
499.00	5.10	531.00	0.43	563.00	0.01	595.00	0.03	627.00	0.27	659.00	0.14	691.00	0.16
500.00	0.62	532.00	0.80	564.00	0.03	596.00	0.04	628.00	0.27	660.00	0.12	692.00	0.85
501.00	14.98	533.00	0.03	565.00	3.84	597.00	0.06	629.00	0.13	661.00	0.06	693.00	0.36

Appendix E: Magnetic Susceptibility
Table 2: Borehole WB027D0

Depth (m)	Av. 3 Values	Depth (m)	Av. 3 Values	Depth (m)	Av. 3 Values	Depth (m)	Av. 3 Values	Depth (m)	Av. 3 Values	Depth (m)	Av. 3 Values	Depth (m)	Av. 3 Values
694.00	0.15	726.00	0.19	758.00	0.42	790.00	0.02	822.00	0.04	854.00	0.02	886.00	0.00
695.00	0.00	727.00	0.18	759.00	0.13	791.00	0.12	823.00	0.04	855.00	0.03	887.00	0.01
696.00	0.16	728.00	0.49	760.00	1.20	792.00	0.03	824.00	0.00	856.00	0.00	888.00	0.16
697.00	0.09	729.00	0.30	761.00	0.43	793.00	0.02	825.00	0.02	857.00	0.73	889.00	0.01
698.00	0.15	730.00	0.07	762.00	0.48	794.00	0.00	826.00	0.01	858.00	0.06	890.00	0.38
699.00	0.16	731.00	0.02	763.00	0.35	795.00	0.00	827.00	0.06	859.00	0.04	891.00	0.00
700.00	0.18	732.00	0.12	764.00	0.36	796.00	0.00	828.00	0.02	860.00	0.05	892.00	0.01
701.00	0.42	733.00	0.24	765.00	0.57	797.00	0.00	829.00	0.02	861.00	0.01	893.00	0.05
702.00	1.02	734.00	0.15	766.00	0.87	798.00	0.00	830.00	0.00	862.00	0.13	894.00	0.07
703.00	0.29	735.00	1.31	767.00	0.67	799.00	0.00	831.00	0.03	863.00	0.11	895.00	0.02
704.00	0.17	736.00	0.14	768.00	0.23	800.00	0.02	832.00	0.02	864.00	0.17	896.00	0.00
705.00	0.18	737.00	0.12	769.00	1.38	801.00	0.01	833.00	0.01	865.00	0.09	897.00	0.00
706.00	0.17	738.00	0.08	770.00	0.80	802.00	0.20	834.00	0.02	866.00	0.09	898.00	0.00
707.00	0.12	739.00	0.02	771.00	2.13	803.00	0.00	835.00	0.05	867.00	0.12	899.00	0.00
708.00	0.08	740.00	0.23	772.00	0.64	804.00	0.00	836.00	0.08	868.00	0.04	900.00	0.06
709.00	0.06	741.00	0.06	773.00	0.41	805.00	0.00	837.00	0.04	869.00	0.04	901.00	0.01
710.00	0.71	742.00	0.30	774.00	0.57	806.00	0.00	838.00	0.04	870.00	0.06	902.00	0.00
711.00	0.70	743.00	0.39	775.00	0.59	807.00	0.00	839.00	0.01	871.00	0.01	903.00	0.04
712.00	0.48	744.00	0.58	776.00	1.57	808.00	0.05	840.00	0.01	872.00	0.04	904.00	0.27
713.00	0.60	745.00	0.58	777.00	0.54	809.00	0.00	841.00	0.03	873.00	0.05	905.00	0.24
714.00	0.41	746.00	0.44	778.00	0.71	810.00	0.08	842.00	0.01	874.00	0.02	906.00	0.15
715.00	0.64	747.00	1.02	779.00	0.97	811.00	0.00	843.00	0.01	875.00	0.05	907.00	0.48
716.00	1.19	748.00	0.53	780.00	0.02	812.00	0.00	844.00	0.06	876.00	0.05	908.00	0.25
717.00	1.02	749.00	1.12	781.00	1.71	813.00	0.00	845.00	0.10	877.00	0.06	909.00	0.11
718.00	0.85	750.00	0.63	782.00	0.78	814.00	0.00	846.00	0.07	878.00	0.04	910.00	4.38
719.00	0.20	751.00	0.01	783.00	1.12	815.00	0.00	847.00	0.07	879.00	0.00	911.00	2.18
720.00	0.16	752.00	0.07	784.00	0.79	816.00	0.02	848.00	0.00	880.00	0.01	912.00	0.13
721.00	0.21	753.00	0.47	785.00	0.36	817.00	0.00	849.00	0.06	881.00	0.04	913.00	0.09
722.00	0.26	754.00	0.73	786.00	0.33	818.00	0.02	850.00	0.16	882.00	0.13	914.00	1.05
723.00	0.33	755.00	0.28	787.00	0.91	819.00	0.02	851.00	0.09	883.00	0.63	915.00	0.03
724.00	0.17	756.00	0.36	788.00	0.08	820.00	0.05	852.00	0.04	884.00	0.20	916.00	0.06
725.00	0.17	757.00	0.52	789.00	0.17	821.00	0.00	853.00	0.05	885.00	0.11	917.00	0.06

Appendix E: Magnetic Susceptibility
Table 2: Borehole WB027D0

Depth (m)	Av. 3 Values	Depth (m)	Av. 3 Values	Depth (m)	Av. 3 Values	Depth (m)	Av. 3 Values	Depth (m)	Av. 3 Values	Depth (m)	Av. 3 Values	Depth (m)	Av. 3 Values
918.00	0.02	950.00	0.67	982.00	3.11	1014.00	0.57	1046.00	0.05	1078.00	0.13	1110.00	6.19
919.00	0.06	951.00	0.20	983.00	0.63	1015.00	4.56	1047.00	0.00	1079.00	13.39	1111.00	0.11
920.00	0.04	952.00	0.00	984.00	1.73	1016.00	0.14	1048.00	0.70	1080.00	13.98	1112.00	1.94
921.00	0.04	953.00	0.24	985.00	2.43	1017.00	3.28	1049.00	4.31	1081.00	0.22	1113.00	6.50
922.00	0.03	954.00	0.18	986.00	0.08	1018.00	9.96	1050.00	6.29	1082.00	11.33	1114.00	20.13
923.00	0.11	955.00	0.13	987.00	0.08	1019.00	7.14	1051.00	4.85	1083.00	13.61	1115.00	5.94
924.00	0.05	956.00	0.14	988.00	4.61	1020.00	12.85	1052.00	1.32	1084.00	18.95	1116.00	3.57
925.00	0.04	957.00	0.19	989.00	2.46	1021.00	0.46	1053.00	8.97	1085.00	0.00	1117.00	0.00
926.00	0.07	958.00	0.11	990.00	0.29	1022.00	0.42	1054.00	9.57	1086.00	0.08	1118.00	0.04
927.00	0.04	959.00	0.19	991.00	3.68	1023.00	0.12	1055.00	22.73	1087.00	4.31	1119.00	0.05
928.00	0.01	960.00	0.04	992.00	6.37	1024.00	14.84	1056.00	4.82	1088.00	8.67	1120.00	0.26
929.00	0.07	961.00	0.09	993.00	0.05	1025.00	0.06	1057.00	17.06	1089.00	0.00	1121.00	0.09
930.00	0.05	962.00	0.22	994.00	0.01	1026.00	0.12	1058.00	30.74	1090.00	24.98	1122.00	0.10
931.00	0.05	963.00	0.17	995.00	2.53	1027.00	0.11	1059.00	23.14	1091.00	0.03	1123.00	1.77
932.00	0.04	964.00	2.03	996.00	0.22	1028.00	10.50	1060.00	22.76	1092.00	0.00	1124.00	0.00
933.00	0.00	965.00	0.18	997.00	0.06	1029.00	0.12	1061.00	18.28	1093.00	20.46	1125.00	0.00
934.00	0.02	966.00	2.10	998.00	2.18	1030.00	0.08	1062.00	13.75	1094.00	18.26	1126.00	5.57
935.00	0.03	967.00	0.05	999.00	4.25	1031.00	0.16	1063.00	11.42	1095.00	11.35	1127.00	7.16
936.00	0.10	968.00	2.92	1000.00	0.14	1032.00	0.15	1064.00	10.89	1096.00	2.54	1128.00	16.55
937.00	0.08	969.00	0.10	1001.00	0.18	1033.00	0.04	1065.00	14.99	1097.00	0.03	1129.00	0.14
938.00	0.18	970.00	2.59	1002.00	0.03	1034.00	0.09	1066.00	1.70	1098.00	0.04	1130.00	30.25
939.00	0.04	971.00	0.03	1003.00	0.22	1035.00	0.07	1067.00	0.11	1099.00	23.01	1131.00	20.83
940.00	0.13	972.00	0.21	1004.00	0.06	1036.00	0.06	1068.00	15.30	1100.00	13.28	1132.00	16.61
941.00	0.08	973.00	2.32	1005.00	0.06	1037.00	0.07	1069.00	10.80	1101.00	6.34	1133.00	27.69
942.00	0.09	974.00	0.71	1006.00	0.10	1038.00	0.01	1070.00	13.51	1102.00	18.53	1134.00	21.95
943.00	0.14	975.00	0.06	1007.00	0.08	1039.00	0.08	1071.00	15.19	1103.00	1.42	1135.00	0.15
944.00	0.10	976.00	1.04	1008.00	0.08	1040.00	0.12	1072.00	14.85	1104.00	16.84	1136.00	0.11
945.00	0.58	977.00	1.43	1009.00	0.20	1041.00	0.62	1073.00	0.07	1105.00	19.10	1137.00	30.59
946.00	0.13	978.00	0.09	1010.00	0.09	1042.00	0.06	1074.00	7.34	1106.00	17.47	1138.00	0.36
947.00	0.17	979.00	1.15	1011.00	0.14	1043.00	0.51	1075.00	14.52	1107.00	13.70	1139.00	0.05
948.00	0.11	980.00	1.79	1012.00	2.23	1044.00	0.00	1076.00	14.20	1108.00	17.91	1140.00	20.97
949.00	0.14	981.00	3.62	1013.00	2.35	1045.00	1.50	1077.00	0.02	1109.00	18.12	1141.00	12.78

Appendix E: Magnetic Susceptibility
Table 2: Borehole WB027D0

Depth (m)	Av. 3 Values	Depth (m)	Av. 3 Values	Depth (m)	Av. 3 Values	Depth (m)	Av. 3 Values	Depth (m)	Av. 3 Values	Depth (m)	Av. 3 Values	Depth (m)	Av. 3 Values
1142.00	0.00	1174.00	0.41	1206.00	0.00								
1143.00	12.77	1175.00	0.18	1207.00	0.11								
1144.00	1.59	1176.00	0.00	1208.00	0.00								
1145.00	2.56	1177.00	0.11	1209.00	0.00								
1146.00	0.04	1178.00	0.00	1210.00	0.00								
1147.00	0.33	1179.00	0.05	1211.00	1.71								
1148.00	0.04	1180.00	0.00										
1149.00	0.03	1181.00	0.00										
1150.00	0.04	1182.00	0.00										
1151.00	0.49	1183.00	0.00										
1152.00	2.55	1184.00	0.00										
1153.00	2.43	1185.00	0.00										
1154.00	32.80	1186.00	0.00										
1155.00	17.27	1187.00	0.00										
1156.00	1.52	1188.00	0.00										
1157.00	8.61	1189.00	0.00										
1158.00	0.04	1190.00	0.00										
1159.00	7.91	1191.00	0.00										
1160.00	24.99	1192.00	0.19										
1161.00	0.00	1193.00	0.00										
1162.00	1.21	1194.00	0.00										
1163.00	4.80	1195.00	0.00										
1164.00	0.23	1196.00	0.00										
1165.00	2.48	1197.00	0.00										
1166.00	0.87	1198.00	0.00										
1167.00	7.10	1199.00	0.00										
1168.00	26.54	1200.00	0.00										
1169.00	0.05	1201.00	0.00										
1170.00	0.02	1202.00	0.00										
1171.00	0.07	1203.00	0.00										
1172.00	0.09	1204.00	0.00										
1173.00	0.07	1205.00	0.00										

Appendix E: Magnetic Susceptibility Interpretation
Figure 2: Borehole WB027D0

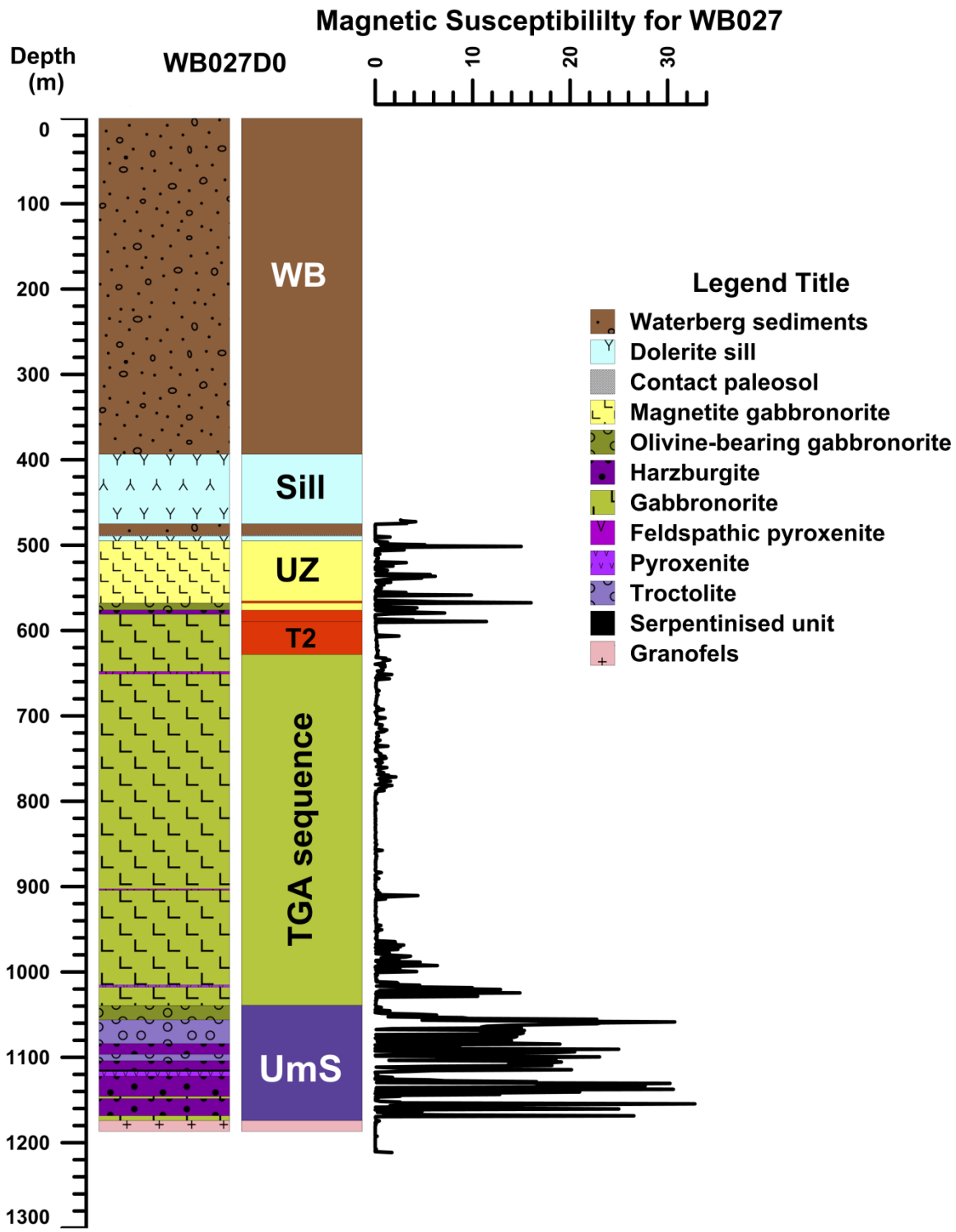

Appendix E: Magnetic Susceptibility
Table 3: Borehole WB099D0

Depth (m)	AV. 3 Values	Depth (m)	AV. 3 Values	Depth (m)	AV. 3 Values	Depth (m)	AV. 3 Values	Depth (m)	AV. 3 Values	Depth (m)	AV. 3 Values	Depth (m)	AV. 3 Values
465.00	0.00	497.00	0.00	529.00	11.50	561.00	0.06	593.00	0.47	625.00	0.17	657.00	1.24
466.00	0.01	498.00	0.00	530.00	0.48	562.00	0.07	594.00	1.03	626.00	0.03	658.00	0.09
467.00	0.01	499.00	0.00	531.00	0.30	563.00	0.07	595.00	7.42	627.00	3.15	659.00	1.14
468.00	0.00	500.00	0.00	532.00	1.26	564.00	0.04	596.00	1.85	628.00	2.59	660.00	1.59
469.00	0.00	501.00	0.00	533.00	0.07	565.00	0.19	597.00	0.99	629.00	1.37	661.00	1.53
470.00	0.00	502.00	0.00	534.00	0.72	566.00	0.15	598.00	0.70	630.00	1.42	662.00	1.64
471.00	0.00	503.00	0.00	535.00	0.28	567.00	0.07	599.00	0.42	631.00	2.13	663.00	2.99
472.00	0.00	504.00	0.00	536.00	0.56	568.00	0.09	600.00	3.03	632.00	2.55	664.00	1.92
473.00	0.00	505.00	0.00	537.00	1.88	569.00	0.08	601.00	0.95	633.00	0.21	665.00	2.01
474.00	0.00	506.00	0.00	538.00	0.57	570.00	0.11	602.00	2.20	634.00	13.30	666.00	1.98
475.00	0.00	507.00	0.00	539.00	0.25	571.00	0.17	603.00	1.12	635.00	0.48	667.00	2.86
476.00	0.00	508.00	0.00	540.00	2.60	572.00	0.46	604.00	0.00	636.00	0.78	668.00	2.94
477.00	0.00	509.00	0.00	541.00	0.05	573.00	0.60	605.00	0.00	637.00	1.04	669.00	2.63
478.00	0.00	510.00	0.00	542.00	9.27	574.00	1.33	606.00	0.06	638.00	3.48	670.00	2.42
479.00	0.00	511.00	0.00	543.00	0.89	575.00	2.81	607.00	0.48	639.00	1.27	671.00	2.99
480.00	0.00	512.00	0.00	544.00	0.69	576.00	1.28	608.00	1.29	640.00	0.68	672.00	2.55
481.00	0.00	513.00	0.00	545.00	0.00	577.00	2.05	609.00	0.05	641.00	1.61	673.00	2.72
482.00	0.00	514.00	0.00	546.00	0.00	578.00	1.26	610.00	0.81	642.00	0.37	674.00	3.73
483.00	0.00	515.00	0.00	547.00	0.07	579.00	0.69	611.00	0.55	643.00	6.03	675.00	2.88
484.00	0.00	516.00	0.00	548.00	0.07	580.00	1.01	612.00	0.09	644.00	3.14	676.00	7.32
485.00	0.00	517.00	0.00	549.00	0.13	581.00	0.80	613.00	0.17	645.00	6.77	677.00	0.00
486.00	0.00	518.00	0.00	550.00	0.00	582.00	0.18	614.00	0.08	646.00	0.47	678.00	0.00
487.00	0.00	519.00	0.00	551.00	6.44	583.00	1.64	615.00	0.23	647.00	1.76	679.00	6.25
488.00	0.00	520.00	L.O.C	552.00	3.35	584.00	0.77	616.00	0.23	648.00	5.74	680.00	0.00
489.00	0.00	521.00	L.O.C	553.00	0.00	585.00	1.04	617.00	0.14	649.00	2.55	681.00	0.00
490.00	0.00	522.00	L.O.C	554.00	0.59	586.00	0.39	618.00	2.11	650.00	1.72	682.00	0.00
491.00	0.00	523.00	L.O.C	555.00	3.20	587.00	2.87	619.00	0.70	651.00	3.96	683.00	5.86
492.00	0.00	524.00	L.O.C	556.00	0.31	588.00	0.43	620.00	0.12	652.00	2.00	684.00	3.01
493.00	0.00	525.00	8.92	557.00	0.27	589.00	6.51	621.00	0.17	653.00	3.29	685.00	0.27
494.00	0.00	526.00	0.14	558.00	0.00	590.00	1.08	622.00	0.14	654.00	11.17	686.00	0.31
495.00	0.00	527.00	0.05	559.00	0.10	591.00	0.42	623.00	0.21	655.00	1.29	687.00	0.06
496.00	0.00	528.00	0.27	560.00	0.18	592.00	0.85	624.00	0.82	656.00	1.36	688.00	0.30

Appendix E: Magnetic Susceptibility
Table 3: Borehole WB099D0

Depth (m)	AV. 3 Values	Depth (m)	AV. 3 Values	Depth (m)	AV. 3 Values	Depth (m)	AV. 3 Values	Depth (m)	AV. 3 Values	Depth (m)	AV. 3 Values	Depth (m)	AV. 3 Values
689.00	0.01	721.00	0.00	753.00	1.32	785.00	0.22	817.00	0.24	849.00	0.08	881.00	0.52
690.00	0.03	722.00	0.00	754.00	0.03	786.00	0.23	818.00	0.13	850.00	0.12	882.00	0.48
691.00	2.67	723.00	0.06	755.00	0.04	787.00	0.20	819.00	0.16	851.00	0.05	883.00	0.37
692.00	0.00	724.00	0.10	756.00	0.03	788.00	0.16	820.00	0.17	852.00	0.14	884.00	0.41
693.00	0.09	725.00	0.05	757.00	0.03	789.00	0.14	821.00	0.16	853.00	0.02	885.00	1.21
694.00	0.03	726.00	0.04	758.00	0.57	790.00	0.15	822.00	0.07	854.00	0.11	886.00	0.60
695.00	0.03	727.00	0.16	759.00	0.37	791.00	0.13	823.00	0.19	855.00	0.13	887.00	0.41
696.00	0.08	728.00	0.07	760.00	1.57	792.00	0.18	824.00	0.17	856.00	0.03	888.00	0.29
697.00	0.01	729.00	0.11	761.00	1.61	793.00	0.18	825.00	0.04	857.00	0.10	889.00	0.22
698.00	0.05	730.00	0.09	762.00	0.94	794.00	0.14	826.00	0.01	858.00	0.01	890.00	0.20
699.00	9.84	731.00	0.03	763.00	0.28	795.00	0.07	827.00	0.03	859.00	0.05	891.00	0.37
700.00	0.38	732.00	0.11	764.00	0.81	796.00	0.14	828.00	0.20	860.00	0.82	892.00	0.08
701.00	3.20	733.00	0.10	765.00	0.31	797.00	0.15	829.00	0.13	861.00	0.34	893.00	0.52
702.00	0.21	734.00	0.09	766.00	0.27	798.00	0.18	830.00	0.05	862.00	0.34	894.00	0.76
703.00	0.09	735.00	0.07	767.00	0.28	799.00	0.11	831.00	0.09	863.00	0.86	895.00	0.33
704.00	0.05	736.00	0.07	768.00	0.37	800.00	0.13	832.00	0.08	864.00	0.76	896.00	0.37
705.00	1.52	737.00	0.06	769.00	0.55	801.00	0.30	833.00	0.06	865.00	0.44	897.00	0.57
706.00	0.18	738.00	0.04	770.00	0.44	802.00	0.15	834.00	0.05	866.00	0.32	898.00	1.22
707.00	0.03	739.00	0.13	771.00	0.69	803.00	0.21	835.00	0.08	867.00	0.51	899.00	6.87
708.00	0.03	740.00	0.10	772.00	0.32	804.00	0.22	836.00	0.08	868.00	0.31	900.00	0.00
709.00	0.01	741.00	0.09	773.00	1.66	805.00	0.23	837.00	0.14	869.00	0.38	901.00	0.13
710.00	0.02	742.00	0.16	774.00	0.41	806.00	0.21	838.00	0.13	870.00	0.38	902.00	0.36
711.00	0.02	743.00	0.16	775.00	0.77	807.00	0.21	839.00	0.12	871.00	0.20	903.00	0.03
712.00	0.00	744.00	0.11	776.00	0.28	808.00	0.18	840.00	0.13	872.00	0.64	904.00	0.37
713.00	0.03	745.00	0.10	777.00	0.28	809.00	0.20	841.00	0.12	873.00	0.81	905.00	0.39
714.00	0.05	746.00	0.47	778.00	0.23	810.00	0.19	842.00	0.12	874.00	0.35	906.00	0.27
715.00	0.03	747.00	0.49	779.00	0.22	811.00	0.28	843.00	0.09	875.00	0.09	907.00	0.23
716.00	0.00	748.00	0.96	780.00	0.24	812.00	0.23	844.00	0.09	876.00	0.14	908.00	0.00
717.00	0.02	749.00	0.77	781.00	0.23	813.00	0.17	845.00	0.10	877.00	0.09	909.00	0.10
718.00	0.00	750.00	2.74	782.00	0.14	814.00	0.23	846.00	0.14	878.00	0.21	910.00	0.17
719.00	0.00	751.00	1.87	783.00	0.21	815.00	0.27	847.00	0.10	879.00	0.18	911.00	0.14
720.00	0.03	752.00	3.10	784.00	0.25	816.00	0.23	848.00	0.29	880.00	0.18	912.00	0.05

Appendix E: Magnetic Susceptibility
Table 3: Borehole WB099D0

Depth (m)	AV. 3 Values	Depth (m)	AV. 3 Values	Depth (m)	AV. 3 Values	Depth (m)	AV. 3 Values	Depth (m)	AV. 3 Values	Depth (m)	AV. 3 Values	Depth (m)	AV. 3 Values
913.00	0.18	945.00	0.18	977.00	0.00	1009.00	0.04	1041.00	0.06	1073.00	0.11	1105.00	0.08
914.00	0.14	946.00	0.20	978.00	0.00	1010.00	0.22	1042.00	0.08	1074.00	0.11	1106.00	0.08
915.00	0.13	947.00	0.17	979.00	0.00	1011.00	0.11	1043.00	0.08	1075.00	0.08	1107.00	0.06
916.00	0.05	948.00	0.00	980.00	0.02	1012.00	0.06	1044.00	0.11	1076.00	0.22	1108.00	0.08
917.00	0.03	949.00	0.15	981.00	0.00	1013.00	0.12	1045.00	0.11	1077.00	0.29	1109.00	0.07
918.00	0.12	950.00	0.06	982.00	0.00	1014.00	0.07	1046.00	0.04	1078.00	0.06	1110.00	0.06
919.00	0.27	951.00	0.14	983.00	0.00	1015.00	0.04	1047.00	0.08	1079.00	0.12	1111.00	0.08
920.00	0.17	952.00	0.25	984.00	0.00	1016.00	0.95	1048.00	0.06	1080.00	0.18	1112.00	0.04
921.00	0.06	953.00	0.20	985.00	0.00	1017.00	0.46	1049.00	0.09	1081.00	0.05	1113.00	0.07
922.00	0.00	954.00	0.14	986.00	0.00	1018.00	0.00	1050.00	0.11	1082.00	0.20	1114.00	0.07
923.00	0.08	955.00	0.06	987.00	0.00	1019.00	0.03	1051.00	0.10	1083.00	0.08	1115.00	0.06
924.00	0.38	956.00	0.21	988.00	0.00	1020.00	0.00	1052.00	0.10	1084.00	0.07	1116.00	0.06
925.00	0.00	957.00	0.08	989.00	0.00	1021.00	0.02	1053.00	0.12	1085.00	0.06	1117.00	0.06
926.00	0.22	958.00	0.19	990.00	0.00	1022.00	0.00	1054.00	0.11	1086.00	0.07	1118.00	0.05
927.00	0.14	959.00	0.04	991.00	0.04	1023.00	0.00	1055.00	0.12	1087.00	0.07	1119.00	0.05
928.00	0.19	960.00	0.10	992.00	0.02	1024.00	0.00	1056.00	0.08	1088.00	0.03	1120.00	0.08
929.00	0.18	961.00	0.10	993.00	0.04	1025.00	0.00	1057.00	0.07	1089.00	0.08	1121.00	0.07
930.00	0.10	962.00	0.04	994.00	0.06	1026.00	0.04	1058.00	0.11	1090.00	0.05	1122.00	1.82
931.00	0.16	963.00	0.07	995.00	0.29	1027.00	0.01	1059.00	0.11	1091.00	0.08	1123.00	3.09
932.00	0.19	964.00	0.10	996.00	0.00	1028.00	0.55	1060.00	0.11	1092.00	0.11	1124.00	1.03
933.00	0.40	965.00	0.08	997.00	0.10	1029.00	4.88	1061.00	0.10	1093.00	0.07	1125.00	0.03
934.00	0.09	966.00	0.14	998.00	0.12	1030.00	12.39	1062.00	0.13	1094.00	0.05	1126.00	1.51
935.00	0.09	967.00	0.06	999.00	0.00	1031.00	0.08	1063.00	0.14	1095.00	0.07	1127.00	1.72
936.00	0.26	968.00	0.07	1000.00	0.05	1032.00	0.06	1064.00	0.26	1096.00	0.07	1128.00	2.28
937.00	0.13	969.00	0.01	1001.00	0.04	1033.00	0.07	1065.00	0.27	1097.00	1.74	1129.00	2.86
938.00	0.13	970.00	0.00	1002.00	0.06	1034.00	2.15	1066.00	0.09	1098.00	0.07	1130.00	3.52
939.00	0.18	971.00	0.00	1003.00	0.03	1035.00	0.68	1067.00	0.14	1099.00	0.10	1131.00	3.50
940.00	0.15	972.00	0.00	1004.00	0.40	1036.00	0.07	1068.00	0.10	1100.00	0.10	1132.00	3.25
941.00	0.26	973.00	0.00	1005.00	0.53	1037.00	0.08	1069.00	0.06	1101.00	0.09	1133.00	0.01
942.00	0.28	974.00	0.00	1006.00	0.44	1038.00	0.06	1070.00	0.10	1102.00	0.06	1134.00	0.01
943.00	0.02	975.00	0.00	1007.00	0.34	1039.00	0.06	1071.00	0.14	1103.00	0.06	1135.00	0.98
944.00	0.18	976.00	0.00	1008.00	0.00	1040.00	5.47	1072.00	0.14	1104.00	0.07	1136.00	0.04

Appendix E: Magnetic Susceptibility
Table 3: Borehole WB099D0

Depth (m)	AV. 3 Values	Depth (m)	AV. 3 Values	Depth (m)	AV. 3 Values	Depth (m)	AV. 3 Values	Depth (m)	AV. 3 Values	Depth (m)	AV. 3 Values	Depth (m)	AV. 3 Values
1137.00	0.09	1169.00	1.86	1201.00	3.53	1233.00	0.10	1265.00	0.07	1297.00	2.01	1329.00	0.08
1138.00	0.03	1170.00	3.03	1202.00	0.02	1234.00	0.46	1266.00	0.49	1298.00	3.63	1330.00	0.08
1139.00	1.73	1171.00	2.67	1203.00	2.20	1235.00	0.02	1267.00	1.81	1299.00	0.32	1331.00	0.07
1140.00	1.48	1172.00	3.81	1204.00	1.27	1236.00	0.09	1268.00	1.96	1300.00	0.15	1332.00	2.13
1141.00	3.76	1173.00	4.11	1205.00	0.59	1237.00	0.07	1269.00	1.95	1301.00	0.18	1333.00	1.56
1142.00	1.66	1174.00	3.44	1206.00	1.56	1238.00	0.10	1270.00	1.51	1302.00	4.54	1334.00	0.56
1143.00	2.60	1175.00	2.91	1207.00	0.50	1239.00	0.07	1271.00	3.81	1303.00	1.09	1335.00	1.01
1144.00	2.73	1176.00	3.34	1208.00	1.95	1240.00	0.09	1272.00	3.70	1304.00	5.24	1336.00	0.38
1145.00	0.30	1177.00	0.04	1209.00	0.79	1241.00	0.04	1273.00	3.43	1305.00	4.53	1337.00	0.16
1146.00	3.42	1178.00	2.70	1210.00	0.59	1242.00	0.03	1274.00	2.84	1306.00	3.29	1338.00	0.64
1147.00	5.28	1179.00	1.62	1211.00	5.89	1243.00	0.10	1275.00	4.95	1307.00	0.11	1339.00	2.01
1148.00	7.12	1180.00	4.06	1212.00	3.29	1244.00	0.04	1276.00	6.64	1308.00	3.89	1340.00	0.00
1149.00	5.36	1181.00	2.57	1213.00	1.80	1245.00	0.05	1277.00	8.68	1309.00	0.26	1341.00	0.00
1150.00	0.56	1182.00	0.05	1214.00	5.78	1246.00	0.09	1278.00	26.43	1310.00	0.08	1342.00	0.02
1151.00	0.00	1183.00	0.00	1215.00	9.72	1247.00	0.10	1279.00	31.78	1311.00	0.09	1343.00	0.23
1152.00	0.00	1184.00	0.00	1216.00	10.48	1248.00	0.00	1280.00	19.69	1312.00	0.08		
1153.00	0.00	1185.00	3.28	1217.00	0.19	1249.00	0.05	1281.00	7.19	1313.00	1.51		
1154.00	0.02	1186.00	3.03	1218.00	2.17	1250.00	0.13	1282.00	18.91	1314.00	0.06		
1155.00	0.01	1187.00	1.26	1219.00	8.33	1251.00	0.06	1283.00	3.61	1315.00	0.16		
1156.00	0.00	1188.00	0.48	1220.00	3.28	1252.00	5.01	1284.00	L.O.C	1316.00	0.64		
1157.00	0.01	1189.00	0.91	1221.00	10.28	1253.00	0.70	1285.00	L.O.C	1317.00	0.10		
1158.00	0.02	1190.00	1.33	1222.00	1.64	1254.00	0.01	1286.00	45.63	1318.00	0.62		
1159.00	0.02	1191.00	1.78	1223.00	3.76	1255.00	2.52	1287.00	1.83	1319.00	0.34		
1160.00	0.03	1192.00	0.48	1224.00	1.19	1256.00	0.04	1288.00	23.55	1320.00	0.48		
1161.00	0.04	1193.00	3.34	1225.00	1.07	1257.00	1.12	1289.00	L.O.C	1321.00	0.06		
1162.00	0.02	1194.00	4.07	1226.00	1.17	1258.00	1.46	1290.00	L.O.C	1322.00	0.03		
1163.00	3.29	1195.00	1.07	1227.00	6.64	1259.00	2.91	1291.00	5.33	1323.00	0.21		
1164.00	2.80	1196.00	5.57	1228.00	8.81	1260.00	3.36	1292.00	2.06	1324.00	0.09		
1165.00	0.11	1197.00	1.77	1229.00	14.94	1261.00	1.99	1293.00	5.02	1325.00	0.03		
1166.00	0.09	1198.00	1.65	1230.00	1.76	1262.00	1.12	1294.00	2.61	1326.00	0.06		
1167.00	2.57	1199.00	0.44	1231.00	3.10	1263.00	2.13	1295.00	4.53	1327.00	0.02		
1168.00	2.34	1200.00	1.60	1232.00	0.11	1264.00	1.65	1296.00	5.73	1328.00	0.02		

Appendix E: Magnetic Susceptibility Interpretation
Figure 3: Borehole WB099D0

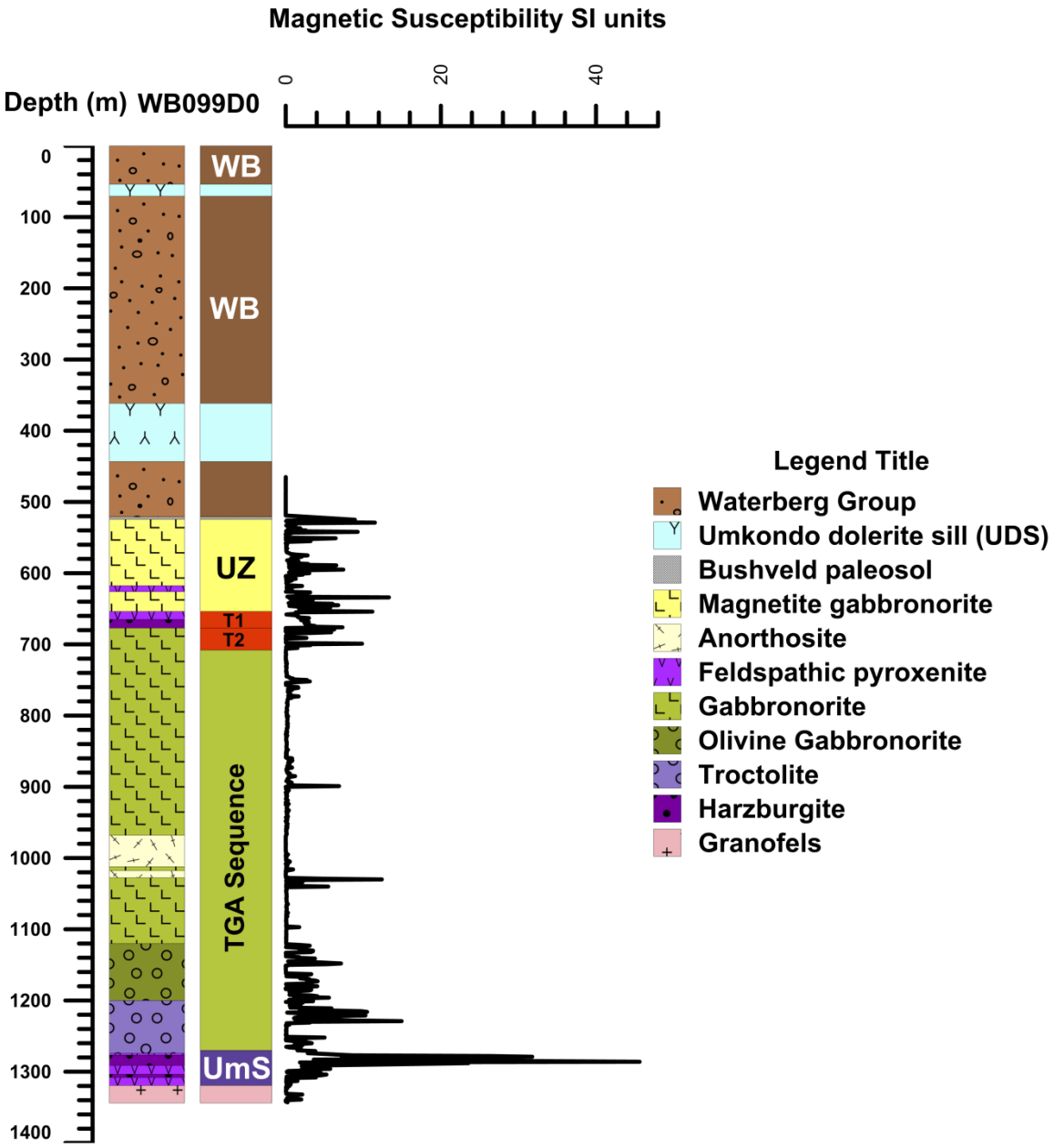

Appendix E: Magnetic Susceptibility
Table 4: Borehole WE001D0

Depth (m)	Av. 3 Values	Depth (m)	Av. 3 Values	Depth (m)	Av. 3 Values	Depth (m)	Av. 3 Values	Depth (m)	Av. 3 Values	Depth (m)	Av. 3 Values	Depth (m)	Av. 3 Values
352.00	0.00	384.00	0.01	416.00	2.86	448.00	0.86	480.00	0.54	512.00	0.09	544.00	0.05
353.00	0.00	385.00	0.00	417.00	1.20	449.00	0.36	481.00	0.70	513.00	0.15	545.00	0.06
354.00	0.00	386.00	0.02	418.00	0.80	450.00	1.14	482.00	0.14	514.00	0.16	546.00	0.02
355.00	0.00	387.00	0.14	419.00	4.37	451.00	0.87	483.00	0.28	515.00	0.20	547.00	0.36
356.00	0.00	388.00	0.10	420.00	0.15	452.00	0.75	484.00	0.22	516.00	0.22	548.00	0.02
357.00	0.00	389.00	0.29	421.00	0.79	453.00	0.36	485.00	0.32	517.00	0.20	549.00	0.17
358.00	0.00	390.00	5.49	422.00	0.50	454.00	0.88	486.00	0.34	518.00	0.31	550.00	0.58
359.00	0.00	391.00	4.66	423.00	0.32	455.00	0.94	487.00	0.14	519.00	0.42	551.00	0.12
360.00	0.00	392.00	0.13	424.00	1.10	456.00	0.15	488.00	1.91	520.00	0.58	552.00	0.11
361.00	0.00	393.00	9.60	425.00	0.07	457.00	0.34	489.00	0.21	521.00	0.33	553.00	0.18
362.00	0.00	394.00	0.79	426.00	0.24	458.00	2.85	490.00	0.17	522.00	1.27	554.00	0.10
363.00	0.00	395.00	0.05	427.00	0.48	459.00	0.29	491.00	0.16	523.00	0.41	555.00	0.34
364.00	0.00	396.00	0.07	428.00	0.31	460.00	0.64	492.00	1.56	524.00	0.59	556.00	0.44
365.00	0.00	397.00	0.02	429.00	0.46	461.00	0.88	493.00	0.62	525.00	0.52	557.00	0.28
366.00	0.00	398.00	0.00	430.00	0.43	462.00	0.35	494.00	0.54	526.00	0.19	558.00	1.00
367.00	0.00	399.00	0.47	431.00	0.13	463.00	1.74	495.00	0.14	527.00	0.56	559.00	0.24
368.00	0.00	400.00	7.68	432.00	1.15	464.00	0.73	496.00	0.29	528.00	0.20	560.00	0.05
369.00	0.00	401.00	0.67	433.00	0.43	465.00	0.03	497.00	0.40	529.00	0.23	561.00	0.22
370.00	0.00	402.00	0.12	434.00	0.22	466.00	0.07	498.00	0.21	530.00	0.07	562.00	0.00
371.00	0.00	403.00	0.24	435.00	0.91	467.00	0.20	499.00	0.14	531.00	0.22	563.00	0.09
372.00	0.02	404.00	0.04	436.00	0.43	468.00	0.49	500.00	0.15	532.00	1.36	564.00	0.09
373.00	L.O.C	405.00	0.07	437.00	1.69	469.00	0.35	501.00	0.18	533.00	0.14	565.00	0.16
374.00	0.00	406.00	0.55	438.00	0.38	470.00	0.53	502.00	0.24	534.00	0.29	566.00	0.15
375.00	0.00	407.00	0.35	439.00	1.87	471.00	0.62	503.00	0.75	535.00	0.29	567.00	0.11
376.00	0.00	408.00	0.82	440.00	1.04	472.00	0.37	504.00	0.39	536.00	0.15	568.00	0.19
377.00	0.00	409.00	0.39	441.00	1.96	473.00	0.35	505.00	0.13	537.00	0.15	569.00	0.16
378.00	0.03	410.00	0.73	442.00	7.06	474.00	0.39	506.00	1.19	538.00	2.68	570.00	0.36
379.00	0.00	411.00	0.49	443.00	0.35	475.00	0.63	507.00	0.20	539.00	0.75	571.00	0.41
380.00	0.02	412.00	0.28	444.00	0.22	476.00	0.46	508.00	0.36	540.00	0.13	572.00	0.39
381.00	0.00	413.00	0.71	445.00	0.71	477.00	0.56	509.00	0.29	541.00	0.08	573.00	0.44
382.00	0.04	414.00	1.65	446.00	0.58	478.00	0.33	510.00	0.24	542.00	0.02	574.00	0.17
383.00	0.00	415.00	2.59	447.00	0.41	479.00	0.49	511.00	0.28	543.00	0.36	575.00	0.38

Appendix E: Magnetic Susceptibility
Table 4: Borehole WE001D0

Depth (m)	Av. 3 Values	Depth (m)	Av. 3 Values	Depth (m)	Av. 3 Values	Depth (m)	Av. 3 Values	Depth (m)	Av. 3 Values	Depth (m)	Av. 3 Values	Depth (m)	Av. 3 Values
576.00	2.75	608.00	0.46	640.00	1.23	672.00	69.67	704.00	0.14	736.00	L.O.C	768.00	65.64
577.00	10.02	609.00	0.36	641.00	6.08	673.00	15.35	705.00	L.O.C	737.00	26.47	769.00	40.12
578.00	4.34	610.00	0.45	642.00	0.08	674.00	49.02	706.00	0.94	738.00	0.32	770.00	1.61
579.00	0.14	611.00	3.98	643.00	35.41	675.00	19.07	707.00	0.35	739.00	2.59	771.00	36.64
580.00	0.16	612.00	5.15	644.00	47.66	676.00	0.40	708.00	2.32	740.00	76.93	772.00	72.15
581.00	0.26	613.00	9.05	645.00	54.50	677.00	L.O.C	709.00	9.52	741.00	36.42	773.00	27.32
582.00	6.13	614.00	1.01	646.00	0.06	678.00	L.O.C	710.00	24.39	742.00	44.82	774.00	26.78
583.00	2.68	615.00	6.74	647.00	0.54	679.00	42.93	711.00	0.05	743.00	0.44	775.00	8.52
584.00	6.18	616.00	9.31	648.00	2.62	680.00	9.61	712.00	0.44	744.00	38.35	776.00	0.28
585.00	0.23	617.00	7.56	649.00	40.75	681.00	41.76	713.00	0.42	745.00	46.26	777.00	0.13
586.00	0.15	618.00	0.90	650.00	31.60	682.00	10.15	714.00	0.12	746.00	47.36	778.00	0.64
587.00	0.11	619.00	0.00	651.00	L.O.C	683.00	14.45	715.00	0.00	747.00	73.58	779.00	1.65
588.00	0.00	620.00	0.00	652.00	L.O.C	684.00	L.O.C	716.00	L.O.C	748.00	55.30	780.00	0.63
589.00	0.11	621.00	0.07	653.00	L.O.C	685.00	0.34	717.00	0.23	749.00	23.64	781.00	13.25
590.00	0.19	622.00	0.04	654.00	42.48	686.00	0.20	718.00	31.77	750.00	1.87	782.00	27.38
591.00	0.24	623.00	0.00	655.00	32.56	687.00	0.32	719.00	L.O.C	751.00	0.47	783.00	0.41
592.00	0.08	624.00	0.08	656.00	25.29	688.00	6.36	720.00	8.66	752.00	0.14	784.00	4.53
593.00	0.08	625.00	17.92	657.00	L.O.C	689.00	12.06	721.00	0.28	753.00	66.72	785.00	29.17
594.00	0.00	626.00	14.08	658.00	0.67	690.00	L.O.C	722.00	29.15	754.00	10.16	786.00	0.06
595.00	0.13	627.00	0.00	659.00	2.63	691.00	0.05	723.00	23.38	755.00	0.32	787.00	0.05
596.00	0.06	628.00	0.15	660.00	0.41	692.00	12.79	724.00	19.51	756.00	0.05	788.00	1.19
597.00	0.11	629.00	8.25	661.00	0.19	693.00	1.52	725.00	14.31	757.00	4.46	789.00	1.04
598.00	0.02	630.00	0.00	662.00	0.00	694.00	0.57	726.00	0.11	758.00	0.32	790.00	1.51
599.00	0.15	631.00	6.23	663.00	0.43	695.00	0.55	727.00	26.65	759.00	20.75	791.00	0.10
600.00	0.00	632.00	0.06	664.00	0.19	696.00	2.17	728.00	21.36	760.00	2.88	792.00	1.10
601.00	11.93	633.00	0.01	665.00	0.01	697.00	0.09	729.00	6.85	761.00	1.70	793.00	0.85
602.00	5.01	634.00	0.08	666.00	L.O.C	698.00	0.51	730.00	0.15	762.00	0.43	794.00	0.00
603.00	0.00	635.00	1.71	667.00	L.O.C	699.00	L.O.C	731.00	6.91	763.00	30.12	795.00	28.47
604.00	0.15	636.00	1.67	668.00	0.23	700.00	10.05	732.00	0.85	764.00	41.63	796.00	0.20
605.00	0.25	637.00	1.29	669.00	0.14	701.00	1.77	733.00	1.97	765.00	47.90	797.00	2.98
606.00	4.20	638.00	2.13	670.00	0.00	702.00	3.38	734.00	4.58	766.00	7.03	798.00	0.05
607.00	0.14	639.00	6.12	671.00	29.79	703.00	0.68	735.00	47.82	767.00	0.31	799.00	0.21

Appendix E: Magnetic Susceptibility
Table 4: Borehole WE001D0

Depth (m)	Av. 3 Values	Depth (m)	Av. 3 Values	Depth (m)	Av. 3 Values	Depth (m)	Av. 3 Values	Depth (m)	Av. 3 Values	Depth (m)	Av. 3 Values
800.00	0.48	810.00	0.02	820.00	0.00	830.00	0.00	840.00	0.05	850.00	0.32
801.00	0.25	811.00	0.39	821.00	0.94	831.00	1.59	841.00	0.18		
802.00	0.18	812.00	0.10	822.00	0.55	832.00	0.00	842.00	0.00		
803.00	1.00	813.00	0.03	823.00	0.78	833.00	0.00	843.00	0.12		
804.00	8.95	814.00	0.44	824.00	0.45	834.00	0.00	844.00	1.05		
805.00	4.65	815.00	0.25	825.00	2.52	835.00	0.00	845.00	2.50		
806.00	3.27	816.00	0.02	826.00	0.00	836.00	0.00	846.00	0.04		
807.00	0.24	817.00	0.00	827.00	0.00	837.00	0.00	847.00	0.85		
808.00	0.10	818.00	0.00	828.00	0.00	838.00	0.25	848.00	8.47		
809.00	0.07	819.00	0.02	829.00	0.05	839.00	0.02	849.00	1.31		

Appendix E: Magnetic Susceptibility Interpretation
Figure 4: Borehole WE001D0

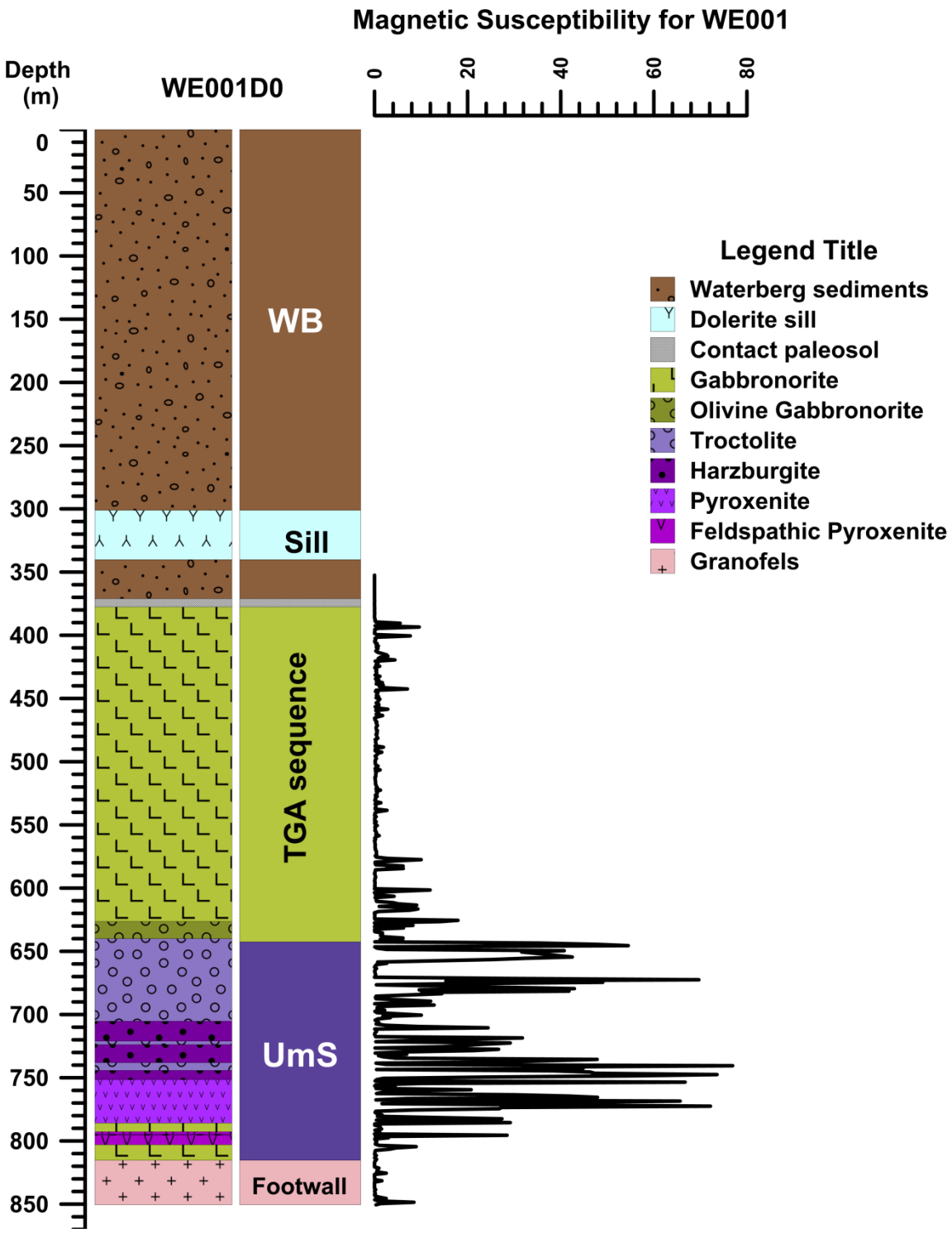

Appendix E: Magnetic Susceptibility
Table 5: Borehole WE027D0

Depth (m)	Av. 3 Values	Depth (m)	Av. 3 Values	Depth (m)	Av. 3 Values	Depth (m)	Av. 3 Values	Depth (m)	Av. 3 Values	Depth (m)	Av. 3 Values	Depth (m)	Av. 3 Values
536.00	0.00	568.00	1.89	600.00	0.57	632.00	1.56	664.00	1.47	696.00	2.89	728.00	0.02
537.00	0.04	569.00	0.04	601.00	2.77	633.00	0.83	665.00	1.43	697.00	2.65	729.00	0.00
538.00	0.00	570.00	0.02	602.00	6.37	634.00	0.52	666.00	0.92	698.00	4.41	730.00	0.00
539.00	0.00	571.00	0.02	603.00	0.04	635.00	0.79	667.00	0.93	699.00	1.03	731.00	14.36
540.00	0.00	572.00	6.87	604.00	0.00	636.00	0.33	668.00	0.70	700.00	2.36	732.00	0.02
541.00	0.00	573.00	5.34	605.00	0.53	637.00	0.55	669.00	1.03	701.00	5.18	733.00	0.00
542.00	0.00	574.00	2.80	606.00	0.31	638.00	0.64	670.00	4.17	702.00	4.68	734.00	0.03
543.00	0.00	575.00	6.33	607.00	0.42	639.00	0.54	671.00	4.63	703.00	4.70	735.00	0.00
544.00	0.00	576.00	0.36	608.00	0.57	640.00	0.48	672.00	4.19	704.00	5.42	736.00	1.03
545.00	0.00	577.00	1.12	609.00	0.64	641.00	1.63	673.00	5.87	705.00	0.18	737.00	0.00
546.00	0.00	578.00	0.06	610.00	0.37	642.00	2.05	674.00	5.91	706.00	0.60	738.00	0.16
547.00	0.00	579.00	0.19	611.00	0.87	643.00	0.18	675.00	3.44	707.00	5.69	739.00	0.08
548.00	0.00	580.00	0.69	612.00	0.13	644.00	0.78	676.00	1.78	708.00	1.18	740.00	0.06
549.00	0.00	581.00	5.21	613.00	0.97	645.00	0.63	677.00	1.17	709.00	0.14	741.00	1.16
550.00	0.00	582.00	1.86	614.00	2.74	646.00	1.78	678.00	1.07	710.00	2.44	742.00	0.66
551.00	0.00	583.00	0.06	615.00	0.12	647.00	1.59	679.00	0.20	711.00	0.15	743.00	0.08
552.00	0.00	584.00	0.22	616.00	0.00	648.00	0.88	680.00	3.85	712.00	0.35	744.00	0.41
553.00	0.00	585.00	0.60	617.00	3.62	649.00	1.65	681.00	4.48	713.00	3.40	745.00	4.41
554.00	0.00	586.00	0.63	618.00	0.02	650.00	0.62	682.00	0.66	714.00	2.94	746.00	2.55
555.00	0.00	587.00	0.21	619.00	0.00	651.00	1.24	683.00	1.75	715.00	0.08	747.00	2.37
556.00	0.00	588.00	0.38	620.00	41.94	652.00	0.91	684.00	3.91	716.00	1.20	748.00	0.40
557.00	0.02	589.00	0.00	621.00	0.22	653.00	0.13	685.00	4.73	717.00	1.72	749.00	1.10
558.00	5.05	590.00	1.72	622.00	1.47	654.00	0.04	686.00	2.74	718.00	0.76	750.00	0.94
559.00	8.74	591.00	0.70	623.00	0.25	655.00	0.08	687.00	3.09	719.00	9.68	751.00	4.55
560.00	6.90	592.00	0.78	624.00	0.01	656.00	0.07	688.00	0.25	720.00	1.62	752.00	1.04
561.00	1.23	593.00	0.26	625.00	1.54	657.00	0.14	689.00	0.06	721.00	0.00	753.00	0.82
562.00	4.05	594.00	0.37	626.00	0.50	658.00	0.36	690.00	5.17	722.00	0.00	754.00	2.80
563.00	2.11	595.00	0.17	627.00	2.22	659.00	1.96	691.00	2.84	723.00	0.09	755.00	1.08
564.00	4.71	596.00	0.11	628.00	0.04	660.00	1.83	692.00	2.36	724.00	5.14	756.00	0.05
565.00	5.05	597.00	0.07	629.00	1.29	661.00	0.80	693.00	2.28	725.00	0.62	757.00	0.54
566.00	2.94	598.00	0.40	630.00	0.97	662.00	0.72	694.00	3.67	726.00	0.12	758.00	5.01
567.00	3.22	599.00	0.27	631.00	0.02	663.00	1.50	695.00	1.80	727.00	0.00	759.00	3.66

Appendix E: Magnetic Susceptibility
Table 5: Borehole WE027D0

Depth (m)	Av. 3 Values	Depth (m)	Av. 3 Values	Depth (m)	Av. 3 Values	Depth (m)	Av. 3 Values	Depth (m)	Av. 3 Values	Depth (m)	Av. 3 Values	Depth (m)	Av. 3 Values
760.00	4.65	792.00	2.21	862.00	4.87	894.00	0.00	926.00	0.13	958.00	0.94	990.00	0.00
761.00	1.40	797.00	4.36	863.00	0.33	895.00	6.01	927.00	1.16	959.00	1.43	991.00	0.01
762.00	0.80	802.00	5.63	864.00	0.45	896.00	0.25	928.00	3.38	960.00	0.26	992.00	0.00
763.00	2.25	809.00	0.05	865.00	0.21	897.00	0.51	929.00	1.94	961.00	2.11	993.00	0.00
764.00	1.42	810.00	0.07	866.00	1.89	898.00	0.44	930.00	1.72	962.00	1.93	994.00	0.01
765.00	2.22	811.00	0.86	867.00	3.60	899.00	0.03	931.00	2.33	963.00	2.50	995.00	2.11
766.00	2.07	816.00	2.00	868.00	0.00	900.00	1.81	932.00	2.85	964.00	1.56	1000.00	5.30
767.00	2.44	821.00	2.88	869.00	0.65	901.00	0.82	933.00	0.33	965.00	2.22	1005.00	1.01
768.00	1.12	826.00	2.55	870.00	0.07	902.00	1.19	934.00	1.85	966.00	1.66	1010.00	4.97
769.00	0.08	831.00	2.55	871.00	1.55	903.00	3.35	935.00	2.19	967.00	3.54	1015.00	6.86
770.00	0.95	836.00	3.98	872.00	0.04	904.00	0.49	936.00	1.84	968.00	2.23	1020.00	7.35
771.00	2.90	841.00	1.33	873.00	0.01	905.00	0.99	937.00	2.14	969.00	2.10	1025.00	4.62
772.00	1.57	842.00	0.75	874.00	2.36	906.00	0.86	938.00	1.21	970.00	2.98	1030.00	7.05
773.00	1.36	843.00	0.00	875.00	1.76	907.00	0.54	939.00	0.61	971.00	2.59	1035.00	7.08
774.00	1.25	844.00	0.01	876.00	0.85	908.00	0.12	940.00	4.07	972.00	4.32	1040.00	6.39
775.00	0.61	845.00	1.24	877.00	1.75	909.00	0.95	941.00	0.11	973.00	2.04	1045.00	6.98
776.00	0.35	846.00	0.01	878.00	0.91	910.00	0.99	942.00	3.00	974.00	7.08	1050.00	5.01
777.00	2.53	847.00	0.14	879.00	1.60	911.00	0.28	943.00	3.07	975.00	2.09	1055.00	6.29
778.00	2.39	848.00	0.25	880.00	1.34	912.00	0.72	944.00	1.54	976.00	3.25	1060.00	9.88
779.00	1.97	849.00	2.59	881.00	0.61	913.00	0.77	945.00	2.67	977.00	1.96	1065.00	6.08
780.00	1.16	850.00	3.48	882.00	1.01	914.00	1.70	946.00	2.35	978.00	1.51	1070.00	9.07
781.00	0.34	851.00	1.28	883.00	1.43	915.00	0.88	947.00	4.84	979.00	2.71	1075.00	5.80
782.00	0.64	852.00	1.14	884.00	1.44	916.00	0.52	948.00	2.66	980.00	2.56	1080.00	7.80
783.00	1.44	853.00	0.13	885.00	2.43	917.00	0.79	949.00	0.04	981.00	0.00	1085.00	9.02
784.00	1.24	854.00	1.21	886.00	2.29	918.00	0.38	950.00	3.12	982.00	4.26	1090.00	6.02
785.00	0.69	855.00	0.18	887.00	0.41	919.00	0.49	951.00	2.91	983.00	0.00	1095.00	5.13
786.00	1.39	856.00	0.11	888.00	0.09	920.00	0.88	952.00	1.75	984.00	0.00	1100.00	4.36
787.00	1.29	857.00	4.98	889.00	90.73	921.00	0.99	953.00	1.41	985.00	0.00	1105.00	4.33
788.00	0.62	858.00	0.03	890.00	7.42	922.00	0.24	954.00	2.01	986.00	0.02	1110.00	7.30
789.00	0.99	859.00	1.16	891.00	14.24	923.00	1.61	955.00	6.77	987.00	0.04	1115.00	6.64
790.00	0.24	860.00	0.55	892.00	1.30	924.00	1.39	956.00	1.38	988.00	0.01	1120.00	1.32
791.00	0.25	861.00	4.37	893.00	15.12	925.00	0.56	957.00	0.81	989.00	0.00	1125.00	7.10

Appendix E: Magnetic Susceptibility
Table 5: Borehole WE027D0

Depth (m)	Av. 3 Values	Depth (m)	Av. 3 Values	Depth (m)	Av. 3 Values	Depth (m)	Av. 3 Values	Depth (m)	Av. 3 Values	Depth (m)	Av. 3 Values	Depth (m)	Av. 3 Values
1130.00	7.37	1259.00	0.45	1291.00	3.20	1323.00	0.08	1355.00	0.60	1387.00	0.10	1419.00	0.51
1135.00	7.26	1260.00	3.40	1292.00	0.82	1324.00	0.13	1356.00	0.00	1388.00	0.04	1420.00	0.02
1140.00	8.80	1261.00	0.59	1293.00	0.06	1325.00	0.49	1357.00	0.11	1389.00	0.10	1421.00	0.01
1145.00	7.49	1262.00	0.51	1294.00	0.84	1326.00	0.11	1358.00	0.20	1390.00	0.46	1422.00	0.13
1150.00	7.85	1263.00	0.08	1295.00	1.38	1327.00	0.10	1359.00	0.24	1391.00	0.16	1423.00	0.18
1155.00	7.92	1264.00	0.39	1296.00	0.17	1328.00	4.53	1360.00	0.05	1392.00	0.09	1424.00	0.31
1160.00	7.55	1265.00	0.55	1297.00	1.36	1329.00	2.88	1361.00	0.10	1393.00	0.33	1425.00	0.05
1165.00	8.24	1266.00	0.14	1298.00	2.22	1330.00	2.45	1362.00	0.07	1394.00	0.92	1426.00	0.08
1170.00	9.04	1267.00	1.86	1299.00	0.16	1331.00	3.05	1363.00	0.07	1395.00	0.38	1427.00	0.65
1175.00	8.36	1268.00	0.31	1300.00	1.82	1332.00	3.49	1364.00	0.07	1396.00	0.22	1428.00	0.24
1180.00	7.81	1269.00	1.22	1301.00	0.01	1333.00	1.69	1365.00	0.04	1397.00	0.00	1429.00	1.38
1185.00	8.05	1270.00	0.05	1302.00	0.01	1334.00	5.53	1366.00	0.17	1398.00	0.07	1430.00	1.44
1190.00	7.90	1271.00	0.09	1303.00	0.09	1335.00	5.68	1367.00	0.14	1399.00	0.01	1431.00	1.06
1195.00	7.76	1272.00	2.31	1304.00	0.48	1336.00	17.60	1368.00	0.12	1400.00	0.06	1432.00	1.78
1200.00	0.25	1273.00	0.29	1305.00	1.11	1337.00	11.37	1369.00	0.11	1401.00	0.38	1433.00	6.12
1205.00	7.47	1274.00	0.00	1306.00	0.10	1338.00	0.00	1370.00	0.11	1402.00	0.08	1434.00	1.89
1210.00	7.62	1275.00	0.65	1307.00	0.35	1339.00	0.05	1371.00	0.09	1403.00	0.05	1435.00	0.95
1215.00	6.95	1276.00	0.00	1308.00	0.53	1340.00	0.24	1372.00	0.12	1404.00	0.33	1436.00	0.81
1220.00	6.82	1277.00	0.00	1309.00	0.27	1341.00	0.04	1373.00	0.04	1405.00	0.11	1437.00	1.59
1225.00	6.69	1278.00	0.05	1310.00	0.02	1342.00	0.01	1374.00	0.04	1406.00	0.05	1438.00	1.09
1230.00	5.38	1279.00	1.22	1311.00	1.49	1343.00	0.12	1375.00	0.04	1407.00	0.01	1439.00	0.03
1235.00	6.28	1280.00	0.05	1312.00	0.27	1344.00	0.03	1376.00	0.11	1408.00	0.04	1440.00	0.02
1240.00	4.25	1281.00	0.09	1313.00	0.51	1345.00	0.24	1377.00	0.01	1409.00	0.05	1441.00	0.14
1245.00	2.14	1282.00	2.31	1314.00	0.04	1346.00	0.21	1378.00	0.02	1410.00	0.11	1442.00	0.60
1250.00	6.93	1283.00	0.03	1315.00	0.07	1347.00	0.22	1379.00	0.06	1411.00	0.02	1443.00	0.18
1252.00	1.67	1284.00	0.90	1316.00	0.04	1348.00	0.47	1380.00	0.06	1412.00	1.72	1444.00	0.13
1253.00	1.29	1285.00	0.02	1317.00	0.07	1349.00	0.22	1381.00	0.04	1413.00	0.27	1445.00	8.41
1254.00	0.04	1286.00	0.09	1318.00	0.08	1350.00	0.41	1382.00	4.57	1414.00	0.57	1446.00	0.31
1255.00	1.00	1287.00	1.90	1319.00	0.04	1351.00	0.36	1383.00	1.27	1415.00	0.58	1447.00	0.01
1256.00	0.00	1288.00	1.07	1320.00	0.02	1352.00	0.66	1384.00	21.43	1416.00	5.09	1448.00	13.04
1257.00	0.15	1289.00	1.77	1321.00	0.04	1353.00	0.33	1385.00	28.90	1417.00	2.15	1449.00	0.65
1258.00	0.00	1290.00	1.57	1322.00	0.05	1354.00	0.42	1386.00	31.21	1418.00	0.65	1450.00	1.08

Appendix E: Magnetic Susceptibility
Table 5: Borehole WE027D0

Depth (m)	Av. 3 Values	Depth (m)	Av. 3 Values	Depth (m)	Av. 3 Values	Depth (m)	Av. 3 Values	Depth (m)	Av. 3 Values	Depth (m)	Av. 3 Values	Depth (m)	Av. 3 Values
1451.00	8.81	1456.00	0.03	1461.00	12.16	1466.00	9.12	1471.00	0.00	1476.00	0.00		
1452.00	3.80	1457.00	3.59	1462.00	0.78	1467.00	0.00	1472.00	0.00	1477.00	0.00		
1453.00	6.23	1458.00	3.96	1463.00	0.00	1468.00	12.62	1473.00	0.00				
1454.00	18.05	1459.00	7.32	1464.00	0.00	1469.00	0.89	1474.00	0.00				
1455.00	4.07	1460.00	28.76	1465.00	18.27	1470.00	31.27	1475.00	0.00				

Appendix E: Magnetic Susceptibility Interpretation
Figure 5: Borehole WE027D0

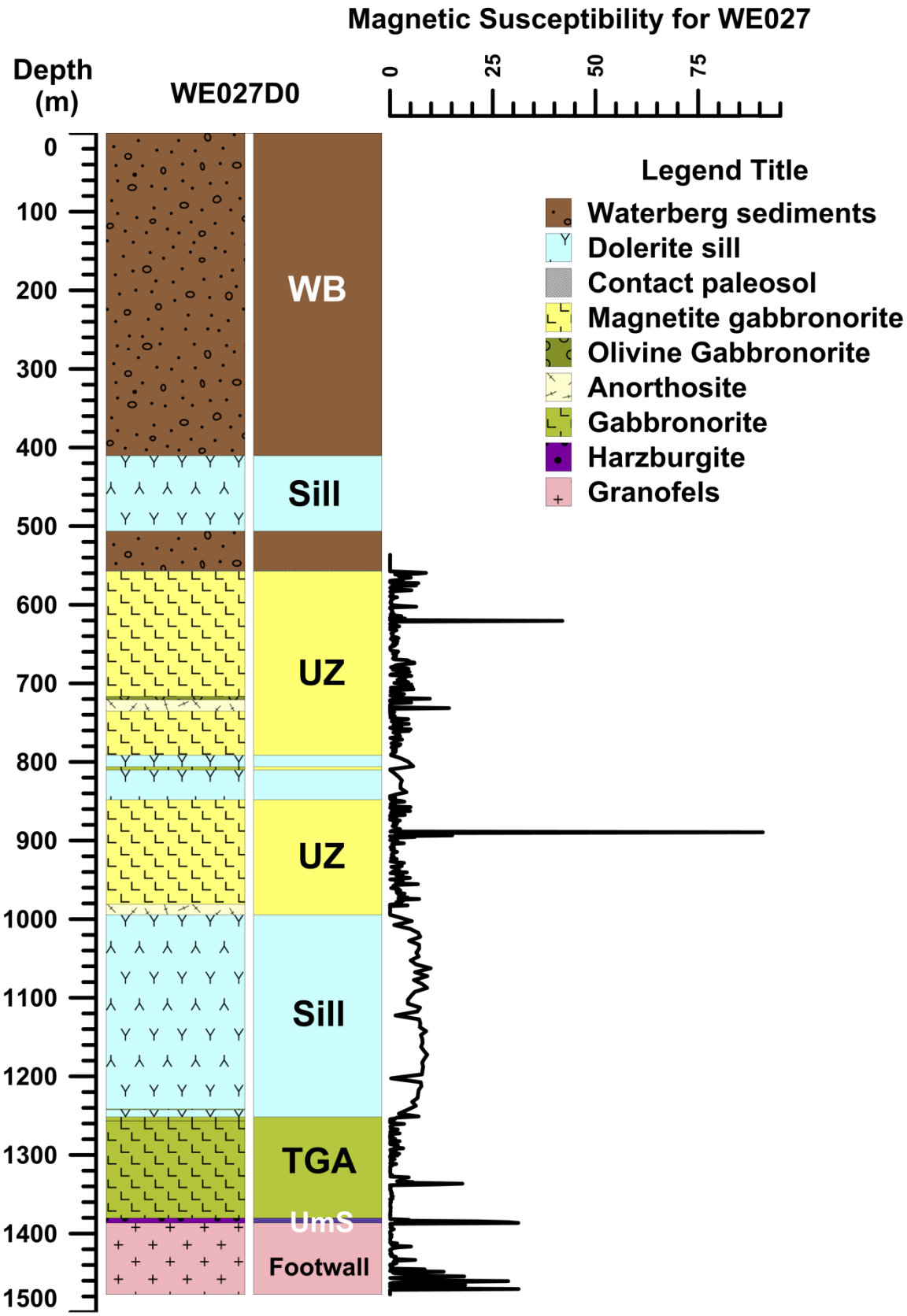

Appendix E: Magnetic Susceptibility
Table 6: Borehole WE035D0

Depth (m)	Av. 3 Values	Depth (m)	Av. 3 Values	Depth (m)	Av. 3 Values	Depth (m)	Av. 3 Values	Depth (m)	Av. 3 Values	Depth (m)	Av. 3 Values	Depth (m)	Av. 3 Values
358.00	0.00	390.00	0.37	422.00	0.09	454.00	0.03	486.00	0.07	518.00	0.09	550.00	0.05
359.00	0.00	391.00	0.69	423.00	0.09	455.00	0.06	487.00	0.05	519.00	0.10	551.00	0.04
360.00	0.00	392.00	2.52	424.00	0.11	456.00	0.20	488.00	0.01	520.00	4.34	552.00	0.08
361.00	0.00	393.00	0.61	425.00	0.15	457.00	0.26	489.00	0.00	521.00	0.04	553.00	0.09
362.00	0.00	394.00	2.76	426.00	0.15	458.00	0.04	490.00	0.01	522.00	0.00	554.00	0.03
363.00	0.00	395.00	0.74	427.00	0.25	459.00	0.18	491.00	0.00	523.00	0.01	555.00	0.04
364.00	0.00	396.00	0.04	428.00	0.68	460.00	0.12	492.00	0.04	524.00	0.19	556.00	0.09
365.00	0.00	397.00	0.48	429.00	0.21	461.00	0.06	493.00	0.07	525.00	0.11	557.00	0.05
366.00	0.00	398.00	0.12	430.00	0.34	462.00	0.00	494.00	1.18	526.00	0.11	558.00	2.36
367.00	0.00	399.00	0.21	431.00	0.69	463.00	0.05	495.00	0.28	527.00	L.O.C	559.00	0.75
368.00	0.00	400.00	0.31	432.00	0.25	464.00	0.02	496.00	2.64	528.00	5.36	560.00	4.53
369.00	0.00	401.00	0.28	433.00	0.08	465.00	0.05	497.00	0.31	529.00	3.39	561.00	2.82
370.00	0.02	402.00	1.61	434.00	0.07	466.00	0.01	498.00	0.08	530.00	0.03	562.00	1.17
371.00	0.01	403.00	0.45	435.00	0.13	467.00	0.02	499.00	0.15	531.00	0.15	563.00	1.71
372.00	0.00	404.00	0.69	436.00	0.12	468.00	0.02	500.00	0.03	532.00	0.03	564.00	0.43
373.00	0.00	405.00	0.14	437.00	0.31	469.00	0.00	501.00	0.01	533.00	5.26	565.00	0.02
374.00	0.01	406.00	0.06	438.00	0.27	470.00	0.00	502.00	0.03	534.00	0.19	566.00	0.05
375.00	0.13	407.00	0.00	439.00	0.13	471.00	0.12	503.00	0.04	535.00	2.17	567.00	3.34
376.00	1.94	408.00	0.87	440.00	0.46	472.00	0.09	504.00	0.04	536.00	0.09	568.00	0.16
377.00	0.01	409.00	0.44	441.00	0.70	473.00	0.00	505.00	0.06	537.00	1.48	569.00	1.01
378.00	1.93	410.00	0.44	442.00	0.08	474.00	0.15	506.00	0.04	538.00	0.03	570.00	4.63
379.00	0.56	411.00	0.93	443.00	0.17	475.00	1.29	507.00	0.09	539.00	7.97	571.00	L.O.C
380.00	2.53	412.00	1.60	444.00	0.15	476.00	0.30	508.00	0.06	540.00	1.56	572.00	1.05
381.00	2.82	413.00	0.24	445.00	0.14	477.00	0.01	509.00	0.13	541.00	8.60	573.00	12.98
382.00	0.37	414.00	0.30	446.00	0.09	478.00	0.06	510.00	0.08	542.00	2.13	574.00	L.O.C
383.00	0.13	415.00	1.24	447.00	0.21	479.00	0.03	511.00	0.10	543.00	1.78	575.00	7.39
384.00	0.22	416.00	0.33	448.00	0.98	480.00	0.06	512.00	0.06	544.00	0.03	576.00	0.62
385.00	0.12	417.00	0.25	449.00	0.11	481.00	0.19	513.00	0.08	545.00	0.01	577.00	0.79
386.00	0.31	418.00	0.09	450.00	0.42	482.00	0.12	514.00	0.05	546.00	0.03	578.00	5.57
387.00	0.40	419.00	0.11	451.00	0.38	483.00	0.10	515.00	4.93	547.00	0.02	579.00	L.O.C
388.00	0.85	420.00	0.14	452.00	0.23	484.00	0.12	516.00	0.03	548.00	0.78	580.00	0.28
389.00	0.54	421.00	0.10	453.00	0.07	485.00	0.07	517.00	0.07	549.00	0.21	581.00	0.57

Appendix E: Magnetic Susceptibility
Table 6: Borehole WE035D0

Depth (m)	Av. 3 Values	Depth (m)	Av. 3 Values	Depth (m)	Av. 3 Values	Depth (m)	Av. 3 Values	Depth (m)	Av. 3 Values	Depth (m)	Av. 3 Values	Depth (m)	Av. 3 Values
582.00	L.O.C	614.00	16.39	646.00	0.55	678.00	0.03	710.00	0.02				
583.00	L.O.C	615.00	0.09	647.00	0.43	679.00	0.04	711.00	0.08				
584.00	L.O.C	616.00	0.15	648.00	0.47	680.00	0.77	712.00	0.05				
585.00	0.04	617.00	0.02	649.00	0.26	681.00	0.48	713.00	0.13				
586.00	0.03	618.00	0.11	650.00	3.51	682.00	0.06	714.00	0.08				
587.00	L.O.C	619.00	0.07	651.00	0.05	683.00	0.08	715.00	0.08				
588.00	L.O.C	620.00	0.25	652.00	0.05	684.00	0.00	716.00	0.19				
589.00	L.O.C	621.00	0.03	653.00	1.00	685.00	0.05	717.00	0.05				
590.00	0.06	622.00	3.87	654.00	0.04	686.00	0.08	718.00	1.36				
591.00	L.O.C	623.00	0.26	655.00	0.05	687.00	0.03	719.00	0.25				
592.00	L.O.C	624.00	0.11	656.00	0.11	688.00	0.06	720.00	0.06				
593.00	L.O.C	625.00	0.68	657.00	0.07	689.00	1.16	721.00	0.08				
594.00	L.O.C	626.00	0.06	658.00	0.04	690.00	0.29	722.00	0.09				
595.00	L.O.C	627.00	0.06	659.00	0.00	691.00	2.07	723.00	0.08				
596.00	0.29	628.00	0.09	660.00	0.03	692.00	1.18	724.00	0.54				
597.00	3.07	629.00	0.19	661.00	0.00	693.00	0.55	725.00	1.43				
598.00	8.87	630.00	0.24	662.00	0.00	694.00	0.07	726.00	0.24				
599.00	4.06	631.00	0.00	663.00	0.00	695.00	1.76	727.00	0.56				
600.00	3.41	632.00	0.30	664.00	0.00	696.00	2.55	728.00	0.06				
601.00	0.30	633.00	0.01	665.00	0.01	697.00	0.73	729.00	4.14				
602.00	L.O.C	634.00	0.02	666.00	0.26	698.00	0.05	730.00	5.29				
603.00	0.04	635.00	0.00	667.00	0.01	699.00	0.04	731.00	2.58				
604.00	0.06	636.00	0.06	668.00	0.08	700.00	0.10						
605.00	0.11	637.00	0.08	669.00	0.35	701.00	0.01						
606.00	0.06	638.00	1.72	670.00	0.26	702.00	0.09						
607.00	15.16	639.00	0.09	671.00	0.25	703.00	0.04						
608.00	10.55	640.00	0.08	672.00	0.82	704.00	0.03						
609.00	0.72	641.00	0.08	673.00	0.56	705.00	0.07						
610.00	0.32	642.00	0.07	674.00	0.09	706.00	0.04						
611.00	0.41	643.00	0.41	675.00	0.33	707.00	0.16						
612.00	0.20	644.00	0.36	676.00	0.01	708.00	0.05						
613.00	7.32	645.00	0.10	677.00	0.24	709.00	0.06						

Appendix E: Magnetic Susceptibility Interpretation
Figure 6: Borehole WE035D0

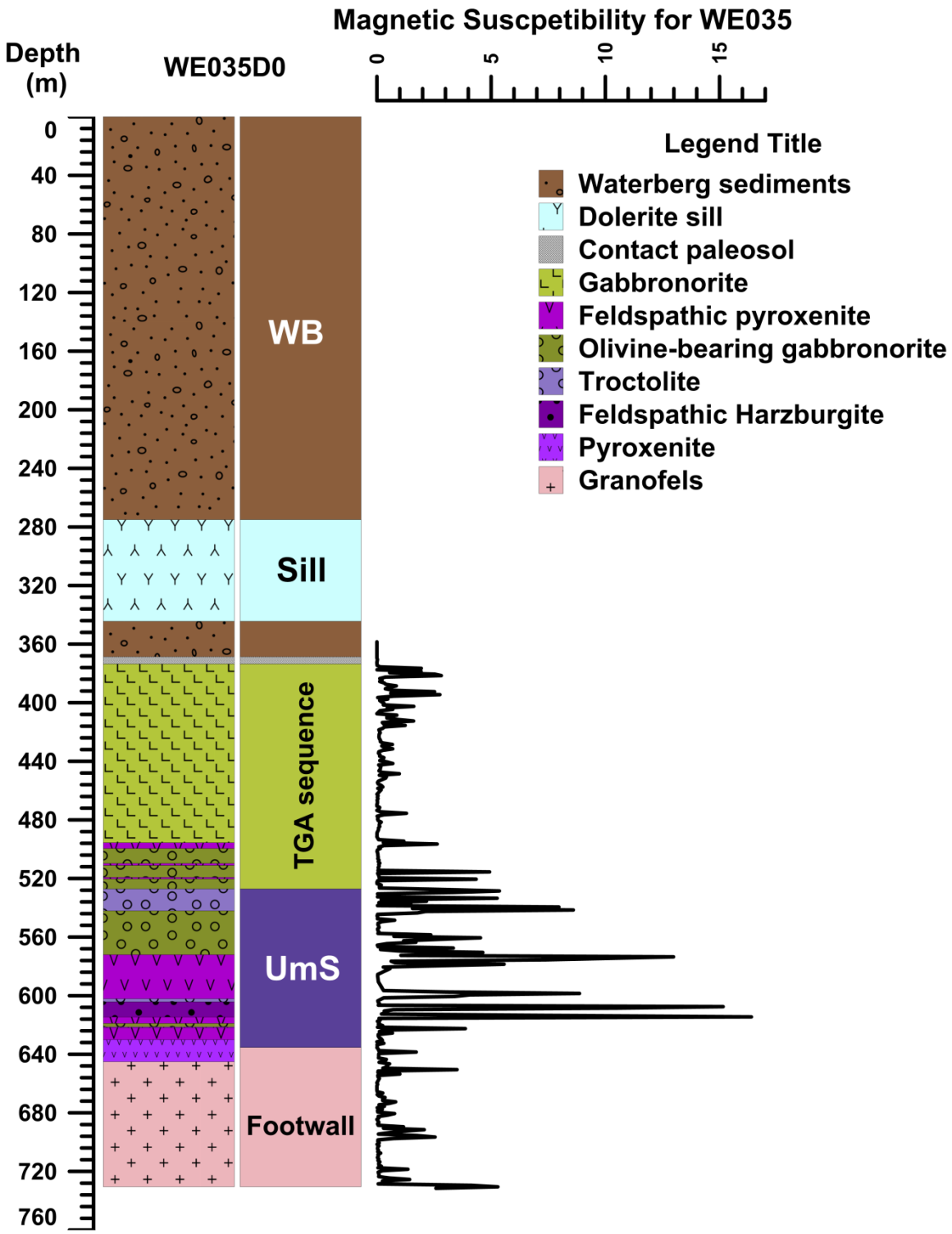

Appendix E: Magnetic Susceptibility

Table 7: Borehole LAP 31 from the Aurora Project

Depth (m)	Av. 3 Values	Depth (m)	Av. 3 Values	Depth (m)	Av. 3 Values	Depth (m)	Av. 3 Values	Depth (m)	Av. 3 Values	Depth (m)	Av. 3 Values
16.0	2.89	41.0	3.92	66.0	26.87	91.0	29.57	116.0	0.19	141.0	0.11
17.0	2.77	42.0	4.84	67.0	0.64	92.0	6.30	117.0	8.26	142.0	29.83
18.0	7.40	43.0	5.77	68.0	3.38	93.0	11.50	118.0	1.21	143.0	0.19
19.0	3.68	44.0	6.43	69.0	2.24	94.0	0.17	119.0	1.83	144.0	166.67
20.0	10.47	45.0	8.44	70.0	0.93	95.0	0.44	120.0	0.58	145.0	562.33
21.0	7.44	46.0	9.00	71.0	1.59	96.0	0.10	121.0	1.04	146.0	0.70
22.0	2.92	47.0	5.60	72.0	116.67	97.0	3.37	122.0	8.47	147.0	0.28
23.0	3.13	48.0	6.12	73.0	7.82	98.0	0.20	123.0	0.60	148.0	76.40
24.0	8.85	49.0	10.57	74.0	4.67	99.0	0.63	124.0	2.44	149.0	0.21
25.0	1.68	50.0	8.60	75.0	2.78	100.0	2.43	125.0	2.91	150.0	384.00
26.0	5.41	51.0	8.25	76.0	1.32	101.0	3.39	126.0	0.43	151.0	67.60
27.0	8.87	52.0	15.47	77.0	0.16	102.0	29.03	127.0	69.87	152.0	0.26
28.0	9.17	53.0	9.49	78.0	0.19	103.0	9.44	128.0	36.40	153.0	1.79
29.0	6.51	54.0	5.11	79.0	0.33	104.0	22.33	129.0	0.24	154.0	0.19
30.0	6.71	55.0	8.31	80.0	0.24	105.0	0.25	130.0	17.30	155.0	0.45
31.0	10.63	56.0	27.77	81.0	0.17	106.0	0.31	131.0	1.61	156.0	0.29
32.0	8.09	57.0	2.27	82.0	0.97	107.0	0.33	132.0	4.78	157.0	0.06
33.0	3.45	58.0	6.65	83.0	0.42	108.0	30.73	133.0	0.14	158.0	47.13
34.0	7.41	59.0	8.41	84.0	0.50	109.0	2.26	134.0	7.10	159.0	15.93
35.0	5.08	60.0	12.57	85.0	1.02	110.0	1.49	135.0	0.41	160.0	0.41
36.0	4.33	61.0	7.74	86.0	8.73	111.0	36.10	136.0	0.11	161.0	0.20
37.0	6.74	62.0	98.00	87.0	13.27	112.0	6.31	137.0	8.81	162.0	0.49
38.0	3.34	63.0	9.45	88.0	0.34	113.0	4.83	138.0	0.16	163.0	1.60
39.0	3.86	64.0	7.91	89.0	7.33	114.0	3.91	139.0	0.28	164.0	0.93
40.0	6.70	65.0	8.43	90.0	15.43	115.0	0.35	140.0	964.67	165.0	0.17

Appendix E: Magnetic Susceptibility
Table 7: Borehole LAP 31 from the Aurora Project

Depth (m)	Av. 3 Values	Depth (m)	Av. 3 Values	Depth (m)	Av. 3 Values	Depth (m)	Av. 3 Values	Depth (m)	Av. 3 Values	Depth (m)	Av. 3 Values
166.0	1.18	191.0	2.45	216.0	16.97	241.0	0.41	266.0	0.44	291.0	0.28
167.0	85.20	192.0	1.64	217.0	50.53	242.0	0.40	267.0	0.31	292.0	1.50
168.0	0.25	193.0	0.74	218.0	3.38	243.0	0.38	268.0	0.35	293.0	0.52
169.0	0.98	194.0	1.10	219.0	0.61	244.0	0.33	269.0	0.21	294.0	0.72
170.0	704.00	195.0	3.14	220.0	0.31	245.0	0.43	270.0	0.30	295.0	0.42
171.0	0.00	196.0	1.64	221.0	0.54	246.0	0.27	271.0	0.28	296.0	0.39
172.0	0.33	197.0	4.20	222.0	3.36	247.0	0.36	272.0	0.33	297.0	2.98
173.0	0.14	198.0	4.66	223.0	19.87	248.0	0.27	273.0	0.33	298.0	2.62
174.0	14.33	199.0	0.58	224.0	42.80	249.0	2.76	274.0	0.55	299.0	0.32
175.0	8.17	200.0	0.21	225.0	3.75	250.0	1.93	275.0	0.25	300.0	0.20
176.0	41.73	201.0	18.90	226.0	2.14	251.0	1.00	276.0	0.37	301.0	4.87
177.0	0.16	202.0	210.67	227.0	11.03	252.0	0.40	277.0	0.37	302.0	4.11
178.0	0.16	203.0	294.33	228.0	0.43	253.0	0.22	278.0	0.38	303.0	0.45
179.0	0.21	204.0	254.33	229.0	0.47	254.0	0.41	279.0	0.39	304.0	0.41
180.0	0.15	205.0	196.00	230.0	0.29	255.0	0.36	280.0	1.06	305.0	0.25
181.0	0.14	206.0	8.04	231.0	0.25	256.0	0.51	281.0	0.94	306.0	0.25
182.0	0.13	207.0	0.17	232.0	0.77	257.0	0.26	282.0	0.55	307.0	0.38
183.0	45.33	208.0	0.34	233.0	1.82	258.0	0.43	283.0	0.34	308.0	0.52
184.0	3.38	209.0	0.92	234.0	0.39	259.0	0.42	284.0	0.94	309.0	0.32
185.0	0.08	210.0	0.25	235.0	0.83	260.0	0.35	285.0	0.96	310.0	0.25
186.0	0.39	211.0	0.22	236.0	1.80	261.0	0.43	286.0	0.90	311.0	0.26
187.0	0.20	212.0	0.17	237.0	0.26	262.0	1.87	287.0	0.31	312.0	0.60
188.0	0.28	213.0	29.07	238.0	L.O.C	263.0	0.48	288.0	0.35	313.0	4.72
189.0	0.20	214.0	5.16	239.0	415.00	264.0	55.27	289.0	0.42	314.0	2.64
190.0	8.09	215.0	34.63	240.0	0.23	265.0	182.33	290.0	0.56	315.0	0.81

Appendix E: Magnetic Susceptibility

Table 7: Borehole LAP 31 from the Aurora Project

Depth (m)	Av. 3 Values	Depth (m)	Av. 3 Values	Depth (m)	Av. 3 Values	Depth (m)	Av. 3 Values	Depth (m)	Av. 3 Values	Depth (m)	Av. 3 Values
316.0	0.30	341.0	1.15	366.0	0.41	391.0	1.13	416.0	0.86		
317.0	1.11	342.0	2.31	367.0	0.46	392.0	1.12	417.0	4.12		
318.0	3.47	343.0	1.38	368.0	0.59	393.0	0.79	418.0	2.60		
319.0	0.42	344.0	0.73	369.0	0.36	394.0	1.35	419.0	2.47		
320.0	3.76	345.0	0.42	370.0	0.54	395.0	1.55	420.0	4.14		
321.0	0.95	346.0	0.36	371.0	0.68	396.0	1.35	421.0	1.13		
322.0	1.99	347.0	0.35	372.0	0.55	397.0	1.39	422.0	3.04		
323.0	5.40	348.0	1.10	373.0	0.77	398.0	0.90	423.0	2.60		
324.0	7.40	349.0	0.36	374.0	0.51	399.0	7.59	424.0	6.01		
325.0	1.75	350.0	0.47	375.0	0.62	400.0	8.34	425.0	6.37		
326.0	1.32	351.0	0.41	376.0	0.50	401.0	3.12	426.0	6.61		
327.0	1.55	352.0	0.36	377.0	1.92	402.0	0.83	427.0	4.22		
328.0	17.17	353.0	0.42	378.0	0.47	403.0	0.74	428.0	4.55		
329.0	9.77	354.0	0.12	379.0	1.07	404.0	0.26	429.0	9.14		
330.0	40.00	355.0	0.30	380.0	0.31	405.0	0.45	430.0	8.51		
331.0	32.47	356.0	0.43	381.0	0.17	406.0	0.34	431.0	4.74		
332.0	0.23	357.0	0.54	382.0	0.27	407.0	1.53	432.0	0.24		
333.0	0.37	358.0	2.65	383.0	0.65	408.0	5.77	433.0	0.12		
334.0	16.33	359.0	2.69	384.0	0.24	409.0	1.64				
335.0	3.65	360.0	1.09	385.0	0.30	410.0	1.76				
336.0	0.38	361.0	1.52	386.0	1.11	411.0	0.74				
337.0	5.44	362.0	0.34	387.0	0.43	412.0	0.70				
338.0	6.47	363.0	2.62	388.0	0.80	413.0	0.59				
339.0	10.93	364.0	1.98	389.0	5.50	414.0	2.38				
340.0	3.93	365.0	0.34	390.0	0.45	415.0	1.00				

Appendix E: Magnetic Susceptibility Interpretation
Figure 7: LAP 31 Aurora Project

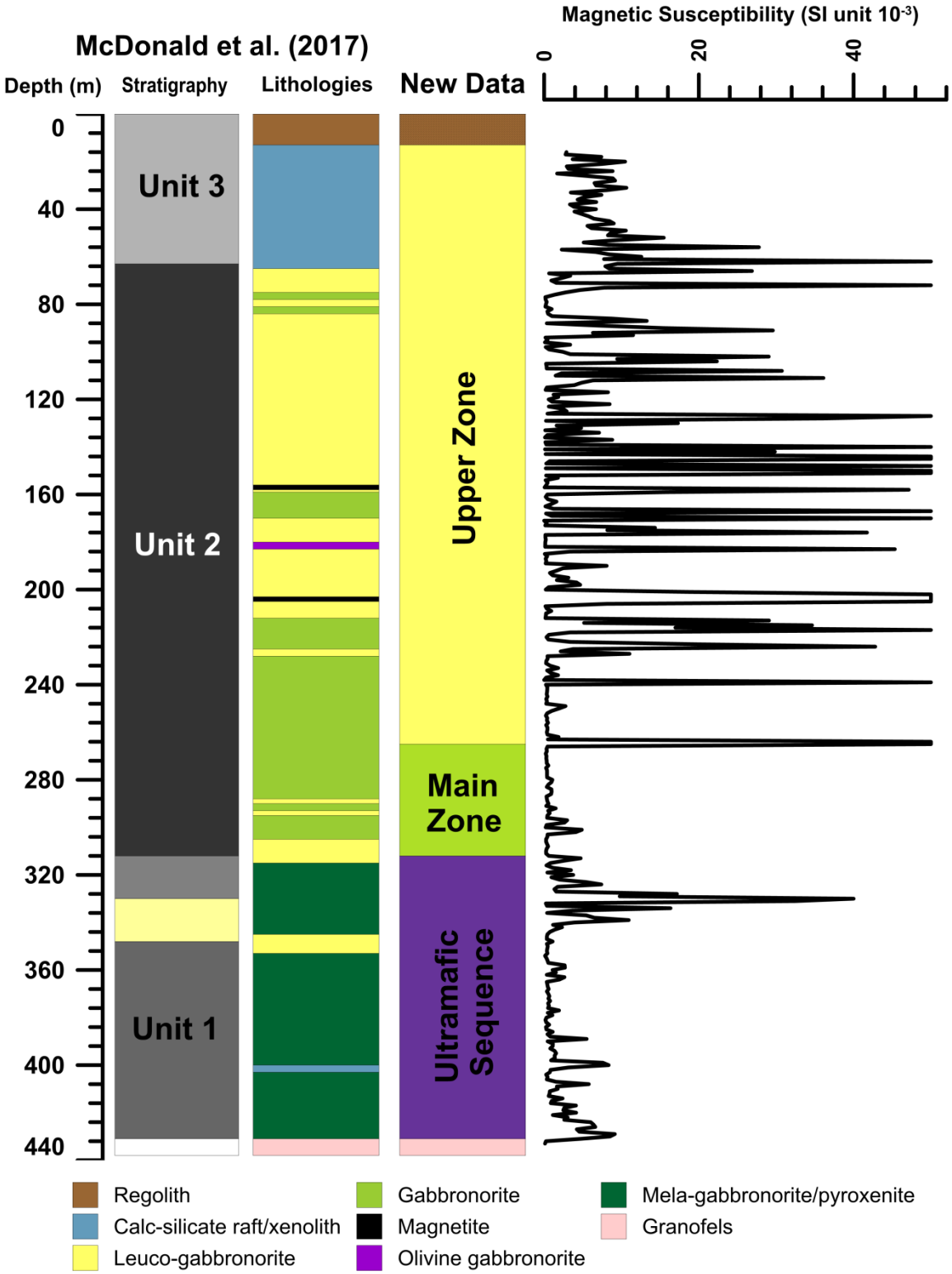

Appendix F

Whole-Rock Geochemistry Major and Trace Elements

WB017D0

WB027D0

WB099D0

WE001D0

WE027D0

WE035D0

Appendix F: Whole-Rock Geochemistry Major and Trace Elements
Table 1: Borehole WB017D0

Major-Element Geochemistry for Borehole WB017D0																
Depth (m)	Rock Type	SiO_2 wt. %	Al_2O_3 wt. %	Fe_2O_3 wt. %	FeO wt. %	MnO wt. %	MgO wt. %	CaO wt. %	Na_2O wt. %	K_2O wt. %	TiO_2 wt. %	P_2O_5 wt. %	Cr_2O_3 wt. %	NiO wt. %	TOTAL wt. %	LOI
156.36	Dolerite	54.60	15.66	1.03	8.36	0.19	7.14	9.17	1.89	1.10	0.67	0.09	0.02	0.01	99.94	2.57
198.55	Magnetite Gabbronorite	52.48	18.12	1.03	8.37	0.12	6.94	10.25	2.24	0.26	0.29	0.02	0.04	0.02	100.19	2.00
201.20	Magnetite Gabbronorite	52.37	7.54	1.64	13.25	0.28	15.27	8.20	0.88	0.22	0.36	0.02	0.07	0.04	100.14	0.64
206.29	Magnetite Gabbronorite	51.88	12.94	1.31	10.57	0.22	12.45	8.73	1.55	0.13	0.23	0.02	0.05	0.03	100.10	0.15
253.66	Magnetite Gabbronorite	48.64	14.47	1.59	12.87	0.21	12.83	6.86	1.62	0.17	0.22	0.02	0.01	0.06	99.54	1.64
294.00	Magnetite Gabbronorite	44.56	13.43	1.98	16.03	0.23	15.58	6.56	1.39	0.18	0.25	0.02	0.01	0.09	100.33	0.20
303.43	Gabbronorite	50.61	17.02	1.10	8.94	0.18	8.85	10.81	1.92	0.14	0.37	0.02	0.06	0.02	100.06	0.42
311.60	Gabbronorite	51.37	24.58	0.46	3.72	0.07	5.32	10.78	2.89	0.54	0.09	0.02	0.04	0.01	99.88	1.58
465.00	Pyroxenite	51.78	9.30	1.58	12.78	0.25	16.01	7.14	0.90	0.09	0.23	0.02	0.07	0.05	100.21	0.90
532.00	Gabbronorite	51.04	21.91	0.65	5.31	0.11	7.35	11.33	2.07	0.16	0.13	0.02	0.02	0.02	100.13	0.86
539.20	Feldspathic Pyroxenite	44.65	14.01	2.19	17.74	0.27	7.07	8.57	1.97	0.16	2.70	0.42	0.02	0.03	99.79	-0.13
633.00	Pegmatoidal unit	47.99	21.57	0.63	5.11	0.11	5.35	17.19	1.87	0.08	0.13	0.02	0.01	0.02	100.08	4.75
649.25	Olivine Gabbronorite	44.45	11.98	1.84	14.95	0.24	18.43	6.89	1.16	0.10	0.10	0.02	0.01	0.12	100.31	1.46
658.00	Gabbronorite	49.90	21.54	0.50	4.02	0.10	5.45	15.86	2.23	0.13	0.15	0.01	0.04	0.01	99.93	1.89
682.50	Gabbronorite	50.07	21.13	0.70	5.67	0.13	6.84	13.05	2.09	0.08	0.14	0.02	0.02	0.02	99.94	1.37
700.28	Anorthosite	43.28	21.06	0.59	4.79	0.15	8.13	21.29	0.12	0.06	0.17	0.02	0.02	0.02	99.70	20.81
711.88	Anorthosite	50.09	20.50	0.67	5.45	0.14	5.76	15.25	1.47	0.62	0.15	0.02	0.02	0.02	100.17	15.22
730.05	Leuco Gabbronorite	50.68	19.43	0.67	5.48	0.12	7.82	13.53	1.88	0.10	0.16	0.02	0.03	0.02	99.95	1.13
765.27	Olivine Gabbronorite	49.85	18.92	0.63	5.13	0.12	9.74	13.60	1.51	0.09	0.14	0.02	0.11	0.03	99.87	2.60
965.52	Gabbronorite	50.68	20.42	0.59	4.81	0.10	9.66	11.74	1.60	0.16	0.13	0.02	0.12	0.02	100.05	0.71
988.74	Troctolite	45.70	15.75	1.11	8.99	0.14	17.86	9.25	1.00	0.15	0.10	0.02	0.12	0.10	100.30	4.18
1003.74	Harzburgite	47.12	8.30	1.26	10.22	0.22	27.02	5.25	0.32	0.05	0.07	0.01	0.38	0.14	100.36	5.98
1015.29	Troctolite	48.48	24.66	0.42	3.38	0.07	6.78	13.64	2.03	0.31	0.08	0.02	0.09	0.02	99.98	2.25
1019.05	Harzburgite	46.23	11.72	1.11	8.97	0.15	24.71	6.20	0.48	0.16	0.06	0.01	0.12	0.17	100.07	6.77
1051.00	Pyroxenite	51.65	5.18	1.69	13.65	0.24	22.50	3.75	0.42	0.05	0.15	0.02	0.31	0.36	99.96	0.45
1072.80	Pyroxenite	49.97	13.46	1.60	12.96	0.18	14.07	6.09	1.10	0.11	0.15	0.01	0.22	0.12	100.02	0.16
1077.90	Granofels	59.75	15.65	0.73	5.97	0.12	8.60	4.23	3.43	0.97	0.14	0.09	0.09	0.03	99.82	2.53
1086.70	Granofels	64.24	21.70	0.08	0.63	0.01	0.28	6.09	6.06	0.38	0.07	0.04	0.00	0.00	99.57	0.64

Appendix F: Whole-Rock Geochemistry Major and Trace Elements
Table 1: Borehole WB017D0

Trace-Element Geochemistry for Borehole WB017D0

Depth (m)	Rock Type	Sc (ppm)	V (ppm)	Cr (ppm)	Co (ppm)	Ni (ppm)	Cu (ppm)	Zn (ppm)	Ga (ppm)	Rb (ppm)	Sr (ppm)	Y (ppm)	Zr (ppm)	Nb (ppm)	Mo (ppm)	Ba (ppm)	Pb (ppm)	Th (ppm)	U (ppm)
156.36	Dolerite	30.42	174.99	82.92	45.49	87.62	74.03	112.50	16.02	42.88	345.64	19.44	91.95	5.17	0.63	477.19	19.46	3.27	d.l.
198.55	Magnetite Gabbronorite	33.93	173.77	190.73	59.85	150.58	81.80	46.40	16.07	4.94	194.84	6.79	13.84	2.36	0.37	100.20	3.22	d.l.	d.l.
201.20	Magnetite Gabbronorite	53.69	241.08	383.94	92.87	260.11	71.50	99.29	9.22	8.41	74.99	11.42	23.93	3.45	1.31	80.62	2.51	d.l.	d.l.
206.29	Magnetite Gabbronorite	38.10	151.98	275.18	69.24	194.64	63.78	77.46	11.63	4.07	156.51	7.16	11.86	3.47	0.20	78.14	3.52	d.l.	d.l.
253.66	Magnetite Gabbronorite	23.43	86.01	56.75	107.55	464.59	60.53	89.16	11.88	6.55	174.67	3.73	15.57	3.74	0.90	78.34	4.52	d.l.	d.l.
294.00	Magnetite Gabbronorite	13.56	76.53	64.66	134.76	699.57	56.68	105.59	11.86	7.69	156.39	3.79	13.82	4.70	1.88	78.15	3.03	0.11	d.l.
303.43	Gabbronorite	34.88	170.87	383.81	57.03	170.97	58.42	61.39	12.18	5.00	186.21	6.29	14.61	3.01	0.13	66.32	4.01	0.28	d.l.
311.60	Gabbronorite	18.08	41.87	252.24	25.69	96.30	51.92	29.14	15.86	13.96	306.05	2.09	16.28	1.59	0.21	186.59	4.31	d.l.	d.l.
465.00	Pyroxenite	41.63	177.63	470.75	89.25	352.67	118.83	101.14	8.35	3.60	87.88	8.17	9.53	2.53	0.68	30.00	4.17	d.l.	d.l.
532.00	Gabbronorite	20.39	76.56	97.40	41.53	140.62	71.09	38.89	16.49	4.56	222.37	4.96	10.77	1.71	0.00	58.09	5.53	d.l.	d.l.
539.20	Feldspathic Pyroxenite	37.25	614.05	81.89	72.64	189.67	305.91	146.21	20.04	5.64	190.69	21.59	27.31	8.16	0.75	87.14	2.72	d.l.	d.l.
633.00	Pegmatoidal unit	23.18	59.51	30.65	33.36	141.25	50.61	45.40	15.99	3.33	239.00	4.14	12.13	2.36	0.67	36.73	4.99	d.l.	d.l.
649.25	Olivine Gabbronorite	18.74	56.61	14.66	155.12	865.77	135.40	98.80	10.12	3.68	118.85	3.16	6.86	2.85	0.60	38.65	2.16	d.l.	d.l.
658.00	Gabbronorite	41.07	127.05	202.95	28.88	113.64	40.94	27.62	14.34	2.34	278.55	6.68	8.58	1.37	0.03	40.42	3.93	d.l.	d.l.
682.50	Gabbronorite	30.44	102.41	85.75	42.85	146.54	118.41	42.00	16.56	2.32	362.43	4.83	8.12	1.42	0.39	41.57	2.32	d.l.	d.l.
700.28	Anorthosite	35.96	109.14	86.41	44.90	143.82	24.73	28.71	10.58	2.67	54.16	5.02	5.82	0.26	0.50	2.66	4.24	d.l.	d.l.
711.88	Anorthosite	25.94	88.68	90.03	30.56	104.72	40.82	31.22	12.10	19.22	123.14	4.09	6.32	1.21	0.05	70.52	2.69	d.l.	d.l.
730.05	Leuco Gabbronorite	30.92	123.74	174.59	38.40	145.53	69.21	40.20	13.75	3.42	245.43	6.85	9.47	2.26	0.37	41.63	3.11	2.44	d.l.
765.27	Olivine Gabbronorite	31.58	117.80	728.67	49.45	185.98	19.79	38.11	11.49	3.87	295.22	3.35	6.76	0.82	0.23	37.15	2.71	d.l.	d.l.
965.52	Gabbronorite	24.98	82.96	760.52	41.96	183.64	15.42	35.50	13.75	5.24	174.47	3.25	9.68	1.24	0.38	55.48	1.59	0.41	d.l.
988.74	Troctolite	18.02	48.53	757.96	97.47	793.96	37.03	62.83	9.17	5.95	132.49	1.34	5.19	1.46	1.13	37.65	0.97	0.54	d.l.
1003.74	Harzburgite	18.40	67.01	2192.61	126.86	1076.96	6.41	74.89	4.43	3.95	55.20	0.51	2.62	0.88	0.14	2.30	3.63	d.l.	d.l.
1015.29	Troctolite	20.55	44.80	627.74	29.59	157.20	28.70	23.40	13.36	9.91	556.18	0.88	6.54	1.15	0.20	112.54	2.52	2.82	d.l.
1019.05	Harzburgite	15.74	43.01	687.44	112.27	1269.23	4.27	51.80	4.69	8.69	104.83	0.26	3.15	0.29	0.21	19.59	6.58	0.21	d.l.
1051.00	Pyroxenite	38.01	208.55	2118.90	175.26	2819.35	1282.28	88.87	5.44	5.39	36.94	3.34	6.83	2.01	0.86	21.07	8.29	0.03	d.l.
1072.80	Pyroxenite	37.33	333.70	1431.24	67.98	881.34	208.00	103.92	12.28	7.24	189.36	2.02	5.44	0.79	0.79	60.76	6.23	d.l.	d.l.
1077.90	Granofels	11.13	58.34	560.34	24.74	248.79	145.05	79.85	18.74	58.28	475.84	4.83	8.08	2.63	0.57	171.64	18.66	4.04	d.l.
1086.70	Granofels	2.28	8.82	19.41	0.55	6.89	9.42	10.35	21.82	8.60	1692.94	2.29	81.79	1.69	0.51	292.24	10.26	8.12	d.l.

Appendix F: Whole-Rock Geochemistry Major and Trace Element
Table 2: Borehole WB027D0

Major-Element Geochemistry for Borehole WB027D0																
Depth (m)	Rock Type	SiO_2 wt. %	Al_2O_3 wt. %	Fe_2O_3 wt. %	FeO wt. %	MnO wt. %	MgO wt. %	CaO wt. %	Na_2O wt. %	K_2O wt. %	TiO_2 wt. %	P_2O_5 wt. %	Cr_2O_3 wt. %	NiO wt. %	TOTAL wt. %	LOI wt. %
490.60	Bushveld paleosol	58.33	24.27	0.67	5.47	0.05	4.48	0.58	0.50	5.00	0.20	0.02	0.03	0.03	99.64	4.78
520.63	Olivine Gabbronorite	49.06	14.69	1.52	12.26	0.24	9.07	9.77	1.83	0.15	1.18	0.02	0.02	0.03	99.84	0.52
537.64	Gabbronorite	49.43	22.06	0.81	6.56	0.14	5.19	12.62	2.36	0.18	0.67	0.03	0.01	0.02	100.07	0.18
606.00	Gabbronorite	49.78	19.72	0.96	7.82	0.13	7.72	10.65	1.98	0.18	0.18	0.04	0.01	0.26	99.46	0.91
622.00	Gabbronorite	51.65	16.82	0.82	6.69	0.16	9.46	12.20	1.86	0.14	0.20	0.02	0.02	0.02	100.07	0.18
649.20	Pyroxenite	52.18	8.09	1.14	9.27	0.23	14.73	13.29	0.86	0.06	0.23	0.02	0.04	0.04	100.18	0.06
815.20	Gabbronorite	50.49	21.36	0.63	5.03	0.14	5.88	13.94	2.02	0.08	0.22	0.03	0.03	0.02	99.85	5.98
881.00	Gabbronorite	51.12	19.05	0.76	6.21	0.13	8.75	12.04	1.78	0.12	0.15	0.02	0.03	0.02	100.21	0.54
889.00	Gabbronorite	52.17	22.45	0.55	4.39	0.10	4.94	13.89	0.63	0.70	0.12	0.02	0.02	0.01	99.97	14.77
928.48	Gabbronorite	51.42	15.63	0.86	6.95	0.16	12.15	11.22	1.35	0.10	0.18	0.02	0.11	0.03	100.17	0.50
939.50	Gabbronorite	50.56	23.37	0.48	3.90	0.08	6.45	12.66	2.08	0.30	0.12	0.02	0.05	0.01	100.07	0.77
1060.50	Harzburgite	44.18	7.68	1.54	12.42	0.22	27.26	5.59	0.40	0.10	0.13	0.02	0.55	0.18	100.24	6.34
1090.70	Olivine Pyroxenite	42.70	8.71	1.37	11.11	0.19	28.01	7.53	0.45	0.25	0.04	0.02	0.03	0.20	100.62	15.61
1092.00	Troctolite	46.79	14.68	0.99	8.02	0.16	17.41	10.73	0.94	0.23	0.10	0.01	0.18	0.10	100.34	3.78
1116.10	Harzburgite	46.13	1.90	0.76	6.19	0.09	44.26	0.25	0.08	0.05	0.06	0.01	0.28	0.37	100.45	13.26
1152.20	Troctolite	44.10	10.27	1.53	12.35	0.18	22.63	6.70	0.34	0.24	0.08	0.02	0.04	0.45	98.93	6.45
1174.70	Granofels	57.59	21.77	0.37	3.00	0.04	1.81	5.81	7.24	0.71	0.06	0.03	0.01	0.48	98.92	3.71
1178.10	Granofels	53.60	13.78	0.58	4.67	0.12	7.92	16.10	1.88	0.85	0.12	0.04	0.05	0.02	99.73	20.16

Appendix F: Whole-Rock Geochemistry Major and Trace Element
Table 2: Borehole WB027D0

Trace-Element Geochemistry for WB027D0																			
Depth (m)	Rock Type	Sc (ppm)	V (ppm)	Cr (ppm)	Co (ppm)	Ni (ppm)	Cu (ppm)	Zn (ppm)	Ga (ppm)	Rb (ppm)	Sr (ppm)	Y (ppm)	Zr (ppm)	Nb (ppm)	Mo (ppm)	Ba (ppm)	Pb (ppm)	Th (ppm)	U (ppm)
490.60	Bushveld paleosol	22.14	35.69	185.73	44.57	222.70	0.09	44.78	16.51	201.15	64.66	5.22	10.64	0.10	0.12	2104.49	11.24	d.l.	d.l.
520.63	Olivine Gabbronorite	40.69	382.52	39.67	74.20	189.53	49.30	99.18	15.63	4.93	149.24	13.07	23.99	1.10	0.70	72.68	6.41	d.l.	d.l.
537.64	Gabbronorite	30.05	242.43	55.22	38.81	135.57	90.85	42.17	16.43	4.73	234.08	7.21	14.66	1.09	0.92	78.01	3.68	d.l.	d.l.
606.00	Gabbronorite	25.98	87.56	67.70	94.60	2074.37	3096.35	47.35	14.74	7.29	194.21	5.49	13.06	0.30	0.30	62.09	7.55	d.l.	d.l.
622.00	Gabbronorite	39.25	142.43	56.63	51.03	178.88	68.64	50.89	12.84	4.21	176.16	8.45	11.86	0.79	0.67	59.04	3.17	d.l.	d.l.
649.20	Pyroxenite	58.51	228.23	204.13	75.94	287.29	97.38	62.95	8.43	2.66	73.80	8.68	10.36	1.29	1.19	25.71	3.15	d.l.	d.l.
815.20	Gabbronorite	31.29	115.33	159.82	32.53	117.98	39.95	45.73	14.90	2.95	141.64	5.51	12.91	0.99	1.18	20.66	4.93	d.l.	d.l.
881.00	Gabbronorite	28.45	111.42	169.74	41.80	149.04	42.32	50.40	14.30	2.81	183.94	5.33	7.90	1.23	1.05	52.08	3.51	d.l.	d.l.
889.00	Gabbronorite	18.00	59.73	58.16	20.97	63.63	5.93	28.10	12.11	17.68	28.68	3.19	6.35	1.10	0.16	26.24	3.39	d.l.	d.l.
928.48	Gabbronorite	38.56	134.61	645.37	53.02	215.75	22.39	51.95	12.65	2.49	151.16	5.82	7.16	1.42	0.67	41.25	3.18	d.l.	d.l.
939.50	Gabbronorite	20.22	69.17	267.56	30.31	107.02	18.06	30.61	15.71	7.41	224.83	3.12	5.22	0.55	0.50	77.15	2.98	d.l.	d.l.
1060.50	Harzburgite	19.13	85.56	2776.78	129.49	1378.87	28.92	87.04	5.39	3.05	60.39	3.03	6.08	0.27	0.42	27.44	6.31	d.l.	d.l.
1090.70	Olivine Pyroxenite	11.22	18.94	161.37	135.37	1318.05	17.78	59.73	3.10	9.22	345.72	0.51	3.20	0.44	0.48	36.04	2.99	d.l.	d.l.
1092.00	Troctolite	25.41	79.27	1052.97	88.48	776.19	50.26	56.56	9.79	7.43	141.82	3.16	4.91	0.61	0.85	45.61	4.44	d.l.	d.l.
1116.10	Harzburgite	6.57	31.23	1300.70	83.71	2415.40	5.43	26.78	1.02	4.51	7.91	1.57	2.66	0.04	0.28	6.08	5.18	d.l.	d.l.
1152.20	Troctolite	14.68	53.60	219.42	135.63	2840.78	1242.38	82.76	7.16	10.59	67.46	1.78	2.88	0.45	0.04	42.66	6.47	d.l.	d.l.
1174.70	Granofels	2.26	11.77	66.64	79.52	3055.39	1620.87	28.57	21.27	21.42	701.14	0.24	22.02	1.03	0.26	249.03	26.82	6.07	d.l.
1178.10	Granofels	12.44	32.09	187.70	21.12	131.00	7.60	11.78	11.45	20.18	650.33	1.84	35.67	0.34	0.54	321.88	2.29	6.79	d.l.

Appendix F: Whole-Rock Geochemistry Major and Trace Elements
Table 3: Borehole WB099D0

Major-Element Geochemistry for WB099D0																
Depth (m)	Rock Type	SiO_2 wt. %	Al_2O_3 wt. %	Fe_2O_3 wt. %	FeO wt. %	MnO wt. %	MgO wt. %	CaO wt. %	Na_2O wt. %	K_2O wt. %	TiO_2 wt. %	P_2O_5 wt. %	Cr_2O_3 wt. %	NiO wt. %	TOTAL wt. %	LOI
527.85	Gabbronorite	50.87	20.64	0.56	4.57	0.12	6.99	14.64	1.88	0.09	0.14	0.02	0.05	0.02	100.59	0.73
551.80	Gabbronorite	50.29	23.28	0.56	4.54	0.09	5.20	13.93	2.29	0.19	0.18	0.07	0.02	0.02	100.66	0.60
566.48	Gabbronorite	50.55	23.68	0.61	4.91	0.10	5.60	12.47	2.25	0.15	0.12	0.02	0.01	0.02	100.49	2.09
602.26	Gabbronorite	50.85	23.54	0.57	4.62	0.10	5.02	12.86	2.43	0.18	0.18	0.03	0.01	0.02	100.40	0.87
619.80	Feldspathic Pyroxenite	52.15	10.15	1.19	9.60	0.23	14.96	10.72	1.10	0.07	0.18	0.02	0.05	0.04	100.44	1.14
628.50	Gabbronorite	51.18	23.72	0.63	5.08	0.10	5.22	11.48	2.69	0.22	0.11	0.02	0.01	0.02	100.47	0.59
671.57	Olivine-bearing Gabbronorite	46.03	15.30	1.46	11.79	0.20	14.37	8.81	1.56	0.11	0.10	0.02	0.01	0.08	99.83	0.19
675.84	Olivine-bearing Gabbronorite	43.99	11.00	1.95	15.79	0.26	19.02	7.06	1.09	0.10	0.12	0.03	0.01	0.13	100.54	1.11
698.67	Magnetite Gabbronorite	49.03	18.81	0.95	7.72	0.13	7.25	12.69	1.94	0.15	0.21	0.02	0.01	0.39	99.32	0.81
699.40	Feldspathic Pyroxenite	49.80	12.33	1.39	11.30	0.20	13.36	9.44	1.00	0.08	0.15	0.01	0.02	0.42	99.50	1.12
700.02	Magnetite Gabbronorite	48.56	16.06	1.31	10.60	0.16	10.28	9.92	1.38	0.16	0.13	0.02	0.02	0.48	99.06	1.20
705.50	Magnetite Gabbronorite	49.50	18.75	1.08	8.78	0.14	8.32	10.53	1.84	0.15	0.15	0.02	0.01	0.34	99.62	0.82
711.80	Magnetite Gabbronorite	51.39	19.17	0.73	5.89	0.13	8.45	12.35	1.95	0.13	0.18	0.03	0.02	0.02	100.44	0.30
734.58	Magnetite Gabbronorite	51.56	19.22	0.71	5.75	0.13	7.78	12.69	2.09	0.14	0.18	0.03	0.02	0.02	100.30	0.30
736.00	Gabbronorite	50.57	21.10	0.69	5.55	0.12	7.04	13.07	1.99	0.18	0.12	0.04	0.01	0.02	100.49	3.01
825.73	Leuco-gabbronorite	50.71	23.09	0.47	3.82	0.09	5.82	13.95	2.18	0.12	0.11	0.02	0.02	0.01	100.41	1.77
900.03	Anorthosite	56.71	24.94	0.24	1.92	0.05	1.60	9.76	4.06	0.84	0.12	0.02	0.00	0.00	100.27	2.57
924.40	Leuco-gabbronorite	50.72	25.00	0.42	3.40	0.07	3.89	13.31	2.51	0.25	0.16	0.02	0.01	0.01	99.76	0.90
1009.00	Leuco-gabbronorite	50.83	23.75	0.52	4.23	0.08	4.95	13.35	2.28	0.14	0.15	0.02	0.01	0.01	100.33	1.28
1021.18	Leuco-gabbronorite	50.46	22.41	0.58	4.72	0.10	6.69	13.68	1.90	0.11	0.15	0.02	0.03	0.02	100.87	0.91
1126.18	Olivine-bearing Gabbronorite	49.78	16.60	0.93	7.56	0.14	13.96	9.91	1.24	0.10	0.12	0.02	0.09	0.06	100.52	0.88
1145.51	Feldspathic Pyroxenite	49.71	8.71	1.35	10.93	0.21	22.76	5.68	0.66	0.09	0.13	0.02	0.20	0.10	100.54	1.83
1169.70	Olivine-bearing Gabbronorite	51.59	17.68	0.86	6.95	0.15	11.22	10.02	1.53	0.12	0.15	0.02	0.08	0.03	100.38	1.60
1172.62	Olivine-bearing Gabbronorite	48.47	13.19	1.15	9.31	0.17	18.20	8.47	0.99	0.13	0.13	0.02	0.10	0.09	100.41	1.41
1193.50	Olivine-bearing Gabbronorite	46.59	15.17	1.18	9.52	0.16	17.98	8.54	1.03	0.11	0.07	0.02	0.08	0.10	100.53	1.99
1215.48	Olivine-bearing Gabbronorite	45.55	10.20	1.36	11.02	0.19	24.00	6.92	0.67	0.07	0.08	0.02	0.10	0.13	100.32	3.81
1228.50	Olivine-bearing Gabbronorite	44.29	10.48	1.44	11.64	0.19	25.36	6.01	0.80	0.06	0.07	0.02	0.05	0.16	100.56	2.11
1270.16	Olivine pyroxenite	53.63	7.71	1.49	12.10	0.25	17.39	5.74	1.36	0.15	0.40	0.13	0.13	0.10	100.58	0.32
1280.17	Olivine pyroxenite	47.93	6.12	1.27	10.26	0.19	29.58	3.94	0.46	0.05	0.12	0.02	0.26	0.20	100.38	0.64
1282.67	Olivine-bearing Gabbronorite	42.22	7.04	1.55	12.54	0.21	31.09	4.42	0.57	0.05	0.07	0.02	0.10	0.24	100.10	0.98
1292.13	Feldspathic Pyroxenite	48.67	4.61	0.91	7.37	0.14	35.51	2.60	0.22	0.04	0.11	0.02	0.39	0.25	100.85	2.61
1315.77	Feldspathic Pyroxenite	54.86	4.26	1.16	9.42	0.20	25.33	4.59	0.37	0.06	0.13	0.02	0.31	0.12	100.83	0.53
1324.53	Granofels	51.78	12.14	0.94	7.60	0.16	17.10	8.97	1.05	0.37	0.15	0.04	0.17	0.08	100.54	2.00
1333.85	Granofels	53.62	13.84	0.95	7.67	0.16	11.86	9.56	1.99	0.24	0.17	0.06	0.07	0.08	100.27	1.27

Appendix F: Whole-Rock Geochemistry Major and Trace Elements
Table 3: Borehole WB099D0

Trace-Element Geochemistry for WB099D0																			
Depth (m)	Rock Type	Sc (ppm)	V (ppm)	Cr (ppm)	Co (ppm)	Ni (ppm)	Cu (ppm)	Zn (ppm)	Ga (ppm)	Rb (ppm)	Sr (ppm)	Y (ppm)	Zr (ppm)	Nb (ppm)	Mo (ppm)	Ba (ppm)	Pb (ppm)	Th (ppm)	U (ppm)
527.85	Gabbronorite	31.96	104.21	276.68	36.05	117.16	29.82	31.25	15.12	2.59	191.80	4.72	6.19	2.79	0.67	46.69	9.03	1.83	d.l.
551.80	Gabbronorite	26.43	87.40	111.82	37.71	147.22	102.57	32.66	15.84	7.50	233.29	5.17	14.57	3.03	0.19	83.34	3.92	4.06	d.l.
566.48	Gabbronorite	22.79	64.59	90.55	36.58	166.99	188.77	36.56	15.91	3.01	221.47	3.43	4.45	2.92	0.98	59.17	3.64	1.17	d.l.
602.26	Gabbronorite	26.52	81.75	51.29	30.84	128.79	104.81	44.21	15.78	4.87	236.92	3.53	8.58	2.92	0.65	54.83	7.79	2.78	d.l.
619.80	Feldspathic Pyroxenite	51.99	179.17	205.39	81.16	289.03	68.72	71.48	8.63	2.32	99.00	5.30	6.02	2.37	0.02	29.13	4.23	d.l.	d.l.
628.50	Gabbronorite	18.69	52.97	33.33	39.51	133.07	84.95	46.58	17.97	4.69	279.15	2.88	5.11	1.38	0.40	84.18	5.92	d.l.	d.l.
671.57	Olivine-bearing Gabbronorite	21.90	67.67	57.50	119.08	593.98	180.42	77.14	11.47	4.64	154.91	2.32	4.50	0.69	0.06	28.46	4.17	d.l.	d.l.
675.84	Olivine-bearing Gabbronorite	18.16	61.79	36.51	148.80	912.02	149.21	109.13	8.27	5.04	108.07	3.13	11.03	2.70	d.l.	33.06	5.75	d.l.	d.l.
698.67	Magnetite Gabbronorite	36.03	144.73	77.59	88.77	2658.22	6556.85	43.88	13.40	4.35	185.25	5.02	13.02	2.33	0.72	75.36	11.44	d.l.	d.l.
699.40	Feldspathic Pyroxenite	40.27	151.15	133.62	118.62	2869.89	6180.29	77.15	9.10	3.61	109.03	3.67	4.77	2.28	1.22	30.64	12.50	d.l.	d.l.
700.02	Magnetite Gabbronorite	32.85	109.91	93.70	128.29	3312.69	9900.96	64.60	11.76	6.55	165.34	5.34	6.40	1.61	0.93	58.97	14.48	d.l.	d.l.
705.50	Magnetite Gabbronorite	23.61	101.71	48.19	92.95	2367.91	6496.37	59.68	15.81	5.40	189.73	4.40	6.78	1.04	0.37	57.15	12.89	d.l.	d.l.
711.80	Magnetite Gabbronorite	33.70	111.51	66.92	47.95	176.84	61.50	43.34	14.60	5.17	190.92	5.87	10.23	1.30	0.66	56.74	4.84	d.l.	d.l.
734.58	Magnetite Gabbronorite	29.46	113.56	58.41	39.87	148.75	76.77	38.88	14.65	4.33	195.83	6.17	9.94	1.79	0.24	60.70	3.25	d.l.	d.l.
736.00	Gabbronorite	27.19	72.87	40.36	33.81	134.38	43.57	41.67	14.49	5.32	192.13	4.76	7.05	0.67	0.63	52.79	4.11	d.l.	d.l.
825.73	Leuco-gabbronorite	24.49	71.74	99.07	26.51	99.30	30.21	25.53	17.66	3.58	222.87	3.68	2.67	0.29	0.78	50.97	4.76	0.59	d.l.
900.03	Anorthosite	12.92	39.31	9.76	8.56	23.37	22.98	21.48	20.13	24.05	274.37	4.05	34.20	d.l.	d.l.	172.99	5.95	8.08	d.l.
924.40	Leuco-gabbronorite	25.48	69.82	43.78	18.80	52.41	11.90	23.90	17.15	7.65	250.19	3.88	13.78	0.82	0.46	78.52	4.24	d.l.	d.l.
1009.00	Leuco-gabbronorite	28.02	80.16	81.43	23.07	72.80	18.67	27.40	18.24	4.89	222.32	4.74	10.08	0.32	0.59	65.51	6.00	d.l.	d.l.
1021.18	Leuco-gabbronorite	28.56	88.57	176.71	34.41	123.18	24.31	34.59	14.75	4.46	191.17	3.80	6.35	0.00	d.l.	52.01	6.26	d.l.	d.l.
1126.18	Olivine-bearing Gabbronorite	25.12	78.35	594.02	78.13	405.96	22.93	51.48	10.81	5.12	144.62	3.41	5.29	1.75	d.l.	43.02	3.63	d.l.	d.l.
1145.51	Feldspathic Pyroxenite	29.12	94.54	1226.35	108.11	677.00	62.04	87.42	6.13	5.54	71.56	4.08	6.64	3.50	0.15	19.25	2.74	d.l.	d.l.
1169.70	Olivine-bearing Gabbronorite	26.57	101.45	534.71	48.24	205.80	49.97	52.08	12.99	2.86	163.59	4.85	5.68	2.77	0.22	63.37	6.82	0.49	d.l.
1172.62	Olivine-bearing Gabbronorite	26.34	87.22	557.46	103.70	639.14	46.31	70.30	8.83	4.48	114.76	4.13	6.95	2.02	d.l.	32.21	7.67	d.l.	d.l.
1193.50	Olivine-bearing Gabbronorite	19.82	48.85	490.80	103.11	705.06	58.45	66.86	8.33	4.90	128.72	1.67	2.45	1.92	d.l.	32.55	4.89	d.l.	d.l.
1215.48	Olivine-bearing Gabbronorite	18.70	60.56	564.33	125.89	1011.25	10.09	73.74	5.95	2.97	81.84	0.72	2.70	2.89	d.l.	27.35	5.56	d.l.	d.l.
1228.50	Olivine-bearing Gabbronorite	13.15	37.26	295.02	137.66	1217.79	45.13	77.76	7.18	3.52	88.76	1.17	3.49	3.50	0.53	31.60	4.82	0.43	d.l.
1270.16	Olivine pyroxenite	32.67	164.37	845.29	90.85	699.49	202.58	115.93	10.32	6.80	143.14	12.31	9.93	4.47	0.14	81.26	4.68	d.l.	d.l.
1280.17	Olivine pyroxenite	18.75	69.31	1592.96	119.75	1471.53	37.83	79.96	3.78	4.19	48.36	0.69	6.49	3.17	d.l.	26.08	6.69	0.15	d.l.
1282.67	Olivine-bearing Gabbronorite	14.30	34.19	551.73	157.27	1777.50	21.86	94.57	4.54	3.08	64.27	0.36	2.58	2.90	0.34	22.46	4.05	d.l.	d.l.
1292.13	Feldspathic Pyroxenite	15.73	62.96	2388.51	99.20	1899.45	58.18	59.81	3.79	3.62	32.46	0.78	7.40	1.08	0.39	24.44	6.30	0.96	d.l.
1315.77	Feldspathic Pyroxenite	27.93	102.64	2001.94	80.76	936.99	63.95	96.64	5.13	4.63	29.49	2.38	4.37	0.65	d.l.	17.19	5.82	d.l.	d.l.
1324.53	Granofels	35.34	109.88	1066.72	74.65	622.76	90.16	65.90	15.13	14.95	129.65	2.28	18.09	1.66	0.50	155.78	7.03	0.97	d.l.
1333.85	Granofels	33.90	119.05	392.48	65.86	536.65	354.48	72.35	12.61	9.49	163.89	6.64	14.44	1.05	d.l.	90.93	8.94	1.21	d.l.

Appendix F: Whole-Rock Geochemistry Major and Trace Elements
Table 4: Borehole WE001D0

Major-Element Geochemistry for WE001D0																
Depth (m)	Rock Type	SiO_2 wt. %	Al_2O_3 wt. %	Fe_2O_3 wt. %	FeO wt. %	MnO wt. %	MgO wt. %	CaO wt. %	Na_2O wt. %	K_2O wt. %	TiO_2 wt. %	P_2O_5 wt. %	Cr_2O_3 wt. %	NiO wt. %	TOTAL wt. %	LOI
378.64	Bushveld paleosol	68.55	15.43	0.70	5.67	0.09	5.90	0.27	0.15	2.64	0.18	0.02	0.04	0.03	99.66	4.68
432.14	Gabbronorite	54.03	18.01	0.75	6.13	0.25	6.04	9.06	2.99	0.26	1.66	0.52	0.02	0.02	99.73	3.01
603.23	Olivine Gabbronorite	49.88	19.29	0.70	5.72	0.12	11.29	11.08	1.57	0.18	0.14	0.02	0.11	0.03	100.13	2.14
636.22	Gabbronorite	49.20	17.27	0.82	6.64	0.14	13.70	10.75	1.08	0.14	0.11	0.01	0.07	0.06	99.99	2.58
642.00	Olivine Gabbronorite	45.84	16.17	1.15	9.34	0.17	20.91	5.62	0.73	0.16	0.12	0.02	0.03	0.10	100.38	7.06
644.40	Olivine Gabbronorite	46.00	17.07	0.97	7.90	0.14	16.62	9.62	0.98	0.13	0.07	0.02	0.13	0.10	99.76	4.06
675.00	Harzburgite	42.72	10.31	1.42	11.53	0.19	27.81	4.88	0.14	0.10	0.11	0.02	0.28	0.34	99.84	8.77
699.97	Harzburgite	45.44	7.48	1.40	11.32	0.19	28.34	4.82	0.33	0.16	0.08	0.02	0.18	0.35	100.10	5.47
730.75	Troctolite	47.66	7.15	0.96	7.83	0.15	31.71	4.00	0.21	0.08	0.12	0.02	0.43	0.18	100.49	7.53
754.95	Gabbronorite	52.32	7.32	1.25	10.11	0.23	22.78	5.41	0.40	0.15	0.16	0.01	0.30	0.09	100.51	4.17
784.10	Olivine Gabbronorite	45.64	7.14	1.57	12.65	0.21	27.23	4.71	0.57	0.08	0.13	0.02	0.12	0.20	100.27	5.88
827.05	Granofels	74.24	15.37	0.04	0.36	0.01	0.44	1.58	6.93	0.58	0.03	0.04	0.00	0.00	99.58	1.07
845.65	Olivine Gabbronorite	51.72	5.41	0.63	5.18	0.09	31.23	5.22	0.23	0.11	0.09	0.02	0.35	0.15	100.42	3.07

Appendix F: Whole-Rock Geochemistry Major and Trace Elements
Table 4: Borehole WE001D0

Trace-Element Geochemistry for WE001D0																			
Depth (m)	Rock Type	Sc (ppm)	V (ppm)	Cr (ppm)	Co (ppm)	Ni (ppm)	Cu (ppm)	Zn (ppm)	Ga (ppm)	Rb (ppm)	Sr (ppm)	Y (ppm)	Zr (ppm)	Nb (ppm)	Mo (ppm)	Ba (ppm)	Pb (ppm)	Th (ppm)	U (ppm)
378.64	Bushveld paleosol	34.25	53.34	266.85	51.03	228.29	2.53	59.13	10.92	87.24	18.02	3.44	8.81	0.95	0.05	1229.48	10.50	0.29	d.l.
432.14	Gabbronorite	25.00	183.44	116.44	31.03	124.25	124.36	37.15	13.71	9.47	190.43	13.25	60.50	12.90	0.49	88.27	4.82	2.78	d.l.
603.23	Olivine Gabbronorite	25.06	85.94	707.97	49.22	266.98	27.47	39.97	14.24	5.79	188.49	3.42	10.05	1.44	0.29	59.64	5.19	d.l.	d.l.
636.22	Gabbronorite	22.39	83.85	387.62	65.64	450.05	43.75	43.11	11.31	4.90	216.23	3.45	6.81	0.87	0.36	36.37	7.11	d.l.	d.l.
642.00	Olivine Gabbronorite	12.13	50.91	180.20	80.93	758.85	2.33	54.40	8.77	6.74	187.83	2.98	10.15	1.10	0.54	30.91	4.46	d.l.	d.l.
644.40	Olivine Gabbronorite	14.47	43.42	699.89	97.63	740.79	51.59	57.27	10.34	6.85	135.02	0.10	3.55	0.82	0.12	31.83	5.00	d.l.	d.l.
675.00	Harzburgite	9.65	41.76	1158.60	145.16	2256.36	878.55	55.76	7.16	8.02	55.75	0.33	6.60	1.02	0.72	28.50	3.70	d.l.	d.l.
699.97	Harzburgite	13.79	48.40	993.60	161.81	2590.20	893.30	81.68	5.09	7.53	69.30	1.26	5.59	1.46	0.82	31.30	6.19	d.l.	d.l.
730.75	Troctolite	17.25	67.53	2185.18	81.52	1368.71	13.10	73.86	5.75	5.79	52.99	1.12	3.02	0.00	0.68	28.34	5.08	d.l.	d.l.
754.95	Gabbronorite	29.11	125.48	1891.69	88.41	701.63	117.76	83.81	6.59	8.16	59.15	2.70	4.31	1.47	0.17	30.00	5.53	d.l.	d.l.
784.10	Olivine Gabbronorite	15.06	58.31	620.29	130.41	1493.72	125.83	90.70	6.53	4.41	53.65	3.06	6.05	1.70	0.07	37.37	5.21	d.l.	d.l.
827.05	Granofels	1.39	0.76	4.25	3.92	4.89	3.70	3.35	14.27	16.63	455.77	2.28	24.48	0.95	0.54	188.34	19.08	3.60	d.l.
845.65	Olivine Gabbronorite	16.96	48.42	2030.09	84.67	1211.22	5.46	56.64	4.80	4.01	53.27	5.61	9.13	2.23	0.38	37.32	2.62	d.l.	d.l.

Appendix F: Whole-Rock Geochemistry Major and Trace Elements
Table 5: Borehole WE027D0

Major-Element Geochemistry for Borehole WE027D0																
Depth (m)	Rock Types	SiO2 wt. %	TiO2 wt. %	Al2O3 wt. %	Fe2O3 wt. %	FeO wt. %	MnO wt. %	MgO wt. %	CaO wt. %	Na2O wt. %	K2O wt. %	P2O5 wt. %	Cr2O3 wt. %	NiO wt. %	TOTAL wt. %	LOI
553.96	Waterberg sediments	85.33	0.27	7.88	0.41	3.29	0.03	0.26	0.13	0.08	2.18	0.05	0.02	0.00	99.93	1.38
556.35	Bushveld paleosol/Shale	48.51	0.54	37.46	1.07	8.63	0.06	0.75	0.53	0.54	2.65	0.02	0.04	0.02	100.81	3.17
565.00	Gabbronorite	50.62	0.29	24.54	0.60	4.84	0.09	3.57	12.77	2.75	0.23	0.03	0.02	0.01	100.35	0.42
570.56	Olivine-bearing Gabbronorite	50.13	0.27	19.01	0.90	7.31	0.14	8.36	10.41	3.11	0.57	0.03	0.05	0.02	100.31	3.31
578.27	Olivine-bearing Gabbronorite	48.66	0.55	25.61	0.72	5.82	0.09	3.48	12.59	2.69	0.25	0.02	0.01	0.02	100.52	0.45
580.59	Olivine-bearing Gabbronorite	49.58	0.14	26.14	0.50	4.05	0.07	3.41	13.74	2.63	0.22	0.02	0.02	0.03	100.54	0.55
586.00	Gabbronorite	49.80	0.32	26.17	0.50	4.07	0.07	2.83	13.39	2.68	0.20	0.02	0.02	0.01	100.09	0.38
588.78	Olivine-bearing Gabbronorite	50.60	0.19	25.40	0.52	4.21	0.10	2.93	11.30	3.72	0.85	0.06	0.01	0.01	99.89	2.19
594.58	Gabbronorite	50.36	0.18	23.44	0.54	4.41	0.09	4.82	13.50	2.39	0.18	0.04	0.03	0.02	99.99	0.38
602.36	Gabbronorite	49.77	0.22	19.30	0.91	7.34	0.14	8.28	12.27	1.85	0.17	0.02	0.04	0.04	100.35	0.54
622.20	Gabbronorite	50.58	0.15	25.31	0.40	3.26	0.07	3.11	14.54	2.64	0.24	0.02	0.02	0.01	100.35	0.56
631.16	Olivine-bearing Gabbronorite	50.67	0.32	23.68	0.56	4.53	0.10	3.70	12.48	2.93	1.14	0.05	0.02	0.02	100.19	2.39
635.40	Gabbronorite	50.36	0.22	21.54	0.69	5.57	0.11	5.97	13.17	2.14	0.16	0.02	0.04	0.04	100.03	0.41
658.08	Gabbronorite	50.85	0.25	17.70	0.79	6.41	0.14	8.61	12.99	1.98	0.17	0.02	0.06	0.02	99.99	0.81
693.21	Olivine-bearing Gabbronorite	47.65	0.12	17.93	1.24	10.03	0.17	11.35	10.10	1.68	0.20	0.02	0.03	0.07	100.59	0.41
724.80	Olivine-bearing Gabbronorite	49.66	0.16	20.76	0.77	6.25	0.11	6.97	11.91	2.60	0.47	0.02	0.02	0.02	99.71	2.83
748.42	Gabbronorite	50.24	0.20	22.01	0.70	5.66	0.12	6.13	13.28	2.06	0.27	0.02	0.04	0.02	100.75	0.64
785.20	Olivine-bearing Gabbronorite	49.75	0.18	22.13	0.71	5.77	0.11	6.25	12.42	1.97	1.01	0.03	0.03	0.02	100.39	1.64
808.34	Olivine-bearing Gabbronorite	49.84	0.19	22.80	0.64	5.22	0.09	5.63	12.11	2.35	1.48	0.02	0.03	0.02	100.42	2.99
849.60	Olivine-bearing Gabbronorite	48.74	0.16	16.42	1.23	9.99	0.17	12.51	9.14	1.54	0.30	0.02	0.04	0.06	100.35	0.82
888.37	Troctolite	35.83	6.36	18.77	2.52	20.41	0.18	3.08	9.55	2.15	0.22	0.93	0.03	0.06	100.10	0.13
891.52	Gabbronorite	51.39	0.39	16.73	0.98	7.96	0.16	8.70	11.23	2.38	0.29	0.04	0.02	0.02	100.31	1.81
929.57	Olivine-bearing Gabbronorite	49.68	0.21	19.83	0.87	7.05	0.13	8.58	11.24	2.02	0.41	0.02	0.04	0.04	100.11	1.32
962.39	Olivine-bearing Gabbronorite	46.42	0.16	12.25	1.66	13.42	0.22	16.24	8.06	1.15	0.18	0.02	0.03	0.09	99.93	0.27
987.21	Olivine-bearing Gabbronorite	50.42	0.14	23.83	0.49	3.99	0.08	5.13	12.73	2.20	1.56	0.02	0.03	0.02	100.65	2.35
994.04	Olivine-bearing Gabbronorite	50.42	0.22	21.75	0.50	4.06	0.10	5.02	12.44	2.81	2.70	0.02	0.04	0.02	100.10	4.06
1252.15	Olivine-bearing Gabbronorite	48.80	0.17	10.45	1.26	10.21	0.20	18.44	9.50	0.84	0.22	0.02	0.04	0.08	100.23	0.65
1282.94	Gabbronorite	50.96	0.17	17.03	0.88	7.14	0.16	10.13	12.42	1.51	0.09	0.01	0.05	0.04	100.60	0.53
1345.20	Gabbronorite	50.12	0.12	22.08	0.57	4.63	0.10	6.81	13.85	1.75	0.12	0.02	0.03	0.02	100.22	0.52
1381.20	Olivine-bearing Gabbronorite	48.31	0.10	9.77	1.21	9.84	0.20	25.11	4.91	0.32	0.24	0.02	0.10	0.10	100.23	5.64
1385.41	Harzburgite	45.34	0.08	5.55	1.50	12.19	0.16	30.87	4.15	0.12	0.05	0.02	0.10	0.25	100.39	8.31
1386.66	Harzburgite	47.18	0.09	5.53	1.49	12.08	0.17	29.41	3.89	0.17	0.04	0.02	0.11	0.21	100.37	5.83
1393.60	Granofels	50.92	0.11	12.37	1.01	8.16	0.15	17.33	8.49	0.71	0.21	0.01	0.26	0.16	99.89	1.24
1403.92	Granofels	51.58	0.10	12.69	1.02	8.24	0.17	17.48	6.87	0.84	0.43	0.02	0.15	0.17	99.75	1.61

Appendix F: Whole-Rock Geochemistry Major and Trace Elements
Table 5: Borehole WE027D0

Trace-Element Geochemistry for Borehole WE027D0																			
Depth (m)	Rock Types	Sc (ppm)	Sr (ppm)	V (ppm)	Cr (ppm)	Co (ppm)	Ni (ppm)	Cu (ppm)	Zn (ppm)	Ga (ppm)	Rb (ppm)	Y (ppm)	Zr (ppm)	Nb (ppm)	Mo (ppm)	Ba (ppm)	Pb (ppm)	Th (ppm)	U (ppm)
553.96	Waterberg sediments	4.31	32.24	35.65	58.24	5.47	14.53	4.88	6.02	8.05	64.21	13.27	104.36	4.26	0.51	620.45	13.31	13.66	d.l.
556.35	Bushveld paleosol/Shale	28.60	191.47	104.72	211.63	17.42	139.76	0.40	70.56	30.71	84.91	4.16	27.84	2.95	0.79	1619.26	55.44	d.l.	d.l.
565.00	Gabbronorite	24.80	254.09	101.91	54.39	22.32	61.35	51.25	37.00	17.94	4.44	6.80	18.00	1.65	1.07	137.50	4.99	d.l.	d.l.
570.56	Olivine-bearing Gabbronorite	37.45	245.72	164.77	247.71	55.06	166.43	102.99	57.98	15.03	17.89	10.34	19.60	2.96	0.08	326.29	10.48	d.l.	d.l.
578.27	Olivine-bearing Gabbronorite	19.76	253.59	133.16	17.54	39.52	149.27	101.17	39.50	17.44	4.79	5.39	24.98	2.95	0.40	106.07	3.73	d.l.	d.l.
580.59	Olivine-bearing Gabbronorite	17.80	246.57	44.61	41.64	33.89	197.25	279.82	29.34	15.75	2.23	4.22	11.49	0.96	0.99	87.28	4.75	d.l.	d.l.
586.00	Gabbronorite	20.56	250.16	103.59	67.00	24.79	68.59	66.90	29.48	16.64	2.85	3.99	16.52	0.60	0.40	106.41	3.59	d.l.	d.l.
588.78	Olivine-bearing Gabbronorite	15.52	362.56	72.56	65.98	25.82	61.14	40.54	38.78	15.55	20.69	6.08	14.39	0.20	0.36	602.74	4.06	d.l.	d.l.
594.58	Gabbronorite	25.85	228.82	93.51	155.53	31.69	101.36	78.13	30.93	16.39	2.55	4.84	13.86	0.79	0.02	101.13	4.45	d.l.	d.l.
602.36	Gabbronorite	32.27	181.28	122.18	214.87	56.64	252.61	146.13	50.43	12.34	2.83	6.53	10.73	0.56	0.85	61.11	2.70	d.l.	d.l.
622.20	Gabbronorite	25.96	244.00	88.31	50.41	18.45	71.92	57.55	24.35	18.01	4.87	7.69	19.70	1.16	0.27	92.99	2.35	d.l.	d.l.
631.16	Olivine-bearing Gabbronorite	24.95	290.35	119.87	123.63	26.80	118.21	109.02	37.18	14.16	45.10	5.04	14.73	1.78	0.18	238.66	5.75	d.l.	d.l.
635.40	Gabbronorite	29.88	200.53	118.15	195.18	38.18	233.28	316.34	37.27	14.10	3.29	6.30	12.41	2.54	1.13	56.23	2.98	d.l.	d.l.
658.08	Gabbronorite	38.53	180.71	151.94	322.22	45.77	172.75	61.60	42.17	13.63	3.81	8.21	18.04	1.08	0.05	55.77	1.40	d.l.	d.l.
693.21	Olivine-bearing Gabbronorite	19.72	179.43	73.53	70.31	94.51	460.96	406.37	69.86	14.42	6.56	2.82	4.52	0.86	0.27	59.41	5.32	d.l.	d.l.
724.80	Olivine-bearing Gabbronorite	34.36	249.93	112.49	97.78	38.73	130.29	30.85	55.15	13.49	20.14	6.85	7.86	0.64	0.94	72.02	5.92	d.l.	d.l.
748.42	Gabbronorite	26.55	210.78	102.49	176.12	37.95	132.97	66.53	36.12	15.28	9.71	7.64	11.58	0.14	0.05	68.81	2.56	d.l.	d.l.
785.20	Olivine-bearing Gabbronorite	21.61	246.92	91.87	147.12	41.56	162.57	59.10	41.20	14.00	42.83	6.39	11.83	1.44	0.64	144.36	5.28	0.76	d.l.
808.34	Olivine-bearing Gabbronorite	24.04	225.33	96.94	155.85	41.19	131.31	65.39	44.65	14.52	63.17	6.98	10.51	0.25	0.31	227.17	5.78	d.l.	d.l.
849.60	Olivine-bearing Gabbronorite	24.07	158.76	84.67	205.09	92.11	424.69	78.14	69.55	10.09	12.78	5.56	10.17	1.14	0.56	70.54	5.61	d.l.	d.l.
888.37	Troctolite	25.17	232.22	758.32	75.99	87.98	466.03	773.20	214.79	26.20	8.89	26.80	39.97	23.50	0.01	113.23	6.41	d.l.	d.l.
891.52	Gabbronorite	37.03	177.11	179.72	67.03	40.66	158.42	14.73	61.38	15.65	8.54	11.58	35.56	2.09	0.07	91.39	3.54	d.l.	d.l.
929.57	Olivine-bearing Gabbronorite	25.15	211.46	104.83	197.40	55.03	227.14	56.91	51.50	13.44	14.76	6.16	16.50	2.39	0.32	101.53	4.08	d.l.	d.l.
962.39	Olivine-bearing Gabbronorite	24.72	124.66	105.91	165.72	122.73	629.57	131.90	91.97	11.84	6.63	5.48	10.03	2.77	0.75	48.97	5.88	d.l.	d.l.
987.21	Olivine-bearing Gabbronorite	27.17	241.79	97.95	153.16	25.35	107.09	43.09	30.05	16.47	71.52	4.97	8.88	1.83	0.49	169.88	4.69	0.10	d.l.
994.04	Olivine-bearing Gabbronorite	38.68	237.02	152.36	190.23	29.77	115.32	13.22	41.88	14.28	116.88	6.62	9.77	1.74	0.06	503.24	10.13	d.l.	d.l.
1252.15	Olivine-bearing Gabbronorite	39.95	89.99	135.06	161.98	100.40	596.98	38.87	69.32	7.52	10.10	7.15	6.78	2.14	0.96	31.89	6.49	d.l.	d.l.
1282.94	Gabbronorite	35.48	146.56	140.70	118.30	53.88	216.79	47.39	50.79	12.02	4.30	6.69	4.74	2.44	0.30	37.91	4.26	d.l.	d.l.
1345.20	Gabbronorite	27.03	183.74	94.71	116.20	31.07	124.58	33.19	30.42	13.25	3.99	5.34	5.71	2.25	0.15	29.06	3.09	d.l.	d.l.
1381.20	Olivine-bearing Gabbronorite	23.39	43.50	87.49	516.31	88.91	728.37	41.06	105.88	7.20	9.21	3.83	3.41	2.17	0.14	50.57	2.72	d.l.	d.l.
1385.41	Harzburgite	17.44	22.96	58.34	606.87	120.46	1689.42	8.52	39.41	2.90	2.56	1.98	2.94	2.36	0.25	3.87	5.73	0.70	d.l.
1386.66	Harzburgite	20.02	26.17	70.79	602.90	128.81	1489.17	1.86	64.47	3.47	4.21	1.99	4.21	2.00	1.20	16.71	1.34	d.l.	d.l.
1393.60	Granofels	32.10	99.37	106.83	1697.81	106.41	1031.19	266.69	51.00	7.14	10.11	1.87	4.29	2.19	0.39	42.32	3.95	d.l.	d.l.
1403.92	Granofels	30.61	231.47	103.87	1016.48	95.89	1127.53	836.58	60.41	7.32	15.28	1.34	3.51	0.67	0.14	89.41	8.18	d.l.	d.l.

Appendix F: Whole-Rock Geochemistry Major and Trace Elements
Table 6: Borehole WE035D0

Major-Element Geochemistry for Borehole WE035																
Depth (m)	Rock Type	SiO_2 wt. %	Al_2O_3 wt. %	Fe_2O_3 wt. %	FeO wt. %	MnO wt. %	MgO wt. %	CaO wt. %	Na_2O wt. %	K_2O wt. %	TiO_2 wt. %	P_2O_5 wt. %	Cr_2O_3 wt. %	NiO wt. %	TOTAL wt. %	LOI
369.90	Conglomerate/ Mudstone	50.27	30.12	1.05	8.51	0.04	2.00	0.42	0.68	6.50	0.30	0.02	0.11	0.03	100.05	5.03
377.53	Bushveld paleosol/Shale	51.69	15.98	0.65	5.29	0.24	10.34	12.58	2.48	0.55	0.23	0.02	0.13	0.03	100.21	3.71
393.80	Gabbronorite	52.06	15.79	0.90	7.33	0.16	11.24	10.81	1.67	0.15	0.20	0.03	0.09	0.04	100.47	1.02
399.70	Gabbronorite	50.80	19.49	0.67	5.41	0.12	8.87	12.32	1.83	0.33	0.15	0.02	0.09	0.02	100.12	2.11
457.65	Gabbronorite	50.89	18.15	0.69	5.61	0.12	10.74	11.82	1.59	0.12	0.13	0.02	0.16	0.03	100.06	3.78
488.30	Olivine-bearing Gabbronorite	51.48	16.14	0.84	6.81	0.15	13.55	8.31	2.26	0.33	0.14	0.02	0.16	0.04	100.22	4.66
505.10	Gabbronorite	51.88	15.59	0.81	6.58	0.14	14.57	9.18	1.32	0.10	0.12	0.01	0.16	0.05	100.53	3.39
515.30	Olivine-bearing Gabbronorite	47.74	14.53	0.99	8.06	0.17	17.88	9.32	0.53	0.38	0.10	0.02	0.12	0.10	99.93	4.95
523.30	Gabbronorite	48.76	21.75	0.55	4.49	0.12	9.55	12.49	2.21	0.35	0.11	0.02	0.09	0.03	100.51	5.10
529.15	Olivine-bearing Gabbronorite	47.43	15.37	0.92	7.48	0.14	17.31	10.40	0.90	0.15	0.10	0.02	0.14	0.09	100.44	3.47
536.46	Olivine-bearing Gabbronorite	48.59	13.62	1.00	8.12	0.17	19.30	8.34	0.73	0.19	0.10	0.01	0.15	0.09	100.41	3.29
544.67	Olivine-bearing Gabbronorite	46.91	13.65	1.11	8.96	0.17	20.89	7.27	0.57	0.32	0.07	0.02	0.17	0.11	100.21	4.61
545.40	Gabbronorite	49.26	21.20	0.56	4.57	0.10	9.41	12.97	1.64	0.34	0.13	0.02	0.10	0.04	100.36	2.98
561.26	Poikilitic Troctolite	47.11	15.28	1.07	8.63	0.14	18.59	8.24	0.80	0.11	0.09	0.02	0.20	0.11	100.38	3.84
572.41	Poikilitic Troctolite	45.88	10.83	1.29	10.44	0.18	23.87	6.39	0.40	0.35	0.14	0.03	0.30	0.16	100.26	5.75
596.73	Poikilitic Troctolite	44.72	9.04	1.42	11.48	0.20	27.36	5.10	0.21	0.20	0.13	0.03	0.27	0.19	100.35	8.31
603.70	Harzburgite	42.86	15.99	1.04	8.38	0.17	22.17	9.46	0.07	0.07	0.06	0.02	0.04	0.15	100.48	9.39
604.60	Poikilitic Troctolite	43.41	10.37	1.39	11.25	0.21	29.49	4.10	0.08	0.04	0.06	0.02	0.05	0.22	100.67	10.65
606.40	Poikilitic Troctolite	43.13	7.32	1.48	12.02	0.19	33.53	2.03	0.04	0.03	0.05	0.02	0.05	0.27	100.18	11.32
609.90	Poikilitic Troctolite	45.17	8.39	1.23	9.93	0.19	27.22	6.12	0.09	0.09	0.05	0.01	0.06	0.45	99.01	9.11
613.40	Harzburgite	43.68	9.48	1.33	10.80	0.16	29.16	4.60	0.16	0.20	0.05	0.02	0.39	0.26	100.29	8.74
616.68	Olivine-bearing Pyroxenite	51.22	8.94	1.05	8.54	0.17	25.04	4.35	0.31	0.05	0.10	0.02	0.35	0.14	100.28	3.28
630.20	Feldspathic Pyroxenite	51.18	15.54	0.86	6.98	0.16	14.07	9.30	1.36	0.29	0.11	0.02	0.15	0.13	100.14	1.44
641.06	Feldspathic Pyroxenite	54.22	3.78	1.22	9.91	0.23	26.12	3.84	0.33	0.04	0.15	0.01	0.30	0.14	100.31	0.36
650.62	Granofels	52.70	6.48	0.67	5.40	0.13	30.92	2.81	0.37	0.12	0.12	0.02	0.38	0.15	100.28	4.14
678.40	Granofels	54.84	5.56	1.30	10.57	0.19	23.53	2.08	0.97	0.14	0.19	0.03	0.37	0.15	99.90	0.72

Appendix F: Whole-Rock Geochemistry Major and Trace Elements
Table 6: Borehole WE035D0

Trace-Element Geochemistry for Borehole WE034D0

Depth (m)	Rock Type	Sc (ppm)	V (ppm)	Cr (ppm)	Co (ppm)	Ni (ppm)	Cu (ppm)	Zn (ppm)	Ga (ppm)	Rb (ppm)	Sr (ppm)	Y (ppm)	Zr (ppm)	Nb (ppm)	Mo (ppm)	Ba (ppm)	Pb (ppm)	Th (ppm)	U (ppm)
369.90	Conglomerate/ Mudstone	43.72	44.31	668.00	31.47	204.73	0.73	17.64	21.14	176.08	47.75	8.67	20.30	1.79	0.29	1890.94	34.36	d.l.	d.l.
377.53	Bushveld paleosol/Shale	42.01	153.85	791.67	48.82	203.63	34.87	67.68	9.75	15.96	166.92	7.40	13.03	1.60	0.73	337.94	16.50	d.l.	d.l.
393.80	Gabbronorite	39.32	128.22	522.69	54.89	248.40	112.79	57.68	11.37	3.68	161.06	5.80	22.18	0.97	0.89	84.80	4.31	d.l.	d.l.
399.70	Gabbronorite	32.21	96.47	588.05	41.49	174.29	16.72	39.71	11.79	7.10	216.79	5.49	9.13	0.11	0.34	164.20	4.39	d.l.	d.l.
457.65	Gabbronorite	34.22	102.99	951.99	46.46	229.35	22.31	41.00	11.75	2.86	149.01	4.71	6.69	0.33	0.12	40.57	5.09	d.l.	d.l.
488.30	Olivine-bearing Gabbronorite	29.89	113.25	1006.70	57.93	298.29	29.60	49.09	11.39	10.76	202.09	4.39	4.38	0.57	0.14	105.90	10.74	d.l.	d.l.
505.10	Gabbronorite	28.20	98.01	1042.63	67.97	349.63	15.95	48.39	9.84	2.55	232.83	3.17	3.23	0.03	0.27	53.85	4.65	0.13	d.l.
515.30	Olivine-bearing Gabbronorite	16.80	62.34	702.44	104.20	762.23	20.56	65.73	8.32	11.65	190.31	3.66	4.50	1.46	0.36	72.19	7.40	d.l.	d.l.
523.30	Gabbronorite	23.71	83.38	813.32	40.36	200.35	7.18	39.54	11.87	10.91	352.52	2.90	3.60	1.21	0.08	83.13	4.79	d.l.	d.l.
529.15	Olivine-bearing Gabbronorite	24.48	58.78	803.07	88.39	661.86	4.42	47.24	8.33	6.67	142.22	3.13	3.20	0.65	0.61	32.25	2.69	d.l.	d.l.
536.46	Olivine-bearing Gabbronorite	22.00	70.53	820.79	89.25	691.25	24.13	57.69	8.33	6.87	116.42	3.21	3.39	0.38	0.58	29.14	5.04	0.76	d.l.
544.67	Olivine-bearing Gabbronorite	15.70	52.70	991.59	106.81	841.76	33.19	64.06	7.61	10.94	131.75	1.75	1.97	d.l.	d.l.	44.11	6.14	d.l.	d.l.
545.40	Gabbronorite	28.20	86.01	624.06	51.74	336.43	22.71	44.77	12.25	10.70	296.53	4.76	6.29	0.96	0.89	120.60	10.05	3.97	d.l.
561.26	Poikilitic Troctolite	16.02	56.37	1120.63	99.04	845.21	19.29	57.56	8.97	5.51	148.06	1.86	3.03	0.00	0.16	29.69	3.39	0.34	d.l.
572.41	Poikilitic Troctolite	16.57	60.06	1505.47	128.40	1179.82	7.44	67.04	6.46	12.80	92.62	3.94	12.73	0.91	0.17	49.93	6.87	d.l.	d.l.
596.73	Poikilitic Troctolite	12.68	44.85	1321.16	136.59	1424.01	20.92	73.14	6.50	8.45	72.05	0.95	8.86	1.97	d.l.	49.96	4.61	d.l.	d.l.
603.70	Harzburgite	8.64	22.25	232.84	105.76	1203.10	d.l.	60.99	6.01	2.99	41.58	d.l.	3.89	1.77	d.l.	28.95	7.07	d.l.	d.l.
604.60	Poikilitic Troctolite	6.90	16.96	206.44	122.74	1485.95	d.l.	77.58	5.29	2.71	7.62	d.l.	4.14	1.69	d.l.	10.86	3.23	d.l.	d.l.
606.40	Poikilitic Troctolite	6.21	16.64	208.72	138.20	1828.99	d.l.	65.49	3.18	3.27	5.39	d.l.	3.92	1.58	d.l.	3.01	4.26	d.l.	d.l.
609.90	Poikilitic Troctolite	9.04	22.58	384.14	142.81	2712.00	1141.85	113.53	5.94	3.68	6.14	d.l.	2.55	1.15	d.l.	21.88	7.49	d.l.	d.l.
613.40	Harzburgite	11.38	32.90	1667.29	149.27	1768.23	634.87	66.03	4.71	5.30	75.68	0.35	1.74	1.23	1.21	40.02	7.04	d.l.	d.l.
616.68	Olivine-bearing Pyroxenite	21.31	80.40	2117.67	89.75	1026.49	56.51	67.47	6.17	3.86	90.69	1.63	2.00	0.66	0.02	18.90	7.13	d.l.	d.l.
630.20	Feldspathic Pyroxenite	30.32	101.24	987.61	71.08	890.02	1017.19	63.65	10.89	9.56	276.19	2.48	2.50	0.54	d.l.	121.40	10.39	d.l.	d.l.
641.06	Feldspathic Pyroxenite	26.77	115.47	2013.03	78.58	1078.73	35.29	117.17	5.04	1.84	27.10	4.39	5.78	2.15	0.85	15.79	8.59	d.l.	d.l.
650.62	Granofels	18.89	62.96	2154.50	65.58	1127.38	d.l.	43.86	6.12	5.31	39.58	3.59	4.55	0.65	0.38	48.58	5.63	d.l.	d.l.
678.40	Granofels	30.89	130.84	2335.61	69.05	1131.81	6.17	215.96	17.53	10.24	85.72	9.28	11.28	5.74	d.l.	106.26	7.95	0.49	d.l.

Appendix G

Amendment Tables

WB017D0

WB027D0

WB099D0

WE001D0

WE027D0

WE035D0

Appendix G: Amendment Table
Table 1: Borehole WB017D0

Bh.I.D	Sample #	Core log Classification	Petrological Classification	Geochemical Classification
WB017	30.80-31.00	Waterberg Sediments	Arkose (Waterberg Sediments)	Waterberg Sediments
WB017	93.78-93.96	Waterberg Sediments	Banded Arkose (Waterberg Sediments)	Waterberg Sediments
WB017	141.23-141.64	Waterberg Sediments	Pebble-Conglomerate (Waterberg Sediments)	Waterberg Sediments
WB017	156.36-156.54	Dolerite/Sill	Dolerite (Sill)	Dolerite (sill)
WB017	198.55-198.81	Ferro Gabbro	Ferro Gabbro	Ferro Gabbro
WB017	201.20-201.42	Ferro Gabbro	Ferro Gabbro	Ferro Gabbro
WB017	206.29-206.57	Magnetite bearing Gabbronorite	Gabbronorite	Magnetite Gabbronorite
WB017	253.66-253.86	Magnetite bearing Gabbronorite	Magnetite bearing Gabbronorite	Magnetite Gabbronorite
WB017	294.00-294.21	Magnetite bearing Gabbronorite	Olivine-bearing Gabbronorite	Magnetite Gabbronorite
WB017	303.43-303.70	Gabbronorite	Gabbronorite	Gabbronorite
WB017	311.16-311.40	Gabbronorite	Pegmatoidal Gabbronorite	Gabbronorite
WB017	465.00.465.20	Pyroxenite	Melo-Gabbronorite	Pyroxenite
WB017	532.00-532.30	Gabbronorite	Gabbronorite	Gabbronorite
WB017	539.20-539.45	Feldspathic pyroxenite (pegmatoidal unit)	Altered Gabbronorite	Feldspathic Pyroxenite
WB017	633.00-633.21	Pegmatoidal unit	Pegmatoidal Gabbronorite	Gabbronorite
WB017	649.25-649.50	Olivine bearing Gabbronorite/ Harzburgite	Harzburgite	Olivine Gabbronorite
WB017	658.00-658.25	Pegmatoidal unit/leuco gabbronorite	Gabbronorite	Gabbronorite
WB017	682.50-682.71	Altered Gabbronorite	Gabbronorite	Gabbronorite
WB017	700.28-700.52	Anorthosite	Altered Anorthosite	Anorthosite
WB017	711.88-712.10	Spotted Anorthosite	Altered Anorthosite	Anorthosite
WB017	730.26-730.65	Leuco Gabbronorite	Olivine-bearing Gabbronorite	Leuco Gabbronorite
WB017	765.27-765.64	Altered Gabbronorite	Olivine-bearing Gabbronorite	Olivine Gabbronorite
WB017	842.74-842.53	Olivine bearing Gabbronorite	Gabbronorite	Gabbronorite
WB017	965.52-965.70	Gabbronorite/leuco Gabbronorite	Gabbronorite	Troctolite
WB017	988.74-988.94	Troctolite	Harzburgite	Harzburgite
WB017	1003.74-1003.95	Harzburgite	Harzburgite	Troctolite
WB017	1015.29-1015.50	Troctolite	Harzburgite	Harzburgite
WB017	1019.26-1019.50	Troctolite/Harzburgite	Troctolite	Pyroxenite
WB017	1051.00-1051.21	Sulphide bearing pyroxenite	Pyroxenite	Pyroxenite
WB017	1072.80-1073.00	Pyroxenite	Pyroxenite	Pyroxenite
WB017	1077.90-1078.10	Vein pyroxenite/feldspars and quartz	Plagioclase-feldspar vein	Plagioclase-feldspar vein
WB017	1086.70-1086.90	Granofels	Granofels (Felsic unit)	Granofels (Felsic unit)

Appendix G: Amendment Table
Table 2: Borehole WB027D0

Bh.I.D	Sample #	Core log Classification	Petrological Classification	Geochemical Classification
WB027	488.00-488.10	Waterberg Sediments with large pebble	Altered Volcanic Clastic Rock	waterberg Sediments
WB027	490.60-490.80	Shale with gabbroic texture (contact)	Palaesol	Palaesol
WB027	520.63-520.80	Pegmatoidal unit	Pegmatoidal Gabbronorite	Olivine Gabbronorite
WB027	537.64-537.85	Magnetite bearing gabbronorite	Gabbronorite	Gabbronorite
WB027	606.00-606.20	Sulphides bearing gabbronorite	Gabbronorite	Gabbronorite
WB027	622.00-622.20	Gabbronorite	Gabbronorite	Gabbronorite
WB027	649.20-649.40	Pyroxenite	Olivine-bearing Pyroxenite	Pyroxenite
WB027	815.20-815.30	Altered Gabbronorite	Altered Gabbronorite	Gabbronorite
WB027	881.00-881.25	Gabbronorite	Gabbronorite	Gabbronorite
WB027	889.00-889.10	Anorthosite	Altered Anorthosite	Gabbronorite
WB027	928.48-928.70	Norite	Gabbronorite	Gabbronorite
WB027	939.50-939.70	Mottled Norite	Mottle Norite	Gabbronorite
WB027	1060.50-1060.70	Troctolite with oikocryst of Opx	Harzburgite	Harzburgite
WB027	1090.70-1090.90	Altered Harzburgite (xenolith)	Altered Harzburgite (xenolith)	Olivine Pyroxenite
WB027	1092.00-1092.20	Olivine Norite/ Troctolite	Altered Troctolite	Troctolite
WB027	1116.10-1116.22	Harzburgite Completely serpentinised	Serpentinite (Altered Harzburgite)	Harzburgite
WB027	1152.20-1152.40	Harzburgite	Altered Serpentinised Harzburgite	Troctolite
WB027	1174.70-1174.80	Granofels	Granofels	Granofels
WB027	1178.10-1178.20	Granofels (altered epidotisation)	Granofels	Granofels

Appendix G: Amendment Table
Table 3: Borehole WB099D0

Bh.I.D	Sample #	Core log Classification	Petrological Classification	Geochemical Classification
WB099	527.85-528.06	Magnetite Gabbronorite	Gabbronorite	Gabbronorite
WB099	551.80-552.00	Magnetite Gabbronorite	Magnetite-bearing Gabbronorite	Gabbronorite
WB099	566.48-566.66	Magnetite Gabbronorite	Magnetite-bearing Gabbronorite	Gabbronorite
WB099	602.26-602.43	Magnetite Gabbronorite (T-reef)	Magnetite-bearing Gabbronorite	Gabbronorite
WB099	619.80-620.00	Feldspathic pyroxenite (T-reef)	Olivine-bearing Feldspathic Pyroxenite	Feldspathic Pyroxenite
WB099	628.50-628.68	Magnetite Gabbronorite (T-reef)	Magnetite-bearing Gabbronorite	Gabbronorite
WB099	671.57-671.74	Feldspathic pyroxenite (T-reef)	Olivine-bearing Gabbronorite	Olivine-bearing Gabbronorite
WB099	675.84-676.04	Gabbronorite (T-reef)	Olivine-bearing Gabbronorite	Olivine-bearing Gabbronorite
WB099	698.67-698.84	Gabbronorite (T-reef) Sulphides	Gabbronorite	Magnetite Gabbronorite
WB099	699.40-699.60	Feldspathic pyroxenite (T-reef) Sulphides	Gabbronorite	Feldspathic Pyroxenite
WB099	700.02-700.37	Gabbronorite (T-reef) Sulphides	Gabbronorite	Magnetite Gabbronorite
WB099	705.50-705.75	Feldspathic pyroxenite (T-reef) Sulphides	Olivine-bearing Gabbronorite	Magnetite Gabbronorite
WB099	711.80-711.96	Gabbronorite (T-reef)	Gabbronorite	Magnetite Gabbronorite
WB099	734.58-734.79	Gabbronorite	Olivine-bearing Gabbronorite	Magnetite Gabbronorite
WB099	763.00-763.22	Gabbronorite	Gabbronorite	Gabbronorite
WB099	825.73-825.88	Leuco-gabbronorite	Leuco-Gabbronorite	Leuco-gabbronorite
WB099	900.03-900.18	Mottled Anorthosite	Anorthosite	Anorthosite
WB099	924.40-924.60	Norite	Leuco-Gabbronorite	Leuco-gabbronorite
WB099	1009.00-1009.17	Leuco-gabbronorite	Altered Leuco-Gabbronorite	Leuco-gabbronorite
WB099	1021.18-1021.32	Gabbronorite	Gabbronorite	Leuco-gabbronorite
WB099	1069.70-1069.90	Leuco-gabbronorite	Olivine-bearing Gabbronorite	Olivine-bearing Gabbronorite
WB099	1126.18-1126.38	Olivine bearing pyroxenite	Olivine-bearing Gabbronorite	Feldspathic Pyroxenite
WB099	1145.51-1145.83	Olivine bearing feldspathic pyroxenite (F-zone)	Poikilitic Troctolite	Olivine-bearing Gabbronorite
WB099	1172.62-1172.86	Poikilitic Troctolite (F-zone)	Poikilitic Troctolite	Olivine-bearing Gabbronorite
WB099	1193.50-1193.77	Poikilitic Troctolite (F-zone)	Poikilitic Troctolite	Olivine-bearing Gabbronorite
WB099	1215.48-1215.80	Poikilitic Troctolite (F-zone)	Poikilitic Troctolite	Olivine-bearing Gabbronorite
WB099	1228.50-1228.77	Poikilitic Troctolite (F-zone)	Poikilitic Troctolite	Olivine-bearing Gabbronorite
WB099	1270.16-1270.41	Feldspathic Pyroxenite (F-zone)	Feldspathic Pyroxenite	Olivine pyroxenite
WB099	1280.17-1280.51	Olivine bearing Feldspathic Pyroxenite (F-zone)	Harzburgite	Olivine pyroxenite
WB099	1282.67-1283.01	Feldspathic Harzburgite (F-zone)	Feldspathic Harzburgite	Olivine-bearing Gabbronorite
WB099	1292.13-1292.43	Feldspathic Pyroxenite (F-zone)	Harzburgite	Feldspathic Pyroxenite
WB099	1315.77-1316.00	Pyroxenite (F-zone)	Olivine-bearing Pyroxenite	Feldspathic Pyroxenite
WB099	1324.53-1324.74	Pegmatoidal unit (F-zone)	Feldspathic Pyroxenite	Granofels (pyroxenite unit)
WB099	1333.85-1334.09	Granofels (Basement)	Altered Olivine-bearing Pyroxenite (Granofels)	Granofels (pyroxenite unit)

Appendix G: Amendment Table
Table 4: Borehole WE001D0

Bh.I.D	Sample #	Core log Classification	Petrological Classification	Geochemical Classification
WE001	367.19-367.35	Waterberg Sediments with pebbles	Sandstone (Waterberg Sediments)	Waterberg Sediments
WE001	378.64-378.75	Shale (Waterberg and Bushveld contact)	Palaesol	Palaesol
WE001	432.14-432.19	Gabbronorite (contact with pegmatoidal unit)	Altered Magnetite-bearing Gabbronorite	Gabbronorite
WE001	432.58-432.69	Pegmatoidal unit (gabbronorite)	Pegmatoidal Gabbronorite	Olivine Gabbronorite
WE001	603.23-603.43	Gabbronorite	Olivine-bearing Gabbronorite	Gabbronorite
WE001	636.22-636.32	Olivine bearing Gabbronorite	Altered Troctolite	Olivine Gabbronorite
WE001	642.00-642.08	Altered Troctolite	Altered Poikilitic Troctolite	Olivine Gabbronorite
WE001	644.40-644.60	Troctolite	Altered Poikilitic Troctolite	Harzburgite
WE001	675.00-675.10	Troctolite with large olivine grains	Altered Harzburgite	Harzburgite
WE001	699.97-700.17	Harzburgite with large oikocryst of Opx	Altered Harzburgite	Troctolite
WE001	730.75-730.90	Altered Harzburgite	Altered Poikilitic Harzburgite	Gabbronorite
WE001	752.99-753.25	Olivine bearing Gabbronorite	Altered Poikilitic Harzburgite	Olivine Gabbronorite
WE001	754.95-755.10	Altered pyroxenite with bands	Poikilitic Troctolite	Olivine Gabbronorite
WE001	784.10-784.20	Troctolite with sulphides	Poikilitic Troctolite	Olivine Gabbronorite
WE001	787.80-787.95	Gabbronorite	Altered Gabbronorite	Gabbronorite
WE001	827.05-827.20	Granofels (quartz and feldspar)	Granofels (Felsic unit)	Granofels
WE001	845.65-845.84	Granofels (serpentinisation)	Granofels (pyroxene-rich unit)	Granofels

Appendix G: Amendment Table
Table 5: Borehole WE027D0

Bh.I.D	Sample #	Core log Classification	Petrological Classification	Geochemical Classification
WE027	553.96-554.17	Conglomerate (waterberg)	Sandstone (Waterberg Sediments)	Waterberg Sediments
WE027	556.35-556.64	Paleosol (Gabbroic texture) Contact	Palaesol	Palaesol (Contact)
WE027	565.00-565.28	Gabbronorite	Magnetite-bearing Gabbronorite	Gabbronorite
WE027	570.56-570.73	Altered Leuco-Gabbronorite	Altered Olivine-bearing Gabbronorite	Olivine-bearing Gabbronorite
WE027	578.27-578.45	Magnetite Gabbronorite	Leuco-Gabbronorite	Olivine-bearing Gabbronorite
WE027	580.59-580.80	Magnetite Gabbronorite	Leuco-Gabbronorite	Olivine-bearing Gabbronorite
WE027	586.00-586.21	Magnetite Gabbronorite	Magnetite-bearing Gabbronorite	Gabbronorite
WE027	588.78-589.00	Altered Leuco-Gabbronorite	Altered Leuco-Gabbronorite	Olivine-bearing Gabbronorite
WE027	594.58-594.80	Magnetite Gabbronorite	Gabbronorite	Gabbronorite
WE027	602.36-602.60	Magnetite Gabbronorite	Magnetite-bearing Gabbronorite	Gabbronorite
WE027	622.20-622.45	Gabbronorite	Leuco-Gabbronorite	Gabbronorite
WE027	631.16-631.43	Leuco-gabbronorite/ anorthosite	Altered Olivine-bearing Gabbronorite	Olivine-bearing Gabbronorite
WE027	635.40-635.61	Gabbronorite	Magnetite-bearing Gabbronorite	Gabbronorite
WE027	658.08-658.30	Gabbronorite	Magnetite-bearing Gabbronorite	Gabbronorite
WE027	693.21-693.52	Gabbronorite	Olivine-bearing Gabbronorite	Olivine-bearing Gabbronorite
WE027	724.80-725.13	Pegmatoidal Gabbronorite	Pegmatoidal Gabbronorite	Olivine-bearing Gabbronorite
WE027	748.42-748.75	Gabbronorite	Magnetite-bearing Gabbronorite	Gabbronorite
WE027	785.20-785.50	Magnetite Gabbronorite	Olivine-bearing Gabbronorite	Olivine-bearing Gabbronorite
WE027	808.34-808.57	Leuco-gabbronorite/ anorthosite	Altered Leuco-Gabbronorite	Olivine-bearing Gabbronorite
WE027	849.60-849.80	Magnetite Gabbronorite	Olivine-bearing Gabbronorite	Olivine-bearing Gabbronorite
WE027	888.37-888.70	Magnetite Gabbronorite	Magnetite-bearing Gabbronorite	Troctolite
WE027	891.52-891.78	Pegmatoidal Magnetite Gabbronorite	Pegmatoidal Gabbronorite	Gabbronorite
WE027	929.57-929.87	Magnetite Gabbronorite	Magnetite-bearing Gabbronorite	Olivine-bearing Gabbronorite
WE027	962.39-962.71	Magnetite Gabbronorite	Poikilitic Troctolite	Olivine-bearing Gabbronorite
WE027	987.21-987.43	Anorthosite	Altered Anorthosite/Leuco-Gabbronorite	Olivine-bearing Gabbronorite
WE027	994.04-994.23	Pegmatoidal Anorthosite	Altered Pegmatoidal Anorthosite	Olivine-bearing Gabbronorite
WE027	1252.15-1252.36	Olivine Gabbronorite	Olivine-bearing Gabbronorite	Olivine-bearing Gabbronorite
WE027	1282.94-1283.12	Gabbronorite	Gabbronorite	Gabbronorite
WE027	1345.20-1345.43	Gabbronorite	Leuco-Gabbronorite	Gabbronorite
WE027	1381.20-1381.46	Olivine bearing pyroxenite	Altered Poikilitic Troctolite	Olivine-bearing Gabbronorite
WE027	1385.60-1385.41	Poikilitic Feldspathic Harzburgite	Altered Feldspathic Harzburgite	Harzburgite
WE027	1386.66-1386.86	Poikilitic Feldspathic Harzburgite	Altered Feldspathic Harzburgite	Harzburgite
WE027	1393.60-1393.81	Granofels (feldspathic pyroxenite)	Granofels (pyroxenite-rich unit)	Granofels (pyroxenite unit)
WE027	1403.92-1404.20	Granofels (feldspathic pyroxenite)	Granofels (pyroxenite-rich unit)	Granofels (pyroxenite unit)

Appendix G: Amendment Table
Table 6: Borehole WE035D0

Bh.I.D	Sample #	Core log Classification	Petrological Classification	Geochemical Classification
WE035	368.55-368.76	Conglomerate/ Mudstone (Waterberg)	Sandstone (Waterberg Sediments)	Waterberg Sediments
WE035	369.90-370.00	Paleosol (gabbroic texture) Contact	Palaesol	Palaesol
WE035	377.53-377.76	Olivine Gabbronorite	Gabbronorite	Gabbronorite
WE035	393.80-394.15	Gabbronorite (pegmatitic)	Gabbronorite	Gabbronorite
WE035	399.70-399.91	Olivine Gabbronorite	Olivine-bearing Gabbronorite	Gabbronorite
WE035	457.65-457.79	Olivine Gabbronorite	Gabbronorite	Olivine-bearing Gabbronorite
WE035	488.30-488.55	Leuco-gabbronorite (altered)	Altered Gabbronorite	Gabbronorite
WE035	505.10-505.20	Olivine norite	Gabbronorite	Olivine-bearing Gabbronorite
WE035	515.30-515.46	Olivine norite	Olivine-bearing Gabbronorite	Gabbronorite
WE035	523.30-523.55	Leuco-gabbronorite (altered)	Altered Olivine-bearing Gabbronorite	Olivine-bearing Gabbronorite
WE035	529.15-529.39	Poikilitic Troctolite (F-zone)	Poikilitic Troctolite	Olivine-bearing Gabbronorite
WE035	536.46-536.68	(Leuco) Poikilitic Troctolite (F-zone)	Olivine-bearing Gabbronorite	Olivine-bearing Gabbronorite
WE035	544.67-544.92	(Leuco) Poikilitic Troctolite (F-zone)	Poikilitic Troctolite	Gabbronorite
WE035	545.40-545.60	Leuco-gabbronorite (altered)	Altered Leuco-Gabbronorite	Poikilitic Troctolite
WE035	561.26-561.48	(Leuco) Poikilitic Troctolite (F-zone)	Poikilitic Troctolite	Poikilitic Troctolite
WE035	572.41-572.74	Poikilitic Troctolite (F-zone)	Poikilitic Troctolite	Poikilitic Troctolite
WE035	596.73-596.96	Poikilitic Troctolite (F-zone)	Poikilitic Troctolite	Harzburgite
WE035	603.70-603.94	(Leuco) Poikilitic Troctolite (F-zone)	Altered Poikilitic Troctolite	Poikilitic Troctolite
WE035	604.60-604.80	Poikilitic Troctolite (F-zone)	Altered Poikilitic Troctolite	Poikilitic Troctolite
WE035	606.40-606.60	Altered Harzburgite (F-zone)	Altered Harzburgite	Poikilitic Troctolite
WE035	609.90-610.15	Altered Feldspathic Harzburgite (F-zone)	Altered Harzburgite	Harzburgite
WE035	613.40-613.16	Troctolite (F-zone)	Altered Harzburgite	Olivine-bearing Pyroxenite
WE035	616.68-616.90	Olivine bearing feldspathic pyroxenite (F-zone)	Feldspathic Pyroxenite	Feldspathic Pyroxenite
WE035	630.20-630.50	Olivine bearing feldspathic pyroxenite (F-zone)	Gabbronorite	Gabbronorite
WE035	641.06-641.32	Feldspathic pyroxenite (F-zone)	Feldspathic Pyroxenite	Feldspathic Pyroxenite
WE035	650.62-650.82	Serpentinised Granofels	Granofels (Pyroxenite-rich unit)	Granofels (Pyroxenite unit)
WE035	678.40-678.65	Granofels	Granofels (Pyroxenite-rich unit)	Granofels (Pyroxenite unit)

Appendix H

Mineral Chemistry of Orthopyroxene and Clinopyroxene

WB099D0

WE027D0

WE035D0

Table 1: Borehole WB099D0 Orthopyroxenite Mineral Chemistry

Chemical composition of orthopyroxene (wt. %) of Borehole WB099D0												
Depth (m)	**Na_2O**	**K_2O**	**SiO_2**	**Al_2O_3**	**MgO**	**FeO**	**TiO_2**	**CaO**	**NiO**	**MnO**	**Cr_2O_3**	**Total**
527.85	0.007	0.009	52.216	1.254	23.739	20.080	0.180	0.780	0.082	0.368	0.071	**98.786**
543.80	0.028	0.016	53.983	1.135	25.166	16.823	0.348	2.098	0.068	0.355	0.095	**100.115**
543.80	0.009	0.015	54.867	0.939	27.688	17.011	0.166	0.607	0.047	0.332	0.064	**101.745**
543.80	0.004	0.011	53.819	1.368	25.816	18.925	0.211	0.579	0.083	0.329	0.034	**101.179**
551.80	0.025	0.035	53.063	1.422	23.288	18.825	0.242	2.158	0.049	0.424	0.000	**99.531**
551.80	0.004	0.004	53.535	1.102	22.479	21.014	0.346	1.175	0.048	0.399	0.010	**100.116**
551.80	0.001	0.011	53.675	1.432	25.559	18.130	0.166	0.749	0.087	0.420	0.000	**100.230**
558.60	0.005	0.042	54.125	1.278	23.307	19.953	0.223	1.173	0.020	0.375	0.033	**100.534**
558.60	0.016	0.011	56.527	1.026	25.074	21.083	0.044	0.808	0.069	0.520	0.071	**105.249**
558.60	0.000	0.021	53.379	1.212	24.163	18.775	0.149	0.680	0.060	0.380	0.073	**98.892**
566.48	0.021	0.012	53.523	1.343	23.995	19.575	0.243	1.801	0.027	0.362	0.000	**100.902**
566.48	0.000	0.014	53.362	1.054	23.694	20.494	0.151	1.576	0.033	0.376	0.057	**100.811**
566.48	0.000	0.010	54.197	1.133	23.555	20.638	0.167	1.313	0.061	0.380	0.071	**101.525**
593.10	0.003	0.030	53.089	1.184	22.429	20.421	0.120	0.770	0.000	0.473	0.006	**98.525**
602.26	0.002	0.023	53.517	0.966	23.728	20.851	0.075	0.765	0.077	0.407	0.044	**100.455**
619.18	0.011	0.003	54.357	1.169	24.670	17.783	0.091	1.759	0.069	0.357	0.034	**100.303**
619.18	0.000	0.023	54.450	1.166	25.028	17.413	0.030	0.779	0.043	0.371	0.033	**99.336**
622.25	0.045	0.000	54.012	1.147	23.611	19.751	0.163	1.870	0.085	0.410	0.011	**101.105**
622.25	0.000	0.037	54.478	1.188	25.596	17.507	0.119	0.762	0.076	0.406	0.073	**100.242**
622.25	0.000	0.009	53.627	1.258	23.341	18.228	0.193	0.723	0.066	0.432	0.036	**97.913**
628.50	0.000	0.010	53.131	1.077	23.741	21.979	0.240	0.786	0.062	0.491	0.000	**101.517**
628.50	0.024	0.017	52.788	1.089	21.774	22.258	0.285	0.735	0.011	0.443	0.052	**99.476**
628.50	0.010	0.013	53.089	0.856	22.853	21.527	0.120	0.502	0.064	0.457	0.042	**99.533**
632.80	0.003	0.014	52.848	0.778	21.650	22.303	0.088	0.506	0.039	0.565	0.005	**98.799**
653.00	0.014	0.032	51.704	1.263	25.942	19.632	0.151	1.259	0.023	0.396	0.007	**100.423**
653.00	0.046	0.022	52.866	1.341	25.698	18.167	0.015	1.086	0.078	0.432	0.048	**99.799**
653.00	0.003	0.032	53.315	1.365	25.486	18.866	0.197	0.789	0.093	0.358	0.119	**100.623**
653.00	0.006	0.012	50.622	1.374	23.911	18.994	0.197	0.715	0.044	0.387	0.117	**96.379**

Table 1: Borehole WB099D0 Orthopyroxenite Mineral Chemistry

Chemical composition of orthopyroxene (wt. %) of Borehole WB099D0												
Depth (m)	**Na_2O**	**K_2O**	**SiO_2**	**Al_2O_3**	**MgO**	**FeO**	**TiO_2**	**CaO**	**NiO**	**MnO**	**Cr_2O_3**	**Total**
671.57	0.025	0.026	53.173	1.364	23.925	18.935	0.210	0.893	0.038	0.414	0.035	**99.038**
671.57	0.007	0.009	53.762	1.352	24.657	18.683	0.196	0.884	0.062	0.428	0.013	**100.053**
671.57	0.014	0.029	53.812	1.301	25.529	17.896	0.151	0.825	0.062	0.370	0.128	**100.117**
675.84	0.018	0.027	54.819	1.258	26.272	18.249	0.348	0.754	0.017	0.374	0.006	**102.142**
690.00	0.000	0.018	53.901	1.227	23.562	19.786	0.089	1.752	0.050	0.387	0.022	**100.794**
690.00	0.017	0.015	53.600	1.143	23.538	18.248	0.015	1.674	0.059	0.417	0.041	**98.767**
690.00	0.000	0.026	53.708	1.273	22.738	19.469	0.327	0.800	0.114	0.381	0.008	**98.844**
698.67	0.019	0.015	54.550	1.378	26.580	15.527	0.076	1.741	0.071	0.327	0.026	**100.310**
699.40	0.012	0.011	54.241	1.420	25.041	17.762	0.197	1.342	0.048	0.376	0.021	**100.471**
700.02	0.000	0.004	53.948	1.369	24.609	18.926	0.015	1.845	0.148	0.408	0.021	**101.293**
700.02	0.013	0.000	53.063	0.637	20.976	23.582	0.299	1.237	0.025	0.498	0.004	**100.334**
700.02	0.021	0.012	53.414	1.235	22.908	20.049	0.166	0.683	0.143	0.394	0.011	**99.036**
705.50	0.031	0.010	53.664	1.331	23.515	19.216	0.151	1.725	0.108	0.387	0.069	**100.207**
705.50	0.015	0.010	53.322	1.135	24.161	19.679	0.181	0.920	0.073	0.452	0.000	**99.948**
705.50	0.013	0.032	53.685	1.369	24.294	20.377	0.241	0.817	0.104	0.360	0.064	**101.356**
709.80	0.000	0.000	53.526	1.060	24.921	20.373	0.270	0.729	0.044	0.428	0.019	**101.370**
711.80	0.038	0.044	54.001	1.111	24.567	17.441	0.257	1.360	0.068	0.428	0.053	**99.368**
711.80	0.000	0.029	54.240	0.799	24.483	18.562	0.166	0.681	0.038	0.444	0.047	**99.489**
711.80	0.007	0.010	53.942	1.306	24.502	18.926	0.045	0.593	0.052	0.402	0.034	**99.819**
714.50	0.018	0.039	34.250	12.378	21.260	16.666	0.000	0.529	0.078	0.195	0.035	**85.448**
714.50	0.000	0.020	33.672	12.621	21.571	18.321	0.000	0.395	0.065	0.274	0.006	**86.945**
716.50	0.011	0.014	53.503	0.952	24.216	18.528	0.310	0.846	0.059	0.437	0.019	**98.895**
716.50	0.018	0.018	53.287	1.043	24.355	19.037	0.206	0.719	0.013	0.421	0.001	**99.118**
718.20	0.017	0.014	53.452	0.938	23.816	20.045	0.164	1.179	0.030	0.416	0.006	**100.077**
718.20	0.002	0.010	53.573	0.954	25.080	18.771	0.105	0.788	0.044	0.463	0.024	**99.814**
718.20	0.000	0.024	54.042	1.403	25.095	20.191	0.075	0.662	0.052	0.379	0.050	**101.973**
725.20	0.025	0.018	53.808	1.107	23.305	19.093	0.149	1.649	0.073	0.429	0.038	**99.694**
725.20	0.021	0.024	53.457	1.307	23.880	19.072	0.179	0.682	0.089	0.413	0.040	**99.164**
734.58	0.027	0.039	53.924	1.164	23.936	17.860	0.257	1.596	0.053	0.349	0.042	**99.247**
734.58	0.008	0.020	53.771	0.925	23.737	18.585	0.181	0.771	0.035	0.443	0.024	**98.500**

Table 1: Borehole WB099D0 Orthopyroxenite Mineral Chemistry

Chemical composition of orthopyroxene (wt. %) of Borehole WB099D0												
Depth (m)	**Na_2O**	**K_2O**	**SiO_2**	**Al_2O_3**	**MgO**	**FeO**	**TiO_2**	**CaO**	**NiO**	**MnO**	**Cr_2O_3**	**Total**
734.58	0.000	0.025	54.170	0.985	24.494	21.109	0.105	0.698	0.058	0.427	0.000	**102.071**
735.40	0.011	0.020	52.553	1.022	23.318	19.757	0.060	0.748	0.024	0.391	0.046	**97.950**
735.40	0.001	0.006	53.870	0.982	24.907	19.823	0.165	0.718	0.024	0.445	0.016	**100.957**
739.58	0.022	0.039	53.499	0.793	24.262	19.180	0.195	0.970	0.075	0.448	0.028	**99.511**
739.58	0.000	0.006	53.254	0.963	23.902	17.940	0.241	0.853	0.017	0.436	0.037	**97.649**
739.58	0.000	0.043	53.330	0.883	23.788	20.218	0.285	0.774	0.051	0.438	0.015	**99.825**
739.58	0.004	0.016	53.489	1.071	24.411	19.005	0.165	0.631	0.096	0.435	0.008	**99.331**
750.10	0.005	0.025	54.306	1.512	26.785	13.751	0.271	1.834	0.039	0.403	0.013	**98.944**
750.10	0.002	0.001	54.712	1.408	26.870	13.541	0.150	1.060	0.055	0.294	0.065	**98.158**
751.90	0.011	0.020	54.019	0.990	24.785	18.623	0.211	0.637	0.062	0.490	0.024	**99.872**
763.00	0.046	0.016	53.318	1.088	25.275	19.330	0.121	0.887	0.056	0.370	0.000	**100.507**
763.00	0.004	0.026	55.827	1.477	28.184	14.312	0.107	0.673	0.017	0.342	0.008	**100.977**
765.00	0.017	0.007	54.916	1.375	25.502	14.376	0.000	0.886	0.071	0.399	0.070	**97.619**
765.00	0.011	0.018	54.915	1.037	26.498	16.328	0.074	0.790	0.000	0.350	0.030	**100.051**
765.00	0.000	0.000	54.689	1.270	26.342	15.752	0.000	0.699	0.083	0.299	0.000	**99.134**
772.00	0.025	0.030	53.485	1.242	23.453	19.172	0.060	1.429	0.019	0.445	0.080	**99.440**
787.90	0.026	0.000	54.570	0.926	25.998	16.492	0.194	0.852	0.064	0.346	0.000	**99.468**
787.90	0.000	0.021	54.033	1.110	26.018	17.634	0.223	0.757	0.003	0.352	0.034	**100.185**
787.90	0.035	0.022	54.569	1.128	25.839	16.580	0.268	0.696	0.037	0.366	0.063	**99.603**
825.73	0.024	0.019	53.434	1.034	24.784	18.237	0.090	1.721	0.062	0.387	0.000	**99.792**
825.73	0.000	0.025	52.490	0.823	24.929	18.954	0.000	0.690	0.054	0.385	0.064	**98.414**
825.73	0.021	0.000	54.465	0.901	24.545	18.732	0.120	0.672	0.056	0.393	0.003	**99.908**
858.10	0.024	0.021	53.384	1.135	24.127	19.367	0.194	1.902	0.051	0.429	0.035	**100.669**
858.10	0.015	0.014	53.484	0.921	23.941	19.848	0.776	1.760	0.031	0.445	0.050	**101.285**
858.10	0.007	0.024	53.884	1.230	24.775	20.291	0.298	0.780	0.059	0.413	0.038	**101.799**
875.30	0.036	0.024	54.204	1.040	23.528	17.920	0.166	2.883	0.025	0.360	0.079	**100.265**
875.30	0.012	0.046	53.146	1.027	24.185	19.224	0.256	1.130	0.051	0.390	0.032	**99.499**
875.30	0.000	0.029	53.647	0.908	24.219	19.967	0.300	0.640	0.051	0.410	0.056	**100.227**
879.20	0.024	0.015	53.770	0.970	24.339	18.567	0.075	1.874	0.094	0.440	0.052	**100.220**
879.20	0.000	0.013	54.165	1.203	24.495	20.031	0.120	0.615	0.061	0.390	0.057	**101.150**

Table 1: Borehole WB099D0 Orthopyroxenite Mineral Chemistry

Chemical composition of orthopyroxene (wt. %) of Borehole WB099D0												
Depth (m)	**Na_2O**	**K_2O**	**SiO_2**	**Al_2O_3**	**MgO**	**FeO**	**TiO_2**	**CaO**	**NiO**	**MnO**	**Cr_2O_3**	**Total**
879.20	0.011	0.016	53.962	1.068	24.263	19.786	0.120	0.604	0.006	0.366	0.042	**100.244**
892.90	0.035	0.026	53.283	1.082	22.502	17.627	0.163	1.994	0.041	0.448	0.048	**97.249**
892.90	0.000	0.000	53.306	1.257	22.301	18.398	0.236	1.428	0.093	0.425	0.000	**97.444**
896.00	0.000	0.013	53.042	1.098	22.919	20.415	0.059	0.779	0.061	0.422	0.039	**98.847**
896.00	0.016	0.012	53.105	0.975	22.333	21.263	0.326	0.776	0.025	0.405	0.000	**99.236**
896.00	0.011	0.016	53.682	1.019	22.959	19.830	0.148	0.771	0.041	0.419	0.040	**98.936**
924.40	0.000	0.009	53.392	1.171	23.503	16.291	0.182	1.612	0.000	0.442	0.043	**96.645**
952.00	0.011	0.031	53.472	1.055	22.969	19.601	0.059	2.075	0.057	0.426	0.047	**99.803**
952.00	0.003	0.038	53.166	1.176	22.729	19.829	0.059	1.216	0.044	0.419	0.097	**98.776**
952.00	0.000	0.008	53.372	1.317	23.568	19.437	0.294	0.691	0.029	0.396	0.095	**99.207**
967.10	0.028	0.009	31.358	11.911	20.405	17.449	0.015	1.428	0.070	0.279	0.107	**83.059**
1009.00	0.013	0.023	53.397	1.260	23.831	20.383	0.257	1.886	0.010	0.360	0.046	**101.466**
1009.00	0.015	0.013	52.530	1.069	22.914	20.361	0.181	1.679	0.086	0.416	0.024	**99.288**
1015.90	0.013	0.024	54.013	1.080	25.955	18.571	0.344	0.682	0.079	0.344	0.043	**101.148**
1021.18	0.014	0.033	54.767	1.395	26.892	16.472	0.106	1.606	0.021	0.340	0.139	**101.785**
1021.18	0.019	0.012	54.491	1.045	23.954	20.002	0.015	1.391	0.036	0.419	0.020	**101.404**
1021.18	0.006	0.013	54.540	1.347	25.978	16.426	0.273	1.126	0.040	0.334	0.064	**100.147**
1045.80	0.012	0.011	55.251	1.173	26.219	15.281	0.135	1.547	0.083	0.305	0.000	**100.017**
1045.80	0.000	0.015	56.144	1.450	25.981	16.135	0.165	0.781	0.057	0.297	0.101	**101.126**
1066.80	0.050	0.016	53.422	1.591	24.550	15.012	0.271	2.033	0.059	0.330	0.220	**97.554**
1066.80	0.053	0.021	54.275	1.672	24.811	16.563	0.000	1.514	0.034	0.353	0.269	**99.565**
1066.80	0.022	0.030	54.787	1.529	27.526	16.230	0.240	0.587	0.021	0.393	0.180	**101.545**
1069.70	0.021	0.023	55.269	1.536	26.440	17.530	0.182	0.611	0.008	0.345	0.266	**102.231**
1073.80	0.036	0.015	54.568	1.294	25.591	16.736	0.119	0.747	0.070	0.365	0.218	**99.759**
1073.80	0.022	0.022	54.867	0.913	26.488	16.511	0.193	0.538	0.043	0.399	0.191	**100.187**
1081.90	0.018	0.000	54.118	1.160	26.378	16.407	0.091	0.616	0.069	0.323	0.203	**99.383**
1095.15	0.017	0.011	55.644	1.466	28.739	13.361	0.122	1.781	0.022	0.295	0.452	**101.910**
1095.15	0.007	0.005	55.449	1.888	29.174	15.283	0.000	0.597	0.072	0.276	0.524	**103.275**
1095.15	0.000	0.007	55.169	1.210	27.875	15.031	0.212	0.589	0.054	0.327	0.230	**100.704**
1095.15	0.010	0.000	55.723	0.893	27.804	16.516	0.227	0.544	0.048	0.355	0.163	**102.283**

Table 1: Borehole WB099D0 Orthopyroxenite Mineral Chemistry

Chemical composition of orthopyroxene (wt. %) of Borehole WB099D0												
Depth (m)	**Na_2O**	**K_2O**	**SiO_2**	**Al_2O_3**	**MgO**	**FeO**	**TiO_2**	**CaO**	**NiO**	**MnO**	**Cr_2O_3**	**Total**
1108.38	0.022	0.003	54.327	1.413	26.098	14.857	0.104	2.048	0.097	0.278	0.253	**99.500**
1108.38	0.001	0.008	55.056	1.407	26.740	15.345	0.194	0.753	0.116	0.305	0.283	**100.208**
1108.38	0.002	0.025	54.364	1.518	25.904	17.601	0.089	0.719	0.052	0.341	0.286	**100.901**
1119.70	0.010	0.024	53.642	1.894	24.451	16.270	0.178	1.363	0.056	0.314	0.516	**98.718**
1119.70	0.000	0.035	54.169	1.249	25.609	17.509	0.222	0.591	0.019	0.316	0.218	**99.937**
1119.70	0.018	0.021	54.355	1.565	27.177	15.190	0.223	0.566	0.075	0.344	0.334	**99.868**
1126.18	0.025	0.005	53.326	1.608	26.283	15.342	0.091	1.539	0.062	0.289	0.359	**98.929**
1126.18	0.002	0.014	54.143	1.394	26.884	16.181	0.166	0.997	0.084	0.310	0.053	**100.228**
1145.51	0.052	0.017	54.686	1.741	27.587	11.725	0.168	2.324	0.041	0.255	0.306	**98.902**
1145.51	0.015	0.012	54.609	1.598	27.076	13.252	0.106	1.477	0.070	0.357	0.307	**98.879**
1145.51	0.000	0.003	54.473	1.839	28.372	13.784	0.000	1.374	0.060	0.307	0.346	**100.558**
1148.60	0.017	0.015	55.061	1.897	28.947	13.557	0.075	0.896	0.073	0.309	0.383	**101.230**
1148.60	0.006	0.009	55.400	1.538	27.439	12.682	0.225	0.653	0.083	0.314	0.218	**98.567**
1200.90	0.000	0.025	55.432	2.193	27.745	13.887	0.241	1.337	0.087	0.295	0.380	**101.622**
1200.90	0.008	0.025	55.221	2.226	29.793	13.304	0.000	0.665	0.089	0.224	0.534	**102.089**
1223.30	0.052	0.026	53.918	2.445	29.324	11.816	0.089	1.265	0.085	0.225	1.085	**100.330**
1223.30	0.015	0.034	54.321	0.960	23.105	19.890	0.206	0.963	0.000	0.484	0.033	**100.011**
1233.00	0.000	0.371	29.721	17.605	21.060	16.342	0.059	0.026	0.052	0.235	1.261	**86.732**
1268.20	0.136	0.028	47.052	0.002	19.371	20.171	0.000	0.571	0.366	0.220	0.000	**87.917**
1270.16	0.000	0.019	55.286	0.638	25.007	18.563	0.106	0.913	0.041	0.359	0.106	**101.038**
1270.16	0.000	0.035	54.806	0.673	26.125	18.547	0.076	0.532	0.006	0.411	0.133	**101.344**
1270.16	0.025	0.007	54.167	0.565	25.560	18.516	0.137	0.404	0.033	0.352	0.120	**99.886**
1280.17	0.026	0.002	55.293	2.354	28.911	11.109	0.000	1.881	0.045	0.253	0.617	**100.491**
1280.17	0.024	0.009	54.923	2.454	28.171	10.446	0.108	0.950	0.065	0.219	0.644	**98.013**
1280.17	0.000	0.036	55.411	2.359	30.564	11.615	0.108	0.706	0.086	0.214	0.541	**101.640**
1292.13	0.002	0.027	55.437	1.655	30.768	9.903	0.244	0.614	0.084	0.255	0.355	**99.344**
1292.13	0.006	0.020	55.443	2.028	30.861	11.124	0.015	0.594	0.091	0.290	0.303	**100.775**
1292.13	0.026	0.000	55.552	1.996	31.949	8.815	0.122	0.440	0.097	0.189	0.657	**99.843**
1292.13	0.013	0.018	55.270	2.258	31.455	10.546	0.000	0.371	0.112	0.205	0.228	**100.476**
1314.50	0.022	0.024	55.939	1.469	32.239	12.768	0.184	0.697	0.145	0.280	0.155	**103.922**

Table 1: Borehole WB099D0 Orthopyroxenite Mineral Chemistry

Chemical composition of orthopyroxene (wt. %) of Borehole WB099D0												
Depth (m)	**Na_2O**	**K_2O**	**SiO_2**	**Al_2O_3**	**MgO**	**FeO**	**TiO_2**	**CaO**	**NiO**	**MnO**	**Cr_2O_3**	**Total**
1315.77	0.041	0.000	56.354	1.467	31.380	10.744	0.123	1.240	0.078	0.161	0.444	**102.032**
1315.77	0.008	0.022	56.186	1.286	31.756	10.269	0.107	0.513	0.134	0.163	0.343	**100.787**
1315.77	0.000	0.014	56.040	1.468	30.258	12.325	0.199	0.476	0.106	0.248	0.347	**101.481**
1321.00	0.000	0.025	54.654	1.441	31.774	12.280	0.153	1.215	0.107	0.220	0.355	**102.224**
1321.00	0.000	0.024	56.269	0.916	32.274	9.576	0.123	0.473	0.108	0.165	0.110	**100.038**
1321.00	0.269	0.059	59.545	0.783	28.447	4.705	0.000	0.058	0.072	0.147	0.206	**94.291**
1324.53	0.000	0.023	55.298	1.349	27.834	13.802	0.183	1.012	0.091	0.292	0.193	**100.077**
1324.53	0.009	0.026	55.782	1.425	29.076	12.186	0.183	0.613	0.073	0.250	0.176	**99.799**
1324.53	0.022	0.021	55.769	1.383	29.151	12.646	0.122	0.555	0.069	0.259	0.159	**100.156**
1333.85	0.055	0.000	52.837	1.401	29.039	15.551	0.319	1.566	0.048	0.307	0.082	**101.205**
1333.85	0.000	0.020	54.155	0.815	25.003	19.258	0.196	1.417	0.040	0.396	0.107	**101.407**
1333.85	0.007	0.017	55.843	1.128	28.160	15.061	0.046	0.601	0.115	0.291	0.012	**101.281**

Table 2: Borehole WB099D0 Clinopyroxene Mineral Chemistry

Chemical Composition of Clinopyroxene (wt.%) from WB099D0												
Depth (m)	**Na_2O**	**K_2O**	**SiO_2**	**Al_2O_3**	**MgO**	**FeO**	**TiO_2**	**CaO**	**NiO**	**MnO**	**Cr_2O_3**	**Total**
527.35	0.310	0.028	53.054	2.151	14.194	10.209	0.221	20.522	0.000	0.242	0.018	**100.949**
527.35	0.303	0.028	53.427	2.580	14.961	9.207	0.570	21.571	0.049	0.245	0.015	**102.956**
527.35	0.231	0.020	52.730	2.333	15.511	7.538	0.475	21.782	0.000	0.183	0.297	**101.100**
527.85	0.218	0.005	53.209	2.227	15.609	6.524	0.376	21.671	0.024	0.180	0.113	**100.156**
527.85	0.264	0.021	53.062	1.853	14.151	8.404	0.219	22.159	0.029	0.160	0.248	**100.570**
527.85	0.284	0.014	53.487	1.899	15.418	6.797	0.220	22.370	0.067	0.209	0.055	**100.820**
539.50	0.277	0.011	52.486	2.247	15.705	6.313	0.411	21.637	0.031	0.195	0.109	**99.422**
539.50	0.253	0.023	52.937	2.217	15.000	6.497	0.300	21.906	0.033	0.194	0.196	**99.556**
539.50	0.248	0.021	52.931	2.406	15.583	5.712	0.142	22.067	0.029	0.128	0.119	**99.386**
539.50	0.201	0.025	52.839	1.722	15.115	6.888	0.253	22.291	0.000	0.200	0.149	**99.683**
551.80	0.264	0.030	53.133	2.329	15.438	7.270	0.470	21.541	0.000	0.169	0.125	**100.769**
551.80	0.273	0.020	53.057	1.963	15.258	7.076	0.094	22.208	0.047	0.192	0.173	**100.361**
558.60	0.237	0.030	53.238	2.096	15.864	7.987	0.408	20.685	0.044	0.197	0.144	**100.930**
558.60	0.312	0.009	53.094	2.547	14.516	7.952	0.126	21.458	0.083	0.169	0.101	**100.367**
566.48	0.279	0.030	53.177	1.643	14.474	7.089	0.188	21.892	0.030	0.224	0.142	**99.168**
566.48	0.267	0.009	53.378	1.830	15.031	7.132	0.282	21.965	0.043	0.158	0.186	**100.281**
566.48	0.245	0.010	53.704	1.563	15.121	6.977	0.313	21.972	0.000	0.204	0.143	**100.252**
566.48	0.269	0.016	53.588	1.639	15.792	7.460	0.438	22.083	0.029	0.181	0.119	**101.614**
593.10	0.350	0.031	51.855	3.573	15.075	7.100	0.362	20.579	0.038	0.135	0.073	**99.171**
593.10	0.283	0.024	53.052	2.463	15.065	7.391	0.173	21.871	0.048	0.194	0.080	**100.644**
593.10	0.273	0.005	53.189	1.773	14.662	8.564	0.267	21.952	0.000	0.197	0.089	**100.971**
599.20	0.265	0.008	52.286	2.169	13.796	9.059	0.172	21.564	0.000	0.210	0.056	**99.585**
599.20	0.237	0.018	52.566	1.967	14.549	7.409	0.252	21.744	0.021	0.224	0.029	**99.016**
599.20	0.258	0.000	52.552	1.966	14.082	8.598	0.236	21.869	0.008	0.224	0.003	**99.796**
602.26	0.288	0.004	52.493	2.184	14.162	8.624	0.250	21.569	0.003	0.305	0.032	**99.914**
602.26	0.224	0.040	53.273	1.556	14.691	7.909	0.298	22.082	0.019	0.179	0.000	**100.271**
602.26	0.230	0.024	53.419	1.584	14.756	7.858	0.376	22.108	0.018	0.196	0.037	**100.606**
619.18	0.266	0.022	52.159	1.906	15.871	8.616	0.174	20.495	0.044	0.207	0.069	**99.829**

Table 2: Borehole WB099D0 Clinopyroxene Mineral Chemistry

Chemical Composition of Clinopyroxene (wt.%) from WB099D0												
Depth (m)	**Na_2O**	**K_2O**	**SiO_2**	**Al_2O_3**	**MgO**	**FeO**	**TiO_2**	**CaO**	**NiO**	**MnO**	**Cr_2O_3**	**Total**
619.18	0.566	0.071	54.133	2.466	15.567	7.124	0.365	20.665	0.009	0.229	0.113	**101.308**
619.18	0.413	0.041	53.641	1.954	16.006	7.738	0.269	21.143	0.042	0.164	0.074	**101.485**
619.18	0.336	0.025	53.110	2.299	15.708	6.406	0.207	22.190	0.045	0.133	0.086	**100.545**
628.50	0.251	0.033	53.409	1.705	15.436	7.825	0.188	21.994	0.040	0.223	0.140	**101.244**
632.80	0.220	0.013	52.301	2.240	14.797	9.019	0.174	20.612	0.010	0.226	0.089	**99.701**
632.80	0.276	0.002	51.750	2.267	14.168	7.488	0.523	21.164	0.028	0.186	0.031	**97.883**
632.80	0.290	0.005	53.235	2.211	14.720	8.285	0.475	21.843	0.056	0.239	0.058	**101.417**
632.80	0.322	0.011	52.999	2.029	14.458	8.336	0.459	21.879	0.051	0.266	0.027	**100.837**
642.00	0.253	0.012	51.429	1.937	13.782	8.781	0.459	21.725	0.062	0.225	0.022	**98.687**
642.00	0.239	0.014	52.785	2.248	15.014	7.513	0.159	21.954	0.074	0.217	0.128	**100.345**
642.00	0.243	0.002	52.892	2.442	15.299	7.946	0.222	22.013	0.005	0.182	0.150	**101.396**
653.00	0.349	0.025	52.379	2.186	14.828	8.658	0.235	20.713	0.035	0.215	0.135	**99.758**
653.00	0.336	0.020	52.379	2.276	14.390	8.505	0.282	20.891	0.063	0.153	0.104	**99.399**
667.10	0.083	0.023	0.058	0.012	0.191	0.242	0.000	54.451	0.009	0.528	0.037	**55.634**
671.57	0.536	0.123	47.188	2.151	13.053	6.251	0.381	18.346	0.030	0.146	0.036	**88.241**
671.57	0.310	0.027	51.549	2.235	14.135	7.867	0.539	20.915	0.025	0.176	0.045	**97.823**
671.57	0.355	0.027	52.280	2.348	15.241	8.116	0.380	21.099	0.040	0.226	0.051	**100.163**
671.57	0.352	0.037	52.303	2.286	15.169	7.465	0.349	21.275	0.044	0.266	0.131	**99.677**
675.84	0.371	0.023	51.483	2.408	15.194	7.952	0.459	20.338	0.032	0.225	0.028	**98.513**
675.84	0.365	0.002	53.302	2.281	15.526	8.696	0.253	20.633	0.036	0.172	0.021	**101.287**
675.84	0.375	0.045	52.023	2.435	15.251	7.283	0.364	21.437	0.054	0.220	0.032	**99.519**
690.00	0.206	0.020	52.463	1.793	14.685	8.708	0.547	20.864	0.058	0.221	0.075	**99.640**
690.00	0.298	0.011	52.597	1.918	14.269	7.692	0.251	21.791	0.064	0.257	0.072	**99.220**
690.00	0.245	0.037	52.447	1.911	14.308	7.458	0.408	21.938	0.035	0.214	0.080	**99.081**
698.67	0.268	0.020	51.620	2.234	13.840	9.095	0.616	20.379	0.032	0.239	0.036	**98.379**
698.67	0.299	0.040	52.139	2.170	14.489	8.239	0.317	21.229	0.068	0.191	0.074	**99.255**
698.67	0.315	0.001	52.698	2.366	15.060	6.085	0.191	21.814	0.025	0.206	0.058	**98.819**
699.40	0.312	0.035	52.479	2.336	15.419	7.205	0.191	21.577	0.008	0.240	0.051	**99.853**
699.40	0.292	0.000	52.117	2.320	14.997	7.352	0.159	21.907	0.053	0.231	0.049	**99.477**
699.40	0.274	0.012	52.542	2.058	14.959	7.451	0.285	22.144	0.065	0.167	0.127	**100.084**

Table 2: Borehole WB099D0 Clinopyroxene Mineral Chemistry

Chemical Composition of Clinopyroxene (wt.%) from WB099D0												
Depth (m)	**Na_2O**	**K_2O**	**SiO_2**	**Al_2O_3**	**MgO**	**FeO**	**TiO_2**	**CaO**	**NiO**	**MnO**	**Cr_2O_3**	**Total**
702.00	0.228	0.024	51.889	1.929	14.606	7.874	0.362	21.339	0.017	0.193	0.062	**98.523**
702.00	0.298	0.031	51.837	2.109	14.364	8.239	0.142	21.692	0.057	0.247	0.060	**99.076**
702.00	0.271	0.019	51.540	2.026	14.385	7.736	0.315	21.703	0.096	0.226	0.128	**98.445**
702.00	0.290	0.005	51.419	2.280	13.505	8.194	0.283	21.897	0.097	0.273	0.043	**98.286**
705.50	0.338	0.020	52.961	2.198	15.213	8.323	0.488	21.268	0.033	0.216	0.050	**101.108**
705.50	0.311	0.000	52.090	2.331	14.839	7.735	0.316	21.913	0.080	0.225	0.067	**99.907**
709.80	0.315	0.018	52.696	1.798	14.805	7.998	0.581	21.705	0.027	0.202	0.066	**100.211**
709.80	0.294	0.000	53.139	1.762	14.979	8.090	0.518	21.756	0.008	0.181	0.054	**100.781**
709.80	0.388	0.012	53.574	1.951	14.843	8.115	0.330	22.010	0.000	0.230	0.058	**101.511**
714.50	0.325	0.017	52.191	1.986	15.348	7.649	0.409	21.960	0.058	0.202	0.046	**100.191**
714.50	0.311	0.019	52.328	1.874	14.796	7.236	0.268	22.001	0.050	0.253	0.062	**99.198**
714.50	0.370	0.034	51.726	1.909	14.408	7.196	0.646	22.040	0.032	0.169	0.052	**98.582**
716.50	0.331	0.038	53.192	2.199	14.855	7.965	0.602	21.987	0.006	0.186	0.071	**101.432**
716.50	0.324	0.016	52.286	1.975	15.293	7.492	0.618	22.226	0.062	0.200	0.040	**100.532**
716.50	0.306	0.006	53.021	1.529	15.402	7.762	0.254	22.240	0.029	0.165	0.006	**100.720**
718.20	0.323	0.012	52.747	2.134	14.501	8.388	0.549	21.114	0.031	0.242	0.033	**100.074**
718.20	0.370	0.015	52.727	2.087	14.536	8.050	0.612	21.549	0.023	0.208	0.067	**100.244**
718.20	0.320	0.026	53.267	2.001	15.003	8.314	0.361	21.945	0.047	0.204	0.037	**101.525**
723.40	0.302	0.022	52.177	1.943	14.783	7.673	0.459	21.652	0.019	0.203	0.046	**99.279**
723.40	0.317	0.037	52.385	2.073	14.787	8.065	0.380	21.723	0.046	0.207	0.041	**100.061**
725.20	0.281	0.021	51.981	2.070	15.145	8.171	0.501	19.605	0.036	0.201	0.041	**98.053**
725.20	0.372	0.022	52.394	2.227	14.428	8.545	0.313	20.921	0.042	0.202	0.073	**99.539**
725.20	0.331	0.019	52.389	1.921	14.574	7.212	0.706	21.715	0.025	0.239	0.090	**99.221**
739.58	0.301	0.000	51.550	2.160	14.958	9.448	0.503	20.370	0.028	0.148	0.042	**99.508**
739.58	0.325	0.033	52.487	1.972	15.072	7.619	0.394	21.824	0.019	0.191	0.019	**99.955**
739.58	0.300	0.018	51.132	2.060	16.802	7.936	0.694	21.846	0.000	0.164	0.051	**101.003**
751.90	0.337	0.015	53.352	2.170	14.329	7.999	0.487	21.094	0.033	0.227	0.000	**100.043**
751.90	0.328	0.029	52.846	2.453	14.119	8.624	0.267	21.358	0.030	0.257	0.000	**100.311**
765.00	0.238	0.028	53.389	1.718	15.813	6.767	0.286	21.805	0.058	0.200	0.018	**100.320**
765.00	0.247	0.018	53.119	2.179	15.680	6.035	0.397	21.877	0.000	0.173	0.104	**99.829**

Table 2: Borehole WB099D0 Clinopyroxene Mineral Chemistry

Chemical Composition of Clinopyroxene (wt.%) from WB099D0												
Depth (m)	**Na_2O**	**K_2O**	**SiO_2**	**Al_2O_3**	**MgO**	**FeO**	**TiO_2**	**CaO**	**NiO**	**MnO**	**Cr_2O_3**	**Total**
765.00	0.275	0.001	53.357	2.091	15.312	7.465	0.570	21.994	0.031	0.202	0.060	**101.358**
772.00	0.296	0.012	52.426	2.066	14.694	7.747	0.235	21.330	0.000	0.164	0.049	**99.019**
772.00	0.296	0.024	52.191	2.268	14.259	7.742	0.627	21.724	0.000	0.221	0.074	**99.426**
772.00	0.225	0.039	52.952	1.190	14.959	7.307	0.110	21.742	0.027	0.179	0.017	**98.747**
787.90	0.324	0.009	52.287	2.279	15.419	7.081	0.286	21.604	0.020	0.201	0.161	**99.671**
787.90	0.334	0.019	51.646	2.174	15.343	7.034	0.254	21.716	0.007	0.213	0.191	**98.931**
799.00	0.271	0.007	53.227	1.371	15.552	7.687	0.250	20.303	0.081	0.265	0.035	**99.049**
799.00	0.255	0.000	52.238	1.927	14.423	7.546	0.423	21.406	0.033	0.177	0.092	**98.520**
803.60	0.356	0.029	51.197	2.484	14.150	8.099	0.613	20.805	0.059	0.222	0.034	**98.048**
803.60	0.347	0.029	51.773	1.862	13.731	7.636	0.394	21.737	0.003	0.188	0.083	**97.783**
825.73	0.317	0.041	52.691	1.747	15.727	7.303	0.444	21.850	0.127	0.190	0.050	**100.487**
825.73	0.236	0.021	52.676	1.536	15.029	7.570	0.206	22.088	0.072	0.250	0.049	**99.733**
825.73	0.298	0.007	52.822	1.649	15.261	7.117	0.301	22.091	0.045	0.172	0.100	**99.863**
858.10	0.372	0.002	53.622	2.549	15.849	5.572	0.315	22.498	0.014	0.200	0.659	**101.652**
875.30	0.314	0.009	52.192	1.860	14.917	8.530	0.409	21.030	0.038	0.207	0.112	**99.618**
875.30	0.242	0.004	52.910	1.296	15.249	7.500	0.379	21.799	0.000	0.180	0.031	**99.590**
886.38	0.277	0.002	52.224	2.002	14.879	10.665	0.551	19.101	0.027	0.239	0.029	**99.996**
886.38	0.336	0.009	51.359	1.826	14.256	8.018	0.317	21.991	0.024	0.216	0.034	**98.386**
892.90	0.293	0.000	51.367	1.880	15.000	8.501	0.474	21.136	0.000	0.229	0.027	**98.907**
892.90	0.331	0.046	50.716	2.353	13.585	7.549	0.523	21.260	0.044	0.217	0.006	**96.630**
892.90	0.261	0.015	51.890	1.608	14.845	7.553	0.301	21.570	0.011	0.202	0.008	**98.264**
915.10	0.314	0.008	52.514	2.098	15.221	7.101	0.505	22.148	0.063	0.187	0.088	**100.247**
915.10	0.373	0.034	52.675	2.264	15.768	7.094	0.411	22.427	0.034	0.176	0.077	**101.333**
924.40	0.299	0.028	52.493	1.832	15.642	9.600	0.458	19.699	0.076	0.261	0.094	**100.482**
924.40	0.355	0.002	52.293	2.140	14.755	9.030	0.395	20.300	0.022	0.223	0.098	**99.613**
924.40	0.288	0.026	51.943	1.810	14.555	7.602	0.491	21.814	0.049	0.206	0.044	**98.828**
936.75	0.312	0.043	52.373	1.227	15.426	8.053	0.173	20.890	0.011	0.210	0.087	**98.805**
936.75	0.325	0.028	51.974	1.852	14.656	7.527	0.378	21.327	0.030	0.271	0.065	**98.433**
936.75	0.308	0.036	51.553	1.914	14.156	7.876	0.567	21.568	0.025	0.225	0.077	**98.305**
967.10	0.278	0.016	51.835	1.823	13.033	7.475	0.267	21.673	0.062	0.219	0.213	**96.894**

Table 2: Borehole WB099D0 Clinopyroxene Mineral Chemistry

Chemical Composition of Clinopyroxene (wt.%) from WB099D0												
Depth (m)	**Na_2O**	**K_2O**	**SiO_2**	**Al_2O_3**	**MgO**	**FeO**	**TiO_2**	**CaO**	**NiO**	**MnO**	**Cr_2O_3**	**Total**
1009.00	0.282	0.018	51.612	1.830	14.615	7.500	0.508	21.752	0.000	0.206	0.012	**98.335**
1009.00	0.280	0.011	51.636	1.975	14.894	8.473	0.285	21.861	0.000	0.133	0.008	**99.556**
1015.90	0.293	0.003	53.360	1.949	14.956	7.869	0.565	21.832	0.000	0.201	0.103	**101.131**
1015.90	0.289	0.019	53.049	1.913	15.143	7.878	0.392	21.896	0.064	0.248	0.091	**100.982**
1015.90	0.294	0.035	53.626	1.711	15.203	7.592	0.204	21.980	0.005	0.161	0.062	**100.873**
1021.18	0.342	0.014	51.859	2.164	14.754	8.098	0.173	21.472	0.022	0.212	0.194	**99.304**
1021.18	0.373	0.016	52.317	2.321	14.803	7.127	0.426	21.575	0.065	0.181	0.186	**99.390**
1021.18	0.274	0.024	53.346	2.339	16.437	5.995	0.047	21.973	0.085	0.138	0.198	**100.856**
1028.80	0.313	0.015	52.235	2.141	15.949	6.269	0.286	21.545	0.051	0.225	0.053	**99.082**
1045.80	0.325	0.024	52.934	2.008	15.654	6.648	0.377	21.588	0.048	0.155	0.097	**99.858**
1045.80	0.335	0.031	53.219	2.406	15.841	6.387	0.236	22.100	0.012	0.124	0.236	**100.927**
1045.80	0.333	0.018	52.703	2.328	15.411	6.615	0.424	22.354	0.011	0.166	0.154	**100.517**
1066.80	0.321	0.018	53.182	2.451	17.315	8.353	0.188	18.623	0.007	0.192	0.458	**101.108**
1066.80	0.293	0.020	53.171	2.605	15.672	6.161	0.173	20.995	0.015	0.120	0.430	**99.655**
1066.80	0.359	0.026	53.069	2.610	15.840	6.799	0.330	21.138	0.037	0.187	0.446	**100.841**
1066.80	0.376	0.000	53.239	2.206	15.696	6.355	0.582	21.924	0.009	0.157	0.175	**100.719**
1069.70	0.259	0.012	52.146	2.015	16.783	8.522	0.316	18.376	0.000	0.177	0.326	**98.932**
1069.70	0.381	0.017	52.458	2.311	15.506	6.763	0.270	21.929	0.064	0.159	0.390	**100.248**
1070.00	0.417	0.054	54.646	2.444	14.742	0.000	0.000	21.420	0.006	0.225	0.015	**93.969**
1070.00	0.280	0.014	52.205	2.254	14.576	7.129	0.190	21.661	0.019	0.203	0.041	**98.572**
1070.00	0.318	0.028	52.512	2.012	15.741	7.162	0.222	22.032	0.042	0.244	0.083	**100.396**
1070.00	0.337	0.025	52.759	1.934	15.141	7.141	0.365	22.115	0.027	0.191	0.048	**100.083**
1073.80	0.306	0.005	50.937	2.431	14.848	6.966	0.269	20.691	0.065	0.217	0.547	**97.282**
1073.80	0.330	0.026	51.312	2.316	15.191	6.608	0.302	21.445	0.034	0.173	0.378	**98.115**
1073.80	0.258	0.015	51.537	2.122	14.909	6.442	0.381	21.831	0.033	0.150	0.426	**98.104**
1073.80	0.334	0.023	51.843	2.299	15.255	6.803	0.381	21.914	0.044	0.176	0.448	**99.520**
1081.90	0.343	0.023	51.818	2.303	14.921	6.676	0.362	21.154	0.035	0.205	0.567	**98.407**
1081.90	0.327	0.040	51.542	2.310	14.762	6.093	0.237	21.773	0.031	0.171	0.633	**97.919**
1095.15	0.239	0.016	51.422	2.436	15.125	6.061	0.347	21.671	0.073	0.154	0.331	**97.875**
1095.15	0.319	0.005	52.283	2.433	15.548	5.781	0.300	21.804	0.025	0.222	0.338	**99.058**

Table 2: Borehole WB099D0 Clinopyroxene Mineral Chemistry

Chemical Composition of Clinopyroxene (wt.%) from WB099D0												
Depth (m)	**Na_2O**	**K_2O**	**SiO_2**	**Al_2O_3**	**MgO**	**FeO**	**TiO_2**	**CaO**	**NiO**	**MnO**	**Cr_2O_3**	**Total**
1095.15	0.302	0.000	51.449	2.603	15.178	5.378	0.490	22.133	0.064	0.186	0.596	**98.379**
1119.70	0.323	0.022	52.538	2.340	15.115	6.082	0.413	22.055	0.028	0.163	0.298	**99.377**
1126.18	0.317	0.013	51.967	2.500	16.743	6.939	0.190	20.131	0.053	0.213	0.347	**99.413**
1126.18	0.400	0.024	51.975	2.589	16.174	6.047	0.270	21.164	0.023	0.116	0.469	**99.251**
1126.18	0.367	0.011	51.488	2.316	15.170	0.017	0.064	22.286	0.016	0.200	0.219	**92.154**
1200.90	0.328	0.015	52.983	1.936	14.821	8.111	0.330	21.878	0.015	0.168	0.013	**100.598**
1268.20	0.280	0.000	52.894	2.291	15.673	6.107	0.409	22.083	0.031	0.159	0.163	**100.090**
1270.16	0.411	0.020	52.398	1.782	16.430	9.855	0.331	18.784	0.043	0.232	0.211	**100.497**
1315.77	0.356	0.017	53.461	2.457	15.967	4.589	0.267	21.781	0.005	0.151	0.659	**99.710**
1315.77	0.360	0.026	53.293	2.604	15.972	5.099	0.189	22.149	0.078	0.113	0.563	**100.446**
1315.77	0.381	0.026	53.495	2.292	16.413	4.249	0.236	22.335	0.045	0.112	0.645	**100.229**
1324.53	0.328	0.023	52.188	2.570	16.531	6.112	0.253	20.609	0.075	0.194	0.385	**99.268**
1324.53	0.445	0.019	52.491	2.670	15.311	5.730	0.111	21.626	0.000	0.202	0.305	**98.910**
1324.53	0.359	0.027	54.588	2.665	15.537	5.106	0.143	22.300	0.078	0.152	0.439	**101.394**
1324.53	0.312	0.021	52.483	2.805	16.461	5.346	0.238	22.413	0.089	0.125	0.490	**100.783**

Table 3: Borehole WE027D0 Orthopyroxene Mineral Chemistry

Chemical Composition of Orthopyroxene (wt. %) for WE027D0												
Depth (m)	**Na_2O**	**K_2O**	**SiO_2**	**Al_2O_3**	**MgO**	**FeO**	**TiO_2**	**CaO**	**NiO**	**MnO**	**Cr_2O_3**	**Total**
562.80	0.030	0.039	52.015	1.207	20.170	23.510	0.135	1.970	0.030	0.481	0.000	**99.587**
562.80	0.000	0.027	51.726	0.981	19.865	24.539	0.134	0.689	0.008	0.547	0.002	**98.518**
565.00	0.020	0.025	52.147	1.029	19.886	24.740	0.134	0.797	0.000	0.601	0.019	**99.398**
572.60	0.015	0.012	53.249	1.572	25.203	17.240	0.091	1.205	0.112	0.362	0.099	**99.160**
572.60	0.019	0.043	53.289	1.233	25.361	17.419	0.030	1.027	0.061	0.347	0.050	**98.879**
574.40	0.007	0.026	54.464	1.432	26.720	17.573	0.076	0.624	0.110	0.400	0.094	**101.526**
578.27	0.000	0.023	52.290	1.116	22.128	23.258	0.271	0.688	0.062	0.454	0.000	**100.290**
586.00	0.034	0.024	52.930	1.348	22.156	21.585	0.105	0.838	0.000	0.426	0.097	**99.543**
586.00	0.025	0.009	52.312	1.558	20.858	24.491	0.000	0.655	0.017	0.438	0.134	**100.497**
594.80	0.029	0.000	52.548	1.171	22.430	21.819	0.060	1.406	0.120	0.402	0.091	**100.076**
602.36	0.014	0.016	52.935	1.595	23.261	20.137	0.045	0.844	0.116	0.379	0.100	**99.442**
605.00	0.008	0.030	53.129	1.067	22.757	22.066	0.299	0.795	0.056	0.429	0.057	**100.693**
605.00	0.000	0.026	53.231	0.947	23.820	21.832	0.284	0.752	0.061	0.438	0.022	**101.413**
605.00	0.019	0.028	53.035	1.001	23.194	20.709	0.165	0.615	0.077	0.434	0.035	**99.312**
605.00	0.013	0.026	52.920	0.988	23.095	21.899	0.090	0.551	0.011	0.420	0.000	**100.013**
610.50	0.029	0.027	53.754	1.177	23.937	22.783	0.195	1.125	0.074	0.544	0.038	**103.683**
610.50	0.024	0.030	52.597	1.089	22.442	22.608	0.045	0.725	0.017	0.516	0.025	**100.118**
626.00	0.020	0.026	53.932	1.617	23.809	20.130	0.151	1.801	0.008	0.396	0.081	**101.971**
635.40	0.024	0.017	53.381	1.200	22.492	20.125	0.211	1.236	0.051	0.438	0.047	**99.222**
635.40	0.002	0.016	53.105	1.046	22.575	21.117	0.390	0.793	0.047	0.431	0.064	**99.586**
635.40	0.005	0.022	53.121	1.285	22.257	22.507	0.060	0.616	0.062	0.410	0.079	**100.424**
644.50	0.066	0.014	53.992	1.309	21.561	21.009	0.105	1.933	0.024	0.423	0.053	**100.489**
644.50	0.005	0.007	52.364	1.156	21.329	21.853	0.269	0.756	0.050	0.415	0.080	**98.284**
658.08	0.011	0.025	52.840	1.222	23.797	20.841	0.197	0.903	0.045	0.407	0.068	**100.356**
658.08	0.001	0.013	53.153	1.378	24.129	20.167	0.106	0.762	0.089	0.464	0.100	**100.362**
658.08	0.013	0.007	53.029	1.337	24.218	19.526	0.152	0.650	0.038	0.477	0.079	**99.526**
669.00	0.019	0.009	52.929	1.531	23.889	19.991	0.105	0.813	0.059	0.346	0.088	**99.779**
669.00	0.010	0.016	52.786	1.114	24.617	19.641	0.196	0.723	0.067	0.471	0.042	**99.683**

Table 3: Borehole WE027D0 Orthopyroxene Mineral Chemistry

Chemical Composition of Orthopyroxene (wt. %) for WE027D0												
Depth (m)	**Na_2O**	**K_2O**	**SiO_2**	**Al_2O_3**	**MgO**	**FeO**	**TiO_2**	**CaO**	**NiO**	**MnO**	**Cr_2O_3**	**Total**
669.00	0.007	0.027	53.242	1.411	24.189	19.802	0.105	0.710	0.033	0.477	0.000	**100.003**
674.00	0.026	0.043	52.495	1.173	21.792	21.753	0.165	1.978	0.028	0.451	0.072	**99.976**
674.00	0.005	0.011	52.479	1.314	23.346	21.200	0.255	0.642	0.031	0.478	0.015	**99.776**
686.00	0.035	0.014	52.118	1.191	22.774	21.501	0.045	0.895	0.052	0.469	0.000	**99.094**
686.00	0.003	0.012	51.738	1.279	22.895	20.588	0.242	0.858	0.017	0.445	0.026	**98.103**
686.00	0.010	0.016	52.206	1.266	23.547	20.573	0.181	0.779	0.052	0.514	0.059	**99.203**
714.00	0.016	0.009	52.165	1.292	23.492	21.718	0.196	1.130	0.017	0.436	0.012	**100.483**
714.00	0.000	0.014	52.279	1.202	23.194	22.537	0.000	0.767	0.066	0.487	0.000	**100.546**
742.00	0.019	0.027	52.206	1.325	21.395	22.010	0.256	0.930	0.060	0.533	0.088	**98.849**
742.00	0.005	0.017	52.286	1.039	22.912	23.427	0.060	0.866	0.058	0.472	0.053	**101.195**
748.42	0.028	0.029	52.377	1.766	21.554	20.418	0.091	1.884	0.034	0.448	0.132	**98.761**
748.42	0.011	0.022	51.058	1.355	21.772	20.432	0.227	1.244	0.052	0.458	0.085	**96.716**
748.42	0.000	0.025	52.882	1.561	23.878	19.048	0.152	0.770	0.075	0.351	0.146	**98.888**
758.50	0.009	0.031	56.888	0.814	31.471	11.146	0.229	0.929	0.040	0.244	0.281	**102.082**
758.50	0.000	0.049	51.307	0.763	22.085	12.038	0.000	0.458	0.020	0.271	0.200	**87.191**
766.00	0.028	0.024	54.158	1.776	24.728	19.676	0.227	1.526	0.035	0.407	0.200	**102.785**
766.00	0.011	0.015	53.860	0.812	23.062	18.867	0.166	0.588	0.041	0.420	0.027	**97.869**
777.00	0.025	0.006	51.049	0.960	21.010	21.661	0.196	0.730	0.063	0.437	0.013	**96.150**
777.00	0.002	0.000	52.803	1.207	22.765	21.401	0.106	0.683	0.028	0.396	0.009	**99.400**
777.00	0.001	0.007	53.480	0.898	23.640	20.946	0.197	0.676	0.073	0.433	0.028	**100.379**
785.20	0.013	0.025	53.086	1.531	22.831	20.534	0.271	2.070	0.022	0.415	0.071	**100.869**
785.20	0.014	0.021	53.328	1.002	22.781	21.647	0.210	0.917	0.047	0.431	0.048	**100.446**
785.20	0.005	0.017	54.073	1.254	23.413	21.010	0.150	0.914	0.088	0.459	0.094	**101.477**
849.60	0.012	0.031	53.824	1.516	24.541	18.504	0.166	0.865	0.062	0.362	0.094	**99.977**
849.60	0.000	0.032	53.891	1.712	23.910	18.214	0.045	0.785	0.043	0.395	0.112	**99.139**
859.00	0.004	0.018	53.568	1.438	24.824	19.766	0.166	1.030	0.070	0.406	0.018	**101.308**
859.00	0.000	0.004	53.661	1.387	24.720	18.408	0.362	0.808	0.063	0.424	0.017	**99.854**
866.00	0.013	0.013	53.603	1.464	26.362	18.790	0.151	0.683	0.089	0.379	0.077	**101.624**
866.00	0.012	0.005	54.041	1.428	25.850	17.781	0.197	0.583	0.069	0.443	0.069	**100.478**
873.00	0.019	0.028	53.579	1.543	24.807	15.785	0.000	2.078	0.041	0.334	0.164	**98.378**

Table 3: Borehole WE027D0 Orthopyroxene Mineral Chemistry

Chemical Composition of Orthopyroxene (wt. %) for WE027D0												
Depth (m)	**Na_2O**	**K_2O**	**SiO_2**	**Al_2O_3**	**MgO**	**FeO**	**TiO_2**	**CaO**	**NiO**	**MnO**	**Cr_2O_3**	**Total**
873.00	0.034	0.000	53.007	1.633	24.403	18.328	0.241	1.821	0.021	0.338	0.156	**99.982**
879.00	0.014	0.026	52.707	1.438	26.976	16.944	0.304	0.843	0.054	0.394	0.133	**99.833**
879.00	0.000	0.011	53.463	1.339	27.151	17.432	0.122	0.760	0.073	0.356	0.062	**100.769**
879.00	0.000	0.035	52.968	1.504	26.559	17.601	0.122	0.726	0.098	0.427	0.050	**100.090**
888.87	0.009	0.009	52.166	1.115	21.902	21.799	0.211	0.839	0.000	0.563	0.007	**98.620**
888.87	0.012	0.013	53.635	1.676	24.731	18.761	0.000	0.696	0.055	0.440	0.147	**100.166**
888.87	0.012	0.022	53.097	1.454	23.478	20.724	0.227	0.642	0.030	0.393	0.082	**100.161**
894.50	0.000	0.020	53.009	1.650	24.721	20.295	0.045	0.552	0.001	0.454	0.121	**100.868**
917.00	0.031	0.023	53.429	1.285	24.555	18.239	0.061	1.978	0.050	0.498	0.105	**100.254**
924.00	0.003	0.015	54.073	1.635	25.927	16.834	0.152	1.100	0.136	0.377	0.042	**100.294**
924.00	0.003	0.014	53.544	1.525	24.905	19.628	0.045	0.629	0.060	0.455	0.120	**100.928**
929.57	0.002	0.019	53.015	1.456	23.225	18.541	0.106	1.202	0.029	0.401	0.088	**98.084**
929.57	0.012	0.019	52.490	1.410	22.531	20.109	0.182	1.120	0.074	0.398	0.040	**98.385**
929.57	0.000	0.029	53.324	1.480	24.349	18.141	0.197	0.720	0.044	0.478	0.083	**98.845**
940.90	0.003	0.026	52.776	1.557	24.760	16.988	0.030	0.961	0.072	0.342	0.127	**97.642**
940.90	0.006	0.044	52.663	1.558	24.862	18.244	0.015	0.695	0.040	0.353	0.106	**98.586**
946.50	0.081	0.024	52.918	1.387	24.227	19.048	0.227	2.031	0.034	0.403	0.035	**100.415**
946.50	0.003	0.027	53.340	1.440	24.898	19.868	0.030	0.718	0.028	0.448	0.040	**100.840**
957.00	0.042	0.024	52.980	1.601	24.451	18.407	0.000	2.032	0.069	0.355	0.098	**100.059**
957.00	0.042	0.009	52.532	1.585	22.754	20.114	0.196	1.553	0.037	0.407	0.099	**99.328**
957.00	0.000	0.013	53.121	1.426	25.390	19.808	0.422	0.768	0.027	0.340	0.118	**101.433**
962.39	0.000	0.011	53.621	1.964	25.774	17.539	0.198	1.326	0.064	0.330	0.165	**100.992**
962.39	0.048	0.000	53.261	1.601	24.066	19.287	0.076	0.974	0.052	0.356	0.142	**99.863**
962.39	0.000	0.000	53.589	1.510	24.934	17.960	0.122	0.923	0.074	0.388	0.059	**99.559**
964.00	0.000	0.016	52.895	1.546	24.187	18.149	0.030	1.286	0.041	0.396	0.084	**98.630**
964.00	0.004	0.010	48.682	1.250	22.349	17.834	0.150	0.969	0.034	0.356	0.069	**91.707**
964.00	0.049	0.023	53.495	1.392	24.718	19.119	0.331	0.738	0.037	0.443	0.038	**100.383**
967.50	0.017	0.022	53.326	1.559	25.444	17.944	0.226	1.583	0.005	0.323	0.047	**100.496**
971.50	0.017	0.011	53.485	1.490	24.975	19.648	0.151	0.794	0.044	0.423	0.055	**101.093**
978.50	0.023	0.008	53.856	1.535	26.100	17.299	0.000	1.194	0.050	0.313	0.075	**100.453**

Table 3: Borehole WE027D0 Orthopyroxene Mineral Chemistry

Chemical Composition of Orthopyroxene (wt. %) for WE027D0												
Depth (m)	**Na_2O**	**K_2O**	**SiO_2**	**Al_2O_3**	**MgO**	**FeO**	**TiO_2**	**CaO**	**NiO**	**MnO**	**Cr_2O_3**	**Total**
978.50	0.026	0.020	53.428	1.633	25.908	17.409	0.136	1.086	0.080	0.356	0.204	**100.286**
1252.15	0.029	0.029	55.566	1.442	28.224	14.488	0.243	0.826	0.083	0.327	0.033	**101.290**
1252.15	0.000	0.026	55.028	1.557	27.953	15.494	0.137	0.796	0.053	0.324	0.056	**101.424**
1252.15	0.023	0.011	54.990	1.516	27.319	16.829	0.197	0.760	0.081	0.290	0.050	**102.066**
1259.00	0.000	0.018	53.754	1.379	26.889	17.978	0.076	1.151	0.077	0.292	0.049	**101.663**
1259.00	0.008	0.027	53.839	1.493	26.506	16.802	0.000	0.856	0.101	0.321	0.064	**100.017**
1259.00	0.026	0.011	52.724	1.463	26.582	17.890	0.046	0.798	0.000	0.000	0.000	**99.540**
1265.00	0.032	0.009	53.665	1.422	25.416	17.453	0.272	1.598	0.037	0.418	0.019	**100.341**
1265.00	0.024	0.027	54.197	1.494	26.312	18.676	0.091	0.780	0.062	0.391	0.021	**102.075**
1265.00	0.015	0.000	54.462	1.094	26.693	18.303	0.272	0.720	0.050	0.426	0.046	**102.081**
1282.94	0.010	0.023	53.300	1.430	23.077	17.519	0.076	2.013	0.024	0.360	0.065	**97.897**
1282.94	0.026	0.013	53.180	1.522	24.727	17.736	0.213	1.611	0.093	0.371	0.074	**99.566**
1282.94	0.013	0.014	53.430	1.344	25.063	19.489	0.258	0.802	0.050	0.363	0.044	**100.870**
1288.00	0.000	0.003	54.626	1.465	26.896	16.843	0.091	0.916	0.074	0.301	0.000	**101.215**
1288.00	0.021	0.016	53.985	1.351	26.029	18.025	0.227	0.833	0.076	0.383	0.042	**100.988**
1304.00	0.003	0.034	53.640	1.437	25.853	14.874	0.107	0.967	0.056	0.362	0.053	**97.386**
1304.00	0.014	0.015	53.484	1.292	24.493	19.475	0.121	0.659	0.083	0.448	0.037	**100.121**
1314.50	0.015	0.019	53.878	1.434	25.517	17.245	0.136	1.304	0.070	0.346	0.000	**99.964**
1314.50	0.000	0.029	52.921	1.168	23.996	20.613	0.255	0.755	0.008	0.459	0.008	**100.212**
1317.00	0.012	0.016	52.794	1.665	25.069	18.937	0.030	1.498	0.083	0.378	0.070	**100.552**
1317.00	0.005	0.013	53.261	1.167	25.821	19.881	0.030	0.495	0.036	0.424	0.024	**101.157**
1331.50	0.010	0.026	52.958	1.584	25.510	16.792	0.045	0.755	0.046	0.405	0.056	**98.187**
1345.20	0.026	0.024	53.136	1.449	24.664	17.955	0.244	1.989	0.068	0.354	0.000	**99.909**
1345.20	0.021	0.020	52.923	1.489	25.778	18.553	0.182	0.686	0.074	0.357	0.063	**100.146**
1348.00	0.007	0.017	51.716	5.777	27.672	17.629	0.000	0.287	0.039	0.235	0.235	**103.614**
1355.50	0.002	0.008	54.832	1.469	28.678	15.179	0.000	1.612	0.029	0.332	0.034	**102.175**
1355.50	0.006	0.008	55.366	1.350	29.398	15.588	0.091	0.596	0.049	0.353	0.045	**102.850**
1355.50	0.001	0.020	55.939	0.956	30.075	14.979	0.183	0.493	0.057	0.367	0.040	**103.110**
1366.00	0.028	0.012	53.927	1.385	26.113	18.522	0.196	0.811	0.072	0.417	0.008	**101.491**
1366.00	0.036	0.019	55.007	1.613	27.577	17.944	0.136	0.808	0.044	0.380	0.036	**103.600**

Table 3: Borehole WE027D0 Orthopyroxene Mineral Chemistry

Chemical Composition of Orthopyroxene (wt. %) for WE027D0												
Depth (m)	**Na_2O**	**K_2O**	**SiO_2**	**Al_2O_3**	**MgO**	**FeO**	**TiO_2**	**CaO**	**NiO**	**MnO**	**Cr_2O_3**	**Total**
1376.00	0.000	0.017	53.903	1.386	25.988	17.124	0.106	0.953	0.020	0.377	0.061	**99.935**
1376.00	0.000	0.031	55.795	1.183	27.853	18.245	0.257	0.682	0.053	0.335	0.047	**104.481**
1376.00	0.009	0.043	54.217	1.288	25.585	18.226	0.106	0.618	0.025	0.362	0.000	**100.479**
1381.20	0.031	0.027	55.945	1.560	30.078	11.004	0.046	1.640	0.042	0.274	0.066	**100.713**
1381.20	3.970	0.063	66.527	20.261	5.560	2.138	0.000	0.198	0.019	0.019	0.043	**98.798**
1385.60	0.056	0.026	55.821	2.412	30.451	9.964	0.123	1.900	0.085	0.190	0.551	**101.579**
1385.60	0.015	0.005	55.917	1.848	30.165	11.287	0.215	1.343	0.042	0.256	0.160	**101.253**
1391.50	0.039	0.011	55.577	1.315	30.981	11.914	0.076	0.866	0.096	0.305	0.231	**101.411**
1391.50	0.010	0.011	54.827	1.317	29.505	12.638	0.137	0.615	0.109	0.297	0.234	**99.700**
1391.50	0.025	0.028	55.581	1.482	30.365	13.210	0.137	0.498	0.132	0.319	0.208	**101.985**
1392.50	0.017	0.012	53.556	1.327	26.769	16.594	0.000	1.064	0.058	0.443	0.228	**100.068**
1393.60	0.000	0.015	55.094	1.378	27.188	15.238	0.107	1.599	0.056	0.329	0.047	**101.051**
1393.60	0.025	0.035	55.938	1.907	29.950	12.455	0.107	1.181	0.093	0.230	0.435	**102.356**
1393.60	0.000	0.021	55.487	1.409	28.688	14.089	0.000	0.628	0.043	0.274	0.329	**100.968**
1400.50	0.022	0.005	54.410	1.466	29.478	12.145	0.000	0.405	0.042	0.317	0.238	**98.528**
1400.50	0.000	0.019	54.872	1.278	30.596	12.646	0.000	0.398	0.027	0.317	0.254	**100.407**
1400.50	0.000	0.015	54.609	1.326	29.882	12.764	0.061	0.367	0.026	0.207	0.283	**99.540**
1403.92	0.020	0.010	55.784	1.377	28.813	13.370	0.184	0.532	0.062	0.270	0.138	**100.560**
1403.92	0.040	0.009	55.794	1.062	29.533	13.675	0.092	0.495	0.079	0.246	0.166	**101.191**
1403.92	0.028	0.025	55.843	1.145	29.844	13.115	0.077	0.490	0.070	0.245	0.196	**101.078**
1408.00	0.000	0.006	54.392	1.474	29.538	14.859	0.076	0.997	0.037	0.324	0.201	**101.904**
1408.00	0.015	0.026	54.430	1.147	29.020	14.751	0.336	0.569	0.108	0.327	0.181	**100.910**
1408.00	0.032	0.022	55.958	1.158	29.786	14.616	0.352	0.431	0.062	0.332	0.194	**102.943**
1411.00	0.019	0.027	56.260	1.253	30.281	14.507	0.061	1.453	0.085	0.276	0.282	**104.504**
1416.00	0.010	0.013	50.797	6.537	25.652	17.253	0.333	0.466	0.040	0.213	0.194	**101.508**
1416.00	0.017	0.028	50.222	6.701	24.612	16.616	0.212	0.440	0.048	0.184	0.335	**99.415**
1416.00	0.011	0.045	51.453	5.791	26.315	15.262	0.228	0.152	0.017	0.262	0.211	**99.747**
1416.80	0.000	0.016	52.062	4.384	25.525	16.732	0.197	0.628	0.059	0.265	0.176	**100.044**
1416.80	0.004	0.033	51.866	4.372	25.934	17.265	0.136	0.619	0.044	0.221	0.332	**100.826**
1416.80	0.020	0.000	52.512	4.239	26.586	16.111	0.167	0.524	0.059	0.262	0.247	**100.727**

Table 3: Borehole WE027D0 Orthopyroxene Mineral Chemistry

Chemical Composition of Orthopyroxene (wt. %) for WE027D0												
Depth (m)	**Na_2O**	**K_2O**	**SiO_2**	**Al_2O_3**	**MgO**	**FeO**	**TiO_2**	**CaO**	**NiO**	**MnO**	**Cr_2O_3**	**Total**
1421.00	0.002	0.021	55.104	0.808	28.127	14.803	0.077	1.763	0.021	0.226	0.179	**101.131**
1421.00	0.022	0.030	54.423	1.058	27.519	14.892	0.107	0.589	0.070	0.299	0.228	**99.237**
1433.50	0.036	0.008	53.678	1.376	23.213	20.525	0.135	0.778	0.063	0.376	0.115	**100.303**
1433.50	0.000	0.014	54.419	1.025	24.773	20.889	0.210	0.672	0.060	0.416	0.080	**102.558**
1454.00	0.000	0.015	55.418	1.468	31.082	11.126	0.246	0.945	0.065	0.371	0.050	**100.786**
1454.00	0.000	0.000	54.744	1.819	31.881	10.890	0.200	0.359	0.098	0.418	0.049	**100.458**
13856.00	0.019	0.000	56.010	2.277	31.932	10.876	0.031	0.923	0.118	0.270	0.495	**102.951**

Table 4: Borehole WE027D0 Clinopyroxene Mineral Chemistry

Chemical Composition for Clinopyroxene (wt. %) for WE027D0												
Depth (m)	**Na_2O**	**K_2O**	**SiO_2**	**Al_2O_3**	**MgO**	**FeO**	**TiO_2**	**CaO**	**NiO**	**MnO**	**Cr_2O_3**	**Total**
562.80	0.302	0.009	50.910	2.241	12.443	10.691	0.473	21.175	0.000	0.276	0.029	**98.549**
562.80	0.281	0.020	50.968	2.415	12.703	9.827	0.694	21.264	0.032	0.243	0.075	**98.522**
562.80	0.303	0.017	51.253	2.218	13.158	9.739	0.505	21.408	0.001	0.282	0.071	**98.955**
566.90	0.344	0.022	52.478	2.280	15.264	8.353	0.236	20.472	0.037	0.207	0.020	**99.713**
566.90	0.343	0.018	52.334	2.257	15.222	7.876	0.504	21.068	0.063	0.170	0.051	**99.906**
566.90	0.339	0.013	52.291	2.358	14.485	7.690	0.378	21.667	0.074	0.200	0.078	**99.573**
574.40	0.348	0.021	52.004	2.598	14.227	7.498	0.331	21.479	0.068	0.194	0.219	**98.987**
574.40	0.367	0.005	52.126	2.547	14.206	7.225	0.268	21.526	0.038	0.182	0.218	**98.708**
574.40	0.401	0.000	52.645	2.540	14.472	6.568	0.458	21.695	0.062	0.220	0.129	**99.190**
577.30	0.325	0.016	52.088	2.553	14.435	9.869	0.315	20.494	0.058	0.264	0.181	**100.598**
577.30	0.297	0.023	51.831	2.331	14.025	9.019	0.316	21.799	0.087	0.268	0.135	**100.131**
583.50	0.359	0.041	52.082	2.321	13.474	8.527	0.488	21.299	0.018	0.198	0.101	**98.908**
583.50	0.280	0.033	53.024	1.964	14.621	8.213	0.237	22.019	0.066	0.200	0.104	**100.761**
605.00	0.303	0.020	51.995	2.491	13.783	8.669	0.393	21.124	0.101	0.180	0.141	**99.200**
605.00	0.342	0.021	51.780	2.325	14.367	8.909	0.535	21.176	0.036	0.222	0.143	**99.856**
605.00	0.325	0.013	51.955	2.383	14.145	8.815	0.613	21.435	0.021	0.227	0.223	**100.155**
610.50	0.274	0.036	52.463	1.070	13.966	8.184	0.174	21.758	0.036	0.192	0.083	**98.236**
610.70	0.311	0.034	50.727	2.476	13.608	8.886	0.142	20.109	0.040	0.247	0.114	**96.694**
613.16	0.361	0.017	52.381	2.176	13.417	9.807	0.455	21.282	0.000	0.227	0.058	**100.181**
613.16	0.268	0.015	51.465	2.649	13.773	9.608	0.581	21.420	0.039	0.187	0.139	**100.144**
644.50	0.365	0.036	47.295	1.886	11.321	9.085	0.504	20.576	0.037	0.222	0.065	**91.392**
644.50	0.376	0.037	52.058	2.700	13.881	8.985	0.378	21.213	0.030	0.235	0.092	**99.985**
644.50	0.351	0.024	53.200	2.012	13.476	9.359	0.347	21.509	0.000	0.233	0.063	**100.574**
674.00	0.376	0.012	51.495	2.268	13.450	8.823	0.190	21.334	0.056	0.304	0.140	**98.448**
674.00	0.326	0.027	51.774	2.494	13.506	8.883	0.569	21.567	0.037	0.188	0.038	**99.409**
686.00	0.318	0.011	52.007	2.667	14.416	8.576	0.613	20.297	0.053	0.193	0.141	**99.292**
686.00	0.372	0.034	50.900	2.561	13.556	8.903	0.581	20.829	0.008	0.225	0.148	**98.117**
714.00	0.265	0.002	52.305	1.600	13.948	10.763	0.173	19.880	0.039	0.287	0.000	**99.262**

Table 4: Borehole WE027D0 Clinopyroxene Mineral Chemistry

Chemical Composition for Clinopyroxene (wt. %) for WE027D0												
Depth (m)	**Na_2O**	**K_2O**	**SiO_2**	**Al_2O_3**	**MgO**	**FeO**	**TiO_2**	**CaO**	**NiO**	**MnO**	**Cr_2O_3**	**Total**
714.00	0.270	0.024	51.724	2.554	13.856	10.807	0.236	20.584	0.071	0.245	0.101	**100.472**
723.00	0.274	0.024	50.915	2.582	13.404	8.929	0.774	21.243	0.014	0.235	0.033	**98.427**
723.00	0.272	0.023	51.113	2.468	13.171	9.424	0.647	21.725	0.033	0.231	0.030	**99.137**
723.00	0.222	0.029	52.001	1.558	13.067	9.605	0.142	22.109	0.015	0.343	0.009	**99.100**
724.80	0.283	0.035	52.723	2.728	14.476	8.519	0.427	21.297	0.005	0.276	0.061	**100.830**
724.80	0.201	0.005	52.665	2.131	14.101	7.416	0.253	21.673	0.059	0.200	0.050	**98.754**
742.00	0.296	0.018	52.477	2.563	14.501	7.849	0.237	21.271	0.029	0.215	0.298	**99.754**
742.00	0.231	0.002	53.111	1.629	15.090	7.942	0.316	21.560	0.000	0.235	0.267	**100.383**
758.50	0.778	0.021	53.401	1.589	16.264	4.801	0.191	21.176	0.062	0.152	0.702	**99.137**
766.00	0.217	0.049	51.345	2.168	13.870	8.881	0.111	20.174	0.082	0.235	0.097	**97.229**
777.00	0.256	0.021	51.615	2.148	13.739	10.389	0.219	19.902	0.058	0.285	0.144	**98.776**
777.00	0.344	0.008	50.411	2.531	13.777	9.033	0.660	21.075	0.039	0.225	0.166	**98.269**
808.34	0.259	0.024	54.647	2.525	13.709	7.420	0.300	20.792	0.072	0.172	0.073	**99.993**
879.00	0.145	0.000	54.331	1.083	17.172	6.448	0.238	20.130	0.025	0.242	0.029	**99.843**
879.00	0.318	0.019	52.518	2.349	15.277	7.003	0.222	21.613	0.035	0.204	0.050	**99.608**
888.00	0.733	0.019	41.190	29.357	0.018	0.861	0.000	21.581	0.024	0.081	0.037	**93.901**
888.00	0.276	0.045	53.290	2.028	16.682	4.648	0.000	21.814	0.067	0.125	0.156	**99.131**
894.50	0.315	0.000	53.041	2.261	14.288	8.461	0.315	21.822	0.038	0.255	0.074	**100.870**
894.50	0.322	0.003	52.508	2.103	14.222	8.155	0.284	21.961	0.000	0.225	0.116	**99.899**
910.00	0.342	0.027	52.860	2.253	14.947	7.588	0.520	21.704	0.000	0.203	0.169	**100.613**
910.00	0.267	0.007	52.164	2.151	14.437	6.829	0.442	21.762	0.071	0.173	0.216	**98.519**
910.00	0.341	0.031	52.448	2.175	14.910	6.608	0.158	21.819	0.011	0.174	0.221	**98.896**
910.00	0.321	0.009	52.057	2.338	14.580	7.192	0.142	21.945	0.033	0.164	0.229	**99.010**
917.00	0.402	0.020	51.739	2.746	14.201	7.941	0.427	20.854	0.057	0.165	0.102	**98.654**
917.00	0.306	0.016	52.294	2.174	14.636	8.302	0.521	21.471	0.008	0.173	0.013	**99.914**
917.00	0.305	0.029	51.892	1.856	14.110	8.369	0.442	21.575	0.021	0.219	0.050	**98.868**
924.00	0.330	0.019	52.867	2.515	15.135	9.204	0.425	20.983	0.062	0.204	0.034	**101.778**
924.00	0.236	0.018	53.746	0.972	15.152	7.394	0.000	22.062	0.025	0.196	0.017	**99.818**
940.90	0.347	0.015	52.354	2.684	15.087	7.454	0.174	21.462	0.023	0.204	0.118	**99.922**
940.90	0.352	0.030	52.494	2.693	14.864	7.495	0.505	21.848	0.000	0.195	0.032	**100.508**

Table 4: Borehole WE027D0 Clinopyroxene Mineral Chemistry

Chemical Composition for Clinopyroxene (wt. %) for WE027D0												
Depth (m)	**Na_2O**	**K_2O**	**SiO_2**	**Al_2O_3**	**MgO**	**FeO**	**TiO_2**	**CaO**	**NiO**	**MnO**	**Cr_2O_3**	**Total**
940.90	0.347	0.032	52.355	2.334	14.980	7.532	0.284	21.872	0.009	0.223	0.098	**100.066**
946.50	0.308	0.025	52.343	2.336	14.674	8.515	0.504	21.372	0.024	0.240	0.068	**100.409**
946.50	0.359	0.003	51.863	2.498	15.146	7.110	0.205	21.924	0.036	0.218	0.283	**99.645**
964.00	0.379	0.011	51.788	2.626	15.013	7.378	0.331	21.059	0.021	0.158	0.109	**98.873**
964.00	0.338	0.000	52.326	2.585	15.041	7.212	0.236	21.535	0.023	0.240	0.095	**99.631**
978.50	0.393	0.022	52.077	2.256	14.867	8.068	0.426	20.649	0.079	0.311	0.089	**99.237**
987.21	0.257	0.025	53.261	1.491	14.824	7.100	0.317	21.471	0.000	0.238	0.058	**99.042**
994.04	0.006	0.000	44.726	23.114	0.661	1.002	0.000	24.923	0.000	0.027	0.070	**94.529**
1259.00	0.335	0.000	52.421	2.696	14.811	6.878	0.380	22.392	0.000	0.189	0.103	**100.205**
1265.00	0.333	0.023	51.727	2.166	12.793	9.689	0.346	21.103	0.044	0.176	0.146	**98.546**
1265.00	0.323	0.024	52.123	2.261	12.655	10.188	0.377	21.246	0.024	0.257	0.079	**99.557**
1265.00	0.220	0.017	49.185	1.830	12.303	9.915	0.393	21.332	0.000	0.246	0.000	**95.441**
1303.50	0.218	0.021	53.031	1.410	15.108	8.744	0.221	21.273	0.000	0.221	0.002	**100.249**
1303.50	0.266	0.012	52.789	2.016	14.911	7.554	0.285	21.655	0.055	0.251	0.106	**99.900**
1304.00	0.297	0.000	51.056	2.353	13.393	9.224	0.676	20.528	0.023	0.264	0.000	**97.814**
1304.00	0.319	0.021	52.343	2.113	14.848	7.905	0.426	21.718	0.018	0.151	0.005	**99.867**
1331.50	0.314	0.022	53.061	2.371	15.842	7.180	0.316	21.405	0.052	0.216	0.162	**100.941**
1331.50	0.361	0.012	52.582	2.605	15.932	6.712	0.285	22.002	0.000	0.148	0.032	**100.671**
1348.00	0.350	0.002	51.038	2.263	14.425	7.080	0.634	21.230	0.014	0.211	0.075	**97.322**
1348.00	0.334	0.030	51.556	1.883	13.920	7.265	0.222	21.693	0.034	0.226	0.092	**97.255**
1355.50	0.258	0.020	53.339	1.760	16.609	6.643	0.206	20.764	0.003	0.152	0.074	**99.828**
1355.50	0.283	0.003	53.524	1.457	15.772	6.887	0.111	21.964	0.059	0.174	0.080	**100.314**
1366.00	0.322	0.013	51.245	2.073	15.189	7.848	0.634	21.323	0.002	0.174	0.030	**98.853**
1366.00	0.325	0.032	51.733	2.341	15.028	7.571	0.222	21.864	0.043	0.126	0.013	**99.298**
1366.00	0.305	0.018	52.143	2.183	15.255	7.227	0.270	22.090	0.061	0.191	0.063	**99.806**
1376.00	0.191	0.057	50.789	1.852	15.220	10.203	0.580	20.431	0.031	0.241	0.097	**99.692**
1376.00	0.328	0.041	52.907	2.151	14.941	7.688	0.347	21.921	0.002	0.196	0.042	**100.564**
1376.00	0.274	0.011	53.207	1.426	15.816	7.033	0.284	22.313	0.052	0.134	0.082	**100.632**
1386.30	0.355	0.008	53.693	2.689	16.763	4.013	0.270	22.351	0.069	0.163	0.379	**100.753**
1386.30	0.328	0.030	53.621	2.686	16.491	4.434	0.079	22.826	0.070	0.098	0.394	**101.057**

Table 4: Borehole WE027D0 Clinopyroxene Mineral Chemistry

Chemical Composition for Clinopyroxene (wt. %) for WE027D0												
Depth (m)	**Na_2O**	**K_2O**	**SiO_2**	**Al_2O_3**	**MgO**	**FeO**	**TiO_2**	**CaO**	**NiO**	**MnO**	**Cr_2O_3**	**Total**
1391.50	0.300	0.000	52.560	2.487	16.338	4.775	0.174	22.586	0.032	0.169	0.443	**99.864**
1392.50	0.405	0.028	53.656	1.389	15.721	7.766	0.411	21.332	0.053	0.152	0.122	**101.035**
1454.00	0.455	0.016	51.847	3.051	15.709	5.182	0.553	20.844	0.047	0.238	0.110	**98.052**
1454.00	0.554	0.016	51.795	3.290	15.647	5.237	0.443	21.514	0.006	0.177	0.107	**98.786**
1454.00	0.518	0.007	52.463	2.822	15.460	4.971	0.301	21.930	0.030	0.170	0.053	**98.725**

Table 5: Borehole WE035D0 Orthopyroxene Mineral Chemistry

Chemical Composition of Orthopyroxene (wt. %) for WE035D0												
Depth (m)	**Na_2O**	**K_2O**	**SiO_2**	**Al_2O_3**	**MgO**	**FeO**	**TiO_2**	**CaO**	**NiO**	**MnO**	**Cr_2O_3**	**Total**
419.50	0.024	0.023	54.778	1.149	26.518	16.147	0.106	0.583	0.040	0.356	0.173	**99.897**
421.00	0.005	0.013	54.614	1.650	27.221	15.200	0.227	2.003	0.075	0.390	0.311	**101.709**
421.00	0.022	0.010	53.932	1.415	27.244	16.999	0.122	0.738	0.020	0.407	0.244	101.153
421.00	0.000	0.015	54.546	1.553	26.566	16.250	0.045	0.582	0.077	0.373	0.282	**100.289**
421.00	0.007	0.014	54.634	1.478	27.646	16.379	0.000	0.533	0.043	0.341	0.251	**101.326**
437.30	0.020	0.011	54.400	1.505	27.765	13.713	0.046	1.172	0.011	0.329	0.225	**99.197**
488.30	0.018	0.028	54.727	1.391	27.752	14.731	0.015	1.680	0.020	0.328	0.088	**100.778**
488.30	0.003	0.000	54.426	1.424	26.614	15.780	0.152	1.527	0.037	0.317	0.101	**100.381**
496.40	0.000	0.002	54.371	1.463	28.480	14.308	0.061	0.656	0.037	0.350	0.148	**99.876**
501.30	1.122	0.046	30.476	11.079	22.659	13.963	0.030	0.516	0.066	0.210	0.482	**80.649**
501.30	0.066	0.019	37.317	10.709	23.935	13.471	0.000	0.448	0.061	0.153	0.422	**86.601**
501.30	0.214	0.015	48.297	6.794	26.040	10.670	0.031	0.413	0.090	0.126	0.283	**92.973**
505.10	0.058	0.024	55.737	1.504	28.172	13.502	0.000	2.049	0.074	0.313	0.312	**101.745**
505.10	0.021	0.013	55.819	1.517	28.666	13.247	0.152	1.634	0.029	0.319	0.243	**101.660**
515.00	0.054	0.025	54.227	1.700	29.845	10.370	0.015	1.876	0.081	0.284	0.301	**98.778**
515.00	0.014	0.018	54.343	2.051	28.853	12.527	0.184	1.780	0.080	0.280	0.462	**100.592**
515.00	0.009	0.018	54.109	1.570	30.170	12.661	0.168	0.856	0.069	0.286	0.354	**100.270**
527.00	0.040	0.008	53.988	2.194	28.888	12.654	0.168	1.506	0.058	0.233	0.516	**100.253**
527.00	0.017	0.005	54.100	2.245	30.377	12.040	0.000	0.847	0.043	0.296	0.426	**100.396**
530.00	0.004	0.026	54.325	1.667	29.518	12.652	0.199	1.330	0.074	0.268	0.302	**100.365**
530.00	0.012	0.024	55.778	1.811	31.513	11.528	0.230	1.039	0.014	0.254	0.568	**102.771**
532.00	0.008	0.024	54.848	1.543	30.048	12.230	0.169	1.819	0.094	0.318	0.304	**101.405**
532.00	0.019	0.021	54.800	2.149	31.315	11.554	0.138	0.953	0.085	0.300	0.603	**101.937**
537.30	0.011	0.023	56.921	1.596	32.231	13.588	0.046	0.784	0.068	0.325	0.155	**105.748**
540.00	0.023	0.020	39.038	10.633	26.553	9.889	0.000	1.177	0.291	0.151	0.086	**87.861**
540.00	0.041	0.037	37.550	8.697	27.975	10.963	0.000	0.746	0.265	0.135	0.065	**86.474**
540.00	0.061	0.018	39.297	3.537	33.855	9.683	0.000	0.271	0.150	0.158	0.002	**87.032**
545.40	0.012	0.027	54.852	1.205	27.814	15.062	0.228	0.688	0.057	0.278	0.072	**100.295**

Table 5: Borehole WE035D0 Orthopyroxene Mineral Chemistry

Chemical Composition of Orthopyroxene (wt. %) for WE035D0												
Depth (m)	**Na_2O**	**K_2O**	**SiO_2**	**Al_2O_3**	**MgO**	**FeO**	**TiO_2**	**CaO**	**NiO**	**MnO**	**Cr_2O_3**	**Total**
550.60	0.011	0.013	55.102	1.620	31.663	11.875	0.061	0.830	0.057	0.350	0.281	**101.863**
550.60	0.004	0.024	55.199	1.785	30.915	11.639	0.123	0.728	0.023	0.267	0.293	**101.000**
550.60	0.000	0.000	55.121	1.740	31.371	12.217	0.077	0.503	0.040	0.340	0.209	**101.618**
567.40	0.000	0.032	53.425	1.994	29.582	12.633	0.000	0.572	0.049	0.253	0.317	**98.857**
572.41	0.024	0.022	55.409	2.053	30.143	11.309	0.168	1.970	0.033	0.266	0.605	**102.002**
600.00	0.016	0.032	54.710	1.978	32.156	11.673	0.000	0.877	0.067	0.270	0.536	**102.315**
602.50	0.038	0.011	54.325	1.833	29.960	12.021	0.015	1.237	0.078	0.270	0.403	**100.191**
616.68	0.023	0.022	55.553	1.836	31.301	9.666	0.138	0.701	0.082	0.171	0.355	**99.848**
616.68	0.000	0.016	56.999	1.719	31.955	10.099	0.168	0.589	0.039	0.220	0.407	**102.211**
616.68	0.000	0.013	55.923	1.825	31.304	9.503	0.061	0.581	0.108	0.227	0.467	**100.012**
620.50	0.044	0.027	53.119	2.513	26.933	16.767	0.152	0.607	0.080	0.434	0.167	**100.843**
620.50	0.023	0.018	54.164	0.916	25.675	19.759	0.227	0.575	0.064	0.491	0.105	**102.017**
620.50	0.000	0.004	53.775	0.896	26.063	17.736	0.167	0.539	0.068	0.404	0.114	**99.766**
624.50	0.012	0.000	55.357	1.178	31.480	11.567	0.107	0.558	0.111	0.246	0.336	**100.952**
624.50	0.009	0.015	55.655	1.373	31.792	12.021	0.092	0.553	0.100	0.334	0.370	**102.314**
629.70	0.015	0.015	54.734	1.019	26.778	16.990	0.121	0.680	0.092	0.342	0.098	**100.884**
629.70	0.000	0.017	54.977	1.368	28.801	15.197	0.076	0.635	0.101	0.341	0.246	**101.759**
629.70	0.000	0.026	55.412	1.256	30.631	13.350	0.137	0.465	0.051	0.316	0.193	**101.837**
630.20	0.005	0.012	55.826	1.437	30.143	12.248	0.000	1.243	0.082	0.281	0.245	**101.522**
630.20	0.033	0.034	55.222	1.267	28.105	12.636	0.259	0.640	0.093	0.315	0.280	**98.884**
630.20	0.009	0.011	55.793	1.627	28.516	13.686	0.091	0.508	0.062	0.315	0.216	**100.834**
637.00	0.000	0.000	55.373	1.682	31.022	10.528	0.246	1.337	0.116	0.211	0.372	**100.887**
637.00	0.000	0.018	54.834	1.531	30.290	10.626	0.276	0.745	0.146	0.226	0.277	**98.969**
641.06	0.000	0.036	56.475	1.319	29.915	11.386	0.000	0.814	0.160	0.252	0.154	**100.511**
641.06	0.018	0.000	56.640	1.291	29.469	10.790	0.076	0.740	0.153	0.197	0.233	**99.607**
644.20	0.005	0.024	54.736	1.943	30.051	10.649	0.183	1.242	0.106	0.187	0.416	**99.542**
644.20	0.007	0.001	55.037	1.570	31.114	11.331	0.259	0.735	0.093	0.227	0.376	**100.750**
644.20	0.009	0.019	54.900	1.653	30.459	10.673	0.168	0.660	0.091	0.196	0.399	**99.227**
650.62	0.054	0.008	57.233	1.689	34.073	5.773	0.368	1.763	0.100	0.113	0.433	**101.607**
650.62	0.013	0.042	57.816	1.525	34.432	6.092	0.000	1.172	0.120	0.163	0.429	**101.804**

Table 5: Borehole WE035D0 Orthopyroxene Mineral Chemistry

Chemical Composition of Orthopyroxene (wt. %) for WE035D0												
Depth (m)	**Na_2O**	**K_2O**	**SiO_2**	**Al_2O_3**	**MgO**	**FeO**	**TiO_2**	**CaO**	**NiO**	**MnO**	**Cr_2O_3**	**Total**
650.62	0.014	0.018	57.587	1.594	35.247	6.437	0.107	0.945	0.114	0.148	0.455	**102.666**
650.62	0.038	0.017	57.662	1.582	33.829	5.898	0.322	0.911	0.117	0.166	0.341	**100.883**
678.40	0.018	0.037	55.694	1.537	28.432	12.999	0.136	1.246	0.087	0.290	0.357	**100.833**
678.40	0.000	0.008	55.597	1.213	28.438	14.327	0.121	0.629	0.144	0.256	0.243	**100.976**
678.40	0.012	0.028	56.369	0.856	30.009	12.838	0.151	0.547	0.088	0.186	0.428	**101.512**
678.40	0.000	0.038	55.761	1.112	28.736	14.005	0.136	0.515	0.145	0.252	0.455	**101.155**

Appendix H: Mineral Chemistry
Table 6: Borehole WE035D0 Clinopyroxene Mineral Chemistry

Chemical Composition of Clinopyroxene (wt. %) for WE035D0												
Depth (m)	**Na_2O**	**K_2O**	**SiO_2**	**Al_2O_3**	**MgO**	**FeO**	**TiO_2**	**CaO**	**NiO**	**MnO**	**Cr_2O_3**	**Total**
377.53	0.359	0.016	52.091	1.865	14.163	7.260	0.364	22.146	0.080	0.636	0.201	**99.181**
399.70	0.126	0.023	54.195	0.347	15.116	5.061	0.000	23.466	0.033	0.210	0.153	**98.730**
402.30	0.316	0.012	53.987	1.723	15.840	6.626	0.348	21.842	0.046	0.218	0.262	**101.220**
402.30	0.317	0.020	52.169	2.170	14.136	6.863	0.727	21.467	0.073	0.203	0.385	**98.530**
402.30	0.318	0.032	52.467	1.858	15.004	7.113	0.332	21.414	0.021	0.173	0.312	**99.044**
402.30	0.368	0.021	52.023	2.336	14.362	7.195	0.695	21.289	0.033	0.206	0.409	**98.937**
419.50	0.319	0.008	52.280	2.509	15.259	6.480	0.380	22.346	0.033	0.185	0.632	**100.431**
419.50	0.349	0.034	52.290	2.560	14.816	6.545	0.221	21.902	0.017	0.212	0.539	**99.485**
419.50	0.373	0.023	51.354	2.575	14.498	6.634	0.395	21.846	0.031	0.174	0.647	**98.550**
419.50	0.376	0.015	51.825	2.245	15.099	7.160	0.253	21.492	0.018	0.162	0.423	**99.068**
419.50	0.344	0.029	51.888	2.189	14.557	6.323	0.253	21.367	0.029	0.151	0.510	**97.640**
421.00	0.258	0.004	50.972	2.247	14.448	6.099	0.237	22.034	0.051	0.164	0.566	**97.080**
421.00	0.311	0.026	52.489	2.284	14.970	6.409	0.474	21.873	0.000	0.162	0.477	**99.475**
421.00	0.318	0.014	52.535	1.904	15.078	6.267	0.348	21.668	0.008	0.143	0.403	**98.686**
437.30	0.342	0.003	51.796	2.643	15.232	5.271	0.396	21.797	0.016	0.164	0.590	**98.250**
437.30	0.267	0.021	52.895	2.427	15.191	5.426	0.253	21.713	0.048	0.105	0.402	**98.748**
457.65	0.311	0.033	52.571	2.577	15.365	6.387	0.317	22.176	0.091	0.186	0.403	**100.417**
515.00	0.372	0.028	51.672	2.652	15.762	4.481	0.396	22.116	0.086	0.102	0.691	**98.358**
530.00	0.789	0.021	42.304	30.547	0.013	0.939	0.000	21.507	0.012	0.000	0.000	**96.132**
530.00	0.217	0.000	38.256	25.408	0.227	6.482	0.095	20.725	0.018	0.369	0.000	**91.797**
534.00	0.330	0.020	52.385	2.302	16.606	5.221	0.729	21.790	0.000	0.177	0.179	**99.739**
543.00	0.419	0.035	51.757	2.745	15.978	5.391	0.317	21.661	0.000	0.179	0.678	**99.160**
550.60	0.246	0.035	50.175	1.388	16.244	4.107	0.382	23.912	0.008	0.148	0.062	**96.707**
550.60	0.081	0.005	54.427	0.925	16.510	3.722	0.064	23.019	0.030	0.104	0.112	**98.999**
567.40	0.418	0.022	52.113	2.781	16.008	5.159	0.348	21.670	0.068	0.185	0.959	**99.731**
578.00	0.420	0.011	51.325	3.179	15.121	4.893	0.237	21.813	0.013	0.147	1.095	**98.254**
578.00	0.474	0.025	52.071	3.105	15.127	4.345	0.127	21.655	0.062	0.211	1.114	**98.316**
578.00	0.438	0.008	51.778	3.159	15.163	4.978	0.127	21.431	0.084	0.153	1.071	**98.390**

Table 6: Borehole WE035D0 Clinopyroxene Mineral Chemistry

Chemical Composition of Clinopyroxene (wt. %) for WE035D0												
Depth (m)	**Na_2O**	**K_2O**	**SiO_2**	**Al_2O_3**	**MgO**	**FeO**	**TiO_2**	**CaO**	**NiO**	**MnO**	**Cr_2O_3**	**Total**
600.00	0.405	0.008	52.152	3.218	15.915	4.760	0.143	21.746	0.047	0.146	1.066	**99.606**
600.00	0.383	0.010	52.289	3.123	15.891	4.658	0.063	21.281	0.007	0.077	1.104	**98.886**
629.70	0.181	0.009	54.091	0.420	15.520	5.020	0.048	22.846	0.039	0.187	0.127	**98.488**
629.70	0.353	0.005	52.320	2.711	15.867	6.527	0.126	20.202	0.059	0.168	0.476	**98.814**
637.00	0.173	0.040	53.750	0.780	17.069	3.376	0.016	23.737	0.016	0.149	0.170	**99.276**
650.62	0.024	0.034	37.465	24.192	2.905	6.171	0.000	19.693	0.000	0.120	0.016	**90.620**